frontiers | Research Topics

Novel biomarkers in tumor immunity and immunotherapy

Edited by
Takaji Matsutani, Esra Akbay and Eyad Elkord

Published in
Frontiers in Immunology
Frontiers in Oncology

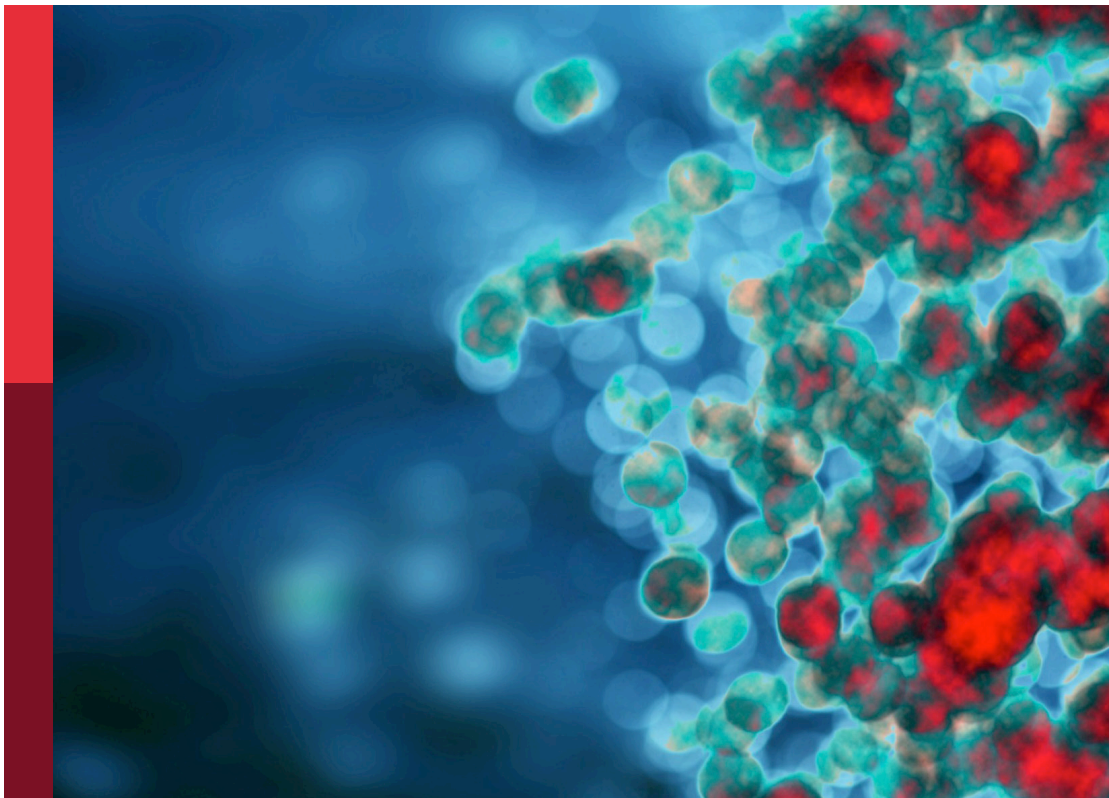

ISSN 1664-8714
ISBN 978-2-8325-4794-6
DOI 10.3389/978-2-8325-4794-6

About Frontiers

Frontiers is more than just an open access publisher of scholarly articles: it is a pioneering approach to the world of academia, radically improving the way scholarly research is managed. The grand vision of Frontiers is a world where all people have an equal opportunity to seek, share and generate knowledge. Frontiers provides immediate and permanent online open access to all its publications, but this alone is not enough to realize our grand goals.

Frontiers journal series

The Frontiers journal series is a multi-tier and interdisciplinary set of open-access, online journals, promising a paradigm shift from the current review, selection and dissemination processes in academic publishing. All Frontiers journals are driven by researchers for researchers; therefore, they constitute a service to the scholarly community. At the same time, the *Frontiers journal series* operates on a revolutionary invention, the tiered publishing system, initially addressing specific communities of scholars, and gradually climbing up to broader public understanding, thus serving the interests of the lay society, too.

Dedication to quality

Each Frontiers article is a landmark of the highest quality, thanks to genuinely collaborative interactions between authors and review editors, who include some of the world's best academicians. Research must be certified by peers before entering a stream of knowledge that may eventually reach the public - and shape society; therefore, Frontiers only applies the most rigorous and unbiased reviews. Frontiers revolutionizes research publishing by freely delivering the most outstanding research, evaluated with no bias from both the academic and social point of view. By applying the most advanced information technologies, Frontiers is catapulting scholarly publishing into a new generation.

What are Frontiers Research Topics?

Frontiers Research Topics are very popular trademarks of the *Frontiers journals series*: they are collections of at least ten articles, all centered on a particular subject. With their unique mix of varied contributions from Original Research to Review Articles, Frontiers Research Topics unify the most influential researchers, the latest key findings and historical advances in a hot research area.

Find out more on how to host your own Frontiers Research Topic or contribute to one as an author by contacting the Frontiers editorial office: frontiersin.org/about/contact

Novel biomarkers in tumor immunity and immunotherapy

This ebook is split into several files; this is part one of the ebook, please see the overview text of the Research Topic page to access the second part of the ebook.

Topic editors

Takaji Matsutani — Maruho, Japan

Esra Akbay — University of Texas Southwestern Medical Center, United States

Eyad Elkord — University of Salford, United Kingdom

Citation

Matsutani, T., Akbay, E., Elkord, E., eds. (2024). *Novel biomarkers in tumor immunity and immunotherapy*. Lausanne: Frontiers Media SA.

doi: 10.3389/978-2-8325-4794-6

Table of contents

frontiers | Frontiers in Immunology

TYPE Editorial
PUBLISHED 08 April 2024
DOI 10.3389/fimmu.2024.1405082

OPEN ACCESS

EDITED AND REVIEWED BY
Peter Brossart,
University of Bonn, Germany

*CORRESPONDENCE
Takaji Matsutani
matsutani_fhu@mii.maruho.co.jp
Eyad Elkord
eyad.elkord@xjtlu.edu.cn

RECEIVED 22 March 2024
ACCEPTED 27 March 2024
PUBLISHED 08 April 2024

CITATION
Matsutani T, Akbay E and Elkord E (2024) Editorial: Novel biomarkers in tumor immunity and immunotherapy.
Front. Immunol. 15:1405082.
doi: 10.3389/fimmu.2024.1405082

Editorial: Novel biomarkers in tumor immunity and immunotherapy

Takaji Matsutani[1]*, Esra Akbay[2] and Eyad Elkord[3,4]*

[1]Translational Research Department, Drug Development Laboratories, Kyoto R&D Center, Maruho Co., Ltd., Kyoto, Japan, [2]Department of Pathology, University of Texas Southwestern Medical Center, Dallas, TX, United States, [3]Department of Biological Sciences, School of Science, Xi'an Jiaotong-Liverpool University, Suzhou, Jiangsu, China, [4]Biomedical Research Center, School of Science, Engineering and Environment, University of Salford, Manchester, United Kingdom

KEYWORDS

biomarker, ICI, bioinformatics, tumor immunology, transcriptome, microbiome

Editorial on the Research Topic
Novel biomarkers in tumor immunity and immunotherapy

In this Research Topic, numerous researchers reported novel biomarkers and methodologies for predicting the efficacy of cancer immunotherapy across various cancers. Additionally, a wide spectrum of fundamental research has been conducted, leading to the discovery of biomarkers. Alongside traditional immunological analyses, a diverse array of methodologies such as bulk RNA-Seq, scRNA-Seq, and bacterial flora analysis have been employed. Moreover, state-of-the-art bioinformatics technologies have been effectively utilized in biomarker discovery. These investigations not only unveil intriguing new discoveries facilitated by cutting-edge technologies but also hold significant promise for shaping the future landscape of tumor immunology.

We are pleased to present this successful Research Topic to the scientific community. This Research Topic comprises six reviews and forty-one original papers. Four systemic reviews on predicting response to immune checkpoint inhibitors (ICI) were published: Qian et al. conducted a meta-analysis, affirming that plasma EBV DNA levels serve as reliable biomarkers for predicting favorable responses to ICI treatment in nasopharyngeal cancer patients, Rugambwa et al. established an association between high neutrophil-lymphocyte and platelet-lymphocyte ratios and poorer ICI treatment outcomes, and Fejza et al. presented accumulating evidence indicating extracellular matrix molecules as biomarkers identifying patients benefiting from ICI treatment. Shi et al. compared various predictive biomarker testing methods for ICI efficacy, while Wu et al. reviewed small molecule inhibitors for KRAS mutant cancers. Fonseca-Montaño et al. delved into the significance of long-non coding RNAs (lncRNAs) in breast cancer and their latest findings. These reviews furnish insights into the current status of previous studies in the realm of tumor immunology, aiding in the recognition and anticipation of forthcoming challenges.

Biomarkers encompass cancer-specific and cancer-nonspecific markers applicable across diverse cancer types. Within this purview, several intriguing factors have been identified as treatment response and prognosis markers in pan-cancer patients. Dong et al. revealed the multifaceted role of Proteasome Activator Complex Subunit 3 (PSME3) in tumors, establishing it as a pan-cancer prognostic marker. Lin et al. proposed Glioma pathogenesis related-2 (GLIPR2) as a promising novel biomarker and tumor suppressor.

Liu et al. examined the functional attributes of Tubulin epsilon and delta complex 2 (TEDC2) in human tumors, identifying TEDC2 as a prognostic marker across various tumor types. Li et al. elucidated the role of disulfidoptosis-related genes (DRGs) in pan-cancer prognosis and their interplay with immunity, constructing a prognostic model utilizing various bioinformatics and machine learning techniques. Zhu et al. highlighted that high expression of Origin recognition complex 6 (ORC6) could serve as a prognostic biomarker in pan-cancer patients. Wei et al. showed the positive correlation between elevated expression levels of IFN-γ-related genes and drug sensitivity, emphasizing the pivotal role of IFN-γ in tumor immunotherapy. Pan et al. reported on the involvement of integrin-binding sialic acid protein (IBSP), a member of the small integrin-binding ligand N-linked glycoprotein (SIBLING) family, in tumorigenesis across various cancers, proposing IBSPs as prognostic biomarkers and immunotherapy targets in pan-cancer. Wu et al. delineated the prognostic potential of the Ferroptosis-related gene Hypermethylated in Cancer 1 (HIC1) in various cancers, indicative of its utility in predicting cancer prognosis, immunotherapy response, and drug sensitivity. Li et al. demonstrated the significant correlation of Thymosin beta-10 (TMSB10) with the tumor microenvironment and immune regulatory factors, advocating its role as a predictive marker for therapeutic response in cancer patients. Huang et al. identified Four Jointed Box 1 (FJX1) as a novel prognostic factor crucial in tumor immunity based on comparative expression profile analysis. Sun et al. established an association between dysregulation of the proprotein convertase subtilisin/kexin-9 (PCSK9) and poor clinical outcomes, suggesting its potential as a robust pan-cancer biomarker. These studies link these genes previously not directly linked to oncogenesis or tumor immunity to immune regulation and suggest potential role as biomarkers.

Studies focusing on specific tumors have unveiled several therapeutic and prognostic markers in hepatocellular carcinoma (HCC). Shi et al. developed the PCD Index (PCDI), comprising programmed cell death-related genes, as a prognostic and treatment response predictor in HCC. Zhang et al. observed elevated expression of DnaJ heat shock protein family member C8 (DNAJC8) in HCC tissues, correlating with poor prognosis and demonstrating its oncogenic role. Jiang et al. identified a significant correlation between CD93 expression and the prognosis of liver hepatocellular carcinoma patients. Xu et al. elucidated abnormal T follicular helper cell infiltration associated with forkhead box M1 (FOXM1) as a crucial prognostic factor in HCC patients.

Prominent biomarkers have also emerged from studies on lung adenocarcinoma (LUAD) and lung squamous cell carcinoma (LUSC). Li et al. focused on coagulation- and macrophage-associated (COMAR) genes, constructing a COMAR risk score model predictive of prognosis and clinical outcome in LUAD patients. Zhu et al. identified twelve HUB genes via Weighted Gene Coexpression Network Analysis (WGCNA), potentially implicated in LUAD progression via immune-related signaling pathways. Wu et al. derived LUSC-specific differentially expressed gene signatures (7-DEGs) with prognostic significance for LUSC patients.

A multitude of original and intensive investigations have explored valid biomarkers across a diverse array of tumors. Li et al. identified hub biomarkers closely associated with gastric cancer (GC) using microarray data and algorithmic approaches. Cai et al. delineated the multifaceted role of Fibroblast activation protein (FAP) in gastrointestinal cancer progression. Deng et al. developed a prognostic panel using hypoxia-related genes, predicting clinical prognosis and treatment efficacy in GC. Chen et al. devised a prognostic score model based on tumor microenvironment (TME)-related genes, effectively predicting breast cancer patient prognosis and chemotherapy efficacy. Wei et al. employed immune- and cancer-associated fibroblast (CAF)-associated genes (ICRGs) to prognosticate and evaluate immunotherapy efficacy in colorectal adenocarcinoma patients. Hailang et al. identified the gene encoding mitochondrial Aspartyl-tRNA synthetase 2 (DARS2) as a prognostic biomarker in bladder cancer. Dong et al. unveiled the impact of necroptosis-associated myeloid lineages on the immune landscape of pancreatic cancer through scRNA-Seq analysis. Liu et al. conducted LASSO and Cox regression analyses on angiogenesis-related genes (ARGs) in soft-tissue sarcomas (STS) to establish a novel ARG signature (ARSig). Their study demonstrated that ARSig holds promise as an independent prognostic predictor for STS. Li et al. demonstrated that C15orf48, an inflammatory response-related gene, could be a potential biomarker for tumor prognosis and a target for immunotherapy in thyroid cancer. Jiang et al. identified two immunogenic cell death (ICD) subtypes through consensus clustering analysis and constructed an ICD prognostic signature capable of predicting overall survival in patients with renal clear cell carcinoma.

Recent insights underscore the pivotal role of the gut microbiota in the cancer microenvironment and its influence on the efficacy of immunotherapies such as ICIs. Multiple studies have been dedicated to this research area. Zhao et al. reported that enrichment of the gut microbiota, particularly Lachnoclostridium, correlates with the presence of intratumoral tertiary lymphoid structures (TLS) in HCC patients. Gorgulho et al. proposed an immune-microbial score comprising the relative abundance of CD3+HLADR+, NLR, and enterobacteria, which demonstrated predictive capability for therapeutic response to ICIs. Hamada et al. identified bacteria implicated in the efficacy of ICIs and immune-related adverse events (irAEs), suggesting promise for developing a marker to predict cancer immunotherapy efficacy through gut microbiota and fecal transplantation applications.

Several novel and useful biomarkers have emerged from serological methods. Hou et al. identified serum cytokines and the neutrophil-to-lymphocyte ratio as effective biomarkers for predicting the efficacy of ICIs in gastric cancer. Liu et al. introduced an inflammatory prognostic index (InPI) based on three inflammatory markers in patients with relapsed/refractory multiple myeloma (R/R MM) treated with CAR-T therapy, demonstrating its validity as a prognostic biomarker. Raza et al. identified novel immunosuppressive/stimulatory soluble mediators as surrogate and predictive biomarkers of tissue PD-L1 (TPD-L1) status, treatment response, and progression-free survival (PFS) in NSCLC patients treated with ICI.

Many studies have shown that the development of new methods and a multifaceted approach can help in the development of new

biomarkers. Ohkuma et al. developed a highly sensitive quantitative immunohistochemical method employing phosphor-integrated dots (PID) for evaluating PD-L1 expression quantitatively. Utilizing this method, they were able to detect PD-L1 expression in the tumors of a subgroup of patients with a favorable prognosis with ICI. Zhang et al. established an alternative splicing (AS) prognostic signature based on AS subtypes in clear cell carcinoma (ccRCC), emphasizing the importance of the AS-SF network, inclusive of splicing factors (SFs), in studying regulatory mechanisms. Yang et al. introduced the CRP-albumin-lymphocyte (CALLY) index, which combines C-reactive protein (CRP), albumin, and lymphocytes, demonstrating its superior prognostic value compared to classical prognostic factors in colorectal cancer patients. Liu et al. introduced a novel biomarker for breast cancer, a nectin-4-specific scFv, with diagnostic and therapeutic applications, recognizing nectin-4 expressed by breast cancer cells *in vitro* and *ex vivo*. Zhou et al. identified CD26lowPD-1+ CD8 T cells associated with acute myeloid leukemia (AML) progression and described the prognostic significance of CD26 in AML. Inaba et al. suggested amino acid polymorphisms of HLA class II molecules and HLA-DP5 as genetic predictors of ICI-T1DM in type 1 diabetes induced by ICIs. Wang et al. demonstrated the utility of 18F-fluorodeoxyglucose positron emission tomography (18F-FDG PET) as an imaging biomarker for predicting pathologic response and prognosis in patients with unresectable hepatocellular carcinoma treated with lenvatinib and PD-1 as a conversion therapy.

The compilation of studies in this Research Topic explores various facets of tumor immunology, focusing on identifying novel biomarkers and predictive methods for cancer immunotherapy across diverse cancer types. Researchers employ advanced technologies to uncover promising biomarkers with implications for treatment response and prognosis in cancer patients. Systematic reviews and original papers shed light on the multifaceted landscape of tumor immunology, exploring biomarkers ranging from traditional immunological markers to emerging candidate biomarkers. Notably, investigations extend beyond cancer-specific markers, revealing the involvement of interesting molecules in cancer progression. Moreover, studies elucidate the role of the gut microbiota in modulating the tumor microenvironment and response to immunotherapy, offering insights into potential therapeutic interventions. Serological methods offer valuable biomarkers, while technological advancements, including quantitative immunohistochemical methods, enhance prognostic accuracy. This comprehensive body of work not only highlights the current state of tumor immunology research but also paves the way for future advancements in cancer diagnosis, prognosis, and treatment.

Author contributions

TM: Writing – original draft, Writing – review & editing. EA: Writing – review & editing. EE: Writing – review & editing.

Acknowledgments

We would like to thank all the authors who participated in the *Novel biomarkers in tumor immunity and immunotherapy* Research Topic, each of the reviewers for their careful peer review and valuable assistance, and the editorial office of the Frontier Journal. We thank Dr. Dennis O Adeegbe for his significant contribution to the conception and editing the proposal of this Research Topic.

Conflict of interest

Author TM is employed by the company Maruho Co., Ltd.

The remaining authors declare that the research was conducted in the absence of any commercial or financial relationships that could be construed as a potential conflict of interest.

The author(s) declared that they were an editorial board member of Frontiers, at the time of submission. This had no impact on the peer review process and the final decision.

Publisher's note

frontiers | Frontiers in Immunology

TYPE Original Research
PUBLISHED 09 March 2023
DOI 10.3389/fimmu.2023.1131870

OPEN ACCESS

EDITED BY
Takaji Matsutani,
Repertoire Genesis, Inc., Japan

REVIEWED BY
Shoib Sarwar Siddiqui,
University of Hertfordshire,
United Kingdom
Xiao-yuan Li,
The Affiliated Hospital of Qingdao
University, China

*CORRESPONDENCE
Chaolin Li
kone_lcl@foxmail.com
Hao Shi
JNFY_shihao@163.com

SPECIALTY SECTION
This article was submitted to
Cancer Immunity
and Immunotherapy,
a section of the journal
Frontiers in Immunology

RECEIVED 26 December 2022
ACCEPTED 23 February 2023
PUBLISHED 09 March 2023

CITATION
Li C, Tang Y, Li Q, Liu H, Ma X, He L and
Shi H (2023) The prognostic and immune
significance of C15orf48 in pan-cancer and
its relationship with proliferation and
apoptosis of thyroid carcinoma.
Front. Immunol. 14:1131870.
doi: 10.3389/fimmu.2023.1131870

The prognostic and immune significance of C15orf48 in pan-cancer and its relationship with proliferation and apoptosis of thyroid carcinoma

Chaolin Li[1]*, Yan Tang[2], Qin Li[1], Haiyan Liu[1], Xiaoying Ma[1], Liu He[3] and Hao Shi[3]*

[1]Department of Obstetrics, Jinniu District Maternal and Child Health Hospital, Chengdu, China, [2]Department of Medical Laboratory, Jinniu District Maternal and Child Health Hospital, Chengdu, China, [3]Department of Pediatrics, Jinniu District Maternal and Child Health Hospital, Chengdu, China

Background: C15orf48 was recently identified as an inflammatory response-related gene; however there is limited information on its function in tumors. In this study, we aimed to elucidate the function and potential mechanism of action of C15orf48 in cancer.

Methods: We evaluated the pan-cancer expression, methylation, and mutation data of C15orf48 to analyze its clinical prognostic value. In addition, we explored the pan-cancer immunological characteristics of C15orf48, especially in thyroid cancer (THCA), by correlation analysis. Additionally, we conducted a THCA subtype analysis of C15orf48 to determine its subtype-specific expression and immunological characteristics. Lastly, we evaluated the effects of C15orf48 knockdown on the THCA cell line, BHT101, by *in vitro* experimentation.

Results: The results of our study revealed that C15orf48 is differentially expressed in different cancer types and that it can serve as an independent prognostic factor for glioma. Additionally, we found that the epigenetic alterations of C15orf48 are highly heterogeneous in several cancers and that its aberrant methylation and copy number variation are associated with poor prognosis in multiple cancers. Immunoassays elucidated that C15orf48 was significantly associated with macrophage immune infiltration and multiple immune checkpoints in THCA, and was a potential biomarker for PTC. In addition, cell experiments showed that the knockdown of C15orf48 could reduce the proliferation, migration, and apoptosis abilities of THCA cells.

Conclusions: The results of this study indicate that C15orf48 is a potential tumor prognostic biomarker and immunotherapy target, and plays an essential role in the proliferation, migration, and apoptosis of THCA cells.

KEYWORDS

C15orf48, THCA, immunity therapy, apoptosis, biomarkers

1 Introduction

Cancer is a major public health concern worldwide (1). Studies show that approximately 3.21 million people died of cancer in 2022 (2). According to the latest assessment of the American Cancer Society, it is estimated that 609,820 people will die of cancer in the USA in 2023 (3). However, developments in immunotherapy, such as immune checkpoint (ICP)-targeting monoclonal antibodies and chimeric antigen receptor T cell therapy, have led to improvements in cancer treatment and prognosis (4, 5). Although these therapies have achieved great success in some cancers, such as breast cancer (BRCA) and glioblastoma (6, 7), their efficacy and post-treatment survival rates are low, especially for some metastatic cancers (8). Several studies have explored the common immunological features of cancers to determine the underlying mechanisms of tumorigenesis and progression (9); however, single cancer-targeting studies limit our understanding of the multifaceted nature of the cancer-related genes and features. Therefore, studies on the macroscopic 'pan-cancer' perspective might help reveal the underlying mechanism of tumorigenesis in malignant cancers (10–12).

C15orf48 (also known as Normal Mucosa of Esophagus-Specific Gene 1 protein [NMES1] and Modulator of Cytochrome C Oxidase during Inflammation [MOCCI]) was initially found to be downregulated in human esophageal squamous cell carcinoma (13), while another study found that it contributed to the development of colon cancer (14). C15orf48 forms a part of complex IV in the mitochondrial respiratory chain and interacts with multiple subunits in complexes I and IV (15, 16). Specifically, C15orf48 is a homolog of the NDUFA4 subunit of cytochrome C oxidase (complex IV), which replaces NDUFA4 in complex IV during inflammation, thereby reducing the membrane potential of mitochondria and reducing the production of reactive oxygen species (ROS), thus inhibiting immune response (17, 18). The inflammatory tumor microenvironment (TME) induced by chronic inflammation can greatly promote tumorigenesis (19). However, the potential role of C15orf48 has only been explored in esophageal squamous cell carcinoma and colon cancer, thus limiting the information on the role of C15orf48 in pan-cancer epigenetic changes, immunological characteristics, and prognosis. Therefore, in this study, we analyzed the pan-cancer expression level, methylation, single-cell mutation, copy number variation (CNV), and prognostic role of C15orf48. Additionally, by using multiple algorithms, we assessed the pan-cancer immunological signature of C15orf48 and its association with immunotherapy response. In addition, we analyzed the specific immunological characteristics, related functions, and subtype characteristics of C15orf48 in thyroid cancer (THCA) and verified the results by *in vitro* experimentation. The results of our study will help reveal the potential role of C15orf48 in tumor immunology and provide new directions for immunotherapy research.

2 Materials and method

2.1 Data collection

The mRNA expression profiles and clinical data of 33 cancers were downloaded from the Cancer Genome Atlas (TCGA) database (https://portal.gdc.cancer.gov/), and the mRNA expression profiles of normal tissues were downloaded from the Genotype-Tissue Expression (GTEx) database (https://www.gtexportal.org/home/) and Human Protein Atlas (HPA) database (https://www.proteinatlas.org/). Cell line gene expression matrices for tumors were obtained from the Cancer Cell Line Encyclopedia dataset (CCLE, https://portals.broadinstitute.org/ccle/about). The CNV data of 11,495 samples were downloaded from the TCGA database and processed by Genomic Identification of Significant Targets in Cancer v2.0. We also downloaded the level 4 single nucleotide variation (SNV) dataset and Illumina HumanMethylation 450k level 3 data of all TCGA samples processed by MuTect2 (20). The glioblastoma dataset, CGGA325, was downloaded from the Chinese Glioma Genome Atlas (CGGA) database (http://www.cgga.org.cn/) (21). Lastly, tumor mutation burden (TMB) and microsatellite instability (MSI) data were derived from studies by Vesteinn Thorsson et al. and Russell Bonneville et al., respectively (22, 23). Abbreviations and sample information are provided in Supplementary Table 1.

2.2 Pan-cancer differential expression, prognosis, and epigenetic analysis of C15orf48

The HPA and GTEx data were used to analyze the expression of C15orf48 in the normal tissues. C15orf48 cancer cell line expression levels were analyzed using CCLE data, and C15orf48 single-cell expression was analyzed using HPA and Tumor Immune Single-cell Hub (TISCH) data (http://tisch.comp-genomics.org/). The expression profiles of TCGA and GTEx were integrated and the differential expression of C15orf48 in tumor and normal tissues was compared. Thereafter, the samples from 33 cancer types were divided into high- and low-expression groups according to the median expression of C15orf48. Thereafter, the R package "survival" was used to compare the survival time and survival status of the two groups. The *p*-values and hazard ratios (HR, with 95% confidence intervals [CI]), for the Kaplan–Meier curves, were derived by log-rank test and univariate cox regression analysis. The time-dependent receiver operating characteristic (timeROC) analysis was used to compare the prediction accuracy of C15orf48, while univariate and multivariate cox regression analyses were used to assess its value as an independent prognostic factor.

We assessed the C15orf48 methylation levels of normal and pan-cancer tumor tissues and divided the tumor samples into high-

and low-methylation groups according to the median C15orf48 methylation level. Spearman correlation analysis was used to obtain the correlation between C15orf48 mRNA expression and methylation level. Thereafter, the R package "survival" was used to compare the survival time and survival status of the two groups. The pan-cancer C15orf48 SNV data were visualized using the R package "maftools". In addition, we assessed the pan-cancer C15orf48 CNV data and its association with pan-cancer prognosis. We also assessed the correlation of C15orf48 with pan-cancer TMB and MSI and the correlation between C15orf48 and 44 marker genes of three classes of RNA modifications (m1A, m5C, and m6A).

2.3 Association between C15orf48 and pan-cancer immune cell infiltration and immunotherapy response

The stromal, immune, and ESTIMATE scores of each tumor sample were calculated according to C15orf48 expression, using the R package "Estimation of STromal and Immune cells in MAlignant Tumor tissues using Expression data" (ESTIMATE) v1.0.13 (24). We used 5 algorithms, including single-sample Gene Set Enrichment Analysis (ssGSEA), Cell-type Identification by Estimating Relative Subsets of RNA Transcripts (CIBERSORT), Tumor IMmune Estimation Resource (TIMER), Estimating the Proportion of Immune and Cancer cells (EPIC), and Microenvironment Cell Populations (MCP)-counter, to determine the correlation between C15orf48 and pan-cancer ICI. We also evaluated the response of C15orf48 high- and low-expression groups to programmed cell death protein 1 (PD-1) and cytotoxic T-lymphocyte associated protein 4 (CTLA4) immunotherapy (25) from the Cancer Immunome Atlas data (TCIA, https://tcia.at/home).

2.4 Immunological characteristics, functional enrichment, and subtype characteristics of C15orf48 in THCA

Based on a study by Charoentong et al. (25), we obtained 122 immune modulators and evaluated their correlation with C15orf48 mRNA expression in THCA. The anti-cancer immune state reflects the various activities of the cancer immune cycle. We used the Tracking Tumor Immunophenotype (TIP) database (http://biocc.hrbmu.edu.cn/TIP/) to assess the anti-cancer immune status at 7 different stages of the tumor immune cycle, including the release of cancer cell antigens (step 1), cancer antigen presentation (step 2), priming and activation (step 3), trafficking of immune cells to tumors (step 4), ICI in tumors (step 5), recognition of cancer cells by T cells (step 6), and killing of cancer cells (step 7) (26). We used 7 algorithms, including CIBERSORT under absolute mode (CIBERSORT-ABS), MCP-counter, quantification of the Tumor Immune contexture from human RNA-seq data (quantIseq), TIMER, xCell, EPIC, and Tumor-Immune System Interactions database (TISIDB, http://cis.hku.hk/TISIDB/index.php), to calculate the level of ICI of C15orf48 in THCA. The list of genes for the immune process was obtained from the AmiGO 2 portal (http://amigo.geneontology.org/amigo). The correlation between C15orf48 and the immune process was determined using the R package "Gene set variation analysis" (GSVA). In addition, we also calculated the correlation between immune cell marker genes and C15orf48 in THCA.

The Search Tool for Retrieval of Interacting Genes/Proteins (STRING) database (https://string-db.org/) was used to analyze the protein interaction network of C15orf48. The differential expression of C15orf48 high- and low-expression groups in THCA was studied using the R package "Limma" v3.40.2. Furthermore, the R package "ClusterProfiler" was used for Gene Ontology (GO) and Kyoto Encyclopedia of Genes and Genomes (KEGG) enrichment analyses. In addition, we collected the gene sets from the relevant pathways (27) and calculated the correlation between gene expression and pathways according to the ssGSEA algorithm. We also evaluated the expression level of C15orf48, the immune signature, and response to immunotherapy among different THCA subtypes, such as papillary thyroid carcinoma (PTC) and follicular thyroid carcinoma (FTC).

2.5 Cell culture, real-time quantitative reverse transcription PCR, and western blotting analyses

The human THCA cell line, BHT101, was purchased from Shanghai Jinyuan Biotechnology (Shanghai, China) and cultured in the indicated medium with 10% phosphate buffer saline (PBS). The cells were incubated at 37°C and 5% CO_2. Total RNA was extracted with TRIzol reagent (Invitrogen, USA) and reverse transcribed with random primers using Hiscipt III 1st strand cDNA synthesis kit (Vazyme, Nanjing, China) according to the manufacturer's instructions. The following primers were used for qRT-PCR: GAPDH forward primer: 3'-GGAGCGAGATCCCTCCAAAAT-5', reverse primer: 3'-GGCTGTTGTCATACTTCTCATGG-5' and C15orf48 forward primer: 3'-AACTCATTCCCTTGGTG GTGTTCAT-5', reverse primer: 3'-CTCGTCATTTGGTCACC CTTTGGAC-5'.

The cells were transfected with C15orf48 siRNA, harvested, washed thrice with PBS, and collected by centrifugation. Total protein extracts were prepared in radioimmunoprecipitation assay (RIPA) buffer supplemented with proteinase inhibitors (R0010, Solarbio). Anti-C15orf48 (NBP1-98391, Novus Biologicals) and anti-GAPDH (60004-1-Ig, Proteintech) antibodies were used for western blot analysis according to the manufacturer's instructions. Goat anti-mouse IgG-HRP (SA00001-1, Proteintech) and goat anti-rabbit IgG-HRP (SA00001-2, Proteintech) were used as secondary antibodies. GAPDH was used as a protein loading control. The signals were visualized using the enhanced chemiluminescence (ECL) reagent (4A Biotech, China).

2.6 Cell counting kit-8 analysis

BHT101 cells transfected with C15orf48 siRNA were digested once they reached 90% confluency and inoculated into 96-well culture plates at 5000 cells/well and 5 wells/group. Thereafter, the cells were cultured in a 37°C and 5% CO_2 incubator and analyzed at 0, 24, 48, and 72 h using the CCK-8 kit (WLA074, China).

2.7 Wound healing test

BHT101 cells were inoculated in 6-well plates and transfected with C15orf48 siRNA. Thereafter, the cells were scraped with a 200 µl pipette tip. The cell surface was cleaned with a serum-free medium and the cell fragments were removed. The cells were then observed and photographed under a 40× microscope and their positions in the photos were recorded. Subsequently, cells in each group were placed in a 37°C and 5% CO_2 incubator for 24 and 48 h, after which they were photographed and recorded. Lastly, the mobility of each group was calculated.

2.8 Transwell migration and apoptotic assay

A 24-well Transwell chamber (8 µm aperture; Corning Costar, USA) was prepared overnight at 4°C and inoculated with 200 µl of cell suspension containing 100,000 cells/mL. A culture medium (700 µl) containing 10% fetal bovine serum was poured into the lower chamber. After 24 h of incubation at 37°C and 5% CO_2, the cells were fixed using 4% paraformaldehyde at room temperature for 20 mins, stained with 0.5% crystal violet dye for 5 mins, and the cell count was recorded.

BHT101 cells were harvested and resuspended in a binding buffer. Thereafter, the cells were stained with Annexin V-FITC/PI Apoptosis Detection kit (Vazyme, Nanjing, China) according to the manufacturer's instructions. The cells were then analyzed by flow cytometry (Cytoflex, Beckman) and the data were analyzed using CytExpert Software.

2.9 Statistical analysis

All the analysis methods and R packages were implemented using R version 4.1.0, except for the online website tools. Wilcoxon rank-sum test was used to calculate differential expression in normal and tumor samples. Univariate cox regression analysis was done with the "forestplot" R package. We used the Spearman correlation method to perform correlation analysis between C15orf48 transcript levels and immune checkpoint gene expression, TMB levels, and MSI status. Data from cell experiments were analyzed using GraphPad Prism (version 9.0.0) for Windows. All the experiments were repeated in triplicate. Student's t-test was used to assess statistical significance. P values less than 0.05 were considered statistically significant. *$p < 0.05$; **$p < 0.01$; ***$p < 0.001$.

3 Results

3.1 Pan-cancer expression of C15orf48

Analysis of the HPA and GTEx datasets revealed higher expression of C15orf48 in the colon, small intestine, esophagus, and other normal tissues (Figure 1A). Additionally, C15orf48 protein expression was significantly elevated in multiple cancers (Supplementary Figures 1A, B). Furthermore, the single-cell analysis revealed cell-specific expression of C15orf48. Analysis of the HPA single-cell dataset and TISCH online dataset revealed that C15orf48 was significantly overexpressed in macrophages (Figures 1B, C). Moreover, we observed a significant enrichment of C15orf48 in macrophages in some datasets that received immunotherapy (Supplementary Figures 1C, D). Furthermore, correlation analysis between C15orf48 expression and immune cell clustering revealed that C15orf48 is a part of cluster 25 monocytes—inflammatory response with confidence 1 (Figure 1D). Moreover, analysis of the cancer cell lines revealed high expression of C15orf48 in specific cancer types, such as pancreatic cancer, kidney cancer, and colorectal cancer (Figure 1E). Additionally, analysis of the integrated TCGA and GTEx data revealed a significantly high expression of C15orf48 in multiple cancers, including THCA (Figure 1F). These results were further validated by the pan-cancer C15orf48 expression data (platform: GPL570; HG-U133_Plus_2) obtained from the Gene Expression Omnibus (GEO) database (Figure 1G).

3.2 C15orf48 is an independent prognostic factor for glioma

Pan-cancer prognostic analysis revealed that C15orf48 was significantly associated with the prognosis of multiple cancers (Figure 2A). Specifically, high expression of C15orf48 was significantly associated with shorter overall survival (OS), progression-free survival (PFS), disease-specific survival (DSS), and disease-free interval (DFI) in low-grade gliomas (LGGs) (Figures 2B–E). Furthermore, high expression of C15orf48 was significantly associated with shorter OS and DSS in liver hepatocellular carcinoma, lung adenocarcinoma, and pancreatic adenocarcinoma (PAAD) (Supplementary Figure 2A). In addition, varying degrees of prognostic correlations were also observed in head and neck squamous cell carcinoma, skin cutaneous melanoma, BRCA, colon adenocarcinoma, mesothelioma, and prostate adenocarcinoma (PRAD) (Supplementary Figure 2A). Considering its significant association with glioma prognosis, we further evaluated the clinical significance of C15orf48 in glioma. The results showed that C15orf48 was significantly enriched in high-grade glioma, non-1p/19q deletion state, wild-type, and non- O (6)-methylguanine-DNA-methyltransferase (MGMT) promoter methylated samples in both TCGA and CGGA datasets (Supplementary Figure 2B). These results indicated that C15orf48 was highly enriched in more malignant gliomas. In addition, we combined the clinical and expression data of TCGA-glioblastoma multiforme (GBM) and

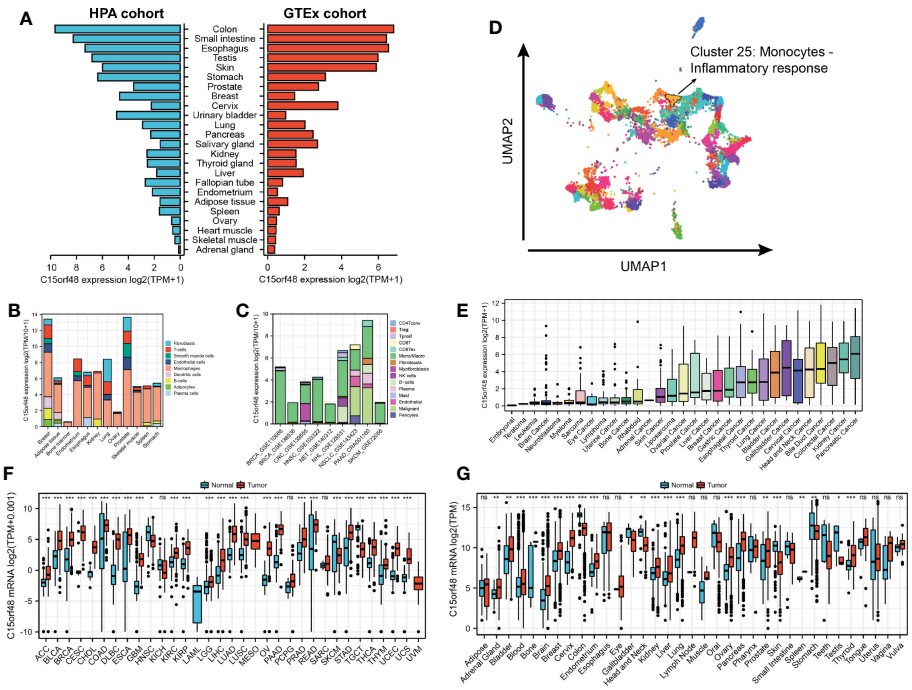

FIGURE 1
(A) Expression level of C15orf48 in normal tissues (HPA+GTEx datasets); **(B)** C15orf48 expression levels in single cells (HPA datasets); **(C)** C15orf48 expression levels in single cells (TISCH datasets); **(D)** C15orf48 is part of cluster 25 Monocytes - Inflammatory response; **(E)** Expression levels of C15orf48 in cancer cell lines (CCLE datasets); **(F)** Differences in the expression of C15orf48 between normal and cancerous tissues (TCGA+GTEx datasets); **(G)** Differences in the expression of C15orf48 between normal and cancerous tissues (GEO datasets). *p < 0.05; **p < 0.01; ***p < 0.001; NS, No Significance.

TCGA-LGG and then evaluated the association between C15orf48 gene expression and patient survival time and survival status. The results showed that glioma patients with high C15orf48 expression had a significantly higher mortality rate with the 1-, 2-, and 3-y mortality prediction areas under the curve (AUC) values of 0.822, 0.801, and 0.804, respectively (Figures 2F–H). These results were further validated using the CGGA database (Figures 2I–K). Lastly, univariate and multivariate cox regression analysis of TCGA and CGGA datasets revealed that C15orf48 can serve as an independent prognostic factor for glioma (Tables 1, 2).

3.3 Pan-cancer epigenetic variations of C15orf48

We further explored the methylation levels of C15orf48 to determine its epigenetic regulation. As shown in Figure 3A, C15orf48 exhibits differential methylation levels in various cancer and normal tissues. Furthermore, the methylation level of C15orf48 was negatively correlated with its mRNA expression to varying degrees in all cancers (Supplementary Figure 3A). Somatic mutations of C15orf48 were primarily missense mutations and the overall somatic mutation rate of C15orf48 was <1%, with the highest mutation rate in rectum adenocarcinoma (READ, 0.76%) (Figure 3B). The CNV of C15orf48 in different tumors was highly heterogeneous (Figure 3C), among which we analyzed both homozygous and heterozygous deletions and amplification. The results showed that heterozygous amplification was prevalent in kidney chromophobe (KICH) and testicular germ cell tumors (TGCT), while heterozygous deletion was prevalent in uterine carcinosarcoma, READ, LUAD, and ovarian serous cystadenocarcinoma. Moreover, the prognostic analysis showed that a high methylation level of C15orf48 was significantly associated with shorter OS, PFS, and DSS in adenoid cystic carcinoma, whereas, a low methylation level of C15orf48 was significantly associated with the poor prognosis of esophageal carcinoma (ESCA), kidney renal clear cell carcinoma (KIRC), acute myeloid leukemia, LGG, and PRAD (Figure 3D; Supplementary Figure 3B). In addition, deletion mutation of C15orf48 was significantly associated with poor prognosis of KIRC, sarcoma (SARC), and THCA, while amplification of C15orf48 was significantly associated with poor prognosis of LGG and uterine corpus endometrial carcinoma (Figure 3E; Supplementary Figure 3C). TMB and MSI are closely associated with clinical treatment and tumor markers. The expression of C15orf48 was significantly correlated with TMB in ESCA, PAAD, LGG, SARC, THCA, etc. (Figure 3F) and significantly correlated with MSI in ESCA, PAAD, SARC, LGG, etc. (Figure 3G). Furthermore, marker genes of C15orf48 and RNA modification showed different degrees of correlation in different cancers (Figure 3H).

10.3389/fimmu.2023.1131870

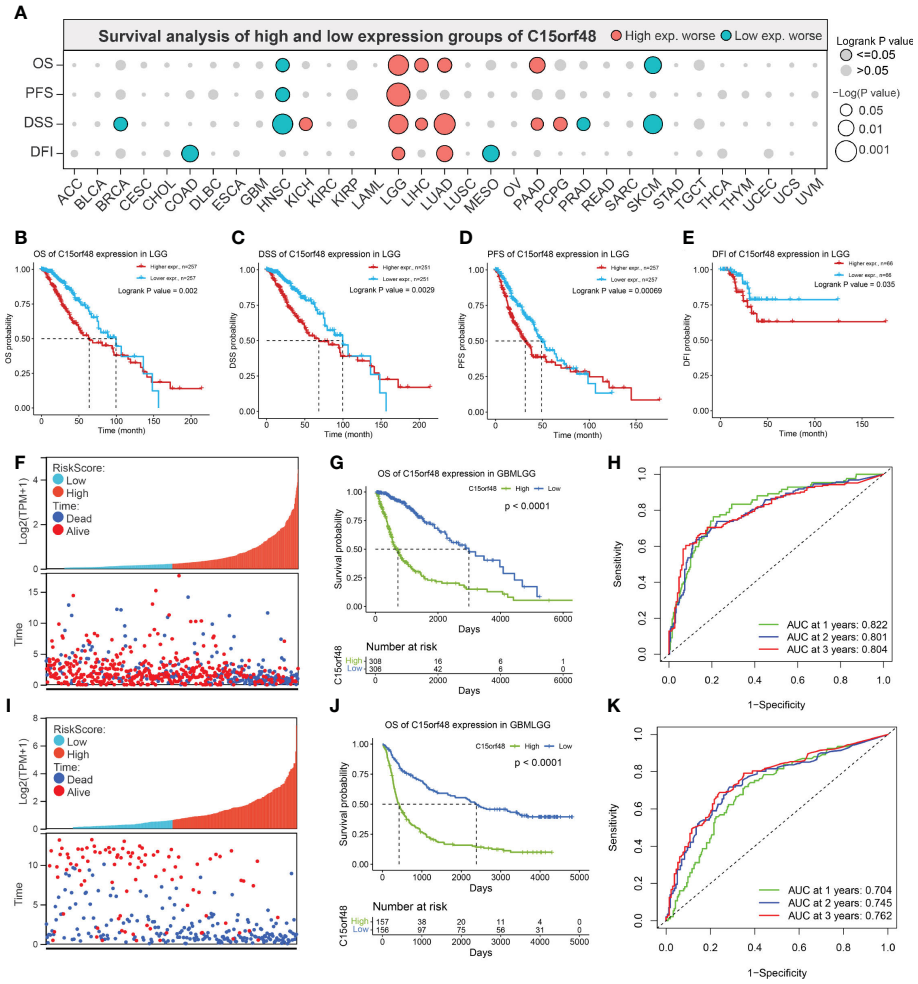

FIGURE 2
(A) Prognosis of C15orf48 in pan-cancer; **(B-E)** High expression of C15orf48 was significantly correlated with shorter OS, DSS, PFS, and DFI of LGG; **(F-H)** Relationship between C15orf48 expression and glioma prognosis score, survival analysis and ROC analysis (TCGA-GBMLGG datasets); **(I–K)** Relationship between C15orf48 expression and glioma prognosis score, survival analysis and ROC analysis (CGGA325 datasets).

3.4 Association between C15orf48 and pan-cancer ICI and immunotherapy response

C15orf48 has a strong positive correlation with immune cells and stromal cells in several cancers, including TGCT, GBM, THCA, etc. (Figure 4A) and with ICPs in TGCT, THCA, KICH, etc. (Figure 4B). Several algorithms, including ssGSEA (Figure 4C), CIBERSORT, TIMER, EPIC, and MCP-counter (Supplementary Figures 4A–D), were used to assess the association of C15orf48 with pan-cancer ICI, and the results revealed that C15orf48 is positively correlated to various levels of ICI in THCA, KICH, TGCT, etc. In addition, C15orf48 was significantly positively correlated with the infiltration scores of major histocompatibility complex (MHC) and

TABLE 1 Univariate and multivariate analyzes of OS prognostic parameters in the TCGA database.

Variable	Univariate analysis		Multivariate analysis	
	HR (95% CI)	*p* value	HR (95% CI)	*p* value
C15orf48	1.501 (1.405-1.604)	2.28E-33	1.114 (1.000-1.241)	0.049
Age	5.043 (3.348-7.596)	9.82E-15	3.605 (2.273-5.716)	5.03E-08
WHO grade	9.544 (6.813-13.371)	2.70E-39	3.957 (2.398-6.530)	7.40E-08
1p/19q Codel	0.220 (0.130-0.375)	2.31E-08	0.397 (0.223-0.705)	0.002
MGMT status	0.312 (0.225-0.433)	2.96E-12	0.627 (0.433-0.909)	0.014

10.3389/fimmu.2023.1131870

TABLE 2 Univariate and multivariate analyzes of OS prognostic parameters in the CGGA database.

Variable	Univariate analysis		Multivariate analysis	
	HR (95% CI)	*p* value	HR (95% CI)	*p* value
C15orf48	2.876 (2.089-3.958)	9.17E-11	1.438 (1.023-2.022)	0.036
Age	1.614 (1.214-2.145)	0.001	1.068 (0.791-1.440)	0.668
WHO grade	4.885 (3.634-6.566)	8.02E-26	3.082 (2.239-4.242)	5.08E-12
1p/19q Codel	0.170 (0.104-0.277)	1.25E-12	0.256 (0.154-0.426)	1.48E-07
MGMT status	0.830 (0.632-1.089)	0.178		

effector cells in TGCT, THCA, and SARC, while it was significantly negatively correlated with the infiltration scores of ICPs and immunosuppressive cells (Supplementary Figure 4E).

Furthermore, we determined the effect of C15orf48 on pan-cancer immunotherapy response. Immunophenoscore (IPS) was used to evaluate the immunotherapy response between the C15orf48 high- and low-expression groups (25), and the results revealed that the C15orf48 high-expression group showed strong immunogenicity upon receiving PD-1, CTLA4, and combination therapy (Figure 4D). In addition, we further evaluated the predictive role of C15orf48 on cancer therapy response using the ROC Plotter database (https://www.rocplot.org/) (28), and the results revealed that C15orf48 was highly expressed in BRCA patients responding to chemotherapy and the AUC value of 5-y recurrence-free survival (RFS) reached 0.645. Moreover, in patients receiving taxane treatment, the AUC of 5-y RFS reached 0.81 (Figure 4E).

3.5 Immunological characteristics, functions, and subtype distribution of C15orf48 in THCA

We observed a strong positive association between C15orf48 and multiple immune modulators (Figure 5A). Some key

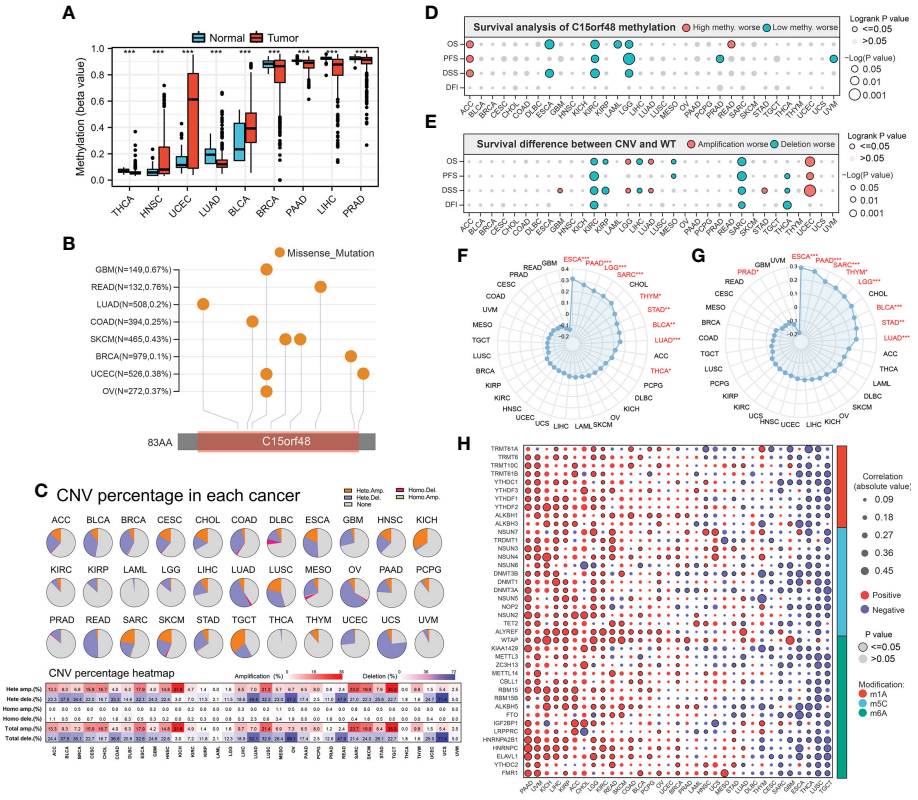

FIGURE 3
(A) Differential methylation levels of C15orf48 in normal and tumor tissues in pan-cancer; **(B)** Somatic mutation levels of C15orf48 in pan-cancer; **(C)** Copy number variation levels of C15orf48 in pan-cancer; **(D)** The relationship between methylation of C15orf48 and prognosis in pan-cancer; **(E)** The relationship between copy number variation of C15orf48 and prognosis in pan-cancer; **(F)** Relationship between C15orf48 and tumor mutational burden in pan-cancer; **(G)** Relationship between C15orf48 and microsatellite instability in pan-cancer; **(H)** Correlation between C15orf48 and RNA-modifying genes in pan-cancer. *p < 0.05; **p < 0.01; ***p < 0.001.

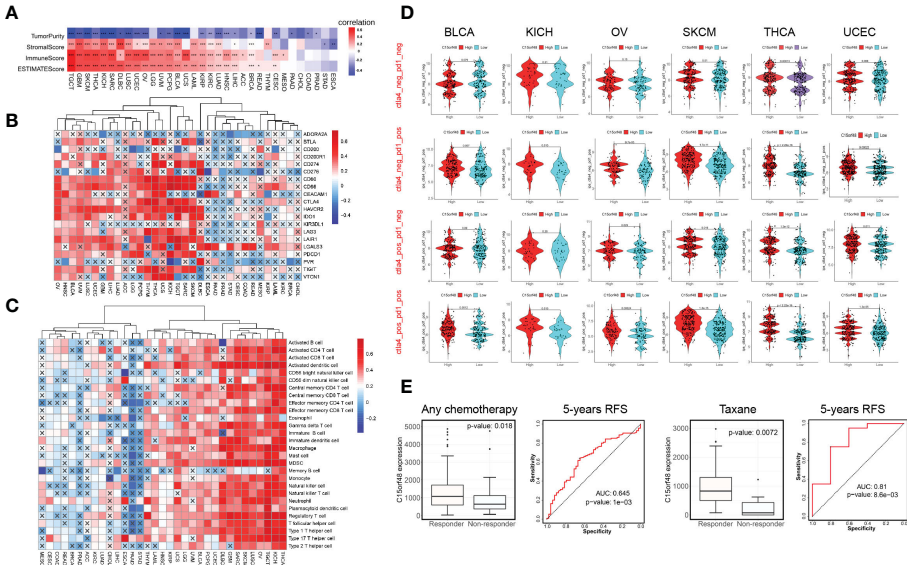

FIGURE 4
(A) Correlation between C15orf48 and tumor purity, stromal, immune, and ESTIMATE scores in pan-cancer; **(B)** Correlation between C15orf48 and immune checkpoints in pan-cancer; **(C)** Correlation between C15orf48 and immune cell infiltration in pan-cancer (ssGSEA); **(D)** Correlation between C15orf48 and immunotherapy response in pan-cancer; **(E)** Box plots show the C15orf48 expression differences between responders and non-responders, and ROC presents the predictive accuracy of patient therapeutic response by C15orf48 levels on the ROCplotter online website.
*P < 0.05; **P < 0.01; ***P < 0.001.

monocyte/macrophage chemokines (CCL7, CCL22, etc.) were upregulated in the C15orf48 high-expression group, promoting inflammatory response and monocyte/macrophage phagocytosis in THCA. Additionally, a large number of MHC molecules were significantly upregulated in THCA in the C15orf48 high-expression group, indicating strong antigen presentation and processing capabilities. Moreover, we observed that the C15orf48 high-expression group has a stronger anti-cancer immune status in most immune cycle steps, including priming and activation (step 3), trafficking of immune cells to tumors (step 4), ICI in tumors (step 5), and killing of cancer cells (step 7) (Figure 5B). The stronger immune status of the C15orf48 high-expression group may further enhance ICI in the THCA-TME. Furthermore, we observed that C15orf48 expression was negatively correlated with the recognition of cancer cells by T cells (step 6), suggesting that the high expression of C15orf48 may reduce the recognition-ability of T cell receptors. The analysis of ICI level showed that in most algorithms, C15orf48 was positively correlated with 5 types of ICIs, including CD8+ T cell, NK cell, and macrophage infiltrations (Figure 5C). Expression abundance analysis revealed a significant positive correlation between C15orf48 and marker genes of these infiltrating cells (Figure 5E), especially macrophages (CD11B and CD45) (Figure 5F). In addition, C15orf48 was also strongly positively correlated with multiple ICPs in THCA (Figure 5G). Moreover, GSVA analysis showed that C15orf48 was significantly correlated with several immune processes, including immune response against tumor cells, cytokine production, and T cell-mediated immune response in THCA (Figure 5D).

Furthermore, we explored the functions of C15orf48 in THCA using protein interaction and gene expression data. C15orf48 protein interaction data was obtained from the STRING database (Figure 6A). Differential gene expression analysis identified a total of 235 upregulated and 89 downregulated genes in THCA (Figure 6B). GO enrichment analysis revealed that the differentially expressed genes (DEGs) were primarily enriched in cell adhesion, transmembrane movement, and immune-related activities, while KEGG enrichment analysis revealed that the DEGs were enriched in PI3K-Akt signaling and cytokine interaction pathways (Figure 6C). Pathway analysis showed that C15orf48 had a significant positive correlation with inflammatory response, apoptosis, P53 pathway, ferroptosis, etc. and a significant negative correlation with nitrogen metabolism (Figure 6E). Considering that the apoptosis gene set includes pro-apoptotic genes and apoptosis-inhibiting genes, we analyzed the correlation between each apoptosis-related gene and C15orf48. The results showed that C15orf48 was significantly positively correlated with multiple anti-apoptotic factors including baculoviral IAP repeat containing 3 (BIRC3) and B-cell CLL/lymphoma 2 like 1 (BCL2L1), and significantly negatively correlated with pro-apoptotic factors such as caspase 9 (CASP9) and programmed cell death 4 (PDCD4) (Supplementary Figure 5C). Considering the high correlation between C15orf48 and ferroptosis, we assessed the correlation between C15orf48 and 484 ferroptosis-related genes, obtained from the FerrDB database (http://www.zhounan.org/ferrdb/current/) (29). The results showed that 322 genes were significantly differentially expressed, among which 68 genes were significantly positively correlated with C15orf48 (35 driver genes, 2 marker genes, and 31 repressor genes) (Figures 6D, F). In addition, we analyzed the co-expression of C15orf48 using Co-essentiality (http://coessentiality.net/) (30), and the results revealed the

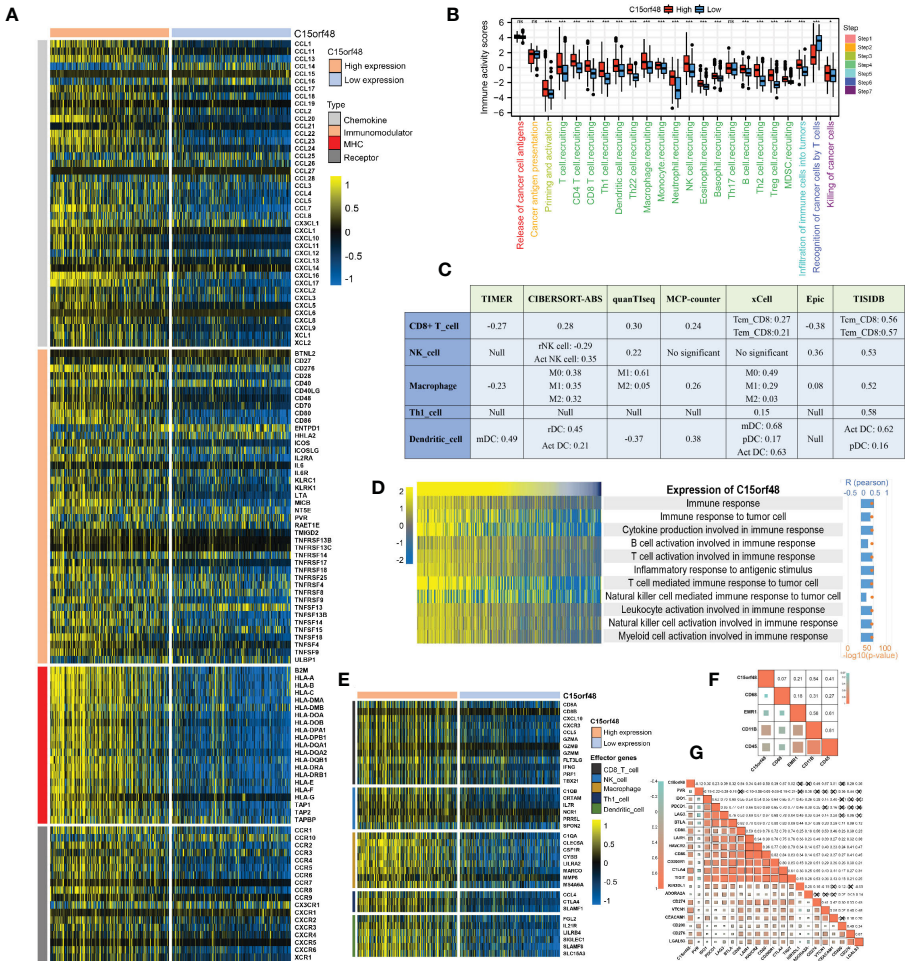

FIGURE 5
(A) Correlation between C15orf48 and 122 immune modulators (chemokines, receptors, MHC and immunostimulants) in THCA; **(B)** Differences in the various steps of the cancer immunity cycle between high- and low-C15orf48 groups; **(C)** Seven algorithms evaluate the correlation between C15orf48 and immune cell infiltration in THCA; **(D)** GSVA assesses the relevance of C15orf48 to some immune pathways; **(E)** Differences in the effector genes of the tumor-associated immune cells between high- and low-C15orf48 groups; **(F)** Correlation between C15orf48 and macrophage marker genes in THCA; **(G)** Correlation between immune checkpoints and C15orf48 in THCA. *p < 0.05; **p < 0.01; ***p < 0.001; NS, No Significance

presence of 56 neighborhood genes of C15orf48, which were primarily enriched in lipid and amino acid metabolism (Supplementary Figures 5A, B).

Subtype analysis showed that C15orf48 was significantly enriched in PTC. The ROC curve revealed the expression specificity of C15orf48 in PTC subtypes, with the AUC value of 70.9% (P <0.0001) (Figures 7A, B), suggesting that C15orf48 may serve as a potential biomarker of PTC subtypes. In addition, compared with FTC, PTC subtypes had higher immune scores (Figure 7C), and ICI analysis showed that C15orf48 in the PTC group had a significant correlation with various immune cells (Figure 7D). The correlation of C15orf48 with ICPs was higher in the PTC group (Figures 7E, F), thus compared with the FTC group, the PTC C15orf48 high-expression group benefited more from ICB (ICP blockade) treatment (Figure 7I). Furthermore, we assessed the association of C15orf48 with ferroptosis genes in both the subtypes and found a relatively higher correlation between C15orf48 and ferroptosis in the PTC group (Figures 7G, H).

3.6 Effects of C15orf48 on proliferation, migration, and apoptosis of THCA cells

We first analyzed the CCLE data and observed that C15orf48 expression was the highest in BHT101 cells (Figure 8A). Therefore, BHT101 cells were selected for subsequent experiments. We transfected BHT101 cells with two siRNA knockout vectors and conducted RT-PCR and western blot analyses. The results revealed that compared with the control group, the expression of mRNA and protein expression in the transfected group were lower, with siRNA1 showing higher knockout efficiency (Figures 8B, C). Therefore, siRNA1 was selected for subsequent experiments. The CCK-8 analysis after siRNC and siRNA1 transfection revealed that the proliferation ability of cells was significantly reduced after 24 h of C15orf48 knockout (siRNC: 0.62 ± 0.020, siRNA1: 0.50 ± 0.002) (Figure 8D). Additionally, the healing and migration abilities of the BHT101 cells were significantly weakened after C15orf48 knockout, as revealed by the cell scratch and Transwell assays, respectively

10.3389/fimmu.2023.1131870

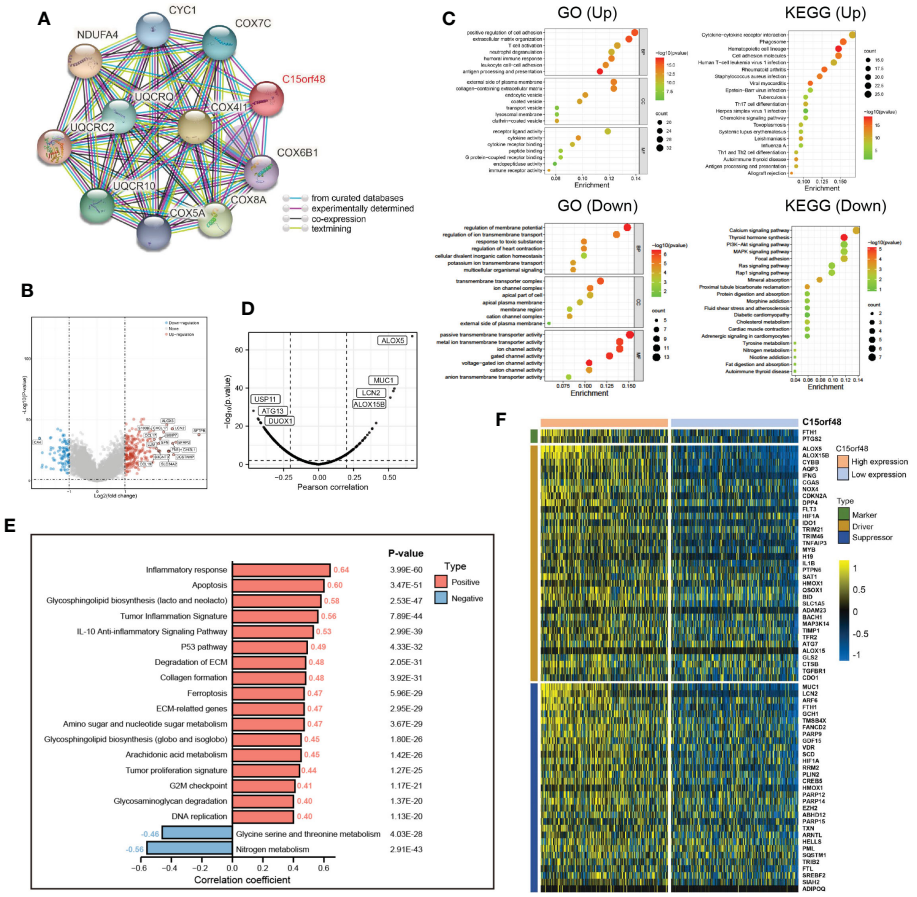

FIGURE 6
(A) The protein interaction network of C15orf48; **(B)** Volcano map of differential genes in C15orf48 high and low expression groups; **(C)** GO and KEGG functional enrichment analysis; **(D)** Correlation between C15orf48 and ferroptosis-related genes in THCA; **(E)** Correlation between C15orf48 and some pathways in THCA; **(F)** Expression of ferroptosis-related genes positively correlated with C15orf48 in THCA.

(Figures 8E, F). Lastly, the apoptosis assay showed that the knockdown of C15orf48 significantly increased the rate of apoptosis of BHT101 cells (siRNC: 25.34 ± 2.624, siRNA1: 34.53 ± 2.278) (Figures 8G, H).

4 Discussion

Mitochondrial dysfunction is a hallmark of immune-mediated inflammatory diseases (31). C15orf48, as part of complex IV of the mitochondrial respiratory chain, is important in the inflammatory response. Clayton et al. demonstrated that the expression of C15orf48 is a conserved response to inflammatory signals and occurs in multiple inflammation-related pathways (18). Significant upregulation of C15orf48 was observed in both rheumatoid arthritis and COVID-19 and was associated with the expression of related macrophage subsets (18). Chronic inflammation is critical for promoting tumor development and drug resistance (32). Specifically, chronic inflammation is associated with immunosuppression. Therefore, it provides a favorable microenvironment for tumor occurrence, development, and metastasis (33). In addition, treatment-induced chronic inflammation contributes to treatment resistance and cancer progression. The inflammatory TME is a key determinant of the efficacy of conventional chemotherapy (radiotherapy and chemotherapy) and immunotherapy (34, 35). However, there is limited information about the role of C15orf48 in tumors.

In our study, we evaluated the pan-cancer expression level of C15orf48 and found that it was significantly upregulated in most tumors, possibly owing to its association with the inflammatory response. Furthermore, the single-cell analysis revealed its immune cell-specific expression in macrophages, suggesting its role in promoting monocyte/macrophage phagocytosis in tumors. Survival analysis showed that C15orf48 was significantly correlated with OS, PFS, DSS, and DFI of multiple cancers, especially glioma. Further univariate and multivariate analyzes revealed that C15orf48 can serve as an independent prognostic factor for glioma. Furthermore, C15orf48 was significantly enriched in malignant gliomas, suggesting its role in promoting the malignant development of gliomas. Altogether, these results illustrate the importance of C15orf48 in tumorigenesis and prognosis. Spisák et al. observed a significant downregulation of C15orf48 methylation in colon cancer tumors (14). Furthermore, analysis of TCGA methylation data revealed the pan-cancer

10.3389/fimmu.2023.1131870

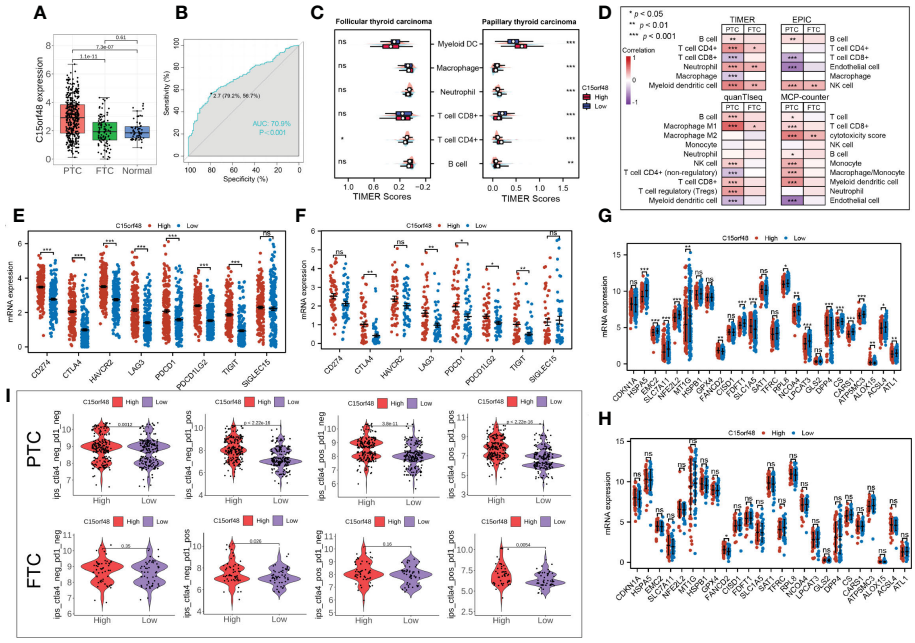

FIGURE 7
(A) Expression levels of C15orf48 in THCA subtypes; **(B)** ROC curves reveal high expression specificity of C15orf48 in PTC subtypes; **(C)** The immune scoring results of different subtypes of THCA (TIMER); **(D)** Correlation between C15orf48 and immune cell infiltration in different THCA isoforms; **(E)** Correlation between C15orf48 and immune checkpoints in PTC subtypes; **(F)** Correlation between C15orf48 and immune checkpoints in FTC subtypes; **(G)** Correlation between C15orf48 and ferroptosis-related genes in PTC subtypes; **(H)** Correlation between C15orf48 and ferroptosis-related genes in FTC subtypes; **(I)** Immunotherapy response results of two subtypes of THCA. *P < 0.05; **P < 0.01; ***P < 0.001, ns, no significance.

epigenetic changes of C15orf48 and found that the methylation level of C15orf48 was downregulated in multiple cancers, including THCA and kidney cancer. Moreover, we observed a significant negative correlation between C15orf48 methylation levels and mRNA expression in most cancers, suggesting that the methylation level of C15orf48 mediates their abnormal expression, which may play an important role in cancer progression. Furthermore, CNV analysis revealed that the frequency of copy number alterations in the C15orf48 gene was highly heterogeneous. CNV is an important part of genome structural variation, affecting the expression of protein-coding and non-coding genes and the activity of various signaling pathways. More importantly, aberrant methylation of C15orf48 and CNVs leads to poor prognosis in multiple cancers, and it is suggested that epigenetic changes of C15orf48 may promote the progression of some cancers. The TME is critical in the immune response of cancer patients, and the level of ICI is significantly correlated with tumor development (36, 37). The results of the immune analysis showed that C15orf48 was significantly associated with the immune response of THCA, TGCT, LIHC, etc. In addition, C15orf48 was significantly associated with immunotherapy response in several cancers and may serve as a potential target for immunotherapy. Considering that high expression of C15orf48 is associated with higher anticancer immunity but negatively correlated with T cell immunity. Thus, if C15orf48 is targeted in mouse models, increased anticancer immunity but decreased T cell immunity may be observed. In human beings, researchers may observe a similar phenomenon, although the magnitude of the effect may be different. However, this requires further research to understand the potential effects of targeting C15orf48 on both anti-cancer immunity and T cell immunity in human beings.

In China, the incidence of THCA has increased the most in recent years (38). Considering the abnormal expression of C15orf48 in THCA and its strong correlation with the immune response, we focused on analyzing the role of C15orf48 in THCA. C15orf48 was significantly associated with multiple immune modulators, especially some chemokines and MHC molecules. Some chemokines recruit immunosuppressive cells, including macrophages and myeloid-derived suppressor cells, to the TME to create an immunosuppressive but pro-tumor environment, thereby undermining the efficacy of immunotherapies, such as anti-PD1. These results underscore the strong association of C15orf48 with immune responses in THCA. Anti-cancer immune status comprehensively reflects the outcome of immune regulation in the TME. We observed a significant positive correlation between C15orf48 and several steps of the cancer immune cycle. For example, macrophage and monocyte recruitment were significantly increased in the C15orf48 high-expression group, which may be due to a significant increase in macrophage infiltration. In addition, C15orf48 expression was significantly negatively correlated with the recognition of cancer cells by T cells (step 6), which may be due to the significantly high expression of multiple inhibitory ICPs in THCA in the C15orf48 high-expression group. It also suggests that the high expression of C15orf48 may reduce the recognition ability of T cell receptors. The overexpression of inhibitory ICPs, such as PD-1/PD-L1, in the

10.3389/fimmu.2023.1131870

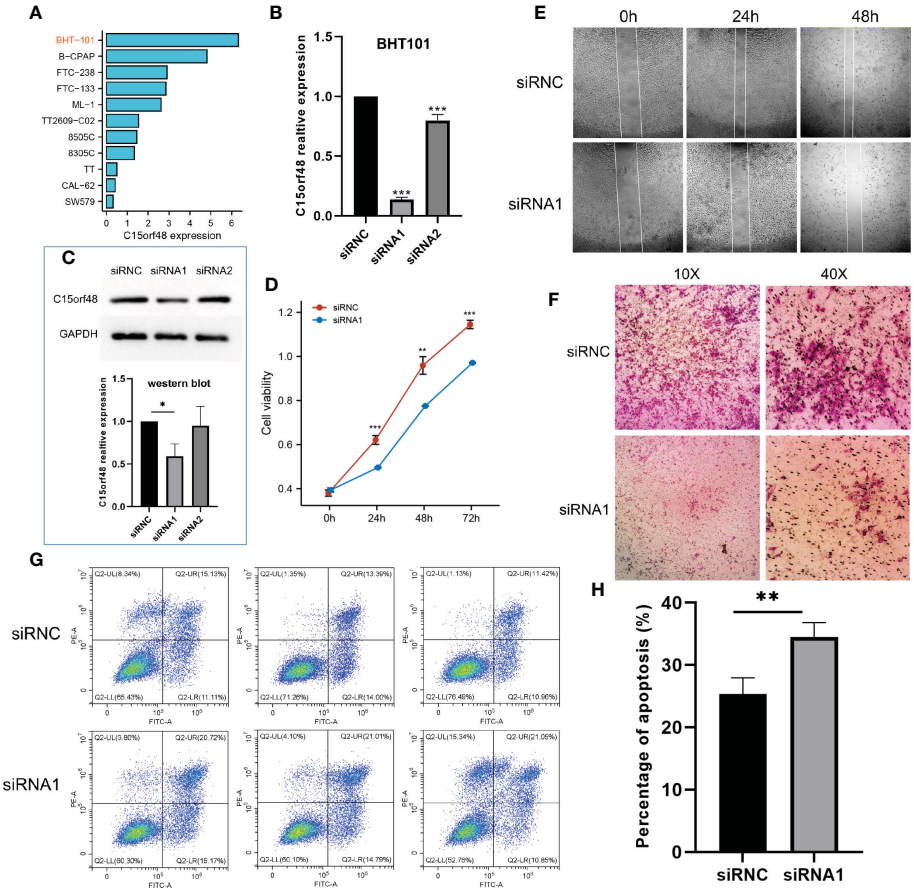

FIGURE 8
Effect of C15orf48 knockdown on THCA cell line BHT101, all experiments were performed in triplicate. **(A)** Expression levels of C15orf48 in different THCA cell lines; **(B)** RT-PCR verification of the knockout efficiency of C15orf48 in BHT101 cells; **(C)** The knockout efficiency of C15orf48 in BHT101 cells was verified by Western blot, and the figure below shows the statistical difference analysis of three repeated experiments; **(D)** CCK8 assay to analyze the effect of knocking out C15orf48 on cell proliferation; **(E)** Analysis of the effect of knocking out C15orf48 on cell healing ability by cell scratch test; **(F)** Transwell assay to analyze the effect of knocking out C15orf48 on cell migration; **(G)** Analysis of cell apoptosis changes by flow cytometry; **(H)** The percentage of apoptotic cells in the two groups. *P < 0.05; **P < 0.01; ***P < 0.001.

C15orf48 high-expression group, may form a persistent inflammatory TME (39). These results indicate that ICB treatment may be effective for the C15orf48 high-expression group, but not the low-expression group. Pathway analysis showed that C15orf48 was significantly associated with various pathways, such as apoptosis, P53 pathway, and ferroptosis, which are critical in cancer development and immunotherapy (40, 41).

Subtype studies have revealed heterogeneity among the different subtypes in THCA. Our results revealed that C15orf48 was highly expressed in PTC and could potentially serve as a biomarker for PTC. PTC is derived from the acinar cells of the thyroid gland, accounting for more than 80% of THCA, and has a relatively low malignancy, while FTC is more aggressive, with more common distant metastasis and vascular invasion (42–44). Immune scoring reveals specific immune signatures among different subtypes. C15orf48 was involved in several immune responses in PTC and was significantly associated with multiple ICPs and ICI. *In vitro* experiments revealed that C15orf48 knockout significantly reduced the proliferation, migration, and apoptosis abilities of BHT101 cells. Based on these results, we speculate that the C15orf48-related apoptosis may be the mitochondrial/cytochrome c-mediated apoptosis pathway; however, further experimental studies are required to verify this hypothesis.

In conclusion, the results of our study revealed that C15orf48 is a potential tumor prognostic biomarker and immunotherapy target. We found that the pan-cancer epigenetic alterations of C15orf48 are highly heterogeneous and that aberrant methylation and copy number variation of C15orf48 is associated with poor prognosis in several cancers. We also found that C15orf48 was significantly associated with macrophage infiltration and multiple ICPs in THCA and can serve as a potential biomarker for PTC. Lastly, we found that *in vitro* knockdown of C15orf48 reduced the proliferation, migration, and apoptosis abilities of the THCA cell line. Our study still has some limitations. First of all, our immunological research on C15orf48 is only limited to bioinformatics analysis, lacking corresponding laboratory data. Second, the research on THCA is not deep enough, and there is a lack of specific mechanism studies, and more in-depth studies are

needed to provide more insights. The findings of our study may help to understand the role of C15orf48 in pan-cancer tumorigenesis and progression, especially in THCA, and provide the basis for further immunotherapy research

Data availability statement

The original contributions presented in the study are included in the article/Supplementary Material. Further inquiries can be directed to the corresponding authors.

Author contributions

CL and HS conceived the initial research project. QL, HL, and XM performed the statistical analysis and explained the data together with CL. YT and LH assisted CL in completing the cell experiment. CL wrote the first draft of the manuscript. All authors have read and agreed to the published version of the manuscript.

Funding

This research was funded by the Science and Technology Innovation Project of Maternal and Child Medicine of Sichuan Province (2020ZD07) and the Medical Research Project of Chengdu Municipal Health Commission (2020211, 2020173).

Acknowledgments

We thank Bullet Edits Limited for the linguistic editing and proofreading of the manuscript.

Conflict of interest

The authors declare that the research was conducted in the absence of any commercial or financial relationships that could be construed as a potential conflict of interest.

Publisher's note

Supplementary material

The Supplementary Material for this article can be found online at: https://www.frontiersin.org/articles/10.3389/fimmu.2023.1131870/full#supplementary-material

References

1. Sung H, Ferlay J, Siegel RL, Laversanne M, Soerjomataram I, Jemal A, et al. Global cancer statistics 2020: GLOBOCAN estimates of incidence and mortality worldwide for 36 cancers in 185 countries. *CA Cancer J Clin* (2021) 71(3):209–49. doi: 10.3322/caac.21660

2. Xia C, Dong X, Li H, Cao M, Sun D, He S, et al. Cancer statistics in China and united states, 2022: Profiles, trends, and determinants. *Chin Med J (Engl)* (2022) 135 (5):584–90. doi: 10.1097/CM9.0000000000002108

3. Siegel RL, Miller KD, Wagle NS, Jemal A. Cancer statistics, 2023. *CA Cancer J Clin* (2023) 73(1):17–48. doi: 10.3322/caac.21763

4. Chen SY, Mamai O, Akhurst RJ. TGFβ: Signaling blockade for cancer immunotherapy. *Annu Rev Cancer Biol* (2022) 6(1):123–46. doi: 10.1146/annurev-cancerbio-070620-103554

5. Wang H, Xu T, Huang Q, Jin W, Chen J. Immunotherapy for malignant glioma: Current status and future directions. *Trends Pharmacol Sci* (2020) 41(2):123–38. doi: 10.1016/j.tips.2019.12.003

6. Domchek SM, Postel-Vinay S, Im SA, Park YH, Delord JP, Italiano A, et al. Olaparib and durvalumab in patients with germline BRCA-mutated metastatic breast cancer (MEDIOLA): An open-label, multicentre, phase 1/2, basket study. *Lancet Oncol* (2020) 21(9):1155–64. doi: 10.1016/S1470-2045(20)30324-7

7. Smith C, Lineburg KE, Martins JP, Ambalathingal GR, Neller MA, Morrison B, et al. Autologous CMV-specific T cells are a safe adjuvant immunotherapy for primary glioblastoma multiforme. *J Clin Invest* (2020) 130(11):6041–53. doi: 10.1172/JCI138649

8. Joshua AM, Monzon JG, Mihalcioiu C, Hogg D, Smylie M, Cheng T. A phase 2 study of tremelimumab in patients with advanced uveal melanoma. *Melanoma Res* (2015) 25(4):342–7. doi: 10.1097/CMR.0000000000000175

9. Mu L, Han Z, Yu S, Wang A, Chen D, Kong S, et al. Pan-cancer analysis of ASB3 and the potential clinical implications for immune microenvironment of glioblastoma multiforme. *Front Immunol* (2022) 21(13):842524. doi: 10.3389/fimmu.2022.842524

10. Saidak Z, Soudet S, Lottin M, Salle V, Sevestre MA, Clatot F, et al. A pan-cancer analysis of the human tumor coagulome and its link to the tumor immune microenvironment. *Cancer Immunol Immun* (2021) 70(4):923–33. doi: 10.1007/s00262-020-02739-w

11. Lee JK, Sivakumar S, Schrock AB, Madison R, Fabrizio D, Gjoerup O, et al. Comprehensive pan-cancer genomic landscape of KRAS altered cancers and real-world outcomes in solid tumors. *NPJ Precis Oncol* (2022) 6(1):91. doi: 10.1038/s41698-022-00334-z

12. Zhang ZF. A comprehensive prognostic and immune infiltration analysis of EXOC3L1 in pan-cancer. *Front Genet* (2022) 21(13):1044100. doi: 10.3389/fgene.2022.1044100

13. Zhou J, Wang H, Lu A, Hu G, Luo A, Ding F, et al. A novel gene, NMES1, downregulated in human esophageal squamous cell carcinoma. *Int J Cancer* (2002) 101 (4):311–6. doi: 10.1002/ijc.10600

14. Spisák S, Kalmár A, Galamb O, Wichmann B, Sipos F, Péterfia B, et al. Genome-wide screening of genes regulated by DNA methylation in colon cancer development. *PloS One* (2012) 7(10):e46215. doi: 10.1371/journal.pone.0046215

15. Floyd BJ, Wilkerson EM, Veling MT, Minogue CE, Xia C, Beebe ET, et al. Mitochondrial protein interaction mapping identifies regulators of respiratory chain function. *Mol Cell* (2016) 63(4):621–32. doi: 10.1016/j.molcel.2016.06.033

16. Endou M, Yoshida K, Hirota M, Nakajima C, Sakaguchi A, Komatsubara N, et al. Coxfa4l3, a novel mitochondrial electron transport chain complex 4 subunit protein, switches from Coxfa4 during spermatogenesis. *Mitochondrion* (2020) 52:1–7. doi: 10.1016/j.mito.2020.02.003

17. Lee CQE, Kerouanton B, Chothani S, Zhang S, Chen Y, Mantri CK, et al. Coding and non-coding roles of MOCCI (C15ORF48) coordinate to regulate host inflammation and immunity. *Nat Commun* (2021) 12(1):2130. doi: 10.1038/s41467-021-22397-5

18. Clayton SA, Daley KK, MacDonald L, Fernandez-Vizarra E, Bottegoni G, O'Neil JD, et al. Inflammation causes remodeling of mitochondrial cytochrome c oxidase mediated by the bifunctional gene C15orf48. *Sci Adv* (2021) 7(50):eabl5182. doi: 10.1126/sciadv.abl5182

19. Zhao H, Wu L, Yan G, Chen Y, Zhou M, Wu Y, et al. Inflammation and tumor progression: Signaling pathways and targeted intervention. *Signal Transduct Target Ther* (2021) 6(1):263. doi: 10.1038/s41392-021-00658-5

20. Beroukhim R, Mermel CH, Porter D, Wei G, Raychaudhuri S, Donovan J, et al. The landscape of somatic copy-number alteration across human cancers. *Nature* (2010) 463(7283):899–905. doi: 10.1038/nature08822

21. Zhao Z, Zhang KN, Wang Q, Li G, Zeng F, Zhang Y, et al. Chinese Glioma genome atlas (CGGA): A comprehensive resource with functional genomic data from Chinese glioma patients. *Genom Proteom Bioinf* (2021) 19(1):1–12. doi: 10.1016/j.gpb.2020.10.005

22. Thorsson V, Gibbs DL, Brown SD, Wolf D, Bortone DS, Ou Yang TH, et al. The immune landscape of cancer. *Immunity* (2019) 51(2):411–2. doi: 10.1016/j.immuni.2019.08.004

23. Bonneville R, Krook MA, Kautto EA, Miya J, Wing MR, Chen HZ, et al. Landscape of microsatellite instability across 39 cancer types. *JCO Precis Oncol* (2017) 2017:PO.17.00073. doi: 10.1200/PO.17.00073

24. Yoshihara K, Shahmoradgoli M, Martínez E, Vegesna R, Kim H, Torres-Garcia W, et al. Inferring tumour purity and stromal and immune cell admixture from expression data. *Nat Commun* (2013) 4:2612. doi: 10.1038/ncomms3612

25. Charoentong P, Finotello F, Angelova M, Mayer C, Efremova M, Rieder D, et al. Pan-cancer immunogenomic analyses reveal genotype-immunophenotype relationships and predictors of response to checkpoint blockade. *Cell Rep* (2017) 18 (1):248–62. doi: 10.1016/j.celrep.2016.12.019

26. Xu L, Deng C, Pang B, Zhang X, Liu W, Liao G, et al. TIP: A web server for resolving tumor immunophenotype profiling. *Cancer Res* (2018) 78(23):6575–80. doi: 10.1158/0008-5472.CAN-18-0689

27. Wei J, Huang K, Chen Z, Hu M, Bai Y, Lin S, et al. Characterization of glycolysis-associated molecules in the tumor microenvironment revealed by pan-cancer tissues and lung cancer single cell data. *Cancers (Basel)* (2020) 12(7):1788. doi: 10.3390/cancers12071788

28. Fekete JT, Győrffy B. ROCplot.org: Validating predictive biomarkers of chemotherapy/hormonal therapy/anti-HER2 therapy using transcriptomic data of 3,104 breast cancer patients. *Int J Cancer* (2019) 145(11):3140–51. doi: 10.1002/ijc.32369

29. Zhou N, Bao J. FerrDb: A manually curated resource for regulators and markers of ferroptosis and ferroptosis-disease associations. *Database (Oxford)* (2020) 1(2020): baaa021. doi: 10.1093/database/baaa021

30. Wainberg M, Kamber RA, Balsubramani A, Meyers RM, Sinnott-Armstrong N, Hornburg D, et al. A genome-wide atlas of co-essential modules assigns function to uncharacterized genes. *Nat Genet* (2021) 53(5):638–49. doi: 10.1038/s41588-021-00840-z

31. Garaude J. Reprogramming of mitochondrial metabolism by innate immunity. *Curr Opin Immunol* (2019) 56:17–23. doi: 10.1016/j.coi.2018.09.010

32. Vasan N, Baselga J, Hyman DM. A view on drug resistance in cancer. *Nature* (2019) 575:299–309. doi: 10.1038/s41586-019-1730-1

33. Shacter E, Weitzman SA. Chronic inflammation and cancer. *Oncology* (2002) 16:217–26.

34. Schaue D, Micewicz ED, Ratikan JA, Xie MW, Cheng G, McBride WH. Radiation and inflammation. *Semin Radiat Oncol* (2015) 25(1):4–10. doi: 10.1016/j.semradonc.2014.07.007

35. Guthrie GJ, Charles KA, Roxburgh CS, Horgan PG, McMillan DC, Clarke SJ. The systemic inflammation-based neutrophil-lymphocyte ratio: experience in patients with cancer. *Crit Rev Oncol Hematol* (2013) 88(1):218–30. doi: 10.1016/j.critrevonc.2013.03.010

36. Fan J, To KKW, Chen ZS, Fu L. ABC Transporters affects tumor immune microenvironment to regulate cancer immunotherapy and multidrug resistance. *Drug Resist Update* (2023) 30(66):100905. doi: 10.1016/j.drup.2022.100905

37. Huntington ND, Cursons J, Rautela J. The cancer-natural killer cell immunity cycle. *Nat Rev Cancer* (2020) 20(8):437–54. doi: 10.1038/s41568-020-0272-z

38. Li M, Zheng R, Dal Maso L, Zhang S, Wei W, Vaccarella S. Mapping overdiagnosis of thyroid cancer in China. *Lancet Diabetes Endo* (2021) 9(6):330–2. doi: 10.1016/S2213-8587(21)00083-8

39. Spranger S, Spaapen RM, Zha Y, Williams J, Meng Y, Ha TT, et al. Up-regulation of PD-L1, IDO, and T (regs) in the melanoma tumor microenvironment is driven by CD8(+) T cells. *Sci Transl Med* (2013) 5(200):200ra116. doi: 10.1126/scitranslmed.3006504

40. Kwan K, Castro-Sandoval O, Gaiddon C, Storr T. Inhibition of p53 protein aggregation as a cancer treatment strategy. *Curr Opin Chem Biol* (2022) 24(72):102230. doi: 10.1016/j.cbpa.2022.102230

41. Tong X, Tang R, Xiao M, Xu J, Wang W, Zhang B, et al. Targeting cell death pathways for cancer therapy: Recent developments in necroptosis, pyroptosis, ferroptosis, and cuproptosis research. *J Hematol Oncol* (2022) 15(1):174. doi: 10.1186/s13045-022-01392-3

42. Boucai L, Seshan V, Williams M, Knauf JA, Saqcena M, Ghossein RA, et al. Characterization of subtypes of BRAF-mutant papillary thyroid cancer defined by their thyroid differentiation score. *J Clin Endocrinol Metab* (2022) 107(4):1030–9. doi: 10.1210/clinem/dgab851

43. Nguyen XV, Roy Choudhury K, Tessler FN, Hoang JK. Effect of tumor size on risk of metastatic disease and survival for thyroid cancer: Implications for biopsy guidelines. *Thyroid* (2018) 28(3):295–300. doi: 10.1089/thy.2017.0526

44. Puliafito I, Esposito F, Prestifilippo A, Marchisotta S, Sciacca D, Vitale MP, et al. Target therapy in thyroid cancer: Current challenge in clinical use of tyrosine kinase inhibitors and management of side effects. *Front Endocrinol (Lausanne)* (2022) 8 (13):860671. doi: 10.3389/fendo.2022.860671

frontiers | Frontiers in Immunology

TYPE Original Research
PUBLISHED 30 March 2023
DOI 10.3389/fimmu.2023.1131496

OPEN ACCESS

EDITED BY
Takaji Matsutani,
Repertoire Genesis, Inc., Japan

REVIEWED BY
Jingjing Xie,
University of California, Davis, United States
Li-Da Wu,
Nanjing Medical University, China

*CORRESPONDENCE
Han-Ping Shi
shihp@ccmu.edu.cn

†These authors have contributed equally to this work and share first authorship

SPECIALTY SECTION
This article was submitted to Cancer Immunity and Immunotherapy, a section of the journal Frontiers in Immunology

RECEIVED 25 December 2022
ACCEPTED 20 March 2023
PUBLISHED 30 March 2023

CITATION
Yang M, Lin S-Q, Liu X-Y, Tang M, Hu C-L, Wang Z-W, Zhang Q, Zhang X, Song M-M, Ruan G-T, Zhang X-W, Liu T, Xie H-L, Zhang H-Y, Liu C-A, Zhang K-P, Li Q-Q, Li X-R, Ge Y-Z, Liu Y-Y, Chen Y, Zheng X and Shi H-P (2023) Association between C-reactive protein-albumin-lymphocyte (CALLY) index and overall survival in patients with colorectal cancer: From the investigation on nutrition status and clinical outcome of common cancers study. *Front. Immunol.* 14:1131496. doi: 10.3389/fimmu.2023.1131496

Association between C-reactive protein-albumin-lymphocyte (CALLY) index and overall survival in patients with colorectal cancer: From the investigation on nutrition status and clinical outcome of common cancers study

Ming Yang[1,2,3,4†], Shi-Qi Lin[1,2,3,4,5†], Xiao-Yue Liu[1,2,3,4†], Meng Tang[1,2,3,4], Chun-Lei Hu[1,2,3,4], Zi-Wen Wang[1,2,3,4], Qi Zhang[1,2,3,4], Xi Zhang[1,2,3,4], Meng-Meng Song[1,2,3,4], Guo-Tian Ruan[1,2,3,4], Xiao-Wei Zhang[1,2,3,4], Tong Liu[1,2,3,4], Hai-Lun Xie[1,2,3,4], He-Yang Zhang[1,2,3,4], Chen-An Liu[1,2,3,4], Kang-Ping Zhang[1,2,3,4], Qin-Qin Li[1,2,3,4], Xiang-Rui Li[1,2,3,4], Yi-Zhong Ge[1,2,3,4,5], Yu-Ying Liu[1,2,3,4], Yue Chen[1,2,3,4,5], Xin Zheng[1,2,3,4] and Han-Ping Shi[1,2,3,4*]

[1]Department of Gastrointestinal Surgery/Department of Clinical Nutrition, Beijing Shijitan Hospital, Capital Medical University, Beijing, China, [2]National Clinical Research Center for Geriatric Diseases, Xuanwu Hospital, Capital Medical University, Beijing, China, [3]Key Laboratory of Cancer Foods for Special Medical Purpose (FSMP) for State Market Regulation, Beijing, China, [4]Beijing International Science and Technology Cooperation Base for Cancer Metabolism and Nutrition, Beijing, China, [5]The Second Affiliated Hospital and Yuying Children's Hospital of Wenzhou Medical University, Wenzhou, China

Background: Colorectal cancer (CRC) is among the most common malignant cancers worldwide, and its development is influenced by inflammation, nutrition, and the immune status. Therefore, we combined C-reactive protein (CRP), albumin, and lymphocyte, which could reflect above status, to be the CRP-albumin-lymphocyte (CALLY) index, and evaluated its association with overall survival (OS) in patients with CRC.

Methods: The clinicopathological and laboratory characteristics of 1260 patients with CRC were collected from the Investigation on Nutrition Status and Clinical Outcome of Common Cancers (INSCOC) study. Cox regression analysis was performed to assess the association between the CALLY index and OS. A nomogram including sex, age, the CALLY index and TNM stage was constructed. The Concordance Index (C-index) was utilized to evaluate the prognostic value of the CALLY index and classical CRC prognostic factors, such as modified Glasgow prognostic score (mGPS), neutrocyte to lymphocyte ratio (NLR), systemic immune inflammation index (SII), and platelet to lymphocyte

ratio (PLR), as well as to assess the prognostic value of the nomogram and TNM stage.

Results: Multivariate Cox regression analyses demonstrated that the CALLY index was independently associated with OS in patients with CRC [Hazard ratio (HR) = 0.91, 95% confidence interval (CI) = 0.87-0.95, *P*<0.001]. The CALLY index showed the highest prognostic value (C-index = 0.666, 95% CI = 0.638-0.694, *P*<0.001), followed by mGPS, NLR, SII, and PLR. The nomogram demonstrated higher prognostic value (C-index = 0.784, 95% CI = 0.762-0.807, *P*<0.001) than the TNM stage.

Conclusion: The CALLY index was independently associated with OS in patients with CRC and showed higher prognostic value than classical CRC prognostic factors. The nomogram could provide more accurate prognostic prediction than TNM stage.

KEYWORDS

colorectal cancer, prognosis, inflammation, nutrition, immune

Introduction

Colorectal cancer (CRC) is one of the most common malignant cancers worldwide and its incidence has been increasing in recent years, posing a significant threat to human health (1, 2). Previous studies have identified several prognostic factors, including neutrophil-to-lymphocyte ratio (NLR), platelet-to-lymphocyte ratio (PLR), systemic immune inflammation index (SII), and modified Glasgow prognostic score (mGPS) (3–5). However, due to their limitations, these factors alone may not provide enough prognostic information to improve survival prediction or select effective treatment strategies. To improve outcomes for patients with CRC, better predictive factors are needed to guide therapy decisions.

Previous studies have shown that the development of CRC is influenced by numerous factors, including the inflammation level, nutritional status, and immune function. The cancer-associated systemic inflammatory response is a critical indicator of tumor progression, and patients with CRC and higher levels of inflammation have a higher risk of death than those with lower levels of inflammation (4, 6). Nutritional status also plays an important role in the prognosis of patients with CRC, with several studies indicating that poor nutrition is linked to poorer overall survival (OS) for patients with CRC (7–9). In addition, good immune function is the main defense against CRC progression. It has been reported that the prognosis of patients with CRC and poor immune function is far worse than that of those with good immune function. Based on the above theories and studies, we believe that an indicator that comprehensively reflects the level of inflammation, nutritional status, and immune function could better predict the prognosis of patients with CRC.

In clinical and past studies, hematological indicators are often used to reflect the inflammation level, nutritional status and immune function of patients with CRC. First, C-reactive protein (CRP) is a common clinical indicator that can reflect the inflammatory levels of patients with CRC (10). Second, serum albumin has been used as an index of nutritional status in clinics for decades (11). Third, lymphocyte count is a traditional biomarker that reflects immune function (12). Finally, we have found that the CRP-albumin-lymphocyte (CALLY) index (a parameter developed by Hiroya Iida et al.) combines CRP, albumin, and lymphocyte, and is a prognostic factor for patients with liver cancer (13).

In this study, we explored the association between the CALLY index and the prognosis of patients with CRC. To determine the superiority and necessity of the CALLY index, we compared its prognostic value to that of classical CRC prognostic factors such as NLR, PLR, SII, and mGPS. Additionally, based on the sex, age, the CALLY index and TNM stage, we developed a nomogram model. We believe that the nomogram could complement the limitations of TNM stage and provide a more accurate prognostic prediction.

Methods

Study population

The main methods, results and a specific description of the Investigation on Nutrition Status and Clinical Outcome of Common Cancers (INSCOC) study have been published previously (14). Between January 1, 2012, and October 31, 2020, the INSCOC study enrolled patients who met the inclusion criteria, which included being at least 18 years of age, having a pathological diagnosis of cancer, providing written informed consent, and maintaining consciousness throughout the study. Patients with acquired immune deficiency syndrome, mental or cognitive impairment, or who were organ transplant recipients were

excluded from participation. Cases in which patients required more than two hospitalizations during the study were considered single cases.

This was a purely observational study on patients with cancer, without any assignment or intervention. Written informed consent was obtained from all subjects and/or their legal guardians for study participation. The Medical Ethical Review Committees and Institutional Review Boards of the participating registered hospitals approved this study. This study conformed to the Declaration of Helsinki. The study was registered with the Chinese Clinical Trial Registry (http://www.chictr.org.cn) on December 24, 2018 (registration number: ChiCTR1800020329).

From the INSCOC study, 1396 patients with CRC were enrolled into this study. A total of 136 patients without data on critical variables, including age (23 patients), CRP levels (52 patients), lymphocyte counts (27 patients), and serum albumin levels (24 patients) were excluded from the study (Figure 1). Ultimately, 1,260 patients were included in this study.

Patient characteristics and outcomes

Data on the following demographic and clinicopathological features were collected within 48 h of admission: sex, age, height, weight, smoking status, alcohol consumption, TNM stage, Karnofsky performance status score (KPS), scored patient-generated subjective global assessment (PG-SGA), neutrocyte counts, lymphocyte counts, platelet counts, serum albumin levels, CRP levels, serum creatinine (Scr) levels, blood urea nitrogen (Bun) levels, total cholesterol (Tchol) levels, triglyceride levels, high-density lipoprotein cholesterol (HDL-C) levels, low-density lipoprotein cholesterol (LDL-C) levels, fasting blood glucose (FBG) levels, total bilirubin (Tbil) levels, direct bilirubin (Dbil) levels, aspartate transferase (AST) levels and alanine aminotransferase (ALT) levels. The standard for smoking and drinking were defined as smoking >20 cigarettes in a lifetime and drinking regularly over the past year, respectively. TNM staging followed the guidelines of the American Joint Committee on Cancer. The laboratory tests were performed using the same protocol and reference range nationwide in China. The primary endpoint was patient death due to any reason.

The criteria of mGPS were presented in Supplemental Table 1. The method of calculating the CALLY index, NLR, PLR and SII were as follows (13):

$$\text{CALLY index}: \ \text{Albumin} \times \text{Lymphocyte} \div (\text{CRP} \times 10)$$

$$\text{NLR}: \ \text{Neutrocyte} \div \text{Lymphocyte}$$

$$\text{PLR}: \ \text{Platelet} \div \text{Lymphocyte}$$

$$\text{SII}: \ \text{Neutrocyte} \times \text{Platelet} \div \text{Lymphocyte}$$

Statistical analysis

Data were presented as simple percentages or as medians with interquartile ranges (IQRs). Fisher's exact test or chi-square tests were used to assess baseline characteristics. Student's t-tests were used to analyze continuous variables with normal distributions, while the Mann-Whitney test was used for continuous variables with non-normal distributions.

Receiver operating characteristic (ROC) curve was used to determine the cut-off point of the CALLY index, which was 1.47 (Supplemental Figure 1). Univariate and multivariate Cox proportional hazards regression models were used to calculate hazard ratios (HR) and their 95% confidence intervals (CI) for each variable in three models (Models 1, 2, and 3). Model 1 was not adjusted for any covariates. Model 2 was adjusted for sex, age, BMI, and TNM stage. Model 3 was adjusted for sex, age, BMI, TNM stage, smoking status, alcohol consumption, KPS and PG-SGA.

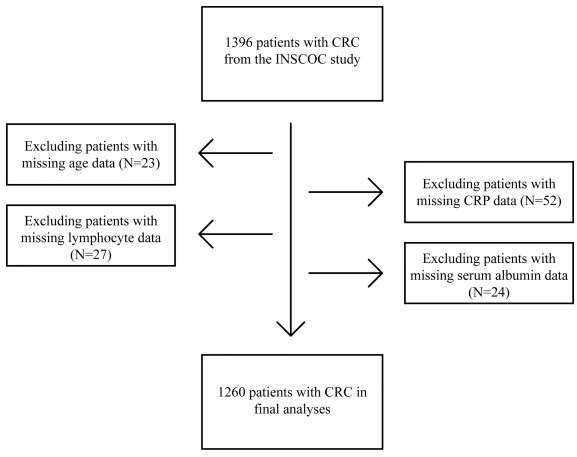

FIGURE 1
Procedures for selection of study participants with CRC from the INSCOC study. CRC, colorectal cancer; INSCOC, Investigation on Nutrition Status and Clinical Outcome of Common Cancers; CRP, C-reactive protein.

Stratified analysis was conducted in each stratifications and sensitivity analysis was conducted after excluding patients with a survival time of less than 1 year to confirm the stability of the association between the CALLY index and OS. Interaction analysis was used to evaluate the interaction between the CALLY index and covariates. Correlation analysis was used to evaluate the relationship between the CALLY index and classical CRC prognostic factors (NLR, PLR, SII and mGPS).

Concordance Index (C-index) and area under the ROC curve (AUC) were used to evaluate the prognostic value of the CALLY index and classical CRC prognostic factors (NLR, PLR, SII and mGPS). C-index, AUC and time-dependent ROC were used to evaluate the prognostic value of the nomogram and TNM stage.

A *P* value less than 0.05 was considered statistically significant. All statistical analyses were performed using R software, version 4.1.1.

Results

Patient characteristics

Of all the patients, the median age was 60 years (IQR, 52 to 67 years); the median BMI was 22.58 kg/m^2 (IQR, 20.55 to 24.84 kg/m^2); the median CALLY index was 1.35 (IQR, 0.27 to 2.82). 60.9% (767/1260) of the patients were men. 5.6% (71/1260), 20.6% (259/1260), 35.1% (442/1260) and 38.7% (488/1260) of the patients were in stage I, II, III, and IV, respectively. Compared to patients with low CALLY index, patients with high CALLY index had higher proportion of male, TNM stage IV, smoker and drinker, lower proportion of TNM stage I, II and III, older age, higher PG-SGA, neutrocyte counts and platelet counts, and lower BMI, KPS, TC levels, triglyceride levels, HDL-C levels and LDL-C levels. The baseline characteristics were summarized in Table 1.

Prognostic role of the CALLY index

Univariate and multivariate Cox regression analyses indicated that the CALLY index was negatively related to the risk of death (Supplemental Figure 2). Patients with high CALLY index had a lower death risk (HR = 0.45, 95% CI = 0.36-0.56, *P* <0.001) compared to those with low CALLY index (Table 2, Supplemental Figure 3). When the CALLY index was divided into 4 quartiles (1st quartile: CALLY index<0.27; 2nd quartile: 0.27≤ CALLY index<1.35; 3rd quartile: 1.35≤ CALLY index<2.82; 4th quartile: CALLY index ≥2.82), patients in the 2nd quartile (HR = 0.69, 95% CI =0.53-0.88, *P* = 0.004), 3rd quartile (HR = 0.46, 95% CI =0.34-0.61, *P*<0.001), and 4th quartile (HR = 0.32, 95% CI = 0.23-0.45, *P*<0.001) had a significantly lower risk of death compared to those in the 1st quartile (Table 2).

Stratified, interaction, sensitivity and correlation analyses

Results of stratified analysis suggested that the association between the CALLY index and OS was stable in various stratifications, which were divided by the covariates such as sex (men *vs.* women), age (less than 65 years *vs.* 65 years or more), BMI (less than 24 kg/m^2 *vs.* 24 kg/m^2 or more), smoking status (Yes *vs.* No), alcohol consumption (Yes *vs.* No), PG-SGA (less than 4 *vs.* 4 or more), tumor stage (I/II/III *vs.* IV) and KPS (less than 90 *vs.* 90 or more) (Figure 2). None of the above covariates had an interaction with the CALLY index (all *P* for interaction >0.050).

After excluding patients with a survival time of less than one year, the results of sensitivity analysis showed that a higher CALLY index was significantly associated with a lower risk of death (HR = 0.92, 95% CI =0.88-0.96, *P*<0.001) (Supplemental Table 2). Results of correlation analysis showed low correlation between the CALLY index and classical CRC prognostic factors [NLR (*r* = -0.207), PLR (*r* = -0.211), SII (*r* = -0.218) and mGPS (*r* = -0.333)] (Supplemental Figure 4).

Prognostic value of the CALLY index and classical CRC prognostic factors (NLR, PLR, SII and mGPS)

As shown in Figure 3, the CALLY index showed the highest prognostic value for patients with CRC, followed by mGPS, NLR, SII and PLR. The C-indices of the CALLY index (C-index = 0.666, 95% CI = 0.638-0.694), mGPS (C-index = 0.623, 95% CI = 0.596-0.650, *P*<0.001), NLR (C-index = 0.614, 95% CI = 0.584-0.644, *P* = 0.001), SII (C-index = 0.611, 95% CI = 0.582-0.641, *P* = 0.001) and PLR (C-index = 0.565, 95% CI = 0.534-0.597, *P*<0.001) were presented in Supplemental Table 3.

Evaluation of the nomogram

Sex, age, the CALLY index and TNM stage were involved the nomogram (Figure 4). The calibration curves of the nomogram showed good agreement with the observed outcomes for patients at 1, 2, and 3 years of OS (Supplemental Figure 5). The nomogram (C-index = 0.784, 95% CI = 0.762-0.807) showed a significantly higher C-index than TNM stage (C-index = 0.727, 95% CI = 0.704-0.750, *P*<0.001) (Supplemental Table 4). As shown in Supplemental Figure 5, the nomogram could better predict OS in patients with CRC than the TNM stage (Figure 5). Based on the nomogram and the TNM stage, the AUCs of time-dependent ROC curves generated were 81.87% and 75.65% for 1 year, 83.31% and 78.33% for 2 years, and 81.95% and 77.65% for 3 years, respectively (Supplemental Figures 6A–C, respectively).

TABLE 1 Characteristics of all patients, patients with high and low CALLY index.

Characteristics	All patients (n = 1260)	Patients with high CALLY index (n = 884)	Patients with low CALLY index (n =376)	*P* value [e]
Sex [a] (male)	767 (60.9)	427 (64.9)	340 (56.5)	0.003
Age [b] (year)	60.00 [52.00, 67.00]	61.00 [53.00, 68.00]	59.00 [51.00, 66.00]	<0.001
BMI [b] (kg/m^2)	22.58 [20.55, 24.84]	22.38 [20.40, 24.68]	22.76 [20.70, 24.97]	0.030
TNM stage [a]				<0.001
I	71 (5.6)	34 (5.2)	37 (6.1)	
II	259 (20.6)	128 (19.5)	131 (21.8)	
III	442 (35.1)	188 (28.6)	254 (42.2)	
IV	488 (38.7)	308 (46.8)	180 (29.9)	
Smoking status [a,c] (Yes)	509 (40.4)	291 (44.2)	218 (36.2)	0.005
Alcohol consumption [a,d] (Yes)	269 (21.3)	158 (24.0)	111 (18.4)	0.019
KPS [b]	90.00 [80.00, 90.00]	80.00 [80.00, 90.00]	90.00 [80.00, 90.00]	<0.001
PG-SGA [b]	6.00 [2.00, 9.00]	7.00 [4.00, 10.00]	4.00 [2.00, 7.00]	<0.001
Neutrocyte [b] ($\times10^9$/L)	3.55 [2.50, 4.97]	4.20 [2.90, 6.00]	3.02 [2.30, 4.00]	<0.001
Lymphocyte [b] ($\times10^9$/L)	1.44 [1.08, 1.83]	1.25 [0.90, 1.61]	1.63 [1.30, 2.00]	<0.001
Platelet [b] ($\times10^9$/L)	212 [164, 271]	225 [171, 291]	200 [161, 250]	<0.001
Albumin [b] (median [IQR])	39.75 [35.77, 42.70]	36.80 [33.40, 40.38]	41.75 [39.30, 44.10]	<0.001
CRP [b] (median [IQR])	3.67 [2.68, 17.20]	16.10 [6.12, 43.72]	2.88 [0.86, 3.20]	<0.001
Scr [b] (μmol/L)	68.0 [55.1, 80.0]	69.0 [55.0, 80.9]	67.0 [55.5, 78.2]	0.333
Bun [b] (mmol/L)	5.02 [3.98, 6.22]	5.00 [3.85, 6.36]	5.03 [4.10, 6.17]	0.615
Tchol [b] (mmol/L)	4.48 [3.86, 5.27]	4.38 [3.69, 5.15]	4.66 [4.06, 5.40]	<0.001
Triglyceride [b] (mmol/L)	1.35 [1.00, 1.82]	1.30 [0.96, 1.73]	1.39 [1.02, 1.96]	0.011
HDL-C [b] (mmol/L)	1.16 [0.97, 1.38]	1.12 [0.92, 1.31]	1.22 [1.02, 1.45]	<0.001
LDL-C [b] (mmol/L)	2.81 [2.26, 3.32]	2.75 [2.15, 3.32]	2.88 [2.34, 3.33]	0.017
FBG [b] (mmol/L)	5.32 [4.86, 6.13]	5.39 [4.83, 6.46]	5.28 [4.88, 5.87]	0.066
Tbil [b] (μmol/L)	10.9 [8.3, 15.2]	10.7 [8.0, 15.1]	11.3 [8.6, 15.2]	0.176
Dbil [b] (μmol/L)	3.0 [2.1, 4.2]	3.2 [2.2, 4.6]	3.0 [2.1, 3.8]	<0.001
AST [b] (U/L)	22 [17, 29]	22 [17, 30]	22 [18, 29]	0.631
ALT [b] (U/L)	19 [13, 29]	19 [12, 29]	19 [14, 29]	0.104

CALLY, C-reactive protein–albumin–lymphocyte; BMI, body mass index; KPS, Karnofsky performance status score; PG-SGA, Scored Patient-Generated Subjective Global Assessment; Scr, serum creatinine; Bun, blood urea nitrogen; Tchol, total cholesterol; HDL-C, high-density lipoprotein cholesterol; LDL-C, low-density lipoprotein cholesterol; FBG, fasting blood glucose; Tbil, total bilirubin; Dbil, direct bilirubin; AST, aspartate transferase; ALT, alanine aminotransferase.

[a]Categorical variables are presented as number (percentage).

[b]Continuous variables are presented as median [interquartile range].

[c]The standard is to smoke more than 20 cigarettes in a lifetime.

[d]The standard is regular drinking in the past year.

[e]The P value was for patients with high and low CALLY index.

Discussion

In this study, we identified a specific association between the CALLY index and the prognosis in patients with CRC. We found that an increase in the CALLY index could significantly predict a decrease in the risk of death and that the CALLY index had a higher prognostic value than classical CRC prognostic factors (NLR, PLR, SII, and mGPS). We also developed a nomogram that includes sex, age, the

10.3389/fimmu.2023.1131496

TABLE 2 Associations between the CALLY index and OS in patients with CRC.

CALLY index	Model 1 [a]		Model 2 [b]		Model 3 [c]	
	HR (95% CI)	*P* value	HR (95% CI)	*P* value	HR (95% CI)	*P* value
Continues	0.87 (0.83, 0.91)	<0.001	0.90 (0.86, 0.93)	<0.001	0.91 (0.87, 0.95)	<0.001
Low [d]	Reference		Reference		Reference	
High [d]	0.36 (0.29, 0.44)	<0.001	0.42 (0.33, 0.52)	<0.001	0.45 (0.36, 0.56)	<0.001
Quartile 1 [e]	Reference		Reference		Reference	
Quartile 2 [e]	0.71 (0.56, 0.90)	0.005	0.62 (0.48, 0.79)	<0.001	0.69 (0.53, 0.88)	0.004
Quartile 3 [e]	0.41 (0.31, 0.54)	<0.001	0.40 (0.30, 0.53)	<0.001	0.46 (0.34, 0.61)	<0.001
Quartile 4 [e]	0.25 (0.19, 0.34)	<0.001	0.29 (0.21, 0.40)	<0.001	0.32 (0.23, 0.45)	<0.001
***P* for trend**	0.63 (0.58, 0.69)	<0.001	0.65 (0.59, 0.72)	<0.001	0.68 (0.62, 0.76)	<0.001

CALLY, C-reactive protein–albumin–lymphocyte; OS, overall survival; CRC, colorectal cancer; HR, hazard ratio; CI, confidence interval; KPS, Karnofsky performance status score; PG-SGA, Scored Patient-Generated Subjective Global Assessment.
[a]Model 1 was not adjusted for any covariates.
[b]Model 2 was adjusted for sex, age, body mass index, and TNM stage.
[c]Model 3 was adjusted for sex, age, body mass index, TNM stage, smoking status, alcohol consumption, KPS and PG-SGA.
[d]Low:<1.47; High: ≥1.47.
[e]Quartile 1:<0.27; Quartile 2: ≥0.27 and<1.35; Quartile 3: ≥1.35 and<2.82; Quartile 4: ≥2.82.

CALLY index and TNM stage to provide accurate predictions. Importantly, this nomogram outperformed the frequently used TNM stage in the clinic when predicting survival outcomes.

The CALLY index consists of CRP, serum albumin and lymphocyte, which can represent inflammation level, nutrition status and immune function, respectively, while inflammation, nutrition, and immunity play important roles in the progression of CRC. Hence, we will discuss the significant association between the CALLY index and OS in patients with CRC from three aspects: inflammation level, nutrition status, and immune function.

CRC is usually accompanied by varying degrees of systemic inflammation, which will influence the incidence and progression of

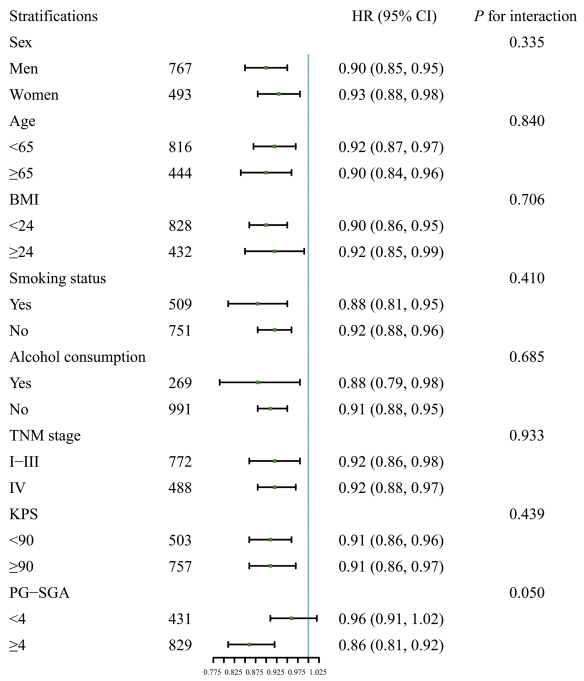

FIGURE 2
Association between the CALLY index and OS in patients with CRC in different stratifications including sex (men *vs.* women), age (less than 65 years *vs.* 65 years or more), BMI (less than 24 kg/m^2 *vs.* 24 kg/m^2 or more), smoking status (Yes *vs.* No), alcohol consumption (Yes *vs.* No), PG-SGA (less than 4 *vs.* 4 or more), tumor stage (I/II/III *vs.* IV), and KPS (less than 90 *vs.* 90 or more). Models were adjusted for sex, age, BMI, smoking status, alcohol consumption, TNM stage, KPS and PG-SGA, but not adjusted for the stratification variable. HR, Hazard ratio; CI, confidence interval; BMI, body mass index; KPS, Karnofsky performance status score; PG-SGA, Scored Patient-Generated Subjective Global Assessment; CALLY, C-reactive protein-albumin-lymphocyte; OS, overall survival; CRC, colorectal cancer.

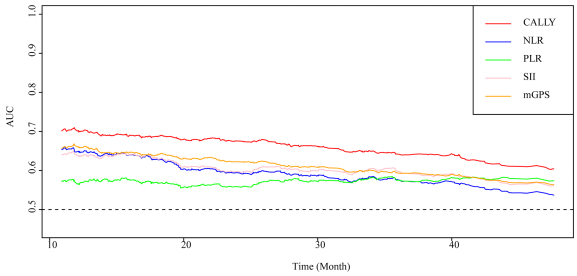

FIGURE 3
AUC of the CALLY index and classical CRC prognostic factors in patients with CRC. AUC, area under the ROC curve; ROC, receiver operating characteristic; CALLY, C-reactive protein-albumin-lymphocyte; CRC, colorectal cancer; mGPS, modified Glasgow prognostic score; NLR, neutrocyte to lymphocyte ratio; SII, systemic immune inflammation index; PLR, platelet to lymphocyte ratio.

CRC (15). Research showed that inflammation could promote the development and metastasis of CRC through oxidative stress (yields products of oxidative stress such as modified DNA and lipid peroxidation products, and plays an important role in the incidence of CRC), nuclear factor-kappa B (regulating the synthesis of pro-inflammatory cytokines and adhesion molecules), and inflammatory factors such as tumor necrosis factor-alpha, and pro-inflammatory cytokines interleukin (IL) 6 and IL-1 (activating Akt and Wnt, two signaling pathways that was associated with CRC incidence), thus, accelerating disease progression and worsening the survival of patients with CRC (16–24). CRP is a commonly used inflammatory index in clinic (10). Previous studies have shown that elevated CRP represents a more severe inflammatory state, which is associated with a worse prognosis in patients with CRC (5). In our study, a lower CALLY index (representing higher CRP) was associated with a higher risk of death in patients with CRC, which is consistent with research and theories mentioned above.

In addition to inflammation, the roles of nutrition status in the occurrence and development of CRC could not be ignored (7, 8). On one hand, CRC cells affect the absorption and utilization of nutrients through inflammation and metabolic processes, making patients with CRC are prone to malnutrition (25, 26). On the other hand, due to the gastrointestinal symptoms, which affect the appetite and eating, most of the patients with CRC have varying degrees of malnutrition risk (25). Moreover, in conditions such as surgery, trauma, chronic debilitating diseases, and aging, protein synthesis may not occur normally after ingestion of nutrients, leading to anabolic resistance and higher risk of malnutrition in patients with CRC (27). Previous studies have demonstrated that patients with CRC show a weakened response to muscle protein synthesis after injection of a mixture of amino acids (28). Malnutrition in patients with CRC will directly or indirectly affect the prognosis of patients through various ways. First, malnutrition leads to the lack of energy and materials required by the body, gradually unable to maintain basic metabolic activities, eventually resulting in patients with CRC being “starved to death” (29). Second, studies have shown that patients with better nutritional status have higher tolerance for surgery, chemotherapy, and radiotherapy, and the curative effect is better than that of patients with poor nutritional status (30, 31). Serum albumin is a very convenient and intuitive nutritional index (the higher the albumin level, the better the nutritional status) (32). Patients with CRC and hypoalbuminemia are more likely to have unhealthy body composition and poor long-term outcomes (33). Our results indicated that a higher CALLY index (representing higher serum albumin) was associated with a better prognosis in patients

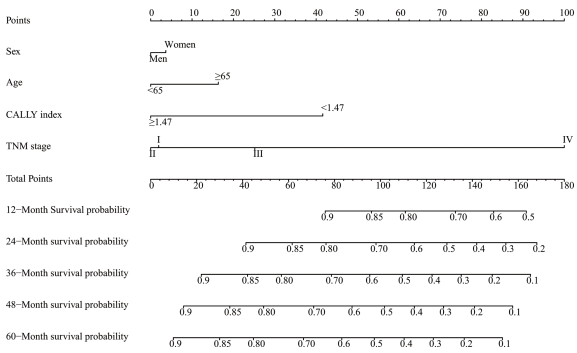

FIGURE 4
A proposed nomogram for predicting median survival time and survival probability in patients with CRC. Sex, age, the CALLY index and TNM stage were included in the constructed nomogram. To use the nomogram, a line is drawn upward to the Points axis to determine the number of points received for each variable. Sum of these points makes the total points. For total points, a line is drawn from the Total Points axis downward to the survival axes to determine the estimated median survival time and survival probability. CRC, colorectal cancer; CALLY, C-reactive protein-albumin-lymphocyte.

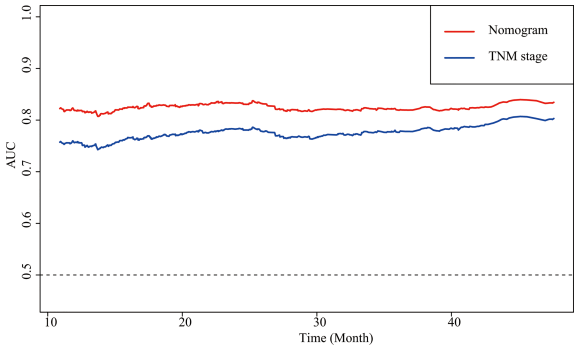

FIGURE 5
AUCs of the nomogram and the TNM stage in patients with CRC. AUC, area under the ROC curve; ROC, receiver operating characteristic; CRC, colorectal cancer.

with CRC, which is consistent with research and theories mentioned above.

In addition to inflammation level and nutrition status, another factor that must be mentioned that affects the occurrence and development of CRC is immune function. The tumorigenesis process involves different kinds of immune cells. Cancer inhibitory effects occur when lymphocytes are stimulated, such as classically follicular T helper cells, interferon-ϒ producing T $CD8^+$, B lymphocytes and so on (34–40). For example, B lymphocytes could be observed in many cancers and have associations with better prognosis (40). Furthermore, a combination of T and B lymphocytes can induce an effective anti-cancer immune response, as shown B lymphocytes associated with T $CD8^+$ lymphocytes shown (40). Additionally, tumor-infiltrating B lymphocytes have associations with better prognosis in various tumor types (41). In addition to lymphocytes themselves, cytokines secreted by lymphocytes also have anti-tumor effects (42). For example, immunoglobulin E antibodies showed anticancer properties (43). Moreover, based on tumor type, stage, and location, alarmins play different roles in promoting or inhibiting tumor progression (40, 44). In addition, epigenetic changes mediated by microRNA have been shown to influence the development of cancer and immune response (45). In clinical settings, lymphocytes are a representative and commonly used immune index (46). It has also been shown in previous studies that circulating lymphocytes can improve cancer patient outcomes by enhancing cancer immune surveillance, inhibiting cancer cell proliferation, and improving tumor chemoprevention (47, 48). While in the tumor microenvironment, T cell deficiency indicated disruptions in immune regulation and antitumor function (49). Patients with a low lymphocyte count had a shorter survival time than those with a high lymphocyte count (46). In our study, lymphocytes were used as part of the CALLY index. Our results showed that the increment of the CALLY index (increased lymphocyte count) was positively correlated with the improvement of OS in patients with CRC.

Inflammation level, nutrition status and immune function not only affect cancer, but their interactions cannot be ignored, and these interactions would further promote the progression of cancer. Firstly, a higher level of inflammation indicated high levels of cytokines such as IL-1, and IL-6, tumor necrosis factor-alpha and CRP, which greatly accelerates the consumption of nutrition, leading to malnutrition and the progression of CRC (50). Secondly, by activating tumor associated macrophages, myeloid-derived suppressive cells, $Cd4^+Foxp3^+$Treg cells or Th17 cells, inflammation could impair the immune response within tumors, promoting immune deficiency and cancer progression (51). Moreover, given the key roles of nutrition in determining the fate and functions of immune cells, malnutrition could induce an impaired immune response, which have great promotion roles on cancer incidence and progression and finally shorten OS (52). More than that, studies have shown that poor nutritional status could lead to increased levels of inflammation in patients with CRC by gut microbiota, resulting in an increased risk of death (53). To sum up, inflammation, nutrition and immunity interact to produce a complex vicious circle, which further promotes the progress of cancer. We use the CALLY index to combine the representative indicators of inflammation (CRP), nutrition (serum albumin) and immune (lymphocyte), which could not only fully utilize the prognostic value of these three indicators, but also make use of their interaction to comprehensively predict the prognosis.

The results of the stratified and sensitivity analyses indicated that the significant association between the CALLY index and OS in patients with CRC was stable and reliable. The results of the correlation analysis showed low correlation between the CALLY index and classical CRC prognostic factors (NLR, PLR, SII and mGPS), which indicated that the CALLY index can provide clinicians with different and novel prognosis prediction from classical CRC prognostic factors. Moreover, the C-indices and AUC of the CALLY index, NLR, PLR, SII and mGPS clearly showed that CALLY index had the highest prognostic value, which demonstrated the privilege of the CALLY index.

Throughout the world, the TNM stage serves as the most commonly used postoperative staging evaluation system, and is instrumental in treatment and follow-up after surgery (54–56). However, patients with the same TNM stage, often have significant survival heterogeneity, and the TNM stage is inadequate in predicting individual prognoses (57, 58). We believe the reason for the inadequacy of TNM stage is that it only examines the pathology postoperatively and does not consider the basic difference, such as sex and age, and cancer prognostic relative

factor, such as inflammation levels, nutrition status and immune function (59, 60). Hence, we developed a nomogram by combining the sex, age, the CALLY index and TNM stage. The C-indices and AUC of the nomogram and TNM stage indicated that the nomogram showed significant higher prognostic value than TNM stage alone. We believe that our nomogram can complement the limitations of TNM stage and help assess the prognosis of patients with CRC more individually and accurately.

To the best of our knowledge, the present study is the first study with the largest number of participants to comprehensively evaluate the association between the CALLY index and survival in patients with CRC. However, the present study has several potential concerns or limitations that are worth mentioning. First, CRP level, albumin level and lymphocyte count were only evaluated at the baseline. More frequent evaluations could enable a more accurate assessment of the association between the CALLY index and the death risk of CRC. Moreover, because the study findings were obtained based on the sample size determined by the INSCOC study conducted from 2012 to 2020, the findings need to be validated in another study with larger and different population. Additionally, due to the scope limitation of laboratory tests used in the INSCOC study, the covariates included in the analysis were limited. Moreover, due to the limitation of external database and the number of study population, we could not conduct external verification and internal verification. In the future, we will conduct more in-depth clinical and laboratory studies with more participants and more confounders to further investigate the underlying mechanisms.

Conclusion

In summary, CALLY index could be used as independent prognostic factors and showed better prognosis prediction ability than classical CRC prognostic factors (NLR, PLR, SII and mGPS) in patients with CRC. We proposed a nomogram that complemented the shortage of the TNM stage and showed better prognosis prediction ability than the TNM stage. We believe that our nomogram could guide clinicians to facilitate clinical decision-making, individualized treatment, and disease management more accurately and specifically.

Data availability statement

The raw data supporting the conclusions of this article will be made available by the authors, without undue reservation.

Ethics statement

The studies involving human participants were reviewed and approved by Medical Ethical Review Committees and Institutional Review Boards of the participating registered hospitals. The patients/participants provided their written informed consent to participate in this study.

Author contributions

HP-S: Conceptualization, Methodology. MY: Data curation, Writing- Original draft preparation. X-YL: Visualization, Investigation, Data curation. S-QL: Software. MT: Validation, Visualization. C-LH: Writing-Reviewing and Editing. Z-WW: Supervision, Investigation. QZ: Writing-Reviewing and Editing. XiZ: Writing-Reviewing and Editing. M-MS: Writing-Reviewing and Editing. G-TR: Supervision, Investigation. X-WZ: Supervision, Investigation. TL: Software. H-LX: Writing-Reviewing and Editing. H-YZ: Supervision, Investigation. K-PZ: Software. Q-QL: Supervision, Investigation. X-RL: Supervision, Investigation. Y-ZG: Supervision, Investigation. Y-YL: Writing-Reviewing and Editing. YC: Supervision, Investigation. XinZ: Supervision, Investigation. All authors contributed to the article and approved the submitted version.

Funding

This work was supported by the National Key Research and Development Program (2022YFC2009600) to Dr. HP-S.

Acknowledgments

We would like to thank the all the patients and their families for participating in the study, and INSCOC project members for their substantial work on data collecting and follow up. We would like to thank TopEdit (www.topeditsci.com) for its linguistic assistance during the preparation of this manuscript.

Conflict of interest

The authors declare that the research was conducted in the absence of any commercial or financial relationships that could be construed as a potential conflict of interest.

Publisher's note

Supplementary material

The Supplementary Material for this article can be found online at: https://www.frontiersin.org/articles/10.3389/fimmu.2023.1131496/full#supplementary-material

References

1. Siegel RL, Miller KD, Fuchs HE, Jemal A. Cancer statistics, 2022. *CA Cancer J Clin* (2022) 72(1):7–33. doi: 10.3322/caac.21708

2. Keum N, Giovannucci E. Global burden of colorectal cancer: emerging trends, risk factors and prevention strategies. *Nat Rev Gastroenterol Hepatol* (2019) 16 (12):713–32. doi: 10.1038/s41575-019-0189-8

3. Takamizawa Y, Shida D, Boku N, Nakamura Y, Ahiko Y, Yoshida T, et al. Nutritional and inflammatory measures predict survival of patients with stage IV colorectal cancer. *BMC Cancer.* (2020) 20(1):1092. doi: 10.1186/s12885-020-07560-3

4. Feliciano EMC, Kroenke CH, Meyerhardt JA, Prado CM, Bradshaw PT, Kwan ML, et al. Association of systemic inflammation and sarcopenia with survival in nonmetastatic colorectal cancer: Results from the c SCANS study. *JAMA Oncol* (2017) 3(12):e172319. doi: 10.1001/jamaoncol.2017.2319

5. Chen JH, Zhai ET, Yuan YJ, Wu KM, Xu JB, Peng JJ, et al. Systemic immune-inflammation index for predicting prognosis of colorectal cancer. *World J Gastroenterol* (2017) 23(34):6261–72. doi: 10.3748/wjg.v23.i34.6261

6. Schmitt M, Greten FR. The inflammatory pathogenesis of colorectal cancer. *Nat Rev Immunol* (2021) 21(10):653–67. doi: 10.1038/s41577-021-00534-x

7. Cavagnari MAV, Silva TD, Pereira MAH, Sauer LJ, Shigueoka D, Saad SS, et al. Impact of genetic mutations and nutritional status on the survival of patients with colorectal cancer. *BMC Cancer.* (2019) 19(1):644. doi: 10.1186/s12885-019-5837-4

8. Guo L, Wang C, Qiu X, Pu X, Chang P. Colorectal cancer immune infiltrates: Significance in patient prognosis and immunotherapeutic efficacy. *Front Immunol* (2020) 11:1052. doi: 10.3389/fimmu.2020.01052

9. Craig SG, Humphries MP, Alderdice M, Bingham V, Richman SD, Loughrey MB, et al. Immune status is prognostic for poor survival in colorectal cancer patients and is associated with tumour hypoxia. *Br J Cancer.* (2020) 123(8):1280–8. doi: 10.1038/s41416-020-0985-5

10. Sproston NR, Ashworth JJ. Role of c-reactive protein at sites of inflammation and infection. *Front Immunol* (2018) 9:754. doi: 10.3389/fimmu.2018.00754

11. Eckart A, Struja T, Kutz A, Baumgartner A, Baumgartner T, Zurfluh S, et al. Relationship of nutritional status, inflammation, and serum albumin levels during acute illness: A prospective study. *Am J Med* (2020) 133(6):713–22 e7. doi: 10.1016/j.amjmed.2019.10.031

12. Fleisher TA, Oliveira JB. Functional and molecular evaluation of lymphocytes. *J Allergy Clin Immunol* (2004) 114(2):227–34. doi: 10.1016/j.jaci.2004.06.001

13. Muller L, Hahn F, Mahringer-Kunz A, Stoehr F, Gairing SJ, Michel M, et al. Immunonutritive scoring for patients with hepatocellular carcinoma undergoing transarterial chemoembolization: Evaluation of the CALLY index. *Cancers (Basel)* (2021) 13(19):5018. doi: 10.3390/cancers13195018

14. Xu H, Song C, Wang C, Fu Z, Guo Z, Lin Y, et al. Investigation on nutrition status and clinical outcome of patients with common cancers in Chinese patients: a multicenter prospective study protocol. *Int J Clin Trials* (2020) 7(2):94–102. doi: 10.18203/2349-3259.ijct20201052

15. Kraus S, Arber N. Inflammation and colorectal cancer. *Curr Opin Pharmacol* (2009) 9(4):405–10. doi: 10.1016/j.coph.2009.06.006

16. Lushchak VI. Free radicals, reactive oxygen species, oxidative stress and its classification. *Chem Biol Interact* (2014) 224:164–75. doi: 10.1016/j.cbi.2014.10.016

17. Valavanidis A, Vlachogianni T, Fiotakis C. 8-hydroxy-2' -deoxyguanosine (8-OHdG): A critical biomarker of oxidative stress and carcinogenesis. *J Environ Sci Health C Environ Carcinog Ecotoxicol Rev* (2009) 27(2):120–39. doi: 10.1080/10590500902885684

18. Mihajlovic M, Gojkovic T, Vladimirov S, Miljkovic M, Stefanovic A, Vekic J, et al. Changes in lecithin: cholesterol acyltransferase, cholesteryl ester transfer protein and paraoxonase-1 activities in patients with colorectal cancer. *Clin Biochem* (2019) 63:32–8. doi: 10.1016/j.clinbiochem.2018.11.010

19. Liu H, Liu X, Zhang C, Zhu H, Xu Q, Bu Y, et al. Redox imbalance in the development of colorectal cancer. *J Cancer.* (2017) 8(9):1586–97. doi: 10.7150/jca.18735

20. Li F, Zhang J, Arfuso F, Chinnathambi A, Zayed ME, Alharbi SA, et al. NF-kappaB in cancer therapy. *Arch Toxicol* (2015) 89(5):711–31. doi: 10.1007/s00204-015-1470-4

21. Donath MY, Shoelson SE. Type 2 diabetes as an inflammatory disease. *Nat Rev Immunol* (2011) 11(2):98–107. doi: 10.1038/nri2925

22. Kaler P, Godasi BN, Augenlicht L, Klampfer L. The NF-kappaB/AKT-dependent induction of wnt signaling in colon cancer cells by macrophages and IL-1beta. *Cancer Microenviron* (2009) 2(1):69–80. doi: 10.1007/s12307-009-0030-y

23. Roszkowski K, Jozwicki W, Blaszczyk P, Mucha-Malecka A, Siomek A. Oxidative damage DNA: 8-oxoGua and 8-oxodG as molecular markers of cancer. *Med Sci Monit* (2011) 17(6):CR329–CR33. doi: 10.12659/MSM.881805

24. Kojima M, Morisaki T, Sasaki N, Nakano K, Mibu R, Tanaka M, et al. Increased nuclear factor-kB activation in human colorectal carcinoma and its correlation with tumor progression. *Anticancer Res* (2004) 24(2B):675–81. Available at: https://ar.iiarjournals.org/content/24/2B/675.long

25. van der Werf A, Arthey K, Hiesmayr M, Sulz I, Schindler K, Laviano A, et al. The determinants of reduced dietary intake in hospitalised colorectal cancer patients. *Support Care Cancer.* (2018) 26(6):2039–47. doi: 10.1007/s00520-018-4044-1

26. Martinez-Escribano C, Arteaga Moreno F, Perez-Lopez M, Cunha-Perez C, Belenguer-Varea A, Cuesta Peredo D, et al. Malnutrition and increased risk of adverse outcomes in elderly patients undergoing elective colorectal cancer surgery: A case-control study nested in a cohort. *Nutrients* (2022) 14(1):207. doi: 10.3390/nu14010207

27. Biolo G, Cederholm T, Muscaritoli M. Muscle contractile and metabolic dysfunction is a common feature of sarcopenia of aging and chronic diseases: from sarcopenic obesity to cachexia. *Clin Nutr* (2014) 33(5):737–48. doi: 10.1016/j.clnu.2014.03.007

28. Williams JP, Phillips BE, Smith K, Atherton PJ, Rankin D, Selby AL, et al. Effect of tumor burden and subsequent surgical resection on skeletal muscle mass and protein turnover in colorectal cancer patients. *Am J Clin Nutr* (2012) 96(5):1064–70. doi: 10.3945/ajcn.112.045708

29. Baracos VE, Martin L, Korc M, Guttridge DC, Fearon KCH. Cancer-associated cachexia. *Nat Rev Dis Primers* (2018) 4:17105. doi: 10.1038/nrdp.2017.105

30. Paccagnella A, Morello M, Da Mosto MC, Baruffi C, Marcon ML, Gava A, et al. Early nutritional intervention improves treatment tolerance and outcomes in head and neck cancer patients undergoing concurrent chemoradiotherapy. *Support Care Cancer.* (2010) 18(7):837–45. doi: 10.1007/s00520-009-0717-0

31. Paccagnella A, Morassutti I, Rosti G. Nutritional intervention for improving treatment tolerance in cancer patients. *Curr Opin Oncol* (2011) 23(4):322–30. doi: 10.1097/CCO.0b013e3283479c66

32. Cabrerizo S, Cuadras D, Gomez-Busto F, Artaza-Artabe I, Marin-Ciancas F, Malafarina V. Serum albumin and health in older people: Review and meta analysis. *Maturitas* (2015) 81(1):17–27. doi: 10.1016/j.maturitas.2015.02.009

33. Wei Y, Xu H, Dai J, Peng J, Wang W, Xia L, et al. Prognostic significance of serum lactic acid, lactate dehydrogenase, and albumin levels in patients with metastatic colorectal cancer. *BioMed Res Int* (2018) 2018:1804086. doi: 10.1155/2018/1804086

34. Sica A, Mantovani A. Macrophage plasticity and polarization: *in vivo* veritas. *J Clin Invest* (2012) 122(3):787–95. doi: 10.1172/JCI59643

35. Pan C, Wang Y, Liu Q, Hu Y, Fu J, Xie X, et al. Phenotypic profiling and prognostic significance of immune infiltrates in esophageal squamous cell carcinoma. *Oncoimmunology* (2021) 10(1):1883890. doi: 10.1080/2162402X.2021.1883890

36. Bottcher JP, Bonavita E, Chakravarty P, Blees H, Cabeza-Cabrerizo M, Sammicheli S, et al. NK cells stimulate recruitment of cDC1 into the tumor microenvironment promoting cancer immune control. *Cell* (2018) 172(5):1022–37 e14. doi: 10.1016/j.cell.2018.01.004

37. Ghaemdoust F, Keshavarz-Fathi M, Rezaei N. Natural killer cells and cancer therapy, what we know and where we are going. *Immunotherapy* (2019) 11(14):1231–51. doi: 10.2217/imt-2019-0040

38. Gu-Trantien C, Loi S, Garaud S, Equeter C, Libin M, de Wind A, et al. CD4(+) follicular helper T cell infiltration predicts breast cancer survival. *J Clin Invest* (2013) 123(7):2873–92. doi: 10.1172/JCI67428

39. Yue W, Lin Y, Yang X, Li B, Liu J, He R. Thymic stromal lymphopoietin (TSLP) inhibits human colon tumor growth by promoting apoptosis of tumor cells. *Oncotarget* (2016) 7(13):16840–54. doi: 10.18632/oncotarget.7614

40. Jensen-Jarolim E, Bax HJ, Bianchini R, Crescioli S, Daniels-Wells TR, Dombrowicz D, et al. AllergoOncology: Opposite outcomes of immune tolerance in allergy and cancer. *Allergy* (2018) 73(2):328–40. doi: 10.1111/all.13311

41. Inoue S, Leitner WW, Golding B, Scott D. Inhibitory effects of b cells on antitumor immunity. *Cancer Res* (2006) 66(15):7741–7. doi: 10.1158/0008-5472.CAN-05-3766

42. Della Valle L, Gatta A, Farinelli A, Scarano G, Lumaca A, Tinari N, et al. Allergooncology: an expanding research area. *J Biol Regul Homeost Agents* (2020) 34 (2):319–26. doi: 10.23812/19-418-63-E

43. Nakamura M, Souri EA, Osborn G, Laddach R, Chauhan J, Stavraka C, et al. IgE activates monocytes from cancer patients to acquire a pro-inflammatory phenotype. *Cancers (Basel)* (2020) 12(11):3376. doi: 10.3390/cancers12113376

44. Jensen-Jarolim E, Bax HJ, Bianchini R, Capron M, Corrigan C, Castells M, et al. AllergoOncology - the impact of allergy in oncology: EAACI position paper. *Allergy* (2017) 72(6):866–87. doi: 10.1111/all.13119

45. Lin S, Gregory RI. MicroRNA biogenesis pathways in cancer. *Nat Rev Cancer.* (2015) 15(6):321–33. doi: 10.1038/nrc3932

46. Iseki Y, Shibutani M, Maeda K, Nagahara H, Tamura T, Ohira G, et al. The impact of the preoperative peripheral lymphocyte count and lymphocyte percentage in patients with colorectal cancer. *Surg Today* (2017) 47(6):743–54. doi: 10.1007/s00595-016-1433-2

47. Matiello J, Dal Pra A, Zardo L, Silva R, Berton DC. Impacts of post-radiotherapy lymphocyte count on progression-free and overall survival in patients with stage III lung cancer. *Thorac Cancer.* (2020) 11(11):3139–44. doi: 10.1111/1759-7714.13621

48. Dunn GP, Old LJ, Schreiber RD. The immunobiology of cancer immunosurveillance and immunoediting. *Immunity* (2004) 21(2):137–48. doi: 10.1016/j.immuni.2004.07.017

49. Siska PJ, Rathmell JC. T Cell metabolic fitness in antitumor immunity. *Trends Immunol* (2015) 36(4):257–64. doi: 10.1016/j.it.2015.02.007

50. Utariani A, Rahardjo E, Perdanakusuma DS. Effects of albumin infusion on serum levels of albumin, proinflammatory cytokines (TNF-, IL-1, and IL-6), CRP, and MMP-8; tissue expression of EGRF, ERK1, ERK2, TGF-, collagen, and MMP-8; and wound healing in sprague dawley rats. *Int J Inflam* (2020) 2020:3254017. doi: 10.1155/2020/3254017

51. Zamarron BF, Chen W. Dual roles of immune cells and their factors in cancer development and progression. *Int J Biol Sci* (2011) 7(5):651–8. doi: 10.7150/ijbs.7.651

52. Kedia-Mehta N, Finlay DK. Competition for nutrients and its role in controlling immune responses. *Nat Commun* (2019) 10(1):2123. doi: 10.1038/s41467-019-10015-4

53. Maraj M, Kusnierz-Cabala B, Dumnicka P, Gala-Bladzinska A, Gawlik K, Pawlica-Gosiewska D, et al. Malnutrition, inflammation, atherosclerosis syndrome (MIA) and diet recommendations among end-stage renal disease patients treated with maintenance hemodialysis. *Nutrients* (2018) 10(1):69. doi: 10.3390/nu10010069

54. Sano T, Coit DG, Kim HH, Roviello F, Kassab P, Wittekind C, et al. Proposal of a new stage grouping of gastric cancer for TNM classification: International gastric cancer association staging project. *Gastric Cancer*. (2017) 20(2):217–25. doi: 10.1007/s10120-016-0601-9

55. Wang Y, Xuan Z, Wang B, Zhang D, Zhang C, Wang J, et al. EphA3 downregulation by hypermethylation associated with lymph node metastasis and TNM stage in colorectal cancer. *Dig Dis Sci* (2019) 64(6):1514–22. doi: 10.1007/s10620-018-5421-9

56. Cserni G, Chmielik E, Cserni B, Tot T. The new TNM-based staging of breast cancer. *Virchows Arch* (2018) 472(5):697–703. doi: 10.1007/s00428-018-2301-9

57. Liu Q, Lian P, Luo D, Cai S, Li Q, Li X. Combination of carcinoembryonic antigen with the American joint committee on cancer TNM staging system in rectal cancer: a real-world and large population-based study. *Onco Targets Ther* (2018) 11:5827–34. doi: 10.2147/OTT.S171433

58. Li J, Guo BC, Sun LR, Wang JW, Fu XH, Zhang SZ, et al. TNM staging of colorectal cancer should be reconsidered by T stage weighting. *World J Gastroenterol* (2014) 20(17):5104–12. doi: 10.3748/wjg.v20.i17.5104

59. Hayama T, Ozawa T, Asako K, Kondo R, Ono K, Okada Y, et al. Impact of colon cancer location on the prognostic significance of nutritional indexes and inflammatory markers. *In Vivo*. (2021) 35(2):1261–9. doi: 10.21873/invivo.12377

60. Hayama T, Hashiguchi Y, Okada Y, Ono K, Nemoto K, Shimada R, et al. Significance of the 7th postoperative day neutrophil-to-lymphocyte ratio in colorectal cancer. *Int J Colorectal Dis* (2020) 35(1):119–24. doi: 10.1007/s00384-019-03463-3

frontiers | Frontiers in Immunology

TYPE Systematic Review
PUBLISHED 31 March 2023
DOI 10.3389/fimmu.2023.1146898

OPEN ACCESS

EDITED BY
Eyad Elkord,
University of Salford, United Kingdom

REVIEWED BY
Xiaolong Wang,
Temple University, United States
Guichuan Lai,
Chongqing Medical University, China

*CORRESPONDENCE
Yunxia Tao
tyx876@163.com

†These authors have contributed equally to this work and share first authorship

This article was submitted to Cancer Immunity and Immunotherapy, a section of the journal Frontiers in Immunology

SPECIALTY SECTION
RECEIVED 18 January 2023
ACCEPTED 21 March 2023
PUBLISHED 31 March 2023

CITATION
Qian X, Chen H and Tao Y (2023) Biomarkers predicting clinical outcomes in nasopharyngeal cancer patients receiving immune checkpoint inhibitors: A systematic review and meta-analysis. *Front. Immunol.* 14:1146898. doi: 10.3389/fimmu.2023.1146898

Biomarkers predicting clinical outcomes in nasopharyngeal cancer patients receiving immune checkpoint inhibitors: A systematic review and meta-analysis

Xiaoyan Qian[1†], Haizhu Chen[2,3†] and Yunxia Tao[4*]

[1]Department of Oncology, Henan Provincial People's Hospital, People's Hospital of Zhengzhou University, People's Hospital of Henan University, Zhengzhou, China, [2]Breast Tumor Centre, Guangdong Provincial Key Laboratory of Malignant Tumor Epigenetics and Gene Regulation, Department of Medical Oncology, Sun Yat-sen Memorial Hospital, Sun Yat-sen University, Guangzhou, China, [3]Phase I Clinical Trial Centre, Guangdong Provincial Key Laboratory of Malignant Tumor Epigenetics and Gene Regulation, Department of Medical Oncology, Sun Yat-sen Memorial Hospital, Sun Yat-sen University, Guangzhou, China, [4]Department of Oncology, The Affiliated Hospital of Xuzhou Medical University, Xuzhou, Jiangsu, China

Background: Optimal biomarkers to select patients who will benefit most from immunotherapy remain lacking in nasopharyngeal cancer (NPC). This systematic review and meta-analysis aimed to evaluate the association between various biomarkers and clinical outcomes in NPC patients treated with immune checkpoint inhibitors (ICIs).

Methods: Systematic searches of PubMed, Embase, Cochrane Library, and Web of Science databases were performed up to October 2022. Studies evaluating the association between biomarkers and intended outcomes of ICIs were included. The pooled odds ratio (OR) and hazard ratio (HR) with 95% confidence intervals (CIs) were calculated, respectively, for the objective response rate (ORR) and progression-free survival (PFS) under fixed or random-effect models.

Results: A total of 15 studies involving 1,407 patients were included. The pooled analysis indicated that NPC patients with lower plasma Epstein-Barr virus (EBV) DNA level at baseline (OR = 2.14, 95% CI: 1.46-3.14, $P < 0.001$), decreased EBV DNA load during immunotherapy (OR = 4.57, 95% CI: 2.24-9.34, $P = 0.002$) and higher programmed cell death-ligand 1 (PD-L1) expression (OR = 2.35, 95% CI: 1.36-4.09, $P = 0.002$) had superior ORR than the counterparts. No significant differences of ORR were observed between positive PD-L1 expression and negative PD-L1 expression (OR = 1.50, 95% CI: 0.92-2.45, $P = 0.104$), as well as higher tumor mutation burden (TMB) and lower TMB (OR = 1.62, 95% CI: 0.41-6.44, $P = 0.494$). Patients with lower plasma EBV DNA level at baseline obtained a significant benefit on PFS than those with higher plasma EBV DNA level (HR = 0.52, 95% CI: 0.42-0.63, $P < 0.001$). There were no differences in PFS between decreased EBV DNA load and increased EBV DNA load during immunotherapy (HR = 0.51, 95% CI: 0.22-1.17, $P = 0.109$), higher PD-L1 expression and lower PD-

L1 expression (HR = 0.65, 95% CI: 0.42-1.01, *P* = 0.054), positive PD-L1 expression and negative PD-L1 expression (HR = 0.90, 95% CI: 0.64-1.26, *P* = 0.531), lower TMB and higher TMB (HR = 0.84, 95% CI: 0.51-1.38, *P* = 0.684).

Conclusion: Lower baseline plasma EBV DNA level, decreased plasma EBV DNA during immunotherapy, and higher PD-L1 expression are reliable biomarkers predicting better response to ICIs treatment. Lower baseline plasma EBV DNA level was also associated with longer PFS. It is warranted to further explore and better illuminate the utility of these biomarkers in future clinical trials and real-world practice.

Systematic review registration: https://www.crd.york.ac.uk/PROSPERO/, identifier CRD42022324434.

KEYWORDS

immune checkpoint inhibitors, nasopharyngeal cancer, biomarker, Epstein-Barr virus, PD-L1 expression, tumor mutation burden, immunotherapy, meta-analysis

1 Introduction

Now is an exciting era of development in immune checkpoint inhibitors (ICIs), which have also exhibited encouraging anti-tumor activity for patients with nasopharyngeal cancer (NPC) in recent years (1–4). However, as one of the most common head and neck malignant tumors in Southeast Asia, especially in southern China (5, 6), NPC has no well-established biomarkers for ICIs up to date.

The widely used biomarker, Epstein-Barr virus (EBV), played an important role in the development and progression of NPC (7, 8). However, it is obscure whether plasma EBV DNA level correlates with the anti-tumor activity of ICIs. Some studies showed that lower baseline plasma EBV DNA level was associated with better objective response rate (ORR) and progression-free survival (PFS) compared with the higher EBV DNA level for NPC patients treated with ICIs (3, 9). Other trials, however, did not demonstrate consistent results, in which patients achieved identical clinical benefits regardless of the EBV DNA level (2).

The predictive value of commonly used biomarkers for ICI efficacy, such as programmed cell death-ligand 1 (PD-L1) expression and tumor mutation burden (TMB), is also unclear in NPC. PD-L1 expression was reported to be associated with clinical outcomes in patients with NPC who received chemoradiotherapy, but the utility for ICI efficacy was not well interpreted. Compared with other solid tumors, the level of TMB is relatively lower in NPC (10, 11). Some studies suggested that NPC patients with lower TMB could also achieve clinical benefits with anti-PD-1/PD-L1 therapies as those with higher TMB (9, 12).

So far, there has been no pooled analysis exploring the impact of EBV DNA, PD-L1 expression, and TMB on the clinical outcomes of ICIs for NPC. Herein, we performed a comprehensive systematic review and meta-analysis with recently accumulated evidence to evaluate the association between the three biomarkers and clinical outcomes in NPC patients treated with ICIs.

2 Methods

This systematic review and meta-analysis were conducted according to the Preferred Reporting Items for Systematic reviews and Meta-Analyses (PRISMA) guidelines (13) and were registered on the International Prospective Register of Systematic Reviews (PROSPERO) (register ID: CRD42022324434).

2.1 Literature search strategy and eligible study selection

Literature search for studies was performed from electronic databases, including PubMed, Embase, Cochrane Library, and Web of Science databases, by two independent investigators (XYQ and YXT) up to October 10, 2022. The Subject headings and main keywords included: (a) “nasopharyngeal carcinoma”, “nasopharyngeal cancer” or “cancer of nasopharynx”; (b) “immune checkpoint inhibitor”, “immunotherapy”, “anti-PD-1” or “anti-PD-L1”. The complete literature search strategy was displayed in Supplementary Table S1.

The main criteria for eligibility are as follows: (1) studies in which NPC patients were treated with ICI monotherapy, or ICI combined with chemotherapy/radiotherapy; (2) studies in which the association between plasma EBV DNA level, PD-L1 expression, TMB and clinical outcomes (ORR, PFS) of ICIs was evaluated; (3) studies in which the related data could be extracted directly or calculated indirectly; (5) studies that were written in English. Exclusion criteria are as follows: (1) studies that were reviews, case reports, comments, or letters; (2) studies that were performed on animals or cells; (3) studies that lacked sufficient information. Two investigators (XYQ and YXT) conducted the study search and selection independently. If there was any disagreement, the third investigator (HZC) reassessed the studies.

2.2 Data extraction and quality assessment

We extracted the following information from the eligible studies (1) characteristics of studies (first author, publication year, area, type of studies, sample size, follow-up time); (2) characteristics of patients (age, sex, study drugs, biomarkers). (3) clinical outcomes (ORR and PFS), hazard ratios (HRs), and their corresponding 95% confidence intervals (CIs) for PFS. If the HRs and 95% CIs were not provided directly in the study, Engauge Digitizer software (version 11.1) was applied to extract the coordinates of points on the Kaplan-Meier curves. When the results in both univariate and multivariate analyses were available, results from the multivariate analysis were preferred. The cut-off values of plasma EBV DNA levels, PD-L1 expression, and TMB varied across studies. For plasma EBV DNA and TMB, the lower group was identified by the value of lower than the cut-off in each study, otherwise, it was defined as the higher group. When one study reported more than one category by different cut-off values, one of the results was collected. For PD-L1 expression, two comparative models were applied: higher vs. lower and positive vs. negative. The PD-L1 higher and lower category were identified according to the cut-off value in each study: Yang et al. (3), Ma et al. (2), and Park et al. (12) using 10%, Yang et al. (14) using 15%, while Wang et al. (9) using 25%. The PD-L1 positive and negative categories were identified by a cut-off value of 1%. Two investigators (XYQ and YXT) conducted the data extraction independently.

The quality of the studies included was evaluated by Newcastle-Ottawa (NOS) assessment scale criteria, which involved the selection, comparability, and outcomes of the studies (15). The total scores ranged from 0 to 9 points, and the quality criteria were evaluated as follows: poor quality (< 5 points); medium quality (5-7 points); high quality (> 7 points).

2.3 Statistical analysis

The predictive value of EBV DNA, PD-L1 expression, and TMB was assessed in NPC patients treated with ICIs. The categorical meta-analysis was performed by comparing lower plasma EBV DNA level with higher EBV DNA level at baseline, decreased plasma EBV DNA load with increased EBV DNA load during ICIs treatment, higher PD-L1 expression in tissue with lower PD-L1 expression, positive PD-L1 expression in tissue with negative PD-L1 expression, and higher TMB in tissue with lower TMB. The impacts of these biomarkers on the clinical outcomes of ICIs were measured by ORR and PFS. Odds ratio (OR) and 95% CI was applied for the pooled analysis of ORR, with HR and 95% CI for PFS.

Cochran's Q test and Higgins I^2 statistic were used to evaluate the heterogeneity among studies (16, 17). For the Q test, a P value < 0.05 was considered significant heterogeneity. For I^2 statistics, heterogeneity was assessed as follows: low (I^2 < 25%), moderate (25% ≤ I^2 < 50%), and high (I^2 ≥ 50%). When there was no significant heterogeneity (P value of Q test ≥ 0.05 and I^2 statistic < 50%), a fixed-effect model was performed for the pooled analysis, otherwise, a random-effect model was used. Publication bias was examined by the Funnel plot (18, 19). Sensitivity analysis was conducted by omitting study by study sequentially. Stata version 15.0 was applied to conduct the statistical analyses. A two-sided P value < 0.05 was considered a statistically significant difference.

3 Results

3.1 Systematic search and study selection

A total of 2440 records were identified through the electronic databases, with 361 from PubMed, 854 from Embase, 102 from Cochrane, and 1123 from Web of Science. The detailed procedure of literature screening is shown in Figure 1. There were 15 relevant studies identified for inclusion in the final analysis (2–4, 9, 12, 14, 20–28), with 13 published articles and 2 conference abstracts, including 1,407 patients.

The quality assessment of the included studies using the Newcastle-Ottawa scale is presented in Supplementary Table S2. Two studies were graded as medium quality, with a quality score of 7. Fourteen studies were graded as high quality, with 2 studies scoring 8 and 11 studies scoring 9.

3.2 Patients' characteristics

Of the 15 included studies, 13 studies assessed more than one predictive biomarker. Table 1 presents the baseline characteristics of the studies included in the systematic review and meta-analysis, including EBV DNA(n=10), dynamic EBV DNA(n=5), PD-L1 (n=7), and TMB(n=6). The median age of patients ranged from 44 to 57 years old. The majority of patients were male. All the NPC patients enrolled were recurrence or metastatic diseases. The median follow-up time of the included studies ranged from 5.8 months to 24.7 months.

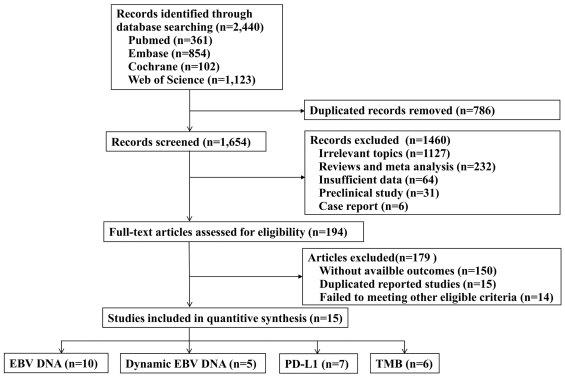

FIGURE 1
Flow chart of the literature search strategy and eligible study selection process. EBV, Epstein-Barr virus; PD-L1, programmed cell death-ligand 1; TMB, tumor mutation burden.

TABLE 1 Baseline characteristics of the studies included in the systematic review and meta-analysis.

Biomarker	Outcomes	Cut-off value	Study	Region	Type of study	Treatment	Stage	The line of treatment	Sample	Median age (range)	Male (%)	Median follow-up (months)
EBV DNA	ORR	NR	Yang 2021 (14)	China	Prospective (phase II)	Camrelizumab	recurrent or metastatic	>2	156	48 (23–71)	124 (79.5)	14.2 (0.7–27.6)
EBV DNA	PFS	NR	Yang 2021 (3)	China	Prospective (phase III)	Camrelizumab combined with chemo (GP)	recurrent or metastatic	1	134	52 (40–58)	113 (84.0)	10.2 (IQR:7.7–12.7)
EBV DNA	PFS	10,000IU/mL	Xu J 2022 (20)	China	Prospective (phase II)	Toripalimab	recurrent or metastatic	>2	179	46 (22-71)	148 (82.7)	NR
EBV DNA	ORR	10,000IU/mL	Wang 2021 (9)	China	Prospective (phase II)	Toripalimab	recurrent or metastatic	>2	190	46 (22-71)	158 (83.2)	NR
EBV DNA	PFS	1,500 copies/mL	Hua 2021 (21)	China	Prospective (phase II)	Toripalimab combined with radiocherapy	recurrence	1	25	49(IQR: 43.5–52.5)	18 (72.0)	14.6 (IQR: 13.1–16.2)
EBV DNA	ORR	19,000 copies/mL	Even 2021 (22)	France	Prospective (phase II)	Spartalizumab(PDR001)	recurrent or metastatic	>1	82	51 (21–74)	68 (82.9)	NR
EBV DNA	ORR, PFS	30,000 copies/mL	Fang 2018 (23)	China	Prospective (phase I)	Cohort1: Camrelizumab monotherapy	recurrent or metastatic	>1	93	45 (38–52)	75 (81.0)	9.9 (IQR:8.1–11.7)
EBV DNA	ORR, PFS	30,000 copies/mL	Fang 2018 (23)	China	Prospective (phase I)	Cohort2: Camrelizumab combination	recurrent or metastatic	>1	22	44 (34–51)	17 (74.0)	10.2 (IQR:9.7–10.8)
EBV DNA	ORR, PFS	50,000copies/mL	Xu L 2022 (26)	China	Prospective (phase I/II)	Camrelizumab or Nivolumab	recurrent or metastatic	≥1	57	47(25-72)	43 (75.4)	5.8
EBV DNA	ORR	1,000 copies/mL	Shi 2022 (4)	China	Prospective (phase II)	KL-A167	recurrent or metastatic	>1	132	49 (26–68)	109 (82.6)	21.7(95%CI: 19.8–22.5)
Dynamic EBV DNA	ORR, PFS	30,000 copies/mL	Fang 2018 (23)	China	Prospective (phase I)	Cohort1: Camrelizumab monotherapy	recurrent or metastatic	>1	93	45 (38–52)	75 (81.0)	9.9 (IQR:8.1–11.7)
Dynamic EBV DNA	ORR	1,000 copies/mL	Shi 2022 (4)	China	Prospective (phase II)	KL-A167	recurrent or metastatic	>1	132	49 (26–68)	109 (82.6)	21.7(95%CI: 19.8–22.5)
Dynamic EBV DNA	ORR	NR	Chiang 2022 (28)	Hong Kong, China	Prospective (phase II)	Bintrafusp alfa	recurrent or metastatic	>1	38	NR	NR	14.9 (1.6-23.3)
Dynamic EBV DNA	PFS	NR	Yang 2021 (3)	China	Prospective (phase III)	Camrelizumab combined with chemo (GP)	recurrent or metastatic	1	134	52 (40–58)	113 (84.0)	10.2 (IQR:7.7–12.7)
Dynamic EBV DNA	PFS	NR	Chen 2022 (27)	China	Prospective (phase II)	Toripalimab combined with chemoradiotherapy	metastatic	≥1	22	54.5 (IQR: 40.5-57.5)	15 (68.2)	NR

(Continued)

10.3389/fimmu.2023.1146898

TABLE 1 Continued

Biomarker	Outcomes	Cut-off value	Study	Region	Type of study	Treatment	Stage	The line of treatment	Sample	Median age (range)	Male (%)	Median follow-up (months)
PD-L1	ORR	1%,10%	Yang 2021 (14)	China	Prospective (phase II)	Camrelizumab	recurrent or metastatic	>2	156	48 (23–71)	124 (79.5)	14.2 (0.7–27.6)
PD-L1	ORR	1%,10%	Ma 2018 (2)	Hong Kong, China	Prospective (phase II)	Nivolumab	recurrent or metastatic	>1	45	57(37-76)	35 (77.8)	12.5 (2.2-22.0)
PD-L1	ORR, PFS	1%, 25%	Wang 2021 (9)	China	Prospective (phase II)	Toripalimab	recurrent or metastatic	>2	190	46(22-71)	158 (83.2)	NR
PD-L1	ORR, PFS	1%,10%	Park 2020 (12)	America	Retrospective	anti-PD-1 antibody therapy	recurrent or metastatic	≥1	42	50 (15–74)	31 (73.8)	13.7 (2.1–55.3)
PD-L1	ORR	1%	Shi 2022 (4)	China	Prospective (phase II)	KL-A167	recurrent or metastatic	>1	132	49 (26–68)	109 (82.6)	21.7(95%CI: 19.8–22.5)
PD-L1	PFS	1%	Hua 2021 (21)	China	Prospective (phase II)	Toripalimab combined with radiocherapy	recurrence	1	25	49(IQR: 43.5–52.5)	18 (72.0)	14.6 (IQR: 13.1–16.2)
PD-L1	PFS	1%, 5%	Mai 2021 (24)	China	Prospective (phase III)	Toripalimab combined with chemo(GP)	recurrent or metastatic	1	130	46(19–72)	124 (85.0)	17.9
TMB	ORR, PFS	2.1muts/Mb	Park 2020 (12)	America	Retrospective	anti-PD-1 antibody therapy	recurrent or metastatic	≥1	42	50 (15–74)	31 (73.8)	13.7 (2.1–55.3)
TMB	ORR, PFS	4muts/Mb	Xu L 2022 (26)	China	Prospective (phase I/II)	Camrelizumab or Nivolumab	recurrent or metastatic	≥1	57	47(25-72)	43 (75.4)	5.8
TMB	PFS	2.9muts/Mb	Wang 2021 (9)	China	Prospective (phase II)	Toripalimab	recurrent or metastatic	>2	190	46(22-71)	158 (83.2)	NR
TMB	PFS	NR	Hua 2021 (21)	China	Prospective (phase II)	Toripalimab combined with radiocherapy	recurrence	1	25	49(IQR: 43.5–52.5)	18 (72.0)	14.6 (IQR: 13.1–16.2)
TMB	PFS	NR	Fang 2018 (23)	China	Prospective (phase I)	Cohort1: Camrelizumab monotherapy	recurrent or metastatic	>1	93	45 (38–52)	75 (81.0)	9.9 (IQR:8.1–11.7)
TMB	PFS	NR	Ma 2021 (25)	China	Prospective (phase I)	Camrelizumab or Nivolumab	recurrent or metastatic	>1	60	46 (23–73)	95 (76.6)	24.7 (95%CI:23.3-26.6)

EBV, Epstein-Barr virus; PD-L1, programmed cell death-ligand 1; TMB, tumor mutation burden; ORR, objective response rate; PFS, progression-free survival; GP, gemcitabine and cisplatin; NR, not reported; IQR, interquartile range; CI, confidence interval.

10.3389/fimmu.2023.1146898

3.3 Pooled analysis of ORR

After pooled analysis, patients with lower plasma EBV DNA level at baseline had superior ORR than those with higher plasma EBV DNA level (OR = 2.14, 95%CI: 1.46-3.14, $P < 0.001$, Figure 2A). Compared with patients harboring increased plasma EBV DNA load during immunotherapy, those with decreased EBV DNA load obtained a significant benefit on ORR (OR = 4.57, 95% CI: 2.24-9.34, $P < 0.001$, Figure 2B). There was no heterogeneity among the studies included.

In the pooled analysis, higher PD-L1 expression was associated with increased ORR than lower PD-L1 expression (OR = 2.35, 95% CI: 1.36-4.09, $P = 0.002$, Figure 2C). Nevertheless, there was no significant difference between positive PD-L1 expression and negative PD-L1 expression as for ORR (OR = 1.50, 95%CI: 0.92-2.45, $P = 0.104$, Figure 2D). No evidence of heterogeneity was observed among the analysis.

The pooled OR for ORR was 1.62 (95% CI: 0.41–6.44, $P = 0.494$), which indicated that patients with lower TMB had a comparable ORR with those with higher TMB. A moderate level of heterogeneity ($I^2 = 30.3\%$, $P = 0.231$, Figure 2E) was observed among the studies included.

3.4 Pooled analysis of PFS

According to the fixed effects model, patients with lower plasma EBV DNA level at baseline had longer PFS (HR = 0.52, 95% CI: 0.42–0.63, $P < 0.001$, Figure 3A) than those with higher plasma EBV DNA level. Patients with decreased plasma EBV DNA load during immunotherapy did not show a significant benefit on PFS than those with increased plasma EBV DNA load (HR=0.51, 95% CI:0.22–1.17, $P=0.109$; Figure 3B) by the random-effect model.

The pooled analysis showed that patients with higher PD-L1 expression had a tendency towards longer PFS than those with lower PD-L1 expression, while this did not reach a statistical difference (HR = 0.65, 95% CI: 0.42-1.01, $P = 0.054$, Figure 3C), There was no difference in PFS between positive PD-L1 expression and negative PD-L1 expression (HR = 0.90, 95% CI: 0.64-1.26, $P = 0.531$, Figure 3D). No evidence of heterogeneity was observed among the analysis.

The forest map did not show that patients with higher TMB have a lower risk of disease progression than those with lower TMB (HR = 0.84, 95% CI: 0.51-1.38, $P = 0.484$, Figure 3E) based on a random-effect model.

3.5 Sensitivity analysis

The sensitivity analysis, which was conducted by removing one study at each time, showed that the pooled results were not significantly influenced by any single study (Supplementary Figures S1, S2). Considering the relatively limited number of included studies for PFS of PD-L1 expression and ORR of TMB, sensitivity analysis was not applied to test the potential heterogeneity.

3.6 Publication bias

There was a slight asymmetrical according to the funnel plot for PFS of TMB. There was no obvious publication bias for the other pooled analysis when tested by funnel plot (Figures 4, 5).

4 Discussion

Though immunotherapy has become an increasingly attractive approach for patients with NPC, the optimal biomarkers to select patients who will benefit most from ICIs remain lacking. To our best knowledge, this meta-analysis is the first and the most comprehensive one that focused on the biomarkers predicting the clinical outcomes of patients with NPC receiving ICIs. In this study, we analyzed the association between plasma EBV DNA level at baseline, dynamic change of plasma EBV DNA level during immunotherapy, PD-L1 expression, TMB, and intended outcomes (ORR and PFS) of ICIs in NPC.

The role of plasma EBV DNA as a clinically useful biomarker in the detection, guiding chemotherapy and radiotherapy, surveillance, and prognostication for NPC has been well established (8, 29, 30). However, it is controversial whether the plasma EBV DNA level was associated with the clinical outcomes of ICIs. Notably, our study observed that NPC patients with lower plasma EBV DNA level at baseline had higher ORR and longer median PFS compared with patients with higher EBV DNA level. In addition, post-treatment EBV DNA decrease was correlated with a better response to ICIs in NPC. One possible underlying mechanism for the pretreatment and the dynamic change of plasma EBV DNA level as a potential indicator for clinical outcomes of NPC patients receiving ICIs might be the tumor evasion from the immune system. The EBV encoding latent membrane proteins and noncoding RNA molecules, limit the actions of interferon and block antigen presentation, which allows NPC cells to escape immune recognition and avoid immune (31, 32). As a result, a heavy load at baseline or an increase post-treatment of plasma EBV DNA level could be correlated with a higher number of NPC tumor cells escaping immune recognition, thus resulting in poor outcomes for patients treated with ICIs (33). Taken together, plasma EBV DNA may pave a way towards the precision immunotherapy approach in NPC. More studies investigating the biological mechanisms underlying those associations are worthwhile to be conducted in the near future.

The predictive value of PD-L1 expression, the most extensively studied biomarker for immunotherapy, though proved to be a useful biomarker in predicting the efficacy of ICIs in lung cancer, esophageal cancer, and other solid carcinomas (34, 35), was still inconclusive in NPC. In our study, no difference was observed with respect to ORR and PFS between positive and negative PD-L1 expression (a cutoff of 1%) in NPC patients receiving ICIs. However, when using a higher cut-off value, a better ORR was observed in high PD-L1 expression. These results manifest that PD-L1 expression has certain predictive utility in NPC, and further considerable studies are warranted to explore the optimal cut-off

10.3389/fimmu.2023.1146898

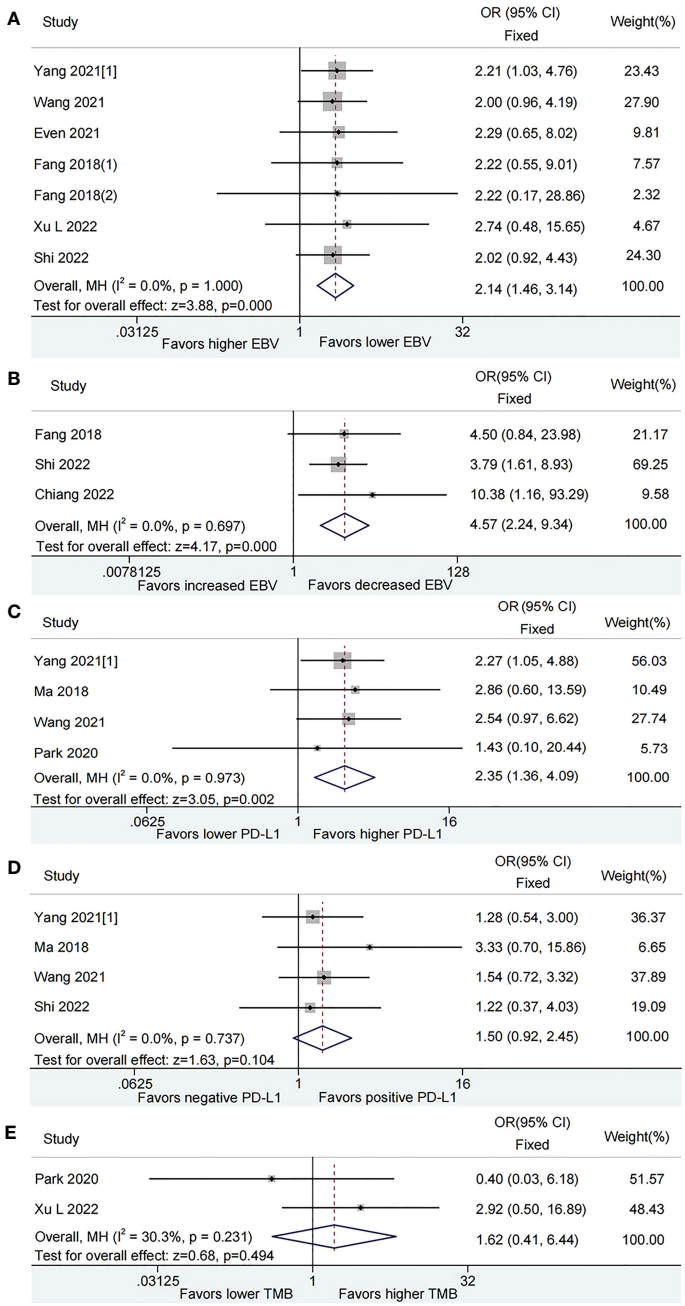

FIGURE 2
Meta-analysis of the association between biomarkers and objective response rate (ORR). **(A)** baseline plasma Epstein-Barr virus (EBV) DNA level and ORR; **(B)** Dynamic plasma EBV DNA load during immunotherapy and ORR; **(C)** programmed cell death-ligand 1 (PD-L1) expression [higher vs. lower] and ORR; **(D)** PD-L1 expression [positive vs. negative] and ORR; **(E)** tumor mutation burden (TMB) and ORR.

value of PD-L1 expression to better illuminate the association between PD-L1 expression and outcomes of ICIs.

TMB was emerging as a potential biomarker for immunotherapy in recent decades. Previous studies suggested that higher TMB was associated with a higher number of tumor-neoantigens presented on major histocompatibility complex class (MHC) molecules, which facilitated immune recognition and the response to anti-tumor immunotherapy (36). Our study found that there was no significant correlation between TMB and clinical outcomes in NPC patients receiving ICIs. This may be due to the variable cut-off values of TMB across studies and the distinct tumor microenvironment of NPC from other solid tumors. The relationship between TMB and response to ICIs remains challenging in NPC.

Notably, additional cohort studies explored the association between other biomarkers (eg, human leukocyte antigen [HLA], MHC and the effect on ICIs. In the CAPTAIN trial, a high MHC-II + cell density in the stroma was found to be associated with improved disease control rate (DCR), longer median PFS, and OS (14). In an international and multicenter study of nivolumab (NCI-

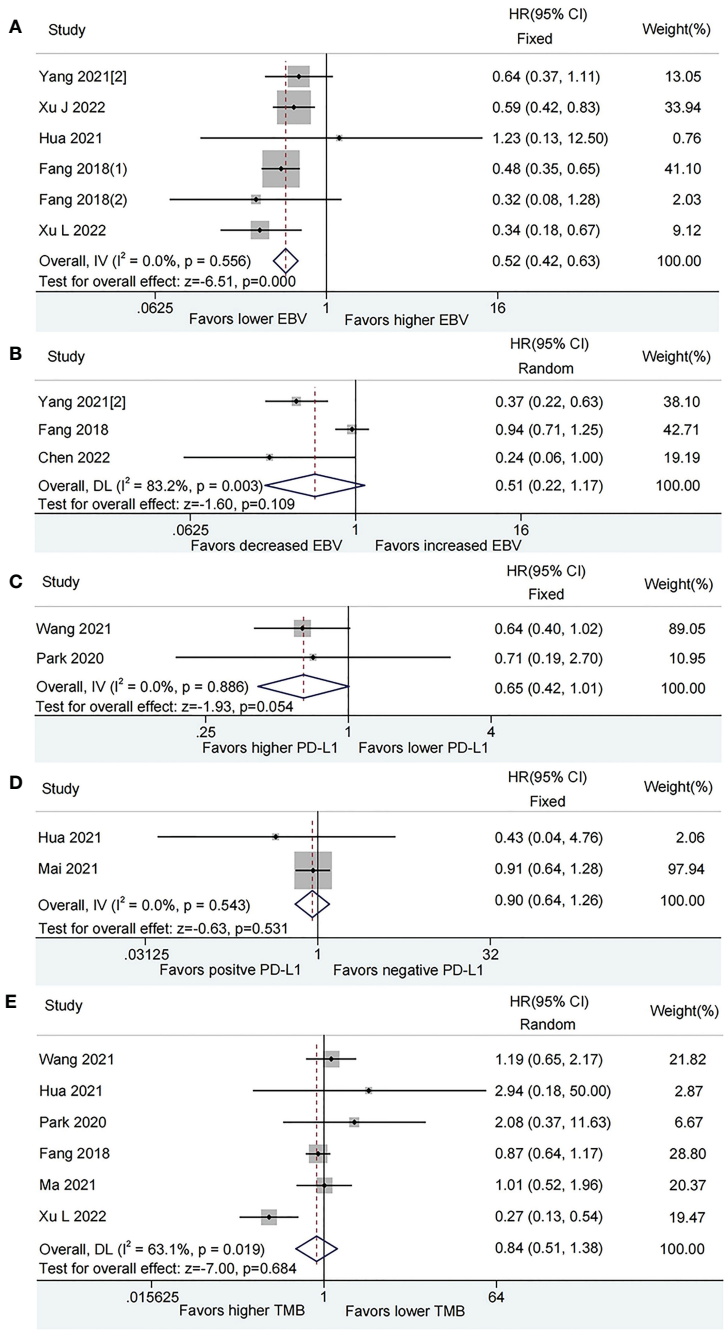

FIGURE 3
Meta-analysis of the association between biomarkers and progression-free survival (PFS). **(A)** baseline plasma Epstein-Barr virus (EBV) DNA level and PFS; **(B)** Dynamic plasma EBV DNA load during immunotherapy and PFS; **(C)** programmed cell death-ligand 1 (PD-L1) expression [higher vs. lower] and PFS; **(D)** PD-L1 expression [positive vs. negative] and PFS; **(E)** tumor mutation burden (TMB) and PFS.

9742), they observed that loss of HLA-A and HLA-B was associated with better survival than patients with HLA-A– and HLA-B–intact tumors (2). However, relevant studies were limited, and there was relatively inadequate power to conduct a meta-analysis. Substantial efforts are needed to elucidate the role of these biomarkers in predicting response and prognosis for NPC patients receiving ICIs.

Besides, the definition of biomarkers has been expanded greatly with the evolution of bioinformatics. A combination of ICI prediction methods with tumor prognostic markers at the molecular level has been well applied in multiple carcinomas (37–41). Chi and colleagues established a multi-biomarker prognostic model based on natural killer cell-associated genes in head and neck squamous cell carcinoma (HNSCC) (37). Chen et al. assessed tumor microenvironment (TME) through virtual microdissection of gene expression profiles, classifying the TME of NPC into three immune subtypes to predict immunotherapy responses and prognosis (42). Undoubtedly, these approaches provide new perspectives for evaluating the response and prognosis of immunotherapy.

10.3389/fimmu.2023.1146898

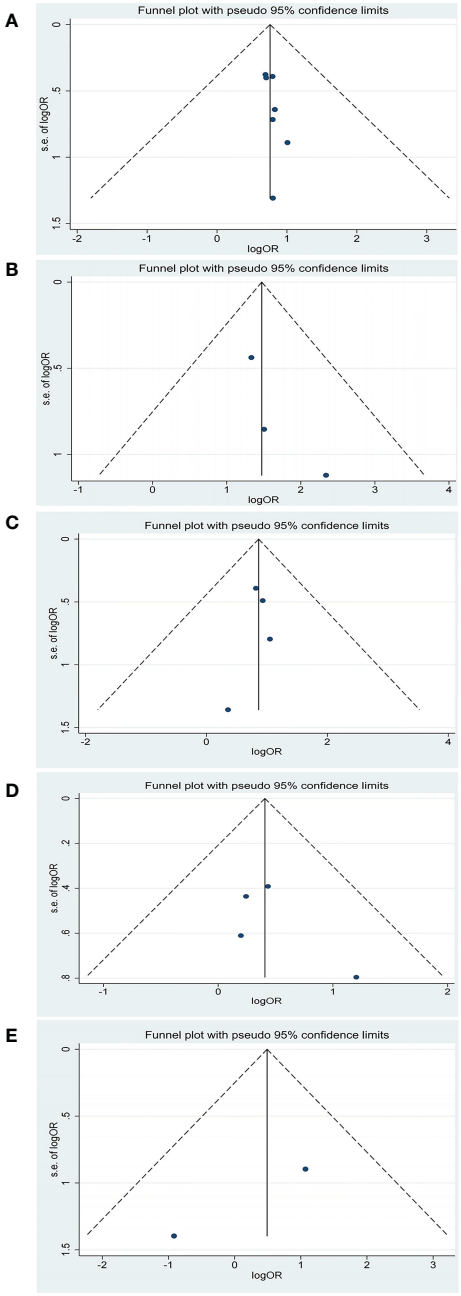

FIGURE 4
Funnel plot of objective response rate (ORR) for studies reporting biomarkers. **(A)** baseline plasma Epstein-Barr virus (EBV) DNA level; **(B)** dynamic plasma EBV DNA load during immunotherapy; **(C)** programmed cell death-ligand 1 (PD-L1) expression (higher vs. lower); **(D)** PD-L1 expression (positive vs. negative); **(E)** tumor mutation burden (TMB).

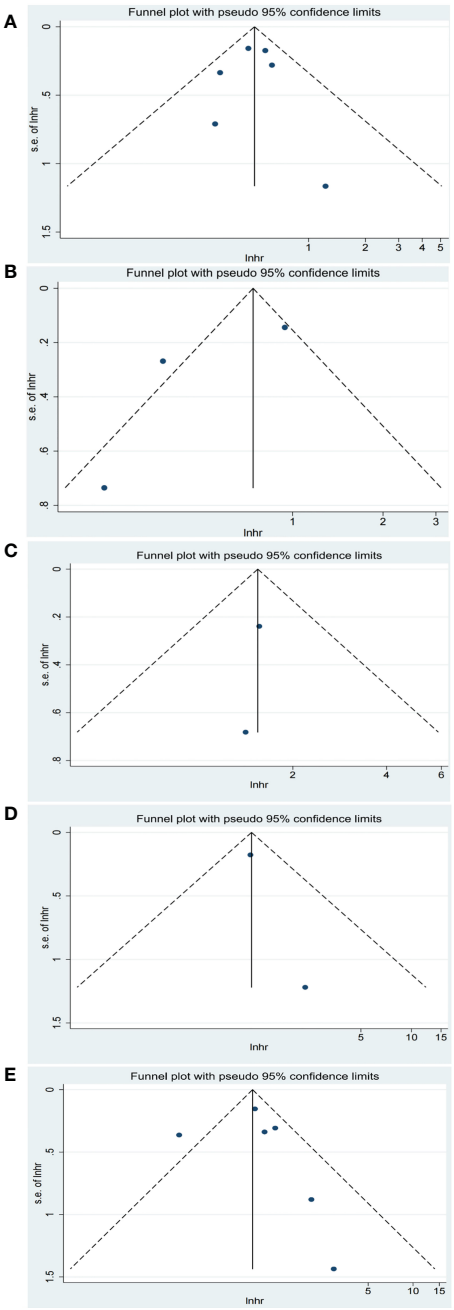

FIGURE 5
Funnel plot of progression-free survival (PFS) for studies reporting biomarkers. **(A)** baseline plasma EBV DNA level; **(B)** dynamic plasma EBV DNA load during immunotherapy; **(C)** programmed cell death-ligand 1 (PD-L1) expression (higher vs. lower); **(D)** PD-L1 expression (positive vs. negative); **(E)** tumor mutation burden (TMB).

Biomarkers of EBV DNA, PD-L1, and TMB in this study have their advantages. First, they are affordable in price. Secondly, the detection technology is mature and easy to be widely used in clinical. Third, the detection of plasma EBV DNA was non-invasive and can be monitored dynamically.

Several limitations should be considered in this meta-analysis. First of all, the number of studies included in each biomarker for each outcome was relatively small. Only two studies were included in the pooled analysis for PFS of PD-L1 expression and ORR of TMB, and the relatively limited number of included studies may limit the power of analysis. Secondly, the majority of the studies included were from China, which may lead to some inevitable sources of bias. However, this may be due to the fact that the endemic regions of NPC are extremely unbalanced, with 72.8% of new cases in Southeast Asia. The age-standardized rate was 3.0 per 100,000 in China, while 0.4 per 100,000 in white populations (5, 6). The essential reason for publication

bias may be the incentives that researchers are more likely to report statistically significant results to be accepted for publication and publishers are more likely to publish studies with statistically significant findings. Thirdly, though overall survival (OS) is also an important outcome to be investigated, the studies reporting the effect of biomarkers on OS were limited to conducte a pooled analysis.

5 Conclusion

In conclusion, lower baseline plasma EBV DNA level, decreased EBV DNA load during immunotherapy, and higher PD-L1 expression are reliable biomarkers predicting better response to ICIs treatment. Lower baseline plasma EBV DNA level was also associated with longer PFS. It is warranted to further explore and better illuminate the utility of these biomarkers in future clinical trials and real-world practice.

Data availability statement

The original contributions presented in the study are included in the article/Supplementary Material. Further inquiries can be directed to the corresponding author.

Author contributions

XQ, HC and YT designed the study, performed the systematic search and selected eligible studies. XQ and HC analyzed the data. XQ wrote the manuscript. HC and YT revised the manuscript. All authors contributed to the article and approved the submitted version.

Conflict of interest

The authors declare that the research was conducted in the absence of any commercial or financial relationships that could be construed as a potential conflict of interest.

Publisher's note

Supplementary material

The Supplementary Material for this article can be found online at: https://www.frontiersin.org/articles/10.3389/fimmu.2023.1146898/full#supplementary-material

References

1. Hsu C, Lee SH, Ejadi S, Even C, Cohen RB, Le Tourneau C, et al. Safety and antitumor activity of pembrolizumab in patients with programmed death-ligand 1-positive nasopharyngeal carcinoma: Results of the KEYNOTE-028 study. *J Clin Oncol* (2017) 35(36):4050–6. doi: 10.1200/JCO.2017.73.3675

2. Ma BBY, Lim WT, Goh BC, Hui EP, Lo KW, Pettinger A, et al. Antitumor activity of nivolumab in recurrent and metastatic nasopharyngeal carcinoma: An international, multicenter study of the Mayo clinic phase 2 consortium (NCI-9742). *J Clin Oncol* (2018) 36(14):1412–8. doi: 10.1200/JCO.2017.77.0388

3. Yang Y, Qu S, Li J, Hu C, Xu M, Li W, et al. Camrelizumab versus placebo in combination with gemcitabine and cisplatin as first-line treatment for recurrent or metastatic nasopharyngeal carcinoma (CAPTAIN-1st): A multicentre, randomised, double-blind, phase 3 trial. *Lancet Oncol* (2021) 22(8):1162–74. doi: 10.1016/S1470-2045(21)00302-8

4. Shi Y, Qin X, Peng X, Zeng A, Li J, Chen C, et al. Efficacy and safety of KL-A167 in previously treated recurrent or metastatic nasopharyngeal carcinoma: A multicenter, single-arm, phase 2 study. *Lancet Regional Health – Western Pac* (2023) 31:100617 doi: 10.1016/j.lanwpc.2022.100617

5. Sung H, Ferlay J, Siegel RL, Laversanne M, Soerjomataram I, Jemal A, et al. Global cancer statistics 2020: GLOBOCAN estimates of incidence and mortality worldwide for 36 cancers in 185 countries. *CA Cancer J Clin* (2021) 71(3):209–49. doi: 10.3322/caac.21660

6. Chen YP, Chan ATC, Le QT, Blanchard P, Sun Y, Ma J. Nasopharyngeal carcinoma. *Lancet* (2019) 394(10192):64–80. doi: 10.1016/S0140-6736(19)30956-0

7. Lee AWM, Lee VHF, Ng WT, Strojan P, Saba NF, Rinaldo A, et al. A systematic review and recommendations on the use of plasma EBV DNA for nasopharyngeal carcinoma. *Eur J Cancer* (2021) 153:109–22. doi: 10.1016/j.ejca.2021.05.022

8. You R, Liu YP, Lin M, Huang PY, Tang LQ, Zhang YN, et al. Relationship of circulating tumor cells and Epstein-Barr virus DNA to progression-free survival and overall survival in metastatic nasopharyngeal carcinoma patients. *Int J Cancer* (2019) 145(10):2873–83. doi: 10.1002/ijc.32380

9. Wang FH, Wei XL, Feng J, Li Q, Xu N, Hu XC, et al. Efficacy, safety, and correlative biomarkers of toripalimab in previously treated recurrent or metastatic nasopharyngeal carcinoma: A phase II clinical trial (POLARIS-02). *J Clin Oncol* (2021) 39(7):704–12. doi: 10.1200/JCO.20.02712

10. Yarchoan M, Albacker LA, Hopkins AC, Montesion M, Murugesan K, Vithayathil TT, et al. PD-L1 expression and tumor mutational burden are independent biomarkers in most cancers. *JCI Insight* (2019) 4(6): e126908. doi: 10.1172/jci.insight.126908

11. Samstein RM, Lee CH, Shoushtari AN, Hellmann MD, Shen R, Janjigian YY, et al. Tumor mutational load predicts survival after immunotherapy across multiple cancer types. *Nat Genet* (2019) 51(2):202–6. doi: 10.1038/s41588-018-0312-8

12. Park JC, Durbeck J, Boudadi K, Ho WJ, Kang H. The efficacy of anti-PD-1 immune checkpoint inhibitor in nasopharyngeal carcinoma. *Oral Oncol* (2020) 108:104935. doi: 10.1016/j.oraloncology.2020.104935

13. Moher D, Liberati A, Tetzlaff J, Altman DG, Group P. Preferred reporting items for systematic reviews and meta-analyses: the PRISMA statement. *BMJ* (2009) 339: b2535. doi: 10.1136/bmj.b2535

14. Yang Y, Zhou T, Chen X, Li J, Pan J, He X, et al. Efficacy, safety, and biomarker analysis of camrelizumab in previously treated recurrent or metastatic nasopharyngeal carcinoma (CAPTAIN study). *J Immunother Cancer* (2021) 9(12): e003790. doi: 10.1136/jitc-2021-003790

15. Stang A. Critical evaluation of the Newcastle-Ottawa scale for the assessment of the quality of nonrandomized studies in meta-analyses. *Eur J Epidemiol* (2010) 25 (9):603–5. doi: 10.1007/s10654-010-9491-z

16. Huedo-Medina TB, Sanchez-Meca J, Marin-Martinez F, Botella J. Assessing heterogeneity in meta-analysis: Q statistic or I2 index? *Psychol Methods* (2006) 11 (2):193–206. doi: 10.1037/1082-989X.11.2.193

17. Higgins JP, Thompson SG, Deeks JJ, Altman DG. Measuring inconsistency in meta-analyses. *BMJ* (2003) 327(7414):557–60. doi: 10.1136/bmj.327.7414.557

18. Begg CB, Mazumdar M. Operating characteristics of a rank correlation test for publication bias. *Biometrics* (1994) 50(4):1088–101. doi: 10.2307/2533446

19. Egger M, Davey Smith G, Schneider M, Minder C. Bias in meta-analysis detected by a simple, graphical test. *BMJ* (1997) 315(7109):629–34. doi: 10.1136/bmj.315.7109.629

20. Xu JY, Wei XL, Ren C, Zhang Y, Hu YF, Li JY, et al. Association of plasma Epstein-Barr virus DNA with outcomes for patients with recurrent or metastatic nasopharyngeal carcinoma receiving anti-programmed cell death 1 immunotherapy. *JAMA Netw Open* (2022) 5(3):e220587. doi: 10.1001/jamanetworkopen.2022.0587

21. Hua Y, You R, Wang Z, Huang P, Lin M, Ouyang Y, et al. Toripalimab plus intensity-modulated radiotherapy for recurrent nasopharyngeal carcinoma: An open-label single-arm, phase II trial. *J Immunother Cancer* (2021) 9(11):e003290. doi: 10.1136/jitc-2021-003290

22. Even C, Wang HM, Li SH, Ngan RK, Dechaphunkul A, Zhang L, et al. Phase II, randomized study of spartalizumab (PDR001), an anti-PD-1 antibody, versus chemotherapy in patients with Recurrent/Metastatic nasopharyngeal cancer. *Clin Cancer Res* (2021) 27(23):6413–23. doi: 10.1158/1078-0432.CCR-21-0822

23. Fang W, Yang Y, Ma Y, Hong S, Lin L, He X, et al. Camrelizumab (SHR-1210) alone or in combination with gemcitabine plus cisplatin for nasopharyngeal carcinoma: Results from two single-arm, phase 1 trials. *Lancet Oncol* (2018) 19(10):1338–50. doi: 10.1016/S1470-2045(18)30495-9

24. Mai HQ, Chen QY, Chen D, Hu C, Yang K, Wen J, et al. Toripalimab or placebo plus chemotherapy as first-line treatment in advanced nasopharyngeal carcinoma: A multicenter randomized phase 3 trial. *Nat Med* (2021) 27(9):1536–43. doi: 10.1038/s41591-021-01444-0

25. Ma Y, Chen X, Wang A, Zhao H, Lin Q, Bao H, et al. Copy number loss in granzyme genes confers resistance to immune checkpoint inhibitor in nasopharyngeal carcinoma. *J Immunother Cancer* (2021) 9(3):e002014. doi: 10.1136/jitc-2020-002014

26. Xu L, Ma Y, Fang C, Peng Z, Gao F, Moll JM, et al. Genomic and microbial factors affect the prognosis of anti-pd-1 immunotherapy in nasopharyngeal carcinoma. *Front Oncol* (2022) 12:953884 doi: 10.3389/fonc.2022.953884

27. Chen SY, Chen M, Rui Y, Hua Y, Zou X, Wang ZQ. Efficacy and safety of chemotherapy plus subsequent locoregional radiotherapy and toripalimab in de novo metastatic nasopharyngeal carcinoma. *J Clin Oncol* (2022) 40(16):6025. doi: 10.1200/JCO.2022.40.16_suppl.6025

28. Chiang CL, Lam TC, Li CBJ, Li WS, Chan SK, Lee YPY, et al. Antitumor activity of bintrafusp alfa in previously treated patients with recurrent or metastatic nasopharyngeal cancer (NPC): A single arm, prospective phase II trial. *J Clin Oncol* (2022) 40(16):e18029. doi: 10.1200/JCO.2022.40.16_suppl.e18029

29. Chan ATC, Hui EP, Ngan RKC, Tung SY, Cheng ACK, Ng WT, et al. Analysis of plasma Epstein-Barr virus DNA in nasopharyngeal cancer after chemoradiation to identify high-risk patients for adjuvant chemotherapy: A randomized controlled trial. *J Clin Oncol* (2018) 36(31):3091–100. doi: 10.1200/JCO.2018.77.7847

30. Trevisiol C, Gion M, Vaona A, Fabricio ASC, Roca E, Licitra L, et al. The appropriate use of circulating EBV-DNA in nasopharyngeal carcinoma: Comprehensive clinical practice guidelines evaluation. *Oral Oncol* (2021) 114:105128. doi: 10.1016/j.oraloncology.2020.105128

31. Wang M, Yu F, Wu W, Wang Y, Ding H, Qian L. Epstein-Barr Virus-encoded microRNAs as regulators in host immune responses. *Int J Biol Sci* (2018) 14(5):565–76. doi: 10.7150/ijbs.24562

32. Shah KM, Stewart SE, Wei W, Woodman CB, O'Neil JD, Dawson CW, et al. The EBV-encoded latent membrane proteins, LMP2A and LMP2B, limit the actions of interferon by targeting interferon receptors for degradation. *Oncogene* (2009) 28 (44):3903–14. doi: 10.1038/onc.2009.249

33. Dunn GP, Bruce AT, Ikeda H, Old LJ, Schreiber RD. Cancer immunoediting: from immunosurveillance to tumor escape. *Nat Immunol* (2002) 3(11):991–8. doi: 10.1038/ni1102-991

34. Brahmer J, Reckamp KL, Baas P, Crino L, Eberhardt WE, Poddubskaya E, et al. Nivolumab versus docetaxel in advanced squamous-cell non-Small-Cell lung cancer. *N Engl J Med* (2015) 373(2):123–35. doi: 10.1056/NEJMoa1504627

35. Kojima T, Shah MA, Muro K, Francois E, Adenis A, Hsu CH, et al. Randomized phase III KEYNOTE-181 study of pembrolizumab versus chemotherapy in advanced esophageal cancer. *J Clin Oncol* (2020) 38(35):4138–48. doi: 10.1200/JCO.20.01888

36. Verdegaal EM, de Miranda NF, Visser M, Harryvan T, van Buuren MM , Andersen RS, et al. Neoantigen landscape dynamics during human melanoma-T cell interactions. *Nature* (2016) 536(7614):91–5. doi: 10.1038/nature18945

37. Chi H, Xie X, Yan Y, Peng G, Strohmer DF, Lai G, et al. Natural killer cell-related prognosis signature characterizes immune landscape and predicts prognosis of HNSCC. *Front Immunol* (2022) 13:1018685. doi: 10.3389/fimmu.2022.1018685

38. Zhao S, Chi H, Ji W, He Q, Lai G, Peng G, et al. Bioinformatics-based analysis of an anoikis-related gene signature predicts the prognosis of patients with low-grade gliomas. *Brain Sci* (2022) 12(10):1349. doi: 10.3390/brainsci12101349

39. Chi H, Peng G, Yang J, Zhang J, Song G, Xie X, et al. Machine learning to construct sphingolipid metabolism genes signature to characterize the immune landscape and prognosis of patients with uveal melanoma. *Front Endocrinol (Lausanne)* (2022) 13:1056310. doi: 10.3389/fendo.2022.1056310

40. Zhao S, Ji W, Shen Y, Fan Y, Huang H, Huang J, et al. Expression of hub genes of endothelial cells in glioblastoma-a prognostic model for GBM patients integrating single-cell RNA sequencing and bulk RNA sequencing. *BMC Cancer* (2022) 22(1):1274. doi: 10.1186/s12885-022-10305-z

41. Lai G, Zhong X, Liu H, Deng J, Li K, Xie B. A novel m7G-related genes-based signature with prognostic value and predictive ability to select patients responsive to personalized treatment strategies in bladder cancer. *Cancers (Basel)* (2022) 14(21):6025. doi: 10.3390/cancers14215346

42. Chen YP, Lv JW, Mao YP, Li XM, Li JY, Wang YQ, et al. Unraveling tumour microenvironment heterogeneity in nasopharyngeal carcinoma identifies biologically distinct immune subtypes predicting prognosis and immunotherapy responses. *Mol Cancer* (2021) 20(1):14. doi: 10.1186/s12943-020-01292-5

frontiers | Frontiers in Immunology

TYPE Original Research
PUBLISHED 06 April 2023
DOI 10.3389/fimmu.2023.1165004

OPEN ACCESS

EDITED BY
Takaji Matsutani,
Repertoire Genesis, Inc., Japan

REVIEWED BY
Hester Doyle,
Yale University, United States
Erin E. Baschal,
University of Colorado Anschutz Medical Campus, United States

*CORRESPONDENCE
Hidefumi Inaba
inaba@wakayama-med.ac.jp

SPECIALTY SECTION
This article was submitted to Cancer Immunity and Immunotherapy, a section of the journal Frontiers in Immunology

RECEIVED 13 February 2023
ACCEPTED 24 March 2023
PUBLISHED 06 April 2023

CITATION
Inaba H, Morita S, Kosugi D, Asai Y, Kaido Y, Ito S, Hirobata T, Inoue G, Yamamoto Y, Jinnin M, Kimura H, Ota M, Okudaira Y, Nakatani H, Kobayashi T, Iwama S, Arima H and Matsuoka T (2023) Amino acid polymorphisms in human histocompatibility leukocyte antigen class II and proinsulin epitope have impacts on type 1 diabetes mellitus induced by immune-checkpoint inhibitors. *Front. Immunol.* 14:1165004. doi: 10.3389/fimmu.2023.1165004

Amino acid polymorphisms in human histocompatibility leukocyte antigen class II and proinsulin epitope have impacts on type 1 diabetes mellitus induced by immune-checkpoint inhibitors

Hidefumi Inaba[1,2]*, Shuhei Morita[2], Daisuke Kosugi[1], Yuki Asai[1], Yosuke Kaido[1], Saya Ito[1], Tomonao Hirobata[1], Gen Inoue[1], Yuki Yamamoto[3], Masatoshi Jinnin[3], Hiroaki Kimura[4], Masao Ota[5], Yuko Okudaira[6], Hiroyasu Nakatani[7], Tomoko Kobayashi[8], Shintaro Iwama[8], Hiroshi Arima[8] and Takaaki Matsuoka[2]

[1]Department of Diabetes and Endocrinology, Japanese Red Cross Wakayama Medical Center, Wakayama, Japan, [2]The First Department of Medicine, Wakayama Medical University, Wakayama, Japan, [3]Department of Dermatology, Wakayama Medical University, Wakayama, Japan, [4]Department of Pharmaceutical Health Sciences, Kyushu University of Health and Welfare, Nobeoka, Miyazaki, Japan, [5]Department of Medicine, Division of Gastroenterology and Hepatology, Shinshu University School of Medicine, Matsumoto, Japan, [6]HLA Typing Section, GenoDive Pharma Inc., Kanagawa, Japan, [7]Research Department, Biospecimen Laboratories, Inc. Tokyo, Japan, [8]Department of Endocrinology and Diabetes, Nagoya University Graduate School of Medicine, Nagoya, Aichi, Japan

Introduction: Immune-checkpoint inhibitors are effective in various advanced cancers. Type 1 diabetes mellitus induced by them (ICI-T1DM) is a serious complication requiring prompt insulin treatment, but the immunological mechanism behind it is unclear.

Methods: We examined amino acid polymorphisms in human histocompatibility leukocyte antigen (HLA) molecules and investigated proinsulin epitope binding affinities to HLA molecules.

Results and Discussion: Twelve patients with ICI-T1DM and 35 patients in a control group without ICI-T1DM were enrolled in the study. Allele and haplotype frequencies of HLA-*DRB1*04:05, DQB1*04:01*, and most importantly *DPB1*05:01* were significantly increased in patients with ICI-T1DM. In addition, novel amino acid polymorphisms in HLA-DR (4 polymorphisms), in DQ (12 polymorphisms), and in DP molecules (9 polymorphisms) were identified. These amino acid polymorphisms might be associated with the development

10.3389/fimmu.2023.1165004

of ICI-T1DM. Moreover, novel human proinsulin epitope clusters in insulin A and B chains were discovered *in silico* and *in vitro* peptide binding assays to HLA-DP5. In conclusion, significant amino acid polymorphisms in HLA-class II molecules, and conformational alterations in the peptide-binding groove of the HLA-DP molecules were considered likely to influence the immunogenicity of proinsulin epitopes in ICI-T1DM. These amino acid polymorphisms and HLA-DP5 may be predictive genetic factors for ICI-T1DM.

KEYWORDS

human histocompatibility leukocyte antigen, immune-checkpoint inhibitors, immune-related adverse events, type 1 diabetes mellitus, proinsulin

Introduction

Immune-checkpoint inhibitors (ICIs) are effective agents in various cancers; however, immune-related adverse events (irAEs) often occur during treatment with ICIs (1–5). Major endocrine irAEs include pituitary irAE (3), thyroid irAE (4), and ICI-induced type 1 diabetes mellitus (ICI-T1DM). ICI-T1DM is an especially critical irAE due to the possibility of acute damage to pancreatic β-cells (5). Qiu et al. reported that anti-insulin antibody was observed in 7 patients with ICI-T1DM (3 patients with fulminant type 1 diabetes, and 4 patients with acute type 1 diabetes) (6). One patient with ICI-T1DM exhibited anti-insulin antibody positivity in our study (5). Proinsulin is cleaved into insulin and C-peptide in pancreatic β-cells at secretion (7), we thus hypothesized that proinsulin could be a major autoantigen in ICI-T1DM.

We have previously identified thyrotropin receptor epitopes to HLA-DR molecules in Graves' disease *in silico*, *in vitro*, and human studies (8, 9). Further, we have also previously in part examined of histocompatibility leukocyte antigen (HLA) alleles and haplotypes in ICI-T1DM. However, immunological mechanisms in ICI-T1DM are largely unknown due to the rarity of the disease (0.8% prevalence among ICI-treated patients (5).

In the current study, novel amino acid polymorphisms in HLA class II molecules in patients with ICI-T1DM, and *in vitro* proinsulin epitope binding affinities to HLA-DP molecules were revealed. These genetic factors may be utilized for prediction of ICI-T1DM, and also contribute to elucidate the mechanism of cancer immunotherapy and ICI-T1DM. Therefore, current study offers novel management and monitoring options for cancer immunotherapy.

Patients and methods

Patients

Patients were recruited from the Japanese Red Cross Society Wakayama Medical Center (JRCW), Wakayama Medical University Hospital (WMU), and Nagoya University (NU). Patients with advanced malignant diseases who received ICI treatment were examined during 2016-2021. ICI treatments included anti-PD-1 antibody (nivolumab or pembrolizumab), anti-PD-L1 antibody (durvalumab or atezolizumab), or anti-CTLA-4 antibody (ipilimumab) following nivolumab (5, 10). The study protocol was approved by the JRCW, WMU, and NU Institutional Ethical Review Boards, and written informed consent was obtained from all participants.

Assessment of irAEs and ICI-T1DM

Assessment of irAEs was made based on the descriptions and grading scales of the *National Cancer Institute (NCI) Common Terminology Criteria for Adverse Events version 3.0*. Diagnostic criteria for T1DM were based on the hyperglycemic symptoms, and continuous requirement of insulin therapy irrespective of autoimmune diabetes-related autoantibodies (11). ICI-controls were defined as those who were treated with ICI but did not develop any irAEs including T1DM (5, 10). Healthy Japanese individuals were used as general controls (12–14), and participants had no clinical or demographic differences and they had the same ethnic background.

HLA-genotyping and amino acid sequences

DNA extracted from blood was genotyped in HLA-*A, B, C, DRB1, DQB1*, and *DPB1* alleles by the next-generation sequence method and a Luminex system with WAKFlow HLA typing kits (GenoDive Pharma, Kanagawa, Japan) as previously described (5, 12–14). Allele frequencies were determined by direct counting and three-locus (DRB1~DQB1~DPB1) haplotype frequencies were obtained by maximum likelihood methods as previously described (http://cmpg.unibe.ch/software/arlequin3/) (5, 12–14). Amino acid sequences were downloaded from (https://www.ebi.ac.uk/ipd/imgt/hla/).

Prediction of human proinsulin-peptides binding affinities to HLA-DP5 and HLA-DP15

In silico binding of human proinsulin (AA 1-110) (NP_000198.1) derived peptide to HLA-DP5 molecule (HLA-*DPA1*02:02*, HLA-*DPB1*05:01*) and a control allele, HLA-DP15 molecule (HLA-*DPA1*02:02*, HLA-*DPB1*15:01*: not previously reported as susceptible or protective allele) were predicted by NetMHCIIpan software version 4.0. The %RANK threshold for strong binders was set as <5%. The peptides with a 5-50%RANK threshold were set as intermediate binders.

In vitro human proinsulin peptides binding assay to HLA-DP5 and HLA-DP15

Fifteen-mer peptides derived from human proinsulin were synthesized based on the predicted affinities to HLA-DP5: 1) strong binders, 2) intermediate binders, and 3) others to cover the entire sequence (PEPscreen® peptide library, ProImmune, Oxford, UK). Peptides that were known to have high affinities with HLA-DP5 and HLA-DP15 were also synthesized. The synthesized peptides were subjected to an *in vitro* peptide binding assay (ProImmune REVEAL® MHC class II-peptide binding assay: (ProImmune, Oxford, UK) using recombinant HLA-DP5 and HLA-DP15 proteins.Detection of binding peptides is based on the presence or absence of the native conformation of the MHC-peptide complex in an immunoassay. Each test peptide was given a 'REVEAL SCORE' relative to positive control peptides, which were known to bind HLA-DP5 or HLA-DP15 with high affinity (signal of known positive control peptide which was known to bind each HLA-DP with high affinity, divided by each test peptide x 100%). The high-throughput assay quantifies the ability of the test peptides to bind to HLA-DP5 and HLA-DP15. The results of the three separate assays were in close agreement and are presented as an average of the results.

Three-dimensional modeling of the HLA-class II molecules

Three-dimensional modeling of HLA-class II molecules (HLA-DR, HLA-DQ, and HLA-DP) was downloaded from the Protein Data Bank database (15), and visualized with PyMOL (16).

Statistical analysis

Differences between the two groups were analyzed by a Mann-Whitney U test. The association of allele frequencies was analyzed using Fisher's exact test. Frequencies of HLA alleles and amino acid polymorphisms were analyzed by univariate and multivariate logistic regression analysis with stepwise selection of covariates. Bonferroni test was applied if the variables were significant. Statistical analyses were performed using JMP, version 15 (SAS Institute Inc., Cary, N.C., USA). P values < 0.05 were considered to be statistically significant.

Results

Clinical characteristics of patients with ICI-T1DM

A total of twelve patients with ICI-T1DM (six patients from JRC, two patients from WMU, and four patients from NU) were identified and enrolled in the study (Tables 1A, 1B; Supplementary Table 1). Clinical profiles of seven patients with ICI-T1DM were partly described previously (5). Thirty-five independent ICI-controls (13 from WMU and 22 from NU) were prospectively identified as subjects without irAE and were analyzed. Anti-GAD65 antibody was negative for patients measured. Patient #6 only developed insulin autoantibodies (IAA).

HLA alleles and haplotypes analysis

The plasma glucose levels of patients with ICI-T1DM and HLA typing results are summarized in Table 1B. We have used HLA-class I and II four-digit allelic typing results in the allele or haplotype analysis (Tables 2A–E; Supplementary Table 2A–C). Allele frequencies of HLA-*DRB1*04:05* (Table 2A) and HLA-*DQB1*04:01* (Table 2B), both alleles in complete linkage disequilibrium, were significantly higher in patients with ICI-T1DM than in general controls and also in ICI-controls. HLA-*DPB1*05:01* allele frequency was more significantly associated with an increased risk of ICI-T1DM when compared with general controls and also in ICI-controls (P=0.005 and 0.004, respectively) (Table 2C).

In haplotype analysis, HLA-*DRB1*04:05-DQB1*04:01* haplotype frequency was significantly higher in patients with ICI-T1DM than those of general controls and also in ICI-controls (P=0.026 and 0.003, respectively) (Table 2D). HLA-*DRB1*04:05-DQB1*04:01-DPB1*05:01* haplotype frequency was significantly higher in patients with ICI-T1DM than those of general controls and also in ICI-controls (P=0.006 and 0.002, respectively) (Table 2E).

Of all significant HLA alleles and haplotypes, notably, only HLA-*DQB1*04:01* and HLA-*DPB1*05:01* allele frequencies were significantly increased in patients with ICI-T1DM compared with ICI-controls after Bonferroni correction (Pc=0.033 and Pc=0.04, respectively) (Tables 2B, 2C). Then the allele frequencies of HLA-*DQB1*04:01* and HLA-*DPB1*05:01* were compared in conditional multiple logistic regression analysis (Table 2F).

Both allele frequencies were found to be significantly increased in ICI-T1DM, P=0.023 for HLA-*DQB1*04:01* and P=0.016 for HLA-*DPB1*05:01* (Table 2F). Note that the result also indicates the equivocal importance of following 3 factors: HLA-*DQB1*04:01*, HLA-*DRB1*04:05*, and HLA-*DRB1*04:05-DQB1*04:01* haplotype, due to the complete linkage disequilibrium between HLA-

TABLE 1A Clinical characteristics of the patients with ICI-T1DM.

Patient	Age (year)	Gender	Cancer	ICI	Number of ICI treatment cycle	Time of onset of ICI-T1DM (weeks)	HbA1c at onset (%)	Casual PG at onset (mg/dl)	PH of diabetes	Other irAEs	Comorbidities	Anti-GAD65 Ab/ Insulin Ab	Tumor response	Continuation of ICI
1	70	M	NSCLC	P	3	9	6	**564**	No	Eczema	Dyslipidemia	Ne/Ne	PR	Continued
2	80	M	NSCLC	P	11	37	**7.3**	**420**	No	IP, Grade1	Hypertension	Ne/Ne	PR	Continued
3	79	M	NSCLC	P	4	12	5.3	**404**	No	None	Hashimoto's thyroiditis	Ne/ND	PR	Discontinued
4	71	M	NSCLC	P	9	31	**8.7**	**491**	T2DM	None	Hypertension	Ne/Ne	PR	Continued
5	72	M	SCLC	D	2	6	**6.5**	**502**	No	None	None	Ne/Ne	PR	Continued
6	80	F	MM	N/ Ipi	N, 20 cycles, then Ipi once	N 60w, Ipi 3w, total 63	**7.7**	**639**	No	None	Hypertension	Ne/Po	CR	Continued
7	78	M	MM	N	14	29	**8.5**	**940**	No	None	Hypertension	Ne/Ne	CR	Continued
8	70	F	RCC	P	4	40	**10.6**	**616**	T2DM	THY	Hypertension	Ne/ND	PR	Discontinued
9	75	M	NSCLC	P	7	29	7.6	**684**	T2DM	None	Atrial fibrillation	Ne/Ne	PD	Discontinued
10	71	F	MM	N	9	21	6.3	**489**	No	None	Hypertension	Ne/Ne	PD	Continued
11	66	M	NSCLC	N/ A	N, 18 cycles, then A once	N 75w, A 2w, total 77w	6.9	**1041**	No	None	Hyperuricemia	Ne/Ne	PD	Continued
12	55	M	NSCLC	N	51	121	9.4	**278**	T2DM	None	None	Ne/Ne	PD	Discontinued

M, male; F, female; Cancer, underlying cancer; ICI, type of ICI; P, pembrolizumab; N, nivolumab; Ipi, ipilimumab; D, durvalumab; A, atezolizumab; N/Ipi, N then ipi; N/A, N then A.
PH, past history; PG, plasma glucose; T2DM, type 2 diabetes mellitus.
MM, malignant melanoma; NSCLC, Non-small cell lung cancer; SCLC, small cell lung cancer; RCC, renal cell carcinoma; IP, interstitial pneumonitis; THY, thyroiditis.
ND, not determined; Ab, autoantibody; Ne, Negative; Po, Positive; CR, complete response; PR, partial response; PD, progressive disease.
Abnormal values are shown in bold. Partial data of patients 1-7 was previously reported in ref (5).

10.3389/fimmu.2023.1165004

10.3389/fimmu.2023.1165004

TABLE 1B The plasma glucose levels of ICI-T1DM patients and their summarized HLA typing results.

Patient	Casual PG at onset (mg/dl)	HLA-DRB1		HLA-DQB1		HLA-DPB1		HLA-DR-DQ haplotype 1		HLA-DR-DQ haplotype 2		HLA-DR-DQ-DP haplotype 1			HLA-DR-DQ-DP haplotype 2		
1	**564**	***04:05**	*09:01	*03:03	***04:01**	***05:01**	***05:01**	**DRB1*04:05**	**DQB1*04:01**	DRB1*09:01	DQB1*03:03	**DRB1*04:05**	**DQB1*04:01**	**DPB1*05:01**	DRB1*09:01	DQB1*03:03	**DPB1*05:01**
2	**420**	***04:05**	*04:06	*03:02	***04:01**	*02:01	***05:01**	**DRB1*04:05**	**DQB1*04:01**	DRB1*04:06	DQB1*03:02	**DRB1*04:05**	**DQB1*04:01**	**DPB1*05:01**	DRB1*04:06	DQB1*03:02	DPB1*02:01
3	**404**	*09:01	*14:54	*03:03	*05:03	*04:02	***05:01**	DRB1*09:01	DQB1*03:03	DRB1*14:54	DQB1*05:03	DRB1*09:01	DQB1*03:03	DPB1*04:02	DRB1*14:54	DQB1*05:03	**DPB1*05:01**
4	**491**	***04:05**	*08:02	*03:02	***04:01**	***05:01**	*19:01	**DRB1*04:05**	**DQB1*04:01**	DRB1*08:02	DQB1*03:02	**DRB1*04:05**	**DQB1*04:01**	DPB1*19:01	DRB1*08:02	DQB1*03:02	**DPB1*05:01**
5	**502**	***04:05**	*08:03	***04:01**	*06:01	***05:01**	***05:01**	**DRB1*04:05**	**DQB1*04:01**	DRB1*08:03	DQB1*06:01	**DRB1*04:05**	**DQB1*04:01**	**DPB1*05:01**	DRB1*08:03	DQB1*06:01	**DPB1*05:01**
6	**639**	***04:05**	*12:01	*03:01	***04:01**	***05:01**	***05:01**	**DRB1*04:05**	**DQB1*04:01**	DRB1*12:01	DQB1*03:01	**DRB1*04:05**	**DQB1*04:01**	**DPB1*05:01**	DRB1*12:01	DQB1*03:01	**DPB1*05:01**
7	**940**	*08:03	*08:03	*06:01	*06:01	***05:01**	***05:01**	DRB1*08:03	DQB1*06:01	DRB1*08:03	DQB1*06:01	DRB1*08:03	DQB1*06:01	**DPB1*05:01**	DRB1*08:03	DQB1*06:01	**DPB1*05:01**
8	**616**	***04:05**	*11:01	*03:01	***04:01**	*02:01	***05:01**	**DRB1*04:05**	**DQB1*04:01**	DRB1*11:01	DQB1*03:01	**DRB1*04:05**	**DQB1*04:01**	**DPB1*05:01**	DRB1*11:01	DQB1*03:01	DPB1*02:01
9	**684**	*09:01	*14:03	*03:01	*03:03	***05:01**	***05:01**	DRB1*09:01	DQB1*03:03	DRB1*14:03	DQB1*03:01	DRB1*09:01	DQB1*03:03	**DPB1*05:01**	DRB1*14:03	DQB1*03:01	**DPB1*05:01**
10	**489**	*09:01	*15:02	*03:03	*06:01	*02:01	*09:01	DRB1*09:01	DQB1*03:03	DRB1*15:02	DQB1*06:01	DRB1*09:01	DQB1*03:03	DPB1*02:01	DRB1*15:02	DQB1*06:01	DPB1*09:01
11	**1041**	***04:05**	*13:02	***04:01**	*06:04	***05:01**	***05:01**	**DRB1*04:05**	**DQB1*04:01**	DRB1*13:02	DQB1*06:04	**DRB1*04:05**	**DQB1*04:01**	**DPB1*05:01**	DRB1*13:02	DQB1*06:04	**DPB1*05:01**
12	**278**	***04:05**	*11:01	*03:01	***04:01**	***05:01**	*14:01	**DRB1*04:05**	**DQB1*04:01**	DRB1*11:01	DQB1*03:01	**DRB1*04:05**	**DQB1*04:01**	**DPB1*05:01**	DRB1*11:01	DQB1*03:01	DPB1*14:01

PG, plasma glucose; Abnormal values and HLA-DRB1*04:05, DQB1*04:01, and DPB1*05:01 are shown in bold.

*DRB1*04:05* and HLA-*DQB1*04:01* in the current study population (Table 2F).

Amino acid polymorphisms in each HLA-class II molecules

Further, univariate logistic regression analysis was thoroughly performed to examine relationships between ICI-T1DM and amino acid polymorphisms at HLA-DRβ1 (237 amino acid positions) (Supplementary Table 3A), DQβ1 (237 amino acid positions) (Supplementary Table 3B, and DPβ1 (229 amino acid positions) (Supplementary Table 3C). The amino acid polymorphisms with significance are indicated as yellow in the tables and they underwent further evaluation. Of those, amino acid carriages at amino acid positions 9, 57, 86, and 96 of HLA-DRβ1 were significantly different between the patients with ICI-T1DM and ICI-controls (Supplementary Table 4A, B). Glu (E) was significantly more frequently observed than Trp (W) (represented as E>W, the same applies hereafter) at position 9 (Figure 1A), Ser (S) > Asp (D) at position 57 (Figure 1B), Gly (G) > Val (V) at position 86 (Figure 1C), and Tyr (Y) > Gln (Q) at position 96 of HLA-DRβ1 in ICI-T1DM (Figure 1D).

Regarding HLA-DQβ1, amino acids carriages at amino acid positions 56, 70, 203, and 53-84-85-89-140-181-182-220-221 (each amino acid in complete linkage disequilibrium) of HLA-DQβ1 were significantly different between the patients with ICI-T1DM and ICI-controls (Supplementary Tables 5A, B). Leu (L) > Pro (P) at position 56 (Figure 2A), E > G at position 70 (Figure 2B), Ile (I) > V at position 203 (Figure 2C), and Leu-Gln-Leu-Thr-Thr-Gln-Asn-His-His (L-Q-L-T-T-Q-N-H-H) > Gln-Glu-Val-Gly-Ala-Gln-Ser-Arg-Gln (Q-E-V-G-A-Q-S-R-Q) at positions 53-84-85-89-140-181-182-220-221 of HLA-DQβ1 in ICI-T1DM (Figure 2D).

Moreover, amino acids carriages at amino acid positions 35, 55, 205, and 84-85-86-87-96-170 (each amino acid in complete linkage disequilibrium) of HLA-DPβ1 were significantly different between the patients with ICI-T1DM and ICI-controls (Supplementary Tables 6A, B). L > Phe (F) at position 35 (Figure 3A), E > D at position 55 (Figure 3B), Met (M) > V at position 205 (Figure 3C), and Asp-Glu-Ala-Val-Lys-Ile (D-E-A-V-K-I) > Gly-Gly-Pro-Met-Arg-Thr (G-G-P-M-R-T) at positions 84-85-86-87-96-170 of HLA-DPβ1 in ICI-T1DM (Figure 3D).

After Bonferroni correction for all significant amino acid polymorphisms, β57 at HLA-DRβ1 (Pc=0.046 by Bonferroni correction, shown with #) (Figure 1B), and β205 at HLA-DPβ1 were significantly increased in patients with ICI-T1DM compared with ICI-controls (Pc=0.011 by Bonferroni correction, shown with #) (Figure 3C).

To investigate the importance of amino acid polymorphisms mentioned above in detail (Figures 1–3), a stepwise selection of covariate amino acid residues was applied in multivariate logistic analysis across the HLA-DR, DQ, and DP (Table 3). Subsequently, β205 at HLA-DPβ1 was found to be most significant among them.

Differences in amino acids at HLA-*DPB1*05:01* and *DPB1*15:01* were shown in Supplementary Table 3C and

10.3389/fimmu.2023.1165004

TABLE 2A Allele frequencies of HLA-DR in patients with ICI-T1DM and controls.

	ICI-T1DM (*N*=24)		ICI-Controls (*N*=70)		*1Controls (*N*=618644)	ICI-T1DM vs general controls				ICI-T1DM vs ICI-controls				ICI-controls vs general controls		
allele	*n*	F (%)	*n*	F (%)	F (%)	*2 *P*	*3 *Pc*	OR	95% CI	*2 *P*	*3 *Pc*	OR	95% CI	*2 *P*	OR	95% CI
DRB1*01:01	0	0.0	5	7.1	5.65	NS				NS				NS		
DRB1*04:01	0	0.0	0	0.0	1.03	NS				NS				NS		
DRB1*04:03	0	0.0	5	7.1	3.13	NS				NS				NS		
DRB1*04:05	8	33.3	5	7.1	13.41	**0.03**	NS	3.34	1.26–9.20	**0.003**	NS	6.50	1.95–21.60	NS		
DRB1*04:06	1	4.2	3	4.3	3.28	NS				NS				NS		
DRB1*04:10	0	0.0	2	2.9	2.12	NS				NS				NS		
DRB1*08:02	1	4.2	4	5.7	4.29	NS				NS				NS		
DRB1*08:03	3	12.5	5	7.1	7.93	NS				NS				NS		
DRB1*09:01	4	16.7	8	11.4	14.6	NS				NS				NS		
DRB1*10:01	0	0.0	1	1.4	0.48	NS				NS				NS		
DRB1*11:01	2	8.3	2	2.9	2.49	NS				NS				NS		
DRB1*11:06	0	0.0	1	1.4	0.002	NS				NS				NS		
DRB1*12:01	1	4.2	3	4.3	3.68	NS				NS				NS		
DRB1*12:02	0	0.0	2	2.9	1.69	NS				NS				NS		
DRB1*13:02	1	4.2	6	8.6	6.34	NS				NS				NS		
DRB1*14:03	1	4.2	1	1.4	1.63	NS				NS				NS		
DRB1*14:05	0	0.0	2	2.9	2.14	NS				NS				NS		
DRB1*14:06	0	0.0	0	0.0	1.54	NS				NS				NS		
DRB1*14:54	1	4.2	0	0.0	3.49	NS				NS				NS		
DRB1*15:01	0	0.0	8	11.4	7.88	NS				NS				NS		
DRB1*15:02	1	4.2	6	8.6	10.27	NS				NS				NS		
DRB1*16:02	0	0.0	1	1.4	0.82	NS				NS				NS		
Others	0	0.0	0	0.0	2.11	NS				NS				NS		
total	24	100.00	70	100.00	100.00											

Alleles with frequencies more than 1.0% in controls were included to the analysis (22 alleles). N, n, number of the alleles.
F, frequency of the allele; OR, odds ratio; CI, confidence interval; NS, not significant.
P values less than 0.05 are shown in bold.
*1 General control subjects: Japanese Society for Histocompatibility and Immunogenetics: http://jshi.umin.ac.jp/standarization/file/JSHI-hyokiallele-2022list.pdf :JSHI2022 ref (12).
http://jshi.umin.ac.jp/standarization/file/JSHI-hyokiallele-2022list.pdf
*2 Each allele frequency was analyzed using Fisher's exact test with 2 x2 contingency tables.
*3 Pc: Bonferroni correction.
95%CI: 95% confidence intervals.

Supplementary Table 6C). Of those, amino acid at positions 85 and 86 compose pocket 1 (P1) of peptide-binding groove on the HLA molecule, and amino acid at position 9 composes P9 (Figure 4).

Amino acid residues located in the nine peptide-binding grooves (referred to as pockets) were previously described (17, 18). Amino acids at positions 9 and 57 of HLA-DRβ1 compose P9, and the amino acid at position 86 composes P1 as well (Figures 1A, B, C, 4, 5A). The amino acid at position 70 of HLA-DQβ1 is associated with P4, and amino acids at positions 85 and 89 of HLA-DQβ1 compose P1 as well (Figures 2B, D, 4, 5B). Amino acids at positions 85 and 86 of HLA-DPβ1 compose P1 (Figure 3D, 4, 5C).

Epitope predictions and *in vitro* binding of human proinsulin peptides to HLA-DP5 and HLA-DP15

Regarding binding of HLA-DP5 and human proinsulin, binding affinity of the signal peptide (AA 1-24) was predicted to be low

10.3389/fimmu.2023.1165004

TABLE 2B Allele frequencies of HLA-DQB1 in patients with ICI-T1DM and controls.

	ICI-T1DM (*N*=24)		ICI-Controls (*N*=70)		*1Controls (*N*=1483)	ICI-T1DM vs general controls				ICI-T1DM vs ICI-controls				ICI-controls vs general controls		
allele	*n*	F (%)	*n*	F (%)	F (%)	*2 *P*	*3 *Pc*	OR	95% CI	*2 *P*	*3 *Pc*	OR	95% CI	*2 *P*	OR	95% CI
DQB1*03:01	4	16.7	6	8.6	11.43	NS				NS				NS		
DQB1*03:02	2	8.3	10	14.3	9.59	NS				NS				NS		
DQB1*03:03	4	16.7	11	15.7	15.54	NS				NS				NS		
DQB1*04:01	8	33.3	5	7.1	12.9	**0.03**	NS	3.34	1.26–9.20	**0.003**	**0.033**	6.50	1.95–21.60	NS		
DQB1*04:02	0	0.0	4	5.7	4.21	NS				NS				NS		
DQB1*05:01	0	0.0	5	7.1	6.58	NS				NS				NS		
DQB1*05:02	0	0.0	1	1.4	2.64	NS				NS				NS		
DQB1*05:03	1	4.2	3	4.3	3.94	NS				NS				NS		
DQB1*06:01	4	16.7	11	15.7	19.08	NS				NS				NS		
DQB1*06:02	0	0.0	8	11.4	7.15	NS				NS				NS		
DQB1*06:04	1	4.2	6	8.6	5.18	NS				NS				NS		
Others	0	0	0	0.0	1.76	NS				NS				NS		
total	24	100.00	70	100.00	100.00											

Alleles with frequencies more than 1.0% in controls were included to the analysis (11 alleles). N, n, number of the alleles.
F, frequency of the allele; OR, odds ratio; CI, confidence interval; NS, not significant.
P values less than 0.05 are shown in bold.
*1 General control subjects: Japanese Society for Histocompatibility and Immunogenetics: http://jshi.umin.ac.jp/standarization/file/JSHI-hyokiallele-2022list.pdf :JSHI2022 ref (12).
http://jshi.umin.ac.jp/standarization/file/JSHI-hyokiallele-2022list.pdf
*2 Each allele frequency was analyzed using Fisher's exact test with 2 x2 contingency tables.
*3 Pc: Bonferroni correction.
95%CI: 95% confidence intervals.

TABLE 2C Allele frequencies of HLA-DPB1 in patients with ICI-T1DM and controls.

	ICI-T1DM (*N*=24)		ICI-Controls (*N*=70)		*1Controls (*N*=1483)	ICI-T1DM vs general controls				ICI-T1DM vs ICI-controls				ICI-controls vs general controls		
allele	*n*	F (%)	*n*	F (%)	F (%)	*2 *p*	*3 *Pc*	OR	95% CI	*2 *p*	*3 *Pc*	OR	95% CI	*2 *p*	OR	95% CI
DPB1*02:01	3	12.5	17	24.3	24.11	NS				NS				NS		
DPB1*02:02	0	0.0	6	8.6	3.41	NS				NS				NS		
DPB1*03:01	0	0.0	6	8.6	3.98	NS				NS				NS		
DPB1*04:01	0	0.0	6	8.6	5.06	NS				NS				NS		
DPB1*04:02	1	4.2	7	10.0	9.78	NS				NS				NS		
DPB1*05:01	17	70.8	24	34.3	38.4	**0.005**	NS	3.96	1.54–10.18	**0.004**	**0.04**	4.66	1.73–12.48	NS		
DPB1*09:01	1	4.2	2	2.9	9.95	NS				NS				NS		
DPB1*13:01	0	0.0	1	1.4	1.96	NS				NS				NS		
DPB1*14:01	1	4.2	1	1.4	1.48	NS				NS				NS		
DPB1*19:01	1	4.2	0	0.0	0.74	NS				NS				NS		
Others	0	0.0	0	0.0	1.13	NS				NS				NS		
total	24	100.00	70	100.00	100.00											

Alleles with frequencies more than 1.0% in controls were included to the analysis (10 alleles). N, n, number of the alleles.
F, frequency of the allele; OR, odds ratio; CI, confidence interval; NS, not significant.
P values less than 0.05 are shown in bold.
*1 General control subjects: Japanese Society for Histocompatibility and Immunogenetics: http://jshi.umin.ac.jp/standarization/file/JSHI-hyokiallele-2022list.pdf :JSHI2022 ref (12).
http://jshi.umin.ac.jp/standarization/file/JSHI-hyokiallele-2022list.pdf
*2 Each allele frequency was analyzed using Fisher's exact test with 2 x2 contingency tables.
*3 Pc: Bonferroni correction.
95%CI: 95% confidence intervals.

10.3389/fimmu.2023.1165004

TABLE 2D Haplotype frequencies of HLA-DRB1-DQB1 in patients with ICI-T1DM.

Haplotype	ICI-T1DM (*N*=24)		ICI-Controls (*N*=70)		*1Controls (*N*=2992)	ICI-T1DM vs general controls				ICI-T1DM vs ICI-controls				ICI-controls vs general controls		
DRB1-DQB1	*n*	F (%)	*n*	F (%)	F (%)	*2 *P*	*3 *Pc*	OR	95% CI	*2 *P*	*3 *Pc*	OR	95% CI	*2 *P*	OR	95% CI
*01:01*05:01	0	0.0	4	5.7	6.05	NS				NS				NS		
*01:01*05:03	0	0.0	1	1.4	0.00	NS				NS				NS		
*04:01-*03:01	0	0.0	0	0.0	1.00	NS				NS				NS		
*04:03-*03:02	0	0.0	5	7.1	2.67	NS				NS				NS		
*04:05-*04:01	8	33.3	5	7.1	12.83	**0.026**	NS	3.67	1.33–10.19	**0.003**	NS	6.20	1.95–21.60	NS		
*04:06-*03:02	1	4.2	3	4.3	3.14	NS				NS				NS		
*04:10-*04:02	0	0.0	2	2.9	1.84	NS				NS				NS		
*08:02-*03:02	1	4.2	2	2.9	2.51	NS				NS				NS		
*08:02-*04:02	0	0.0	2	2.9	2.34	NS				NS				NS		
*08:03-*06:01	3	12.5	5	7.1	8.16	NS				NS				NS		
*09:01-*03:03	4	16.7	8	11.4	14.47	NS				NS				NS		
*10:01-*05:01	0	0.0	1	1.4	0.50	NS				NS				NS		
*11:01-*03:01	2	8.3	1	1.4	2.74	NS				NS				NS		
*11:01-*03:03	0	0.0	1	1.4	0.07	NS				NS				NS		
*11:06-*03:01	0	0.0	1	1.4	0.00	NS				NS				NS		
*12:01-*03:01	1	4.2	4	5.7	2.61	NS				NS				NS		
*12:01-*03:03	0	0.0	1	1.4	0.84	NS				NS				NS		
*12:02-*03:01	0	0.0	0	0.0	1.87	NS				NS				NS		
*13:02-*06:04	1	4.2	6	8.6	5.18	NS				NS				NS		
*14:03-*03:01	1	4.2	1	1.4	1.20	NS				NS				NS		
*14:05-*05:03	0	0.0	2	2.9	1.97	NS				NS				NS		
*14:06-*03:01	0	0.0	0	0.0	1.24	NS				NS				NS		
*14:54-*05:02	0	0.0	0	0.0	1.64	NS				NS				NS		
*14:54-*05:03	1	4.2	0	0.0	1.94	NS				NS				NS		
*15:01-*06:02	0	0.0	9	12.9	7.15	NS				NS				NS		
*15:02-*06:01	1	4.2	5	7.1	10.86	NS				NS				NS		
*16:02-*05:02	0	0.0	1	1.4	0.77	NS				NS				NS		
Others	0	0.0	0	0.0	4.41	NS				NS				NS		
total	24	100.00	70	100.00	100.00											

Haplotypes with frequencies more than 1.0% in controls were included to the analysis (27 haplotypes). N, n, number of the haplotypes.
*1 Control subjets: HLA LABORATORY, Japan INC: http://hla.or.jp/med/frequency_search/ja/haplo/ ref (11).
*2 Each haplotype frequency was analyzed using Fisher's exact test with 2 x2 contingency tables.
*3 Pc: Bonferroni correction.
F, frequency of the haplotype; NS, not significant.
P values less than 0.05 are shown in bold.
95%CI: 95% confidence intervals.

(possessing high %RANK) (Table 4) (Figure 6A). In the remaining region (AA 25-110), two epitope candidate regions (AA 43-60 and AA 53-67) were predicted. Five peptides in the regions were strong binders. Other 13 peptides were predicted as intermediate binders. In addition to the 18 peptides, 16 overlapping peptides were synthesized to cover the whole portion. Subsequently, a total of 34 overlapping 15-mer human proinsulin-derived peptides were synthesized and subjected to *in vitro* peptide binding assay

10.3389/fimmu.2023.1165004

TABLE 2E Haplotype frequencies of HLA-DRB1-DQB1-DPB1 in patients with ICI-T1DM.

Haplotype	ICI-T1DM (*N*=24)		ICI-Controls (*N*=70)		*1Controls (*N*=2938)	ICI-T1DM vs general controls				ICI-T1DM vs ICI-controls				ICI-controls vs general controls		
DRB1-DQB1-DPB1	*n*	F (%)	*n*	F (%)	F (%)	*2 *P*	*3 *Pc*	OR	95% CI	*2 *P*	*3 *Pc*	OR	95% CI	*2 *P*	OR	95% CI
*15:02-*06:01-*09:01	1	4.2	2	2.86	8.88	NS				NS				NS		
*04:05-*04:01-*05:01	7	29.2	3	4.29	7.32	**0.006**	NS	5.47	1.77–17.04	**0.002**	NS	9.20	2.31–36.13	NS		
*09:01-*03:03-*05:01	2	8.3	4	5.71	6.77	NS				NS				NS		
*09:01-*03:03-*02:01	1	4.2	1	1.43	5.28	NS				NS				NS		
*01:01-*05:01-*04:02	0	0.0	4	5.71	4.08	NS				NS				NS		
*13:02-*06:04-*04:01	0	0.0	5	7.14	3.68	NS				NS				NS		
*08:03-*06:01-*05:01	3	12.5	3	4.29	3.54	NS				NS				NS		
*15:01-*06:02-*02:01	0	0.0	2	2.86	3.06	NS				NS				NS		
*15:01-*06:02-*05:01	0	0.0	3	4.29	3.03	NS				NS				NS		
*04:05-*04:01-*02:01	0	0.0	0	0.00	2.28	NS				NS				NS		
*08:03-*06:01-*02:01	0	0.0	0	0.00	1.91	NS				NS				NS		
*08:02-*03:02-*05:01	1	4.2	2	2.86	1.84	NS				NS				NS		
*08:03-*06:01-*02:02	0	0.0	2	2.86	1.60	NS				NS				NS		
*04:05-*04:01-*04:02	0	0.0	0	0.00	1.53	NS				NS				NS		
*12:01-*03:01-*05:01	1	4.2	0	0.00	1.43	NS				NS				NS		
*04:06-*03:02-*02:01	1	4.2	2	2.86	1.33	NS				NS				NS		
*04:06-*03:02-*05:01	0	0.0	1	1.43	1.12	NS				NS				NS		
*12:02-*03:01-*05:01	0	0.0	1	1.43	1.09	NS				NS				NS		
*11:01-*03:01-*05:01	0	0.0	1	1.43	1.06	NS				NS				NS		
*01:01-*05:01-*05:01	0	0.0	1	1.43	1.02	NS				NS				NS		
*04:03-*03:02-*02:01	0	0.0	1	1.43	1.02	NS				NS				NS		
*11:01-*03:01-*02:01	1	4.2	0	0.00	0.99	NS				NS				NS		
*14:03-*03:01-*05:01	1	4.2	1	1.43	0.95	NS				NS				NS		

(Continued)

10.3389/fimmu.2023.1165004

TABLE 2E Continued

Haplotype	ICI-T1DM (*N*=24)		ICI-Controls (*N*=70)		*1Controls (*N*=2938)	ICI-T1DM vs general controls				ICI-T1DM vs ICI-controls				ICI-controls vs general controls		
DRB1-DQB1-DPB1	*n*	F (%)	*n*	F (%)	F (%)	*2 *P*	*3 *Pc*	OR	95% CI	*2 *P*	*3 *Pc*	OR	95% CI	*2 *P*	OR	95% CI
*15:02-*06:01-*02:01	0	0.0	3	4.29	0.92	NS				NS				NS		
*14:54-*05:03-*05:01	1	4.2	0	0.00	0.85	NS				NS				NS		
*04:05-*04:01-*03:01	0	0.0	1	1.43	0.75	NS				NS				NS		
*12:01-*03:03-*05:01	0	0.0	1	1.43	0.75	NS				NS				NS		
*15:02-*06:01-*05:01	0	0.0	1	1.43	0.72	NS				NS				NS		
*09:01-*03:03-*04:02	1	4.2	2	2.86	0.65	NS				NS				NS		
*14:05-*05:03-*02:01	0	0.0	2	2.86	0.65	NS				NS				NS		
*08:02-*04:02-*05:01	0	0.0	1	1.43	0.58	NS				NS				NS		
*04:10-*04:02-*03:01	0	0.0	2	2.86	0.55	NS				NS				NS		
*08:02-*04:02-*02:01	0	0.0	1	1.43	0.51	NS				NS				NS		
*15:01-*06:02-*13:01	0	0.0	1	1.43	0.44	NS				NS				NS		
*12:02-*03:01-*02:01	0	0.0	1	1.43	0.37	NS				NS				NS		
*04:05-*04:01-*19:01	1	4.2	0	0.00	0.37	NS				NS				NS		
*13:02-*06:04-*05:01	1	4.2	0	0.00	0.36	NS				NS				NS		
*04:03-*03:02-*03:01	0	0.0	1	1.43	0.34	NS				NS				NS		
*16:02-*05:02-*02:02	0	0.0	1	1.43	0.31	NS				NS				NS		
*12:01-*03:01-*02:01	0	0.0	1	1.43	0.31	NS				NS				NS		
*15:01-*06:02-*03:01	0	0.0	1	1.43	0.27	NS				NS				NS		
*09:01-*03:03-*02:02	0	0.0	1	1.43	0.24	NS				NS				NS		
*10:01-*05:01-*02:01	0	0.0	1	1.43	0.24	NS				NS				NS		
*04:05-*04:01-*02:02	0	0.0	1	1.43	0.17	NS				NS				NS		
*04:03-*03:02-*04:02	0	0.0	1	1.43	0.14	NS				NS				NS		
*04:05-*04:01-*14:01	0	0.0	0	0.00	0.10	NS				NS				NS		

(Continued)

10.3389/fimmu.2023.1165004

TABLE 2E Continued

Haplotype	ICI-T1DM (*N*=24)		ICI-Controls (*N*=70)		*1Controls (*N*=2938)	ICI-T1DM vs general controls				ICI-T1DM vs ICI-controls				ICI-controls vs general controls		
DRB1-DQB1-DPB1	*n*	F (%)	*n*	F (%)	F (%)	*2 *P*	*3 *Pc*	OR	95% CI	*2 *P*	*3 *Pc*	OR	95% CI	*2 *P*	OR	95% CI
*15:01-*06:02-*04:01	0	0.0	1	1.43	0.07	NS				NS				NS		
*04:03-*03:02-*02:02	0	0.0	1	1.43	0.03	NS				NS				NS		
*12:01-*03:03-*02:01	0	0.0	1	1.43	0.03	NS				NS				NS		
*13:02-*06:04-*03:01	0	0.0	1	1.43	0.03	NS				NS				NS		
*11:01-*03:03-*14:01	1	4.2	1	1.43	0.03	NS				NS				NS		
*01:01*05:03-*05:01	0	0.0	1	1.43	0.00	NS				NS				NS		
*11:06-*03:01-*05:01	0	0.0	1	1.43	0.00	NS				NS				NS		
Others	0	0.0	0	0.00	24.40	NS				NS				NS		
total	24	100.00	70	100.00	100.00											

Haplotypes with frequencies more than 1.0% in controls were included to the analysis (53 haplotypes). N, n, number of the haplotypes.
*1 Control subjets: HLA LABORATORY, Japan INC: http://hla.or.jp/med/frequency_search/ja/haplo/ ref (11).
*2 Each haplotype frequency was analyzed using Fisher's exact test with 2 x2 contingency tables.
*3 Pc: Bonferroni correction.
F, frequency of the haplotype; NS, not significant.
P values less than 0.05 are shown in bold.
95%CI: 95% confidence intervals.

(Table 4). Besides, proinsulin epitope binding predictions to HLA-DP15 were similarly shown in Table 4. The proinsulin binding predictions to HLA-DR5 or to HLA-DP15 were different, but all portions in proinsulin including C-peptide region (AA57-87) showed binding predictions to both alleles.

Then *in vitro* peptide binding assay was conducted, and remarkably, in the insulin B chain (AA25-54) and insulin A chain (AA90-110), two clusters were identified (peptides 6-10: AA 29-57 as cluster 1 and peptides 31-34: AA 84-110 as cluster 2) for HLA-DP5 and also for HLA-DP15 (Table 4) (Figure 6B). Moreover, peptides in the C-peptide region (AA57-87) bound to neither HLA-DP5 nor HLA-DP15.

Discussion

A total of 47 patients with malignancies who had been treated with ICI were subjected to HLA typing by next generation sequencing. T1DM developed in twelve and the remaining thirty-five served as controls. In allele and haplotype analyses, the patients had an increase of HLA-*DRB1*04:05*, *DQB1*04:01*, and in particular of *DPB1*05:01*. Indeed, 17/24 (71%) alleles were *DPB1*05:01* among the patients compared with 24/70 (34%) in the controls. Moreover, significant amino acid polymorphisms at HLA-DR, DQ, and DP allele were identified that might contribute to the development of ICI-T1DM, probably with conformational

TABLE 2F Multiple logistic regression analysis of HLA-alleles in ICI-T1DM patients and ICI-controls.

HLA allele	Predicted score	Standard error	P-value	Odds ratio	95%CI
HLA-*DQB1*04:01* (completely in linkage disequilibrium with HLA-*DRB1*04:05*)	0.755	0.333	**0.023**	4.53	1.22–16.7
HLA-*DPB1*05:01*	0.647	0.268	**0.016**	3.65	1.27–10.44

95%CI: 95% confidence intervals.
P values less than 0.05 are shown in bold.

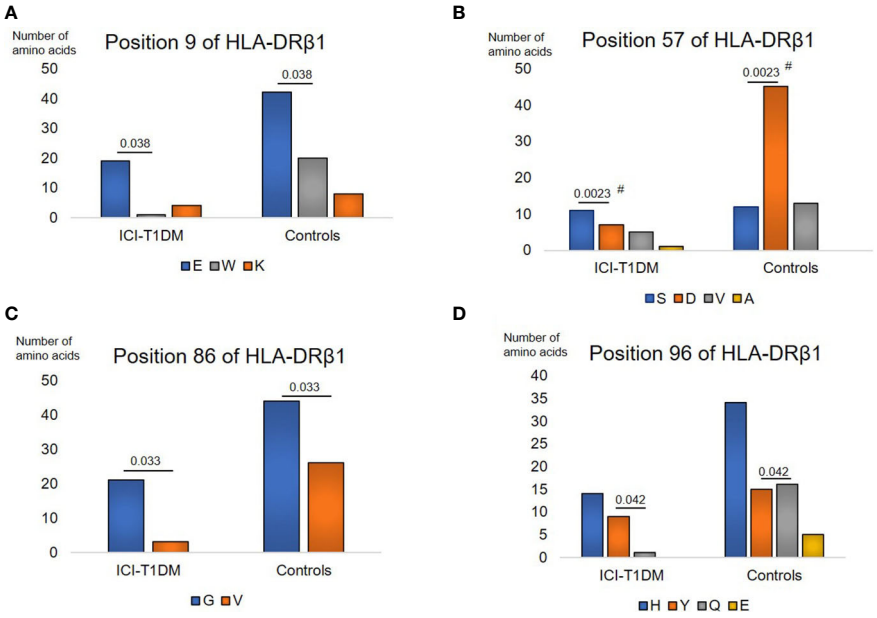

FIGURE 1
Prevalence of amino acid carriages at residues of HLA-DRB1 allele in patients with ICI-T1DM and ICI-controls (shown as controls) **(A–D)**. Prevalence of amino acid at position 9, E, Glutamic acid vs W, Tryptophan, P=0.038. OR 9.05, 95% CI: 1.13-72.43 **(A)**, position 57, S, Serine vs D, Aspartic acid, P=0.0023. OR 5.89, 95%CI: 1.88-18.46 **(B)**, position 86, G, Glycine vs V, Valine, P=0.033. OR 4.14, 95%CI: 1.12-15.23 **(C)**, and position 96, Y, Tyrosine vs Q, Glutamine, P=0.042. Odds ratio of 9.60, 95%CI: 1.08-85.16 **(D)** are shown. After Bonferroni correction for all significant amino acid polymorphisms among HLA-DRB1 alleles, only amino acid position 57 on HLA-DRB1 allele **(B)** was significantly different (Pc=0.046 after Bonferroni correction, shown with #).

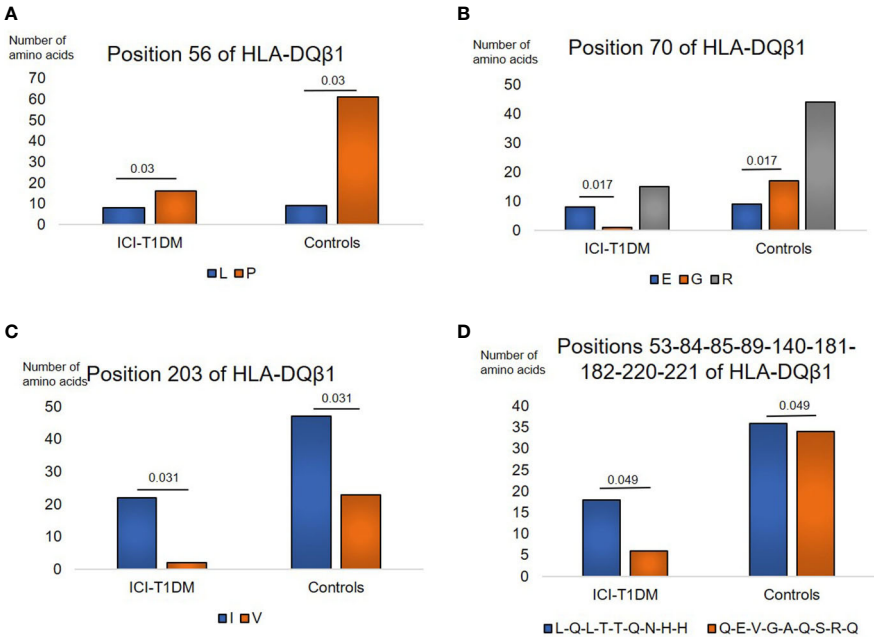

FIGURE 2
Similarly, prevalence of amino acid carriages at residues of HLA-DQB1 allele in patients with ICI-T1DM and ICI-controls **(A–D)**. Prevalence of amino acid at position 56, L, Leucine vs P, Proline, P=0.03. OR 3.39, 95%CI: 1.13-10.18 **(A)**, position 70, E, Glutamic acid vs G, Glycine, P=0.017. OR 15.11, 95%CI: 1.62-140.58 **(B)**, position 203, I, Isoleucine vs V, Valine, P=0.031. OR 5.38, 95%CI: 1.16-24.89 **(C)**, and positions 53-84-85-89-140-181-182-220-221, L-Q-L-T-T-Q-N-H-H, Leucine-Glutamine-Leucine-Threonine-Threonine-Glutamine-Asparagine-Histidine-Histidine vs Q-E-V-G-A-Q-S-R-Q, Glutamine-Glutamic acid-Valine-Glycine-Alanine-Glutamine-Serine-Arginine-Glutamine, P=0.049. OR 2.83, 95%CI: 1.01-7.98 **(D)** are shown. After Bonferroni correction for all significant amino acid polymorphisms among HLA-DQB1 alleles, no amino acid polymorphisms were significantly different.

10.3389/fimmu.2023.1165004

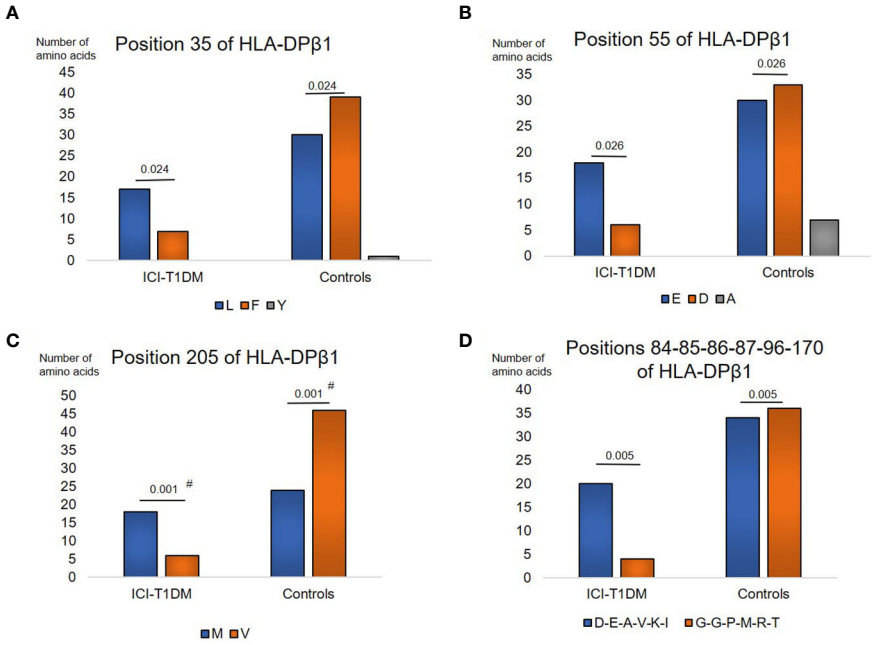

FIGURE 3
Then, prevalence of amino acid carriages at residues of HLA-DPB1 allele in patients with ICI-T1DM and ICI-controls **(A–D)**. Prevalence of amino acid at position 35, L, Leucine vs F, Phenylalanine, P=0.024. OR 3.16, 95%CI: 1.16-8.59 **(A)**, position 55, E, Glutamic acid vs D, Aspartic acid, P=0.026. OR 3.3, 95%CI: 1.16-9.41 **(B)**, position 205, M, Methionine vs V, Valine, P=0.001. OR 5.75, 95%CI: 2.02-16.39 **(C)**, and positions 84-85-86-87-96-170, D-E-A-V-K-I, Aspartic acid-Glutamic acid-Alanine-Valine-Lysine-Isoleucine vs G-G-P-M-R-T, Glycine-Glycine-Proline-Methionine-Arginine-Tryptophan, P=0.005. OR 5.29, 95%CI: 1.64-17.08 **(D)** are shown. OR, odds ratio; 95%CI, 95% confidence interval; Note that due to the statistical analyses employed, each P value was the same value in the respective figures. After Bonferroni correction for significant amino acid polymorphisms among HLA-DPB1 alleles, only amino acid position 205 on HLA-DP allele **(C)** were significantly different (Pc=0.011 after Bonferroni correction, shown with #).

TABLE 3 Stepwise selection and multivariate regression analysis of amino acid polymorphisms across HLA-class II alleles in ICI-T1DM patients and ICI-controls.

Amino acid position	HLA-chain	Amino acid	Compared amino acid	Predicted score	Test statistics by Wald method	P-value	Selection	Standard error	Odds ratio	95% CI
9	HLA-DRβ1	K and E	W	0	0.044	0.833				
9	HLA-DRβ1	K	E	0	0.070	0.965				
57	HLA-DRβ1	A and S	V and D	0	1.369	0.242				
57	HLA-DRβ1	A	S	0	2.479	0.290				
57	HLA-DRβ1	V	D	0	0.109	0.947				
86	HLA-DRβ1	G	V	0.556	2.499	0.114	Selected	0.352	3.039	0.765–12.061
96	HLA-DRβ1	Y and H	Q and E	0.924	2.919	0.088	Selected	0.541	2.519	0.873–7.269
96	HLA-DRβ1	Y	H	0	1.219	0.270				
96	HLA-DRβ1	Q	E	0	0.485	0.486				

(Continued)

10.3389/fimmu.2023.1165004

TABLE 3 Continued

Amino acid position	HLA-chain	Amino acid	Compared amino acid	Predicted score	Test statistics by Wald method	P-value	Selection	Standard error	Odds ratio	95% CI
53-84-85-89-140-181-182-220-221	HLA-DQβ1	L-Q-L-T-T-Q-N-H-H	Q-E-V-G-A-Q-S-R-Q	0	0.213	0.644				
56	HLA-DQβ1	L	P	0	0.415	0.519				
70	HLA-DQβ1	E	R and G	0	0.415	0.519				
70	HLA-DQβ1	R	G	0	0.002	0.999				
203	HLA-DQβ1	I	V	0	0.445	0.505				
35	HLA-DPβ1	L	F and Y	0	2.348	0.125				
35	HLA-DPβ1	F	Y	0	0.019	0.991				
55	HLA-DPβ1	E	D and A	0	1.440	0.230				
55	HLA-DPβ1	D	A	0	2.583	0.275				
84-85-86-87-96-170	HLA-DPβ1	D-E-A-V-K-I	G-G-P-M-R-T	0	0.709	0.400				
205	HLA-DPβ1	M	V	0.69	6.001	**0.014***	Selected	0.282	3.976	1.318–11.998

K, Lysine; E, Glutamic acid; A, Alanine; S, Serine; V, Valine; G, Glycine; Y, Tyrosine; H, Histidine; Q, Glutamine; L, Leucine; R, Arginine; I, Isoleucine; F, Phenylalanine; D, Aspartic acid; M, Methionine; W, Tryptophan; P, Proline; T, Threonine; N, Asparagine; C, Cysteine.
A stepwise selection (cut-off P value at 0.2) of covariate amino acid residues is shown.
*β205 at HLA-DPβ1 was found to be significant (P=0.014, sensitivity 0.75, specificity 0.73, and Area Under the Curve, 0.782)
95%CI: 95% confidence intervals.

alterations in the peptide-binding groove in each HLA-class II molecule. HLA-DP5 was found to be more strongly related to amino acid polymorphisms. As the peptide-binding groove dictate peptide binding, we scanned proinsulin *in silico* as a hypothetical autoantigen and novel human proinsulin epitope clusters in insulin B and A chains were discovered for HLA-DP *in vitro*. Our findings are promising suggestion of a possible association between HLA and ICI-T1DM through proinsulin peptide binding studies.

In comparison with our previous study (5), the current study was conducted on a larger scale with confirmation of HLA-*DPB1*05:01* predominance in ICI-T1DM than those of general controls and ICI-controls with the same ethnic background. Current study may also support other reports describing that HLA-DR4 alleles are increased in patients with ICI-T1DM in the United States (21, 22), although these studies are not at the detailed allelic levels. Based on the conditional multiple regression analysis, in addition to HLA-*DPB1*05:01* allele, alleles of HLA-*DRB1*04:05* and *DQB1*04:01, and* HLA-*DRB1*04:05-DQB1*04:01* haplotype were found to be susceptible to ICI-T1DM (Tables 2A–E) . HLA-*DRB1*04:05-DQB1*04:01* haplotype and HLA-*DRB1*04:05-DQB1*04:01-DPB1*05:01* haplotype predominance in ICI-T1DM also suggested that HLA-DP5 controls immune reaction of HLA-*DR* and *DQ* as mentioned below.

Then we disentangled amino acid polymorphisms at positions 9 and 57 (P9) and 86 (P1) of HLA-DRβ1, position 70 (P4 and P7) and positions 85 and 89 (P1) of HLA-DQβ1, and positions 85 and 86 (P1) of HLA-DPβ1 (Figures 5A–C). These amino acids contribute to the formation of the peptide-binding grooves on HLA-class II molecules, therefore may functionally contribute to the epitope presentations. Notably, patients with ICI-T1DM in Japan have been reported to have HLA-*DRB1*11:01/*13:02* (23), *DRB1*04:05* (24–26), *DRB1*04:06* (26), and *DRB1*09:01* (25), and all of patients above had G86 at HLA-DRβ1. Particularly, both HLA-*DRB1*04:05* and *DRB1*09:01* have G86 at HLA-DRβ1, and were reported to be associated with T1DM (27). Conversely, HLA-*DRB1*15:01*, a protective allele for T1DM has V86 at HLA-DRβ1 (27), and HLA-*DRB1*15:01* was not seen in patients with ICI-T1DM in the current study. Therefore, G86 and V86 seemed to be disease-promotion and protection alleles, respectively, at HLA-DRβ1, in association with (P1). Todd, et al. reported strongly conserved Asp (D) at position 57 (P1, P9) of HLA-DQβ1 with disease susceptibility in patients with T1DM (28), and D at position 57 (P1, P9) of HLA-DRβ1 seemed to play a strong protective role in ICI-T1DM in the current study (Figure 5A). Then, stepwise selection and multivariate analysis revealed that β205 at HLA-DPβ1 was most important

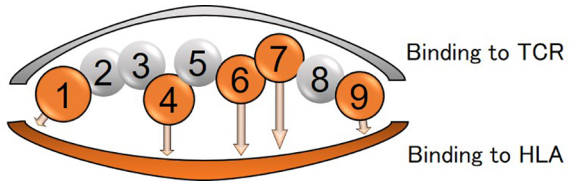

FIGURE 4
Peptide-binding grooves in an HLA class-II molecule (amino acid position 1-9) are shown. Amino acids in positions 1, 4, 6, 7, and 9 bind to HLA and those in positions 2, 3, 5, and 8 are assumed to be outward facing in order to stimulate the T-cell receptor (TCR).

(Table 3). Therefore, we speculated the amino acid polymorphism β205 at HLA-DPβ, which locates outside of the peptide-binding groove in HLA-DPβ1, may be related to interactions such as HLA-DM, or to alterations in signal transduction within the HLA molecule.

Taken together, significances of HLA-DP5 in ICI-T1DM were observed. Next, we conducted human proinsulin peptide binding prediction to HLA-DP molecules to ensure effective epitope presentation in ICI-T1DM (Table 4) (Figure 6A). Predicted binding affinities and *in vitro* binding results were quite different for HLA-DP5, especially in the C-peptides region, for reasons unknown (Figures 6A, B). Remarkably, insulin B chain epitope (cluster 1): AA 29-57, and the insulin A chain epitope (cluster 2): AA 84-110 were established *in vitro* binding assay (Figure 6B). Among them, peptide 9 (AA 42-56), VCGERGFFYTPKTRR (core sequence underlined), was predicted as intermediate binders and also exhibited the strongest *in vitro* peptide binding, thus is mostly expected to be immunogenic T-cell epitope. Insulin peptide B9-23 (AA 33-47) has been reported to be a major autoantigen to induce immunity in the nonobese diabetic mouse, and is also included in the cluster 1 (19). Mannering et al. reported that cells transfected with HLA-*DRB1*04:05* presented insulin A1–13 (AA 88-102) which is the identical to the peptide 32 (20). HLA-DP15 has not been reported as a risk allele in ICI-T1DM, but showed similar *in vitro* proinsulin epitopes to HLA-DP5 (cluster 1 and cluster 2) (Figure 6B). Despite the dissimilarities in amino acid sequence between HLA-*DPB1*05:01* and HLA-*DPB1*15:01*, the importance of epitope cluster 1 and cluster 2 was reinforced across the alleles *in silico* and *in vitro* (Supplementary Table 6C).

In the development of ICI-T1DM, we hypothesized that the inhibition of immune-checkpoint molecules by ICI induced immunity to pancreatic β-cells, as observed in thyroid follicular epithelial cells during thyroid irAE (5, 29). Antibody-dependent cellular cytotoxicity by ICIs, by cytotoxic T-cells (30), or by both of them, would contribute to the development of ICI-T1DM. We speculate that ICI-T1DM-predisposing HLA may also be involved with malignant diseases. Proinsulin epitope, as well as tumor-associated antigen/neoantigen, could be bound to peptide-binding cleft of HLA, and cross-presented on the surface of antigen-presenting cells due to molecular mimicry (3, 4, 9). Another important topic is the correlation of ICI treatment effectivity and ICI-T1DM. Considering that 8/12 (75%) were ICI-responders in ICI-T1DM group and that generally only 20-30% are responders, common mechanisms between ICI treatment and ICI-T1DM were suggested. Therefore, HLA seemed to be associated with both ICI treatment outcome and risk for an endocrine adverse event. Considering that proinsulin is processing into insulin A chain and B chain, and that epitope clusters were identified in the two chains, evaluation of IAA in the time course may be of interest. As well, anti-GAD65 antibody titers in the course seem to be important.

This study has limitations. Firstly, we have tested proinsulin binding to HLA-DP. Binding studies for HLA-DR and HLA-DQ molecules are also desirable. Secondly, more evidence of immunogenicity of HLA-DP5 from *in vitro* and *in vivo* experiments in comparison with HLA-DR/DQ are preferable to confirm the peptide binding data in this study. Thirdly, better investigation of the frequency of HLA-*DPB1*05:01*, irrespective of ICI treatment is still desirable. Finally, the study consists of a small

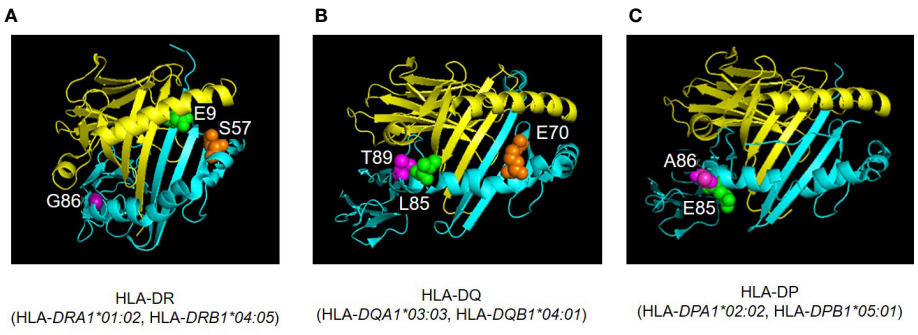

FIGURE 5
Three-dimensional illustration of ICI-T1DM risk-associated amino acid positions were identified in the current study. The crystal structures of HLA-DR **(A)**, HLA-DQ **(B)**, and HLA-DP **(C)** molecules are established based on Protein Data Bank entries 4IS6, 2NNA, and 3WEX, respectively. The structure of extracellular domains of HLA-class IIα and IIβ chains are shown in yellow and cyan, respectively. Amino acid polymorphic sites are shown as spheres. Amino acid position 9 (E, Glutamic acid, green) and 57 (S, Serine, orange) are located in pocket 9 of HLA-DR molecule (HLA-*DRA1*01:02*, HLA-*DRB1*04:05*) **(A)**. Amino acid position 86 (G, Glycine, purple) composes pocket 1 **(A)**. Amino acid position 70 (E, Glutamic acid, orange) is associated with both pocket 4 of HLA-DQ (HLA-*DQA1*03:03*, HLA-*DQB1*04:01*) **(B)**. The HLA-DQβ1 amino acid positions 85 (L, Leucine, green) and 89 (T, Threonine, purple) compose pocket 1 of HLA-DQ molecule **(B)**. Amino acid positions 85 (Glu, Glutamic acid, green) and 86 (A, Alanine, purple) compose pocket 1 of HLA-DP molecule (HLA-*DPA1*02:02*, HLA-*DPB1*05:01*) **(C)**. Pocket: peptide-binding groove pocket.

TABLE 4 Human proinsulin-derived peptides and their affinities to HLA-DP5 and HLA-DP15 *in silico* and *in vitro*.

																	Predicted binding score (shown as % RANK)		In vitro binding score (shown as REVEAL score)		%RANK note	REVEAL score note	References
ID	Position	Amino acid sequences of synthesized peptides															DP15	DP5	DP15	DP5	DP5	DP5	
1	*1-15	**M**	**A**	**L**	**W**	**M**	**R**	**L**	**L**	P	L	L	A	L	L	A	22.17	76.22	16.1	6.1			
2	*7-21	L	L	P	**L**	**L**	**A**	**L**	**L**	**A**	**L**	**W**	**G**	P	D	P	73.14	92.69	0.4	0.4			
3	*13-27	L	L	A	L	**W**	**G**	**P**	**D**	**P**	**A**	**A**	**A**	**F**	V	N	44.91	62.68	0.1	0.2			
4	*19-33	P	D	P	**A**	**A**	**A**	**F**	**V**	**N**	**Q**	**H**	**L**	C	G	S	41.54	63.13	0	0			
5	*25-39	F	V	N	**Q**	**H**	**L**	**C**	**G**	**S**	**H**	**L**	**V**	E	A	L	82.17	87.5	0.3	0.2			
6	***29-43**	H	L	C	G	S	H	**L**	**V**	**E**	**A**	**L**	**Y**	**L**	**V**	**C**	63.42	95	14.2	4.6		**Cluster 1**	
7	***33-47**	S	H	**L**	**V**	**E**	**A**	**L**	**Y**	**L**	**V**	**C**	G	E	R	G	33.96	80.96	9.1	3.6			(19)
8	***37-51**	E	A	L	**Y**	**L**	**V**	**C**	**G**	**E**	**R**	**G**	**F**	F	Y	T	67.91	75.54	17.3	8.9			
9	***42-56**	V	C	G	E	R	G	**F**	**F**	**Y**	**T**	**P**	**K**	**T**	**R**	**R**	32.28	20.09	37.4	26.8	IB		
10	***43-57**	C	G	E	R	G	**F**	**F**	**Y**	**T**	**P**	**K**	**T**	**R**	**R**	E	10.81	4.24	17.2	9.5	SB		
11	*44-58	G	E	R	G	**F**	**F**	**Y**	**T**	**P**	**K**	**T**	**R**	**R**	E	A	4.62	1.43	0.4	0.2	SB		
12	*45-59	E	R	G	**F**	**F**	**Y**	**T**	**P**	**K**	**T**	**R**	**R**	E	A	E	3.37	0.71	0	0	SB		
13	*46-60	R	G	**F**	**F**	**Y**	**T**	**P**	**K**	**T**	**R**	**R**	E	A	E	D	5.96	3.74	0	0	SB		
14	*47-61	G	**F**	**F**	**Y**	**T**	**P**	**K**	**T**	**R**	**R**	E	A	E	D	L	16.23	15.52	0	0	IB		
15	*48-62	F	F	**Y**	**T**	**P**	**K**	**T**	**R**	**R**	**E**	**A**	E	D	L	Q	50.27	49.79	0	0	IB		
16	*49-63	F	Y	T	**P**	**K**	**T**	**R**	**R**	**E**	**A**	**E**	**D**	L	Q	V	59.35	51.18	0	0			
17	*50-64	Y	T	P	K	T	R	**R**	**E**	**A**	**E**	**D**	**L**	**Q**	**V**	**G**	55.66	26.85	0	0	IB		
18	*51-65	T	P	K	T	R	**R**	**E**	**A**	**E**	**D**	**L**	**Q**	**V**	**G**	Q	42.39	7.81	0	0.3	IB		
19	*52-66	P	K	T	R	**R**	**E**	**A**	**E**	**D**	**L**	**Q**	**V**	**G**	Q	V	38.06	5.25	0	0.1	IB		
20	*53-67	K	T	R	**R**	**E**	**A**	**E**	**D**	**L**	**Q**	**V**	**G**	Q	V	E	35.72	4.26	0	0	SB		
21	*54-68	T	R	**R**	**E**	**A**	**E**	**D**	**L**	**Q**	**V**	**G**	Q	V	E	L	55.52	23.95	0	0	IB		
22	*59-73	E	D	**L**	**Q**	**V**	**G**	**Q**	**V**	**E**	**L**	**G**	G	G	P	G	45.97	70.3	0	0			
23	*64-78	G	Q	**V**	**E**	**L**	**G**	**G**	**G**	**P**	**G**	**A**	G	S	L	Q	94.37	95	0	0			
24	*69-83	G	G	G	P	G	**A**	**G**	**S**	**L**	**Q**	**P**	**L**	**A**	**L**	E	77.82	84.31	0	0			

(Continued)

10.3389/fimmu.2023.1165004

TABLE 4 Continued

ID	Position	Amino acid sequences of synthesized peptides															Predicted binding score (shown as % RANK)		In vitro binding score (shown as REVEAL score)		%RANK note	REVEAL score note	References
																	DP15	DP5	DP15	DP5	DP5	DP5	
25	*74-88	A	G	S	**L**	**Q**	**P**	**L**	**A**	**L**	**E**	**G**	**S**	L	Q	K	36.67	29.36	0	0	IB		
26	*75-89	G	S	L	Q	P	**L**	**A**	**L**	**E**	**G**	**S**	**L**	**Q**	**K**	R	35.2	10.52	0	0.1	IB		
27	*76-90	S	L	Q	P	**L**	**A**	**L**	**E**	**G**	**S**	**L**	**Q**	**K**	R	G	24.48	5.07	0	0	IB		
28	*77-91	L	Q	P	**L**	**A**	**L**	**E**	**G**	**S**	**L**	**Q**	**K**	R	G	I	26.62	5.24	0	0	IB		
29	*78-92	Q	P	**L**	**A**	**L**	**E**	**G**	**S**	**L**	**Q**	**K**	R	G	I	V	43.33	9.38	0	0.1	IB		
30	*79-93	P	**L**	**A**	**L**	**E**	**G**	**S**	**L**	**Q**	**K**	R	G	I	V	E	65.94	37.94	0	0	IB		
31	***84-98**	G	S	L	Q	**K**	**R**	**G**	**I**	**V**	**E**	**Q**	**C**	**C**	T	S	91.03	86.88	1.1	0.5		**Cluster 2**	
32	***88-102**	K	R	G	**I**	**V**	**E**	**Q**	**C**	**C**	**T**	**S**	**I**	C	S	L	94.91	91.7	16.3	9.9			(20)
33	***92-106**	V	E	Q	C	**C**	**T**	**S**	**I**	**C**	**S**	**L**	**Y**	**Q**	L	E	95	95	1.5	0.5			
34	***96-110**	C	T	S	**I**	**C**	**S**	**L**	**Y**	**Q**	**L**	**E**	**N**	Y	C	N	95	94.28	10.1	2.6			

Core 9 amino acids in the prediction for HLA-DP5 are shown in bold.
SB, strong binders for HLA-DP5: %RANK<5; IB, intermediate binder for HLA-DP5: %RANK was between 5 to 50.
K, Lysine; E, Glutamic acid; A, Alanine; S, Serine; V, Valine; G, Glycine; Y, Tyrosine; H, Histidine;
Q, Glutamine; L, Leucine; R, Arginine; I, Isoleucine; F, Phenylalanine; D, Aspartic acid; M, Methionine;
W, Tryptophan; P, Proline; T, Threonine; N, Asparagine; C, Cysteine
Peptide numbers within B chain (AA25-54) and A chain (AA90-110) are shown in bold lines.

10.3389/fimmu.2023.1165004

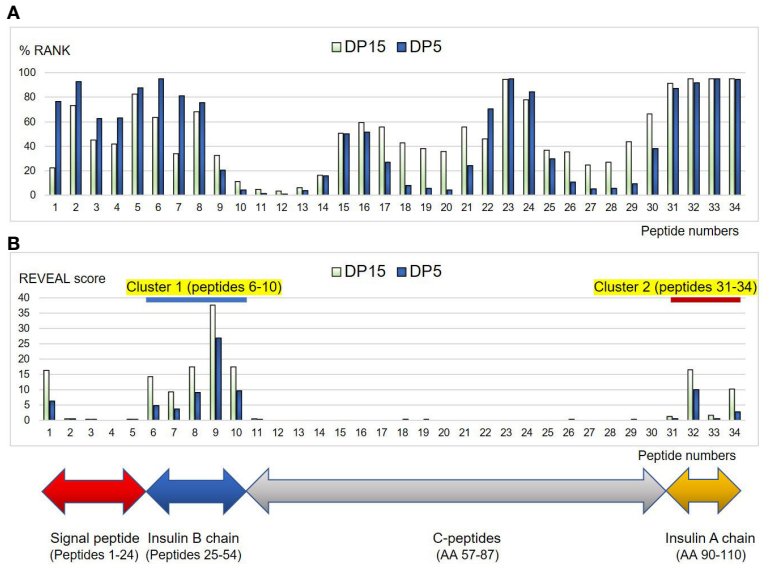

FIGURE 6
Binding affinities of the peptides derived from human proinsulin to HLA-DP5 (HLA-*DPA1*02:02*, HLA-*DPB1*05:01*) or HLA-DP15 (HLA-*DPA1*02:02*, HLA-*DPB1*15:01*) molecules are shown as %RANK *in silico* **(A)**, and shown as REVEAL score *in vitro* **(B)**. Horizontal numbers indicate peptide numbers used in the study (shown in Table 4). Note that lower %RANK means predicted strong binder *in silico*, and higher REVEAL score indicates peptide with high affinity *in vitro*. Cluster 1 (peptides 6-10) and Cluster 2 (peptide 31-34) were shown with blue and red line, respectively.

sample size, so more data with increased numbers may help to establish our results.

In conclusion, HLA-DP5 as a predisposition molecule, and significant amino acid polymorphisms at HLA-class II molecules in patients with ICI-T1DM were established in this study. Based on the *silico* and *in vitro* proinsulin peptide-binding study, conformational changes in the peptide-binding groove of the HLA-DP molecules may influence the immunogenicity of proinsulin epitopes in ICI-T1DM. These genetic factors may be utilized for prediction of ICI-T1DM, and also could contribute to elucidation of the mechanism of cancer immunotherapy and ICI-T1DM. Therefore, current study offers safer and more effective management and monitoring options for cancer immunotherapy. Further investigations are warranted to elucidate the relation of ICI- treatment effectiveness and development of ICI-T1DM.

Data availability statement

The datasets presented in this study can be found in online repositories. The names of the repository/repositories and accession number(s) can be found in the article/Supplementary Material.

Ethics statement

The studies involving human participants were reviewed and approved by Red Cross Society Wakayama Medical Center (JRCW), Wakayama Medical University Hospital (WMU), and Nagoya University (NU). The patients/participants provided their written informed consent to participate in this study. Written informed consent was obtained from the individual(s) for the publication of any potentially identifiable images or data included in this article.

Author contributions

HI: Conceptualization, designed the study. original draft preparation. SM: Visualization, writing- reviewing and editing. All authors performed the clinical studies statistically analyzed the data and wrote the manuscript. All authors approved the final version of the manuscript for publication. All authors contributed to the article and approved the submitted version.

Funding

This work was partially supported by the Takeda Science Foundation, the Japanese Foundation for Multidisciplinary Treatment of Cancer, Japan Diabetes Foundation, and the Grant-in-Aid for Scientific Research from the Ministry of Education, Science, Sports, and Culture, Japan (20K17541 and 21K08544).

Acknowledgments

We are indebted to Dr. Hidetoshi Inoko (Tokai University) for technical advice. We acknowledge proofreading and editing by Benjamin Phillis at the Clinical Study Support Center, Wakayama Medical University.

Conflict of interest

Author YO was employed by GenoDive Pharma Inc. Author HN was employed by Biospecimen Laboratories, Inc. Author SIw has received personal fees from Ono Pharmaceutical Co. Ltd., Bristol-Myers Squibb, Chugai Pharmaceutical Co., Ltd. and MSD K.K. outside of this study. Author HA received grants from Ono

Pharmaceutical Co., Ltd., MSD K.K., and Chugai Pharmaceutical Co., Ltd., and personal fees from Ono Pharmaceutical Co., Ltd., Bristol– Myers Squibb and MSD K.K. outside of this study.

The remaining authors declare that the research was conducted in the absence of any commercial or financial relationships that could be construed as a potential conflict of interest.

Publisher's note

All claims expressed in this article are solely those of the authors and do not necessarily represent those of their affiliated organizations, or those of the publisher, the editors and the reviewers. Any product that may be evaluated in this article, or claim that may be made by its manufacturer, is not guaranteed or endorsed by the publisher.

Supplementary material

The Supplementary Material for this article can be found online at: https://www.frontiersin.org/articles/10.3389/fimmu.2023.1165004/full#supplementary-material

References

1. Arima H, Iwama S, Inaba H, Ariyasu H, Makita N, Otsuki M, et al. Management of immune-related adverse events in endocrine organs induced by immune checkpoint inhibitors: clinical guidelines of the Japan endocrine society. *Endocr J* (2019) 66(7):581–6. doi: 10.1507/endocrj.EJ19-0163

2. Inaba H, Ariyasu H, Takeshima K, Iwakura H, Akamizu T. Comprehensive research on thyroid diseases associated with autoimmunity: autoimmune thyroid diseases, thyroid diseases during immune-checkpoint inhibitors therapy, and immunoglobulin-G4-associated thyroid diseases. *Endocr J* (2019) 66(10):843–52. doi: 10.1507/endocrj.EJ19-0234

3. Inaba H, Ariyasu H, Iwakura H, Ueda Y, Kurimoto C, Takeshima K, et al. Comparative analysis of HLA between idiopathic and anti-PD-1 antibody induced isolated ACTH deficiency: A pilot study. *Clin Endocrinol (Oxf)* (2019) 91(6):786–92. doi: 10.1111/cen.14082

4. Inaba H, Ariyasu H, Iwakura H, Kurimoto C, Takeshima K, Morita S, et al. Distinct clinical features and prognosis between persistent and temporary thyroid dysfunctions by immune-checkpoint inhibitors. *Endocr J* (2021) 68(2):231–41. doi: 10.1507/endocrj.EJ20-0371

5. Inaba H, Kaido Y, Ito S, Hirobata T, Inoue G, Sugita T, et al. Human leukocyte antigens and biomarkers in type 1 diabetes mellitus induced by immune-checkpoint inhibitors. *Endocrinol Metab (Seoul)* (2022) 37(1):84–95. doi: 10.3803/EnM.2021.1282

6. Qiu J, Luo S, Yin W, Guo K, Xiang Y, Li X, et al. Characterization of immune checkpoint inhibitor-associated fulminant type 1 diabetes associated with autoantibody status and ethnic origin. *Front Immunol* (2022) 13:968798. doi: 10.3389/fimmu.2022.968798

7. Kemmler W, Peterson JD, Rubenstein AH, Steiner DF. On the biosynthesis, intracellular transport and mechanism of conversion of proinsulin to insulin and c-peptide. *Diabetes* (1972) 21(2 Suppl):572–81. doi: 10.2337/diab.21.2.S572

8. Inaba H, Martin W, De Groot AS, Qin S, De Groot LJ. Thyrotropin receptor epitopes and their relation to histocompatibility leukocyte antigen-DR molecules in graves' disease. *J Clin Endocrinol Metab* (2006) 91(6):2286–94. doi: 10.1210/jc.2005-2537

9. Inaba H, Martin W, Ardito M, De Groot AS, De Groot LJ. The role of glutamic or aspartic acid in position four of the epitope binding motif and thyrotropin receptor-extracellular domain epitope selection in graves' disease. *J Clin Endocrinol Metab 95* (2010) 6):2909–16. doi: 10.1210/jc.2009-2393

10. Kobayashi T, Iwama S, Sugiyama D, Yasuda Y, Okuji T, Ito M, et al. Anti-pituitary antibodies and susceptible human leukocyte antigen alleles as predictive biomarkers for pituitary dysfunction induced by immune checkpoint inhibitors. *J Immunother Cancer* (2021) 9(5):e002493. doi: 10.1136/jitc-2021-002493

11. Kawasaki E, Maruyama T, Imagawa A, Awata T, Ikegami H, Uchigata Y, et al. Diagnostic criteria for acute-onset type 1 diabetes mellitus: Report of the committee of Japan diabetes society on the research of fulminant and acute-onset type 1 diabetes mellitus. *J Diabetes Investig* (2014) 5(1):115–8. doi: 10.1111/jdi.12119

12. Imanishi T, Akaza T, Kimura A, Tokunaga K, Gojobori T. Allele and haplotype frequencies for HLA and complement loci in various ethnic groups. In: Tsuji K, Aizawa M, Sasazuki T, editors. *HLA 1991: Proceedings of the eleventh international histocompatibility workshop and conference*. Oxford, UK: Oxford University Press (1992). p. 1065–220.

13. HLA LABORATORY and Japan INC . Available at: http://hla.or.jp/med/frequency_search/ja/haplo/ (Accessed October 10, 2022).

14. Japanese Society for Histocompatibility and Immunogenetics. Available at: http://jshi.umin.ac.jp/standarization/JSHI-hyokiallele-2022list.pdf/ (Accessed October 10, 2022).

15. wwPDB consortium. Protein data bank: the single global archive for 3D macromolecular structure data. *Nucleic Acids Res* (2019) 47(D1):D520–8. doi: 10.1093/nar/gky949

16. DeLano WL. *The PyMOL molecular graphics system*. San Carlos (CA: DeLano Scientific, San Carlos (2002).

17. Sarri CA, Giannoulis T, Moutou KA, Mamuris Z. HLA class II peptide-binding-region analysis reveals funneling of polymorphism in action. *Immunol Lett* (2021) 238:75–95. doi: 10.1016/j.imlet.2021.07.005

18. Bondinas GP, Moustakas AK, Papadopoulos GK. The spectrum of HLA-DQ and HLA-DR alleles, 2006: a listing correlating sequence and structure with function. *Immunogenetics* (2007) 59(7):539–53. doi: 10.1007/s00251-007-0224-8

19. Moriyama H, Abiru N, Paronen J, Sikora K, Liu E, Miao D, et al. Evidence for a primary islet autoantigen (preproinsulin 1) for insulitis and diabetes in the nonobese diabetic mouse. *Proc Natl Acad Sci U.S.A.* (2003) 100(18):10376–81. doi: 10.1073/pnas.1834450100

20. Mannering SI, Harrison LC, Williamson NA, Morris JS, Thearle DJ, Jensen KP, et al. The insulin a-chain epitope recognized by human T cells is posttranslationally modified. *J Exp Med* (2005) 202(9):1191–7. doi: 10.1084/jem.20051251

21. Stamatouli AM, Quandt Z, Perdigoto AL, Clark PL, Kluger H, Weiss SA, et al. Collateral damage: Insulin-dependent diabetes induced with checkpoint inhibitors. *Diabetes* (2018) 67(8):1471–80. doi: 10.2337/dbi18-0002

22. Akturk HK, Couts KL, Baschal EE, Karakus KE, Van Gulick RJ, Turner JA, et al. Analysis of human leukocyte antigen DR alleles, immune-related adverse events, and survival associated with immune checkpoint inhibitor use among patients with advanced malignant melanoma. *JAMA Netw Open* (2022) 5(12):e2246400. doi: 10.1001/jamanetworkopen.2022.46400

23. Miyoshi Y, Ogawa O, Oyama Y. Nivolumab, an anti-programmed cell death-1 antibody, induces fulminant type 1 diabetes. *Tohoku J Exp Med* (2016) 239(2):155–8. doi: 10.1620/tjem.239.155

24. Okamoto M, Okamoto M, Gotoh K, Masaki T, Ozeki Y, Ando H, et al. Fulminant type 1 diabetes mellitus with anti-programmed cell death-1 therapy. *J Diabetes Investig* (2016) 7(6):915–8. doi: 10.1111/jdi.12531

25. Usui Y, Udagawa H, Matsumoto S, Imai K, Ohashi K, Ishibashi M, et al. Association of serum anti-GAD antibody and HLA haplotypes with type 1 diabetes mellitus triggered by nivolumab in patients with non-small cell lung cancer. *J Thorac Oncol* (2017) 12(5):e41–3. doi: 10.1016/j.jtho.2016.12.015

26. Ishikawa K, Shono-Saito T, Yamate T, Kai Y, Sakai T, Shimizu F, et al. A case of fulminant type 1 diabetes mellitus, with a precipitous decrease in pancreatic volume, induced by nivolumab for malignant melanoma: analysis of HLA and CTLA-4 polymorphisms. *Eur J Dermatol* (2017) 27(2):184–5. doi: 10.1684/ejd.2016.2923

27. Kawabata Y, Ikegami H. Genetics of fulminant type 1 diabetes. *Diabetol Int* (2020) 11(4):315–22. doi: 10.1007/s13340-020-00468-0

28. Todd JA, Bell JI, McDevitt HO. HLA-DQ beta gene contributes to susceptibility and resistance to insulin-dependent diabetes mellitus. *Nature* (1987) 329(6140):599–604. doi: 10.1038/329599a0

29. Iwama S, Kobayashi T, Yasuda Y, Arima H. Immune checkpoint inhibitor-related thyroid dysfunction. *Best Pract Res Clin Endocrinol Metab* (2022) 36(3):101660. doi: 10.1210/clinem/dgab829

30. Yoneda S, Imagawa A, Hosokawa Y, Baden MY, Kimura T, Uno S, et al. T-Lymphocyte infiltration to islets in the pancreas of a patient who developed type 1 diabetes after administration of immune checkpoint inhibitors. *Diabetes Care* (2019) 42 (7):e116–8. doi: 10.2337/dc18-2518

frontiers | Frontiers in Immunology

TYPE Original Research
PUBLISHED 19 April 2023
DOI 10.3389/fimmu.2023.1169071

OPEN ACCESS

EDITED BY
Esra Akbay,
University of Texas Southwestern Medical Center, United States

REVIEWED BY
Said Dermime,
National Center for Cancer Care and Research, Qatar
Simrit Parmar,
University of Texas MD Anderson Cancer Center, United States

*CORRESPONDENCE
Zhenyu Li
lizhenyumd@163.com
Kailin Xu
lihmd@163.com
Chong Chen
cchen@xzhmu.edu.cn

†These authors have contributed equally to this work and share first authorship

SPECIALTY SECTION
This article was submitted to Cancer Immunity and Immunotherapy, a section of the journal Frontiers in Immunology

RECEIVED 18 February 2023
ACCEPTED 03 April 2023
PUBLISHED 19 April 2023

CITATION
Liu Y, Jie X, Nian L, Wang Y, Wang C, Ma J, Jiang J, Wu Q, Qiao J, Chen W, Cao J, Yan Z, Shi M, Cheng H, Zhu F, Sang W, Li D, Chen C, Xu K and Li Z (2023) A combination of pre-infusion serum ferritin, CRP and IL-6 predicts outcome in relapsed/refractory multiple myeloma patients treated with CAR-T cells. *Front. Immunol.* 14:1169071. doi: 10.3389/fimmu.2023.1169071

A combination of pre-infusion serum ferritin, CRP and IL-6 predicts outcome in relapsed/refractory multiple myeloma patients treated with CAR-T cells

Yang Liu[1,2,3†], Xingxing Jie[1,2,3†], Li Nian[1,2,3†], Ying Wang[1,2,3], Congyue Wang[1,2,3], Jin Ma[1,2,3], Jingjing Jiang[1,2,3], Qingyun Wu[1,2,3], Jianlin Qiao[1,2,3], Wei Chen[1,2,3], Jiang Cao[1,2,3], Zhiling Yan[1,2,3], Ming Shi[4], Hai Cheng[1,2,3], Feng Zhu[1,2,3], Wei Sang[1,2,3], Depeng Li[1,2,3], Chong Chen[1,2,3*], Kailin Xu[1,2,3*] and Zhenyu Li[1,2,3*]

[1]Blood Diseases Institute, Xuzhou Medical University, Xuzhou, Jiangsu, China, [2]Department of Hematology, The Affiliated Hospital of Xuzhou Medical University, Xuzhou, Jiangsu, China, [3]Jiangsu Key Laboratory of Bone Marrow Stem Cells, Xuzhou, Jiangsu, China, [4]Cancer Institute, Xuzhou Medical University, Xuzhou, Jiangsu, China

Background: Chimeric antigen receptor - T (CAR-T) cell therapy has shown remarkable efficacy in patients with relapsed/refractory multiple myeloma (R/R MM). However, a subset of patients still experienced progression or relapse, and the predictors of prognosis are little known. We analyzed the inflammatory markers before CAR-T cell infusion, to clarify their correlation with survival and toxicity.

Methods: This study involved 109 R/R MM patients who received CAR-T therapy between June 2017 and July 2021. Inflammatory markers, including ferritin, c-reactive protein (CRP), and interleukin-6 (IL-6) before CAR-T cell infusion were detected and then categorized by quartiles. Adverse events and clinical outcomes were compared between patients with upper quartile of inflammatory markers and patients with lower three quartiles of inflammatory markers. An inflammatory prognostic index (InPI) based on these three inflammatory markers was developed in this study. Patients were divided into 3 groups according to the InPI score, progression-free survival (PFS) and overall survival (OS) were compared among the groups. In addition, we explored the correlation between cytokine release syndrome (CRS) and pre-infusion inflammatory markers.

Results: We found that the pre-infusion high ferritin (hazard ratio [HR], 3.382; 95% confidence interval [CI], 1.667 to 6.863; P = .0007), high CRP (HR, 2.043; 95% CI, 1.019 to 4.097; P = .044), and high IL-6 (HR, 3.298; 95% CI, 1.598 to 6.808; P = .0013) were significantly associated with inferior OS. The formula of the InPI score was based on the HR value of these 3 variables. Three risk groups were formed: (good, 0 to 0.5 point; intermediate, 1 to 1.5 points; poor, 2 to 2.5 points). Median OS for patients with good, intermediate, and poor InPI was not reached, 24 months, and 4 months, respectively, and median PFS was 19.1

months, 12.3 months, and 2.9 months, respectively. In the cox proportional hazards model, poor InPI remained an independent prognostic factor for PFS and OS. Pre-infusion ferritin was negatively associated with CAR T-cell expansion normalized to baseline tumor burden. Spearman correlation analysis showed that pre-infusion ferritin and IL-6 levels positively correlated with the grade of CRS (P = .0369 and P = .0117, respectively). The incidence of severe CRS was higher in patients with high IL-6 compared with patients with low IL-6 (26% *vs*. 9%, P = .0405). Pre-infusion ferritin, CRP and IL-6 were positively correlated with each peak values within the first month after infusion.

Conclusions: Our results suggest that patients with elevated inflammation markers before CAR-T cell infusion are more likely to have poor prognosis.

KEYWORDS

chimeric antigen receptor T cell, relapsed/refractory, multiple myeloma, prognostic predictor, inflammation

Introduction

Chimeric antigen receptor - T (CAR – T) cells, which could recognize and kill tumor cells through major histocompatibility complex (MHC)-unrestricted pattern, is very promising in the era of immunotherapy (1). Multiple clinical trials have demonstrated unprecedented response rates of anti-BCMA CAR-T therapy in relapsed/refractory multiple myeloma (R/R MM) patients, regardless of previous treatment, ISS stage and cytogenetic risk (2). However, there was significant discrepancy in respect to long-term outcomes, and some patients experienced early progression or relapse (3, 4). Efforts have been made to boost and prolong the efficacy, including *in vitro* enriching memory phenotype T cells through culturing CAR-T cells with PI3K inhibitors (5), combination of γ-secretase inhibitor to increase the BCMA expression on the surface of MM cells (6) and "armed" CAR-T cells to transform an immune-suppressive signal into an immune-stimulatory signal (7).

Although the improvement of CAR-T cells and the exploration of new targets are undoubtedly critical, the identification of prognostic markers is also needed to help us distinguishing patients with poor prognosis for early intervention. It is generally believed that inflammation is critical for the oncogenesis and progression of tumor (8). A peripheral pro-inflammatory status has been reported to be related with worse outcomes in tumor patients treated with immune checkpoint inhibitors (9–11). Inflammatory markers, such as ferritin, c-reactive protein (CRP) and interleukin-6 (IL-6) have been widely proved to be related with cytokine release syndrome (CRS) during CAR-T cell therapy (12–15). The occurrence of severe CRS is associated with high early mortality (16), and the CRS-related complications such as delayed hematopoietic recovery, coagulopathy and cardiac disorders will also dispose patients to poor outcomes (17–19). To date, there are limited data regarding the correlation of circulating inflammatory markers and the prognosis of CAR-T therapy in the setting of MM. Herein, we conducted a retrospective study to clarify their correlation in a relatively large cohort of 109 R/R MM patients.

Patients and methods

Study population

This retrospective study included 109 patients with R/R MM treated with anti-BCMA CAR-T cells alone (Chinese Clinical Trial Registry, ChiCTR-1900026219) or combined with anti-CD19 CAR-T cells (ChiCTR-OIC-17011272) at the Affiliated Hospital of Xuzhou Medical University between June 2017 and July 2021. This study was approved by the Ethics Committee of Affiliated Hospital of Xuzhou Medical University and was conducted in accordance with the Declaration of Helsinki. The detailed inclusion and exclusion criteria could refer to previous studies (20, 21). Lymphodepletion conditioning chemotherapy was carried out in all patients, the regimen was fludarabine (30 mg/m^2/d, days -5 to -3) and cyclophosphamide (750 mg/m^2/d, day -5).

Data collection and therapeutic evaluation

Disease characteristics of patients were collected at enrollment, including age, gender, MM type, prior treatment, cytogenetic abnormalities. Laboratory data was obtained by retrieving electronic medical records. Baseline lactate dehydrogenase, albumin and beta-2 microglobulin data were defined as the latest data within 15 days prior to lymphodepletion. Baseline values of ferritin, CRP, and IL-6 were collected within 3 days before the CAR-T cell infusion, peak values were collected during the first month after infusion. CAR-T cell counts in peripheral blood were

measured by flow cytometry at day 7, day 14, day 21, and day 28 post infusion. Efficacy was assessed according to the International Myeloma Working Group criteria (22). The severity of cytokine release syndrome (CRS) was evaluated according to the ASTCT consensus (23).

Statistical analysis

The deadline of follow-up for this study was August 31, 2022. OS was defined as the time from CAR T-cell infusion to death of any cause. Progression-free survival (PFS) was calculated from infusion to disease progression or death. Duration of response (DOR) was defined as the time from first partial response (PR) to progression or death. Quartile analysis was used to define the patients with high ferritin, high CRP and high IL-6, i.e., the upper quartile defined as high value, the lower three quartiles defined as low value. The difference between categorical variables was analyzed by Fisher's exact test. The correlation between continuous variables was calculated by Spearman's rank-order test. The log-rank test was used to compare the survival difference between groups. Factors with a P value <.2 or with clinical significance were included in the multivariate cox proportional hazards model. Two-sided P value <.05 was considered statistically significant. Statistical analysis was performed using SPSS 19.0 (IBM Corp., Armonk, NY, USA).

Results

Patient characteristics

Baseline characteristics of 109 patients with R/R MM treated with CAR-T cells are summarized in Table 1. The median age was 57 years (range, 30 to 70 years). 59% of the patients were male. At enrollment, 32 (29%) of the patients had extramedullary disease (EMD), 22 (20%) had high-risk cytogenetics aberrations, 37 (34%) had revised international staging system (R-ISS) stage III diseases. Patients had a median of 4 lines of prior therapy. A total of 28% patients received prior autologous hematopoietic stem cell transplantation. The pre-infusion median ferritin was 469.2ng/mL (interquartile range [IQR], 251.8 – 882.3 ng/mL), and 62 (57%) patients had ferritin above the upper limit of normal (ULN). Median CRP was 5mg/L (IQR, 1.9 – 20.3 mg/L), and above the ULN in 53 (49%) patients. Median IL-6 was 7.6pg/mL (IQR, 3 – 14.1 pg/mL), and above the ULN in 55 (50%) patients.

Correlation between pre-infusion inflammatory markers and patient characteristics

Quartiles method was used to classify patients with high ferritin (> 882.3 ng/mL), high CRP (> 20.3 mg/L) and high IL-6 (> 14.1 pg/mL), i.e., the upper quartile was defined as high value. We then analyzed the correlation between these inflammatory markers and patients' clinical and biological indicators. Both age, gender, high-risk cytogenetic, prior treatment and disease stage had no correlation with high-level pre-infusion inflammatory markers (Table S1). Interestingly, a significant higher proportion of patients with light chain myeloma had high ferritin (46% *vs.* 17%, $P = .0021$), high CRP (39% *vs.* 20%, $P = .039$), and high IL-6 (39% *vs.* 20%, $P = .039$) compared with those with non-light chain myeloma (Table S1). Patients with high ferritin had a higher tumor burden (median plasma cells in bone marrow, 38% *vs* 11%, $P = .003$) than those with low ferritin, also, there was a weak but significant association between ferritin levels and tumor burden (Spearman r = 0.2543, $P = .0076$) (Table S1 and Figure S1). However, we found

TABLE 1 Baseline characteristics of 109 patients.

Variable	Overall (N = 109)
Age, years, median (range)	57 (30 - 72)
Gender, Male, n (%)	64 (59%)
Extramedullary disease, n (%)	32 (29%)
MM type, n (%)	
IgG	47 (43%)
IgA	22 (20%)
IgD	8 (7%)
Light chain	28 (26%)
Nonsecretory	4 (4%)
High-risk cytogenetics*, n (%)	22 (20%)
R-ISS, n (%)	
Stage I + II	72 (66%)
Stage III	37 (34%)
High tumor burden†, n (%)	27 (25%)
Prior lines of therapy, median (range)	4 (1 - 17)
Prior ASCT, n (%)	31 (28%)
CAR construct, n (%)	
CD19 + BCMA	66 (61%)
BCMA	43 (39%)
Pre-infusion ferritin, ng/mL, median (range)	469.2 (14.6 - 5000)
Pre-infusion CRP, mg/L, median (range)	5 (0.2 – 241.7)
Pre-infusion IL-6, pg/mL, median (range)	7.6 (1 - 60)
Pre-LD LDH, U/L, median (range)	205 (110 - 2101)
Pre-LD β2-MG, ng/ml, median (range)	2970 (838 - 20000)
Pre-LD albumin, g/L, median (range)	39.3 (22.1 - 60.1)

*High-risk: presence of del(17p) and/or translocation t (4;14) and/or translocation t (14;16).
†High tumor burden: defined as ≥ 50% clonal plasma cells or bone marrow plasma cells.
R-ISS, revised - international staging system; ASCT, autologous hematopoietic stem cell transplantation; CRP, c-reactive protein; IL-6, interleukin-6; Pre-LD, pre - lymphodepletion; LDH, lactate dehydrogenase; β2-MG, beta-2 microglobulin.

no correlation between pre-infusion CRP and IL-6 with tumor burden.

Relationship between pre-infusion inflammatory markers and treatment response

The overall response rate was 85% (93/109) within 3 months after the infusion of CAR-T cells. Seventy-nine patients achieved a very good partial response (VGPR) or better response, and these patients had lower pre-infusion ferritin and IL-6, but not statistically significant (Figure S2). Except for high ferritin tended to be associated with decreased VGPR or better response rate (59% *vs.* 77%, P = .087), we found no significant association between other inflammatory markers and response rates (Table S2).

We further evaluated if there was a relationship between pre-infusion inflammatory markers and *in vivo* CAR T-cell expansion. However, Pre-infusion ferritin, CRP, and IL-6 were not associated directly with *in vivo* CAR T-cell expansion at indicated time points (days 7, 14, 21, and 28 post infusion) (Figure S3). Interestingly, ferritin, but not CRP and IL-6, was significantly (P <.05) but modestly (Spearman r < -0.3) associated with lower CAR T-cell expansion normalized to baseline tumor burden at days 7, 14, and 21 post infusion (Figures 1, S4).

High inflammatory markers were associated with decreased PFS and OS

The patients with high ferritin had significantly poorer OS and PFS compared with those with low ferritin (median OS: 14 months *vs.* 50.2 months, HR 3.382, P = .0007; median PFS: 5.7 months *vs.* 19

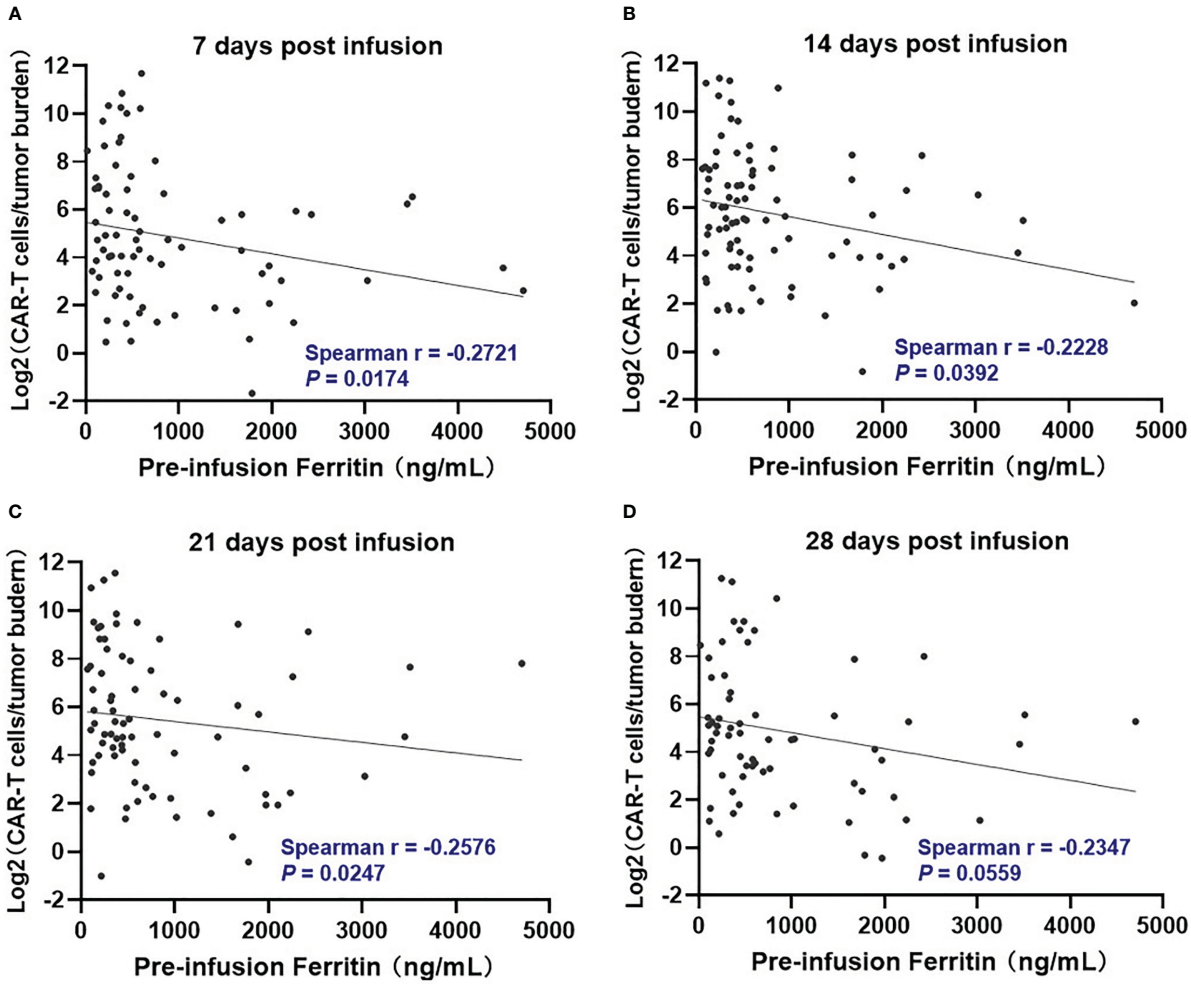

FIGURE 1
Correlation between pre-infusion ferritin and *in vivo* CAR T-cell expansion normalized to tumor burden during the first month following CAR-T cell infusion. At day 7, 14, and 21 post infusion **(A–C)**, CAR-T cell expansion normalized to baseline tumor burden was negatively correlated with ferritin, and the correlation did not remain at day 28 **(D)**. Tumor burden was defined as percentage of plasma cells in bone marrow. Spearman r value was calculated using the Spearman's correlation test.

months, HR 2.611, P = .0015) (Figures 2A, 3A). High IL-6 also had similar adverse effects on OS and PFS (median OS: 14 months *vs.* not reached (NR), HR 3.298, P = .0013; median PFS: 8.4 months *vs.* 17.8 months, HR 2.026, P = .018) (Figures 2C, 3C). Patients with high CRP had inferior OS than patients with low CRP (median of 15.4 months *vs.* 36.5 months, HR 2.043, P = .044), but the difference in PFS was not significant (median of 10.3 months *vs.* 16.5 months, HR 1.261, P = .4142) (Figures 2B, 3B).

Based on the HR values of ferritin, CRP and IL-6, inflammatory prognostic index (InPI) was developed, 0.5 point was assigned to high CRP, and 1 point was each assigned to high ferritin and high IL-6. According to the InPI score, patients were divided into 3 risk categories: good, 0 to 0.5 point; intermediate, 1 to 1.5 points; poor, 2 to 2.5 points. 67 (61%) of the patients had good InPI, 30 (28%) had intermediate InPI, and 12 (11%) had poor InPI. The median OS for patients with good, intermediate, and poor InPI was NR, 24 months (95% CI, 17.3 months to 30.7 months), and 4 months (95% CI, 0 to 9.4 months), respectively, and median PFS was 19.1 months (95% CI, 12.2 months to 26.0 months), 12.3 months (95% CI, 9.8 months to 14.9 months), and 2.9 months (95% CI, 0 to 6.8 months), respectively (both P <.0001) (Figures 2D, 3D).

To further determine whether InPI index was an independent prognostic factor for PFS and OS, we introduced potential influence covariates, including age, gender, EMD, number of therapy lines, type of MM, high-risk cytogenetic, R-ISS stage, tumor burden and InPI into cox proportional hazard model. The results showed that high InPI score still had independent adverse influence on OS (P = .009) and PFS (P = .01) even after adjusting for tumor burden (Table 2). In addition, high tumor burden was independent risk factor for PFS (HR: 2.512, 95% CI: 1.408 – 4.48, P = .002) and OS (HR: 2.249, 95% CI: 1.091 – 4.637, P = .028). EMD was independent risk factor for OS (HR: 2.077, 95% CI: 1.015 – 4.251, P = .046).

High inflammatory markers were associated with decreased DOR

Pre-infusion increases in ferritin and IL-6, but not CRP, were significantly associated with decreased DOR (HR 2.269, 95% CI 1.152 to 4.469, P = .0179, for high ferritin; HR 2.224, 95% CI 1.130 to 4.377, P = .0207, for high IL-6) (Figures S5A–C). The median

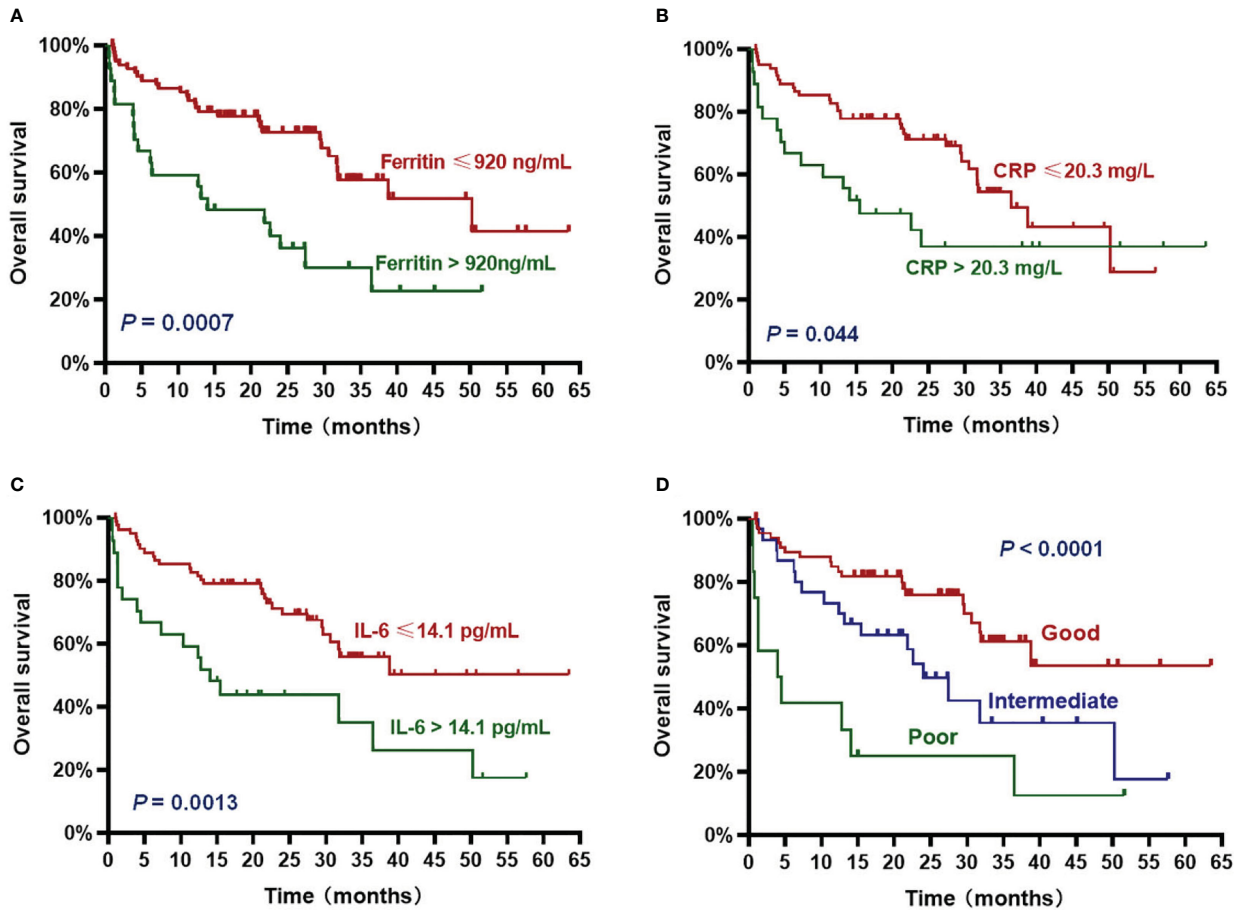

FIGURE 2
Overall survival (OS) according to inflammatory markers and InPI index. The patients with ferritin > 920 ng/mL **(A)**, CRP > 20.3 mg/L **(B)**, IL-6 > 14.1 pg/mL **(C)** and intermediate to poor InPI **(D)** had inferior OS. Survival curves were drawn according to the Kaplan-Meier method. The log-rank test was used to compare the difference in survival probability between two groups.

DOR for patients with good, intermediate, and poor InPI was 21.1 months (95% CI, 14.1 months to 28.1 months), 13.8 months (95% CI, 6.4 months to 21.2 months), and 4 months (95% CI, 1.2 months to 6.8 months), respectively (Figure S5D).

The correlation between pre-infusion inflammatory markers and CRS

Of all patients, 91% experienced CRS. Grade 3 or higher CRS, defined as severe CRS, occurred in 14 (13%) patients. Median time to onset of CRS was 7d (0 – 28d), median duration of CRS was 4d (1d - 25d). Patients with lower pre-infusion concentration of ferritin and IL-6 were more likely to develop non-severe CRS than severe CRS (Table 3). When considering the severity of CRS as continuous variable, the levels of pre-infusion serum IL-6 (Spearman r = 0.241, $P = .0117$) and ferritin (Spearman r = 0.2, $P = .0369$) were positively correlated with the grade of CRS, no correlation was found between CRP concentration and CRS grade (Figures 4A–C). In addition, there was no correlation between inflammatory markers and the onset time of CRS or duration of CRS (Figures 4D–I). Furthermore, we found that the levels of pre-infusion ferritin, CRP and IL-6 were positively correlated with the post-infusion peak values of each of these markers (Spearman r = 0.49, $P < .0001$; Spearman r = 0.428, $P < .0001$; Spearman r = 0.352, $P = .0002$; respectively) (Figures 5A, E, I). Pre-infusion ferritin correlated with the peak values of CRP and IL-6 (Figures 5B, C), but the peak ferritin did not correlate with pre-infusion CRPand IL-6 (Figures 5D, G). There were positive correlations between IL-6 and CRP, regardless of baseline and peak values (Figures 5F, H). The InPI score also had positive correlation with the post-infusion peak levels of ferritin, CRP and IL-6 (Figures 5J–L).

Discussion

Due to the high financial cost and the potentially life-threatening toxicities, it is of particular importance to early identify patients who will not benefit or less benefit from CAR-T cell therapy. Except for EMD, there are still no validated biomarkers for predicting prognosis in R/R MM patients following CAR-T therapy.

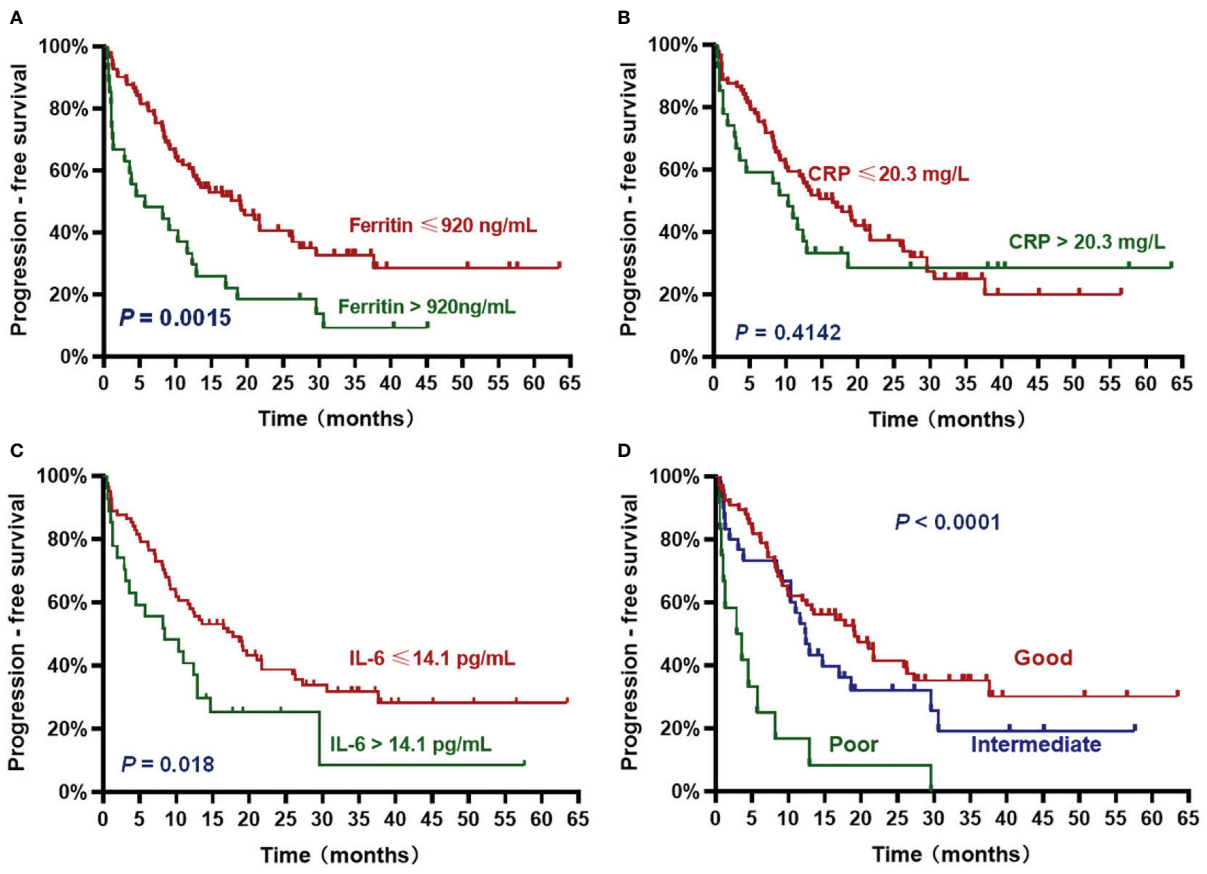

FIGURE 3
Progression-free survival (PFS) according to inflammatory markers and InPI index. The patients with ferritin > 920 ng/mL **(A)**, IL-6 > 14.1 pg/mL **(C)** and intermediate to poor InPI **(D)** had inferior PFS. No significant association was found between CRP and PFS **(B)**. Survival curves were drawn according to the Kaplan-Meier method. The log-rank test was used to compare the difference in survival probability between two groups.

TABLE 2 Univariate and multivariate analysis of PFS and OS.

	Progression-free survival (PFS)				Overall survival (OS)			
	Univariate		Multivariate		Univariate		Multivariate	
	HR (95% CI)	P	HR (95% CI)	P	HR (95% CI)	P	HR (95% CI)	P
Age, >60 years	0.888 (0.548 – 1.44)	0.6301			0.9689 (0.519 – 1.808)	0.9209		
Gender, male	1.117 (0.699 – 1.783)	0.644			1.059 (0.590 – 1.901)	0.8482		
Prior lines of therapy, ≥ 6	1.359 (0.802 – 2.305)	0.2541			1.317 (0.687 – 2.524)	0.4069		
MM type, Light chain	1.456 (0.839 – 2.528)	0.182			2.165 (1.075- 4.36)	0.0305	1.909 (0.915 – 3.983)	0.085
Extramedullary disease	1.788 (1.03 – 3.103)	0.039			2.727 (1.347 - 5.519)	0.0053	2.077 (1.015 – 4.251)	0.046
Cytogenetics, high-risk	1.67 (0.88 – 3.168)	0.1167			1.614 (0.749 – 3.48)	0.2218		
High tumor burden	3.456 (1.867 – 6.399)	< 0.0001	2.512 (1.408 – 4.48)	0.002	2.68 (1.315 – 5.463)	0.0067	2.249 (1.091 – 4.637)	0.028
Pre-LD LDH, > ULN	1.252 (0.7771 – 2.018)	0.3555			0.9592 (0.5322 – 1.729)	0.8896		
Pre-LD β2-MG, ≥ 5500ng/ml	1.295 (0.7013 – 2.393)	0.4083			2.386 (1.121 – 5.078)	0.024		
Pre-LD serum albumin, < 35 g/L	1.43 (0.847 – 2.415)	0.1806			1.39 (0.7329 – 2.637)	0.3132		
R-ISS, stage III	1.159 (0.709 – 1.893)	0.5562			1.266 (0.691 – 2.318)	0.4459		
InPI		<0.0001		0.009		<0.0001		0.01
good	Ref.		Ref.		Ref.		Ref.	
intermediate	1.367 (0.813 – 2.298)	0.238	1.095 (0.608 – 1.971)	0.762	2.102 (1.106 – 3.996)	0.023	1.412 (0.672 – 2.967)	0.362
poor	4.199 (2.177 – 8.102)	<0.0001	3.689 (1.571 – 8.664)	0.003	4.957 (2.316 – 10.61)	<0.0001	4.85 (1.736 – 13.553)	0.003

InPI, inflammatory prognostic index; ULN, upper limit of normal.

TABLE 3 Association between pre-infusion inflammatory markers and CRS.

	No-severe CRS	Severe CRS	P
Ferritin			0.1063
> 920 ng/mL (n = 27)	21 (78%)	6 (22%)	
≤ 920 ng/mL (n = 82)	74 (90%)	8 (10%)	
C-reactive protein			0.329
> 20.3 mg/L (n = 27)	22 (81%)	5 (19%)	
≤ 20.3 mg/L (n = 82)	73 (89%)	9 (11%)	
Interleukin-6			0.0405
> 14.1 pg/mL (n = 27)	20 (74%)	7 (26%)	
≤ 14.1 pg/mL (n = 82)	75 (91%)	7 (9%)	

Severe CRS defined as grade 3 or higher CRS.
Two-sided P values were calculated using the Fisher's exact test.

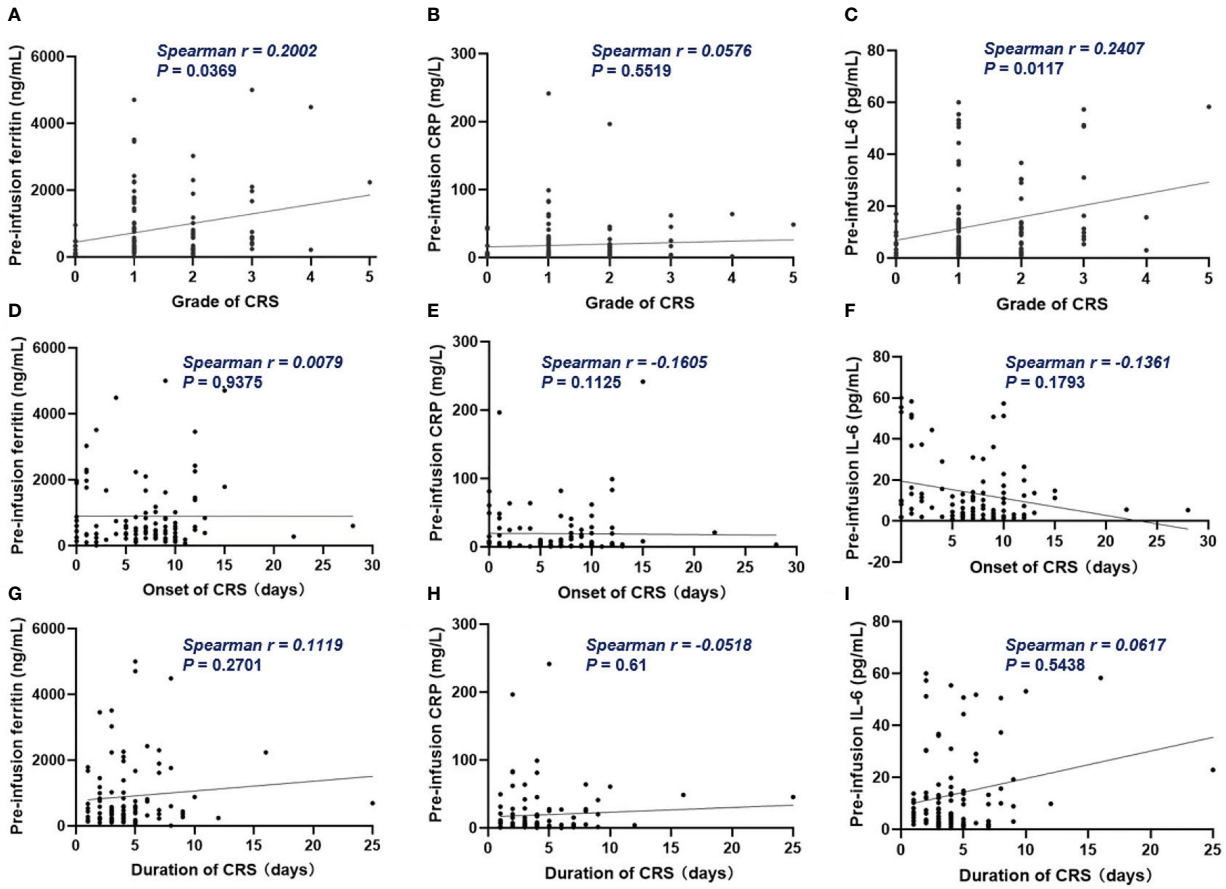

FIGURE 4
The correlation between inflammatory markers and CRS. **(A, C)** Pre-infusion ferritin and IL-6 correlated with the grade of CRS. **(B)** Pre-infusion CRP had no correlation with the grade of CRS. **(D–I)** The pre-infusion ferritin, CRP and IL-6 had no correlation with the onset and the duration of CRS. Spearman r value was calculated using the Spearman's correlation test.

A cohort of 17 patients treated with LCAR-B38M revealed that EMD and anti-CAR T antibody constituted risk factors for early recurrence and progression (24). Que and colleagues found that the patients who had more than 6 lines of prior therapy had shorter PFS and OS, but when incorporating EMD into multivariate analysis, > 6 lines of therapy lost its predictive value, only EMD being an independently significant prognostic factor (25). Recently, zhang et al. reported that EMD, light chain type, high-risk cytogenetics, and > 3 prior therapeutic lines were independent risk factors of PFS, ECOG score of 2 and light chain type were independent risk factors of OS (26). Our results also showed that EMD was an independent risk factor that associated with OS. Besides, light chain type MM was identified as one of the risk factors for inferior OS in the univariate analysis, a marginal significant correlation remained in the multivariate analysis, though the exact mechanism is not clear. We think it deserve further study to verify and make clear of these findings.

An in-depth analysis from ZUMA-1 study in large B-cell lymphoma demonstrated that the levels of ferritin and IL-6 before CAR-T cell infusion had negative correlation with durable remission rates (27). One real world study of Axicabtagene Ciloleucel in patients with R/R B-cell non-Hodgkin lymphoma suggested that low CRP levels at baseline was associated with better response (28). However, the effect of inflammation on the prognosis of CAR-T therapy has not been reported in myeloma patients. Hence, we conducted a *post-hoc* analysis to elucidate their correlation. Our study proved that both pre-infusion high ferritin, high IL-6, and high CRP were risk factors for long-term survival, and patients with high ferritin and high IL-6 had shorter duration of remission. Further, we established a scoring system based on these three inflammatory indicators, defined as InPI index in this context. The InPI index helped us distinguished three groups of patients with different prognosis, the patients with a score of 2 to 2.5 points had the worst survival. Since high inflammation might partly be a proxy for disease burden or aggressive disease, we therefore brought variables that pertain to disease burden into multivariate analysis to determine the independent effect of InPI index. The results showed that after account for high tumor burden and EMD, poor InPI remained an independent predictor for durable remission and survival.

Inflammation has been extensively studied in the malignant progression of tumors, either by acting on cancerous cells or by

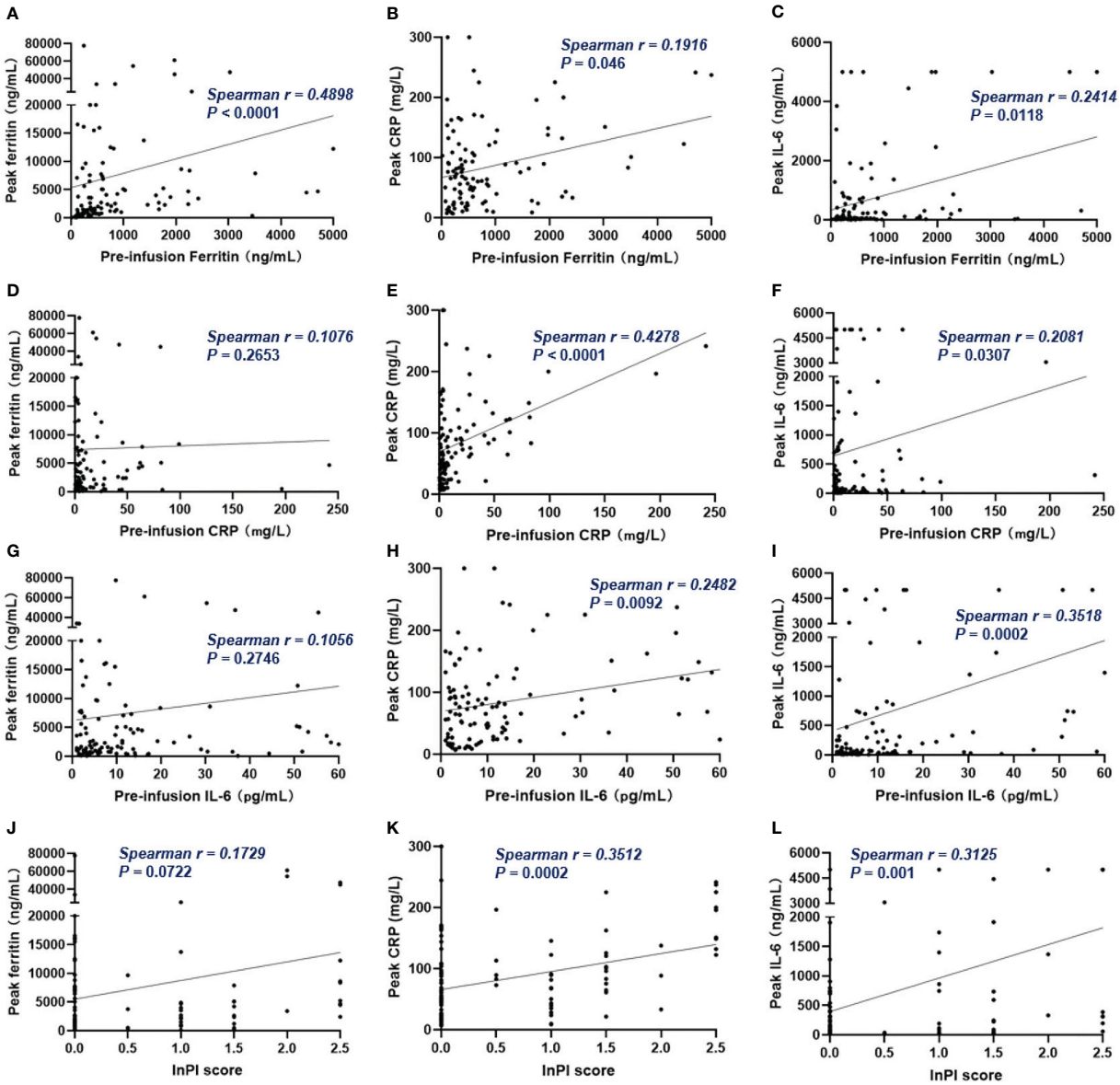

FIGURE 5
The correlation between pre-infusion inflammatory markers, InPI score and the post-infusion peak inflammatory markers. **(A–C)** Pre-infusion levels of ferritin correlated with the peak values of ferritin, CRP and IL-6. **(D, G)** Pre-infusion CRP and IL-6 had no correlation with peak ferritin. **(E, F)** Pre-infusion CRP correlated with peak CRP and IL-6. **(H, I)** Pre-infusion IL-6 correlated with peak CRP and IL-6. **(J–L)** InPI score positively correlated with peak ferritin, CRP, and IL-6. Spearman r value was calculated using the Spearman's correlation test.

acting on anti-tumor immunity (29, 30). The pro-inflammatory cytokine IL-6 might impair anti-tumor immunity through multi-aspect. It could restrict the differentiation of Th1 cells and decrease the production of interferon-γ, resulting in less mounting of CD8+ cytotoxic T cells in anti-tumor response (31). Besides, IL-6 could promote the differentiation of Th2 and Th17 cells, thereby tilt anti-tumor immune response to an immunosuppressive response (32, 33). Acute phase proteins such as CRP, fibrinogen and ferritin could be rapidly synthesized in liver after the stimulation of IL-6 (34). Our study also showed that high-level ferritin at baseline might adversely influence *in vivo* CAR-T amplification. These and our results led to a hypothesis that inflammation might be one of the most relevant factors for disease progression and long-term survival in CAR-T therapy, partially by affecting the activation and expansion of effector T cells.

Despite the superior efficacy of CAR-T therapy, its benefits might be offset by the serious adverse effects after infusion. CRS and immune effector cell-associated neurotoxicity syndrome (ICANS) are common adverse effects which are associated with endothelial activation injury and cytokine release. Due to the low incidence of ICANS in our center, we did not further discuss it. According to our recently published data, the occurrence of severe CRS was

associated with poorer survival (15). Therefore, it is necessary to identify patients who will develop severe CRS preemptively. In this study, we found that the patients with high ferritin and IL-6 before CAR-T infusion had increased rates of severe CRS, and these inflammatory markers' baseline levels positively correlated with the peak values after infusion. Peak levels of inflammatory markers had been reported to be correlated with the occurrence and the severity of CRS (35–38). Hay and colleagues reported that the pre-existing endothelial activation before conditioning and CAR-T cell infusion might increase the risk of severe CRS in patients receiving anti-CD19 CAR-T treatment (39). Researchers from University of Pennsylvania found that blood vessel endothelial cells are a key source of IL-6 during CRS (40). Together, these findings indicated that elevated pre-infusion inflammation might increase the risk of developing severe CRS. Although the small sample size of severe CRS in our cohort may limit the statistical power to detect the effect of pre-infusion inflammation on CRS, these might be important markers of concern. As the current predictive power of peak inflammatory markers usually occurs after severe symptoms have already appeared.

To our knowledge, this is the first study to illustrate the importance of pre-infusion inflammation on prognosis in R/R MM patients receiving CAR-T cell therapy. However, there are some limitations to our study. It is a single-center retrospective study. We had limited data to interpret the effect of inflammation at the time of apheresis on prognosis. In addition, because our findings were from a retrospective study, we did not take special interventions to ameliorate inflammation before CAR-T cell infusion. We also appreciate that there will be prospective studies to validate our findings by using commercial CAR-T products.

Conclusion

In conclusion, pre-infusion inflammation markers were useful predictors of durable remission and long-term survival, and might be risk factors for the subsequent development of severe CRS. Our data suggest that treating patients' pre-infusion inflammation earlier in their course may improve durability of response to CAR-T cell therapy.

Data availability statement

The raw data supporting the conclusions of this article will be made available by the authors, without undue reservation.

Ethics statement

The studies involving human participants were reviewed and approved by Ethics committee of the Affiliated Hospital of Xuzhou Medical University. The patients/participants provided their written informed consent to participate in this study.

Author contributions

ZL, KX and CC designed the study. YW, WC, JC, ZY, HC, FZ, WS, QW, CC and DL were responsible for patient enrollment. YL, XJ, LN, CW, JM and JJ collected the data. MS was responsible for the generation of CAR-T cells. YL and LN performed statistical analysis. YL wrote the manuscript. ZL, JQ, CC and KX revised the manuscript. All authors contributed to the article and approved the submitted version.

Funding

This work was supported by funding from the National Natural Science Foundation of China (grant 81770223, 82171762 and 82270232), Research and practice innovation program for Postgraduates of Jiangsu Province (KYCX22_2940).

Acknowledgments

We would like to thank all the patients and their families who participated in this study.

Conflict of interest

The authors declare that the research was conducted in the absence of any commercial or financial relationships that could be construed as a potential conflict of interest.

Publisher's note

Supplementary material

The Supplementary Material for this article can be found online at: https://www.frontiersin.org/articles/10.3389/fimmu.2023.1169071/full#supplementary-material

References

1. Benmebarek MR, Karches CH, Cadilha BL, Lesch S, Endres S, Kobold S, et al. Killing mechanisms of chimeric antigen receptor (CAR) T cells. *Int J Mol Sci* (2019) 20 (6). doi: 10.3390/ijms20061283

2. Parikh RH, Lonial S. Chimeric antigen receptor T-cell therapy in multiple myeloma: a comprehensive review of current data and implications for clinical practice. *CA Cancer J Clin* (2023). doi: 10.3322/caac.21771

3. Munshi NC, Anderson LJ, Shah N, Madduri D, Berdeja J, Lonial S, et al. Idecabtagene vicleucel in relapsed and refractory multiple myeloma. *N Engl J Med* (2021) 384(8):705–16. doi: 10.1056/NEJMoa2024850

4. Martin T, Usmani SZ, Berdeja JG, Agha M, Cohen AD, Hari P, et al. Ciltacabtagene autoleucel, an anti-b-cell maturation antigen chimeric antigen receptor T-cell therapy, for Relapsed/Refractory multiple myeloma: CARTITUDE-1 2-year follow-up. *J Clin Oncol* (2022) 41(6):1265-74. doi: 10.1200/JCO.22.00842

5. Raje NS, Shah N, Jagannath S, Kaufman JL, Siegel DS, Munshi NC, et al. Updated clinical and correlative results from the phase I CRB-402 study of the BCMA-targeted CAR T cell therapy bb21217 in patients with relapsed and refractory multiple myeloma. *Blood* (2021) 138(Supplement 1):548. doi: 10.1182/blood-2021-146518

6. Cowan AJ, Pont M, Dukesather B, TurtleMBBS CJ, Till BG, Nagengast AM, et al. Efficacy and safety of fully human bcma CAR T cells in combination with a gamma secretase inhibitor to increase bcma surface expression in patients with relapsed or refractory multiple myeloma. *Blood* (2019) 134(Supplement 1):204. doi: 10.1182/blood-2019-129405

7. Liu H, Lei W, Zhang C, Yang C, Wei J, Guo Q, et al. CD19-specific CAR T cells that express a PD-1/CD28 chimeric switch-receptor are effective in patients with PD-L1-positive b-cell lymphoma. *Clin Cancer Res* (2021) 27(2):473–84. doi: 10.1158/1078-0432.CCR-20-1457

8. Coussens LM, Werb Z. Inflammation and cancer. *Nature* (2002) 420(6917):860–7. doi: 10.1038/nature01322

9. Mezquita L, Auclin E, Ferrara R, Charrier M, Remon J, Planchard D, et al. Association of the lung immune prognostic index with immune checkpoint inhibitor outcomes in patients with advanced non-small cell lung cancer. *JAMA Oncol* (2018) 4 (3):351–7. doi: 10.1001/jamaoncol.2017.4771

10. Laino AS, Woods D, Vassallo M, Qian X, Tang H, Wind-Rotolo M, et al. Serum interleukin-6 and c-reactive protein are associated with survival in melanoma patients receiving immune checkpoint inhibition. *J Immunother Cancer* (2020) 8(1). doi: 10.1136/jitc-2020-000842

11. Keegan A, Ricciuti B, Garden P, Cohen L, Nishihara R, Adeni A, et al. Plasma IL-6 changes correlate to PD-1 inhibitor responses in NSCLC. *J Immunother Cancer* (2020) 8(2):e678. doi: 10.1136/jitc-2020-000678

12. Greenbaum U, Strati P, Saliba RM, Torres J, Rondon G, Nieto Y, et al. CRP and ferritin in addition to the EASIX score predict CAR-t-related toxicity. *Blood Adv* (2021) 5(14):2799–806. doi: 10.1182/bloodadvances.2021004575

13. Tedesco VT, Mohan C. Biomarkers for predicting cytokine release syndrome following CD19-targeted CAR T cell therapy. *J Immunol* (2021) 206(7):1561–8. doi: 10.4049/jimmunol.2001249

14. Teachey DT, Lacey SF, Shaw PA, Melenhorst JJ, Maude SL, Frey N, et al. Identification of predictive biomarkers for cytokine release syndrome after chimeric antigen receptor T-cell therapy for acute lymphoblastic leukemia. *Cancer Discov* (2016) 6(6):664–79. doi: 10.1158/2159-8290.CD-16-0040

15. Wang X, Zhao L, Wang J, Yao Y, Wang J, Ji S, et al. Correlation of cytokine release syndrome with prognosis after chimeric antigen receptor T cell therapy: analysis of 54 patients with relapsed or refractory multiple myeloma. *Front Immunol* (2022) 13:814548. doi: 10.3389/fimmu.2022.814548

16. Hernani R, Benzaquen A, Solano C. Toxicities following CAR-T therapy for hematological malignancies. *Cancer Treat Rev* (2022) 111:102479. doi: 10.1016/j.ctrv.2022.102479

17. Qi K, Yan Z, Cheng H, Chen W, Wang Y, Wang X, et al. An analysis of cardiac disorders associated with chimeric antigen receptor T cell therapy in 126 patients: a single-centre retrospective study. *Front Oncol* (2021) 11:691064. doi: 10.3389/fonc.2021.691064

18. Li H, Zhao L, Sun Z, Yao Y, Li L, Wang J, et al. Prolonged hematological toxicity in patients receiving BCMA/CD19 CAR-t-cell therapy for relapsed or refractory multiple myeloma. *Front Immunol* (2022) 13:1019548. doi: 10.3389/fimmu.2022.1019548

19. Jiang H, Liu L, Guo T, Wu Y, Ai L, Deng J, et al. Improving the safety of CAR-T cell therapy by controlling CRS-related coagulopathy. *Ann Hematol* (2019) 98(7):1721–32. doi: 10.1007/s00277-019-03685-z

20. Yan Z, Cao J, Cheng H, Qiao J, Zhang H, Wang Y, et al. A combination of humanised anti-CD19 and anti-BCMA CAR T cells in patients with relapsed or refractory multiple myeloma: a single-arm, phase 2 trial. *Lancet Haematol* (2019) 6(10): e521–9. doi: 10.1016/S2352-3026(19)30115-2

21. Wang Y, Li C, Xia J, Li P, Cao J, Pan B, et al. Humoral immune reconstitution after anti-BCMA CAR T-cell therapy in relapsed/refractory multiple myeloma. *Blood Adv* (2021) 5(23):5290–9. doi: 10.1182/bloodadvances.2021004603

22. Palumbo A, Rajkumar SV, San MJ, Larocca A, Niesvizky R, Morgan G, et al. International myeloma working group consensus statement for the management, treatment, and supportive care of patients with myeloma not eligible for standard autologous stem-cell transplantation. *J Clin Oncol* (2014) 32(6):587–600. doi: 10.1200/JCO.2013.48.7934

23. Lee DW, Santomasso BD, Locke FL, Ghobadi A, Turtle CJ, Brudno JN, et al. ASTCT consensus grading for cytokine release syndrome and neurologic toxicity associated with immune effector cells. *Biol Blood Marrow Transplant* (2019) 25(4):625–38. doi: 10.1016/j.bbmt.2018.12.758

24. Xu J, Chen LJ, Yang SS, Sun Y, Wu W, Liu YF, et al. Exploratory trial of a biepitopic CAR T-targeting b cell maturation antigen in relapsed/refractory multiple myeloma. *Proc Natl Acad Sci U S A* (2019) 116(19):9543–51. doi: 10.1073/pnas.1819745116

25. Que Y, Xu M, Xu Y, Almeida V, Zhu L, Wang Z, et al. Anti-BCMA CAR-T cell therapy in Relapsed/Refractory multiple myeloma patients with extramedullary disease: a single center analysis of two clinical trials. *Front Immunol* (2021) 12:755866. doi: 10.3389/fimmu.2021.755866

26. Zhang M, Zhou L, Zhao H, Zhang Y, Wei G, Hong R, et al. Risk factors associated with durable progression-free survival in patients with relapsed or refractory multiple myeloma treated with anti-BCMA CAR T-cell therapy. *Clin Cancer Res* (2021) 27(23):6384–92. doi: 10.1158/1078-0432.CCR-21-2031

27. Locke FL, Rossi JM, Neelapu SS, Jacobson CA, Miklos DB, Ghobadi A, et al. Tumor burden, inflammation, and product attributes determine outcomes of axicabtagene ciloleucel in large b-cell lymphoma. *Blood Adv* (2020) 4(19):4898–911. doi: 10.1182/bloodadvances.2020002394

28. Jacobson CA, Hunter B, Armand P, Kamihara Y, Ritz J, Rodig SJ, et al. Axicabtagene ciloleucel in the real world: outcomes and predictors of response, resistance and toxicity. *Blood* (2018) 132(Supplement 1):92. doi: 10.1182/blood-2018-99-117199

29. Greten FR, Grivennikov SI. Inflammation and cancer: triggers, mechanisms, and consequences. *Immunity* (2019) 51(1):27–41. doi: 10.1016/j.immuni.2019.06.025

30. Shalapour S, Karin M. Pas de deux: control of anti-tumor immunity by cancer-associated inflammation. *Immunity* (2019) 51(1):15–26. doi: 10.1016/j.immuni.2019.06.021

31. Diehl S, Anguita J, Hoffmeyer A, Zapton T, Ihle JN, Fikrig E, et al. Inhibition of Th1 differentiation by IL-6 is mediated by SOCS1. *Immunity* (2000) 13(6):805–15. doi: 10.1016/S1074-7613(00)00078-9

32. Bettelli E, Carrier Y, Gao W, Korn T, Strom TB, Oukka M, et al. Reciprocal developmental pathways for the generation of pathogenic effector TH17 and regulatory T cells. *Nature* (2006) 441(7090):235–8. doi: 10.1038/nature04753

33. De Monte L, Reni M, Tassi E, Clavenna D, Papa I, Recalde H, et al. Intratumor T helper type 2 cell infiltrate correlates with cancer-associated fibroblast thymic stromal lymphopoietin production and reduced survival in pancreatic cancer. *J Exp Med* (2011) 208(3):469–78. doi: 10.1084/jem.20101876

34. Tanaka T, Narazaki M, Kishimoto T. IL-6 in inflammation, immunity, and disease. *Cold Spring Harb Perspect Biol* (2014) 6(10):a16295. doi: 10.1101/cshperspect.a016295

35. Yan Z, Zhang H, Cao J, Zhang C, Liu H, Huang H, et al. Characteristics and risk factors of cytokine release syndrome in chimeric antigen receptor T cell treatment. *Front Immunol* (2021) 12:611366. doi: 10.3389/fimmu.2021.611366

36. Turtle CJ, Hanafi LA, Berger C, Gooley TA, Cherian S, Hudecek M, et al. CD19 CAR-T cells of defined CD4+:CD8+ composition in adult b cell ALL patients. *J Clin Invest* (2016) 126(6):2123–38. doi: 10.1172/JCI85309

37. Wang Z, Han W. Biomarkers of cytokine release syndrome and neurotoxicity related to CAR-T cell therapy. *biomark Res* (2018) 6:4. doi: 10.1186/s40364-018-0116-0

38. Norelli M, Camisa B, Barbiera G, Falcone L, Purevdorj A, Genua M, et al. Monocyte-derived IL-1 and IL-6 are differentially required for cytokine-release syndrome and neurotoxicity due to CAR T cells. *Nat Med* (2018) 24(6):739–48. doi: 10.1038/s41591-018-0036-4

39. Hay KA, Hanafi LA, Li D, Gust J, Liles WC, Wurfel MM, et al. Kinetics and biomarkers of severe cytokine release syndrome after CD19 chimeric antigen receptor-modified T-cell therapy. *Blood* (2017) 130(21):2295–306. doi: 10.1182/blood-2017-06-793141

40. Obstfeld AE, Frey NV, Mansfield K, Lacey SF, June CH, Porter DL, et al. Cytokine release syndrome associated with chimeric-antigen receptor T-cell therapy: clinicopathological insights. *Blood* (2017) 130(23):2569–72. doi: 10.1182/blood-2017-08-802413

frontiers | Frontiers in Immunology

TYPE Original Research
PUBLISHED 26 April 2023
DOI 10.3389/fimmu.2023.1140328

OPEN ACCESS

EDITED BY
Takaji Matsutani,
Repertoire Genesis, Inc., Japan

REVIEWED BY
Ziwei Zeng,
University of Heidelberg, Germany
Huocong Huang,
University of Texas Southwestern Medical Center, United States

*CORRESPONDENCE
Chunhui Sun
sunchh6@mail.sysu.edu.cn
Changhua Zhang
zhchangh@mail.sysu.edu.cn

†These authors have contributed equally to this work

SPECIALTY SECTION
This article was submitted to Cancer Immunity and Immunotherapy, a section of the journal Frontiers in Immunology

RECEIVED 08 January 2023
ACCEPTED 12 April 2023
PUBLISHED 26 April 2023

CITATION
Deng C, Deng G, Chu H, Chen S, Chen X, Li X, He Y, Sun C and Zhang C (2023) Construction of a hypoxia-immune-related prognostic panel based on integrated single-cell and bulk RNA sequencing analyses in gastric cancer. *Front. Immunol.* 14:1140328. doi: 10.3389/fimmu.2023.1140328

Construction of a hypoxia-immune-related prognostic panel based on integrated single-cell and bulk RNA sequencing analyses in gastric cancer

Cuncan Deng[1†], Guofei Deng[1†], Hongwu Chu[1†], Songyao Chen[1], Xiancong Chen[1], Xing Li[1], Yulong He[1,2], Chunhui Sun[1,2*] and Changhua Zhang[1,2*]

[1]Digestive Diseases Center, The Seventh Affiliated Hospital, Sun Yat-sen University, Shenzhen, China, [2]Guangdong Provincial Key Laboratory of Digestive Cancer Research, The Seventh Affiliated Hospital of Sun Yat-sen University, Shenzhen, Guangdong, China

Introduction: Gastric cancer (GC) is the fifth most common tumor, contributing to the third-highest number of cancer-related deaths. Hypoxia is a major feature of the tumor microenvironment. This study aimed to explore the influence of hypoxia in GC and establish a hypoxia-related prognostic panel.

Methods: The GC scRNA-seq data and bulk RNA-seq data were downloaded from the GEO and TCGA databases, respectively. AddModuleScore() and AUCell() were used to calculate module scores and fractions of enrichment for hypoxia-related gene expression in single cells. Least absolute shrinkage and selection operator cox (LASSO-COX) regression analysis was utilized to build a prognostic panel, and hub RNAs were validated by qPCR. The CIBERSORT algorithm was adopted to evaluate immune infiltration. The finding of immune infiltration was validated by a dual immunohistochemistry staining. The TIDE score, TIS score and ESTIMATE were used to evaluate the immunotherapy predictive efficacy.

Results: Hypoxia-related scores were the highest in fibroblasts, and 166 differentially expressed genes were identified. Five hypoxia-related genes were incorporated into the hypoxia-related prognostic panel. 4 hypoxia-related genes (including POSTN, BMP4, MXRA5 and LBH) were significantly upregulated in clinical GC samples compared with the normal group, while APOD expression decreased in GC samples. Similar results were found between cancer-associated fibroblasts (CAFs) and normal fibroblasts (NFs). A high hypoxia score was associated with advanced grade, TNM stage, N stage, and poorer prognosis. Decreased antitumor immune cells and increased cancer-promoting immune cells were found in patients with high hypoxia scores. Dual immunohistochemistry staining showed high expression of CD8 and ACTA2 in gastric cancer tissue. In addition, the high hypoxia score group possessed higher TIDE scores, indicating poor immunotherapy benefit. A high hypoxia score was also firmly related to sensitivity to chemotherapeutic drugs.

Discussion: This hypoxia-related prognostic panel may be effective in predicting the clinical prognosis, immune infiltrations, immunotherapy, and chemotherapy in GC.

KEYWORDS

gastric cancer, hypoxia, prognostic panel, immune infiltration, immune therapy

1 Introduction

Gastric cancer (GC) is the fifth most prevalent cancer globally, causing the third most cancer-related death worldwide (1). Exceeding 1 million individuals have been diagnosed with GC, and 784000 deaths were caused by GC worldwide in 2018. Although some advances have been achieved in both diagnosis and therapy, the survival rate of GC is still unsatisfactory in many countries (2). The current dilemma of gastric cancer includes the lack of effective early diagnosis, poor clinical outcomes, and high metastasis and recurrence rates.

The tumor microenvironment consists of inflammatory cells, cancer-associated fibroblasts (CAFs), nerves, and vascular endothelial cells (3). The interaction of components in the tumor microenvironment promotes tumour progression. Hypoxia is a vital feature of the tumor microenvironment (TME) in solid tumors and is associated with various cancer features, such as metabolic reprogramming, impaired immune response, and increased genomic instability (4). Hypoxia can enhance tumor cell proliferation, immune escape, and inflammation, induce angiogenesis and activate invasion, consequently leading to the aggression, metastasis, and drug resistance of gastric cancer (5, 6). Hypoxia is associated with tumor malignancy progression, treatment resistance, and poor clinical prognostic outcomes for patients (7). Hypoxia-related genes improve proliferation and distant metastasis through the miR-30c-2-3p/LOX axis in GC (8). The downregulation of miR-4521 caused by hypoxia inhibits the progression of gastric carcinoma by regulating the expression of IGF2 and FOXM1 (9). The lncRNA-CBSLR, which is induced by hypoxia, regulates ferroptosis in gastric cancer by modulating CBS through a m6A-YTHDF2-dependent mechanism (10). SERPINE1 and EFNA3 might be hypoxia-related prognostic factors in GC (11). Hypoxia-induced lncRNAs could facilitate the invasion of GC by interacting with SNAI1 (12).

At present, several studies have elaborated on the mechanism by which hypoxia regulates the physiological changes in gastric cancer, but the mechanism needs further elucidation. Elucidating the hypoxia-related pathogenesis and identifying effective biomarkers of gastric cancer are meaningful for improving the diagnosis, prevention and management of GC.

In this study, we aimed to develop a hypoxia-related prognostic panel to predict the immune microenvironment (TME) in GC patients. First, GC scRNA-seq data were obtained from the GEO database, and bulk RNA-seq data were obtained from the TCGA database. The hypoxia hallmark genes were utilized to calculate the hypoxia score and AUC value. Least absolute shrinkage and selection operator Cox (LASSO-COX) regression analysis was utilized to build a novel hypoxia score-related prognostic panel. The CIBERSORT algorithm was manipulated to analyze the relationship between the infiltration of immune cells and the hypoxia score. The tumor immune dysfunction and exclusion (TIDE) score and T-cell-inflamed signature (TIS) score were used to evaluate the immunotherapy predictive efficacy of the hypoxia score.

2 Methods

2.1 Data acquisition

The processing flow of this research is shown in Figure 1. The GC scRNA-seq data GSE183904 were accessed from the GEO database (https://www.ncbi.nlm.nih.gov/geo/), which included 10 normal tissue samples, 26 GC tissue samples, 3 peritoneum tissue samples from GC patients and 1 normal peritoneum tissue sample. Bulk RNA-seq data for GC were accessed from the TCGA database (https://portal.gdc.cancer.gov/) comprising 32 normal tissues and 375 gastric cancer tissues. Clinical data and survival data were also retrieved.

2.2 Processing of scRNA-seq data

GC scRNA-seq data were analyzed by using the single-cell analysis R package "Seurat". The preliminary data screening process was carried out according to this standard: the number of genes detected in a single cell was more than 200 and less than 5,000, and the mitochondrial gene count was 20%.

The SCTransform() function of the Seurat package was utilized to preprocess and reduce the batch effect to integrate different single-cell transcriptome samples, and 5000 highly variable genes were chosen by SelectIntegrationFeatures() for anchoring. Then, RunPCA() was adopted to reduce the dimension of PCA with dim = 20 to further reduce dimensionality with the UMAP method according to ElbowPlot(), and the resolution was set to 0.4 for cluster analysis using the FindClusters() function. Uniform Manifold Approximation and Projection (UMAP) is an algorithm that reduces dimensionality by mapping a high-dimensional probability distribution to a low-dimensional space. Finally, we identified 10 cell types based on typical cell markers.

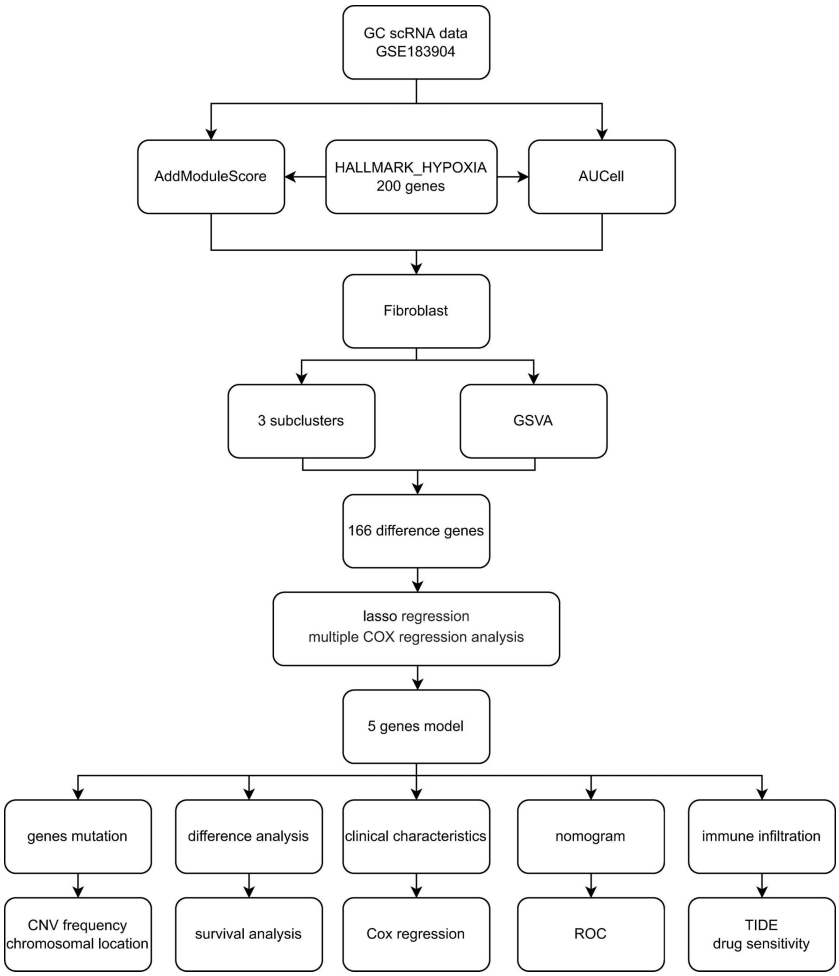

FIGURE 1
Flowchart of the study.

2.3 Score according to hypoxia-related hallmark genes

To calculate module scores and the fraction of enrichment for hypoxia-related gene expression in single cells, AddModuleScore() and AUCell() were performed. The hypoxia hallmark gene was downloaded from the Molecular Signatures Database (http://www.gsea-msigdb.org/gsea/msigdb/index.jsp), which incorporates 200 genes widely employed in cancer research. We calculated the hypoxia score and AUC value in each cell type with the 200 hypoxia-related hallmark genes.

2.4 Gene set variation analysis

GSVA was used to sequence the different genes in normal and GC tissue, aiming at evaluating the enrichment of hallmark gene sets in the differential gene list. DEGs were screened using FindMarkers(), with the expression ratio of the least differential genes set to 0.25. The hallmark gene sets were accessed from the MSigDB database with the R package "msigdbr", species = "Homo sapiens", category = "H".

2.5 Least absolute shrinkage and selection operator cox regression analysis

To formulate the hypoxia-based prognostic panel, LASS analysis was employed to select reliable genes related to the clinical outcome of GC patients from the TCGA cohort. We calculated the hypoxia score for every GC patient with the following formula: score= Σ coefficient mRNAn * expression level mRNA. Patients were divided into two groups according to the calculated scores. Follow-up analysis will focus on patients with different hypoxia scores.

2.6 Clinical specimen collection and ethics approval

Gastric cancer and normal samples were accessed from the Seventh Hospital of Sun Yat-sen University. The sample collection procedure was approved by the Sun Yat-sen University Health Science Institution Review Board (No. KY-2022-051-02). All tissues were preserved at -80 degrees for further study.

2.7 Cell isolation and cell culture

The GC cell line MKN45 and normal control GES1 cells were purchased from Shanghai Institute of Cell Biology, Chinese Academy of Sciences (Shanghai, China). MKN45 and GES1 cells were cultured using RPMI 1640 medium (Gibco) containing 10% fetal bovine serum (FBS, Nanjing BioChannel Biotechnology Co., Ltd., China) in a 37°C, 5% CO2 environment.

To isolate cancer-associated fibroblasts and normal fibroblasts (NFs), gastric cancer tissues and normal tissues were obtained from the Seventh Hospital of Sun Yat-sen University respectively. The tissues were washed three times with PBS containing 1% penicillin streptomycin. The tissue was cut into 1-3 mm pieces using surgical scissors and then digested by adding collagenase IV and shaking for 1-2 hours at 37°C. The precipitate was obtained by centrifugation at 1000 rpm for 10 minutes and the red blood cells were then lysed by adding erythrocyte lysis solution(C3702, Beyotime, China). Digestion was terminated by the addition of a high sugar Dulbecco's Modified Eagle Medium (11965092, DMEM, Gibco) containing 10% serum and 1% penicillin and streptomycin. The obtained cells are cultured in a CO2 incubator at 37°C with 5% CO2.

2.8 Real-time PCR analysis of hub RNAs identified by LASSO

Several hub RNAs were identified by LASSO analysis. The expression of these hub RNAs was detected by qPCR. Total RNA was extracted from the gastric tissues and cell lines (including GES1 cells, MKN45 cells, NFs and CAFs) with the AG RNAex Pro RNA reagent (Accurate Biology, CAT#AG21102) following the manufacturer's instructions. cDNA was synthesized using Evo M-MLV reverse transcription master mix (Accurate Biology, CAT# AG11706). qPCR was conducted utilizing a SYBR Green Pro Tag HS premixed qPCR kit (Accurate Biology, CAT# AG11701). The relative expression of the hub RNAs was calculated using the $2^{-\Delta\Delta Ct}$ method. mRNA expression was normalized to β-actin. The primer sequences of all RNAs used for qPCR are recorded in Table S1.

2.9 Hypoxia-related gene analysis

The "findMarkers" function within the Seurat package was utilized to investigate the expression levels of five genes across distinct cell types in single-cell sequencing data. Kaplan-Meier analysis of selected hypoxia-related genes in the TCGA-GC cohort. GEPIA2 database (http://gepia2.cancer-pku.cn/) to explored the associations between CAFs markers (ACTA2, FAP) and genes included in the prognostic panel in gastric cancer.

2.10 Univariate and multivariate Cox regression analysis

To verify whether the hypoxia score was an independent prognostic factor, we performed a Cox regression analysis. The variables included in the univariate Cox regression analysis included age, sex, tumor grade, TNM stage and hypoxia score, and significant factors were included in the multivariate Cox regression analysis. The results are shown in a forest diagram.

2.11 Clinical correlation and survival analysis

For a deeper understanding of the relationship between the hypoxia score and clinical features, clinical correlation analysis was conducted among patients in different groups. Furthermore, we utilized Kaplan–Meier (K-M) analysis to find differences in OS outcomes between the high- and low-score groups. A time-dependent receiver operating characteristic (ROC) curve was generated to determine the predictive ability of the risk model.

2.12 Immune cell infiltration

To analyze the relationship between the infiltration of immune cells and the hypoxia score, the CIBERSORT (HTTPS://cibersort.stanford.edu/) (13) algorithm was adopted to evaluate the infiltration of immune cells in TCGA-GC patients. The Wilcoxon test was applied to analyze the difference in infiltrated immune cells between the high- and low-score groups. The infiltration difference of some functional cells in different score groups was also evaluated with the same method.

2.13 Dual immunohistochemistry staining

The finding of immune infiltration was validated by a dual immunohistochemistry staining. A dual immunohistochemistry staining kit (#DS-0003, ZSGB-BIO, China) was used following the manufacturer's protocols to assess the association of CD8+ T cell and CAFs in GC tissues. The sections of GC tissue, which had been fixed in formalin and embedded in paraffin, were subjected to deparaffinization in xylene 20 minutes after being heated in an oven at 65°C for 2 hours. Following this, they were rehydrated in 100%, 95%, 85%, and 75% alcohol for 2 minutes each. Antigen retrieval was performed with Citrate solution. All slides were blocked with goat serum buffer at 37°C for 30 min and then incubated with CAFs marker Anti-ACTA2 (1:100, Genxspan, #GXP6460) and CD8 (1:100, Huabio, # ET1606-31) primary antibodies at 4°C overnight. The next day, the slides were incubated with AP-labeled Rabbit and HRP-labeled mouse secondary antibodies at 37°C for 1 hours. Then, the related products were detected with DAB and RED respectively. The nuclei were stained for 1 to 2 minutes using hematoxylin. Finally, the sections were dehydrated, transparent and sealed with gum. The slides were viewed with a microscope and images captured.

2.14 Immunotherapy prediction

To predict the prognostic value of hypoxia scores in immunotherapy patients, time-dependent receiver operating

characteristic (ROC) curve analysis was adopted to acquire the area under the curve (AUC). In addition, the tumor immune dysfunction and exclusion (TIDE) score and T-cell-inflamed signature (TIS) score were downloaded online (HTTP://tide.dfci.harvard.edu/) to compare the prognosis among the hypoxia scores, TIDE, and TIS by multiple ROC curves.

2.15 Analysis of the purity of tumors using ESTIMATE

The Estimation of Stromal and Immune cells in Malignant Tumours using Expression data (ESTIMATE) algorithm was employed to calculate the scores of stromal cells, immune cells and tumor cells in the different hypoxia score groups (14). The contents of immune cells and stromal cells in the tumor microenvironment (TME) were obtained for further analysis of the relationship between the hypoxia score and the purity of the tumor.

2.16 Drug sensitivity analysis

The sensitivity of different drugs was predicted in GC patients in the high-hypoxia score subgroup and low-hypoxia score subgroup. The R package pRRophetic was employed to predict drug sensitivity. Significant differences in IC50 between the high and low hypoxia score subgroups were evaluated with the Wilcoxon signed-rank test. The result was visualized with the package "ggplot2".

2.17 Statistical analysis

R software (version 4.1.2; https://www.R-project.org) and associated R packages were applied in data management, such as the "limma" package for difference analysis between different groups and the "Survminer" package for survival analysis. The Wilcoxon test was conducted to compare the differences among distinct groups. The Spearman correlation method was conducted to calculate the correlation coefficient. All statistical analyses were bilateral, P<0.05. 0.05 was considered statistically significant.

3 Result

3.1 Annotation of cell types and hypoxia score

A total of 73981 cells and 26571 genes were screened from GSE183904. Ten cell types were annotated according to typical cell markers (Figure 2A). The cell markers for annotation are shown in Figure 2B. Hypoxia-related scores and AUCs were the highest in fibroblasts compared with other cell types based on the AddmoduleScore function (Figure 2C) and AUCell (Figure 2D). Therefore, fibroblasts were extracted for subsequent analysis. Three

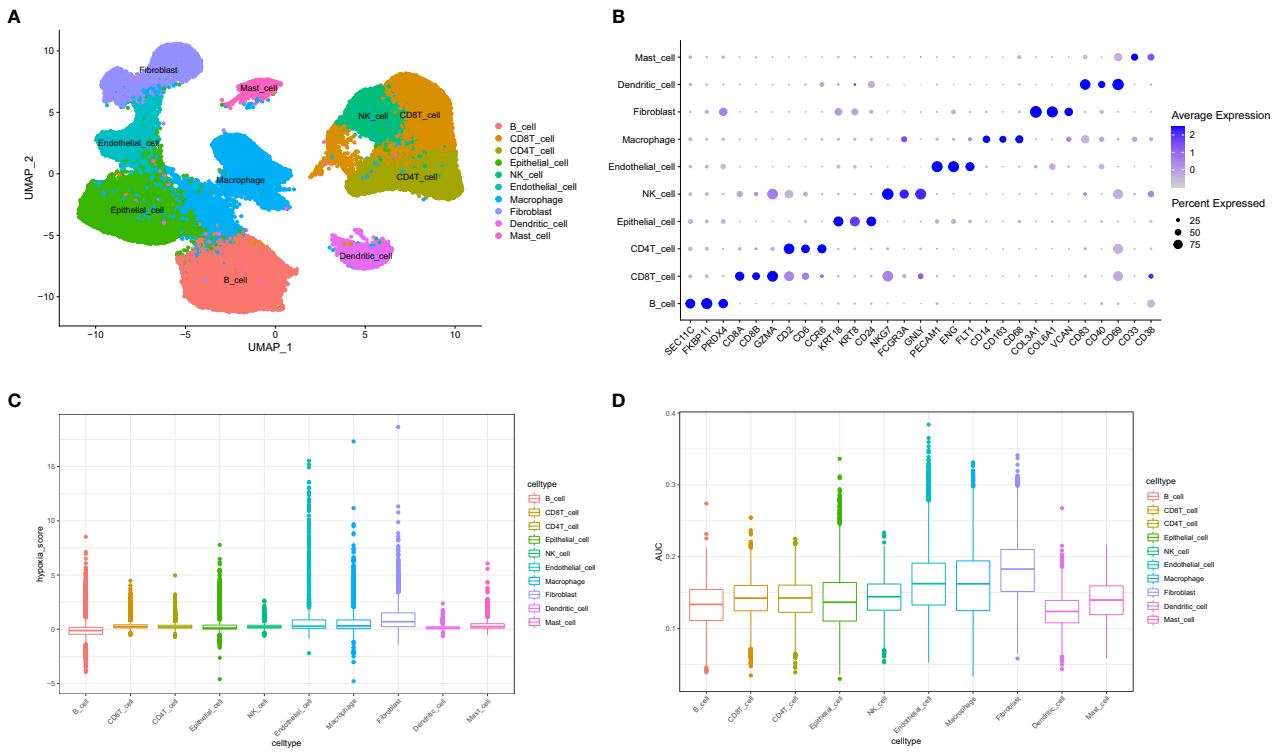

FIGURE 2
Overview of single-cell data. **(A)** UMAP of ten different cell types of samples. **(B)** Cell markers used to identify cell types. **(C)** Hypoxia score calculated by the AddModuleScore function. **(D)** Hypoxia-related AUC calculated by the AUCell function.

clusters were obtained by secondary clustering of fibroblasts (Figure 3A). Then, the GSVA enrichment score was determined for each cell in the fibroblast subcluster, and the results indicated that the hypoxia-related hallmark was enriched in Cluster 2 of fibroblasts (Figure 3B).

3.2 Differential gene analysis

The DEGs between fibroblast Cluster 2 and other clusters were screened by the FindMarkers function (logFC>1, p value<0.05, Minpct = 0.25). 166 differentially expressed genes in cluster 2 CAFs between normal and gastric cancer group were identified that were used for follow-up analysis. The volcano map of the differentially expressed genes is shown in Figure 3C. LASSO-Cox regression analysis was conducted to identify the hub genes. The change trajectory of genes is shown in Figures 3D, E. Finally, 5 genes were screened as hypoxia-related genes to construct the hypoxia-related prognostic model, including APOD, BMP4, POSTN, MXRA5 and LBH.

3.3 qPCR validation and Kaplan–Meier analysis of genes included in LASSO model

The differentially expressed genes in the LASSO model were analyzed. Clinical gastric cancer samples were collected to perform qPCR. In terms of expression level, 4 hypoxia-related genes (including POSTN, BMP4, MXRA5 and LBH) were significantly upregulated in clinical GC samples compared with the normal group, while APOD expression decreased in GC samples (TCGA cohort-Figure 4A; clinical samples-Figure 4B). Furthermore, the expression of these hub genes was detected by PCR in cell lines. Consistent with the tissue results, POSTN, BMP4, MXRA5 and LBH were significantly upregulated and APOD was decreased in MKN45 cells compared with normal control cells (Figure 4C). Besides, we detected the expressions of genes included in the prognostic panel in NFs and CAFs. The CAFs marker ACTA2 and FAP significantly upregulated in CAFs compared with NFs. POSTN, BMP4, MXRA5 and LBH were significantly upregulated and APOD was decreased in CAFs compared with NFs (Figure 4D).

We further explored the expressions of these 5 genes in the scRNA-seq data. The results showed that these genes were highly expressed in fibroblast but also expressed in other cells, including Endothelial cell, epithelial cell, B cell, CD4 T cell and CD8 T cell et al. (Figures 4E–I).

Furthermore, Kaplan–Meier (K-M) analysis was performed to explore the correlation between RNA expression and survival in GC. The result showed that high APOD, POSTN, MXRA5 and LBH expression was related to a poor prognosis in GC while high BMP4 expression was associated with a higher survival rate (Figures 4J–N).

There were many differentially expressed genes in cluster 2 CAFs compared with other cluster CAFs and the genes were listed in Table S2. Since ACTA2 and FAP were the well-known markers of CAFs, the correlation between CAFs markers (ACTA2 and FAP) and hypoxia-related prognostic panel (including APOD, POSTN, BMP4, MXRA5 and LBH) were analysed using GEPIA2 database. The results were showed in Figure S1.

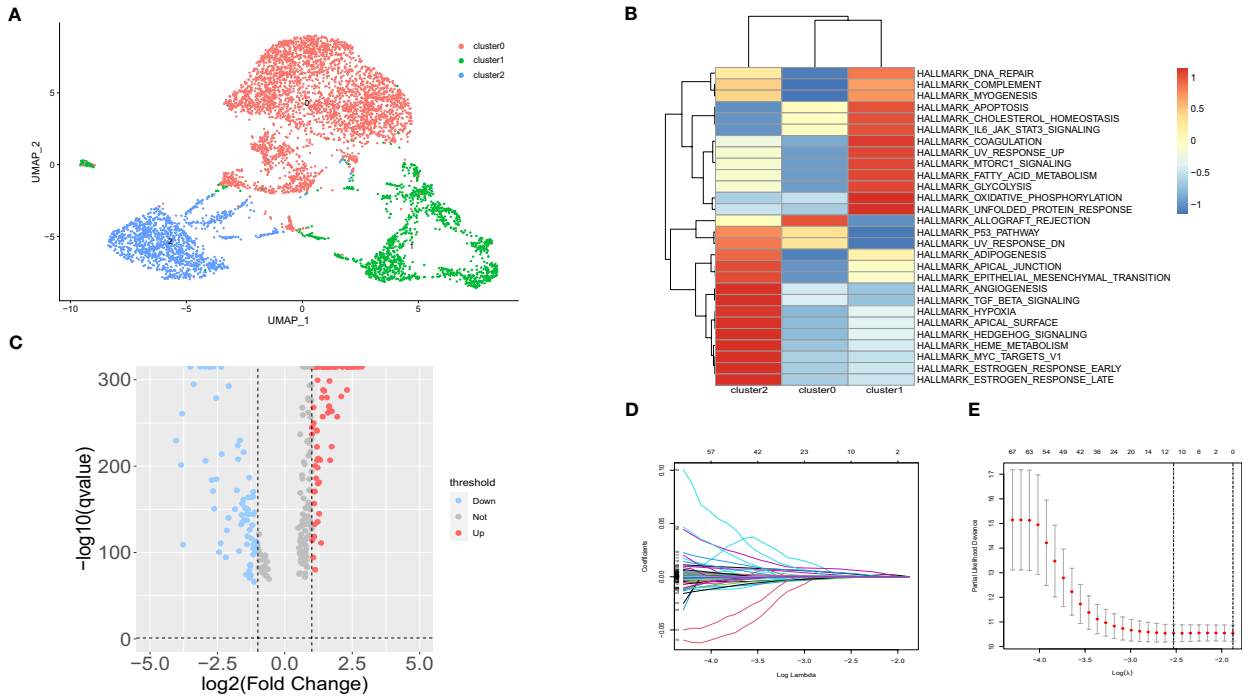

FIGURE 3
Subpopulation analysis in fibroblast subtypes. **(A)** UMAP of 3 fibroblast clusters. **(B)** Hallmarks enriched by GSVA in 3 fibroblast clusters. **(C)** Volcano maps of up- and downregulated genes in fibroblast Cluster 2. **(D)** LASSO coefficient distribution of each independent gene. **(E)** The partial likelihood deviance in LASSO Cox regression analysis.

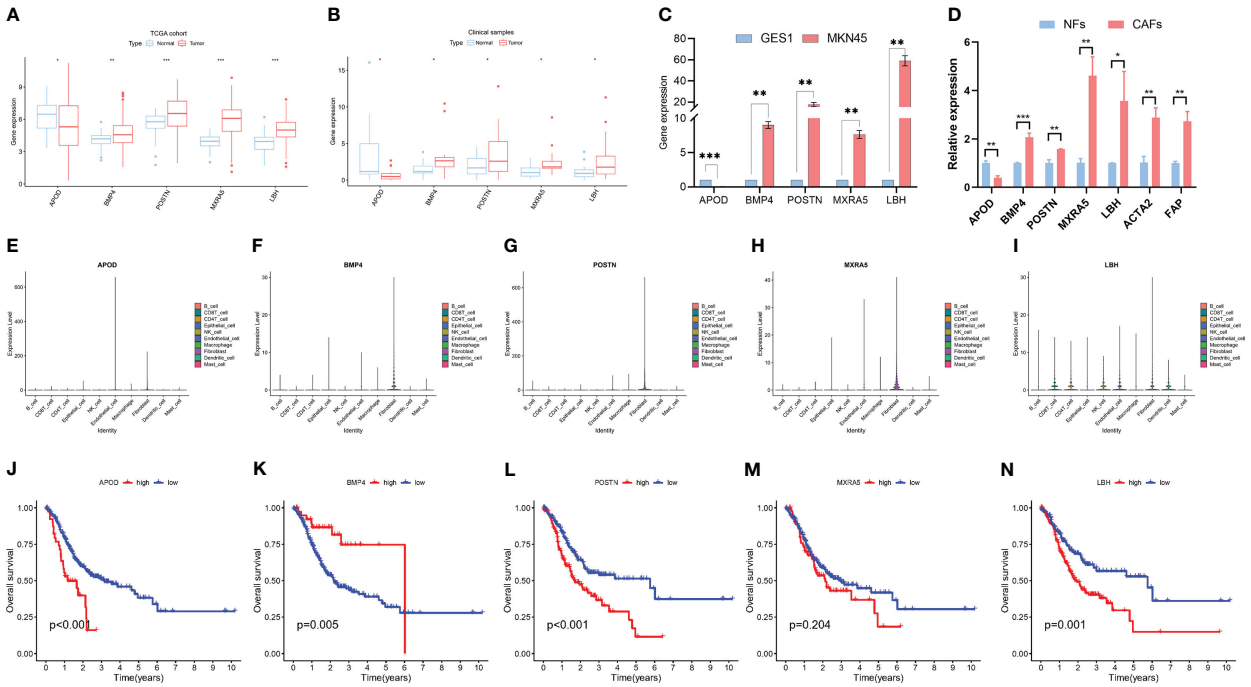

FIGURE 4
Characteristics of 5 hypoxia-related genes in gastric cancer. **(A)** Expression differences of 5 hypoxia-related genes in normal and gastric cancer tissues in the TCGA dataset. **(B)** Validation of the expression of 5 hub genes by PCR in clinical patients. **(C)** Validation of the expression of 5 hub genes by PCR in cell lines. **(D)** Validation of the expression of 5 hub genes by PCR in NFs and CAFs. **(E–I)**. The expressions of 5 hub genes in different cells according to scRNA-seq data. **(J–N)**. Kaplan–Meier analysis of patients in high- and low- expression groups of these 5 hub genes. * means p<0.05; ** means p<0.01; *** means p<0.001.

3.4 Clinicopathologic characteristics analysis and model construction

According to the results of LASSO-Cox regression analysis, the hypoxia score was calculated using gene expression and coefficients. TCGA-GC patients were divided into high and low groups according to the median hypoxia score. According to univariate Cox regression analysis, TNM stage, T stage, N stage and hypoxia scores were significantly related to the prognosis of gastric cancer (Figure 5A). In further exploration, Figure 5B shows that the hypoxia score was an independent prognostic factor in multivariate Cox regression analysis. The clinicopathologic characteristics of GC patients in the TCGA cohort showed a significant difference in age, TNM grade, TNM stage and T stage between the high and low hypoxia score groups (Figures 5C–F, S2A). There was no significant difference in N stage, M stage or gender (Figures S2B-D). KM survival analysis showed a significantly poorer prognosis in the higher hypoxia score group than in the low hypoxia score group (Figure 5G). The results of survival analysis for each candidate gene are shown in Figure S3. Figure 5H shows the relationship between the hypoxia score and patient survival status, and higher scores suggest a worse prognosis. Finally, we used the selected hypoxia-related genes to build a prognostic correlation prediction nomogram (Figure 5I). As the ROC curve shows, the hypoxia-related gene model could effectively predict the prognosis of GC patients, and the area under the curve (AUC) value reached 0.679 at 1 year, 0.676 at 2 years, and 0.716 at 3 years (Figure 5J).

3.5 Association between immune infiltration and hypoxia score

CIBERSORT was used to estimate the infiltration of 22 immune cells in the TCGA-GC cohort, and then the difference in immune cell infiltration in the different hypoxia score groups was explored. The results showed that antitumour immune cells (including activated NK cells or CD8+ T cells) were fewer in the high hypoxia score patients, while cancer-promoting immune cells such as resting NK cells and M2 macrophages were increased in the high score group (Figures 6A, B). The majority of functional immune cells infiltrated the high hypoxia score group, indicating that the hypoxia score was closely related to the immune microenvironment. The correlation analysis between hypoxia genes and immune cells is shown in Figure S4A, which indicated that M2 macrophages and activated B cells were positively correlated with the hypoxia score, while neutrophils and activated memory CD4 T cells were the opposite (Figures S4B-4E).

This LASSO model was built based on the DEGs in cluster 2 CAFs. To validate the relationship of CAFs and immune infiltration, we used double-staining immunohistochemistry to detect the CAF marker ACTA2 and the CD8+ T cell marker CD8.The result showed that the expression of ACTA2 was upregulated in the gastric cancer accompanied with the high expression of CD8. This result showed that CAFs is associated with immune infiltration (Figure 6D).

10.3389/fimmu.2023.1140328

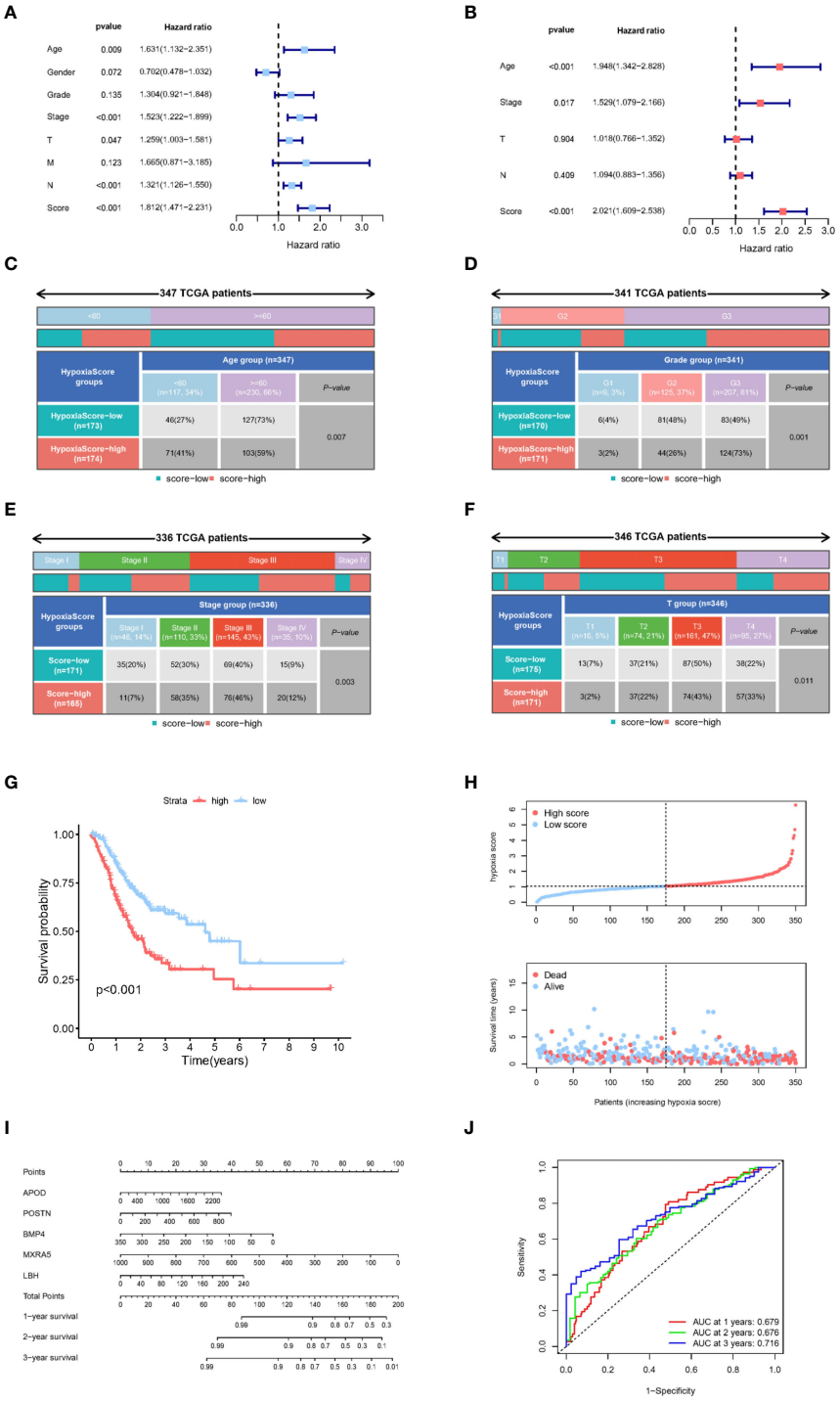

FIGURE 5
Clinical characteristics of the hypoxia-related gene model. **(A)** Univariate Cox regression analysis of clinical characteristics and hypoxia scores. **(B)** Multivariate Cox regression analysis of significant clinical characteristics and hypoxia scores. **(C–F)**. Age, grade, tumour stage and T stage were significantly different between the two hypoxia score subgroups. **(G)** Kaplan–Meier analysis of patients in different hypoxia score groups. **(H)** Relationship between survival status and hypoxia score in TCGA-GC patients. **(I)** The nomogram constructed with 5 hypoxia-related genes to predict the 1-, 3-, and 5-year OS in GC patients in the TCGA cohort. **(J)** ROC curves of key hypoxia genes for predicting 1-, 3-, and 5-year OS in the TCGA cohort.

3.6 Immunotherapy predictive efficacy of the hypoxia score

The Tumour Immune Dysfunction and Exclusion (TIDE) algorithm was adopted to test the interactions between candidate genes and cytotoxic T-cell function. The TIDE predictive score is positively related to immune evasion, proving resistance to immunotherapy. According to the ROC curve, the hypoxia score is a better prognostic panel than the TIDE score or the TIS score (Figure 6C). In the TCGA-GC cohort, the TIDE score of the high

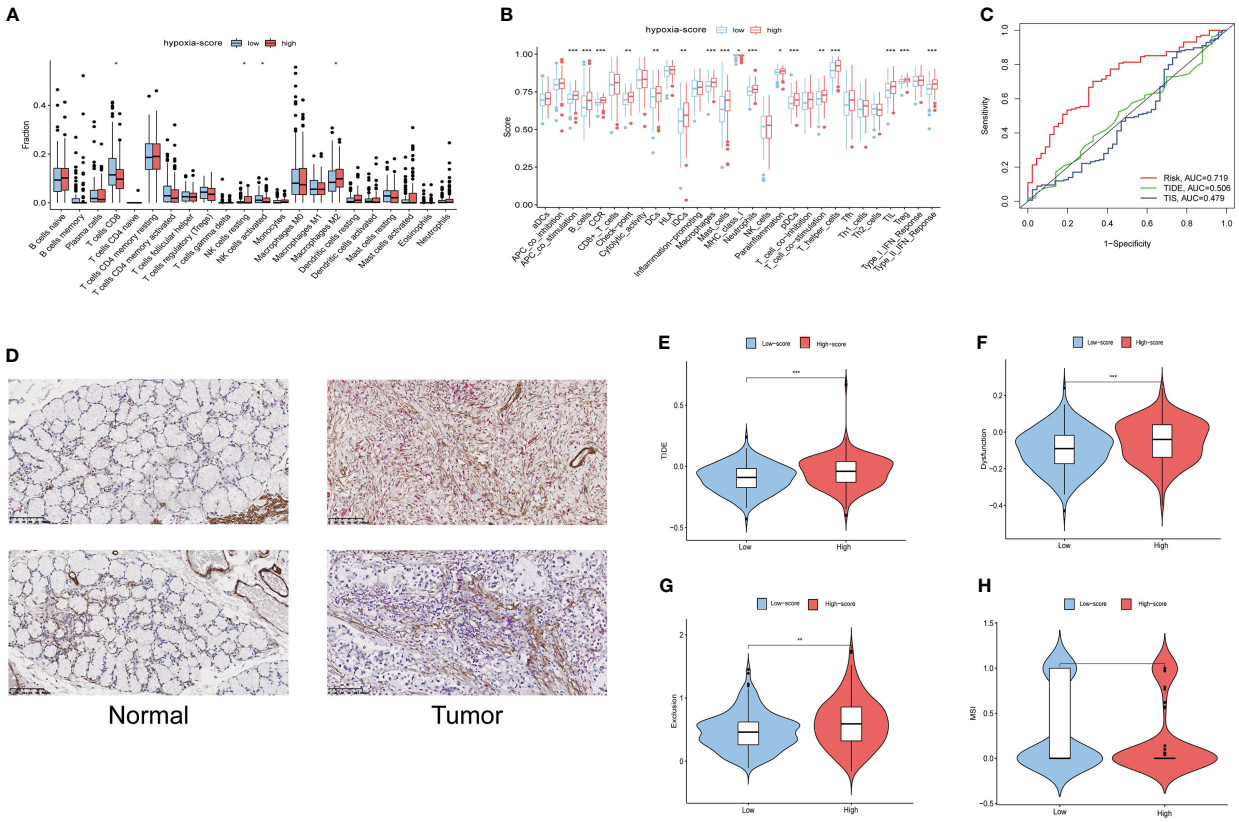

FIGURE 6
Immune infiltration and prognostic values of immunotherapy in different hypoxia score groups. **(A)** The fractions of 22 immune cells between the low and high hypoxia score groups by the CIBERSORT method. **(B)** The scores of 29 functional cells between the low and high hypoxia score groups. **(C)** ROC curves of the hypoxia score, TIDE and TIS to predict the OS of GC patients in TCGA cohorts. **(D)** The finding of immune infiltration was validated by a dual immunohistochemistry staining(ACTA2 and CD8). **(E–H)**. Differences in TIDE, T-cell exclusion score, T-cell dysfunction score and MSI in the two hypoxia score subgroups. * means p<0.05; ** means p<0.01; *** means p<0.001.

hypoxia score group was significantly higher than that of the low score group (Figure 6E). Furthermore, the T-cell exclusion scores (Figure 6F) and the T-cell dysfunction score (Figure 6G) were significantly different between the two hypoxia score subgroups, except for the MSI score (Figure 6H). These results indicated that patients with a high hypoxia score show poor immunotherapy benefit, which is consistent with the findings of previous studies. Survival analysis suggests that patients with a high hypoxia score have a poor prognosis (15).

According to the ESTIMAT algorithm, the patients with high hypoxia scores also had higher tumour purity than the patients with low hypoxia scores (Figure 7A). Tumour mutational burden (TMB) was defined as the total number of somatic mutations detected in every one million bases. Studies have shown that patients with a high tumour mutational burden are more likely to benefit from ICI treatment. The expression of TMB was remarkably upregulated in the low hypoxia score group compared with the high hypoxia score group (Figure 7B). Moreover, we observed that a low hypoxia score was associated with MSI-H status, while a high CAFS score was associated with microsatellite stable (MSS) status (Figures 7C, D).

3.7 Drug sensitivity

Furthermore, we explored the relationship between the hypoxia score and the effectiveness of chemotherapy for GC treatment. We discovered that a high hypoxia score was associated with a lower half inhibitory concentration (IC50) of chemotherapeutics, including axitinib, bexarotene, lenalidomide, nilotinib, temsirolimus and vinblastine (Figures 7E–J, P<0.05). Therefore, our study indicated that the hypoxia score could serve as a potential effective predictor of chemotherapy sensitivity prediction.

4 Discussion

Gastric cancer, the third major cause of cancer-related deaths worldwide, exhibits a worse clinical prognosis and elevated metastasis rate. The hypoxic TME is present in almost all solid tumors and profoundly affects the progression of gastric cancer (10). A hypoxic tumor microenvironment is one of the characteristics of gastric cancer. Gastric cancer cells in the microenvironment can influence the biological properties of

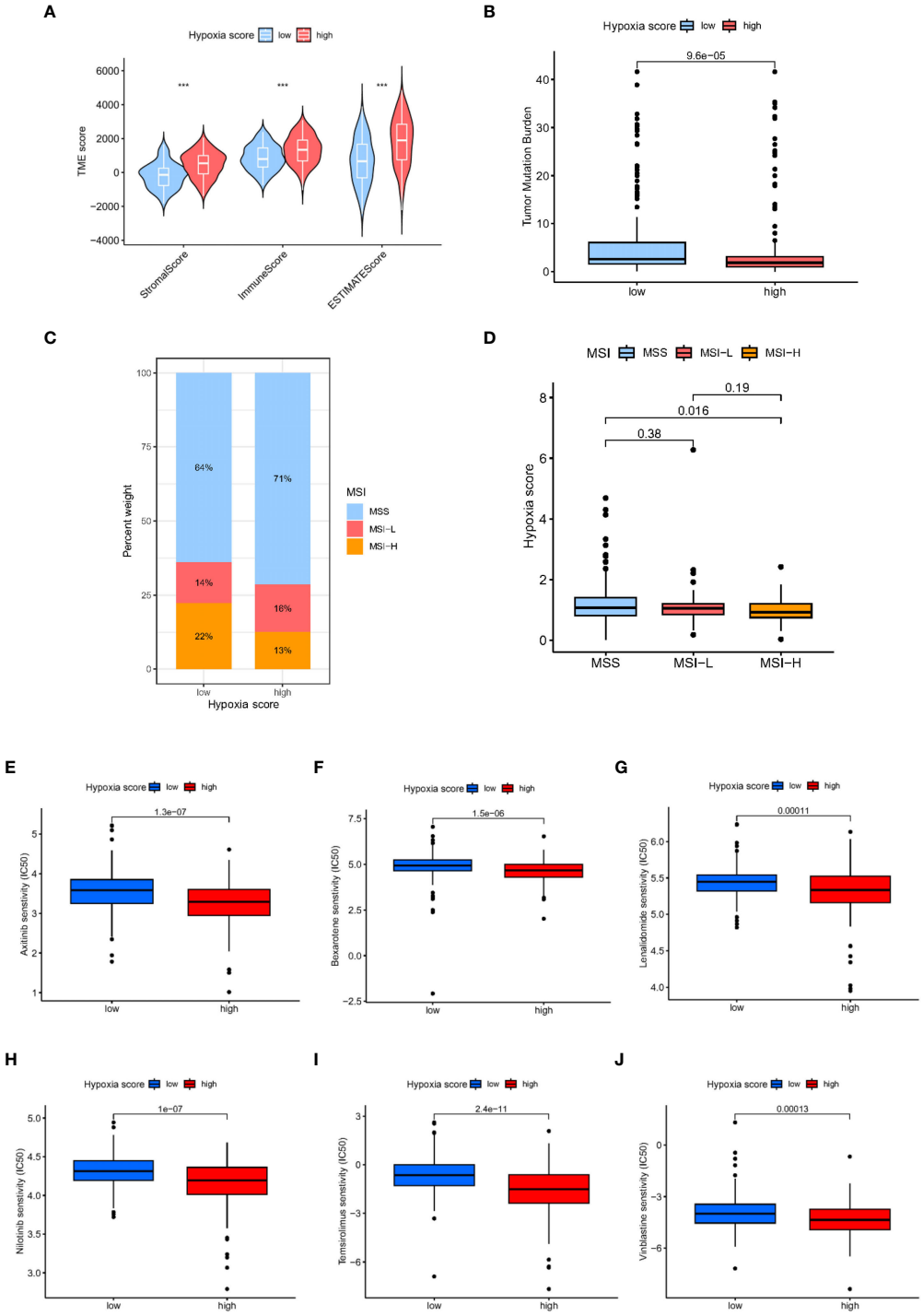

FIGURE 7
Analysis of tumour microenvironment and drug sensitivity in patients with different hypoxia scores. **(A)** TME scores in patients with different hypoxia scores based on ESTIMATE. **(B)** The TMB in different hypoxia score groups. **(C, D)** Relationship between hypoxia score and MSI. **(E)** Relationship between hypoxia score and tumour stemness index. **(E–J)**: Sensitivity analysis of hypoxia scores and antineoplastic drugs.

tumor cells by affecting the expression of certain transcription factors and tumor-associated genes to adapt to the hypoxic environment. Tumours are usually tolerant to anticancer drugs under hypoxic conditions. Although hypoxia has been reported to participate in proliferation, aggression, metastasis and drug resistance, the deeper mechanisms remain to be elucidated.

In our study, 10 cell types were identified from GC scRNA-seq data, and hypoxia-related scores were the highest in fibroblasts. The tumor microenvironment contains miscellaneous cells, including fibroblasts, immune cells, nerves, and vascular endothelial cells, which can interact with cancer cells (16). Cancer-associated fibroblasts (CAFs) are one of the most abundant constituents of

the cancer microenvironment. Tumour-associated fibroblasts interact with tumor cells and other stromal components, such as immune cells, to promote gastric cancer progression. Activated CAFs can produce chemokines, extracellular matrix, growth factors and metabolites. These molecules can interact with tumor cells and facilitate tumor growth and inflammatory responses through direct contact or in a paracrine manner. Tumour cells switch their metabolic state between oxidative phosphorylation and glycolysis by establishing metabolic interactions with CAFs. In the hypoxic environment, tumor cells exhibit the Warburg effect, but in the normoxic environment, they exhibit the reverse Warburg effect. Metabolic interactions between CAFs and tumor cells facilitate the proliferation and metastasis of gastric cancer (17). CAFs usually play a tumor-promoting role, but recent studies have found that CAFs may also have an inhibitory effect on tumor progression (18, 19).

To further clarify the mechanism of hypoxia in gastric cancer, we screened differentially expressed genes in fibroblasts and used LASSO-Cox analysis to construct a novel hypoxia-related prognostic panel. As a result, 5 hypoxia-related genes (including APOD, POSTN, BMP4, MXRA5, and LBH) were included in the prognostic model. In agreement with our results, genes involved in this prognostic panel were significant in hypoxia-related physiological processes. APOD is a potential biomarker of hypoxia and is involved in immune responses (20). APOD is included in a novel necrosis-related gene model for predicting the prognosis of gastric adenocarcinoma and is closely associated with the immune microenvironment of cold tumors (21). In glioma, POSTN may regulate resistance to anti-VEGF-A therapy by upregulating the expression of TGFβ1 and HIF1α (22). POSTN is implicated in promoting metastasis of ovarian cancer via its ability to enhance M2 macrophages and cancer-associated fibroblasts through integrin-mediated activation of the NF-κB and TGF-β2 signaling pathways (23). Zhong et al. reported that BMP4 may play an important role in regulating glycolysis in hepatocellular carcinoma cells under hypoxia and hypoglycemia (24). BMP4 Promotes Tumor Progression in Bladder Cancer by Inducing M2 Macrophage Polarization (25). Hypoxia could accelerate malignant progression in glioma by promoting the expression of LBH (26). LBH inhibits cellular migration, invasion and epithelial-mesenchymal transition in nasopharyngeal carcinoma via downregulating αB-crystallin expression (27). MXRA5 was involved in a 6-gene prognostic stratification system which can be used to evaluate the prognostic risk (28). These genes involved in our prognostic panel are closely associated with hypoxia or immune cells and could promote tumor progression.

According to this five-gene prognostic panel constructed by LASSO-Cox regression analysis, TCGA-GC patients were classified into high and low hypoxia score groups. We found a remarkable difference in grade, TNM stage and N stage between the high and low hypoxia score groups. Patients with higher hypoxia scores have a significantly poorer prognosis than individuals with low hypoxia scores. The ROC curve shows that the hypoxia-related prognostic panel could effectively predict the prognosis of GC patients. These results indicated that hypoxia is a poor prognostic factor for gastric cancer. Consistent with a previous study, studies showed that the hypoxia-induced factor HIF-1α could facilitate the migration, proliferation, invasion, and tumor angiogenesis of gastric cancer cells (29). Hypoxia is involved in GC cell proliferation, migration and invasion through activation and upregulation of NHE1 (30). Hypoxia influences the expression of a variety of genes (including HIF-1α and von Hippel Lindau protein (pVHL)), resulting in the progression of cancer (31, 32).

Hypoxia is an essential feature of the TME [6], while immune infiltration is another prominent feature (33, 34). In our study, we found that antitumor immune cells, including CD8+ T cells and activated NK cells, were less abundant in the high hypoxia score patients, while cancer-promoting immune cells, such as resting NK cells and M2 macrophages, were more abundant in the high score group. The TIDE score, T-cell dysfunction scores and exclusion score of the high hypoxia score group were significantly increased compared with those of the hypoxia score subgroups. These results suggest that patients with a high hypoxia score show poor immunotherapy benefit, which is consistent with the results of a previous study. A signature of genes related to both hypoxia and immune response has been developed for the purpose of predicting the risk stratification and survival outcomes in individuals with triple-negative breast cancer (35). Hypoxia significantly upregulates PD-L1 expression in immune cells in a HIF-1α-dependent manner (36). Hypoxia promotes the activity of immunosuppressive cells and immune escape, mediating adaptation to the hypoxic environment in cancer cells (37, 38). Hypoxia is firmly associated with an immunosuppressive microenvironment and can promote gastric cancer progression.

In addition to the TIDE score, the IPS can also reflect the expression level of immune checkpoints, which can reflect the response sensitivity to ICI treatment. An effective model of patient selection based on hypoxia prior to ICI treatment of gastric cancer has not been established. Our study indicated that the expression of immune checkpoints (ICs) is closely related to the hypoxia score, which was remarkably higher in the low hypoxia score group. Patients in the low-score group are more likely to stimulate an immune response and were sensitive to immunotherapy. Consistent with our results, previous studies proved that hypoxia inhibited immune surveillance by regulating the expression of immune checkpoints comprising CTLA-4, PD-1 or PD-L1 (39). Hypoxia is an obstacle to tumor immunotherapy (40). This hypoxia-related prognostic model may be meaningful for guiding clinical immunotherapy.

Furthermore, we wondered whether the usage of a combination of chemotherapy and immunotherapy in GC had better efficacy. Therefore, we explored the chemotherapy sensitivity of various agents in the high and low hypoxia score subgroups of gastric cancer patients. Our study discovered that the high hypoxia score group had a high potential for ICI response to chemotherapeutics, including axitinib, bexarotene, lenalidomide, nilotinib, temsirolimus and vinblastine. According to the hypoxia score, these drugs predicted possible potential for therapeutic drugs under certain conditions (41, 42).

Our study innovatively combines single-cell sequencing data with a hypoxia gene set to build a novel prognostic model for gastric cancer. We innovatively found that the hypoxia-related gene set was enriched in cluster 2 cancer-associated fibroblasts (CAFs), and constructed a novel prognostic model by using the differential

genes in this group of cells through LASSO algorithm. There were several limitations in our study. First, some data lack clinical follow-up information, which needs further experimental research and a larger sample size for verification. In addition, a direct clinical application test of the prognostic model is needed. We will further verify the predictive ability of this prognostic model through clinical samples in subsequent studies.

5 Conclusion

A novel five-element hypoxia-related panel established based on single-cell and bulk RNA sequencing is a potential biomarker for gastric cancer prognostic prediction. This hypoxia-related prognostic panel was firmly associated with immune infiltration, immunotherapy and chemotherapy. This study may provide potential targets for GC therapy, but more experimental research is needed.

Data availability statement

The datasets presented in this study can be found in online repositories. The names of the repository/repositories and accession number(s) can be found within the article/Supplementary Materials.

Ethics statement

The studies involving human participants were reviewed and approved by Sun Yat-sen University Health Science Institution Review Board. The patients/participants provided their written informed consent to participate in this study.

Author contributions

Conceptualization: CD and CZ; data curation, methodology, and software: CD, GD, and HC; supervision and funding acquisition: YH, CS, and CZ; project administration and validation: SC, XC, and XL; writing-original draft: CD and GD; writing – review and editing: CS and CZ. All authors contributed to the article and approved the submitted version.

Funding

This study was supported by the Shenzhen Key Medical discipline Construction Fund (SZXK016), the Shenzhen excellent Science and Technology Innovation Talent training project (RCBS20210706092410002), Guangdong Provincial Key Laboratory of Digestive Cancer Research (No. 2021B1212040006), Shenzhen Sustainable Project (KCXFZ202002011010593), National Natural Science Foundation of China (82073148), Shenzhen Fundamental Research Program (JCYJ20190809190601671) and Sanming Project of Medicine in Shenzhen (No. SZSM201911010).

Conflict of interest

The authors declare that the research was conducted in the absence of any commercial or financial relationships that could be construed as a potential conflict of interest.

Publisher's note

All claims expressed in this article are solely those of the authors and do not necessarily represent those of their affiliated organizations, or those of the publisher, the editors and the reviewers. Any product that may be evaluated in this article, or claim that may be made by its manufacturer, is not guaranteed or endorsed by the publisher.

Supplementary material

The Supplementary Material for this article can be found online at: https://www.frontiersin.org/articles/10.3389/fimmu.2023.1140328/full#supplementary-material

References

1. Smyth EC, Nilsson M, Grabsch HI, van Grieken NC, Lordick F. Gastric cancer. *Lancet* (2020) 396(10251):635–48. doi: 10.1016/S0140-6736(20)31288-5

2. Machlowska J, Baj J, Sitarz M, Maciejewski R, Sitarz R. Gastric cancer: epidemiology, risk factors, classification, genomic characteristics and treatment strategies. *Int J Mol Sci* (2020) 21(11):4012. doi: 10.3390/ijms21114012

3. Rojas A, Araya P, Gonzalez I, Morales E. Gastric tumor microenvironment. *Adv Exp Med Biol* (2020) 1226:23–35. doi: 10.1007/978-3-030-36214-0_2

4. Choudhry H, Harris AL. Advances in hypoxia-inducible factor biology. *Cell Metab* (2018) 27(2):281–98. doi: 10.1016/j.cmet.2017.10.005

5. Gilkes DM, Semenza GL, Wirtz D. Hypoxia and the extracellular matrix: drivers of tumour metastasis. *Nat Rev Cancer* (2014) 14(6):430–9. doi: 10.1038/nrc3726

6. Shida M, Kitajima Y, Nakamura J, Yanagihara K, Baba K, Wakiyama K, et al. Impaired mitophagy activates mtROS/HIF-1α interplay and increases cancer aggressiveness in gastric cancer cells under hypoxia. *Int J Oncol* (2016) 48(4):1379–90. doi: 10.3892/ijo.2016.3359

7. King R, Hayes C, Donohoe CL, Dunne MR, Davern M, Donlon NE. Hypoxia and its impact on the tumour microenvironment of gastroesophageal cancers. *World J Gastrointest Oncol* (2021) 13(5):312–31. doi: 10.4251/wjgo.v13.i5.312

8. Li Z, Shi L, Li X, Wang X, Wang H, Liu Y. RNF144A-AS1, a TGF-β1- and hypoxia-inducible gene that promotes tumor metastasis and proliferation via targeting the miR-30c-2-3p/LOX axis in gastric cancer. *Cell Biosci* (2021) 11(1):177. doi: 10.1186/s13578-021-00689-z

9. Zhang H, Deng T, Liu R, Ning T, Yang H, Liu D, et al. CAF secreted miR-522 suppresses ferroptosis and promotes acquired chemo-resistance in gastric cancer. *Mol Cancer* (2020) 19(1):43. doi: 10.1186/s12943-020-01168-8

10. Yang H, Hu Y, Weng M, Liu X, Wan P, Hu Y, et al. Hypoxia inducible lncRNA-CBSLR modulates ferroptosis through m6A-YTHDF2-dependent modulation of CBS in gastric cancer. *J Adv Res* (2022) 37:91–106. doi: 10.1016/j.jare.2021.10.001

11. Pei JP, Zhang CD, Yusupu M, Zhang C, Dai DQ. Screening and validation of the hypoxia-related signature of evaluating tumor immune microenvironment and predicting prognosis in gastric cancer. *Front Immunol* (2021) 12:705511. doi: 10.3389/fimmu.2021.705511

12. Zhang J, Jin HY, Wu Y, Zheng ZC, Guo S, Wang Y, et al. Hypoxia-induced LncRNA PCGEM1 promotes invasion and metastasis of gastric cancer through regulating SNAI1. *Clin Transl Oncol* (2019) 21(9):1142–51. doi: 10.1007/s12094-019-02035-9

13. Newman AM, Liu CL, Green MR, Gentles AJ, Feng W, Xu Y, et al. Robust enumeration of cell subsets from tissue expression profiles. *Nat Methods* (2015) 12 (5):453–7. doi: 10.1038/nmeth.3337

14. Yoshihara K, Shahmoradgoli M, Martínez E, Vegesna R, Kim H, Torres-Garcia W, et al. Inferring tumour purity and stromal and immune cell admixture from expression data. *Nat Commun* (2013) 4(1):2612. doi: 10.1038/ncomms3612

15. Lin Z, Song J, Gao Y, Huang S, Dou R, Zhong P, et al. Hypoxia-induced HIF-1α/lncRNA-PMAN inhibits ferroptosis by promoting the cytoplasmic translocation of ELAVL1 in peritoneal dissemination from gastric cancer. *Redox Biol* (2022) 52:102312. doi: 10.1016/j.redox.2022.102312

16. Oya Y, Hayakawa Y, Koike K. Tumor microenvironment in gastric cancers. *Cancer Sci* (2020) 111(8):2696–707. doi: 10.1111/cas.14521

17. Wanandi SI, Ningsih SS, Asikin H, Hosea R, Neolaka GMG. Metabolic interplay between tumour cells and cancer-associated fibroblasts (CAFs) under hypoxia versus normoxia. *Malays J Med Sci* (2018) 25(3):7–16. doi: 10.21315/mjms2018.25.3.2

18. Mizutani Y, Kobayashi H, Iida T, Asai N, Masamune A, Hara A, et al. Meflin-positive cancer-associated fibroblasts inhibit pancreatic carcinogenesis. *Cancer Res* (2019) 79(20):5367–81. doi: 10.1158/0008-5472.CAN-19-0454

19. Rhim AD, Oberstein PE, Thomas DH, Mirek ET, Palermo CF, Sastra SA, et al. Stromal elements act to restrain, rather than support, pancreatic ductal adenocarcinoma. *Cancer Cell* (2014) 25(6):735–47. doi: 10.1016/j.ccr.2014.04.021

20. Beemelmanns A, Zanuzzo FS, Xue X, Sandrelli RM, Rise ML, Gamperl AK. The transcriptomic responses of Atlantic salmon (Salmo salar) to high temperature stress alone, and in combination with moderate hypoxia. *BMC Genomics* (2021) 22(1):261. doi: 10.1186/s12864-021-07464-x

21. Khan M, Lin J, Wang B, Chen C, Huang Z, Tian Y, et al. A novel necroptosis-related gene index for predicting prognosis and a cold tumor immune microenvironment in stomach adenocarcinoma. *Front Immunol* (2022) 13:968165. doi: 10.3389/fimmu.2022.968165

22. Park SY, Piao Y, Jeong KJ, Dong J, de Groot JF. Periostin (POSTN) regulates tumor resistance to antiangiogenic therapy in glioma models. *Mol Cancer Ther* (2016) 15(9):2187–97. doi: 10.1158/1535-7163.MCT-15-0427

23. Lin SC, Liao YC, Chen PM, Yang YY, Wang YH, Tung SL, et al. Periostin promotes ovarian cancer metastasis by enhancing M2 macrophages and cancer-associated fibroblasts via integrin-mediated NF-κB and TGF-β2 signaling. *J BioMed Sci* (2022) 29(1):109. doi: 10.1186/s12929-022-00888-x

24. Zhong J, Kang Q, Cao Y, He B, Zhao P, Gou Y, et al. BMP4 augments the survival of hepatocellular carcinoma (HCC) cells under hypoxia and hypoglycemia conditions by promoting the glycolysis pathway. *Am J Cancer Res* (2021) 11(3):793–811.

25. Martínez VG, Rubio C, Martínez-Fernández M, Segovia C, López-Calderón F, Garín MI, et al. BMP4 induces M2 macrophage polarization and favors tumor progression in bladder cancer. *Clin Cancer Res* (2017) 23(23):7388–99. doi: 10.1158/1078-0432.CCR-17-1004

26. Zhang KN, Zeng F, Chai RC, Chen J, Jiang T. Hypoxia induced LBH overexpression accelerates malignant progression in glioma. *EBioMedicine* (2019) 49:4–5. doi: 10.1016/j.ebiom.2019.10.021

27. Wu A, Zhang L, Luo N, Zhang L, Li L, Liu Q. Limb-bud and heart (LBH) inhibits cellular migration, invasion and epithelial-mesenchymal transition in nasopharyngeal carcinoma via downregulating αB-crystallin expression. *Cell Signal* (2021) 85:110045. doi: 10.1016/j.cellsig.2021.110045

28. Liang L, Li J, Yu J, Liu J, Xiu L, Zeng J, et al. Establishment and validation of a novel invasion-related gene signature for predicting the prognosis of ovarian cancer. *Cancer Cell Int* (2022) 22(1):118. doi: 10.1186/s12935-022-02502-4

29. Chen J, Zhang M, Ma Z, Yuan D, Zhu J, Tuo B, et al. Alteration and dysfunction of ion channels/transporters in a hypoxic microenvironment results in the development and progression of gastric cancer. *Cell Oncol (Dordr)* (2021) 44(4):739–49. doi: 10.1007/s13402-021-00604-1

30. Paehler Vor der Nolte A, Chodisetti G, Yuan Z, Busch F, Riederer B, Luo M, et al. Na(+)/H(+) exchanger NHE1 and NHE2 have opposite effects on migration velocity in rat gastric surface cells. *J Cell Physiol* (2017) 232(7):1669–80. doi: 10.1002/jcp.25758

31. Ucaryilmaz Metin C, Ozcan G. The HIF-1α as a potent inducer of the hallmarks in gastric cancer. *Cancers (Basel)* (2022) 14(11):2711. doi: 10.3390/cancers14112711

32. Ding XF, Chen J, Zhou J, Chen G, Wu YL. Never-in-mitosis a-related kinase 8, a novel target of von-Hippel-Lindau tumor suppressor protein, promotes gastric cancer cell proliferation. *Oncol Lett* (2018) 16(5):5900–6. doi: 10.3892/ol.2018.9328

33. Sundar R, Qamra A, Tan ALK, Zhang S, Ng CCY, Teh BT, et al. Transcriptional analysis of immune genes in Epstein-Barr virus-associated gastric cancer and association with clinical outcomes. *Gastric Cancer* (2018) 21(6):1064–70. doi: 10.1007/s10120-018-0851-9

34. Lazăr DC, Avram MF, Romoşan I, Cornianu M, Tăban S, Goldiş A. Prognostic significance of tumor immune microenvironment and immunotherapy: novel insights and future perspectives in gastric cancer. *World J Gastroenterol* (2018) 24(32):3583–616. doi: 10.3748/wjg.v24.i32.3583

35. Yang X, Weng X, Yang Y, Zhang M, Xiu Y, Peng W, et al. A combined hypoxia and immune gene signature for predicting survival and risk stratification in triple-negative breast cancer. *Aging (Albany NY)* (2021) 13(15):19486–509. doi: 10.18632/aging.203360

36. Noman MZ, Desantis G, Janji B, Hasmim M, Karray S, Dessen P, et al. PD-L1 is a novel direct target of HIF-1α, and its blockade under hypoxia enhanced MDSC-mediated T cell activation. *J Exp Med* (2014) 211(5):781–90. doi: 10.1084/jem.20131916

37. Zhang H, Lu H, Xiang L, Bullen JW, Zhang C, Samanta D, et al. HIF-1 regulates CD47 expression in breast cancer cells to promote evasion of phagocytosis and maintenance of cancer stem cells. *Proc Natl Acad Sci U S A.* (2015) 112(45):E6215–23. doi: 10.1073/pnas.1520032112

38. Siska PJ, Rathmell JC. T Cell metabolic fitness in antitumor immunity. *Trends Immunol* (2015) 36(4):257–64. doi: 10.1016/j.it.2015.02.007

39. Hu M, Li Y, Lu Y, Wang M, Li Y, Wang C, et al. The regulation of immune checkpoints by the hypoxic tumor microenvironment. *PeerJ* (2021) 9:e11306. doi: 10.7717/peerj.11306

40. Daniel SK, Sullivan KM, Labadie KP, Pillarisetty VG. Hypoxia as a barrier to immunotherapy in pancreatic adenocarcinoma. *Clin Transl Med* (2019) 8(1):10. doi: 10.1186/s40169-019-0226-9

41. Oh DY, Doi T, Shirao K, Lee KW, Park SR, Chen Y, et al. Phase I study of axitinib in combination with cisplatin and capecitabine in patients with previously untreated advanced gastric cancer. *Cancer Res Treat* (2015) 47(4):687–96. doi: 10.4143/crt.2014.225

42. Said R, Ye Y, Hong DS, Naing A, Falchook G, Fu S, et al. Phase I clinical trial of lenalidomide in combination with 5-fluorouracil, leucovorin, and oxaliplatin in patients with advanced cancer. *Cancer Chemother Pharmacol* (2016) 77(3):575–81. doi: 10.1007/s00280-015-2952-z

frontiers | Frontiers in Immunology

TYPE Original Research
PUBLISHED 03 May 2023
DOI 10.3389/fimmu.2023.1164724

OPEN ACCESS

EDITED BY
Esra Akbay,
University of Texas Southwestern Medical Center, United States

REVIEWED BY
Shaheen Khan,
University of Texas Southwestern Medical Center, United States
Ruthee Bayer,
Northwell Health, United States

*CORRESPONDENCE
Kiyoshi Yoshimura
kyoshim1@med.showa-u.ac.jp

†These authors have contributed equally to this work

RECEIVED 13 February 2023
ACCEPTED 03 April 2023
PUBLISHED 03 May 2023

CITATION
Hamada K, Isobe J, Hattori K, Hosonuma M, Baba Y, Murayama M, Narikawa Y, Toyoda H, Funayama E, Tajima K, Shida M, Hirasawa Y, Tsurui T, Ariizumi H, Ishiguro T, Suzuki R, Ohkuma R, Kubota Y, Sambe T, Tsuji M, Wada S, Kiuchi Y, Kobayashi S, Kuramasu A, Horiike A, Kim Y-G, Tsunoda T and Yoshimura K (2023) *Turicibacter* and *Acidaminococcus* predict immune-related adverse events and efficacy of immune checkpoint inhibitor.
Front. Immunol. 14:1164724.
doi: 10.3389/fimmu.2023.1164724

Turicibacter and *Acidaminococcus* predict immune-related adverse events and efficacy of immune checkpoint inhibitor

Kazuyuki Hamada[1,2†], Junya Isobe[3†], Kouya Hattori[4,5], Masahiro Hosonuma[1,6,7,8], Yuta Baba[6], Masakazu Murayama[6,7,8,9], Yoichiro Narikawa[6,7,8,9], Hitoshi Toyoda[6,7,8,10], Eiji Funayama[11], Kohei Tajima[6,12], Midori Shida[6], Yuya Hirasawa[1], Toshiaki Tsurui[1], Hirotsugu Ariizumi[1], Tomoyuki Ishiguro[1], Risako Suzuki[1], Ryotaro Ohkuma[1], Yutaro Kubota[1], Takehiko Sambe[13], Mayumi Tsuji[7,8], Satoshi Wada[14], Yuji Kiuchi[7,8], Shinichi Kobayashi[15], Atsuo Kuramasu[6], Atsushi Horiike[1], Yun-Gi Kim[4], Takuya Tsunoda[1] and Kiyoshi Yoshimura[1,6*]

[1]Division of Medical Oncology, Department of Medicine, Showa University School of Medicine, Tokyo, Japan, [2]Department of Chest Surgery, School of Medicine, Fukushima Medical University, Fukushima, Japan, [3]Department of Hospital Pharmaceutics, School of Pharmacy, Showa University, Tokyo, Japan, [4]Research Center for Drug Discovery and Faculty of Pharmacy and Graduate School of Pharmaceutical Sciences, Keio University, Tokyo, Japan, [5]Division of Biochemistry, Faculty of Pharmacy and Graduate School of Pharmaceutical Sciences, Keio University, Tokyo, Japan, [6]Department of Clinical Immuno Oncology, Clinical Research Institute for Clinical Pharmacology and Therapeutics, Showa University, Tokyo, Japan, [7]Department of Pharmacology, Showa University School of Medicine, Tokyo, Japan, [8]Pharmacological Research Center, Showa University, Tokyo, Japan, [9]Department of Otorhinolaryngology-Head and Neck Surgery, Showa University School of Medicine, Tokyo, Japan, [10]Department of Orthopedic Surgery, School of Medicine, Showa University, Tokyo, Japan, [11]Division of Pharmacology, Department of Pharmacology, School of Pharmacy, Showa University, Tokyo, Japan, [12]Department of Gastroenterological Surgery, Tokai University School of Medicine, Kanagawa, Japan, [13]Division of Clinical Pharmacology, Department of Pharmacology, Showa University School of Medicine, Tokyo, Japan, [14]Department of Clinical Diagnostic Oncology, Clinical Research Institute for Clinical Pharmacology and Therapeutics, Showa University, Tokyo, Japan, [15]Clinical Research Institute for Clinical Pharmacology and Therapeutics, Showa University, Tokyo, Japan

Introduction: Immune checkpoint inhibitors have had a major impact on cancer treatment. Gut microbiota plays a major role in the cancer microenvironment, affecting treatment response. The gut microbiota is highly individual, and varies with factors, such as age and race. Gut microbiota composition in Japanese cancer patients and the efficacy of immunotherapy remain unknown.

Methods: We investigated the gut microbiota of 26 patients with solid tumors prior to immune checkpoint inhibitor monotherapy to identify bacteria involved in the efficacy of these drugs and immune-related adverse events (irAEs).

10.3389/fimmu.2023.1164724

Results: The genera *Prevotella* and *Parabacteroides* were relatively common in the group showing efficacy towards the anti-PD-1 antibody treatment (effective group). The proportions of *Catenibacterium* (P = 0.022) and *Turicibacter* (P = 0.049) were significantly higher in the effective group than in the ineffective group. In addition, the proportion of *Desulfovibrion* (P = 0.033) was significantly higher in the ineffective group. Next, they were divided into irAE and non-irAE groups. The proportions of *Turicibacter* (P = 0.001) and *Acidaminococcus* (P = 0.001) were significantly higher in the group with irAEs than in those without, while the proportions of *Blautia* (P = 0.013) and the unclassified *Clostridiales* (P = 0.027) were significantly higher in the group without irAEs than those with. Furthermore, within the Effective group, *Acidaminococcus* and *Turicibacter* (both P = 0.001) were more abundant in the subgroup with irAEs than in those without them. In contrast, *Blautia* (P = 0.021) and *Bilophila* (P= 0.033) were statistically significantly more common in those without irAEs.

Discussion: Our Study suggests that the analysis of the gut microbiota may provide future predictive markers for the efficacy of cancer immunotherapy or the selection of candidates for fecal transplantation for cancer immunotherapy.

KEYWORDS

clinical efficacy, gut microbiota, immune checkpoint inhibitors, immune-related adverse events, PD-1 inhibitor, *Turicibacter*, *Acidaminococcus*

1 Introduction

Approximately 40 trillion bacteria of 1,000 types are thought to coexist in the human intestine, with the intestinal microflora weighing 1.5–2 kg (1). It is not known how these intestinal bacteria originally came to coexist with humans. The formation of the human intestinal microbiota begins immediately after birth. The intestinal microbiota formed during the neonatal period is not invariant throughout life, and the constituent bacteria change with age (2). Additionally, it has been reported that the microbiota is affected by various environmental factors, such as the duration of gestation, mode of delivery, and mode of breastfeeding (3). Gut microbiota is known to differ across racial or ethnic groups (4).

Moreover, the pattern of the intestinal microbiota also varies with the content of the long-term diet (5). Enterotypes are classified by similar populations (5, 6). For instance, type B is dominated by the genus *Bacteroides*, while type P is dominated by the genus *Prevotella*.

When the composition of this bacterial layer is disrupted, diseases such as inflammatory bowel disease, rheumatic disease, obesity, diabetes, atopy, allergies, etc., are triggered. Such dysbiosis may also have a severe impact on cancer (7). With advances in dysbiosis research, the concepts of "good bacteria" and "bad bacteria" are now used less frequently (8–14). Additionally, due to recent technological advances, next-generation sequencing analysis of intestinal bacteria has become possible, resulting in accumulating information on the microbiota constitution in various disease groups, including cancers (8, 9, 15–18).

A fairly recent advance in cancer treatment involves the use of immune checkpoint inhibitors (ICIs). One such treatment is the use of anti-PD-1/PD-L1 antibodies, which primarily inhibit the negative regulatory mechanisms between a tumor and the T cells. This is called the effector phase. In contrast, anti-CTLA-4 antibodies, another form of ICI treatment, maintain T cell activation by blocking inhibitory signals from dendritic cells in lymph nodes (19). This is referred to as the priming phase.

Groups in the US and France have reported that certain gut bacteria may modulate the clinical efficacy of anti-PD-1 antibodies (8, 9, 13). However, the gut microbiota influencing ICI efficacy reported by each group differed, and no common bacteria were identified. The differences in microbiota associated with racial/ethnic groups or with long-term diet may have influenced the above findings. Nevertheless, increasing evidence indicates that microbiota constitution may be highly correlated with the therapeutic efficacy of ICIs (20–22). Moreover, intestinal bacteria may be involved in many types of cancer, including esophageal and gastric cancer (23). Furthermore, it has been reported that the administration of antibiotics has a robust negative effect on intestinal bacteria and thereby, on the therapeutic effect of ICIs (24, 25)

While the effect of the microbiota on ICI efficacy has been reported in various countries, it has not yet been reported in Japanese individuals, who reportedly have a higher proportion of *Bifidobacterium* in the gut microbiota than individuals from the US. Thus, in this study, we investigated the gut microbiota of Japanese cancer patients treated with ICI monotherapy to identify bacteria involved in ICI efficacy and in the occurrence of immune-related adverse events.

Abbreviations: ICI, immune checkpoint inhibitor; irAE, Immune-related adverse event; ORR, overall response rate; PD, progressive disease; PFS, progression-free survival; PR, partial response; SCFA, short-chain fatty acid; SD, stable disease.

2 Methods

2.1 Patients

The study was approved by the Ethics Committee of Showa University School of Medicine (Approval No. 2165). The participants in this study were 26 cancer patients treated with nivolumab or pembrolizumab from 2018 to 2021 at the Division of Medical Oncology, Showa University Hospital, who gave written consent to participate. There were 14 non-small cell lung cancer patients, nine stomach cancer patients, two malignant melanoma patients, and one bladder cancer patient.

2.2 Clinical evaluation methods

Patients underwent ICI treatment as per the following regimen: 240 mg Nivolumab in the form of a 30-minute intravenous injection (IV) infusion every 2 weeks. Treatment efficacy was defined as partial response (PR) and stable disease (SD) at 1 year after the start of ICI treatment. In contrast, progressive disease (PD) was defined as a lack of efficacy. Efficacy was evaluated using the durable clinical response as in PR and SD as efficacy, and PD as inefficacy.

Immune-related adverse events (irAEs) of Grade 2 or higher, evaluated using the National Cancer Institute Common Terminology Criteria for Adverse Events (version 4.0), during the 1-year follow-up period were considered as irAEs.

2.3 Bacterial analysis

Fecal samples were collected before treatment within three weeks of starting the therapy using a stool collection kit containing guanidine (TechnoSuruga Laboratory, Shizuoka, Japan). Fecal samples were stored at -80°C until further analysis. DNA was extracted using the QIAamp PowerFecal Pro DNA Kit (QIAGEN, Hilden, Germany) according to the manufacturer's instructions. MetaGenome analysis was performed on a next-generation sequencer (MySeq: Illumina, San Diego, CA, USA) to analyze the 16S V3 and V4 regions of ribosomal RNA genes. Quiime2 (https://qiime2.org/) was used to identify the bacteria. In this study, an exploratory statistical analysis was performed on the differences in bacterial abundance between groups to reveal new insights and identify potential directions for future research. Statistical analysis was performed by using the Mann–Whitney U-test in the JMP pro software (SAS, Tokyo, JAPAN).

3 Results

3.1 Composition of the bacterial flora in each case

The bacterial florae (genus level) in the stool of each patient with solid cancer (n=26), before the start of anti-PD-1 antibody therapy, are shown in Figures 1A, B, respectively. The relative abundance of the different genera, where the total is 100%, is shown in Figures 1C, D.

3.2 Differences in gut microbiota composition in patients with and without a durable clinical response

The group with a good clinical response, including SD, at 1 year after ICI administration was defined as the Effective group (n=16), while the other group was defined as the Ineffective group (n=10). The mean intestinal microbiota of these two groups is shown in bar graphs, with the vertical axis representing the percentage of bacteria that could be discriminated at the genus level (Figure 2A), with the sum of all bacteria constituting 100%. Individual bacteria are indicated by color in Figure 2B.

In Figure 2C, the bacteria shown in Figure 2A are shown in a phylogenetic diagram, with phylogeny color-coded according to the efficacy (effective vs. ineffective) of the anti-PD-1 antibody. *Prevotella* and *Parabacteroides* were relatively common in the effective group, although the same genera were also found in the ineffective group (Figure 2C).

3.3 Analysis of the top-20 most abundant enterobacterial genera

Next, we selected only those bacteria that represented more than 0.1% of the total number of bacteria in each group and expressed the sum of the bacteria as a percentage of 100%. The percentage of the intestinal microflora is shown as a bar graph in Figures 2D, E. The top-5 most abundant genera in the Effective group were *Bacteroides*, *Parabacteroides*, *Streptococcus*, and *Parabacteroides*, while in the Ineffective group, *Bacteroides*, unclassified Enterobacteriaceae, *Lactobacillus*, *Streptococcus*, and *Parabacteroides* were most abundant (Table 1A).

Differences in the top-20 genera composing the microbiota between the Effective and Ineffective groups were then statistically compared. *Catenibacterium* ($P = 0.022$) and *Turicibacter* ($P = 0.049$) were overrepresented in the Effective group when compared to the Ineffective group (Figure 3A; Tables 2A, B).

3.4 Differences in intestinal microbiota composition according to presence or absence of immune-related adverse events

Patients were categorized into two groups: irAE (n=12) and non-irAE (n=14). The irAEs observed in this study were as follows: Hypothyroidism in 4 cases, Rash in 4 cases, Oral Mucositis in 1 case, Type 1 Diabetes in 1 case, Hypopituitarism in 2 cases, Pneumonitis in 2 cases, Infusion Reaction in 1 case, and Asthma in 1 case. A history of autoimmune diseases was present in 2 cases (Table S1). The mean intestinal microbiota compositions in those with and without Grade 2 or higher irAEs during the course of treatment are shown in Figure 4, where the vertical axis shows the sum of all bacteria at the discriminable genus level as 100%. The vertical axis shows the bacterial flora at the genus level in Figure 4A, while their individual names are shown by color in Figure 4B.

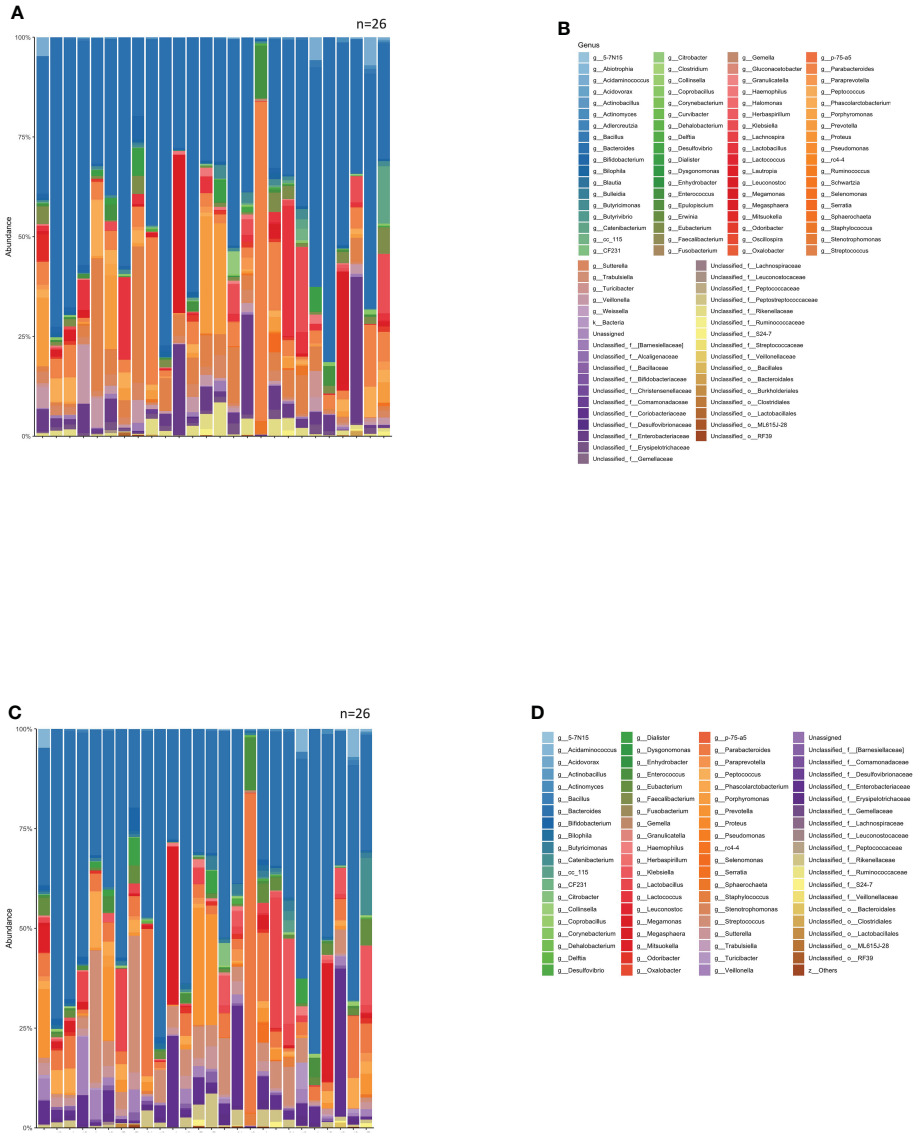

FIGURE 1
Relative abundance of intestinal bacteria in each patient before initiation of anti-PD-1 antibody therapy. **(A)** Percentage of bacteria at discernible genus level in the total stool of each patient. **(B)** Names of the bacteria represented in the bar graph in **(A)**. **(C)** Bar graph showing the proportions of the bacteria in **(A)** that were found in 0.1% or more of the stools, summed to 100%. **(D)** Names of bacteria shown in **(C)**.

In Figure 4C, bacteria shown in Figure 4A are represented in a phylogenetic tree, which is color-coded according to the presence or absence of irAEs to anti-PD-1 antibody (Figure 4C).

3.5 Analysis of the top-20 most abundant genera according to the presence or absence of immune-related adverse events

Next, the average intestinal microbiota was calculated by summing (to 100%) the bacteria in Figure 4A of which 0.1% or more were associated with irAEs, whereas the remaining were not (Figures 4D, E). The Top 20 bacteria are shown in Table 1B. Particular attention was paid to the top 3%, which consisted of the following six bacteria. In other words, the top-5 most abundant genera in the irAE group were *Bacteroides*, *Parabacteroides*, *Streptococcus*, *Phascolarctobacterium*, and *Veillonella*, while those in the group without irAE were *Bacteroides*, *Parabacteroides*, *Streptococcus*, *Prevotella*, and *Megamonas*.

Statistically differences in the top-20 most abundant genera were analyzed between the irAE and without irAE groups. In the irAE group, *Turicibacter* (P = 0.001) and *Acidaminococcus* (P = 0.001) were more abundant than in the no-irAE group. In contrast, *Blautia* (P = 0.013) and unclassified Clostridiales (P = 0.028) were statistically more common in the no-irAE group (Figure 3B; Tables 2C, D).

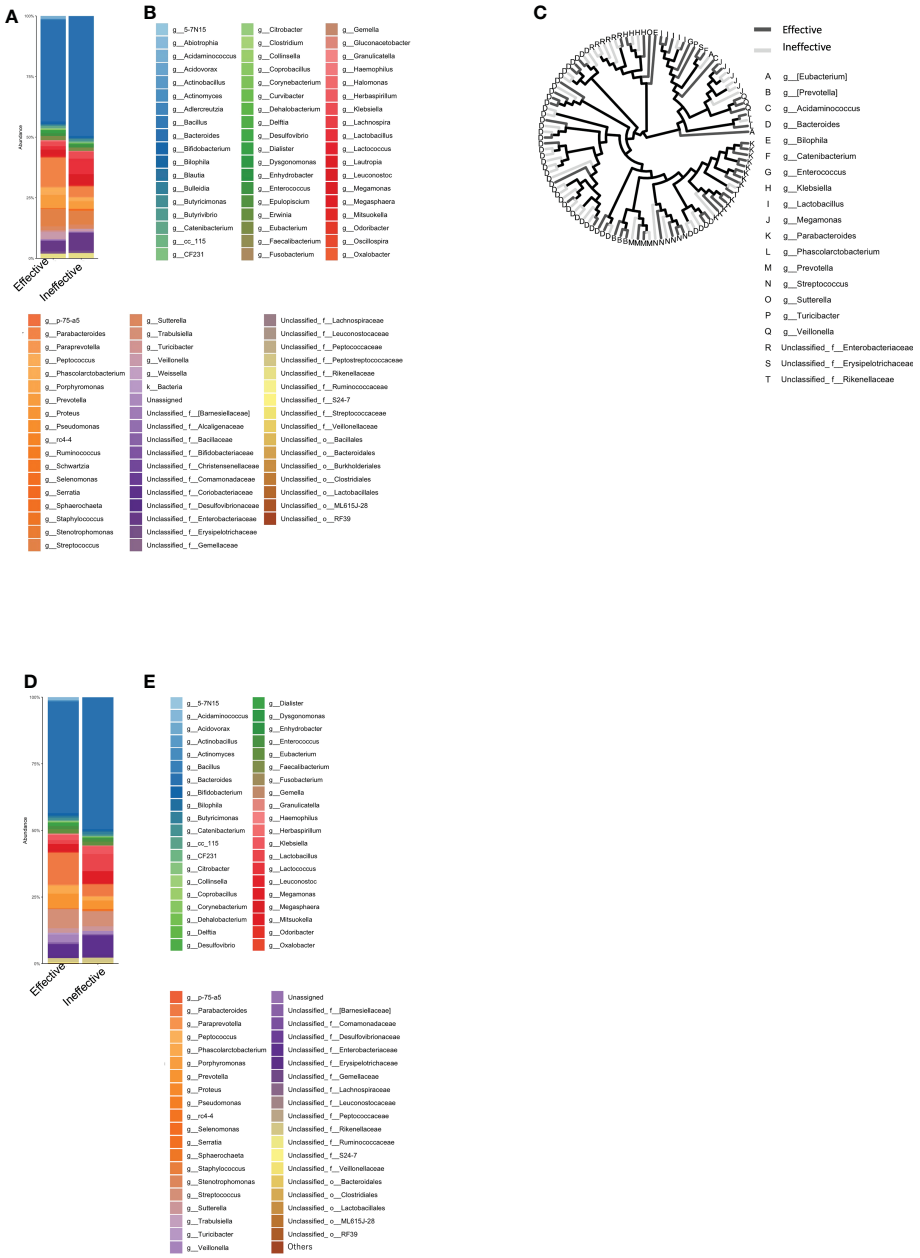

FIGURE 2
Percentage composition of microbiota in groups based on the therapeutic efficacy of anti-PD-1 antibody treatment in cancer patients. **(A)** Relative abundance (%, composition) of bacteria at the genus level in the Effective and Ineffective treatment groups. **(B)** Names of bacteria shown in **(A)**. **(C)** Bacterial tree diagram, with the dark gray and light gray lines indicating the bacteria found in the Effective Ineffective groups, respectively. **(D)** Bar graph showing the bacterial composition of the microbiota in the Effective and Ineffective groups. Bacteria that were found in more than 0.1% of the cases were summed to 100%. **(E)** Names of bacteria shown in **(C)**.

3.6 Differences in gut microbiota composition in the Effective group with and without immune-related adverse events

The mean intestinal microbiota in the Effective group was divided into subgroups: those with (n=10) and those without Grade 2 or higher irAEs (n=6) (Figures 5A, B). Color-coded phylogenetic trees are based on the presence or absence of irAEs to anti-PD-1 antibody in the Effective group (Figure 5C). The top-5 most abundant genera associated with treatment efficacy without irAEs were *Bacteroides*, *Parabacteroides*, *Prevotella*, *Streptococcus*, and *Megamonas*. Bacteria associated with treatment efficacy, but with irAEs were *Bacteroides*, *Parabacteroides*, *Streptococcus*, unclassified *Enterobacteriaceae*, and *Veillonella* (Table 1C).

10.3389/fimmu.2023.1164724

TABLE 1 Percentage of predominant bacteria (%) in the treatment response, immune-related adverse events (irAEs), and irAEs in the treatment response group.

(A) Top-20 bacteria by treatment effect at genus level		
Abundance (%)	Effective	Ineffective
g:Parabacteroides	11.951	4.290
g:Prevotella	5.408	2.961
g:Veillonella	2.945	1.099
g:Phascolarctobacterium	3.007	1.249
g:Streptococcus	7.132	5.611
g:Acidaminococcus	1.176	0.015
g:Dialister	1.264	0.188
g:Turicibacter	0.635	0.038
g:Catenibacterium	0.897	0.476
g:Mitsuokella	0.409	0.000
g:Porphyromonas	0.045	0.292
g:cc_115	0.039	0.293
Unclassified_ f:Rikenellaceae	1.525	1.813
g:Butyricimonas	0.575	0.944
g:Serratia	0.028	0.491
g:Klebsiella	1.938	2.915
g:Megamonas	1.776	4.111
Unclassified_ f:Enterobacteriaceae	4.312	7.351
g:Lactobacillus	1.434	6.377
g:Bacteroides	41.783	49.238
(B) Top-20 bacteria at genus level, by presence/absence of immune-related adverse events (irAEs)		
Abundance (%)	No irAE	With irAE
g:Megamonas	4.951	0.018
g:Prevotella	6.159	2.494
g:Parabacteroides	9.809	8.066
Unclassified_ f:Rikenellaceae	2.339	0.815
g:Streptococcus	7.147	5.848
g:Sutterella	2.143	1.201
g:Enterococcus	1.606	0.669
Unclassified_ f:[Barnesiellaceae]	0.737	0.202
g:Lactobacillus	3.574	3.057
g:Butyricimonas	0.940	0.456
g:Klebsiella	2.213	2.431
g:Coprobacillus	0.105	0.360
g:Citrobacter	0.018	0.522
g:Mitsuokella	0.003	0.543
g:Turicibacter	0.030	0.843

(Continued)

TABLE 1 Continued

(B) Top-20 bacteria at genus level, by presence/absence of immune-related adverse events (irAEs)		
Abundance (%)	No irAE	With irAE
g:Catenibacterium	0.340	1.197
g:Acidaminococcus	0.008	1.571
g:Phascolarctobacterium	1.544	3.249
g:Veillonella	1.411	3.197
g:Bacteroides	39.495	50.665
(C) Top-20 bacteria at genus level, by presence/absence of immune-related adverse events (irAEs) in cases with effective treatment		
Abundance (%)	Effective without irAE	Effective with irAE
g:Parabacteroides	16.834	9.021
g:Prevotella	9.937	2.691
g:Megamonas	4.711	0.015
g:Enterococcus	2.488	0.310
g:Streptococcus	8.127	6.536
Unclassified_ f:Rikenellaceae	2.509	0.935
g:Sutterella	2.506	1.197
g:Dialister	2.069	0.781
Unclassified_ f:[Barnesiellaceae]	1.068	0.224
g:Bifidobacterium	1.296	0.555
g:Citrobacter	0.000	0.621
g:Mitsuokella	0.006	0.651
g:Turicibacter	0.025	1.000
g:Phascolarctobacterium	2.171	3.508
g:Catenibacterium	0.000	1.436
g:Acidaminococcus	0.000	1.881
g:Veillonella	1.606	3.749
g:Klebsiella	0.305	2.917
Unclassified_ f:Enterobacteriaceae	1.571	5.956
g:Bacteroides	33.174	46.948

3.7 Analysis of the top-20 most abundant enterobacteria in the effective group

Next, we selected the bacteria that accounted for more than 0.1% of the total the gut microbiota, and showed the mean intestinal microbiota of the groups with and without irAEs as a percentage (Figures 5D, E). *Bacteroides*, unclassified *Enterobacteriaceae*, *Klebsiella*, *Veillonella*, and *Acidaminococcus* were predominant in the group with irAEs. In the group without irAEs, *Parabacteroides Prevotella*, *Megamonas*, *Enterococcus*, and *Streptococcus* were more abundant. The Effective group was then divided into the irAE and no-irAE subgroups, and statistically differences between the two subgroups were analyzed. *Acidaminococcus* (P = 0.001) and *Turicibacter* (P = 0.001) were more abundant in the irAE subgroup within the Effective group. In contrast, *Blautia* (P = 0.021) and *Bilophila* (P= 0.033) were more common in the no-irAE subgroup than in the irAE subgroup within the Effective group (Figure 3C; Tables 2E, F).

3.8 Alpha-diversity of gut microbiota

There were no statistically differences in alpha-diversity between the Effective and Ineffective groups (Figure 6A), with and without irAEs (Figure 6B), and with and without irAEs in the Effective group (Figure 6C).

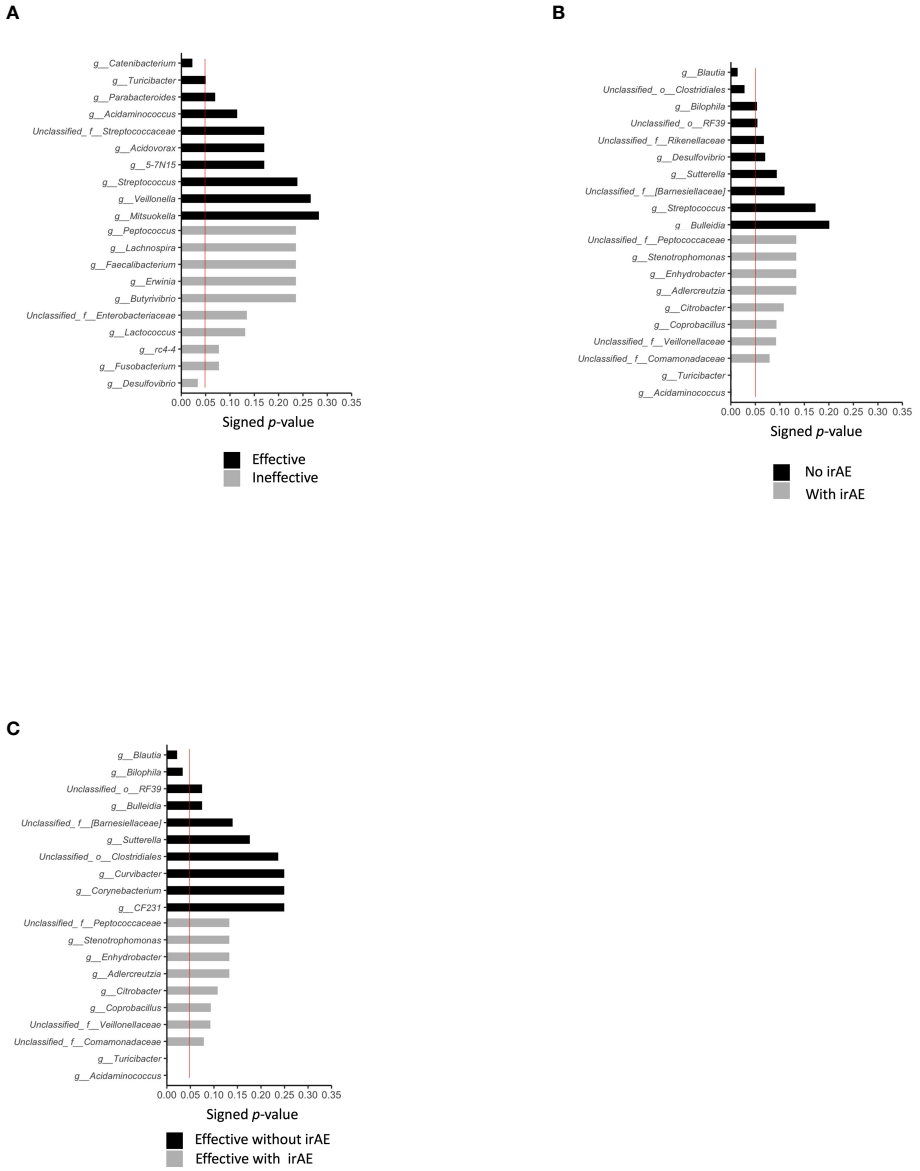

FIGURE 3
Statistically significant differences in intestinal bacteria. We compared the statistical significance of differences in bacteria in the presence or absence of treatment effect, presence or absence of irAE, and presence or absence of irAE within the effective treatment group, using the Mann–Whitney Utest. The red line indicates a P value of 0.05. **(A)** Top-10 bacteria by treatment effect at the genus level. **(B)** Top-10 bacteria by irAE at genus level **(C)** Top-10 bacteria by genus level according to the presence/absence of irAE in cases showing effective treatment response to anti-PD-1 antibody.

TABLE 2 Statistically significant differences in gut microbiota between groups.

(A) Top-20 bacteria at genus level, in descending order of P value by treatment response	
Efective	*p*-value
g:Catenibacterium	0.022
g:Turicibacter	0.049
g:Parabacteroides	0.068
g:Acidaminococcus	0.113

(Continued)

TABLE 2 Continued

(A) Top-20 bacteria at genus level, in descending order of P value by treatment response	
Efective	*p*-value
g:5-7N15	0.168
g:Acidovorax	0.168
Unclassified_ f:Streptococcaceae	0.168
g:Streptococcus	0.235

(Continued)

10.3389/fimmu.2023.1164724

TABLE 2 Continued

(A) Top-20 bacteria at genus level, in descending order of P value by treatment response	
Efective	*p*-value
g:Veillonella	0.262
g:Bulleidia	0.278
g:Mitsuokella	0.278
g:Trabulsiella	0.278
Unclassified_ f:Peptococcaceae	0.278
Unclassified_ f:Comamonadaceae	0.338
Unclassified_ f:Veillonellaceae	0.338
g:Haemophilus	0.382
g:Phascolarctobacterium	0.392
g:Leuconostoc	0.421
g:Abiotrophia	0.476
g:Clostridium	0.476
(B) Top-20 bacteria at genus level, in descending order of P value by treatment non-response	
Ineffective	*p*-value
Unclassified_ o:Clostridiales	0.018
g:Desulfovibrio	0.033
g:Fusobacterium	0.077
g:rc4-4	0.077
g:Lactococcus	0.130
Unclassified_ f:Enterobacteriaceae	0.134
g:Butyrivibrio	0.235
g:Erwinia	0.235
g:Faecalibacterium	0.235
g:Lachnospira	0.235
g:Peptococcus	0.235
g:Proteus	0.235
g:Pseudomonas	0.235
g:Selenomonas	0.235
Unclassified_ f:Leuconostocaceae	0.235
Unclassified_ o:Burkholderiales	0.235
g:Serratia	0.265
g:Megamonas	0.335
g:Ruminococcus	0.353
g:Bacteroides	0.363

(Continued)

TABLE 2 Continued

(C) Top-20 bacteria at genus level, in decreasing order of P value by absence of immune-related adverse events (irAEs)C	
No irAE	*p*-value
g:Blautia	0.013
Unclassified_ o:Clostridiales	0.027
g:Bilophila	0.053
Unclassified_ o:RF39	0.054
Unclassified_ f:Rikenellaceae	0.067
g:Desulfovibrio	0.070
g:Sutterella	0.094
Unclassified_ f:[Barnesiellaceae]	0.109
g:Streptococcus	0.172
g:Bulleidia	0.200
g:CF231	0.200
g:Fusobacterium	0.200
g:Herbaspirillum	0.200
g:rc4-4	0.200
Unclassified_ f:Desulfovibrionaceae	0.200
Unclassified_ o:ML615J-28	0.200
g:Parabacteroides	0.297
g:Enterococcus	0.321
g:Dialister	0.357
g:Megamonas	0.362
(D) Top-20 bacteria at genus level, in decreasing order of P value by presence of immune-related adverse events (irAEs)	
With irAE	*p*-value
g:Acidaminococcus	0.001
g:Turicibacter	0.001
Unclassified_ f:Comamonadaceae	0.078
Unclassified_ f:Veillonellaceae	0.092
g:Coprobacillus	0.093
g:Citrobacter	0.108
g:Adlercreutzia	0.133
g:Enhydrobacter	0.133
g:Stenotrophomonas	0.133
Unclassified_ f:Peptococcaceae	0.133
Unclassified_ o:Lactobacillales	0.133
g:Bacteroides	0.144

(Continued)

10.3389/fimmu.2023.1164724

TABLE 2 Continued

(D) Top-20 bacteria at genus level, in decreasing order of P value by presence of immune-related adverse events (irAEs)	
With irAE	*p*-value
g:Catenibacterium	0.163
g:Veillonella	0.211
g:Granulicatella	0.251
g:Abiotrophia	0.315
g:Clostridium	0.315
g:Dysgonomonas	0.315
g:Halomonas	0.315
g:Oxalobacter	0.31587
(E) Top-20 bacteria at genus level, in order of decreasing P-value by absence of immune-related adverse events (irAEs) in cases showing effective treatment response to anti-PD-1 antibody	
Effective without irAE	*p*-value
g:Blautia	0.021
g:Bilophila	0.033
g:Bulleidia	0.073
Unclassified_ o:RF39	0.073
Unclassified_ f:[Barnesiellaceae]	0.137
g:Sutterella	0.173
Unclassified_ o:Clostridiales	0.232
g:CF231	0.245
g:Corynebacterium	0.245
g:Curvibacter	0.245
g:Epulopiscium	0.245
g:Gemella	0.245
g:Gluconacetobacter	0.245
g:Herbaspirillum	0.245
g:Lautropia	0.245
g:Weissella	0.245
Unclassified_ f:Bifidobacteriaceae	0.245
Unclassified_ f:Desulfovibrionaceae	0.245
Unclassified_ f:Peptostreptococcaceae	0.245
Unclassified_ o:Bacillales	0.245
(F) Top-20 bacteria at genus level, in order of decreasing P-value by presence of immune-related adverse events (irAEs) in cases showing effective treatment response to anti-PD-1 antibody	
Effective with irAE	*p*-value
g:Acidaminococcus	0.001

(Continued)

TABLE 2 Continued

(F) Top-20 bacteria at genus level, in order of decreasing P-value by presence of immune-related adverse events (irAEs) in cases showing effective treatment response to anti-PD-1 antibody	
Effective with irAE	*p*-value
g:Turicibacter	0.001
Unclassified_ f:Comamonadaceae	0.078
Unclassified_ f:Veillonellaceae	0.092
g:Coprobacillus	0.093
g:Citrobacter	0.108
g:Adlercreutzia	0.133
g:Enhydrobacter	0.133
g:Stenotrophomonas	0.133
Unclassified_ f:Peptococcaceae	0.133
Unclassified_ o:Lactobacillales	0.133
g:Bacteroides	0.144
g:Catenibacterium	0.163
g:Veillonella	0.211
g:Granulicatella	0.251
g:Abiotrophia	0.315
g:Clostridium	0.315
g:Dysgonomonas	0.315
g:Halomonas	0.315
g:Oxalobacter	0.315

Statistical analyses were performed by the Mann–Whitney U-test between two groups.

4 Discussion

We found that *Prevotella* and *Parabacteroides* were relatively common in the Effective group. In the overall cohort, *Turicibacter* (P = 0.001) and *Acidaminococcus* (P = 0.001) were more abundant in the irAE group. In contrast, *Blautia* (P = 0.013) and unclassified Clostridiales (P = 0.028) were more prevalent in the no-irAE group. Similarly, within the Effective group, *Acidaminococcus* and *Turicibacter* (both P = 0.001) were more abundant in the subgroup with irAEs than in those without, while *Blautia* (P = 0.021) and *Bilophila* (P= 0.033) were more commonly found in those without irAEs.

Bifidobacterium, *Lactobacillus*, phylum Bacteroidetes, *Akkermansia muciniphila*, and *Faecalibacterium* have been reported as bacteria involved in the beneficial effect of ICI (8, 10–14, 18). On the other hand, *Prevotella* and *Fusobacterium nucleatum* have been reported as a bacterial flora with negative effects in cancer immunity, such as cancer recurrence (8, 10–14, 18). In previous studies, the genera *Bacteroidetes* and *Lactobacillus* have been reported as bacteria associated with ICI efficacy. One possible reason for the difference in results between our study and previous

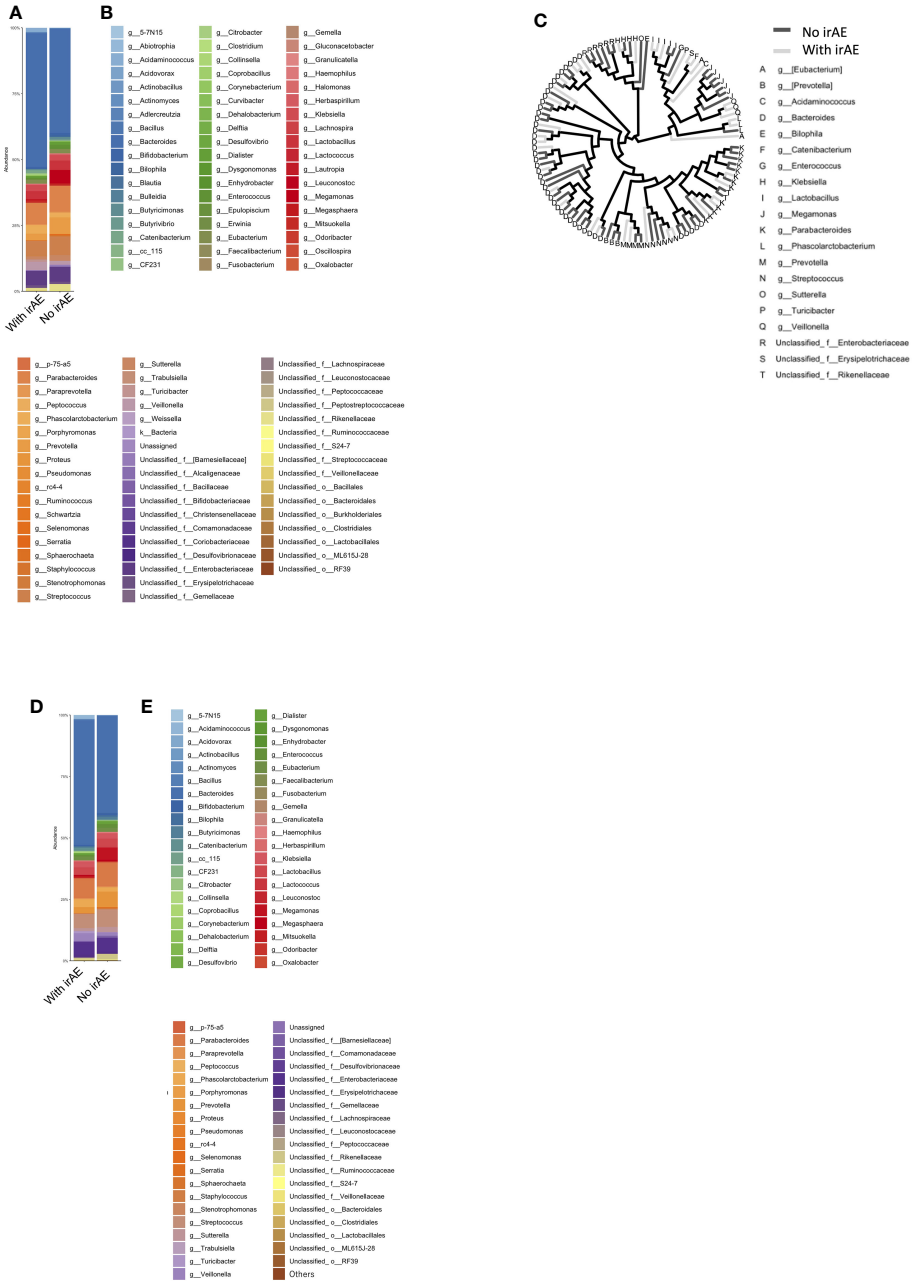

FIGURE 4
Microbiota composition according to the presence or absence of immune-related adverse events (ir-AEs). **(A)** Relative abundance (%, composition) of bacteria at the genus level in the irAE- and no-irAE groups. **(B)** Names of bacteria shown in **(A)**. **(C)** Bacterial tree, with dark gray lines indicating bacteria found in the no-irAE group and light gray lines indicating bacteria found in the irAE group. **(D)** Bar graph showing the microbiota composition in each group, where the sum of all the bacteria found in more than 0.1% of the cases in each group were summed to 100%. **(E)** Names of bacteria shown in **(D)**.

studies may be that microbiota composition differs by race and region. It has been reported that the composition of the human intestinal microbiota in healthy individuals was significantly diverse across 12 countries: Japan, Denmark, Spain, USA, China, Sweden, Russia, Venezuela, Malawi, Austria, France, and Peru (26). In particular, the gut microbiota of the Japanese was reported to be different from those of other populations (26). Specifically, Japanese have more *Bifidobacterium* and fewer *Bacteroidetes* and *Prevotella* than Americans (26).

In the present study, the genera *Parabacteroides* and *Prevotella* were more abundant in the Effective group without irAEs than those with irAEs, although there was no statistically difference in abundance (%). *Parabacteroides* and *Prevotella* are underrepresented in the Japanese population (26). The high prevalence of *Parabacteroides* and *Prevotella*

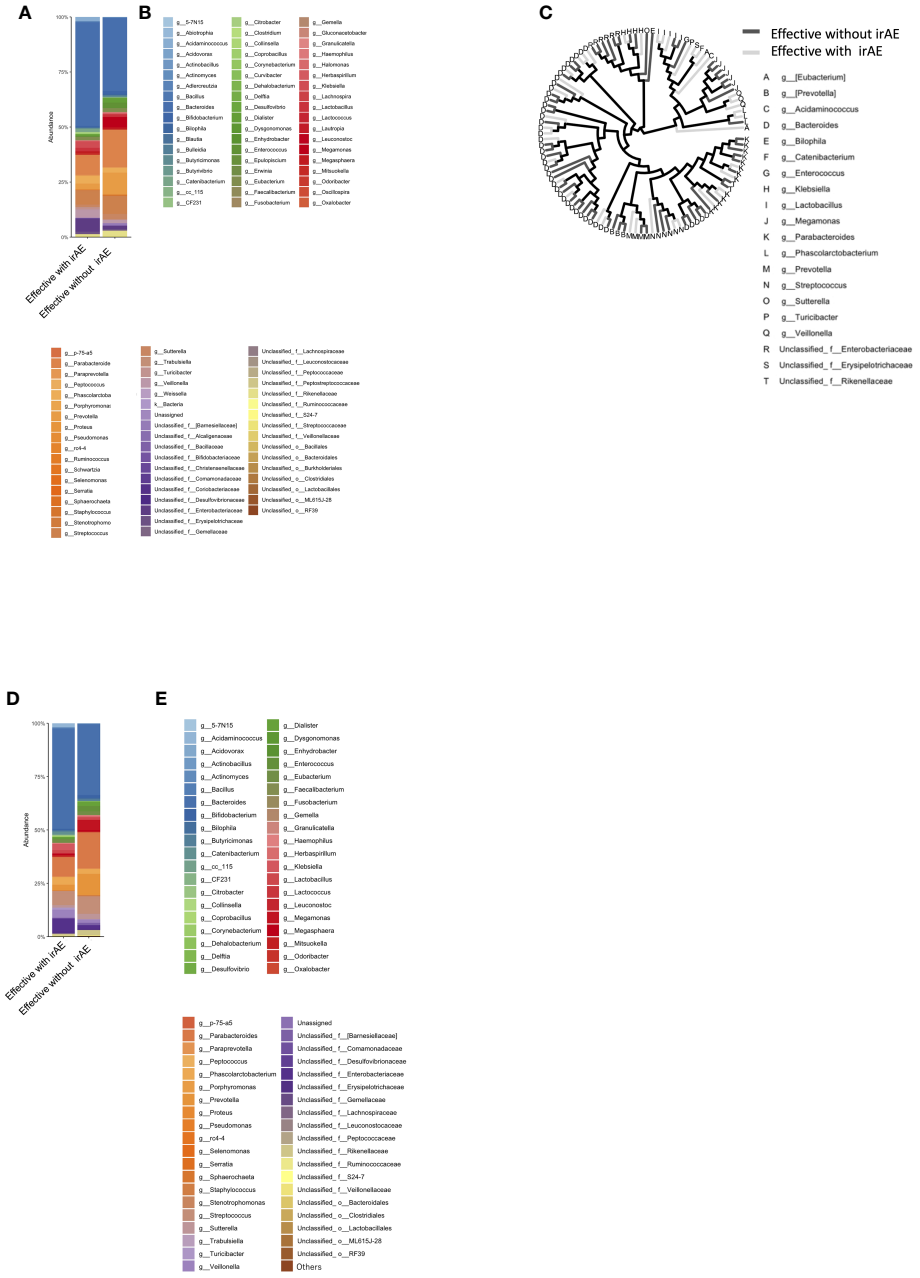

FIGURE 5
Bacterial proportions in the microbiota in the group showing an effective response to anti-PD-1 antibody, with and without irAE. **(A)** Relative abundance (%, composition) of bacteria at discriminable genus level in patients with and without irAE who responded to anti-PD-1 antibody treatment. **(B)** Names of bacteria shown in **(A)**. **(C)** Bacterial tree, with dark gray lines indicating bacteria found in the no-irAE group and light gray lines indicating bacteria found in the irAE group. **(D)** Bar graph showing the proportion of bacteria in each group, where the sum of all the bacteria found in more than 0.1% of the cases in each group were summed to 100%. **(E)** Names of bacteria shown in **(D)**.

in the top tier in our study is very interesting, since these may therefore be biomarkers of therapeutic efficacy without irAEs for Japanese patients receiving ICI. *Parabacteroides distasonis* was reported to be abundant in intestinal bacteria in French patients with non-small cell lung cancer and renal cell carcinoma in a population treated using anti-PD-1 antibodies, with a PFS of less than 3 months (9).

Peng et al. reported that *Prevotella* spp. increased in Chinese patients after the treatment of gastrointestinal cancer with anti-PD-1/PD-L1 agents. In particular, the relative amount of *Prevotella* spp. increased in responders (27). The group with a higher *Prevotella* abundance had a longer PFS than the group with lower abundance. Conversely, the group with a higher abundance of *Bacteroides* had a shorter PFS (27). However, Gopalakrishnan et al. reported a high presence of *Prevotella histicola* in American melanoma non-responders. In addition, they found that patients with high levels of *Bacteroides* had a shorter PFS (8).

10.3389/fimmu.2023.1164724

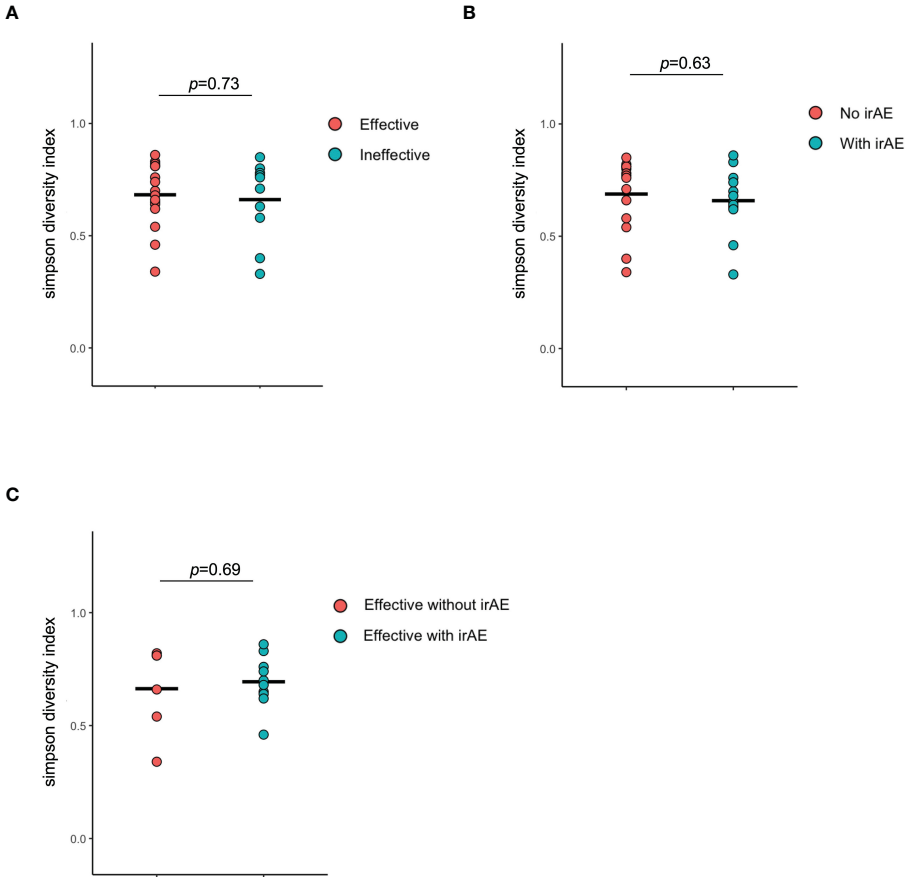

FIGURE 6
Alpha diversity of the intestinal microbiota. **(A)** Comparison of Simpson diversity index between effective and ineffective groups. **(B)** Comparison of Simpson diversity index between responders and non-responders in terms of immune-related adverse effects. **(C)** Comparison of Simpson diversity index between responders and non-responders in terms of immune-related adverse effects in the effective group.

The mechanism by which *Prevotella* spp. exert an antitumor effect is unknown. In the present study, *Prevotella* spp. were more common in the group that showed efficacy during ICI treatment. The genus *Prevotella* and its related metabolites, and their positive effects on immunity, should be elucidated in future studies.

In the present study, *Bacteroidetes* and *Lactobacillus* were more abundant in the Ineffective group. The high prevalence of *Bacteroidetes* in this group was consistent with the study by Peng et al. (27). In another study, the genera *Bacteroidetes* and *Lactobacillus* were reported as bacteria associated with ICI efficacy. The reason for the differences in results may be that the organisms involved in the efficacy of ICIs may differ by country or type of carcinoma.

The most important result of the present study was the identification of bacteria with a high abundance (%) in the gut microbiota showing statistically significant differences between groups with and without treatment response or with and without irAEs. These are candidate bacteria that may influence anti-PD-1 antibody therapy.

Catenibacterium had a statistically significant higher percentage in the Effective than in the Ineffective group.

Interestingly, *Turicibacter* was statistically significantly overrepresented in the Effective group, irAE group, and irAE subgroup within the Effective group. *Turicibacter* may be involved in overall immune activation.

Acidaminococcus may be strongly involved in irAE, since it was statistically significantly more abundant in the irAE group and the irAE subgroup within the Effective group. *Acidaminococcus* was shown in a Taiwanese study to be associated with hepatocellular carcinoma treated with anti-PD-1/anti-PD-L1in responder, in some cases in combination with angiogenesis inhibitors, and in patients with controlled disease (objective response or SD for ≥ 16 weeks) (28). In the present study, its proportion was statistically significantly higher in patients with irAE and in the effective population with irAEs. Future studies should elucidate the mechanisms involved in anti-PD-1 antibody therapy, including the related metabolites, to elucidate the effects of these bacteria on antitumor immunity.

The involvement of bacterial metabolites has been suggested as a mechanism by which the gut microbiota influences the immune system. For example, the genus *Bacteroidetes* is capable of inducing IgA production, in addition to producing various short-chain fatty acids. *Lactobacillus* is a lactic acid-producing bacterium. All of these bacteria are short-chain fatty acid (SCFA) producers, which are considered to be beneficial for ICI treatment. SCFAs are considered to activate and regulate immunity. The related mechanism is mainly

determined by their receptors, however, much about this process remains unknown. SCFAs play important roles in human immunity and homeostasis, such as induction of regulatory T cells, type 1 helper T cells, and maintenance of intestinal epithelial cell proliferation (29). However, its relationship with antitumor effects in particular remains to be elucidated. Interestingly, SCFAs produced by bacteria fermenting dietary fiber as a nutrient source are certainly involved, highlighting the importance of studies on the significance of including fiber in the diet and on the effect of each SCFA on immunity. In addition to SCFAs, other metabolites produced by intestinal bacteria have also been studied extensively in recent years. However, facultative anaerobic bacteria have few enzymes that can digest dietary fiber, and utilize sources of nutrients that are abundant in Westernized diets, such as monosaccharides, disaccharides, fats, proteins, and alcohols, instead of dietary fiber (30).

Although SCFAs are generally known to increase antitumor activity, some data suggest that they may inhibit some conditions and types. For instance, a mouse study showed that sodium butyrate inhibited anti-CTLA-4-induced dendritic cell maturation and T-cell priming (31). Further studies are needed to elucidate the mechanisms by which individual SCFAs affect cancer immunity. In fact, individual SCFAs differ in their immune activity. The details of the effects of SCFAs need to be clarified in future studies (28).

If the immune state in which irAEs are likely to occur and the immune state in which efficacy is likely to be demonstrated can be inferred by analyzing intestinal bacteria, it will be possible to induce a state in which irAEs are unlikely to occur and ICI efficacy is likely to be demonstrated by administering various treatments, including modification of the intestinal microflora. At the very least, if these bacteria can be used as biomarkers, it will facilitate therapeutic strategies, particularly in terms of the management of side effects. Nevertheless, our study was limited by the small number of patients and more cases need to be accumulated.

In conclusion, in the present study, we found that *Catenibacterium* was significantly more abundant in the gut microbiota of patients with solid tumors prior to starting treatment with anti-PD-1 antibody monotherapy in the group in which the ICI was effective than in those in whom it was ineffective. *Turicibacter* was also more abundant in the effective group. *Acidaminococcus* was statistically significantly more abundant in the irAE group and in the irAE subgroup within the Effective group, suggesting that *Acidaminococcus* is strongly involved in irAE. The gut microbiota may be an effective biomarker for predicting the efficacy of anti-PD-1 antibody therapy and of irAE. The results of our study differ from those of previously reported studies on the gut microbiota in the US. This highlights the importance of examining the association between the gut microbiota and efficacy of anti-PD-1 antibody therapy by race and region.

Data availability statement

The original contributions presented in the study are publicly available. This data can be found here: https://figshare.com/articles/dataset/The_abundance_of_gut_microbiota_in_Japanese_patients_with_solid_tumors/22654954.

Ethics statement

The studies involving human participants were reviewed and approved by The Ethics Committee of Showa University School of Medicine (Approval No. 2165). The patients/participants provided their written informed consent to participate in this study.

Author contributions

KaH and JI were contributed equally. KaH, JI, and KY designed, performed investigation, analyzed data, and wrote the paper; KoH, MH, YB, MM, YN, HT, EF, KT, MS, YH, ToT, HA, TI, RS, RO, and YKu collected the clinical data of the patients and gave technical support. TS, MT, SW, YKi, SK, AK, AH, Y-GK, and TaT supervised the findings of this work and reviewed the manuscript. All authors contributed to the article and approved the submitted version.

Acknowledgments

We thank Kyoko Homma and Mayu Kato for their management of the sample collection. The authors would like to thank Editage (www.editage.com) for English language editing. The authors are grateful to Eisuke Inoue for advice on statistical analysis.

Conflict of interest

The authors declare that the research was conducted in the absence of any commercial or financial relationships that could be construed as a potential conflict of interest.

Publisher's note

Supplementary material

The Supplementary Material for this article can be found online at: https://www.frontiersin.org/articles/10.3389/fimmu.2023.1164724/full#supplementary-material

References

1. Sender R, Fuchs S, Milo R. Revised estimates for the number of human and bacteria cells in the body. *PloS Biol* (2016) 14:e1002533. doi: 10.1371/journal.pbio.1002533

2. Arboleya S, Binetti A, Salazar N, Fernández N, Solís G, Hernández-Barranco A, et al. Establishment and development of intestinal microbiota in preterm neonates. *FEMS Microbiol Ecol* (2012) 79:763–72. doi: 10.1111/j.1574-6941.2011.01261.x

3. Bäckhed F, Roswall J, Peng Y, Feng Q, Jia H, Kovatcheva-Datchary P, et al. Dynamics and stabilization of the human gut microbiome during the first year of life. *Cell Host Microbe* (201) 5 17::852. doi: 10.1016/j.chom.2015.05.012

4. Hester CM, Jala VR, Langille MG, Umar S, Greiner KA, Haribabu B. Fecal microbes, short chain fatty acids, and colorectal cancer across racial/ethnic groups. *World J Gastroenterol* (2015) 21:2759–69. doi: 10.3748/wjg.v21.i9.2759

5. Arumugam M, Raes J, Pelletier E, Le Paslier D, Yamada T, Mende DR, et al. Enterotypes of the human gut microbiome. *Nature* (2011) 473:174–80. doi: 10.1038/nature09944

6. Vandeputte D, Kathagen G, D'Hoe K, Vieira-Silva S, Valles-Colomer M, Sabino J, et al. Quantitative microbiome profiling links gut community variation to microbial load. *Nature* (2017) 551:507–11. doi: 10.1038/nature24460

7. Cani PD. Gut microbiota - at the intersection of everything? *Nat Rev Gastroenterol Hepatol* (2017) 14:321–2. doi: 10.1038/nrgastro.2017.54

8. Gopalakrishnan V, Spencer CN, Nezi L, Reuben A, Andrews MC, Karpinets TV, et al. Gut microbiome modulates response to anti-PD-1 immunotherapy in melanoma patients. *Science* (2018) 359:97–103. doi: 10.1126/science.aan4236

9. Routy B, Le Chatelier E, Derosa L, Duong CPM, Alou MT, Daillère R, et al. Gut microbiome influences efficacy of PD-1-based immunotherapy against epithelial tumors. *Science* (2018) 359:91–7. doi: 10.1126/science.aan3706

10. Gevers D, Kugathasan S, Denson LA, Vázquez-Baeza Y, Van Treuren W, Ren B, et al. The treatment-naive microbiome in new-onset crohn's disease. *Cell Host Microbe* (2014) 15:382–92. doi: 10.1016/j.chom.2014.02.005

11. Ahn J, Sinha R, Pei Z, Dominianni C, Wu J, Shi J, et al. Human gut microbiome and risk for colorectal cancer. *J Natl Cancer Inst* (2013) 105:1907–11. doi: 10.1093/jnci/djt300

12. Lepage P, Häsler R, Spehlmann ME, Rehman A, Zvirbliene A, Begun A, et al. Twin study indicates loss of interaction between microbiota and mucosa of patients with ulcerative colitis. *Gastroenterology* (2011) 141:227–36. doi: 10.1053/j.gastro.2011.04.011

13. Matson V, Fessler J, Bao R, Chongsuwat T, Zha Y, Alegre ML, et al. The commensal microbiome is associated with anti-PD-1 efficacy in metastatic melanoma patients. *Science* (2018) 359:104–8. doi: 10.1126/science.aao3290

14. Dubin K, Callahan MK, Ren B, Khanin R, Viale A, Ling L, et al. Intestinal microbiome analyses identify melanoma patients at risk for checkpoint-blockade-induced colitis. *Nat Commun* (2016) 7:10391. doi: 10.1038/ncomms10391

15. Lynch SV, Pedersen O. The human intestinal microbiome in health and disease. *N Engl J Med* (2016) 375:2369–79. doi: 10.1056/NEJMra1600266

16. Liu L, Zhang J, Cheng Y, Zhu M, Xiao Z, Ruan G, et al. Gut microbiota: a new target for T2DM prevention and treatment. *Front Endocrinol (Lausanne)* (2022) 13:958218. doi: 10.3389/fendo.2022.958218

17. Matson V, Chervin CS, Gajewski TF. Cancer and the microbiome-influence of the commensal microbiota on cancer, immune responses, and immunotherapy. *Gastroenterology* (2021) 160:600–13. doi: 10.1053/j.gastro.2020.11.041

18. Baruch EN, Youngster I, Ben-Betzalel G, Ortenberg R, Lahat A, Katz L, et al. Fecal microbiota transplant promotes response in immunotherapy-refractory melanoma patients. *Science* (2021) 371:602–9. doi: 10.1126/science.abb5920

19. Ribas A. Tumor immunotherapy directed at PD-1. *N Engl J Med* (2012) 366:2517–9. doi: 10.1056/NEJMe1205943

20. Vétizou M, Pitt JM, Daillère R, Lepage P, Waldschmitt N, Flament C, et al. Anticancer immunotherapy by CTLA-4 blockade relies on the gut microbiota. *Science* (2015) 350:1079–84. doi: 10.1126/science.aad1329

21. Sivan A, Corrales L, Hubert N, Williams JB, Aquino-Michaels K, Earley ZM, et al. Commensal bifidobacterium promotes antitumor immunity and facilitates anti-PD-L1 efficacy. *Science* (2015) 350:1084–9. doi: 10.1126/science.aac4255

22. Wang Y, Wiesnoski DH, Helmink BA, Gopalakrishnan V, Choi K, DuPont HL, et al. Fecal microbiota transplantation for refractory immune checkpoint inhibitor-associated colitis. *Nat Med* (2018) 24:1804–8. doi: 10.1038/s41591-018-0238-9

23. Schwabe RF, Jobin C. The microbiome and cancer. *Nat Rev Cancer* (2013) 13:800–12. doi: 10.1038/nrc3610

24. Derosa L, Hellmann MD, Spaziano M, Halpenny D, Fidelle M, Rizvi H, et al. Negative association of antibiotics on clinical activity of immune checkpoint inhibitors in patients with advanced renal cell and non-small-cell lung cancer. *Ann Oncol* (2018) 29:1437–44. doi: 10.1093/annonc/mdy103

25. Hamada K, Yoshimura K, Hirasawa Y, Hosonuma M, Murayama M, Narikawa Y, et al. Antibiotic usage reduced overall survival by over 70% in non-small cell lung cancer patients on anti-PD-1 immunotherapy. *Anticancer Res* (2021) 41:4985–93. doi: 10.21873/anticanres.15312

26. Nishijima S, Suda W, Oshima K, Kim SW, Hirose Y, Morita H, et al. The gut microbiome of healthy Japanese and its microbial and functional uniqueness. *DNA Res* (2016) 23:125–33. doi: 10.1093/dnares/dsw002

27. Peng Z, Cheng S, Kou Y, Wang Z, Jin R, Hu H, et al. The gut microbiome is associated with clinical response to anti-PD-1/PD-L1 immunotherapy in gastrointestinal cancer. *Cancer Immunol Res* (2020) 8:1251–61. doi: 10.1158/2326-6066.CIR-19-1014

28. Shen YC, Lee PC, Kuo YL, Wu WK, Chen CC, Lei CH, et al. An exploratory study for the association of gut microbiome with efficacy of immune checkpoint inhibitor in patients with hepatocellular carcinoma. *J Hepatocell Carcinoma* (2021) 8:809–22. doi: 10.2147/JHC.S315696

29. Sun M, Wu W, Liu Z, Cong Y. Microbiota metabolite short chain fatty acids, GPCR, and inflammatory bowel diseases. *J Gastroenterol* (2017) 52:1–8. doi: 10.1007/s00535-016-1242-9

30. Skelly AN, Sato Y, Kearney S, Honda K. Mining the microbiota for microbial and metabolite-based immunotherapies. *Nat Rev Immunol* (2019) 19:305–23. doi: 10.1038/s41577-019-0144-5

31. Coutzac C, Jouniaux J-M, Paci A, Schmidt J, Mallardo D, Seck A, et al. Systemic short chain fatty acids limit antitumor effect of CTLA-4 blockade in hosts with cancer. *Nat Commun* (2020) 11:2168. doi: 10.1038/s41467-020-16079-x

frontiers | Frontiers in Immunology

TYPE Original Research
PUBLISHED 05 May 2023
DOI 10.3389/fimmu.2023.1151967

OPEN ACCESS

EDITED BY
Takaji Matsutani,
Repertoire Genesis, Inc., Japan

REVIEWED BY
Xiaoli Lan,
Huazhong University of Science and Technology, China
Hongcheng Shi,
Fudan University, China

*CORRESPONDENCE
Guangyu Ma
mgy301@163.com
Ruimin Wang
wrm@yeah.net
Shichun Lu
lusc_301@163.com

†These authors have contributed equally to this work

RECEIVED 27 January 2023
ACCEPTED 25 April 2023
PUBLISHED 05 May 2023

CITATION
Wang G, Zhang W, Luan X, Wang Z, Liu J, Xu X, Zhang J, Xu B, Lu S, Wang R and Ma G (2023) The role of ^{18}F–FDG PET in predicting the pathological response and prognosis to unresectable HCC patients treated with lenvatinib and PD-1 inhibitors as a conversion therapy.
Front. Immunol. 14:1151967.
doi: 10.3389/fimmu.2023.1151967

The role of ^{18}F–FDG PET in predicting the pathological response and prognosis to unresectable HCC patients treated with lenvatinib and PD-1 inhibitors as a conversion therapy

Guanyun Wang[1,2†], Wenwen Zhang[3†], Xiaohui Luan[1,4], Zhanbo Wang[5], Jiajin Liu[1], Xiaodan Xu[1], Jinming Zhang[1], Baixuan Xu[1], Shichun Lu[3*], Ruimin Wang[1*] and Guangyu Ma[1*]

[1]Department of Nuclear Medicine, The First Medical Centre, Chinese People's Liberation Army (PLA) General Hospital, Beijing, China, [2]Nuclear Medicine Department, Beijing Friendship Hospital, Capital Medical University, Beijing, China, [3]Faculty of Hepato-Pancreato-Biliary Surgery, Chinese People's Liberation Army (PLA) General Hospital/Institute of Hepatobiliary Surgery of Chinese People's Liberation Army/Key Laboratory of Digital Hepetobiliary Surgery, People's Liberation Army, Beijing, China, [4]Graduate School, Medical School of Chinese People's Liberation Army (PLA), Beijing, China, [5]Department of Pathology, The First Medical Centre, Chinese People's Liberation Army (PLA) General Hospital, Beijing, China

Purpose: To investigate the diagnostic value of ^{18}F-fluorodeoxyglucose positron emission tomography (^{18}F-FDG PET), as an imaging biomarker, for predicting pathological response and prognosis of unresectable hepatocellular carcinoma (HCC) patients treated with Lenvatinib and programmed cell death protein 1 (PD-1) inhibitors as a conversion therapy.

Methods: A total of 28 unresectable HCC patients with BCLC stage B or C were treated with Lenvatinib and PD-1 inhibitors before surgery. The ^{18}F-FDG PET/CT scans were acquired before pre- (scan-1) and post-conversion therapy (scan-2). The maximum standardized uptake value (SUVmax), TLR (tumor-to-normal liver standardized uptake value ratio), and the percentages of post-treatment changes in metabolic parameters (ΔSUVmax [%] and ΔTLR [%]) were calculated. Major pathological response (MPR) was identified based on the residual viable tumor in the resected primary tumor specimen (≤10%). Differences in the progression-free survival (PFS) and overall survival (OS) stratified by ΔTLR were examined by the Kaplan-Meier method.

Results: 11 (11/28, 39.3%) patients were considered as MPR responders and 17 (17/28, 60.7%) patients as non-MPR responders after conversion therapy. ΔSUVmax (-70.0 [-78.8, -48.8] vs. -21.7 [-38.8, 5.7], respectively; P<0.001) and ΔTLR (-67.6 [-78.1, -56.8] vs. -18.6 [-27.9, 4.0], respectively; P<0.001) were reduced in the responder group than those in the non-responder group. According to the results of the receiver operating characteristic curve analysis,

ΔTLR showed an excellent predictive value for the MPR of primary HCC lesions (area under curve=0.989, with the optimal diagnostic threshold of -46.15). When using ΔTLR of -21.36% as a threshold, patients with ΔTLR-based metabolic response had superior PFS (log-rank test, *P*=0.001) and OS (log-rank test, *P*=0.016) compared with those without ΔTLR-based metabolic response.

Conclusion: ^{18}F-FDG PET is a valuable tool for predicting pathological response and prognosis of unresectable HCC patients treated by Lenvatinib combined with PD-1 as a conversion therapy.

KEYWORDS

unresectable hepatocellular carcinoma, conversion therapy, major pathological response, prognosis, ^{18}F-FDG PET

Introduction

Primary liver cancer is the sixth most common cancer and the third leading cause of cancer death worldwide (1). Hepatocellular carcinoma (HCC), as the most common type of primary liver malignancy in the world (75-85% of cases), has shown an increasing prevalence rate globally (2). Although surgical resection is a potentially curative treatment for patients with HCC, the majority of these patients are already in the advanced stage of HCC, and only 40-50% of patients in developed countries with regular physical examination are diagnosed at an early stage (3). Because of liver dysfunction, advanced stage or poor performance, more than half of HCC patients are not candidates of radical resection, resulting in poor prognosis (4, 5).

Non-surgical local or systemic treatment is the predominant choice for most advanced HCC patients (6). In recent years, non-surgical treatment of liver cancer, particularly systemic therapy, has progressed. Especially, for some advanced HCC patients, the original unresectable lesions can be changed to resectable lesions through systemic therapy, which is also called conversion therapy (6). Anti-angiogenic drugs, such as tyrosine kinase inhibitors (TKIs), combined with immunotherapies (e.g., programmed cell death protein 1 [PD-1]) have become an important choice for unresectable or intermediate and advanced HCC, and for conversion therapy of potentially resectable HCC (7). Lenvatinib, a multi-target TKI, was approved for the treatment of unresectable HCC in European countries, USA, Japan, and China (8). Lenvatinib inhibited vascular endothelial growth factor (VEGF) and fibroblast growth factor (FGF) pathways, and suppressed the proliferation signals from VEGF receptor (VEGFR) and FGF receptor (FGFR), which were overexpressed in cancer cells (9, 10). As a type of immunotherapy, the PD-1 blocking monoclonal antibodies act directly on immune cells and block the inhibitory T-cell receptor PD-1, and have also been proven to be effective for the treatment of liver cancer (4). Anti-angiogenic drugs combined with immunotherapy can achieve an objective response rate (ORR) of about 30%, and the median survival for patients receiving this type of therapy can be up to 20 months (11–14). As one of the TKIs combined with immunotherapy, Lenvatinib combined with PD-1 inhibitors have also been confirmed to show a certain therapeutic effect (11, 15–20).

When an unresectable HCC patient successfully receives TKIs combined with immunotherapy and surgery, pathological response is a very important indicator for the postoperative recurrence and long-term survival of the patient (6). Studies have shown that the tumor-free survival of HCC patients after resection is related to pathological response, and the tumor-free survival of patients with pathological response is longer (20, 21). However, how to predict pathological response remains to be investigated. In terms of imaging evaluation, the modified Response Evaluation Criteria in Solid Tumors (mRECIST) criteria were the most common standard to evaluate the therapeutic response of liver lesions (22, 23). However, it is still unclear whether mRECIST can predict pathological response and prognosis of HCC patients after conversion therapy. Although ^{18}F-fluorodeoxyglucose positron emission tomography/computed tomography (^{18}F-FDG PET/CT)

Abbreviations: ^{18}F-FDG, ^{18}F-fluorodeoxyglucose; AASLD, American Association for the Study of Liver Diseases; AC, attenuation correction; AFP, alpha fetoprotein; AUC, area under the curve;BCLC, Barcelona clinic liver cancer; BMI, body mass index; CPR, complete pathological response; ECOG PS, Eastern Cooperative Oncology Group Performance Status; FGF, fibroblast growth factor; FLR/SLV, future liver remnant volume to standard liver volume; HCC, hepatocellular carcinoma; irAEs, Immune-related adverse events; mRECIST, modified Response Evaluation Criteria in Solid Tumors; MPR, major pathological response; MVTT, macrovascular tumor thrombi; NPV, negative predictive value; ORR, objective response rate; OS, overall survival; OSEM, ordered subset expectation maximization algorithm; PD-1, programmed cell death protein 1; PET, positron emission tomography; PFS, progression free survival; PLR, portal vein tumor thrombus-to-normal liver standardized uptake value ratio; PVTT, portal vein tumor thrombus; PPV, positive predictive value; PTR, pathological treatment response; ROC, receiver operating characteristic; ROI, region of interest; SUVmax, maximum standardized uptake value; TILs, tumor-infiltrating lymphocytes; TKIs, tyrosine kinase inhibitors; TLR, tumor-to-normal liver standardized uptake value ratio; VEGF, vascular endothelial growth factor; VOI, volume of interest.

has exhibited a poor sensitivity for the detection of HCC compared with other solid tumors (24), ^{18}F-FDG PET/CT has still been used for accurate staging, predicting therapeutic response, and detecting recurrence of HCC (25). In recent years, the metabolic parameters of ^{18}F-FDG PET have shown a great value in predicting pathological response and prognosis of various malignant tumors after neoadjuvant therapy (26–28). However, there is no study on the metabolic parameters of ^{18}F-FDG PET in predicting pathological response and prognosis of unresectable HCC patients undergoing conversion therapy. The present study aimed to explore the value of ^{18}F-FDG PET in predicting pathological response and prognosis of unresectable HCC patients treated with Lenvatinib combined with PD-1 inhibitors as conversion therapy.

Materials and methods

Patients

This single-center retrospective study was based on a prospective, single-center, single-arm, investigator-initiated, clinical trial study, which was registered at http://www.chictr.org.cn/ (ChiCTR1900023914), and it was approved by the Ethics Committee of the General Hospital of the People's Liberation Army (Beijing, China). All patients were informed and signed the informed consent form before ^{18}F-FDG PET/CT. The study was performed in accordance with the Declaration of Helsinki.

Between July 2019 and March 2023, unresectable HCC patients who underwent pre-treatment and post-treatment ^{18}F-FDG PET/CT in the General Hospital of the People's Liberation Army were retrospectively recruited. The inclusion criteria were as follows:(a) Patients older than 18 years and without a history of other malignance; (b) The diagnosis of HCC was pathologically confirmed by fine-needle biopsy or in accordance with the clinical diagnosis criteria of the American Association for the Study of Liver Diseases (AASLD) (29); (c) Patients who were diagnosed with unresectable HCC, and conversion therapy (combination of Lenvatinib and PD-1 inhibitors) could be performed after clinical evaluation; (d) ^{18}F-FDG PET/CT was performed within 2 weeks prior to conversion therapy and within 3 weeks prior to surgery; I No other anti-tumor therapy was given during the treatment using Lenvatinib combined with PD-1 inhibitors, and the drugs were not terminated or changed during the therapy; (f) All patients underwent surgery and had definite postoperative pathological diagnosis; (g) High-quality ^{18}F-FDG PET/CT images that could be used for diagnosis.

PET/CT scanning

All patients underwent ^{18}F-FDG PET/CT (Biograph 64; GE Healthcare, New York, NY, USA). Patients were fasted for 6 h with plasma glucose levels under 11.1 mmol/L, and rested for at least 20 min in a quiet waiting room before intravenous administration of ^{18}F-FDG (^{18}F-FDG was produced by our department, with a radiochemical purity of >95%). Patients were injected with ^{18}F-FDG at a dose of 3.70-4.44 MBq/kg (0.10-0.12 mCi/kg). PET/CT scan was performed after 60 min, beginning from the skull base to the upper femur in free-breathing mode. The low-dose CT (LDCT) parameters were as follows: voltage=120 kV, current=100 mAs, rotation=0.8, layer thickness=5 mm, and pitch=1. The parameters of PET included 3-dimensional mode, 2 min/bed (30% overlap), 4-5 beds/person, three iterations, 21 subsets, and Gaussian filter half-height width of 4.0 mm. Images were reconstructed with CT attenuation correction (CTAC) using the ordered subset expectation maximization (OSEM) algorithm.

Image analysis

Multiparametric analysis prototype (GE Healthcare), a dedicated prototypic post-processing tool, was used for image analysis. Quantitative analyses were performed by two experienced nuclear medicine physicians (WGY and MGY) who were blinded to patients' clinical data. If there were discrepancies between the two physicians, the process would be repeated two weeks later to reach a consensus. Areas with abnormal uptake of ^{18}F-FDG on PET and/or abnormal density on CT were defined as lesions. A two-dimensional region of interest (ROI) was delineated manually according to the boundary of the HCC lesion and portal vein tumor thrombus (PVTT) on each layer of transaxial CT images to form a three-dimensional volume of interest (VOI). Contrast-enhanced magnetic resonance imaging (MRI)/CT was used to accurately determine the VOI. The VOI was applied to the corresponding PET images, which were registered to CT images. To measure a normal liver activity, 3 non-overlapping spherical 1-cm (3)-sized VOIs were drawn in the normal liver on the axial PET images, avoiding the HCC areas on dynamic CT. The SUVmax (maximum standard uptake value) in HCC and PVTT for each patient was calculated by placing a spherical VOI over the sites of the HCC lesions and PVTT. Using the SUVmax of HCC and PVTT and mean SUV of the normal liver, TLR (tumor-to-normal liver standardized uptake value ratio, SUVmax of the tumor/SUVmean of the normal liver parenchyma) and PLR (PVTT-to-normal liver standardized uptake ratio, SUVmax of the PVTT/SUVmean of the normal liver parenchyma) were calculated for each patient. There were no significant differences in terms of SUVmean of the liver parenchyma between the MPR responder group and non-MPR responder group (pre-treatment: 2.41 ± 0.25 vs. 2.60 ± 0.33, P = 0.122; post-treatment: 2.38 ± 0.4 vs. 2.31 ± 0.41, P = 0.637).

The percentages of post-treatment changes in metabolic parameters were calculated as follows:

$$\Delta\text{SUVmax}(\%) = \frac{\text{SUVmax of post-treatment} - \text{SUVmax of pre-treatment}}{\text{SUVmax of pre-treatment}} \times 100\,\%$$

$$\Delta\text{TLR}(\%) = \frac{\text{TLR of post-treatment} - \text{TLR of pre-treatment}}{\text{TLR of pre-treatment}} \times 100\,\%$$

$$\Delta\text{PLR}(\%) = \frac{\text{PLR of post-treatment} - \text{PLR of pre-treatment}}{\text{PLR of pre-treatment}} \times 100\,\%$$

Furthermore, ΔSUVmax and ΔTLR of primary HCC lesions, and ΔPLR of PVTT were recorded, respectively.

Systemic therapy

Conversion therapy mainly included Lenvatinib and PD-1 inhibitors. Patients were treated with intravenous infusion of anti-PD-1 antibodies (dose, 200-240 mg for different drugs), and the vast majority of the data were collected under four treatment regimens (Pembrolizumab 200 mg/q3w, Sintilimab 200 mg/q3w, Toripalimab 240 mg/q3w, and Tislelizumab 200mg/q3w). Lenvatinib was given orally (8 or 12 mg/day, depending on the patient's weight < 60 or ≥ 60 kg.

Follow-up during systemic therapy and radiological assessment

All patients were treated regularly and were monitored to assess their response to systemic therapy. Patients' complete blood count, thyroid, cardiac, liver, renal, adrenal functions, and tumor markers prior to each cycle of PD-1 treatment were assessed. After 3 cycles of treatment with PD-1 inhibitors, tumor response of the patients was evaluated (according to RECIST ver. 1.1 (30) and mRECIST (22) criteria: complete response [CR], partial response [PR], stable disease [SD], and progressive disease [PD], and the resectability of liver cancer was investigated by contrast-enhanced MRI/CT and chest CT. The patients were categorized into responders (CR or PR) and non-responders (SD or PD) according to mRECIST. Immune-related adverse events (irAEs) were assessed using the National Cancer Institute's Common Terminology Criteria for Adverse Events (ver. 4.0) (31, 32) (Table S1).

Criteria for successful conversion therapy

The criteria for successful conversion therapy were summarized as follows (33): (a) Child-Pugh grade A; (b) Eastern Cooperative Oncology Group Performance Status (ECOG PS) score ≤ 1; (c) Shrinkage or disappearance of metastatic lymph nodes, and the remaining lymph nodes can be removed; (d) No new extrahepatic metastases; I Intact vascular structure (including the inflow and outflow) of the reserved liver; (f) The expected ratio of future liver remnant volume to standard liver volume (FLR/SLV) after resection of tumor-bearing liver is ≥40% in compromised livers and 35% in normal livers. All patients who met the criteria for successful conversion therapy would be informed of the benefits and risks of surgery.

Histopathological assessment of tumor regression

Surgical specimens were analyzed by two experienced pathologists who were blinded to the patients' treatment and outcomes. The pathological treatment response (PTR) was classified based on the tumor cellularity. The primary tumors and PPVT were recorded. Major pathological response (MPR, ≤10% residual viable tumor) or complete pathological response (CPR, no residual viable tumor) following immunotherapy was used as endpoints in the great majority of clinical trials (34, 35). Whether patients reached CPR or MPR through HCC lesions and PVTT (if present) was comprehensively considered.

We categorized all patients according to their pathological response into MPR responder and non-MPR responder groups.

Postoperative therapy and follow-up

Patients continued to receive therapy according to the pathological results and their personal conditions at 4-6 weeks after surgery and clinical evaluation. Serum tumor biomarkers were examined every cycle, and imaging examinations (contrast-enhanced MRI/CT or abdominal ultrasound) were performed every 3 months to monitor HCC recurrence. HCC recurrence was defined as the presence of radiological evidence of new intra- and/or extra-hepatic tumors (36). According to the guidelines, post-recurrence treatments were administered (6). The time of recurrence and death was recorded, respectively.

Statistical analysis

Quantitative data were expressed as median (interquartile range [IQR]) or mean ± standard deviation (SD). Qualitative data were expressed as number of cases and percentage (n [%]). Homogeneity of variance of the data was verified using Levene's test, and normal distribution of the data by Shapiro–Wilk test. The student's *t*-test or Mann-Whitney U test was used to compare ^{18}F-FDG PET/CT metabolic parameters among different groups. The categorical variables were analyzed by the Fisher's exact test or the Chi-square test. The optimal cut-off values for continuous variables were estimated using receiver operating characteristic (ROC) curve analysis with the area under the curve (AUC), and sensitivity, specificity, positive predictive value (PPV), and negative predictive value (NPV) were calculated, respectively. PTR was compared with ^{18}F-FDG PET/CT metabolic parameters using Spearman correlation analysis.

The metabolic parameters were dichotomized according to specific cutoff values, which were determined by using ROC curve analysis. Progression-free survival (PFS) was determined as the interval from the start of conversion therapy to the date of disease relapse/progression. Overall survival (OS) was defined as the interval between the conversion therapy and death from any cause. All patients were followed up for at least 6 months (i.e., 2 of 28 patients who was followed up for shorter than 8 months was excluded). Kaplan Meier was used to plot the survival curve and log-rank test of PFS and OS difference was used to evaluate the significance.

The statistical analysis was performed using SPSS 24.0 (IBM, Armonk, NY, USA) and R 4.0.2 (Bell Laboratories, Holmdel, NJ, USA) software. All statistical tests were two-sided and the significance level was set at P=0.05.

Results

Patients' characteristics

Eventually, 28 patients underwent surgical excision after successful conversion therapy in our study (24 men; median age: 58.0 years, IQR: 51.8–61.8 years; Figure 1). Among them, 11 (11/28, 39.3%) and 17 (17/28, 60.7%) patients were assigned to MPR responder group and non-MPR responder group, respectively. In addition, 5 of 11 patients in the MPR responder group achieved CPR. There was no significant difference in baseline characteristics between MPR responder group and non-MPR responder group in terms of general status (age, gender, body mass index [BMI], alcohol abuse, history of liver diseases, and ECOG PS score), clinical data (Barcelona clinic liver cancer [BCLC] stage, Child-Pugh score, and baseline alpha fetoprotein [AFP] level), imaging findings (tumor diameter, cirrhosis, macroscopic portal vein invasion, extrahepatic metastases), surgical findings (strategy of hepatectomy and R0 resection) and the type of PD-1 inhibitors. The post-treatment AFP level (normal or abnormal), number of tumor and the distribution of mRECIST were significantly different between the two groups (P=0.025, P=0.025 and P=0.001, respectively; Table 1). Due to the impact of conversion therapy, only two patients in MPR responder group determined the degree of pathological differentiation, both of whom were poorly differentiated; Among patients in non-MPR responder group, 10 were moderately differentiated, 5 were moderately poorly differentiated, and 1 was poorly differentiated. The median time between the start of conversion therapy and surgery was 107.0 days (IQR: 92.3-133.8 days), the median cycle of conversion therapy was 5.0 (IQR: 4.0-5.8), the median time between the pre-treatment ^{18}F-FDG PET/CT and the start of conversion therapy was 4.0 days (IQR: 2.0-7.0 days), the median time between post-treatment ^{18}F-FDG PET/CT and surgery was 6 days (IQR: 3.3-8.8 days), and the median time between two ^{18}F-FDG PET/CT was 104.5 days (IQR: 90.0-132.3 days). Supplementary Table 2 shows the details of patients' conversion therapy and surgery.

Tumor metabolic parameters of ^{18}F–FDG PET indicated a significant difference between MPR responder and non–MPR responder groups and predicted pathological response of MPR patients

Pre-treatment ^{18}F-FDG PET metabolic parameters were compared between responder group and non-responder group, and there was a significant difference in SUVmax (11.6 [8.7, 16.7] vs. 6.7 [4.5, 10.8], respectively; P=0.028) and TLR (5.1 [3.9, 6.5] vs. 2.3 [1.8, 4.0], respectively; P=0.022) on pre-treatment scan. The metabolic parameters of post-treatment scan showed no significant difference between MPR responder group and non–MPR responder group (P=0.053 and 0.059 for SUVmax and TLR, respectively). ΔSUVmax (%) (-70.0 [-78.8, -48.8] vs. -21.7 [-38.8, 5.7], respectively; P<0.001) and ΔTLR (%) (-67.6 [-78.1, -56.8] vs. -18.9 [-27.9, 2.6], respectively; P<0.001) were significantly lower in the MPR responder group than those in the non–MPR responder group after conversion therapy (Table 2).

Compared mRECIST and other ^{18}F-FDG PET metabolic parameters, ΔTLR (%) showed the largest AUC (AUC=0.989, 95% confidence interval [CI]: 0.962-1.000), with the optimal diagnostic threshold of -46.15. The sensitivity, specificity, PPV, and NPV were 0.909 (0.571-0.995), 1.000 (0.771-1.000), 1.000 (0.655-1.000), and 0.944 (0.706-0.997), respectively (Table 3 and Figure 2). The relationship between the ΔTLR (%) and the mRECIST criteria and pathological response is detailed in Figure 3.

Correlation between ^{18}F-FDG PET metabolic parameters and pathological response

The Spearman correlation analysis was carried out to explore the relationship between ^{18}F-FDG PET metabolic parameters and pathological response. The results showed that ΔTLR (%), ΔSUVmax (%), TLR (Scan 1), SUVmax (Scan 1), and SUVmax

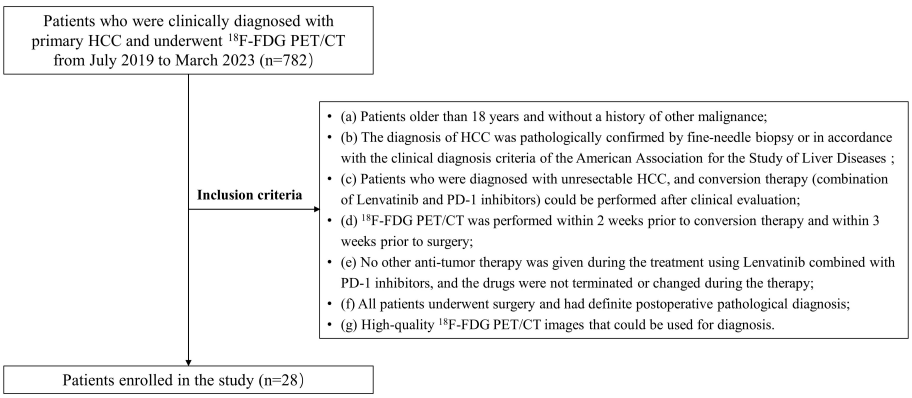

FIGURE 1
The flow diagram of study. HCC, Hepatocellular carcinoma; ^{18}F-FDG PET/CT, ^{18}F-fluorodeoxyglucose positron emission tomography/computed tomography.

10.3389/fimmu.2023.1151967

TABLE 1 Baseline Clinical and Pathologic Characteristics.

Characteristics	Responder (n=11)	Non-Responder (n=17)	*P*
General status			
Age	58.0 (51.0-66.0)	58.0 (48.5-61.0)	0.453*
Sex			
Male	11 (100%)	13 (77%)	0.132
Female	0 (0%)	4 (23%)	
BMI	25.0 (22.9-25.9)	23.4 (22.4-25.1)	0.241*
Alcohol abuse	5 (46%)	9 (53%)	0.699
History of liver diseases			0.172
None	1 (9%)	3 (17%)	
Hepatitis B	10 (91%)	9 (53%)	
Hepatitis C	0 (0%)	4 (24%)	
Other	0 (0%)	1 (6%)	
ECOG Performance Status			1.000
0	11 (100%)	17 (100%)	
≥1	0 (0%)	0 (0%)	
Clinical data			
BCLC stage			0.619
B	1 (9%)	4 (23.5%)	
C	10 (91%)	13 (76.5%)	
Child-Pugh score			0.701
A5	6 (54.5%)	11 (65%)	
A6	5 (45.5%)	6 (35%)	
Pre-treatment AFP (ng/mL)			1.000
<400	5 (45.5%)	7 (41%)	
≥400	6 (54.5%)	10 (59%)	
Post-treatment AFP			0.025
Normal	8 (73%)	5 (29%)	
Abnormal	3 (27%)	12 (71%)	
Treatment times (cycle)	5.0 (5.0-6.0)	4.0 (3.0-5.0)	0.089*
Imaging findings			
Tumor diameter (mm)	108.0 (73.0-120.0)	86.0 (54.5-113.5)	0.317*
Cirrhosis	8 (73%)	10 (59%)	0.689
Macroscopic portal vein invasion	6 (54.5%)	11 (65%)	0.701
Extrahepatic metastases	8 (73%)	6 (35%)	0.053
Tumor number			0.025
Single	8 (73%)	5 (29%)	
Multiple	3 (27%)	12 (71%)	
mRECIST			0.001
CR	8 (73%)	0 (0%)	

(Continued)

TABLE 1 Continued

Characteristics	Responder (n=11)	Non-Responder (n=17)	*P*
PR	2 (18%)	10 (59%)	
SD	1 (9%)	6 (35%)	
PD	0 (0%)	1 (6%)	
Operation Findings			
Strategy of hepatectomy			0.591
Anatomic resection	6 (54.5%)	11 (65%)	
Non-anatomic resection	5 (45.5%)	6 (35%)	
R0 resection	11 (100%)	17 (100%)	1.000
Pathological differentiation			
Well	–	0	
Moderately-Well	–	0	
Moderately	–	11 (65%)	
Moderately-Poorly	–	5 (29%)	
Poorly	2 (18%)	1 (6%)	
PD-1 inhibitors			0.840
Pembrolizumab	1 (9%)	1 (6%)	
Sintilimab	9 (82%)	14 (82%)	
Tislelizumab	0 (0%)	1 (6%)	
Toripalimab	1 (9%)	1 (6%)	

*Data are medians with interquartile ranges or numbers of participants with percentages.
*Student t test
BMI, Body mass index; BCLC stage, Barcelona Clinic Liver Cancer stage; ECOG PS, Eastern Cooperative Oncology Group performance status; AFP, Alpha fetoprotein; mRECIST, modified Response Evaluation Criteria in Solid Tumors; CR, Complete response; PR, Partial response; SD, Stable disease; PD, Progressive disease.

(Scan 2) were correlated with pathological response, with correlation coefficients (rs) of -0.83, -0.75, 0.49, 0.47, and -0.38, respectively ($P<0.05$). The TLR(Scan 2) showed a lower correlation (r=-0.37), whereas no significant difference was found ($P>0.05$). The results are displayed in Figure 4.

Prognostic value of ^{18}F-FDG PET on PFS and OS

The follow-up ended in February 15, 2023. Twopatients waere not included in the analysis due to short follow-up time. During the follow-up period, 19/26 (73.1%) patients showed a disease progression, and median follow-up was 14.7 (IQR:6.6-23.6) months; 7/26 (26.9%) patients died, and median follow-up was 27.6 (IQR: 12.7-31.1) months. When ΔTLR of -46.15% was used as a threshold, patients with ΔTLR-based metabolic response had no superior PFS (log-rank test, $P=0.112$) and OS (log-rank test, $P=0.218$) compared with those without a ΔTLR-based metabolic response. According to ROC analysis, when ΔTLR of -21.36% was used as a threshold, patients with ΔTLR-based metabolic response had superior PFS (log-rank test, $P=0.001$) and OS (log-rank test, $P=0.016$) compared with those without ΔTLR-based metabolic response (Figure 5). Patients' follow-up data are summarized in Supplementary Table S3.

^{18}F-FDG PET identified PVTT involvement

In this study, 17 of 28 (60.7%) patients had macroscopic portal vein invasion. The number of residual tumor cells in PVTT was analyzed in 14 patients. Among them, 9 (9/14, 64.3%) patients were considered as PVTT CPR-responders and 5 (5/14, 35.7%) patients were PVTT CPR-non-responders. The metabolic parameters of pre-treatment scan, post-treatment scan, and the percentage of change in pre-treatment scan and post-treatment scan showed no significant difference between the responder group and the non-responder group (Table 4).

Discussion

To our knowledge, this is the first study to report the role of ^{18}F-FDG PET in predicting pathological response and prognosis of unresectable HCC patients after treated by Lenvatinib in

TABLE 2 The difference of ^{18}F-FDG PET parameters between MPR responders and non-MPR responders in primary lesion.

Parameter	MPR Responders (n=11)	Non-MPR responders (n=17)	*P*
Pre-treatment scan (Scan 1)			
SUVmax	11.6 (8.7, 16.7)	6.7 (4.5, 10.8)	0.028*
TLR	5.1 (3.9, 6.5)	2.3 (1.8, 4.0)	0.022*
Post-treatment scan (Scan 2)			
SUVmax	3.9 (3.1, 4.2)	5.9 (3.5, 8.7)	0.053#
TLR	1.7 (1.4, 1.8)	2.6 (1.4, 3.9)	0.059#
The percentage changes (Δ%) between pre-treatment scan and post-treatment scan			
ΔSUVmax (%)	-70.0 (-78.8, -48.8)	-21.7 (-38.8, 5.7)	<0.001*
ΔTLR (%)	-67.6 (-78.1, -56.8)	-18.9 (-27.9, 2.6)	<0.001#

Data are medians with interquartile ranges in parentheses.
*Student t test; #Mann-Whitney test
MPR, Major pathological response; SUVmax, Max standard uptake value; TLR, Tumor-to-normal liver standardized uptake value ratio.

combination with PD-1 inhibitors as conversion therapy. The results suggested that the differences between the TLR (ΔTLR, %) of pre-treatment ^{18}F-FDG PET and post-treatment ^{18}F-FDG PET were promising imaging biomarkers for pathological response and prognosis of primary unresectable HCC after treated with the PD-1 blockade in combination with Lenvatinib as conversion therapy. However, ^{18}F-FDG PET was not a predictive factor of PVTT pathological response.

CPR has been proven to be an important prognostic factor for patients with multiple malignancies after treatment and surgery, including HCC (37, 38). However, for patients with unresectable HCC, there are few options to achieve CPR, thus, MPR is a good alternative. MPR, defined as equal to 10% residual tumor following neoadjuvant therapy, has also been used as a prognostic factor of malignant tumors, such as non-small cell lung cancer (39), pancreatic cancer (40), and melanoma (41). The possible reason is that patients may not need a complete pathological resolution of the tumor burden to experience clinical benefits, because the main mechanism of the clinical benefits of immunotherapy-based conversion therapy is to initiate an anti-tumor immune response that may systematically seek and destroy microscopic tumor deposits that may lead to tumor recurrence (34). Compared with the traditional RECIST (ver. 1.1) criteria, mRECIST criteria based on CT or MRI were developed to better evaluate the response of liver lesions (6), and they possess some advantages in terms of assessing the degree of pathological response (42). After the treatment takes effect, tumor necrosis appears first, while absorption is relatively slow. Due to the histological and biological changes caused by tumor necrosis, mRECIST criteria are more appropriate for imaging evaluation of conversion therapy (7). However, some studies have shown that mRECIST criteria are only appropriate for assessing pathological response of HCC patients receiving neo-adjuvant therapy before liver transplantation (43). For treatment response, the metabolic parameters of ^{18}F-FDG PET also play an important role in predicting HCC (44–46). However, no study has analyzed the

TABLE 3 Differential diagnostic efficiency of ^{18}F-FDG PET metabolic parameters and mRECIST criteria between MPR-responders and MPR-non-responders.

Parameter	Cut-off	AUC	Sensitivity	Specificity	PPV	NPV
Pre-treatment scan (Scan 1)						
SUVmax	8.14	0.775 (0.601-0.950)	0.909 (0.571-0.995)	0.647 (0.386-0.847)	0.625 (0.359-0.738)	0.917 (0.598-0.996)
TLR	3.84	0.791 (0.621-0.962)	0.818 (0.478-0.968)	0.765 (0.498-0.922)	0.692 (0.389-0.896)	0.867 (0.584-977)
The percentage changes (Δ%) between pretreatment scan and post-treatment scan						
ΔSUVmax (%)	-40.26	0.941 (0.858-1.000)	0.909 (0.571-0.995)	0.824 (0.558-0.953)	0.769 (0.460-0.938)	0.933 (0.660-0.997)
ΔTLR (%)	-46.15	0.989 (0.962-1.000)	0.909 (0.571-0.995)	1.000 (0.771-1.000)	1.000 (0.655-1.000)	0.944 (0.706-0.997)
mRECIST	–	0.660 (0.457-0.864)	0.909 (0.571-0.995)	0.412 (0.194-0.665)	0.500 (0.279-0.721)	0.875 (0.467-0.993)

mRECIST: CR or PR vs. SD or PD
MPR, Major pathological response; AUC, Area under the curve; PPV, Positive predictive value; NPV, Negative predictive value; TLR, Tumor-to-normal liver standardized uptake value ratio.

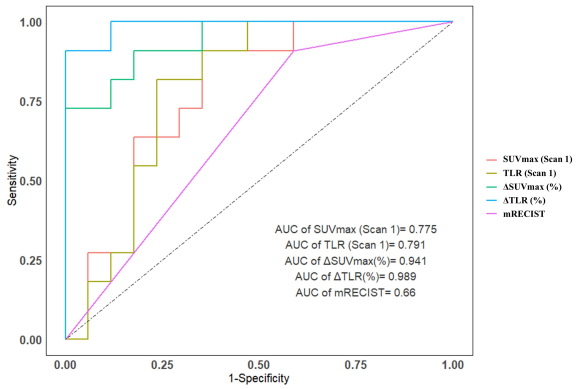

FIGURE 2
The area under the ROC curve for predicting major pathological response for SUVmax (Scan 1), TLR (Scan 1), ΔTLRand ΔSUVmax was 0.775, 0.791, 0.941 and 0.989, respectively, both are above the mRECIST criteria (0.660).

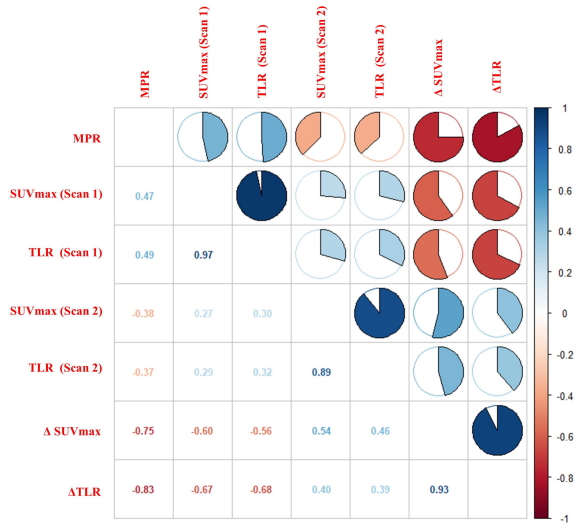

FIGURE 4
Correlation between ^{18}F-FDG PET metabolic parameters and pathological response. The figure showed a strong correlation between ΔTLR and MPR (r = -0.83, P< 0.01).

pathological response of ^{18}F-FDG PET in patients with unresectable HCC after receiving Lenvatinib in combination with PD-1 inhibitors as conversion therapy.

Our previous study indicated that pre-treatment TLR was a potent marker to predict pathological response of HCC patients (BCLC stage C) treated with Lenvatinib and PD-1 inhibitors as conversion therapy (33). In the present study, it was found that pre-treatment TLR could predict MPR (AUC=0.791, sensitivity=81.8%, specificity=76.5%), which is similar to our previous study. One explanation is that the FDG uptake is positively correlated with the content of tumor-infiltrating lymphocytes (TILs), especially T cells (47–49). Besides, the high FDG uptake in HCC may be a valuable predictor of an extremely rapid response to Lenvatinib (50). This may explain the relationship between the high FDG uptake and pathological response, and it is also because more TILs are accumulated in responders' HCC lesions, and they may more strongly promote the local and systematic enhancement of T cell-mediated anti-tumor immunity by TKIs combined with immunotherapy than non-responders. Therefore, the therapeutic effect of responders was better. This suggested to some extent why

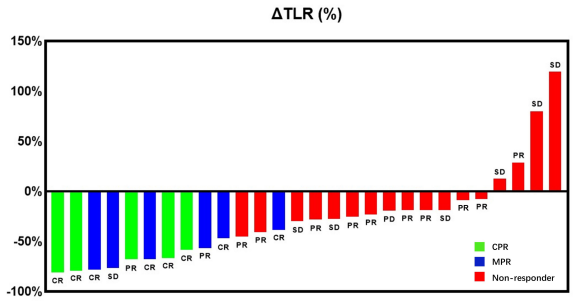

FIGURE 3
Waterfall plot presenting the percentage of change in primary tumor TLR from baseline to on-treatment per individual patient and the preoperative primary HCC lesions of patients determined by mRECIST criteria. Bar color indicates CPR response (green), MPR response (blue) or non-response (red).

there was a greater difference in FDG uptake between pre-treatment and post-treatment ^{18}F-FDG PET, and the patient was more likely to achieve MPR. Our results showed that ΔTLR (cut-off value: -46.15%) was the best parameter to predict pathological response of primary HCC lesions, and it was more accurate than mRECIST criteria (Figure 6). However, in our patients, four patients showed an increase in ΔTLR. But all four patients were in the non–MPR responder group, and their treatment cycles were relatively short, ranging from 3-5 cycles. All four patients had relapsed, and two died. The reason may be that although the volume of the tumor has decreased, the surviving tumor cells have stronger activity and stronger metabolism compared to before, leading to an increase in FDG uptake, which may lead to postoperative recurrence in these patients. Therefore, using ^{18}F-FDG PET to evaluate the conversion therapy effectiveness of unresectable HCC patients at different time points may also help to find a more accurate surgical time. ^{18}F-FDG PET may provide more reliable imaging predictors for the timing of operation for unresectable HCC patients treated with Lenvatinib and PD-1 inhibitors as conversion therapy.

As pathological response is associated with prognosis of HCC patients, we hypothesized that FDG metabolic parameters can also predict the prognosis of unresectable HCC patients after receiving Lenvatinib in combination with PD-1 inhibitors as conversion therapy. There are limited data of biomarkers to help decision-making and guide the treatment of advanced HCC (51), and there is no imaging biomarker for prognosis of patients with unresectable HCC after conversion therapy. The present study revealed that ΔTLR (cut-off value: -21.36%) was also an indicator to predict PFS and OS of patients receiving Lenvatinib in combination with PD-1 inhibitors as conversion therapy. Previous studies have shown that the more obvious the reduction of FDG uptake, the better the prognosis (PSF or/and OS) of patients with other malignant tumors treated with TKIs or immunotherapy (52–55). Our present study indicated a potential imaging biomarker of the therapeutic efficacy

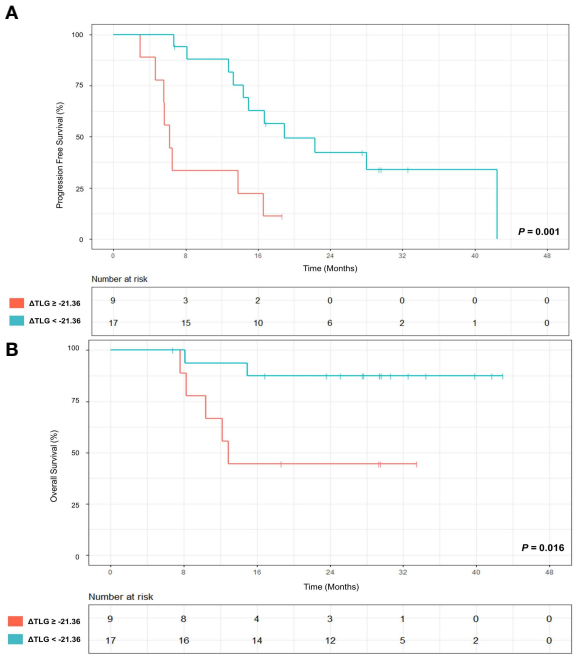

FIGURE 5
(A) Progression-free survival (PFS) of patients with ≥ 21.36% decrease in TLR at primary tumor site (red) from baseline to on-treatment and patients without ≥ 21.36% decrease (green). **(B)** Overall survival (OS) of patients with ≥21.36% decrease in TLR at primary tumor site (red) from baseline to on-treatment and patients without ≥21.36% decrease (green). *P* values were calculated using log-rank test.

and prognosis of patients with advanced HCC after treated by conversion therapy.

However, our study found that metabolic parameters of PET could not predict pathological response of PVTT. PVTT plays a major role in the prognosis and clinical staging of HCC (56, 57), some studies have shown that HCC patients with PVTT after neo-adjuvant therapy still have better survival outcomes than those without neo-adjuvant therapy (58, 59). Huang et al. demonstrated that the ORR of Lenvatinib combined with PD-1 inhibitors was 54.5% for macrovascular tumor thrombi (MVTT) and 32.8% for hepatic tumors, and among 17 MVTT patients who achieved ORR, 6 (18.1%) patients underwent surgery (60). Postoperative pathology indicated that 66.7% of patients with PVTT achieved pathological complete necrosis. This confirmed that the conversion therapy of Lenvatinib combined with PD-1 inhibitors had a promising therapeutic effect on PVTT. Therefore, biomarkers are also needed to evaluate pathological response of patients with PVTT. It has been reported that FDG uptake has diagnostic and prognostic value for HCC PVTT (61, 62). However, the components in the tumor thrombus are more complex than the original tumor. After treatment for the tumor thrombus, there may still be many tumor-infiltrating inflammatory cells, which may lead to the increased FDG uptake, disabling metabolic parameters to predict pathological response of patients with PVTT. It is noteworthy that fewer patients were included in this study, and bias was inevitable. More studies are still required to verify our findings.

The present study has some limitations. First, it was a retrospective single-center study and the number of enrolled patients was small. This may bias the study results. However, due to the low proportion of unresectable HCC patients treated with Lenvatinib and PD-1 Inhibitors as a conversion therapy and successfully undergo conversion surgery (63–65), few patients could be included in our study. Second, the follow-up was short, and a longer follow-up period is needed to examine whether ^{18}F-FDG PET metabolic parameters on primary tumors can predict survival outcomes of HCC patients after treated with Lenvatinib in combination with PD-1 inhibitors as conversion therapy, followed by surgery. Third, only pathological treatment

TABLE 4 The difference of ^{18}F-FDG PET metabolic parameters between CPR-responders and CPR-non-responders in PVTT.

Parameter	CPR-Responders (n=9)	CPR-Non-responders (n=5)	*P*
Pre-treatment scan (Scan 1)			
SUVmax	9.2 (5.5, 10.1)	6.5 (5.2, 12.1)	0.970*
PLR	3.6 (1.9, 3.8)	2.4 (1.9, 4.2)	0.709*
Post-treatment scan (Scan 2)			
SUVmax	2.2 (2.0, 2.4)	2.7 (2.1, 5.0)	0.147#
PLR	0.9 (0.8, 1.2)	1.4 (0.9, 2.0)	0.056*
The percentage changes (Δ%) between pretreatment scan and post-treatment scan			
ΔSUVmax (%)	-76.7 (-79.5, -57.9)	-55.9 (-73.2, -32.6)	0.496*
ΔPLR (%)	-67.4 (-79.5, -47.1)	-41.9 (-63.6, -23.2)	0.210*

Data are medians with interquartile ranges in parentheses.
*Student t test; #Mann-Whitney test
CPR, complete pathological response; SUVmax, Max standard uptake value; PLR, PVTT-to-normal liver standardized uptake value ratio.

response of the primary tumor and PVTT was assessed, and there is still a lack of evidence on extrahepatic metastases. Especially, in our study, except for ^{18}F-FDG PET, we found that there was a significant difference between MPR responder group and non-MPR responder group in whether the post-treatment AFP levels were normal. This may also provide biomarkers for predicting pathological response, but more research is still needed. Fourth, due to the small number of patients, we were unable to analyze more related factors and predicting biomarker in the survival analysis, such as tumor responses, PVTT, male, baseline AFP level and liver disease history (51, 60, 65, 66). It is therefore essential to comprehensively analyze the related factors in the future large-scale research. Fifthly, since the pathological results of most patients in MPR responder group did not indicate the

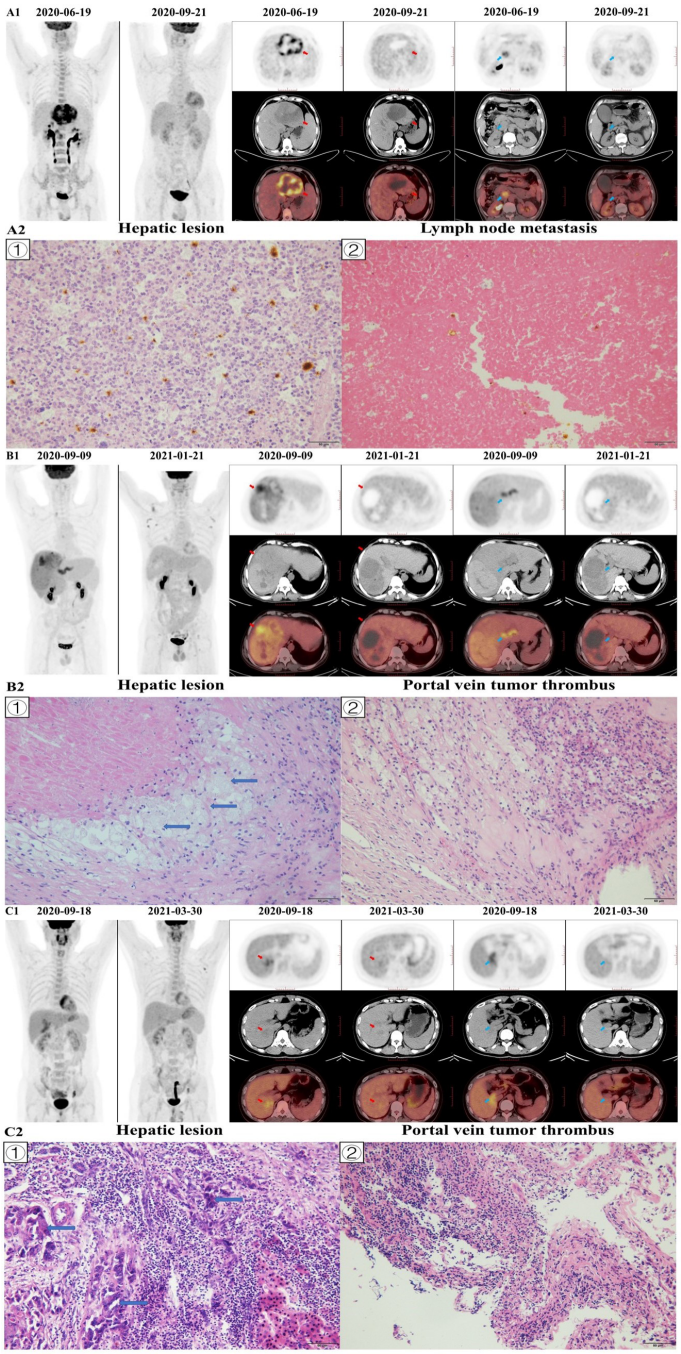

FIGURE 6 (Continued)

FIGURE 6 (Continued)
Image A1 shows a 51-year-old man with BCLC-C stage hepatocellular carcinoma in the left hepatic lobe (red arrow), and the patient was accompanied by lymph node metastasis (blue arrow). The hepatic lesion of pre-treatment ^{18}F-FDG PET/CT (2020–06–19) showed that tumor-to-normal liver standardized uptake value ratio (TLR) was 8.21, and the hepatic lesion of post-treatment ^{18}F-FDG PET/CT (2020–09–21) showed that TLR was 1.80. The percentage of change in TLR was -78.08. The baseline AFP level was 960.4 ng/mL, the baseline tumor diameter was 106 mm, and the Child-Pugh score was 5. The patient had no history of hepatitis and drinking, while had a history of liver cirrhosis. After conversion therapy (4 cycles of Lenvatinib and Sintilimab), the AFP level decreased to 2.95 ng/mL and the tumor diameter decreased to 85 mm. The patient underwent left hemihepatectomy and lymph node dissection, and histopathological evaluation of response revealed major histopathological response to therapy (residual viable tumor cells rate =8%; Image A2 ①), and no residual tumor tissue was found in metastatic lymph nodes; Image A2 ②). The patient died of myocardial infarction 14.9 months later, and there was no recurrence during the follow-up period. Image A2 shows: ① the hepatic tumor, with a small number of tumor cells, some visible mitotic figures, surrounded by a large number of lymphocyte infiltration (×200); ② showed a large number of necrotic tissues in metastatic lymph nodes and cell aggregation (×200). Image B1 shows a 51-year-old man with BCLC-C stage hepatocellular carcinoma in the right hepatic lobe (red arrow), and the patient was accompanied by portal vein tumor thrombus (PVTT; blue arrow). The hepatic lesion of pre-treatment ^{18}F-FDG PET/CT (2020–09–09) showed that TLR was 4.22, and the hepatic lesion of post-treatment ^{18}F–FDG PET/CT (2021–01–21) showed that TLR was 1.37. The hepatic lesion of pre-treatment ^{18}F-FDG PET/CT (2020–09–09) showed that PVTT-to-normal liver standardized uptake value ratio (PLR) was 3.85, and the hepatic lesion of post-treatment ^{18}F-FDG PET/CT (2021–01–21) showed that PLR was 0.87. The percentage of change in TLR and PLR was -67.61 and -77.44, respectively. The baseline AFP level was 86.78 ng/mL, the baseline tumor diameter 190 mm, and the Child-Pugh score 6. The patient had no history of hepatitis, while had a history of liver cirrhosis. After conversion therapy (4 cycles of Lenvatinib and Sintilimab), the AFP level decreased to 1.88 ng/mL and the tumor diameter decreased to 127 mm. The patient underwent right hemihepatectomy and PVTT resection. The histopathologic evaluation of primary liver lesion response indicated major histopathological response to therapy (residual viable tumor cells rate<5%; Image B2 ①) and the histopathological evaluation of PVTT response revealed complete histopathological response to therapy (residual viable tumor cells rate=0%; Image B2 ②). No recurrence or death occurred during the follow-up period. Image B2 shows: ① showed the hepatic tumor with no viable tumor cells but foam cells aggregation (blue arrows), and scattered lymphocyte infiltration (×200); ② showed a large area of necrosis in the PVTT, with a large number of inflammatory cell infiltration and foam cell reaction around it, and no obvious viable tumor cells (×200). Image C1 shows a 38-year-old man with BCLC-C stage hepatocellular carcinoma in the right hepatic lobe (red arrow), and the patient was accompanied by portal vein tumor thrombus (blue arrow). The hepatic lesion of pre-treatment ^{18}F-FDG PET/CT (2020–09–18) showed that TLR was 1.94, and the hepatic lesion of post-treatment ^{18}F-FDG PET/CT (2021–03–30) showed that TLR was 1.39. The hepatic lesion of pre-treatment ^{18}F-FDG PET/CT (2020–09–18) showed that PLR was 2.20, and the hepatic lesion of post-treatment ^{18}F-FDG PET/CT (2021–03–30) showed that PLR was 1.35. The percentage of change in TLR and PLR was -28.08 and -38.59, respectively. The baseline AFP level was 289.4 ng/mL, the baseline tumor diameter 48 mm, and the Child-Pugh score 5. The patient had no history of hepatitis, while had a history of liver cirrhosis. After conversion therapy (9 cycles of Lenvatinib and Sintilimab), the AFP level decreased to 35.04 ng/mL and the tumor diameter decreased to 23 mm. The patient underwent S7 segmentectomy and PVTT resection. The histopathological evaluation of response revealed no major histopathological response to therapy (residual viable tumor cells rate =85%; Image C2 ①) and the histopathological evaluation of portal vein tumor thrombus response indicated no complete histopathological response to therapy (residual viable tumor cells rate=50%; Image C2 ②). No recurrence or death occurred during the follow-up period. Image C2 shows: ① showed the tumor cell with degeneration, deep staining of the nucleus, obvious atypia (blue arrows), and a large number of lymphocyte infiltration around (×200); ② showed PVTT, visible tumor cells with some cancer tissue degeneration, visible hemorrhage necrosis and foam cell aggregation (×200).

tumor differentiation, the impact of HCC differentiation on ^{18}F-FDG uptake could not be considered. In the future, we will design prospective studies with a longer follow-up and a larger sample size to verify the role of ^{18}F-FDG PET in predicting pathological response and prognosis of unresectable HCC patients after treated by Lenvatinib in combination with PD-1 inhibitors as conversion therapy.

Conclusions

In conclusion, the results of this study suggest that ^{18}F-FDG PET is a precious tool for predicting pathological response and prognosis of patients with primary unresectable HCC after treated by Lenvatinib combined with PD-1 inhibitors as conversion therapy. Our study provided valuable markers for clinical decision-making, preoperative evaluation and prognostic prediction of patients with unresectable HCC.

Data availability statement

The original contributions presented in the study are included in the article/Supplementary Material. Further inquiries can be directed to the corresponding authors.

Ethics statement

The study involving human participants was reviewed and approved by The Ethics Committee of the General Hospital of the People's Liberation Army (Beijing, China). Written informed consent for participation was not required for this study in accordance with the national legislation and the institutional requirements.

Author contributions

Conception and design: GYW, WWZ, BXX, SCL, RMW and GYM. Data collation: GYW, WWZ, XHL, ZBW, JJL and JMZ. Statistical Analysis: GYW, RMW and GYM. Article writing: GYW, WWZ, XHL and XDX. Article revision: JJL, JMZ, BXZ, SCL, RMW and GYM. All authors contributed to the article and approved the submitted version.

Acknowledgments

The authors would like to thank the staffs at Department of Nuclear Medicine and Faculty of Hepato-Pancreato-Biliary Surgery (The First Medical Centre, Chinese PLA General Hospital, Beijing, China) for their assistance in carrying out this study.

Conflict of interest

The authors declare that the research was conducted in the absence of any commercial or financial relationships that could be construed as a potential conflict of interest.

Publisher's note

All claims expressed in this article are solely those of the authors and do not necessarily represent those of their affiliated organizations, or those of the publisher, the editors and the reviewers. Any product that may be evaluated in this article, or claim that may be made by its manufacturer, is not guaranteed or endorsed by the publisher.

Supplementary material

The Supplementary Material for this article can be found online at: https://www.frontiersin.org/articles/10.3389/fimmu.2023.1151967/full#supplementary-material

References

1. Sung H, Ferlay J, Siegel RL, Laversanne M, Soerjomataram I, Jemal A, et al. Global cancer statistics 2020: GLOBOCAN estimates of incidence and mortality worldwide for 36 cancers in 185 countries. *CA Cancer J Clin* (2021) 71(3):209–49. doi: 10.3322/caac.21660

2. Clark T, Maximin S, Meier J, Pokharel S, Bhargava P. Hepatocellular carcinoma: review of epidemiology, screening, imaging diagnosis, response assessment, and treatment. *Curr Probl Diagn Radiol* (2015) 44(6):479–86. doi: 10.1067/j.cpradiol.2015.04.004

3. Pinter M, Peck-Radosavljevic M. Review article: systemic treatment of hepatocellular carcinoma. *Aliment Pharmacol Ther* (2018) 48(6):598–609. doi: 10.1111/apt.14913

4. Zhang L, Ding J, Li HY, Wang ZH, Wu J. Immunotherapy for advanced hepatocellular carcinoma, where are we? *Biochim Biophys Acta Rev Cancer* (2020) 1874(2):188441. doi: 10.1016/j.bbcan.2020.188441

5. Bruix J, Reig M, Sherman M. Evidence-based diagnosis, staging, and treatment of patients with hepatocellular carcinoma. *Gastroenterology* (2016) 150(4):835–53. doi: 10.1053/j.gastro.2015.12.041

6. Sun HC, Zhou J, Wang Z, Liu X, Xie Q, Jia W, et al. Chinese expert consensus on conversion therapy for hepatocellular carcinoma (2021 edition). *Hepatobiliary Surg Nutr* (2022) 11(2):227–52. doi: 10.21037/hbsn-21-328

7. Tang H, Cao Y, Jian Y, Li X, Li J, Zhang W, et al. Conversion therapy with an immune checkpoint inhibitor and an antiangiogenic drug for advanced hepatocellular carcinoma: a review. *Biosci Trends* (2022) 16(2):130–41. doi: 10.5582/bst.2022.01019

8. Al-Salama ZT, Syed YY, Scott LJ. Lenvatinib: a review in hepatocellular carcinoma. *Drugs* (2019) 79(6):665–74. doi: 10.1007/s40265-019-01116-x

9. Matsuki M, Hoshi T, Yamamoto Y, Ikemori-Kawada M, Minoshima Y, Funahashi Y, et al. Lenvatinib inhibits angiogenesis and tumor fibroblast growth factor signaling pathways in human hepatocellular carcinoma models. *Cancer Med* (2018) 7(6):2641–53. doi: 10.1002/cam4.1517

10. Tohyama O, Matsui J, Kodama K, Hata-Sugi N, Kimura T, Okamoto K, et al. Antitumor activity of lenvatinib (e7080): an angiogenesis inhibitor that targets multiple receptor tyrosine kinases in preclinical human thyroid cancer models. *J Thyroid Res* (2014) 2014:638747. doi: 10.1155/2014/638747

11. Finn RS, Ikeda M, Zhu AX, Sung MW, Baron AD, Kudo M, et al. Phase ib study of lenvatinib plus pembrolizumab in patients with unresectable hepatocellular carcinoma. *J Clin Oncol* (2020) 38(26):2960–70. doi: 10.1200/JCO.20.00808

12. Finn RS, Qin S, Ikeda M, Galle PR, Ducreux M, Kim TY, et al. Atezolizumab plus bevacizumab in unresectable hepatocellular carcinoma. *N Engl J Med* (2020) 382 (20):1894–905. doi: 10.1056/ NEJMoa1915745

13. Xu J, Shen J, Gu S, Zhang Y, Wu L, Wu J, et al. Camrelizumab in combination with apatinib in patients with advanced hepatocellular carcinoma (RESCUE): a nonrandomized, open-label, phase II trial. *Clin Cancer Res* (2021) 27(4):1003–11. doi: 10.1158/1078-0432.CCR-20- 2571

14. Ren Z, Xu J, Bai Y, Xu A, Cang S, Du C, et al. Sintilimab plus a bevacizumab biosimilar (IBI305) versus sorafenib in unresectable hepatocellular carcinoma (ORIENT-32): a randomised, open-label, phase 2-3 study. *Lancet Oncol* (2021) 22 (7):977–90. doi: 10.1016/S1470-2045(21)00252-7

15. Kudo M, Ikeda M, Motomura K, Okusaka T, Kato N, Dutcus CE, et al. A phase ib study of lenvatinib (LEN) plus nivolumab (NIV) in patients (Pts) with unresectable hepatocellular carcinoma (uHCC): study 117. *J Clin Oncol* (2020) 38(4_suppl):513–3. doi: 10.1200/JCO.2020.38.4_suppl.513

16. Zhu AX, Finn RS, Ikeda M, Sung MW, Baron AD, Kudo M, et al. A phase ib study of lenvatinib (LEN) plus pembrolizumab (PEMBRO) in unresectable hepatocellular carcinoma (uHCC). *J Clin Oncol* (2020) 38(2020):4519. doi: 10.1200/JCO.2020.38.15_suppl.4519

17. Zhang W, Lu S, Hu B, Wan T, Wang H, Han J, et al. PD-1 inhibitor combined with lenvatinib for unresectable liver cancer as the conversion therapy: an open-label, nonrandomized, phase IV study. *J Clin Oncol* (2021) 39(suppl 15):e16173. doi: 10.1200/JCO.2021.39.15_suppl.e16173

18. Zhang W, Hu B, Han J, Wang Z, Ma G, Ye H, et al. Surgery after conversion therapy with PD-1 inhibitors plus tyrosine kinase inhibitors are effective and safe for advanced hepatocellular carcinoma: a pilot study of ten patients. *Front Oncol* (2021) 11:747950. doi: 10.3389/fonc.2021.747950

19. Zhu XD, Huang C, Shen YH, Ji Y, Ge NL, Qu XD, et al. Downstaging and resection of initially unresectable hepatocellular carcinoma with tyrosine kinase inhibitor and anti-PD-1 antibody combinations. *Liver Cancer* (2021) 10(4):320–9. doi: 10.1159/000514313

20. Zhang W, Hu B, Han J, Wang H, Wang Z, Ye H, et al. A real-world study of PD-1 inhibitors combined with TKIs for HCC with major vascular invasion as the conversion therapy: a prospective, non-randomized, open-label cohort study. *Ann Oncol* (2020) 31:S1307. doi: 10.1016/j.annonc.2020.10.195

21. Yarchoan M, Zhu Q, Durham JN, Gross N, Charmsaz S, Leatherman JM, et al. Feasibility and efficacy of neoadjuvant cabozantinib and nivolumab in patients with borderline resectable or locally advanced hepatocellular carcinoma (HCC). *J Clin Oncol* (2021) 39(3_suppl):335. doi: 10.1200/JCO.2021.39.3_suppl.335

22. Lencioni R, Llovet JM. (mRECIST) assessment for hepatocellular carcinoma. *Semin Liver Dis* (2010) 30(1):52–60. doi: 10.1055/s-0030-1247132

23. Llovet JM, Lencioni R. mRECIST for HCC: performance and novel refinements. *J Hepatol* (2020) 72(2):288–306. doi: 10.1016/j.jhep.2019.09.026

24. Hong CM, Ahn BC, Jang YJ, Jeong SY, Lee SW, Lee J. Prognostic value of metabolic parameters of 18F-FDG PET/CT and apparent diffusion coefficient of MRI in hepatocellular carcinoma. *Clin Nucl Med* (2017) 42(2):95–9. doi: 10.1097/RLU.0000000000001478

25. Kim YI, Paeng JC, Cheon GJ, Suh KS, Lee DS, Chung JK, et al. Prediction of posttransplantation recurrence of hepatocellular carcinoma using metabolic and volumetric indices of 18F-FDG PET/CT. *J Nucl Med* (2016) 57(7):1045–51. doi: 10.2967/jnumed.115.170076

26. Tian F, Shen G, Deng Y, Diao W, Jia Z. The accuracy of (18)F-FDG PET/CT in predicting the pathological response to neoadjuvant chemotherapy in patients with breast cancer: a meta-analysis and systematic review. *Eur Radiol* (2017) 27(11):4786–96. doi: 10.1007/s00330-017-4831-y

27. Vos JL, Zuur CL, Smit LA, de Boer JP, Al-Mamgani A, van den Brekel MWM, et al. [(18)F]FDG-PET accurately identifies pathological response early upon neoadjuvant immune checkpoint blockade in head and neck squamous cell carcinoma. *Eur J Nucl Med Mol Imaging* (2022) 49(6):2010–22. doi: 10.1007/s00259-021-05610-x

28. Rufini V, Collarino A, Calcagni ML, Meduri GM, Fuoco V, Pasciuto T, et al. The role of (18)F-FDG-PET/CT in predicting the histopathological response in locally advanced cervical carcinoma treated by chemo-radiotherapy followed by radical surgery: a prospective study. *Eur J Nucl Med Mol Imaging* (2020) 47(5):1228–38. doi: 10.1007/s00259-019-04436-y

29. Marrero JA, Kulik LM, Sirlin CB, Zhu AX, Finn RS, Abecassis MM, et al. Diagnosis, staging, and management of hepatocellular carcinoma: 2018 practice guidance by the american association for the study of liver diseases. *Hepatology* (2018) 68(2):723–50. doi: 10.1002/hep.29913

30. Eisenhauer EA, Therasse P, Bogaerts J, Schwartz LH, Sargent D, Ford R, et al. New response evaluation criteria in solid tumours: revised RECIST guideline (version 1.1). *Eur J Cancer* (2009) 45(2):228–47. doi: 10.1016/j.ejca.2008.10.026

31. Institute NC. *Common terminology criteria for adverse events*. Available at: http://ctepcancergov/protocolDevelopment/electronic_applications/ctchtm. (Accessed 14 Jun 2011).

32. Kudo M, Finn RS, Qin S, Han KH, Ikeda K, Piscaglia F, et al. Lenvatinib versus sorafenib in first-line treatment of patients with unresectable hepatocellular carcinoma: a randomised phase 3 noninferiority trial. *Lancet* (2018) 391(10126):1163–73. doi: 10.1016/S0140-6736(18)30207-1

33. Wang G, Zhang W, Chen J, Luan X, Wang Z, Wang Y, et al. Pretreatment metabolic parameters measured by (18)F-FDG PET to predict the pathological treatment response of HCC patients treated with PD-1 inhibitors and lenvatinib as a conversion therapy in BCLC stage c. *Front Oncol* (2022) 12:884372. doi: 10.3389/fonc.2022.884372

34. Stein JE, Lipson EJ, Cottrell TR, Forde PM, Anders RA, Cimino-Mathews A, et al. Pan-tumor pathologic scoring of response to PD-(L)1 blockade. *Clin Cancer Res* (2020) 26(3):545–51. doi: 10.1158/1078-0432.CCR-19-2379

35. Xia Y, Tang W, Qian X, Li X, Cheng F, Wang K, et al. Efficacy and safety of camrelizumab plus apatinib during the perioperative period in resectable hepatocellular carcinoma: a single-arm, open label, phase II clinical trial. *J Immunother Cancer* (2022) 10:e004656. doi: 10.1136/jitc-2022-004656

36. Lim C, Salloum C, Chalaye J, Lahat E, Costentin CE, Osseis M, et al. 18F-FDG PET/CT predicts microvascular invasion and early recurrence after liver resection for hepatocellular carcinoma: a prospective observational study. *HPB (Oxford)* (2019) 21(6):739–47. doi: 10.1016/j.hpb.2018.10.007

37. Allard MA, Sebagh M, Ruiz A, Guettier C, Paule B, Vibert E, et al. Does pathological response after transarterial chemoembolization for hepatocellular carcinoma in cirrhotic patients with cirrhosis predict outcome after liver resection or transplantation? *J Hepatol* (2015) 63(1):83–92. doi: 10.1016/j.jhep.2015.01.023

38. Yang Y, Dang Z, Lu P, Qian Y, Lin K, Pan Z, et al. Impact of pathological response after preoperative transcatheter arterial chemoembolization (TACE) on incidences of microvascular invasion and early tumor recurrence in hepatocellular carcinoma: a multicenter propensity score matching analysis. *Hepatobiliary Surg Nutr* (2022) 11(3):386–99. doi: 10.21037/hbsn-20-700

39. Hellmann MD, Chaft JE, William WN Jr, Rusch V, Pisters KM, Kalhor N, et al. Pathological response after neoadjuvant chemotherapy in resectable non-small-cell lung cancers: proposal for the use of major pathological response as a surrogate endpoint. *Lancet Oncol* (2014) 15(1):e42–50. doi: 10.1016/S1470-2045(13)70334-6

40. Truty MJ, Kendrick ML, Nagorney DM, Smoot RL, Cleary SP, Graham RP, et al. Factors predicting response, perioperative outcomes, and survival following total neoadjuvant therapy for Borderline/Locally advanced pancreatic cancer. *Ann Surg* (2021) 273(2):341–9. doi: 10.1097/SLA.0000000000003284

41. Stein JE, Soni A, Danilova L, Cottrell TR, Gajewski TF, Hodi FS, et al. Major pathologic response on biopsy (MPRbx) in patients with advanced melanoma treated with anti-PD-1: evidence for an early, on-therapy biomarker of response. *Ann Oncol* (2019) 30(4):589–96. doi: 10.1093/annonc/mdz019

42. Edeline J, Boucher E, Rolland Y, Vauléon E, Pracht M, Perrin C, et al. Comparison of tumor response by response evaluation criteria in solid tumors (RECIST) and modified RECIST in patients treated with sorafenib for hepatocellular carcinoma. *Cancer* (2012) 118(1):147–56. doi: 10.1002/cncr.26255

43. Vicentin I, Mosconi C, Garanzini E, Sposito C, Serenari M, Buscemi V, et al. Inter-center agreement of mRECIST in transplanted patients for hepatocellular carcinoma. *Eur Radiol* (2021) 31(12):8903–12. doi: 10.1007/s00330-021-08088-1

44. Song MJ, Bae SH, Lee SW, Song DS, Kim HY, Yoo IeR, et al. 18F-fluorodeoxyglucose PET/CT predicts tumour progression after transarterial chemoembolization in hepatocellular carcinoma. *Eur J Nucl Med Mol Imaging* (2013) 40(6):865–73. doi: 10.1007/s00259-013-2366-2

45. Kucuk ON, Soydal C, Araz M, Bilgic S, Ibis E. Prognostic importance of 18F-FDG uptake pattern of hepatocellular cancer patients who received SIRT. *Clin Nucl Med* (2013) 38(7):e283–289. doi: 10.1097/RLU.0b013e3182867f17

46. Song MJ, Bae SH, Yoo leR, Park CH, Jang JW, Chun HJ, et al. Predictive value of (1)(8)F-fluorodeoxyglucose PET/CT for transarterial chemolipiodolization of hepatocellular carcinoma. *World J Gastroenterol* (2012) 18(25):3215–22. doi: 10.3748/wjg.v18.i25.3215

47. Lopci E, Toschi L, Grizzi F, Rahal D, Olivari L, Castino GF, et al. Correlation of metabolic information on FDG-PET with tissue expression of immune markers in patients with non-small cell lung cancer (NSCLC) who are candidates for upfront surgery. *Eur J Nucl Med Mol Imaging* (2016) 43(11):1954–61. doi: 10.1007/s00259-016-3425-2

48. Wofford JA, Wieman HL, Jacobs SR, Zhao Y, Rathmell JC. IL-7 promotes Glut1 trafficking and glucose uptake *via* STAT5-mediated activation of akt to support t-cell survival. *Blood* (2008) 111(4):2101–11. doi: 10.1182/blood-2007-06-096297

49. Itoh S, Yoshizumi T, Kitamura Y, Yugawa K, Iseda N, Shimagaki T, et al. Impact of metabolic activity in hepatocellular carcinoma: association with immune status and vascular formation. *Hepatol Commun* (2021) 5(7):1278–89. doi: 10.1002/hep4.1715

50. Kawamura Y, Kobayashi M, Shindoh J, Kobayashi Y, Kasuya K, Sano T, et al. (18)F-fluorodeoxyglucose uptake in hepatocellular carcinoma as a useful predictor of an extremely rapid response to lenvatinib. *Liver Cancer* (2020) 9(1):84–92. doi: 10.1159/000503577

51. Llovet JM, Kelley RK, Villanueva A, Singal AG, Pikarsky E, Roayaie S, et al. Hepatocellular carcinoma. *Nat Rev Dis Primers* (2021) 7(1):6. doi: 10.1038/s41572-020-00240-3

52. Valerio L, Guidoccio F, Giani C, Tardelli E, Puccini G, Puleo L, et al. [18F]-FDG-PET/CT correlates with the response of radiorefractory thyroid cancer to lenvatinib and patient survival. *J Clin Endocrinol Metab* (2021) 106(8):2355–66. doi: 10.1210/clinem/dgab278

53. Shao D, Cheng Y, Yuan ZS, Jiang BY, Wang SX. Value of interim (18)F-FDG PET/CT for predicting progression-free survival in stage B/IV EGFR-mutant non-small-cell lung cancer patients with EGFR-TKI therapy. *Lung Cancer* (2020) 149:137–43. doi: 10.1016/j.lungcan.2020.09.020

54. Sachpekidis C, Kopp-Schneider A, Pan L, Papamichail D, Haberkorn U, Hassel JC. Interim [(18)F]FDG PET/CT can predict response to anti-PD-1 treatment in metastatic melanoma. *Eur J Nucl Med Mol Imaging* (2021) 48(6):1932–43. doi: 10.1007/s00259-020-05137-7

55. Ito K, Teng R, Schöder H, Humm JL, Ni A, Michaud L, et al. (18)F-FDG PET/CT for monitoring of ipilimumab therapy in patients with metastatic melanoma. *J Nucl Med* (2019) 60(3):335–41. doi: 10.2967/jnumed.118.213652

56. Li SH, Wei W, Guo RP, Shi M, Guo ZX, Chen ZY, et al. Long-term outcomes after curative resection for patients with macroscopically solitary hepatocellular carcinoma without macrovascular invasion and an analysis of prognostic factors. *Med Oncol* (2013) 30(4):696. doi: 10.1007/s12032-013-0696-3

57. Sun J, Guo R, Bi X, Wu M, Tang Z, Lau WY, et al. Guidelines for diagnosis and treatment of hepatocellular carcinoma with portal vein tumor thrombus in china (2021 edition). *Liver Cancer* (2022) 11(4):315–28. doi: 10.1159/000523997

58. Li N, Feng S, Xue J, Wei XB, Shi J, Guo WX, et al. Hepatocellular carcinoma with main portal vein tumor thrombus: a comparative study comparing hepatectomy with or without neoadjuvant radiotherapy. *HPB (Oxford)* (2016) 18(6):549–56. doi: 10.1016/j.hpb.2016.04.003

59. Wei X, Jiang Y, Zhang X, Feng S, Zhou B, Ye X, et al. Neoadjuvant three-dimensional conformal radiotherapy for resectable hepatocellular carcinoma with portal vein tumor thrombus: a randomized, open-label, multicenter controlled study. *J Clin Oncol* (2019) 37(24):2141–51. doi: 10.1200/JCO.18.02184

60. Huang C, Zhu XD, Shen YH, Wu D, Ji Y, Ge NL, et al. Organ specific responses to first-line lenvatinib plus anti-PD-1 antibodies in patients with unresectable hepatocellular carcinoma: a retrospective analysis. *biomark Res* (2021) 9(1):19. doi: 10.1186/s40364-021-00274-z

61. Ahn SJ, Park MS, Kim KA, Park JY, Kim I, Kang WJ, et al. (1)(8)F-FDG PET metabolic parameters and MRI perfusion and diffusion parameters in hepatocellular carcinoma: a preliminary study. *PloS One* (2013) 8(8):e71571. doi: 10.1371/journal.pone.0071571

62. Lee JW, Hwang SH, Kim DY, Han KH, Yun M. Prognostic value of FDG uptake of portal vein tumor thrombosis in patients with locally advanced hepatocellular carcinoma. *Clin Nucl Med* (2017) 42(1):e35–40. doi: 10.1097/RLU.0000000000001422

63. Zhu XD, Huang C, Shen YH, Xu B, Ge NL, Ji Y, et al. Hepatectomy after conversion therapy using tyrosine kinase inhibitors plus anti-PD-1 antibody therapy for patients with unresectable hepatocellular carcinoma. *Ann Surg Oncol* (2023) 30(5):2782–90. doi: 10.1245/s10434-022-12530-z

64. Xu B, Zhu XD, Shen YH, Zhu JJ, Liu J, Li ML, et al. Criteria for identifying potentially resectable patients with initially oncologically unresectable hepatocellular carcinoma before treatment with lenvatinib plus an anti-PD-1 antibody. *Front Immunol* (2022) 13:1016736. doi: 10.3389/fimmu.2022.1016736

65. Yi Y, Sun BY, Weng JL, Zhou C, Zhou CH, Cai MH, et al. Lenvatinib plus anti-PD-1 therapy represents a feasible conversion resection strategy for patients with initially unresectable hepatocellular carcinoma: a retrospective study. *Front Oncol* (2022) 12:1046584. doi: 10.3389/fonc.2022.1046584

66. Cheng AL, Qin S, Ikeda M, Galle PR, Ducreux M, Kim TY, et al. Updated efficacy and safety data from IMbrave150: atezolizumab plus bevacizumab vs. sorafenib for unresectable hepatocellular carcinoma. *J Hepatol* (2022) 76(4):862–73. doi: 10.1016/j.jhep.2021.11.030

frontiers | Frontiers in Immunology

TYPE Correction
PUBLISHED 22 May 2023
DOI 10.3389/fimmu.2023.1219757

OPEN ACCESS

EDITED AND REVIEWED BY
Takaji Matsutani,
Repertoire Genesis, Inc., Japan

*CORRESPONDENCE
Guangyu Ma
mgy301@163.com
Ruimin Wang
wrm@yeah.net
Shichun Lu
lusc_301@163.com

†These authors have contributed equally to this work

RECEIVED 09 May 2023
ACCEPTED 12 May 2023
PUBLISHED 22 May 2023

CITATION
Wang G, Zhang W, Luan X, Wang Z, Liu J, Xu X, Zhang J, Xu B, Lu S, Wang R and Ma G (2023) Corrigendum: The role of 18F–FDG PET in predicting the pathological response and prognosis to unresectable HCC patients treated with lenvatinib and PD-1 inhibitors as a conversion therapy.
Front. Immunol. 14:1219757.
doi: 10.3389/fimmu.2023.1219757

Corrigendum: The role of 18F–FDG PET in predicting the pathological response and prognosis to unresectable HCC patients treated with lenvatinib and PD-1 inhibitors as a conversion therapy

Guanyun Wang[1,2†], Wenwen Zhang[3†], Xiaohui Luan[1,4], Zhanbo Wang[5], Jiajin Liu[1], Xiaodan Xu[1], Jinming Zhang[1], Baixuan Xu[1], Shichun Lu[3*], Ruimin Wang[1*] and Guangyu Ma[1*]

[1]Department of Nuclear Medicine, The First Medical Centre, Chinese People's Liberation Army (PLA) General Hospital, Beijing, China, [2]Nuclear Medicine Department, Beijing Friendship Hospital, Capital Medical University, Beijing, China, [3]Faculty of Hepato-Pancreato-Biliary Surgery, Chinese People's Liberation Army (PLA) General Hospital/Institute of Hepatobiliary Surgery of Chinese People's Liberation Army/Key Laboratory of Digital Hepetobiliary Surgery, People's Liberation Army, Beijing, China, [4]Graduate School, Medical School of Chinese People's Liberation Army (PLA), Beijing, China, [5]Department of Pathology, The First Medical Centre, Chinese People's Liberation Army (PLA) General Hospital, Beijing, China

KEYWORDS

unresectable hepatocellular carcinoma, conversion therapy, major pathological response, prognosis, ^{18}F-FDG PET

A corrigendum on

The role of 18F–FDG PET in predicting the pathological response and prognosis to unresectable HCC patients treated with lenvatinib and PD-1 inhibitors as a conversion therapy

by Wang G, Zhang W, Luan X, Wang Z, Liu J, Xu X, Zhang J, Xu B, Lu S, Wang R and Ma G (2023). *Front. Immunol.* 14:1151967. doi: 10.3389/fimmu.2023.1151967

In the published article, there was an error in the formula in the manuscript.

A correction has been made to **Materials and Methods**, Image analysis, Paragraph 2. This sentence previously stated:

"The percentages of post-treatment changes in metabolic parameters were calculated as follows:

$$\Delta\text{SUVmax}\,(\,\%\,) = \frac{\text{SUVmax of pre-treatment} - \text{SUVmax of post-treatment}}{\text{SUVmax of pretreatment}} \times 100\,\%$$

$$\Delta\text{TLR}(\,\%\,) = \frac{\text{TLR of pre-treatment} - \text{TLR of post-treatment}}{\text{TLR of pre-treatment}} \times 100\,\%$$

$$\Delta PLR(\%) = \frac{\text{PLR of pre-treatment} - \text{PLR of post-treatment}}{\text{PLR of pre-treatment}} \times 100\%"$$

The corrected sentence appears below:

"The percentages of post-treatment changes in metabolic parameters were calculated as follows:

$$\Delta SUVmax(\%) = \frac{\text{SUVmax of post-treatment} - \text{SUVmax of pre-treatment}}{\text{SUVmax of pre-treatment}} \times 100\%$$

$$\Delta TLR(\%) = \frac{\text{TLR of post-treatment} - \text{TLR of pre-treatment}}{\text{TLR of pre-treatment}} \times 100\%$$

$$\Delta PLR(\%) = \frac{\text{PLR of post-treatment} - \text{PLR of pre-treatment}}{\text{PLR of pre-treatment}} \times 100\%"$$

The authors apologize for this error and state that this does not change the scientific conclusions of the article in any way. The original article has been updated.

Publisher's note

frontiers | Frontiers in Immunology

TYPE Original Research
PUBLISHED 10 May 2023
DOI 10.3389/fimmu.2023.1138524

OPEN ACCESS

EDITED BY
Esra Akbay,
University of Texas Southwestern Medical Center, United States

REVIEWED BY
Galal Metwally,
Zagazig University, Egypt
Abhijit Maji,
University of Texas Southwestern Medical Center, United States

*CORRESPONDENCE
Lei Meng
menglei0901@126.com
Xue Pan
405465029@qq.com

†These authors share first authorship

RECEIVED 05 January 2023
ACCEPTED 26 April 2023
PUBLISHED 10 May 2023

CITATION
Xu Z, Pei C, Cheng H, Song K, Yang J, Li Y, He Y, Liang W, Liu B, Tan W, Li X, Pan X and Meng L (2023) Comprehensive analysis of FOXM1 immune infiltrates, m6a, glycolysis and ceRNA network in human hepatocellular carcinoma.
Front. Immunol. 14:1138524.
doi: 10.3389/fimmu.2023.1138524

Comprehensive analysis of FOXM1 immune infiltrates, m6a, glycolysis and ceRNA network in human hepatocellular carcinoma

Ziwu Xu[1,2†], Chaozhu Pei[2†], Haojie Cheng[2], Kaixin Song[1], Junting Yang[1], Yuhang Li[1], Yue He[1], Wenxuan Liang[1], Biyuan Liu[3], Wen Tan[4], Xia Li[5], Xue Pan[1*] and Lei Meng[1*]

[1]School of Pharmacy, Hunan University of Chinese Medicine, Changsha, China, [2]College of Biology, Hunan University, Changsha, China, [3]School of Medical, Hunan University of Chinese Medicine, Changsha, China, [4]Department of Pathology, Changsha Hospital of Traditional Chinese Medicine, Changsha Eighth Hospital, Changsha, China, [5]Department of General Surgery, People's Hospital of Hunan Province, Changsha, China

Background: Forkhead box M1 (FOXM1) is a member of the Forkhead box (Fox) transcription factor family. It regulates cell mitosis, cell proliferation, and genome stability. However, the relationship between the expression of FOXM1 and the levels of m6a modification, immune infiltration, glycolysis, and ketone body metabolism in HCC has yet to be fully elucidated.

Methods: Transcriptome and somatic mutation profiles of HCC were downloaded from the TCGA database. Somatic mutations were analyzed by maftools R package and visualized in oncoplots. GO, KEGG and GSEA function enrichment was performed on FOXM1 co-expression using R. We used Cox regression and machine learning algorithms (CIBERSORT, LASSO, random forest, and SVM-RFE) to study the prognostic value of FOXM1 and immune infiltrating characteristic immune cells in HCC. The relationship between FOXM1 and m6A modification, glycolysis, and ketone body metabolism were analyzed by RNA-seq and CHIP-seq. The competing endogenous RNA (ceRNA) network construction relies on the multiMiR R package, ENCORI, and miRNET platforms.

Results: FOXM1 is highly expressed in HCC and is associated with a poorer prognosis. At the same time, the expression level of FOXM1 is significantly related to the T, N, and stage. Subsequently, based on the machine learning strategies, we found that the infiltration level of T follicular helper cells (Tfh) was a risk factor affecting the prognosis of HCC patients. The high infiltration of Tfh was significantly related to the poor overall survival rate of HCC. Besides, the CHIP-seq demonstrated that FOXM1 regulates m6a modification by binding to the promoter of IGF2BP3 and affects the glycolytic process by initiating the transcription of HK2 and PKM in HCC. A ceRNA network was successfully obtained, including FOXM1 - has-miR-125-5p – DANCR/MIR4435-2HG ceRNA network related to the prognosis of HCC.

Conclusion: Our study implicates that the aberrant infiltration of Tfh associated with FOXM1 is a crucial prognostic factor for HCC patients. FOXM1 regulates genes related to m6a modification and glycolysis at the transcriptional level. Furthermore, the specific ceRNA network can be used as a potential therapeutic target for HCC.

KEYWORDS

FoxM1, hepatocellular carcinoma, immune infiltration, m6A modification, glycolysis

1 Introduction

Liver cancer is the third most prevalent malignancy, mainly comprising hepatocellular carcinoma (HCC, also known as LIHC) and intrahepatic cholangiocarcinoma (ICC), of which incidence and mortality rates are increasing worldwide (1). HCC accounts for approximately 75% ~ 90% of all liver cancer cases and is a significant cancer type with a poor prognosis (2). Despite the latest advances in HCC screening and treatment modalities, conventional curative treatments are generally ineffective for HCC because most HCC patients present at an advanced stage to an extent when they are diagnosed (3). Therefore, researching the in-depth investigations of the underlying tumorigenesis and tumor development mechanisms of HCC for screening and prevention is paramount.

The FOXM1 transcription factors are crucial for G1–S and G2–M cell cycle phase progression and mitotic spindle integrity (4). In tumor cells, the expression and the transcriptional activity of FOXM1 are typically upregulated, and overexpression of FOXM1 has been involved in almost all major hallmarks of cancer, manifesting an oncogenic function (5). On the one hand, FOXM1 promotes cancer development by transactivating the expression of its target genes during transcription. On the other hand, FOXM1 may play an oncogenic role that functions within protein interaction networks and protein complexes to activate different oncogenic pathways (6). The strategy of targeting transcription factors has been considered a promising approach in tumor therapy (7). Regarding the multiple biological functions of FOXM1, it has been proven to be a potential therapeutic target for cancer (8), while there are no FDA-approved FOXM1 targeting drugs in oncology treatment.

This study analyzed TCGA data of hepatocellular carcinoma patients for gene RNA-seq expression and clinical information. It used multidimensional analysis to provide an understanding of expression patterns and functional networks to the expression of FOXM1. Use machine learning methods to screen potential diagnostic FOXM1-related infiltrating immune cells in HCC. Evaluating the relationship between differential FOXM1 expression and m6a and glycolysis/KBM-related genes and a comprehensive analysis of genome-wide FOXM1 binding sites in Huh-7 cell lines predicts FOXM1-driven m6a and glycolysis/KBM gene regulation. Finally, FOXM1 was used as the core molecule to predict its associated ceRNA network. To provide a theoretical basis for discovering possible molecular pathways of FOXM1. The schematic diagram of the research design is shown in Figure 1.

2 Method

2.1 Ethics statement

This study proposal has been approved by the Ethics Committee of Changsha Hospitalof Traditional Chinese Medicine (Changsha Elghth Hospltal) and conducted in accordance with the research principles described in the Helsinki Declaration.

2.2 Data collection and preprocessing

The GDC download tool (https://portal.gdc.cancer.gov) from the Cancer Genome Atlas (TCGA) database was used to download the transcriptome data and clinical follow-up data for liver cancer (TCGA-liver hepatocellular carcinoma, LIHC). Each gene expression was normalized using the transcripts per kilobase of exon model per Million mapped reads (TPM) metric. Then we kept the expression matrix of 56,494 genes containing 50 normal and 374 tumor samples. The GSE84006 HCC array datasets containing 38 paired samples were downloaded from the gene expression omnibus (GEO) database (https://www.ncbi.nlm.nih.gov/geo/). When multiple probes correspond to the same gene symbol, the maximum value was considered the final value. The somatic variants in Mutation Annotation Format (MAF) were downloaded from TCGA, and Maftools (9) R package was used for the integrative analysis of somatic variants. The CHIP-seq data is a bigwig and bed file of the Huh-7 cell line that was downloaded in the GSE176383 dataset with reference GRch38primary assembly and visualized by IGV software. Every CHIP-seq peak was called at a false discovery rate (FDR) < 0.05.

2.3 Differentially expressed genes screening

The original expression data of TCGA were transformed with log2, and differentially expressed genes (DEGs) were identified by

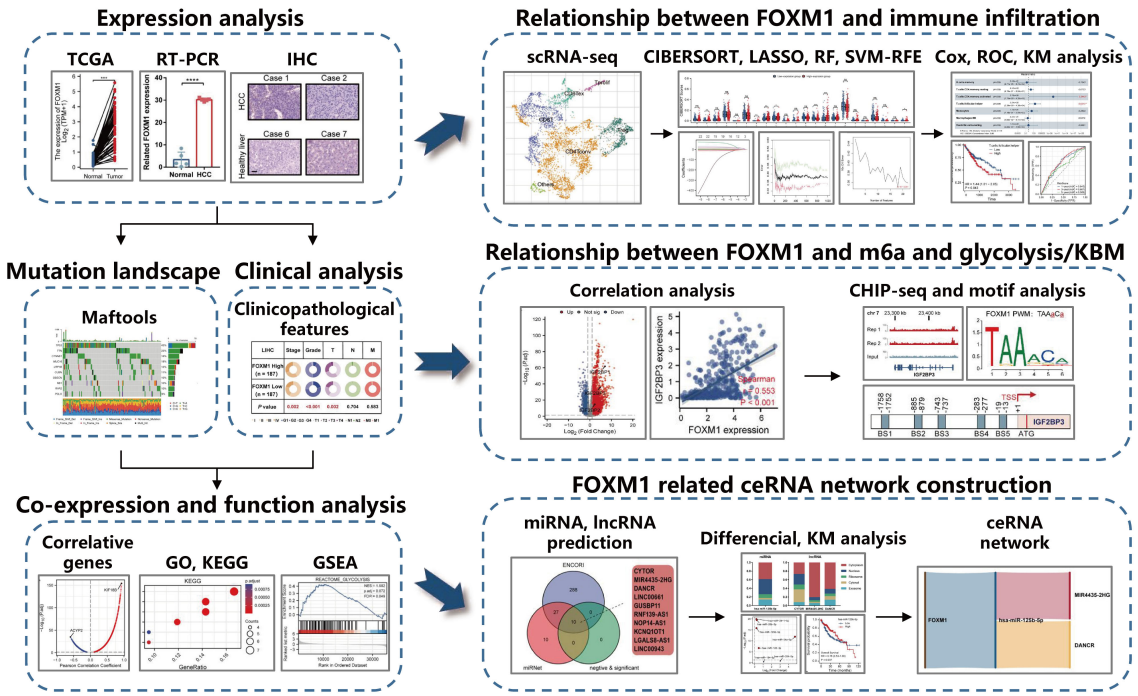

FIGURE 1
Schematic diagram of the study design.

the DESeq2 package of R language (9) under the criteria of |log2FC| > log2(2) and $P < 0.05$.

2.4 RNA extraction and RT-PCR

The total RNA of patients' tissues was isolated from cells using RNA easy fast tissue/cell kit (TIANGEN, China, DP451). Use Prime Script RT reagent kit (TIANGEN, China, KR118-02) for reverse transcription, and then use SYBR Prime Script RT PCR kit (TIANGEN, China, FP209-02) for RT-PCR. Use β-Actin as an internal reference and the $2^{-\triangle\triangle Ct}$ method to calculate the results. FOXM1 primer sequences: forward primer 5'- GCTTGCCAG AGTCCTTTTTGC -3' and reverse primer 5'- CCACCTGAG TTCTCGTCAATGC -3'. β-Actin primer sequences: forward primer 5'- CATGTACGTTGCTATCCAGGC -3' and reverse primer 5'- CTCCTTAATGTCACGCACGAT -3'.

2.5 Immunohistochemistry

HCC tissues from five patients with HCC and five patients with healthy livers were fixed with 4% paraformaldehyde, dehydrated, paraffin-embedded, and prepared into tissue chips. After dewaxing and hydration, a 10 mM sodium citrate antigen repair solution was used at 95°C for 15 min for antigen repair. Then endogenous peroxidase was blocked by 3% H2O2 for 30 min at room temperature. Nonspecific antigens were blocked with 5% BSA in PBS for 30 min. The mouse monoclonal antibodies of FOXM1 (1:200, Cell Signaling Technology, USA, 20459) were incubated overnight at 4°C. Next, secondary antibody binding was detected with goat anti-mouse IgG-HRP (1:2000, Beyotime, China, A0216). DAB and hematoxylin were then used for staining. Images were photographed with a microscope.

2.6 Co-expression analysis

Based on the LinkedOmics platform (10) (http://www.linkedomics.org/admin.php) using the Pearson correlation test method for RNA-Seq, FOXM1 positive and negative co-expression genes were screened under the condition of FDR < 005. The protein-protein interactions PPI network for FOXM1 and its neighbor genes was constructed using the String platform (https://cn.string-db.org/). The R package clusterProfiler (11) was used to process the Genome Ontology (GO) and Kyoto Encyclopedia of Genes and Genomes (KEGG) pathway analysis of FOXM1 co-expression genes.

2.7 Gene set enrichment analysis

Based on the clusterProfiler package (11), gene set enrichment analysis (GSEA) (12) was carried out for further underlying mechanism analysis of FOXM1. Patients in the LIHC cohort were stratified into low or high groups based on gene expression, using the median expression as the cut-off value. The high-expression was compared with the low-expression group by GSEA analysis. The c2.cp.v7.2.symbols.gmt [Curated] was selected as annotated gene set.

2.8 Machine learning and immune infiltration analysis

To uncover the potential role of FOXM1 on the single-cell level, the Tumor Immune Single-cell Hub (TISCH) database (13) (http://tisch.comp-genomics.org/home/) was employed to analyze the correlation between FOXM1 expression and immune cells. Furthermore, We utilized the Least absolute shrinkage and selection operator (LASSO), random forest (RF), and support vector machine-recursive feature elimination (SVM-RFE) to figure out the key immune cells from 22 immune cells by the CIBERSORT (14) algorithm. First, we performed the CIBERSORT algorithms to quantify immune cells' activity or enrichment levels in LIHC tumor tissues. Subsequently, the "glmnet," "randomForest," and "e1071" R package was performed with the CIBERSORT scores of FOXM1 high and low group and follow-up data of each patient to carry out the LASSO, SVM-RFE, and RF analysis of immune cells, respectively. The overlapping immune cells of three algorithms were further screened with multivariate Cox regression analysis, and the key immune cells were evaluated by ROC curve.

2.9 CeRNA network analysis

The multiMiR R package was used for exploring microRNA (miRNA) that has been experientially validated to interact with FOXM1. The long non-coding RNA (lncRNA) interaction with screened miRNA was predicted by ENCORI (15) platform (https://rna.sysu.edu.cn/encori/index.php) and miRNet (16) platform (https://www.mirnet.ca/). Besides, the subcellular localization of ceRNA was analyzed by the lncLocator (17) platform. According to the ceRNA hypothesis, mRNA and lncRNA negatively correlate to miRNA, RNA expression analysis, and overall survival analysis in the LIHC cohort to construct the ceRNA network.

2.10 Statistical analysis

All statistical analyses in this study were conducted using GraphPad Prism 7.0 and R. The correlation between diagnostic gene expression levels and clinical factors was determined using unpaired Student's t-tests for continuous variables and Fisher's exact tests for categorical variables. To analyze the data normalization, a non-parametric statistical analysis was performed. Data with non-parametric characteristics were analyzed with the Kruskal-Wallis or Wilcoxon two-sample test. A two-sided $P < 0.05$ was considered to indicate statistical significance for all analyses.

3 Result

3.1 FOXM1 expression and mutation analysis

The progression of HCC is usually accompanied by abnormal gene expression and poor prognosis. Expression of FOXM1 in matched HCC tissues was found to be higher than that in adjacent samples (Figure 2A). Data from the RT-PCR revealed a consistent trend (Figure 2B). IHC analysis demonstrated that FOXM1 was mainly overexpressed in the nucleus, consistent with its role as a transcription factor (Figure 2C). We used the maftools package to screen the 10 genes with the highest mutation frequencies in the FOXM1 high and low expression groups, respectively (Figures 2D, E). The results showed a high frequency of mutations in TP53, TTN, CTNNB1, MUC16, and PCLO in the high FOXM1 expression group. These mutated genes are known biomarkers of HCC and are of great value for evaluating the malignant tumor progression or therapeutic response (18). The critical genes in HCC progression were usually correlated with cancer stages and patient prognosis. Patients with HCC showed more advanced stage, grade, and T stage in the FOXM1 high-expression group (Figure 2F) and shorter overall and disease-free survival (Figure 2G) outcomes.

3.2 Enrichment analysis of FOXM1 co-expressed genes

To better understand the biological function of FOXM1, we obtained the correlation between each gene and FOXM1 using the LinkedOmics database and analyzed the enrichment of the top 100 genes. There were 8027 genes positively correlated with FOXM1, and 3610 genes negatively correlated with FXOM1 under FDR < 0.05 (Figure 3A). The heat map shows the top 50 positively (Figure 3B) and negatively (Figure 3C) associated genes with FOXM1, respectively. Kinesin family member 18B (KIF18B) expression was positively correlated with the expression of FOXM1, suggesting FOXM1 may have similar regulatory functions to KIF18B. Acylphosphatase 2 (ACYP2) had the highest negative correlation coefficient, probably because it plays opposite roles to FOXM1 in different functional pathways. We further performed the STRING database to study the protein-protein interaction (PPI) network of FOXM1 (Figure 3D). For the more biological function of FOXM1, Gene Ontology (GO) and Kyoto Encyclopedia of Genes and Genomes (KEGG) enrichment analysis was performed. The result indicated that those genes positively correlated with FOXM were positively associated with the cell cycle and cell division (Figure 3E). In contrast, genes negatively associated with FOXM1 in HCC samples were more related to various metabolic pathways (Figure 3F).

3.3 Gene set enrichment analysis of FOXM1

To further characterize the potential function of FOXM1, GSEA was performed. We separated the LIHC cohort samples into a high-expressed group and a low-expressed group according to the expression level of FOXM1 to identify the gene sets associated with FOXM1. The GSEA results showed that cell cycle checkpoints (FDR = 0.016), regulation of TP53 activity (FDR = 0.016), and immunoregulatory interactions between a lymphoid and a non-lymphoid cell (FDR = 0.016) were upregulated in FOXM1 high-

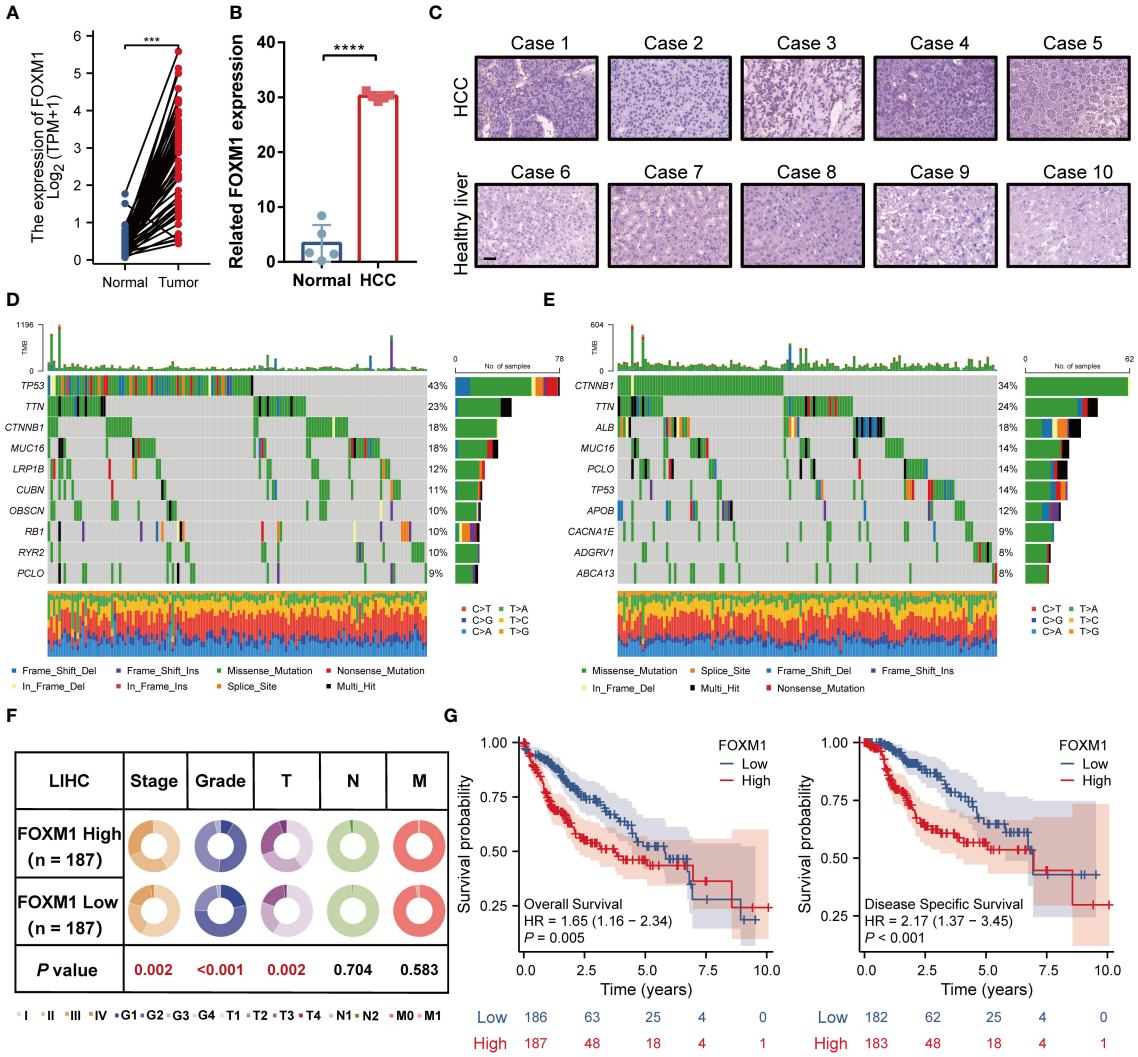

FIGURE 2
FOXM1 is highly expressed in HCC and is associated with high-frequency mutation and poor prognosis. **(A)** FOXM1 expression level in TCGA databases. **(B)** Difference of expression of FOXM1 in clinical samples. **(C)** The protein level of FOXM1 in healthy liver and primary HCC samples was detected by immunohistochemistry, bar 10 μm. The landscape profile of the top 10 mutated genes in the FOXM1 high expression group **(D)** and FOXM1 low expression group **(E)** from the TCGA database. **(F)** The proportion difference of clinical indices (including tumor, node, metastasis stages, and pathological grade) in the FOXM1 high and low expression groups from the TCGA LIHC dataset. **(G)** Prognostic relationship (OS and DFS) between FOXM1 and patients with HCC. (***p < 0.001, ****p < 0.0001).

expression cluster. On the contrary, the low-expressed FOXM1 group was enriched for genes implicated in DNA methylation (FDR = 0.031), glycolysis (FDR = 0.049), and ketone body metabolism (FDR = 0.019) (Figure 4). Sustaining proliferative signaling, deregulating cellular metabolism, and avoiding immune destruction are the hallmarks of cancer (19). According to GSEA results, we further evaluated the association of FOXM1 in immune infiltration and glycolysis and KBM.

3.4 Correlations of FOXM1 expression with immune infiltration

Based on the scRNA-seq TISCH database, we obtained five independent HCC datasets for single-cell analysis to explore the correlation between immune cell distribution and FOXM1 expression levels at the single-cell level (Figure 5A). In the LIHC_GSE98638 dataset, higher levels of FOXM1 expression were found in proliferating T cells (T prolif) (Figures 5A, B). The distribution and expression of FOXM1 in different immune cells were obtained from the clustered plots of scRNA-seq (Figure 5C). Those results indicated that FOXM1 expression levels were significantly correlated with immune cell types and their proportions in HCC.

3.5 Identification of key immune cells associated with FOXM1

Immune infiltration profoundly affects tumor progression, and the composition of tumor-infiltrating immune cells has been

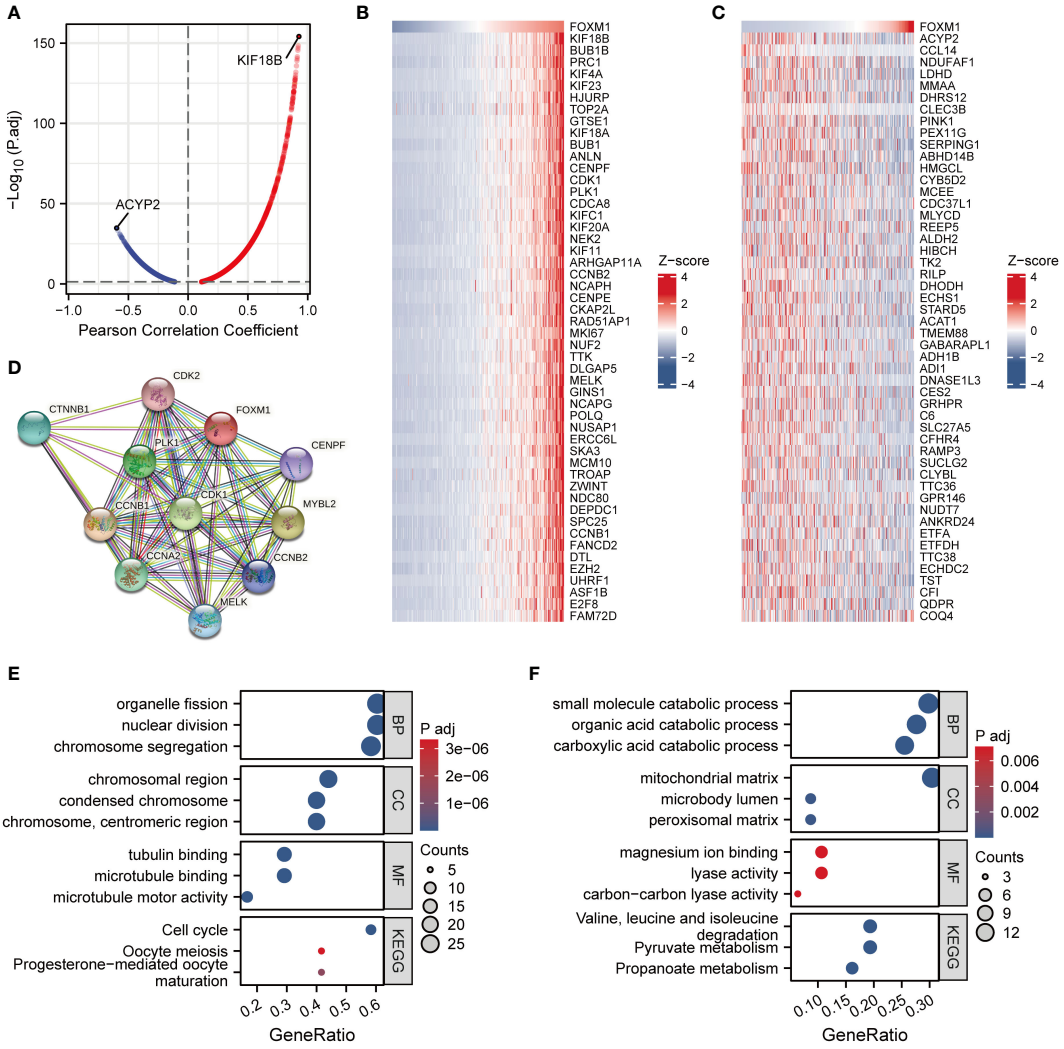

FIGURE 3
Co-expression network analysis and enrichment analysis of FOXM1 in LIHC. **(A)** Volcano map of correlative genes of FOXM1. **(B)** Heat map of Top50 positive co-expression genes with FOXM1. **(C)** Heat map of top50 negative co-expression genes with FOXM1. **(D)** PPI network analysis of FOXM1. Gene ontology and KEGG analysis for genes belonging to the co-expression with strongest positive **(E)** and negative correlation **(F)** with FOXM1.

identified as a critical factor influencing tumor therapy success (20). The CIBERSORT deconvolution algorithm obtains the percentage of infiltration of 22 immune cells in each HCC sample. Grouping comparison of FOXM1 expression showed that there were seven different types of infiltrating immune cells, namely B cells memory ($p < 0.01$), T cell CD4 memory activated ($p < 0.01$), Tfh cells ($p < 0.01$), T cell regulation (Tregs) ($p < 0.05$), monocytes ($p < 0.001$), macrophage M0 ($p < 0.001$), and neutrophils ($p<0.05$) (Figure 6A). The following study performed LASSO, RF, and SVM-RFE analysis on 22 immune cell infiltration. The penalty parameter was tuned by 10-fold cross-validation in LASSO logistic regression, which selected eight immune cells as the feature (Figures 6B, C). The RF diagnosis model was developed with ntree = 500 and mtry = 6 and obtained 19 key immune cells (Figure 6D). Besides, the SVM-RFE algorithm was applied to identify the best feature of the immune cell combination (Figure 6E**).** Overall, marker genes acquired based on the above three algorithms were intersected to obtain seven key immune cells (B cells memory, T cells CD4 memory resting, T cells CD4 memory activated, Tfh cells, monocytes, macrophages M0, and dendritic cells resting) were selected for subsequent analysis (Figure 6F). The correlation analysis showed FOXM1 expression is negatively correlated with T cells CD4 memory resting (Cor = -0.05), monocytes (Cor = -0.16), and significantly positively correlated with B cells memory (Cor = 0.14), T cells CD4 memory activated (Cor = 0.13), Tfh cells (Cor = 0.18), macrophages M0 (Cor = 0.20), and dendritic cells resting (Cor = 0.18) (Figure 6G).

3.6 The clinical manifestations of key immune cells

We further included seven immune characteristics in the multivariate Cox regression. The results showed that T cells CD4 memory resting and Tfh cells were the key immune landscapes associated with FOXM1 (Figure 7A). We then performed the time

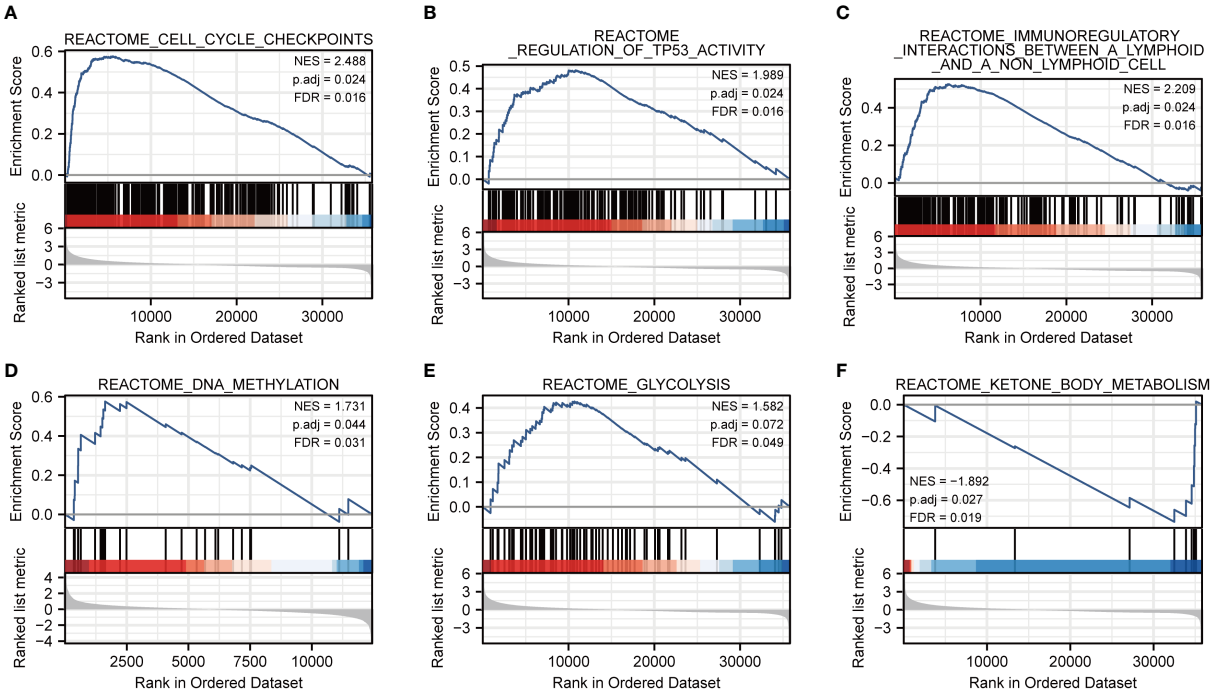

FIGURE 4
Co-expression network analysis and enrichment analysis of FOXM1 in LIHC. **(A)** Cell cycle checkpoints. **(B)** Regulation of TP53 activity. **(C)** Immunoregulatory interactions between a lymphoid and a non-lymphoid cell. **(D)** DNA methylation. **(E)** Glycolysis. **(F)** Ketone body metabolism.

ROC analysis to clarify the specificity and sensitivity of the key immune cells. The areas under the curve (AUCs) of 1, 3, and 5-year OS were 0.645, 667, and 0.589, indicating that the prediction model was credible (Figure 7B). We further investigated the prognostic ability of immune cells associated with FOXM1. We performed Kaplan-Meier analysis on FOXM1 associated immune cells and found that the low infiltration of Tfh cells was significantly associated with the poor prognosis of HCC patients (Figure 7C). Tfh cell infiltration in the high-expression group was considerably higher than in the FOXM1 low-expression group (Figure 7D). Furthermore, the Tfh cells infiltration significantly correlates with the FOXM1 expression (Figure 7E). Taken together, the abnormal infiltration of Tfh cells associated with FOXM1 is a critical factor in predicting the prognosis of HCC patients.

3.7 Correlations of FOXM1 expression with m6a-related genes

Modifying m6a is a reversible chemical modification on mRNA, which regulates gene expression, controls many cellular and biological processes, and is implicated in human carcinogenesis (21). We first analyzed the TCGA LIHC cohort and GSE62232 data sets to evaluate the correlations between the expression of FOXM1 and m6a-related genes in LIHC (Figure 8A). The result shows that FOXM1 expression was significantly positively correlated with most m6a-related genes, including HNRNPA2B1, HNRNPC, IGF2BP1, IGF2BP2, IGF2BP3, METTL3, RBM15B, WTAP, YTHDF1 and YTHDF3 ($p < 0.001$). To determine whether m6a modifications differ from changes in FOXM1 expression, we assessed the relationships between the FOXM1 high and low groups. The result showed that compared with the low expression group, all the m6a-related genes' expression increased in the high expression group except ZC3H13 (Figure 8B). By differential analysis, we obtained the m6a-related genes IGF2BP1, IGF2BP2, and IGF2BP3 that are upregulated in HCC (Figure 8C). After that, among the identified DEGs above, three genes were positively correlated with FOXM1, shared by the TCGA and GEO datasets (Figure 8D). To corroborate the function of FOXM1 in regulating m6a, the following CHIP-seq analysis was performed in Huh-7. In the analysis of overlapping m6a-related genes, we found that FOXM1 was enriched in the promoter region of IGF2BP1, IGF2BP3, and IGF2BP3 genes (Figure 8E). Based on the motif sequence of FOXM1 (Figure 8F) predicted by the FootprintDB database (22) (https://footprintdb.eead.csic.es/index.php), five FOXM1 binding sites (BS1, -1752 to - 1758; BS2, - 879 to -885; BS3, - 737 to – 743; BS4, -277 to - 283 and BS5, - 13 to - 19) were analyzed to exist in the IGF2BP3 promoter (Figure 8G). Besides, there was a high correlation between FOXM1 and IGF2BP1, IGF2BP3, and IGF2BP3 (Figure 8H). Kaplan-Meier survival curve demonstrates the prognostic value of IGF2BP3 (Figure 8I). These results laterally reflect the biological activity of FOXM1 in regulating the transcriptional level of m6a-related genes.

3.8 Correlations of FOXM1 expression with glycolytic/KBM-related genes

Based on pathway enrichment analysis, FOXM1 is involved in a range of metabolic pathways in LIHC. The current study analyzed the

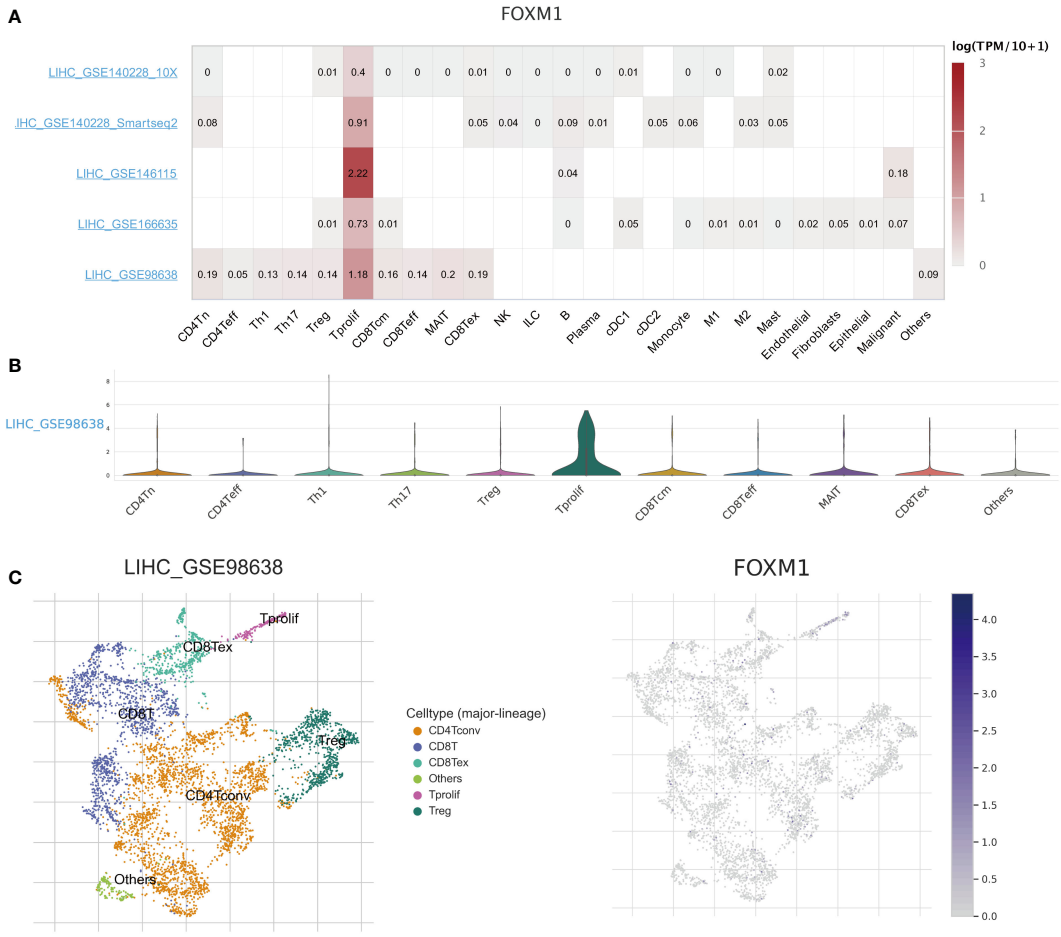

FIGURE 5
The scRNA-seq analysis of the expression of FOXM1 in different immune cells of HCC. **(A)** Heatmap of the correlation of FOXM1 with immune cell infiltration levels in the independent scRNA-seq database. **(B)** Violin plot of FOXM1 and immune cell infiltration. **(C)** Single-cell atlas of all cells in GSE98638 dataset and the expression and distribution of FOXM1.

correlation of glycolytic and ketone body metabolism (KBM) related genes with FOXM1 expression. Glycolysis and ketone bodies metabolic related genes were manually retrieved from the Molecular Signatures Database v 7.1 (MSigDB) (23). By analyzing the TCGA LIHC cohort and GSE62232 data sets, the correlations between the expression of FOXM1 and glycolytic-related genes were significantly positively correlated, including ALDOA, ENO1, HK2, PGAM1, PKM, TPI1, and as for KBM-related genes (Figure 9A). The KBM related genes was ACAT1, ACSS3, BDH1, BDH2, HMGCL, HMGCLL1, HMGCS2 significant negative correlated with FOXM1 (Figure 9A). Moreover, we further analyzed the differential expression of glycolytic/KBM-related genes between the high and low expression of FOXM1 (Figure 9B). The result showed that compared with the low expression group, the expression of glycolysis-related genes, including ALDOA, ENO1, ENO2, HK2, PFKP, PGAM1, PGAM2, PGK1, PKM, TPI1, and KBM-related genes were increased in the high-expression group. In contrast, there was a decrease in the high-expression group of KBM related genes, including ACAT1 ACSS3 BDH1 HMGCL, HMGCLL1, and HMGCS2. Volcano plots revealed that glycolytic-related genes were upregulated, and more KBM-related genes were downregulated in HCC (Figure 9C). We next matched the DEGs to the positive correlation genes in the correlation result of Figure 9A. In summary, seven genes were overlapping (Figure 9D). Subsequent CHIP-seq analysis revealed significant peaks of FOXM1 in the HK2, and PKM gene promoter regions, suggesting that FOXM1 is involved in the transcription of these genes in Huh-7 cells (Figure 9E). Moreover, the motifs of three FOXM1 binding sites were detected in the promoters of HK2 and PKM genes, respectively (Figure 9F). The scatter plot shows the correlation between glycolytic/KBM-related genes (Figure 9G). Together with Kaplan-Meier curve analysis, HK2 and PKM were significantly relevant with poor prognosis of HCC (Figure 9H). These 21 genes were involved in transforming this substance on the metabolic pathways, among which HK2 and PKM participated in the reaction process of glucose to Glucose-6-phosphate (G-6-P) and phosphoenolpyruvate (PEP) to pyruvate as metabolic enzymes, respectively (Figure 9I).

3.9 Construction of FOXM1-related ceRNA network

The hypothesis of ceRNA that is involved in tumorigenesis has been validated by various experiments (24). In this study, we carried

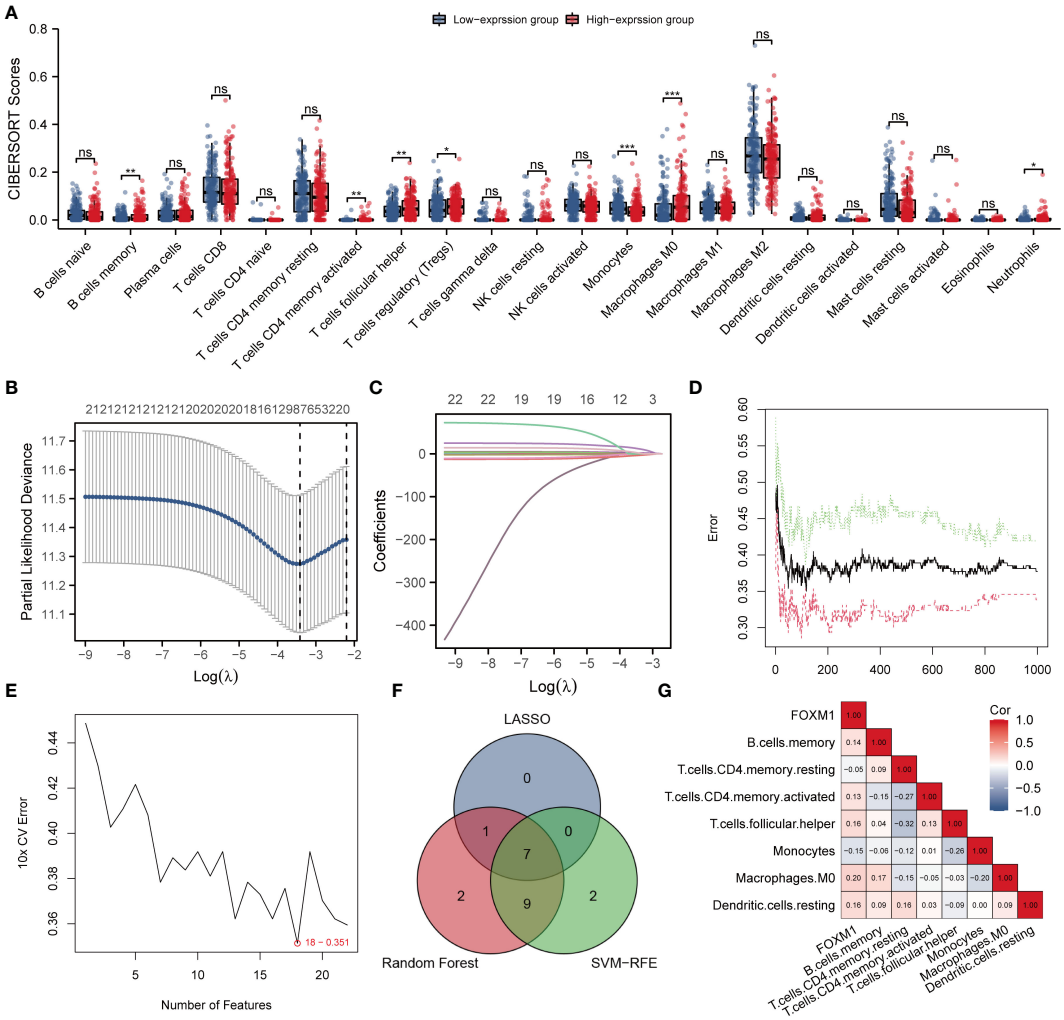

FIGURE 6
Identification of the key infiltrated immune cells by machine learning. **(A)** Differences in immune infiltration between FOXM1 high and low expression groups. **(B)** Penalty plot of 22 immune cells in the LASSO model, error bars represent standard error. **(C)** Distribution of LASSO coefficients for 22 immune cells. **(D)** The error variation of the RF algorithm, red and green represent the error rate of high and low FOXM1 expression groups, and black represents the overflow error rate. **(E)** Identification of 22 immune cells through the SVM-RFE algorithm. **(F)** 7 immune cell types were identified by LASSO and RF algorithms. **(G)** Correlation graph between the infiltration level of 7 immune cells and the expression level of the FOXM1 gene. (*p < 0.05, **p < 0.01, ***p < 0.001, ns not significant).

out an analysis of the FOXM1-related ceRNA network in LIHC. Based on the multiMIR R package, 65 experimentally validated miRNA interacting with FOXM1 had been retrieved. Since miRNA expression and ceRNA (mRNA, lncRNA, etc.) expression take on a negative trend according to the ceRNA hypothesis, there were 5 targeting miRNA that had been screened in the matched miRNA (Figure 10A). The significantly expressed miRNA had been identified through the transcript-level differential analysis expression profiles of the selected miRNA integrated from the TCGA project in paracancerous and hepatic tumor tissue (Figure 10B). Kaplan-Meier analysis revealed that only hsa-miR-125b-5p low-expressed played a significant role in LIHC patients' poor prognosis (Figure 10C). Further, the lncRNA interaction with miRNA was predicted, and the Venn diagram demonstrates the interacting lncRNA by retrieving the differentially expressed miRNA from the ENCORI and miRNet database (Figure 10D). Followed difference analysis of the lncRNA that significantly negatively correlated with miRNA in the database intersection was also done (Figure 10E). We consistently utilized Kaplan-Meier analysis on the screened lncRNA in the ceRNA network, finding that CYTOR, DANCR, and MIR4435-2HG were related to prognosis (Figure 10F). Besides, the subcellular localization of ceRNA components can be a possible influential factor in ceRNA activity and contributes to human diseases, including cancer (24). Since the ceRNA network mainly exists in the cytoplasm, we further analyzed the lncRNA cellular distribution by performing the lncLocator platform (Figure 10G). Predicting that MIR4435-2HG and DANCR were mainly distributed in the cytoplasm, but CYTOR was located primarily on cytosol. These data indicated that the FOXM1-related lncRNA-miRNA-mRNA triple regulatory

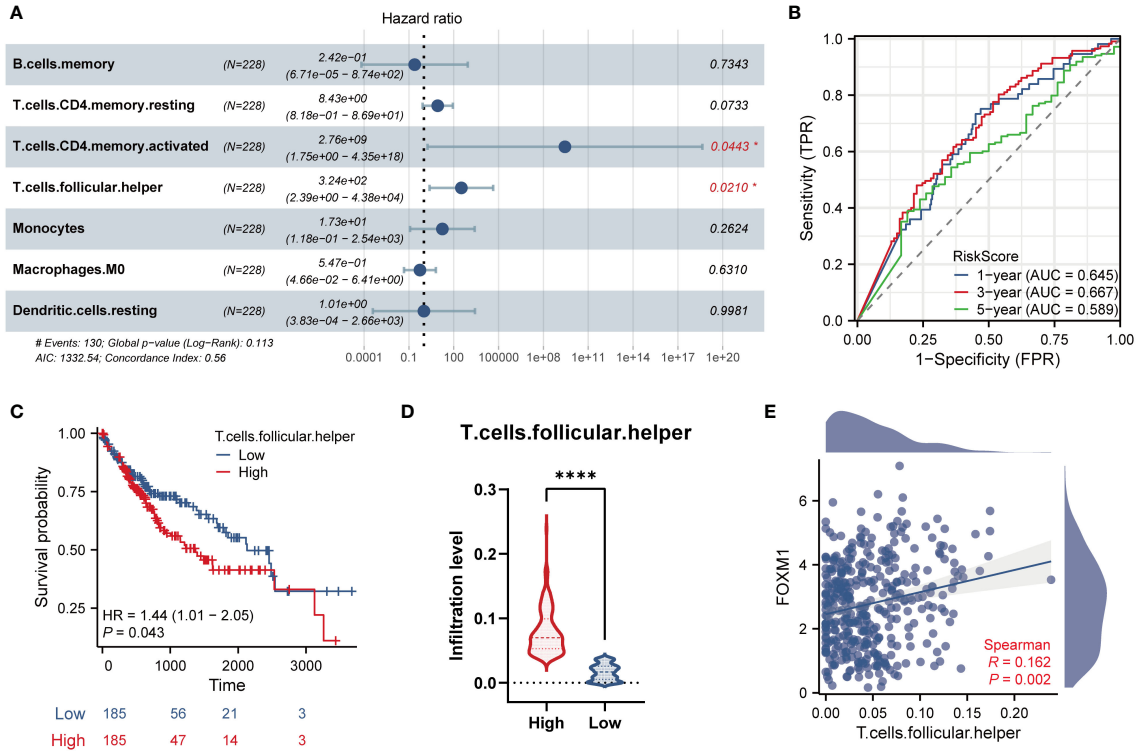

FIGURE 7
Validation and survival analysis of the key infiltrated immune cells. **(A)** Multivariate Cox Forest plots related to the prognosis of 7 key immune cells. **(B)** The AUC values of the time ROC curves. **(C)** The Kaplan-Meier curve of Tfh cells infiltration level and overall survival. **(D)** The violin plot of Tfh cells infiltration in FOXM1 high and low expression groups. **(E)** The scatter plot of the correlation between the infiltration level of Tfh cells and the FOXM1 expression. (*p < 0.05, ****p < 0.0001).

networks constructed from the RNAs, which MIR4435-2HG and DANCR act as ceRNAs to improve the expression of FOXM1 through sponging hsa-miR-125b-5p (Figure 10H).

4 Discussion

The FOX gene family is an evolutionarily conserved gene family that encodes approximately 50 transcription factors in the human genome (25). These critical transcription factors broadly regulate gene transcription and involve various biological processes (26). FOXM1 is the only member of the FOXM subfamily known for its functionality in promoting the G1-S and the G2-M cell cycle transition (27). It is mainly detected along with the growth of cells (5). Additionally, FOXM1 is crucial in tumor development and is associated with poor prognosis (28). Current studies have identified FOXM1 as a tumor-specific biomarker with powerful predictive prognostic capacity in HCC (29, 30). In this study, FOXM1 is highly expressed in HCC, related to advanced TNM staging and poor prognosis, consistent with the study (31). We analyzed the relationship between the FOXM1 expression and the prognosis, survival rate, tumor stage, and lymph node metastasis of HCC patients through TCGA data. HCC patients with high FOXM1 expression have a low survival rate significantly related to lymph node metastases and HCC clinical stage.

FOXM1 was first identified as a protein that regulates cell cycle and proliferation (32). While with the developed understanding of cancer mechanisms, novel hallmarks have been further expanded (33). In the analysis of FOXM1 co-expression in RNA-seq data from HCC patients, KIF18B had a positive correlation with FOXM1. As reported, KIF18B is a molecular motor protein that destabilizes astral microtubules during mitosis (34), which promotes tumor development in various cancers and is associated with poor prognosis (35). Moreover, KIF18B and FOXM1 similarly mediate DNA double-strand break repair (34) and participate in the cell cycle and DNA replication (36). KIF18B is also closely associated with infiltrating immune cells (37). These results imply that FOXM1 may have similar biological functions to KIF18B. Research reports ACYP2, which we found is negatively associated with FOXM1, whose polymorphisms are related to changes in plasma telomerase levels (21). The SNPs of ACYP2 can serve as risk and protective factors in HCC, respectively (38). However, the discussion on the relationship between the ACYP2 gene and cancer is still relatively scarce. In turn, enrichment analysis was performed of the gene set. The positively correlated group had several significantly enriched categories, including cell cycle and cell division. In contrast, the negatively correlated group enriched genes related to the catabolic process and metabolism. Besides, the GSEA of FOXM1 indicated that the pathways of cell cycle checkpoints, regulation of TP53 activity, immunoregulatory

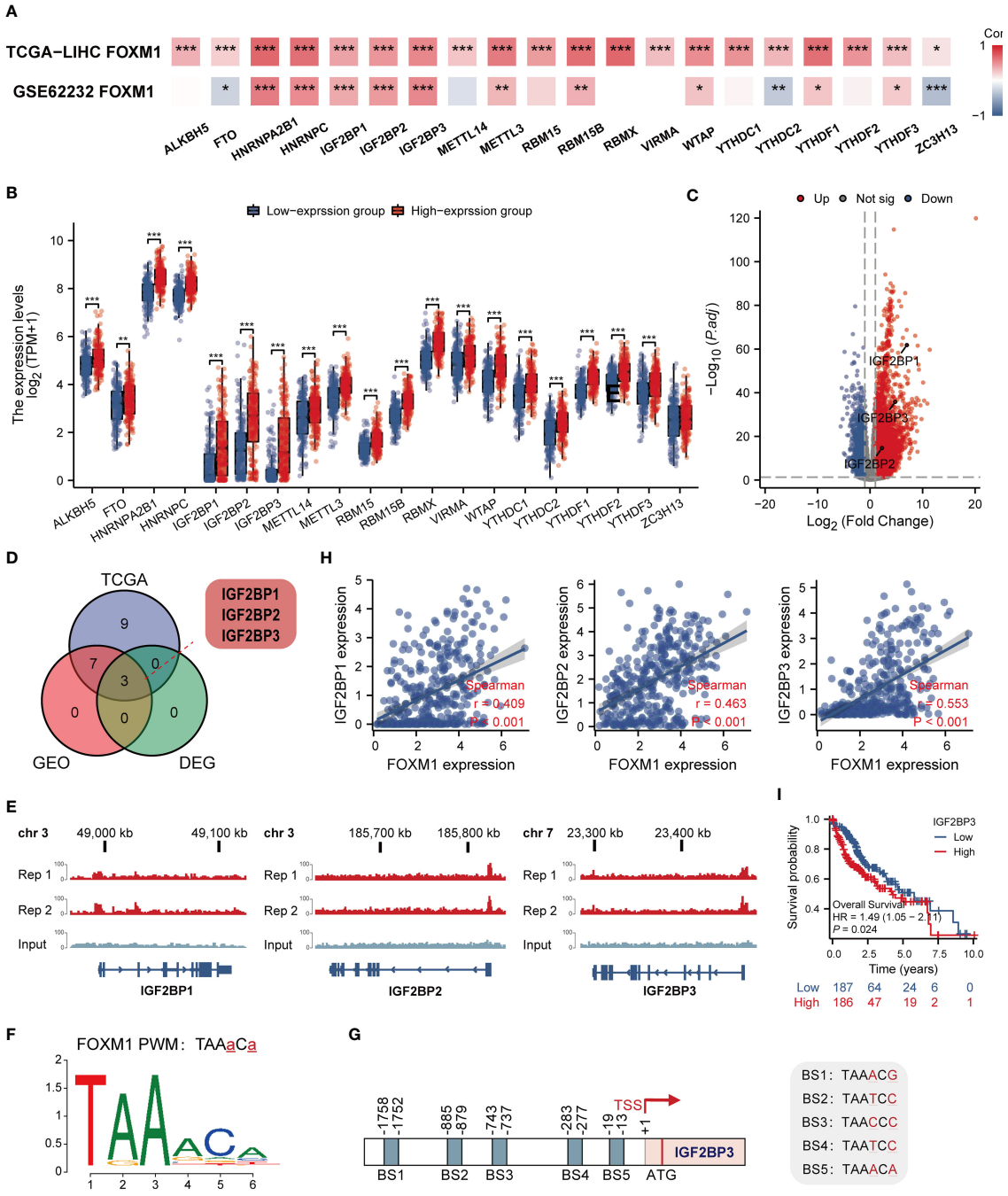

FIGURE 8
FOXM1 is highly correlated with m6a-related genes and has the ability to potentially transcribe IGF2BP1, IGF2BP2 and IGF2BP3. **(A)** Heat map of the correlation between FOXM1 and m6a-related genes expression. **(B)** Differences in m6a-related gene between FOXM1 high and low expression groups. **(C)** Volcano plots of mRNA that were differentially expressed between HCC and normal tissues. **(D)**Venn diagram of m6A-related genes positively associated with FOXM1 and DEGs in HCC. **(E)** Genome browser screenshots of the FOXM1 binding sites. The test group has two replicates, and the peaks shown are statistically significant. **(F)** Map of FOXM1 binding site sequence. **(G)** Schematic illustration of the potential FOXM1 binding sites (BS) in the IGF2BP3 promoter. **(H)** The scatter plot shows the correlation between the overlapping genes and FOXM1. **(I)** Kaplan-Meier overall survival curves of IGF2BP3. (*p < 0.05, **p < 0.01, ***p < 0.001).

interactions between a lymphoid and a non-lymphoid cell, DNA methylation, glycolysis were up-regulated, and downregulation of ketone body metabolism. These results suggest that FOXM1 may exert metabolic and immune biological functions in the process of cancer. In this article, we focus on the relationship of FOXM1 in immune infiltration, m6a modification, and glycolysis/KBM, as previous studies have associated these pathways with HCC progression and metastasis.

The immune cells in the tumor microenvironment have a complex biological relationship with tumor cells and may lead to tumor development or suppression, resulting in differential immunotherapeutic responses (39). In scRNA-seq analysis, we

10.3389/fimmu.2023.1138524

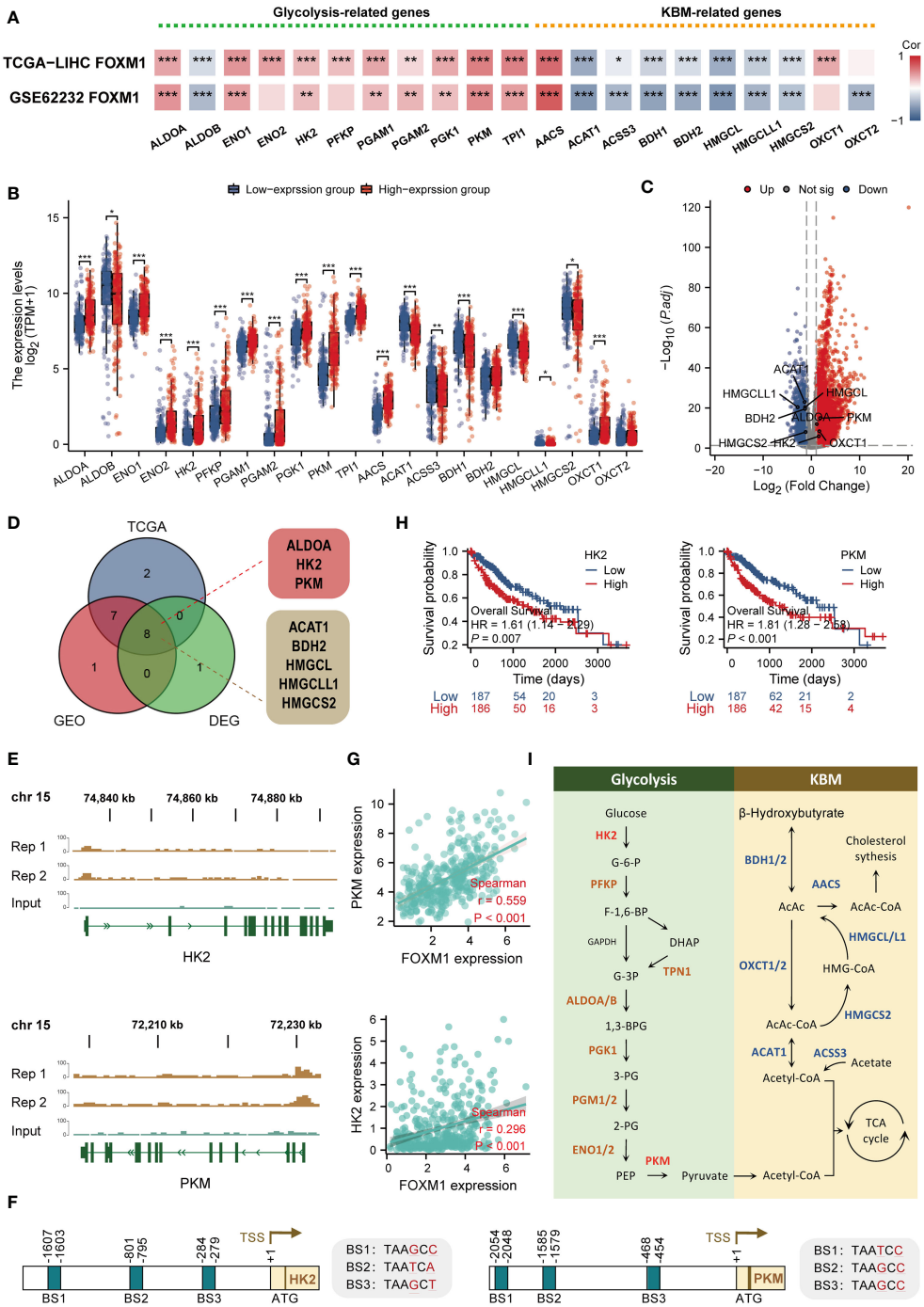

FIGURE 9
FOXM1 is highly correlated with glycolysis/KBM-related genes and has the ability to potentially transcribe HK2 and PKM. **(A)** Heat map of the correlation between FOXM1 and glycolysis/KBM-related gene expression. **(B)** Differences in glycolysis/KBM-related genes between FOXM1 high and low expression groups. **(C)** Volcano plots of mRNA that were differentially expressed between HCC and normal tissues. **(D)**Venn diagram of glycolysis/KBM-related genes positively associated with FOXM1 and DEGs in HCC. **(E)** Genome browser screenshots of the FOXM1 binding sites. The test group has two replicates, and the peaks shown are statistically significant. **(F)** Schematic model illustrating the glycolysis and KBM pathway. **(G)** The scatter plot shows the correlation between the overlapping genes and FOXM1. **(H)** Kaplan-Meier overall survival curves of HK2 and PKM. **(I)** Diagram showing the position of the recognized promoter sites in FOXM1. The selected signature genes are marked in the pathway, with glycolytic enzymes in brown, ketone bodies metabolic genes in blue, and the FOXM1-bindin genes highlighted in red. (*p < 0.05, **p < 0.01, ***p < 0.001).

evaluated the association between infiltrating immune cells and FOXM1 in HCC tissues and found that FOXM1 was mainly distributed in T prolif cells. The relationship between FOXM1 and the promotion of B cell proliferation (40) and induction of M2 macrophage polarization (41) in non-cancerous conditions has been reported. FOXM1 has also been found to recruit macrophage migration in FOXM1 in lung cancer (42). If only the biological functions of FOXM1 in the cell cycle and cell proliferation are

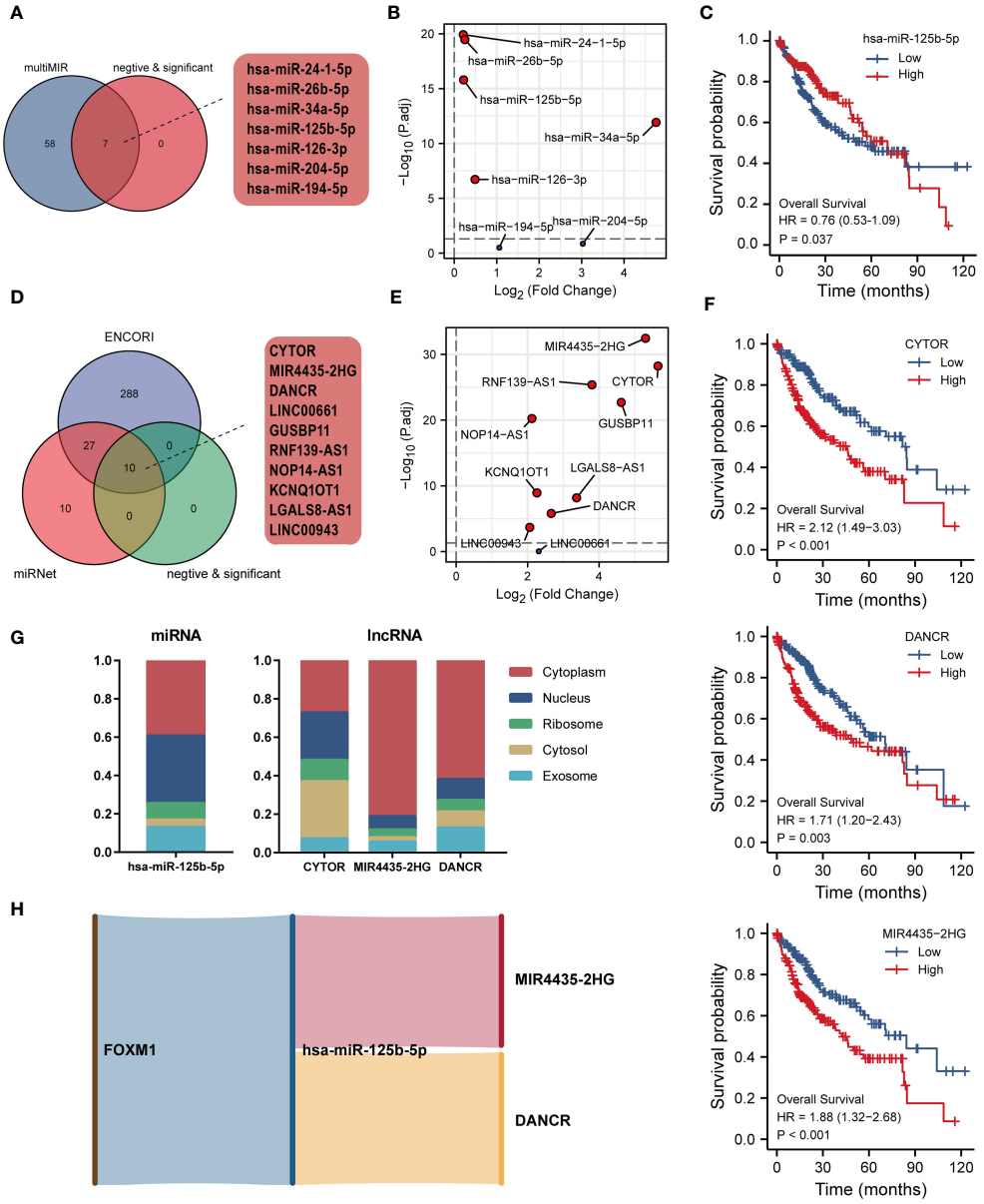

FIGURE 10
Construction of ceRNA network of FOXM1 in LIHC. **(A)** Venn diagram of miRNA interacting with FOXM1. **(B)** Differential expression of interacted miRNA in TCGA LIHC cohort. **(C)** Kaplan-Meier curve of hsa-miR-125b-5p. **(D)** Venn diagram of lncRNA interacting with hsa-miR-125b-5p. **(E)** Differential expression of interacted lncRNA in TCGA LIHC cohort. **(F)** Kaplan-Meier curve of CYTOR, DANCR, MIR4435-2HG. **(G)** The subcellular localization of screened miRNA and lncRNA. **(H)** Sankey diagram of the ceRNA (mRNA-miRNA-lncRNA) network.

considered, it is not surprising that FOXM1 is predominantly expressed in T-proliferating cells. However, FOXM1 does not solely promote immune cell infiltration in tumors; it also can suppress the maturation of BMDCs *via* direct activation of Wnt5a and weakened promotion of T-cell proliferation (43). Therefore, it still suggests the relevance of FOXM1 to immune infiltration and the bias of FOXM1 expression in different types of infiltrating immune cells. Besides, based on the CIBERSORT algorithm, FOXM1 expression was positively correlated with T cell CD4 memory activated, Tfh cells, and Tregs in T cell subsets infiltration. Given the complex relationships between immune cells in the tumor microenvironment, we predicted the immune cells with prognostic value. Further machine learning (LASSO, RF, and SVM-RFE algorithms) analysis found that seven immune infiltrating cells were significantly associated with patients with hepatocellular carcinoma in the FOXM1 expression subgroup. Cox regression and Kaplan-Meier analysis showed that high invasion of Tfh cells was associated with poor prognosis in HCC patients.

Tfh cells are a specific subpopulation of $CD4^+$ T cells that help B lymphocytes produce an adequate antibody response to various pathogens (44). Nonetheless, Increasing evidence for the increase of Tfh cells was associated with poor prognosis (45, 46), and the rate of Tfh cell infiltration is higher in late-stage patients than in early-stage patients. Tfh cells also have known roles in the origin of T cell

malignancies and assist malignant B cells (47). Besides, Tfh cells exacerbate immune-related adverse events, such as immune checkpoint blockade (ICB) and autoimmunity during cancer immunotherapy (48). Research on FOXM1 and immune regulation has been reported. FOXM1 selectively upregulates PD-L1 expression by directly binding to the PD-L1 promoter in the nucleus (49). High glucose microenvironment can activate CD27 transcription and expression in $CD8^+$ T cells *via* the mTOR-FOXM1 pathway, thereby significantly enhancing the immunocidal effect of $CD8^+$ T cells (50). This study also found a correlation between FOXM1 and immune cell infiltration. Moreover, the abnormal infiltration of the Tfh cells associated with FOXM1 may be a key predictor of HCC based on various machine-learning algorithms.

Regarding m6a modification, the most abundant mRNA modification plays different roles in various biological processes by affecting gene expression post-transcriptionally in eukaryotes (51). The m6a modification is a highly dynamic and reversible process involving enzymes responsible for the installation of modifications called "Writers," the removal of methylation called "Erasers," and the recognition of modifications called "Readers" (52). However, m6a is often dysregulated in various types of cancer, leading to tumorigenesis, progression, and metastasis (53). Therefore, understanding the correlation between m6a modification of FOXM1 is rewarding to understanding the regulation mechanism of FOXM1 in LIHC. This study found that most m6a-related genes were positively correlated with FOXM1 expression, and IGF2BP family proteins (IGF2BP1/2/3) were differentially upregulated in HCC. Considering the transcriptional function of FOXM1 as a transcription factor regulating gene transcription, we explored the interaction of FOXM1 with the DNA promoter regions of these three genes in CHIP-seq data of FOXM1 in the Huh-7 cell line. Kaplan-Meier curves identified IGF2BP3 as having a prognostic value in hepatocellular carcinoma. Further analysis revealed five potential FOXM1 binding sequences in its promoter region, which has not been reported.

IGF2BP family proteins are highly expressed during embryonic development and are essential in embryogenesis, while IGF2BP1 and IGF2BP3 are not expressed in normal adult tissues (54). However, in cancer tissues, IGF2BP1 and IGF2BP3 both tested positive. Compared with IGF2BP3, IGF2BP1 has a more complex role in cancer, possessing both pro- and anti-cancer effects, and therefore, IGF2BP3 correlates better with cancer progression (55)., suggesting the importance of further studies on FOXM1 regulation of IGF2BP3. IGF2BP3 can interact with mRNA (53), non-coding RNA (57), and protein (58), respectively. Current studies on FOXM1 and methylation revolve around FOXM1 being methylated, including ALKBH5 demethylation of FOXM1 nascent transcripts (59) and YTHDF1 recognition and binding to m6A-modified FOXM1 mRNA (60), but rarely research has been done on FOXM1 regulating m6a modification. Overall, we predict FOXM1 may affect the messaging of m6a modification by regulating IGF2BP3 transcription.

Metabolic reprogramming is a well-established hallmark of cancer (19). Numerous studies have shown that enhanced glycolysis predicts poor prognosis and promotes tumor progression, immune evasion, and drug resistance in different cancer types (61). The switch from oxidative phosphorylation (OXPHOS) to glycolysis, which is called the "Warburg effect," is one of the phenomena of cancer (62). Nowadays, targeting the biochemical targets of glycolysis and their potent antagonists or inhibitors with promising anti-cancer effects has become potential therapeutic drug strategies (63). Ketone bodies function as an alternative energy source without glucose, in which fatty acids are mobilized and converted by the liver into ketone bodies to power the body (64). Considering the OXPHOS dysfunction in tumor cells, ketogenic diets (KD) target altered glucose metabolism in cancer cells, further disrupting energy metabolism and adversely affecting tumor cell proliferation (65). In this study, we evaluated the association of FOXM1 with genes related to glycolysis and KBM. FOXM1 expression was positively correlated with most glycolysis-related genes and conversely negatively correlated with KBM-relate genes. By correlation and differential expression analysis, we screened three glycolysis-related genes and five KBM-related genes, indicating that FOXM1 is associated with glycolysis and the KBM process. Among them, we newly analyzed three sequences predicted to bind to FOXM1 in the promoter regions of HK2 and PKM genes, implying that FOXM1 affects the glycolytic biological process in cells by regulating the transcription of HK2 and PKM.

Available studies have shown that there are three critical rate-limiting enzymes in the glycolytic process, namely hexokinase (HK), phosphofructokinase (PFK), and pyruvate kinase (PK), which are essential control nodes of the glycolytic process, and important targets for cancer therapy (66). HK is the first rate-limiting enzyme in glycolysis. The current study found that HK2 is highly expressed in tumors, and its expression level is closely related to the malignancy of the tumor (67). In addition to the glycolytic function of HK2, more and more novel non-classical effects are being discovered. Nuclear-localized HK2 regulates stem/progenitor cell function and differentiation independently of its kinase and metabolic functions (68). Besides, when glycolysis in cellular metabolism is exuberant, HK2 can phosphorylate IκBa in tumor cells, leading to IκBa degradation and NF-κB activation-dependent increase in PD-L1 expression to evade tumor immunity (69). PKM is another rate-limiting enzyme in glycolysis. In mammals, four tissue-specific pyruvate kinases exist, including PKL, PKR, PKM1, and PKM2 (70). The PKM gene forms PKM1 and PKM2 through variable splicing. Unlike constitutively active PKM1, PKM2 is activated only when cellular levels of the allosteric activator increase. Most cancer cells predominantly express PKM2 over PKM1, and PKM2 is mainly found in highly proliferative cells with high anabolic requirements, especially in tumors and embryonic tissues (71). Additionally, the increased expression of PKM2 in tumors was significantly correlated with the prognosis of tumors (72). The involvement of FOXM1 in the glycolytic process has been reported (73, 74). Still, it has not been shown that FOXM1 affects the glycolytic process at the transcriptional level by regulating the expression of HK2 and PKM. This study predicted that FOXM1 binds to the HK2 and PKM promoter regions, providing direction for subsequent studies.

The ceRNA network is a post-transcriptional regulation mediated by miRNA that links the functions of coding and noncoding RNAs. Through the competitive binding of lncRNA or circular RNA to miRNA, the ceRNA network regulates the mRNA expression, potentially affecting the biological process and causing various

diseases (75). A previous study has found that FOXM1 plays a core gene in the ceRNA network of HCC (76). In this study, we first searched for miRNAs with experimentally demonstrated FOXM1 interactions and screened them for differential and survival analysis to obtain has-miR-125b-5p. lncRNAs with differential expression and significant prognostic correlation were predicted by pairing has-miR-125b-5p to obtain CYTOR, MIR4435-2HG, and DANCR. Finally, considering that the specific functions of lncRNAs are closely related to their intracellular location and that ceRNA acts mainly in the cytoplasm (17), identified MIR4435-2HG and DANCR as potential target lncRNAs by subcellular localization analysis in the ceRNA network. Has-miR-125b-5p is reported to be downregulated with poor prognosis in HCC patients, and overexpression of has-miR-125b-5p inhibited the proliferation, migration, and invasion of HCC by targeting TXNRD1 (77). MIR4435-2HG was upregulated in HCC, facilitating the progression of liver cancer (78) and promoting cancer cell proliferation (79). Furthermore, DANCR facilitated HCC cell progression by sponging miR-125b-5p through MAPK pathway activation (80). The above studies further suggested the verification of our analysis. In summary, the ceRNA network based on interactions between FOXM1 to hsa-miR-125b-5p to MIR4435-2HG/DANCR was constructed to reveal the gene interaction profile in LIHC.

Data availability statement

The original contributions presented in the study are included in the article/supplementary material. Further inquiries can be directed to the corresponding authors.

Ethics statement

The studies involving human participants were reviewed and approved by the Ethics Committee of Changsha Hospital of Traditional Chinese Medicine (Changsha Eighth Hospital). Written informed consent to participate in this study was provided by the participants' legal guardian/next of kin.

Author contributions

Conceptualization, ZX and HC. Data curation, ZX, CP and KS. Formal analysis, ZX, CP and JY. Funding acquisition, XP and LM. Investigation, YL and YH. Methodology, ZX, CP, HC and BL. Project administration, XP and LM. Resources, ZX, XL and WL. Software, ZX and CP. Supervision, XP and LM. Writing-original draft, ZX and CP. Writing-review & editing, ZX and LM. All authors contributed to the article and approved the submitted version.

Funding

This research was funded by University level scientific research fund of Hunan University of Traditional Chinese Medicine (2021XJJJ017), Changsha Natural Science Foundation (No. kq2014085), Hunan Provincial Administration of Traditional Chinese Medicine (No.2021065), Hunan Provincial Department of Education Research Project (No.20C1408), The Key Discipline of Biological Engineering in the Fourteenth Five-year Plan of Hunan University of Chinese Medicine. [XiaoXingFaGuiZi-2023-No.2] and Pharmaceutical Open Fund of Domestic First-class Disciplines(cultivation) of Hunan Province.

Conflict of interest

The authors declare that the research was conducted in the absence of any commercial or financial relationships that could be construed as a potential conflict of interest.

Publisher's note

References

1. Sung H, Ferlay J, Siegel RL, Laversanne M, Soerjomataram I, Jemal A, et al. Global cancer statistics 2020: GLOBOCAN estimates of incidence and mortality worldwide for 36 cancers in 185 countries. *CA A Cancer J Clin* (2021) 71:209–49. doi: 10.3322/caac.21660

2. Chaudhary K, Poirion OB, Lu L, Huang S, Ching T, Garmire LX. Multimodal meta-analysis of 1,494 hepatocellular carcinoma samples reveals significant impact of consensus driver genes on phenotypes. *Clin Cancer Res* (2019) 25:463–72. doi: 10.1158/1078-0432.CCR-18-0088

3. Zhang H, Zhang W, Jiang L, Chen Y. Recent advances in systemic therapy for hepatocellular carcinoma. *biomark Res* (2022) 10:3. doi: 10.1186/s40364-021-00350-4

4. Nandi D, Cheema PS, Jaiswal N, Nag A. FoxM1: repurposing an oncogene as a biomarker. *Semin Cancer Biol* (2018) 52:74–84. doi: 10.1016/j.semcancer.2017.08.009

5. Halasi M, Gartel AL. FOX(M1) news–it is cancer. *Mol Cancer Ther* (2013) 12:245–54. doi: 10.1158/1535-7163.MCT-12-0712

6. Gartel AL. FOXM1 in cancer: interactions and vulnerabilities. *Cancer Res* (2017) 77:3135–9. doi: 10.1158/0008-5472.CAN-16-3566

7. Darnell JE. Transcription factors as targets for cancer therapy. *Nat Rev Cancer* (2002) 2:740–9. doi: 10.1038/nrc906

8. Borhani S, Gartel AL. FOXM1: a potential therapeutic target in human solid cancers. *Expert Opin Ther Targets* (2020) 24:205–17. doi: 10.1080/14728222.2020.1727888

9. Love MI, Huber W, Anders S. Moderated estimation of fold change and dispersion for RNA-seq data with DESeq2. *Genome Biol* (2014) 15:550. doi: 10.1186/s13059-014-0550-8

10. Vasaikar SV, Straub P, Wang J, Zhang B. LinkedOmics: analyzing multi-omics data within and across 32 cancer types. *Nucleic Acids Res* (2018) 46:D956–63. doi: 10.1093/nar/gkx1090

11. Yu G, Wang L-G, Han Y, He Q-Y. clusterProfiler: an r package for comparing biological themes among gene clusters. *OMICS: A J Integr Biol* (2012) 16:284–87. doi: 10.1089/omi.2011.0118

12. Subramanian A, Tamayo P, Mootha VK, Mukherjee S, Ebert BL, Gillette MA, et al. Gene set enrichment analysis: a knowledge-based approach for interpreting genome-wide expression profiles. *Proc Natl Acad Sci USA* (2005) 102:15545–50. doi: 10.1073/pnas.0506580102

13. Han Y, Wang Y, Dong X, Sun D, Liu Z, Yue J, et al. TISCH2: expanded datasets and new tools for single-cell transcriptome analyses of the tumor microenvironment. *Nucleic Acids Res* (2023) 51:D1425–31. doi: 10.1093/nar/gkac959

14. Chen B, Khodadoust MS, Liu CL, Newman AM, Alizadeh AA. Profiling tumor infiltrating immune cells with CIBERSORT. *Methods Mol Biol* (2018) 1711:243–59. doi: 10.1007/978-1-4939-7493-1_12

15. Li J-H, Liu S, Zhou H, Qu L-H, Yang J-H. starBase v2.0: decoding miRNA-ceRNA, miRNA-ncRNA and protein–RNA interaction networks from large-scale CLIP-seq data. *Nucl Acids Res* (2014) 42:D92–7. doi: 10.1093/nar/gkt1248

16. Chang L, Zhou G, Soufan O, Xia J. miRNet 2.0: network-based visual analytics for miRNA functional analysis and systems biology. *Nucleic Acids Res* (2020) 48:W244–51. doi: 10.1093/nar/gkaa467

17. Cao Z, Pan X, Yang Y, Huang Y, Shen H-B. The lncLocator: a subcellular localization predictor for long non-coding RNAs based on a stacked ensemble classifier. *Bioinformatics* (2018) 34:2185–94. doi: 10.1093/bioinformatics/bty085

18. Kong F, Kong D, Yang X, Yuan D, Zhang N, Hua X, et al. Integrative analysis of highly mutated genes in hepatitis b virus-related hepatic carcinoma. *Cancer Med* (2020) 9:2462–79. doi: 10.1002/cam4.2903

19. Hanahan D. Hallmarks of cancer: new dimensions. *Cancer Discovery* (2022) 12:31–46. doi: 10.1158/2159-8290.CD-21-1059

20. Li Y, McGrail DJ, Xu J, Mills GB, Sahni N, Yi S, et al. Gene regulatory network perturbation by genetic and epigenetic variation. *Trends in Biochemical Sciences* (2018) 43:576–92. doi: 10.1016/j.tibs.2018.05.002

21. Chen M, Wong C-M. The emerging roles of N6-methyladenosine (m6A) deregulation in liver carcinogenesis. *Mol Cancer* (2020) 19:44. doi: 10.1186/s12943-020-01172-y

22. Contreras-Moreira B, Sebastian A. FootprintDB: analysis of plant cis-regulatory elements, transcription factors, and binding interfaces. In: Hehl R, editor. *Plant synthetic promoters. methods in molecular biology*. New York, NY: Springer New York (2016). p. 259–77. doi: 10.1007/978-1-4939-6396-6_17

23. Qian L, Li Y, Cao Y, Meng G, Peng J, Li H, et al. Pan-cancer analysis of glycolytic and ketone bodies metabolic genes: implications for response to ketogenic dietary therapy. *Front Oncol* (2021) 11:689068. doi: 10.3389/fonc.2021.689068

24. Qi X, Zhang D-H, Wu N, Xiao J-H, Wang X, Ma W. ceRNA in cancer: possible functions and clinical implications. *J Med Genet* (2015) 52:710–8. doi: 10.1136/jmedgenet-2015-103334

25. Carlsson P, Mahlapuu M. Forkhead transcription factors: key players in development and metabolism. *Dev Biol* (2002) 250:1–23. doi: 10.1006/dbio.2002.0780

26. Wang J, Li W, Zhao Y, Kang D, Fu W, Zheng X, et al. Members of FOX family could be drug targets of cancers. *Pharmacol Ther* (2018) 181:183–96. doi: 10.1016/j.pharmthera.2017.08.003

27. Wierstra I, Alves J. FOXM1, a typical proliferation-associated transcription factor. *Biol Chem* (2007) 388:1257–74. doi: 10.1515/BC.2007.159

28. Song B-N, Chu I-S. A gene expression signature of FOXM1 predicts the prognosis of hepatocellular carcinoma. *Exp Mol Med* (2018) 50:e418–8. doi: 10.1038/emm.2017.159

29. Wang D, Liu J, Liu S, Li W. Identification of crucial genes associated with immune cell infiltration in hepatocellular carcinoma by weighted gene Co-expression network analysis. *Front Genet* (2020) 11:342. doi: 10.3389/fgene.2020.00342

30. Sun H-C, Li M, Lu J-L, Yan D-W, Zhou C-Z, Fan J-W, et al. Overexpression of forkhead box M1 protein associates with aggressive tumor features and poor prognosis of hepatocellular carcinoma. *Oncol Rep* (2011) 25:1533–9. doi: 10.3892/or.2011.1230

31. Wei G, Yang X, Lu H, Zhang L, Wei Y, Li H, et al. Prognostic value and immunological role of FOXM1 in human solid tumors. *Aging* (2022) 14:9128–48. doi: 10.18632/aging.204394

32. Ye H, Kelly TF, Samadani U, Lim L, Rubio S, Overdier DG, et al. Hepatocyte nuclear factor 3/fork head homolog 11 is expressed in proliferating epithelial and mesenchymal cells of embryonic and adult tissues. *Mol Cell Biol* (1997) 17:1626–41. doi: 10.1128/MCB.17.3.1626

33. Hanahan D, Weinberg RA. Hallmarks of cancer: the next generation. *Cell* (2011) 144:646–74. doi: 10.1016/j.cell.2011.02.013

34. Luessing J, Sakhteh M, Sarai N, Frizzell L, Tsanov N, Ramberg KO, et al. The nuclear kinesin KIF18B promotes 53BP1-mediated DNA double-strand break repair. *Cell Rep* (2021) 35:109306. doi: 10.1016/j.celrep.2021.109306

35. Zhao F, Feng Y, Zhang X, Liu X, Li A. Kinesin superfamily member 18B (KIF18B) promotes cell proliferation in colon adenocarcinoma. *CMAR* (2020) 12:12769–78. doi: 10.2147/CMAR.S261894

36. Zhang L, Zhu G, Wang X, Liao X, Huang R, Huang C, et al. Genome–wide investigation of the clinical significance and prospective molecular mechanisms of kinesin family member genes in patients with lung adenocarcinoma. *Oncol Rep* (2019), 1017–34. doi: 10.3892/or.2019.7236

37. Qiu M, Wang Q, Li Q, Zhu L, Li Y, Yang S, et al. KIF18B is a prognostic biomarker and correlates with immune infiltrates in pan-cancer. *Front Mol Biosci* (2021) 8:559800. doi: 10.3389/fmolb.2021.559800

38. Chen Z, Sun Y, Xu Z, Xu J, Li J, Yan M, et al. *ACYP2* polymorphisms are associated with the risk of liver cancer in a han Chinese population. *Oncotarget* (2017) 8:67723–31. doi: 10.18632/oncotarget.18574

39. Lv B, Wang Y, Ma D, Cheng W, Liu J, Yong T, et al. Immunotherapy: reshape the tumor immune microenvironment. *Front Immunol* (2022) 13:844142. doi: 10.3389/fimmu.2022.844142

40. Lefebvre C, Rajbhandari P, Alvarez MJ, Bandaru P, Lim WK, Sato M, et al. A human b-cell interactome identifies MYB and FOXM1 as master regulators of proliferation in germinal centers. *Mol Syst Biol* (2010) 6:377. doi: 10.1038/msb.2010.31

41. Yang Y, Zhang B, Yang Y, Peng B, Ye R. FOXM1 accelerates wound healing in diabetic foot ulcer by inducing M2 macrophage polarization through a mechanism involving SEMA3C/NRP2/Hedgehog signaling. *Diabetes Res Clin Pract* (2022) 184:109121. doi: 10.1016/j.diabres.2021.109121

42. Balli D, Ren X, Chou F-S, Cross E, Zhang Y, Kalinichenko VV, et al. Foxm1 transcription factor is required for macrophage migration during lung inflammation and tumor formation. *Oncogene* (2012) 31:3875–888. doi: 10.1038/onc.2011.549

43. Zhou Z, Chen H, Xie R, Wang H, Li S, Xu Q, et al. Epigenetically modulated FOXM1 suppresses dendritic cell maturation in pancreatic cancer and colon cancer. *Mol Oncol* (2019) 13:873–93. doi: 10.1002/1878-0261.12443

44. Crotty S. T Follicular helper cell biology: a decade of discovery and diseases. *Immunity* (2019) 50:1132–48. doi: 10.1016/j.immuni.2019.04.011

45. Gutiérrez-Melo N, Baumjohann D. T Follicular helper cells in cancer. *Trends Cancer* (2023) 9:309–25. doi: 10.1016/j.trecan.2022.12.007

46. Anderson NM, Simon MC. The tumor microenvironment. *Curr Biol* (2020) 30:R921–5. doi: 10.1016/j.cub.2020.06.081

47. Madhi H, Lee J, Choi YE, Li Y, Kim MH, Choi Y, et al. FOXM1 inhibition enhances the therapeutic outcome of lung cancer immunotherapy by modulating PD-L1 expression and cell proliferation. *Advanced Sci* (2022) 9:2202702. doi: 10.1002/advs.202202702

48. Hu B, Yu M, Ma X, Sun J, Liu C, Wang C, et al. IFNα potentiates anti–PD-1 efficacy by remodeling glucose metabolism in the hepatocellular carcinoma microenvironment. *Cancer Discovery* (2022) 12:1718–41. doi: 10.1158/2159-8290.CD-21-1022

49. Petri BJ, Klinge CM. m6A readers, writers, erasers, and the m6A epitranscriptome in breast cancer. *J Mol Endocrinol* (2023) 70:e220110. doi: 10.1530/JME-22-0110

50. Cao J, Mu Q, Huang H. The roles of insulin-like growth factor 2 mRNA-binding protein 2 in cancer and cancer stem cells. *Stem Cells Int* (2018) 2018:1–15. doi: 10.1155/2018/4217259

51. Wang P-F, Wang X, Liu M, Zeng Z, Lin C, Xu W, et al. The oncogenic functions of insulin-like growth factor 2 mRNA-binding protein 3 in human carcinomas. *CPD* (2020) 26:3939–54. doi: 10.2174/1381612826666200413080936

52. Zhang J, Yang K, Bu J, Yan J, Hu X, Liu K, et al. IGF2BP3 promotes progression of gallbladder carcinoma by stabilizing KLK5 mRNA in N6-methyladenosine-dependent binding. *Front Oncol* (2022) 12:1035871. doi: 10.3389/fonc.2022.1035871

53. Jin P, Huang Y, Zhu P, Zou Y, Shao T, Wang O. CircRNA circHIPK3 serves as a prognostic marker to promote glioma progression by regulating miR-654/IGF2BP3 signaling. *Biochem Biophys Res Commun* (2018) 503:1570–4. doi: 10.1016/j.bbrc.2018.07.081

54. Tran T, Bassi J, Nibber N, Philipp J, Draper J, Lin T, et al. The RNA binding protein IGF2BP3 is required for MLL-AF4 mediated leukemogenesis. *Blood* (2020) 136:21–2. doi: 10.1182/blood-2020-143181

55. Zhang S, Zhao BS, Zhou A, Lin K, Zheng S, Lu Z, et al. m6A demethylase ALKBH5 maintains tumorigenicity of glioblastoma stem-like cells by sustaining FOXM1 expression and cell proliferation program. *Cancer Cell* (2017) 31:591–606.e6. doi: 10.1016/j.ccell.2017.02.013

56. Chen H, Yu Y, Yang M, Huang H, Ma S, Hu J, et al. YTHDF1 promotes breast cancer progression by facilitating FOXM1 translation in an m6A-dependent manner. *Cell Biosci* (2012) 12:19. doi: 10.1186/s13578-022-00759-w

57. Jiang Z, Liu Z, Li M, Chen C, Wang X. Increased glycolysis correlates with elevated immune activity in tumor immune microenvironment. *EBioMedicine* (2019) 42:431–42. doi: 10.1016/j.ebiom.2019.03.068

58. Yu L, Chen X, Sun X, Wang L, Chen S. The glycolytic switch in tumors: how many players are involved? *J Cancer* (2017) 8:3430–40. doi: 10.7150/jca.21125

59. Ganapathy-Kanniappan S, Geschwind J-FH. Tumor glycolysis as a target for cancer therapy: progress and prospects. *Mol Cancer* (2013) 12:152. doi: 10.1186/1476-4598-12-152

60. Puchalska P, Crawford PA. Metabolic and signaling roles of ketone bodies in health and disease. *Annu Rev Nutr* (2021) 41:49–77. doi: 10.1146/annurev-nutr-111120-111518

61. Feng S, Wang H, Liu J, Aa J, Zhou F, Wang G. Multi-dimensional roles of ketone bodies in cancer biology: opportunities for cancer therapy. *Pharmacol Res* (2019) 150:104500. doi: 10.1016/j.phrs.2019.104500

62. Sun X, Peng Y, Zhao J, Xie Z, Lei X, Tang G. Discovery and development of tumor glycolysis rate-limiting enzyme inhibitors. *Bioorganic Chem* (2021) 112:104891. doi: 10.1016/j.bioorg.2021.104891

63. Zhang Z-F, Feng X-S, Chen H, Duan Z-J, Wang L-X, Yang D, et al. Prognostic significance of synergistic hexokinase-2 and beta2-adrenergic receptor expression in human hepatocelluar carcinoma after curative resection. *BMC Gastroenterol* (2016) 16:57. doi: 10.1186/s12876-016-0474-8

64. Thomas G, Garcia Prat L, Gronda M, Hurren R, MacLean N, Wang X, et al. The metabolic enzyme hexokinase 2 localizes to the nucleus in AML and normal

hematopoietic Stem/Progenitor cells to maintain stemness. *Blood* (2018) 132:2795–5. doi: 10.1182/blood-2018-99-110021

65. Guo D, Tong Y, Jiang X, Meng Y, Jiang H, Du L, et al. Aerobic glycolysis promotes tumor immune evasion by hexokinase2-mediated phosphorylation of IκBα. *Cell Metab* (2022) 34:1312–1324.e6. doi: 10.1016/j.cmet.2022.08.002

66. Lee Y, Min JK, Kim J, Cap KC, Islam R, Hossain AJ, et al. Multiple functions of pyruvate kinase M2 in various cell types. *J Cell Physiol* (2022) 237:128–48. doi: 10.1002/jcp.30536

67. Mazurek S. Pyruvate kinase type M2: a key regulator of the metabolic budget system in tumor cells. *Int J Biochem Cell Biol* (2011) 43:969–80. doi: 10.1016/j.biocel.2010.02.005

68. Zhao R, Li L, Yang J, Niu Q, Wang H, Qin X, et al. Overexpression of pyruvate kinase M2 in tumor tissues is associated with poor prognosis in patients with hepatocellular carcinoma. *Pathol Oncol Res* (2020) 26:853–60. doi: 10.1007/s12253-019-00630-3

69. Wang Y, Hou J, He D, Sun M, Zhang P, Yu Y, et al. The emerging function and mechanism of ceRNAs in cancer. *Trends Genet* (2016) 32:211–24. doi: 10.1016/j.tig.2016.02.001

70. Luo Y, Li H, Huang H, Xue L, Li H, Liu L, et al. Integrated analysis of ceRNA network in hepatocellular carcinoma using bioinformatics analysis. *Med (Baltimore)* (2021) 100:e26194. doi: 10.1097/MD.0000000000026194

71. Hua S, Quan Y, Zhan M, Liao H, Li Y, Lu L. miR-125b-5p inhibits cell proliferation, migration, and invasion in hepatocellular carcinoma *via* targeting TXNRD1. *Cancer Cell Int* (2019) 19:203. doi: 10.1186/s12935-019-0919-6

72. Zhu Y, Li B, Xu G, Han C, Xing G. lncRNA MIR4435–2HG promotes the progression of liver cancer by upregulating B3GNT5 expression. *Mol Med Rep* (2021) 25:38. doi: 10.3892/mmr.2021.12554

73. Kong Q, Liang C, Jin Y, Pan Y, Tong D, Kong Q, et al. The lncRNA MIR4435-2HG is upregulated in hepatocellular carcinoma and promotes cancer cell proliferation by upregulating miRNA-487a. *Cell Mol Biol Lett* (2019) 24:26. doi: 10.1186/s11658-019-0148-y

74. Yang L, Jiang M-N, Liu Y, Wu C-Q, Liu H. Crosstalk between lncRNA DANCR and miR-125b-5p in HCC cell progression. *Tumori* (2021) 107:504–13. doi: 10.1177/0300891620977010

75. Lu J, Kang X, Wang Z, Zhao G, Jiang B. The activity level of follicular helper T cells in the peripheral blood of osteosarcoma patients is associated with poor prognosis. *Bioengineered* (2022) 13:3751–9. doi: 10.1080/21655979.2022.2031387

76. Ng KW, Marshall EA, Enfield KS, Martin SD, Milne K, Pewarchuk ME, et al. Somatic mutation-associated T follicular helper cell elevation in lung adenocarcinoma. *OncoImmunology* (2018) 7:e1504728. doi: 10.1080/2162402X.2018.1504728

77. Koh CWQ, Goh YT, Goh WSS. Atlas of quantitative single-base-resolution N6-methyl-adenine methylomes. *Nat Commun* (2019) 10:5636. doi: 10.1038/s41467-019-13561-z

78. Huang H, Weng H, Chen J. m6A modification in coding and non-coding RNAs: roles and therapeutic implications in cancer. *Cancer Cell* (2020) 37:270–88. doi: 10.1016/j.ccell.2020.02.004

79. Cheng Y, Sun F, Thornton K, Jing X, Dong J, Yun G, et al. FOXM1 regulates glycolysis and energy production in multiple myeloma. *Oncogene* (2022) 41:3899–911. doi: 10.1038/s41388-022-02398-4

80. Shang R, Pu M, Li Y, Wang D. FOXM1 regulates glycolysis in hepatocellular carcinoma by transactivating glucose transporter 1 expression. *Oncol Rep* (2017) 37:2261–9. doi: 10.3892/or.2017.5472

frontiers | Frontiers in Immunology

TYPE Original Research
PUBLISHED 15 May 2023
DOI 10.3389/fimmu.2023.1157100

OPEN ACCESS

EDITED BY
Eyad Elkord,
University of Salford, United Kingdom

REVIEWED BY
Vasyl Nagibin,
National Academy of Sciences of Ukraine, Ukraine
Jonghwa Won,
ABL Bio/Sang Hoon Lee, Republic of Korea
Dorota Kwapisz,
Early Phase Institute, Poland

*CORRESPONDENCE
Said Demime
sdermime@hamad.qa

RECEIVED 02 February 2023
ACCEPTED 13 April 2023
PUBLISHED 15 May 2023

CITATION
Raza A, Mohsen R, Kanbour A, Zar Gul AR, Philip A, Vijayakumar S, Hydrose S, Prabhu KS, Al-Suwaidi AK, Inchakalody VP, Merhi M, Abo El-Ella DM, Tauro MA, Akbar S, Al-Bozom I, Abualainin W, Al-Abdulla R, Sirriya SA, Hassnad S, Uddin S, Mohamed Ibrahim MI, Al Homsi U and Demime S (2023) Serum immune mediators as novel predictors of response to anti-PD-1/PD-L1 therapy in non-small cell lung cancer patients with high tissue-PD-L1 expression.
Front. Immunol. 14:1157100.
doi: 10.3389/fimmu.2023.1157100

Serum immune mediators as novel predictors of response to anti-PD-1/PD-L1 therapy in non-small cell lung cancer patients with high tissue-PD-L1 expression

Afsheen Raza[1,2], Reyad Mohsen[1], Aladdin Kanbour[1], Abdul Rehman Zar Gul[1], Anite Philip[1], Suma Vijayakumar[1], Shereena Hydrose[1,2], Kirti S. Prabhu[3], Aisha Khamis Al-Suwaidi[1,2], Varghese Philipose Inchakalody[1,2], Maysaloun Merhi[1,2], Dina M. Abo El-Ella[1,2], Melissa Annrose Tauro[4], Shayista Akbar[5], Issam Al-Bozom[6], Wafa Abualainin[7], Rajaa Al-Abdulla[6], Shaza Abu Sirriya[7], Suparna Hassnad[8], Shahab Uddin[9,10], Mohamed Izham Mohamed Ibrahim[11], Ussama Al Homsi[1] and Said Demime[1,2,5]*

[1]Department of Medical Oncology, National Center for Cancer Care and Research, Hamad Medical Corporation, Doha, Qatar, [2]Translational Cancer Research Facility, Translational Research Institute, Academic Health System, Hamad Medical Corporation, Doha, Qatar, [3]Translational Research Institute (TRI), Academic Health System, Hamad Medical Corporation, Doha, Qatar, [4]Department of Human Genetics, Sidra Medical and Research Center, Doha, Qatar, [5]College of Health and Life Sciences, Hamad Bin Khalifa University, Doha, Qatar, [6]Department of Laboratory Medicine and Pathology, Hamad Medical Corporation, Doha, Qatar, [7]Diagnostic Genomic Division , Department of Laboratory Medicine and Pathology, Hamad Medical Corporation, Doha, Qatar, [8]Department of Radiation Oncology, National Center for Cancer Care and Research, Hamad Medical Corporation, Doha, Qatar, [9]Translational Research Institute and Dermatology Institute, Academic Health System, Hamad, Medical Corporation, Doha, Qatar, [10]Laboratory Animal Research Center, Qatar University, Doha, Qatar, [11]Clinical Pharmacy and Practice Department, College of Pharmacy, Qatar University (QU) Health, Qatar University, Doha, Qatar

Background: Non-small cell lung cancer (NSCLC) is the leading cause of cancer-related morbidity and mortality worldwide. Immune checkpoint inhibitors (ICIs) including anti-PD-1 and anti-PD-L1 antibodies, have significantly changed the treatment outcomes with better overall survival, but only 15-40% of the patients respond to ICIs therapy. The search for predictive biomarkers of responses is warranted for better clinical outcomes. We aim here to identify pre-treatment soluble immune molecules as surrogate biomarkers for tissue PD-L1 (TPD-L1) status and as predictors of response to anti-PD-1/PD-L1 therapy in NSCLC patients. Sera from 31 metastatic NSCLC patients, eligible for anti-PD-1/PD-L1 or combined chemoimmunotherapy, were collected prior to treatment. Analysis of soluble biomarkers with TPD-L1 status showed significant up/down regulation of the immune inhibitory checkpoint markers (sSiglec7, sSiglec9, sULBP4 and sPD-L2) in patients with higher TPD-L1 (TPD-L1 >50%) expression. Moreover,

correlation analysis showed significant positive linear correlation of soluble PD-L1 (sPD-L1) with higher TPD-L1 expression. Interestingly, only responders in the TPD-L1 >50% group showed significant down regulation of the immune inhibitory markers (sPD-L2, sTIMD4, sNectin2 and CEA). When responders vs. non-responders were compared, significant down regulation of other immune inhibitory biomarkers (sCD80, sTIMD4 and CEA) was recorded only in responding patients. In this, the optimal cut-off values of CD80 <91.7 pg/ml and CEA <1614 pg/ml were found to be significantly associated with better progression free survival (PFS). Indeed, multivariate analysis identified the cutoff-value of CEA <1614 pg/ml as an independent predictor of response in our patients. We identified here novel immune inhibitory/stimulatory soluble mediators as potential surrogate/predictive biomarkers for TPD-L1 status, treatment response and PFS in NSCLC patients treated with anti-PD-1/PD-L1 therapy.

KEYWORDS

non-small cell lung cancer, anti-PD-1, anti-PD-L1, tissue PD-L1, predictive soluble biomarkers, CEA

Introduction

Lung Cancer is the second most common cancer and a leading cause of cancer-related deaths (a total of 18% of cancer deaths) worldwide. In 2020, 2.2 million new cancer cases and 1.8 million deaths were reported for lung cancer. The 5-year survival rate is poor, ranging between 10-20% in developed countries (1).

Non-small cell lung cancer (NSCLC) is the most common cancer type, accounting for approximately 85% of lung cancer cases (2). Treatment management includes surgical removal, adjuvant chemotherapy, radiotherapy, and molecular-targeted therapies for patients with driver mutations (3). However, in a cohort of metastatic NSCLC patients with wild type epidermal growth factor receptor (EGFR), anaplastic lymphoma kinase (ALK) gene and tumor tissue expressing programmed death ligand-1(TPD-L1), treatment mainly comprises of FDA approved immune checkpoint inhibitors (ICIs), anti-programmed death protein 1/programmed death ligand 1 (PD-1/PD-L1) (4). ICIs are mainly monoclonal antibodies that target immune checkpoints, PD-1, and PD-L1 and block their pathways to help unleash a robust anti-tumor response [5]. Although ICIs have been shown to improve the overall survival in NSCLC patients, limited response rates, ranging between 15-40%, have been documented (5). Several intrinsic and extrinsic factors circulating within the host tumor microenvironment such as regulatory T cells (T regs), myeloid derived suppressor cells (MDSCs), M2 macrophages, immune checkpoints, cytokines and chemokines, have been associated with manipulation of immune response to facilitate tumor progression (6). On the other hand, it is postulated that soluble forms of immune checkpoint T and Natural killer (NK) cell receptors/ligands such as soluble programmed death protein 1 (sPD-1), soluble programmed death ligand 1 (sPD-L1), soluble programmed death ligand 2 (sPD-L2), soluble T cell immunoglobulin domain and mucin domain 3 (sTIM3), soluble UL16 binding protein 1/4 (sULBP-1/4), soluble Natural killer group 2D receptor and ligands sNKG2DL may affect treatment dynamics, either in an immune inhibitory or immune stimulatory manner (7–9). Some of the immune modulatory mechanisms associated with soluble forms include their binding to the treatment active site to hinder treatment efficacy, activation of immune suppressive molecules, inhibition of Interleukin-2 (IL-2) production/T cell activation, T cell apoptosis, upregulation of Tumor necrosis factor-α (TNF-α)/Interferon-gamma (IFN-γ) and early activation of $CD8^+$ T cells leading either to tumor immune escape or control (10–13). In anti-PD-1/PD-L1 treated NSCLC patients, a limited number of studies have associated soluble immune checkpoint markers with prognosis, response to treatment, and overall survival (14–19). The results from these studies indicate a potential role of soluble immune checkpoint mediators as biomarkers for patient stratification (responding vs. non-responding patients) and treatment dynamics. However, most studies have focused mainly on sPD-1 and sPD-L1, indicating a lack of data on other soluble T and NK immune checkpoint markers and their role in prognosis or prediction of response.

In addition to soluble T and NK markers, several studies have also reported on the role of tumor secreted antigens, such as Carcinoembryonic Antigen (CEA), Cytokeratin Fragment 19 (CYFRA21-1), and Carbohydrate Antigen 125 (CA-125), as biomarkers in some tumor types (20–22). These soluble antigens are expressed in various cancers, and some of them are widely used for clinical assessment and treatment monitoring in chemotherapyIn ICI-treated patients, limited number of studies have documented the role of circulating tumor antigens as dynamic biomarkers (23–27). However, the utility of these biomarkers in assessing immunotherapy efficacy in NSCLC patients is still poorly

explored, indicating a significant knowledge gap on their role as potential predictive/prognostic biomarkers.

In addition to soluble biomarkers, tissue markers have also been reported as predictors of response. To date, TPD-L1, measured by the immunohistochemistry (IHC) technique, is the only predictive marker approved by FDA as a companion diagnostic for anti-PD-1 antibody treatment in advanced NSCLC. To date, several randomized controlled trials have associated various TPD-L1 tumor proportional scores (TPS) such as ≥1%, ≥5%, ≥10%, and ≥50% with clinical efficacy endpoints such as overall survival (OS), progression-free survival (PFS) and objective response rate (ORR) (28, 29). However, conflicting data regarding the utility of TPD-L1 TPS has been reported, with some trials reporting it as a powerful predictive marker for OS while others indicate limited value of this marker (30–33). In lieu of this, limited studies have investigated the linear relationship of TPD-L1 expression with soluble biomarkers and clinical response in ICI-treated NSCLC patients to understand the role of soluble mediators as surrogate markers for TPD-L1 (34–36). This is an essential area of research since finding non-invasive surrogate markers for tissue can have various advantages, such as ease of sampling, longitudinal monitoring, and limited heterogeneity.

Pre-treatment assessment of dynamic biomarkers is an essential timeline as it helps understand the correlation of baseline biomarkers with disease/treatment dynamics (37, 38). It is well documented that early markers of response can serve as powerful tools for patient stratification and prediction of response (39–41). For ICI-treatment in NSCLC patients, the significance of pre-treatment biomarkers is of utmost importance as this cohort of patients has limited treatment options, and early response prediction can facilitate better patient management.

We aimed here to identify pre-treatment soluble immune checkpoint and circulating tumor antigens as surrogate/predictive markers in TPD-L1 expressing patients and to determine the role of soluble markers as predictors of response in anti-PD-1/PD-L1 treated NSCLC patients.

Methods

Study population and data collection

This prospective study was conducted at the National Center for Cancer Care and Research (NCCCR), Hamad Medical Corporation (HMC), Doha, Qatar, from September 2020 to July 2022. A total of 31 metastatic advanced-stage NSCLC patients eligible for treatment with anti-PD-1 (Nivolumab, Pembrolizumab), anti-PD-L1 (Durvalumab) monotherapy or combined chemoimmunotherapy (Carboplatin + Pemetrexed + Pembrolizumab) were enrolled in the study. Demographics and clinical characteristics of all patients, including age, gender, ethnicity, smoking history, histology, stage, differentiation status, Eastern Cooperative Oncology Group performance status (ECOG PS), genetic aberrations, Tissue PD-L1 expression, metastasis sites, previous lines of radiotherapy/chemotherapy, imaging and clinical response were extracted from electronic health record system of HMC (CERNER®).

Written informed consent was obtained from all eligible participants per Declaration of Helsinki and good clinical practice guidelines. The study was approved by the Institutional Review Board of HMC (MOPH-HMC-020).

Sample collection

Blood sample (10 ml) was collected from eligible patients before anti-PD-1/anti-PD-L1 monotherapy or combined chemoimmunotherapy treatment in BD Vacutainer SST II Advance Serum tubes (Becton Dickenson, USA). The tubes were centrifuged at 1300 g for 10 minutes and the extracted serum was cryopreserved at -80°C until further analysis.

Measurement of soluble immune checkpoint mediators and circulating tumor biomarkers

According to manufacturers' instruction, the level of soluble immune checkpoint T and NK cell mediators was detected using the Immuno-Oncology Checkpoint 14-Plex Human ProcartaPlex Panel 1, Panel 2, and Immuno-Oncology Checkpoint 9-Plex Human ProcartaPlex Panel 3 (ThermoFisher Scientific, USA). The 37 analytes tested included CD27, CD28, 4-1BB, GITR, HVEM, BTLA, CD80, CTLA-4, IDO, LAG-3, PD-1, PD-L1, PD-L2, TIM-3, MICA, MICB, Perforin, ULBP-1, ULBP-3, ULBP-4, Arginase, NT5E, Tactile, ECadherin, Nectin-2, PVR, Siglec-7, Siglec-9, B7-H6, B7-H3, IAP, BLAST-1,OX40, ICOS Ligand, TIMD-4, S100A8/A9, and VISTA.

The level of the circulating tumor biomarkers, CA-125, CA-15-3, CA-19-9, CEA, and CYFRA-21, was detected according to manufacturers' instruction, using the customized MILLIPLEX Human Circulating Cancer Biomarker Panel 1 kit (Merck KGaA, Germany).

The concentration of serum immune checkpoint mediators and circulating tumor biomarkers was measured by Luminex Bio-Plex 200 system (BIO-RAD). Acquisition and data analysis were performed by Bio-plex Manager TM version 6.2 software. Analyte concentrations in patients were calculated against a seven-point standard curve using a five-parametric fit algorithm in xPONENT v4.0.3.

Measurement of PD-L1 expression in tumor tissue

TPD-L1 expression was performed in the CAP-accredited Department of Laboratory Medicine and Pathology (DLMP), HMC, Qatar, as part of routine diagnostic testing. TPD-L1 expression was assessed, as per manufacturers' instructions, on formalin-fixed, paraffin-embedded (FFPE) tissue, by a qualitative immunohistochemical assay (DAKO PD-L1 IHC 22C3 pharmDx)

using monoclonal mouse Anti-PD-L1, Clone 22C3 on Automated Autostainer Link 48 (Dako, USA). Briefly, following incubation with the primary monoclonal antibody to TPD-L1 or the Negative Control Reagent (NCR), specimens were incubated with a Linker antibody specific to the host species of the primary antibody, and then incubated with a ready-to-use visualization reagent, consisting of secondary antibody molecules and horseradish peroxidase molecules coupled to a dextran polymer backbone. The enzymatic conversion of the subsequently added chromogen resulted in the precipitation of a visible reaction product at the site of the antigen. The entire slide was evaluated by an independent pathologist using a light microscope objective of 10-40X. To ensure run quality control, the slides were examined in the order of hematoxylin and eosin (H&E), control cell line slide, positive control tissue slides, negative control tissue, patient tissue slide stained using the NCR, and patient tissue slide stained using the PD-L1 primary antibody slides. For TPD-L1 scoring, a minimum of 100 viable tumor cells, negative and positive controls, were tested for quality control and test validity. TPD-L1 protein expression was determined by using Tumor Proportion Score (TPS), which is the percentage of viable tumor cells showing partial or complete membrane staining. The specimen was considered PD-L1 weak positive if membrane staining of TPS≥ 1% but < 50% of the viable tumor cells was observed, high PD-L1 (strongly positive) if TPS≥ 50% of the viable tumor cells exhibited membrane staining at any intensity. The intensity was evaluated as follows: No staining scored as "0", Weak staining as "1+", Moderate staining as "2+", Strong staining as "3+". The specimen was considered PD-L1 positive if ≥1% of the viable tumor cells exhibited membrane staining at any intensity (regardless of degree intensity, 1+, 2+, 3+). Representative TPD-L1 negative, TPD-L1<50% and TPD-L1>50% IHC images (400 x magnifications) are shown in Figure 1A.

Next generation sequencing for determination of genetic aberrations

Next Generation Sequencing to detect genetic aberrations was performed in the CAP-accredited Department of Laboratory Medicine and Pathology (DLMP), HMC, Qatar, as part of routine diagnostic testing. The NGS Oncomine Focus Assay was performed for the samples. A total of 52 genes were tested to cover hotspots and copy number variations (CNVs) by DNA sequencing and most targeted gene fusions by RNA sequencing in a single workflow within the same NGS panel. The tumor area was collected from slides of a formalin-fixed paraffin-embedded (FFPE) specimen; this area was identified by the consultant pathologist from which genomic DNA/RNA was extracted and analyzed by using Next Generation Sequencing NGS – Ion S5 (Oncomine Focus Assay). The data generated were analyzed for alterations in the Hotspot genes and fusion drivers.

Clinical assessment of response

Response to treatment was assessed *via* PET-CT imaging data and clinical assessment per RECIST criteria. Progression-free survival (PFS) was defined as the period from blood sample collection (before the first dose of anti-PD-1/PD-L1/Combined chemoimmunotherapy) to the date of clinical and radiological disease progression or death by any cause observed within 6-8 months from the start of the treatment.

Statistical analysis

Statistical analysis was performed using GraphPad Prism version 9.3.2 (GraphPad Software, Inc., USA). Descriptive statistics including median (IQR), 95% CI and frequencies (%) were used for analysis of demographics and soluble biomarker concentrations. Mann-Whitney U test was used for analyzing differences in biomarkers expression levels in TPD-L1 groups, treatment response, and response in different treatment types. The correlation between TPD-L1 and soluble biomarkers was determined by Pearson correlation. Cut-off values of soluble biomarkers were estimated by receiver operating characteristic (ROC) curve. Association of cut-off values with demographic/clinical characteristics was performed by Fisher exact test. Survival curves were plotted using the Kaplan-Meier method and compared using the log-rank test. Univariate and multivariate analyses of Progression-free survival (PFS) were performed using the Cox Proportional Hazard regression model with hazards ratio (HR) and 95%CI. The results were considered statistically significant if $p<0.05$ was observed.

Results

Demographic and clinical characteristics

A total of 31 advanced-stage, metastatic NSCLC patients were enrolled in the study. The demographic and clinical characteristics of patients are shown in Table 1. Anti-PD-1 treatment was administered to 48% of the patients (Pembrolizumab 35%, Nivolumab 13%), while 10% of the patients were treated with anti-PD-L1 (Durvalumab). The remaining 42% of the patients were treated with combined chemoimmunotherapy *(*Pembrolizumab+Carboplatin+Pemetrexed). Response to treatment was observed in 48% (n=15) of the patients, while 52% of the patients (n=16) were categorized as non-responders (Table 1).

Expression of soluble immune checkpoints/circulating tumor antigens and patients' characteristics

The concentration of soluble immune checkpoints/circulating tumor antigens was successfully detected, and median + Interquartile (IQR) values of tested biomarkers are shown in Supplementary table 1.

Expression of TPD-L1 in enrolled patients

TPD-L1 expression was observed in 74% (n=23), while 26% (n=8) of the patients were found to be negative. For further analysis, TPD-L1 positive patients were stratified into two groups: TPD-L1<50% (n=6) and TPD-L1>50% (n=17). Representative images for TPD-L1 negative, TPD-L1<50% and TPD-L1>50% are shown in Figure 1A.

Soluble biomarkers and TPD-L1

Comparison of the expression level of soluble biomarkers between TPD-L1 negative vs. positive groups showed no significant change. However, comparison of TPD-L1<50% and >50% groups showed significant changes in various soluble markers. In the TPD-L1>50% group, significant downregulation of the immune inhibitory checkpoint markers, sSiglec7 (p=0.011*), sSiglec9 (p=0.003**), sULBP4 (p=0.008**) and significant up-regulation of sPD-L2 (p=0.015*) was observed (Figure 1B). The result indicates that high TPD-L1 expression could induce secretion of the soluble Natural Killer (NK) and T cell immune inhibitory checkpoint markers for immune regulation of anti-tumor response.

The median (IQR) values of soluble biomarkers in TPDL-1<50% and TPD-L1>50% groups are given in supplementary Table 2.

Correlation between soluble immune checkpoint biomarkers and TPD-L1 >50% group

Pearson correlation analysis was performed to understand the linear relationship of TPD-L1 expression with up/down regulated soluble markers sSiglec7, sSiglec9, sULBP4, and sPD-L2. In addition to these markers, correlation analysis between TPD-L1 and sPD-L1 was also performed to determine if there is an existing relationship between the tissue and the secreted form of PD L1. No significant correlation between TPD-L1 >50% group and sSiglec7, sSiglec9, sULBP4, sPDL2 was noted. However, a moderate positive linear correlation (r =0.4857) was observed between the immune inhibitory marker, sPD-L1, and TPD-L1 >50%, with a significance value of p=0.048* (Figure 1C). This indicates that TPD-L1 expression levels are directly proportional to the concentration of sPD-L1 i.e., as TPD-L1 expression increases above 50%, the concentration of sPD-L1 also increases, making sPD-L1 a potential surrogate marker for longitudinal monitoring of TPD-L1.

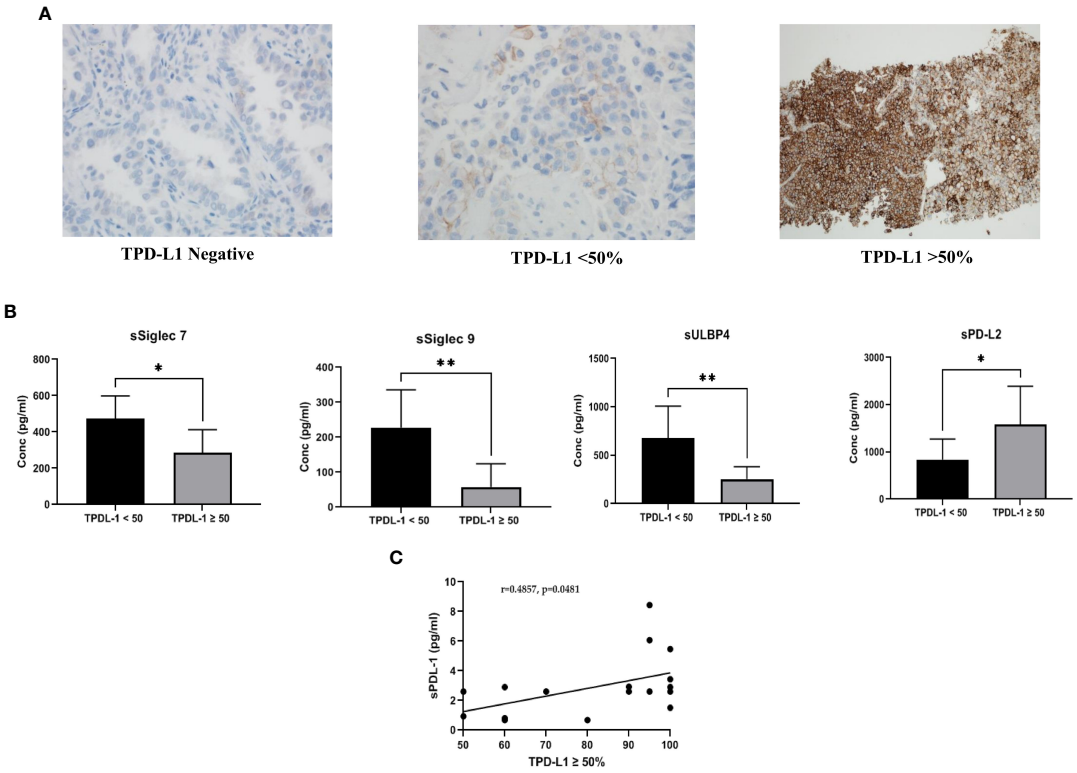

FIGURE 1
(A) Representative images of PD-L1 expression on tumor tissue: Tissue PD-L1 negative, tissue PD-L1<50% and tissue PD-L1>50% was observed by immunohistochemistry using DAKO PD-L1 IHC 22C3 pharmDx assay **(B)** Comparison of soluble immune biomarker expression between TPD-L1 low (<50%) and TPD-L1 high (>50%) groups: Significant down regulation of immune inhibitory checkpoint markers, sSiglec7 (p=0.011*), sSiglec9 (p=0.003**), sULBP4 (p=0.008**) and significant up regulation of sPD-L2 (p=0.015*) was observed in high TPD-L1 (>50%) expressing group **(C)** Pearson correlation showed significant moderate positive linear correlation (r =0.4857, p=0.048*) between the immune inhibitory marker, soluble PD-L1 and high TPD-L1(>50%) expressing group.

10.3389/fimmu.2023.1157100

TABLE 1 Patient characteristics (all, responders and non-responders) and their association with treatment response.

Patient Characteristics	Patients n=31 (%)	Responders (R) n=15 (%)	Non-Responders (NR) n=16 (%)	Association analysis R. vs. NR (p value)
Age in years (Median, range)	59 (40-80)			
<60	16 (52)	5 (33)	11 (69)	0.756
>60	15 (48)	10 (67)	5 (31)	
Gender				
Male	26 (84)	12 (80)	14 (88)	0.6539
Female	5 (16)	3 (20)	2 (12)	
Ethnicity				
Arabs	14 (45)	8 (53)	6 (38)	0.4795
Non-Arabs	17 (55)	7 (47)	10 (62)	
Smoking history				
Never	10 (32)	6 (40)	4 (25)	0.4578
Current/Former	21 (68)	9 (60)	12 (75)	
Histology				
Adenocarcinoma	27 (87)	13 (87)	14 (88)	0.999
Squamous cell carcinoma	4 (13)	2 (13)	2 (12)	
Stages				
Stage 3	7 (23)	6 (40)	1 (6)	*0.0373**
Stage 4	24 (77)	9 (60)	15 (94)	
Differentiation status				
Well differentiated	10 (32)	4 (27)	5 (31)	0.999
Poorly differentiated	21 (68)	11 (73)	11 (69)	
ECOG PS				
0-1	26 (84)	13 (87)	13 (81)	0.999
>2	5 (16)	2 (13)	3 (19)	
Genetic alterations				
EGFR				
Wild type	28 (90)	14 (100)	14 (88)	0.999
Mutated	1 (3)	–	1 (6)	
Unknown	2 (7)	–	2 (12)	
ALK				
Wild type	27 (87)	14 (93)	13 (81)	0.451
Mutated	1 (3)	1 (7)	–	
Unknown	3 (10)	–	3 (19)	
ERBB3				
Wild type	28 (90)	14 (93)	14 (88)	0.999
Mutated	3 (10)	1 (7)	2 (12)	
KRAS				
Wild type	28 (90)	13 (87)	15 (94)	0.5996

(Continued)

TABLE 1 Continued

Patient Characteristics	Patients n=31 (%)	Responders (R) n=15 (%)	Non-Responders (NR) n=16 (%)	Association analysis R. vs. NR (p value)
Mutated	3 (10)	2 (13)	1 (6)	
PDL-1 TPS				
Negative	8 (26)	1 (7)	7 (44)	
TPD-L1 Positive < 50%	6 (26)	3 (21)	3 (33)	
TPD-L1Positive >50%	17 (74)	11 (79)	6 (66)	0.6430
Brain metastasis	17 (74)			
Present	15 (48)	8 (53)	7 (44)	0.7244
Absent	16 (52)	7 (47)	9 (56)	
Liver Metastasis				
Present	7 (23)	1 (7)	6 (38)	0.0829
Absent	24 (77)	14 (93)	10 (62)	
Pulmonary Metastasis				
Present	21 (68)	8 (53)	13 (81)	0.1351
Absent	10 (32)	7 (47)	3 (19)	
Previous history of radiotherapy				
Yes	14 (45)	9 (60%)	8 (50)	0.7224
No	17 (55)	6 (40%)	8 (50)	
Previous lines of chemotherapy				
0	8 (26)	5 (33%)	3 (19)	0.4331
>1	23 (74)	10 (66%)	13 (81)	
Treatment type				
Anti-PD-1 (Pembrolizumab/Nivolumab)	15	6 (40)	9 (56)	0.2059
Anti-PD-L1(Durvalumab)	3 (10)	3 (20)	0 (0)	
Chemoimmunotherapy (Pembrolizumab+Carboplatin+Pemetrexed)	13 (42)	6 (40)	7 (44)	0.999 (anti-PD-1) 0.2125 (anti-PD-L1)

ECOG PS, Eastern Cooperative Oncology Group performance status; EGFR, Epidermal Growth factor receptor; ALK, Anaplastic lymphoma kinase; ERBB3, Erb-b2 receptor tyrosine kinase 3; KRAS, Kirsten rat sarcoma viral oncogene homolog; PD-L1, programmed death-ligand 1; PD-1, Programmed cell death Protein 1; TPS, Tumor Proportion score.

Expression of soluble biomarkers in TPD-L1 >50% group and their role in treatment response

A comparison of the expression of soluble biomarkers with treatment response was performed in TPD-L1 groups. In TPD-L1 >50% group, comparison between responders (n=6) and non-responders (n=11) showed significant down regulation of immune inhibitory markers sPD-L2 (p=0.008**), sTIMD4 (p=0.040*), sNectin2 (p=0.012*) and CEA (p=0.024*) in responding patients (Figure 2). Our study results imply that in patients expressing TPD-L1 >50%, T cell immune checkpoint and circulating tumor antigens may play a role in immune modulation and tumor response. As such, these biomarkers may have utility as predictive biomarkers of response in this cohort. No significant expression of soluble biomarkers with treatment response was observed in TPD-L1 positive/negative groups and TPD-L1 <50% group (data not shown). The median (IQR) values of soluble biomarkers in responders vs. non-responders in the TPD-L1>50% group is given in Supplementary Table 2.

Association of patient characteristics with treatment response

Based on imaging and clinical status as per RECIST criteria, the enrolled participants were stratified as responders (n=15) and non-responders (n=16). Association of treatment response with demographic/clinical characteristics showed significant association of disease stage 4 (p=0.037*) with non-responders. No other demographics/clinical characteristics were associated with treatment response (Table 1).

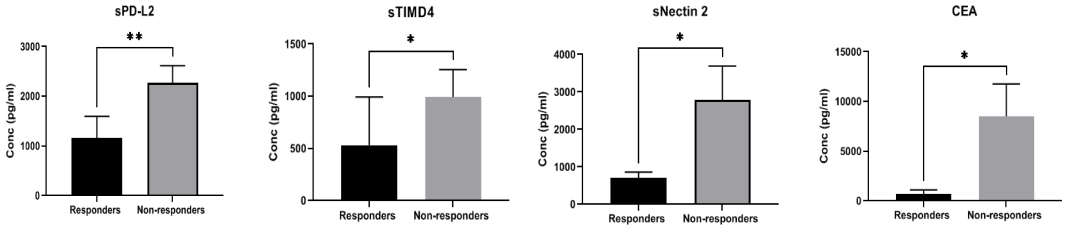

FIGURE 2
Comparison of soluble biomarker expression between responders (n=6) and non-responders (n=11) in high TPD-L1(>50%) group showed significant down regulation of immune inhibitory markers sPD-L2 (p=0.008**), sTIMD4 (p=0.040*), sNectin2 (p=0.012*) and CEA (p=0.024*) in responding patients.

Soluble biomarkers and their association with treatment response in anti-PD-1/PD-L1 monotherapy and chemo-immunotherapy group

Treatment types utilized for patients included monotherapy with anti-PD1 (Nivolumab, Pembrolizumab), anti-PD-L1 (Durvalumab) and combination chemoimmunotherapy (Carboplatin +Pemetrexed + Pembrolizumab). Due to the different treatment types, we stratified the patients into two groups. Group 1 comprised all patients who received anti-PD-1 and anti-PD-L1 monotherapy (anti-PD-1/PD-L1 monotherapy group: Nivolumab+Pembrolizumab+Durvalumab: n=18), whereas Group 2 included all patients who received combination chemoimmunotherapy (n=13).

The expression of soluble biomarkers was analyzed as follows a) responding patients in Group 1 (n=9) vs. Group 2 (n=6) and b) non-responding patients in Group 1 (n=9) vs. Group 2 (n=7). Interesting results were observed with both groups' significant up/down-regulation of soluble biomarkers. In "responding" patients, the immune inhibitory checkpoint marker sPD-1, was significantly downregulated (p=0.012*) in Group 1 compared to Group 2. On the other hand, in "non-responding" patients, the immune suppressive biomarker S100A8/A9 (p=0.0084**) was significantly upregulated in Group 1 compared to Group 2. Our results clearly identify soluble biomarkers that can discriminate treatment response in different treatment groups and thus serve as predictive biomarkers (Figure 3A). Median (IQR) values of soluble biomarkers in responding and non-responding patients in Group 1 and Group 2 is given in Supplementary Table 3.

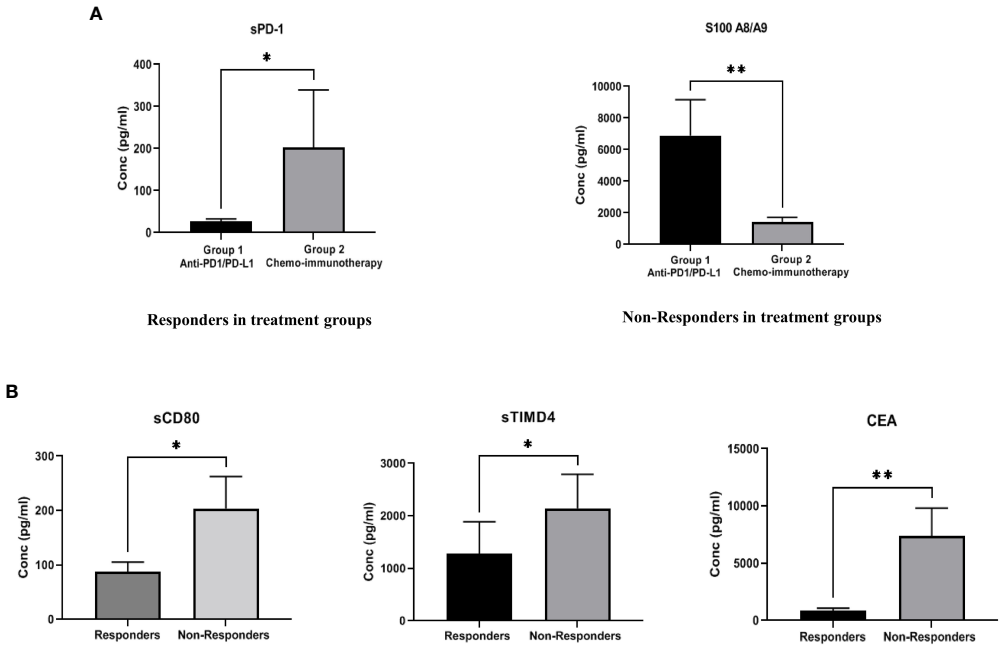

FIGURE 3
(A) Comparison of soluble biomarker expression between responders and non-responders in two treatment groups-Group 1 (anti-PD-1/PD-L1 monotherapy group), Group 2 (combination chemoimmunotherapy group). In "responding" patients, the immune inhibitory checkpoint marker sPD-1, was significantly down regulated (p=0.012*) in Group 1 as compared to Group 2. In "non-responding" patients, the immune suppressive biomarker S100A8/A9 (p=0.0084**) was significantly up regulated in Group 1 as compared to Group 2 **(B)** Comparison of soluble biomarker expression between all responders vs. all non-responders irrespective of treatment type. Significant down regulation of the immune inhibitory biomarkers sCD80 (p=0.023*), sTIMD4 (p=0.033*) and CEA (p=0.008**) in "responding" patients was observed.

Comparison of soluble biomarkers in responders and non-responders irrespective of treatment types

To identify generalized biomarkers of response in NSCLC patients treated with ICI, we compared the expression of soluble biomarkers in responders (n=15) vs. non-responders (n=16), irrespective of treatment groups. The results showed significant downregulation of the immune inhibitory biomarkers sCD80 (p=0.023*), sTIMD4 (p=0.033*), and CEA (p=0.008**) in "responding" patients indicating that these biomarkers may be playing a rather generalized but extensive role in immune modulation and treatment response to ICI therapy (Figure 3B). The median (IQR) values of soluble biomarkers between responders and non-responders, irrespective of treatment types, is given in supplementary Table 4.

Determination of optimal cut-off values of soluble biomarkers to discriminate responders from non-responders

The generalized soluble biomarkers that showed significant association with treatment response (irrespective of treatment types), including CD80, TIMD4, and CEA, were further analyzed by Receiver Operator Characteristic Curve (ROC) to determine their optimal cut-offs. It was found that the optimal cut-off value for soluble biomarkers to discriminate responders from non-responders were as follows: CD80 <91.7pg/ml (AUC: 0.7262, 95% CI: 0.535-0.917, sensitivity: 73%, specificity: 71%); TIMD4 <600pg/ml (AUC: 0.7250, 95% CI: 0.543 to 0.907, sensitivity: 75%, specificity: 66%); CEA <1614pg/ml (AUC: 0.778, 95% CI: 0.586-0.969, sensitivity: 67%, specificity: 83%) (Figure 4A). The cut-off values were further analyzed for their association with PFS in patients.

Association of soluble immune checkpoint/ circulating tumor antigens with progression free survival

The association of higher than cut-off and lower than cut-off values of the soluble biomarkers CD80, TIMD4, and CEA with PFS was determined using Kaplan Meier (log-rank) test. It was observed that patients having higher than cut-off values of CD80 and CEA had poor PFS (median survival of 4 months and 3.5 months, respectively). On the other hand, patients having CD80 cut-off value of lower than 91.7 pg/ml (HR: 2.873, 95% CI: 1.078-7.658, p=0.042*) and CEA cut-off value of lower than 1614 pg/ml (HR: 2.566, 95% CI: 0.131-1.160, p=0.037*) were significantly associated with better progression-free survival (Figure 4B). No significant association of TIMD4 cut-off value with PFS was observed (HR: 2.699, 95% CI: 1.012-7.202, p=0.05) (Figure 4B).

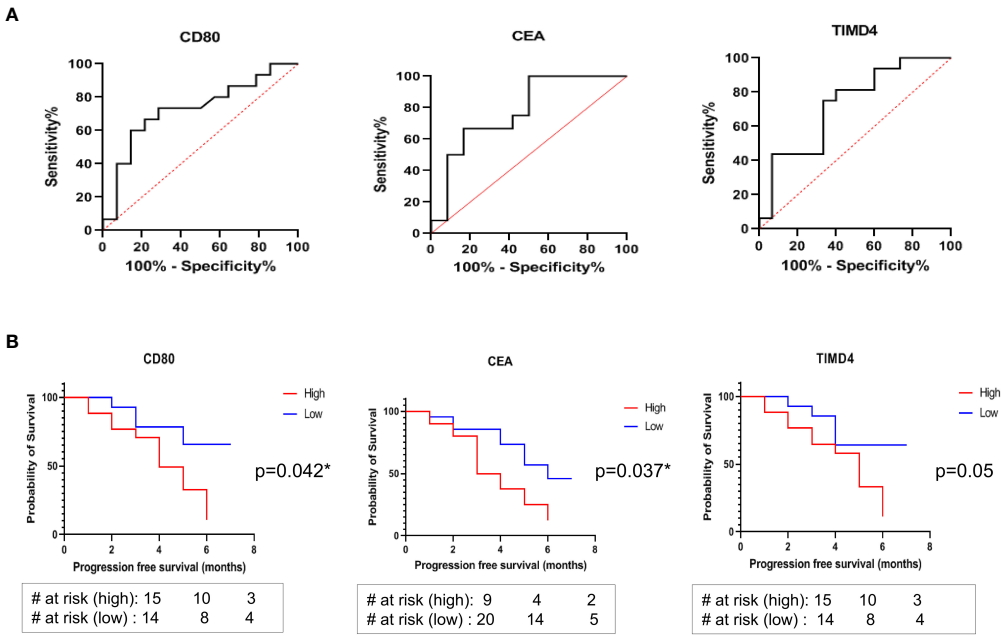

FIGURE 4
(A) ROC curves to discriminate responders from non-responders identified optimal cut-off values of soluble biomarkers: CD80 <91.7pg/ml, AUC: 0.7262, sensitivity: 73%, specificity: 71%; TIMD4 <600pg/ml, AUC: 0.7250, sensitivity: 75%, specificity: 66%; CEA <1614pg/ml AUC: 0.778, sensitivity: 67%, specificity: 83% **(B)** Kaplan Meier (log rank) analysis for association of cut-off values with progression free survival showed that patients having CD80 cut-off value of lower than 91.7 pg/ml (HR: 2.873, 95% CI: 1.078-7.658, p=0.042*) and CEA cut-off value of lower than 1614 pg/ml (HR: 2.566, 95% CI: 0.131-1.160, p=0.037*) were significantly associated with better progression free survival. No significant association of TIMD4 cut-off value with PFS was observed (HR: 2.699, 95% CI: 1.012-7.202, p=0.05).

Cox proportional hazard regression analysis

To assess the impact of patient characteristics and soluble biomarkers as independent predictive factors of PFS, univariate and multivariate analysis by Cox Proportional Hazard Regression was performed. Multivariate analysis showed that age <60 years (HR 4.856 [95% CI: 1.244-23.10]; p=0.031) and CEA lower than the cut-off value of 1614 pg/ml (HR 0.1834 [95% CI: 0.04-0.65]; p=0.012) are independent predictors of better progression-free survival in patients (Table 2).

Discussion

We have identified in this study immune inhibitory/stimulatory soluble mediators as a potential surrogate/predictive biomarker for TPD-L1 status, treatment response, and progression-free survival in NSCLC patients treated with anti-PD-1/PD-L1. This a pilot study and the results showed a significant association of circulating tumor antigen, CEA, and several NK and T cell immune checkpoint markers with TPD-L1 expression and treatment response. To the best of our knowledge, this is the first study that extensively examines the role of NK/T cell immune checkpoint biomarkers/circulating tumor antigens with regards to TPD-L1 expression and treatment response in this cohort of patients.

We first aimed to identify and understand the role of various NK and T cell immune checkpoint serum markers as surrogate biomarkers/predictors of response with respect to TPD-L1 status. TPD-L1 is the only FDA approved companion diagnostic, predictive marker to assess the eligibility of NSCLC patients for ICI treatment (42). The ICI treatments for NSCLC include anti-PD-1, anti-PD-L1, or combined chemoimmunotherapy. Although TPD-L1 assessment is not a pre-requisite for all ICI treatments, several clinical trials have evaluated its role in predicting survival benefits for ICI-treated NSCLC patients (43). A large-scale meta-analysis on fifteen randomized controlled trials showed that patients with high TPD-L1 expression (>50%) exhibited improved overall response rates and subsequently benefitted from anti-PD-1/PD-L1 therapy (33). However, TPD-L1 expression could not predict survival benefits in patients on combined chemoimmunotherapy (33). This variability in predicting immunotherapy efficacy is possibly due to its inherent limitations, including inadequate tissue sampling, tumor heterogeneity, variable testing parameters, and evolutionary changes in TPD-L1 expression (induced by prior treatment lines), making its utility in clinical settings unclear. On the other hand, liquid biopsy, with its fundamental characteristics, such as noninvasiveness, incorporating tumor heterogeneity, ease of longitudinal monitoring *via* multiple sampling, and representation of systemic biomarker expression, could serve as an essential component to assess immunotherapy efficacy (44). Furthermore, its utility as a surrogate marker for TPD-L1 expression can help in longitudinal treatment monitoring. Our results showed that in patients with TPD-L1 >50% expression, significant downregulation of the soluble NK immune inhibitory markers Siglec-7 and-9, ULBP4 and significant upregulation of the soluble T cell immune inhibitory marker PD-L2 was observed. The role of these markers in immune regulation is well documented. Siglecs (Sialic acid-binding immunoglobulin-like lectins) are a family of receptors, present mainly on immune cells (45),. Siglec receptors recognize sialoglycan ligands on cell membranes and lead to eventual dephosphorylation of downstream immune pathways leading to inhibition of cellular activation (45). In tumors, the immune suppressive microenvironment helps facilitate this inhibition *via* aberrant expression of sialoglycan ligands on tumor cells and Siglec receptor overexpression on immune cells (46, 47). A strong receptor-ligand binding leads to immune inhibition and tumor escape (46, 47). Studies have shown that Siglec-7 and -9 are abundantly present in NK cells, and their interaction with sialoglycan ligands (on tumor cells) inhibits NK cell activation (48). Enhanced expression of siglec-7 and -9 in peripheral $CD8^+$ T cells and tumor tissues have been observed in NSCLC, melanoma, and colon cancers (49, 50). Moreover, a study on NSCLC patients observed that high Siglec-9 expression on infiltrating $CD8^+$ T cells was associated with increased expression of PD-L1, co-expression of inhibitory receptors PD-1, TIM-3, Lag3, and reduced production of inflammatory cytokines leading to an exhausted T cell phenotype and poor survival in patients (50–52). In lieu of this, our results show a different pattern. Serum-derived Siglec-7 and -9 were downregulated in patients exhibiting TPD-L1 >50% expression. Since we could not determine the expression of Siglecs in the tumor tissue, it is possible that Siglecs were overexpressed within the tumor tissue, subsequently leading to high PD-L1 expression.

TABLE 2 Uni- and multivariate analysis of Progression free survival by Cox proportional Hazards model.

	Univariate analysis		Multivariate analysis	
Variables	HR (95% CI)	p value	HR (95% CI)	p value
Age (>60 vs.<60)	3.034 (1.094-9.691)	0.041*	4.856 (1.244-23.10)	0.031*
PDL-1 TPS (Positive vs. Negative)	2.891 (1.024-7.849)	0.037*	2.019 (0.679-5.728)	0.188
Liver Metastasis (Absent vs. Present)	4.199 (1.310-13.38)	0.013*	2.351 (0.607-8.938)	0.204
CEA (High vs. Low)	0.357 (0.129-0.984)	0.042*	0.183 (0.04-0.65)	0.012*

However, with their release into the circulation as soluble forms, other factors within the TME may have come into play for their downregulation and modulation. Down-regulation of Siglecs has been associated with augmentation of anti-tumor responses. In this, studies in mice deficient in Siglecs-E (the functional equivalent of human Siglec-9) showed increased *in vivo* killing of tumor cells and enhanced immunosurveillance (53). The same study showed that polymorphisms in human Siglec-9 contributed to its reduced binding to cancer cells, leading to improved survival in NSCLC patients (53). Therefore, we postulate that downregulation of soluble Siglecs in circulation in our cohort may indicate their role in the anti-tumor response. However, since no study on serum Siglecs and TPD-L1 has been reported, we could not corroborate our data with previous studies. Larger studies on this aspect could provide a better understanding of these Siglecs in TPD-L1 expression and immune regulation.

Another marker, UL16-binding protein 4 (ULBP4) was found to be significantly down regulated in patients expressing TPD-L1>50%. Mainly, NK cell–mediated cytotoxicity is regulated *via* the binding of NK group 2 member D (NKG2D) activating receptors with their ligands, such as the ULBP family (ULBP1-6) (54, 55). ULBP ligand expression is observed to be low in non-malignant cells (56, 57). However, in tumors, ULBP 1-6 ligands are aberrantly expressed, leading to modulation of anti-tumor responses (56, 57). Specifically, secreted forms of ULBP4 (generated *via* alternative splicing) have been reported to bind to NKG2D receptor, thus initiating its internalization for NK cell-acquired dysfunction and reduced NK cytotoxicity for tumor immune escape (58–60). Moreover, studies have reported that as ULBP4 ligand secretion increases, it induces the expansion of immune suppressive T cells, thus creating a favorable environment for tumor growth (61). On the other hand, studies on glioma and nasopharyngeal carcinoma have documented contrasting results, showing that upregulation of the cytokines TGF-β/IFN-γ and increased PD-L1 expression can lead to selective downregulation of ULBP3 and 4 to facilitate tumor escape (62–64). Our results agree with this notion showing that as PD-L1 expression increases, ULBP4 expression decreases, possibly playing its role in immune modulation. However, since the role of soluble ULBP4 with respect to PD-L1 expression in ICI-treated NSCLC patients has not been reported yet, we believe that our results could allow further studies to explore this aspect in detail.

In addition to NK markers, the T cell immune inhibitory checkpoint ligand PD-L2 was found to be upregulated in the TPD-L1 >50% group. PD-L2 that serves as second ligand for PD-1 and is involved in T cell regulation *via* decreased cytokine production and inhibition of T cell receptor (TCR)-mediated proliferation (65). Studies on lung and melanoma have shown that simultaneous expression of PD-L1 with PD-L2 is an important concept and could be one of the mechanisms utilized by tumor cells for immune evasion and tumor progression (66, 67). In fact, a study on ovarian cancer reported that blocking both PD-L1 and PD-L2 could help to overcome resistance to ICI treatment by unleashing the immune responses, thus indicating a clear role of both ligands in immune regulation (68). In our study, we observed simultaneous upregulation of sPD-L2 with TPD-L1 expression, indicating a possible synergistic effect for tumor response. Though tissue PD-L2 was not tested in our cohort, we assume that soluble PD-L2 (generated *via* splicing event of membrane-bound PD-L2) may indicate its presence within the tumor tissue. Also, as our result indicates concurrent up regulation of both markers (PD-L1 and PD-L2), we propose the utility of sPD-L2 as a surrogate marker for tissue PD-L1 and PD-L2. However, since limited studies on sPD-L2 are available in the literature, our assumption on the dualistic role of TPD-L1 and soluble PD-L2 in anti-tumor response needs further validation.

To understand if any linear relation exists between the up/down regulated soluble markers Siglec-7,-9, ULBP4 and PD-L2, Pearson correlation analysis was performed. We did not find any of these markers to correlate with TPD-L1. However, we did correlation analysis of sPD-L1 with TPD-L1 with the concept that since sPD-L1 is a spliced variant secreted by membrane-bound PD-L1, a linear relationship could exist between the two markers. Interestingly, correlation analysis between serum PD-L1 and TPD-L1 >50% showed a moderate positive relationship indicating that increased serum concentration of PD-L1 could be associated with increased PD-L1 expression in tissues. This is an important finding and allows the assumption that serum PD-L1 could be utilized as a surrogate marker for TPD-L1 status for longitudinal monitoring in patients on ICI treatment. Studies showing a significant positive correlation between the two markers have been reported, thus corroborating our observation (69, 70).

Furthermore, we aimed to identify specific biomarkers that could help stratify responding from non-responding patients in TPD-L1 >50% group. This is important as the identification of early biomarkers of response could help treatment management in this group. In responding patients with TPD-L1 >50% expression, the immune inhibitory markers sPD-L2, sTIMD4, sNectin2 and CEA were significantly downregulated. sPD-L2 is a spliced variant of membrane-bound PD-L2 that retains the ability to bind to its membrane-bound PD-1 receptor for immune regulation (71). Studies on the prognostic value of sPD-L2 in NSCLC are very limited. Only one study on 22 patients was carried out that evidenced better survival in patients with low pre-treatment sPD-L2 expression (18, 72). Moreover, co-expression of sPD-L2 with other soluble mediators such as PD-L1, CD137, TIM-3 BTLA-4 and CEA has been associated with favorable clinical response indicating a synergistic effect of these soluble mediators with each other to induce modulatory effects within the tumor microenvironment (18, 72). In our study, we observed downregulation of sPD-L2 with other soluble immune inhibitory markers such as sTIMD4, sNectin2, and CEA indicating the plausibility of a synergistic mechanism of soluble markers with each other thus enabling anti-tumor response in high tissue PD-L1 expressing patients. Further studies on these markers would enable a better understanding on this inference.

Besides sPD-L2, the NK associated ligand, sNectin2 was also found to be down regulated in high tissue PD-L1 responding patients. Nectin-2 is a immunoglobulin-like cell-to-cell adhesion protein that acts in a stimulatory or inhibitory manner Several studies on serum Nectin-2 have associated its overexpression with aggressiveness and metastasis in various cancers including colon, breast, esophageal and lung indicating its role as a prognostic and

predictive biomarker in cancers (73–76). Moreover, blockade *via* anti-Nectin-2 monoclonal antibodies can induce antibody-dependent cellular cytotoxicity (ADCC) with robust anti-tumor response in breast and ovarian cancers, indicating its role in immune regulation (77, 78). Similar results were observed for Esophageal squamous cell carcinoma (ESCC) where knockdown of Nectin−2 in ESCC cell lines was associated with effective suppression of cell migration and invasion (75). Our results corroborate with these studies, and we postulate that high TPD-L1 could lead to immune-inflamed TME with downregulation of sNectin-2 as an anti-tumor response mechanism in responding patients of this cohort.

Our results also showed downregulation of the immune inhibitory marker TIMD4 (T Cell Immunoglobulin and Mucin Domain Containing 4) in TPD-L1 >50% group. TIMD4 is a cell-surface glycoprotein and in cancers including renal cell carcinoma, diffuse large B-cell lymphoma, pancreatic cancer, and glioma, expression of TIMD4 has been associated with enhanced apoptosis, reduced clonogenic ability of cancer cells, and better survival (79–82). In NSCLC, a comprehensive study documented the role of TIMD4 overexpression in the promotion of lung cancer cell proliferation and poor overall survival (83). Although the mechanism of TIMD4-mediated cancer progression remains unknown, the study showed that mutation in the TIMD4 RGD motif reduces cancer progression (83). We presuppose here (based on the mechanism of action of TIMD4) that high PD-L1 expression could have influenced the TME to induce downregulation of circulating TIMD4 as an active anti-tumor response mechanism in responding patients.

In addition to T and NK cell markers, we also found circulating tumor antigen CEA to be downregulated in the high TPD-L1 group. CEA is a serum glycoprotein and is a well-established prognostic and predictive tumor marker utilized for treatment monitoring in various cancers (84–86). In lung cancers, elevated CEA levels have been associated with tumor size, lymph node status, stage of disease, and treatment monitoring (87). Studies on ICI-treated NSCLC patients' have associated high pre-treatment levels of CEA with worse PFS and OS (23, 25, 27). Moreover, a study on the correlation between CEA and PD-L1 has reported CEA as an independent prognostic indicator of worse OS in the PD-L1-positive group (88). On the other hand, a more specific role of CEA and immune modulation *via* PD-L1 has recently been documented (89–94). Several studies on T cell–bispecific antibody (CEA-TCB) targeting CEA and T cell receptor have shown interesting results in syngeneic tumor models, cell lines, *in vivo* humanized mice, and patients (89–94). CEA-TCB specifically induced T cell-mediated killing of CEA-expressing tumors by converting a non-inflamed PD-L1 negative tumor to a highly inflamed PD-L1 positive tumor (89–94). In our study, responding patients with high tissue PD-L1 showed down-regulation of CEA. Based on previous studies discussed above including low pre-treatment CEA associated with response and elevated PD-L1 expression inducing an immune hot/inflamed TME, we postulate that in our cohort high PD-L1 expression may have led to downregulation of CEA thus facilitating an efficient anti-tumor response.

The second aim of our study was to understand the role of soluble biomarkers as early predictors of response in NSCLC patients on ICI treatment. We stratified our analysis into various aspects, as discussed below. Firstly, we sought to identify early predictive biomarkers of response in patients on different therapeutic regimens (anti-PD-1/PD-L1 monotherapy group vs. chemoimmunotherapy group). In the anti-PD-1/PD-L1 monotherapy group, we identified two immune suppressive markers to be significantly associated with response. In responding patients, immune inhibitory checkpoint marker sPD-1 was found to be significantly downregulated. sPD-1 is a spliced variant of membranous PD-1 that retains its PD-L1 binding domain and can thus bind to membranous PD-L1 and PD-L2. This binding facilitates several immune modulatory effects, including early activation of $CD8^+$ T cells, blocking of PD-L1 expression on tumor cells, and essentially reducing T cell inhibition (11, 95). On the other hand, some studies have documented its role in tumor immune escape *via* its ability to bind with membrane-bound PD-1 and in turn, compete with therapeutic anti-PD-1 monoclonal antibodies for their PD-1 binding site (95). The successful binding of sPD-1, instead of anti-PD-1 antibodies, leads to suboptimal efficacy/reduced bioavailability of therapeutic monoclonal antibodies (95). In ICI-treated NSCLC patients, the role of sPD-1 is still unclear and is described in a dynamic context (18, 19, 96). Mainly, dynamic increase in sPD-1 after anti-PD-1 treatment has been significantly associated with disease progression, indicating that as sPD-1 levels increase, it strengthens T cell inhibition and cancer immune evasion, thus resulting in poor outcome (18, 19, 96). Our result shows that in the anti-PD-1/PD-L1 group, low pre-treatment sPD-1 levels are associated with patients' response to treatment. We postulate that low expression of sPD-1 may induce a weak affinity for membranous PD-1 thus allowing benefit to therapeutic anti-PD-1 antibodies to effectively bind and induce an active anti-tumor response. However, since we did not assess its modulation after treatment, we cannot comment on its dynamic role in immune regulation (as described in earlier studies). Our group is conducting a study on pre- and post-treatment sPD-1 levels which may give better insight into this aspect.

We also identified S100A8/A9 as a biomarker in non-responding patients on anti-PD-1/PD-L1 monotherapy. In tumors, pro-inflammatory S100A8/A9 production helps sustain MDSC accumulation for maintaining immune suppressive TME and facilitating tumor immune escape (97, 98). In lung cancers, S100A8/A9 overexpression has been implicated in the promotion of pre-metastatic niches, anchorage-independent invasion, and tumor cell proliferation (99, 100). Several studies on NSCLC have also associated overexpression of S100A8/A9 with poor survival and a high relapse rate (100–103). Moreover, the blockade of S100A8/A9 by anti-S100A8/A9 monoclonal antibodies demonstrated significant inhibition of lung metastasis in a mouse model (104). With respect to anti-PD-1 treatment, studies on head and neck, gastric, and melanoma have reported high levels of S100A8/A9 in non-responding patients indicating its role in ICI treatment resistance (105–108). However, studies on the role of S100A8/A9

in NSCLC patients treated with immune checkpoint inhibitors are limited. One single study, conducted on extracellular vesicle (EVs) proteins in 31 ICI-treated NSCLC patients, reported dynamic modulation of S100A8 with increased baseline associated with increased chemotaxis of myeloid cells (S100A8) while decreased expression (after treatment) was associated with inhibition of myeloid cell chemotaxis with induction of treatment response (109). Our result supports such a mechanism where the increased expression of S100A8/A9 may lead to increased chemotaxis of myeloid cells, and this resulted in immune suppression and resistance to the response. Additionally, results from other cancers (described above) corroborate with our study findings indicating the significance of S100A8/A9 as a novel predictive biomarker in ICI-treated NSCLC patients.

Having identified discriminatory markers in different treatment types, we intended to evaluate the predictive biomarkers of response irrespective of the treatment types used. This objective aimed to identify generalized biomarkers that could help to stratify responders vs. non-responders in patients on any type of ICI regimen. We observed downregulation of sCD80, CEA and sTIMD4 in responding patients. For TIMD4, the optimal value of <600 pg/ml was found to discriminate responders from non-responders with sensitivity and specificity of 75 to 66%, respectively. However, this optimal value could not be associated significantly with PFS. As discussed earlier, the mechanism of TIMD4 is still unclear. However, its low expression has been associated with better overall survival in NSCLC, indicating its potential as a prognostic/predictive biomarker (81, 83, 110). Since our results did not show its association with the response (as observed in previous studies), we hypothesize that synergistic expression of circulating immune modulatory molecules such as CD80, CEA, etc., with TIMD4 may be playing their role in influencing its association. Furthermore, it is possible that the role of TIMD4 as a predictive biomarker may be associated with its dynamic modulation in pre- and post-treatment samples.

In addition to sTIMD4, an optimal cut-off value of sCD80 level (<91.7 pg/ml) was found to be able to discriminate responders from non-responders and PFS. Briefly, soluble CD80 is generated *via* splicing of membranous CD80 (111). Though sCD80 lacks a transmembrane domain, it can still bind to CTLA-4, CD28 and activated T cells (111). Based on its ability to interact with both co-stimulatory (CD28) and co-inhibitory (CTLA-4) molecules, its role in immune modulation is contradictory. Its engagement with CD28 and PD-L1 is associated with T cell activation, while it's binding with CTLA-4 can lead to co-inhibition of T cells leading to tumor immune escape and progression (112, 113). Moreover, sCD80 can compete with membrane-bound mCD80 on antigen-presenting cells thus reducing its co-stimulatory effects on T cells making the tumor invisible to the immune cells (114). Studies on prostate cancer, hematological malignancies, renal cell carcinoma, and NSCLC have associated low serum CD80 expression with progression-free survival while high levels are associated with enhanced invasiveness and poor prognosis (115–118). In this context, our results corroborate with previous findings. However, in our study, multivariate analysis did not identify sCD80 as an independent predictive biomarker in this cohort. This could be due to the inherent characteristic of this marker to form intricate, complex relationships with other checkpoints such as PD-L1, CD28, and CTLA4, making it a dynamic rather than an independent marker (119, 120). Larger comprehensive studies on sCD80 will help to provide a better understanding of this marker in ICI- treated NSCLC patients.

Our study identified CEA as a highly robust predictive biomarker in the ICI-treated NSCLC patient cohort. The optimal cut-off value of CEA <1614 pg/ml was associated with not only its ability to discriminate responders vs. non-responders but also with PFS and as an independent predictor of response. The role of CEA in its prognostic/predictive capacity has been documented for several cancers (23, 25, 27). However, limited studies have reported on this important tumor marker in ICI-treated NSCLC patients. Results from these studies showed high baseline CEA levels followed by a decrease of more than or equal to 20% within 4-6 weeks of immunotherapy treatment to be associated with response (23, 25, 27). Our study is the first to associate a specific cut-off, observed prior to treatment, to be associated with response prediction. As CEA is a routinely used marker in diagnostic settings, its utility in ICI treatment is complemented by this cut-off-value that could help in the early stratification of patients for efficient treatment management. Moreover, the mechanism of CEA in immune modulation (discussed earlier) further evidences its potential as a robust predictive biomarker in NSCLC patients treated with ICI.

The main limitation of this study is that we were unable to evaluate serum levels of immunosuppressive factors in a control group of individuals without NSCLC with approximately the same age and comorbidity profile as the patients. Since comorbidities such as atherosclerosis, inflammatory diseases, metabolic disorders, lifestyle and age are important factors of immune landscape change and can significantly influence the level of immunosuppressive mediators and cells in the blood, this could give a broader understanding of the immune mediators. However, due to the scope of study focusing only on patients and non-availability of healthy controls of same age and comorbidity profile as the patients, we were unable to assess this aspect.

Conclusions

Identifying soluble, non-invasive immune oncology and tumor antigens as biomarkers of response in ICI treated-NSCLC cohort is an emerging and exciting field that can help better understand immune regulatory mechanisms and their role in anti-tumor responses. This understanding can help to stratify responding patients from non-responding ones early in the treatment timeline thus aiding in robust treatment management. We were able to identify NK/T cell markers as biomarkers for TPD-L1 and CEA as robust predictive biomarkers of response in the ICI-treated NSCLC patient cohort. We have presented several novel early biomarkers concerning TPD-L1 expression and treatment response that have not been reported in previous studies, which is the main strength of this study. However, limitations of the study include a small sample size in a single-center study. We tried to

overcome these limitations with robust analysis with recommendation that our study results serve as a foundation for large-scale studies for better patient stratification and management.

Data availability statement

The original contributions presented in the study are included in the article/Supplementary Material. Further inquiries can be directed to the corresponding author.

Ethics statement

The studies involving human participants were reviewed and approved by The Institutional Review Board, Medical Research Center, Hamad Medical Corporation, Doha, Qatar. The patients/participants provided their written informed consent to participate in this study.

Author contributions

Conceptualization, supervision, validation: AR, RM, AK, SD. Data curation, formal analysis, Software: AR, MI. Funding acquisition: AR, SD. Investigation, methodology, resources: AR, SA, AZ, SH, KP, AA-S, IA-B, WA, RA-A, SAS, SH. Project administration: AR, AP, SV, SH, MT. Visualization, roles/writing - original draft: AR. Writing - review & editing: AR, MM, VP, SU, SD, UA. All authors contributed to the article and approved the submitted version.

Funding

This research was funded by Academic Health System, Medical Research Center, Hamad Medical Corporation, Doha, Qatar, grant number MRC-01-20-507 and the Article Processing Charges was funded by Academic Health System, Medical Research Center, Hamad Medical Corporation, Doha, Qatar. The funders were not involved in the study design, collection, analysis, interpretation of data, the writing of this article or the decision to submit it for publication.

Acknowledgments

We would like to acknowledge all the enrolled patients for their participation.

Conflict of interest

Authors AR, RM, AK, AZ, AP, SV, SH, KP, AA-S, D-AE, VP, MM, IA-B, WA, RA-A, SAS, SH, SU, UA, SD were employed by Hamad Medical Corporation.

The remaining authors declare that the research was conducted in the absence of any commercial or financial relationships that could be construed as a potential conflict of interest.

Publisher's note

Supplementary material

The Supplementary Material for this article can be found online at: https://www.frontiersin.org/articles/10.3389/fimmu.2023.1157100/full#supplementary-material

References

1. Sung H, Ferlay J, Siegel RL, Laversanne M, Soerjomataram I, Jemal A, et al. Global cancer statistics 2020: GLOBOCAN estimates of incidence and mortality worldwide for 36 cancers in 185 countries. *CA Cancer J Clin* (2021) 71(3):209–49. doi: 10.3322/caac.21660

2. Siegel RL, Miller KD, Jemal A. Cancer statistics, 2019. *CA Cancer J Clin* (2019) 69 (1):7–34. doi: 10.3322/caac.21551

3. Daga A, Ansari A, Patel S, Mirza S, Rawal R, Umrania V. Current drugs and drug targets in non-small cell lung cancer: limitations and opportunities. *Asian Pac J Cancer Prev* (2015) 16(10):4147–56. doi: 10.7314/APJCP.2015.16.10.4147

4. Twomey JD, Zhang B. Cancer immunotherapy update: FDA-approved checkpoint inhibitors and companion diagnostics. *AAPS J* (2021) 23(2):39. doi: 10.1208/s12248-021-00574-0

5. Berghmans T, Durieux V, Hendriks LEL, Dingemans AM. Immunotherapy: from advanced NSCLC to early stages, an evolving concept. *Front Med (Lausanne)* (2020) 7:90. doi: 10.3389/fmed.2020.00090

6. Sharma P, Hu-Lieskovan S, Wargo JA, Ribas A. Primary, adaptive, and acquired resistance to cancer immunotherapy. *Cell* (2017) 168(4):707–23. doi: 10.1016/j.cell.2017.01.017

7. Pilla L, Maccalli C. Immune profiling of cancer patients treated with immunotherapy: advances and challenges. *Biomedicines* (2018) 6(3):76. doi: 10.3390/biomedicines6030076

8. Matsuo N, Azuma K, Hattori S, Ohtake J, Kawahara A, Ishii H, et al. Association between soluble immune mediators and tumor responses in patients with nonsmall cell lung cancer treated with anti-PD-1 inhibitor. *Int J Cancer* (2019) 144(5):1170–9. doi: 10.1002/ijc.31923

9. Raza A, Merhi M, Relecom A, Fernandes Q, Inchakalody V, Gul ARZ, et al. Evolving dynamic biomarkers for prediction of immune responses to checkpoint inhibitors in cancer. *Adv Precis Med Oncol* (2020). doi: 10.5772/intechopen.96494

10. Gu D, Ao X, Yang Y, Chen Z, Xu X. Soluble immune checkpoints in cancer: production, function and biological significance. *J Immunother Cancer* (2018) 6(1):132. doi: 10.1186/s40425-018-0449-0

11. He L, Zhang G, He Y, Zhu H, Zhang H, Feng Z. Blockade of B7-H1 with sPD-1 improves immunity against murine hepatocarcinoma. *Anticancer Res* (2005) 25 (5):3309–13.

12. Kuipers H, Muskens F, Willart M, Hijdra D, van Assema FB, Coyle AJ, et al. Contribution of the PD-1 ligands/PD-1 signaling pathway to dendritic cell-mediated

CD4+ T cell activation. *Eur J Immunol* (2006) 36(9):2472–82. doi: 10.1002/eji.200635978

13. Song MY, Park SH, Nam HJ, Choi DH, Sung YC. Enhancement of vaccine-induced primary and memory CD8(+) T-cell responses by soluble PD-1. *J Immunother* (2011) 34(3):297–306. doi: 10.1097/CJI.0b013e318210ed0e

14. Costantini A, Julie C, Dumenil C, Helias-Rodzewicz Z, Tisserand J, Dumoulin J, et al. Predictive role of plasmatic biomarkers in advanced non-small cell lung cancer treated by nivolumab. *Oncoimmunology* (2018) 7(8):e1452581. doi: 10.1183/13993003.congress-2018.OA3302

15. Okuma Y, Wakui H, Utsumi H, Sagawa Y, Hosomi Y, Kuwano K, et al. Soluble programmed cell death ligand 1 as a novel biomarker for nivolumab therapy for non-small-cell lung cancer. *Clin Lung Cancer* (2018) 19(5):410–7 e1. doi: 10.1016/j.cllc.2018.04.014

16. Bonomi M, Ahmed T, Addo S, Kooshki M, Palmieri D, Levine BJ, et al. Circulating immune biomarkers as predictors of the response to pembrolizumab and weekly low dose carboplatin and paclitaxel in NSCLC and poor PS: an interim analysis. *Oncol Lett* (2019) 17(1):1349–56. doi: 10.3892/ol.2018.9724

17. Tiako Meyo M, Jouinot A, Giroux-Leprieur E, Fabre E, Wislez M, Alifano M, et al. Predictive value of soluble PD-1, PD-L1, VEGFA, CD40 ligand and CD44 for nivolumab therapy in advanced non-small cell lung cancer: a case-control study. *Cancers (Basel)* (2020) 12(2):473. doi: 10.3390/cancers12020473

18. Zizzari IG, Di Filippo A, Scirocchi F, Di Pietro FR, Rahimi H, Ugolini A, et al. Soluble immune checkpoints, gut metabolites and performance status as parameters of response to nivolumab treatment in NSCLC patients. *J Pers Med* (2020) 10(4):208. doi: 10.3390/jpm10040208

19. Ohkuma R, Ieguchi K, Watanabe M, Takayanagi D, Goshima T, Onoue R, et al. Increased plasma soluble PD-1 concentration correlates with disease progression in patients with cancer treated with anti-PD-1 antibodies. *Biomedicines* (2021) 9(12):1929. doi: 10.3390/biomedicines9121929

20. Hao C, Zhang G, Zhang L. Serum CEA levels in 49 different types of cancer and noncancer diseases. *Prog Mol Biol Transl Sci* (2019) 162:213–27. doi: 10.1016/bs.pmbts.2018.12.011

21. Moriyama J, Oshima Y, Nanami T, Suzuki T, Yajima S, Shiratori F, et al. Prognostic impact of CEA/CA19-9 at the time of recurrence in patients with gastric cancer. *Surg Today* (2021) 51(10):1638–48. doi: 10.1007/s00595-021-02248-y

22. Zhang J, Wei Q, Dong D, Ren L. The role of TPS, CA125, CA15-3 and CEA in prediction of distant metastasis of breast cancer. *Clin Chim Acta* (2021) 523:19–25. doi: 10.1016/j.cca.2021.08.027

23. Dal Bello MG, Filiberti RA, Alama A, Orengo AM, Mussap M, Coco S, et al. The role of CEA, CYFRA21-1 and NSE in monitoring tumor response to nivolumab in advanced non-small cell lung cancer (NSCLC) patients. *J Transl Med* (2019) 17(1):74. doi: 10.1186/s12967-019-1828-0

24. Lang D, Haslinger W, Akbari K, Scala M, Hergan B, Asel C, et al. Serum tumor marker dynamics as predictive biomarkers in NSCLC chemo-immunotherapy and mono-immunotherapy maintenance: a registry-based descriptive study. *Lung Cancer (Auckl)* (2020) 11:113–21. doi: 10.2147/LCTT.S286228

25. Zhang Z, Yuan F, Chen R, Li Y, Ma J, Yan X, et al. Dynamics of serum tumor markers can serve as a prognostic biomarker for Chinese advanced non-small cell lung cancer patients treated with immune checkpoint inhibitors. *Front Immunol* (2020) 11:1173. doi: 10.3389/fimmu.2020.01173

26. Clevers MR, Kastelijn EA, Peters BJM, Kelder H, Schramel F. Evaluation of serum biomarker CEA and Ca-125 as immunotherapy response predictors in metastatic non-small cell lung cancer. *Anticancer Res* (2021) 41(2):869–76. doi: 10.21873/anticanres.14839

27. Muller M, Hoogendoorn R, Moritz RJG, van der Noort V, Lanfermeijer M, Korse CM, et al. Validation of a clinical blood-based decision aid to guide immunotherapy treatment in patients with non-small cell lung cancer. *Tumour Biol* (2021) 43(1):115–27. doi: 10.3233/TUB-219007

28. Postow MA, Callahan MK, Wolchok JD. Immune checkpoint blockade in cancer therapy. *J Clin Oncol* (2015) 33(17):1974–82. doi: 10.1200/JCO.2014.59.4358

29. Abdel-Rahman O. Correlation between PD-L1 expression and outcome of NSCLC patients treated with anti-PD-1/PD-L1 agents: a meta-analysis. *Crit Rev Oncol Hematol* (2016) 101:75–85. doi: 10.1016/j.critrevonc.2016.03.007

30. Borghaei H, Paz-Ares L, Horn L, Spigel DR, Steins M, Ready NE, et al. Nivolumab versus docetaxel in advanced nonsquamous non-Small-Cell lung cancer. *N Engl J Med* (2015) 373(17):1627–39. doi: 10.1056/NEJMoa1507643

31. Carbone DP, Reck M, Paz-Ares L, Creelan B, Horn L, Steins M, et al. First-line nivolumab in stage IV or recurrent non-Small-Cell lung cancer. *N Engl J Med* (2017) 376(25):2415–26. doi: 10.1056/NEJMoa1613493

32. Zhao Q, Xie R, Lin S, You X, Weng X. Anti-PD-1/PD-L1 antibody therapy for pretreated advanced or metastatic nonsmall cell lung carcinomas and the correlation between PD-L1 expression and treatment effectiveness: an update meta-analysis of randomized clinical trials. *BioMed Res Int* (2018) 2018:3820956. doi: 10.1155/2018/3820956

33. Xu Y, Wan B, Chen X, Zhan P, Zhao Y, Zhang T, et al. The association of PD-L1 expression with the efficacy of anti- PD-1/PD-L1 immunotherapy and survival of non-small cell lung cancer patients: a meta-analysis of randomized controlled trials. *Trans Lung Cancer Res* (2019) 8(4):413–28. doi: 10.21037/tlcr.2019.08.09

34. Li C, Li C, Zhi C, Liang W, Wang X, Chen X, et al. Clinical significance of PD-L1 expression in serum-derived exosomes in NSCLC patients. *J Transl Med* (2019) 17(1):355. doi: 10.1186/s12967-019-2101-2

35. Oh SY, Kim S, Keam B, Kim TM, Kim DW, Heo DS. Soluble PD-L1 is a predictive and prognostic biomarker in advanced cancer patients who receive immune checkpoint blockade treatment. *Sci Rep* (2021) 11(1):19712. doi: 10.1038/s41598-021-99311-y

36. Yang Q, Chen M, Gu J, Niu K, Zhao X, Zheng L, et al. Novel biomarkers of dynamic blood PD-L1 expression for immune checkpoint inhibitors in advanced non-Small-Cell lung cancer patients. *Front Immunol* (2021) 12:665133. doi: 10.3389/fimmu.2021.665133

37. Relecom A, Merhi M, Inchakalody V, Uddin S, Rinchai D, Bedognetti D, et al. Emerging dynamics pathways of response and resistance to PD-1 and CTLA-4 blockade: tackling uncertainty by confronting complexity. *J Exp Clin Cancer Res* (2021) 40(1):74. doi: 10.1186/s13046-021-01872-3

38. Dermime S, Merhi M, Merghoub T. Editorial: dynamic biomarkers of response to anti-immune checkpoint inhibitors in cancer. *Front Immunol* (2021) 12:781872. doi: 10.3389/fimmu.2021.781872

39. Zhang N, Liang R, Gensheimer MF, Guo M, Zhu H, Yu J, et al. Early response evaluation using primary tumor and nodal imaging features to predict progression-free survival of locally advanced non-small cell lung cancer. *Theranostics* (2020) 10(25):11707–18. doi: 10.7150/thno.50565

40. Oitaben A, Fonseca P, Villanueva MJ, Garcia-Benito C, Lopez-Lopez A, Garrido-Fernandez A, et al. Emerging blood-based biomarkers for predicting immunotherapy response in NSCLC. *Cancers (Basel)* (2022) 14(11):2626. doi: 10.3390/cancers14112626

41. Wang M, Zhai X, Li J, Guan J, Xu S, Li YY, et al. The role of cytokines in predicting the response and adverse events related to immune checkpoint inhibitors. *Front Immunol* (2021) 12. doi: 10.3389/fimmu.2021.670391

42. Wang Y, Tong Z, Zhang W, Zhang W, Buzdin A, Mu X, et al. FDA-Approved and emerging next generation predictive biomarkers for immune checkpoint inhibitors in cancer patients. *Front Oncol* (2021) 11:683419. doi: 10.3389/fonc.2021.683419

43. Paz-Ares L, Luft A, Vicente D, Tafreshi A, Gumus M, Mazieres J, et al. Pembrolizumab plus chemotherapy for squamous non-Small-Cell lung cancer. *N Engl J Med* (2018) 379(21):2040–51. doi: 10.1056/NEJMoa1810865

44. Rossi G, Russo A, Tagliamento M, Tuzi A, Nigro O, Vallome G, et al. Precision medicine for NSCLC in the era of immunotherapy: new biomarkers to select the most suitable treatment or the most suitable patient. *Cancers (Basel)* (2020) 12(5):1125. doi: 10.3390/cancers12051125

45. Duan S, Paulson JC. Siglecs as immune cell checkpoints in disease. *Annu Rev Immunol* (2020) 38:365–95. doi: 10.1146/annurev-immunol-102419-035900

46. Chen Z, Yu M, Guo L, Zhang B, Liu S, Zhang W, et al. Tumor derived SIGLEC family genes may play roles in tumor genesis, progression, and immune microenvironment regulation. *Front Oncol* (2020) 10:586820. doi: 10.3389/fonc.2020.586820

47. Bull C, den Brok MH, Adema GJ. Sweet escape: sialic acids in tumor immune evasion. *Biochim Biophys Acta* (2014) 1846(1):238–46. doi: 10.1016/j.bbcan.2014.07.005

48. Jandus C, Boligan KF, Chijioke O, Liu H, Dahlhaus M, Demoulins T, et al. Interactions between siglec-7/9 receptors and ligands influence NK cell-dependent tumor immunosurveillance. *J Clin Invest* (2014) 124(4):1810–20. doi: 10.1172/JCI65899

49. Haas Q, Boligan KF, Jandus C, Schneider C, Simillion C, Stanczak MA, et al. Siglec-9 regulates an effector memory CD8(+) T-cell subset that congregates in the melanoma tumor microenvironment. *Cancer Immunol Res* (2019) 7(5):707–18. doi: 10.1158/2326-6066.CIR-18-0505

50. Stanczak MA, Siddiqui SS, Trefny MP, Thommen DS, Boligan KF, von Gunten S, et al. Self-associated molecular patterns mediate cancer immune evasion by engaging siglecs on T cells. *J Clin Invest* (2018) 128(11):4912–23. doi: 10.1172/JCI120612

51. Wherry EJ, Kurachi M. Molecular and cellular insights into T cell exhaustion. *Nat Rev Immunol* (2015) 15(8):486–99. doi: 10.1038/nri3862

52. Thommen DS, Schreiner J, Muller P, Herzig P, Roller A, Belousov A, et al. Progression of lung cancer is associated with increased dysfunction of T cells defined by coexpression of multiple inhibitory receptors. *Cancer Immunol Res* (2015) 3(12):1344–55. doi: 10.1158/2326-6066.CIR-15-0097

53. Laubli H, Pearce OM, Schwarz F, Siddiqui SS, Deng L, Stanczak MA, et al. Engagement of myelomonocytic siglecs by tumor-associated ligands modulates the innate immune response to cancer. *Proc Natl Acad Sci U S A* (2014) 111(39):14211–6. doi: 10.1073/pnas.1409580111

54. Eagle RA, Trowsdale J. Promiscuity and the single receptor: NKG2D. *Nat Rev Immunol* (2007) 7(9):737–44. doi: 10.1038/nri2144

55. Cosman D, Mullberg J, Sutherland CL, Chin W, Armitage R, Fanslow W, et al. ULBPs, novel MHC class I-related molecules, bind to CMV glycoprotein UL16 and stimulate NK cytotoxicity through the NKG2D receptor. *Immunity* (2001) 14(2):123–33. doi: 10.1016/S1074-7613(01)00095-4

56. Kong Y, Cao W, Xi X, Ma C, Cui L, He W. The NKG2D ligand ULBP4 binds to TCRgamma9/delta2 and induces cytotoxicity to tumor cells through both TCRgammadelta and NKG2D. *Blood* (2009) 114(2):310–7. doi: 10.1182/blood-2008-12-196287

57. Conejo-Garcia JR, Benencia F, Courreges MC, Khang E, Zhang L, Mohamed-Hadley A, et al. Letal, a tumor-associated NKG2D immunoreceptor ligand, induces activation and expansion of effector immune cells. *Cancer Biol Ther* (2003) 2(4):446–51. doi: 10.4161/cbt.2.4.479

58. Zoller T, Wittenbrink M, Hoffmeister M, Steinle A. Cutting an NKG2D ligand short: cellular processing of the peculiar human NKG2D ligand ULBP4. *Front Immunol* (2018) 9:620. doi: 10.3389/fimmu.2018.00620

59. Cao W, Xi X, Wang Z, Dong L, Hao Z, Cui L, et al. Four novel ULBP splice variants are ligands for human NKG2D. *Int Immunol* (2008) 20(8):981–91. doi: 10.1093/intimm/dxn057

60. Arreygue-Garcia NA, Daneri-Navarro A, del Toro-Arreola A, Cid-Arregui A, Gonzalez-Ramella O, Jave-Suarez LF, et al. Augmented serum level of major histocompatibility complex class I-related chain a (MICA) protein and reduced NKG2D expression on NK and T cells in patients with cervical cancer and precursor lesions. *BMC Cancer* (2008) 8:16. doi: 10.1186/1471-2407-8-16

61. Groh V, Smythe K, Dai Z, Spies T. Fas-ligand-mediated paracrine T cell regulation by the receptor NKG2D in tumor immunity. *Nat Immunol* (2006) 7 (7):755–62. doi: 10.1038/ni1350

62. Xu Y, Zhou L, Zong J, Ye Y, Chen G, Chen Y, et al. Decreased expression of the NKG2D ligand ULBP4 may be an indicator of poor prognosis in patients with nasopharyngeal carcinoma. *Oncotarget* (2017) 8(26):42007–19. doi: 10.18632/oncotarget.14917

63. Zhang X, Rao A, Sette P, Deibert C, Pomerantz A, Kim WJ, et al. IDH mutant gliomas escape natural killer cell immune surveillance by downregulation of NKG2D ligand expression. *Neuro Oncol* (2016) 18(10):1402–12. doi: 10.1093/neuonc/now061

64. Eisele G, Wischhusen J, Mittelbronn M, Meyermann R, Waldhauer I, Steinle A, et al. TGF-beta and metalloproteinases differentially suppress NKG2D ligand surface expression on malignant glioma cells. *Brain* (2006) 129(Pt 9):2416–25. doi: 10.1093/brain/awl205

65. Latchman Y, Wood CR, Chernova T, Chaudhary D, Borde M, Chernova I, et al. PD-L2 is a second ligand for PD-1 and inhibits T cell activation. *Nat Immunol* (2001) 2 (3):261–8. doi: 10.1038/85330

66. Larsen TV, Hussmann D, Nielsen AL. PD-L1 and PD-L2 expression correlated genes in non-small-cell lung cancer. *Cancer Commun (Lond)* (2019) 39(1):30. doi: 10.1186/s40880-019-0376-6

67. Obeid JM, Erdag G, Smolkin ME, Deacon DH, Patterson JW, Chen L, et al. PD-L1, PD-L2 and PD-1 expression in metastatic melanoma: correlation with tumor-infiltrating immune cells and clinical outcome. *Oncoimmunology* (2016) 5(11): e1235107. doi: 10.1080/2162402X.2016.1235107

68. Miao YR, Thakkar KN, Qian J, Kariolis MS, Huang W, Nandagopal S, et al. Neutralization of PD-L2 is essential for overcoming immune checkpoint blockade resistance in ovarian cancer. *Clin Cancer Res* (2021) 27(15):4435–48. doi: 10.1158/1078-0432.CCR-20-0482

69. Shimada Y, Matsubayashi J, Kudo Y, Maehara S, Takeuchi S, Hagiwara M, et al. Serum-derived exosomal PD-L1 expression to predict anti-PD-1 response and in patients with non-small cell lung cancer. *Sci Rep* (2021) 11(1):7830. doi: 10.1038/s41598-021-87575-3

70. Murakami S, Shibaki R, Matsumoto Y, Yoshida T, Goto Y, Kanda S, et al. Association between serum level soluble programmed cell death ligand 1 and prognosis in patients with non-small cell lung cancer treated with anti-PD-1 antibody. *Thorac Cancer* (2020) 11(12):3585–95. doi: 10.1111/1759-7714.13721

71. He XH, Liu Y, Xu LH, Zeng YY. Cloning and identification of two novel splice variants of human PD-L2. *Acta Biochim Biophys Sin (Shanghai)* (2004) 36(4):284–9. doi: 10.1093/abbs/36.4.284

72. Gao J, Qiu X, Li X, Fan H, Zhang F, Lv T, et al. Expression profiles and clinical value of plasma exosomal Tim-3 and galectin-9 in non-small cell lung cancer. *Biochem Biophys Res Commun* (2018) 498(3):409–15. doi: 10.1016/j.bbrc.2018.02.114

73. Ak N, Serilmez M, Üçüncü MZ, Bademler S, Vatansever S. Nectin-2 and nectin-4 adhesion molecules in patients with breast cancer. *Turkish J Oncol* (2021) 36(2):165–70. doi: 10.5505/tjo.2021.2697

74. Erturk K, Karaman S, Dagoglu N, Serilmez M, Duranyildiz D, Tas F. Serum nectin-2 and nectin-4 are diagnostic in lung cancer: which is superior? *Wien Klin Wochenschr* (2019) 131(17-18):419–26. doi: 10.1007/s00508-019-01537-4

75. Li M, Qiao D, Pu J, Wang W, Zhu W, Liu H. Elevated nectin-2 expression is involved in esophageal squamous cell carcinoma by promoting cell migration and invasion. *Oncol Lett* (2018) 15(4):4731–6. doi: 10.3892/ol.2018.7953

76. Karabulut M, Gunaldi M, Alis H, Afsar CU, Karabulut S, Serilmez M, et al. Serum nectin-2 levels are diagnostic and prognostic in patients with colorectal carcinoma. *Clin Transl Oncol* (2016) 18(2):160–71. doi: 10.1007/s12094-015-1348-1

77. Sim YH, Um YJ, Park JY, Seo MD, Park SG. A novel antibody-drug conjugate targeting nectin-2 suppresses ovarian cancer progression in mouse xenograft models. *Int J Mol Sci* (2022) 23(20):12358. doi: 10.3390/ijms232012358

78. Oshima T, Sato S, Kato J, Ito Y, Watanabe T, Tsuji I, et al. Nectin-2 is a potential target for antibody therapy of breast and ovarian cancers. *Mol Cancer* (2013) 12:60. doi: 10.1186/1476-4598-12-60

79. Shi B, Chu J, Huang T, Wang X, Li Q, Gao Q, et al. The scavenger receptor MARCO expressed by tumor-associated macrophages are highly associated with poor pancreatic cancer prognosis. *Front Oncol* (2021) 11:771488. doi: 10.3389/fonc.2021.771488

80. Li Y, Zhang PY, Yang ZW, Ma F, Li FX. TIMD4 exhibits regulatory capability on the proliferation and apoptosis of diffuse large b-cell lymphoma cells *via* the wnt/beta-catenin pathway. *J Gene Med* (2020) 22(8):e3186. doi: 10.1002/jgm.3186

81. Yano H, Motoshima T, Ma C, Pan C, Yamada S, Nakayama T, et al. The significance of TIMD4 expression in clear cell renal cell carcinoma. *Med Mol Morphol* (2017) 50(4):220–6. doi: 10.1007/s00795-017-0164-9

82. Li W, Li X, Xu S, Ma X, Zhang Q. Expression of Tim4 in glioma and its regulatory role in LN-18 glioma cells. *Med Sci Monit* (2016) 22:77–82. doi: 10.12659/MSM.894963

83. Zhang Q, Wang H, Wu X, Liu B, Liu W, Wang R, et al. TIM-4 promotes the growth of non-small-cell lung cancer in a RGD motif-dependent manner. *Br J Cancer* (2015) 113(10):1484–92. doi: 10.1038/bjc.2015.323

84. Nakamura Y, Shida D, Tanabe T, Takamizawa Y, Imaizumi J, Ahiko Y, et al. Prognostic impact of preoperatively elevated and postoperatively normalized carcinoembryonic antigen levels following curative resection of stage I-III rectal cancer. *Cancer Med* (2020) 9(2):653–62. doi: 10.1002/cam4.2758

85. Zhao W, Li X, Wang W, Chen B, Wang L, Zhang N, et al. Association of preoperative serum levels of CEA and CA15-3 with molecular subtypes of breast cancer. *Dis Markers* (2021) 2021:5529106. doi: 10.1155/2021/5529106

86. Baqar AR, Wilkins S, Staples M, Angus Lee CH, Oliva K, McMurrick P. The role of preoperative CEA in the management of colorectal cancer: a cohort study from two cancer centres. *Int J Surg* (2019) 64:10–5. doi: 10.1016/j.ijsu.2019.02.014

87. Nasralla A, Lee J, Dang J, Turner S. Elevated preoperative CEA is associated with subclinical nodal involvement and worse survival in stage I non-small cell lung cancer: a systematic review and meta-analysis. *J Cardiothorac Surg* (2020) 15(1):318. doi: 10.1186/s13019-020-01353-2

88. Cui Y, Li X, Du B, Diao Y, Li Y. PD-L1 in lung adenocarcinoma: insights into the role of (18)F-FDG PET/CT. *Cancer Manag Res* (2020) 12:6385–95. doi: 10.2147/CMAR.S256871

89. Sam J, Colombetti S, Fauti T, Roller A, Biehl M, Fahrni L, et al. Combination of T-cell bispecific antibodies with PD-L1 checkpoint inhibition elicits superior anti-tumor activity. *Front Oncol* (2020) 10:575737. doi: 10.3389/fonc.2020.575737

90. Del Rivero J, Donahue RN, Marte JL, Gramza AW, Bilusic M, Rauckhorst M, et al. A case report of sequential use of a yeast-CEA therapeutic cancer vaccine and anti-PD-L1 inhibitor in metastatic medullary thyroid cancer. *Front Endocrinol (Lausanne)* (2020) 11:490. doi: 10.3389/fendo.2020.00490

91. Bacac M, Klein C, Umana P. CEA TCB: a novel head-to-tail 2:1 T cell bispecific antibody for treatment of CEA-positive solid tumors. *Oncoimmunology* (2016) 5(8): e1203498. doi: 10.1080/2162402X.2016.1203498

92. Bacac M, Fauti T, Sam J, Colombetti S, Weinzierl T, Ouaret D, et al. A novel carcinoembryonic antigen T-cell bispecific antibody (CEA TCB) for the treatment of solid tumors. *Clin Cancer Res* (2016) 22(13):3286–97. doi: 10.1158/1078-0432.CCR-15-1696

93. Osada T, Patel SP, Hammond SA, Osada K, Morse MA, Lyerly HK. CEA/CD3-bispecific T cell-engaging (BiTE) antibody-mediated T lymphocyte cytotoxicity maximized by inhibition of both PD1 and PD-L1. *Cancer Immunol Immunother* (2015) 64(6):677–88. doi: 10.1007/s00262-015-1671-y

94. Osada T, Hsu D, Hammond S, Hobeika A, Devi G, Clay TM, et al. Metastatic colorectal cancer cells from patients previously treated with chemotherapy are sensitive to T-cell killing mediated by CEA/CD3-bispecific T-cell-engaging BiTE antibody. *Br J Cancer* (2010) 102(1):124–33. doi: 10.1038/sj.bjc.6605364

95. Khan M, Zhao Z, Arooj S, Fu Y, Liao G. Soluble PD-1: predictive, prognostic, and therapeutic value for cancer immunotherapy. *Front Immunol* (2020) 11:587460. doi: 10.3389/fimmu.2020.587460

96. Sorensen SF, Demuth C, Weber B, Sorensen BS, Meldgaard P. Increase in soluble PD-1 is associated with prolonged survival in patients with advanced EGFR-mutated non-small cell lung cancer treated with erlotinib. *Lung Cancer* (2016) 100:77–84. doi: 10.1016/j.lungcan.2016.08.001

97. Srivastava MK, Andersson A, Zhu L, Harris-White M, Lee JM, Dubinett S, et al. Myeloid suppressor cells and immune modulation in lung cancer. *Immunotherapy* (2012) 4(3):291–304. doi: 10.2217/imt.11.178

98. Zwadlo G, Bruggen J, Gerhards G, Schlegel R, Sorg C. Two calcium-binding proteins associated with specific stages of myeloid cell differentiation are expressed by subsets of macrophages in inflammatory tissues. *Clin Exp Immunol* (1988) 72(3):510–5.

99. Sumardika IW, Chen Y, Tomonobu N, Kinoshita R, Ruma IMW, Sato H, et al. Neuroplastin-beta mediates S100A8/A9-induced lung cancer disseminative progression. *Mol Carcinog* (2019) 58(6):980–95. doi: 10.1002/mc.22987

100. Hiratsuka S, Watanabe A, Sakurai Y, Akashi-Takamura S, Ishibashi S, Miyake K, et al. The S100A8-serum amyloid A3-TLR4 paracrine cascade establishes a pre-metastatic phase. *Nat Cell Biol* (2008) 10(11):1349–55. doi: 10.1038/ncb1794

101. Perego M, Tyurin VA, Tyurina YY, Yellets J, Nacarelli T, Lin C, et al. Reactivation of dormant tumor cells by modified lipids derived from stress-activated neutrophils. *Sci Transl Med* (2020) 12(572):eabb5817. doi: 10.1126/scitranslmed.abb5817

102. Liu Y, Cui J, Tang YL, Huang L, Zhou CY, Xu JX. Prognostic roles of mRNA expression of S100 in non-Small-Cell lung cancer. *BioMed Res Int* (2018) 2018:9815806. doi: 10.1155/2018/9815806

103. Huang H, Huang Q, Tang T, Gu L, Du J, Li Z, et al. Clinical significance of calcium-binding protein S100A8 and S100A9 expression in non-small cell lung cancer. *Thorac Cancer* (2018) 9(7):800–4. doi: 10.1111/1759-7714.12649

104. Kinoshita R, Sato H, Yamauchi A, Takahashi Y, Inoue Y, Sumardika IW, et al. Newly developed anti-S100A8/A9 monoclonal antibody efficiently prevents lung tropic cancer metastasis. *Int J Cancer* (2019) 145(2):569–75. doi: 10.1002/ijc.31982

105. Zhou X, Fang D, Liu H, Ou X, Zhang C, Zhao Z, et al. PMN-MDSCs accumulation induced by CXCL1 promotes CD8(+) T cells exhaustion in gastric cancer. *Cancer Lett* (2022) 532:215598. doi: 10.1016/j.canlet.2022.215598

106. Rad Pour S, Pico de Coana Y, Demorentin XM, Melief J, Thimma M, Wolodarski M, et al. Predicting anti-PD-1 responders in malignant melanoma from the frequency of S100A9+ monocytes in the blood. *J Immunother Cancer* (2021) 9(5): e002171. doi: 10.1136/jitc-2020-002171

107. Kwak T, Wang F, Deng H, Condamine T, Kumar V, Perego M, et al. Distinct populations of immune-suppressive macrophages differentiate from monocytic myeloid-derived suppressor cells in cancer. *Cell Rep* (2020) 33(13):108571. doi: 10.1016/j.celrep.2020.108571

108. Wagner NB, Weide B, Gries M, Reith M, Tarnanidis K, Schuermans V, et al. Tumor microenvironment-derived S100A8/A9 is a novel prognostic biomarker for advanced melanoma patients and during immunotherapy with anti-PD-1 antibodies. *J Immunother Cancer* (2019) 7(1):343. doi: 10.1186/s40425-019-0828-1

109. Brocco D, Lanuti P, Pieragostino D, Cufaro MC, Simeone P, Bologna G, et al. Phenotypic and proteomic analysis identifies hallmarks of blood circulating extracellular vesicles in NSCLC responders to immune checkpoint inhibitors. *Cancers (Basel)* (2021) 13(4):585. doi: 10.3390/cancers13040585

110. Chen S, Wang Y, Liu W, Liang Y, Wang Y, Wu Z, et al. N-glycosylation at Asn291 stabilizes TIM-4 and promotes the metastasis of NSCLC. *Front Oncol* (2022) 12:730530. doi: 10.3389/fonc.2022.730530

111. Kakoulidou M, Giscombe R, Zhao X, Lefvert AK, Wang X. Human soluble CD80 is generated by alternative splicing, and recombinant soluble CD80 binds to CD28 and CD152 influencing T-cell activation. *Scand J Immunol* (2007) 66(5):529–37. doi: 10.1111/j.1365-3083.2007.02009.x

112. Haile ST, Dalal SP, Clements V, Tamada K, Ostrand-Rosenberg S. Soluble CD80 restores T cell activation and overcomes tumor cell programmed death ligand 1-mediated immune suppression. *J Immunol* (2013) 191(5):2829–36. doi: 10.4049/jimmunol.1202777

113. Butte MJ, Keir ME, Phamduy TB, Sharpe AH, Freeman GJ. Programmed death-1 ligand 1 interacts specifically with the B7-1 costimulatory molecule to inhibit T cell responses. *Immunity* (2007) 27(1):111–22. doi: 10.1016/j.immuni.2007.05.016

114. Zang X, Allison JP. The B7 family and cancer therapy: costimulation and coinhibition. *Clin Cancer Res* (2007) 13(18 Pt 1):5271–9. doi: 10.1158/1078-0432.CCR-07-1030

115. Wang Q, He Y, Li W, Xu X, Hu Q, Bian Z, et al. Soluble immune checkpoint-related proteins in blood are associated with invasion and progression in non-small cell lung cancer. *Front Immunol* (2022) 13:887916. doi: 10.3389/fimmu.2022.887916

116. Wang Q, Ye Y, Yu H, Lin SH, Tu H, Liang D, et al. Immune checkpoint-related serum proteins and genetic variants predict outcomes of localized prostate cancer, a cohort study. *Cancer Immunol Immunother* (2021) 70(3):701–12. doi: 10.1007/s00262-020-02718-1

117. Frigola X, Inman BA, Lohse CM, Krco CJ, Cheville JC, Thompson RH, et al. Identification of a soluble form of B7-H1 that retains immunosuppressive activity and is associated with aggressive renal cell carcinoma. *Clin Cancer Res* (2011) 17(7):1915–23. doi: 10.1158/1078-0432.CCR-10-0250

118. Hock BD, Starling GC, Patton WN, Salm N, Bond K, McArthur LT, et al. Identification of a circulating soluble form of CD80: levels in patients with hematological malignancies. *Leuk Lymphoma* (2004) 45(10):2111–8. doi: 10.1080/10428190410001712199

119. Sugiura D, Maruhashi T, Okazaki IM, Shimizu K, Maeda TK, Takemoto T, et al. Restriction of PD-1 function by cis-PD-L1/CD80 interactions is required for optimal T cell responses. *Science* (2019) 364(6440):558–66. doi: 10.1126/science.aav7062

120. Lu D, Ni Z, Liu X, Feng S, Dong X, Shi X, et al. Beyond T cells: understanding the role of PD-1/PD-L1 in tumor-associated macrophages. *J Immunol Res* (2019) 2019:1919082. doi: 10.1155/2019/1919082

10.3389/fimmu.2023.1157100

Glossary

ADCC	Antibody-Dependent Cellular Cytotoxicity
ALK	Anaplastic Lymphoma Kinase;CA-125, Carbohydrate Antigen 125
CD80	Cluster of Differentiation 80;CEA, Carcinoembryonic Antigen
CYFRA21-1	Cytokeratin Fragment 19
DC	Dendritic cells;DNAM-1, DNAX accessory molecule 1;ECOG PS, Eastern Cooperative Oncology Group performance status
EGFR	Epidermal Growth Factor Receptor;ERBB3, Erb-b2 receptor tyrosine kinase 3;ICIs, Immune Checkpoint Inhibitors
IFN-γ	Interferon-Gamma
IHC	Immunohistochemistry
IL-2	Interleukin-2
ITIM	Immunoreceptor Tyrosine-based Inhibition Motif
KRAS	Kirsten rat sarcoma viral oncogene homolog
MDSCs	Myeloid Derived Suppressor Cells
Nectin2	Poliovirus receptor-related 2
NK	Natural killer
NKG2DL	Natural Killer Group 2D Receptor and Ligands
NSCLC	Non-small cell lung cancer
ORR	Objective Response Rate
OS	Overall Survival
PD-1	Programmed Death Protein 1
PD-L1	Programmed Death Ligand 1
PD-L2	Programmed Death Ligand 2
PFS	Progression Free Survival
PVRIG	PVR-related Ig domain
RECIST	Response Evaluation Criteria In Solid Tumors
RGD	Arginine-Glycine-Aspartic acid
ROC	Receiver Operator characteristic curve
S100A8/A9	S100 calcium-binding protein A8/A9
SHP-1/SHP-2	Src Homology 1/2
Siglec7	Sialic acid binding immunoglobulin-like lectin 7
Siglec9	Sialic acid binding immunoglobulin-like lectin 9;T regs, T regulatory cells
TACTILE	T cell activation, increased late expression
TGF-β	Transforming growth factor-β
TIGIT	T-cell immunoglobulin and ITIM domain
TIM3	T cell Immunoglobulin Domain and Mucin domain 3
TIMD4	T-cell immunoglobulin and mucin domain containing 4
TME	Tumor microenvironment
TNF-α	Tumor necrosis factor-α
TPD-L1	Tissue Programmed Death Ligand-1;TPS, Tumor proportional scores
ULBP-1/4	UL16 binding protein ¼.

frontiers | Frontiers in Immunology

TYPE Original Research
PUBLISHED 18 May 2023
DOI 10.3389/fimmu.2023.1170539

OPEN ACCESS

EDITED BY
Takaji Matsutani,
Repertoire Genesis, Inc., Japan

REVIEWED BY
Galal Metwally,
Zagazig University, Egypt
Augustine k. Ballah,
First Affiliated Hospital of Jinan University, China

*CORRESPONDENCE
Yajie Zhao
zyjie5977@csu.edu.cn

RECEIVED 21 February 2023
ACCEPTED 10 May 2023
PUBLISHED 18 May 2023

CITATION
Li Z, Li Y, Tian Y, Li N, Shen L and Zhao Y (2023) Pan-cancer analysis identifies the correlations of Thymosin Beta 10 with predicting prognosis and immunotherapy response.
Front. Immunol. 14:1170539.
doi: 10.3389/fimmu.2023.1170539

Pan-cancer analysis identifies the correlations of Thymosin Beta 10 with predicting prognosis and immunotherapy response

Zhanzhan Li[1], Yanyan Li[2], Yifu Tian[3], Na Li[1], Liangfang Shen[1] and Yajie Zhao[4,5]*

[1]Department of Oncology, Xiangya Hospital, Central South University, Changsha, Hunan, China, [2]Department of Nursing, Xiangya Hospital, Central South University, Changsha, Hunan, China, [3]Department of Pathology, Xiangya Hospital, Central South University, Changsha, Hunan, China, [4]Department of Nuclear Medicine, Xiangya Hospital, Central South University, Changsha, Hunan, China, [5]National Clinical Research Center for Geriatric Disorders, Xiangya Hospital, Central South University, Changsha, Hunan, China

Introduction: The biological function and prognosis roles of thymosin β(TMSB) 10 are still unclear in pan-cancer.

Methods: We retrieved The Cancer Genome Atlas and Genotype-tissue expression datasets to obtain the difference of TMSB10 expression between pan-cancer and normal tissues, and analyzed the biological function and prognosis role of TMSB10 in pan-cancer by using cBioPortal Webtool.

Results: The expression of TMSB10 in tumor tissues was significantly higher than normal tissues, and showed the potential ability to predict the prognosis of patients in Pan-cancer. It was found that TMSB10 was significantly correlated with tumor microenvironment, immune cell infiltration and immune regulatory factor expression. TMSB10 is involved in the regulation of cellular signal transduction pathways in a variety of tumors, thereby mediating the occurrence of tumor cell invasion and metastasis. Finally, TMSB10 can not only effectively predict the anti-PD-L1 treatment response of cancer patients, but also be used as an important indicator to evaluate the sensitivity of chemotherapy. In vitro, low expression of TMSB10 inhibited clonogenic formation ability, invasion, and migration in glioma cells. Furthermore, TMSB10 may involve glioma immune regulation progression by promoting PD-L1 expression levels via activating STAT3 signaling pathway.

Conclusions: Our results show that TMSB10 is abnormally expressed in tumor tissues, which may be related to the infiltration of immune cells in the tumor microenvironment. Clinically, TMSB10 is not only an effective prognostic factor for predicting the clinical treatment outcome of cancer patients, but also a promising biomarker for predicting the effect of tumor immune checkpoint inhibitors (ICIs) and chemotherapy in some cancers.

KEYWORDS

TMSB10, pan-cancer, immunotherapy, prognosis, immune infiltration

Introduction

The thymosin β(TMSB)family members, including TMSB4, TMSB10 and TMSB15, which were originally identified from the thymus. The functions of TMSB mainly to inhibit actin polymerization and disrupt F-actin formation. TMSB10 contains 40-44 amino acid protein and is mainly localized in cytoplasm, which has multiple physiological functions in humans, such as early organ development, apoptosis, proliferation, migration, angiogenesis (1).

Several studies have found that up-regulated expression of TMSB10 is associated with metastasis and invasion in a variety of solid cancers. For example, Overexpression of TMSB10 by activating the AKT/FOXO signaling pathway *in vitro* and *in vivo* could promote proliferation, invasion, and migration of breast cancer (2–4). By mediating the transformation and proliferation of pI3k/AKT signaling pathway, TMSB10 could promote lung adenocarcinoma (2–4). TMSB10 induces renal cell carcinoma by regulating renal epithelial mesenchymal transition (2–4). It is also a key factor in promoting the proliferation of papillary thyroid carcinoma (PTC) and epithelial-mesenchymal transition (EMT) progression, by negatively regulating microRNA (5). Recently, several reports have found that TMSB10 may have a closely relationship with immune infiltration, JUN as one of the activating protein-1 (AP-1) transcription factor, it regulates the expression of TMSB10 through transcription by CHIP assay, which could enrich its biological information function (6, 7).

In our study, we conducted a pan-cancer genomic analysis of TMSB10 across different cancer types by using GTEx and The Cancer Genome Atlas (TCGA) database, evaluating the expression of TMSB10 and its association with the prognosis of patients with different cancers. Furthermore, we examined the relationship between TMSB10 expression and the immune cell infiltration score, immune checkpoints, immune activation genes, immune inhibition genes and the response of immunotherapy and chemotherapy. Finally, we validated our findings *in vitro*. Our research aims to provide a new understanding of TMSB10 in Pan-cancer. The results show that TMSB10 has the potential to affect the tumor microenvironment, cancer immunotherapy and chemotherapy response.

Methods

Data collection and processing

TMSB10 expression in different tissues is based on The Cancer Genome Atlas (TCGA) pan-cancer tissue database and Chinese Glioma Genome Atlas (CGGA), normal human tissue data is based on Genotype-Tissue Expression (GTEx) database, which were downloaded from the UCSC Xena database (https://xenabrowser.net/datapages/) (8). The marked copy number segment, DNA methylation (Illumina human methylation 450), gene expression RNAseq (HTSeq), somatic mutation (SNPx and small INDELs) were also downloaded. The expression profile was converted into transcripts in the format of millions of bases per thousand (TPM) according to the following steps: We call raw data as "read counts", "total reads" are sum of read counts of all genes in each sample. We can obtain a matrix data including genes through the read counts divided by the length of the gene. Finally, we obtained the relative expression data matrix data divided by "total reads", and the data in log2 (TPM+1) format were used for subsequent analysis. All cancer lists with abbreviations was in the Table S1.

Genomic alterations, localization, and interaction of TMSB10 in cancers

Using multifunctional cBioPortal cancer genome database (http://www.cbioportal.org) can identify molecular data in cancer tissue and understand related gene epigenetics, gene expression and protein group (9, 10). In this study, we explored the correlations of TMSB10 mRNA expression and coy number variation in cancer through this database, such as gene alteration frequency, gene mutation, gene amplification and deep deletion. We also visualized the rate of change in the genome through the cBioPortal Webtool.

The Human Protein Atlas (HPA; http://www.proteinatlas.org) database was used to provide the protein level of TMSB10 in human tumor. String (https://string-db.org/) database was used to show the protein-protein interaction network (PPI; http://comppi.linkgroup.hu/) of TMSB10. GeneCards (https://www.genecards.org/) was used to visualize the subcellular locations of TMSB10.

Prognostic and function enrichment analysis

Prognostic factors included overall survival (OS) time, progression-free survival (PFS) time, disease-specific survival (DSS) time, and disease-free interval survival (DFI) time. Kaplan-Meier model and Univariate Cox Regression were used to evaluate the relationship between TMSB10 and pan-cancer.

50 Hallmark gene sets were obtained from the Molecular Signature Database (MSigDB, https://www.gseamsigdb.org/gsea/index.jsp) and the Normalized Enrichment Fraction (NES) and False Discovery Rate (FDR) of biological processes of each cancer were calculated. The R software packages "clusterProfiler" (11) and "GSVA" (12) were used for gene enrichment analysis, and the results were displayed as heat maps in the R software package "ggplot2".

Immune infiltration of TMSB10

Tumor microenvironment (TME) plays an important role in tumor genesis and development. By ImmuneScore, StromalScore and ESTIMATE Score, we found that the higher the ImmuneScore or StromalScore was, the larger the proportion of immune matrix was, which was positively correlated with immune infiltration. ESTIMATE Score is the sum of the Immune Score and Stromal Score, which represents the time of the integral proportional

component of ESTIMATE Score. We evaluated the relationship between TMSB10 mRNA expression and several immune cell subsets, including cancer-associated fibroblast (CAF), B cells, neutrophils, CD4+ T cells, endothelial cells (Endo), eosinophil (Eos), NK T cells, γ/δ T cells, monocytes, macrophages, CD8+ T cells, mast cells, and NK cells across cancers in a heatmap by using the R package "ggplot2".

Immunotherapy prediction

The Spearman correlation analysis was used to analyze the association between TMSB10 and immunotherapy biomarkers. This analysis could also reflect the relationship between TMSB10 and tumor mutation load (TMB) and satellite instability (MSI) in pan-cancer. In order to explore the relationship between TMSB10 and immune checkpoint blockade (ICB), two ICB therapy cohorts, anti-PDL1 (CD274) and CTLA4, were used to verify the ability of TMSB10 in immunotherapy response in renal carcinoma and melanoma. By using the "SURV cut point" of the "SurvMiner" R software package to determine the optimal cutoff value, patients were divided into low-expression TMSB10 group and high-expression TMSB10 group. Chi-square test was used to assess the Overall Survival and Progression Free Survival in the patients with low and high TMSB10 expression.

Chemotherapy sensitivity

The Spearman method was used to analyze the relationship between TMSB10 and chemotherapy sensitivity. IC50, the semi-inhibitory concentration, measures the concentration of 50% of tumor cell apoptosis induced by chemotherapy drugs, it can reflect the tolerance degree of tumor cells to various chemotherapy drugs. The higher of the IC50, the stronger resistant ability of the tumor. IC50 was used to investigate the relationship between TMSB10 and chemotherapy sensitivity. The Connectivity Map (CMap) database (https://portals.broadinstitute.org/cmap/), which could provide the relationship between TMSB10 expression in pan-cancer and specific inhibitors through the heatmap.

Cell lines and western blotting

Human astrocytes were purchased from BIONEED (Beijing, China), and U251 and LN229 were purchased from the BeNa Culture Collection (Beijing). All cells were cultured in DMEM (Sigma-Aldrich, USA) with 10% fetal bovine serum (FBS) at 37 °C with 5% CO_2. TMSB10 and negative control (NC) were synthesized by Santa Cruz Biotechnology (USA). Cell transfection was done using 40 nM *TMSB10* RNA or vector for 24 hours. The cell proteins were extracted using RIPA buffer. Protein concentrations were detected using a BCA kit. Incubation of the membranes was done with rabbit anti-human primary antibodies against TMSB10 (Cell Signaling Technology, USA), E-cadherin, N-cadherin, and Vimentin (Cell Signaling Technology) or β-tubulin (Cell Signaling Technology) as a loading control.

Reverse-transcription quantitative polymerase chain reaction

RT-qPCR was performed as per the guidelines provided by the manufacturer (Takara Bio, Japan). TRIzol kit (Invitrogen, USA) was utilized for total RNA extraction, and cDNA was formed by reverse transcription of 1,000ng RNA in 20μL reaction volume. Santa-Cruz Biotechnology designed the following qPCR primer sequences: reverse 3`- cttatcgaagctggcgattt -5` and forward 5`- agtgggagcaccaggatct -3`. SYBR premix Taq and a CFX96 Real-Time PCR Detection System (Bio-Rad, USA) were employed to perform RT-qPCR. For the relative expression quantification of TMSB10, the $2^{-\Delta\Delta CT}$ method was utilized.

Cell migration assay

24-well transwell chambers were utilized to conduct cell migration assay with 600μL DMEM and 10% FBS at the bottom. NC and glioma (U251 and LN229) cells (1×10^5) with transfection of TMSB10 were seeded into upper chambers with 100μL serum-free medium. Cotton swabs were utilized to remove cells on the upper surface of the filter following a whole day of culture. In addition, 4% formaldehyde was utilized to fix lower-surface invading cells, followed by their staining using Giemsa solution.

Cell scratchy assay

Horizontal lines were drawn across the back of a six-well plate using a marker at approximately 0.5–1 cm distance from each other. Approximately 1 x 10^5 NC shRNA and U251 and LN229 TMSB10-overexpressing cells were seeded into the six-well plate. A sterile 200-μL pipette tip was employed to scrape the cell monolayer after two days. This was followed by cell washing thrice using PBS to remove loose cells and adding the serum-free medium, after which cell incubation was done at 37°C with 5% CO_2. Photographs were recorded at 0 and 48 hours.

Clonogenic assay

NCs and U251 and LN229 TMSB10-overexpressing cells were seeded in six-well plates (1×10^5 cells per well). PBS was employed to wash the cells thrice after a period of 14 days, and then they were stained using 0.2% crystal violet. The surviving colonies were identified as those with a cell number greater than 50. Viability data were standardized based on the NC treatment.

Statistical analyses

The Wilcoxon rank-sum test was used to compare the expression difference of TMSB10 between tumor tissues and normal tissues. Paired T test was used to evaluate the protein levels of TMSB10 in clinical GBM samples and adjacent tissues. Univariate Cox regression analysis and Kaplan-Meier method (log-rank test) were used to evaluate the effect of TMSB10 expression on the prognosis of generalized carcinoma. The Spearman correlation analysis was used to predict the efficacy of TMSB10 on immunotherapy checkpoint inhibitors and chemotherapy. Finally, chi-square test was used to compare low and high expression of TMSB10 with specific inhibitors in pan-cancer.

Results

Abnormal expressions of TMSB10 in pan-cancer

By integrating GTEx database, the top three normal tissues with high expression of TMSB10 are ovary, lung, and adipose tissue (Figure 1A). By integrating TCGA database, the expression level of TMSB10 in tumor tissues was higher than the corresponding normal tissues, and the result showed that TMSB10 is highly expressed in 15 tumor types: BLCA, BRCA, CHOL, COAD, ESCA, GBM, HNSC, KIRC, KIRP, LUAD, LUSC, READ, STAD, THCA and UCEC (all P<0.05). By contrast, TMSB10 is lowly expressed in 3 tumor types: KICH、LIHC and PRAD (all P<0.05). (Figure 1B)

Gene alteration levels of TMSB10 in pan-cancer

In view of the abnormal expression of TMSB10 in pan-cancer, we speculate that this phenomenon may be related to the genetic alteration of TMSB10. The result showed that Patients with Sarcoma had the highest "Amplification" frequency of TMSB10 genetic alteration (>3%). Therefore, we further analyzed the expression of TMSB10 in the Sarcoma "Amplification" group, "Diploid" group, "Gain" group and "Shallow Deletion" group, and found that the expression of TMSB10 in the "Diploid" group was significantly higher than "Shallow Deletion" group (Figure 1D). The "Structural Variant" were found in the Mature B-cell Neoplasms with a frequency of about 2%. The "Mutation" type of copy number alteration (CNA) was only found in Pancreatic cancer (Figure 1C).

Interaction and subcellular locations of TMSB10

By searching the ComPPI database, TMSB10 participates in several protein-protein interactions. The most closely related to S100A6 (Figure 1E). By querying the Human Protein Atlas (HPA), the subcellular localization of TMSB10 was mainly located in the cytoskeleton, then followed by cytosol (Figure 1F).

Prognosis roles of TMSB10 in pan-cancer

To further investigate the predictive potential of TMSB10 in pan-cancer, we compared and analyzed four prognostic indicators of 33 cancers, which contained Overall Survival (OS), Progression-Free Survival (PFS), Disease-Specific Survival (DSS) and Disease-Free Interval (DFI). Heat map results showed that TMSB10 was highly correlated with the prognosis of multiple cancers. It is a risk factor for poor prognosis for ACC, BRCA, CESC, COAD, GBM, HNSC, KIRC, LGG, LIHC, LUAD, LUSC, MESO, PAAD, PRAD, SARC, STAD, THCA, THYM, and UVM. In contrast, TMSB10 is a protective factor for BLCA, OV, PCPG, SKCM, and UCEC, and it is not associated with CHOL, DLBC, ESCA and TGCT (Figure 2A). The Forest map results showed that downregulation of TMSB10 expression could prolong the OS of some tumors: LGG (HR=2.250 [95%CI, 1.837-2.756], P<0.001), ACC (HR=2.086 [95%CI, 1.528-2.850], P<0.001), MESO (HR=2.329 [95%CI, 1.492-3.634], P<0.001), KIRC (HR=1.417 [95%CI, 1.124-1.786], P=0.003), PAAD (HR=1.490 [95%CI, 1.143-1.943], P=0.003), LUAD (HR=1.336 [95%CI, P=0.004), LIHC (HR=1.175 [95%CI, 1.046-1.320], P=0.006), GBM (HR=1.470 [95%CI, 1.114-1.939], P=0.006), UNM (HR=2.726 [95%CI, 1.282-5.799], P=0.004). Upregulation of TMSB10 expression could shorten the OS in OV (HR=0.891 [95% CI, 0.830-0.957], P=0.002) (Figure 2B, Figure S1). In addition, we analyzed Kaplan-Meier curves of these tumors which have statistical significance, found that low expression of TMSB10 is an important favorable prognosis marker in many tumors, such as LGG, ACC, MESO, PAAD, LUAD, LIHC, GBM (all P<0.05). In Comparison, we also found that high TMSB10 expression in OV had a favorable prognosis. Therefore, we suppose that TMSB10 has an important value in predicting the prognosis of many cancers (Figures 2C–L).

Gene set variation analysis identified the correlations of TMSB10 with immune response

To further explore the biological processes of TMSB10 in cancer initiation and development, we performed Gene Set Variation Analysis (GSVA) on 33 cancers to evaluate the relationship between TMSB10 and 50 common cancer signaling pathways, tumor immune and inflammatory responses. The results showed the immune and inflammation-related pathways:IL2-STAT5-signaling, Allograft-rejection, Inflammatory Response, IL6-JAK-STAT3-signaling, TNFA-signaling-via-NFKB, IFN-α-Response and IFN-γ-Response, and TMSB10 was significantly and positively enriched in various tumors, especially in BLCA, GBM, KICH, KIRC, PCPG and THCA. These results suggest that TMSB10 may be closely related to the tumor immune microenvironment and immune Response. Our results also showed that TMSB10 was positively enriched in most OV and TGCT signaling-pathways, immune and inflammatory reactions, while negatively enriched in

10.3389/fimmu.2023.1170539

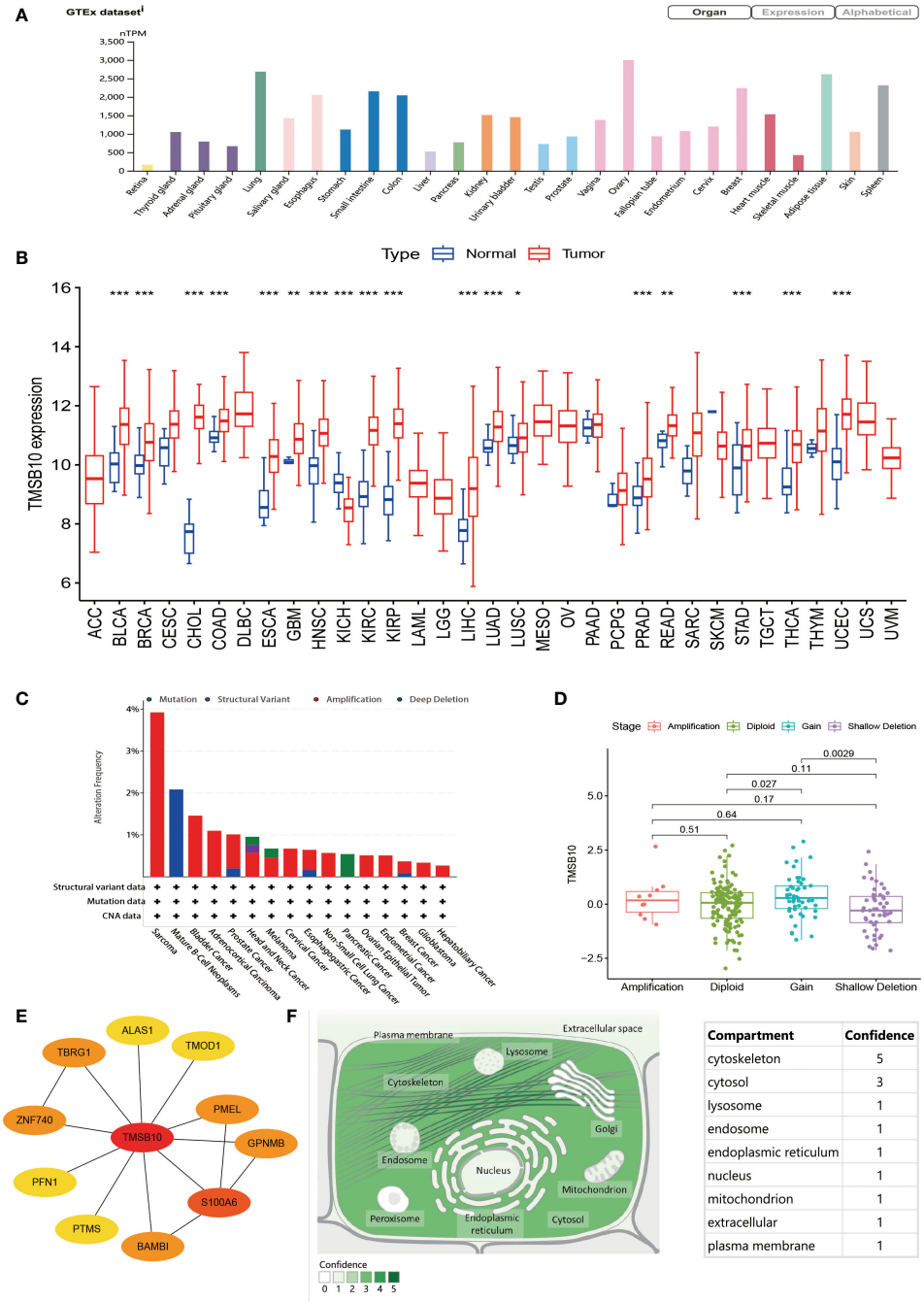

Compartment	Confidence
cytoskeleton	5
cytosol	3
lysosome	1
endosome	1
endoplasmic reticulum	1
nucleus	1
mitochondrion	1
extracellular	1
plasma membrane	1

FIGURE 1
General information of TMSB10. **(A)** Expression level of TMSB in different organ. **(B)** Comparisons of TMSB10 expression levels between tumor and normal tissues. **(C)** Landscapes of TMSB10 in pan-cancer. **(D)** TMSB10 expression of different gene mutations in Sarcoma. **(E)** Protein-protein interaction for TMSB10. **(F)** Subcellular locations of TMSB10. *P<0.05; **P<0.01; ***P<0.001.

READ and THYM. In addition, we found that TMSB10 was positively correlated with Epithelial Mesenchymal Transformation (EMT) in a variety of tumors: ACC, BLCA, BRCA, GBM, KICH, KIRC, LGG, LIHC, LUSC, PAAD, PCPG, SARC, SKCM, TGCT, THCA and SKCM, suggesting that TMSB10 may play an important role in tumor invasion and migration (Figure 3). TMSB10 may exert its function in the development and progression of cancer by regulating tumor microenvironment and mediating tumor-related immune and inflammatory responses.

Tumor microenvironment and immune infiltration Levels of TMSB10 in pan-cancer

Our previous results showed that TMSB10 was associated with tumor immune microenvironment. Therefore, we analyzed the relationship between TMSB10 and tumor immune microenvironment by ESTIMATE score and Enrichment score, and the results verified that TMSB10 was positively correlated with the level of immune cell infiltration in a variety of tumors, especially in KICH、UVM、LGG

10.3389/fimmu.2023.1170539

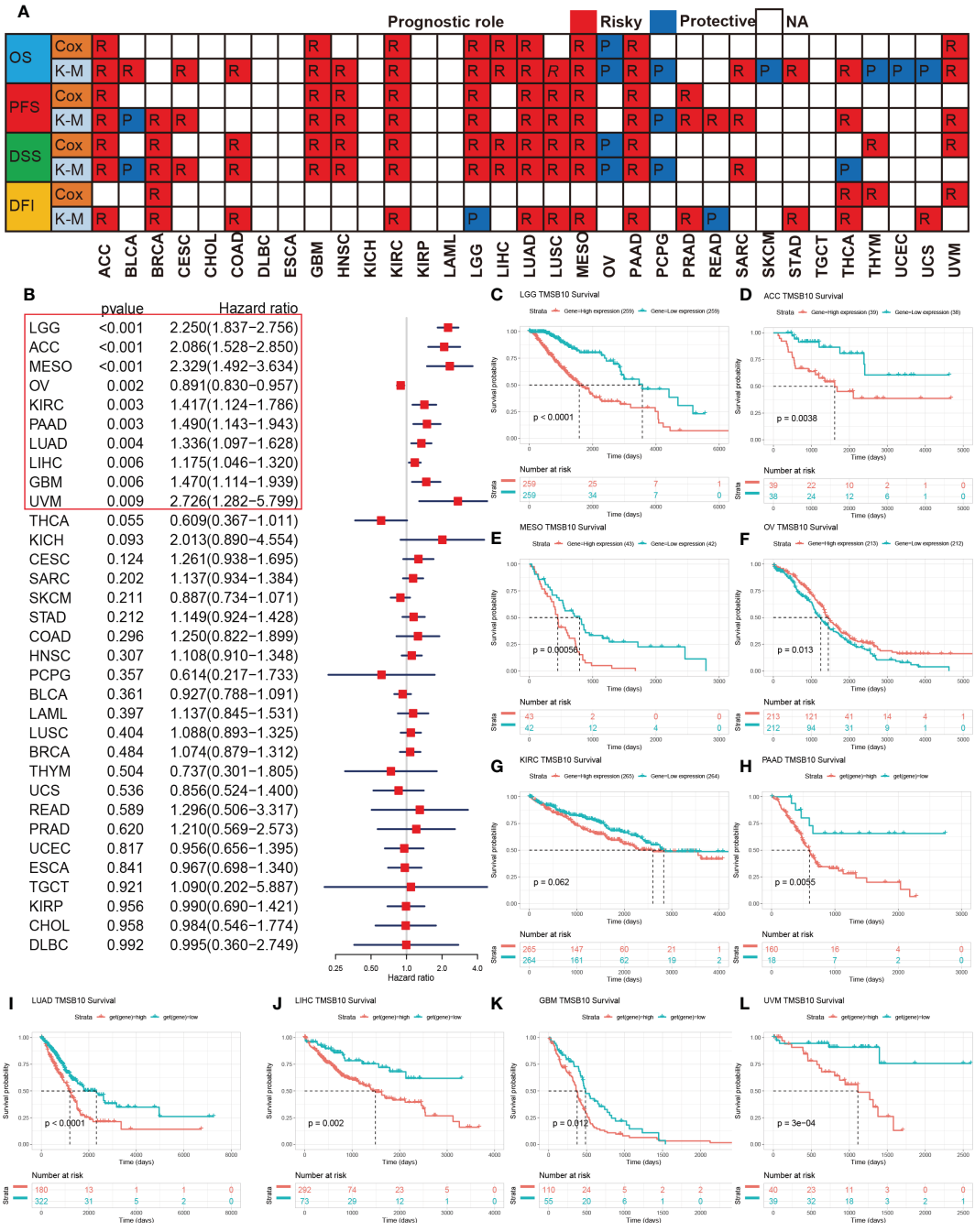

FIGURE 2
Prognosis roles of TMSB10 in pan-cancer. **(A)** Correlations of TMSB10 with OS, PFS, DSS and DFI using cox regression and Kaplan-Meier methods in pan-cancer. **(B)** Forest indicated the correlations of TMSB10 with OS in pan-cancer. **(C-L)** Kaplan-Meier survival curve of OS in LGG, ACC, MESO, OV, KIRC, PAAD, LUAD, LIHC, GBM AND UVM.

and LIHC (Figures 4A, B). The relationship between TMSB10 expression and various immune cell infiltration in pan-cancer was explored by TIMER2.0 database. The results showed that TMSB10 was positively correlated with some immune cells, such as T cells gamma and delta, CD4_Th1 and Th2, macrophage M1 and M2, $CD8^+$ T cells, endothelial cells (Endo), and eosinophils (Eos) (Figure 5). We also explored the correlations of TMSB10 with cell-specific markers in pan-cancer. The Figure S2 presented the results, and we found that TMSB10 was positively associated with these cell-specific markers in LIHC, THCA, TGCT, KICH, LGG, PCPG, SARC, GEM, BLCA, SKCM, and BRCA. Some markers CD14 (monocyte), CD3D (CD4+T cells), CD3E (CD8+T cells), CD68 (macrophage), CST3 (myeloid cells), GNLY (NK cells), KRT18 (epithelial cells), and NKG7 (NK cells) were positively associated with TMSB10 in all cancers.

10.3389/fimmu.2023.1170539

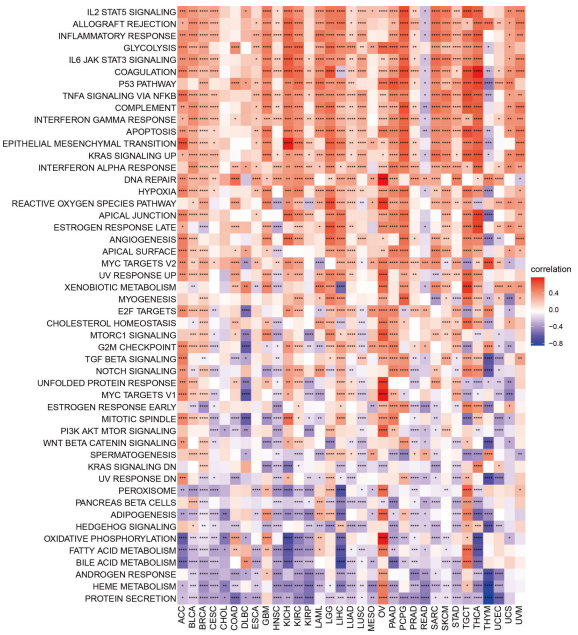

FIGURE 3
Gene set variation analysis of TMSB10 in pan-cancer *P<0.05; **P<0.01; ***P<0.001; ****P<0.0001

Correlations of TMSB10 with immune regulators, TMB and MSI

The Spearman correlation analysis was performed to know the relationship between TMSB10 and 46 immunoregulatory genes (Figure 6A). The results showed that TMSB10 was positively correlated with various tumor immune activation genes, especially in THCA, KICH, PAAD, OV, PCPG, KIRC and LGG, but negatively correlated with THYM and READ. We also found that TMSB10 was positively correlated with multiple tumor immune inhibition genes, especially in UVM, KICH, LIHC, OV, THCA, SKCM, BLCA, LGG, and PCPG, while READ was negatively correlated (Figure 6B). In conclusion, TMSB10 as a "dual-role" is related to both immune activation gene and immune inhibition genes in KICH, THCA and LGG. The interaction of chemokines and their receptors controls the targeted migration of various immune cells, clears the source of infection, promotes wound healing, and destroys the function of abnormal proliferating cells. Our results showed that TMSB10 expression was positively correlated with the expression of multiple chemokines and their receptors, such as THCA, UVM and KICH (Figures 7A, B). In order to further understand the role of TMSB10 in predicting the efficacy of Immune Checkpoint Inhibitor (ICI), we used Tumor Mutation Burden (TMB) and Microsatellite Instability (MIS) to predict the relationship between TMSB10 and the efficacy of immunotherapy.

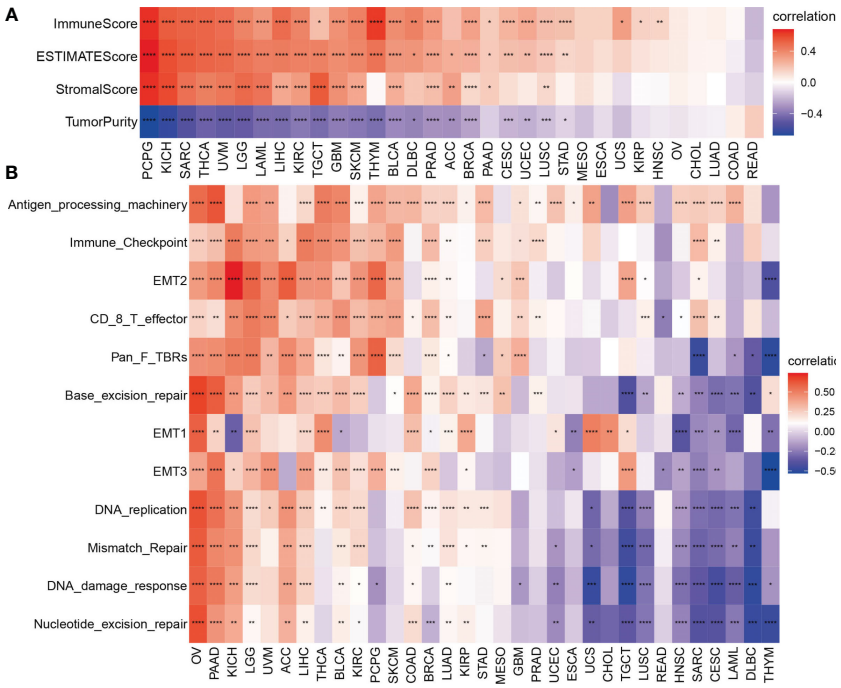

FIGURE 4
Tumor microenvironment analysis of TMSB10 in pan-cancer. **(A)** ESTIMATE method. **(B)** enrichment score method *P<0.05; **P<0.01; ***P<0.001; ****P<0.0001.

10.3389/fimmu.2023.1170539

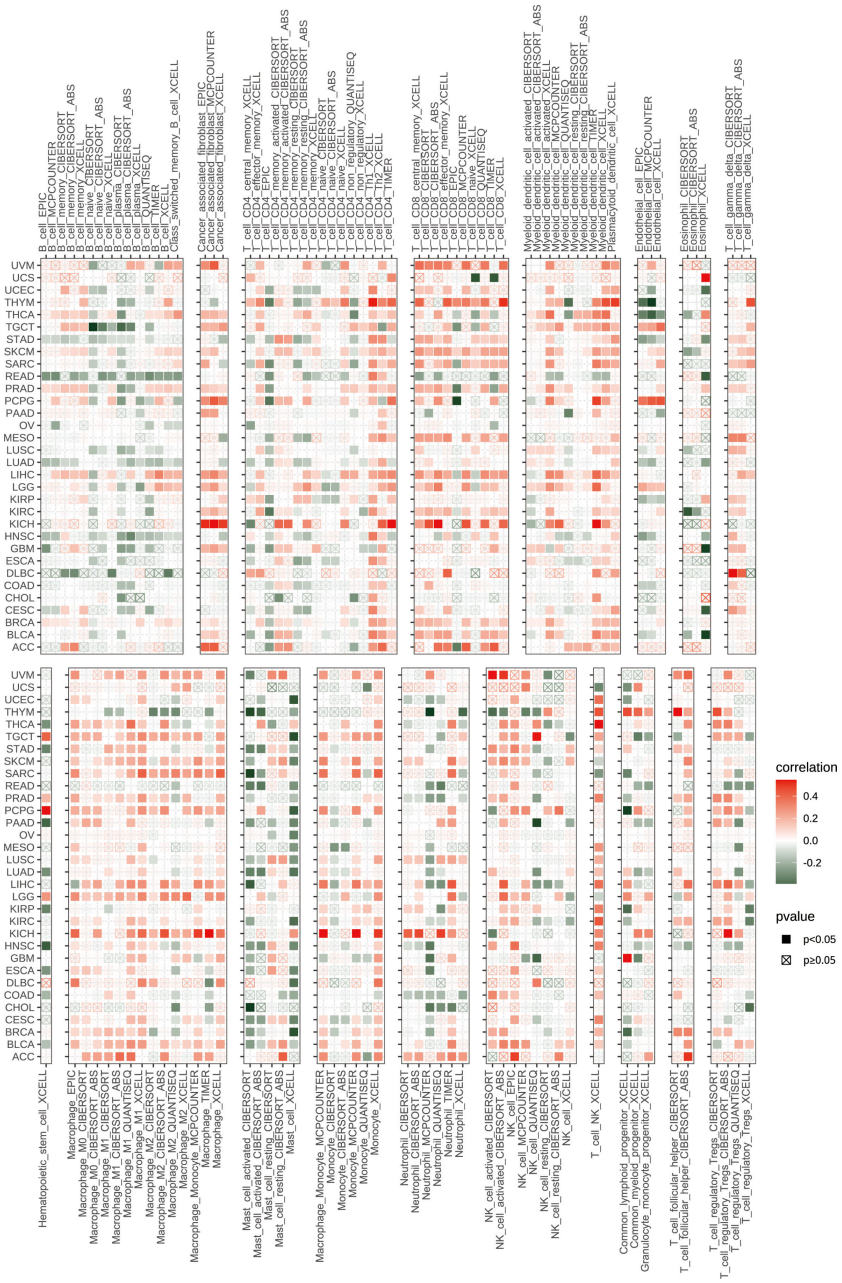

FIGURE 5
Immune infiltration levels of TMSB10 in different immune cells.

The results showed that the expression of TMSB10 in COAD, KIRP, STAD, SKCM, BLCA and BRCA was positively correlated with TMB, and negatively correlated in DLBC, LIHC and CESC (Figure 7C). In addition, the expression of TMSB10 was positively correlated with MSI in HNSC, STAD, THCA, COAD, PRAD and BRCA, and negatively correlated in CHOL, CESC, LUAD, and UVM (Figure 7D). In addition, we found that TMSB10 could effectively predicted the effect of anti-PDL1 (PDCD1), anti-CTLA4 and anti-TIGIT immunotherapy in KIRC, KICH and MESO, and the expression of TMSB10 is positively correlated with immune cell infiltration (Figures 7E–G). These results indicated that TMSB10 may be associated with immune regulation in some cancer.

TMSB10 predicts immunotherapy response

In the Checkmate cohort, the efficacy of immune checkpoint inhibitors (anti-PD-L1) in the TMSB10 high expression group was worse than that in the low expression group (Figures 7H, I), and the OS and PFS in the TMSB10 high expression group were also lower (Figures 7K, L). However, in the GSE78220 cohort, although the

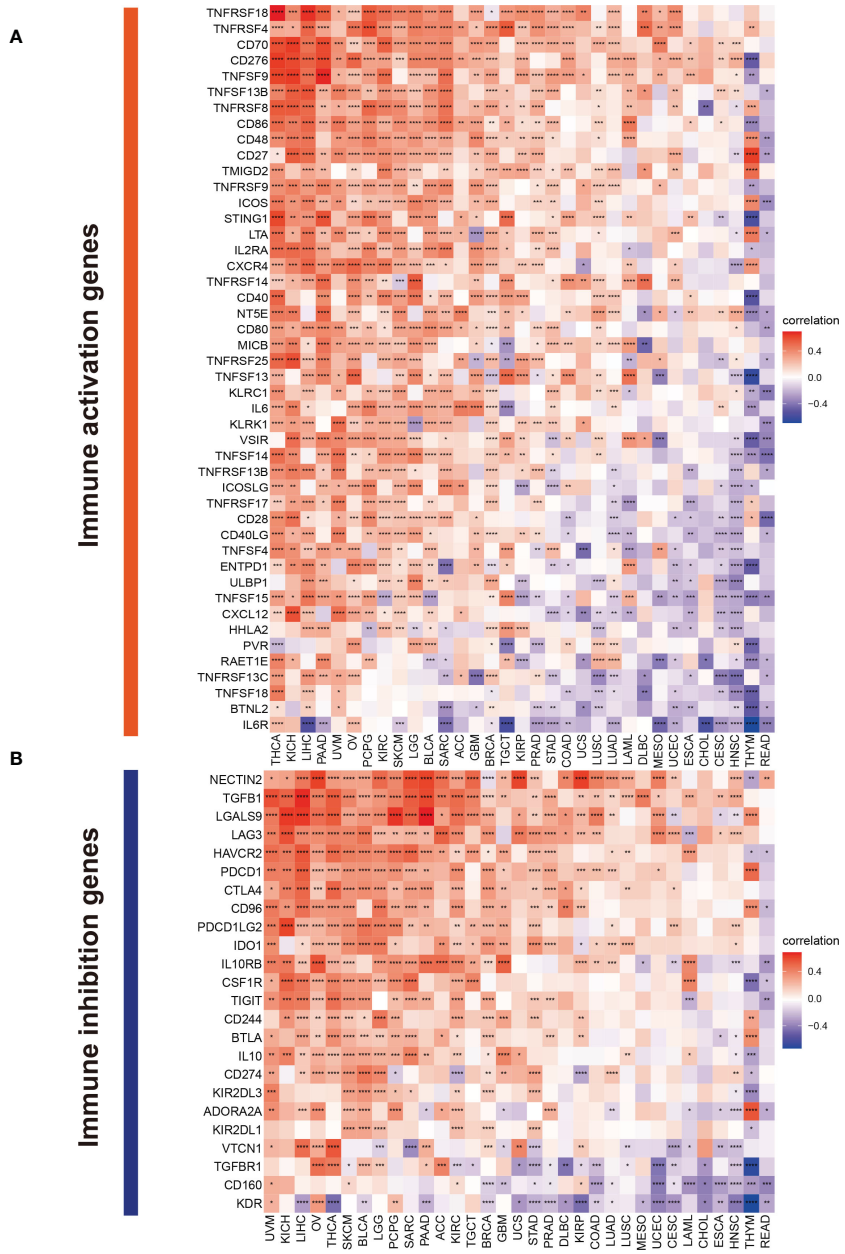

FIGURE 6
Correlations of TMSB10 with immune genes. **(A)** immune activation genes. **(B)** immune inhibition genes *P<0.05; **P<0.01; ***P<0.001; ****P<0.0001.

efficacy of anti-PD-L1 therapy was worse in the TMSB10 high expression group, there was no significant effect on OS (Figures 7J, M). TMSB10 may be used as an effective marker to predict the efficacy of immune checkpoint inhibitors in some cancer.

Effect of TMSB10 on chemotherapy sensitivity

The relationship between gene expression and the efficacy of chemotherapy was reflected in the immune infiltration correlation plot. We selected the top 6 small molecule compounds with chemotherapy resistance/sensitivity as examples, and the results showed that the expression of TMSB10 was positively correlated with some chemotherapy resistance, especially in Sorafenib, LGK 974, Vorinostat, AZD5991, TAF1 and AZD1208. However, TMSB10 was positively associated with sensitivity to some chemotherapy, especially in ZM447439, BI-2536, JQ1, Nu7441, Tozasertib and Dasatinib (Figure S3, Table S2).

TMSB10 promotes glioma progression by regulating PD-L1 expression *via* IL6/JAK/STAT3 signaling pathway

We further explored the function role of TMSB10 in glioma through cell experiments. In CGGA, high-expressed TMSB10 was associated with poor OS (Figure 8A) and PFS (Figure 8B). Next, we compared the

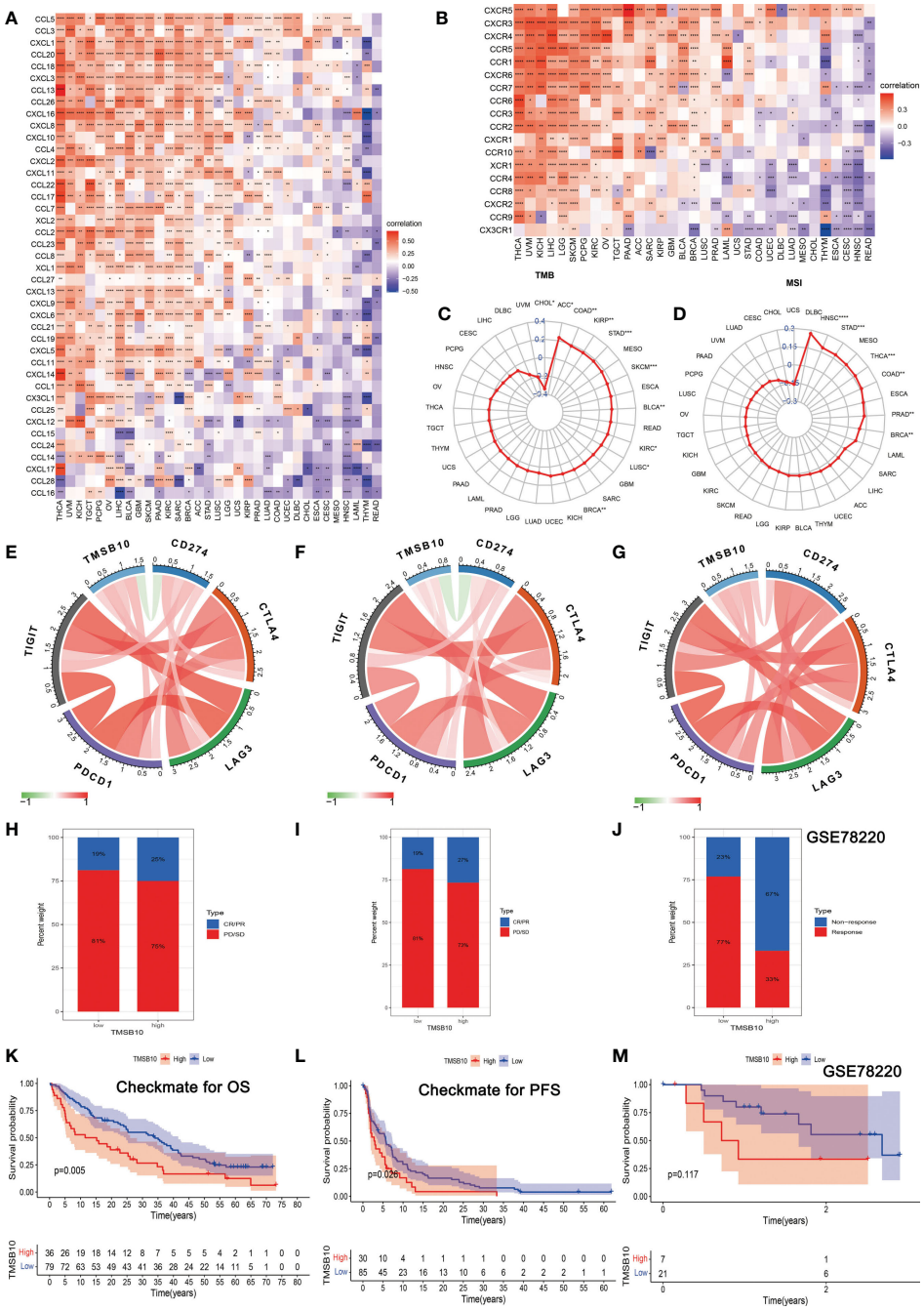

FIGURE 7
Correlations of TMSB10 with chemokines and immune checkpoint key genes and its effect on immunotherapy. **(A, B)** Associations between TMSB10 and chemokines and its receptors (*P<0.05, **P<0.01, ***P<0.001). **(C, D)** Correlations of TMSB10 with TMB and MSI levels. **(E-G)** Associations between TMSB10 with immune checkpoint key genes in KIRC, KICH, and Melanoma. **(H-K)** Effects of TMSB10 expression on anti-PD-L1 treatment responses and OS in Checkmate cohorts. **(I-L)** Effects of TMSB10 expression on anti-PD-L1 treatment response and PFS in Checkmate cohorts. **(J, M)** Effects of TMSB10 expression on anti-PD-L1 treatment response and OS in GSE78220 cohorts. *P<0.05; **P<0.01; ***P<0.001; ****P<0.0001.

TMSB10 expression level among different grade, and we found glioma patients with advanced grade had higher TMSB10 expression (Figure 8C, P=1.3e-36). Finally, univariate, and multivariate cox regression showed that TMSB10 was an independent prognosis factor for glioma (univariate: HR=1.337, 95%CI: 1.243-1.439, P<0.001, Figure 8D; Multivariate: HR=1.095, 95%CI: 1.04-1.194, P=0.041, Figure 8E).

Then, we built glioma cells of TMSB10 low expression (Figures 9A, B). We found low expression of TMSB10 inhibited clonogenic formation ability, invasion, migration *in vitro* (Figures 9C–J). Furthermore, the correlation analyses indicated that TMSB10 were positively associated with PD-L1 expression level in primary and recurrent glioma (Figures 10A, B). The pathways enrichment analysis indicated TMSB10 was positively associated with IL6/JAK/STAT3 signaling pathway (Figure S4), and we also found TMSB10 was positively associated with IL-6 in patients with primary/recurrent glioma (Figures S5A-H, grade III: r=0.46, P<0.001, grade IV: r=0.317,

10.3389/fimmu.2023.1170539

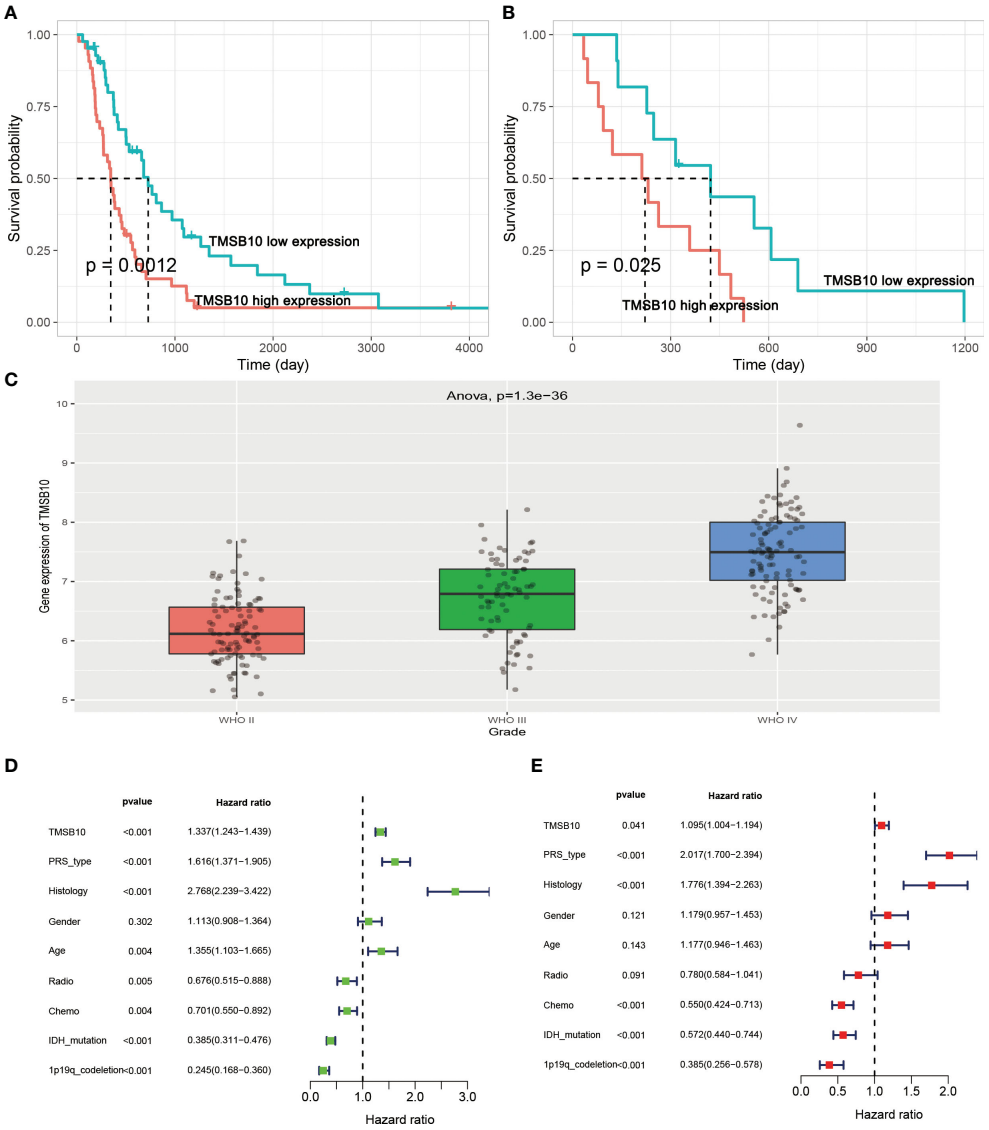

FIGURE 8
TMSB10 is an independent prognosis factor in glioma. **(A, B)** High-expressed TMSB10 is associated with poor OS and PFS**(C)** TMSB10 increased with grade. **(D, E)** Univariate and multivariate cox regression indicated that TMSB10 was associated with prognosis in glioma.

P=0.003). Western blot indicated that PD-L1 and p-STAT3 expression levels were significantly down-regulated after TMSB10 knock down (Figures 10C, D). qPCR also indicated that mRNA levels of PD-L1 and IL6 were down-regulated after TMSB10 knock down (Figures 10E, F). Furthermore, we found PD-L1 expression and p-STAT3 levels were increased in TMSB10-knock down cells using IL-6 stimulating for 36 hours (Figures S6A–C). TMSB10 may involve glioma immune regulation progression by promoting PD-L1 expression levels *via* activating STAT3 signaling pathway.

Discussion

Immune checkpoint inhibitors (ICIs) play an important role in the maintenance of tolerance and tissue damage caused by immune response by regulating the number and function of antigen-specific T cells. The immune checkpoints mainly include programmed death-1 (PD-1), cytotoxic T lymphocyte associated antigen 4 (CTLA-4), T cell Immunoglobulin domain and Mucindomain-3 (TIM-3), which can induce immunosuppressive responses of T cells and promote T cell failure by binding with corresponding ligands on the surface of tumor cells. Prompting tumor cells to evade the immune system's surveillance (13, 14). At present, the monoclonal antibodies that block the interaction of PD-L1/PD-1 have been clinically approved for many solid cancer immunotherapy, especially refractory or advanced tumors. However, although antibody drugs have been used wildly in the clinical cure, the curative effective is still not satisfied enough, the effective rate of PD-1/PD-L1 inhibitor treatment is only 20%-40% in many solid tumors (15, 16), which emphasizes the necessity of developing new immune checkpoints to predict the prognosis of cancer immunotherapy. In our study, we proved that TMSB10 could become a hopeful prognosis biomarker in pan-cancer,

10.3389/fimmu.2023.1170539

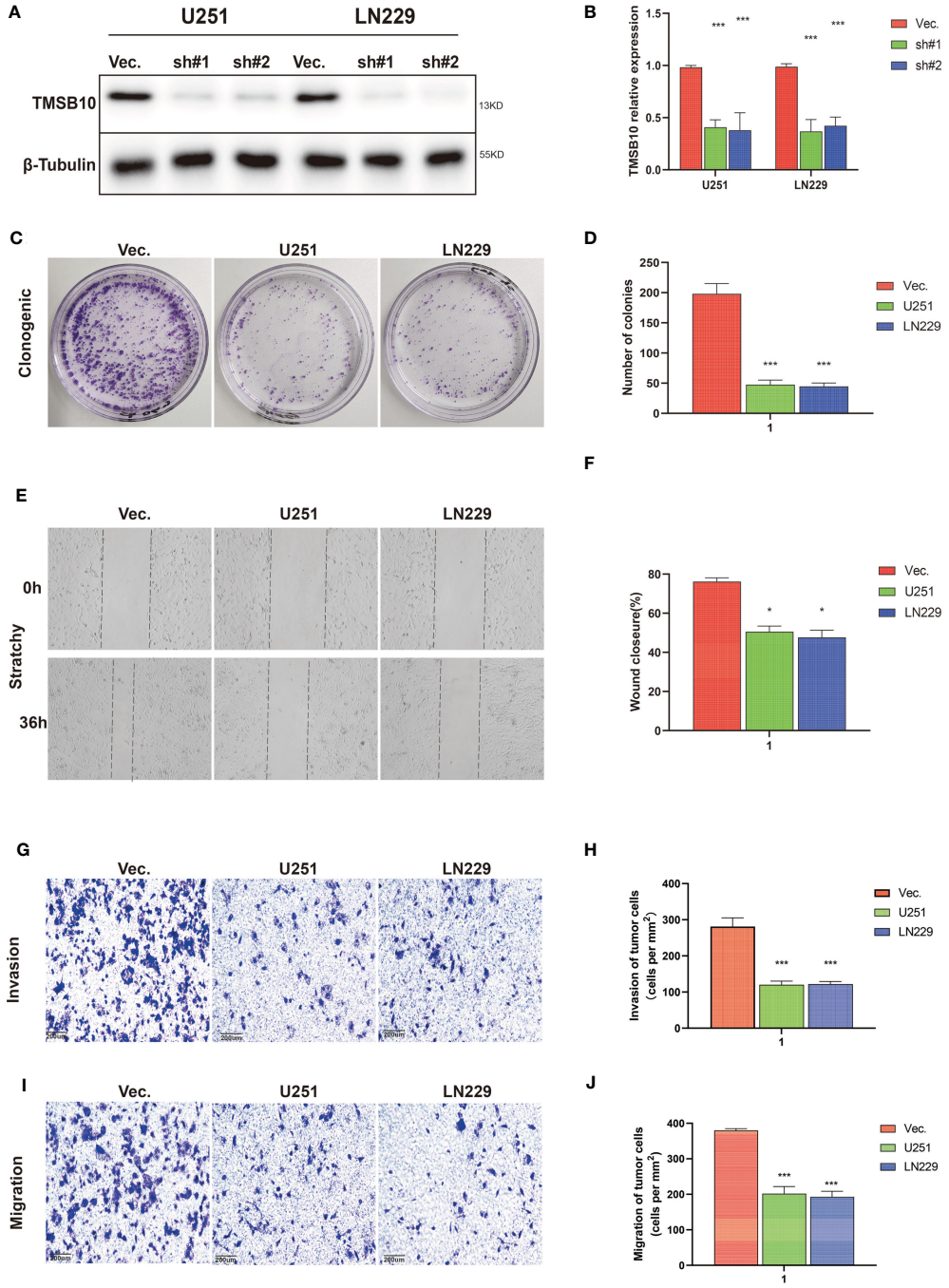

FIGURE 9
TMSB10 involves in glioma progression. **(A, B)** Establishment of TMSB10 knock out cells. **(C, D)** Low expression of TMSB10 inhibited the clonogenic formation ability of glioma cells. **(E , F)** Low expression of TMSB10 inhibited migration of glioma cells. **(G–J)** Low expression of TMSB10 inhibits the invasion and migration of glioma cells. *P<0.05; ***P<0.001.

especially in the response of cancer immunotherapy and chemotherapy in the future.

According to our study, the expression level of TMSB10 is not only different in normal tissues, but it was higher in many tumor tissues by integrating GTEx and TCGA database. Our result showed that TMSB10 is highly expressed in 15 tumor types and lowly expressed in 3 tumor types. Our findings are consistent with most previous studies that have shown that overexpression of TMSB10 is closely related to the occurrence and development of gastric cancer, breast cancer, bladder cancer and hepatocellular carcinoma (2, 17–19). In the Landscapes, it was found that sarcoma had the highest gene alteration frequency of TMSB10 in pan-cancer and we analyzed the expression of TMSB10 in different gene mutations in sarcomas, the result showed that Diploid and Shallow Deletion were two of the highest incidence of mutation types.

Then, we analyzed the clinical prognostic with the expression level of TMSB10 in 33 cancers. Our results showed that TMSB10 was highly correlated with the prognosis of multiple cancers. High

10.3389/fimmu.2023.1170539

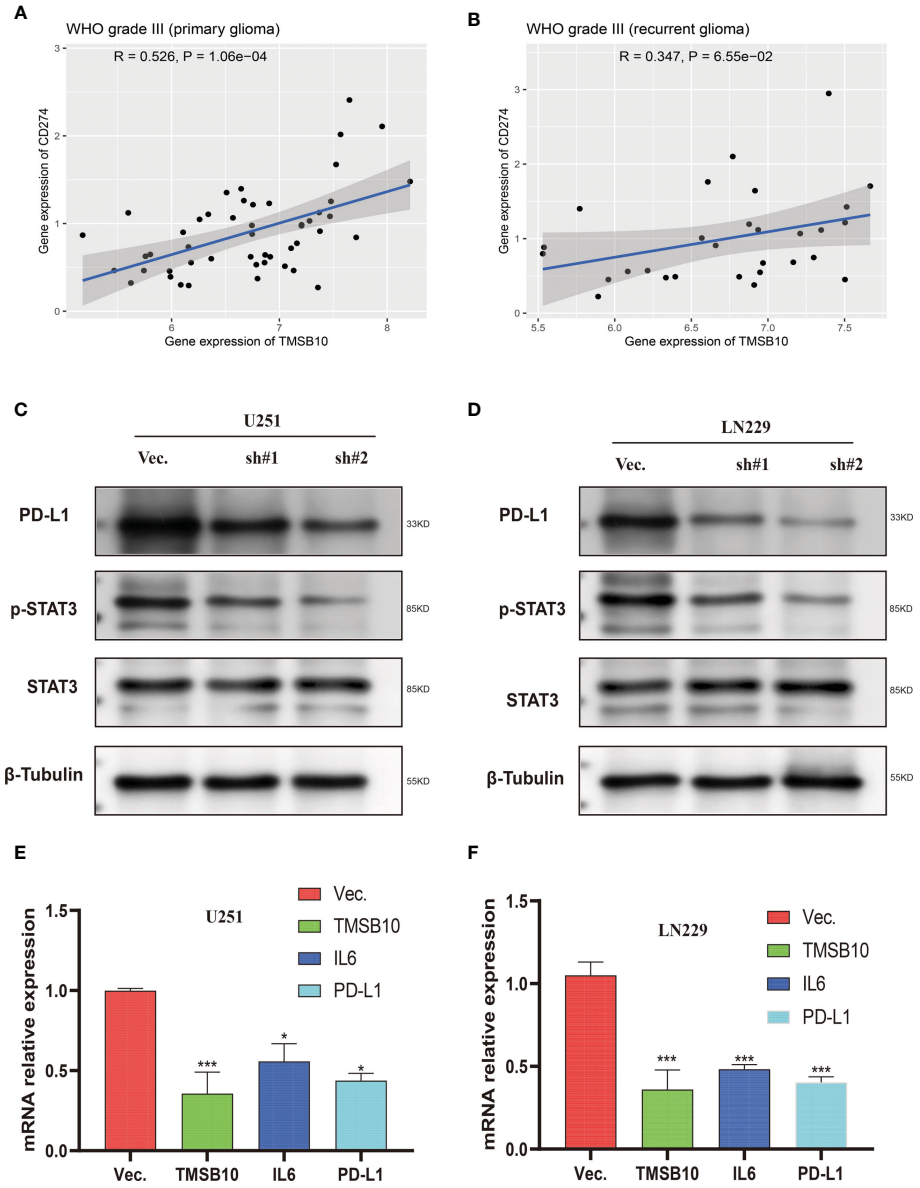

FIGURE 10
Low expression of TMSB10 inhibited PD-L1 expression *via* regulating STAT3 signaling. **(A, B)** TMSB10 was positively associated with PD-L1 in primary and recurrent glioma. **(C, D)** Western blot indicated PD-L1 and p-STAT3 were down-regulated after TMSB10 inhibition in glioma cells. **(E, F)** q-PCR indicated IL6 and PD-L1 were low expressed after TMSB10 inhibited. **P*<0.05; ****P*<0.001.

expression of TMSB10 could predict a poor prognosis in 19 cancers, and low expression of TMSB10 could predict a positive prognosis in 5 cancers. Our results also showed that downregulation of TMSB10 expression could prolong the OS of 9 tumors, and upregulation of TMSB10 expression could shorten the OS in 1 tumor. Upregulation of TMSB10 is involved in a variety of signaling pathways related to tumor invasion and metastasis, leading to unsatisfied survival rate of patients. Therefore, we suppose that TMSB10 has an important value in predicting the prognosis of many cancers.

In recent years, tumor microenvironment has received more and more attention because it plays a key role in tumor immune escape, distant metastasis, treatment resistance and targeted therapy response (20, 21). We explored the relationship between tumor microenvironment and TMSB10 expression in pan-cancer. The GSVA results showed that TMSB10 expression closely related to immune and inflammation-related pathways in many tumors and positively correlated with EMT in a variety of tumors, and TMSB10 was positively correlated with the level of immune cell infiltration in a variety of tumors, especially in KICH、UVM、LGG and LIHC. TMSB10 was positively correlated with the infiltration levels of various immune cells, such as T cells, B cells, CD8+T cells, endothelial cells (Endo), and eosinophils (Eos). These results suggested that TMSB10 is associated with tumor immune microenvironment.

Next, we hope to know the relationship between TMSB10 expression and immunoregulatory genes. Our results showed that upregulate TMSB10 expression was related with immune activation genes in 7 tumors, and upregulate TMSB10 expression was related

with immune inhibition genes in 9 tumors. In addition, TMSB10 as a "dual-role" is related to both immune activation gene and immune inhibition genes in KICH, THCA and LGG. Our results showed that TMSB10 expression was positively correlated with the expression of multiple chemokines and their receptors in THCA, UVM and KICH. We used the TMB and MIS to predict the relationship between TMSB10 and the efficacy of immunotherapy. The results showed that the expression of TMSB10 in COAD, KIRP, STAD, SKCM, BLCA and BRCA was positively correlated with TMB, and negatively correlated in DLBC, LIHC and CESC. And the expression of TMSB10 was positively correlated with MSI in HNSC, STAD, THCA, COAD, PRAD and BRCA, and negatively correlated in CHOL, CESC, LUAD, and UVM. In addition, we found that TMSB10 could effectively predicted the effect of anti-PDL1, anti-CTLA4 and anti-TIGIT immunotherapy in KIRC KICH, and MESO, and the expression of TMSB10 is positively correlated with immune cell infiltration. To validate our findings, we performed the experiments *in vitro* and found low expression of TMSB10 inhibited clonogenic formation ability, invasion, and migration in glioma cells. Furthermore, TMSB10 may involve glioma immune regulation progression by promoting PD-L1 expression levels *via* activating STAT3 signaling pathway in glioma cells. Therefore, we hypothesized that TMSB10 could be an effective biomarker to predict the efficacy of immune checkpoint inhibitors in pan-cancer.

Finally, we verified the expression of TMSB10 could reflect immunotherapy and chemotherapy responses in some tumors, especially in KIRC, KICH and MESO. Our results showed that the efficacy of anti-PD-L1 in the TMSB10 high expression group was worse than that in the low expression group in KIRC and KICH, and the OS and PFS in the TMSB10 high expression group were also lower. However, in the GSE78220 cohort, although the efficacy of anti-PD-L1 therapy was worse in the TMSB10 high expression group, there was no significant effect on OS. We further found that the expression of TMSB10 has a closely relationship with chemotherapy resistance and sensitivity.

Previous study also explored the function roles of TMSB10 in pan-cancer (22). Both previous and our study had bioinformatics analyses and experiment validations. However, there are remarkedly differences between previous study and our study. For bioinformatics analyses, previous study only presented the pan-cancer expression pattern and biological and immunomodulatory function of TMSB10, and most of results focus on glioma. But our study included prognosis analyses, pathway enrichment, tumor microenvironment and immune infiltration, immune checkpoints, immune activation genes, immune inhibition genes, chemokines and their receptor genes, tumor mutation burden, and microsatellite instability in pan-cancer. We also explored the effect of TMSB10 on immunotherapy in real world cohort data. We showed a huge landscape in pan-cancer, which is completely different from previous study. For experiments validation, we admitted that previous study presented more details, but we have different findings for TMSB10 in glioma. Previous study explored the TMSB10 promoted glioma progression *via* YAP1/AKT/ERK1/2, but we explored the TMSB10 promoted glioma progression *via* IL6/JAK/STAT3 signaling pathway. But we both proved that TMSB10 can be a potential immunotherapy target point in glioma. Gene regulation is a complex process, and we provide a different view and enriched the molecular mechanism in glioma.

There are several limitations to our study. First, the association with protein levels needs to be tested *in vivo*. Second, validation can be performed with other public datasets to further support our current findings. Third, anti-tumor activity can be measured by targeting TMSB10, and the role of TMSB10 in immune checkpoints and its effect on chemotherapy sensitivity can be validated in conjunction with more clinical trials.

In conclusion, we performed a comprehensive evaluation of TMSB10, revealing its potential role as a prognostic indicator for patients in immunomodulatory and therapeutic efficacy. TMSB10 may become a novel target for tumor immunotherapy and chemotherapy.

Data availability statement

The original contributions presented in the study are included in the article/Supplementary Material. Further inquiries can be directed to the corresponding author.

Ethics statement

Ethical approval was not provided for this study on human participants because Data of Human was from publica data. The ethics committee waived the requirement of written informed consent for participation.

Author contributions

ZL designed this study and directed the research group in all aspects, including planning, execution, and analysis of the study. YZ drafted the manuscript. YL and NL collected the data. ZL provided the statistical software, performed the data analysis. YT and NL arranged the Figures and Tables. ZL and LS revised the manuscript. All authors contributed to the article and approved the submitted version.

Funding

This study was supported by the National Natural Science Foundation of China (ZL: No.82003239);, and National key clinical specialty (2209090720).

Conflict of interest

The authors declare that the research was conducted in the absence of any commercial or financial relationships that could be construed as a potential conflict of interest.

Publisher's note

Supplementary material

The Supplementary Material for this article can be found online at: https://www.frontiersin.org/articles/10.3389/fimmu.2023.1170539/full#supplementary-material

SUPPLEMENTARY FIGURE 1
The correlations of TMSB10 with PFI **(A)**, DFI **(B)** and DSS **(C)** in cancers.

SUPPLEMENTARY FIGURE 2
Correlations of TMSB10 with cell-specific markers in pan-cancer.

SUPPLEMENTARY FIGURE 3
Correlations of TMSB10 with Chemotherapy sensitivity. **(A)** Top 6 compounds showing resistant to TMSB10. **(B)** Top 6 compounds showing sensitivity to TMSB10.

SUPPLEMENTARY FIGURE 4
Pathways enrichment analysis of TMSB10.

SUPPLEMENTARY FIGURE 5
TMSB10 was positively associated with IL-6 in primary and recurrent glioma **(A-H)**.

SUPPLEMENTARY FIGURE 6
IL-6 affect the PD-L1 **(A)** and p-STAT3 levels **(B, C)**.

References

1. Safer D, Golla R, Nachmias VT. Isolation of a 5-kilodalton actin-sequestering peptide from human blood platelets. *Proc Natl Acad Sci U S A.* (1990) 87:2536–40. doi: 10.1073/pnas.87.7.2536

2. Zhang X, Ren D, Guo L, Wang L, Wu S, Lin C, et al. Thymosin beta 10 is a key regulator of tumorigenesis and metastasis and a novel serum marker in breast cancer. *Breast Cancer Res* (2017) 19:15. doi: 10.1186/s13058-016-0785-2

3. Zeng J, Yang X, Yang L, Li W, Zheng Y. Thymosin beta10 promotes tumor-associated macrophages M2 conversion and proliferation *via* the PI3K/Akt pathway in lung adenocarcinoma. *Respir Res* (2020) 21:328. doi: 10.1186/s12931-020-01587-7

4. Pan Q, Cheng G, Liu Y, Xu T, Zhang H, Li B. TMSB10 acts as a biomarker and promotes progression of clear cell renal cell carcinoma. *Int J Oncol* (2020) 56:1101–14. doi: 10.3892/ijo.2020.4991

5. Yang C, Liu Y, Fang K. Thymosin beta10 mediates the effects of microRNA-184 in the proliferation and epithelial-mesenchymal transition of BCPAP cells. *Exp Ther Med* (2021) 22:742. doi: 10.3892/etm.2021.10174

6. Wang C, He Y, You Z, Chen X. TMSB10 promotes progression of clear cell renal cell carcinoma *via* JUN transcription regulation. *Ann Clin Lab Sci* (2022) 52:230–9. doi: 10.3892/ijo.2020.499

7. Shaulian E. AP-1–the jun proteins: oncogenes or tumor suppressors in disguise? *Cell Signal* (2010) 22:894–9. doi: 10.1016/j.cellsig.2009.12.008

8. Goldman MJ, Craft B, Hastie M, Repecka K, McDade F, Kamath A, et al. Visualizing and interpreting cancer genomics data *via* the xena platform. *Nat Biotechnol* (2020) 38:675–8. doi: 10.1038/s41587-020-0546-8

9. Haeussler M, Zweig AS, Tyner C, Speir ML, Rosenbloom KR, Raney BJ, et al. The UCSC genome browser database: 2019 update. *Nucleic Acids Res* (2019) 47:D853–8. doi: 10.1093/nar/gky1095

10. Gao J, Aksoy BA, Dogrusoz U, Dresdner G, Gross B, Sumer SO, et al. Integrative analysis of complex cancer genomics and clinical profiles using the cBioPortal. *Sci Signal* (2013) 6:l1. doi: 10.1126/scisignal.2004088

11. Yu G, Wang LG, Han Y, He QY. clusterProfiler: an r package for comparing biological themes among gene clusters. *Omics* (2012) 16:284–7. doi: 10.1089/omi.2011.0118

12. Hanzelmann S, Castelo R, Guinney J. GSVA: gene set variation analysis for microarray and RNA-seq data. *BMC Bioinf* (2013) 14:7. doi: 10.1186/1471-2105-14-7

13. Lin X, Lu X, Luo G, Xiang H. Progress in PD-1/PD-L1 pathway inhibitors: from biomacromolecules to small molecules. *Eur J Med Chem* (2020) 186:111876. doi: 10.1016/j.ejmech.2019.111876

14. Fourcade J, Sun Z, Pagliano O, Chauvin JM, Sander C, Janjic B, et al. PD-1 and Tim-3 regulate the expansion of tumor antigen-specific CD8(+) T cells induced by melanoma vaccines. *Cancer Res* (2014) 74:1045–55. doi: 10.1158/0008-5472.CAN-13-2908

15. Borghaei H, Paz-Ares L, Horn L, Spigel DR, Steins M, Ready NE, et al. Nivolumab versus docetaxel in advanced nonsquamous non-Small-Cell lung cancer. *N Engl J Med* (2015) 373:1627–39. doi: 10.1056/NEJMoa1507643

16. Robert C, Long GV, Brady B, Dutriaux C, Maio M, Mortier L, et al. Nivolumab in previously untreated melanoma without BRAF mutation. *N Engl J Med* (2015) 372:320–30. doi: 10.1056/NEJMoa1412082

17. Yan Z, Yan Q, Song Y, Wang L. TMSB10, a potential prognosis prediction biomarker, promotes the invasion and angiogenesis of gastric cancer. *J Gastroenterol Hepatol* (2021) 36:3102–12. doi: 10.1111/jgh.15576

18. Song C, Su Z, Guo J. Thymosin beta 10 is overexpressed and associated with unfavorable prognosis in hepatocellular carcinoma. *Biosci Rep* (2019) 39:BSR20182355. doi: 10.1042/BSR20182355

19. Wang B, Wang Z, Zhang T, Yang G. Overexpression of thymosin beta10 correlates with disease progression and poor prognosis in bladder cancer. *Exp Ther Med* (2019) 18:3759–66. doi: 10.3892/etm.2019.8006

20. Paluskievicz CM, Cao X, Abdi R, Zheng P, Liu Y, Bromberg JS. T Regulatory cells and priming the suppressive tumor microenvironment. *Front Immunol* (2019) 10:2453. doi: 10.3389/fimmu.2019.02453

21. Quail DF, Joyce JA. Microenvironmental regulation of tumor progression and metastasis. *Nat Med* (2013) 19:1423–37. doi: 10.1038/nm.3394

22. Xiong Y, Qi Y, Pan Z, Wang S, Li B, Feng B, et al. Pancancer landscape analysis of the thymosin family identified TMSB10 as a potential prognostic biomarker and immunotherapy target in glioma. *Cancer Cell Int* (2022) 22:294. doi: 10.1186/s12935-022-02698-5

frontiers | Frontiers in Immunology

TYPE Original Research
PUBLISHED 30 May 2023
DOI 10.3389/fimmu.2023.1183440

OPEN ACCESS

EDITED BY
Esra Akbay,
University of Texas Southwestern Medical Center, United States

REVIEWED BY
Degao Chen,
Army Medical University, China
Kangsan Kim,
University of Texas Southwestern Medical Center, United States

*CORRESPONDENCE
Qinghua Jiang
qhjiang@hit.edu.cn
Yu Li
liyugene@hit.edu.cn
Huan Nie
nh1212@hit.edu.cn

†These authors have contributed equally to this work

RECEIVED 10 March 2023
ACCEPTED 18 May 2023
PUBLISHED 30 May 2023

CITATION
Cai J, Yang D, Sun H, Xiao L, Han F, Zhang M, Zhou L, Jiang M, Jiang Q, Li Y and Nie H (2023) A multifactorial analysis of FAP to regulate gastrointestinal cancers progression. *Front. Immunol.* 14:1183440. doi: 10.3389/fimmu.2023.1183440

A multifactorial analysis of FAP to regulate gastrointestinal cancers progression

Jialing Cai†, Depeng Yang†, Handi Sun†, Lixing Xiao, Fang Han, Mengmeng Zhang, Lu Zhou, Meiyi Jiang, Qinghua Jiang*, Yu Li* and Huan Nie*

School of Life Science and Technology, Harbin Institute of Technology, Harbin, Heilongjiang, China

Background: Fibroblast activation protein (FAP) is a cell-surface serine protease that has both dipeptidyl peptidase as well as endopeptidase activities and could cleave substrates at post-proline bond. Previous findings showed that FAP was hard to be detected in normal tissues but significantly up-regulated in remodeling sites like fibrosis, atherosclerosis, arthritis and embryonic tissues. Though increasing evidence has demonstrated the importance of FAP in cancer progression, no multifactorial analysis has been developed to investigate its function in gastrointestinal cancers until now.

Methods: By comprehensive use of datasets from The Cancer Genome Atlas (TCGA), Clinical Proteomic Tumor Analysis Consortium (CPTAC), scTIME Portal and Human Protein Atlas (HPA), we evaluated the carcinogenesis potential of FAP in gastrointestinal cancers, analyzing the correlation between FAP and poor outcomes, immunology in liver, colon, pancreas as well as stomach cancers. Then liver cancer was selected as example to experimentally validate the pro-tumor and immune regulative role of FAP in gastrointestinal cancers.

Results: FAP was abundantly expressed in gastrointestinal cancers, such as LIHC, COAD, PAAD and STAD. Functional analysis indicated that the highly-expressed FAP in these cancers could affect extracellular matrix organization process and interacted with genes like COL1A1, COL1A2, COL3A1 and POSTN. In addition, it was also observed that FAP was positively correlated to M2 macrophages infiltration across these cancers. To verify these findings *in vitro*, we used LIHC as example and over-expressed FAP in human hepatic stellate LX2 cells, a main cell type that produce FAP in tumor tissues, and then investigate its role on LIHC cells as well as macrophages. Results showed that the medium from FAP-over-expressed LX2 cells could significantly promote the motility of MHCC97H and SK-Hep1 LIHC cells, increase the invasion of THP-1 macrophages and induce them into pro-tumor M2 phenotype.

Conclusion: In summary, we employed bioinformatic tools and experiments to perform a comprehensive analysis about FAP. Up-regulation of FAP in gastrointestinal cancers was primarily expressed in fibroblasts and contributes to tumor cells motility, macrophages infiltration and M2 polarization, revealing the multifactorial role of FAP in gastrointestinal cancers progression.

KEYWORDS

FAP, fibroblast, gastrointestinal cancers, immunology, macrophage polarization

Introduction

Gastrointestinal cancers refer to tumors in esophagus, stomach, colon, liver as well as pancreas, currently regarded as one of the most leading cause of cancer death and the major obstruction in cancer treatment (1, 2). Numerous evidences have demonstrated the key role of immune microenvironment in the occurrence and development of gastrointestinal cancers (3), however, the regulatory mechanisms need further exploration. With continuous development and improvement of bioinformatic tools, it is possible to reveal the significance and correlation of specific genes in immune microenvironment regulation, providing an opportunity to evaluate the potential of these genes as novel prognosis markers and treatment target across gastrointestinal cancers (4).

Fibroblast activation protein (FAP) is a constitutively active serine peptidase with both dipeptidyl peptidase and collagenase activity (5). Previous findings revealed that FAP was rare to be detected in healthy tissues, notably, FAP had a high expression trend in some kinds of malignant tumors, such as breast cancer, colorectal cancer and pancreatic cancer (6–10). High expression of FAP in these cancers was reported to estimate worse outcomes in patients and involved in tumor progression via diverse mechanisms. For instance, FAP was found able to promote migration and invasion of cancer cells by binding to ENO1 and activating NF-κB signaling pathway in colorectal adenocarcinoma (COAD) (11). In stomach adenocarcinoma (STAD), high FAP expression in tumor tissues is always accompanied by increased micro-vessel density (12), while after FAP knock-out or pharmacological inhibition, tumor growth and microvascular density could be decreased (13), suggesting that FAP was involved in angiogenesis as well. The effect of FAP in tumor immune system was not investigated until recent years. In a mouse model of pancreatic adenocarcinoma (PAAD), Feig C and colleagues found that the depletion of FAP positive cells contributed to improved anti-CTLA-4 or anti-PD-L1 immunotherapy efficacy, revealing the immune suppressive effect of FAP in cancers (14). Similar findings were also observed in mouse model of COAD and STAD, results showed that co-injection of cancer cells and FAP positive cells led to anti-PD-1 treatment resistance in mice (15, 16). Though these findings suggested a significant role of FAP in gastrointestinal cancers progression, a multifactorial and comprehensive analysis is still needed.

Our current study utilized bioinformatic methods to give a description on the functions of FAP across gastrointestinal cancers and then verified these findings by *in vitro* experiments. Results showed that FAP was up-regulated in gastrointestinal cancers and involved in tumor cell mobility, macrophages infiltration as well as M2 polarization process. The study not only revealed the multifactorial role of FAP in gastrointestinal cancer progression but also provided the first evidence that M2 macrophages played dominant roles underlying FAP immune-suppressive effects, revealing a novel target for future treatment options.

Materials and methods

Gene expression analysis

Data collected from the Cancer Genome Atlas (TCGA) were used to visualize the mRNA expression level of FAP in various human cancers and their normal counterparts. Furthermore, the TISBID website was used to examine the expression of FAP mRNA and the grading of tumors. The relationship between FAP mRNA expression in the normal, tumor and metastasis site was evaluated using TNMplot online server.

Protein expression and immunohistochemistry staining

In order to investigate the expression of FAP protein in different human tumors and their normal counterparts, the UALCAN program was used. UALCAN developed protein expression analysis using data collected from the Clinical Proteomic Tumor Analysis Consortium (CPTAC). The IHC staining images of FAP in different tumor tissues and normal tissues were obtained from HPA (Human Protein Atlas) dataset.

For IHC staining of LIHC tissues from patients, antigens were retrieved by sodium citrate for 10 min. Later the sections were incubated with 5% BSA at room temperature for 1 h to get rid of unspecific bindings. Primary antibodies were diluted with PBS and an overnight incubation was conducted at 4 °C. Following primary antibodies, the sections were washed and incubated by secondary antibodies for 1 h the next day. Afterwards, color reaction was carried out using DAB kit. All images were captured using an optical microscope.

Survival prognosis and ROC diagnosis analysis

Sangerbox webserver was utilized to evaluate the survival outcomes of FAP in different human cancers. To explore the diagnosis value of FAP in various cancers, the pROC R package was used for statistical analysis and ggplot2 R package was used to create the receiver operating characteristic (ROC) curve. ROC curves of FAP with Area Under the Curve (AUC) more than 0.7 was regarded as high diagnostic values in different types of human cancers.

FAP methylation analysis

DNA methylation is a kind of DNA chemical modification and behaves as an essential regulator of gene transcription. FAP DNA methylation analysis using data collected from TCGA database was conducted using UALCAN. Analysis of the correlation between FAP expression and gene promoter methylation was developed for each type of cancer.

Protein-protein interaction and functional enrichment analysis

FAP co-expression data was downloaded from TCGA dataset. $|\log_2 FC| > 1.5$, adj $p < 0.05$ was used as a standard to obtain FAP-correlating genes. These genes were enriched by Gene Ontology (GO) [including biological processes (BP), cellular components (CC), and molecular function (MF)] and KEGG pathway analyses. Then the STRING website was used to acquire top 20 FAP-interacting genes. Vein diagram was used to conduct analysis to compare FAP-correlating and interacting genes in different human cancers. The "Gene_Corr" module of Timer2.0 was used to generate heatmap or correlation curve of FAP-correlating and interacting genes, which contains partial correlation and p value.

Immune reactivity analysis

Estimation of Immune Cells in Malignant Tumor Tissues Using Expression Data (ESTIMATE) is a method to investigate the degree of stroma or immune cell infiltration into tumors according to existing gene expression data. The ESTIMATE was used to estimate immune scores for each tumor. The correlation between FAP expression and immune cell infiltration was calculated using MCPcounter by Sangerbox webserver. In addition, the relationship between FAP and immune check-point, tumor mutation burden (TMB) and microsatellite instability (MSI) was also evaluated using SangerBox webserver.

Single-cell sequencing analysis

The expression of FAP, MRC1 and NOS2 in different cellular component of tumor was obtained and analyzed using scTIME Portal online server. The species and cancer type were first tabbed to select a dataset. Then the gene name was inserted to visualize FAP, MRC1 and NOS2 expression in different cells in malignant tumor. The interactions among fibroblasts, tumor cells and macrophages were also obtained and analyzed using CellphoneDB analysis via scTIME Portal online server.

Cell lines and cell culture

The human hepatic stellate LX2 cell line, liver cancer MHCC97H and SK-Hep1 cell line, monocyte THP-1 cell line was purchased from Stem Cell Bank, Chinese Academy of Sciences. All cells were cultured at 5% CO_2 and 37°C in DMEM or RPMI-1640 medium and routinely examined to exclude mycoplasma contamination by Genetic Testing Biotechnology Corporation (Suzhou, China).

Cell transfection and cell stimulation

FAP plasmid and its corresponding control plasmid were designed and constructed. During transfection, lipofectamine 3000 reagent was used according to the manufacturer's protocol. The culture medium was collected 48 h after transfection and then filtered to remove cellular debris. The culture medium was then transferred to MHCC97H and SK-Hep1 liver cancer cells as well as PMA-treated THP-1 cells. The migration and invasion of cancer cells were detected using wound healing assay and transwell assay. The polarization state of THP-1 cells was detected by qRT-PCR.

Wound healing and transwell assay

For wound healing assay, the MHCC97H and SK-Hep1 cells were planted in 6-well plates at a density of $4\times10\text{^}5$, scratches were made in the middle of the well. The cells were treated with conditioned medium collected from LX2 cells for 48 h, then the wound closure was measured.

For transwell assay, $1.5\times10\text{^}4$ cells were treated with serum-free medium and inoculated in the upper chamber. The LX2 cells were planted in the lower chamber and treated with complete medium. After 24 h culture, cells that migrated across the membrane were stained using 1% crystal violet and photographed.

Quantitative reverse-transcriptase PCR analysis and western blotting

Total RNA was extracted from LX2 and THP-1 cells using TRIzol reagent and 1 μg total RNA was then reverse-transcribed. Quantitative reverse-transcriptase PCR was conducted using a reaction mix of SYBR Green and the relative expression of target genes was compared using ΔΔCt method and GAPDH served as the endogenous gene.

Total protein was lysed from cells by RIPA lysis buffer added with protease inhibitor. Protein concentration was measured using the BCA Protein Assay Kit. SDS-PAGE was used to separate the proteins and PVDF membrane was used to transfer the proteins. 5% skim milk was used to block unspecific bindings at room temperature for 1 h and then primary antibodies were used to incubate the membrane. After overnight incubation, the membrane was washed and incubated with secondary antibodies. Finally, the protein bands were visualized by chemiluminescence system.

Statistical analysis

The experimental data were presented as mean ± S.E.M. and analyzed using Graphpad Prism 7.0 software. The difference between two groups were analyzed using Student's t test. $p < 0.05$ was considered as significant.

Results

FAP is abnormally up-regulated and correlated to poor prognosis in gastrointestinal cancers

First, TCGA dataset was used to examine the expression of FAP mRNA in tumors and adjacent normal tissues. According to our findings, FAP mRNA was increased in most of the tumors (22/31)

(Supplementary Figure 1A). Notably, we noticed that FAP mRNA was commonly increased in gastrointestinal cancers such as LIHC, COAD, PAAD and STAD, which attracted our attention (Figure 1A). In this regard, we further analyzed the expression of FAP at protein level in these gastrointestinal tumors using the National Cancer Institute's CPTAC dataset. Results indicated that the expression of FAP protein was significantly up-regulated in LIHC, COAD, PAAD as compared to their normal counterparts, which was also validated by IHC staining pictures acquired from the Human Protein Atlas (HPA) dataset. The protein expression data of FAP in STAD was not found using CPTAC, higher FAP protein expression was still observed in the IHC staining pictures (Figures 1B, C). Then we intended to investigate whether the up-regulation of FAP in tumor tissues correlated to DNA methylation of FAP promotor using UALCAN online tool. Beta value ranging from 0 (unmethylated) to 1 (fully methylated) in Figure 1D

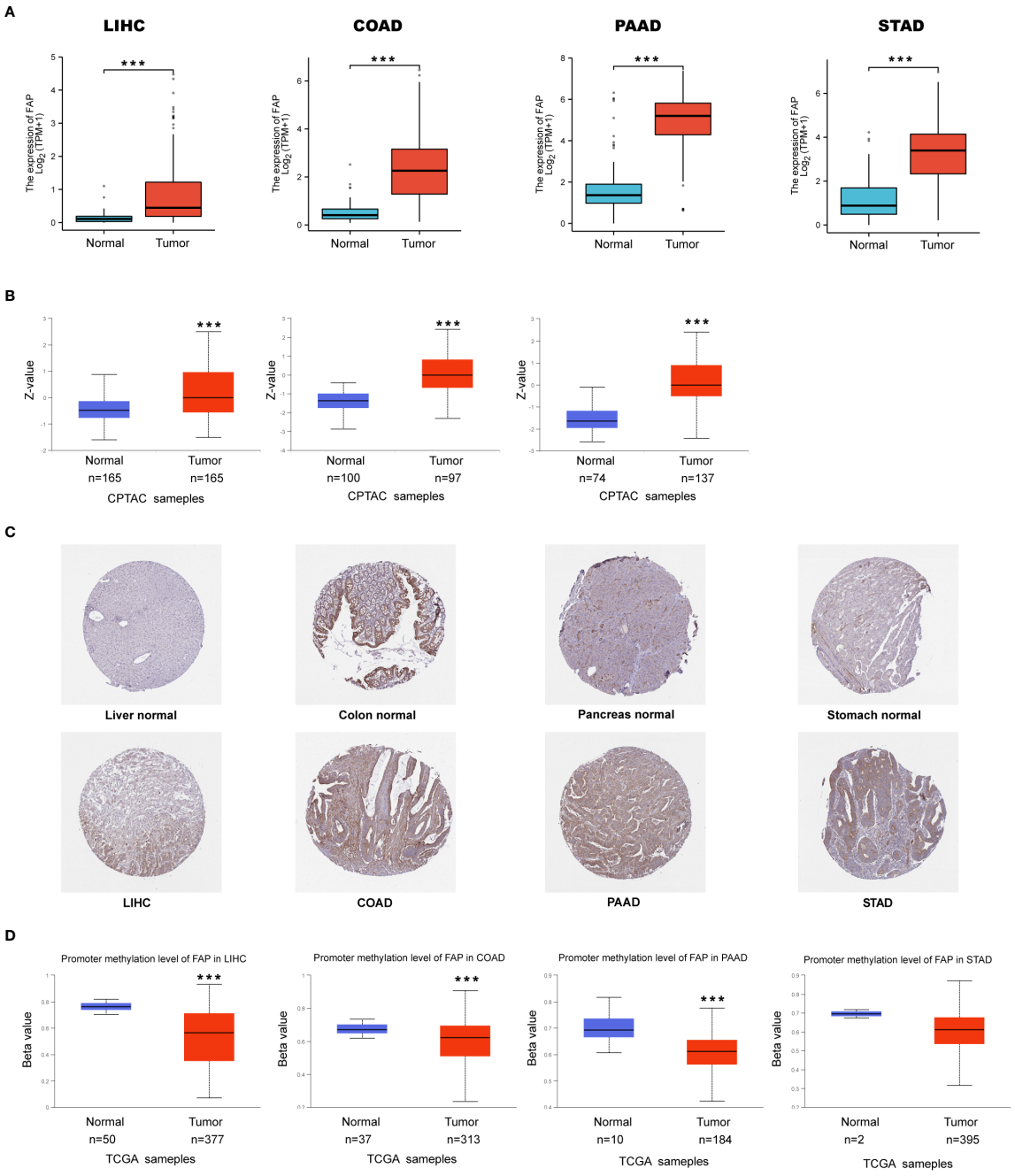

FIGURE 1
FAP up-regulation by DNA methylation in gastrointestinal cancers. **(A)** Expression of FAP mRNA in gastrointestinal cancers. **(B, C)** Expression of FAP protein in gastrointestinal cancers versus normal tissues (left side), and IHC staining for normal tissue (middle) and tumors (right side) from HPA database. **(D)** Differential expression of FAP promotor methylation in gastrointestinal tumors versus normal tissues. ***$p < 0.001$.

indicates the level of DNA methylation, 0.5 to 0.7 indicates hypermethylated, while hypomethylated when the value ranging from 0.25 to 0.3. Our results suggested that the methylation of FAP promotor was significantly lower in LIHC, COAD and PAAD as compared to normal tissues. Though the data showed that DNA methylation at FAP promotor in STAD is unaffected, we speculated that this may be due to limited case numbers since there is still a downregulated tendency (Figure 1D).

Then TNM plot online server was used to compare expression of FAP mRNA in normal, tumor and metastasis sites. Results indicated that FAP mRNA was significantly up-regulated in tumors of liver, colon, pancreas as compared to normal tissues. Furthermore, this pattern would maintain between the metastatic and cancerous sites in colon (Supplementary Figure 1B). Subsequently, we tried to figure out the association between FAP mRNA and cancer stages. By TISDIB online web server, we found that FAP was positively correlated to the disease stage of COAD as well as PAAD (Supplementary Figure 1C). Moreover, FAP could affect the survival probability of gastrointestinal cancer patients and has high diagnostic accuracy in the model of ROC analysis for the cancers (Supplementary Figures 2, 3).

FAP is correlated to extracellular matrix organization in gastrointestinal cancers

Afterwards, it is essential to investigate the functions of FAP across different gastrointestinal cancers. FAP-correlating proteins with $|\log_2 FC| > 1.5$, adj $p < 0.05$ were obtained from TCGA datasets. Totally 872, 822, 245 and 312 genes were identified correlated to FAP in LIHC, COAD, PAAD and STAD, respectively (Figure 2A). To further investigate the functional significance of FAP in these cancers, FAP-correlating proteins obtained from different cancers were reanalyzed using Gene Ontology (GO) enrichment analysis. Results showed that FAP may be closely associated with extracellular matrix or structure organization process across all these four tumors (Figures 2B–F). Undoubtedly, the data also suggested that FAP was involved in specific functions of certain tumor, for instance, FAP is also associated with digestion function in PAAD (Figure 2E).

Then vein diagram identified totally 26 genes that were commonly correlated to FAP expression across these four tumors (Figure 3A). At the meanwhile, top 20 FAP-interacting genes were extracted from STRING database and displayed as a protein-protein interaction network (Figure 3B). After comparing proteins from these two lists, 4 genes including COL1A1, COL1A2, COL3A1 and POSTN were identified both correlated and interacted with FAP in gastrointestinal cancers (Figure 3C). A heatmap created by Timer2.0 then validated significant positive correlation between these four genes and FAP (Figure 3D). Besides, we also used Timer2.0 to obtain correlation analysis plots of all these 4 genes with FAP (Figure 3E): COL1A1 (R = 0.72), COL1A2 (R = 0.79), COL3A1 (R = 0.75) and POSTN (R = 0.76).

FAP is correlated to M2 macrophage infiltration in gastrointestinal cancers

Since extracellular matrix organization process plays crucial roles in building the immune-suppressive tumor microenvironment (TME) (17), then we tried to figure out whether FAP was involved in the immune-regulatory process. We utilized the ESTIMATE algorithm to calculate the correlation between FAP expression and immune scores. Results showed that FAP was positively correlated to immune scores in LIHC, COAD, PAAD and STAD (Figure 4A). In addition, significant correlation between FAP and immune check-points, MSI and TMB also suggested that FAP was involved in cancer immunology (Supplementary Figures 4A–C). We then intended to examine the relationship between FAP and the infiltration of different immune cells using MCPcounter. Results indicated that FAP was significantly correlated to monocyte across all the four gastrointestinal cancers (Figure 4B). Monocytes are the main source of macrophages and FAP was found positively correlated to the infiltration of macrophages across all these cancers (Figure 4C), suggesting that FAP may be involved in cancer immunology by regulating macrophages functions.

As is known, macrophages are a kind of immune cells that could exert opposite effects depending on their polarization phenotypes, with M1 suppressive while M2 promotive on tumor progression. The M1 macrophages usually expressed markers like NOS2 (iNOS), TNF, IL1B, while M2 expressed MRC1 (CD206), Arg-1, IL-10 and so on. By single-cell sequencing analysis, we found that MRC1 was highly and primarily expressed in macrophages across these four gastrointestinal cancers (Supplementary Figures 5A–D). Gene correlation analysis indicated a positive correlation between the expression of FAP and MRC1 in the gastrointestinal cancers (Figure 4D), suggesting that FAP was possibly involved in M2 macrophage infiltration in gastrointestinal cancers.

FAP is primarily expressed in fibroblasts in gastrointestinal cancers

It has been reported that the four FAP-correlating and interacting genes were mainly expressed in fibroblasts of tumors (18, 19), then we intended to investigate whether FAP was also expressed in fibroblasts in gastrointestinal cancers. By using scTIME Portal online server for single-cell sequencing analysis. We found that FAP was exclusively expressed in fibroblasts as well as cancer associated fibroblasts (CAFs) in LIHC (GSE125449) (Figure 5A). Similarly, same conclusions were obtained from single-cell sequencing analysis of COAD (GSE146771), PAAD (cra001160) as well as STAD (phs001818.v1.p1) (Figures 5B–D). By further analysis using CellphoneDB analysis, we found there are strong interactions between fibroblasts and tumor cells as well as macrophages in gastrointestinal cancer tissues (Supplementary Figures 6A–D). These results indicated that FAP was primarily expressed in fibroblasts and its role on tumor progression was achieved via affecting the interaction between fibroblasts, tumor cells and macrophages.

FAP-over-expressed fibroblasts promoted cancer cell motility in LIHC

First, we investigated the role of FAP in fibroblasts on tumor cells *in vitro*. LIHC is one of the gastrointestinal cancers that

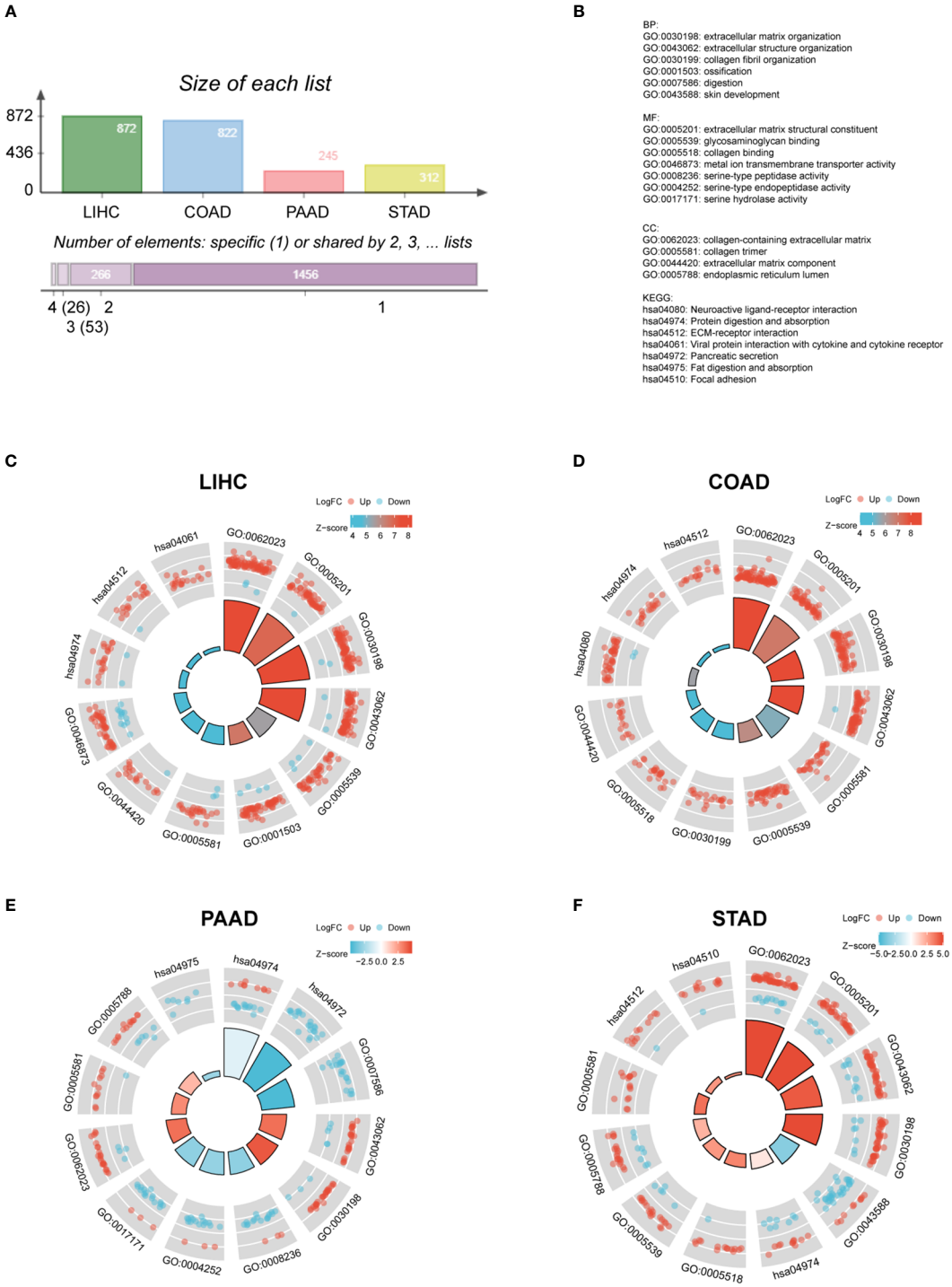

FIGURE 2
GO and KEGG analysis of FAP in different gastrointestinal cancers. **(A)** FAP-correlating genes in different gastrointestinal cancers. **(B)** GO and KEGG functional annotations. GO and KEGG analysis of FAP in **(C)** LIHC. **(D)** COAD. **(E)** PAAD. **(F)** STAD.

influenced by FAP, we overexpressed FAP in human hepatic stellate LX2 cell line, the key source of fibroblast in LIHC and then collected the cell medium 48 h later (Figures 6A, B). The medium was used to treat liver cancer MHCC97H and SK-Hep1 cells for 48 h or 24 h, tumor cell migration and invasion was examined using wound healing test as well as the transwell invasion assay (Figure 6C). Results showed that the conditioned medium from FAP-over-expressed LX2 cells could significantly promote the cell invasion

10.3389/fimmu.2023.1183440

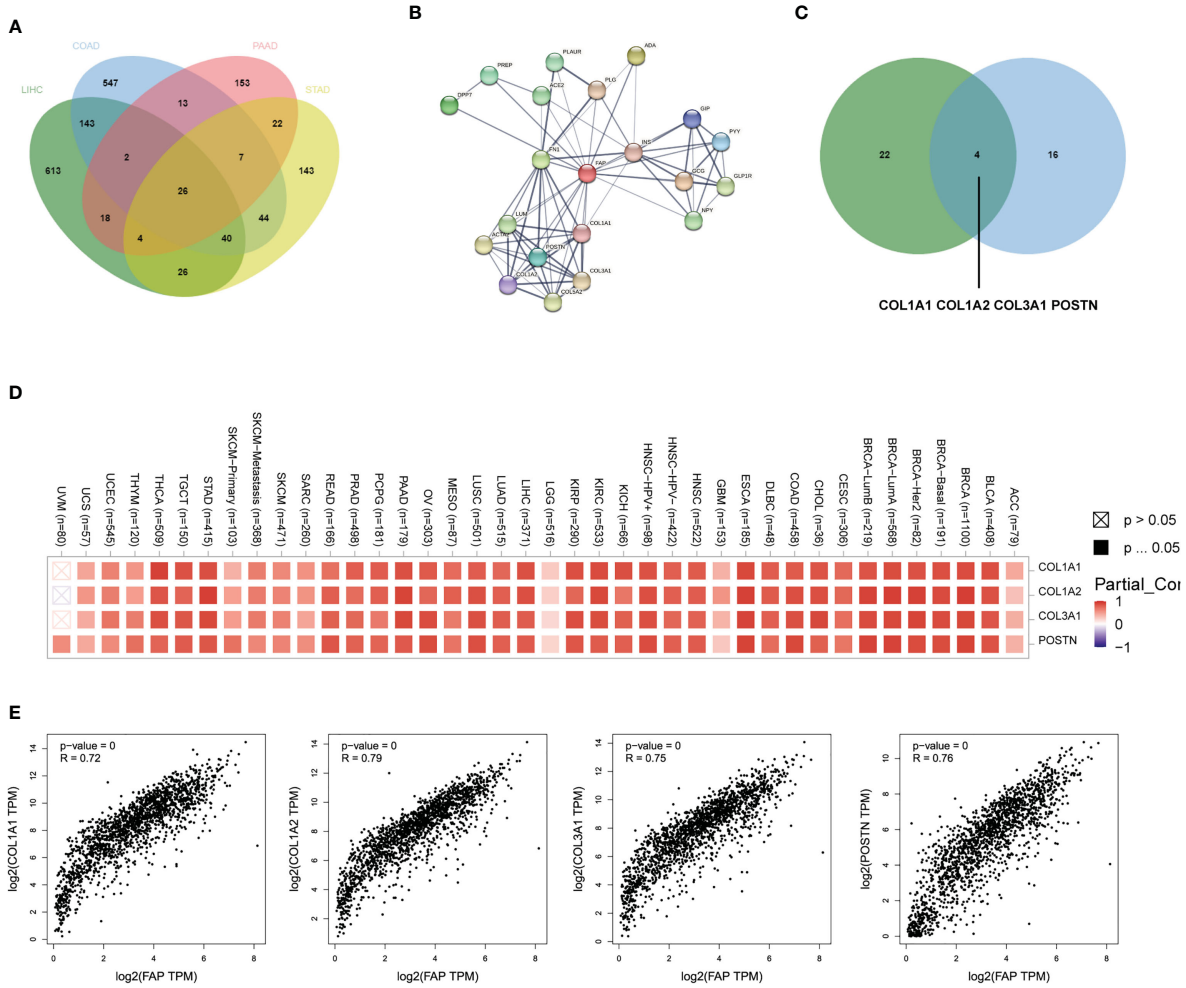

FIGURE 3
FAP-associated protein network interactions in different gastrointestinal cancers. **(A)** FAP-correlating proteins in different gastrointestinal cancers. **(B)** A map of top 20 FAP-interacting proteins analyzed by STRING database. **(C)** Vein diagram showing overlap between FAP-correlating and interacting proteins in different human cancers. **(D)** Heatmap showing both FAP-correlating and interacting proteins in tumor tissues. **(E)** Expression correlation analysis between FAP and FAP-correlating and interacting proteins in tumor tissues.

and migration rate of both MHCC97H and Sk-Hep1 cells as compared to NC group (Figures 6D, E), suggesting that FAP in fibroblast is involved in tumor cell motility process in LIHC.

FAP-over-expressed fibroblasts promoted macrophages infiltration and M2 polarization in LIHC

In LIHC, IHC staining suggested that more M2 macrophages were presented in tumor tissues of patients with high FAP expression (Figure 7A). In *in vitro* experiments, THP-1 monocyte was first treated by PMA for 48 h and then stimulated by the conditioned medium collected from LX2 cells (Figure 7B). The conditioned medium collected from FAP-over-expressed LX2 cells could significantly promote the invasion rate of THP-1 macrophages as compared to the NC group (Figures 7C, D). Then qRT-PCR was conducted to examine M1 or M2 macrophage marker alterations in THP-1 cells. Results showed that conditioned medium from FAP-over-expressed LX2 cells could decrease the expression of M1 markers like iNOS, TNF-α and IL-1β but increase the expression of M2 markers like IL-10 in macrophages as compared to NC group, transforming the macrophages into M2 pro-tumor phenotype (Figure 7E). These results indicated that FAP in fibroblasts is involved in macrophages infiltration and M2 polarization in LIHC

In summary, FAP is primarily expressed in fibroblasts of gastrointestinal cancers and promoted cancer progression via promoting tumor cell motility as well as macrophages infiltration and M2 polarization.

Discussion

FAP is a serine peptidase that share 70% of the sequence identity with the enzyme dipeptidyl-peptidase to facilitate extracellular matrix reorganization and promote tumor malignancies. The current study started with analyzing the

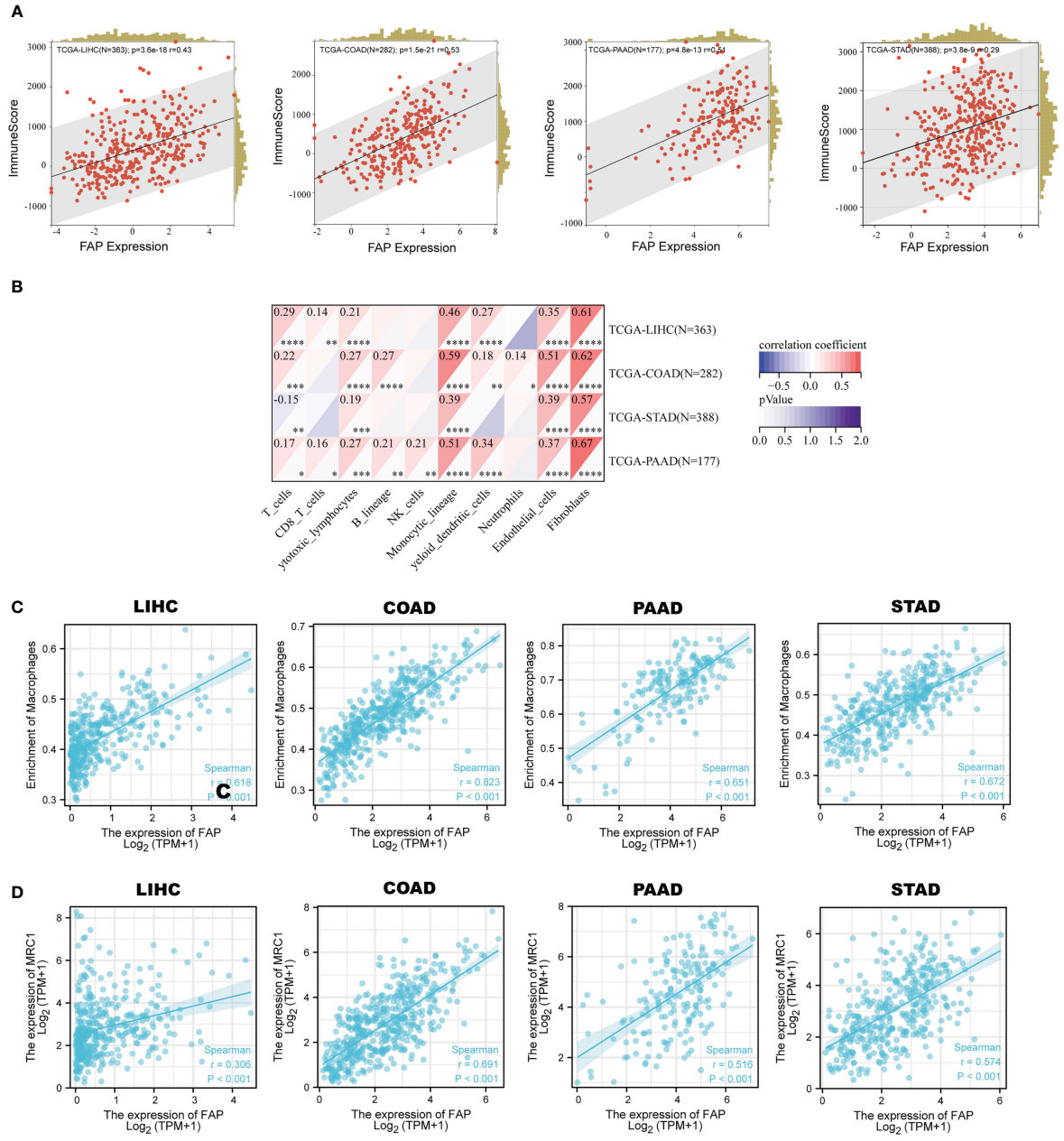

FIGURE 4
Correlation between FAP and M2 macrophages infiltration in gastrointestinal cancers. **(A)** Correlation between FAP expression and immune scores across gastrointestinal cancers. **(B)** Analysis of immune cell infiltration correlated to FAP expression across gastrointestinal cancers. **(C)** Scatter plots showing the correlation between FAP expression and macrophage infiltration in gastrointestinal cancers. **(D)** Scatter plots showing the correlation between FAP expression and M2 macrophage marker MRC1 in gastrointestinal cancers.

mRNA level of FAP in a list of human cancers, where it was found that FAP mRNA was significantly up-regulated in 22 of 31 cancers. Interestingly, we found that FAP mRNA was consistently up-regulated in gastrointestinal cancers including LIHC, COAD, PAAD as well as STAD. Similar findings were observed at protein level via CPTAC and HPA dataset and the expression of FAP positively correlated with poor outcomes of gastrointestinal cancers. As gastrointestinal cancers are increasingly prevalent in the world and possibly account for 20% of cancer cases (20), we suspected that FAP could be a potential gastrointestinal cancer biomarker and instructive for future treatment options.

Previous evidence has already demonstrated a significant role of FAP in tumor progression through multiple mechanisms. For instance, the invasion and migration ability of cancer cells was significantly promoted after coculturing with FAP positive CAFs isolated from the stroma tissue of breast cancer patients (21). Inhibition of FAP via anti-FAP IgG1 antibody or knock-down by siRNA could reverse FAP-mediated migration and invasion promotion (22). Besides, FAP was also involved in angiogenesis of TME, depletion of FAP and dipeptidyl peptidase 4 (DPP4) in CAFs led to decease of vascularization in colorectal cancer, while such effect was not observed when DPP4 was depleted alone (23). In

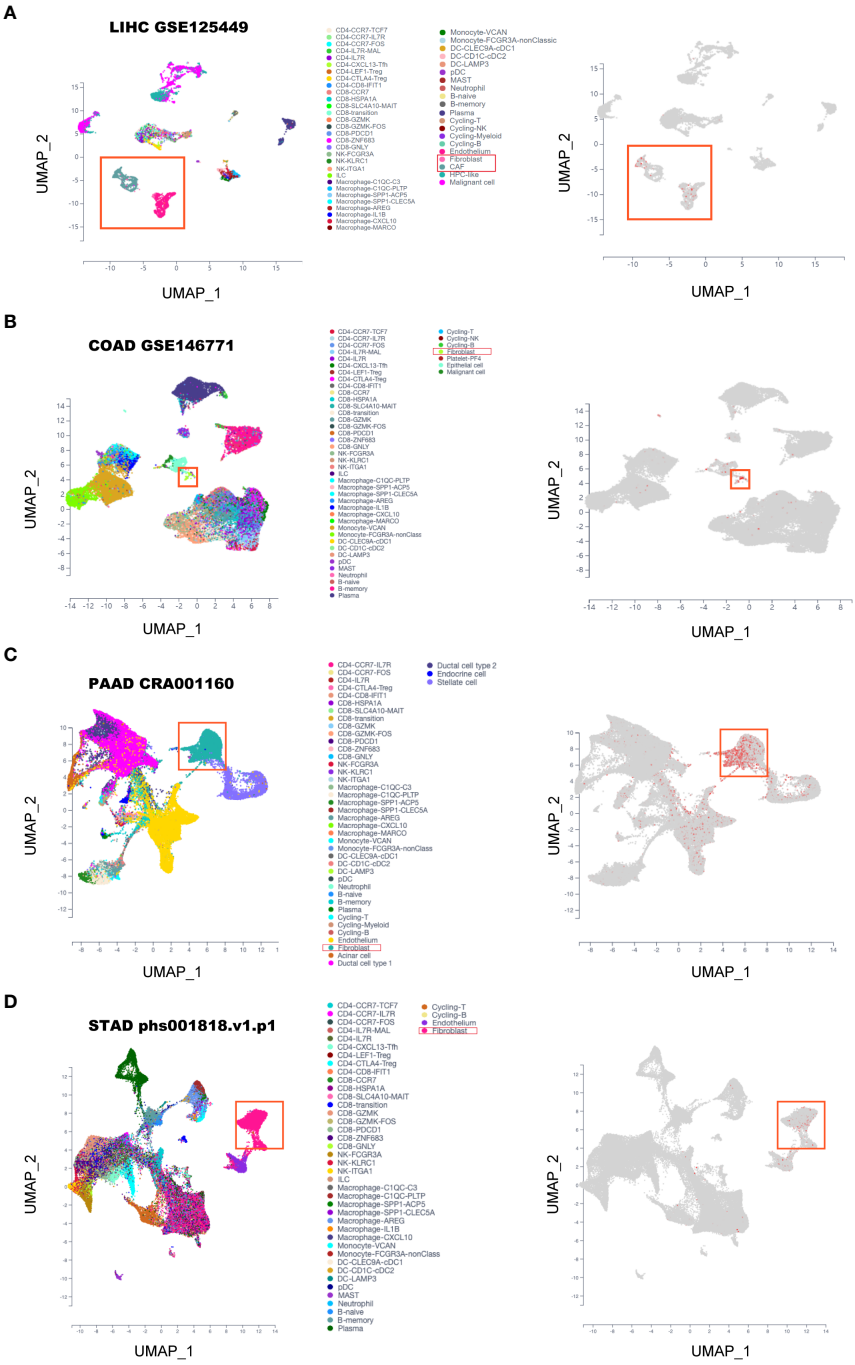

FIGURE 5
Single-cell sequencing analysis of FAP expression in gastrointestinal cancers. **(A)** LIHC. **(B)** COAD. **(C)** PAAD. **(D)** STAD.

the present study, we found that FAP was generally involved in extracellular matrix organization process across all these four gastrointestinal cancers by analyzing FAP-correlated genes in LIHC, COAD, PAAD and STAD. After comparing the commonly correlated genes of FAP across gastrointestinal cancers with top 20 FAP-interacting genes extracted from STRING database, 4 genes including COL1A1, COL1A2, COL3A1 and POSTN were identified both correlated and interacted with FAP. It is noteworthy that all these 4 genes have been demonstrated to be involved in extracellular matrix organization process (18, 19), validating our previous findings.

Since extracellular matrix contributes to the construction of the immune microenvironment surrounding tumor cells (17, 24, 25), we found that FAP was positively correlated to immune scores across different gastrointestinal cancers by the ESTIMATE algorithm, suggesting that FAP is involved in cancer immune regulation. More importantly, we found that FAP was significantly correlated to macrophages infiltration across

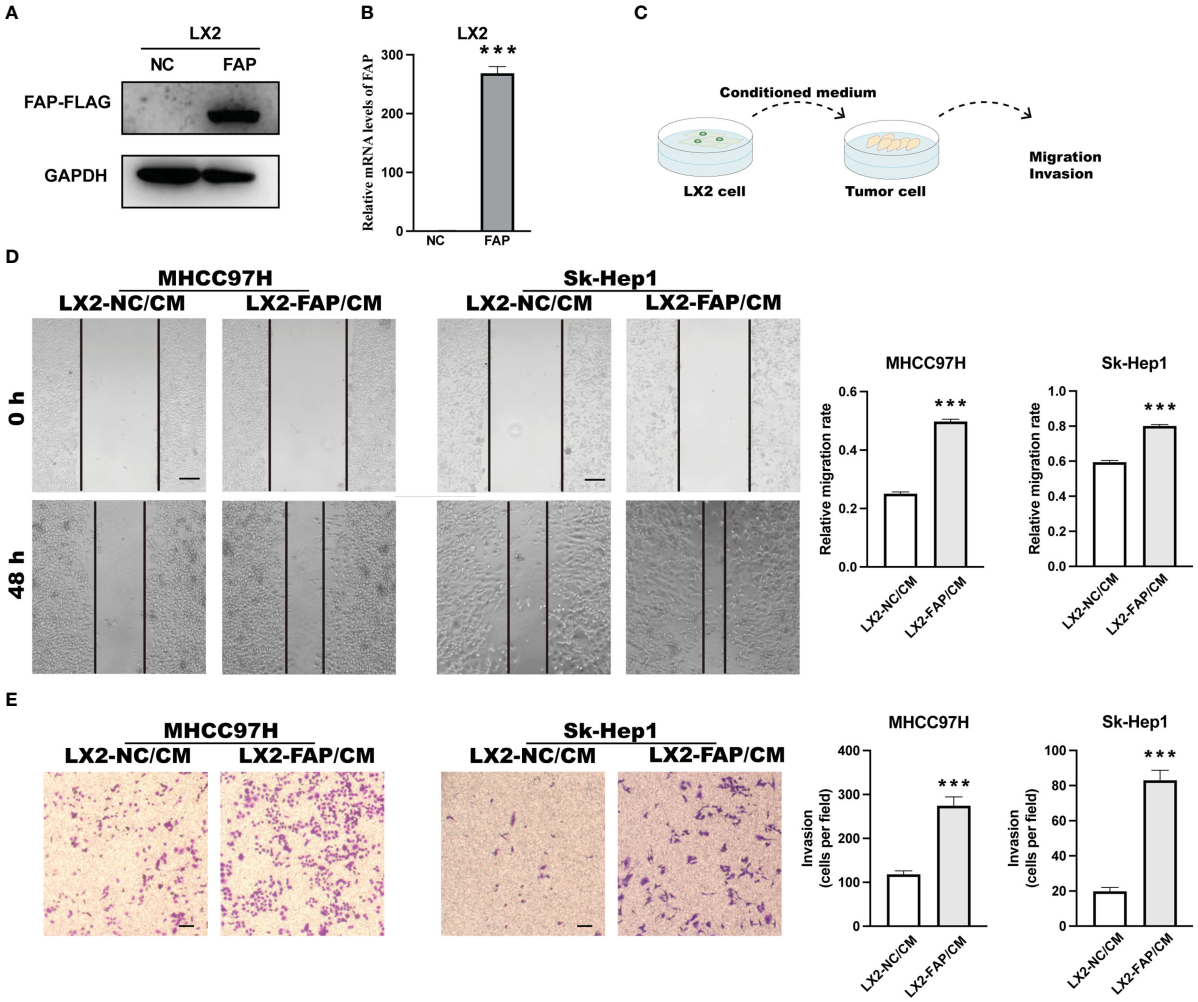

FIGURE 6
Experimental validation of relationship between FAP expression and tumor cell motility in LIHC. **(A, B)** FAP expression after FAP overexpression in human hepatic stellate LX2 cell line. **(C)** Experimental diagram. **(D)** Wound healing assay investigating the effect of FAP on tumor cell migration. **(E)** Transwell assay investigating the effect of FAP on tumor cell invasion. ***$p < 0.001$. Scale bar = 200 μm.

gastrointestinal cancers, suggesting that the immune-regulatory effect of FAP in gastrointestinal cancers is possibly mediated by macrophages. It is commonly accepted that macrophages can be classified into two phenotypes, the classically activated pro-inflammatory M1 phenotype as well as the alternatively activated anti-inflammatory M2 phenotype (26). In most cases, M1 phenotype of macrophages exhibited positive correlation to better prognosis and longer survival times of patients with cancer like lung cancer (27), colon cancer (28), breast cancer (29) and so on, while the M2 phenotype exhibited opposite roles. It is recorded that the majority of macrophages surrounding the tumor exhibited an M2 phenotype and can assist the tumor cells in proliferation, metastasis, angiogenesis, immune escape and drug resistance (30–32). By bioinformatic analysis, we found that FAP was positively correlated to the expression of M2 macrophages marker MRC1 across gastrointestinal cancers, suggesting that FAP may be involved in regulating M2 macrophages in these cancers.

Afterwards, we intended to validate the findings of FAP on macrophages by experiments. FAP was found primarily expressed in fibroblasts across these cancers by single-cell sequencing analysis, verified previous findings that FAP behaves as a marker of CAFs (33). Furthermore, strong interactions have been identified between fibroblasts and macrophages, suggesting that fibroblasts may be involved in regulating macrophages functions across gastrointestinal cancers. For instance, the fibroblasts-derived CSF-1, IL-6 and CCL2 has been found to promote macrophages infiltration and M2 phenotype polarization process in pancreas cancer (34). As for the effect of FAP in fibroblasts on macrophages functions, though FAP in fibroblasts have been demonstrated to be closely located with pro-tumor macrophages in tumor tissues and involved in macrophages migration process (12, 35), the role of FAP on macrophages functions has not been further investigated yet. In the present study, we over-expressed FAP in human hepatic stellate LX2 cells for 48 h and collected medium to treat macrophages. The results showed that medium from FAP-over-expressed LX2 cells could promote the invasion ability of macrophages and increase their transformation into M2-like phenotype, providing the first evidence that FAP is involved in macrophage M2 polarization in

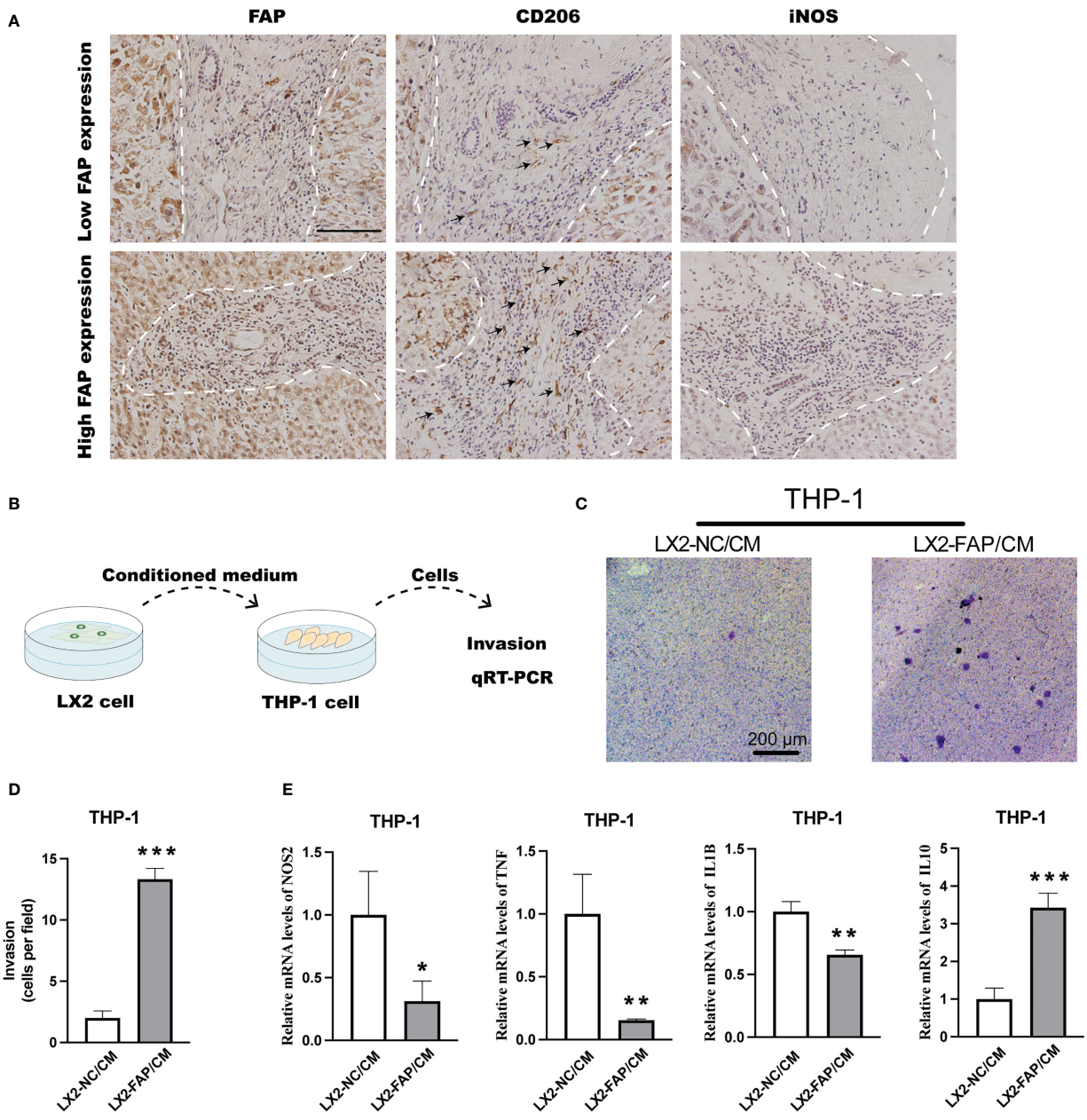

FIGURE 7
Experimental validation of relationship between FAP expression and M2 macrophage polarization. **(A)** IHC staining of FAP, CD206 and iNOS in LIHC tissues. **(B)** Experimental diagram. **(C, D)** Transwell assay investigating the effect of FAP on macrophage invasion. **(E)** Transwell co-culturing system investigating the effect of FAP on M2 macrophage polarization. *$p < 0.05$, **$p < 0.01$, ***$p < 0.001$. Scale bar = 1 mm.

gastrointestinal cancers. Furthermore, we also investigated the effect of FAP in fibroblast on tumor cells. Results showed that medium from FAP-overexpressed LX2 cells could promote tumor cell migration as well as invasion process. Based on these results, we found that the up-regulation of FAP could promote gastrointestinal cancers progression through promoting tumor cell motility as well as macrophages infiltration and M2 polarization.

Although our study is not the first work to demonstrate the significant role of FAP in tumor, there is still some innovations. First, we are the first to give a comprehensive illustration of FAP across gastrointestinal tumors using bioinformatics methods and then validate significant findings using experimental methods. Second, our study laid the foundation for detailed studies of the correlation between FAP expression and diverse immune cell infiltrations, first revealing the role of FAP on inducing M2 macrophages polarization to promote tumor progression across gastrointestinal cancers. Regretful, these results were obtained only focusing on FAP that expressed in fibroblasts, though previous evidence has demonstrated that fibroblasts contribute to main source of FAP in tumor tissues, FAP could also be detected in other kinds of cells like tumor cells, endothelial cells, monocytes, lymphocytes at lower concentration (36, 37), in this regard, their effects in tumor progression cannot be neglected and required more experiments for analysis.

In conclusion, the present study provided the first multifactorial analysis of FAP in gastrointestinal cancers, revealing that the up-regulation of FAP in these cancers is correlated to tumor progression through promoting tumor cell motility as well as macrophages infiltration and M2 polarization. These findings may provide more evidence for FAP as gastrointestinal cancers treatment targets.

Data availability statement

The original contributions presented in the study are included in the article/Supplementary Material. Further inquiries can be directed to the corresponding authors.

Author contributions

JC, DY and HS contributed equally to this work. JC and DY contributed conception and design of the study. HS and LX organized the database. FH, MZ, LZ and MJ performed the statistical analysis. JC, DY and HS wrote the first draft of the manuscript. LX, FH, MZ, LZ and MJ wrote the sections of the manuscript. All authors contributed to manuscript revision, read and approved the submitted version.

Funding

This work was supported by grant from the National Natural Science Foundation of China (31771627 and 32270759) and Interdisciplinary Research Foundation of HIT (No. IR2021102 of HN).

Acknowledgments

Publicly available datasets were used and analyzed in the present study. We sincerely appreciated to the teams of the open source of software or databases involved in this study, including but not limited to Sangerbox, scTIME Portal.

Conflict of interest

The authors declare that the research was conducted in the absence of any commercial or financial relationships that could be construed as a potential conflict of interest.

Publisher's note

Supplementary material

The Supplementary Material for this article can be found online at: https://www.frontiersin.org/articles/10.3389/fimmu.2023.1183440/full#supplementary-material

SUPPLEMENTARY FIGURE 1
Correlation between FAP expression and clinical outcome of gastrointestinal cancers. **(A)** Expression of FAP mRNA in pan-cancers. **(B)** Expression of FAP in normal, tumor and metastatic sites of gastrointestinal cancers. **(C)** Expression of FAP across different stages of gastrointestinal cancers. $^{**}p < 0.01$, $^{***}p < 0.001$

SUPPLEMENTARY FIGURE 2
Cox regression analysis of FAP in pan-cancers. **(A)** LIHC. **(B)** COAD. **(C)** PAAD. **(D)** STAD.

SUPPLEMENTARY FIGURE 3
ROC curves indicating the AUC of FAP in gastrointestinal cancers. **(A)** LIHC. **(B)** COAD. **(C)** PAAD. **(D)** STAD.

SUPPLEMENTARY FIGURE 4
Correlation between FAP and immune check-points, MSI and TMB. **(A)** immune check-points. **(B)** MSI. **(C)** TMB.

SUPPLEMENTARY FIGURE 5
Single-cell sequencing analysis of NOS2 and MRC1 in gastrointestinal cancers. **(E)** LIHC. **(F)** COAD. **(G)** PAAD. **(H)** STAD.

SUPPLEMENTARY FIGURE 6
Single-cell sequencing analysis of fibroblasts and macrophages interactions in gastrointestinal cancers. **(A)** LIHC. **(B)** COAD. **(C)** PAAD. **(D)** STAD.

References

1. Tong Y, Gao H, Qi Q, Liu X, Li J, Gao J, et al. High fat diet, gut microbiome and gastrointestinal cancer. *Theranostics* (2021) 11:5889–910. doi: 10.7150/thno.56157

2. Alese OB, Cook N, Ortega-Franco A, Ulanja MB, Tan L, Tie J, et al. An emerging tool in gastrointestinal cancers. *Am Soc Clin Oncol Educ Book* (2022) 42:1–20. doi: 10.1200/EDBK_349143

3. Man SM. Inflammasomes in the gastrointestinal tract: infection, cancer and gut microbiota homeostasis. *Nat Rev Gastroenterol Hepatol* (2018) 15:721–37. doi: 10.1038/s41575-018-0054-1

4. Cheng X, Wang X, Nie K, Cheng L, Zhang Z, Hu Y, et al. Systematic pan-cancer analysis identifies TREM2 as an immunological and prognostic biomarker. *Front Immunol* (2021) 12:646523. doi: 10.3389/fimmu.2021.646523

5. Mathew S, Scanlan MJ, Mohan Raj BK, Murty VV, Garin-Chesa P, Old LJ, et al. The gene for fibroblast activation protein alpha (FAP), a putative cell surface-bound serine protease expressed in cancer stroma and wound healing, maps to chromosome band 2q23. *Genomics* (1995) 25:335–7. doi: 10.1016/0888-7543(95)80157-H

6. Li M, Younis MH, Zhang Y, Cai W, Lan X. Clinical summary of fibroblast activation protein inhibitor-based radiopharmaceuticals: cancer and beyond. *Eur J Nucl Med Mol Imaging* (2022) 49:2844–68. doi: 10.1007/s00259-022-05706-y

7. Hamson EJ, Keane FM, Tholen S, Schilling O, Gorrell MD. Understanding fibroblast activation protein (FAP): substrates, activities, expression and targeting for cancer therapy. *Proteomics Clin Appl* (2014) 8:454–63. doi: 10.1002/prca.201300095

8. Garin-Chesa P, Old LJ, Rettig WJ. Cell surface glycoprotein of reactive stromal fibroblasts as a potential antibody target in human epithelial cancers. *Proc Natl Acad Sci U.S.A.* (1990) 87:7235–9. doi: 10.1073/pnas.87.18.7235

9. Henry LR, Lee HO, Lee JS, Klein-Szanto A, Watts P, Ross EA, et al. Clinical implications of fibroblast activation protein in patients with colon cancer. *Clin Cancer Res* (2007) 13:1736–41. doi: 10.1158/1078-0432.CCR-06-1746

10. Shi M, Yu DH, Chen Y, Zhao CY, Zhang J, Liu QH, et al. Expression of fibroblast activation protein in human pancreatic adenocarcinoma and its clinicopathological significance. *World J Gastroenterol* (2012) 18:840–6. doi: 10.3748/wjg.v18.i8.840

11. Yuan Z, Hu H, Zhu Y, Zhang W, Fang Q, Qiao T, et al. Colorectal cancer cell intrinsic fibroblast activation protein alpha binds to Enolase1 and activates NF-kappaB pathway to promote metastasis. *Cell Death Dis* (2021) 12:543. doi: 10.1038/s41419-021-03823-4

12. Gao LM, Wang F, Zheng Y, Fu ZZ, Zheng L, Chen LL. Roles of fibroblast activation protein and hepatocyte growth factor expressions in angiogenesis and metastasis of gastric cancer. *Pathol Oncol Res* (2019) 25:369–76. doi: 10.1007/s12253-017-0359-3

13. Santos AM, Jung J, Aziz N, Kissil JL, Pure E. Targeting fibroblast activation protein inhibits tumor stromagenesis and growth in mice. *J Clin Invest* (2009) 119:3613–25. doi: 10.1172/JCI38988

14. Feig C, Jones JO, Kraman M, Wells RJ, Deonarine A, Chan DS, et al. Targeting CXCL12 from FAP-expressing carcinoma-associated fibroblasts synergizes with anti-PD-L1 immunotherapy in pancreatic cancer. *Proc Natl Acad Sci U.S.A.* (2013) 110:20212–7. doi: 10.1073/pnas.1320318110

15. Chen L, Qiu X, Wang X, He J. FAP positive fibroblasts induce immune checkpoint blockade resistance in colorectal cancer via promoting immunosuppression. *Biochem Biophys Res Commun* (2017) 487:8–14. doi: 10.1016/j.bbrc.2017.03.039

16. Wen X, He X, Jiao F, Wang C, Sun Y, Ren X, et al. Fibroblast activation protein-alpha-Positive fibroblasts promote gastric cancer progression and resistance to immune checkpoint blockade. *Oncol Res* (2017) 25:629–40. doi: 10.3727/096504016X14768383625385

17. Sutherland TE, Dyer DP, Allen JE. The extracellular matrix and the immune system: a mutually dependent relationship. *Science* (2023) 379:eabp8964. doi: 10.1126/science.abp8964

18. Lee JS, Mitulovic G, Panahipour L, Gruber R. Proteomic analysis of porcine-derived collagen membrane and matrix. *Materials* (2020) 13(22):5187. doi: 10.3390/ma13225187

19. Li X, Sun Z, Peng G, Xiao Y, Guo J, Wu B, et al. Single-cell RNA sequencing reveals a pro-invasive cancer-associated fibroblast subgroup associated with poor clinical outcomes in patients with gastric cancer. *Theranostics* (2022) 12:620–38. doi: 10.7150/thno.60540

20. Kuntz S, Krieghoff-Henning E, Kather JN, Jutzi T, Hohn J, Kiehl L, et al. Gastrointestinal cancer classification and prognostication from histology using deep learning: systematic review. *Eur J Cancer* (2021) 155:200–15. doi: 10.1016/j.ejca.2021.07.012

21. Gao MQ, Kim BG, Kang S, Choi YP, Park H, Kang KS, et al. Stromal fibroblasts from the interface zone of human breast carcinomas induce an epithelial-mesenchymal transition-like state in breast cancer cells *in vitro*. *J Cell Sci* (2010) 123:3507–14. doi: 10.1242/jcs.072900

22. Teichgraber V, Monasterio C, Chaitanya K, Boger R, Gordon K, Dieterle T, et al. Specific inhibition of fibroblast activation protein (FAP)-alpha prevents tumor progression *in vitro*. *Adv Med Sci* (2015) 60:264–72. doi: 10.1016/j.advms.2015.04.006

23. Fitzgerald AA, Weiner LM. The role of fibroblast activation protein in health and malignancy. *Cancer Metastasis Rev* (2020) 39:783–803. doi: 10.1007/s10555-020-09909-3

24. Xiao Y, Yu D. Tumor microenvironment as a therapeutic target in cancer. *Pharmacol Ther* (2021) 221:107753. doi: 10.1016/j.pharmthera.2020.107753

25. Zhao K, Ma Z, Zhang W. Comprehensive analysis to identify SPP1 as a prognostic biomarker in cervical cancer. *Front Genet* (2021) 12:732822. doi: 10.3389/fgene.2021.732822

26. Pollard JW. Trophic macrophages in development and disease. *Nat Rev Immunol* (2009) 9:259–70. doi: 10.1038/nri2528

27. Ma J, Liu L, Che G, Yu N, Dai F, You Z. The M1 form of tumor-associated macrophages in non-small cell lung cancer is positively associated with survival time. *BMC Cancer* (2010) 10:112. doi: 10.1186/1471-2407-10-112

28. Edin S, Wikberg ML, Oldenborg PA, Palmqvist R. Macrophages: good guys in colorectal cancer. *Oncoimmunology* (2013) 2:e23038. doi: 10.4161/onci.23038

29. Guo L, Cheng X, Chen H, Chen C, Xie S, Zhao M, et al. Induction of breast cancer stem cells by M1 macrophages through Lin-28B-let-7-HMGA2 axis. *Cancer Lett* (2019) 452:213–25. doi: 10.1016/j.canlet.2019.03.032

30. Zhang M, He Y, Sun X, Li Q, Wang W, Zhao A, et al. A high M1/M2 ratio of tumor-associated macrophages is associated with extended survival in ovarian cancer patients. *J Ovarian Res* (2014) 7:19. doi: 10.1186/1757-2215-7-19

31. Talmadge JE, Donkor M, Scholar E. Inflammatory cell infiltration of tumors: Jekyll or Hyde. *Cancer Metastasis Rev* (2007) 26:373–400. doi: 10.1007/s10555-007-9072-0

32. Allavena P, Mantovani A. Immunology in the clinic review series; focus on cancer: tumour-associated macrophages: undisputed stars of the inflammatory tumour microenvironment. *Clin Exp Immunol* (2012) 167:195–205. doi: 10.1111/j.1365-2249.2011.04515.x

33. Dendl K, Koerber SA, Kratochwil C, Cardinale J, Finck R, Dabir M, et al. FAP and FAPI-PET/CT in malignant and non-malignant diseases: a perfect symbiosis? *Cancers* (2021) 13(19):4946. doi: 10.3390/cancers13194946

34. Nagarsheth N, Wicha MS, Zou W. Chemokines in the cancer microenvironment and their relevance in cancer immunotherapy. *Nat Rev Immunol* (2017) 17:559–72. doi: 10.1038/nri.2017.49

35. Han M, Tran TPT, Oh JK. Chronic pancreatitis and cancer risk in a matched cohort study using national claims data in south Korea. *Sci Rep* (2022) 12:5545. doi: 10.1038/s41598-022-09426-z

36. Pure E, Blomberg R. Pro-tumorigenic roles of fibroblast activation protein in cancer: back to the basics. *Oncogene* (2018) 37:4343–57. doi: 10.1038/s41388-018-0275-3

37. Simkova A, Busek P, Sedo A, Konvalinka J. Molecular recognition of fibroblast activation protein for diagnostic and therapeutic applications. *Biochim Biophys Acta Proteins Proteom* (2020) 1868:140409. doi: 10.1016/j.bbapap.2020.140409

frontiers | Frontiers in Oncology

TYPE Original Research
PUBLISHED 30 May 2023
DOI 10.3389/fonc.2023.1170482

OPEN ACCESS

EDITED BY
Esra Akbay,
University of Texas Southwestern Medical Center, United States

REVIEWED BY
Shoib Sarwar Siddiqui,
University of Hertfordshire, United Kingdom
Wei Kang,
The Chinese University of Hong Kong, China

*CORRESPONDENCE
Kangmin Zhuang
zkm1002@126.com
Side Liu
liuside2011@163.com
Yali Zhang
zyl41531@163.com

†These authors have contributed equally to this work and share first authorship

RECEIVED 21 February 2023
ACCEPTED 02 May 2023
PUBLISHED 30 May 2023

CITATION
Huang M, Guo T, Meng Y, Zhou R, Xiong M, Ding J, Zhang Y, Liu S and Zhuang K (2023) Comprehensive analysis of the prognosis and immune effect of the oncogenic protein Four Jointed Box 1. *Front. Oncol.* 13:1170482. doi: 10.3389/fonc.2023.1170482

Comprehensive analysis of the prognosis and immune effect of the oncogenic protein Four Jointed Box 1

Mei Huang[1†], Tian Guo[1†], Yan Meng[1†], Ruling Zhou[1†], Man Xiong[1], Jian Ding[1], Yali Zhang[1*], Side Liu[1,2,3*] and Kangmin Zhuang[1*]

[1]Guangdong Provincial Key Laboratory of Gastroenterology, Department of Gastroenterology, Nanfang Hospital, Southern Medical University, Guangzhou, Guangdong, China, [2]Pazhou Lab, Guangzhou, Guangdong, China, [3]Department of Gastroenterology, Zhuhai People's Hospital (Zhuhai Hospital Affiliated With Jinan University), Zhuhai, Guangdong, China

Background: The Four Jointed Box 1 (FJX1) gene has been implicated in the upregulation of various cancers, highlighting its crucial role in oncology and immunity. In order to better understand the biological function of FJX1 and identify new immunotherapy targets for cancer, we conducted a comprehensive analysis of this gene.

Methods: We analyzed the expression profiles and prognostic value of FJX1 using data from The Cancer Genome Atlas (TCGA) and Genotype-Tissue Expression (GTEx). Copy number alterations (CNAs), mutations, and DNA methylation were analyzed through cBioPortal. The Immune Cell Abundance Identifier (ImmuCellAI) was used to examine the correlation between FJX1 expression and immune cell infiltration. The relationship between FJX1 expression and immune-related genes and immunosuppressive pathway-related genes was analyzed using The Tumor Immune Estimation Resource version 2 (TIMER2). Tumor mutational burden (TMB) and microsatellite instability (MSI) were obtained from TCGA pan-cancer data. The effect of immunotherapy and the IC50 were assessed using IMvigor210CoreBiologies and Genomics For Drug Sensitivity in Cancer (GDSC). Finally, we evaluated the impact of FJX1 on colon cancer cell proliferation and migration through *in vitro* functional experiments.

Results: Our study indicated that FJX1 expression was high in most cancers and was significantly associated with poor prognosis. High FJX1 expression was also linked to significant alterations in CNA, DNA methylation, TMB, and MSI. Positive correlations were found between FJX1 expression and tumor-associated macrophages (TAMs) and with immune-related genes such as TGFB1 and IL-10 and immunosuppressive pathway-related genes such as TGFB1 and WNT1. On the other hand, FJX1 expression showed a negative relationship with CD8+ T cells. Furthermore, high FJX1 expression led to reduced effectiveness of immunotherapy and drug resistance. In colon cancer cells, FJX1 knockdown was found to decrease cell proliferation and migration.

Conclusion: Our research findings demonstrate that FJX1 is a new prognostic factor with a significant role in tumor immunity. Our results highlight the importance of further exploring the potential of targeting FJX1 as a therapeutic strategy in cancer.

KEYWORDS

pan-cancer, FJX1, prognosis, biomarker, immunotherapy

Introduction

Cancer is currently the leading cause of premature death and reduces life expectancy worldwide (1–3). Although traditional treatments have been developed, some patients may become resistant to them (4, 5). Immunotherapy is a promising treatment that can overcome drug resistance and target escape. With the help of public databases, researchers can identify novel immunotherapy targets and therapeutic strategies through pan-cancer analysis of gene expression (6–8).

One potential target for immunotherapy is four jointed box 1 (FJX1), which is closely related to various tumor pathways in other species (9–13). While its biological function and tumor pathogenesis in human cancer are not fully understood, studies have found that FJX1 is highly expressed in several types of cancer, including head and neck cancer, colon cancer, breast cancer, ovarian cancer, and lung cancer (14–18). Additionally, high FJX1 expression has been linked to poor survival in colon cancer and can regulate important proteins in cell cycle progression to enhance proliferation and invasion in nasopharyngeal carcinoma (19–21). Interestingly, a recent study found that FJX1-specific peptides can inhibit the proliferation of high FJX1 expression cancer cells and may serve as a potential immunotherapy for NPC patients (22). These findings suggest that FJX1 may be a candidate diagnostic and prognostic biological target and an immunotherapy target for cancers. Further research in this area may lead to the development of more effective treatments for cancer patients.

In this study, we conducted a comprehensive analysis of the relationship between FJX1 expression and various types of cancer using pan-cancer data from The Cancer Genome Atlas (TCGA) and Genotype-Tissue Expression (GTEx) databases. We also analyzed copy number alteration, mutation status, and DNA methylation of FJX1 using cBioPortal. In addition, we used Immune Cell Abundance Identifier (ImmuCellAI) to examine the correlation between FJX1 expression and immune cell infiltration.

Furthermore, we investigated the association between FJX1 expression and immune-related genes and immunosuppressive pathway-related genes using The Tumor Immune Estimation Resource version2 (TIMER2). We also assessed the tumor mutational burden (TMB) and microsatellite instability (MSI) using TCGA pan-cancer data. Additionally, we examined the immunotherapy effect and IC50 using IMvigor210CoreBiologies and Genomics For Drug Sensitivity in Cancer (GDSC). To validate our findings, we performed functional experiments *in vitro* to determine whether FJX1 promotes colon cancer cell proliferation and migration. We also co-cultured THP1 macrophages with HCT116-siFJX1. Our results indicated that FJX1 is a critical prognostic factor in various cancers and plays a crucial role in tumor immunity. We believe that the pan-cancer analysis of FJX1 can provide new insights into the development of novel therapeutic strategies for cancer treatment.

Materials and methods

FJX1 gene expression analysis

The "ggplot2" R package was used to investigate the FJX1 abnormal expression between 31 types of normal tissue and 33 types of cancer by GTEx (https://commonfund.nih.gov/GTEx) (23) and TCGA (https://portal.gdc.cancer.gov/). We conducted box plots to show the different FJX1 expression between cancerous tissues and paracancerous tissues and in different stages of pathology in numerous tumors, via "ggpubr" and "ggplot" R package, respectively. All the data of TCGA and GTEx for FJX1 were obtained from the UCSC XENA (https://xenabrowser.net/).

Analysis of genetic variation and gene set variation

Genetic variation characteristics of FJX1 were acquired via cBioPortal (https://www.cbioportal.org/) (24), including mutation type, structural variant, and CNA and DNA methylation. Meanwhile, the CNA and DNA methylation correlation with FJX1 mRNA expression were analyzed by the "ggplot2" R package. We explored the correlation between FJX1 and 50 star pathways in HALLMARK via "GSVA score" R package, and a heat map was made via the "ggplot2" R package.

Survival prognosis analysis

The FJX1 expression correlation with prognosis for patients were studied via overall survival (OS), disease-free interval (DFI), disease-specific survival (DSS), and progression-free interval (PFI). The HR

and p-value were displayed via forest diagram. The FJX1 expression correlation with cancer survival were employed via Kaplan–Meier analysis, and the survival curves were manufactured by "survminer" and "survival" R packages.

Immune infiltration and immune modulator genes analysis

We used related metrics including immune score, stromal score, ESTIMATE sore, tumor purity, immune-related pathways, metastasis-related pathways, and DNA damage repair-related pathways to explore the FJX1 expression relation with tumor microenvironment in pan-cancer. Meanwhile, we analyzed the FJX1 expression correlation with immune infiltrating cells in various tumors via ImmuCellAI (http://bioinfo.life.hust.edu.cn/ImmuCellAI#!/) (25). Additionally, we used TIMER2 (http://timer.comp-genomics.org/) (26) to explore the FJX1 expression connection with TMB, MSI, immune-suppressive pathway-related genes, and immune-related genes. The results were all displayed by heat maps made by the "ggplot2" R package.

Immunotherapy analysis

The immunotherapy datasets were obtained from IMvigor210CoreBiologies (http://research-pub.gene.com/IMvigor210CoreBiologies/packageVersions/) to analyze the FJX1 expression relationship with immunotherapy efficacy and overall survival of patients.

Connection between FJX1 and IC50

The connections between FJX1 expression and IC50 of 198 types of drug were analyzed by using the data from GDSC (https://www.cancerrxgene.org/). The first six drugs with positive correlation were selected and used the "ggplot2" R package to make line chart.

Cell culture and treatment

Colon cancer cells from human (HCT116 and SW480) and THP1 were obtained from American Type Culture Collection (ATCC, Manassas, VA, USA). HCT116 and SW480 were cultivated in DMEM (Gbico & Trade,China), and THP1 were cultivated in RPMI-1640 (Gbico & Trade, China). We added 10% fetal bovine serum (FBS, ExCell Bio) in media to feed the cells and incubated the cells in an incubator containing 5% CO_2 at 37°C. For transient transfection, colon cancer cells were transfected with FJX1-siRNA and FJX1-NCRNA using Lipo8000 (Beyotime, Shanghai, China) and DMEM (Gbico & Trade, China), following the manufacturer's instructions. After 48 h, the real-time quantitative PCR (q-PCR) and Western blot (WB) were used to verify transfection efficiency (FJX1-siRNA 5′-GCACUGUAAGG CCAAGUACTT-3′; FJX1-NCRNA 5′-TTCTCCGAACGTGTCACGT-3). For co-culture, we cultivated THP-1 (5×10^5) in a 12-well plate and added 200 ng/ml phorbol-12-myristate-13-acetate (PMA) (MedChemExpress, NJ, USA) for 24 h to differentiate into adhered macrophages and used an inverted microscope to record macrophages morphology. Pretreated colon cancer cells (2×10^5) were seeded in a chamber (0.4 μm pore, Corning, USA), then transferred to the 12-well plate planted with adhered macrophages, and recorded macrophages morphology again after co-culturing for another 24 h. CD80, CD86, and CD163 expressed on co-cultured macrophages were detected by qPCR.

Cell proliferation assay

The pretreated colon cancer cells were planted into a 96-well plate (1×10^3 cells/well). CCK-8 reagent (Yeasen Bio, shanghai, China) was co-incubated with the cells after 24, 48, 72, 96, and 120 h, respectively, according to the manufacturer's instruction. OD450 values were determined via a microplate reader.

Transwell migration assay

We prepared the pretreated colon cancer cells. Complete medium (600 μl) was added in the bottom of a 24-well plate; meanwhile, transwell chambers (0.8 μm pore, Corning, USA) were put in the 24-well plate. A total of 200 μl cell suspension (5×10^4 cells/well) with serum-free medium was planted in transwell chambers. After incubation for 48 h, we used 4% paraformaldehyde to immobilize the cells and 0.1% crystal violet solution for dyeing, then seriously removed the cells in the upper membrane of the chamber with cotton swabs. An upright microscope was used to photograph, and Image J was used to dealt with the results.

Wound healing assay

The pretreated colon cancer cells (1×10^5 cells/well) were seeded into 12-well plate until the cells reached 95% confluence. We used a pipette tip to gain a cross scratch and washed the cells three times with phosphate-buffered saline (PBS). Serum medium (3%) was utilized to cultivate the cells, and the inverted microscope was applied to photograph at 0 and 48 h. The scratch areas were assessed via ImageJ.

Real-time quantitative PCR

Total RNA of colon cancer cells and macrophages was extracted by the TRIzol reagent (Leagene, Beijing, China), and EVO M-MLV RT Premix (Accurate Bio, Hunan, China) was used to perform reverse transcription to obtain objective cDNA. FJX1, TGB1, IL10, CD80, CD86, and CD163 expressions were detected by SYBR Green PCR Master Mix (GenStar, Beijing, China). GAPDH was a control reference, and the classical $2^{-\Delta\Delta Ct}$ method was applied to calculate the relative expression. Primers are detailed in the attachment.

Western blot analysis

FJX1 proteins were extracted from the cells through standard protocols, separated by sodium dodecyl sulfate (SDS)-polyacrylamide gel electrophoresis, and performed Western blot analyses. The chemi-luminescence method was used to detect protein bands. Primary antibody against FJX1 (1:1,000, ABclconal, Wuhan, China) was used. GAPDH (1:10,000, ABclconal, Wuhan, China) was used as a control. The secondary antibodies were anti-rabbit (1:10,000, ABclconal, Wuhan, China) and anti-rat (1:10,000, ABclconal, Wuhan, China).

Statistical analysis

The correlation coefficients are all Pearson, but the Spearman coefficient is used in the correlation analysis of IC50. All experimental data analysis and picture production were done through GraphPad Prism 9.0. Statistical analyses were performed with Student's t-test. Each experiment was repeated three times. All $p < 0.05$ was considered statistically significant.

Results

FJX1 expression status analysis in pan-cancer

The FJX1 expression of cancer tissues correlation with normal tissues were explored by TCGA and GTEx. The FJX1 expression in cancer tissues was significantly higher than in normal tissues, including the adrenocortical carcinoma (ACC), bladder urothelial carcinoma (BLCA), breast invasive carcinoma (BRCA), cholangiocarcinoma (CHOL), COAD, lymphoid neoplasm diffuse large B-cell lymphoma (DLBC), esophageal carcinoma (ESCA), glioblastoma (GBM), head and neck squamous cell carcinoma (HNSC), brain lower grade glioma (LGG), kidney renal clear cell carcinoma (KIRC), kidney renal papillary cell carcinoma (KIRP), liver hepatocellular carcinoma (LIHC), lung squamous cell carcinoma (LUSC), ovarian serous cystadenocarcinoma (OV), pancreatic adenocarcinoma (PAAD), rectum adenocarcinoma (READ), stomach adenocarcinoma (STAD), thyroid carcinoma (THCA), testicular germ cell tumors (TGCT), thymoma (THYM), uterine corpus endometrial carcinoma (UCEC), and uterine carcinosarcoma (UCS). On the contrary, the FJX1 expression in cancer tissues was lower significantly, compared with normal tissues, including the kidney chromophobe (KICH), acute myeloid leukemia (LAML), lung adenocarcinoma (LUAD), prostate adenocarcinoma (PRAD), and skin cutaneous melanoma (SKCM) (Figure 1A). Simultaneously, the radar charts displayed that the mean FJX1 expression in cancers was 7.3, while the mean FJX1 expression in normal tissues was 4.97 (Figures 1B, C). Additionally, we analyzed the FJX1 expression in cancer and para-cancerous tissues. In BLCA, BRCA, CHOL, COAD, ESCA, HNSC,SARC, KIRC, KIRP, LIHC, STAD, and THCA, the FJX1 expression in cancer was significantly higher than in paracancerous tissues. Inversely, FJX1 expression in cancer was lower than in paracancerous tissues only in KICH (Supplementary Figure S1A). We also investigated the FJX1 expression levels in different clinical stages. The FJX1 expression increased with tumor stage in ACC, COAD, ESCA, KIRP, LUAD, and UVM (Supplementary Figure S1B). All the investigations indicated that FJX1 expression was significantly upregulated in most cancers and associated with tumor stage.

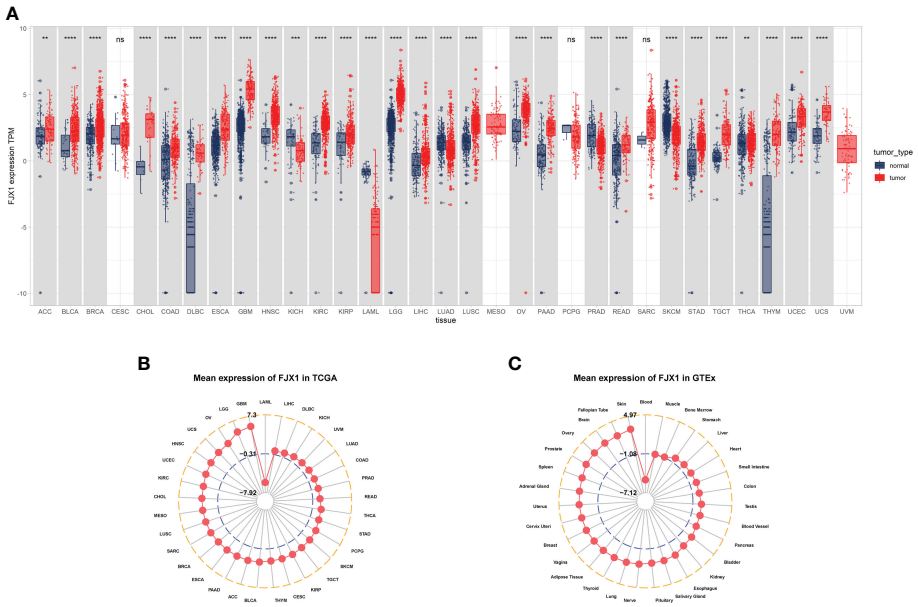

FIGURE 1
FJX1 expression levels vary in different cancers. **(A)** Profiles of FJX1 levels between tumors and normal tissues. **(B)** Expression of FJX1 in 33 types of cancer (TCGA). **(C)** Expression of FJX1 in 31 types of normal tissue (GTEx). The box plots and radar charts were made by "ggplot2" and "ggradar" R package, respectively. *p < 0.05, **p < 0.01, ***p < 0.001, ****p < 0.0001. ns, not significant.

FJX1 CNA and DNA methylation analysis in pan-cancer

The FJX1 gene alterations data were obtained from the cBioPortal, which suggested that the highest alteration frequency of FJX1 was more than 4% and the "amplification" was the primary genetic alteration type in stomach adenocarcinoma. Among the different types of genetic, variation, "mutation" had the highest expression in stomach adenocarcinoma, "amplification" had the highest expression in esophageal adenocarcinoma, and "deep deletion" had the highest expression in prostate adenocarcinoma (Figure 2A). Additionally, we also explored the correlation of FJX1 mRNA expression with CNA and DNA methylation. CNA and FJX1 mRNA expressions were positively correlated in 17 types of cancer, including HNSC, OV, SARC, DLBC, LUSC, GBM, THYM, BLCA, READ, BRCA, SKCM, TGCT, ESCA, LGG, LIHC, LUAD, and STAD (Figure 2B), Meanwhile, the DNA methylation and FJX1 mRNA expression were negatively correlated in 21 types of cancers, including THCA, CESC, LUSC, UCEC, LUAD, LIHC, LGG, HNSC, TGCT, COAD, MESD, UVM, ACC, STAD, SKCM, PRAD, BRCA, DLBC, THYM, SARC, and ESCA (Figure 2C).

FJX1 prognostic value analysis in pan-cancer

A univariate Cox regression model was employed to analyze the FJX1 expression correlation with OS, DSS, DFI, and PFI in multiple cancers. For OS, high FJX1 expression was significantly linked to worse OS in LUAD, MESO, UVM, KIRP, COAD, STAD, HNSC, BLCA, and ACC (Figure 3A). For DSS, low FJX1 expression had a high DSS rate in patients with KIRP, COAD, MESO, UVM, LUAD, HNSC, STAD, and BLCA (Figure 3B). For DFI, in KIRP, PAAD, PRAD, UCS, ESCA, and MESO, lower DFI was significantly related with high FJX1 expression (Figure 3C). For PFI, high FJX1 expression was significantly related to lower PFI in KIRP, UVM, COAD, PRAD, PAAD, LUAD, GBM, and TGCT (Figure 3D). However, in OV, low FJX1 expression implied better OS, DFI, PFI, and DSS ($p<0.05$, Figure 3). Moreover, the survival curve displayed that high FJX1 expression indicated worse overall survival time in 16 types of cancer (Supplementary Figure S2). All the results displayed that FJX1 was a potential novel prognostic biomarker.

Gene set variation analysis of FJX1 in pan-cancer

GSVA were used to investigate the FJX1 expression correlation with 50 stars pathways in HALLMARK. we found that FJX1 had a significantly positive correlation with the first six pathways in various cancers, including "ANGIOGENESIS," "WNT BETA CATENIN SIGNALING," "NOTCH SIGNALING," "EPITHELIAL MESENCHYMAL TRANSITION," "APICAL JUNCTION," and "TGF BETA SIGNALING," which all were closely related to carcinoma and immunity (Supplementary Figure S3).

Immune infiltration and immune modulator genes analysis of FJX1 in pan-cancer

Tumor microenvironment (TME) data were downloaded from TIMER2. As displayed in Supplementary Figure S4A, FJX1 expression was positive relation with stromal score, ESTIMATE sore, and immune score in 17, 14, and 10 kinds of cancer, respectively ($p<0.05$), while there was a negative correlation with tumor purity in 13 kinds of cancer ($p<0.05$). In addition, FJX1 also had significant positive correlation with immune-related pathways and DNA damage repair-related pathways in most cancers (Supplementary Figure S4B).

We used ImmuCellAI and TIMER2 to investigate the FJX1 expression relationship with immune infiltrating cells in various TCGA tumors. FJX1 expression was positive relevant with large number of infiltrated immune cells, such as monocyte cells, NKT, macrophages, and Th2, while there was negative association with CD8+ T cells and B cells in various cancers (Figure 4A). Additionally, we further evaluated the FJX1 expression relationship with different subtypes of immune cell. We discovered that in most cancers, the FJX1 expression positively related with different subtypes of tumor macrophages (TAMs) but negatively related with different subtypes of B and T cells (Figure 4B).

TMB and MSI scores were downloaded to analyze the FJX1 expression relationship with TMB or MSI via TCGA. The results suggested that FJX1 had significant correlation with TMB in ACC, STAD, UCEC, ESCA, DLBC, and CHOL (Figure 5A), with MSI in LUSC, TGCT, KIRP, and BRCA, SKCM, COAD, PAAD, ESCA, UCEC, and STAD (Figure 5B). Furthermore, we also explored the connection of FJX1 expression with immune-related genes (MHC genes, immunosuppressive genes, chemokines, and chemokines receptors) and immunosuppressive pathway-related genes. We found that FJX1 expression was significantly correlation with vast majority of MHC genes (21 types) in most cancers (Figure 6A). Additionally, FJX1 expression was significantly and positively correlated with immunosuppressive genes (TGFB1 and IL-10), chemokines (CCR1 and CCR5), chemokines receptors (CCL2 and CXCL5) (Figures 6B–D), and immunosuppressive pathway-related genes (TFGB1 and WNT1), in most TCGA cancers (Figure 7). Interestingly, TFGB1 and WNT relative pathway activation was associated with immunosuppressive status. All the investigations revealed that FJX1 was closely relevant to the immunosuppressive microenvironment and the matrix microenvironment. It was indicated that high FJX1 expression put patients in an immunosuppressed state.

Immunotherapy analysis of FJX1 in pan-cancer

To investigate whether FJX1 affects the immunotherapy effect in cancer patients, we downloaded the immunotherapy dataset from IMvigor210CoreBiologies and found that in the immunotherapy-

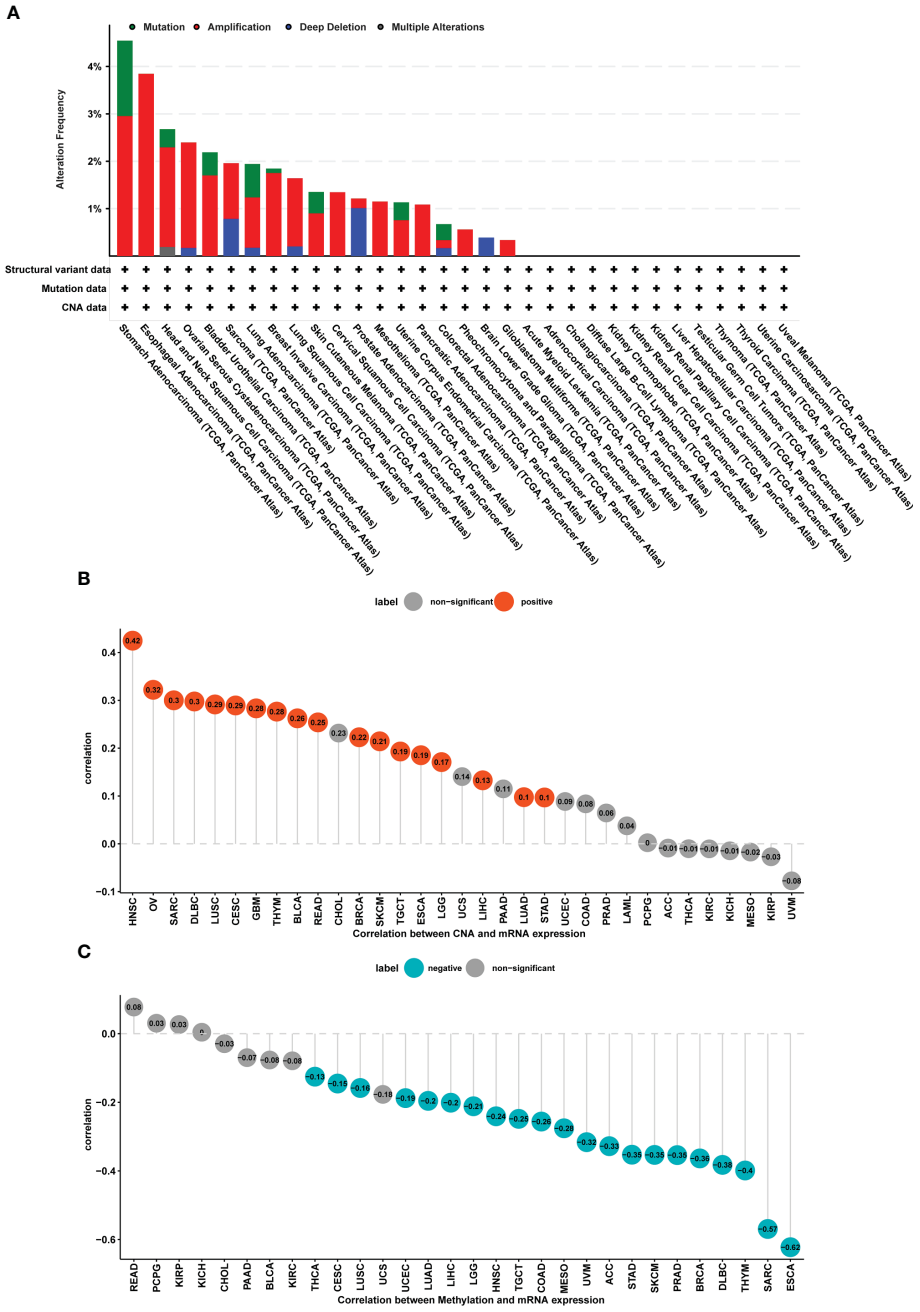

FIGURE 2
CNA and DNA methylation of FJX1 in pan-cancer. **(A)** The structural variant, mutation, and CNA status of FJX1 in TCGA tumors (cBioportal). **(B)** Correlation between CNA and FJX1 mRNA expression. Red color represents significant results ($p < 0.05$). **(C)** Correlation between DNA methylation and FJX1 mRNA expression. Blue color represents significant results ($p < 0.05$). CNA, copy number alteration.

tolerant group, the FJX1 expression was higher compared with immunotherapy-effective group ($p<0.05$) (Supplementary Figure S5A). In addition, we also found that compared with low FJX1 expression, patients in the high FJX1 expression group had worse overall survival ($p=0.00029$) (Supplementary Figure S5B). Furthermore, stable disease (SD)/progressive disease (PD) accounted for 87% and complete remission (CR)/partial remission(PR) accounted for 13% in patients with high FJX1 expression, while SD/PD accounted for 73%, and CR/PR accounted for 27% in patients with low FJX1 expression (Supplementary Figure S5C). All the results suggested that upregulated FJX1 could reduce the efficacy of immunotherapy.

Connection between FJX1 expression and IC50 in pan-cancer

We obtained the data from GDSC to explain the FJX1 expression connection with IC50 of 198 types of drug. As shown in Supplementary Figure S6, FJX1 had significantly positive

10.3389/fonc.2023.1170482

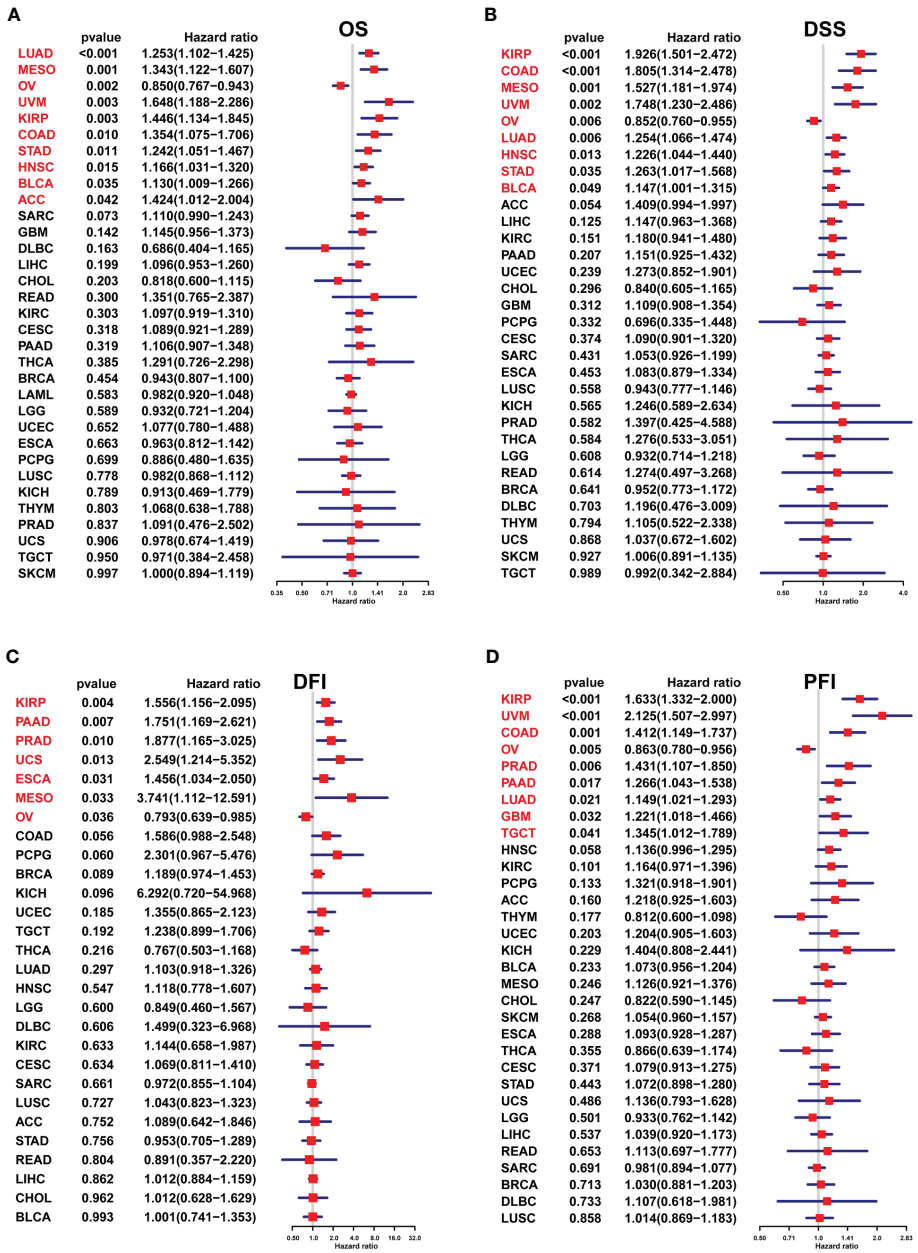

FIGURE 3
Association between the FJX1 expression and prognostic value in pan-cancer. **(A–D)** The forest plots showing the correlation between FJX1 expression and OS, DSS, DFI, and PFI in TCGA cancers. Red color represents significant results ($p < 0.05$).

correlation with IC50 of LGK974, BMS-754807, Crizotinib, AZD5991, Vorinostat, and ML_323, which revealed that patients with high FJX1 expression may develop resistance to these drugs.

FJX1 knockdown weakens the proliferation and migration in COAD cells

The FJX1 was knocked down via transfection with FJX1-siRNA. FJX1 mRNA and FJX1 protein expressions were all lower in the FJX1-siRNA group than in the FJX1-NCRNA group (Figures 8A–C). Meanwhile, TGFB1 and IL10 mRNA relative expression were also lower in the FJX1-siRNA group compared with the FJX1-NCRNA group (Figure 8G). To confirm the biological function of FJX1 in COAD cells, cell proliferation assay, transwell migration assay, and wound healing assay were performed in HCT116 and SW480 cells. The outcomes indicated that the proliferation and migration ability and wound average healing rate of HCT116 and SW480 cells were attenuated in the FJX1-siRNA group compared with the FJX1-NCRNA group (p all <0.05, Figures 8D–F).

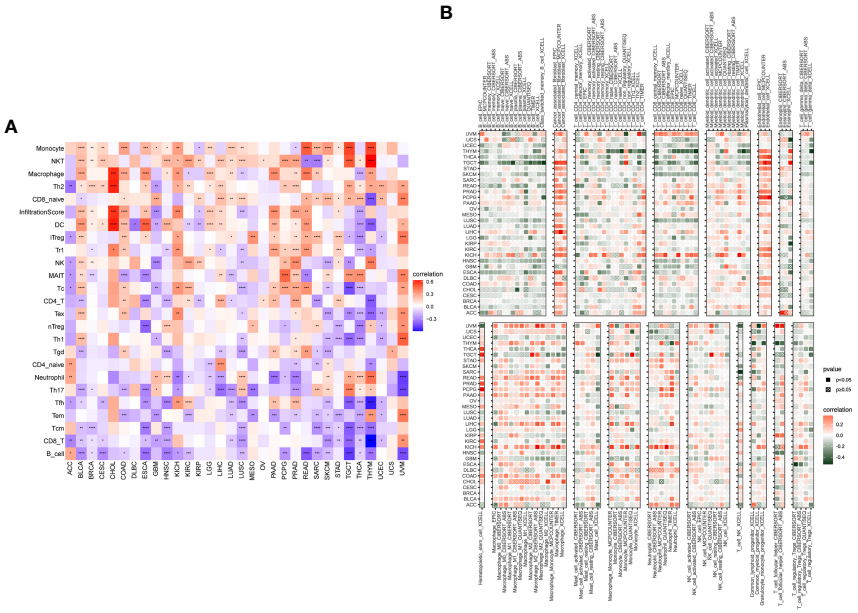

FIGURE 4
Correlation between FJX1 and immune infiltrating cells in TCGA cancers. **(A)** The correlation between FJX1 expression and immune cells. **(B)** The correlation between FJX1 expression and different immune cell subtypes. Red represents positive correlation, blue or dark green represents negative correlation, and the darker the color, the stronger the correlation.*p < 0.05, **p < 0.01, ***p < 0.001, ****p < 0.0001.

THP1 macrophages co-cultured with knocking down FJX1 HCT116 increased CD80/CD163 and CD86/CD163

As shown in Figure 8H, THP1 macrophages were round without antennae. After co-culture with HCT116 bare bead cells and control groups, some THP1 macrophages were elongated and grew antennae, but most of them showed roundness and decreased antennae after co-culture with HCT116-siFJX1. Additionally, according to the results of qPCR, CD80/CD163 and CD86/CD163 were elevated in the knockdown FJX1 group compared with the control group (Figure 8I). This suggested that FJX1 had the potential to induce THP1 macrophages to polarize to M2.

Discussion

Cancer can have a significant impact on a patient's health and quality of life, causing great suffering. Despite advancements in cancer diagnosis and treatment, the overall survival rate for cancer patients remains unsatisfactory (27). Therefore, it is crucial to explore novel strategies for cancer diagnosis and treatment, and pan-cancer analysis can provide new ideas and directions (28). Previous studies have shown that FJX1 is highly expressed in some cancers (14–18), and in colorectal carcinoma, upregulated FJX1 is significantly associated with poor survival (20). Our findings are consistent with these studies, as our pan-cancer analysis revealed high FJX1 expression in 22 types of cancer, and it was correlated

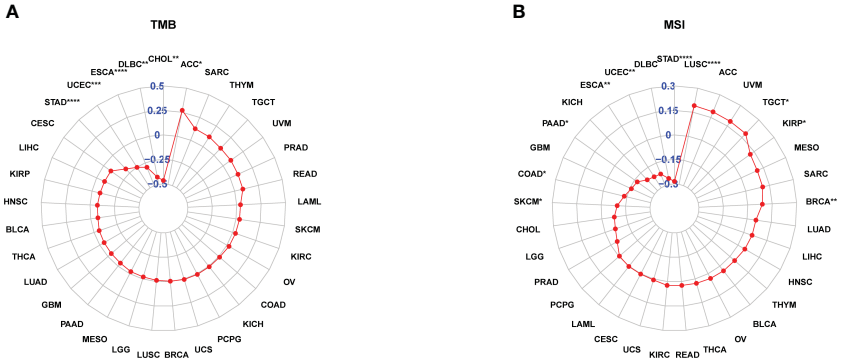

FIGURE 5
FJX1 correlation with TMB and MSI. **(A)** FJX1 was significantly correlated with TMB in ACC, STAD, UCEC, ESCA, DLBC, and CHOL. **(B)** FJX1 has significantly correlation with MSI in LUSC, TGCT, KIRP, BRCA, SKCM, COAD, PAAD, ESCA, UCEC, and STAD. TMB, mutational burden; MSI, microsatellite instability. *p < 0.05, **p < 0.01, ***p < 0.001, ****p < 0.0001.

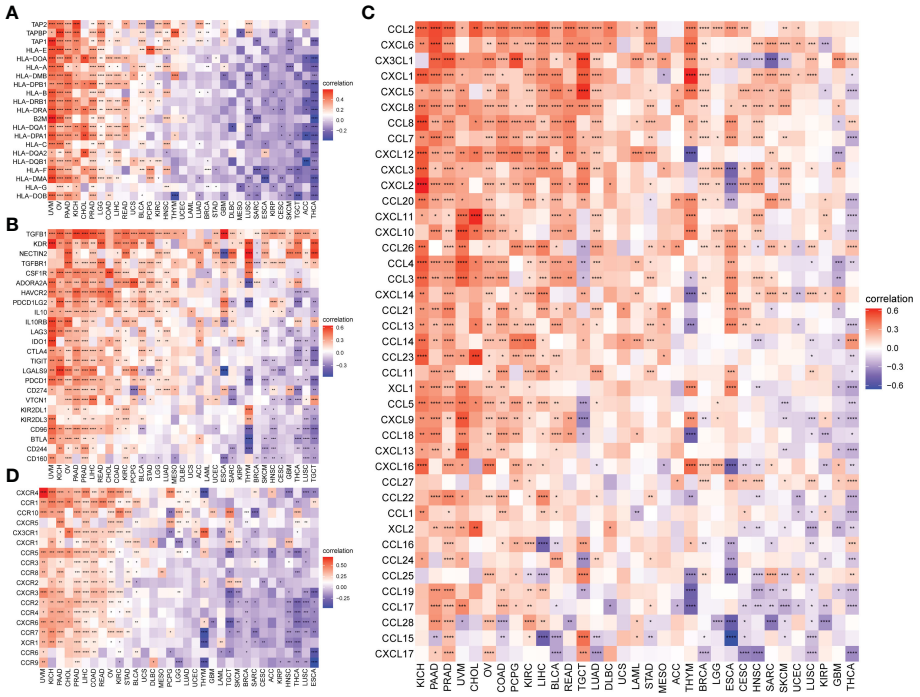

FIGURE 6
Correlation between FJX1 expression and immune-related genes. Correlation between FJX1 and **(A)** MHC genes, **(B)** Immunosuppressive genes, **(C)** chemokines, and **(D)** chemokine receptors. Red represents positive correlation, blue represents negative correlation, and the darker the color, the stronger the correlation.*p < 0.05,**p < 0.01, ***p < 0.001, ****p < 0.0001.

with poor overall survival, disease-specific survival, disease-free interval, progression-free interval, and worse overall survival in some cancers. Therefore, our pan-cancer prognosis value analysis of FJX1 demonstrates that it could be an underlying and novel diagnostic and prognostic biomarker for cancers.

Tumorigenesis is closely associated with various genetic alterations, including mutation, amplification, deep deletion, copy number alteration (CNA), and DNA methylation of genes (29–31). According to our results, FJX1 was found to be altered in 19 types of cancer, with amplification being the most common genetic alteration across different cancer types. Additionally, FJX1 mRNA expression was positively correlated with CNA and negatively correlated with DNA methylation in 18 and 22 types of cancer, respectively. We also discovered that FJX1 is closely linked with cancer and immunity pathways. Previous research has revealed that FJX1 is a direct target of the Hippo-Yes-associated protein in the Hippo-signaling pathway, which regulates cell proliferation and apoptosis (32). Moreover, FJX1 has been shown to promote angiogenesis in colorectal carcinoma and potentiate invasion by regulating planar cell polarity, which is involved in wound repair

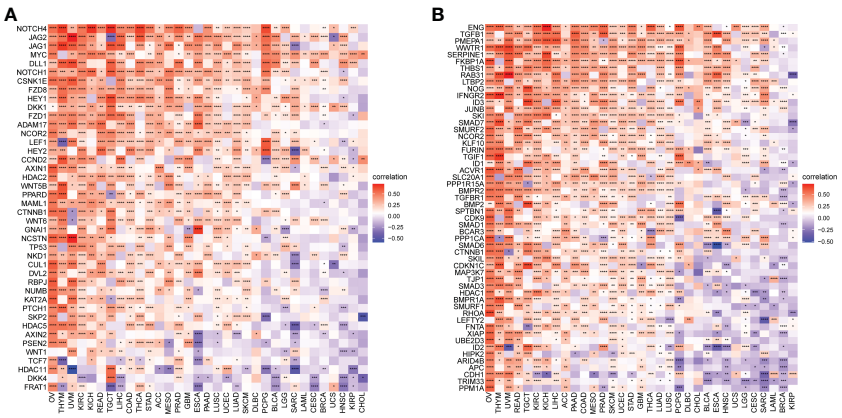

FIGURE 7
Correlation between FJX1 and immunosuppressive pathways-related genes **(A, B)**. Red represents positive correlation, blue represents negative correlation, and the darker the color, the stronger the correlation.*p < 0.05, **p < 0.01, ***p < 0.001, ****p < 0.0001.

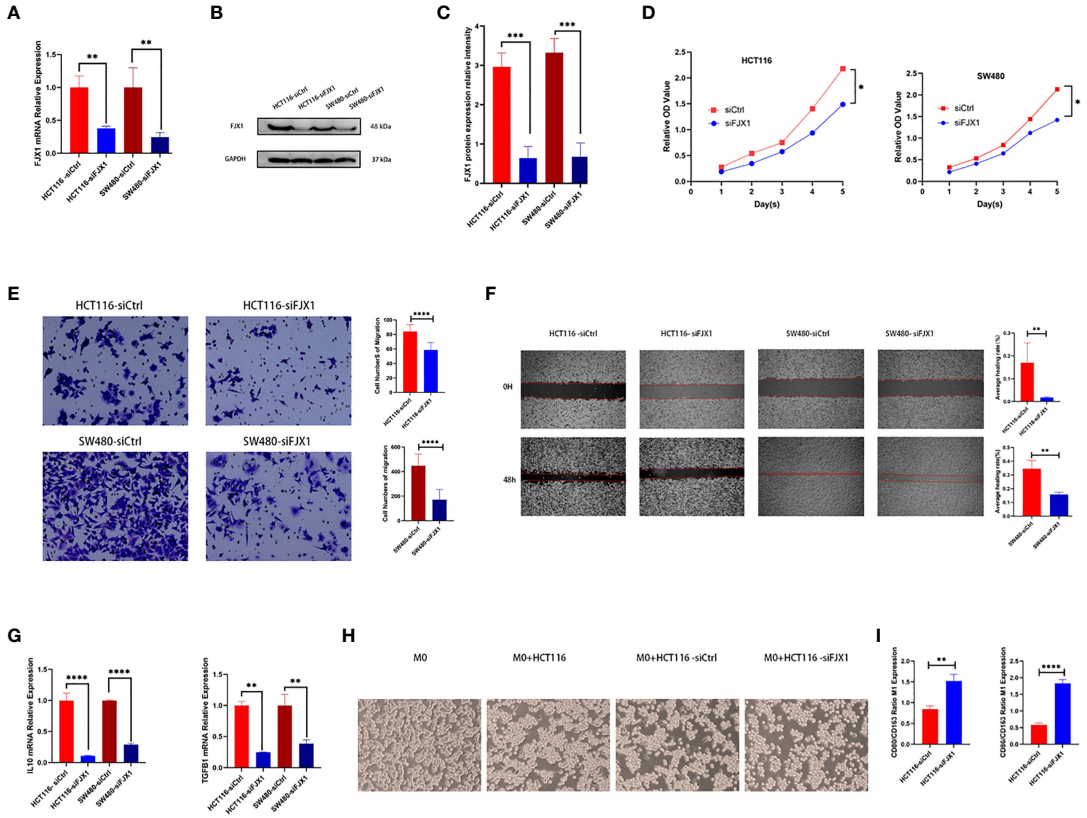

FIGURE 8
Knocking down FJX1 inhibits proliferation and migration in HCT116 and SW480 cells. **(A)** Real-time PCR and **(B, C)** Weston blot determine the efficiency of knocking down FJX1; **(D)** proliferation assay, **(E)** transwell migration assay, and **(F)** wound healing assay shows that knockdown FJX1 significantly weakens proliferation, migration ability, and average healing rate. The cell numbers of migration and average healing rate(%) are shown in histograms. **(G)** TGFB1 and IL10 mRNA relative expression. **(H)** Morphology of macrophages after co-culture with HCT116 in different states. **(I)** CD80/CD163 and CD86/CD163 are increasing in macrophages after co-culture with HCT116-siFJX1. *p < 0.05, **p < 0.01, ***p < 0.001, ****p < 0.0001. Each experiment was repeated three times. Statistical analyses were performed with Student's t-test.

and development (33). Our external experimental results also demonstrated that knocking down FJX1 in colon cancer cells weakened their proliferation and migration. Thus, all these findings suggest that FJX1 is a factor in promoting carcinogenesis.

The tumor microenvironment (TME) exerts a long-lasting impact on tumor cells and plays critical roles in various aspects of tumor biology, including infiltration, invasion, metastasis, and response to immunotherapy (34). Among the cellular components of TME, macrophages are particularly important and are commonly referred to as tumor-associated macrophages (TAMs) (35). TAMs are a heterogeneous population that can exhibit distinct phenotypes, with the M1 type having an anti-tumor function and the M2 type promoting tumor growth and progression. The proportion of M2 TAMs has been shown to correlate with poor prognosis in many types of cancer (36–38). In our study, we found that the expression of FJX1 was significantly associated with monocytes, macrophages, Th2 cells, and NKT cells. Moreover, we observed a positive and significant correlation between FJX1 expression and most macrophage subtypes. Interestingly, we also found that co-culture of THP1 macrophages with HCT116 cells that were transfected with siFJX1 led to morphological changes in macrophages, with decreased antennae and a more rounded shape. Furthermore, the expression of surface markers such as CD80/CD163 and CD86/CD163 was increased in macrophages co-cultured with HCT116-siFJX1 compared to the control group *in vitro*. CD80 and CD86 are typical markers of M1 macrophages, while CD163 is a marker of M2 macrophages (39). Thus, the increased expression of CD80/CD163 and CD86/CD163 in macrophages suggests a decrease in the proportion of CD163+ M2 TAMs and an increase in the proportion of CD80+ or CD86+ M1 TAMs. Collectively, our findings suggest that FJX1 is positively associated with TAMs.

TMB and MSI are important biomarkers for evaluating antitumor responses and predicting the efficacy of tumor immunotherapy, including antibody therapies and checkpoint inhibitors (40, 41). However, cancer cells can develop drug resistance by undergoing immunoediting, which allows them to escape detection and clearance by the immune system (42, 43). Our research suggests that FJX1 plays a significant role in the development of drug resistance in 6 and 10 types of cancer, by affecting TMB and MSI, respectively. Specifically, high expression of FJX1 is associated with a more immunotherapy-tolerant microenvironment and lower overall survival in cancer patients. Furthermore, our results indicate that FJX1 is positively correlated

with the expression of MHC genes, immunosuppressive genes, chemokines, chemokine receptors, and immunosuppressive pathway-related genes in most TCGA cancers. We also found that FJX1 expression is positively associated with TGFB1 and IL-10, which can induce macrophages to M2 polarization and regulate tumor immunology (44). When FJX1 was knocked down in colon cancer cells, the expression of TGFB1 and IL-10 also decreased, suggesting that FJX1 may affect the polarization of macrophages and thus the tumor microenvironment.

Finally, we used GDSC to analyze the connection between FJX1 and IC50 in 198 types of drug and found that high expression of FJX1 is associated with drug resistance. These results suggest that FJX1 is a potential target for the development of immunosuppressants. Overall, our findings provide new insights into the role of FJX1 in cancer immunotherapy and drug resistance.

While our article highlights the significance of FJX1 as a biomarker for carcinogenicity and prognosis in various types of cancer, there are some important limitations to our study. Although previous research suggests that high FJX1 expression is associated with poor prognosis in different tumors, the specific mechanism and role of the tumor immunosuppressive microenvironment have not been fully explored. Therefore, further investigation is necessary to confirm the relationship between FJX1 and the immunosuppressive microenvironment in human cancers. In addition, future studies should also focus on exploring the expression and function of FJX1 in greater detail.

Conclusion

Our study underscores the importance of FJX1 as a potential biomarker for cancer diagnosis and prognosis. High FJX1 expression may contribute to an immunosuppressive microenvironment, and targeting FJX1 could be a promising approach for immunotherapy in cancer treatment.

Data availability statement

The original contributions presented in the study are included in the article/Supplementary Material. Further inquiries can be directed to the corresponding authors.

Author contributions

KMZ conceived the study. KMZ ,SDL and YLZ drafted the manuscript and performed the analysis. YM and JD performed the literature search and collected the data. MX contributed to the in-vitro experiment and revision of manuscript. MH contributed to drafting the manuscript and interpreting data. TG and RLZ contribute to the revision of manuscript. MH, TG, YM and RLZ contribute equally to the research. All authors read and approved the final manuscript.

Funding

This work was financially supported by the National Natural Science Foundation of China (No. 81802965), Provincial Science and Technology Award Project (No. 2017B020209003), Project supported by the President Foundation of Nanfang Hospital, Southern Medical University (Grant No. 2020B020) and the Science and Technology Project in Guangzhou (No. 202102020108, No. 202201011101, No. 2023A04J2373).

Acknowledgments

We would like to acknowledge Pazhou Lab for its support to this research.

Conflict of interest

The authors declare that the research was conducted in the absence of any commercial or financial relationships that could be construed as a potential conflict of interest.

Publisher's note

Supplementary material

The Supplementary Material for this article can be found online at: https://www.frontiersin.org/articles/10.3389/fonc.2023.1170482/full#supplementary-material

References

1. Sung H, Ferlay J, Siegel RL, Laversanne M, Soerjomataram I, Jemal A, et al. Global cancer statistics 2020: GLOBOCAN estimates of incidence and mortality worldwide for 36 cancers in 185 countries. *CA Cancer J Clin* (2021) 71:209–49. doi: 10.3322/caac.21660

2. Bray F, Laversanne M, Weiderpass E, Soerjomataram I. The ever-increasing importance of cancer as a leading cause of premature death worldwide. *Cancer* (2021) 127:3029–30. doi: 10.1002/cncr.33587

3. Vos T. Global burden of 369 diseases and injuries in 204 countries and territories, 1990-2019: a systematic analysis for the global burden of disease study 2019. *Lancet* (2020) 396:1204–22. doi: 10.1016/S0140-6736(20)30925-9

4. Walcher L, Kistenmacher AK, Suo H, Kitte R, Dluczek S, Strauß A, et al. Cancer stem cells-origins and biomarkers: perspectives for targeted personalized therapies. *Front Immunol* (2020) 11:1280. doi: 10.3389/fimmu.2020.01280

5. Park JH, Pyun WY, Park HW. Cancer metabolism: phenotype, signaling and therapeutic targets. *Cells* (2020) 9:2308. doi: 10.3390/cells9102308

6. Abbott M, Ustoyev Y. Cancer and the immune system: the history and background of immunotherapy. *Semin Oncol Nurs* (2019) 35:150923. doi: 10.1016/j.soncn.2019.08.002

7. Colli LM, Machiela MJ, Zhang H, Myers TA, Jessop L, Delattre O, et al. Landscape of combination immunotherapy and targeted therapy to improve cancer management. *Cancer Res* (2017) 77:3666–71. doi: 10.1158/0008-5472.CAN-16-3338

8. Zhang Y, Zhang Z. The history and advances in cancer immunotherapy: understanding the characteristics of tumor-infiltrating immune cells and their therapeutic implications. *Cell Mol Immunol* (2020) 17:807–21. doi: 10.1038/s41423-020-0488-6

9. Strutt H, Mundy J, Hofstra K, Strutt D. Cleavage and secretion is not required for four-jointed function in drosophila patterning. *Development* (2004) 13:881–90. doi: 10.1242/dev.00996

10. Buckles GR, Rauskolb C, Villano JL, Katz FN. Four-jointed interacts with dachs, abelson and enabled and feeds back onto the notch pathway to affect growth and segmentation in the drosophila leg. *Development* (2001) 128:3533–42. doi: 10.1242/dev.128.18.3533

11. Ishikawa HO, Takeuchi H, Haltiwanger RS, Irvine KD. Four-jointed is a golgi kinase that phosphorylates a subset of cadherin domains. *Science* (2008) 321:401–4. doi: 10.1126/science.1158159

12. Bao Y, Hata Y, Ikeda M, Withanage K. Mammalian hippo pathway: from development to cancer and beyond. *J Biochem* (2011) 149:361–79. doi: 10.1093/jb/mvr021

13. Gutierrez-Aviño FJ, Ferres-Marco D, Dominguez M. The position and function of the notch-mediated eye growth organizer: the roles of JAK/STAT and four-jointed. *EMBO Rep* (2009) 10:1051–8. doi: 10.1038/embor.2009.140

14. Ong CA, Shannon NB, Ross-Innes CS, Rueda OM, Hu DE, Kettunen MI, et al. Amplification of TRIM44: pairing a prognostic target with potential therapeutic strategy. *J Natl Cancer Inst* (2014) 106:dju050. doi: 10.1038/embor.2009.140

15. Chang JW, Wei NC, Su HJ, Huang JL, Chen TC, Wu YC, et al. Comparison of genomic signatures of non-small cell lung cancer recurrence between two microarray platforms. *Anticancer Res* (2012) 32:1259–65.

16. Järvinen AK, Autio R, Kilpinen S, Saarela M, Leivo I, Grénman R, et al. High-resolution copy number and gene expression microarray analyses of head and neck squamous cell carcinoma cell lines of tongue and larynx. *Genes Chromosom Cancer* (2008) 47:500–9. doi: 10.1002/gcc.20551

17. Dang W, Zhu Z. MicroRNA-1249 targets four-jointed box kinase 1 and reduces cell proliferation, migration and invasion of colon adenocarcinoma. *J Gene Med* (2020) 22:e3183. doi: 10.1002/jgm.3183

18. Buckanovich RJ, Sasaroli D, O'Brien-Jenkins A, Botbyl J, Hammond R, Katsaros D, et al. Tumor vascular proteins as biomarkers in ovarian cancer. *J Clin Oncol* (2007) 25:852–61. doi: 10.1200/JCO.2006.08.8583

19. Liu L, Huang Y, Li Y, Wang Q, Hao Y, Liu L, et al. FJX1 as a candidate diagnostic and prognostic serum biomarker for colorectal cancer. *Clin Transl Oncol* (2022) 24:1964–74. doi: 10.1007/s12094-022-02852-5

20. Al-Greene NT, Means AL, Lu P, Jiang A, Schmidt CR, Chakravarthy AB, et al. Four jointed box 1 promotes angiogenesis and is associated with poor patient survival in colorectal carcinoma. *PloS One* (2013) 8:e69660. doi: 10.1371/journal.pone.0069660

21. Chai SJ, Ahmad ZM, Gan SP, Rajadurai P, Lim PVH, Ng CC, et al. An oncogenic role for four-jointed box 1 (FJX1) in nasopharyngeal carcinoma. *Dis Markers* (2019) 2019:3857853. doi: 10.1155/2019/3857853

22. Chai SJ, Yap YY, Foo YC, Yap LF, Ponniah S, Teo SH, et al. Identification of four-jointed box 1 (FJX1)-specific peptides for immunotherapy of nasopharyngeal carcinoma. *PloS One* (2015) 10:e130464. doi: 10.1371/journal.pone.0130464

23. Carithers LJ, Ardlie K, Barcus M, Branton PA, Britton A, Buia SA, et al. A novel approach to high-quality postmortem tissue procurement: the GTEx project. *Biopreserv Biobank* (2015) 13:311–9. doi: 10.1089/bio.2015.0032

24. Cerami E, Gao J, Dogrusoz U, Gross BE, Sumer SO, Aksoy BA, et al. The cBio cancer genomics portal: an open platform for exploring multidimensional cancer genomics data. *Cancer Discov* (2012) 2:401–4. doi: 10.1158/2159-8290.CD-12-0095

25. Miao YR, Zhang Q, Lei Q, Luo M, Xie GY, Wang H, et al. ImmuCellAI: a unique method for comprehensive T-cell subsets abundance prediction and its application in cancer immunotherapy. *Adv Sci (Weinh)* (2020) 7:1902880. doi: 10.1002/advs.201902880

26. Li T, Fu J, Zeng Z, Cohen D, Li J, Chen Q, et al. TIMER2.0 for analysis of tumor-infiltrating immune cells. *Nucleic Acids Res* (2020) 48:W509–14. doi: 10.1093/nar/gkaa407

27. Xia C, Dong X, Li H, Cao M, Sun D, He S, et al. Cancer statistics in China and united states, 2022: profiles, trends, and determinants. *Chin Med J (Engl)* (2022) 135:584–90. doi: 10.1097/CM9.0000000000002108

28. Lauri AA, Federico A, Adam A, Hiroyuki A, David JA, Nishant A, et al. Pan-cancer analysis of whole genomes. *Nature* (2020) 578:82–93. doi: 10.1038/s41586-020-1969-6

29. Baylin SB, Jones PA. Epigenetic determinants of cancer. *Cold Spring Harb Perspect Biol* (2016) 8:a019505. doi: 10.1101/cshperspect.a019505

30. Ogawa S. Genetics of MDS. *Blood* (2019) 133:1049–59. doi: 10.1182/blood-2018-10-844621

31. Yamamoto H, Imai K. Microsatellite instability: an update. *Arch Toxicol* (2015) 89:899–921. doi: 10.1007/s00204-015-1474-0

32. Happé H, van der Wal AM, Leonhard WN, Kunnen SJ, Breuning MH, de Heer E, et al. Altered hippo signalling in polycystic kidney disease. *J Pathol* (2011) 224:133–42. doi: 10.1002/path.2856

33. Rock R, Heinrich AC, Schrauth S, Gessler M. Expression of mouse dchs1, fjx1, and fat-j suggests conservation of the planar cell polarity pathway identified in drosophila. *Dev Dyn* (2005) 234:747–55. doi: 10.1002/dvdy.20553

34. Wu K, Lin K, Li X, Yuan X, Xu P, Ni P, et al. Redefining tumor-associated macrophage subpopulations and functions in the tumor microenvironment. *Front Immunol* (2020) 11:01731. doi: 10.3389/fimmu.2020.01731

35. Cheng X, Wang X, Nie K, Cheng L, Zhang Z, Hu Y, et al. Systematic pan-cancer analysis identifies TREM2 as an immunological and prognostic biomarker. *Front Immunol* (2021) 12:646523. doi: 10.3389/fimmu.2021.646523

36. Kim J, Bae JS. Tumor-associated macrophages and neutrophils in tumor microenvironment. *Mediators Inflamm* (2016) 2016:6058147. doi: 10.1155/2016/6058147

37. Pan Y, Yu Y, Wang X, Zhang T. Tumor-associated macrophages in tumor immunity. *Front Immunol* (2020) 11:583084. doi: 10.3389/fimmu.2020.583084

38. Han S, Wang W, Wang S, Yang T, Zhang G, Wang D, et al. Tumor microenvironment remodeling and tumor therapy based on M2-like tumor associated macrophage-targeting nano-complexes. *Theranostics* (2021) 11:2892–916. doi: 10.7150/thno.50928

39. Baumeier C, Escher F, Aleshcheva G, Pietsch H, Schultheiss HP. Plasminogen activator inhibitor-1 reduces cardiac fibrosis and promotes M2 macrophage polarization in inflammatory cardiomyopathy. *Basic Res Cardiol* (2021) 116:1. doi: 10.1007/s00395-020-00840-w

40. Zhong A, Chen T, Xing Y, Pan X, Shi M. FUCA2 is a prognostic biomarker and correlated with an immunosuppressive microenvironment in pan-cancer. *Front Immunol* (2021) 12:758648. doi: 10.3389/fimmu.2021.758648

41. Hu J, Qiu D, Yu A, Deng H, Li H, Yi Z, et al. YTHDF1 is a potential pan-cancer biomarker for prognosis and immunotherapy. *Front Oncol* (2021) 11:607224. doi: 10.3389/fonc.2021.607224

42. Rizzo A, Ricci AD, Brandi G. PD-L1 TMB, MSI, and other predictors of response to immune checkpoint inhibitors in biliary tract cancer. *Cancers (Basel)* (2021) 13:558. doi: 10.3390/cancers13030558

43. O'Donnell JS, Teng M, Smyth MJ. Cancer immunoediting and resistance to T cell-based immunotherapy. *Nat Rev Clin Oncol* (2019) 16:151–67. doi: 10.1038/s41571-018-0142-8

44. Tan S, Li D, Zhu X. Cancer immunotherapy: pros, cons and beyond. *BioMed Pharmacother* (2020) 124:109821. doi: 10.1016/j.biopha.2020.109821

frontiers | Frontiers in Immunology

TYPE Review
PUBLISHED 05 June 2023
DOI 10.3389/fimmu.2023.1194300

OPEN ACCESS

EDITED BY
Eyad Elkord,
University of Salford, United Kingdom

REVIEWED BY
Dongbo Jiang,
Air Force Medical University, China
Zhiyuan Zhang,
Fudan University, China

*CORRESPONDENCE
Marco Antonio Fonseca-Montaño
mfonseca.mntn@gmail.com
Alfredo Hidalgo-Miranda
ahidalgo@inmegen.gob.mx

RECEIVED 26 March 2023
ACCEPTED 24 May 2023
PUBLISHED 05 June 2023

CITATION
Fonseca-Montaño MA, Vázquez-Santillán KI and Hidalgo-Miranda A (2023) The current advances of lncRNAs in breast cancer immunobiology research. *Front. Immunol.* 14:1194300. doi: 10.3389/fimmu.2023.1194300

The current advances of lncRNAs in breast cancer immunobiology research

Marco Antonio Fonseca-Montaño[1,2*], Karla Itzel Vázquez-Santillán[3] and Alfredo Hidalgo-Miranda[1*]

[1]Laboratorio de Genómica del Cáncer, Instituto Nacional de Medicina Genómica (INMEGEN), Mexico City, Mexico, [2]Programa de Doctorado, Posgrado en Ciencias Biológicas, Unidad de Posgrado, Universidad Nacional Autónoma de México (UNAM), Mexico City, Mexico, [3]Laboratorio de Epigenética, Instituto Nacional de Medicina Genómica (INMEGEN), Mexico City, Mexico

Breast cancer is the most frequently diagnosed malignancy and the leading cause of cancer-related death in women worldwide. Breast cancer development and progression are mainly associated with tumor-intrinsic alterations in diverse genes and signaling pathways and with tumor-extrinsic dysregulations linked to the tumor immune microenvironment. Significantly, abnormal expression of lncRNAs affects the tumor immune microenvironment characteristics and modulates the behavior of different cancer types, including breast cancer. In this review, we provide the current advances about the role of lncRNAs as tumor-intrinsic and tumor-extrinsic modulators of the antitumoral immune response and the immune microenvironment in breast cancer, as well as lncRNAs which are potential biomarkers of tumor immune microenvironment and clinicopathological characteristics in patients, suggesting that lncRNAs are potential targets for immunotherapy in breast cancer.

KEYWORDS

breast cancer, immune cells, tumor immune microenvironment, lncRNAs, immune response, biomarker, prognosis

1 Introduction

Breast cancer (BC) is the most frequently diagnosed malignancy and the leading cause of cancer-related death in women worldwide (1, 2). BC is a multifactorial and heterogeneous disease that includes well-defined histological types and protein markers, such as estrogen receptor (ER), progesterone receptor (PR), human epidermal growth factor receptor 2 (HER2), and Ki-67 (1, 3–5). According to the PAM50 gene signature, BC is classified into Luminal A (LA), Luminal B (LB), HER2-enriched, and Basal-like (BL) subtypes. Remarkably, luminal BCs represent around 60 to 70% of diagnosed cases and are frequently associated with improved prognosis, in contrast to non-luminal subtypes (1, 6, 7). Understanding the alterations in specific genes and disrupted signaling pathways involved in BC is essential to unravel the underlying mechanisms of development and progression. In this regard, accumulated evidence has shown recurrent alterations in

diverse genes (i.e., *TP53, ESR1, PIK3CA, PTEN, CDH1, GATA3, CCND1, FGFR1/2, ERBB2, CDKN2A/2B, MYC* and *BRCA1/2)* as well as dysregulations in various signaling pathways (i.e., hormone receptors, DNA damage repair, PI3K/AKT/mTOR, MAPK/ERK, TGF-β, NFκB, WNT/β-Catenin, Notch, Hippo, and SHH), which are associated with cell survival, proliferation, epithelial-mesenchymal transition (EMT), therapy resistance, immune evasion and tumor immune microenvironment (TIME) alterations in BC (1, 8–19).

The TIME consists of dynamic niches where cancer cells coexist and interact with diverse lymphoid (i.e., natural killer (NK) cells, B cells, $CD4^+$ T cells, $CD8^+$ T cells, regulatory T cells, and T follicular helper cells) and myeloid immune cell populations (i.e., dendritic cells (DCs), mast cells, myeloid-derived suppressor cells (MDSCs), M0, M1, M2 macrophages, and neutrophils), as well as with soluble factors secreted by these cells (i.e., cytokines and chemokines) in the extracellular matrix. Notably, the cancer genotype and phenotype have a crucial role in the TIME's composition and functionality, varying depending on the cancer type and clinical stage. In this context, TIME is essential at primary, pre-metastatic, and metastatic sites (20–22). Therefore, the immune context in cancer is associated with prognosis and therapeutic efficacy in patients (23, 24). Previous articles have reviewed the cancer-immunity cycle and the cancer-immune set point for a better understanding of cancer immunobiology (25, 26). Remarkably, several studies have characterized and analyzed the composition and functionality of tumor-infiltrating immune cells (TIICs) across different BC subtypes, evidencing significant associations with prognosis in patients (27–34). Immunotherapies for BC treatment based on CAR T cells, CAR NK cells, immune-checkpoint (IC) inhibitors, cytokine modulation, chemotherapy drugs to induce immunogenic cell death, and personalized vaccines related to tumor-associated antigens are being tested in clinical trials (35). Despite these advances, there is still a lack of knowledge to understand BC immunobiology fully. A fascinating research field focused on long non-coding RNAs (lncRNAs) is being explored in this context.

LncRNAs are non-protein-coding transcripts of more than 200 nucleotides in length and are classified according to their location and orientation relative to protein-coding genes into sense, anti-sense, intronic, intergenic, and bidirectional (36, 37). Notably, lncRNAs are frequently transcribed by RNA polymerase II (Pol II) and III (Pol III). Pol II-transcribed lncRNAs are spliced, bear 7-methyl guanosine caps at the 5' end, and have polyadenylated tails at the 3' end. In contrast, Pol III-transcribed lncRNAs lack caps and poly-A tails. Remarkably, the expression of lncRNAs is lower compared to protein-coding genes. However, lncRNAs exhibit higher tissue and cell specificity, highlighting their regulatory roles (36, 37).

LncRNAs may act in the nucleus or cytoplasm cell fraction, exhibiting a wide range of functions. In a non-pathological context, lncRNAs have essential roles in diverse biological processes, such as regulation of gene expression, chromatin modification, genomic imprinting, and transcriptional and translational processing (36, 37). These functions are mainly achieved due to lncRNA may interact with diverse DNA elements (i.e., exons, introns, and promoters), RNA species (i.e., mRNAs, miRNAs, and other lncRNAs), proteins (i.e., related to epigenetic, transcriptional, translational processes and extracellular vesicles). Previous findings have demonstrated that dysregulation of lncRNAs is associated with cancer biology, evidencing that these molecules are critical modulators of cancer signaling pathways and may act as oncogenes and tumor suppressors, showing versatile and complex roles associated with diverse hallmarks of cancer (38–43). Notably, various reports have evidenced that functional mechanisms and dysregulations associated with various lncRNAs (i.e., SPRY4-IT1, DANCR, PVT1, TUSC8, ATV1, LINC00617, PICART1, APOC1P1-3, SERM, and SERT) are promoters of cell proliferation, invasion, migration, apoptosis, stemness, and drug resistance in BC (44). Particularly, recent investigations have demonstrated the importance of lncRNAs in BC immunobiology, showing that lncRNAs are essential players in the antitumoral immune response, immune evasion mechanisms, and composition and functionality of the TIME. Abnormal expression of lncRNAs has been shown to affect the immune phenotypes across different cancer types, including BC (45–48). In this review, we provide the current advances about the role of lncRNAs as tumor-intrinsic and tumor-extrinsic modulators of the antitumoral immune response and TIME in BC, as well as lncRNAs which are potential biomarkers of the TIME and clinicopathological characteristics in BC patients.

2 LncRNAs as tumor-intrinsic modulators of the antitumoral immune response in BC

Previous research demonstrated that metabolic changes, loss of antigenicity, upregulation of immune inhibitory factors, and alterations in the TIME are important tumor-intrinsic mechanisms of immune evasion and immunotherapy resistance across different cancer types (23, 49, 50). In addition, the dysregulation of oncogenic pathways, such as WNT/β-catenin, MYC, LKB1, PTEN, and TP53, have a crucial role in the promotion and suppression of local antitumor immune response, depending on the cell context and cancer type (8). Prior findings evidenced that *BRCA1, BRCA2*, and *TP53* mutations are associated with high mutational burden, neoantigen load, tumor-infiltrating lymphocyte density, high cytolytic activity, and improved prognosis in BC. Interestingly, the crosstalk between *BRCA1/BRCA2* alterations with NFkB, NOTCH, and PTEN signaling pathways hampers the immune response in BC (51–59). Remarkably, recent studies have evidenced that lncRNAs are critical regulators of cancer immunobiology (45–48). In this regard, the role of diverse lncRNAs as tumor-intrinsic modulators of BC immunobiology has been explored, identifying lncRNAs that function as promoters and suppressors of the antitumoral immune response.

2.1 Tumor-intrinsic lncRNAs as promoters of the antitumoral immune response in BC

Recent findings have evidenced the regulatory roles of lncRNAs as tumor-intrinsic promoters of the antitumoral immune response in BC. Salama et al. identified that triple-negative breast cancers

(TNBC) exhibit a high expression of PD-L1 and a low expression of XIST. Notably, the XIST knockdown promotes an increased expression of PD-L1 in TNBC cells (60). In addition, Zhao et al. evidenced that the XIST knockdown promotes macrophage polarization from M1 to M2, supporting the proliferation and migration of BC cell lines (61). Another research demonstrated that the XIST loss upregulates the c-Met/MSN signaling pathway in TNBC, promoting brain metastasis. Specifically, the XIST loss promotes the microglia reprogramming from M1 to M2 macrophages by exosomal miR-503 releasing, STAT3, and NFκB pathways. Furthermore, BL and TNBC patients have a low expression of XIST, which is associated with poor metastasis-free survival (62). In addition, Hamed et al. showed that the oleuropein compound promotes the expression of XIST and the inhibition of miR194-5p/PD-L1 in TNBC, suggesting the feasibility of modulating the BC immunobiology by targeting lncRNAs and IC inhibitors (63). Overall, XIST is a positive regulator of the antitumoral immune response by preventing PD-L1 expression and M2 macrophage-related phenotypes in BC (Figure 1).

Another study showed that the high expression of KRT19P3 is related to the low expression of PD-L1 and high infiltration of $CD8^+$ T cells in BC, indicating that this lncRNA might have an essential role in the T cell function through the PD-L1 modulation. Also, KRT19P3 decreases proliferation, migration, and invasion *in vitro* (64) (Figure 1). Otherwise, Beltran-Anaya et al. found that LncKLHDC7B is enriched in TNBC immunomodulatory subtype samples with high immunophenoscore values. The silencing of this lncRNA promotes cell migration and invasion while decreasing apoptosis *in vitro*. In addition, the low expression of LncKLHDC7B is associated with recurrence, metastatic events, and reduced survival in TNBC patients (65). In other research, Zhang et al. found that the expression of lncRNA BM466146 positively and negatively correlates with the infiltration level of $CD8^+$ T cells and the Ki-67 index in BC patients, respectively. Particularly, BM466146 could upregulate the CXCL13 expression to recruit $CD8^+$ T cells to the BC immune microenvironment. Also, the overexpression of BM466146 reduces the proliferation *in vitro*, while the high expression of this lncRNA is associated with increased overall survival (OS) in BC patients (66). In addition, an investigation based on an innovative CRISPR activation screening strategy showed that *LINC01198* is suppressed in diverse cancer types, including BC. Additional analyses demonstrated that IFNGR1-related genes, MHC-I protein expression, and STAT1 phosphorylation increase when *LINC01198* is activated in BC cells, while its inhibition decreases the expression of type I IFN pathway-related genes. Specifically, the activation of *LINC01198* promotes the expression of CXCL10, IFN-β, type I IFN receptors, interferon-stimulated genes (ISGs), and the transcriptional activity of NFκB (related to p65 component) *in vitro* (Figure 1). Equally important, the high expression of *LINC01198* is associated with a high score of CD8, IL-2, IL-8, and IL-12 immune signatures and improved OS in BC patients, indicating that *LINC01198* is a promoter of IFN-related antitumoral immune response (67).

2.2 Tumor-intrinsic lncRNAs as suppressors of the antitumoral immune response in BC

Different studies have shown the regulatory roles of lncRNAs as tumor-intrinsic suppressors of the antitumoral immune response in BC. In this context, Salama et al. demonstrated that the TSIX knockdown (a negative regulator of XIST) promotes a reduced expression of PD-L1 in TNBC cells. Moreover, TSIX is highly expressed in TNBC patients with high expression of PD-L1 (60). In another research, Samir et al. exhibited that the increased expression of MALAT1 and miR-182-5p positively modulates the

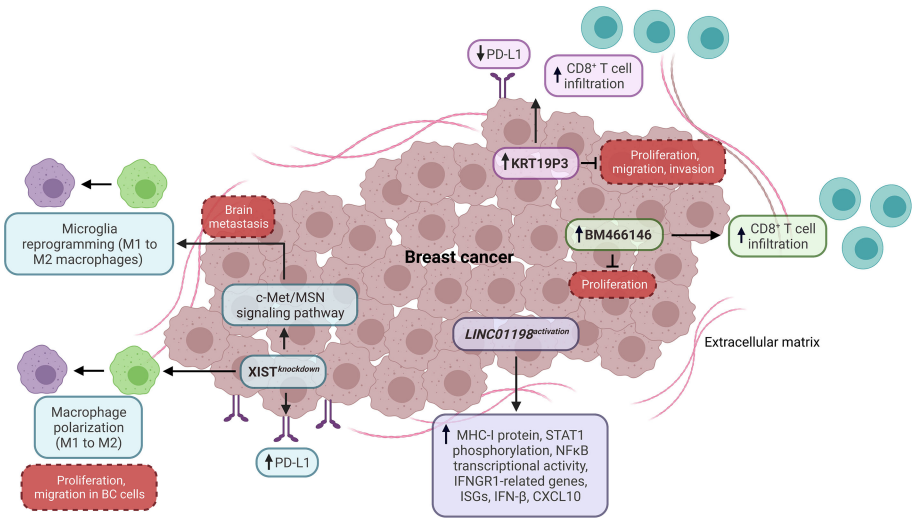

FIGURE 1
Impact of lncRNAs as tumor-intrinsic promoters of the immune response in BC. LncRNAs, including XIST, KRT19P3, BM466146, and LINC01198, function as tumor-intrinsic promoters of the immune response in BC, preventing PD-L1 expression, macrophage polarization, and promoting $CD8^+$ T cell infiltration, as well as the expression of genes and proteins associated with antitumoral immune response. Dashed boxes in red denote cancer-related phenotypes. ISGs, interferon-stimulated genes.

PD-L1 expression through a negative and positive regulation of XIST and TSIX expression, respectively, promoting an immunosuppressive phenotype in TNBC (68). Recent findings showed that MALAT1 knockdown promotes the expression of stress-induced ligands (MICA and MICB) and the repression of immune checkpoints (PD-L1 and B7-H4) in TNBC cells. Also, the MALAT1 knockdown boosts the NK cells-mediated killing and $CD8^+$ T cells-mediated cytotoxic activity *via* miR-34a and miR-17-5p, respectively, indicating that this lncRNA hampers the innate and adaptive immune response in TNBC (69). In another report, Xiping et al. found that MALAT1 knockdown decreases the expression of MYC oncogene and CD47 (a protein that binds to SIRPα and blocks the antigen uptake mediated by macrophages and DCs) in HER2+ and TNBC cells. In addition, the MALAT1 expression promotes proliferation and invasion *in vitro*, supporting the role of this lncRNA in the immune evasion of BC (70). A study showed that the methoxylated quercetin glycoside compound diminishes the MALAT1 expression, altering the immunogenic profile in BC (71). In addition, Wang et al. demonstrated that TINCR is a promoter of immune evasion in BC. Specifically, TINCR acts as a molecular sponge for miR-199a-5p and upregulates the USP20 stability through a ceRNA regulatory mechanism, promoting the upregulation of PD-L1 protein by inhibiting its ubiquitination. Additional analyses revealed that TINCR transcription is promoted through the activation of STAT1 signaling by IFNγ stimulation. Moreover, the TINCR knockdown reduces tumor growth, cell proliferation, migration, and invasion in BC (72).

On the other hand, a comprehensive investigation found that GATA3-AS1 expression enhances the PD-L1 protein levels and promotes cell proliferation and migration of TNBC cells. Particularly, GATA3-AS1 promotes the deubiquitination of PD-L1 protein through the upregulation of COPS5. Besides, the upregulation of GATA3-AS1 is related to a reduced percentage of $CD8^+$ T cells in TNBC, and the high expression of this lncRNA is associated with reduced OS. In contrast, the high level of PD-L1 protein correlates with poor prognosis, large tumor size, and clinical stage in TNBC patients (73) (Figure 2). Another study demonstrated that HEIH is highly expressed in TNBC. At the same time, silencing this lncRNA reduces the expression of miR-939-5p, NOS2, decreases NO production and inhibits cell viability and migration *in vitro*. Moreover, the HEIH silencing increases the expression of MICA and MICB while decreasing the expression of PD-L1, IL-10, and TNFα, suggesting that HEIH significantly promotes immunosuppressive phenotypes in TNBC (74).

Hu et al. evidenced that LINK-A is upregulated in TNBC and negatively correlates with antigen-presenting cells and $CD8^+$ T cell levels in BL BC. Particularly, LINK-A downregulates antigen processing and presentation components (i.e., TPSN, TAP1, TAP2, and CALR) and intrinsic tumor suppressor barriers (Rb and p53), which indicates that this lncRNA promotes tumor immune evasion (Figure 2). Likewise, TNBC patients who are responders to Pembrolizumab have a low expression of LINK-A and high infiltration of $CD8^+$ T cells, in contrast to non-responders. Remarkably, LINK-A inhibition improves the $CD8^+/CD3^+$ T cell infiltration and cytotoxicity, indicating that this lncRNA might be a potential immunosuppressive biomarker and therapeutic target in TNBC patients (75). Wang et al. characterized the function of *IL10RB-DT* through a CRISPR activation screening. They found that the activation of this lncRNA inhibits the transcription of MHC-I and antigen-processing genes in BC cells. Equally important, the *IL10RB-DT* expression is associated with poor survival in BC patients (67). A study about the LINC00624 expression showed that this lncRNA negatively correlates with

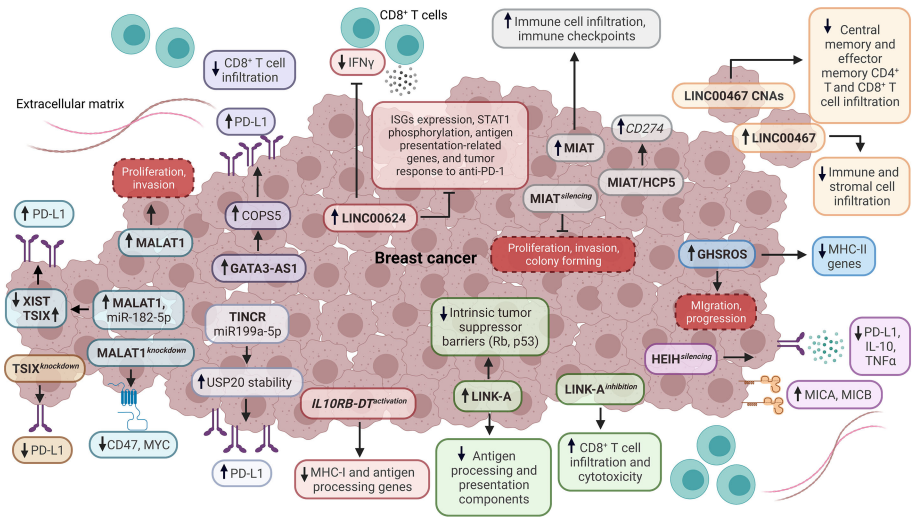

FIGURE 2
Impact of lncRNAs as tumor-intrinsic suppressors of the immune response in BC. Diverse lncRNAs, such as TSIX, TINCR, MALAT1, GATA3-AS1, LINC00624, IL10RB-DT, LINK-A, HEIH, GHSROS, LINC00467, MIAT, and HCP5 function as tumor-intrinsic suppressors of immune response in BC, dysregulating the expression of antigen processing and presentation components, interferon-stimulated genes (ISGs), immune checkpoints, cytokines, stress-induced ligands, STAT1 phosphorylation, tumor suppressor barriers, oncogenes, immunotherapy response, infiltration and functionality of tumor-infiltrating immune cells. Dashed boxes in red denote cancer-related phenotypes. CNAs, copy number amplifications.

type I IFN and antigen processing and presentation pathways *in vitro*. Also, the overexpression of LINC00624 inhibits the ISGs expression and STAT1 phosphorylation *in vitro*. Additionally, IFNα induces the LINC00624 expression, suggesting that this lncRNA is an ISG that is a negative feedback modulator of the IFN signaling pathway (76) (Figure 2). Further analyses demonstrated that ADAR1 interacts with LINC00624, promoting A-to-I substitutions in this lncRNA *in vitro*, which increase after IFNα treatment. Interestingly, the function of the edited LINC00624 depends on ADAR1 to inhibit the IFN response and to promote Lapatinib and anti-HER2 treatment resistance in HER2+ BC cells. Also, tumor cells overexpressing LINC00624 co-cultured with $CD8^+$ T cells inhibit IFNγ production *in vivo*. In contrast, the antigen presentation-related genes, ISGs, and tumor response to anti-PD-1 treatment are inhibited by LINC00624 *in vivo* (76) (Figure 2). This lncRNA is highly expressed in HER2+ BC patients with a non-pathological complete response, and the high expression of LINC00624 is associated with poor disease-free survival (DFS) (76).

Recent research evidenced that the lncRNA MIAT is co-expressed with different genes related to immune cells' regulation, activation, and adhesion. BC patients with high expression of MIAT exhibit a high infiltration of $CD8^+$ T cells, resting memory $CD4^+$ T cells, activated memory $CD4^+$ T cells, gamma-delta T cells, and M1 macrophages. In contrast, the infiltration of plasma cells, activated NK cells, monocytes, M2 macrophages, and activated mast cells are reduced (77). Furthermore, the MIAT expression positively correlates with IC genes like *PDCD1, CD274*, and *CTLA-4*, which are critical players in suppressing the antitumoral response mediated by T cells (Figure 2). Moreover, the high expression of MIAT is associated with clinical stage and lymph node metastasis in serum samples derived from BC patients. The high expression of MIAT is associated with reduced OS in BL BC. In contrast, the high expression of this lncRNA is associated with reduced post-progression survival in LA, LB, and HER2+ BC patients, which indicates a subtype-specific prognostic role of MIAT (77). Additional research confirmed that this lncRNA positively correlates with IC gene expression and its prognostic role associated with OS. Also, MIAT silencing reduces proliferation, colony forming, and invasion, while increasing TNBC cell apoptosis *in vivo*, indicating that MIAT is a promoter of immunosuppressive phenotypes in BC (78). A similar behavior was detected for lncRNA HCP5 in BC. Additional analyses showed that MIAT and HCP5 upregulate the expression of CD274 through a ceRNA mechanism, which involves miR-150-5p sponging in human cancer (78) (Figure 2). Interestingly, Wu et al. found that a ceRNA network composed of BTN3A1-has-miR-20b-5p-HCP5 could have a role in the interaction between BC cells and T cells *in vitro* (79). In this regard, different studies have indicated that ceRNA networks are composed of mRNAs-miRNAs-lncRNAs and are potential modulators of the TIME in BC (80–83).

Another study evidenced that the overexpression of lncRNA GHSROS induces the downregulation of MHC-II genes (*HLA-DRA, HLA-DPB1, HLA-DPA1*, and *HLA-DRB3*) in TNBC cells. In addition, the overexpression of GHSROS is associated with the downregulation of immune-related pathways, including antigen processing and presentation signaling. The expression of GHSROS promotes cell migration *in vitro* and progression *in vivo*, suggesting that this lncRNA is involved in BC immune evasion (84) (Figure 2). In another study, Bo et al. identified a high expression of LINC00467 in metastatic BC and circulating tumor cells. Functional analyses demonstrated that LINC00467 silencing decreases migration and invasion *in vitro*. The high expression of LINC00467 is associated with poor distant metastasis-free survival and relapse-free survival (RFS) in patients across different BC subtypes. Also, the expression of LINC00467 negatively correlates with immune and stromal infiltration in BC. Significantly, the copy number amplifications of LINC00467 are related to low infiltration of central and effector memory $CD4^+$ and $CD8^+$ T cells (Figure 2) and are also associated with poor disease-specific survival and progression-free survival in BC patients (85).

2.3 LncRNAs related to IL-6 in BC

IL-6 is a pleiotropic cytokine that is crucial in the immune response in non-pathological and pathological conditions. IL-6 can antagonize or promote tumor progression depending on the cell context (86–89). Recent studies indicate that some lncRNAs are related to IL-6 in BC. A study showed that lncRNA BCAR4 is recruited to *PTCH1, MUC5AC, TGF-β1*, and *IL-6* promoters to induce their expression in response to CCL21 in BC cells. Also, the *BCAR4* expression promotes migration and invasion *in vitro* (90). Moreover, DeVaux et al. identified that BHLHE40-AS1 promotes migration and invasion in ductal infiltrating BC through a low expression of IL-6 and STAT3 phosphorylation (91). Similarly, Nyati et al. found that lncRNA AU021063 expression is promoted by IL-6/Arid5a signaling. Additional analyses showed that AU021063 induces invasion and metastasis of BC *in vitro* and *in vivo* via upregulation of Trib3 and activation of the Mek/Erk signaling pathway (92).

3 LncRNAs as tumor-extrinsic regulators of the TIME in BC

Different studies have demonstrated that diverse lncRNAs function as tumor-extrinsic factors specifically expressed by diverse immune cell populations to regulate their functionality, which is essential in the TIME and prognosis in BC. Despite recent advances, the role of lncRNAs as extrinsic regulators of the TIME in BC has been only reported in cytotoxic T lymphocytes, regulatory T cells, and tumor-associated macrophages.

3.1 Cytotoxic T lymphocytes

The cytotoxic T lymphocytes (CTLs) are a subpopulation of $CD8^+$ T cells that are the main effectors of the antitumoral immune response (24, 93). Remarkably, the CTLs eliminate cancer cells through perforin and granzyme mechanisms. The functionality of CTLs is mainly suppressed in cancer by the induction of anergy

states and exhaustion phenotypes (93, 94). Therefore, CTLs are frequently associated with improved prognosis in different cancer types (24). Recent studies have evidenced that lncRNAs are crucial regulators of CTLs in the TIME of BC. Although the role of NKILA in non-neoplastic and neoplastic conditions has been recently reviewed (95), different studies have identified critical roles of this lncRNA in CTLs from the TIME of BC. In this regard, Huang et al. found that NKILA is highly expressed in tumor-specific CTLs and Th1 cells, enhancing their sensibility to activation-induced cell death (AICD) compared to Treg and Th2 cells in BC. Specifically, NKILA suppresses the IκBα phosphorylation, p65 nuclear translocation, and transcription of NFκB-target anti-apoptotic genes in CTLs (96). Additional studies have corroborated the role of NKILA as a negative regulator of NFκB in immune cells from BC (97, 98) (Figure 3). Notably, the transcription of NKILA is regulated by calmodulin-induced histone acetylation and STAT1 signaling, and the high levels of NKILA^{hi} tumor-specific CTLs are associated with poor survival in BC patients (96). In contrast, Liu et al. found that the low expression of NKILA is associated with distal metastasis, lymph node status, advanced clinical stage, tumor size, and poor DFS in BC patients (97). Similarly, Wu et al. demonstrated that NKILA silencing promotes TGFβ-induced EMT *in vivo* and the low expression of this lncRNA is associated with poor DFS in BC patients (98) (Figure 3). Therefore, NKILA could exert a context-dependent role as a regulator of NFκB signaling and metastasis, suggesting the potential of this lncRNA as a therapeutic target to modulate the function of tumor-specific T cells in BC. In addition, Yu et al. showed that lncRNA expression and CTLs predict the OS and immunotherapy response in cancer patients stratified by immune groups (99).

3.2 Regulatory T cells

The regulatory T (Treg) cells are a specialized subpopulation of CD4$^+$ T cells characterized by the expression of CD25 and FOXP3. In a non-pathological context, Treg cells suppress the immune response for homeostasis maintaining, self-tolerance, and preventing autoimmune diseases (100). In cancer, Treg cells often promote immunosuppression by expressing IL-10, TGFβ, and CTLA-4. Therefore, Treg cells are frequently associated with poor prognosis in different cancer types (24, 101). Recent research indicates that lncRNAs are important regulators of Treg cells in the TIME of BC. Moallemi-Rad et al. evaluated the Treg cell-related lncRNAs expression from BC in this regard. In particular, RMRP and MAFTRR expression is positively associated with nuclear grade, tubule formation, and tumor size. Conversely, the expression of FLICR differs according to the HER2 levels in BC (102).

SNHG1 and SNHG16 belong to the SNHG lncRNA family, which has a critical oncogenic role in different cancer types (103). Recent findings have evidenced their role as tumor-extrinsic regulators in the TIME of BC. Pei et al. demonstrated that lncRNA SNHG1 is highly expressed on CD4$^+$ T cells from the peripheral blood of BC patients, in contrast to CD4$^+$ T cells from normal donors. Moreover, the SNHG1 knockdown decreases IDO1, Foxp3, and IL-10 expression, essential Treg cell differentiation promoters. In addition, the SNHG1 knockdown reduces the tumor volume in murine models with BC xenografts (104). In another study, Ni et al. identified that lncRNA SNHG16, delivered from BC exosomes, promotes the activation of the TGF-β1/SMAD5 signaling pathway and miR-16-5p downregulation to induce the

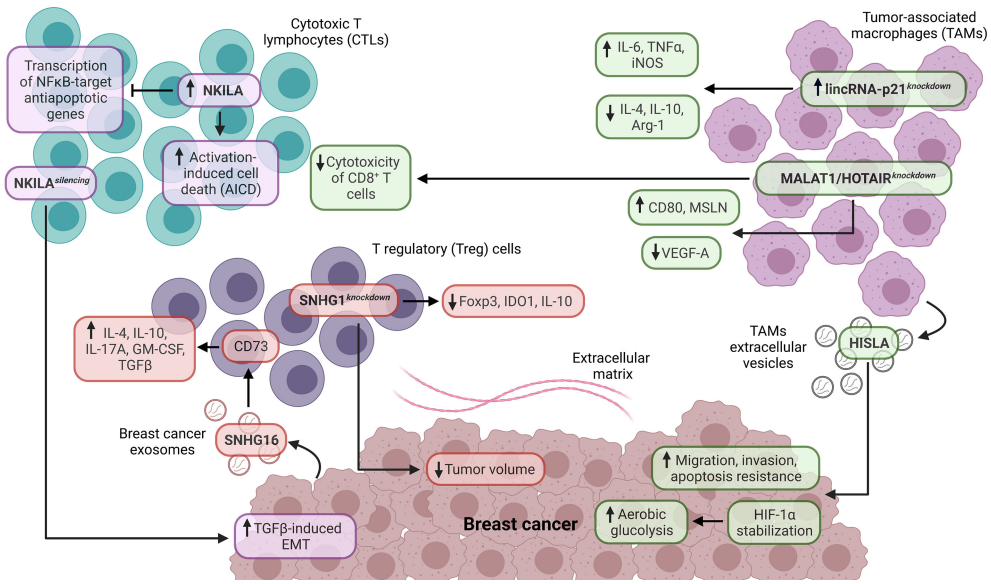

FIGURE 3
Role of lncRNAs as tumor-extrinsic regulators of the TIME in BC. In the TIME of BC, lncRNAs are critical modulators of the functionality in immune cell populations and BC. In this regard, NKILA is associated with cytotoxic T lymphocytes (CTLs), while SNHG1 is related to regulatory T (Treg) cells. In contrast, lincRNA-p21, HOTAIR, and MALAT1 are related to tumor-associated macrophages (TAMs). In addition, the lncRNAs, such as SNHG16, HISLA, MALAT1, and HOTAIR, are expressed by specific cell populations and have a crucial impact on the functionality of target cell populations in the TIME of BC. EMT, epithelial-mesenchymal transition.

upregulation of CD73 in γδ1 Treg cells. The γδ1 Treg cells constitute a high proportion of TIICs in TNBC, ER+PR+, and HER2+ BCs, and the CD73 expression is higher in γδ1 Treg cells derived from BC. Remarkably, $CD73^+$ γδ1 Treg cells exhibit high expression of IL-4, IL-10, IL-17A, GM-CSF, and TGFβ, which are critical immunosuppressive molecules, indicating that $CD73^+$ γδ1 Treg cells have an immunosuppressive role in the TIME of BC (105) (Figure 3).

3.3 Tumor-associated macrophages

Tumor-associated macrophages (TAMs) are a crucial cell component in the TIME (106). According to their functions, TAMs are separated into M1 and M2 macrophages. M1 macrophages have pro-inflammatory and antitumoral functions mediated by the secretion of IL-1β, IL-6, IL-12, TNFα, and reactive oxygen species. Moreover, M1 macrophages are key promoters of Th1-type response and are associated with improved prognosis in different cancer types (21, 24, 106). Conversely, M2 macrophages have anti-inflammatory and pro-tumoral functions mediated by the expression of IL-10, TGFβ, PGE2, PD-L1, and PD-L2, promoting immunosuppression. Therefore, M2 macrophages are strongly associated with poor prognosis in cancer patients (21, 24, 106). Interestingly, recent research indicates that lncRNAs are critical regulators of TAMs in the TIME of BC. Zhou et al. evidenced that lincRNA-p21 is upregulated in TAMs from BC murine models. Moreover, the lincRNA-p21 knockdown in TAMs promotes the production of pro-inflammatory molecules (IL-6 and TNFα), iNOS, and decreases the production of anti-inflammatory molecules (IL-4 and IL-10) and Arg-1, indicating that this lncRNA has an essential role in the TAM polarization *in vivo* (Figure 3). In addition, the lincRNA-p21 knockdown promotes the interaction of MDM2/p53 to activate the NFκB and STAT3 signaling pathways. Interestingly, the lincRNA-p21 knockdown decreases the BC progression and improves survival *in vivo* (107). On the other hand, Chen et al. found that the extracellular vesicle-packaged lncRNA HISLA from TAMs is delivered to TNBC cells, stabilizing HIF-1α (through the inhibition of PHD2/HIF-1α interaction) and enhancing tumoral aerobic glycolysis, suggesting a metabolic reprogramming of BC mediated by cell-cell communication. Also, HISLA promotes migration, invasion, and apoptosis resistance in BC cells (Figure 3). The high expression of this lncRNA is associated with lymph node metastasis and poor DFS in BC patients (108). Another investigation analyzed the relationship between lncRNAs and their immunomodulatory role in TAMs derived from BC. In particular, MALAT1 and HOTAIR are upregulated in TAMs derived from TNBC, HER2+, and hormonal BCs. In these TAMs, the MALAT1 and HOTAIR silencing promotes the upregulation of CD80 and MSLN and the downregulation of VEGF-A. Furthermore, this study showed a cytotoxicity decrease in $CD8^+$ T cells against TNBC cells treated with anti-PD-L1 inhibitor and cultured under conditioned media derived from TAMs with MALAT1 and HOTAIR silencing, indicating the role of both lncRNAs as tumor-extrinsic negative modulators of the antitumoral immune response in BC (109) (Figure 3).

4 LncRNAs as potential biomarkers of the TIME and clinicopathological characteristics in BC

In recent years, several Next-Generation Sequencing (NGS) approaches (i.e. bulk RNA-seq, single cell RNA-seq, whole-genome sequencing and whole-exome sequencing) and bioinformatic tools (i.e., Polysolver, NetMHCpan, CIBERSORTx and MiXCR) have been incorporated for interrogating cancer immunobiology, creating the area known as cancer immunogenomics and immunotranscriptomics (110–114), which includes comprehensive pan-cancer analyses focused on neoantigens prediction (115, 116), MHC class I and class II genes (117, 118), compositional and functional characterization of TIMEs (119, 120), cytolytic activity estimation (121), BCR/TCR repertoires (122) and immunotherapies monitoring (110, 119, 123). Remarkably, large-scale bioinformatics pan-cancer studies have focused on the characterization of lncRNAs as immune-related oncogenic biomarkers and as modifiers of TIMEs, highlighting the potential clinical application of lncRNAs as immunotherapy targets (124, 125). Remarkably, recent findings based on identifying lncRNAs as biomarkers of the TIME and clinicopathological characteristics in BC have gained particular interest. This section highlights relevant studies, primarily based on NGS data mining and bioinformatic approaches, which have explored the role of diverse lncRNAs as individual biomarkers and prognostic models/signatures in the BC immunobiology context.

4.1 Individual lncRNAs

Recent advances in BC patients have revealed that individual lncRNAs are promising biomarkers of the TIME and clinicopathological characteristics. A study found that the expression of lncRNA ST7-AS1 is associated with various signaling pathways, including MYC, KRAS, IL6-JAK-STAT3, and apoptosis signaling pathways. In addition, the expression of ST7-AS1 differentially correlates with elevated levels of diverse lymphoid and myeloid cell populations. The high expression of ST7-AS1 is associated with improved OS, progression-free survival, and disease-specific survival (DSS) in BC patients (126).

Yi et al. observed that the expression of SLC26A4-AS1 is associated with the infiltration of diverse immune cell populations. Notably, high expression of this lncRNA is associated with improved OS and DSS in BC patients (127). A study by Zhao et al. revealed that the expression of lncRNA DRAIC is inversely correlated with the infiltration of DCs and neutrophils. High expression of DRAIC is associated with advanced tumor stage, positive lymph node status, and unfavorable OS and DSS in ER+ BC patients (128). Another research demonstrated that elevated expression of lncRNA TCL6 is associated with various immune-related pathways in BC. TCL6 expression positively correlates with infiltration of neutrophils, DCs, B cells, $CD4^+$ T, and $CD8^+$ T cells, as well as the expression of IC genes, such as *PD-1, PD-L1, PD-L2*, and *CTLA-4*. The low and high expression of TCL6 is associated with poor and improved OS, respectively, in LB BC (129). Similarly,

a recent study demonstrated that high and low expression of LINC00426 is consistently associated with increased and poor OS in LB BC, respectively. Moreover, the LINC00426 expression correlates with the infiltration level of diverse immune cell populations, IC, and cytolytic activity-related genes, evidencing that this lncRNA is an immune phenotype-related biomarker in LB BC (130).

Liu et al. reported that lncRNA OSTN-AS1 positively correlates with B and T cell signaling pathways in BC, involving genes like *PDCD1, CTLA-4, CD79A*, and *CD79B*. High expression of OSTN-AS1 is related to diverse immune functions encompassing cytokines, chemokines, NK cells, B cells, T cells, and others. The high expression of OSTN-AS1 is associated with a favorable prognosis in TNBC patients (131). In another study, De Santiago et al. found that LINC00944 is upregulated in TNBC cells due to ADAR1 loss. This lncRNA is related to immune signaling pathways, such as interferon-gamma response, inflammatory response, IL2-STAT5, and TNFα-NFκB. Also, the LINC00944 expression positively correlates with T cell-associated gene markers (*CD3D, CD3E, CD3G, SH2D1A*, and *TRAT1*) in BC patients. Reduced expression of LINC00944 is associated with diminished T-cell infiltration, while the high expression of this lncRNA is related to the upregulation of anti-apoptotic genes. The high expression of LINC00944 is associated with improved RFS in TNBC patients (132). Similarly, a study identified that lncRNAs RP3-460G2.2, RP11-1008C21.1, and RP5-899E9.1 are correlated with the infiltration of diverse immune cell populations and are strongly associated with macrophage gene markers (*CD68* and *MSR1*) in BC (133).

An investigation revealed a negative correlation between LINC00472 expression and IFNγ, IFNα, and TNFα pathways while exhibiting a positive correlation with p53, ER, and PR pathways in ER+, ER- BCs, and TNBC, implying an association with immunosuppression. Conversely, the opposite correlation was detected for lnc-HLA-DRB1-5 in ER+, ER- BCs, and TNBC (134). Notably, recent research has focused on evaluating the expression and roles of immune-related lncRNAs in different BC subtypes. Mathias et al. highlighted the high expression of LINC01871 in BL BC, which participates in interferon-gamma response, allograft rejection, interferon alpha, inflammatory response, IL6-JAK-STAT3, and IL2-STAT5 signaling. Additionally, the upregulation of LINC01871 was associated with improved OS and progression-free interval (PFI) in BL BC (135).

Similarly, XXYLT1-AS2 exhibits high expression in HER2-enriched BC and correlates with improved PFI in this subtype. This lncRNA positively correlates with allograft rejection, interferon-gamma response, inflammatory response, IL-2, and IL-6 signaling, while negatively correlates with EMT, hypoxia, and myogenesis. Conversely, MEG3 is highly expressed in LA BC and positively correlated with TNFα-NFκB, inflammatory response, allograft rejection, interferon-gamma response, and IL2-STAT5 signaling (135). Furthermore, the lncRNA EBLN3P is highly expressed in LB BC and is associated with improved OS. The expression of EBLN3P negatively correlates with TNFα-NFκB and allograft rejection signaling (135).

Recent findings highlighted LINC01087 as a potential promoter of the antitumoral immune response with high expression in luminal BCs. Specifically, LINC01087 demonstrated a relationship with the NFκB signaling pathway in LA and LB BC. Moreover, this lncRNA is also related to chemoattractants, chemokine, and pattern recognition receptors signaling pathways in LA BC. Elevated expression of LINC01087 downregulates oncogenic network components related to proliferation and adhesion, including the WNT/β-catenin pathway. Remarkably, the high expression of LINC01087 was correlated with improved OS and RFS in LA and LB BC patients (136). On the other hand, a recent study analyzed the expression of immune-related lncRNAs in BC, revealing differences based on hormone status. Notably, the low expression of immune-related lncRNAs ENST0000615051, lnc-DDX31, and LINC02381 was detected in ER+ BC, while reduced expression of lnc-DDX31 was observed in PR+ BC (137). Equally important, an investigation found epigenetically dysregulated lncRNAs associated with immune pathways related to inflammation, cytokines, chemokines, and T cells, depending on the BC subtype. In this context, LINC01983, UCA1, RP11-221J22.1 and RP11-221J22.2 were specific to luminal BCs, while RP1-140K8.5, AC005162.1, AC020916.2 SLC26A4-AS1, and CTC-303L1.2 were specific to BL subtype (138). These findings point out the potential of specific lncRNAs as valuable biomarkers for assessing the TIME and predicting clinical outcomes in BC patients.

4.2 LncRNA prognostic models/signatures

Recent studies have explored the combined roles of diverse immune-related lncRNAs in models/signatures, which are prognostic predictors and markers of immune landscapes in BC, indicating their potential usefulness in clinical settings (139–143). Liu et al. showed that a nomogram, based on seven immune-related lncRNAs, age, clinical stage, ER status, and BC subtype, is a predictor of OS in BC. Also, the study exhibited that low-risk patients have an enrichment of immune pathways associated with inflammation and a correlation between the infiltration of B cells, T cells, and macrophages with the risk score. In contrast, high-risk patients show a high mutational burden (144). Similarly, a signature based on five immune-related lncRNAs predicts the OS and negatively correlates with the infiltration of B cells, T cells, DCs, neutrophils, and macrophages (145). In this context, different immune-related lncRNA models/signatures are predictors of survival and metastatic status. Notably, the lncRNA models/signatures can stratify BC patients based on their risk score, associated with the enrichment of various immune-related pathways, the abundance of diverse immune cell populations, and the expression of different IC genes (Table 1).

Interestingly, different studies have demonstrated a relationship between tumor immune response and ferroptosis, necroptosis, pyroptosis, autophagy, and genomic instability processes (156–161). In this regard, various studies have developed prognostic lncRNA models/signatures related to these processes, which predict the TIME characteristics and immunotherapy response in BC patients (Table 2). Additional lncRNA prognostic models/signatures focused on other biological processes, such as lipid metabolism, hypoxia, glycolysis, EMT, stemness, RNA-binding

TABLE 1 Immune-related lncRNA models/signatures are prognostic predictors and markers of the TIME characteristics in BC.

Number of lncRNAs in the model/signature	Prognostic value in patients	TIME characteristics determined by the model/signature	Reference
4	MFS, OS	A high RS is associated with aDCs, eosinophils, immature B cells, pDCs, Treg cells, and T_H2 cells. A low RS is associated with CD56dim NK cells, monocytes, and neutrophils.	(146)
4	RFS	The signature is associated with leukocytes, lymphocytes, B cells, T cells, cytokines, IFNγ production, antigen receptor, and regulation of different immune and intracellular processes-related pathways.	(147)
5	OS	The lncRNAs negatively correlate with CD4 T cells, CD8 T cells, B cells, DCs, neutrophils, and macrophages.	(145)
5	Metastatic status	The signature correlates with gene markers associated with B cells, naive T cells, effector T cells, resident memory T cells, T_H1 cells, Treg cells, T cell exhaustion, macrophages, TAMs, monocytes, NK cells, neutrophils, and DCs.	(148)
6	OS	A high RS is associated with a low enrichment of CD8 T cells and with dysregulations in the endoplasmic reticulum and antigen processing and presentation pathways. A low RS is associated with high enrichment of CD8 T cells.	(149)
7	OS	The RS negatively correlates with CD8 T cells, resting memory CD4 T cells, naive B cells, and memory B cells. Also, the RS positively correlates with M0 and M2 macrophages. A low RS is associated with the enrichment of IFN response pathways-related genes.	(144)
8	OS	A low RS is associated with the enrichment of positive regulation of immune effector processes, positive regulation of adaptive immune response, positive regulation of lymphocyte activation, regulation of T cell activation, and T cell receptor signaling pathways.	(150)
10	OS, tumor mutational burden, immunotherapy response	A low RS is enriched with different immune-related functions, infiltration of diverse immune cell populations, reduced expression of immune checkpoint genes, poor OS, and high TIDE score compared to the high RS group.	(151)
11	OS	The RS negatively correlates with B cells, $CD4^+$ T cells, $CD8^+$ T cells, DCs, neutrophils, and macrophages.	(152)
13	OS	A high RS positively correlates with plasma cells, M2 macrophages, neutrophils, and low expression of PD-L1. A low RS positively correlates with the infiltration of diverse immune cell populations.	(153)
40	OS	A high RS positively correlates with M0 and M2 macrophages and low expression of *LAG3, CTLA-4, PDCD1*, and *PDCD1LG2*. Also, the high RS negatively correlates with $CD8^+$ T cells.	(154)
56	OS	A low RS is associated with high infiltration of aDCs, B cells, CD8 T cells, DCs, NK CD56dim cells, NK CD56bright cells, pDCs, Tfh, T_H17, T_H2, and Treg cells. Moreover, a low RS is associated with low infiltration of macrophages, Tem, Tcm, Tgd, and T_H1 cells.	(155)

aDCs, activated dendritic cells; CD, cluster of differentiation; DCs, dendritic cells; IFN, interferon; MFS, metastasis-free survival; NK, natural killer; OS, overall survival; pDCs, plasmacytoid dendritic cells; RFS, relapse-free survival; RS, risk score; TAMs, tumor-associated macrophages; Tcm, T central memory cells; Tem, T effector memory cells; Tfh, T follicular helper cells; Tgd, T gamma-delta cells; TH, T helper cells; TIDE, tumor immune dysfunction and exclusion; TIME, tumor immune microenvironment; Treg, regulatory T cells.

proteins, endoplasmic reticulum stress, cuproptosis, lactate, oxidative stress, androgen receptor signaling pathway, mitochondrial function, aging and angiogenesis have also demonstrated to be predictors of immune landscapes characteristics in BC (176–190). However, further studies are mandatory to explore the relationship between these processes with BC immunobiology.

5 Potential limitations and advantages of lncRNAs for BC immunotherapy

Diverse studies have demonstrated the importance of lncRNAs in cancer biology (38–42). As discussed in this review, lncRNAs are critical players in diverse BC-intrinsic and extrinsic immune-related processes. Also, lncRNAs are potential biomarkers of patients' TIME and clinicopathological characteristics. Previous studies have supported the potential usefulness of strategies for targeting lncRNAs in a cancer context. These approaches are mainly focused on post-transcriptional targeting [i.e., RNA-mediated interference (RNAi), Morpholino oligomers, and anti-sense oligonucleotides (ASOs)], modulation of lncRNA-expressing loci via CRISPR/Cas9-based genome editing, transcriptional upregulation through targeting natural anti-sense RNAs, steric inhibition of lncRNA function, and lncRNA tertiary structure disrupting-based strategies (43, 44, 191–193). Notably, a comprehensive study used ASOs to target LINC00624 in HER2+ BC, resulting in the inhibition of proliferation *in vitro* and increasing the expression of innate immune response-related genes in xenograft tumor models, supporting the role of LINC00624 as an inhibitor of the antitumoral immune response (76). In addition, a CRISPR activation screening strategy was recently used to determine the mechanistic role of LINC01198 and IL10RB-DT in BC cells, concluding an association with promoting and suppressing the

TABLE 2 LncRNA models/signatures related to ferroptosis, necroptosis, pyroptosis, autophagy, and genomic instability are prognostic predictors and markers of the TIME characteristics in BC.

Number of lncRNAs in the model/ signature	Prognostic value in patients	TIME characteristics determined by the model/signature	Reference
5 (ferroptosis-related)	RFS	Patients in the high-risk group have low expression of ICs.	(162)
7 (ferroptosis-related)	OS	A high RS is associated with low infiltration of macrophages, DCs, $CD8^+$ T, and B cells.	(163)
8 (ferroptosis-related)	DSS, OS, PFS	Low-risk patients have an enrichment of antigen processing and presentation, NK cell-mediated cytotoxicity, T cell receptor, and chemokine signaling pathways. Also, these patients have a high proportion of tumor-infiltrating $CD8^+$ T cells, activated NK cells, and M1 macrophages and high expression of PD1, PDL1, CTLA-4, LAG3, and TIGIT.	(164)
10 (ferroptosis-related)	OS	Patients in the low-risk group have an enrichment of diverse immune-related processes.	(165)
11 (ferroptosis-related)	OS	A low RS is associated with the enrichment of NK, T, and B cells. A high RS is associated with the enrichment of M1 macrophages and cancer-associated fibroblasts. Patients in the high-risk group have an enrichment of ICs.	(166)
4 (necroptosis-related)	OS	A high RS is negatively associated with infiltration of memory B cells, activated memory $CD4^+$ T cells, $CD8^+$ T cells, aDCs, M0 and M1 macrophages, activated NK cells, plasma cells, Tfh, Treg cells, and positively associated with infiltration of M2 macrophages, resting memory $CD4^+$ T cells, resting DCs, resting mast cells, naive B cells, and eosinophils. A low RS is associated with high expression of 36 ICs, and with enrichment of cell cycle, cytokine-cytokine receptor interaction, chemokine signaling pathway, primary immunodeficiency, and T cell receptor signaling pathway.	(167)
7 (necroptosis-related)	Immunotherapy response	The RS positively correlates with aDCs, M0, and M2 macrophages. Low-risk patients have a high stromal and immune infiltration score and a high TIDE score.	(168)
13 (necroptosis-related)	OS, immunotherapy response	A low RS is associated with high infiltration of naive B cells, monocytes, activated NK cells, plasma cells, $CD4^+$ activated memory T cells, and $CD8^+$ T cells. Patients in the high-risk group have high infiltration of M0 and M2 macrophages and neutrophils. Patients in the low-risk group have an enrichment of ICs like PD-L1, CD28, and CTLA-4. Also, these patients have an enrichment of diverse immune-related processes.	(169)
5 (autophagy-related)	OS	Patients in the low-risk group have an enrichment of antigen processing and presentation and T cell receptor pathways.	(170)
11 (autophagy-related)	OS	A high RS correlates with infiltration of central memory CD8 T cells, Tfh cells, and memory B cells. A low RS correlates with infiltration of activated CD8 T cells, effector memory CD8 T cells, T_H1 cells, activated B cells, immature B cells, NK cells, eosinophils, mast cells, and monocytes.	(171)
8 (pyroptosis-related)	OS, immunotherapy response	Patients in the high-risk group have a low abundance of immune infiltrating cell populations and have inhibition of antigen processing and presentation, apoptosis, B-cell receptor, T-cell receptor, and JAK-STAT pathways. Responding patients have a low RS than non-responding patients to anti-PD-1 treatment.	(172)
10 (pyroptosis-related)	OS	A low RS is associated with a high abundance of $CD8^+$ T cells, activated memory $CD4^+$ T cells, B cells, and NK cells. Patients in the high-risk group have infiltration of Treg cells and M2 macrophages. Patients in the low-risk group have high expression of T cell phenotypic and functional markers, activating immune receptors, IFNγ signature, and IC markers.	(173)
7 (genomic instability-related)	OS, number of somatic mutations	Patients in the high-risk group have low levels of $CD8^+$ T cells and increased levels of M2 macrophages. Moreover, in this group, the CXCL8 expression is positively correlated with M2 macrophages and negatively correlated with CD8 T cells.	(174)
128 (genomic instability-related)	OS, number of somatic mutations	A high RS is positively associated with high expression of negative ICs (CTLA-4, CD276, TIGIT, PVR, HMGB1, TDO2, IDO1, CXCL9, and CXCL10). A low RS is positively associated with the expression of positive ICs (TNFRSF9, TNFRSF14, and TNFRSF18).	(175)

aDCs, activated dendritic cells; CD, cluster of differentiation; DCs, dendritic cells; DSS, disease-specific survival; IC, immune-checkpoint; IFN, interferon; MFS, metastasis-free survival; NK, natural killer; OS, overall survival; PFS, progression-free survival; RFS, relapse-free survival; RS, risk score; Tfh, T follicular helper cells; TH, T helper cells; TIDE, tumor immune dysfunction and exclusion; TIME, tumor immune microenvironment; Treg, regulatory T cells.

antitumoral immune response, respectively (67). These findings highlight lncRNAs as attractive targets for BC immunotherapy. However, some issues must be addressed before incorporating lncRNAs in clinical settings. Firstly, most of the functional studies focused on lncRNAs, in the context of BC immunobiology, are based on targeting strategies, like CRISPR-Cas9, RNAi and ASOs, and routine functional assays *in vitro* and *vivo* (i.e., co-cultures, proliferation, migration and invasion assays). Despite these advances, there is still a gap in our understanding of the exact mechanistic role of lncRNAs; therefore, the incorporation of comprehensive functional approaches and complementary strategies to fully dissect the crosstalk of lncRNAs in signaling pathways, lncRNA tertiary structure, and lncRNAs interactions with diverse RNA species, DNA elements, chromatin, and proteins are mandatory to completely understand the versatile and complex mechanistic roles of lncRNAs in BC immunobiology. Secondly, bioinformatic studies focused on lncRNAs must be validated using experimental methodologies like flow cytometry and multiplex immunofluorescence. Thirdly, we still lack information about the tumor extrinsic roles of diverse lncRNAs in the remaining BC TIME cell components, such as B cells, MDSCs, and neutrophils. Additionally, clinical trials by FDA and EMA are mandatory for validating immune-related prognostic biomarkers and immunotherapy strategies based on lncRNAs in BC, considering the current hurdles associated with non-coding RNA therapeutics, such as on-target specificity, unwanted off-target effects, and delivery systems (43, 44, 192, 194).

Despite these challenges, lncRNAs are promising molecules for BC immunotherapy because different molecules like XIST, LINC001198, TINCR, LINK-A, and HEIH function as promoters or suppressors of the antitumoral immune response at intrinsic and extrinsic levels, demonstrated by *in vivo* and *in vitro* studies. Also, investigations based on NGS data mining from public repositories and bioinformatic analyses have elucidated the role of diverse lncRNAs like DRAIC, OSTN-AS1, LINC00944, and LINC01871 as biomarkers of the TIME and clinicopathological features in BC, highlighting lncRNAs as potential immunotherapy targets. In addition, lncRNA targeting strategies may be combined with current and approved immunotherapies based on protein and cellular targets (i.e., IC inhibitors, cytokine modulation, and immune cell-based therapies) to increase the therapeutic options, improve the response to immunotherapies and consider personalized treatments for BC patients. Also, lncRNAs like GATA3-AS1, LINC00624, TCL6, LINC00426, and MIAT have BC subtype-specific expression that can be useful for proper designing and specific implementation for patients' stratification strategies and immunotherapies based on lncRNAs in BC in the next coming years.

6 Conclusion and perspectives

The dysregulation of lncRNAs has a crucial role in tumorigenesis and cancer progression. Mainly, various studies have reported the relevance of different lncRNAs in alterations of processes associated with cancer immunobiology. In this review, we provided the current advances in the role of lncRNAs as modulators of antitumoral immune response and the TIME in BC, as well as their role as potential biomarkers of the TIME and clinicopathological characteristics in BC patients. The pivotal role of lncRNAs in regulating antigen processing and presentation, ICs expression, infiltration, and functionality of immune cell populations, and their association with diverse prognosis parameters, highlights that lncRNAs are potential biomarkers of immune phenotypes and immunotherapy targets for BC. Limitations in our knowledge of lncRNAs in BC immunobiology are associated with the complexity of thoroughly dissecting their exact mechanistic roles and interactions. Therefore, future lncRNA research based on comprehensive functional strategies, bioinformatics approaches, and clinical trials is mandatory to fully understand the versatile and complex mechanistic and clinical roles of diverse lncRNAs in BC immunobiology. Taken together, the advances in lncRNAs have opened a novel and exciting area to dissect BC immunobiology and its potential therapeutic significance in the next coming years.

Author contributions

Conceptualization, investigation, resources, original draft, figures and tables preparation: MAF-M. Writing and editing: MAF-M. Review and comments: KIV-S. Supervision: AH-M. All authors contributed to the article and approved the submitted version.

Funding

This research was funded by the Consejo Nacional de Ciencia y Tecnología (CONACYT) 708515 grant (scholarship).

Acknowledgments

We thank to Programa de Doctorado en Ciencias Biológicas, UNAM. The authors thank the reviewers for their helpful comments on the manuscript.

Conflict of interest

The authors declare that the research was conducted in the absence of any commercial or financial relationships that could be construed as a potential conflict of interest.

Publisher's note

References

1. Harbeck N, Penault-Llorca F, Cortes J, Gnant M, Houssami N, Poortmans P, et al. Breast cancer. *Nat Rev Dis Prim* (2019) 5(1):66. doi: 10.1038/s41572-019-0111-2

2. Sung H, Ferlay J, Siegel RL, Laversanne M, Soerjomataram I, Jemal A, et al. Global cancer statistics 2020: GLOBOCAN estimates of incidence and mortality worldwide for 36 cancers in 185 countries. *CA Cancer J Clin* (2021) 71(3):209–49. doi: 10.3322/caac.21660

3. Bydoun M, Marcato P, Dellaire G. Breast cancer genomics. In: *Cancer genomics: from bench to personalized medicine*. Elsevier Inc (2013). p. 213–32. doi: 10.1016/B978-0-12-396967-5.00013-X

4. Goldhirsch A, Winer EP, Coates AS, Gelber RD, Piccart-Gebhart M, Thürlimann B, et al. Personalizing the treatment of women with early breast cancer: highlights of the st gallen international expert consensus on the primary therapy of early breast cancer 2013. *Ann Oncol* (2013) 24(9):2206–23. doi: 10.1093/annonc/mdt303

5. Akram M, Iqbal M, Daniyal M, Khan AU. Awareness and current knowledge of breast cancer. *Biol Res* (2017) 50(1):1–23. doi: 10.1186/s40659-017-0140-9

6. Perou CM, Sørile T, Eisen MB, Van De Rijn M, Jeffrey SS, Ress CA, et al. Molecular portraits of human breast tumours. *Nature* (2000) 406(6797):747–52. doi: 10.1038/35021093

7. Bernard PS, Parker JS, Mullins M, Cheung MCU, Leung S, Voduc D, et al. Supervised risk predictor of breast cancer based on intrinsic subtypes. *J Clin Oncol* (2009) 27(8):1160–7. doi: 10.1200/JCO.2008.18.1370

8. Spranger S, Gajewski TF. Impact of oncogenic pathways on evasion of antitumour immune responses. *Nat Rev Cancer* (2018) 18(3):139–47. doi: 10.1038/nrc.2017.117

9. Yousefnia S, Seyed Forootan F, Seyed Forootan S, Nasr Esfahani MH, Gure AO, Ghaedi K. Mechanistic pathways of malignancy in breast cancer stem cells. *Front Oncol* (2020) 10:452(April). doi: 10.3389/fonc.2020.00452

10. Ortega MA, Fraile-Martínez O, Asúnsolo Á, Buján J, García-Honduvilla N, Coca S. Signal transduction pathways in breast cancer: the important role of PI3K/Akt/mTOR. *J Oncol* (2020) 2020:1–11. doi: 10.1155/2020/9258396

11. Tufail M, Cui J, Wu C. Breast cancer: molecular mechanisms of underlying resistance and therapeutic approaches. *Am J Cancer Res* (2022) 12(7):2920–49. doi: 2156-6976/ajcr0143265

12. Shen L, Shi Q, Wang W. Double agents: genes with both oncogenic and tumor-suppressor functions. *Oncogenesis* (2018) 7(3):1–14. doi: 10.1038/s41389-018-0034-x

13. Kontomanolis EN, Koutras A, Syllaios A, Schizas D, Mastoraki A, Garmpis N, et al. Role of oncogenes and tumor-suppressor genes in carcinogenesis: a review. *Anticancer Res* (2020) 40(11):6009–15. doi: 10.21873/anticanres.14622

14. Chen L, Liu S, Tao Y. Regulating tumor suppressor genes: post-translational modifications. *Signal Transduct Target Ther* (2020) 5(1):1–25. doi: 10.1038/s41392-020-0196-9

15. Datta N, Chakraborty S, Basu M, Ghosh MK. Tumor suppressors having oncogenic functions: the double agents. *Cells* (2021) 10(1):1–26. doi: 10.3390/cells10010046

16. Nik-Zainal S, Davies H, Staaf J, Ramakrishna M, Glodzik D, Zou X, et al. Landscape of somatic mutations in 560 breast cancer whole-genome sequences. *Nature* (2016) 534(7605):47–54. doi: 10.1038/nature17676

17. Angus L, Smid M, Wilting SM, van Riet J, Van Hoeck A, Nguyen L, et al. The genomic landscape of metastatic breast cancer highlights changes in mutation and signature frequencies. *Nat Genet* (2019) 51(10):1450–8. doi: 10.1038/s41588-019-0507-7

18. Condorelli R, Mosele F, Verret B, Bachelot T, Bedard PL, Cortes J, et al. Genomic alterations in breast cancer: level of evidence for actionability according to ESMO scale for clinical actionability of molecular targets (ESCAT). *Ann Oncol* (2019) 30(3):365–73. doi: 10.1093/annonc/mdz036

19. Zhou S, Liu S, Zhao L, Sun HX. A comprehensive survey of genomic mutations in breast cancer reveals recurrent neoantigens as potential therapeutic targets. *Front Oncol* (2022) 12:786438(March). doi: 10.3389/fonc.2022.786438

20. Nagarsheth N, Wicha MS, Zou W. Chemokines in the cancer microenvironment and their relevance in cancer immunotherapy. *Nat Rev Immunol* (2017) 17:1–14. doi: 10.1038/nri.2017.49

21. Binnewies M, Roberts EW, Kersten K, Chan V, Fearon DF, Merad M, et al. Understanding the tumor immune microenvironment (TIME) for effective therapy. *Nat Med* (2018) 24(5):541–50. doi: 10.1038/s41591-018-0014-x

22. Wang H, Pan J, Barsky L, Jacob JC, Zheng Y, Gao C, et al. Characteristics of pre-metastatic niche: the landscape of molecular and cellular pathways. *Mol BioMed* (2021) 2(1):1–32. doi: 10.1186/s43556-020-00022-z

23. Pitt JM, Vétizou M, Daillère R, Roberti MP, Yamazaki T, Routy B, et al. Resistance mechanisms to immune-checkpoint blockade in cancer: tumor-intrinsic and -extrinsic factors. *Immunity* (2016) 44(6):1255–69. doi: 10.1016/j.immuni.2016.06.001

24. Bruni D, Angell HK, Galon J. The immune contexture and immunoscore in cancer prognosis and therapeutic efficacy. *Nat Rev Cancer* (2020) 20(11):662–80. doi: 10.1038/s41568-020-0285-7

25. Chen DS, Mellman I. Oncology meets immunology: the cancer-immunity cycle. *Nature* (2013) step 3):1–10. doi: 10.1016/j.immuni.2013.07.012

26. Chen DS, Mellman I. Elements of cancer immunity and the cancer-immune set point. *Nature* (2017) 541(7637):321–30. doi: 10.1038/nature21349

27. Savas P, Salgado R, Denkert C, Sotiriou C, Darcy PK, Smyth MJ, et al. Clinical relevance of host immunity in breast cancer: from TILs to the clinic. *Nat Rev Clin Oncol* (2016) 13(4):228–41. doi: 10.1038/nrclinonc.2015.215

28. Bense RD, Sotiriou C, Piccart-gebhart MJ, Haanen JBAG, Vugt MATM, Van, Vries EGE, et al. Relevance of tumor-infiltrating immune cell composition and functionality for disease outcome in breast cancer. *J Natl Cancer Inst* (2017) 109:1–9. doi: 10.1093/jnci/djw192.

29. Glajcar A, Szpor J, Hodorowicz-zaniewska D, Tyrak KE, Oko K. The composition of T cell infiltrates varies in primary invasive breast cancer of different molecular subtypes as well as according to tumor size and nodal status. *Virchows Arch* (2019) 475:13–23. doi: 10.1007/s00428-019-02568-y

30. Degnim AC, Hoskin TL, Arshad M, Frost MH, Winham SJ, Brahmbhatt RA, et al. Alterations in the immune cell composition in premalignant breast tissue that precede breast cancer development. *Clin Cancer Res* (2017) 23(14):3945–52. doi: 10.1158/1078-0432.CCR-16-2026

31. Graeser M, Feuerhake F, Gluz O, Volk V, Hauptmann M, Jozwiak K, et al. Immune cell composition and functional marker dynamics from multiplexed immunohistochemistry to predict response to neoadjuvant chemotherapy in the WSG-ADAPT-TN trial. *J Immunother Cancer* (2021) 9(5):1–11. doi: 10.1136/jitc-2020-002198

32. Hanamura T, Kitano S, Kagamu H, Yamashita M, Terao M, Tsuda B, et al. Immunological profiles of the breast cancer microenvironment represented by tumor-infiltrating lymphocytes and PD-L1 expression. *Sci Rep* (2022) 12(1):1–10. doi: 10.1038/s41598-022-11578-x

33. Coppola L, Smaldone G, D'aiuto M, D'aiuto G, Mossetti G, Rinaldo M, et al. Identification of immune cell components in breast tissues by a multiparametric flow cytometry approach. *Cancers (Basel)* (2022) 14(16):1–17. doi: 10.3390/cancers14163869

34. Zhang SC, Hu ZQ, Long JH, Zhu GM, Wang Y, Jia Y, et al. Clinical implications of tumor-infiltrating immune cells in breast cancer. *J Cancer* (2019) 10(24):6175–84. doi: 10.7150/jca.35901

35. Salemme V, Centonze G, Cavallo F, Defilippi P, Conti L. The crosstalk between tumor cells and the immune microenvironment in breast cancer: implications for immunotherapy. *Front Oncol* (2021) 11:610303(March). doi: 10.3389/fonc.2021.610303

36. Zhu JJ, Fu HJ, Wu YG, Zheng XF. Function of lncRNAs and approaches to lncRNA-protein interactions. *Sci China Life Sci* (2013) 56(10):876–85. doi: 10.1007/s11427-013-4553-6

37. Chen LL. Linking long noncoding RNA localization and function. *Trends Biochem Sci* (2016) 41(9):761–72. doi: 10.1016/j.tibs.2016.07.003

38. Qiu MT, Hu JW, Yin R, Xu L. Long noncoding RNA: an emerging paradigm of cancer research. *Tumor Biol* (2013) 34(2):613–20. doi: 10.1007/s13277-013-0658-6

39. Bhan A, Soleimani M, Mandal SS. Long noncoding RNA and cancer: a new paradigm. *Cancer Res* (2017) 77(15):1–18. doi: 10.1158/0008-5472.CAN-16-2634

40. Bolha L, Ravnik-Glavač M, Glavač D. Long noncoding RNAs as biomarkers in cancer. *Dis Markers* (2017) 2017:1–14. doi: 10.1155/2017/7243968

41. Schmitt AM, Chang HY. Long noncoding RNAs: At the intersection of cancer and chromatin biology. *Cold Spring Harb Perspect Med* (2017), 1-16. doi: 10.1101/cshperspect.a026492

42. Zhao S, Zhang X, Chen S, Zhang S. Long noncoding RNAs: fine-tuners hidden in the cancer signaling network. *Cell Death Discovery* (2021) 7(1):1–10. doi: 10.1038/s41420-021-00678-8

43. Arun G, Diermeier SD, Spector DL. Therapeutic targeting of long non-coding RNAs in cancer. *Trends Mol Med* (2018) 24(3):257–77. doi: 10.1016/j.molmed.2018.01.001

44. Jin H, Du W, Huang W, Yan J, Tang Q, Chen Y, et al. lncRNA and breast cancer: progress from identifying mechanisms to challenges and opportunities of clinical treatment. *Mol Ther - Nucleic Acids* (2021) 25(September):613–37. doi: 10.1016/j.omtn.2021.08.005

45. Denaro N, Merlano MC, Lo Nigro C. Long noncoding RNAs as regulators of cancer immunity. *Mol Oncol* (2019) 13(1):61–73. doi: 10.1002/1878-0261.12413

46. Luo Y, Yang J, Yu J, Liu X, Yu C, Hu J, et al. Long non-coding RNAs: emerging roles in the immunosuppressive tumor microenvironment. *Front Oncol* (2020) 10:48 (January). doi: 10.3389/fonc.2020.00048

47. Wu M, Fu P, Qu L, Liu J, Lin A. Long noncoding RNAs, new critical regulators in cancer immunity. *Front Oncol* (2020) 10:550987(October). doi: 10.3389/fonc.2020.550987

48. Zhang L, Xu X, Su X. Noncoding RNAs in cancer immunity: functions, regulatory mechanisms, and clinical application. *Mol Cancer* (2020) 19(1):1–12. doi: 10.1186/s12943-020-01154-0

49. Kim SK, Cho SW. The evasion mechanisms of cancer immunity and drug intervention in the tumor microenvironment. *Front Pharmacol* (2022) 13:868695 (May). doi: 10.3389/fphar.2022.868695

50. Spranger S, Gajewski TF. Mechanisms of tumor cell-intrinsic immune evasion. *Annu Rev Cancer Biol* (2018) 2:213–28. doi: 10.1146/annurev-cancerbio-030617-050606

51. Van Verschuer VMT, Hooning MJ, Van Baare-Georgieva RD, Hollestelle A, Timmermans AM, Koppert LB, et al. Tumor-associated inflammation as a potential prognostic tool in BRCA1/2-associated breast cancer. *Hum Pathol* (2015) 46(2):182–90. doi: 10.1016/j.humpath.2014.10.020

52. Kraya AA, Maxwell KN, Wubbenhorst B, Wenz BM, Pluta J, Rech AJ, et al. Genomic signatures predict the immunogenicity of BRCA-deficient breast cancer. *Clin Cancer Res* (2019) 25(14):4363–74. doi: 10.1158/1078-0432.CCR-18-0468

53. Wen WX, Leong CO. Association of BRCA1- and BRCA2-deficiency with mutation burden, expression of PD-L1/ PD-1, immune infiltrates, and T cell-inflamed signature in breast cancer. *PloS One* (2019) 14(4):1–16. doi: 10.1371/journal.pone.0215381

54. Solinas C, Marcoux D, Garaud S, Vitória JR, Van den Eynden G, de Wind A, et al. BRCA gene mutations do not shape the extent and organization of tumor infiltrating lymphocytes in triple negative breast cancer. *Cancer Lett* (2019) 450 (December 2018):88–97. doi: 10.1016/j.canlet.2019.02.027

55. Tung N, Garber JE, Hacker MR, Torous V, Freeman GJ, Poles E, et al. Prevalence and predictors of androgen receptor and programmed death-ligand 1 in BRCA1-associated and sporadic triple-negative breast cancer. *NPJ Breast Cancer* (2016) 2(1):1–7. doi: 10.1038/npjbcancer.2016.2

56. Qi F, Qin WX, Zang YS. Molecular mechanism of triple-negative breast cancer-associated BRCA1 and the identification of signaling pathways. *Oncol Lett* (2019) 17 (3):2905–14. doi: 10.3892/ol.2019.9884

57. Behring M, Vazquez AI, Cui X, Irvin MR, Ojesina AI, Agarwal S, et al. Gain of function in somatic TP53 mutations is associated with immune-rich breast tumors and changes in tumor-associated macrophages. *Mol Genet Genomic Med* (2019) 7(12):1–9. doi: 10.1002/mgg3.1001

58. Li L, Li M, Wang X. Cancer type-dependent correlations between TP53 mutations and antitumor immunity. *DNA Repair (Amst)* (2020) 88(January):1–9. doi: 10.1016/j.dnarep.2020.102785

59. Liu Z, Jiang Z, Gao Y, Wang L, Chen C, Wang X. TP53 mutations promote immunogenic activity in breast cancer. *J Oncol* (2019) 2019:1–19. doi: 10.1155/2019/5952836

60. Salama EA, Adbeltawab RE, El Tayebi HM. XIST and TSIX: novel cancer immune biomarkers in PD-L1-Overexpressing breast cancer patients. *Front Oncol* (2020) 9:1459(January). doi: 10.3389/fonc.2019.01459

61. Zhao Y, Yu Z, Ma R, Zhang Y, Zhao L, Yan Y, et al. lncRNA-Xist/miR-101-3p/KLF6/C/EBPα axis promotes TAM polarization to regulate cancer cell proliferation and migration. *Mol Ther Nucleic Acids* (2021) 23:536–51. doi: 10.1016/j.omtn.2020.12.005

62. Xing F, Liu Y, Wu SY, Wu K, Sharma S, Mo YY, et al. Loss of XIST in breast cancer activates MSN-c-Met and reprograms microglia *via* exosomal miRNA to promote brain metastasis. *Cancer Res* (2018) 78(15):4316–30. doi: 10.1158/0008-5472.CAN-18-1102

63. Hamed MM, Handoussa H, Hussein NH, Eissa RA, Abdel-Aal LK, El Tayebi HM. Oleuropin controls miR-194/XIST/PD-L1 loop in triple negative breast cancer: new role of nutri-epigenetics in immune-oncology. *Life Sci* (2021) 277:1–12. doi: 10.1016/j.lfs.2021.119353

64. Fan Y, Dong X, Li M, Liu P, Zheng J, Li H. LncRNA KRT19P3 is involved in breast cancer cell proliferation, migration and invasion. *Front Oncol* (2022) 11:799082 (January). doi: 10.3389/fonc.2021.799082

65. Beltrán-Anaya FO, Romero-Córdoba S, Rebollar-Vega R, Arrieta O, Bautista-Piña V, Dominguez-Reyes C, et al. Expression of long non-coding RNA ENSG00000226738 (LncKLHDC7B) is enriched in the immunomodulatory triple-negative breast cancer subtype and its alteration promotes cell migration, invasion, and resistance to cell death. *Mol Oncol* (2019) 13(4):909–27. doi: 10.1002/1878-0261.12446

66. Zhang Y, Dong X, Wang Y, Wang L, Han G, Jin L, et al. Overexpression of LncRNA BM466146 predicts better prognosis of breast cancer. *Front Oncol* (2021) 10:628757(January). doi: 10.3389/fonc.2020.628757

67. Wang Y, Zhao Y, Guo W, Yadav GS, Bhaskarla C, Wang Z, et al. Genome-wide gain-of-function screening characterized lncRNA regulators for tumor immune response. *Sci Adv* (2022) 8(49):1–17. doi: 10.1126/sciadv.add0005

68. Samir A, Tawab RA, Eltayebi HM. Long non-coding RNAs XIST and MALAT1 hijack the PD-L1 regulatory signaling pathway in breast cancer subtypes. *Oncol Lett* (2021) 22(593):1–12. doi: 10.3892/ol.2021.12854

69. Mekky RY, Ragab MF, Manie T, Attia AA, Youness RA. MALAT-1: immunomodulatory lncRNA hampering the innate and the adaptive immune arms in triple negative breast cancer. *Transl Oncol* (2023) 31(March):1–9. doi: 10.1016/j.tranon.2023.101653

70. Wang Q, Li G, Ma X, Liu L, Liu J, Yin Y, et al. LncRNA TINCR impairs the efficacy of immunotherapy against breast cancer by recruiting DNMT1 and downregulating MiR-199a-5p *via* the STAT1–TINCR-USP20-PD-L1 axis. *Cell Death Dis* (2023) 14(2):1–12. doi: 10.1038/s41419-023-05609-2

71. Xiping Z, Bo C, Shifeng Y, Feijiang Y, Hongjian Y, Qihui C, et al. Roles of MALAT1 in development and migration of triple negative and her-2 positive breast cancer. *Oncotarget* (2018) 9(2):2255–67. doi: 10.18632/oncotarget.23370

72. Abdel–Latif M, Riad A, Soliman RA, Elkhouly AM, Nafae H, Gad MZ, et al. MALAT–1/p53/miR–155/miR–146a ceRNA circuit tuned by methoxylated quercitin glycoside alters immunogenic and oncogenic profiles of breast cancer. *Mol Cell Biochem* (2022) 477):1281–93. doi: 10.1007/s11010-022-04378-4

73. Zhang M, Wang N, Song P, Fu Y, Ren Y, Li Z, et al. LncRNA GATA3-AS1 facilitates tumour progression and immune escape in triple-negative breast cancer through destabilization of GATA3 but stabilization of PD-L1. *Cell Prolif* (2020) 53 (9):1–13. doi: 10.1111/cpr.12855

74. Nafea H, Youness RA, Abou-Aisha K, Gad MZ. LncRNA HEIH/miR-939-5p interplay modulates triple-negative breast cancer progression through NOS2-induced nitric oxide production. *J Cell Physiol* (2021) 236:5362–72. doi: 10.1002/jcp.30234

75. Hu Q, Ye Y, Chan LC, Li Y, Liang K, Lin A, et al. Oncogenic lncRNA downregulates cancer cell antigen presentation and intrinsic tumor suppression. *Nat Immunol* (2019) 20(7):835–51. doi: 10.1038/s41590-019-0400-7

76. Zhang Q, Xiu B, Zhang L, Chen M, Chi W, Li L, et al. Immunosuppressive lncRNA LINC00624 promotes tumor progression and therapy resistance through ADAR1 stabilization. *J Immunother Cancer* (2022) 10(10):1–15. doi: 10.1136/jitc-2022-004666

77. Ye T, Feng J, Cui M, Yang J, Wan X, Xie D, et al. lncRNA MIAT services as a noninvasive biomarker for diagnosis and correlated with immune infiltrates in breast cancer. *Int J Womens Health* (2021) 13:991–1004. doi: 10.2147/IJWH.S312714

78. Xu S, Wang Q, Kang Y, Liu J, Yin Y, Liu L, et al. Long noncoding RNAs control the modulation of immune checkpoint molecules in cancer. *Cancer Immunol Res* (2020) 8(7):937–51. doi: 10.1158/2326-6066.CIR-19-0696

79. Wu J, Li M, Zhang Y, Cai Y, Zhao G. Molecular mechanism of activated T cells in breast cancer. *Onco Targets Ther* (2018) 11:5015–24. doi: 10.2147/OTT.S173018

80. Wang Y, Zhu M, Guo F, Song Y, Fan X, Qin G. Identification of tumor microenvironment-related prognostic biomarkers in luminal breast cancer. *Front Genet* (2020) 11. doi: 10.3389/fgene.2020.555865

81. Liu S, Song A, Zhou X, Huo Z, Yao S, Yang B, et al. ceRNA network development and tumour-infiltrating immune cell analysis of metastatic breast cancer to bone. *J Bone Oncol* (2020) 24:1–16. doi: 10.1016/j.jbo.2020.100304

82. Peng Z, Su P, Yang Y, Yao X, Zhang Y, Jin F, et al. Identification of CTLA-4 associated with tumor microenvironment and competing interactions in triple negative breast cancer by co-expression network analysis. *J Cancer* (2020) 11:6365–75. doi: 10.7150/jca.46301

83. Wang Z, Yang X, Shen J, Xu J, Pan M, Liu J, et al. Gene expression patterns associated with tumor-infiltrating CD4+ and CD8+ T cells in invasive breast carcinomas. *Hum Immunol* (2021) 82:279–87. doi: 10.1016/j.humimm.2021.02.001

84. Thomas PB, Seim I, Jeffery PL, Gahete MD, Maugham M, Crisp GJ, et al. The long non-coding RNA GHSROS facilitates breast cancer cell migration and orthotopic xenograft tumour growth. *Int J Oncol* (2019) 55:1223–36. doi: 10.3892/ijo.2019.4891

85. Bo H, Zhang W, Zhong X, Chen J, Liu Y, Cheong K, et al. LINC00467, driven by copy number amplification and DNA demethylation, is associated with oxidative lipid metabolism and immune infiltration in breast cancer. *Oxid Med Cell Longev* (2021) 2021:1–27. doi: 10.1155/2021/4586319

86. Chen J, Wei Y, Yang W, Huang Q, Chen Y, Zeng K, et al. IL-6: the link between inflammation, immunity and breast cancer. *Front Oncol* (2022) 12:903800. doi: 10.3389/fonc.2022.903800

87. Kumari N, Dwarakanath BS, Das A, Bhatt AN. Role of interleukin-6 in cancer progression and therapeutic resistance. *Tumor Biol* (2016) 37(9):11553–72. doi: 10.1007/s13277-016-5098-7

88. Rašková M, Lacina L, Kejík Z, Venhauerová A, Skaličková M, Kolář M, et al. The role of IL-6 in cancer cell invasiveness and metastasis–overview and therapeutic opportunities. *Cells* (2022) 11(22):1–23. doi: 10.3390/cells11223698

89. Fisher DT, Appenheimer MM, Evans SS. The two faces of IL-6 in the tumor microenvironment. *Semin Immunol* (2014) 26(1):38–47. doi: 10.1016/j.smim.2014.01.008

90. Xing Z, Lin A, Li C, Liang K, Wang S, Liu Y, et al. LncRNA directs cooperative epigenetic regulation downstream of chemokine signals. *Cell* (2014) 159:1110–25. doi: 10.1016/j.cell.2014.10.013

91. DeVaux RS, Ropri AS, Grimm SL, Hall PA, Herrera EO, Chittur SV, et al. Long noncoding RNA BHLHE40-AS1 promotes early breast cancer progression through modulating IL-6/STAT3 signaling. *J Cell Biochem* (2020) 121(7):3465–78. doi: 10.1002/jcb.29621

92. Nyati KK, Hashimoto S, Singh SK, Tekguc M, Metwally H, Liu YC, et al. The novel long noncoding RNA AU021063, induced by IL-6/Arid5a signaling, exacerbates breast cancer invasion and metastasis by stabilizing Trib3 and activating the Mek/Erk pathway. *Cancer Lett* (2021) 520:295–306. doi: 10.1016/j.canlet.2021.08.004

93. McLane LM, Abdel-Hakeem MS, Wherry EJ. CD8 T cell exhaustion during chronic viral infection and cancer. *Annu Rev Immunol* (2019) 37:457–95. doi: 10.1146/annurev-immunol-041015-055318

94. Prado-Garcia H, Romero-Garcia S. The role of exhaustion in tumor-induced T-cell dysfunction in cancer. *Cancer Immunol A Transl Med Context Second Ed* (2020), 117–32. doi: 10.1007/978-3-030-30845-2_8

95. Hussen BM, Azimi T, Hidayat HJ, Taheri M, Ghafouri-Fard S. NF-KappaB interacting LncRNA: review of its roles in neoplastic and non-neoplastic conditions. *BioMed Pharmacother* (2021) 139:1–8. doi: 10.1016/j.biopha.2021.111604

96. Huang D, Chen J, Yang L, Ouyang Q, Li J, Lao L, et al. NKILA lncRNA promotes tumor immune evasion by sensitizing T cells to activation-induced cell death. *Nat Immunol* (2018) 19(10):1112–25. doi: 10.1038/s41590-018-0207-y

97. Liu B, Sun L, Liu Q, Gong C, Yao Y, Lv X, et al. A cytoplasmic NF-κB interacting long noncoding RNA blocks IκB phosphorylation and suppresses breast cancer metastasis. *Cancer Cell* (2015) 27(3):370–81. doi: 10.1016/j.ccell.2015.02.004

98. Wu W, Chen F, Cui X, Yang L, Chen J, Zhao J, et al. LncRNA NKILA suppresses TGF-β-induced epithelial–mesenchymal transition by blocking NF-κB signaling in breast cancer. *Int J Cancer* (2018) 143:2213–24. doi: 10.1002/ijc.31605

99. Yu Y, Zhang W, Li A, Chen Y, Ou Q, He Z, et al. Association of long noncoding RNA biomarkers with clinical immune subtype and prediction of immunotherapy response in patients with cancer. *JAMA Netw Open* (2020) 3(4):1–12. doi: 10.1001/jamanetworkopen.2020.2149

100. Sakaguchi S, Mikami N, Wing JB, Tanaka A, Ichiyama K, Ohkura N. Regulatory T cells and human disease. *Annu Rev Immunol* (2020) 38:541–66. doi: 10.1146/annurev-immunol-042718-041717

101. Speiser DE, Ho PC, Verdeil G. Regulatory circuits of T cell function in cancer. *Nat Rev Immunol* (2016) 16(10):599–611. doi: 10.1038/nri.2016.80

102. Moallemi-Rad L, Ghorbani A, Dadyar M, Hussen BM, Rasul MF, Eslami S, et al. Expression of treg-associated lncRNAs in breast cancer. *Pathol Res Pract* (2022) 241:1–7. doi: 10.1016/j.prp.2022.154270

103. Zimta AA, Tigu AB, Braicu C, Stefan C, Ionescu C, Berindan-Neagoe I. An emerging class of long non-coding RNA with oncogenic role arises from the snoRNA host genes. *Front Oncol* (2020) 10:389(April). doi: 10.3389/fonc.2020.00389

104. Pei X, Wang X, Li H. LncRNA SNHG1 regulates the differentiation of treg cells and affects the immune escape of breast cancer *via* regulating miR-448/IDO. *Int J Biol Macromol* (2018) 118:24–30. doi: 10.1016/j.ijbiomac.2018.06.033

105. Ni C, Fang QQ, Chen WZ, Jiang JX, Jiang Z, Ye J, et al. Breast cancer-derived exosomes transmit lncRNA SNHG16 to induce CD73+γδ1 treg cells. *Signal Transduct Target Ther* (2020) 5(1):1–14. doi: 10.1038/s41392-020-0129-7

106. Mantovani A, Marchesi F, Malesci A, Laghi L, Allavena P. Tumour-associated macrophages as treatment targets in oncology. *Nat Rev Clin Oncol* (2017) 14(7):399–416. doi: 10.1038/nrclinonc.2016.217

107. Zhou L, Tian Y, Guo F, Yu B, Li J, Xu H, et al. LincRNA-p21 knockdown reversed tumor-associated macrophages function by promoting MDM2 to antagonize* p53 activation and alleviate breast cancer development. *Cancer Immunol Immunother* (2020) 69(5):835–46. doi: 10.1007/s00262-020-02511-0

108. Chen F, Chen J, Yang L, Liu J, Zhang X, Zhang Y, et al. Extracellular vesicle-packaged HIF-1α-stabilizing lncRNA from tumour-associated macrophages regulates aerobic glycolysis of breast cancer cells. *Nat Cell Biol* (2019) 21(4):498–510. doi: 10.1038/s41556-019-0299-0

109. Amer HT, Eissa RA, El Tayebi HM. A cutting-edge immunomodulatory interlinkage between HOTAIR and MALAT1 in tumor-associated macrophages in breast cancer: a personalized immunotherapeutic approach. *Front Mol Biosci* (2022) 9:1032517. doi: 10.3389/fmolb.2022.1032517

110. Liu XS, Mardis ER. Applications of immunogenomics to cancer. *Cell* (2017) 168(4):600–12. doi: 10.1016/j.cell.2017.01.014

111. Finotello F, Rieder D, Hackl H, Trajanoski Z. Next-generation computational tools for interrogating cancer immunity. *Nat Rev Genet* (2019) 20(12):724–46. doi: 10.1038/s41576-019-0166-7

112. Mardis ER. The impact of next-generation sequencing on cancer genomics: from discovery to clinic. *Cold Spring Harb Perspect Biol* (2019) 11(9):1–14. doi: 10.1101/cshperspect.a036269

113. Hammerbacher J, Snyder A. Informatics for cancer immunotherapy. *Ann Oncol* (2017) 28(January):xii56–73. doi: 10.1093/annonc/mdx682

114. Finotello F, Trajanoski Z. Quantifying tumor-infiltrating immune cells from transcriptomics data. *Cancer Immunol Immunother* (2018) 67:1–10. doi: 10.1007/s00262-018-2150-z

115. Turajlic S, Litchfield K, Xu H, Rosenthal R, McGranahan N, Reading JL, et al. Insertion-and-deletion-derived tumour-specific neoantigens and the immunogenic phenotype: a pan-cancer analysis. *Lancet Oncol* (2017) 18(8):1009–21. doi: 10.1016/j.cell.2017.01.014

116. Hashimoto S, Noguchi E, Bando H, Miyadera H, Morii W, Nakamura T, et al. Neoantigen prediction in human breast cancer using RNA sequencing data. *Cancer Sci* (2021) 112(1):465–75. doi: 10.1111/cas.14720

117. Marty R, Kaabinejadian S, Rossell D, Slifker MJ, van de Haar J, Engin HB, et al. MHC-I genotype restricts the oncogenic mutational landscape. *Cell* (2017) 171(6):1–28. doi: 10.1016/j.cell.2017.09.050

118. Schaafsma E, Fugle CM, Wang X, Cheng C. Pan-cancer association of HLA gene expression with cancer prognosis and immunotherapy efficacy. *Br J Cancer* (2021) 125(3):422–32. doi: 10.1038/s41416-021-01400-2

119. Charoentong P, Angelova M, Finotello F, Mayer C, Efremova M, Rieder D, et al. Pan-cancer immunogenomic analyses reveal genotype-immunophenotype relationships and predictors of response to checkpoint blockade. *Cell Rep* (2017) 18(1):248–62. doi: 10.1016/j.celrep.2016.12.019

120. Thorsson V, Gibbs DL, Brown SD, Wolf D, Bortone DS, Ou Yang TH, et al. The immune landscape of cancer. *Immunity* (2018) 48(4):812–830.e14. doi: 10.1016/j.immuni.2018.03.023

121. Rooney MS, Shukla SA, Wu CJ, Getz G, Hacohen N. Molecular and genetic properties of tumors associated with local immune cytolytic activity. *Cell* (2015) 160(1–2):48–61. doi: 10.1016/j.cell.2014.12.033

122. Li B, Li T, Pignon JC, Wang B, Wang J, Shukla SA, et al. Landscape of tumor-infiltrating T cell repertoire of human cancers. *Nat Genet* (2016) 48(7):725–32. doi: 10.1038/ng.3581

123. Zhang Y, Zhang Z. The history and advances in cancer immunotherapy: understanding the characteristics of tumor-infiltrating immune cells and their therapeutic implications. *Cell Mol Immunol* (2020) 17(8):807–21. doi: 10.1038/s41423-020-0488-6

124. Li Y, Jiang T, Zhou W, Li J, Li X, Wang Q, et al. Pan-cancer characterization of immune-related lncRNAs identifies potential oncogenic biomarkers. *Nat Commun* (2020) 11(1):1–13. doi: 10.1038/s41467-020-14802-2

125. Zhang Z, Yan C, Li K, Bao S, Li L, Chen L, et al. Pan-cancer characterization of lncRNA modifiers of immune microenvironment reveals clinically distinct *de novo* tumor subtypes. *NPJ Genomic Med* (2021) 6(1):1–11. doi: 10.1038/s41525-021-00215-7

126. Zhang Z, Zhang H, Li D, Zhou X, Wang J, Zhang Q. LncRNA ST7-AS1 is a potential novel biomarker and correlated with immune infiltrates for breast cancer. *Front Mol Biosci* (2021) 8:604261(April). doi: 10.3389/fmolb.2021.604261

127. Yi W, Shen H, Sun D, Xu Y, Feng Y, Li D, et al. Low expression of long noncoding RNA SLC26A4 antisense RNA 1 is an independent prognostic biomarker and correlate of immune infiltrates in breast cancer. *Med Sci Monit* (2021) 27:1–14. doi: 10.12659/MSM.934522

128. Zhao D, Dong JT. Upregulation of long non-coding RNA DRAIC correlates with adverse features of breast cancer. *Non-coding RNA* (2018) 4(39):1–9. doi: 10.3390/ncrna4040039

129. Zhang Y, Li Z, Chen M, Chen H, Zhong Q, Liang L, et al. lncRNA TCL6 correlates with immune cell infiltration and indicates worse survival in breast cancer. *Breast Cancer* (2020) 27(4):573–85. doi: 10.1007/s12282-020-01048-5

130. Fonseca-Montaño MA, Cisneros-Villanueva M, Coales I, Hidalgo-Miranda A. LINC00426 is a potential immune phenotype-related biomarker and an overall survival predictor in PAM50 luminal b breast cancer. *Front Genet* (2023) 2:1034569(May). doi: 10.3389/fgene.2023.1034569

131. Liu Z, Mi M, Li X, Zheng X, Wu G, Zhang L. lncRNA OSTN-AS1 may represent a novel immune-related prognostic marker for triple-negative breast cancer based on integrated analysis of a ceRNA network. *Front Genet* (2019) 10:850. doi: 10.3389/fgene.2019.00850

132. de Santiago PR, Blanco A, Morales F, Marcelain K, Harismendy O, Sjöberg Herrera M, et al. Immune-related lncRNA LINC00944 responds to variations in ADAR1 levels and it is associated with breast cancer prognosis. *Life Sci* (2021) 268:1–11. doi: 10.1016/j.lfs.2020.118956

133. Bradford JR, Cox A, Bernard P, Camp NJ. Consensus analysis of whole transcriptome profiles from two breast cancer patient cohorts reveals long non-coding RNAs associated with intrinsic subtype and the tumour microenvironment. *PloS One* (2016) 11(9):1–18. doi: 10.1371/journal.pone.0163238

134. Liu D. Identification of a prognostic LncRNA signature for ER-positive, ER-negative and triple-negative breast cancers. *Breast Cancer Res Treat* (2020) 183:95–105. doi: 10.1007/s10549-020-05770-8

135. Mathias C, Muzzi JCD, Antunes BB, Gradia DF, Castro MAA, Carvalho de Oliveira J. Unraveling immune-related lncRNAs in breast cancer molecular subtypes. *Front Oncol* (2021) 11:692170(May). doi: 10.3389/fonc.2021.692170

136. De Palma FDE, Del Monaco V, Pol JG, Kremer M, D'Argenio V, Stoll G, et al. The abundance of the long intergenic non-coding RNA 01087 differentiates between luminal and triple-negative breast cancers and predicts patient outcome. *Pharmacol Res* (2020) 161:1–17. doi: 10.1016/j.phrs.2020.105249

137. Ghafouri-Fard S, Asadi M, Sohrabi B, Arsang-Jang S, Mehravaran E, Taheri M, et al. Down-regulation of a panel of immune-related lncRNAs in breast cancer. *Pathol Res Pract* (2021) 224:1–9. doi: 10.1016/j.prp.2021.153534

138. Zhao H, Liu X, Yu L, Lin S, Zhang C, Xu H, et al. Comprehensive landscape of epigenetic-dysregulated lncRNAs reveals a profound role of enhancers in carcinogenesis in BC subtypes. *Mol Ther Nucleic Acids* (2021) 23:667–81. doi: 10.1016/j.omtn.2020.12.024

139. Sui Y, Ju C, Shao B. A lymph node metastasis-related protein-coding genes combining with long noncoding RNA signature for breast cancer survival prediction. *J Cell Physiol* (2019) 23:1–10. doi: 10.1002/jcp.28600

140. Li H, Liu H, Hao Q, Liu X, Yao Y, Cao M. Oncogenic signaling pathway-related long non-coding RNAs for predicting prognosis and immunotherapy response in breast cancer. *Front Immunol* (2022) 13:891175(August). doi: 10.3389/fimmu.2022.891175

141. Shen S, Chen X, Hu X, Huo J, Luo L, Zhou X. Predicting the immune landscape of invasive breast carcinoma based on the novel signature of immune-related lncRNA. *Cancer Med* (2021) 10:6561–75. doi: 10.1002/cam4.4189

142. Liu B, Zhu N, Huo H, Long J, Ji X, Li J, et al. A 5-pathway signature predicts prognosis based on immune-derived lncRNAs in patients with breast cancer. *J Oncol* (2022) 2022:1–17. doi: 10.1155/2022/2906049

143. Li S, Sun X, Li J, Zheng A, Cao Y, Guo Y, et al. A novel prognostic signature of immune-related long noncoding RNA pairs for tumor-infiltrating immune cells and drug susceptibility in breast cancer. *DNA Cell Biol* (2022) 41(2):103–15. doi: 10.1089/dna.2021.0489

144. Liu Z, Mi M, Li X, Zheng X, Wu G, Zhang L. A lncRNA prognostic signature associated with immune infiltration and tumour mutation burden in breast cancer. *J Cell Mol Med* (2020) 24(21):1–13. doi: 10.1111/jcmm.15762

145. Xiao R, Yang M, Tan Y, Ding R, Li D. Identification of five immune-related lncRNAs predicting survival and tumor microenvironment characteristics in breast cancer. *Comput Math Methods Med* (2021) 2021:1–12. doi: 10.1155/2021/6676692

146. Li YX, Wang SM, Li CQ. Four-lncRNA immune prognostic signature for triple-negative breast cancer. *Math Biosci Eng* (2021) 18(4):3939–56. doi: 10.3934/mbe.2021197

147. Lai J, Chen B, Zhang G, Li X, Mok H, Liao N. Molecular characterization of breast cancer: a potential novel immune-related lncRNAs signature. *J Transl Med* (2020) 18(416):1–10. doi: 10.1186/s12967-020-02578-4

148. Li Q, Yang H, Wang P, Liu X, Lv K, Ye M. XGBoost-based and tumor-immune characterized gene signature for the prediction of metastatic status in breast cancer. *J Transl Med* (2022) 20(1):1–12. doi: 10.1186/s12967-022-03369-9

149. Li Z, Li Y, Wang X, Yang Q. Identification of a six-Immune-Related long non-coding RNA signature for predicting survival and immune infiltrating status in breast cancer. *Front Genet* (2020) 11:680(July). doi: 10.3389/fgene.2020.00680

150. Ma W, Zhao F, Yu X, Guan S, Suo H, Tao Z, et al. Immune-related lncRNAs as predictors of survival in breast cancer: a prognostic signature. *J Transl Med* (2020) 18(442):1–13. doi: 10.1186/s12967-020-02522-6

151. Jiang T, Wang Y, Chen X, Xia W, Xue S, Gu L, et al. Neutrophil extracellular traps (NETs)-related lncRNAs signature for predicting prognosis and the immune microenvironment in breast cancer. *Front Cell Dev Biol* (2023) 11:1117637(February). doi: 10.3389/fcell.2023.1117637

152. Shen Y, Peng X, Shen C. Identification and validation of immune-related lncRNA prognostic signature for breast cancer. *Genomics* (2020) 112:2640–6. doi: 10.1016/j.ygeno.2020.02.015

153. Yang W, Qiu Z, Zhang J, Zhi X, Yang L, Qiu M, et al. Correlation between immune cell infiltration and PD-L1 expression and immune-related lncRNA determination in triple-negative breast cancer. *Front Genet* (2022) 13:878658 (March). doi: 10.3389/fgene.2022.878658

154. Zhu JY, Lyu AQ, Wang ZT, Chan WY, Qin T, Miu KK, et al. Machine learning-devised immune-related lncRNA signature panel predicts the prognosis and immune landscape in breast cancer novel IRLP signature in BRCA. *J Immunol Res* (2022) 2022:1–16. doi: 10.1155/2022/3704

155. Huang Z, Xiao C, Zhang F, Zhou Z, Yu L, Ye C, et al. A novel framework to predict breast cancer prognosis using immune-associated LncRNAs. *Front Genet* (2021) 11:634195. doi: 10.3389/fgene.2020.634195

156. Dang Q, Sun Z, Wang Y, Wang L, Liu Z, Han X. Ferroptosis: a double-edged sword mediating immune tolerance of cancer. *Cell Death Dis* (2022) 13(11):1–16. doi: 10.1038/s41419-022-05384-6

157. Shi L, Liu Y, Li M, Luo Z. Emerging roles of ferroptosis in the tumor immune landscape: from danger signals to anti-tumor immunity. *FEBS J* (2022) 289(13):3655–65. doi: 10.1111/febs.16034

158. Anusha A, Kumar S, Kaushik S, Jyoti A. Necroptosis in immuno-oncology and cancer immunotherapy. *J Pharm Sci Res* (2017) 9(5):662–6. doi: 10.1097/mou.0000000000000337

159. Liu W, Peng J, Xiao M, Cai Y, Peng B, Zhang W, et al. The implication of pyroptosis in cancer immunology: current advances and prospects. *Genes Dis* (2022), 1–12. doi: 10.1016/j.gendis.2022.04.019

160. Xia H, Green DR, Zou W. Autophagy in tumour immunity and therapy. *Nat Rev Cancer* (2021) 21(5):281–97. doi: 10.1038/s41568-021-00344-2

161. Chen M, Linstra R, van Vugt MATM. Genomic instability, inflammatory signaling and response to cancer immunotherapy. *Biochim Biophys Acta - Rev Cancer* (2022) 1877(1):1–15. doi: 10.1016/j.bbcan.2021.188661

162. Wang Y, Xu Y, Zhang Y. A novel ferroptosis-related long noncoding RNA signature for relapse free survival prediction in patients with breast cancer. *Med (United States)* (2022) 101(31):1–10. doi: 10.1097/MD.0000000000029573

163. Wei T, Zhu N, Jiang W, Xing XL. Development and validation of ferroptosis- and immune-related lncRNAs signatures for breast infiltrating duct and lobular carcinoma *Front oncol*. (2022) 12(April):1–11. doi: 10.3389/fonc.2022.844642

164. Zhang K, Ping L, Du T, Liang G, Huang Y, Li Z, et al. A ferroptosis-related lncRNAs signature predicts prognosis and immune microenvironment for breast cancer. *Front Mol Biosci* (2021) 8:678877(June). doi: 10.3389/fmolb.2021.678877

165. Shen S, Yang D, Yang Y, Chen Y, Xiong J, Hu X. A novel prognostic ferroptosis-related lncRNA signature associated with immune landscape in invasive breast cancer. *Dis Markers* (2022) 2022:1–25. doi: 10.1155/2022/9168556

166. Jia CL, Yang F, Li R. Prognostic model construction and immune microenvironment analysis of breast cancer based on ferroptosis-related lncRNAs. *Int J Gen Med* (2021) 14:9817–31. doi: 10.2147/IJGM.S342783

167. Zhang Y, Yue Q, Cao F, Li YQ, Wei Y. Necroptosis-related lncRNA signatures determine prognosis in breast cancer patients. *Sci Rep* (2022) 12(1):1–14. doi: 10.1038/s41598-022-15209-3

168. Chen F, Yang J, Fang M, Wu Y, Su D, Sheng Y. Necroptosis-related lncRNA to establish novel prognostic signature and predict the immunotherapy response in breast cancer. *J Clin Lab Anal* (2022) 36(4):1–11. doi: 10.1002/jcla.24302

169. Tao S, Tao K, Cai X. Necroptosis-associated lncRNA prognostic model and clustering analysis: prognosis prediction and tumor-infiltrating lymphocytes in breast cancer. *J Oncol* (2022) 2022:1–18. doi: 10.1155/2022/7099930

170. Wu Q, Li Q, Zhu W, Zhang X, Li H. Identification of autophagy-related long non-coding RNA prognostic signature for breast cancer. *J Cell Mol Med* (2021) 25:4088–98. doi: 10.1111/jcmm.16378

171. Luo Z, Nong B, Ma Y, Fang D. Autophagy related long non-coding RNA and breast cancer prognosis analysis and prognostic risk model establishment. *Ann Transl Med* (2022) 10(2):58–8. doi: 10.21037/atm-21-6251

172. Liu L, Chen C, Tu G, Peng Y, Shen M, Xu Y, et al. Pyroptosis-related lncRNAs for predicting the prognosis and identifying immune microenvironment infiltration in breast cancer lung metastasis. *Front Cell Dev Biol* (2022) 10:821727. doi: 10.3389/fcell.2022.821727

173. Yang X, Weng X, Yang Y, Jiang ZN. Pyroptosis-related lncRNAs predict the prognosis and immune response in patients with breast cancer. *Front Genet* (2022) 12:792106(March). doi: 10.3389/fgene.2021.792106

174. Lv Z, Wang Q, Liu X, Du Z, Liang W, Liu T, et al. Genetic instability-related lncRNAs predict prognosis and influence the immune microenvironment in breast cancer. *Front Genet* (2022) 13:926984(September). doi: 10.3389/fgene.2022.926984

175. Jiao Y, Li S, Wang X, Yi M, Wei H, Rong S, et al. A genomic instability-related lncRNA model for predicting prognosis and immune checkpoint inhibitor efficacy in breast cancer. *Front Immunol* (2022) 13:929846(August). doi: 10.3389/fimmu.2022.929846

176. Shi GJ, Zhou Q, Zhu Q, Wang L, Jiang GQ. A novel prognostic model associated with the overall survival in patients with breast cancer based on lipid metabolism-related long noncoding RNAs. *J Clin Lab Anal* (2022) 36(6):1–9. doi: 10.1002/jcla.24384

177. Gu P, Zhang L, Wang R, Ding W, Wang W, Liu Y, et al. Development and validation of a novel hypoxia-related long noncoding RNA model with regard to prognosis and immune features in breast cancer. *Front Cell Dev Biol* (2021) 9:796729 (December). doi: 10.3389/fcell.2021.796729

178. Jiang ZR, Yang LH, Jin LZ, Yi LM, Bing PP, Zhou J, et al. Identification of novel cuproptosis-related lncRNA signatures to predict the prognosis and immune microenvironment of breast cancer patients. *Front Oncol* (2022) 12:988680 (September). doi: 10.3389/fonc.2022.988680

179. Li J, Zhang Y, Li C, Wu H, Feng C, Wang W, et al. A lactate-related LncRNA model for predicting prognosis, immune landscape and therapeutic response in breast cancer. *Front Genet* (2022) 13:956246(October). doi: 10.3389/fgene.2022.956246

180. Liu Z, Ren C, Cai J, Yin B, Yuan J, Ding R, et al. A novel aging-related prognostic lncRNA signature correlated with immune cell infiltration and response to immunotherapy in breast cancer. *Molecules* (2023) 28(8):1–22. doi: 10.3390/molecules28083283

181. Wang Y, Gao S, Xu Y, Tang Z, Liu S. A mitochondrial function-related LncRNA signature predicts prognosis and immune microenvironment for breast cancer. *Sci Rep* (2023) 13(1):1–17. doi: 10.1038/s41598-023-30927-y

182. Gao S, Wang Y, Xu Y, Liu S. An angiogenesis-related lncRNA signature is associated with prognosis and tumor immune microenvironment in breast cancer. *J Pers Med* (2023) 13(3):1–23. doi: 10.3390/jpm13030513

183. Zhao J, Ma H, Feng R, Li D, Liu B, Yu Y, et al. A novel oxidative stress-related lncRNA signature that predicts the prognosis and tumor immune microenvironment of breast cancer. *J Oncol* (2022) 2022:1–22. doi: 10.1155/2022/9766954

184. Huang G, Cao H, Liu G, Chen J. Role of androgen receptor signaling pathway-related lncRNAs in the prognosis and immune infiltration of breast cancer. *Sci Rep* (2022) 12(1):1–17. doi: 10.1038/s41598-022-25231-0

185. Zou J, Gu Y, Zhu Q, Li X, Qin L. Identifying glycolysis-related LncRNAs for predicting prognosis in breast cancer patients. *Cancer Biomarkers* (2022) 34(3):393–401. doi: 10.3233/CBM-210446

186. Guo J, Yi X, Ji Z, Yao M, Yang Y, Song W, et al. Development of a prognostic model based on the identification of EMT-related lncRNAs in triple-negative breast cancer. *J Oncol* (2021) 2021:1–18. doi: 10.1155/2021/9219961

187. Qian D, Qian C, Ye B, Xu M, Wu D, Li J, et al. Development and validation of a novel stemness-Index-Related long noncoding RNA signature for breast cancer based on weighted gene Co-expression network analysis. *Front Genet* (2022) 13:760514 (February). doi: 10.3389/fgene.2022.760514

188. Xu S, Xie J, Zhou Y, Liu H, Wang Y, Li Z. Integrated analysis of RNA binding protein-related lncRNA prognostic signature for breast cancer patients. *Genes (Basel)* (2022) 13(2):1–18. doi: 10.3390/genes13020345

189. Cai J, Ji Z, Wu J, Chen L, Zheng D, Chen Y, et al. Development and validation of a novel endoplasmic reticulum stress-related lncRNA prognostic signature and candidate drugs in breast cancer. *Front Genet* (2022) 13:949314. doi: 10.3389/fgene.2022.949314

190. Zhang L, Zhang Y, Bao J, Gao W, Wang D, Pan H. Cuproptosis combined with lncRNAs predicts the prognosis and immune microenvironment of breast cancer. *Comput Math Methods Med* (2022) 2022:1–32. doi: 10.1155/2022/5422698

191. Chen BQ, Dragomir MP, Yang C, Li Q, Horst D, Calin GA. Targeting non-coding RNAs to overcome cancer therapy resistance. *Signal Transduct Target Ther* (2022) 7(1):1–20. doi: 10.1038/s41392-022-00975-3

192. Winkle M, El-Daly SM, Fabbri M, Calin GA. Noncoding RNA therapeutics-challenges and potential solutions. *Nat Rev Drug Discovery* (2021) 20(8):629–51. doi: 10.1038/s41573-021-00219-z

193. Jiang M-C, Ni J-J, Cui W-Y, Wei Z. Emerging roles of lncRNA in cancer and therapeutic opportunities. *Am J Cancer Res* (2019) 9(7):1354–66. doi: 2156-6976/ajcr0097340

194. Pandey GK, Kanduri C. Long non-coding RNAs: tools for understanding and targeting cancer pathways. *Cancers (Basel)* (2022) 14(19):1–18. doi: 10.3390/cancers14194760

frontiers | Frontiers in Immunology

TYPE Original Research
PUBLISHED 09 June 2023
DOI 10.3389/fimmu.2023.1202529

OPEN ACCESS

EDITED BY
Takaji Matsutani,
Repertoire Genesis, Inc., Japan

REVIEWED BY
Ashwin Somasundaram,
University of North Carolina at Chapel Hill, United States
Baohong Liu,
Chinese Academy of Agricultural Sciences, China

*CORRESPONDENCE
Huan Yu
huanhuanyu2006@163.com

†These authors have contributed equally to this work and share first authorship

RECEIVED 08 April 2023
ACCEPTED 30 May 2023
PUBLISHED 09 June 2023

CITATION
Li C, Yang T, Yuan Y, Wen R and Yu H (2023) Bioinformatic analysis of hub markers and immune cell infiltration characteristics of gastric cancer. *Front. Immunol.* 14:1202529. doi: 10.3389/fimmu.2023.1202529

Bioinformatic analysis of hub markers and immune cell infiltration characteristics of gastric cancer

Chao Li[1,2†], Tan Yang[1†], Yu Yuan[1], Rou Wen[2] and Huan Yu[2*]

[1]School of Pharmacy, Tianjin University of Traditional Chinese Medicine, Tianjin, China, [2]School of Pharmacy, Jiangxi University of Traditional Chinese Medicine, Nanchang, China

Background: Gastric cancer (GC) is the fifth most common cancer and the second leading cause of cancer-related deaths worldwide. Due to the lack of specific markers, the early diagnosis of gastric cancer is very low, and most patients with gastric cancer are diagnosed at advanced stages. The aim of this study was to identify key biomarkers of GC and to elucidate GC-associated immune cell infiltration and related pathways.

Methods: Gene microarray data associated with GC were downloaded from the Gene Expression Omnibus (GEO). Differentially expressed genes (DEGs) were analyzed using Gene Ontology (GO), Kyoto Gene and Genome Encyclopedia, Gene Set Enrichment Analysis (GSEA) and Protein–Protein Interaction (PPI) networks. Weighted gene coexpression network analysis (WGCNA) and the least absolute shrinkage and selection operator (LASSO) algorithm were used to identify pivotal genes for GC and to assess the diagnostic accuracy of GC hub markers using the subjects' working characteristic curves. In addition, the infiltration levels of 28 immune cells in GC and their interrelationship with hub markers were analyzed using ssGSEA. And further validated by RT-qPCR.

Results: A total of 133 DEGs were identified. The biological functions and signaling pathways closely associated with GC were inflammatory and immune processes. Nine expression modules were obtained by WGCNA, with the pink module having the highest correlation with GC; 13 crossover genes were obtained by combining DEGs. Subsequently, the LASSO algorithm and validation set verification analysis were used to finally identify three hub genes as potential biomarkers of GC. In the immune cell infiltration analysis, infiltration of activated CD4 T cell, macrophages, regulatory T cells and plasmacytoid dendritic cells was more significant in GC. The validation part demonstrated that three hub genes were expressed at lower levels in the gastric cancer cells.

Conclusion: The use of WGCNA combined with the LASSO algorithm to identify hub biomarkers closely related to GC can help to elucidate the molecular mechanism of GC development and is important for finding new immunotherapeutic targets and disease prevention.

KEYWORDS

gastric cancer (GC), hub markers, immune cell infiltration, WGCNA, LASSO

1 Introduction

GC is one of the most common malignancies in the human digestive tract. According to Global Cancer Statistics, GC has become the fifth most frequently diagnosed cancer and the third leading cause of cancer deaths, making it a major global health crisis (1). In China, the total number of new cases of GC in 2020 was 478,000, ranking 2nd in the number of incidences of malignant tumors and 373,000 deaths, ranking 3rd in the number of deaths from malignant tumors (2). The above figures are sufficient to show that GC is highly malignant, has a low survival rate and poor prognosis and is a serious threat to human health and life.

GC is a malignant disease caused by a combination of factors, such as *Helicobacter pylori* infection, unhealthy lifestyle, genetics and immune cell imbalance. The pathogenesis of GC is still not fully understood, but the activation of proto-oncogenes caused by the abovementioned oncogenic factors is an important molecular mechanism. The molecular mechanisms involved in the pathogenesis of the disease still need to be further elucidated. Clinical treatments for GC based on surgical resection, chemotherapy, radiotherapy or a combination of targeted therapies have difficulty completely removing the tumor lesions, and the tumor is prone to progression or recurrence with high toxic side effects, with a 5-year survival rate of patients as low as 10% to 15% (3–5). It is important to emphasize that GC is usually asymptomatic in the early stages, and some patients are already at an advanced stage when diagnosed, with a survival rate of only 24% (6). Therefore, it is important to develop effective biomarkers for the prognosis of gastric cancer and for targeted therapy.

The tumor microenvironment (TME), due to its key role in cancer progression and drug resistance, has emerged as a potential immunotherapeutic target for a variety of malignancies, including GC. The TME consists of different cell types, including immune and inflammatory cells (lymphocytes and macrophages), stromal cells (fibroblasts, adipocytes and pericytes), small cell organelles, RNA, blood vessels and lymphatic vessels, extracellular matrix (ECM) and secreted proteins. The cells involved in the GC immune microenvironment are called tumor infiltrating immune cells (TIICs) (7). Immunotherapy in the treatment of advanced GC improves survival and is associated with good survival in GC patients, according to the results of the CheckMate 649 case study presented at the European Society for Medical Oncology (ESMO) 2020 virtual meeting (8, 9). However, recent studies have found that abnormal activation of the immune system may also be a key factor in the development of GC (10). In short, tapping into immune cell-related targets is an effective pathway to optimize tumor immunotherapy.

Due to advances in genomic technology, bioinformatics analysis of gene expression profiles has become increasingly popular in molecular mechanistic studies and is playing an increasingly important role in the discovery of disease-specific biomarkers. Weighted gene coexpression network analysis was proposed by Zhang & Horvath in 2005 as a systematic algorithm widely used for bioinformatics data, avoiding the drawbacks of traditional differential gene screening methods, which tend to miss core molecules in the regulatory process and make it difficult to explore the whole biological system, and has been widely used to screen molecular diagnostic markers or therapeutic targets for complex diseases (11, 12). This provides a new way to predict the function of coexpressed genes and to find genes that play a key role in human disease. LASSO is a regression method that allows the calculation of correlation coefficients between variables and more accurate screening of variables (13). There have been a host of studies on screening GC biomarkers based on bioinformatics methods both domestically and internationally, but there are problems with a small sample size and a single data analysis method as well as lack of further experimental verification (14–16). Thus, this article comprehensively utilizes various bioinformatics methods to integrate and analyze gene datasets from multiple platforms, and expand sample size and validated by *in vitro* cellular experiments, for improving the scientific nature of bioinformatics analysis, and in order to more accurately explore the pathogenesis and therapeutic targets of GC, and provide molecular biology basis and new research ideas and directions for subsequent experimental research.

Based on the above, this study used the GSE54129 and GSE65801 datasets to construct a gene weighted coexpression network by the WGCNA algorithm to screen out pivotal modules that are highly relevant to the development of GC, analyze the biological functions of the pivotal modules and use the LASSO regression model to screen key genes and validate them with the GSE118916 dataset, and then further identify important prognostic molecular markers and assess the extent of associated immune cell infiltration, with a view to providing new references for studying the development of GC, potential molecular mechanisms and therapeutic targets. Flowchart of our study was shown Figure 1.

2 Materials and methods

2.1 Expression data and clinical data collection

The flow chart of the study is shown in Figure 1. Acquisition of gene microarray data: Three gastric cancer datasets (GSE54129, GSE65801, GSE118916) were selected from the GEO database of NCBI (https://www.ncbi.nlm.nih.gov/geo/) based on the following three conditions: the samples were from human gastric tissue specimens, a case control group was available, and the number of samples was ≥20 to ensure the representativeness of the datasets. The datasets GSE79973, GSE65801 and GSE118916 were based on GPL570, GPL14550 and GPL15207, respectively. GSE54129 contained 111 cases of cancer and 21 cases of normal tissues; GSE65801 contained 32 cases of cancer and 32 cases of normal tissues; GSE118916 contained 15 cases of cancer and 15 cases of normal tissues. GSE118916 contained 15 cases of cancer and normal tissues. Detailed information is shown in Table 1.

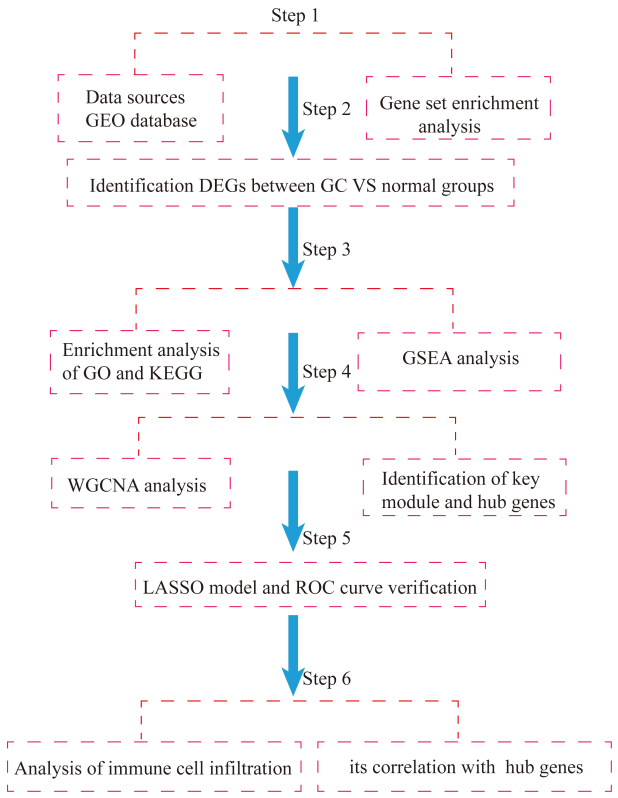

FIGURE 1
Flowchart of integrated bioinformatic analysis of hub markers and immune cell infiltration characteristics of GC.

2.2 Cells

The normal gastric cell line (GES-1) and gastric cancer cell line (MKN-45) were obtained from iCell Bioscience Inc., (Shanghai, China).

2.3 Data processing and analysis

The main analysis software used in this study was Rstudio desktop version, which is based on the Integrated Development Environment (IDE) for the R language, with better visualization, operability and simplicity. R packages are a collection of R language functions, example data and precompiled code. The main R packages used in this study are "WGCNA", "clusterprofiler" and "ggpubr".

2.3.1 Data preprocessing

The downloaded raw data were preprocessed for information extraction, background correction and normalization, construction of gene expression matrices, and conversion of probe names to gene names, followed by the next step of analysis.

2.3.2 Screening of differentially expressed genes (DEGs)

The R language (version 4.1.2) limma data package (Linear Models for Microarray Data) was used to normalize the data and screen for differentially expressed genes. |LogFC|>1 and corrected P<0.05 were used as conditions to screen for upregulated and downregulated genes. The pheatmap and ggplot packages in R language were used to plot heatmaps and volcano maps for DEGs, respectively.

2.3.3 Construction of protein interaction networks

A protein interaction network (PPI) of differential genes was constructed using the String (http://string-db.org/) database, with an interaction score >0.4 as the threshold condition. The PPI network was imported into Cytoscape software for visualization, and the connectivity of the nodes was calculated. The systematic analysis of the interactions of a large number of proteins in biological systems is important for understanding the working principles of proteins in biological systems, the response mechanisms of biological signals and energy substance metabolism in specific physiological states such as diseases, as well as understanding the functional connections between proteins.

2.3.4 Gene Ontology (GO) enrichment analysis of DEGs and Kyoto Encyclopedia of Genes and Genomes (KEGG) pathway analysis

GO analysis is a common method for enrichment studies of gene functions, which are classified into three categories: biological process (BP), molecular function (MF) and cellular component (CC). KEGG is a database that integrates a large amount of information on genomes, diseases, biological pathways and system functions. The GO function analysis and KEGG pathway analysis of differentially expressed genes were performed using the R 4.1.2 software clusterProfiler and enrichplot tools to derive the biological functions of DEGs, setting FDR P<0.05.

TABLE 1 The main features of 3 selected datasets included in this analysis.

Database ID	Platform	Author	Year	Tissue sample	Number of treatment (GC group)	Number of control (normal group)
Training set GSE54129	GPL570	Liu B	2017	Gastric tissue	111	21
GSE65801	GPL14550	Hao L	2015	Gastric tissue	32	32
Validation set GSE118916	GPL15207	Li L	2019	Gastric tissue	15	15

2.3.5 Gene set enrichment analysis

Gene set enrichment analysis (GSEA) is a computational method in which all sequenced genes are first sorted in descending order of difference, and then the input gene set is ranked to determine its enrichment in different biological functions and signaling pathways.

GSEA is a computational method used to determine whether a set of *a priori* defined genes show statistically significant and consistent differences between two biological states. The downloaded GEO matrix files were collated and grouped into GC and normal groups. To verify the functional differences between the normal and GC groups in the dataset, we performed gene function enrichment analysis on the set of genes between the two groups using the gene set enrichment analysis (GSEA) method. The raw data were calculated by R language with corresponding P.adjust, q value, P value and log2 gene expression fold-change (FC). GSEA was performed using the cluster Profiler package, which is available on the Molecular Characterization Database website (https://www.gsea-msigdb.org/gsea/msigdb/index.jsp), to obtain the corresponding analysis. Pathways with |NES|>1, P<0.05 and FDR q<0.25 were generally considered to be significantly different.

2.3.6 Construction of weighted gene coexpression networks

Genes with expression greater than all quartiles of variance were extracted and then imported into the R software platform "WGCNA" package to construct a GC-weighted gene coexpression network. Sample clustering trees were drawn, outlier samples were excluded, and sample numbers in the gene expression matrix were ensured to correspond to sample numbers in the clinical information. The optimal soft threshold β was calculated by the scale-free network, followed by the construction of the adjacency matrix by the power of the β operation. The topological overlap matrix (TOM) was then established to measure the similarity between genes, and the topological overlap matrix was used as the basic element to construct a hierarchical clustering tree. The dynamic hybrid cut method was used to divide and merge the modules and to draw the gene tree. After module partitioning, the module eigengene (ME) was calculated for each module and correlated with the clinical traits of GC patients and normal subjects, and the Pearson correlation coefficient was used to calculate the degree of correlation between the module eigenvectors and the clinical traits of the sample.

2.3.7 Hub gene screening

To find the true core target genes, we took intersections of previously analyzed differential gene datasets and genes from the characterization module with the help of Venn plots. The relevant genes were then screened and used for further analysis.

2.3.8 LASSO regression model building and ROC curve analysis

The LASSO regression model can calculate the correlation coefficients of the independent variables and incorporate the independent variables with coefficients that are not zero into the model, thus achieving dimensionality reduction. It can effectively avoid overfitting in dealing with high-dimensional data, multivariate covariance problems and overall variable selection and provides conditions for extracting characteristic genes. Receiver operating characteristic (ROC) curves are used to evaluate the accuracy of the model. After plotting the ROC curve, the area under the curve (AUC) value can be calculated, which is a probabilistic value that indicates the accuracy of the prediction model; the higher the AUC value, the better the model can classify the sample. In this study, the LASSO regression model was used to screen key genes that were highly correlated with the development of GC, and ROC curves were plotted to evaluate the accuracy of the LASSO regression model.

2.3.9 Analysis of immune cell infiltration and its correlation with characteristic hub genes

Tumor-infiltrating immune cells were assessed using the ssGESA algorithm to estimate the proportion of immune cells in the tumor tissue. These immune cells included macrophage, central memory CD4 T cell, activated CD8 T cell, activated memory CD4 T cell, type 17 T helper cell, neutrophil and 28 other species. To improve accuracy, samples were screened at P< 0.05, and histograms of the proportion of each immune cell in all eligible samples, heatmaps of correlations between immune cells and violin plots of the proportion of immune cells in GC tissue versus normal tissue samples were plotted. Spearman correlation analysis was then used to analyze the association between hub genes and the 28 immune infiltrating cells, with correlation coefficients greater than 0 being positive and correlation coefficients less than 0 being negative, and the absolute value of the correlation coefficient representing strong, weak or no correlation, with $P \leq 0.05$ being considered statistically significant.

2.3.10 Cell culture and RT-qPCR validation

Normal and cancer cells were cultured in RPMI-1640 medium (Gibco) at 37 °C with 5% CO2, and 10% fetal bovine serum (Gibco) and 1% penicillin-streptomycin solution (Gibco) were added to all media, and the cells could be processed for passaging when they were logarithmically grown.

Total RNA was extracted from normal gastric cells (GES-1) and gastric cancer cells (MKN-45) using TRIzol. Real-time fluorescence quantitative PCR was performed using HiScript® II Q RT SuperMix kit and SYBR Green Master Mix (Vazyme, Nanjing, China). Data were normalized to the GAPDH expression level of the internal reference control, and the relative expression levels of hub genes in different groups were calculated using the $2^{-\Delta\Delta Ct}$ method. The primers were synthesized and designed by wuhan huayan Biotechnology CO., LTD (Wuhan, China). The primer sequences are shown in Table 2.

2.3.11 Statistical analysis

Analysis of variance results were obtained by R software (version 4.2.3), and t-test was used for comparison between the two groups, with P<0.05 being a significant difference.

TABLE 2 RT-qPCR primer sequences.

Gene	Primer	Sequence (5′-3′)	PCR Products
Homo GAPDH	Forward	TCAAGAAGGTGGTGAAGCAGG	115bp
	Reverse	TCAAAGGTGGAGGAGTGGGT	
Homo ADH7	Forward	GATGGCACCACCAGATTTACA	282bp
	Reverse	CCTAGATGCACCAGCTGACTTA	
Homo CWH43	Forward	CCCAGGAGGTGTCTACGCT	241bp
	Reverse	CAGTTTTCTCTCATAGGCTTTA	
Homo SCNN1B	Forward	GGAGCGGGACCAAAGCA	125bp
	Reverse	GCAGCCAGACGATGTTA	

3 Results

3.1 Screening of DEGs

After merging and eliminating the batch effect of the GSE54129 and GSE65801 datasets, 133 differentially expressed genes were screened to obtain a heatmap and volcano map using differential genes. In this paper, the differentially expressed genes were analyzed by hierarchical clustering using the"pheatmap" package in R. The top 50 differentially expressed genes heatmap was output, with red representing increasing gene expression levels and green representing decreasing gene expression levels. Differential gene expression profiles existed between the normal control and GC groups (Figure 2A). The volcano plot (Figure 2B) can reflect the overall gene expression, the horizontal coordinate represents -log10 (corrected *P* value), the vertical coordinate represents log (fold change), each point represents a gene, red points represent differential gene expression upregulation, green points represent differential gene expression downregulation, and black points represent differentially expressed genes that are not significant.

3.2 Results of functional enrichment analysis of DEGs and their PPI construction

GO enrichment analysis of 133 differential genes was performed using the clusterProfiler package in R. The differential genes were normalized in terms of biological pathways involved, function and cellular localization (Table 2). The GO analysis showed that these genes were mainly involved in the following biological processes: extracellular matrix organization, extracellular structure organization, external encapsulating structure organization and digestion. The main MF categories included extracellular matrix structural constituent, peptidase regulator activity, extracellular matrix structural constituent conferring tensile strength, and glycosaminoglycan binding. The main CCs were collagen-containing extracellular matrix, endoplasmic reticulum lumen, collagen trimer and basal cells (Figure 3A). KEGG pathway analysis revealed that these genes were mainly enriched in gastric acid secretion, ECM-receptor interaction, protein digestion and absorption and amino acid metabolism (Figure 3B). To further understand the potential connections between the proteins, we constructed a PPI network of DEGs with a PPI enrichment *P* value of <1.0e-16. The network consisted of 263 edges and 131 nodes with tight connections between nodes (Figure 3C). Furthermore, GSEA

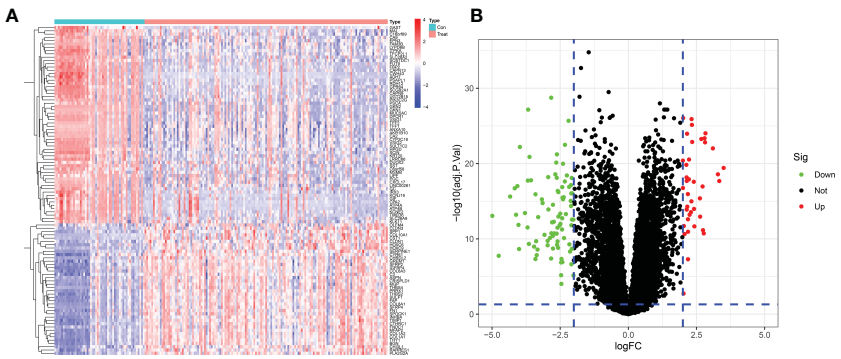

FIGURE 2
Differentially expressed genes between GC patients and healthy controls. **(A)** Heatmap of the top 50 up- and down-regulated genes. **(B)** DEGs volcano plot between healthy controls and GC tissue.

10.3389/fimmu.2023.1202529

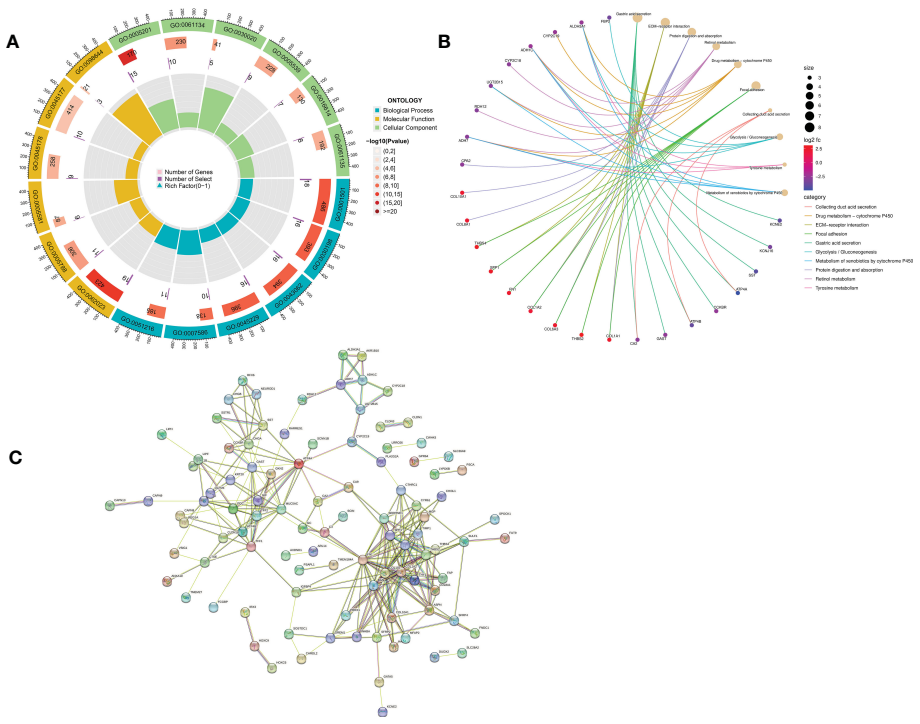

FIGURE 3
Functional enrichment analysis of DEGs and their PPI construction. **(A)** GO enrichment analysis. The first circle indicates the name of the GO; the second circle represents the number of genes on each GO. (The redder the color, the more significant the enrichment of DEGs); the third circle indicates the number of differential genes enriched on each GO term; and the fourth circle represents the proportion of genes. **(B)** KEGG pathway enrichment analysis. The different line colors indicate the different pathways to which they belong. Yellow dots are pathways, with larger dots indicating more genes involved. The other dots represent genes, the redder the gene the higher the expression level in GC patients and vice versa, the bluer the color. The top eight pathways for significant enrichment of differential genes were demonstrated. **(C)** Protein-protein interaction (PPI) network.

showed that the gene set was mainly enriched in the normal group of macrophages, B cells, CD4 T cell, T cell, cytokines and immune organs (Figures 4A, B), and the top 5 significantly enriched gene sets in normal control group and GC group see Table 3 for details.

3.3 Identification of key modules based on WGCNA

The downloaded dataset was first preprocessed, and samples were screened to remove missing values to ensure reliable network construction, yielding 196 samples and 17,348 genes for subsequent analysis in the construction of WGCNA. A hierarchical clustering tree was created based on dynamic hybrid cuts using scale-free coexpression networks and topological overlap. Based on the scale-free topology criterion, the optimal soft threshold $\beta = 6$ was determined based on the scale-free fit index $R^2 = 0.9$. A total of nine modules were obtained by dynamic hybrid cutting (Figures 5A, B), corresponding to the colors black, blue, brown, green, green-yellow, gray, magenta, pink and purple, and the numbers of module genes were 223, 2574, 446, 614, 101, 115, 159, 201 and 125, in that order. The most relevant hub modules to GC

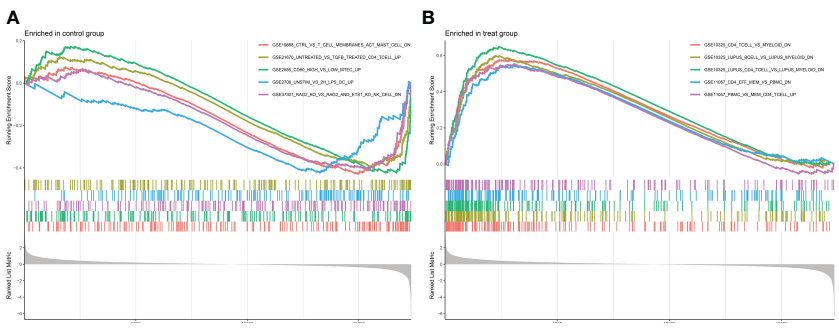

FIGURE 4
Enrichment plot for GSEA. **(A)** Active gene sets in healthy controls. **(B)** Active gene set in GC group.

TABLE 3 Top 5 significantly enriched gene sets in normal control group and GC group.

Gene set name	NES	*p*value	*p*.adjust	qvalues
Enriched in normal control group				
GSE19888 CTRL VS T Cell membranes ACT mast Cell down	-1.692957907	0.000161482	0.001895759	0.001302505
GSE21670 Untreated vs TGFB treated CD4 T Cell up	-1.554264308	0.001274963	0.009257259	0.006360315
GSE2585 CD80 high vs low MTEC up	-1.657193329	0.000254598	0.002690672	0.00184866
GSE2706 Unstim VS 2H LPS DC up	-1.634072618	0.000987185	0.007658545	0.005261899
GSE37301 Rag2 KO VS Rag2 and Ets1 KO NK cell down	-1.593873519	0.000661997	0.005698322	0.003915103
Enriched in treat (GC) group				
GSE10325_CD4 T Cell VS Myeloid down	2.298424482	1.00E-10	1.08E-08	7.44E-09
GSE10325 Lupus B Cell VS Lupus Myeloid down	2.403164632	1.00E-10	1.08E-08	7.44E-09
GSE10325 Lupus CD4 T Cell VS Lupus Myeloid down	2.593696725	1.00E-10	1.08E-08	7.44E-09
GSE11057 CD4 Eff Mem VS Pbmc down	2.176921036	1.00E-10	1.08E-08	7.44E-09
GSE11057 Pbmc VS Mem CD4 T Cell up	2.206216446	1.00E-10	1.08E-08	7.44E-09

were screened by calculating the correlation coefficient (R) and *P* value for each module (Figure 6A). The heatmap from this study shows that the pink module (201 genes) was highly positively correlated with GC (R = 0.63, *P* = 2e-23) (Figures 6B, C), and subsequently, the 201 core genes of the pink module (cor = 0.41, *P* = 1.5e-09) were screened for subsequent analysis based on GS > 0.5 and MM > 0.8 (Figure 6D).

3.4 Screening for hub genes

Thirteen crossover genes were obtained after taking the intersection of the DEG dataset and the gene set in the feature module (Figure 7A). Subsequently, LASSO analysis was used to screen three genes from the crossover genes as pivotal genes for GC, including ADH7, CWH43 and SCNN1B (Figures 7B, C).

3.5 Identification and validation of differential expression analysis of key genes and their diagnostic value

The screened hub genes were extracted for expression to construct differential expression box plots. The differential expression box plot showed that all three key genes were underexpressed in GC patients ($P < 0.001$) (Figure 8A). The AUC areas for the three gene models were 0.868, 0.845 and 0.877, respectively (Figure 9A), indicating that the model is highly accurate and that ADH7, CWH43 and SCNN1B may be involved in affecting the development of GC. Subsequently, the independent dataset GSE118916 was used as the validation dataset to identify their expression levels and diagnostic value to further validate the clinical application of the pivotal genes. The results showed that the expression levels of ADH7, CWH43 and SCNN1B in the GC group were significantly lower than those in healthy controls in the validation set ($P < 0.001$), which was consistent with the results of the training set data (Figure 8B). ROC curves were used to further validate the diagnostic value of the three pivotal genes in the validation dataset. The results showed that ADH7, CWH43 and SCNN1B had high diagnostic value with AUC values of 0.942, 0.987 and 0.964, respectively (Figure 9B).

3.6 Analysis of immune cell infiltration and its correlation with characteristic hub genes

Immune cell infiltration was assessed by the ssGSEA algorithm on tissue samples from the dataset, involving a total of 28 immune cell species. The majority of immune cells were found to be highly infiltrated in GC tissue (Figure 10A). Among them, activated CD4 T cell, activated dendritic cell, CD56 bright natural killer cell, γδ T cell, immature dendritic cell, MDSC, macrophage, mast cell, monocyte, natural killer T cell, natural killer cell, plasmacytoid dendritic cell, regulatory T cell, T follicular helper cell, type 1 helper cell, central memory CD4 T cell and regulatory T cell were extremely significantly increased in GC tissues ($P<0.001$), and activated CD8 T cell ($P=0.006$), neutrophil ($P=0.003$), type 2 helper cell ($P=0.004$) and e 0.004) and effector memory CD8 T cell ($P=0.036$) were also significantly increased in GC tissue. In contrast, activated B cell ($P=0.535$), CD56bright natural killer cell ($P=0.600$), eosinophil ($P=0.284$), immature B cell ($P=0.065$), type 17 T helper cell ($P=0.275$), effector memory CD4 T cell ($P=0.095$), memory B cell ($P=0.182$) and central memory CD8 T cell ($P=0.535$) did not differ significantly in GC tissue (Figure 10B). We then performed a correlation analysis to further explore the association of the hub genes with the 28 immune cells. We found that ADH7, CWH43 and

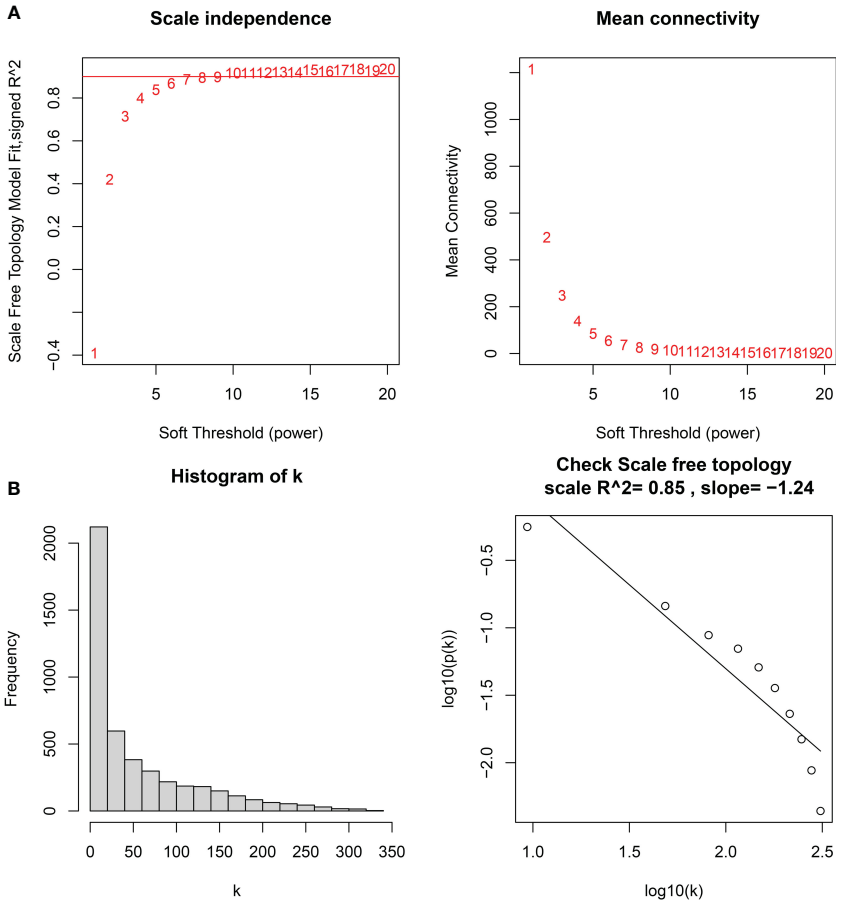

FIGURE 5
(A) Soft thresholds for determining the best scale-free topological model fit index (left) and average connectivity (right), with the red horizontal line indicating R^2 = 0.9. **(B)** The distribution of the connectivity of each node in the network (left) and node degree power distribution (right).

SCNN1B were significantly associated with type 1 helper cell, T follicular helper cell, regulatory T cell, plasmacytoid dendritic cell, natural killer T cell, and natural cells. In addition, CWH43 and SCNN1B were also negatively correlated with type 1 helper cell, macrophages and γδ T cell (P<0.05). Interestingly, SCNN1B was also negatively correlated with activated CD4 T cell (P<0.001, P<0.01, P<0.05). ADH7 and CWH43 were significantly positively correlated with CD56 bright natural killer cell (P<0.05), while SCNN1B was significantly positively correlated with monocyte (P<0.01) (Figure 10C). These results suggest that hub genes may influence malignant tumor progression by regulating the abundance of infiltrating immune cells in the nodal GC tumor microenvironment.

3.7 Expression of hub genes in two groups of cells

To verify our predicted results, we did further validation by *in vitro* cellular experiments. As shown in Figure 11, it was confirmed that ADH7, CWH43 and SCNN1B all showed low expression in gastric cancer cells (p < 0.05). This is consistent with the results of our bioinformatics analysis.

4 Discussion

In recent years, the understanding of the pathogenesis of gastric cancer has been deepened, and a series of targeted drugs have been explored continuously, but the current exploration of gastric cancer targets is not comprehensive and in-depth enough for a multitarget, multilevel systemic therapy (17). Therefore, it is of great clinical importance to expand the research and discovery of potential targets for gastric cancer. Based on the multilevel concept of "disease-phenotype-molecule", combined with the application and development of computer technology and artificial intelligence in the field of medical biology, bioinformatics has become one of the necessary tools for molecular marker research based on big data, which can be used to screen molecular markers related to disease phenotypes (18, 19). Individualized treatment and predictable outcomes of molecular pathways associated with gastric cancer have opened up many research directions, such as the use of molecular markers as useful tools in clinical work to assist in the diagnosis and treatment of gastric cancer patients, to assess the efficacy of treatments and to explore new therapeutic modalities (20, 21).

In this study, we obtained gastric cancer and normal tissue gene microarray datasets from the GEO database and performed DEG

10.3389/fimmu.2023.1202529

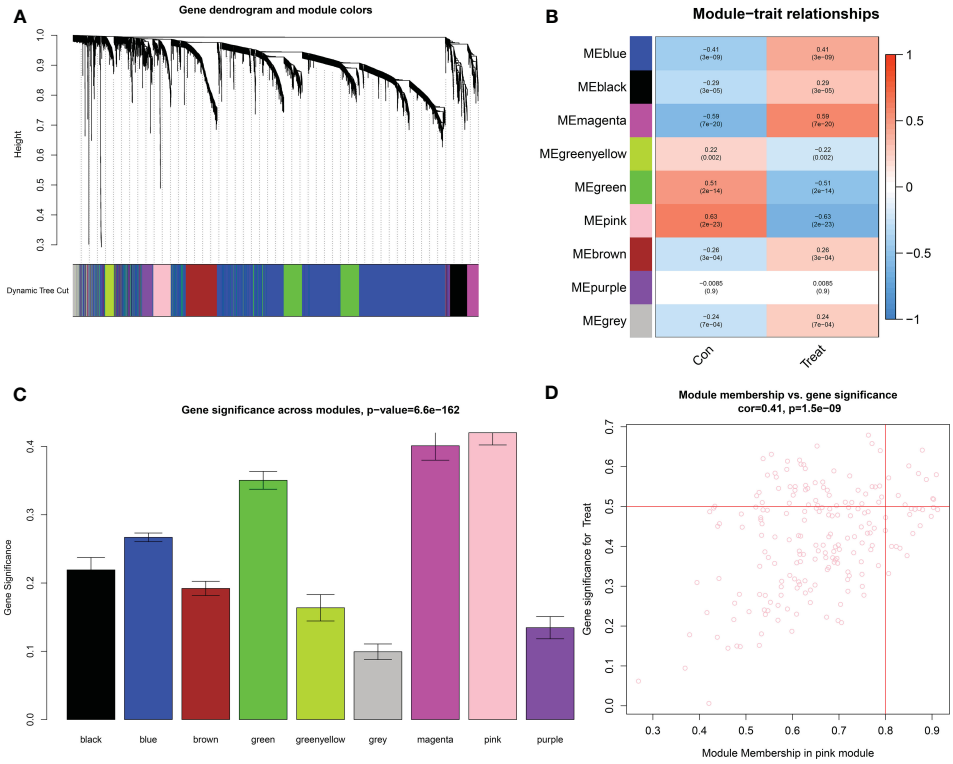

FIGURE 6
Identification of key modules based on WGCNA. **(A)** GC-related gene clustering dendrogram. In the figure, the top half is a hierarchical clustering tree diagram of the genes, and the bottom half is the gene modules, or network modules. Genes with relative relatedness are located on the same or adjacent branches. **(B)** Heatmap of correlation analysis of the modules and clinical traits. **(C)** Gene significance in the modules. **(D)** Scatter plots of GS score and MM for genes in the pink module.

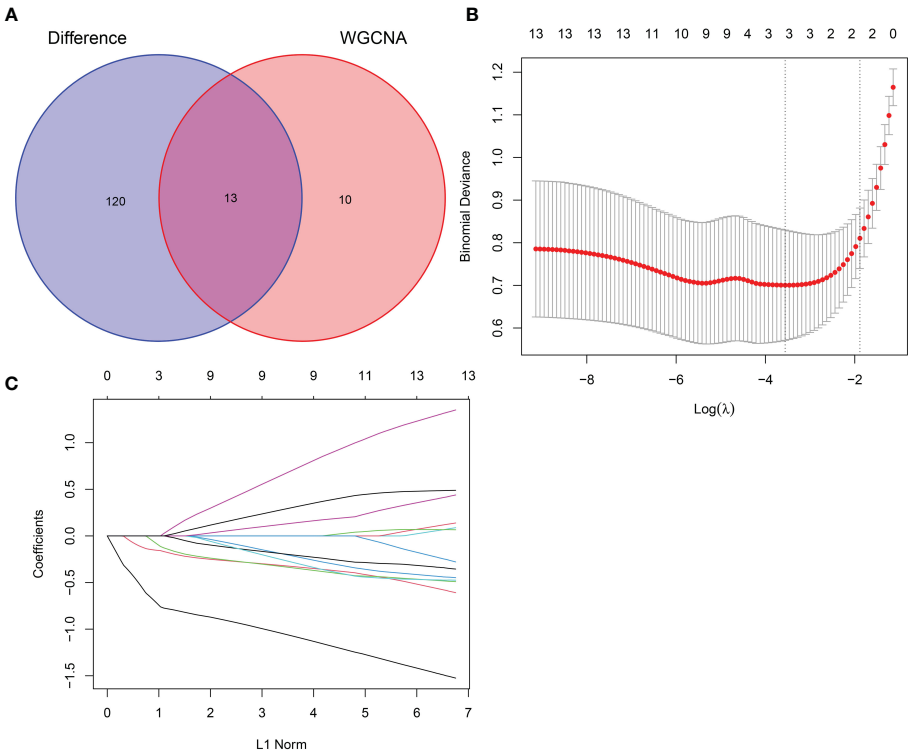

FIGURE 7
LASSO screening for hub genes. **(A)** Venn diagram of intersecting genes between DEGs and the pink module. **(B)** Coefficients distribution trend of LASSO regression. **(C)** Distribution of hub genes in cross validation.

10.3389/fimmu.2023.1202529

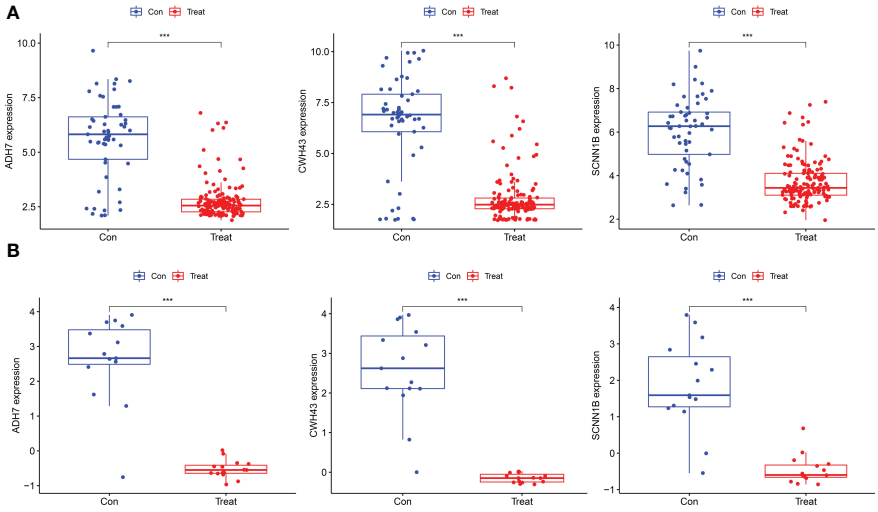

FIGURE 8
Expression levels of the three Hub genes between the normal control and GC groups. **(A)** Boxplot of these hub genes in the training dataset. **(B)** Boxplot of hub genes in the validation dataset. (****P*<0.001).

analysis on these combined datasets. GO and KEGG analyses showed that gastric cancer tissues differed significantly from normal tissue cells in BP, CC, and MF, mainly in biological processes such as collagen catabolic processes, extracellular matrix disassembly, and collagen protofibril tissue synthesis. The differential cellular components included extracellular regions, protein extracellular matrix, collagen trimer, etc., and both BP and CC play an important role in the migration of tumor cells. The extracellular matrix (ECM) is a loose connective tissue located outside the cell and contains a variety of biomolecules, such as collagen, adhesion factors, glycoproteins, and cytokines (22). It is physiologically important in intercellular signaling, intercellular interactions and regulation of cell proliferation, differentiation and migration (23). The ECM has been shown to be an independent risk factor for lymph node metastasis in early gastric cancer. Furthermore, the overall results of KEGG enrichment suggest that GC is accompanied by disturbed gastric acid secretion, amino acid metabolism and energy metabolism. The answer to this phenotype is well documented in the previous literature. Tumor cells are able to survive and proliferate in a nutrient-poor microenvironment through metabolic reprogramming, where abnormal glucose metabolism plays an

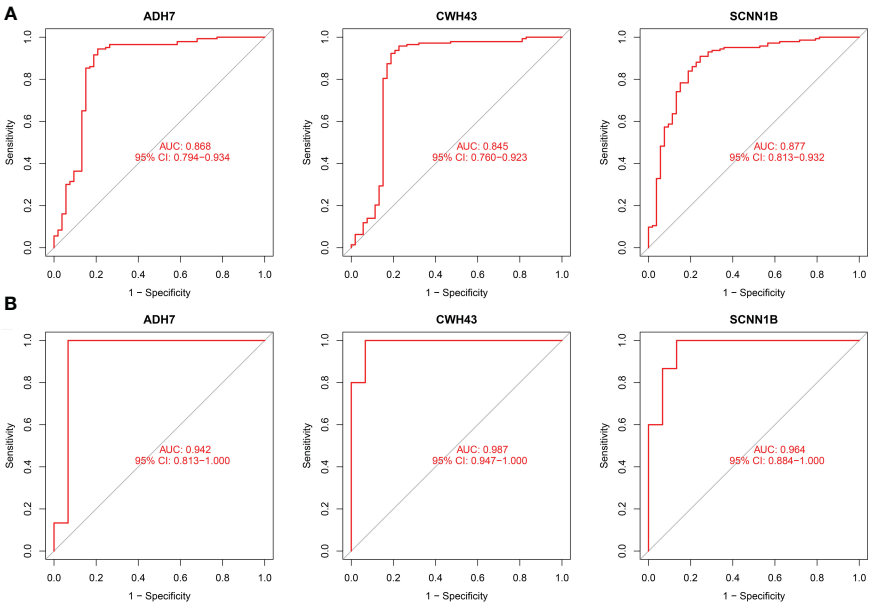

FIGURE 9
Diagnostic value of the three genes. **(A)** ROC curves of hub genes in the training dataset. **(B)** ROC curves of hub genes in the validation dataset.

10.3389/fimmu.2023.1202529

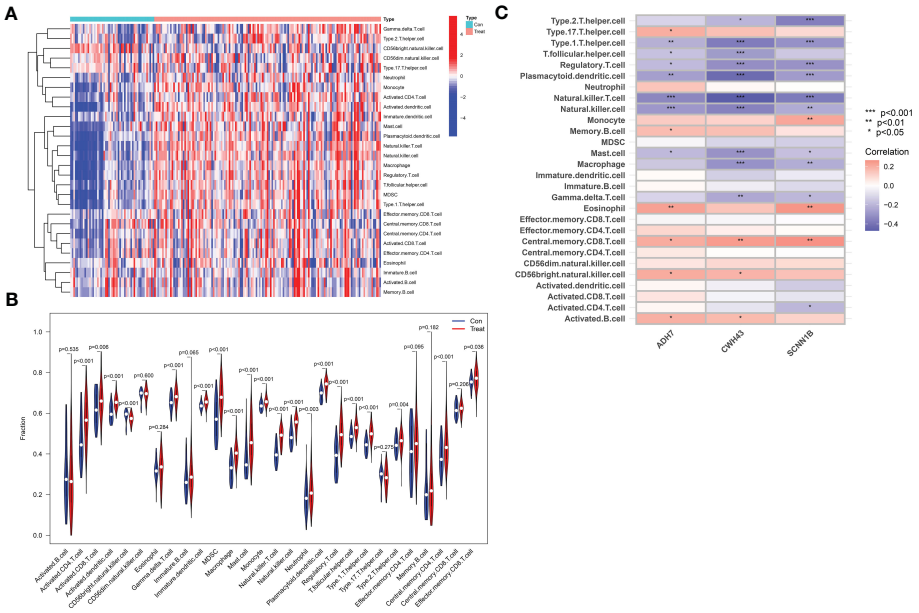

FIGURE 10
Analysis of immune cell infiltration and its correlation with characteristic hub genes. **(A)** Heat map of immune cell infiltration between normal control and GC group **(B)** Violin diagram of the difference in immune cell infiltration between normal controls and GC. **(C)** Analysis of the association of 3 Hub genes with immune cells.

important role in maintaining the malignant character of the tumor (24). Tumor cells obtain the energy necessary for growth and proliferation by glycolysis, even in conditions of adequate oxygen (25). Excessive gastric acid promotes the progression of gastric cancer. Gastrin, an inducer of gastric acid secretion, has been shown to be a valuable screening marker for gastric cancer (26, 27).

Most studies are currently based only on systems biology methods or machine learning algorithms for cancer marker screening. The use of a single systems biology approach or machine learning algorithm for data analysis may lead to some missing data or too much confounding data, so the combination of two or more methods can improve the confidence in the results (28). In this study, three biomarkers, ADH7, CWH43 and SCNN1B, were included in the model that used multiple bioinformatics methods to screen for gastric cancer. Based on the literature available to date, ADH7 belongs to the alcohol dehydrogenase family, a gene expressed mainly in the upper gastrointestinal tract, and has been shown to be involved in the metabolism of xenobiotics by cytochrome P450: it is associated with the metabolism of ethanol that occurs in gastroesophageal tissues and is then absorbed into the bloodstream. In addition, single nucleotide polymorphisms in ADH7 are susceptibility factors for cancer and drug dependence (29). SCNN1B encodes the β subunit of the epithelial sodium channel (ENaC), which is involved in the control of transepithelial transport of water and electrolytes and cell differentiation in different organs. Current studies on ENaC in cancer have shown that in breast cancer and neuroblastoma, SCNN1A gene silencing caused by hypermethylation in the promoter region of the SCNN1A gene, which encodes the α subunit of ENaC, is the main reason for the poor prognosis of patients with these tumors and diseases. Recently, SCNN1B was found to inhibit the growth and metastasis of gastric cancer cells, and the expression level of SCNN1B was positively correlated with the survival rate of gastric cancer patients and reduce the expression level of Glucose-Regulated Protein 78 [GRP78, Recent studies have also found that GRP78 expression is elevated in cancer cells and plays an important role in the development of cancer tumors (30, 31)]. In addition, activation of downstream proteins leads to caspase-dependent apoptosis and cell cycle arrest through induction of the unfolded protein response (UPR) (32–34). A recent study identified CWH43 as a prognosis-related gene in colorectal cancer (CRC), but little is known about its function (35).

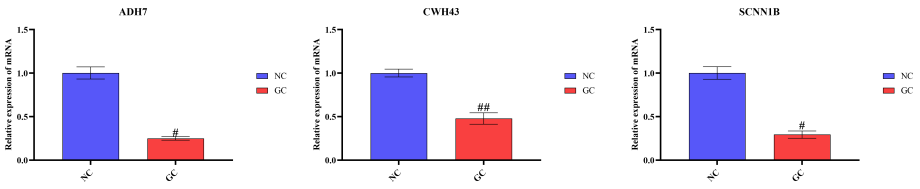

FIGURE 11
RT-qPCR validation of hub gene mRNA in different groups. The data presented are means ± SD (n=3). $^{\#}P$ <0.05 and $^{\#\#}P$ <0.01 relative to the control group.

The GC tumor microenvironment is highly complex and heterogeneous, tumor-associated immune cells play a role in tumorigenesis, development, invasion and metastasis, and the type and proportion of their infiltration are closely related to the clinical outcome of patients (36, 37). Therefore, the investigation of immune cell infiltration and its correlation with characteristic hub genes is also important for the pathogenesis, prevention and treatment of GC. In this study, we used ssGSEA to assess the expression levels and dynamic regulatory processes of 28 immune cell types in GC. The results showed significant differences in the pattern of immune cell infiltration between normal gastric and GC tissues, which to some extent indicated an imbalance in the immune response in GC. Tumor-associated macrophages (TAMs) are important components of the gastric cancer tumor microenvironment, which can influence the malignant biological behavior of gastric cancer and play a key role in gastric carcinogenesis and metastasis (38, 39). In the tumor microenvironment, TAMs secrete a large number of inflammatory factors, growth factors, chemokines and proteases through crosstalk with gastric cancer cells and various other cells, which play an active role in tumor growth, inhibition of apoptosis, angiogenesis and lymphatic metastasis (40, 41). In addition, myeloid inhibitory cells (MDSCs) are diverse bone marrow progenitor cells that produce arginase 1 (ARG1) to promote tumor cell growth and suppress immune cell function (42). CD4 T cells can be differentiated into four main subpopulations: Th1 cells, Th2 cells, regulatory cells (Tregs) and Th17 cells. The imbalance in the ratio of T lymphocytes alters the immune microenvironment of tumors, thus facilitating the proliferation, invasion and metastasis of tumor cells. Immunosuppressive effector cells modulate the intensity of the body's immune response, attenuate immune damage, and mediate immune escape by suppressing the antitumor immune response, thereby promoting tumor progression. Previous studies have shown that a large number of immune cells and inflammatory factors are present in the tumor microenvironment of GC, and the number and phenotype of immune cell subpopulations in GC tissues are closely related to the development of GC and the prognosis of patients (43–45). To further reveal the potential mechanism of the differential expression of hub genes on the predictive value of the immune microenvironment in GC, this study analyzed these markers with infiltrating immune cells and found that the expression of these three biomarkers was significantly and negatively correlated with the level of immune infiltration of immune cells that were significantly upregulated in GC. This suggests that these genes may influence the progression of GC by affecting the level of immune infiltration as well as the interactions between immune cells. In short, these correlations may reveal potential molecular mechanisms underlying GC development and suggest that ADH7, CWH43 and SCNN1B play important roles in the GC immune microenvironment.

Although there are potential suggestions from this study for the early detection of gastric cancer and the corresponding treatment, there are still some limitations to consider. First, the sample size used in this trial may limit the generalizability of the study findings, and therefore, further evaluation in a larger cohort and in a different population would provide stronger evidence. Second, this study primarily utilized retrospective transcriptome analysis data and lacked validation. Therefore, *in vitro*, *in vivo* and prospective data still need to be collected to validate the real-world clinical significance of the identified DEGs and core genes in relation to gastric carcinogenesis, progression and prognosis. Finally, more experiments are needed to elucidate the upstream regulatory pathways and downstream mechanisms of the identified key differentially expressed genes.

In conclusion, the present study screened and validated the key genes ADH7, CWH43 and SCNN1B, which are significantly associated with GC development, based on the GEO public database, through a combination of WGCNA and lasso regression models, providing a molecular basis for the early diagnosis and treatment of GC, as well as for immunotherapy research and the development of new targeted drugs.

Data availability statement

Publicly available datasets were analyzed in this study. This data can be found here: https://www.ncbi.nlm.nih.gov/geo/query/acc.cgi?acc=GSE54129, https://www.ncbi.nlm.nih.gov/geo/query/acc.cgi?acc=GSE65801, https://www.ncbi.nlm.nih.gov/geo/query/acc.cgi?acc=GSE118916.

Author contributions

CL: Conceptualization, Methodology, Software, Writing-Original Draft. TY: Methodology, Validation, Writing-Original Draft. YY: Visualization, Investigation. RW: Formal analysis, Software. HY: Writing-Review & Editing, Supervision, Funding acquisition. All authors contributed to the article and approved the submitted version.

Funding

This work was supported by the National Natural Science Foundation of China (82160749) (82104392).

Acknowledgments

We sincerely acknowledge the GEO database for providing online resources for gene expression and the researchers for uploading their meaningful datasets. We also sincerely appreciate the contributions of all participants to our present study. We thank Elsevier Language Editing Services (https://webshop.elsevier.com/) for polishing this manuscript.

Conflict of interest

The authors declare that the research was conducted in the absence of any commercial or financial relationships that could be construed as a potential conflict of interest.

Publisher's note

References

1. Januszewicz W, Turkot MH, Malfertheiner P, Regula J. A global perspective on gastric cancer screening: which concepts are feasible, and when? *Cancers (Basel)* (2023) 15(3):664. doi: 10.3390/cancers15030664

2. Cao W, Chen HD, Yu YW, Li N, Chen WQ. Changing profiles of cancer burden worldwide and in China: a secondary analysis of the global cancer statistics 2020. *Chin Med J (Engl)* (2021) 134(7):783–91. doi: 10.1097/CM9.0000000000001474

3. Li Y, Wang HC, Wang JS, Sun B, Li LP. Chemokine receptor 4 expression is correlated with the occurrence and prognosis of gastric cancer. *FEBS Open Bio* (2020) 10(6):1149–61. doi: 10.1002/2211-5463.12864

4. Sexton RE, Al Hallak MN, Diab M, Azmi AS. Gastric cancer: a comprehensive review of current and future treatment strategies. *Cancer Metastasis Rev* (2020) 39 (4):1179–203. doi: 10.1007/s10555-020-09925-3

5. Smyth EC, Nilsson M, Grabsch HI, van Grieken NC, Lordick F. Gastric cancer. *Lancet* (2020) 396(10251):635–48. doi: 10.1016/S0140-6736(20)31288-5

6. Banks M, Graham D, Jansen M, Gotoda T, Coda S, di Pietro M, et al. British Society of gastroenterology guidelines on the diagnosis and management of patients at risk of gastric adenocarcinoma. *Gut* (2019) 68(9):1545–75. doi: 10.1136/gutjnl-2018-318126

7. Li K, Zhang A, Li X, Zhang H, Zhao L. Advances in clinical immunotherapy for gastric cancer. *Biochim Biophys Acta Rev Cancer* (2021) 1876(2):188615. doi: 10.1016/j.bbcan.2021.188615

8. Korman LY, Nylen ES, Finan TM, Linnoila RI, Becker KL. Primary culture of the enteric nervous system from neonatal hamster intestine. selection of vasoactive intestinal polypeptide-containing neurons. *Gastroenterology* (1988) 95(4):1003–10. doi: 10.1016/0016-5085(88)90176-x

9. Smyth EC, Cervantes A. Addition of nivolumab to chemotherapy in patients with advanced gastric cancer: a relevant step ahead, but still many questions to answer. *ESMO Open* (2020) 5(6):e001107. doi: 10.1136/esmoopen-2020-001107

10. Ji L, Qian W, Gui L, Ji Z, Yin P, Lin GN, et al. Blockade of beta-Catenin-Induced CCL28 suppresses gastric cancer progression *via* inhibition of treg cell infiltration. *Cancer Res* (2020) 80(10):2004–16. doi: 10.1158/0008-5472.CAN-19-3074

11. Zhang B, Horvath S. A general framework for weighted gene co-expression network analysis. *Stat Appl Genet Mol Biol* (2005) 4 (1), 2005. doi: 10.2202/1544-6115.1128

12. Zhang P, Pei S, Gong Z, Feng Y, Zhang X, Yang F, et al. By integrating single-cell RNA-seq and bulk RNA-seq in sphingolipid metabolism, CACYBP was identified as a potential therapeutic target in lung adenocarcinoma. *Front Immunol* (2023) 14:1115272. doi: 10.3389/fimmu.2023.1115272

13. Lemieux W, Fleischer D, Yang AY, Niemann M, Oualkacha K, Klement W, et al. Dissecting the impact of molecular T-cell HLA mismatches in kidney transplant failure: a retrospective cohort study. *Front Immunol* (2022) 13:1067075. doi: 10.3389/fimmu.2022.1067075

14. Sun C, Chen Y, Kim NH, Lowe S, Ma S, Zhou Z, et al. Identification and verification of potential biomarkers in gastric cancer by integrated bioinformatic analysis. *Front Genet* (2022) 13:911740. doi: 10.3389/fgene.2022.911740

15. Liu B, Ma X, Ha W. Identification of potential prognostic biomarkers associated with macrophage M2 infiltration in gastric cancer. *Front Genet* (2021) 12:827444. doi: 10.3389/fgene.2021.827444

16. Zhang S, Lv M, Cheng Y, Wang S, Li C, Qu X. Immune landscape of advanced gastric cancer tumor microenvironment identifies immunotherapeutic relevant gene signature. *BMC Cancer* (2021) 21(1):1324. doi: 10.1186/s12885-021-09065-z

17. Raoul JL, Moreau-Bachelard C, Gilabert M, Edeline J, Frenel JS. Drug-drug interactions with proton pump inhibitors in cancer patients: an underrecognized cause of treatment failure. *ESMO Open* (2023) 8(1):100880. doi: 10.1016/j.esmoop.2023.100880

18. Chen H, Xu J, Wei S, Jia Z, Sun C, Kang J, et al. RABC: rheumatoid arthritis bioinformatics center. *Nucleic Acids Res* (2023) 51(D1):D1381–7. doi: 10.1093/nar/gkac850

19. Turhon M, Maimaiti A, Gheyret D, Axier A, Rexiati N, Kadeer K, et al. An immunogenic cell death-related regulators classification patterns and immune microenvironment infiltration characterization in intracranial aneurysm based on machine learning. *Front Immunol* (2022) 13:1001320. doi: 10.3389/fimmu.2022.1001320

20. Li S, Yuan L, Xu ZY, Xu JL, Chen GP, Guan X, et al. Integrative proteomic characterization of adenocarcinoma of esophagogastric junction. *Nat Commun* (2023) 14(1):778. doi: 10.1038/s41467-023-36462-8

21. Rezaei Z, Ranjbaran J, Safarpour H, Nomiri S, Salmani F, Chamani E, et al. Identification of early diagnostic biomarkers *via* WGCNA in gastric cancer. *BioMed Pharmacother* (2022) 145:112477. doi: 10.1016/j.biopha.2021.112477

22. Karamanos NK, Theocharis AD, Piperigkou Z, Manou D, Passi A, Skandalis SS, et al. A guide to the composition and functions of the extracellular matrix. *FEBS J* (2021) 288(24):6850–912. doi: 10.1111/febs.15776

23. Bonnans C, Chou J, Werb Z. Remodelling the extracellular matrix in development and disease. *Nat Rev Mol Cell Biol* (2014) 15(12):786–801. doi: 10.1038/nrm3904

24. Lin JX, Lian NZ, Gao YX, Zheng QL, Yang YH, Ma YB, et al. m6A methylation mediates LHPP acetylation as a tumour aerobic glycolysis suppressor to improve the prognosis of gastric cancer. *Cell Death Dis* (2022) 13(5):463. doi: 10.1038/s41419-022-04859-w

25. Hsu PP, Sabatini DM. Cancer cell metabolism: warburg and beyond. *Cell* (2008) 134(5):703–7. doi: 10.1016/j.cell.2008.08.021

26. Maddalo G, Spolverato Y, Rugge M, Farinati F. Gastrin: from pathophysiology to cancer prevention and treatment. *Eur J Cancer Prev* (2014) 23(4):258–63. doi: 10.1097/CEJ.0000000000000008

27. Rao SV, Solum G, Niederdorfer B, Norsett KG, Bjorkoy G, Thommesen L. Gastrin activates autophagy and increases migration and survival of gastric adenocarcinoma cells. *BMC Cancer* (2017) 17(1):68. doi: 10.1186/s12885-017-3055-5

28. Yu R, Zhang J, Zhuo Y, Hong X, Ye J, Tang S, et al. Identification of diagnostic signatures and immune cell infiltration characteristics in rheumatoid arthritis by integrating bioinformatic analysis and machine-learning strategies. *Front Immunol* (2021) 12:724934. doi: 10.3389/fimmu.2021.724934

29. Zhao L, Lei H, Shen L, Tang J, Wang Z, Bai W, et al. Prognosis genes in gastric adenocarcinoma identified by cross talk genes in disease–related pathways. *Mol Med Rep* (2017) 16(2):1232–40. doi: 10.3892/mmr.2017.6699

30. Samanta S, Yang S, Debnath B, Xue D, Kuang Y, Ramkumar K, et al. The hydroxyquinoline analogue YUM70 inhibits GRP78 to induce ER stress-mediated apoptosis in pancreatic cancer. *Cancer Res* (2021) 81(7):1883–95. doi: 10.1158/0008-5472.CAN-20-1540

31. Farshbaf M, Khosroushahi AY, Mojarad-Jabali S, Zarebkohan A, Valizadeh H, Walker PR. Cell surface GRP78: an emerging imaging marker and therapeutic target for cancer. *J Control Release* (2020) 328:932–41. doi: 10.1016/j.jconrel.2020.10.055

32. Qian Y, Wong CC, Xu J, Chen H, Zhang Y, Kang W, et al. Sodium channel subunit SCNN1B suppresses gastric cancer growth and metastasis *via* GRP78 degradation. *Cancer Res* (2017) 77(8):1968–82. doi: 10.1158/0008-5472.CAN-16-1595

33. Lu A, Shi Y, Liu Y, Lin J, Zhang H, Guo Y, et al. Integrative analyses identified ion channel genes GJB2 and SCNN1B as prognostic biomarkers and therapeutic targets for lung adenocarcinoma. *Lung Cancer* (2021) 158:29–39. doi: 10.1016/j.lungcan.2021.06.001

34. Hanukoglu I, Hanukoglu A. Epithelial sodium channel (ENaC) family: phylogeny, structure-function, tissue distribution, and associated inherited diseases. *Gene* (2016) 579(2):95–132. doi: 10.1016/j.gene.2015.12.061

35. Lacalamita A, Piccinno E, Scalavino V, Bellotti R, Giannelli G, Serino G. A gene-based machine learning classifier associated to the colorectal adenoma-carcinoma sequence. *Biomedicines* (2021) 9(12):1937. doi: 10.3390/biomedicines9121937

36. Li Y, Hu X, Lin R, Zhou G, Zhao L, Zhao D, et al. Single-cell landscape reveals active cell subtypes and their interaction in the tumor microenvironment of gastric cancer. *Theranostics* (2022) 12(8):3818–33. doi: 10.7150/thno.71833

37. Qing X, Xu W, Liu S, Chen Z, Ye C, Zhang Y. Molecular characteristics, clinical significance, and cancer immune interactions of angiogenesis-associated genes in gastric cancer. *Front Immunol* (2022) 13:843077. doi: 10.3389/fimmu.2022.843077

38. Lin C, He H, Liu H, Li R, Chen Y, Qi Y, et al. Tumour-associated macrophages-derived CXCL8 determines immune evasion through autonomous PD-L1 expression in gastric cancer. *Gut* (2019) 68(10):1764–73. doi: 10.1136/gutjnl-2018-316324

39. Eum HH, Kwon M, Ryu D, Jo A, Chung W, Kim N, et al. Tumor-promoting macrophages prevail in malignant ascites of advanced gastric cancer. *Exp Mol Med* (2020) 52(12):1976–88. doi: 10.1038/s12276-020-00538-y

40. Zheng P, Li W. Crosstalk between mesenchymal stromal cells and tumor-associated macrophages in gastric cancer. *Front Oncol* (2020) 10:571516. doi: 10.3389/fonc.2020.571516

41. Pan Y, Yu Y, Wang X, Zhang T. Tumor-associated macrophages in tumor immunity. *Front Immunol* (2020) 11:583084. doi: 10.3389/fimmu.2020.583084

42. Ding L, Wan M, Wang D, Cao H, Wang H, Gao P. Myeloid-derived suppressor cells in patients with acute pancreatitis with increased inhibitory function. *Front Immunol* (2022) 13:840620. doi: 10.3389/fimmu.2022.840620

43. Hirahara K, Nakayama T. CD4+ T-cell subsets in inflammatory diseases: beyond the Th1/Th2 paradigm. *Int Immunol* (2016) 28(4):163–71. doi: 10.1093/intimm/dxw006

44. Laine A, Labiad O, Hernandez-Vargas H, This S, Sanlaville A, Leon S, et al. Regulatory T cells promote cancer immune-escape through integrin alphavbeta8-mediated TGF-beta activation. *Nat Commun* (2021) 12(1):6228. doi: 10.1038/s41467-021-26352-2

45. Kalaora S, Nagler A, Wargo JA, Samuels Y. Mechanisms of immune activation and regulation: lessons from melanoma. *Nat Rev Cancer* (2022) 22(4):195–207. doi: 10.1038/s41568-022-00442-9

frontiers | Frontiers in Immunology

TYPE Original Research
PUBLISHED 12 June 2023
DOI 10.3389/fimmu.2023.1178436

OPEN ACCESS

EDITED BY
Takaji Matsutani,
Repertoire Genesis, Inc., Japan

REVIEWED BY
Yifeng Tao,
Carnegie Mellon University, United States
Jie Zhang,
The First Affiliated Hospital of Chongqing Medical University, China
Federica Recine,
Azienda Ospedaliera San Giovanni Addolorata, Italy
Hong-Hui Wang,
Hunan University, China

*CORRESPONDENCE
Shasha He
heshasha611@csu.edu.cn
Zhihong Li
lizhihong@csu.edu.cn

†These authors have contributed equally to this work and share first authorship

RECEIVED 02 March 2023
ACCEPTED 26 May 2023
PUBLISHED 12 June 2023

CITATION
Liu B, Li C, Feng C, Wang H, Zhang H, Tu C, He S and Li Z (2023) Integrative profiling analysis reveals prognostic significance, molecular characteristics, and tumor immunity of angiogenesis-related genes in soft tissue sarcoma. *Front. Immunol.* 14:1178436. doi: 10.3389/fimmu.2023.1178436

Integrative profiling analysis reveals prognostic significance, molecular characteristics, and tumor immunity of angiogenesis-related genes in soft tissue sarcoma

Binfeng Liu[1,2†], Chenbei Li[1,2†], Chengyao Feng[1,2], Hua Wang[1,2], Haixia Zhang[3], Chao Tu[1,2], Shasha He[3*] and Zhihong Li[1,2*]

[1]Department of Orthopaedics, The Second Xiangya Hospital of Central South University, Changsha, Hunan, China, [2]Hunan Key Laboratory of Tumor Models and Individualized Medicine, The Second Xiangya Hospital of Central South University, Changsha, Hunan, China, [3]Department of Oncology, The Second Xiangya Hospital of Central South University, Changsha, Hunan, China

Background: Soft tissue sarcoma (STS) is a class of malignant tumors originating from mesenchymal stroma with a poor prognosis. Accumulating evidence has proved that angiogenesis is an essential hallmark of tumors. Nevertheless, there is a paucity of comprehensive research exploring the association of angiogenesis-related genes (ARGs) with STS.

Methods: The ARGs were extracted from previous literature, and the differentially expressed ARGs were screened for subsequent analysis. Next, the least absolute shrinkage and selection operator (LASSO) and Cox regression analyses were conducted to establish the angiogenesis-related signature (ARSig). The predictive performance of the novel ARSig was confirmed using internal and external validation, subgroup survival, and independent analysis. Additionally, the association of the ARSig with the tumor immune microenvironment, tumor mutational burden (TMB), and therapeutic response in STS were further investigated. Notably, we finally conducted *in vitro* experiments to verify the findings from the bioinformatics analysis.

Results: A novel ARSig is successfully constructed and validated. The STS with a lower ARSig risk score in the training cohort has an improved prognosis. Also, consistent results were observed in the internal and external cohorts. The receiver operating characteristic (ROC) curve, subgroup survival, and independent analysis further indicate that the novel ARSig is a promising independent prognostic predictor for STS. Furthermore, it is proved that the novel ARSig is relevant to the immune landscape, TMB, immunotherapy, and chemotherapy sensitivity in STS. Encouragingly, we also validate that the signature ARGs are significantly dysregulated in STS, and ARDB2 and SRPK1 are closely connected with the malignant progress of STS cells.

Conclusion: In sum, we construct a novel ARSig for STS, which could act as a promising prognostic factor for STS and give a strategy for future clinical decisions, immune landscape, and personalized treatment of STS.

KEYWORDS

soft tissue sarcoma, angiogenesis, prognosis, immune landscape, immunotherapy

Background

Sarcomas are a class of malignant tumors originating from mesenchymal tissue, about 80% of which originate from soft tissue and 20% from bone (1). Among them, soft tissue sarcoma (STS) comprises more than 70 histological subtypes, and the most frequently observed subtypes are leiomyosarcoma, liposarcoma, synovial sarcoma, and rhabdomyosarcoma (2). Although STS is relatively rare, it has a high lethality. According to statistics, more than 5,800 sarcoma patients die yearly in the United States, accounting for 40% of new cases (3). Since it the highly aggressive with early relapse and metastasis, the clinical outcome of STS is not ideal (4). Previous studies have demonstrated that the 5-year survival rate after diagnosis of STS is only 55.5-56.5%, and the patients with metastasis or recurrence are only about 20% (3, 5). Overall, the prognosis of the patient with STS remains dismal, and the development in recent years seems to have gotten stuck in a bottleneck. Therefore, it is urgent to find reliable biomarkers for early diagnosis, risk stratification, and prognosis prediction of STS.

Angiogenesis is the process of forming new blood vessels from pre-existing ones, which offers an adequate metabolic supply and nutrients for tumor growth and is widely considered to play an essential role in tumorigenesis and development (6). With the sustained rapid cellular proliferation and a high metabolic rate of tumor cells, the rapid development of new vascular networks is often required, which is driven by angiogenic factors such as the vascular endothelial growth factor (VEGF) family, hypoxia-inducible factors (HIFs), and fibroblast growth factors (FGFs) (7). Tumor angiogenesis not only supplies nutrients and natural migration pathways for tumors but also promotes tumor progression and regulates the tumor microenvironment (8). Accordingly, targeted tumor angiogenesis therapy has been investigated as a potential anti-tumor therapeutic approach. For instance, anlotinib, a multikinase angiogenesis inhibitor, shows an anti-tumor ability in several STS entities (9). In addition, the identification of promising angiogenesis-related markers and signatures has also been pursued as an attractive strategy for tumor diagnosis and prognostic evaluation. Yuan Yang et al. established a prognosis signature rely on angiogenesis-related genes (ARGs), which can help to predict prognosis, immune infiltration status, and chemotherapy sensitivity in hepatocellular carcinoma (10). However, it remains unclear whether angiogenesis-related signatures (ARSig) can be used in the prognosis and therapy prediction of STS.

Herein, we first constructed a novel signature for STS based on the ARGs, which exhibited excellent predicted performance for the prognosis of STS. Subsequently, the functional enrichment analysis was conducted to investigate the underlying mechanisms. Additionally, the relationships between the ARSig and the tumor immune microenvironment, immune therapy response, and the sensitivity of chemotherapeutic agents were investigated using a serial bioinformatic analysis. It may provide a promising predictor for prognosis prediction and clinical management of STS.

Methods

Data collection

The expression profile, copy number variation (CNV), somatic mutation, and clinical characteristics of the STS cohort were downloaded from The Cancer Genome Atlas database (TCGA, https://www.cancer.gov/aboutnci/organization/ccg/research/structural-genomics/tcga). The individual lacking survival information and other clinicopathological features were excluded from subsequent analysis, and the R package "GeoTcgaData" was utilized to convert ensemble ids to gene symbols. In addition, the expression and clinical data of the three independent cohorts (GSE17674, GSE21050, and GSE71118) were extracted from the Gene Expression Omnibus (GEO, https://www.ncbi.nlm.nih.gov/geo/) database. The clinical information of the above patients is shown in Tables S1-S3. The R package "AnnoProbe" was applied to map probes, and the R package "limma" was applied to calculate the average values of multiple probes. Among them, the GSE17674 gene set was utilized to identify differentially expressed ARGs, while GSE21050 and GSE71118 cohorts were considered external validation cohorts for the validation analysis. For normalization, the RNA-sequencing data was converted by log2. The ARGs were obtained from previous literature, and their detailed information is shown in Table S4 (11, 12).

Identification of differentially expressed ARGs in STS

The R package "limma" was utilized to screen the differential expressed gene with $|\log2FC| \geq 1$ and false discovery rate-adjusted P-value ≤ 0.05 (13, 14). Then, the Venn graph was used to confirm

the DEARGs. The visualization used the volcano plots and heatmaps based on the R package "ggplot2" and "heat map." The principal component analysis (PCA) was performed to explore the distribution differences of samples.

Screening of DEARGs related to the prognosis of STS

To explore the relevance between the DEARGs and the prognosis of STS, we applied the univariate COX regression analysis screening the DEARGs related to prognosis in STS. The screen criteria were set as P-values < 0.05, and these prognostic DEARGs were selected for subsequent signature construction.

Derivation of angiogenesis-related signatures

All TCGA-STS cohorts (n=260) were randomly split into the training cohort (n=130) and testing (n=130) cohort by "caret" package in R software. In the training cohort, the least absolute shrinkage and selection operator (LASSO) regression analysis was performed to identify candidate signature ARGs from the prognostic DEARGs. Subsequently, the candidate signature ARGs were included in the multivariate Cox regression analysis to construct the optimal ARSig. The ARSig risk score of each STS individual was computed as the following: ARSig risk score = β_i*X_i (β_i and X_i represent the regression coefficients and expression level of gene i, respectively). Next, every STS cohort was divided into high- and low-risk groups according to the median risk score of the training cohort. To compare the difference in the overall survival (OS) between the distinct ARSig risk groups, we then performed Kaplan-Meier (KM) survival analysis using the "survival" package. In addition, the receiver operating characteristic (ROC) curve and the area under the curve (AUC) were used to assess the predictive accuracy of the novel ARSig (15). The distribution of ARSig risk score and survival status were plotted in R software.

Evaluation and validation of the novel ARSig

To estimate the credibility of the novel ARSig, we performed the internal and external validation based on the training cohort, the entire cohort, GSE21050, and GSE71118. The above analyses were also conducted in the internal and external validation cohorts. Moreover, the subgroup clinical survival analysis based on different clinical features was performed to investigate the general applicability of the novel ARSig. To assess whether the novel ARSig was an independent indicator of OS in STS, we performed univariate and multivariate Cox regression analyses by combining multiple clinical characteristics. In addition, prognostic signatures for STS based on gene expression were systematically searched from PubMed for predictive performance comparison. Table S5 includes previously published prognostic models collected in this study.

Identification of DEGs and functional enrichment analysis

We performed differential expression analysis and functional enrichment analysis to explore the difference in molecular function between the distinct risk groups. Initially, the differentially expressed genes (DEGs) were screened using the limma package. The criterion for screening DEGs was false discovery rate-adjusted P-value < 0.05 and | logFC | > 0.585. Also, the volcano and heat map was applied to visualize the differential expression analysis results. Subsequently, the functional enrichment analysis based on these DEGs was performed utilizing the "clusterProfiler" package, including Gene Ontology (GO) and Kyoto Encyclopedia of Genes and Genomes (KEGG) analysis (16). The functional enrichment analysis results were visualized using the bubble plot.

Identification of top ten hub genes

The "GOSemSim" package was used to conduct the Friend analysis for screening the hub gene (17). The association between the signature ARGs and each hub gene was investigated utilizing Pearson's correlation analysis. Then, the difference in the expression of these hub genes between the low- and high-risk groups was compared. The KM survival analysis was applied to explore the relationship between the expression of each hub gene and the OS of patients with STS.

Gene set enrichment analysis and Gene set variation analysis

To identify the enriched cellular pathways in the high- and low-risk STS cohort, we performed GSEA and GSVA analyses (18, 19). For GSEA, the KEGG gene set (c2.cp.kegg.v7.4.symbols.gmt) was extracted from The Molecular Signatures Database. Then, the GSEA was carried out using the "clusterProfiler" package, and the result was visualized using the R software. Meanwhile, the R package "GSVA" was applied to conduct GSVA analysis, and the limma package was employed to compare the difference in the enriched pathways between the low- and high-risk groups. The pathways with |logFC| > 0.15 and false discovery rate-adjusted P-value < 0.05 were considered significantly enriched pathways and illustrated in clustered heat maps.

Relationship of ARSig with Tumor Microenvironment, immune checkpoints, and immune cell infiltration in STS

Besides, the association of the novel ARSig with TME and Immune Cell Infiltration was explored in our study. First, we assessed the TME score using the ESTIMATE (Estimation of Stromal and Immune cells in Malignant Tumor tissues using Expression data) algorithm (20). The TME score consists of immune, stromal, and tumor purity scores. Then, the CIBERSORT algorithm was utilized to assess the abundance of

immune infiltrating cells (21). Generally, the immune checkpoint gene expression is closely associated with the sensitivity of immunotherapy. Therefore, we obtained the immune checkpoints from previous literature and compared their expression level between the distinct risk groups. Furthermore, the connection between the TME score and immune cell infiltration with the prognosis of STS was investigated by KM survival analysis.

Mutation and CNV analysis

To explore the relationships between the ARSig and somatic mutations, we analyzed mutation annotation data from the TCGA database using the "maftools" package. Next, the tumor mutation burden (TMB) scores for each STS patient were calculated, and the difference in the TMB scores between the two risk groups was compared by statistical analysis. In addition, the mutations of the genes with mutation Top 20 in the low- and high-risk groups were visualized using waterfall plots. Furthermore, we analyzed the association of the ARSig risk scores with the cancer stem cell (CSC) index.

Immunotherapy response and drug sensitivity analysis

To further guide the treatment selection for STS, we assess the responses to immunotherapy and chemotherapeutic agent in STS. The response to immunotherapy inhibitors (anti-CTAL-4 and anti-PD-L1) of STS patients in the distinct risk groups was evaluated by the Subclass Mapping (SubMap) algorithm (22). The Bonferroni correction was employed to correct the P-value of the test level, and the Bonferroni P-value less than 0.05 was considered a statistical significance. For chemotherapy drug sensitivity comparison, the R package "pRRophetic" was applied to determine the half maximal inhibitory concentration (IC50) (23). Then, the Wilcoxon sign-rank test was applied to compare the IC50 of chemotherapy agents between the two different risk groups.

Establishment of a predictive nomogram

Based on the multivariate Cox progression analysis result, a nomogram composed of independent prognostic factors was constructed using the R package "rms." (24). Additionally, the calibration curve and decision curve analysis (DCA) draws utilizing the R packages "caret" and "rmda", which could assess the predictive reliability of the nomogram. Moreover, we further conducted the ROC curve to estimate the predictive performance of the nomogram by using the "survival ROC" package in R software.

Cell lines and cell culture

The sources of the cell lines used in the present study were all described in previous research (25). All the cell lines were cultured in Dulbecco's modified Eagle's medium (DMEM, Procell) containing 10% fetal bovine serum and 1% penicillin-streptomycin solution. Cell cultures were performed at 37°C in a humidified atmosphere containing 5% CO2.

Quantitative reverse transcription PCR

Total RNA was collected using RNA Express Total RNA Kit (New Cell & Molecular Biotech), and RNA was reverse transcribed utilizing the Revert Aid First Strand cDNA Synthesis Kit (Thermo Scientific), according to the manufacturer's instructions. Next, RT-qPCR was performed by Hieff qPCR SYBR Green Master Mix (High Rox Plus) (YEASEN Biotech Co., Ltd). The GAPDH was applied for the internal reference for normalization. The relative expression of each gene was calculated with the $2^{-\Delta\Delta CT}$ method. The specific primer sequences used in the present study are shown in Table S6.

Cell transfection

Negative control (NC), ADRB2, and SRPK1 siRNAs were purchased from Hanbio (Shanghai, China). SW872 cells were seeded in a 6-well plate. When cell area reached 50%, 50nmol NC, ADRB2, and SRPK1 siRNAs were separately transfected into cells using 5uL Lipofectamine 2000 reagent (Invitrogen) for 12 hours. The sequence of siRNA used in our research is illustrated in Table S7.

Cell proliferation assays

Cell counting kit-8 (CCK-8, New Cell & Molecular Biotech) was used to detect the viability of SW872 cells. SW872 cells were placed in a 96-well plate (2000 cells per well) and incubated overnight. Cells were transfected and cultured for indicated times (0, 24, 48, 72, and 96 hours). In each well was added 10ul CCK-8 solution combining 90ul DMEM containing 10% FBS. After 1.5 hours of incubation, the optical absorbance at 450nm was measured with a microplate reader.

5-Ethynyl-2′-Deoxyuridine assays

EdU assays (RiboBio) were performed to determine cell proliferation. After transfection, SW872 cells were seeded in 14 ul slippers in 12-well plates. After 48 hours of incubation, cells were cultured using 50um EdU reagent (diluted with DMEM containing 10% FBS at 1:1000) for 2 hours at 37°C. Then, fixed with 4% paraformaldehyde (PFA) and stained with Hoechst solution (diluted with DMEM containing 10% FBS at 1:100).

Colony-forming assays

The colony-forming assays were carried out for cell proliferation detection. After transfection, 1000 SW872 cells were

seeded in 6-well plates and cultured for 2 weeks. Cells were fixed in 4% PFA for 15 minutes and stained with 0.2% crystal violet for 15 minutes.

Wound healing assay

Wound healing assays were performed to reveal the migration capacity. SW872 cells were placed in different 6-well plates and underwent transfection when the cell area reached 70%. When cell confluence reached 100%, wound healing assays were performed using a 100ul pipette tip to scratch the cells to make a separate wound. Afterward, wounded cells were washed with PBS, and the remaining cells were cultured in DMEM containing 2% FBS. Migration capacity was evaluated by light microscope by quantifying the area covered by migrated cells at 0 and 48 hours.

Transwell assays for migration

After the above-mentioned transfection, Transwell migration assays were carried out using a 24-well chamber (Corning). Cells (2 x 10^4) were suspended in 100ul DMEM and added to the upper layer of chambers. 700ul DMEM containing 10% FBS was added below the chambers. Cells were cultured for 24 hours at 37°C, and then the upper chambers were cleaned with cotton swabs. SW872 cells penetrated and adhered to the bottom of the chamber and were fixed with 4% PFA for 15 min and stained with 0.5% crystal violet for 15 min. Chambers were imaged under a microscope.

Transwell assays for invasion

After the transfection, Transwell invasion assays were used to examine cell invasion ability. First, 50ul Matrigel (diluted using DMEM containing 10% FBS at 1:8) was loaded in a 24-well chamber (Corning). DMEM containing 10% FBS was added to the lower chamber, and suspension of DMEM containing 5 x 104 cells was added to the upper chamber. After incubation for 24 hours at 37°C, the upper chambers were cleaned with cotton swabs. SW872 cells penetrated and adhered to the bottom of the chamber and were fixed with 4% PFA for 15 min and stained with 0.5% crystal violet for 15 min. Chambers were imaged under a microscope.

Statistical analysis

The R software (version 4.0.1) and GraphPad Prism (version 9.0.0) were used for statistical analysis. The difference between the two distinct risk groups was compared with the Wilcoxon test. A Chi-square test was used to analyze the clinicopathological characteristics of the two risk groups. The difference in the overall survival rate of STS between the high- and low-risk groups were compared using the Log-rank test. The expression of signature ARGs between normal and STS cell line was evaluated by one-way analysis of variance (ANOVA). The Pearson correlation test was applied to explore the correlation between two variables. A P-value less than 0.05 represent a statistically significant difference.

Results

Establishment and validation of the novel ARSig for STS

The flow chart of our study is presented in Figure S1. Initially, we identify 5499 DEGs (3900 upregulated and 1599 downregulated) in the STS cohort through differential expression analysis. The volcano and heat map of these DEGs is presented in Figures 1A, B. The PCA analysis indicates that the STS and normal tissue samples could be clearly separated by the combined expression of these DEGs (Figure 1C). Next, we obtained 1605 ARGs from previous studies. From the intersection between DEGs and ARGs, we identify 511 DEARGs in STS, including 403 upregulated and 108 downregulated ARGs (Figure 1D). The upregulated and downregulated ARGs are shown as cluster heatmaps and volcano plots in Figure S2. Subsequently, we find 116 DEARGs relevant to the prognosis of STS by univariate analysis (Table S8), which are enrolled for the angiogenesis-related signature construction. For ARSig construction, we first screen the candidate prognostic DEARGs through LASSO Cox regression analysis (Figures 1E, F). Next, the multivariate Cox regression analysis is applied to optimize the signature (Figure 1G). As a result, the novel ARSig composed of five prognostic DEARGs (ADRB2, SRPK1, SQSTM1, SULF1, and MAGED1) is established. According to the multivariate analysis results (Table S9), the formula of ARSig risk score calculation is as follows: Risk score = SRPK1* 1.15110386815651 - ADRB2* 0.420077308273549 - SQSTM1* 0.428083645117686 - SULF1* 0.176496892249047 + MAGED1*0.3588603726472 31. Figures 1H, I indicates the risk score and survival status distribution of each STS individual. With the risk score increasing, the number of STS deaths also increases. Consistently, the KM analysis suggests that the STS patients with a lower risk score displayed a significantly improved survival rate than those with a higher risk score (Figure 1J). Furthermore, the AUC of the ROC curve for 1-, 3-, and 5-year survival was 0.835, 0.843, and 0.801, respectively, which indicated the predictive power of the novel ARSig (Figure 1K).

To estimate the predictive robustness of the novel ARSig, we performed internal validation in the testing and the entire STS cohort. As shown in Figures S3-4, we observed similar results in the training and the testing STS cohort. We also use the external cohort (GSE21050 and GSE71118 cohort) to verify the predictive performance of the novel ARSig (Figures 1L-S). Consistent with the results from the internal cohort, the distribution plot and Kaplan–Meier survival analysis indicated that the STS in the low-risk group exhibit a better prognosis than those in the high-risk groups. In aggregate, these results confirmed that the novel ARSig had a promising performance in predicting the prognosis of patients with STS.

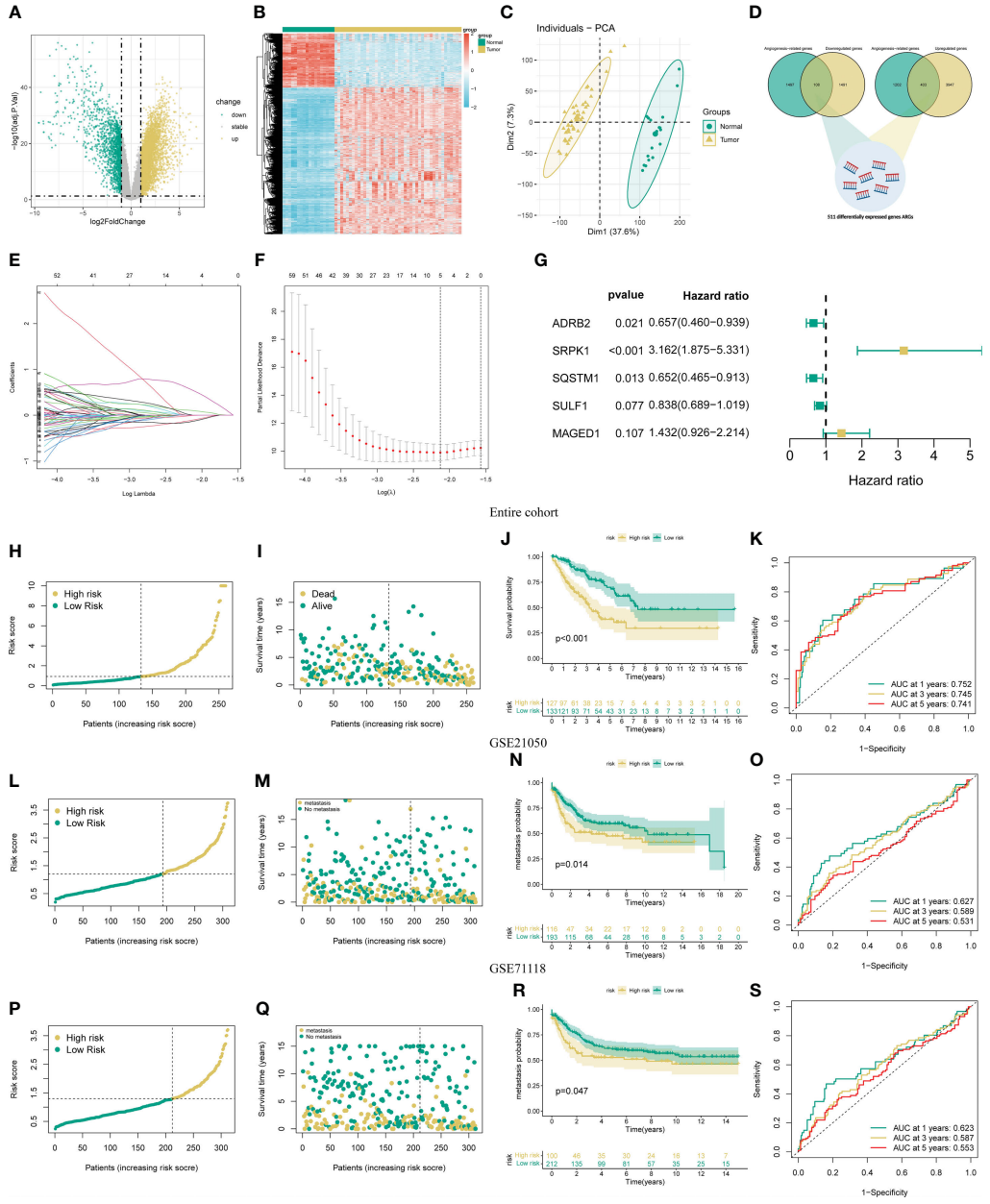

FIGURE 1
Development and validation of the novel ARSigs for the STS cohort. **(A)** Volcano plot of the DEGs **(B)** Heatmap of the DEGs among tumor and normal tissue. **(C)** Principal component analysis (PCA) based on DEGs to distinguish STS from normal tissues. **(D)** Venn diagram among DEGs and ARGs. **(E)** LASSO regression analysis of 116 prognostic DEARGs **(F)** Cross-validation method to select candidate signature genes. **(G)** Multivariate Cox regression analysis of signature gene. **(H-I)** Risk score curve and survival status distribution of STS cohort in the entire group. **(J)** KM survival analysis of the high and low-risk groups in entire groups. **(K)** Assess the prognostic performance of the novel ARSig using the ROC curve in the entire group. **(L-M)** Risk score curve and survival status distribution in the GSE21050 cohort. **(N)** KM survival analysis of the high and low-risk groups in the GSE21050 cohort. **(O)** Assess the prognostic performance of the novel ARSig using the ROC curve in the GSE21050 cohort. **(P-Q)** Risk score curve and survival status distribution in the GSE71118 cohort. **(R)** KM survival analysis of the high and low-risk groups in the GSE71118 cohort. **(S)** Assess the prognostic performance of the novel ARSig using the ROC curve in the GSE71118 cohort.

Evaluating the performance of novel ARSig

To determine the prognostic generality of the novel ARSig, we further compared the risk score between distinct clinical subgroups and carried out a subgroup KM survival analysis. There was no significant difference in the risk score distribution between the distinct clinical subgroup, indicating that the novel ARSig was relatively independent of the clinical characteristics (Figures 2A-E, S5). In addition, the subgroup survival analysis demonstrates that the low-risk group patients have an improved OS comparing to the high-risk subgroup in distinct clinical features (age, gender, margin status, metastasis status, and new tumor events. Figures 2F-J). Importantly, we also implement univariate and multivariate Cox regression analyses to investigate whether the novel ARSig is an

independent prognostic factor for STS patients. The univariate analysis indicates that the risk score, age, margin status, metastasis, and new tumor events are remarkably associated with OS (Figure 2K). Encouragingly, the multivariate analysis result further confirmed that the ARSig risk score is an independent prognostic indicator affecting the OS of STS (Figure 2L). Moreover, we also found that the c-index of our signatures based on ARGs performs better than almost all previous signatures (Figure S6).

To facilitate the clinical application of the novel ARSig, we further construct a nomogram incorporating the ARSig risk score and independent clinical factor. According to the nomogram, we could precisely estimate the 1-year, 3-year, and 5-year survival rates of each STS individual (Figure 2M). Encouragingly, the calibration curves exhibits that the actual values of the 1-, 3-, and 5-year OS match those predicted by the nomograph, indicating the nomogram we built is reliable and accurate (Figure 2N). The 1-, 3-, and 5-year area under the ROC curve of the nomogram are 0.854, 0.763, and 0.787, respectively (Figure 2O). Also, the DCA demonstrates that the nomogram has the best clinical net benefit comparing with other variables (Figure 2P). Overall, these findings show that the novel ARSig is successfully constructed and exhibited reliable and has excellent performance for the OS prediction of STS.

The signature ARGs in STS

Subsequently, we perform the KM survival analysis to investigate the respective prognostic value of each signature ARG. Similarly, we find that the STS patient with mitigation of ADRB2 and SQSTM1 has poorer OS (Figures 3A, B), while the augmented levels of MAGED1, SRPK1, and SULF1 seem to account for a better prognosis in STS (Figures 3C-E). Collectively, these results imply that the abnormal expression of these signature ARGs might be relevant to the prognosis of STS.

Functional enrichment analysis and angiogenesis-related hub genes in STS

To comprehend the difference in the functional pathways among the distinct risk groups, we identify 1006 DEGs between the low- and high-risk groups (Figures 3F, G). Then, the functional enrichment analysis is conducted based on these DEGs. The GO analysis results indicate that these DEGs are mainly enriched in immune-related functions, like humoral immune response, humoral immune response mediated by circulating immunoglobulin, regulation of humoral immune response, immunoglobulin complex, and immunoglobulin receptor binding (Figure 3H). Also, Figure 3I shows the top twenty pathways these DEGs enriched. Among them, the Human T−cell leukemia virus 1 infection, Viral protein interaction with cytokine and cytokine receptors, and Antigen processing and presentation are immune-related, while the Cell adhesion molecules are associated with tumorigenesis. Moreover, we define ten potential hub genes (AHNAK2, GPC2, DBNDD2, OLFM1, SCRG1, TNFAIP8L2, FILIP1L, CYSTM1, PARM1, and NCAPG) in the identified angiogenesis-associated GO progress through the Friend analysis (Figure 3J). We observe a remarkably co-expression relevance between the signature ARGs and these ten hub genes (Figure 3K). Almost all these hub genes display an abnormal expression in the STS compared to normal tissue, except for SCRG1 (Figures 3L-U). Equally, the KM survival also suggests that all ten hub genes exhibit significant prognostic effects in STS (Figure S7).

Exploring the underlying pathways in STS

To further verify the molecular mechanism difference between the distinct risk groups, we perform the GSEA and GSVA analysis. The GSEA shows that the high-risk STS patient mainly associated with tumorigenesis pathways, such as basal cell carcinoma, cell cycle, DNA replication, hedgehog signaling pathway, and Wnt signaling pathway (Figure S8A). Meanwhile, those mainly enriched pathways in the low-risk group are relevant to immunity function (Figure S8B). In the following GSVA analysis, we obtain results consistent with the previous GSEA, such as the low risk mainly concentrated in complement and coagulation cascades, chemokine signaling pathway, and graft versus host disease (Figure 4A). Altogether, these results provide promising clues for inferring the underlying mechanism of the novel ARSig regulating STS progress.

TME and immune cell infiltration analysis

Given these above functional enrichment analysis results and the critical role of tumor immunity in tumor development, we further investigate the immune status among the various ARSig risk groups. Initially, the ESTIMATE analysis indicates that the low-risk STS patients displayed an enhanced immune and stromal score and a lower tumor purity score, hinting the STS cohort in the low-risk group has a better immune infiltration (Figures 4B-D). Also, we find that both the patients with an augmented immune and stromal score or an attenuated tumor purity score exhibits an ameliorated prognosis (Figures 4E-G). Subsequently, we evaluate the infiltrate proportion of the 22 types of immune cells in STS by applying the CIBERSORT algorithm (Figure S9A). We observe that the abundance of naive B cells, CD8 T cells, CD4 memory resting T cells, Monocytes, M1 Macrophage, resting dendritic cells, and resting mast cells are elevated in the low-risk groups, while the infiltration level of $CD4^+$ T cells, Resting NK cells, M0 Macrophage, and activated dendritic cell in the low-risk group is lower than those in the high-risk groups (Figures 4H, I). Besides, there are remarkable correlations between the ARSig risk score and signature ARGs with the proportion of the immune cell infiltration (Figures 4J; S9B). Notably, the KM survival demonstrates an enhanced infiltration level of naive B cells, activated NK cells and CD8 T cells are relevant to an improved prognosis in STS (Figures S9C-E). Contrary, the patients with an increasing abundance of M0 Macrophage, M2 Macrophage, and CD4+ T cells have a poorer OS (Figures S9F-H).

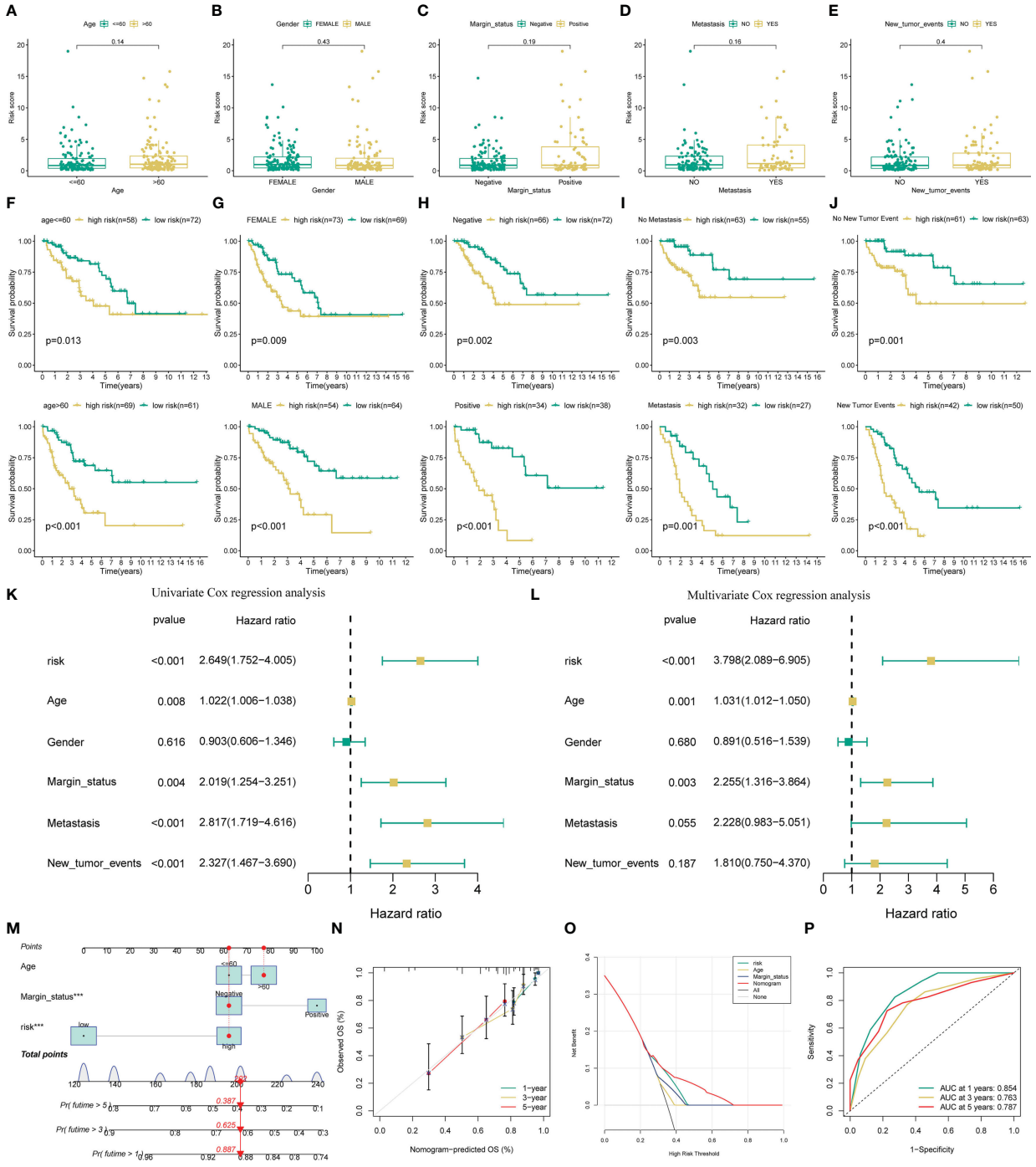

FIGURE 2
Evaluation of the predictive performance of the novel AGSig. **(A-E)** Boxplots of the risk score in STS were stratified by age, gender, margin status, metastasis, and new tumor events, respectively. **(F-J)** Prognostic value of risk score in patients with different ages, gender, margin status, metastasis, and new tumor events, respectively. **(K)** Univariate Cox regression analysis of angiogenesis-related risk score and clinical characteristics. **(L)** Multivariate Cox regression analysis of angiogenesis-related risk score and clinical characteristics. **(M)** A nomogram based on ARSig risk score and independent clinical factor for predicting 1-, 3-, and 5-year OS of STS. **(N)** Calibration curves. **(O)** The ROC curves for nomogram. **(P)** Decision curve analysis plot.

Association of the novel ARSig with tumor mutation burden

Considering the importance of CSC and TMB in tumor generation and development, we explore their association with the novel ARSig. Figures 5A–C indicates the relationship between ARSig risk scores and the CSC index. We find that risk score is positively correlated with the CSC index, and the STS patients with a lower CSC index exhibits an ameliorated prognosis. For TMB, the higher risk is correlated to an elevated TMB score (Figures 5D, E).

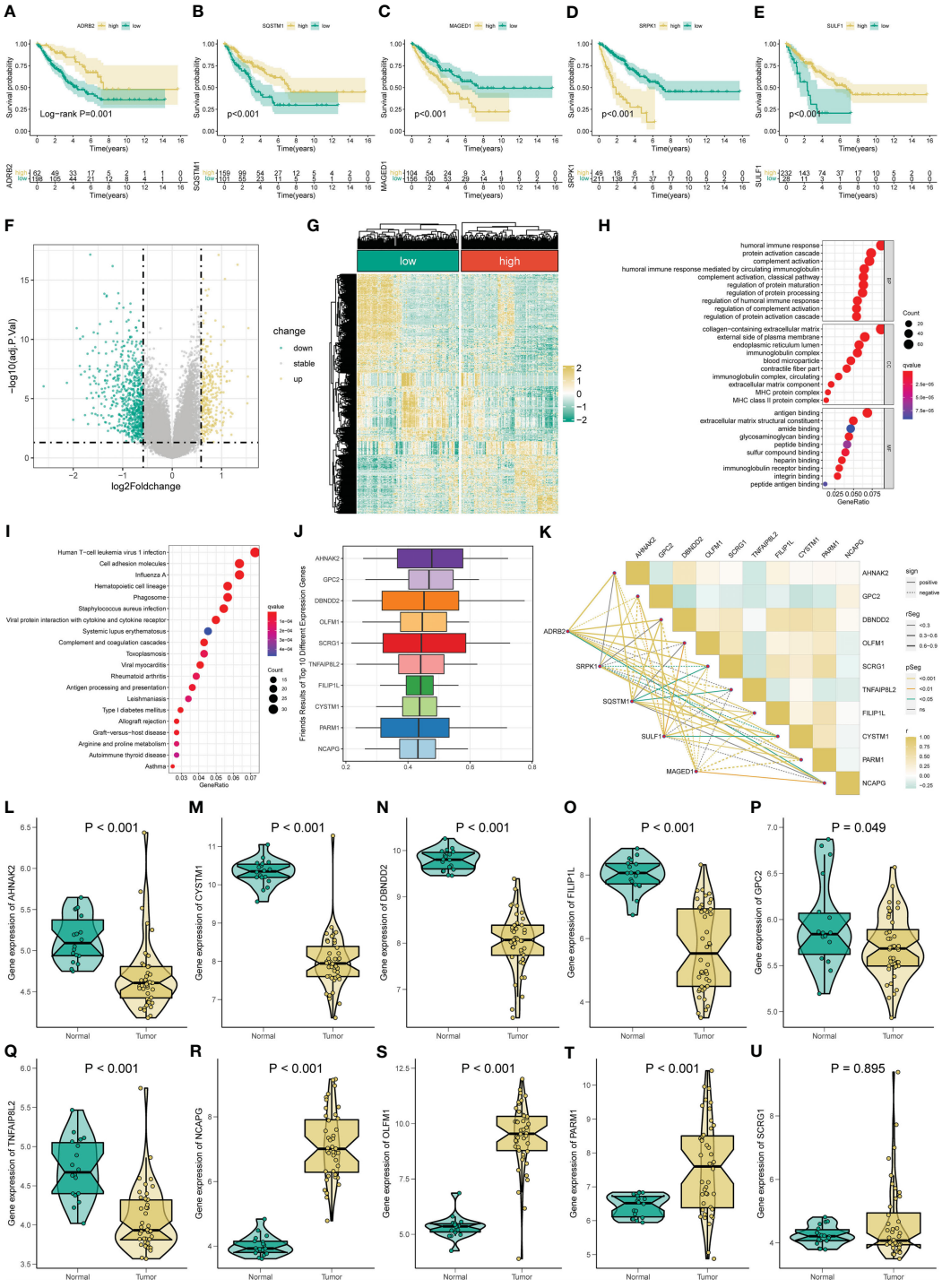

FIGURE 3
Gene functional enrichment analysis of differentially expressed genes between distinct risk groups. KM survival curves for ADRB2 **(A)**, SQSTM1 **(B)**, MAGED1 **(C)**, SRPK1 **(D)**, and SULF1 **(E)**. **(F-G)** The volcano plot and heatmap of DEGs among the low- and high-risk risk group. **(H)** GO enrichment analysis includes a biological process (BP), cellular component (CC), and molecular function (MF). **(I)** KEGG enrichment analysis indicates related genes and pathways. **(J)** The Friends analysis of GO-related genes. **(K)** The correlation between these ten hub genes and each signature ARG. **(L-U)** The expression of these ten hub genes in STS.

Also, the waterfall plot indicates that TP53, TTN, and RB1 are the top three mutation rate genes in the low-risk group (Figure 5F). Similarly, TP53 shows the highest mutation frequency in the high-risk group, followed by ATRX and MUC16 (Figure 5G). Then, we investigate somatic copy number alterations in these signature ARGs and hub genes. Among them, MAGED1, AHNAK2, and TNFAIP8L2 have widespread CNV increases, while OLFM1 and SCRG1 display CNV decreases (Figure 5H). The locations of the CNV alterations in these genes on their respective chromosomes are presented in Figure 5I. We further observe that the high-risk group

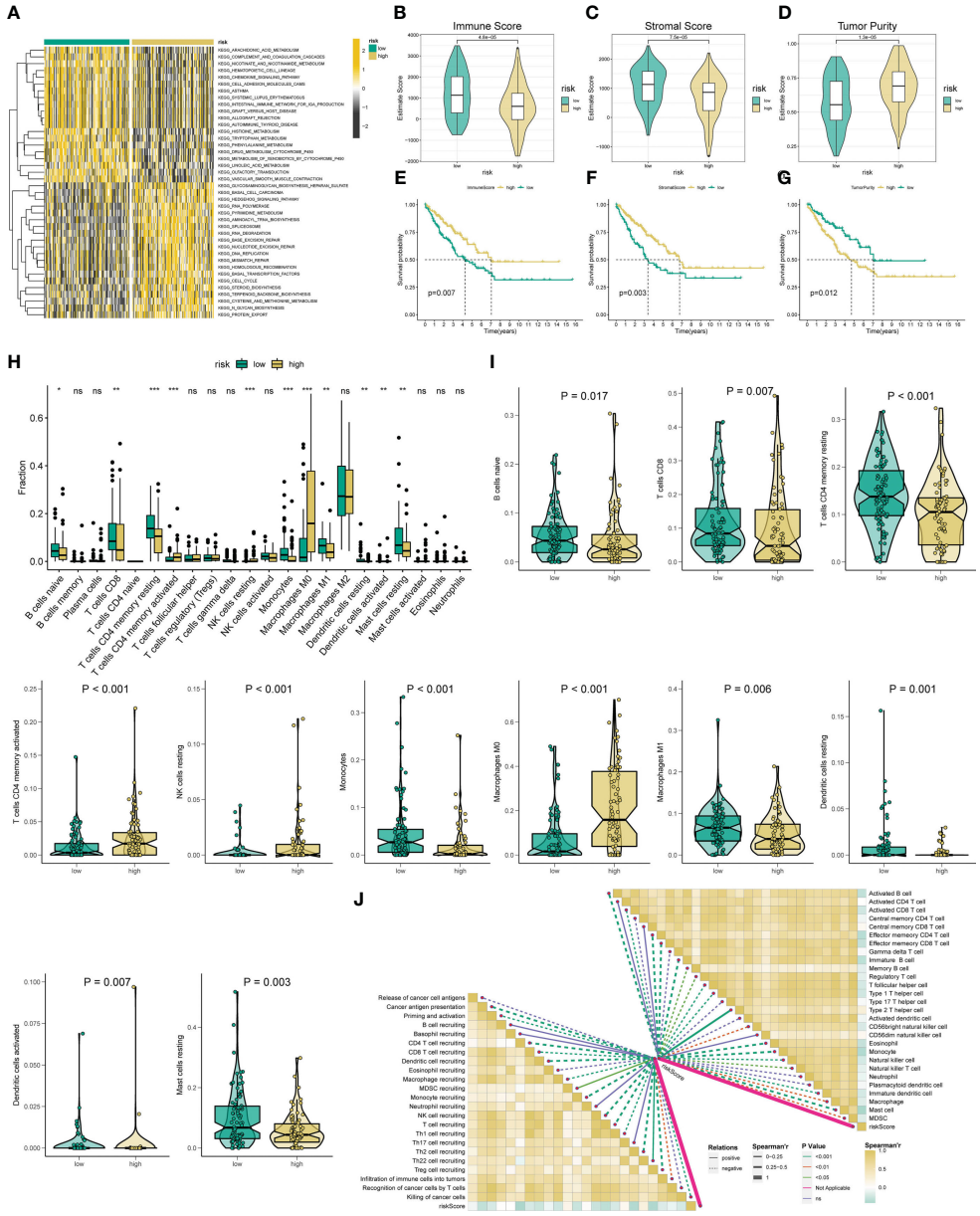

FIGURE 4
Analysis of immune status based on the angiogenesis-related risk score. **(A)** Heat maps of GSVA exhibit signaling pathways between low- and high-risk groups. **(B-D)** Comparison of immune, stromal, and tumor purity scores between the high- and low-risk groups. **(E-G)** Prognostic value of immune, stromal, and tumor purity score in STS. **(H)** The abundance of 22 infiltrating immune cell types in the two risk subgroups. **(I)** The proportion of B cells naive, T cells CD8, T cells CD4 memory resting, T cells CD4 activated, NK cell resting, Monocytes, Macrophage M0, Macrophage M1, Dendritic cell resting, Dendritic cell activated, and Mast cell resting in the different risk groups. **(J)** The correlation between the ARSig risk score and the infiltration of immune cells. * represent P < 0.05, ** represents P < 0.01, *** represents P < 0.001, and ns represent no significance.

company with an elevated frequency of copy number amplification compared to the low-risk group (Figures 5J, K).

Prediction efficacy of the immunotherapy and chemotherapy

Immune checkpoint modulators are known to play a critical role in tumor immunity and immunotherapy. We find that the expression of virtually all immune checkpoints is upregulated in the low-risk group compared with the high-risk group (Figure S10). Therefore, we further assess the response to immune checkpoint inhibitors (CTLA4-blocker and PD1-blocker) in the subgroup classified by ARSig risk score. As present in Figure 6A, the STS patients in the low-risk groups have a better response to PD1-blocker (Bonferroni P-value < 0.05). Equally, we estimate the response of the STS cohort to commonly used chemotherapeutic agents by comparing the difference in IC50 between the distinct

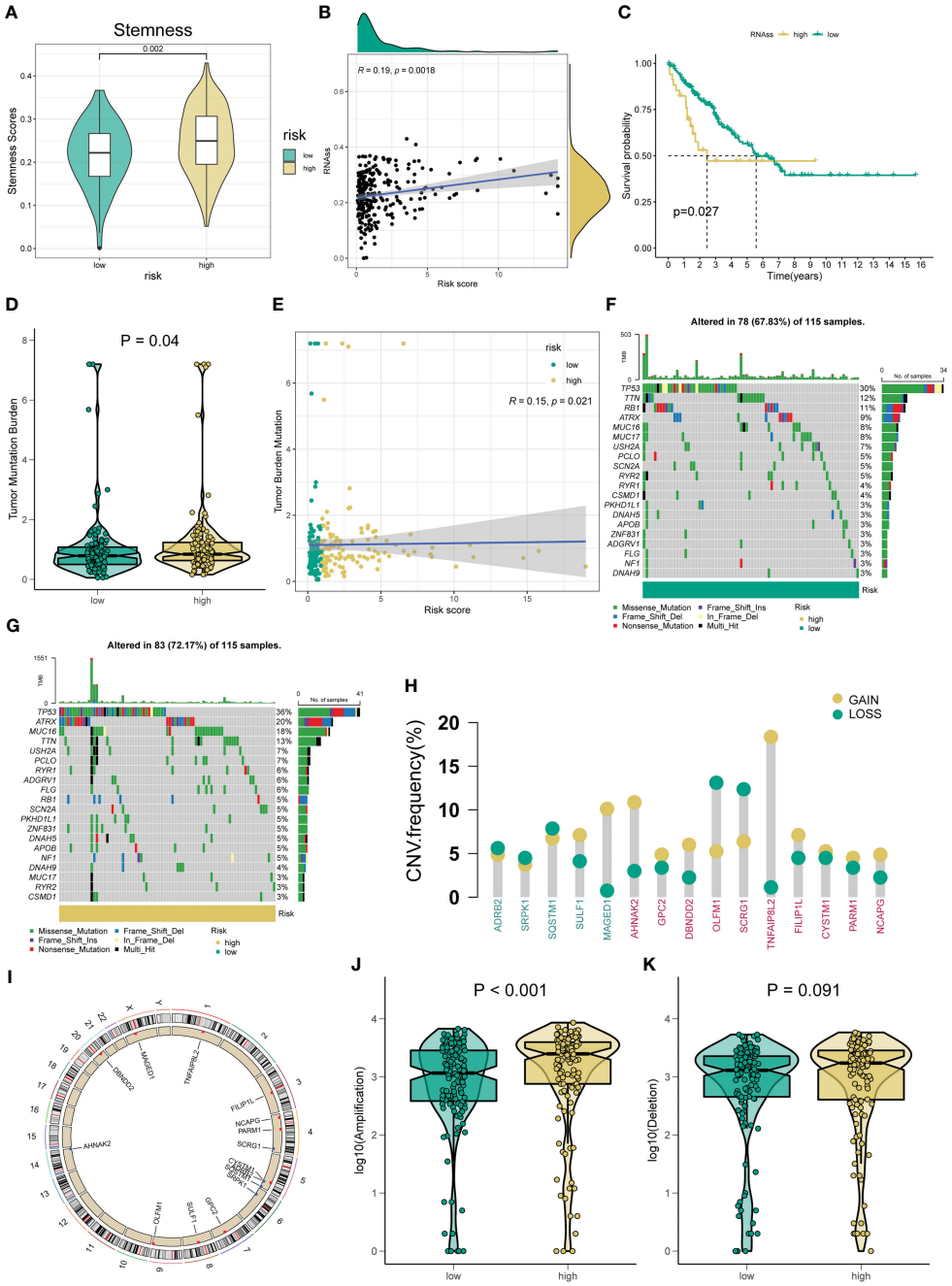

FIGURE 5
Correlation between the novel ARSig and Tumor mutation status. **(A-C)** The relationships between angiogenesis-related risk score and CSC index. **(D)** TMB score among different risk groups. **(E)** The Spearman correlation analysis of the angiogenesis-related risk score and TMB score. **(F-G)** The difference in Mutations between distinct risk groups (the top 20 mutated genes). **(H)** Frequencies of CNV gain, loss, and non-CNV among signature ARGs and ten hub genes. **(I)** The location of signature ARGs and ten hub genes on chromosomes. **(J-K)** The difference in CNV loss and gain between the low- and high-risk groups.

risk groups. The STS cohort in the low-risk group has a higher IC50 of axitinib, cisplatin, cytarabine, docetaxel, doxorubicin, gemcitabine, midostaurin, pazopanib, vinblastine, vinorelbine, and vorinostat than those in the high-risk group (Figures 6B-L). In contrast, the IC50 of lenalidomide, erlotinib, and gefitinib in the low-risk group is lower than those in the high-risk group (Figures 6M-O).

The effect of signature ARGs in STS

Importantly, we verify the expression of each signature ARG in the STS cell lines using RT-qPCR. As shown in Figure S11, we observe that the whole signature ARGs are significantly dysregulated in STS cell lines. Considering that ARDB2 and SRPK1 are aberrantly elevated in the STS, we further explore the

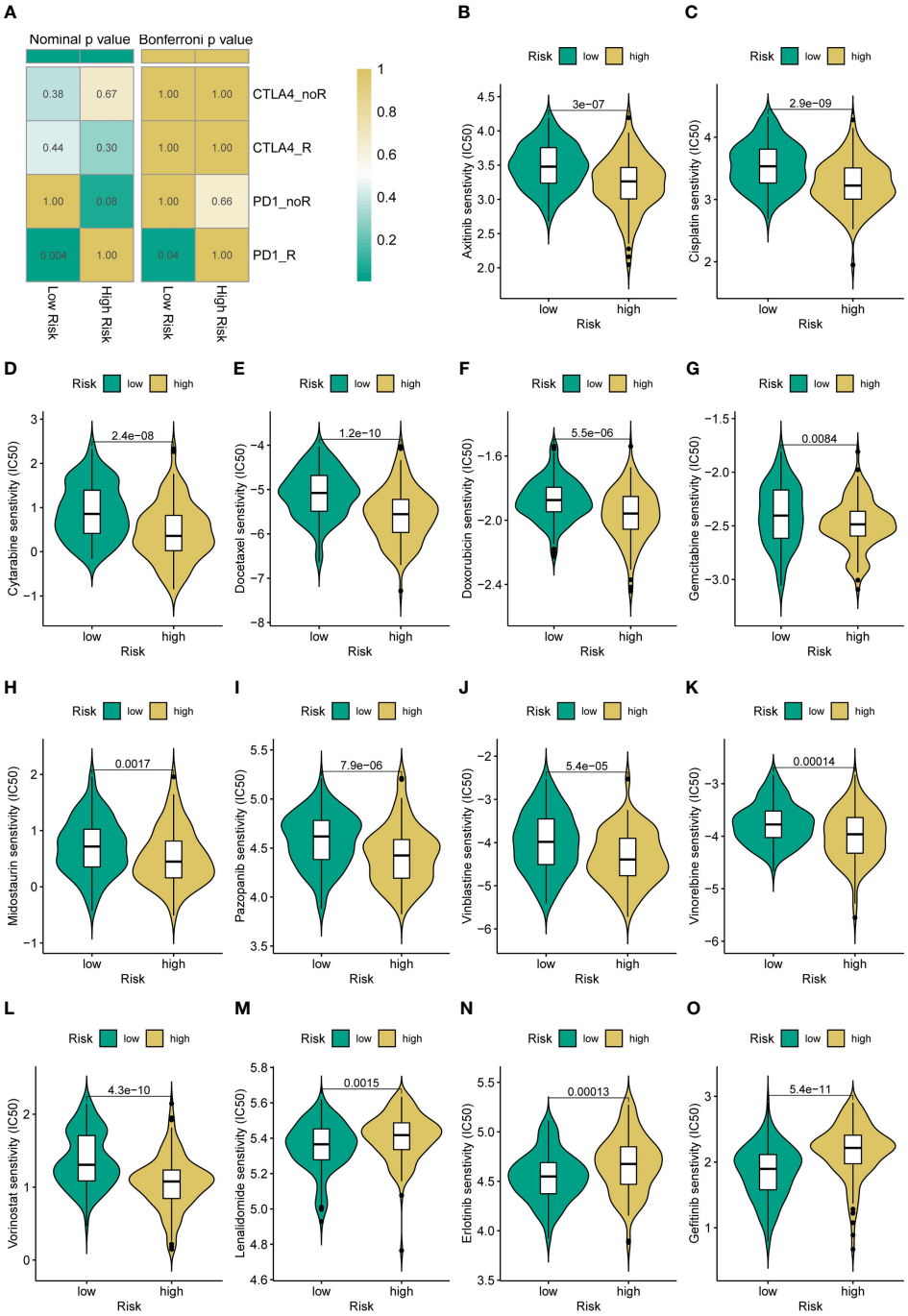

FIGURE 6
Different immunotherapy and chemotherapy sensitivity analyses. **(A)** The immunotherapy responses to immune checkpoint inhibitors in the STS cohort with a different risk score. **(B-O)** Relationships between ARSig risk score and chemotherapeutic sensitivity.

function of ARDB2 and SRPK1 in STS. As shown in Figures 7A, 8A, the expressions of SRPK1 and ARDB2 were significantly down-regulated in SW872 cells after siRNA transfection. The CCK8 results show that the attenuation of SRPK1 and ARDB2 could lead to the slowing down of the proliferation rate of SW872 (Figures 7B, 8B). Consistently, the colony-forming ability of SW872 is attenuated with the downregulation of SRPK1 and ARDB2 (Figures 7C, 8C). Also, compared to negative control groups, the percentage of EdU-positive cells exhibits a downward trend in the siRNA-SRPK1 and siRNA-ARDB2 groups (Figures 7D, 8D). On the other hand, the scratch test indicates that the moving distance of SW872 in the siRNA-SRPK1 and siRNA-ARDB2 group was significantly less than that of the control group (Figures 7E, 8E). Moreover, the transwell migration and invasion assay reveal that the SRPK1 and ARDB2 diminished could inhibit SW872 cell migration and invasion (Figures 7F, G, 8F, G). Hence, these above-mentioned results imply that the abnormal overexpression of ARDB2 and SRPK1 could promotes the malignant phenotype of

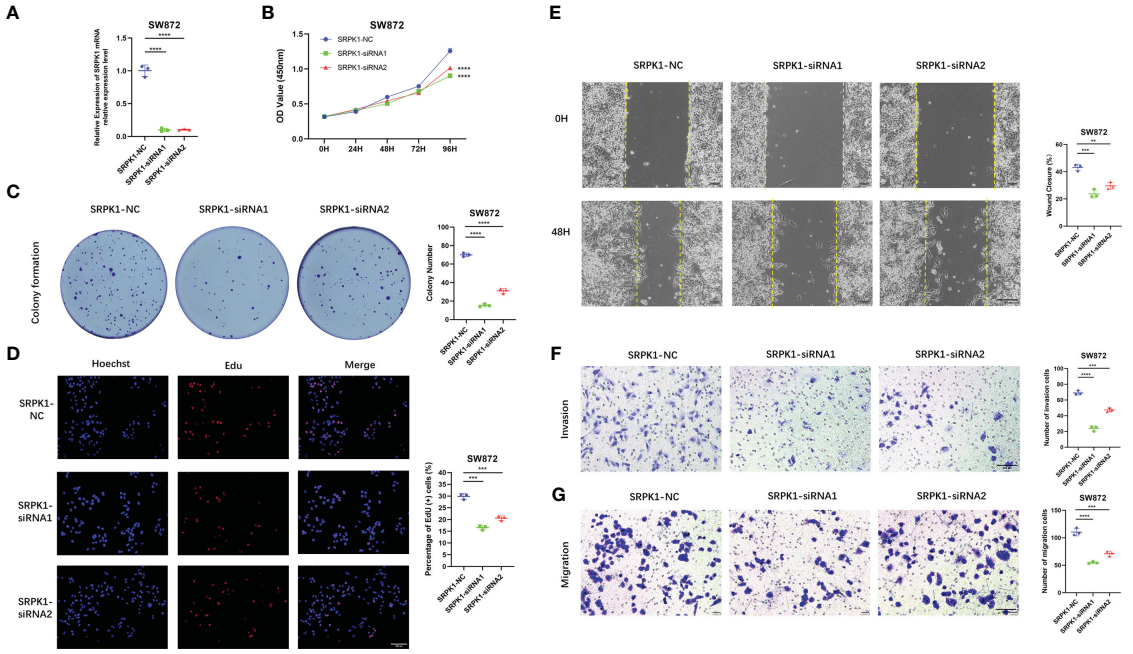

FIGURE 7
Down-regulated SRPK1 inhibits soft tissue sarcoma proliferation, migration, and invasion. **(A)** SRPK1 was transfected with siRNA for 48 hours. **(B)** The cell proliferation rate of NC, SRPK1-siRNA1, and SRPK1-siRNA2 groups were detected by CCK-8 assay. **(C)** Colony formation abilities in NC, SRPK1-siRNA1, and SRPK1-siRNA2 groups. Colony numbers were shown in the corresponding column at the right. **(D)** The cell proliferation rate of NC, SRPK1-siRNA1, and SRPK1-siRNA2 groups was detected using Edu-assay. Percentages of Edu-positive cells were quantified in corresponding columns at right. **(E, F)** The migration ability of NC, S SRPK1-siRNA1, and SRPK1-siRNA2 groups was illustrated by scratch tests and transwell assay for migration. **(G)** The invasion abilities of NC, SRPK1-siRNA1, and SRPK1-siRNA2 groups were demonstrated using transwell assay for invasion. ** represents $P < 0.01$, *** represents $P < 0.001$, and **** represents $P < 0.0001$.

soft tissue sarcoma cells, further validating our bioinformatic analysis results.

Discussion

STS is a heterogeneous malignant disease deriving from mesenchymal, constituting 1% of adult malignancies and 15% of malignant neoplasms in childhood (26). Since the aggressiveness, metastasis, and relapse of tumor, the overall survival rates of STS remain suboptimal. Therefore, it is critical to establish an effective prognostic biomarker for risk stratification and precision prognostic prediction of STS. Angiogenesis has been revealed to play a crucial role in carcinogenesis and progression, which is highly dependent on angiogenic cytokines (27, 28). For instance, the secretion of VEGF is essential to tumor vascularization, and its inhibition disrupts tumor progression (29). HIF1 is a heterodimeric protein consisting of HIF1α and HIF1β subunits, and it is also known to be an important stimulus for tumor angiogenesis (30). In addition, several recent research has demonstrated that the angiogenesis-related gene signature was closely linked to the prognosis of various cancer patients. Xin Qing et al. identified an angiogenesis-associated genes signature, contributing to predicting the prognosis, clinical characteristics and TME of gastric cancer (12). Similarly, the angiogenesis-related gene signature exhibited a promising ability for the prognosis and treatment response prediction of glioblastoma multiforme and will help the therapeutic strategies selection in glioblastoma multiforme (11). However, numerous studies have only evaluated the role of single ARGs in STS. The research systematically elucidates the holistic impact of the combinatorial of diverse ARGs is still lacking.

In the present study, we identified 116 DEARGs with prominent prognosis significance of STS. Subsequently, a novel ARSig consisting of five angiogenesis-associated genes was successfully established using LASSO, univariate, and multivariate COX regression analysis. The novel prognostic ARSig exhibited an effective ability to stratify the prognosis of STS. Our results show that the STS patients in the low-risk groups have an improved prognosis, while the prognosis of STS in the high-risk group is significantly poorer. Next, the prediction performance of the novel ARSig is further confirmed using the ROC curve, internal validation, and subgroup survival analysis. In addition, the univariate and multivariate Cox analysis demonstrate that the ARSig risk score is an independent prognostic predictor for the OS of STS. Encouragingly, a consistent validation result in predicting OS is also founded in the external cohort (GSE21050 and GSE71118), which further corroborate the reliability and potential of our signature. Herein, we construct a novel prognostic signature based on ARGs, which could be used as a reliable and independent marker to help conduct personalized prognostic evaluations in STS.

To further investigate the association of the novel ARSig with STS, we explore the difference in underlying mechanisms between the two distinct risk groups using GSEA and GSVA. Interestingly, we observe that the GSEA and GSVA results both show that the STS patients with a higher risk score mainly enriched in cell cycle, DNA

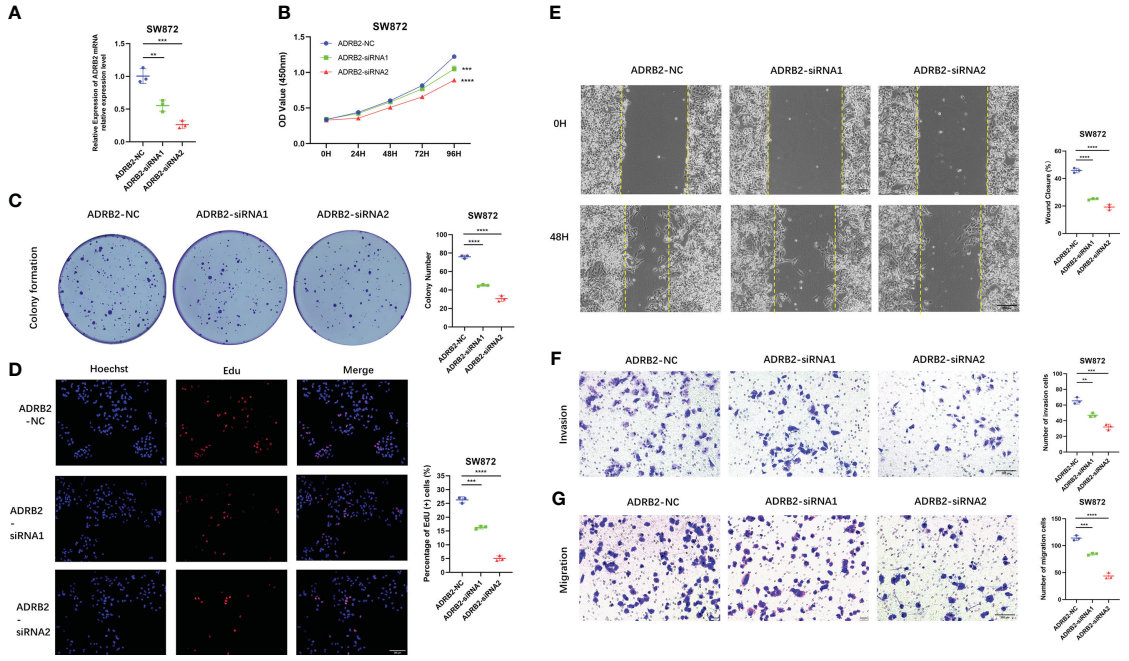

FIGURE 8
Down-regulated ADRB2 inhibits soft tissue sarcoma proliferation, migration, and invasion. **(A)** ADRB2 was transfected with siRNA for 48 hours. **(B)** The cell proliferation rate of NC, ADRB2-siRNA1, and ADRB2-siRNA2 groups was detected by CCK-8 assay. **(C)** Colony formation abilities in NC, ADRB2-siRNA1, and ADRB2-siRNA2 groups. Colony numbers were shown in the corresponding column at the right. **(D)** The cell proliferation rate of NC, ADRB2-siRNA1, and ADRB2-siRNA2 groups was detected using Edu-assay. Percentages of Edu-positive cells were quantified in corresponding columns at right. **(E, F)** The migration ability of NC, ADRB2-siRNA1, and ADRB2-siRNA2 groups was illustrated by scratch tests and transwell assay for migration. **(G)** The invasion abilities of NC, ADRB2-siRNA1, and ADRB2-siRNA2 groups were demonstrated using transwell assay for invasion. ** represents $P < 0.01$, *** represents $P < 0.001$, and **** represents $P < 0.0001$.

replication, and hedgehog signaling pathway. As is known to all, growing evidence has confirmed that these pathways are involved in the progression of various tumors. For instance, PLA2G10 could promote the cell cycle progression of soft tissue leiomyosarcoma cells through upregulated of the expression of cyclin E1 and CDK2 (31). The dysregulated of DNA replication results in abnormal gene phenotypes that trigger normal cells to transform into malignant ones (32). In addition, the hedgehog signaling pathway also plays a vitally important role in the tumor. Dongdong Cheng et al. prove that CNOT1 cooperates with LMNA to aggravate the occurrence of osteosarcoma by regulating the Hedgehog signaling pathway (33). On the contrary, the patients in the low-risk group seem relevant to immune-related responses, which may affect the tumor immunity microenvironment of STS. Given these results and previous studies, it is reasonable to believe that these identify pathways provided novel insights into the relationship between the novel ARSig and tumor biology of STS.

Meanwhile, ten key hub genes (AHNAK2, GPC2, DBNDD2, OLFM1, SCRG1, TNFAIP8L2, FILIP1L, CYSTM1, PARM1, and NCAPG) are determined using the Friend analysis, which is associated with the prognosis of STS. The Friends analysis is a commonly used method for identifying hub genes in the pathway (34). Surprisingly, the functional role of these ten hub genes in tumor has been widely reported in previous studies. AHNAK2 has been shown to be a prognostic marker in papillary thyroid cancer, clear cell renal cell carcinoma (ccRCC), and lung adenocarcinoma (35–37). Minglei Wang et al. reveal that the overexpression of AHNAK2 could drive tumorigenesis and progression of ccRCC by facilitate EMT and cancer cell stemness (36). FILIP1L is a tumor suppressor with diminished expression in various tumors (38). For instance, the downregulation of FILIP1L causes the aberrant stabilization of a centrosome-associated chaperone protein, thereby driving aneuploidy and progression in colorectal adenocarcinoma (39). Guoming Chen et al. demonstrate that GPC2 could sreve as a Potential prognostic, diagnostic, and immunological biomarker in pan-cancer (40). In addition, it is revealed that the elevated TNFAIP8L2 inhibit the survival and proliferation of colorectal cancer cell line, while endogenous TNFAIP8L2 facilitate the tumorigenesis when exposure to dangerous environment (41). NCAPG is overexpressed in cardia adenocarcinoma (CA), which could suppress the apoptosis and advocate the epithelial-mesenchymal transition of the CA cell line via activating the Wnt/β-catenin signaling pathway (42). Consistently, OLFM1 could inhibit the growth and metastasis of colorectal cancer cells through affect the NF-κB signalling pathway (43). Also, the oncogenic potential and important role of PARM1 in leukemogenesis were proved by Cyndia Charfi et al., which could promote anchorage and cell proliferation capacity (44). However, research on the role of SCRG1, DBNDD2 and CYSTM1 in tumorigenesis and development is currently lacking. Collectively, these hub genes exhibit a significant association with tumors, representing a promising clue for future biomarker research in STS.

It has shown that the tumor immune microenvironment is closely relevant to the progression and invasion, with the tumor immune microenvironment receiving considerable attention past

few years (45). In the low-risk group, the immune and stromal scores and the abundance of immune infiltration augmented significantly, indicating the STS cohort with a low-risk score has a better immune status. Consistently, previous research has demonstrated that immune infiltration is an ignored prognostic factor for tumor (46), and the ameliorated immunity status was related to the prognosis of STS (47). Interestingly, we observe a decreased M0 infiltration and enhanced M1 macrophage infiltration degree in the low-risk group, and the STS patient with more M0 and M2 macrophage infiltration degrees has an attenuated prognosis. As we all know, macrophages are very versatile cells with a high degree of plasticity and have various functions in various pathological processes (48). Macrophages are broadly categorized into M1 classically activated macrophages, and M2 alternatively activated macrophages (49). Among them, M1 macrophages have anti-tumour effects, while M2 macrophages have pro-tumour effects (50). Therefore, it is reasonable to believe that the infiltration degree of macrophages may partly account for the different tumor immune microenvironment among distinct risk groups, and the different immune status is closely correlated with the prognosis of STS in different ARGsig risk groups.

Recently, immunotherapy has become a promising strategy, which is expected to become the predominant anti-tumor treatment in the future (51). However, not all malignancies benefit from immunotherapy (52). Therefore, stratifying and differentiating patients is necessary for the effectiveness of immunotherapy (53). In the present study, we observe that the low-risk STS patients had an elevated expression of immune checkpoint genes. Similarly, the STS cohorts with low ARSig risk scores exhibits a positive response for anti-PD1, indicating the novel ARSig has a potential ability to predict response to immunotherapy in STS. Also, chemotherapy is another important alternative therapeutic method for patients with STS (54). We find that the low-risk STS cohort responded better to lenalidomide, erlotinib, and gefitinib, while the high-risk STS patients are more sensitive to axitinib, cisplatin, cytarabine, docetaxel, doxorubicin, gemcitabine, midostaurin, pazopanib, vinblastine, vinorelbine, and vorinostat. It may help clinicians choose an appropriate chemotherapy plan based on the risk score. In general, the novel ARSig we presented may provide insight into the individualized immunotherapy and chemotherapy of STS.

Notably, we finally detect the expression levels and the effect of signature ARGs using *in vitro* experiment in the STS cell line, and the result shows that there was a significant difference in the expression of these ARGs among the STS and control cells, increasing the credibility of our study. It is worth mentioning that some ARGs have been demonstrated to be associated with the malignant progression of cancer. For example, the ARDB2 signaling could facilitate the progression and sorafenib resistance of hepatocellular carcinoma via inhibited autophagic degradation of HIF1α (55). SRPK1 is frequently overexpressed in gastric cancer, resulting in tumor cell growth by regulating the small nucleolar RNA expression (56). Consistently, our study reveals that ARDB2 and SRPK1 could promote the proliferation, migration, and invasion ability of SW872. As a member of ARGs, the specific mechanism by which SRPK1 and ARDB2 play a role in angiogenesis is also worth exploring. Currently, studies have reported that the inhibition of SRPK1 can reduce the expression of pro-angiogenic VEGF, thereby maintaining the production of anti-angiogenic VEGF isoforms (57). Also, Yingwei Chang et al. proved that the SRPK1 could affect the angiogenesis via the PI3K/Akt signaling pathway (58). However, the mechanism of ARDB2 in angiogenesis remains unclear. Hence, these results further confirm the reliability of our study, but the specific mechanisms of ARDB2 and SRPK1 in the angiogenesis of STS are worth further exploration in the future.

Conclusion

Briefly, our study reveals that the identified ARSig is a robust prognostic marker for OS prediction in patients with STS. Furthermore, the stratification base on the novel ARSig could guide the clinical decision, tumor immune microenvironment prediction, personalized immunotherapy and chemotherapy of STS. It is reasonable to believe that our study offers a valuable basis for further research.

Data availability statement

The datasets presented in this study can be found in online repositories. The names of the repository/repositories and accession number(s) can be found within the article/Supplementary Materials.

Author contributions

SH and ZL contributed to the conception and made final approval of the version, BL performed the study concept and design and wrote the manuscript. CL performed the experiment. CF, HW, HZ, and CT helped with data analysis. All authors contributed to the manuscript revision, read, and approved the submitted version.

Funding

This work was supported by the National Natural Foundation of China (82272664, 81902745, 82172500), Hunan Provincial Natural Science Foundation of China (2022JJ30843), the Science and Technology Development Fund Guided by Central Government (2021Szvup169), Hunan Provincial Administration of Traditional Chinese Medicine Project (D2022117), the Scientific Research Program of Hunan Provincial Health Commission (B202304077077), and the Rehabilitation Project of Hunan Disabled Persons' Federation (2022XK0215).

Acknowledgments

We really appreciate the public database TCGA and GEO for allowing access to their data.

Conflict of interest

The authors declare that the research was conducted in the absence of any commercial or financial relationships that could be construed as a potential conflict of interest.

Publisher's note

All claims expressed in this article are solely those of the authors and do not necessarily represent those of their affiliated organizations, or those of the publisher, the editors and the reviewers. Any product that may be evaluated in this article, or claim that may be made by its manufacturer, is not guaranteed or endorsed by the publisher.

Supplementary material

The Supplementary Material for this article can be found online at: https://www.frontiersin.org/articles/10.3389/fimmu.2023.1178436/full#supplementary-material

References

1. Jemal A, Siegel R, Ward E, Murray T, Xu J, Thun MJ. Cancer statistics, 2007. *CA: Cancer J Clin* (2007) 57(1):43–66. doi: 10.3322/canjclin.57.1.43

2. Choi JH, Ro JY. The 2020 WHO classification of tumors of soft tissue: selected changes and new entities. *Adv Anat Pathol* (2021) 28(1):44–58. doi: 10.1097/PAP.0000000000000284

3. Chang L, Asatrian G, Dry SM, James AW. Circulating tumor cells in sarcomas: a brief review. *Med Oncol (Northwood London England)* (2015) 32(1):430. doi: 10.1007/s12032-014-0430-9

4. Aung T, Asam C, Haerteis S. Ion channels in sarcoma: pathophysiology and treatment options. *Pflugers Archiv Eur J Physiol* (2019) 471(9):1163–71. doi: 10.1007/s00424-019-02299-8

5. Savina M, Le Cesne A, Blay JY, Ray-Coquard I, Mir O, Toulmonde M, et al. Patterns of care and outcomes of patients with METAstatic soft tissue SARComa in a real-life setting: the METASARC observational study. *BMC Med* (2017) 15(1):78. doi: 10.1186/s12916-017-0831-7

6. Hanahan D, Weinberg RA. Hallmarks of cancer: the next generation. *Cell* (2011) 144(5):646–74. doi: 10.1016/j.cell.2011.02.013

7. Hoeben A, Landuyt B, Highley MS, Wildiers H, Van Oosterom AT, De Bruijn EA. Vascular endothelial growth factor and angiogenesis. *Pharmacol Rev* (2004) 56(4):549–80. doi: 10.1124/pr.56.4.3

8. Viallard C, Larrivée B. Tumor angiogenesis and vascular normalization: alternative therapeutic targets. *Angiogenesis* (2017) 20(4):409–26. doi: 10.1007/s10456-017-9562-9

9. Chi Y, Fang Z, Hong X, Yao Y, Sun P, Wang G, et al. Safety and efficacy of anlotinib, a multikinase angiogenesis inhibitor, in patients with refractory metastatic soft-tissue sarcoma. *Clin Cancer Res* (2018) 24(21):5233–8. doi: 10.1158/1078-0432.CCR-17-3766

10. Yang Y, Wu G, Li Q, Zheng Y, Liu M, Zhou L, et al. Angiogenesis-related immune signatures correlate with prognosis, tumor microenvironment, and therapeutic sensitivity in hepatocellular carcinoma. *Front Mol Biosciences* (2021) 8:690206. doi: 10.3389/fmolb.2021.690206

11. Wang G, Hu JQ, Liu JY, Zhang XM. Angiogenesis-related gene signature-derived risk score for glioblastoma: prospects for predicting prognosis and immune heterogeneity in glioblastoma. *Front Cell Dev Biol* (2022) 10:778286. doi: 10.3389/fcell.2022.778286

12. Qing X, Xu W, Liu S, Chen Z, Ye C, Zhang Y. Molecular characteristics, clinical significance, and cancer immune interactions of angiogenesis-associated genes in gastric cancer. *Front Immunol* (2022) 13:843077. doi: 10.3389/fimmu.2022.843077

13. Ritchie ME, Phipson B, Wu D, Hu Y, Law CW, Shi W, et al. Limma powers differential expression analyses for RNA-sequencing and microarray studies. *Nucleic Acids Res* (2015) 43(7):e47. doi: 10.1093/nar/gkv007

14. Tu Z, Wu L, Wang P, Hu Q, Tao C, Li K, et al. N6-Methylandenosine-Related lncRNAs are potential biomarkers for predicting the overall survival of lower-grade glioma patients. *Front Cell Dev Biol* (2020) 8:642. doi: 10.3389/fcell.2020.00642

15. Kamarudin AN, Cox T, Kolamunnage-Dona R. Time-dependent ROC curve analysis in medical research: current methods and applications. *BMC Med Res methodology* (2017) 17(1):53. doi: 10.1186/s12874-017-0332-6

16. Wu T, Hu E, Xu S, Chen M, Guo P, Dai Z, et al. clusterProfiler 4.0: a universal enrichment tool for interpreting omics data. *Innovation (Cambridge (Mass))* (2021) 2(3):100141.

17. Liu B, Liu Z, Feng C, Li C, Zhang H, Li Z, et al. Identification of cuproptosis-related lncRNA prognostic signature for osteosarcoma. *Front Endocrinol (Lausanne)* (2022) 13:987942. doi: 10.3389/fendo.2022.987942

18. Subramanian A, Tamayo P, Mootha VK, Mukherjee S, Ebert BL, Gillette MA, et al. Gene set enrichment analysis: a knowledge-based approach for interpreting genome-wide expression profiles. *Proc Natl Acad Sci U S A* (2005) 102(43):15545–50. doi: 10.1073/pnas.0506580102

19. Hänzelmann S, Castelo R, Guinney J. GSVA: gene set variation analysis for microarray and RNA-seq data. *BMC Bioinf* (2013) 14:7. doi: 10.1186/1471-2105-14-7

20. Yoshihara K, Shahmoradgoli M, Martínez E, Vegesna R, Kim H, Torres-Garcia W, et al. Inferring tumour purity and stromal and immune cell admixture from expression data. *Nat Commun* (2013) 4:2612. doi: 10.1038/ncomms3612

21. Chen B, Khodadoust MS, Liu CL, Newman AM, Alizadeh AA. Profiling tumor infiltrating immune cells with CIBERSORT. *Methods Mol Biol (Clifton NJ)* (2018) 1711:243–59. doi: 10.1007/978-1-4939-7493-1_12

22. Jiang P, Gu S, Pan D, Fu J, Sahu A, Hu X, et al. Signatures of T cell dysfunction and exclusion predict cancer immunotherapy response. *Nat Med* (2018) 24(10):1550–8. doi: 10.1038/s41591-018-0136-1

23. Geeleher P, Cox N, Huang RS. pRRophetic: an r package for prediction of clinical chemotherapeutic response from tumor gene expression levels. *PloS One* (2014) 9(9):e107468. doi: 10.1371/journal.pone.0107468

24. Iasonos A, Schrag D, Raj GV, Panageas KS. How to build and interpret a nomogram for cancer prognosis. *J Clin Oncol* (2008) 26(8):1364–70. doi: 10.1200/JCO.2007.12.9791

25. Liu B, Pang K, Feng C, Liu Z, Li C, Zhang H, et al. Comprehensive analysis of a novel cuproptosis-related lncRNA signature associated with prognosis and tumor matrix features to predict immunotherapy in soft tissue carcinoma. *Front Genet* (2022) 13:1063057. doi: 10.3389/fgene.2022.1063057

26. Blay JY, Ray-Coquard I. Sarcoma in 2016: evolving biological understanding and treatment of sarcomas. *Nat Rev Clin Oncol* (2017) 14(2):78–80. doi: 10.1038/nrclinonc.2016.200

27. Shashni B, Nishikawa Y, Nagasaki Y. Management of tumor growth and angiogenesis in triple-negative breast cancer by using redox nanoparticles. *Biomaterials* (2021) 269:120645. doi: 10.1016/j.biomaterials.2020.120645

28. Ash D, Sudhahar V, Youn SW, Okur MN, Das A, O'Bryan JP, et al. The p-type ATPase transporter ATP7A promotes angiogenesis by limiting autophagic degradation of VEGFR2. *Nat Commun* (2021) 12(1):3091. doi: 10.1038/s41467-021-23408-1

29. Roudsari LC, Jeffs SE, Witt AS, Gill BJ, West JL. A 3D poly(ethylene glycol)-based tumor angiogenesis model to study the influence of vascular cells on lung tumor cell behavior. *Sci Rep* (2016) 6:32726. doi: 10.1038/srep32726

30. de Heer EC, Jalving M, Harris AL. HIFs, angiogenesis, and metabolism: elusive enemies in breast cancer. *J Clin Invest* (2020) 130(10):5074–87. doi: 10.1172/JCI137552

31. Tan G, Zhang GY, Xu J, Kang CW, Yan ZK, Lei M, et al. PLA2G10 facilitates the cell-cycle progression of soft tissue leiomyosarcoma cells at least by elevating cyclin E1/CDK2 expression. *Biochem Biophys Res Commun* (2020) 527(2):525–31. doi: 10.1016/j.bbrc.2020.04.043

32. Swanton C. Intratumor heterogeneity: evolution through space and time. *Cancer Res* (2012) 72(19):4875–82. doi: 10.1158/0008-5472.CAN-12-2217

33. Cheng DD, Li J, Li SJ, Yang QC, Fan CY. CNOT1 cooperates with LMNA to aggravate osteosarcoma tumorigenesis through the hedgehog signaling pathway. *Mol Oncol* (2017) 11(4):388–404. doi: 10.1002/1878-0261.12043

34. Wang Z, Cao L, Zhou S, Lyu J, Gao Y, Yang R. Construction and validation of a novel pyroptosis-related four-lncRNA prognostic signature related to gastric cancer and immune infiltration. *Front Immunol* (2022) 13:854785. doi: 10.3389/fimmu.2022.854785

35. Wang M, Li X, Zhang J, Yang Q, Chen W, Jin W, et al. AHNAK2 is a novel prognostic marker and oncogenic protein for clear cell renal cell carcinoma. *Theranostics* (2017) 7(5):1100–13. doi: 10.7150/thno.18198

36. Zheng L, Li S, Zheng X, Guo R, Qu W. AHNAK2 is a novel prognostic marker and correlates with immune infiltration in papillary thyroid cancer: evidence from integrated analysis. *Int Immunopharmacol* (2021) 90:107185. doi: 10.1016/j.intimp.2020.107185

37. Zheng M, Liu J, Bian T, Liu L, Sun H, Zhou H, et al. Correlation between prognostic indicator AHNAK2 and immune infiltrates in lung adenocarcinoma. *Int Immunopharmacol* (2021) 90:107134. doi: 10.1016/j.intimp.2020.107134

38. Kwon M, Libutti SK. Filamin a interacting protein 1-like as a therapeutic target in cancer. *Expert Opin Ther Targets* (2014) 18(12):1435–47.

39. Kwon M, Rubio G, Nolan N, Auteri P, Volmar JA, Adem A, et al. FILIP1L loss is a driver of aggressive mucinous colorectal adenocarcinoma and mediates cytokinesis defects through PFDN1. *Cancer Res* (2021) 81(21):5523–39. doi: 10.1158/0008-5472.CAN-21-0897

40. Chen G, Luo D, Zhong N, Li D, Zheng J, Liao H, et al. GPC2 is a potential diagnostic, immunological, and prognostic biomarker in pan-cancer. *Front Immunol* (2022) 13:857308. doi: 10.3389/fimmu.2022.857308

41. Li Y, Zhang N, Ma C, Xu W, Jin G, Zheng Y, et al. The overexpression of Tipe2 in CRC cells suppresses survival while endogenous Tipe2 accelerates AOM/DSS induced-tumor initiation. *Cell Death Dis* (2021) 12(11):1001. doi: 10.1038/s41419-021-04289-0

42. Zhang X, Zhu M, Wang H, Song Z, Zhan D, Cao W, et al. Overexpression of NCAPG inhibits cardia adenocarcinoma apoptosis and promotes epithelial-mesenchymal transition through the wnt/β-catenin signaling pathway. *Gene* (2021) 766:145163. doi: 10.1016/j.gene.2020.145163

43. Shi W, Ye Z, Zhuang L, Li Y, Shuai W, Zuo Z, et al. Olfactomedin 1 negatively regulates NF-κB signalling and suppresses the growth and metastasis of colorectal cancer cells. *J p* (2016) 240(3):352–65.

44. Charfi C, Levros LCJr., Edouard E, Rassart E. Characterization and identification of PARM-1 as a new potential oncogene. *Mol cancer* (2013) 12:84. doi: 10.1186/1476-4598-12-84

45. An G, Wu F, Huang S, Feng L, Bai J, Gu S, et al. Effects of CCL5 on the biological behavior of breast cancer and the mechanisms of its interaction with tumor−associated macrophages. *Oncol Rep* (2019) 42(6):2499–511.

46. Pagès F, Galon J, Dieu-Nosjean MC, Tartour E, Sautès-Fridman C, Fridman WH. Immune infiltration in human tumors: a prognostic factor that should not be ignored. *Oncogene.* (2010) 29(8):1093–102. doi: 10.1038/onc.2009.416

47. Liu B, Liu Z, Feng C, Tu C. A necroptosis-related lncRNA signature predicts prognosis and indicates the immune microenvironment in soft tissue sarcomas. *Front Genet* (2022) 13:899545. doi: 10.3389/fgene.2022.899545

48. Anderson NR, Minutolo NG, Gill S, Klichinsky M. Macrophage-based approaches for cancer immunotherapy. *Cancer Res* (2021) 81(5):1201–8. doi: 10.1158/0008-5472.CAN-20-2990

49. Orecchioni M, Ghosheh Y, Pramod AB, Ley K. Macrophage polarization: different gene signatures in M1(LPS+) vs. classically and M2(LPS-) vs. alternatively activated macrophages. *Front Immunol* (2019) 10:1084. doi: 10.3389/fimmu.2019.01084

50. Brown JM, Recht L, Strober S. The promise of targeting macrophages in cancer therapy. *Clin Cancer Res* (2017) 23(13):3241–50. doi: 10.1158/1078-0432.CCR-16-3122

51. Wu Z, Li S, Zhu X. The mechanism of stimulating and mobilizing the immune system enhancing the anti-tumor immunity. *Front Immunol* (2021) 12:682435. doi: 10.3389/fimmu.2021.682435

52. Gras Navarro A, Espedal H, Joseph JV, Trachsel-Moncho L, Bahador M, Gjertsen BT, et al. Pretreatment of glioblastoma with bortezomib potentiates natural killer cell cytotoxicity through TRAIL/DR5 mediated apoptosis and prolongs animal survival. *Cancers* (2019) 11(7). doi: 10.3390/cancers11070996

53. Li Y, Zhang X, Liu X, Pan W, Li N, Tang B. Intelligent stimuli-responsive nano immunomodulators for cancer immunotherapy. *Chem science* (2021) 12(9):3130–45. doi: 10.1039/D0SC06557A

54. He L, Yang H, Huang J. The tumor immune microenvironment and immune-related signature predict the chemotherapy response in patients with osteosarcoma. *BMC cancer* (2021) 21(1):581. doi: 10.1186/s12885-021-08328-z

55. Wu FQ, Fang T, Yu LX, Lv GS, Lv HW, Liang D, et al. ADRB2 signaling promotes HCC progression and sorafenib resistance by inhibiting autophagic degradation of HIF1α. *J Hepatol* (2016) 65(2):314–24. doi: 10.1016/j.jhep.2016.04.019

56. Li Y, Yu S, Wang X, Ye X, He B, Quan M, et al. SRPK1 facilitates tumor cell growth via modulating the small nucleolar RNA expression in gastric cancer. *J Cell Physiol* (2019) 234(8):13582–91. doi: 10.1002/jcp.28036

57. Gammons MV, Lucas R, Dean R, Coupland SE, Oltean S, Bates DO. Targeting SRPK1 to control VEGF-mediated tumour angiogenesis in metastatic melanoma. *Br J Cancer* (2014) 111(3):477–85. doi: 10.1038/bjc.2014.342

58. Chang Y, Wu Q, Tian T, Li L, Guo X, Feng Z, et al. The influence of SRPK1 on glioma apoptosis, metastasis, and angiogenesis through the PI3K/Akt signaling pathway under normoxia. *Tumour Biol* (2015) 36(8):6083–93. doi: 10.1007/s13277-015-3289-2

Glossary

STS	Soft tissue sarcoma
VEGF	Vascular endothelial growth factor
HIFs	Hypoxia-inducible factors
FGFs	Fibroblast growth factors
ARGs	Angiogenesis-related genes
ARSig	Angiogenesis-related signatures
CNV	Copy number variation;
TCGA	The Cancer Genome Atlas
GEO	Gene Expression Omnibus
DEARGs	Differential Expressed ARGs
DEGs	Differentially expressed gene
PCA	Principal component analysis
LASSO	least absolute shrinkage and selection operator
OS	Overall survival
KM	Kaplan–Meier
ROC	Receiver operating characteristic
AUC	Area under the curve
GO	Gene Ontology
KEGG	Kyoto Encyclopedia of Genes and Genomes
GSEA	Gene Set Enrichment Analysis
GSVA	Gene set variation analysis
TME	tumor microenvironment
ESTIMATE	Estimation of STromal and Immune cells in Malignant Tumor tissues using Expression data
TMB	Tumor mutation burden
CSC	Cancer Stem Cell
SubMap	Subclass Mapping
IC50	Half of the maximum inhibitory concentration
DMEM	Dulbecco's modified Eagle's medium
RT-qPCR	Quantitative reverse transcription PCR
EdU	5-Ethynyl-2'-Deoxyuridine

frontiers | Frontiers in Immunology

TYPE Original Research
PUBLISHED 14 June 2023
DOI 10.3389/fimmu.2023.1182030

OPEN ACCESS

EDITED BY
Esra Akbay,
University of Texas Southwestern Medical Center, United States

REVIEWED BY
Rui Sha,
First Affiliated Hospital of Wannan Medical College, China
Subhayan Das,
Indian Institute of Technology Kharagpur, India

*CORRESPONDENCE
Tang Liu
liutang1204@csu.edu.cn
Zhihong Li
lizhihong@csu.edu.cn

†These authors have contributed equally to this work and share first authorship

RECEIVED 08 March 2023
ACCEPTED 31 May 2023
PUBLISHED 14 June 2023

CITATION
Wu Y, Lin Z, Tang X, Tong Z, Ji Y, Xu Y, Zhou Z, Yang J, Li Z and Liu T (2023) Ferroptosis-related gene HIC1 in the prediction of the prognosis and immunotherapeutic efficacy with immunological activity.
Front. Immunol. 14:1182030.
doi: 10.3389/fimmu.2023.1182030

Ferroptosis-related gene HIC1 in the prediction of the prognosis and immunotherapeutic efficacy with immunological activity

Yanlin Wu[1†], Zhengjun Lin[1†], Xianzhe Tang[2], Zhongyi Tong[3], Yuqiao Ji[1], Yingting Xu[1], Ziting Zhou[1], Jing Yang[1], Zhihong Li[1*] and Tang Liu[1*]

[1]Department of Orthopedics, The Second Xiangya Hospital, Central South University, Changsha, Hunan, China, [2]Department of Orthopedics, Chenzhou No.1 People's Hospital, Chenzhou, Hunan, China, [3]Department of Pathology, The Second Xiangya Hospital, Central South University, Changsha, Hunan, China

Background: Hypermethylated in Cancer 1 (HIC1) was originally confirmed as a tumor suppressor and has been found to be hypermethylated in human cancers. Although growing evidence has supported the critical roles of HIC1 in cancer initiation and development, its roles in tumor immune microenvironment and immunotherapy are still unclear, and no comprehensive pan-cancer analysis of HIC1 has been conducted.

Methods: HIC1 expression in pan-cancer, and differential HIC1 expression between tumor and normal samples were investigated. Immunohistochemistry (IHC) was employed to validate HIC1 expression in different cancers by our clinical cohorts, including lung cancer, sarcoma (SARC), breast cancer, and kidney renal clear cell carcinoma (KIRC). The prognostic value of HIC1 was illustrated by Kaplan-Meier curves and univariate Cox analysis, followed by the genetic alteration analysis of HIC1 in pan-cancer. Gene Set Enrichment Analysis (GSEA) was conducted to illustrate the signaling pathways and biological functions of HIC1. The correlations between HIC1 and tumor mutation burden (TMB), microsatellite instability (MSI), and the immunotherapy efficacy of PD-1/PD-L1 inhibitors were analyzed by Spearman correlation analysis. Drug sensitivity analysis of HIC1 was performed by extracting data from the CellMiner™ database.

Results: HIC1 expression was abnormally expressed in most cancers, and remarkable associations between HIC1 expression and prognostic outcomes of patients in pan-cancer were detected. HIC1 was significantly correlated with T cells, macrophages, and mast cell infiltration in different cancers. Moreover, GSEA revealed that HIC1 was significantly involved in immune-related biological functions and signaling pathways. There was a close relationship of HIC1 with TMB and MSI in different cancers. Furthermore, the most exciting finding was that HIC1 expression was significantly correlated with the response to PD-1/PD-L1 inhibitors in cancer treatment. We also found that HIC1 was significantly correlated with the sensitivity of several anti-cancer drugs, such as axitinib, batracylin, and nelarabine. Finally, our clinical cohorts further validated the expression pattern of HIC1 in cancers.

Conclusions: Our investigation provided an integrative understanding of the clinicopathological significance and functional roles of HIC1 in pan-cancer. Our findings suggested that HIC1 can function as a potential biomarker for predicting the prognosis, immunotherapy efficacy, and drug sensitivity with immunological activity in cancers.

KEYWORDS

HIC1, pan-cancer, genetic alternation, prognosis, immune microenvironment, immunotherapeutic efficacy, drug sensitivity

Introduction

Cancer is a great threat to human health and is one of the major causes of death, which ubiquitously affects people globally and brings a great economic burden to society (1). Immunotherapy, mainly including immune checkpoint inhibitors (ICIs) and adoptive cell therapy (ACT), has led to the revolution of anti-cancer treatments and attracted the attention of tumor immunology (2). However, only a fraction of cancer patients can respond to current cancer immunotherapies, and most patients have innate or acquired immunotherapeutic resistance (3, 4). The tumor immune microenvironment, including tumor-infiltrating immune cells, and immune-related biomolecules, is critically involved in cancer initiation and development, and recent work has verified novel targets in the tumor immune microenvironment for cancer immunotherapy (5). By dissecting the mechanisms underlying cancer immunotherapy resistance, the tumor immune microenvironment has been confirmed as a major location for immunoresistance to occur (6). Therefore, it is warranted to explore critical modulators mediating the tumor immune microenvironment and novel biomolecules to predict the immunotherapeutic efficacy of cancer patients.

Hypermethylated in Cancer 1 (HIC1), located on chromosome 17p13.3 completely within a CpG island, is a tumor repressor that is widely expressed in normal tissues, however, is generally lowly expressed with methylation in several cancers, such as prostate cancer, breast cancer, and pancreatic cancer (7–9). In 1995, HIC1 was first discovered and was found to be activated by p53 (10). Chen et al. indicated that the loss of HIC1 function could induce the development of cancer by activating the deacetylase SIRT1, subsequently downregulating the expressions of p53 (11). Interacting with several major repression and chromatin remodeling complexes, including CtBP, NuRD, PRC2, and SWI/SNF, HIC1 is recognized as a multifaceted transcriptional repressor. Besides, it has been found that HIC1 is involved in multiple physiological processes and oncology, such as embryonic development, DNA damage repair, and angiogenesis (12). For instance, the abundant methylation status of 11 CpG sites within the HIC1 promoter has been detected in cell lines, tissues, and plasma of patients with prostate cancer compared with normal controls. Restoration of HIC1 expression could suppress the proliferation, migration, and invasion and induce the apoptosis of prostate cancer cells (7). In bladder cancer, ZBTB7A can bind to the HIC1 promoter, and decreased HIC1 expression can promote the malignant behavior of bladder cancer cells (13). Recent work has suggested the regulatory roles of HIC1 in ferroptosis during cancer progression. It has been found that HIC1 controlled several pro-ferroptosis genes transcriptionally, such as HBA1, and promotes ferroptosis in liver cancer (14). Notably, several studies have reported controversial findings indicating the potential oncogenic functions of HIC1 (15). Generally, HIC1 plays a critical role in various cancers, however, there is no pan-cancer analysis of HIC1 and the immune-mediating functions of HIC1 in cancers are largely unknown.

In this research, we presented and validated the HIC1 expression landscape in different cancers, and its association with the prognosis of cancer patients was also explored. Moreover, we also explored the genetic alternation characteristics and the potential biological functions and signaling pathways of HIC1. Furthermore, the potential functions of HIC1 in mediating the tumor immune microenvironment and predicting the immunotherapeutic efficacy and drug sensitivity were further investigated. Our results highlighted that HIC1 plays an important role in the progression and therapy of various cancers, thereby offering new insight into cancer immunotherapy.

Materials and methods

Data collection

The normalized TCGA pan-cancer dataset was downloaded from the UCSC database (https://xena.ucsc.edu/) (16), and the expression data of HIC1 of each sample in 33 cancers was extracted. In addition, expression profiles of different cancer cell lines were also downloaded from the Broad Institute Cancer Cell Line Encyclopedia (CCLE) portal database (https://portals.broadinstitute.org/ccle/about) and HIC1 expression levels in 21 cancer cell lines were also investigated. Moreover, the expression levels of HIC1 in normal tissues were assessed by expression profiles from Genotype-Tissue Expression (GTEx) database (https://www.gtexportal.org/). Differential expression analysis between cancer samples and their corresponding normal samples in the TCGA pan-cancer. Besides, we also confirmed the differential expression of HIC1 between tumor samples in the

TCGA pan-cancer database and normal samples in the GTEx database. Finally, we explored differential HIC1 expression among patients with different clinical stages. The abbreviations of 33 cancer types are presented in Table S1.

Prognostic analysis of HIC1

The correlation of HIC1 expression with overall survival (OS), disease-specific survival (DSS), disease-free survival (DFS), and progression-free survival (PFS) was evaluated through utilizing TCGA pan-cancer survival data by univariate Cox regression analysis, and the results were visualized by forest map. Kaplan–Meier curves with log-rank p values were further employed to illustrate the differential survival outcomes between of high-HIC1 expression and low-HIC1 expression groups in different cancers. R-packages "survival", "survminer", "forestplot", "limma" and "ggpubr" were utilized for this investigation process.

Genetic alternation analysis of HIC1

The genetic mutation characteristics of HIC1 were investigated by utilizing"TCGA Pan-Cancer Atlas Studies" dataset in the online database cbioportal (cBio Cancer Genomics Portal) (http://cbioportal.org) (17). The genetic alteration frequency, mutation type, and copy number alteration (CNA) of HIC1, the mutated sites, and the three-dimensional structure of HIC1 were investigated.

Immune microenvironment assessment

Estimation of Stromal and Immune cells in Malignant Tumor tissues using Expression data (ESTIMATE) analysis was employed to calculate the stromal and immune scores of each tumor sample by "estimate" R package (18). CIBERSORT, a bioinformatics algorithm that can quantify the immune cellular composition of tissue samples according to their gene expression levels, was utilized to explore the correlation between HIC1 and diverse immune cells within the tumor immune microenvironment in different cancer types (18). The relationship between HIC1 expression and infiltrating immune cells was evaluated by utilizing Spearman correlation analysis. TISIDB (http://cis.hku.hk/TISIDB/index.php) is an integrated online portal for the investigation of tumor-immune system interaction. We utilized TISIDB online database to determine the relationship between HIC1 expression and tumor-infiltrating lymphocyte (TILs) expression, major histocompatibility complex (MHC) genes expression, immunoinhibitory/immunostimulator genes expression, chemokines and chemokines receptors expression in human cancers. $|R| > 0.5$, P-value < 0.05 was considered as significantly relative.

Gene set enrichment analysis

GSEA was conducted to explore the possible biological functions and potential signaling pathways modulated by HIC1 in each cancer type. The "gmt" data of the hallmark gene set (h.all.v7.4.symbols.gmt) which consists of 50 hallmark gene sets was extracted from the MSigDB database (https://www.gsea-msigdb.org/gsea/index.jsp). The analysis process was performed and visualized by utilizing R packages "clusterProfiler" (19), "enrichplot", and "ggplot2".

Investigation of HIC1 in predicting immunotherapeutic efficacy

To assess the connection between HIC1 expression and the immunotherapeutic responses to immune checkpoint blockade (ICB), three datasets providing patients with immunotherapy treatment, including GSE78220 (melanoma) (20), GSE67501 (renal cell carcinoma) (21), and IMvigor210 (metastatic urological cancer) extracted from GEO (https://www.ncbi.nlm.nih.gov/geo/) online database were included in our study. The procedure was conducted and the results were visualized utilizing the R-package "ggpubr" and "ggplot2".

Investigation of HIC1 in predicting drug sensitivity

To investigate the correlation between HIC1 expression and drug sensitivity, NCI-60 compound activity data with RNA-seq expression profiles were downloaded from the CellMiner™ online database (https://discover.nci.nih.gov/cellminer/home.do). Drugs approved by FDA were included in our analysis by utilizing R packages "impute", "limma", "ggplot2", and "ggpubr".

Clinical samples and immunohistochemistry

Patient samples were obtained under a Second Xiangya Hospital-approved protocol. Informed consent was obtained from all patients in accordance with the Declaration of Helsinki. HIC1 immunostains in all cancer cases were reviewed and evaluated by pathologists ZY T and P Z. Clinical tumor tissue samples and commercially available tumor tissue chips were stained for HIC1. IHC staining was implemented with HIC1 antibody (1:50; Proteintech, China) based on the manufacturer's protocols. Sections of tumor tissues were deparaffinized and rehydrated. Then, the antigen was retrieved by being immersed in pH=6.0 citrate buffer for 15 minutes at 95°C before incubation with 0.3% hydrogen peroxide for 15 mins at room temperature to block the activity of endogenous peroxidase. Sections were treated with PBS rinsing and 5% normal goat serum blocking for 30 minutes at room temperature before being treated with a primary anti-HIC1 antibody and incubated overnight at 4°C. The proportion of negative (–), weakly positive (+), moderately positive (++), or strongly positive (+++) staining cells and cell staining intensity in five randomly selected fields were counted. The immunoreactivity scores were calculated by multiplying a number representing the

percentage of immunoreactive cells (0+, none; 1+, <25%; 2+, 25%-50%; 3+, 51%-75%; and 4+, 75%-100%.) by the number representing staining intensity (0, negative; 1, weak; 2, moderate; 3, strong). The immunoreactivity scores were obtained by multiplying the scores for distribution and intensity, giving scores in the range of 0-12. IHC images of HIC1 protein expression in four tumor tissues, including colon adenocarcinoma (COAD), breast invasive carcinoma (BRCA), lung squamous cell carcinoma (LUSC), lung adenocarcinoma (LUAD), and their corresponding normal tissues were also downloaded from the HPA database (http://www.proteinatlas.org/). The IHC results were also compared with the protein level of HIC1 in TCGA from the UALCAN database (https://ualcan.path.uab.edu/).

Statistical analysis

All statistical analyses were conducted in R programming, version 4.1.1. The Wilcoxon rank-sum test was used to calculate the gene expression and the methylation level differences between cancerous and normal tissues of each cancer type. The coefficient values were evaluated by Spearman correlation analysis. $P < 0.05$ was considered statistically significant (*$p < 0.05$, **$p < 0.01$, and ***$p < 0.001$).

Results

The expression pattern of HIC1 in pan-cancer

To explore the expression levels of HIC1 across normal tissues and cancers, we analyzed the HIC1 expression of samples in GTEx, CCLE, and TCGA pan-cancer databases. The investigation of HIC1 expression in the GTEx database found that HIC1 was highly expressed in several tissues, such as ovary, uterus, and breast tissues, while was lowly expressed in bone marrow, liver, and pancreas tissues in comparison with other normal tissue samples (Figure 1A). The expression of HIC1 in different cancer cell lines was shown in Figure 1B, which showed that HIC1 was highly expressed in bone, central nervous system, and pleura cancer cell lines compared with other cancer cell lines. As for HIC1 expression in the TCGA pan-cancer dataset, the results showed that HIC1 was highly expressed in thymoma (THYM) and SARC, while was lowly expressed in brain lower grade glioma (LGG) and uveal melanoma (UVM) compare to other cancer types (Figure 1C). Differential expression analysis indicated that HIC1 expression was strongly decreased in tumor samples in comparison with their compared normal samples of TCGA pan-cancer dataset in bladder urothelial carcinoma (BLCA), BRCA, cervical squamous cell carcinoma, and endocervical adenocarcinoma (CESC), COAD, kidney chromophobe (KICH), kidney renal papillary cell carcinoma (KIRP), LUAD, LUSC, thyroid carcinoma (THCA) and uterine corpus endometrial carcinoma (UCEC), while was significantly increased in cholangiocarcinoma (CHOL), head and neck squamous cell carcinoma (HNSC), and KIRC (Figure 2D). Moreover, we also compared the differential expression between cancer samples and their corresponding normal samples in the GTEx database. The results showed that HIC1 was abnormally higher in cancer samples in CHOL, glioblastoma multiforme (GBM), HNSC, KIRC, acute myeloid leukemia (LAML), pancreatic adenocarcinoma (PAAD), and stomach adenocarcinoma (STAD), while was significantly downregulated in adrenocortical carcinoma (ACC), BLCA, BRCA, CESC, COAD, esophageal carcinoma (ESCA), KICH, LGG, LICH, LUAD, LUSC, ovarian serous cystadenocarcinoma (OV), prostate adenocarcinoma (PRAD), skin cutaneous melanoma (SKCM), testicular germ cell tumors (TGCT), THCA, UCEC, and uterine carcinosarcoma (UCS) (Figure 1E). These results indicated that HIC1 expression is abnormally high or low in various types of cancer, suggesting that HIC1 may play a potentially important role in cancer diagnosis. Furthermore, we also investigated the associations of HIC1 with clinical stages in patients with different cancers, and the results indicated patients in advanced clinical stages presented higher HIC1 expression levels in BLCA, ESCA, and STAD, and significant differences in the HIC1 expression among patients with different clinical stages were also detected in BRCA and SKCM (Figure 1F).

Prognostic significance of HIC1

To explore the prognostic significance of HIC1 in pan-cancer, we first conducted the univariate Cox regression analysis to illustrate the associations of HIC1 with OS, DFS, DSS, and PFS in different cancer types. The forest map showed that HIC1 expression was correlated with OS in ACC, KIRP, LGG, UCEC, and UVM. HIC1 was associated with worse OS in ACC (HR, 1.925; 95% CI, 1.171-3.164; P = 0.010), KIRP (HR, 2.886; 95% CI, 1.647-5.058; P < 0.001), LGG (HR, 2.104; 95% CI, 1.164-3.802; P =0.014), and UVM (HR, 9.243; 95% CI, 2.417-35.350; P = 0.001), while was correlated with better OS in UCEC (HR, 0.560; 95% CI, 0.372-0.844; P = 0.006) in the assessment of OS in pan-cancer (Figure 2A). For univariate Cox analysis of DFS, the results indicated that HIC1 was a risk factor in ACC (HR, 2.011; 95% CI, 1.052-3.846; P = 0.035), KICH (HR, 21.421; 95% CI, 1.127-407.252; P = 0.041), and KIRP (HR, 2.623; 95% CI, 1.246-5.524; P = 0.011), while was a protective factor in UCEC (HR, 0.386; 95% CI, 0.219-0.681; P = 0.001) (Figure 2B). The forest map of DSS showed that HIC1 expression was correlated with worse DSS in ACC (HR, 1.975; 95% CI, 1.197-3.257; P = 0.008), KICH (HR, 3.920; 95% CI, 1.199-12.819; P = 0.024), KIRP (HR, 4.199; 95% CI, 2.302-7.660; P < 0.001), LGG (HR, 2.233; 95% CI, 1.205-4.140; P = 0.011), mesothelioma (MESO) (HR, 1.473; 95% CI, 1.010-2.150; P = 0.044) and UVM (HR, 10.227; 95% CI, 2.473-42.295; P = 0.001), while was associated with better DSS in UCEC (HR, 0.497; 95% CI, 0.296-0.835; P = 0.008) (Figure 2C). With regards to PFS, there was a close relationship between HIC1 expression and PFS in CHOL, KICH, KIRP, LGG, STAD, UCEC, and UVM, and HIC1 could serve as a risk regulator for PFS in KICH (HR, 2.635; 95% CI, 1.218-5.702; P = 0.014), KIRP (HR, 2.444; 95% CI, 1.416-4.219; P = 0.001), LGG (HR, 1.867; 95% CI, 1.126-3.097; P = 0.016), STAD (HR, 1.252; 95% CI, 1.011-1.550; P =

10.3389/fimmu.2023.1182030

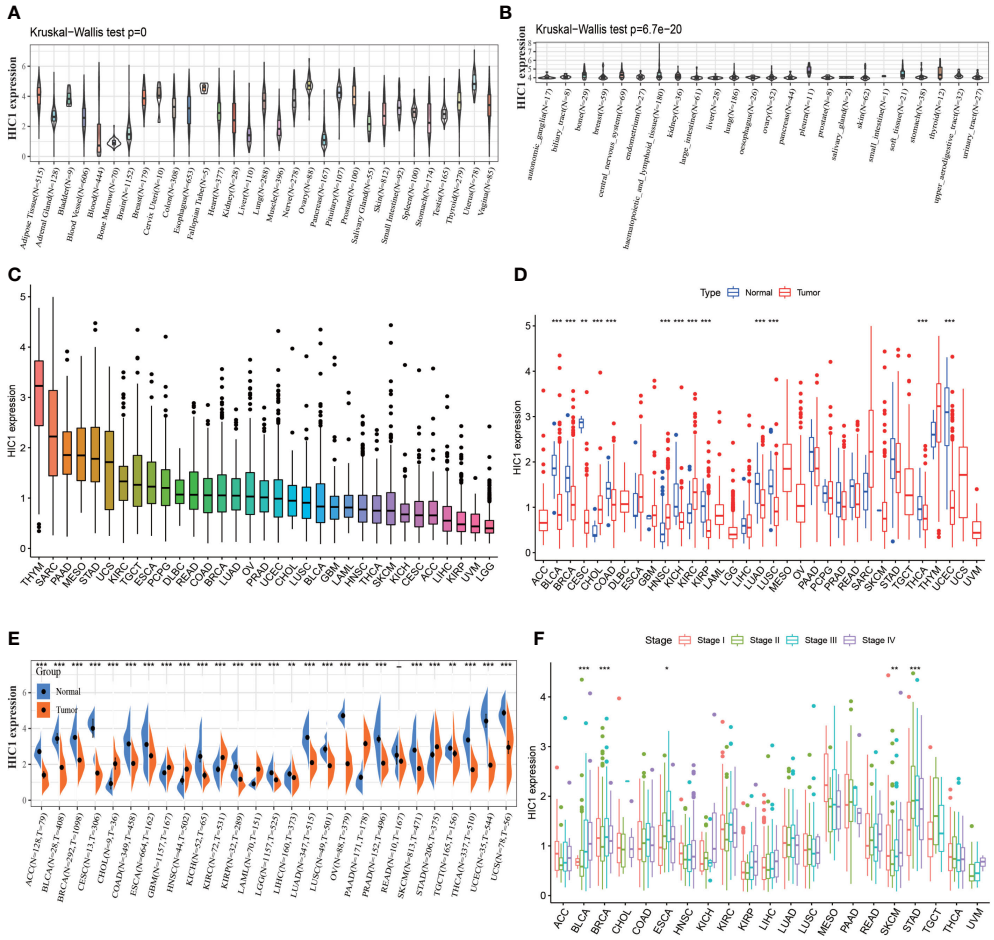

FIGURE 1
The expression pattern of HIC1. **(A)** The expression level of HIC1 in 31 normal tissues from the GTEx database. **(B)** The expression level of HIC1 in 24 tumor cell lines from the CCLE database. **(C)** The expression level of HIC1 in pan-cancer. **(D)** Comparison of HIC1 expression level between cancer and normal samples from TCGA database. **(E)** Comparison of HIC1 expression level between cancer and normal samples from GTEx database. **(F)** The expression level of HIC1 in patients with different WHO stages in various cancer from the TCGA database. *p < 0.05, **p < 0.01, ***p < 0.001.

0.039), and UVM (HR, 8.698; 95% CI, 2.321-32.601; P = 0.001), while could serve as a protective regulator for PFS in CHOL (HR, 0.248; 95% CI, 0.072-0.855; P = 0.027) and UCEC (HR, 0.581; 95% CI, 0.409-0.824; P = 0.002) (Figure 2D).

Next, Kaplan–Meier curves were drawn to compare the differences in the survival time between high HIC1 expression and low HIC1 expression subgroups. The OS Kaplan–Meier curves indicated that patients with high HIC1 expression in ACC (P = 0.015), MESO (P = 0.011), TGCT (P = 0.041), and UVM (P < 0.001) had a shorter survival time, while UCEC patients with high HIC1 expression had a longer survival time (P = 0.010) (Figure 3A). As for DFS Kaplan–Meier curves, we detected that HIC1 expression was linked to shorter survival time in ACC (P = 0.014), whereas was associated with longer survival time in BLCA (P = 0.037) and UCEC (P < 0.001) (Figure 3B). With regards to DSS Kaplan–Meier curves, we found that HIC1 expression was significantly connected with poor DSS in ACC (P = 0.011), KIRP (P = 0.003), and UVM (P < 0.001), while was related to better DSS in pheochromocytoma and paraganglioma (PCPG) (P = 0.004) and UCEC (P = 0.002) (Figure 3C). Finally, the Kaplan–Meier curves of PFS showed that high HIC1 expression predicted poor PFS in ACC (P = 0.027), KIRP (P = 0.004), and UVM (P = 0.002), while predicted better PFS in CHOL (P = 0.018), THCA (P = 0.012) and UCEC (P < 0.001) (Figure 3D). In summary, these results indicated that HIC1 may function as a prognosis-related risk factor in several cancers, including ACC, MESO, KIRP, TGCT, and UVM, and a prognosis-related protective factor in BLCA, CHOL, PCPG, THCA, and UCEC.

Genetic alternation analysis of HIC1

Next, we investigated the genetic alternation characteristics of HIC1 in the cbioportal database. The genetic alternation frequency of HIC1 was approximately 1.1%, and the genetic alternation frequency was higher than 2.5% in 3 cancer types, including CHOL, SARC, and STAD in TCGA pan-cancer cohort (Figure 4A). Deep deletion, amplification, and missense mutation were the major types of genetic alteration of HIC1 in pan-cancer (Figure 4B). Furthermore, we investigated the genetic mutation

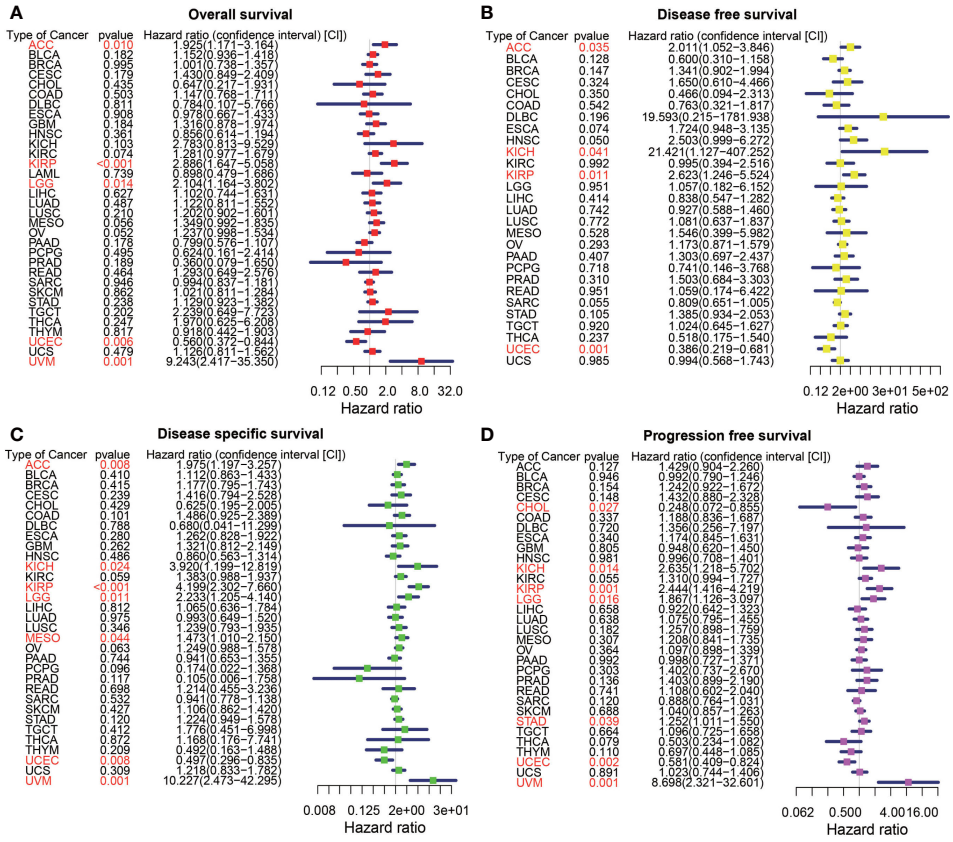

FIGURE 2
The forest map of univariate Cox regression analysis of HIC1. **(A)** The forest map shows the results of univariate Cox regression analysis of HIC1 for OS in TCGA pan-cancer. **(B)** The forest map shows the results of univariate cox regression analysis of HIC1 for DFS in TCGA pan-cancer. **(C)** Forest map shows the results of univariate Cox regression analysis of HIC1 for DSS in TCGA pan-cancer. **(D)** The forest map shows the results of univariate cox regression analysis of HIC1 for PFS in TCGA pan-cancer. Red items indicate statistical significance.

types, sites, and case samples of HIC1. Missense mutation was the most common alternation type of HIC1, while G541R mutation was detected in two samples in PRAD and STAD respectively (Figure 4C). In addition, the putative copy-number alterations of HIC1 from genomic identification of significant targets in cancer (GISTIC) included many types, such as deep deletion, shallow deletion, amplification, and gain function, contributing to the alternations of gene expression (Figure 4D). The genetic alterations of SMURF2P1, IGHV3-74, IGLV3-1, CLIP1-AS1, HNF1A-AS1, LINC01761, LINC02607, TLCD4-RWDD3, DPYD-AS2, and LINC01089 were more commonly occurred in the HIC1-altered group in comparison with unaltered group (Figure 4E).

Gene set enrichment analysis

To investigate the potential biological functions and signaling pathways of HIC1 in the specific cancer type, KEGG pathway and GO functional analyses were performed. The results of KEGG analysis indicated that HIC1 was most commonly involved in the chemokine signaling pathway and cytokine-cytokine receptor interaction, as well as the T cell receptor signaling pathway, calcium signaling pathway, JAK-STAT signaling pathway in different cancer types (Figure 5A). GO analysis found that HIC1 might exert biological functions in calcium ion transport in cancer, and functions on the immune system, including adaptive immune response, activation of immune response, regulation of lymphocyte activation, and T cell activation in cancer biology (Figure 5B). These results indicated that calcium transport and calcium signaling pathway and immune modulatory functions were most commonly involved in HIC1 in cancer biology, suggesting the critical roles of HIC1 in regulating the tumor immune microenvironment.

Correlation of HIC1 expression with the tumor immune microenvironment

To further uncover the potential immunomodulatory functions of HIC1 in tumor immunity, we employed the ESTIMATE algorithm, CIBERSORT algorithm, and TISIDB databases to investigate the correlations of HIC1 with the tumor immune microenvironment in pan-cancer. The results of the ESTIMATE algorithm suggested that HIC1 expression was positively correlated with immune and stromal scores in multiple cancers, including BLCA, CHOL, COAD, ESCA, LUSC, PAAD, PCPG, PRAD, rectum adenocarcinoma (READ), and

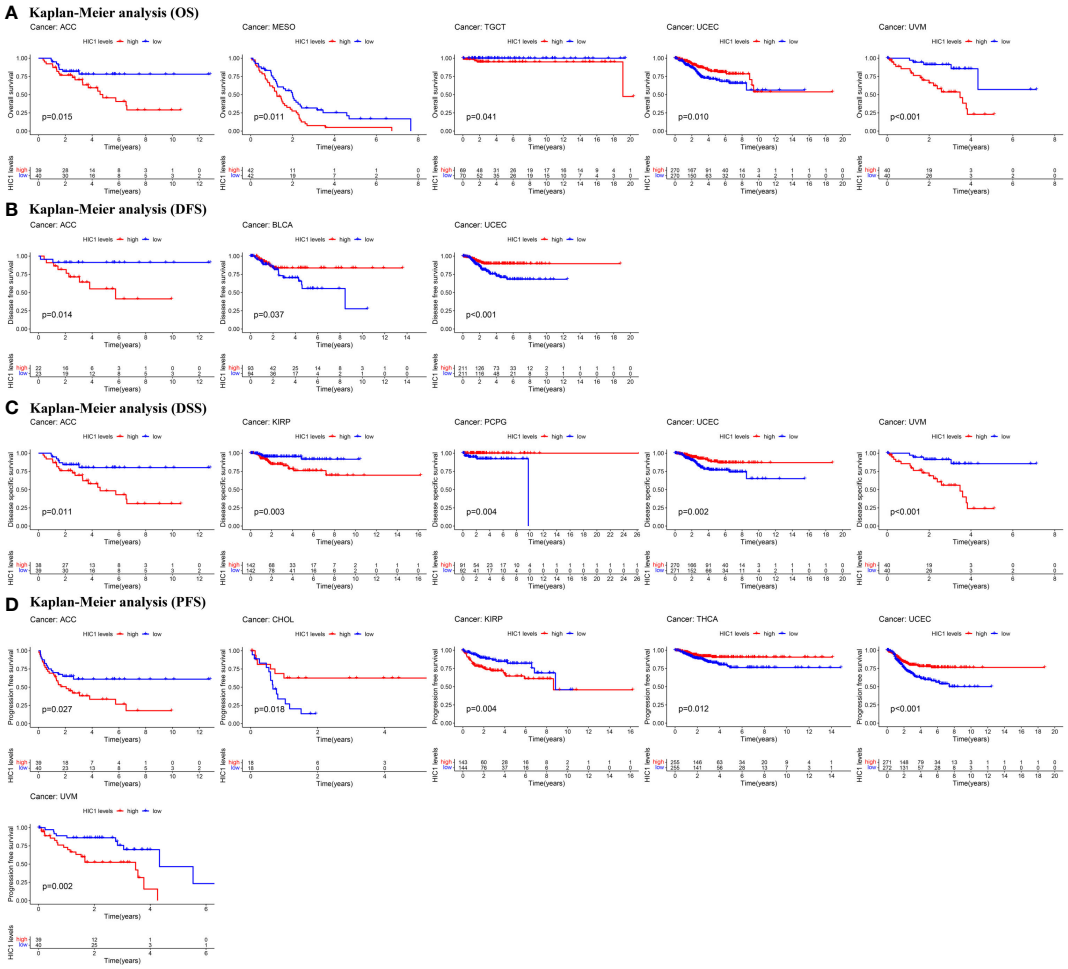

FIGURE 3
Kaplan-Meier survival curves of HIC1 in pan-cancer. **(A)** Kaplan–Meier analysis of the correlation between HIC1 expression and OS in 5 cancer types. **(B)** Kaplan–Meier analysis of the correlation between HIC1 expression and DFS in 3 cancer types. **(C)**Kaplan–Meier analysis of the correlation between HIC1 expression and DSS in 5 cancer types. **(D)** Kaplan–Meier analysis of the correlation between HIC1 expression and PFS in 7 cancer types.

UVM (Figure 6). In addition, there was a positive correlation between HIC1 expression and stromal scores in SARC, SKCM, STAD, TGCT, UCEC, OV, liver hepatocellular carcinoma (LIHC), LUAD, KIRP, HNSC, CESC, and BRCA (Figure S1). Moreover, we utilized CIBERSORT to analyze the abundance of diverse infiltrating immune cells in the specific cancer type. The results showed that HIC1 expression was negatively related to T follicular helper cells infiltration in UCS, THYM, TGCT, and BLCA, and CD4+ memory resting T cells infiltration in ACC and THYM. In particular, there was also a negative correlation of HIC1 expression with B naive cells abundance in TGCT, NK activated cells abundance in CHOL, whereas a positive correlation of HIC1 expression with mast resting cells in ESCA, STAD, and THYM, mast activated cells in KICH, dendritic resting cells in THYM, M1 macrophages in lymphoid neoplasm diffuse large B-cell lymphoma (DLBC), M2 macrophages in SARC, and plasma cells in CHOL (Figure 7). Overall, HIC1 expression was mainly correlated with T cells, B cells, macrophages, and mast cells within the tumor immune microenvironment in multiple cancer types.

Moreover, TISIDB online database was utilized to explore the effects of HIC1 on mediating tumor-infiltrating lymphocytes, the expression of MHC genes, immunoinhibitory/immunostimulator genes, chemokines, and chemokines receptors during cancer progression. There were positive correlations between HIC1 expression and several immunoinhibitory genes, such as TGFB1, ADORA2A, and CSF1R in multiple cancers (Figure 8A). It was also detected that HIC1 expression was positively related to several immunestimulators in different cancers, such as CXCL12 and TNFRSF4, and was negatively connected with IL-6R in TGCT (Figure 8B). Besides, we found that HIC1 expression was positively linked to MHC genes, such as TAPBP in TGCT and HLA-DPB1 in COAD (Figure 8C). In addition, there were positive correlations between HIC1 and lymphocytes, such as macrophages and mast cells in multiple cancers (Figure 8D). With regards to chemokines and chemokines receptors, our results revealed significantly positive correlations of HIC1 with CXCL12 and CCR10 in several cancers (Figures 8E, F). These findings revealed that HIC1 may function as an important mediator of immune-related biomolecules and lymphocytes in the tumor immune microenvironment.

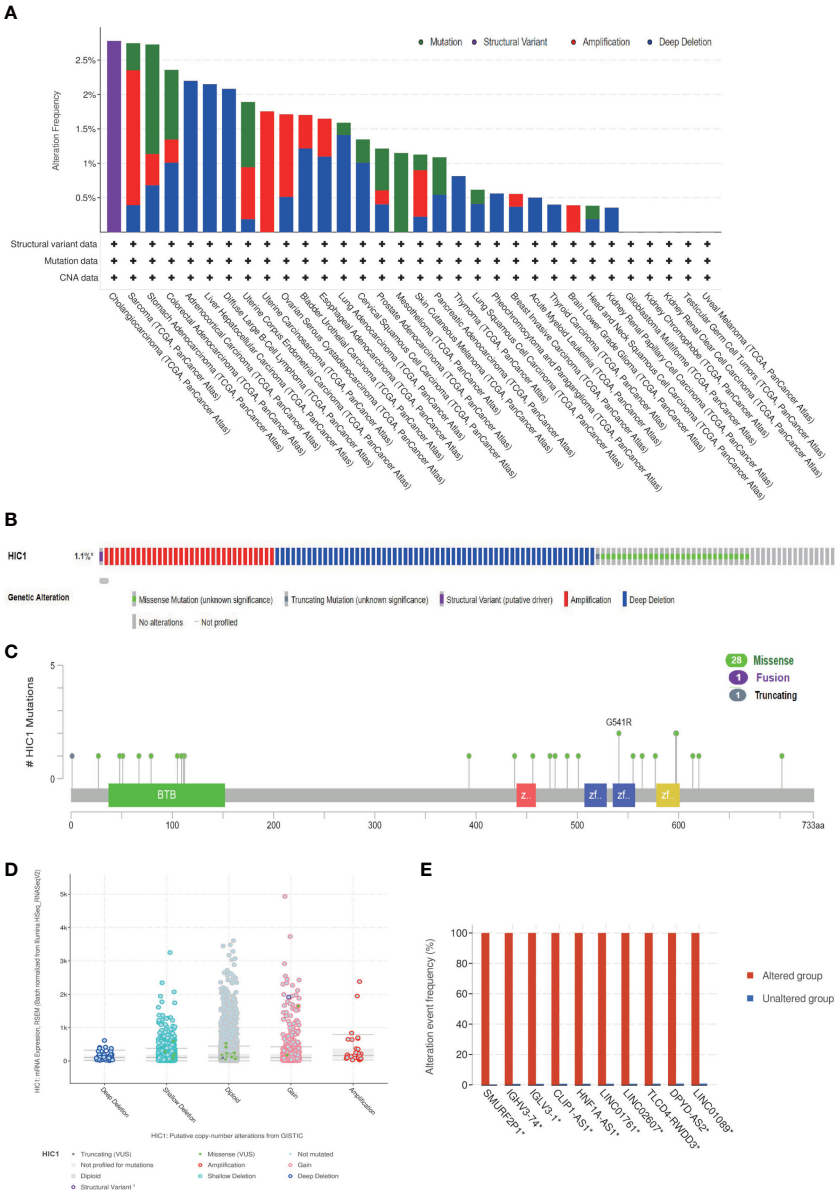

FIGURE 4
The genetic alteration characteristics of HIC1 in pan-cancer. **(A)** The alteration frequency of HIC1 with different types of mutations in different cancer types. **(B)** Different genetic alteration types of HIC1. **(C)** The mutation types, sites, and sample numbers of the HIC1 genetic alterations. **(D)** The correlated alteration types and putative copy-number of HIC1 in pan-cancer. **(E)** Co-occurrence of genetic mutations in tumors with HIC1 alterations.

Correlation of HIC1 with TMB and MSI

To illustrate the predictive value of HIC1 in cancer immunotherapy treatment, we further investigated the relationship of HIC1 expression with TMB and MSI, two biomarkers that are closely connected with cancer immunotherapy efficacy. The radar figure showed that HIC1 expression was negatively connected with MSI level in STAD, READ, SKCM, DLBC, and UCEC (Figure 9B). As for TMB, there was a significantly negative correlation between HIC1 expression and TMB in multiple cancer types, including THCA, STAD, SKCM, PRAD, PAAD, LUSC, LUAD, LIHC, KIRP, HNSC, DLBC, COAD, CHOL, CESC, BRCA, and BLCA, whereas a significantly positive connection in LGG, SARC, and THYM (Figure 9A). These results suggested that HIC1 expression may be correlated with immunotherapeutic responses in these human cancer types.

Correlation between HIC1 expression with immunotherapeutic efficacy

The potential of HIC1 in predicting the immunotherapeutic efficacy of anti-PD-1/PD-L1 treatment for cancer patients was further investigated. A total of 3 cohorts, including GSE78220, GSE67501, and IMvigor210, were included in our study to compare the differential HIC1 expression between immunotherapy-

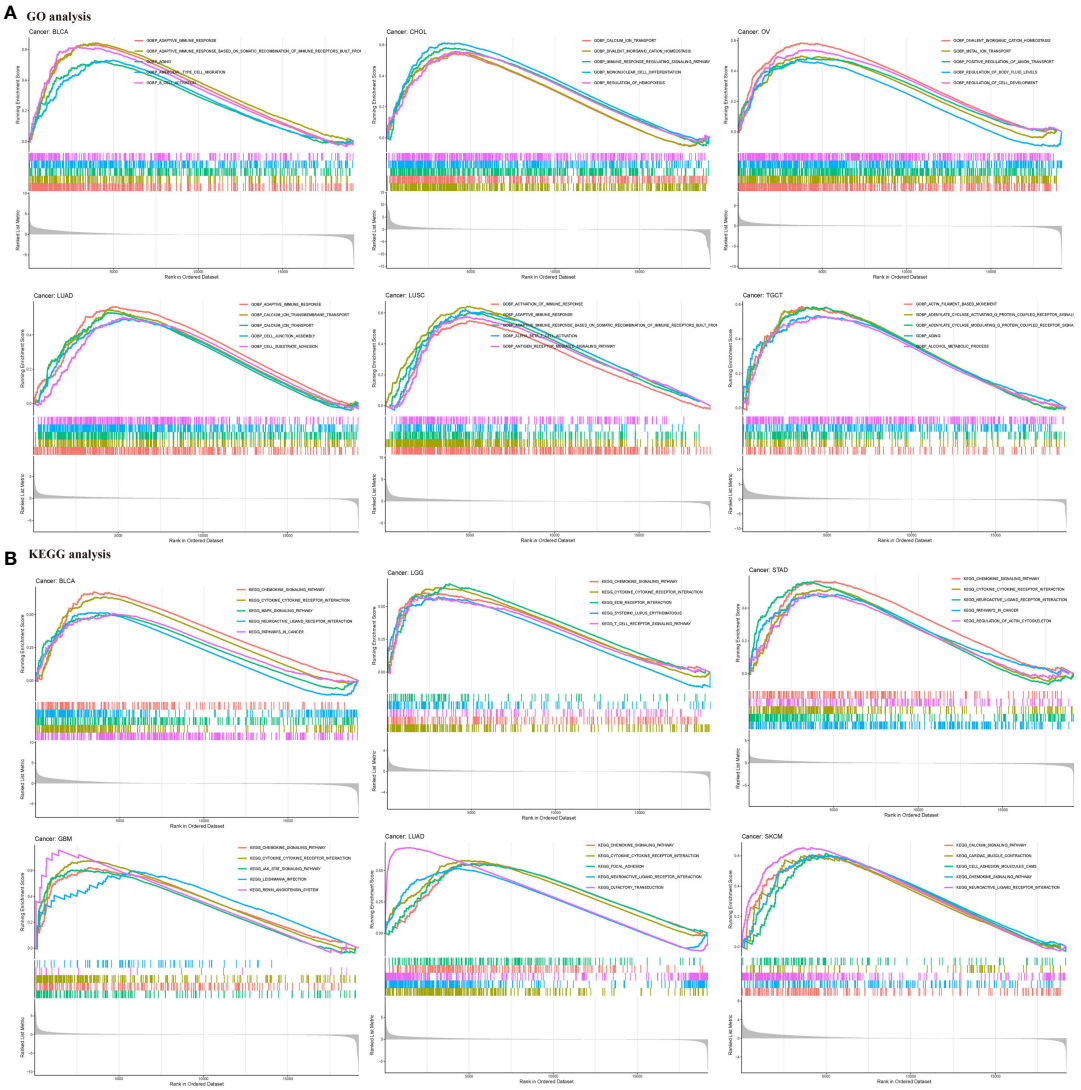

FIGURE 5
GSEA of HIC1. **(A)** GO functional annotation of HIC1 shows that HIC1 might exert biological functions in calcium ion transport in cancer, and modulating immune system. **(B)** KEGG pathway analysis of HIC1 indicated HIC1 was most commonly involved in the chemokine signaling pathway and cytokine-cytokine receptor interaction, as well as T cell receptor signaling pathway, calcium signaling pathway, JAK-STAT signaling pathway in different cancer types. Peaks on the upward curve indicate positive regulation and peaks on the downward curve indicate negative regulation.

responsive and immunotherapy-nonresponsive patients. The results showed that HIC1 expression was significantly higher in patients with nonresponses to immunotherapy in IMvigor210 (Figure 9C) and GSE78220 cohorts (Figure 9D), while there was no static significance in the GSE67501 cohort (Figure 9E). These results indicated that HIC1 could effectively predict the immunotherapy responses for individual cancer patient and might be a novel therapeutic target to overcome immunotherapy resistance.

Drug sensitivity analysis of HIC1

We further explored the potential relationship between HIC1 expression and drug sensitivity by utilizing the CellMiner database. We found that HIC1 expression was positively correlated with the sensitivity to several agents, including rebimastat, zoledronate, nelarabine, axitinib, temsirolimus, and batracylin (Figures 10A–F), while was negatively correlated with the sensitivity to trametinib, cobimetinib, selumetinib, and PD–98059 (Figures 10G–J). Notably, the results indicated that HIC1 might be significantly correlated with the sensitivity to several small molecule inhibitors that have been applied in cancer treatment, such as MEK inhibitors trametinib and PD–98059.

IHC validation of HIC1

The expression of HIC1 was further verified by IHC across 4 different types of cancer by our cohorts, including LUAD, SARC, breast cancer, and KIRC. As shown in Figure 11, HIC1 was detected in all of the examined tumor tissue samples. A strongly positive expression of HIC1 was observed in SARC and KIRC, while low expression of HIC1 was detected in patients with LUAD and breast

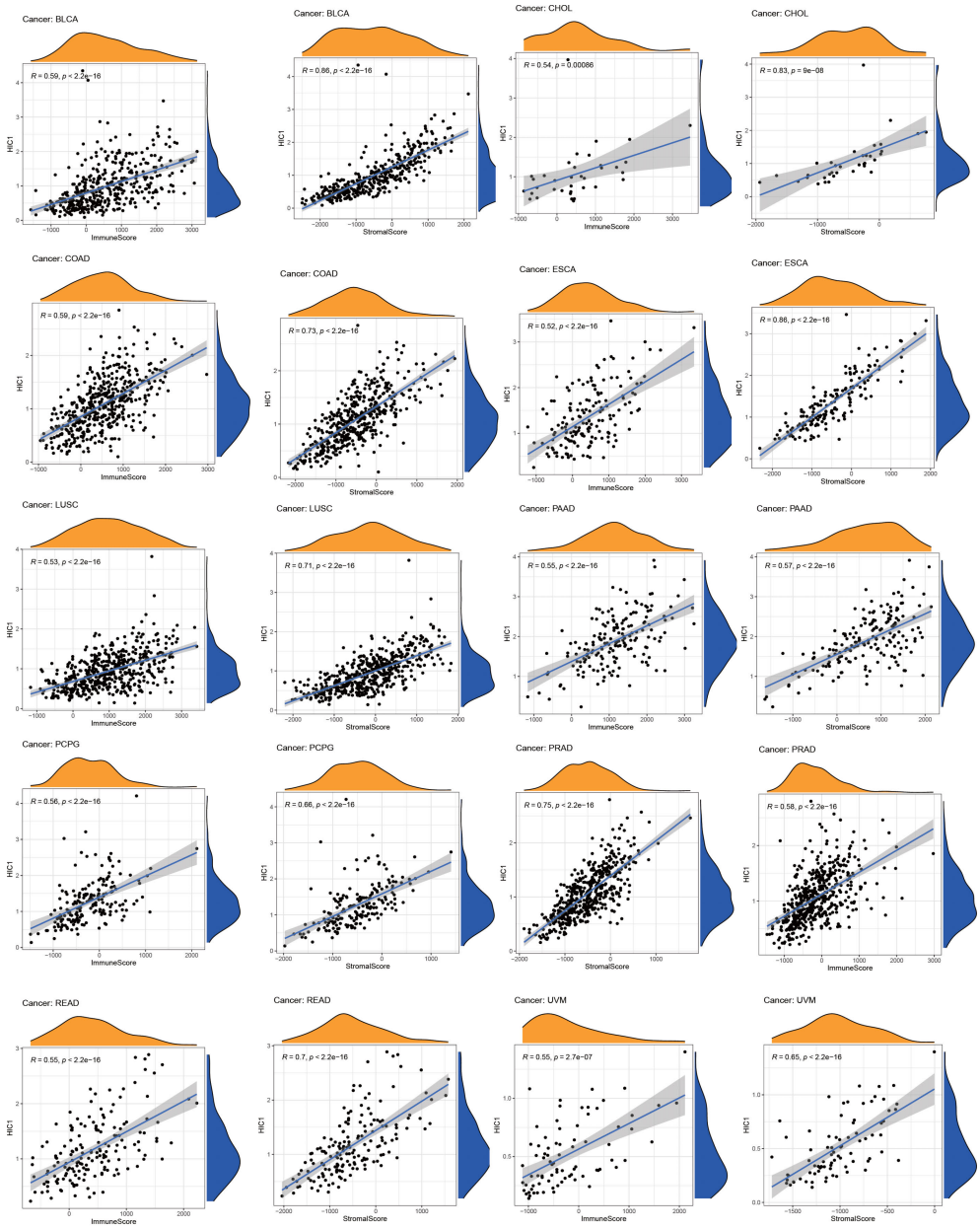

FIGURE 6
The correlation between HIC1 and immune and stromal scores in pan-cancer.

cancer. The immunoreactivity score of each cancer type was presented in Figure 11E. These findings further were generally consistent with previous bioinformatics analysis. In addition, we also obtained IHC results from the HPA database and compared the results with HIC1 protein level in UALCAN. The IHC staining of HIC1 was mainly weakly or negatively expressed in tumor tissue from breast cancer, LUSC, LUAD, and COAD while was relatively higher in their corresponding normal tissues (Figure S2).

Discussion

HIC1 is frequently hypermethylated which lead to the inactivation of HIC1 in the development of tumor. As a direct target gene of P53, HIC1 is associated with the regulation of cell-cycle regulation, thus contributing to tumorigenesis (22). A HIC1-SIRT1-p53 circular loop has been well illustrated. In the circular loop, HIC1 inhibits the transcription of SIRT1 which deacetylates and suppresses the expression of p53, thus resulting in the inactivation of HIC1 in turn (23). Nowadays, the role of HIC1 in several cancers, such as colorectal cancer (24), epithelial ovarian cancer (25) and medulloblastoma (26), have been investigated. Recent work has found that HIC1 can regulate ferroptosis during cancer progression (14, 15, 27). Wang et al. have constructed and validated a novel prognostic signature including 3 ferroptosis-related genes: HIC1, LPCAT3, and DUOX1. *In vitro* experiments revealed that inhibition of HIC1 can promote chemosensitivity and anti-PD1 therapy efficacy through inducing

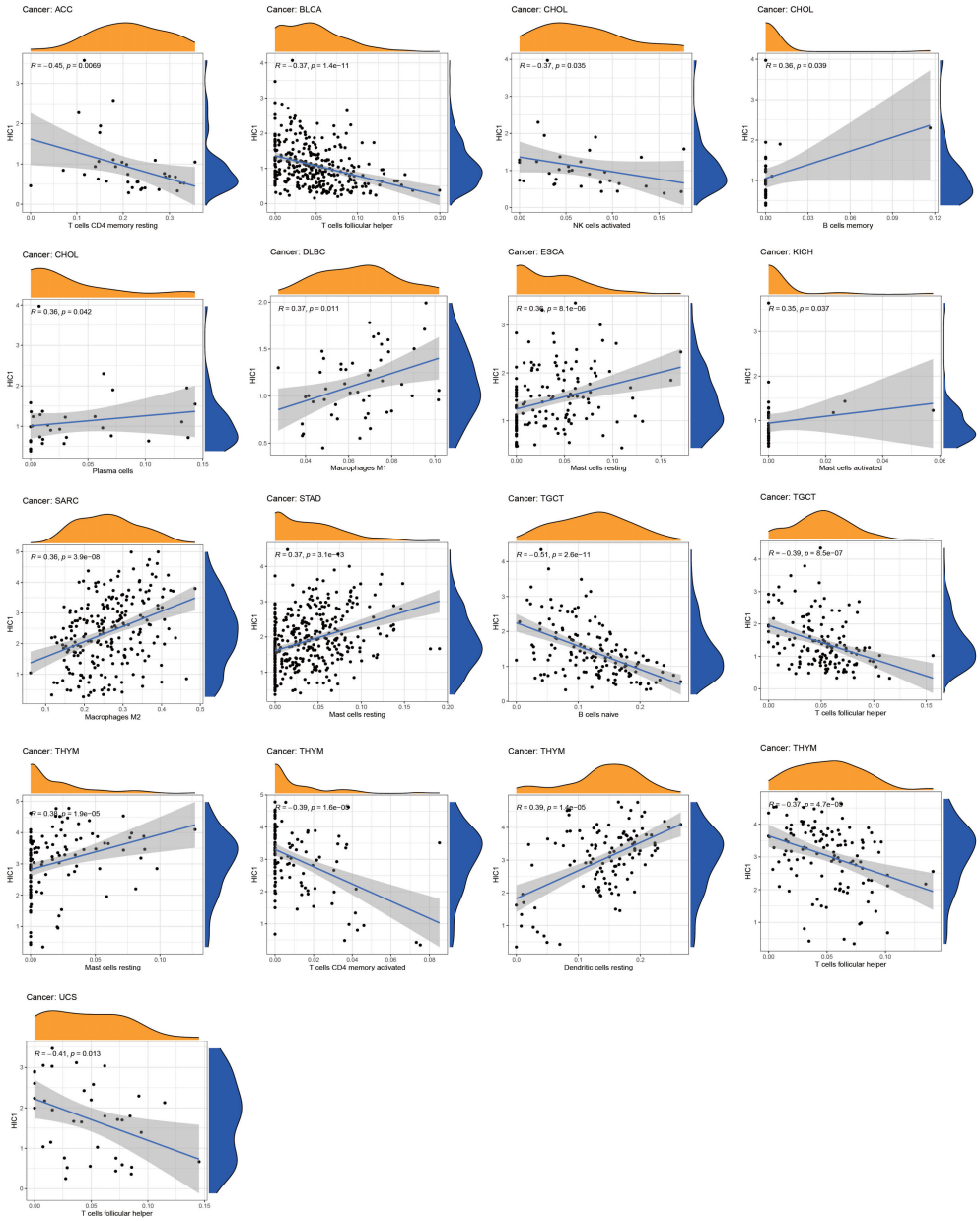

FIGURE 7
The correlation between HIC1 expression and the immune cells infiltration in pan-cancer.

ferroptosis in ovarian cancer cells (15). Notably, ferroptosis has been confirmed to play critical roles in cancer immunotherapy, and ferroptosis activation may be a potential strategy to promote the immunotherapy efficacy (28). For instance, inhibition of APOC1 can increase the M1/M2 macrophage ratio through regulating ferroptosis and improve the anti-PD-1 immunotherapy efficacy for hepatocellular carcinoma (HCC) (29). Wang et al. have found that immunotherapy-activated CD8 + T cells can enhance ferroptosis-specific lipid peroxidation in tumor cells, and that increased ferroptosis further results in the increasing anti-tumor efficacy of immunotherapy (30). However, the roles of HIC1 are inconsistent and controversial among several cancers, there are no pan-cancer analysis of HIC1 and the associations of HIC1 with tumor immune microenvironment and the immunotherapeutic efficacy are still largely unknown. Therefore, we perform a pan-cancer analysis to thoroughly explore the clinical significance of HIC1 as well as its critical roles in tumor immune microenvironment and immunotherapy.

To begin with, we investigated the expression levels and clinical significance of HIC1 in different cancers. The results showed that compared with adjacent normal samples in TCGA, HIC1 expression was significantly decreased in tumor samples in BLCA, BRCA, CESC, COAD, KICH, KIRP, LUAD, LUSC, THCA and UCEC, while was strongly increased in CHOL, HNSC, and KIRC. By comparing HIC1 expression between TCGA tumor samples and GTEx normal samples, upregulation of HIC1 was also detected in GBM, LAML, PAAD, and STAD, and downregulation of HIC1 was also found in ACC, ESCA, LGG, LIHC, OV, PRAD, SKCM, and UCS. These inconsistent findings may be attributed to the application of different algorithms, sample

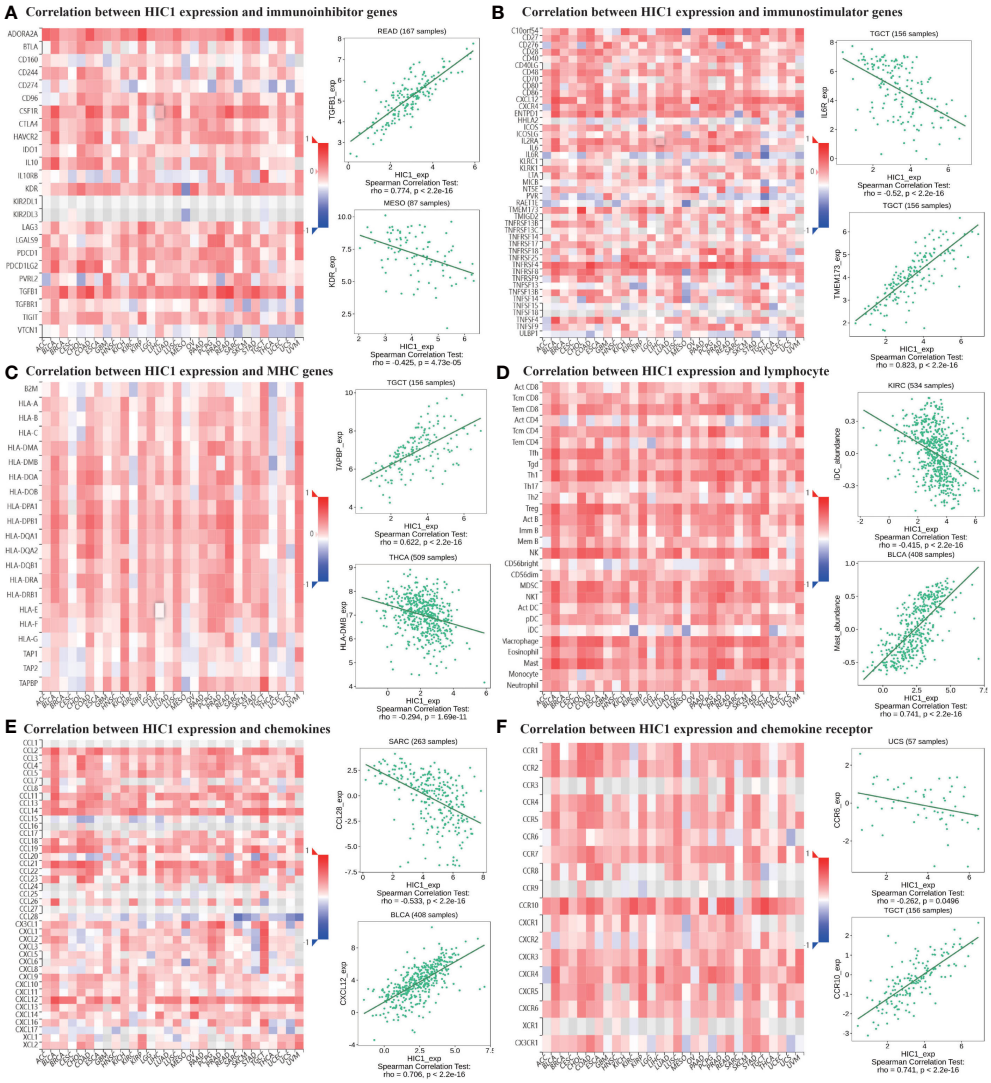

FIGURE 8
The correlation between HIC1 expression and immune-related biomarkers in the TISIDB database. The co-expression heatmaps show the association between HIC1 expression and **(A)** immunoinhibitor genes, **(B)** immunostimulator genes, **(C)** MHC genes, **(D)** lymphocyte, **(E)** chemokines, and **(F)** chemokines receptors in pan-cancer.

sizes and sources in distinct databases, and the insufficient number of normal samples in TCGA may also result in insignificant findings in some cancer types. There was also disparity between HIC1 expression in TCGA tumor tissues and CCLE cancer cell lines, which may be attributed to the fact that there are multiple cell lines in a specific cancer type in CCLE database, and gene expression level is often significantly different among these cell lines *in vitro* experiment. Also, gene expression in cancer patients may change during cancer progression and after receive different treatment options, which may also explain this phenomenon. IHC results in our clinical samples further confirmed the low protein level of HIC1 in breast cancer and LUAD, while the relatively high HIC1 protein expression in KIRC and SARC, which further validates HIC1 expression pattern in bioinformatics analysis. Previous studies have found that HIC1 was downregulated in bladder cancer, and HIC1 can inhibit bladder cancer progression through the YAP signaling pathway (31). HIC1 expression has been found to be silenced only in triple-negative breast cancer compared with other breast cancer molecular subtypes, and HIC1 slicing could facilitate triple-negative breast cancer progression by targeting lipocalin-2 (LCN2) (32). However, Brieger et al. indicated that chromosome 17p13.3 where HIC1 is located on is a region usually lost in HNSC (33) and Eggers et al. showed that HIC1 hypermethylated and inactivated in KIRC (34). These results conflicted with our findings, possibly because of the different sources of samples and heterogeneity, which should be further validated in more large cohorts. With regards to the clinicopathological significance of HIC1, our results found that HIC1 was expressed higher in patients with later clinical stages in BLCA, ESCA, and STAD, indicating that HIC1 may function as a biomarker for predicting disease progression for cancer patients. Zhang et al. have reported that HIC1 expression was negatively related to the clinical stage in patients with liver cancer (14). As determined by pan-cancer prognostic analyses, high HIC1 expression was significantly correlated with improved OS, DFS, DSS, and PFS in ACC, OS, DSS, and PFS in UVM, DSS, and PFS in KIRP,

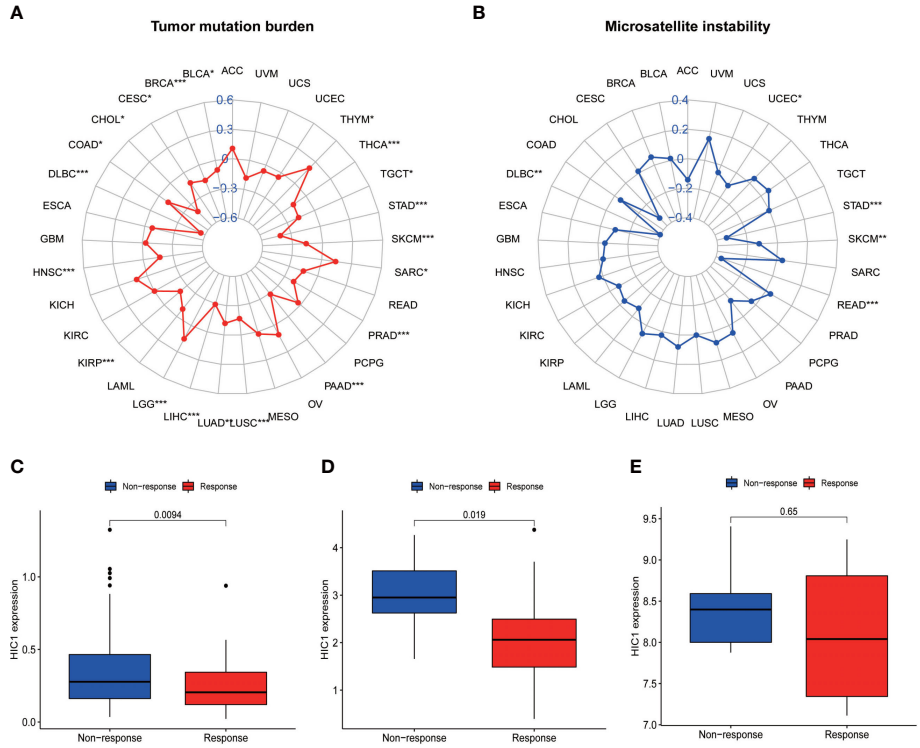

FIGURE 9
The correlation between HIC1 expression and TMB levels, MSI event, and immunotherapeutic efficacy. **(A)** Radar map of the relationship between HIC1 expression and TMB levels. **(B)** Radar map of the relationship between HIC1 expression and MSI event. **(C–E)** The relationship between HIC1 expression and the immunotherapeutic efficacy in IMvigor210 cohort **(C)**, GSE78220 **(D)**, and GSE67501 **(E)**. *p < 0.05, **p < 0.01; ***p < 0.001.

OS in MESO, and TGCT. In contrast, UCEC patients with high HIC1 expression were significantly associated with worse OS DFS, DSS, and PFS. There were also significant associations between CHOL patients with high HIC1 expression and worse PFS, BLCA patients with worse DFS, and PCPG patients, and worse DSS. Combining these results, our studies suggest patients with high HIC1 expression had a better prognosis in ACC, UVM, KIRP, MESO, and TGCT, while had a worse prognosis in UCEC, BLCA, CHOL, and PCPG. Previous studies indicated that overexpression of HIC1 can act as a poor prognostic biomarker for KIRC, while a biomarker for better prognosis in

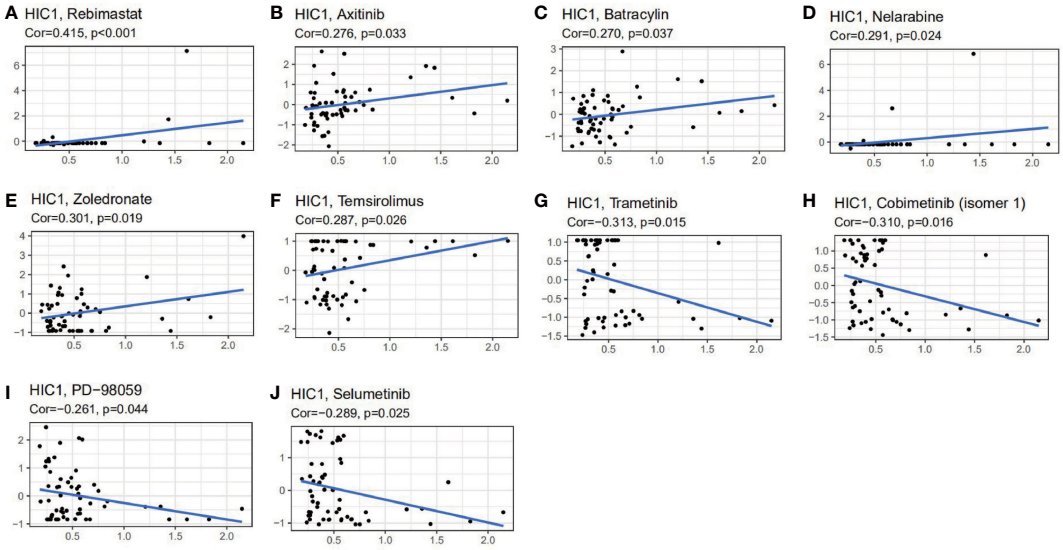

FIGURE 10
The correlation between HIC1 expression and drug sensitivity. The HIC1 was linked to the sensitivity of **(A)** Rebimastat, **(B)** Axitinib, **(C)** Batracylin, **(D)** Nelarabine, **(E)** Zoledronate, **(F)** Temsirolimus, **(G)** Trametinib, **(H)** Cobimetinib, **(I)** PD-98059, and **(J)** Selumetinib.

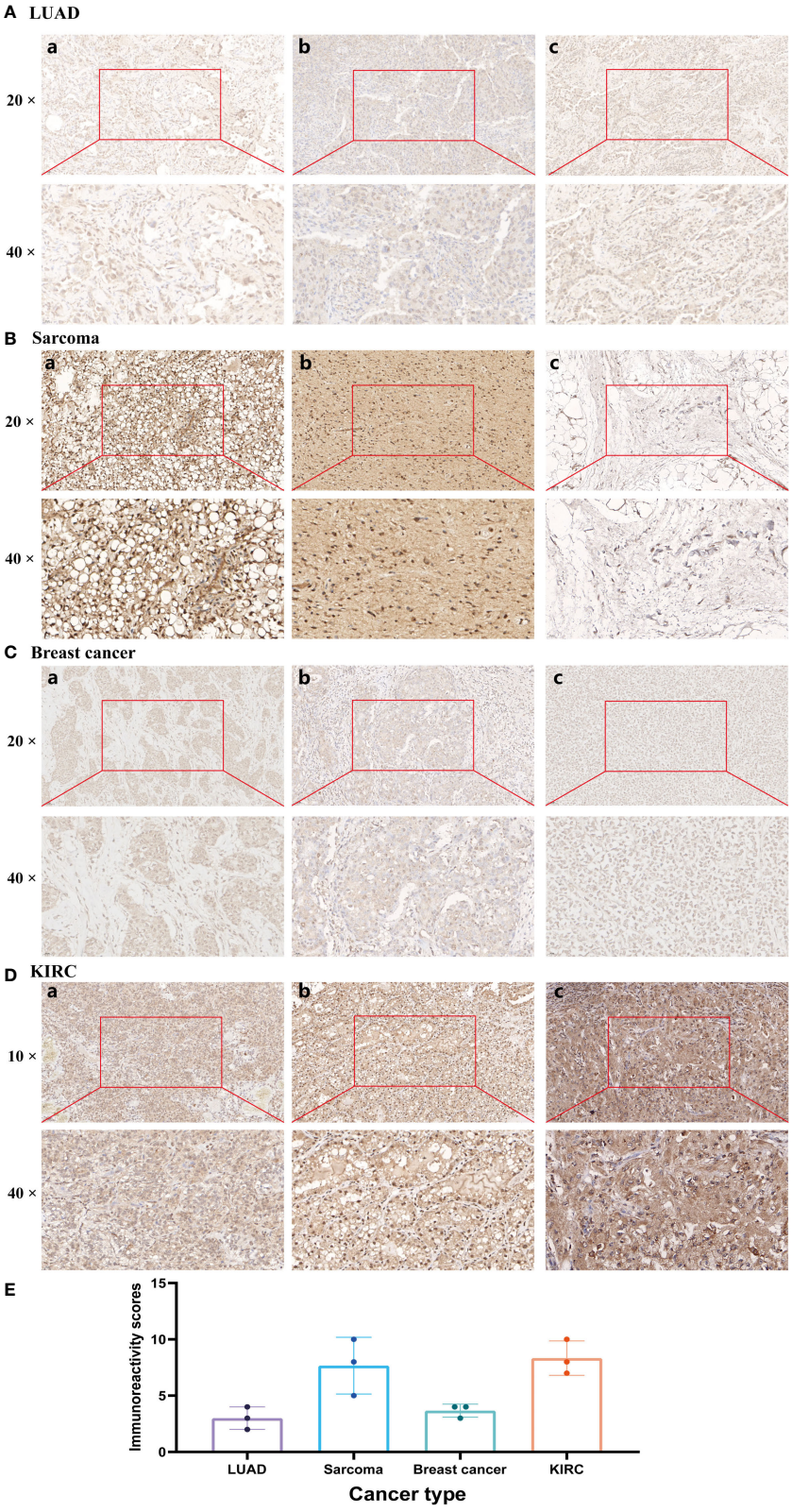

FIGURE 11
Immunohistochemistry validation of HIC1 in different cancers by clinical samples. **(A)** LUAD, **(B)** SARC, **(C)** Breast cancer, **(D)** KIRC, and **(E)** Immunoreactivity score.

pancreatic cancer (9, 34). It has been found that HIC1 is an important contributor to the development and functions of several immune cells, such as T cells and macrophage. Therefore, the associations of HIC1 with cancer prognosis may attribute to its ability to mediate the body's immune response. Overall, these findings indicate that HIC1 may serve different functions in different cancer types, and is a critical prognostic biomarker in several cancers, and monitoring HIC1 expression may help predict the prognosis of cancer patients, which is mutually corroborated by previous studies.

Cancer is usually resulted from genetic alterations and cancer genomes included 4-5 mutations on average (35). Genetic changes play an important role in regulating cancer development and immune tolerance. For instance, mutant PD-L1 with structural variations can contribute to aberrant PD-L1 expression and immunosuppression. The amplifications of JAK2/PD-L1/PD-L2 (9p24.1) can induce constitutive overexpression of PD-L1 and a significant response to immune checkpoint inhibitors (36). In our study, we found that the major types of genetic alteration of HIC1 were deep deletion, amplification, and miss mutation. The genetic alternation frequency of HIC1 was higher than 2.5% in CHOL, which was matched with previous studies (37). It has been found that several CpG-islands (HIC1, OPCML, SFRP1, PTEN, and DcR1) presented a frequency of hypermethylation >28% of CHOL (37). In prostate carcinoma, a high frequency of alterations in the promoter methylation status of HIC1, SFRP2, and DAPK1 was detected in patients with prostate carcinomas of high Gleason Score (GS) (38). Currently, the functions of HIC1 genetic alternations in cancer immunological activity are still largely known and warranted further investigation.

To further explore the biological functions and downstream signaling pathways of HIC1 in different cancer types, we conducted KEGG and GO analysis. Our results suggested that HIC1 plays an important role in the chemokine signaling pathway in several cancers. It has been reported that deletion of HIC1 can contribute to premalignant transformation in the early stage of tumor formation. Moreover, the HIC1-deleted breast cancer cells can secret CXCL14 to its cognate receptor GPR85 on mammary fibroblasts in the microenvironment, and activate fibroblasts through the ERK1/2, Akt, and neddylation signaling pathways, whereas the activated fibroblasts can facilitate breast cancer progression through inducing epithelial-mesenchymal transition (EMT) by the CCL17/CCR4 axis (39). Besides, the results indicated that HIC1 is associated with T cell-related pathways, including the T cell receptor signaling pathway and T cell activation. Previous studies have reported that HIC1 suppresses the function of human induced regulatory T cells (iTreg) by interacting with the transcription factors (TFs) required for the development of Th1/2/17 cells (40). In addition, HIC1 can promote the differentiation of tissue-resident memory T cells (T_{RM} cells) (41). These findings are consistent with our results and confirmed the critical roles of HIC1 in mediating T cell functions. Our results also showed that HIC1 is related to cytokine-cytokine receptor interaction, calcium signaling pathway, MAPK signaling pathway as well as regulating the immune system.

The tumor immune microenvironment has been regarded as an integral part of cancer, which forms a complex tumor microenvironment that supports the growth and metastatic dissemination of cancer cells (42). Importantly, novel targets within the tumor immune microenvironment can help direct and improve the actions of cancer immunotherapies which can reshape the tumor immune microenvironment and restores the capability of immune cells to kill tumor cells. To further reveal the role of HIC1 in the tumor immune microenvironment, we first analyzed the relationship between HIC1 expression and immune and stromal scores by the ESTIMATE algorithm, which presented a positive correlation in multiple cancers, such as BLCA, CHOL, and COAD. Furthermore, we explored the relationship between HIC1 expression levels and the abundance of infiltrating immune cells in the specific cancer type. Our results showed that HIC1 expression was mainly associated with T cells, B cells, macrophages, and mast cells in the tumor immune microenvironment in multiple cancers. Previous studies have indicated the correlation between HIC1 and T cells, including iTreg and T_{RM} cells (40, 41). HIC1 has been found to be upregulated early during the differentiation of human iTreg cells, and HIC1 deficiency can contribute to a significant loss of suppression by iTreg cells with a concomitant upregulation of effector T cell associated genes (40). Besides, HIC1 has been reported to regulate the differentiation of B lymphocytes by inhibiting the transcription of class II transactivator (CIITA) (43). To date, little research has been conducted to investigate the role of HIC1 in mediating immune cells in tumor immune microenvironment, which may be a novel direction for exploring the biological functions in oncology.

TMB is defined as the total number of mutations present in a tumor specimen and reflects cancer mutation quantity (44). High TMB is clinically related to better response for immune checkpoint inhibitors (ICI) and has been acknowledged as a predictive biomarker (45). MSI is also a predictive biomarker for the responses of cancer patients to ICI (46). Narayan G et al. have suggested that the expression level of HIC1 is positively correlated with the frequency of MSI-H in cervical cancer (47). Our results indicated that the expression level of HIC1 is associated with TMB in 20 cancer types and MSI in 5 cancer types, such as STAD, READ, SKCM, and DLBC, suggesting the promising potential of HIC1 as a biomarker for predicting the efficacy of cancer immunotherapy. Furthermore, we identified the role of HIC1 in the immunotherapeutic efficacy in 3 cohorts. Our results illustrated that in patients with metastatic urothelial cancer and melanoma, there was a higher expression level of HIC1 in patients with no-response to PD-1/PD-L1 inhibitors, suggesting that HIC1 may serve as a promising biomarker for predicting the immunotherapy efficacy in melanoma and urothelial cancer. Several studies have explored the clinical significance and functions of HIC1 in metastatic urothelial cancer and melanoma. For instance, it has been reported that HIC1 prohibited the progression of uveal melanoma by activating lncRNA-numb, providing a potential therapeutic target for uveal melanoma (48). In KIRC, patients with lymph node metastases presented a low methylation level of HIC1 compared to patients without lymph node metastases, and hypermethylation of HIC1 can act as a poor prognostic biomarker for renal cell carcinoma (34). In addition, hypermethylation of the HIC1 exacerbated prostate cancer metastasis by inducing epithelial-mesenchymal transition (EMT) mediated by Slug and CXCR4, which contributed to the poor prognosis of prostate cancer patients (39). However, the predictive value of HIC1 for immunotherapeutic

efficacy in these cancers has not been illustrated, which should be further investigated in future studies.

Therefore, HIC1 has the potential to act as a biomarker associated with cancer immunotherapies and predict immunotherapy responses in cancer patients. Dynamic monitoring of HIC1 expression may be a valuable approach to effectively evaluate the immunotherapeutic responses of cancer patients, thus helping choose the most suitable therapy strategy for individual cancer patients. Moreover, we also explore the relationship between HIC1 expression and the anti-cancer drug sensitivity of cancer patients. Koul S et al. have reported that the promoter hypermethylation of HIC1 was involved in the resistance of Male germ cell tumor (GCT) to cisplatin (49). Our findings showed that HIC1 is closely related to the sensitivity of multiple anti-cancer drugs, especially small molecule inhibitors, including MEK inhibitors trametinib and PD–98059, indicating HIC1 plays a critical role in predicting the sensitivity of anti-cancer drugs. Among these drugs whose sensitivity is related to HIC1 expression, zoledronate, and trametinib have been reported to be associated with ferroptosis. In osteosarcoma, zoledronic acid can induce ferroptosis by decreasing ubiquinone and upregulating the expression of HMOX1 or cytochrome P450 oxidoreductase (POR) (50, 51). Besides, zoledronic acid also induced ferroptosis in osteoclasts by suppressing ubiquitination and degradation of p53 through FBXO9 (52). In addition, the combination of the MEK inhibitor trametinib and the autophagy inhibitor hydroxychloroquine (HCQ) could inhibit proliferative activity in Lkb1-deficient Kras-driven lung tumors by inducing ferroptosis (53). Future studies should focus on the roles of HIC1 in mediating cancer drug resistance through the regulation of ferroptosis.

Though we have comprehensively conducted numerous analyses to illustrate and validate the roles of HIC1 in pan-cancer, there are still some limitations in our research. Firstly, although we have validated the expression pattern in our clinical samples, the associations of HIC1 with immunotherapeutic efficacy and anti-cancer drug sensitivity have not been validated in our own cohorts. Secondly, the specific mechanisms by which HIC1 regulates the tumor immune microenvironment remain largely unclear and have not been illustrated in experiments. Therefore, future studies are required to investigate the biological functions of HIC1 in tumor immune microenvironment.

Conclusion

In summary, this comprehensive pan-cancer analysis of HIC1 reveals the expression pattern and role of the ferroptosis-related gene HIC1 in different cancer types. Our findings suggested that HIC1 may serve as a prognostic biomarker, and is related to immune infiltration, immunotherapeutic efficacy, and anti-cancer drug sensitivity in various cancers, thereby providing a theoretical basis for more precise cancer treatment in the future. Further research is needed to verify the specific mechanisms involved.

Data availability statement

The original contributions presented in the study are included in the article/Supplementary Material. Further inquiries can be directed to the corresponding authors.

Ethics statement

The studies involving human participants were reviewed and approved by the Ethics Committee of Second Xiangya Hospital. The patients/participants provided their written informed consent to participate in this study.

Author contributions

YLW and ZJL: writing–original draft, data curation, and formal analysis. ZYT and ZHL: immunohistochemistry analysis. YQJ and ZXT: writing–original draft. YTX, and ZTZ: formal analysis. JY and TL: writing–review and editing, and visualization. TL and ZHL: writing–review and editing, supervision, and funding acquisition. All authors contributed to the article and approved the submitted version.

Funding

This study was supported by grants from the National Natural Science Foundation of China (Grant No.81871783 and 82072441); Hunan Outstanding Youth Fund Project (Grant NO. 2022JJ10095); Chenzhou Municipal Science and Technology Bureau Science and Technology Development Program Project (Grant No. yfzx201910); Natural Science Foundation of Xinjiang Uygur Autonomous Region (NO. 2022D01C565).

Acknowledgments

We acknowledge the TCGA database for providing its platforms and contributors for uploading its meaningful datasets, and Sangerbox online dataset (http://sangerbox.com) for providing some analysis. We acknowledge Dr. Zhou for his contribution to immunohistochemistry analysis.

Conflict of interest

The authors declare that the research was conducted in the absence of any commercial or financial relationships that could be construed as a potential conflict of interest.

Publisher's note

Supplementary material

The Supplementary Material for this article can be found online at: https://www.frontiersin.org/articles/10.3389/fimmu.2023.1182030/full#supplementary-material

SUPPLEMENTARY FIGURE 1
A positive correlation between HIC1 expression and stromal scores in SARC, SKCM, STAD, TGCT, UCEC, OV, LIHC, LUAD, KIRP, HNSC, CESC, and BRCA.

SUPPLEMENTARY FIGURE 2
Comparison of HIC1 gene expression between normal and tumor tissues and immunohistochemistry images in normal and tumor tissues. **(A)** LUSC, **(B)** Breast cancer, **(C)** LUAD, and **(D)** COAD.

References

1. Sung H, Ferlay J, Siegel RL, Laversanne M, Soerjomataram I, Jemal A, et al. Global cancer statistics 2020: GLOBOCAN estimates of incidence and mortality worldwide for 36 cancers in 185 countries. *CA Cancer J Clin* (2021) 71:209–49. doi: 10.3322/caac.21660

2. Zhang Y, Zhang Z. The history and advances in cancer immunotherapy: understanding the characteristics of tumor-infiltrating immune cells and their therapeutic implications. *Cell Mol Immunol* (2020) 17:807–21. doi: 10.1038/s41423-020-0488-6

3. O'Donnell JS, Teng MWL, Smyth MJ. Cancer immunoediting and resistance to T cell-based immunotherapy. *Nat Rev Clin Oncol* (2019) 16:151–67. doi: 10.1038/s41571-018-0142-8

4. Yang Y. Cancer immunotherapy: harnessing the immune system to battle cancer. *J Clin Invest* (2015) 125:3335–7. doi: 10.1172/JCI83871

5. Xiao Y, Yu D. Tumor microenvironment as a therapeutic target in cancer. *Pharmacol Ther* (2021) 221:107753. doi: 10.1016/j.pharmthera.2020.107753

6. Fu T, Dai LJ, Wu SY, Xiao Y, Ma D, Jiang YZ, et al. Spatial architecture of the immune microenvironment orchestrates tumor immunity and therapeutic response. *J Hematol Oncol* (2021) 14:98. doi: 10.1186/s13045-021-01103-4

7. Zheng J, Wang J, Sun X, Hao M, Ding T, Xiong D, et al. HIC1 modulates prostate cancer progression by epigenetic modification. *Clin Cancer Res* (2013) 19:1400–10. doi: 10.1158/1078-0432.CCR-12-2888

8. Wang Y, Weng X, Wang L, Hao M, Li Y, Hou L, et al. HIC1 deletion promotes breast cancer progression by activating tumor cell/fibroblast crosstalk. *J Clin Invest* (2018) 128:5235–50. doi: 10.1172/JCI99974

9. Hu B, Zhang K, Li S, Li H, Yan Z, Huang L, et al. HIC1 attenuates invasion and metastasis by inhibiting the IL-6/STAT3 signalling pathway in human pancreatic cancer. *Cancer Lett* (2016) 376:387–98. doi: 10.1016/j.canlet.2016.04.013

10. Wales MM, Biel MA, Deiry W, Nelkin BD, Issa JP, Cavenee WK, et al. p53 activates expression of HIC-1, a new candidate tumour suppressor gene on 17p13.3. *Nat Med* (1995) 1:570–7. doi: 10.1038/nm0695-570

11. Chen WY, Wang DH, Yen RC, Luo J, Gu W, Baylin SB. Tumor suppressor HIC1 directly regulates SIRT1 to modulate p53-dependent DNA-damage responses. *Cell* (2005) 123:437–48. doi: 10.1016/j.cell.2005.08.011

12. Rood BR, Leprince D. Deciphering HIC1 control pathways to reveal new avenues in cancer therapeutics. *Expert Opin Ther Targets* (2013) 17:811–27. doi: 10.1517/14728222.2013.788152

13. Liu J, Chou Z, Li C, Huang K, Wang X, Li X, et al. ZBTB7A, a miR-144-3p targeted gene, accelerates bladder cancer progression *via* downregulating HIC1 expression. *Cancer Cell Int* (2022) 22:179. doi: 10.1186/s12935-022-02596-w

14. Zhang X, Du L, Qiao Y, Zhang X, Zheng W, Wu Q, et al. Ferroptosis is governed by differential regulation of transcription in liver cancer. *Redox Biol* (2019) 24:101211. doi: 10.1016/j.redox.2019.101211

15. Wang H, Cheng Q, Chang K, Bao L, Yi X. Integrated analysis of ferroptosis-related biomarker signatures to improve the diagnosis and prognosis prediction of ovarian cancer. *Front Cell Dev Biol* (2021) 9:807862. doi: 10.3389/fcell.2021.807862

16. Goldman M, Craft B, Swatloski T, Cline M, Morozova O, Diekhans M, et al. The UCSC cancer genomics browser: update 2015. *Nucleic Acids Res* (2015) 43:D812–817. doi: 10.1093/nar/gku1073

17. Gao J, Aksoy BA, Dogrusoz U, Dresdner G, Gross B, Sumer SO, et al. Integrative analysis of complex cancer genomics and clinical profiles using the cBioPortal. *Sci Signal* (2013) 6:l1. doi: 10.1126/scisignal.2004088

18. Chen B, Khodadoust MS, Liu CL, Newman AM, Alizadeh AA. Profiling tumor infiltrating immune cells with CIBERSORT. *Methods Mol Biol* (2018) 1711:243–59. doi: 10.1007/978-1-4939-7493-1_12

19. Yu G, Wang LG, Han Y, He QY. clusterProfiler: an r package for comparing biological themes among gene clusters. *OMICS* (2012) 16:284–7. doi: 10.1089/omi.2011.0118

20. Hugo W, Zaretsky JM, Sun L, Song C, Moreno BH, Hu-Lieskovan S, et al. Genomic and transcriptomic features of response to anti-PD-1 therapy in metastatic melanoma. *Cell* (2016) 165:35–44. doi: 10.1016/j.cell.2016.02.065

21. Ascierto ML, McMiller TL, Berger AE, Danilova L, Anders RA, Netto GJ, et al. The intratumoral balance between metabolic and immunologic gene expression is associated with anti-PD-1 response in patients with renal cell carcinoma. *Cancer Immunol Res* (2016) 4:726–33. doi: 10.1158/2326-6066.CIR-16-0072

22. Chen W, Cooper TK, Zahnow CA, Overholtzer M, Zhao Z, Ladanyi M, et al. Epigenetic and genetic loss of Hic1 function accentuates the role of p53 in tumorigenesis. *Cancer Cell* (2004) 6:387–98. doi: 10.1016/j.ccr.2004.08.030

23. Tseng RC, Lee CC, Hsu HS, Tzao C, Wang YC. Distinct HIC1-SIRT1-p53 loop deregulation in lung squamous carcinoma and adenocarcinoma patients. *Neoplasia* (2009) 11:763–70. doi: 10.1593/neo.09470

24. Yao J, Yang J, Yang Z, Wang XP, Yang T, Ji B, et al. FBXW11 contributes to stem-cell-like features and liver metastasis through regulating HIC1-mediated SIRT1 transcription in colorectal cancer. *Cell Death Dis* (2021) 12:930. doi: 10.1038/s41419-021-04185-7

25. Singh A, Gupta S, Badarukhiya JA, Sachan M. Detection of aberrant methylation of HOXA9 and HIC1 through multiplex MethyLight assay in serum DNA for the early detection of epithelial ovarian cancer. *Int J Cancer* (2020) 147:1740–52. doi: 10.1002/ijc.32984

26. Briggs KJ, Eberhart CG, Watkins DN. Just say no to ATOH: how HIC1 methylation might predispose medulloblastoma to lineage addiction. *Cancer Res* (2008) 68:8654–6. doi: 10.1158/0008-5472.CAN-08-1904

27. Dai C, Chen X, Li J, Comish P, Kang R, Tang D. Transcription factors in ferroptotic cell death. *Cancer Gene Ther* (2020) 27:645–56. doi: 10.1038/s41417-020-0170-2

28. Zhao L, Zhou X, Xie F, Zhang L, Yan H, Huang J, et al. Ferroptosis in cancer and cancer immunotherapy. *Cancer Commun (Lond)* (2022) 42:88–116. doi: 10.1002/cac2.12250

29. Hao X, Zheng Z, Liu H, Zhang Y, Kang J, Kong X, et al. Inhibition of APOC1 promotes the transformation of M2 into M1 macrophages *via* the ferroptosis pathway and enhances anti-PD1 immunotherapy in hepatocellular carcinoma based on single-cell RNA sequencing. *Redox Biol* (2022) 56:102463. doi: 10.1016/j.redox.2022.102463

30. Wang W, Green M, Choi JE, Gijon M, Kennedy PD, Johnson JK, et al. CD8(+) T cells regulate tumour ferroptosis during cancer immunotherapy. *Nature* (2019) 569:270–4. doi: 10.1038/s41586-019-1170-y

31. Zhou X, Zhang P, Han H, Lei H, Zhang X. Hypermethylated in cancer 1 (HIC1) suppresses bladder cancer progression by targeting yes-associated protein (YAP) pathway. *J Cell Biochem* (2019) 120:6471–81. doi: 10.1002/jcb.27938

32. Cheng G, Sun X, Wang J, Xiao G, Wang X, Fan X, et al. HIC1 silencing in triple-negative breast cancer drives progression through misregulation of LCN2. *Cancer Res* (2014) 74:862–72. doi: 10.1158/0008-5472.CAN-13-2420

33. Brieger J, Pongsapich W, Mann SA, Hedrich J, Fruth K, Pogozelski B, et al. Demethylation treatment restores hic1 expression and impairs aggressiveness of head and neck squamous cell carcinoma. *Oral Oncol* (2010) 46:678–83. doi: 10.1016/j.oraloncology.2010.06.016

34. Eggers H, Steffens S, Grosshennig A, Becker JU, Hennenlotter J, Stenzl A, et al. Prognostic and diagnostic relevance of hypermethylated in cancer 1 (HIC1) CpG island methylation in renal cell carcinoma. *Int J Oncol* (2012) 40:1650–8. doi: 10.3892/ijo.2012.1367

35. ICGC/TCGA Pan-Cancer Analysis of Whole Genomes Consortium. Pan-cancer analysis of whole genomes. *Nature* (2020) 578:82–93. doi: 10.1038/s41586-020-1969-6

36. Gupta S, Cheville JC, Jungbluth AA, Zhang Y, Zhang L, Chen YB, et al. JAK2/PD-L1/PD-L2 (9p24.1) amplifications in renal cell carcinomas with sarcomatoid transformation: implications for clinical management. *Mod Pathol* (2019) 32:1344–58. doi: 10.1038/s41379-019-0269-x

37. Sriraksa R, Zeller C, El-Bahrawy MA, Dai W, Daduang J, Jearanaikoon P, et al. CpG-island methylation study of liver fluke-related cholangiocarcinoma. *Br J Cancer* (2011) 104:1313–8. doi: 10.1038/bjc.2011.102

38. Kilinc D, Ozdemir O, Ozdemir S, Korgali E, Koksal B, Uslu A, et al. Alterations in promoter methylation status of tumor suppressor HIC1, SFRP2, and DAPK1 genes in prostate carcinomas. *DNA Cell Biol* (2012) 31:826–32. doi: 10.1089/dna.2011.1431

39. Hao M, Li Y, Wang J, Qin J, Wang Y, Ding Y, et al. HIC1 loss promotes prostate cancer metastasis by triggering epithelial-mesenchymal transition. *J Pathol* (2017) 242:409–20. doi: 10.1002/path.4913

40. Ubaid U, Andrabi SBA, Tripathi SK, Dirasantha O, Kanduri K, Rautio S, et al. Transcriptional repressor HIC1 contributes to suppressive function of human induced regulatory T cells. *Cell Rep* (2018) 22:2094–106. doi: 10.1016/j.celrep.2018.01.070

41. Crowl JT, Heeg M, Ferry A, Milner JJ, Omilusik KD, Toma C, et al. Tissue-resident memory CD8(+) T cells possess unique transcriptional, epigenetic and functional adaptations to different tissue environments. *Nat Immunol* (2022) 23:1121–31. doi: 10.1038/s41590-022-01229-8

42. Rotte A. Combination of CTLA-4 and PD-1 blockers for treatment of cancer. *J Exp Clin Cancer Res* (2019) 38:255. doi: 10.1186/s13046-019-1259-z

43. Zeng S, Yang Y, Cheng X, Zhou B, Li P, Zhao Y, et al. HIC1 epigenetically represses CIITA transcription in b lymphocytes. *Biochim Biophys Acta* (2016) 1859:1481–9. doi: 10.1016/j.bbagrm.2016.10.003

44. Jardim DL, Goodman A, de Melo Gagliato D, Kurzrock R. The challenges of tumor mutational burden as an immunotherapy biomarker. *Cancer Cell* (2021) 39:154–73. doi: 10.1016/j.ccell.2020.10.001

45. McGrail DJ, Pilié PG, Rashid NU, Voorwerk L, Slagter M, Kok M, et al. High tumor mutation burden fails to predict immune checkpoint blockade response across all cancer types. *Ann Oncol* (2021) 32:661–72. doi: 10.1016/j.annonc.2021.02.006

46. Palmeri M, Mehnert J, Silk AW, Jabbour SK, Ganesan S, Popli P, et al. Real-world application of tumor mutational burden-high (TMB-high) and microsatellite instability (MSI) confirms their utility as immunotherapy biomarkers. *ESMO Open* (2022) 7:100336. doi: 10.1016/j.esmoop.2021.100336

47. Narayan G, Arias-Pulido H, Koul S, Vargas H, Zhang FF, Villella J, et al. Frequent promoter methylation of CDH1, DAPK, RARB, and HIC1 genes in carcinoma of cervix uteri: its relationship to clinical outcome. *Mol Cancer* (2003) 2:24. doi: 10.1186/1476-4598-2-24

48. Cheng G, He J, Zhang L, Ge S, Zhang H, Fan X. HIC1 modulates uveal melanoma progression by activating lncRNA-numb. *Tumour Biol* (2016) 37:12779–89. doi: 10.1007/s13277-016-5243-3

49. Koul S, McKiernan JM, Narayan G, Houldsworth J, Bacik J, Dobrzynski DL, et al. Role of promoter hypermethylation in cisplatin treatment response of male germ cell tumors. *Mol Cancer* (2004) 3:16. doi: 10.1186/1476-4598-3-16

50. Jiacong H, Qirui Y, Haonan L, Yichang S, Yan C, Keng C. Zoledronic acid induces ferroptosis by upregulating POR in osteosarcoma. *Med Oncol* (2023) 40:141. doi: 10.1007/s12032-023-01988-w

51. Ren T, Huang J, Sun W, Wang G, Wu Y, Jiang Z, et al. Zoledronic acid induces ferroptosis by reducing ubiquinone and promoting HMOX1 expression in osteosarcoma cells. *Front Pharmacol* (2022) 13:1071946. doi: 10.3389/fphar.2022.1071946

52. Qu X, Sun Z, Wang Y, Ong HS. Zoledronic acid promotes osteoclasts ferroptosis by inhibiting FBXO9-mediated p53 ubiquitination and degradation. *PeerJ* (2021) 9: e12510. doi: 10.7717/peerj.12510

53. Bhatt V, Lan T, Wang W, Kong J, Lopes EC, Wang J, et al. Inhibition of autophagy and MEK promotes ferroptosis in Lkb1-deficient kras-driven lung tumors. *Cell Death Dis* (2023) 14:61. doi: 10.1038/s41419-023-05592-8

frontiers | Frontiers in Oncology

TYPE Original Research
PUBLISHED 20 June 2023
DOI 10.3389/fonc.2023.1199608

OPEN ACCESS

EDITED BY
Takaji Matsutani,
Repertoire Genesis, Inc., Japan

REVIEWED BY
Xinzhou Deng,
Hubei University of Medicine, China
Chen Huang,
Fujian Provincial Hospital, China

*CORRESPONDENCE
Xingcai Gao
gxc575788@sina.com

†These authors share first authorship

RECEIVED 03 April 2023
ACCEPTED 02 June 2023
PUBLISHED 20 June 2023

CITATION
Zhu A, Pei D, Zong Y, Fan Y, Wei S, Xing Z, Song S, Wang X and Gao X (2023) Comprehensive analysis to identify a novel diagnostic marker of lung adenocarcinoma and its immune infiltration landscape. *Front. Oncol.* 13:1199608. doi: 10.3389/fonc.2023.1199608

Comprehensive analysis to identify a novel diagnostic marker of lung adenocarcinoma and its immune infiltration landscape

Ankang Zhu[1,2†], Dongchen Pei[1†], Yan Zong[1†], Yan Fan[1,2], Shuai Wei[1,2], Zhisong Xing[1,2], Shuailin Song[1,2], Xin Wang[1,2] and Xingcai Gao[1,2*]

[1]The Fifth Affiliated Hospital of Zhengzhou University, Zhengzhou University, Zhengzhou, China, [2]Department of Cardiothoracic Surgery, The Fifth Affiliated Hospital of Zhengzhou University, Zhengzhou University, Zhengzhou, China

Background: Lung cancer continues to be a problem faced by all of humanity. It is the cancer with the highest morbidity and mortality in the world, and the most common histological type of lung cancer is lung adenocarcinoma (LUAD), accounting for about 40% of lung malignant tumors. This study was conducted to discuss and explore the immune-related biomarkers and pathways during the development and progression of LUAD and their relationship with immunocyte infiltration.

Methods: The cohorts of data used in this study were downloaded from the Gene Expression Complex (GEO) database and the Cancer Genome Atlas Program (TCGA) database. Through the analysis of differential expression analysis, weighted gene co-expression network analysis (WGCNA), and least absolute shrinkage and selection operator(LASSO), selecting the module with the highest correlation with LUAD progression, and then the HUB gene was further determined. The Gene Ontology (GO), Kyoto Encyclopedia of Genes and Genomes (KEGG), and Gene Set Enrichment Analysis (GSEA) were then used to study the function of these genes. Single-sample GSEA (ssGSEA) analysis was used to investigate the penetration of 28 immunocytes and their relationship with HUB genes. Finally, the receiver operating characteristic curve (ROC) was used to evaluate these HUB genes accurately to diagnose LUAD. In addition, additional cohorts were used for external validation. Based on the TCGA database, the effect of the HUB genes on the prognosis of LUAD patients was assessed using the Kaplan-Meier curve. The mRNA levels of some HUB genes in cancer cells and normal cells were analyzed by reverse transcription-quantitative polymerase chain reaction (RT-qPCR).

Results: The turquoise module with the highest correlation with LUAD was identified among the seven modules obtained with WGCNA. Three hundred fifty-four differential genes were chosen. After LASSO analysis, 12 HUB genes were chosen as candidate biomarkers for LUAD expression. According to the immune infiltration results, CD4 + T cells, B cells, and NK cells were high in LUAD sample

tissue. The ROC curve showed that all 12 HUB genes had a high diagnostic value. Finally, the functional enrichment analysis suggested that the HUB gene is mainly related to inflammatory and immune responses. According to the RT-qPCR study, we found that the expression of DPYSL2, OCIAD2, and FABP4 in A549 was higher than BEAS-2B. The expression content of DPYSL2 was lower in H1299 than in BEAS-2B. However, the expression difference of FABP4 and OCIAD2 genes in H1299 lung cancer cells was insignificant, but both showed a trend of increase.

Conclusions: The mechanism of LUAD pathogenesis and progression is closely linked to T cells, B cells, and monocytes. 12 HUB genes(ADAMTS8, CD36, DPYSL2, FABP4, FGFR4, HBA2, OCIAD2, PARP1, PLEKHH2, STX11, TCF21, TNNC1) may participate in the progression of LUAD *via* immune-related signaling pathways.

KEYWORDS

lung adenocarcinoma, immune cell infiltration, biomarkers, immune-related pathways, LASSO, RT-qPCR

1 Introduction

Lung cancer is one of the most common cancers in the world. In recent years, the number of new cases has reached a peak, and lung cancer has the highest number of deaths (1, 2). Lung adenocarcinoma has the highest incidence of lung cancer at approximately 40% (3). While one of the reasons for the high mortality of LUAD is that 57% of cases had progressed at the time of testing, when the treatment regimen was limited, with 1-and 5-year survival rates of only 26% and 4%, respectively (4, 5). This result is not satisfactory, and although the rapid development of immunotherapy and targeted therapies in recent years has led to a significant improvement in the outcomes of LUAD patients, the prognosis outcome of LUAD patients is still unsatisfactory (6, 7). Thus, there is a need to investigate and discover novel biomarkers or immune cell infiltration during LUAD progression, which is of extraordinary importance for the early detection, diagnosis, treatment, and better prognosis of LUAD. Despite the diverse pathogenesis and causes of LUAD, extensive clinical evidence and experimental data show that immunocytes and immune-related pathways play various roles in the development of LUAD and the prognostic process. For example, a reduction in CD4 + T cells suppresses the activity of cytotoxic T cells in tumors, thereby restricting LUAD tumor cell growth (6). Programmed cell death 1 (PD-1) is expressed in T cells to suppress peripheral autoimmunity (immune tolerance) (8). M2-polarized macrophages exhibit immunosuppressive activity and promote tumor angiogenesis in LUAD patients (9). Many other molecules are closely associated with LUAD and play an immunological role in tumor progression. Thus, further investigation into the molecular mechanisms of LUAD pathogenesis is still needed.

WGCNA works by analyzing a large number of genes and then putting genes with similar expressions into the same module according to the clustering principle. The most significant advantage of this method over simple cluster analysis is that it is biologically meaningful and allows for effective preliminary screening of genes related to target features (10, 11). In many cases, LASSO algorithms are used to describe the degree of correlation between two related variables. The advantage of this algorithm over the traditional Cox regression and logistic regression lies in its ability to reduce the dimension. Both WGCNA and LASSO regression analysis are commonly used for bioinformatics technology analysis. Moreover, the LASSO analysis of the WGCNA genes can make us more accurate in screening the target feature-related genes (12). In the first step, we screened differentially expressed genes and identified key biomarkers for LUAD progression. Based on the results of the Gene Ontology (GO) of differentially expressed genes and the Kyoto Encyclopedia of Genes and Genomes (KEGG), we found that these DEGs mainly focus on some immune processes and immune pathways related to LUAD. We then used ssGSEA analysis to assess the infiltration of immunocytes in the immune environment in the hope of gaining a clearer understanding of the mechanisms of LUAD progression, and the results may provide a way to understand the pathogenesis of LUAD and find new therapeutic targets.

Abbreviations: LUAD, lung adenocarcinoma; DEGs, Differentially expressed genes; WGCNA,weighted gene co-expression network analysis; GEO, Gene-Expression Omnibus; TCGA, The Cancer Genome Atlas Program; LASSO, Least absolute shrinkage and selection operator; AUC, Area under the curve; ssGSEA, single-sample gene-set enrichment analysis algorithm; GO, Gene Ontology; Tregs, regulatory T cell; PPAR, Peroxisome proliferator-activated receptors; FOXP3, Forkhead box P3; KEGG, Kyoto Encyclopedia of Genes and Genomes; ROC, receiver operating characteristic curve; GSEA, Gene Set Enrichment Analysis.

2 Materials and methods

2.1 Data collection

Microarray expression data and clinical information for LUAD were obtained from the GEO and TCGA databases. There were two cohorts in the treatment group, GSE63459 and GSE176348, with 89 specimens (including 45 tumor samples and 44 normal samples). In addition, external validation using the TCGA-LUAD cohort with 598 samples (including 539 tumor samples and 59 normal samples) was performed. All sequencing information for normal samples comes from adjacent tissues.

2.2 Selection of the DEGs

We used the data normalization and probe annotation from the R software (version 4.2.1) "limma" and "GEOquery" packages for the data of GSE63459 and GSE176348, with P-value < 0.05 and |log fold change (FC) | > 1 for the DEGS screening criteria (13, 14).

2.3 Construction of gene co-expression network

We used the WGCNA to process expression profile data from GSE63459 and GSE176348 datasets to establish a weighted co-expression network. Then we investigated the genes that deviate from the top 25% of the median (10). The data integrity is checked by the 'Good SampleGenes' function. We chose a suitable soft threshold value (β) and validated the ability of the soft threshold value. The matrix data was transformed into an adjacency matrix by us, followed by clustering to identify modules based on the topological overlap. Then, the module feature element (ME) is calculated, the similarly expressed modules are combined into the cluster tree according to the ME, and we draw the hierarchical cluster tree graph. Then, the module and phenotype data are combined, and then the gene significant (GS) and module significant (MS) are calculated; the calculation results are used to evaluate whether the gene and clinical information are essential and to analyze the correlation between the module and the model. In addition, We calculated the module membership (MM) for each gene to analyze the GS values of each module.

2.4 Selection and validation of the HUB genes

The gene with the highest inter-module connectivity was selected as the candidate HUB gene. The GS values for biologically significant genes are also generally higher. Therefore, we chose candidate genes with an absolute GS value> 0.20 and an MM value > 0.80. We then intersected these genes with DEGS using the "glmnet" package in the R software package and used the LASSO analysis to determine the final HUB genes (11). We used box plots to probe the HUB gene expression levels in LUAD samples and healthy samples. With the help of 'MedCalc' software (version 2.0.1), we draw the receiver operating characteristic curves (ROC) to determine these HUB genes' diagnostic specificity and accuracy. A dataset (TCGA-LUAD) is also available for external verification of the HUB gene's expression level and diagnostic value.

2.5 Prognostic analysis

With the help of the "Survival" and "SurvMiner" packages in the "R" software, we divided the samples in TCGA-LUAD into two groups (high and low expression groups) using the median expression of the HUB gene. Lastly, survival curves for HUB and LUAD genes were plotted using the Kaplan-Meier method with the aid of the software package "ggplot2".

2.6 Immunohistochemical staining was performed

Results of immunohistochemical staining of the HUB gene in normal lung tissue and lung cancer specimens from The Human Protein Atlas(www.proteinatlas.org).

2.7 Assessment of immunocytes infiltration and its association with HUB genes

We quantified the infiltration of 28 immunocytes in the GSE63459 and GSE176348 datasets using the ssGSEA algorithm (15). The box plots we established indicate the differences in the expression levels of these immune cells. We also calculated the Spearman correlation of these immune-infiltrating cells with the candidate HUB genes and visualized the calculated results with the 'ggplot2' program package.

2.8 Functional enrichment analysis

We performed GO analysis of DEGs, KEGG analysis, and GSEA analysis through the 'clusterProfiler' and 'enrichplot' package of the R software package (16). We used the immunological signature genomes from the Molecular Signature Database (MsigDB) as the reference, and the significantly enriched genomes had to meet the P <0.05 and the false discovery rate (FDR) q-value <0.05.

2.9 Experimental validation

Several HUB genes (DPYSL2, OCIAD2, and FABP4) were selected for study to verify the HUB genes' role further. Normal human lung epithelial cells (BEAS-2B) and lung adenocarcinoma cells (A549 and H1299) were collected for culture, moreover, extracted RNA from the three cells using the Trizol reagent. For cDNA synthesis, the synthesis was performed using the reverse transcription reagent VAZYME R232. The final PCR reaction was performed on a quantitative real-time PCR instrument. The reaction parameters included the denaturation process

(30s at 95°C), followed by 40 PCR cycles (5s at 95°C and 34s at 60°C). The melting curve of the PCR product was established, and after the amplification reaction, the temperature was slowly heated from 60°C at (95°C, 15s, 60°C, 60s, 95°C, 15 s) to 99°C (instrument automatic ramp rate 0.05°C/s). Quantitative real-time PCR reactions were performed for target and housekeeping genes for each sample. We calculated the relative expression levels of the three genes using the 2 ^ (-δδ ct) method. Since the experimental results of FABP 4 and DPYSL2 were fit to a normal distribution, the analysis was performed using the one-way ANOVA test. We used the Kruskal-Wallis test for statistical analysis for OCIAD2 genes whose results do not conform to the normal distribution (Supplementary file 1). The sequence of the primers is as follows:

DPYSL2, 5'-CCCTGCAGAACATCAACGAC-3' (forward) and 5'-GGCATCTGGAAACGAGTGTG-3' (reverse); OCIAD2, 5'-GTCTGCTCGTGGAAACCAAG-3' (forward) and 5'-CAAGAGACCAGCAAGTGCAAC-3' (reverse); FABP4, 5-GATGACAGGAAAGTCAAGAGCAC-3' (forward) and 5'-GACGCCTTTCATGACGCATTC-3' (reverse); and GADPH,5'-TCTGACTTCAACAGCGACACC-3' (forward) and 5'-CTGTTGCTGTAGCCAAATTCGT-3' (reverse).

3 Results

3.1 Establishment of a co-expression network and selection of key modules

The absolute deviations in the median top 25% of genes were selected for constructing WGCNA, and missing values and outliers in the samples were subsequently removed by cluster analysis. To maintain consistency with the scale-free network, we set the soft threshold β to 5 (scale-free R2 = 0.91; slope =-1.67) (Figures 1A, B). We also analyzed the gene expression in the normal and LUAD samples and plotted the results as a heatmap (Figure 1C). We built a co-expression matrix and obtained seven modules with the help of dynamic hybridization shear (Figure 2A). The relationship between these seven modules and the LUAD and healthy samples is shown in the heatmap. The turquoise module has the highest correlation (cor) (cor = 0.89; P=1e-31) (Figures 2B, C). Moreover, after our correlation analysis, we found that in the turquoise module, GS and MM are also well correlated(cor=1.51; P=1.3e-08) (Figure 2D).

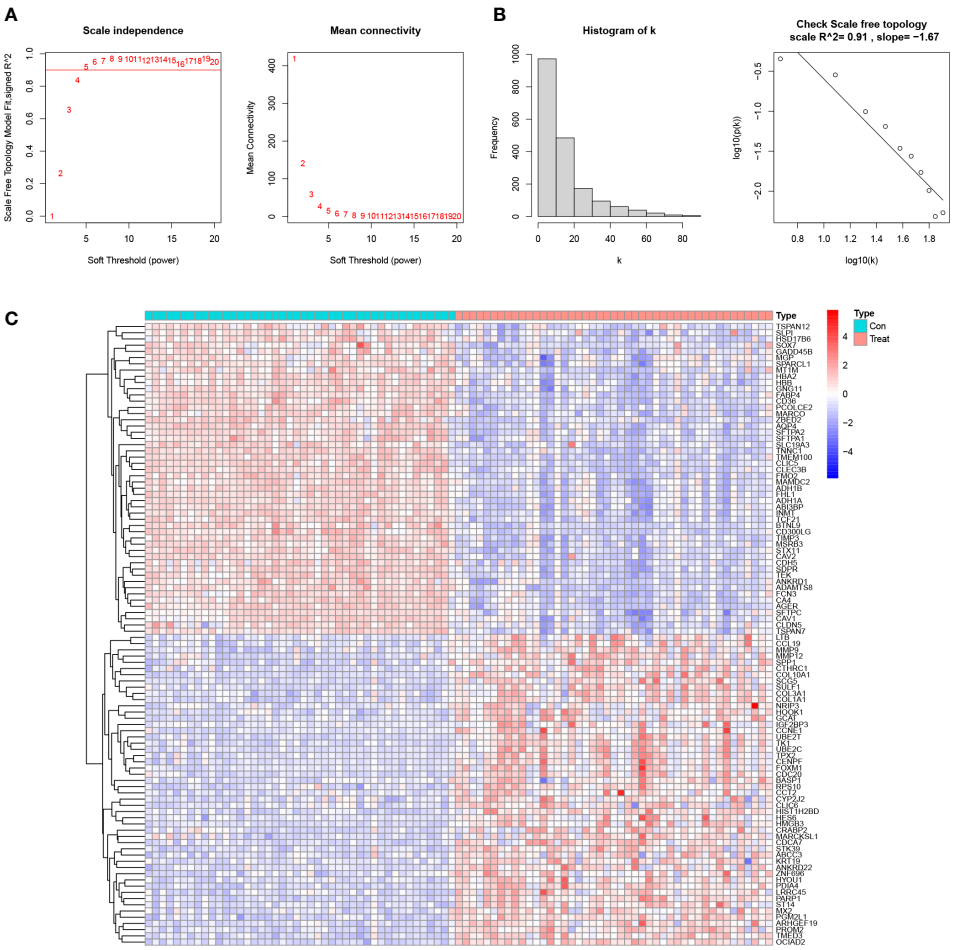

FIGURE 1
Determine the soft threshold ability in WGCNA. **(A)** Scale-free fit index and average connectivity for different soft threshold powers (β). Positions with a correlation coefficient of 0.9 are marked with a red line, corresponding to a soft threshold power of 5. **(B)** Histogram of the connectivity distribution and checking the scale-free topology map. **(C)** Heatmap of the correlation of genes in the experimental and control groups.

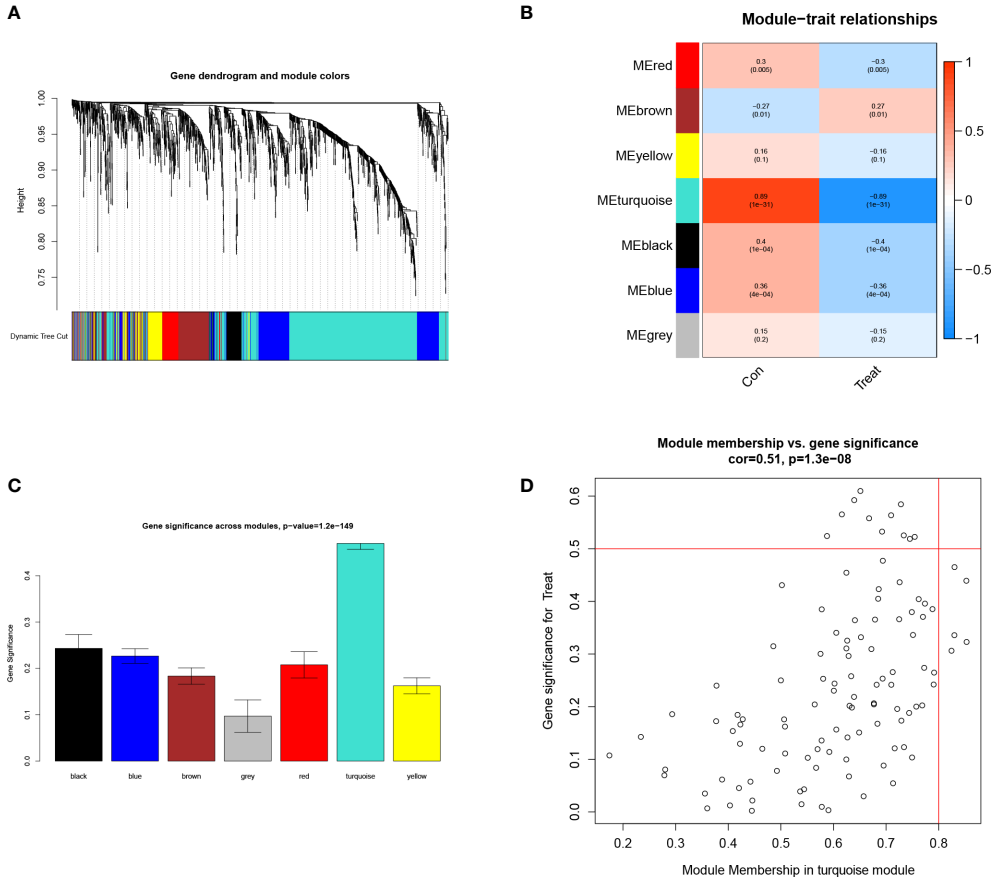

FIGURE 2
Establishment of the WGCNA module. **(A)** Cluster plot of genes in the top 25% of the median absolute deviation. Each color in the horizontal axis corresponds to a module, and each branch in the graph indicates the gene. **(B)** Heat map of the module-characteristic relationship. **(C)** Bar graph of the distribution of average gene significance in different modules. **(D)** Scatterplot depicting the relationship between gene module membership and gene significance in the turquoise module.

3.2 Identification of DEGs and selection of HUB genes

For the DEGs, our filtering criteria were P <0.05 and | logFC |> 1, including 354 differential expressed genes and displaying the results on the volcano plot (Figure 3A). We further selected 87 genes with higher connectivity in the turquoise module using |GS|> 0.20 and |MM|> 0.80 as screening criteria. The results of these two screens were compared, and their intersection was selected as candidate HUB genes, and 85 genes were combined (Figure 3B). Ultimately, after a further screening of these genes using the LASSO analysis, we were able to obtain 12 genes (ADAMTS8, CD36, DPYSL2, FABP4, FGFR4, HBA2, OCIAD2, PARP1, PLEKHH2, STX11, TCF21, TNNC1) (Figures 3C, D).

3.3 Functional enrichment analysis of DEGs

Next, we investigated the function of the DEGs screened above; We performed GO analysis on 354 genes. According to the results, we know that DEGs mainly focus on the regulation of genes or pathways (e.g., transforming growth factor receptor signaling pathway, positive regulation of gene expression, negative regulation of transcription by RNA polymerase II promoter), vascular development (e. g., angiogenesis, angiogenesis, vascular development), immune response and inflammatory response (e. g. inflammation, cellular response of interleukin-1, positive regulation of interleukin-6 production), and even play an essential role in alveolar development (Figure 4). According to the KEGG analysis, We can also learn that DEGs are mainly enriched in the following pathways, pathways of immunological and inflammation-related diseases (AGE-RAGE signaling pathway in diabetic complications, fluid shear stress, and atherosclerosis, rheumatoid arthritis), there are also some immune-related pathways (IL-17 signaling pathway, TNF signal channel, the TGF signaling pathway, PPAR signaling pathway, and other pathways)(Figure 5). The GO analysis and KEGG analysis showed that there are many biological processes and signaling pathways related to the immune-inflammatory response in the development and development of LUAD.

3.4 Immunohistochemical staining of HUB genes in normal tissues and tumor tissues

IHC staining results were paired as shown in Figure 6. On the left of each pair of images is the gene staining in normal lung tissue, and

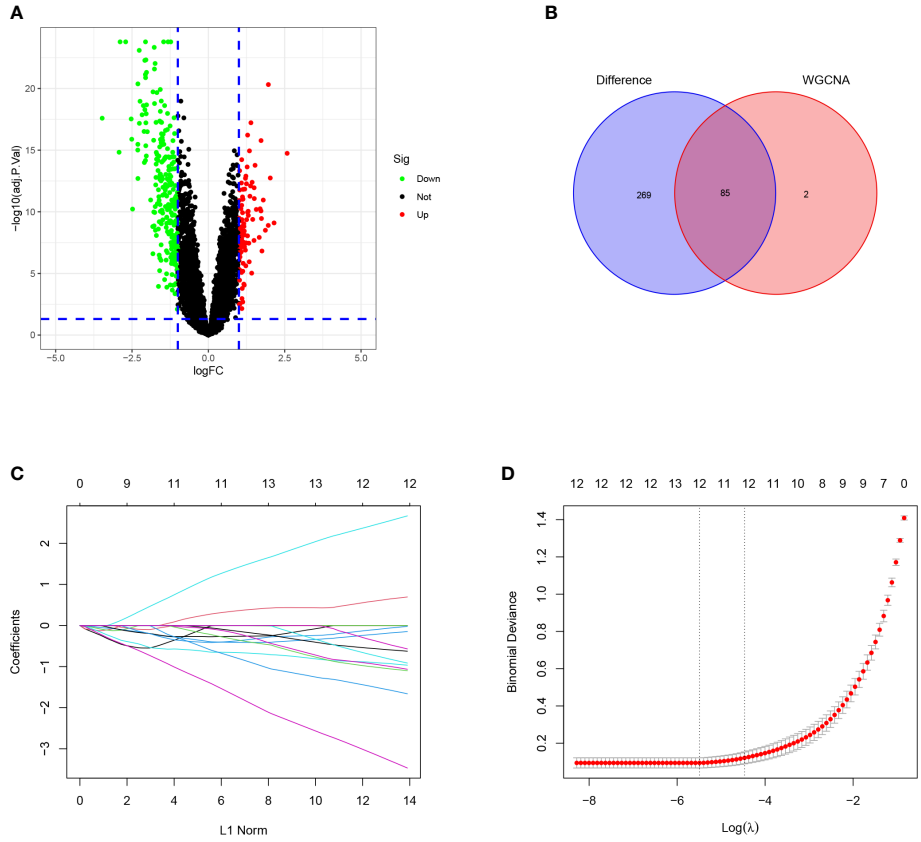

FIGURE 3
Identification of the DEGS and selection of the HUB genes. **(A)** Volcano plot of DEGS between LUAD samples and healthy control tissues. **(B)** A Venn diagram of the intersection of the DEGS and the turquoise module. **(C)** The relationship of partial likelihood bias with log **(L)** changes plotted by LASSO regression in the 10-time cross-validation. **(D)** Distribution of LASSO coefficient for 12 HUB genes in 10-fold cross-validation.

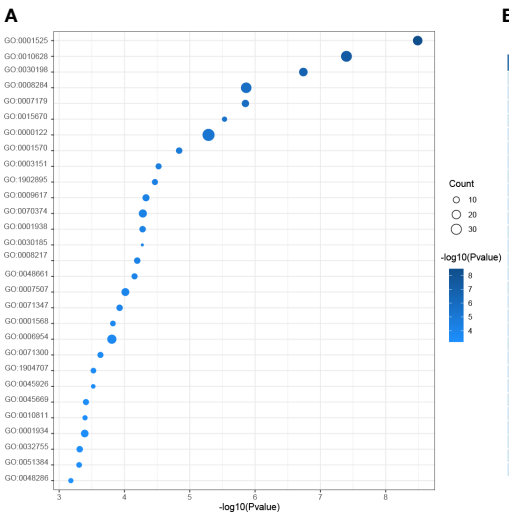

B

ID	Description
GO:0001525	angiogenesis
GO:0010628	positive regulation of gene expression
GO:0030198	extracellular matrix organization
GO:0008284	positive regulation of cell proliferation
GO:0007179	transforming growth factor beta receptor signaling pathway
GO:0015670	carbon dioxide transport
GO:0000122	negative regulation of transcription from RNA polymerase II promoter
GO:0001570	vasculogenesis
GO:0003151	outflow tract morphogenesis
GO:1902895	positive regulation of pri-miRNA transcription from RNA polymerase II promoter
GO:0009617	response to bacterium
GO:0070374	positive regulation of ERK1 and ERK2 cascade
GO:0001938	positive regulation of endothelial cell proliferation
GO:0030185	nitric oxide transport
GO:0008217	regulation of blood pressure
GO:0048661	positive regulation of smooth muscle cell proliferation
GO:0007507	heart development
GO:0071347	cellular response to interleukin-1
GO:0001568	blood vessel development
GO:0006954	inflammatory response
GO:0071300	cellular response to retinoic acid
GO:1904707	positive regulation of vascular smooth muscle cell proliferation
GO:0045926	negative regulation of growth
GO:0045669	positive regulation of osteoblast differentiation
GO:0010811	positive regulation of cell-substrate adhesion
GO:0001934	positive regulation of protein phosphorylation
GO:0032755	positive regulation of interleukin-6 production
GO:0051384	response to glucocorticoid
GO:0048286	lung alveolus development

FIGURE 4
(A) Heatmap of biological process enrichment of DEGs. **(B)** Corresponding annotation for the GO ID.

A

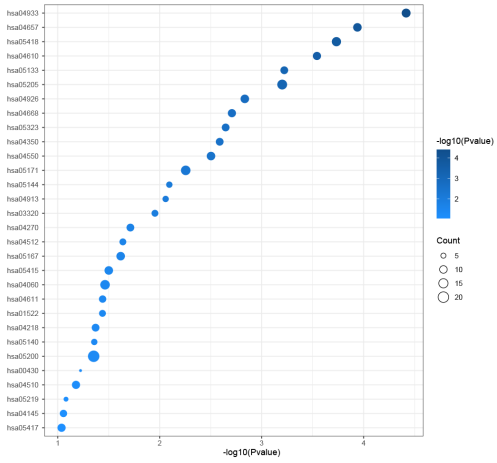

B

ID	Description
hsa04933	AGE-RAGE signaling pathway in diabetic complications
hsa04657	IL-17 signaling pathway
hsa05418	Fluid shear stress and atherosclerosis
hsa04610	Complement and coagulation cascades
hsa05133	Pertussis
hsa05205	Proteoglycans in cancer
hsa04926	Relaxin signaling pathway
hsa04668	TNF signaling pathway
hsa05323	Rheumatoid arthritis
hsa04350	TGF-beta signaling pathway
hsa04550	Signaling pathways regulating pluripotency of stem cells
hsa05171	Coronavirus disease - COVID-19
hsa05144	Malaria
hsa04913	Ovarian steroidogenesis
hsa03320	PPAR signaling pathway
hsa04270	Vascular smooth muscle contraction
hsa04512	ECM-receptor interaction
hsa05167	Kaposi sarcoma-associated herpesvirus infection
hsa05415	Diabetic cardiomyopathy
hsa04060	Cytokine-cytokine receptor interaction
hsa04611	Platelet activation
hsa01522	Endocrine resistance
hsa04218	Cellular senescence
hsa05140	Leishmaniasis
hsa05200	Pathways in cancer
hsa00430	Taurine and hypotaurine metabolism
hsa04510	Focal adhesion
hsa05219	Bladder cancer
hsa04145	Phagosome
hsa05417	Lipid and atherosclerosis

FIGURE 5
(A) Heatmap of signal pathway enrichment of DEGs. **(B)** The KEGG ID corresponds to the annotation.

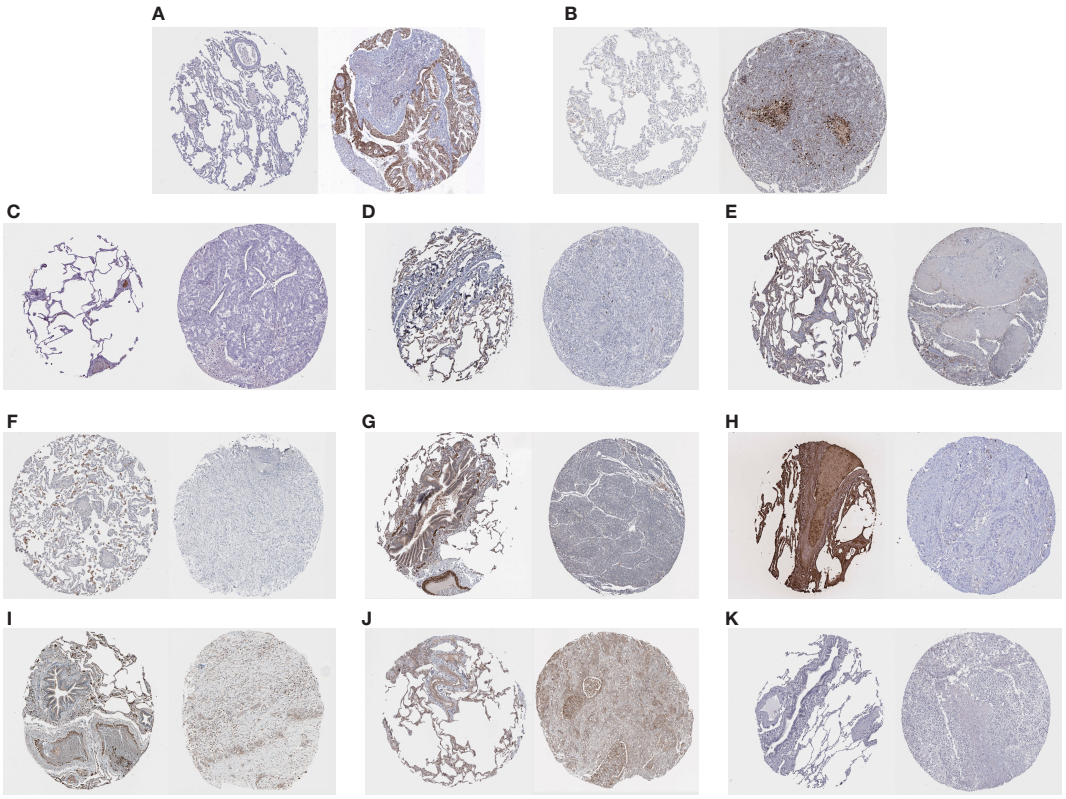

FIGURE 6
(A–K) Results of the immunohistochemical staining of OCIAD2, PARP 1, ADAMTS8, CD36, DPYSL2, FABP4, FGFR4, HBA2, STX11, TCF21, and TNNC 1, on the left of each pair of images, is the staining of genes in normal lung tissue, and on the right is the staining in lung cancer samples.

on the right is the staining in lung cancer samples. We can estimate the expression level of HUB genes, and it is clear that two HUB genes, OCIAD2 and PARP 1, have higher expression in lung cancer samples (Figures 6A, B), while the remaining HUB genes have more expression in normal samples (Figures 6C–K). Unfortunately, we were unable to find the PLEKHH2 staining results, and we will continue to follow up on the results in follow-up studies.

3.5 Validation of HUB gene expression levels and diagnostic value

We assessed the expression levels of the 12 HUB genes by box plots. The results indicated that only OCIAD2, PARP 1 were significantly increased in the control group (Figures 7G, H) (P <0.001), while the other ten genes, ADAMTS8, CD36, DPYSL2,

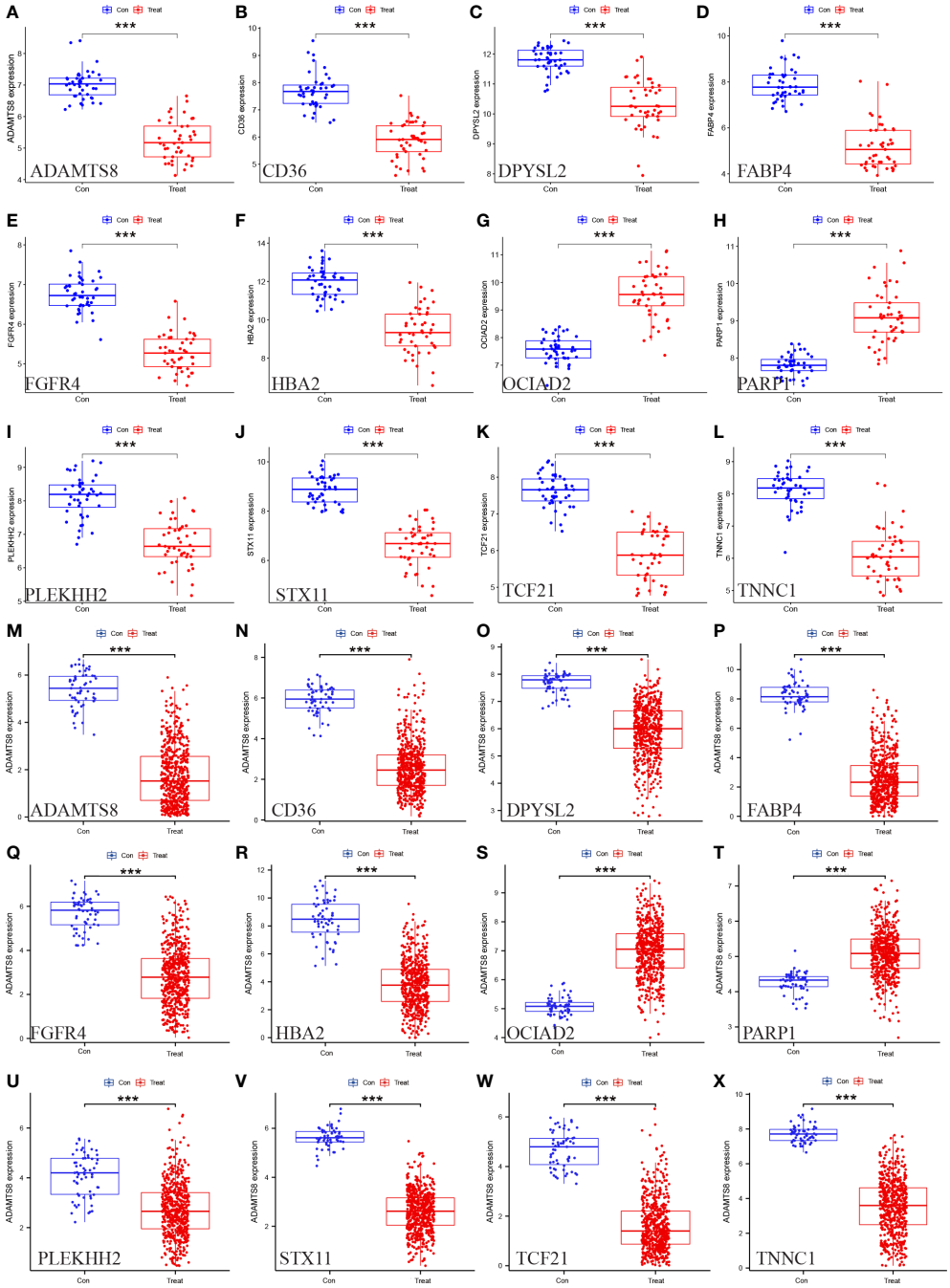

FIGURE 7
Verification of the 12 HUB genes at the gene expression level. **(A–L)** Verification of the HUB genes in the GSE63459 and GSE176348 **(M–X)** Verification of the HUB gene in the TCGA-LUAD cohort (* represents P <0.05, ** represents P <0.01, and *** represents P <0.001).

FABP4, FGFR4, HBA2, PLEKHH2, STX11, TCF21, TNNC1 were higher in the control group (Figures 7A–F, I–L). Next, we also externally verified the expression levels of these 12 HUB genes using the TCGA-LUAD dataset, and validation results were in agreement with our experimental group (Figures 7M–X). In the ROC curve analysis of the 12 HUB genes, the area under the curve (AUC) of the HUB gene represents the sensitivity and specificity of the HUB gene for the diagnosis of LUAD. From the ROC curve, we can know that the AUC values of all 12 HUB genes were> 0.93, indicating the high value of HUB genes for the diagnosis of LUAD (Figure 8A). While in the TCGA-LUAD cohort, the AUC values, except for PAPR 1 and PLEKHH2, were 0.884 and 0.839, respectively. The AUC values for the remaining HUB genes were all> 0.95, which coincident with the findings from our cohort study above (Figure 8B).

3.6 Prognostic analysis of HUB genes

We partitioned LUAD samples into two groups (high and low expression groups) based on the TCGA-LUAD database. Kaplan-Meier curves were performed for the HUB gene in order to analyze its prognostic relationship to LUAD patients. According to the results, the high expression of OCIAD2 and PARP1 is linked to poor prognosis in LUAD patients (Supplementary Figures 1G, H). However, high expression of ADAMTS8, CD36, DPYSL2, PLEKHH2, STX11, and TCF21 tends to lead to better prognosis (Supplementary Figures 1A–F, I–L), which coincides with the difference in expression of these HUB genes in normal samples and lung cancer samples.

3.7 Immune cell infiltration and its correlation with HUB genes

We compared and analyzed the immune cell infiltration of LUAD samples and the control group with the ssGSEA algorithm. The graph shows the distribution of 28 immunocytes in two datasets, GSE63459 and GSE17634 (Figure 9A). Shown according to its results, the CD4+T cells, CD8+T cells, natural killer (NK) cells, and Bcell in LUAD samples were higher than that in normal samples, and this result indicates that these cells play a significant role in the progression of LUAD (Figure 9B). According to the correlation analysis of HUB genes and immune cell infiltration, most of these HUB genes showed a positive correlation with immune infiltrating cells, such as macrophage, CD4 + T cell, CD8 + T cell, and NK cell. CD8 + T cell exerts antitumor effects in a wide range of cancers. It should be noted that OCIAD2 and PARP1 genes are negatively associated with numerous immune cells. This fits with their results leading to the poor prognosis associated with patients with LUAD (Figure 9C).

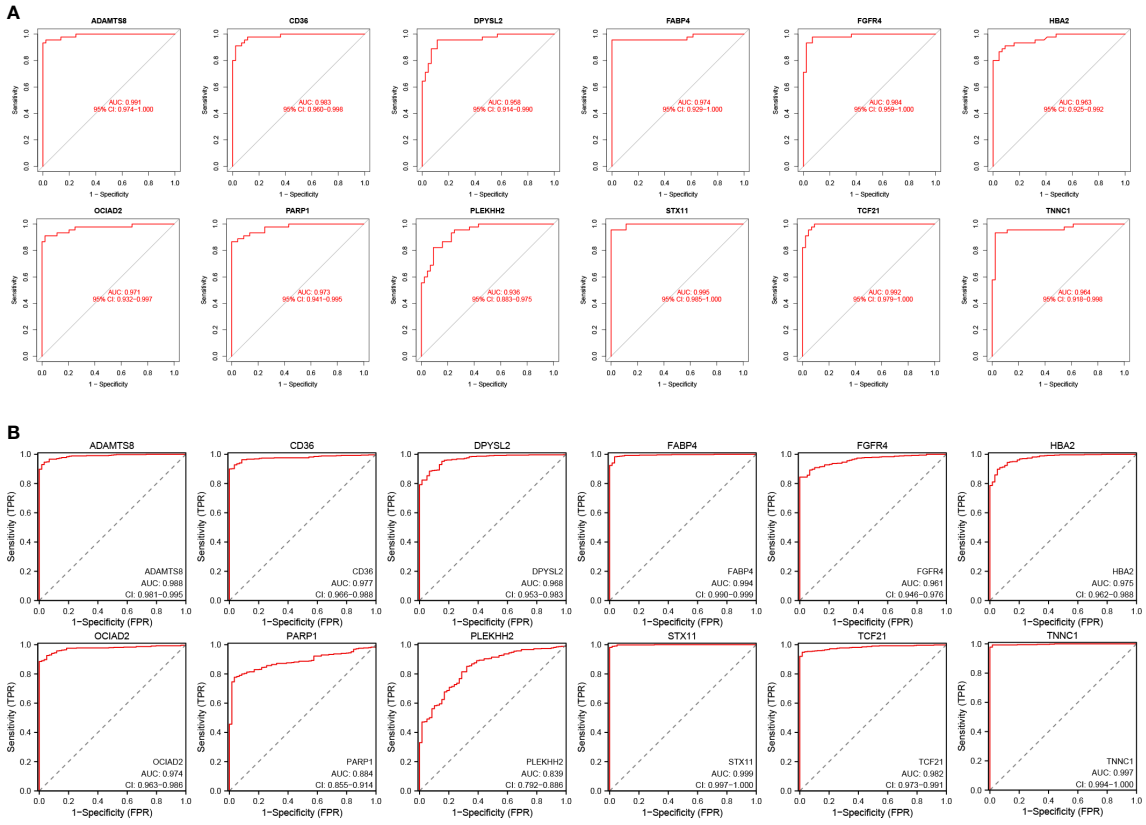

FIGURE 8
Verification of the diagnostic value of the 12 HUB genes. **(A)** Verification of the HUB genes in the GSE63459 and GSE176348 cohorts. **(B)** Validation of the HUB gene in the TCGA-LUAD cohort.

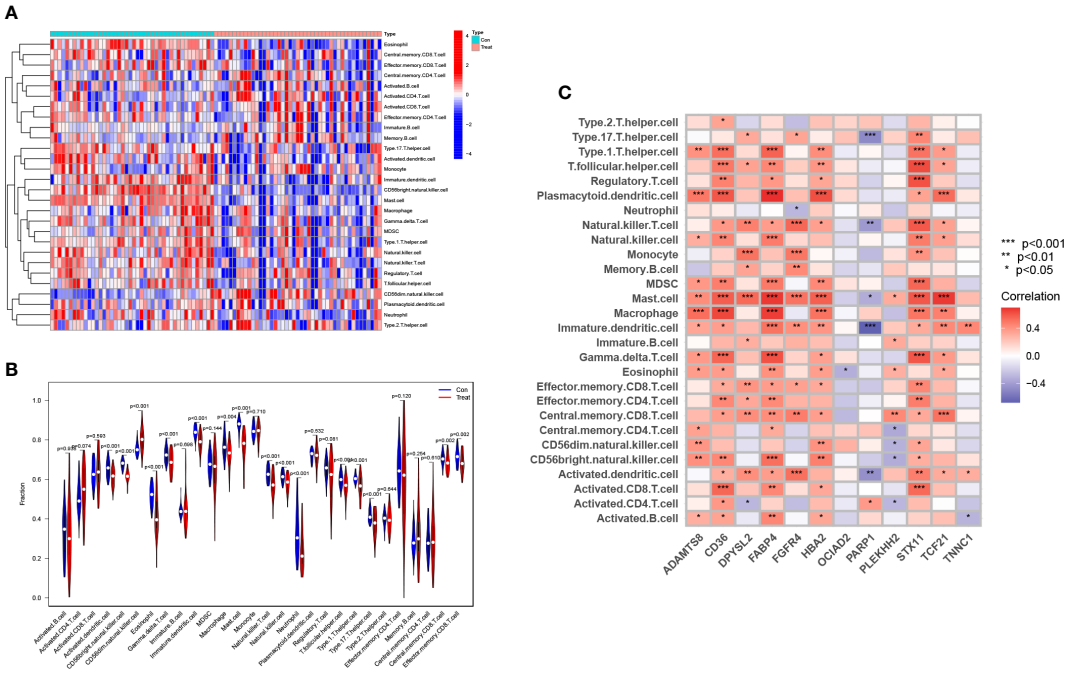

FIGURE 9
Analysis of the immune microenvironment associated with LUAD. Both **(A)** and **(B)** show the distribution of 28 immune cells in the immune microenvironment of normal and LUAD samples. **(C)** The relationship of the 12 HUB genes with the infiltration of multiple immune cells. (* represents P <0.05, ** represents P <0.01, and *** represents P <0.001).

3.8 Enrichment analysis of GSEA immune signature gene sets

To make out that immunogenetics may exist during the progression of LUAD, we have used the immunologically signature gene set in the MsigDB database as a reference standard for DEGS GSEA. A total of 819 gene sets were significantly enriched (|normalized enrichment score (NES)|> 1; FDR Q value <0.05). These genes were mainly concentrated in CD8 T cells, NK Cells, CD4+T cells, monocytes, and regulatory T cells (Supplementary Table S1). Based on the above findings, it appears that many immune genes play an essential role in LUAD progression (Figure 10).

3.9 Detection of mRNA levels of HUB genes by RT-qPCR

After statistical analysis of the PCR results, we found that DPYSL2 (p <0.001), OCIAD2 (p <0.05), and FABP4 (p <0.001) had higher expression in A549 compared to BEAS-2B, showing a statistically significant difference. The expression content of DPYSL2 was lower in H1299 cells compared to t BEAS-2B (p <0.01). Although the expression difference of FABP 4 and OCIAD2 genes in H1299 was not statistically significant, they both showed a trend to increase (Figure 11). These experimental results can better support our study. Nevertheless, the results may require further study with a larger sample size.

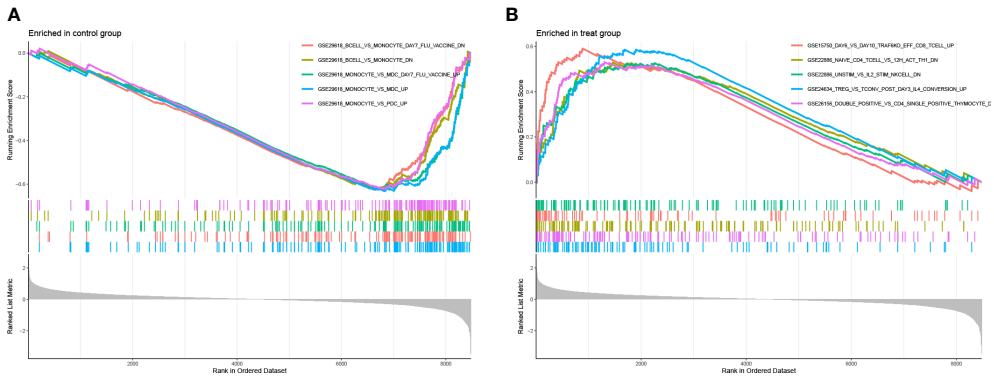

FIGURE 10
(A, B) plots represent the enrichment map of the GSEA immune marker database for the experimental and control groups, respectively.

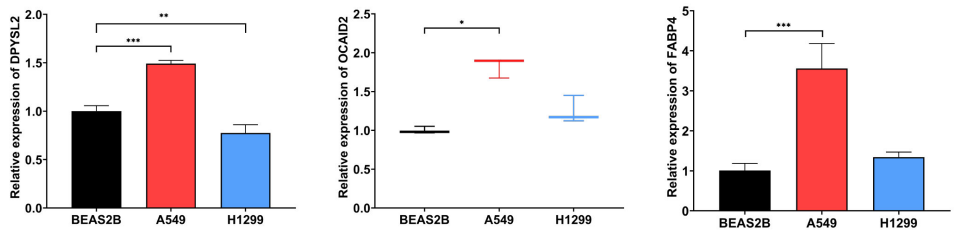

FIGURE 11
The mRNA levels of DPYSL2, OCIAD2, and FABP 4 were measured in human normal lung epithelial cell lines (BEAS-2B) and LUAD cell lines (A549 and H1299), respectively. (* represents P <0.05, ** represents P <0.01, and *** represents P <0.001).

4 Discussion

Using high-throughput microarray technology is a more efficient and accurate bioinformatics method when finding and screening key genes related to the mechanism of cancer development. This technology can also help us diagnose and treat diseases and help us in the design of new drugs. DEG is primarily enriched in leukocyte activation and production, alveolar development, the development of angiogenesis as well as certain immune responses, which are related to the mechanism of LUAD development (17). Analysis of the KEGG showed that DEGs were primarily enriched in immune-related pathways (IL-17 signaling pathway, TNF signal channel, The TGF signaling pathway, PPAR signaling pathway, and other pathways). The cytokine IL-17 can mediate a variety of physiological effects (18, 19). IL-17 is produced primarily by both innate and adaptive immune cells, whose main role is to exert its immune regulatory function by promoting the production of various proinflammatory cytokines and chemokines (IL-6, IL-23, transforming growth factor- β, tumor necrosis factor, etc.), leading to the accumulation of neutrophils and macrophages at the site of inflammation (20–22). IL-17 can stimulate lung tumor growth by promoting angiogenesis and proliferative activation (23, 24). IL-17 in the immune microenvironment can also induce lung cancer metastasis and spread (25). It has also been shown that treatment with a neutralizing anti-IL-17A antibody can reduce the angiogenesis of the tumor as well as reduce the inflammatory response, thereby reducing the growth of lung cancer progression (24, 26). IL-17 is overexpressed in a variety of lung cancer types. During the development of LUAD, the recruitment of numerous neutrophils by IL-17 leads to sustained inflammatory damage (27). All point to a strong link between IL-17 with LUAD progression and prognosis, and these studies are in good agreement with the DEGS enrichment results indicating that there are indeed genes within DEGS that are important in LUAD development.

Traditional DEG-based screening approaches are only capable of local analysis of datasets, which can easily cause the omission and loss of core genes. WGCNA can help us to systematically construct individual biological interaction network maps that can help us to identify core genes that are highly associated with disease prognosis (28, 29). Therefore, we used WGCNA to search for genes highly associated with LUAD and crossed the present results to previous DEGS to obtain highly related and differential genes. After screening these genes by LASSO analysis, the next 12 HUB genes were identified: ADAMTS8, CD36, DPYSL2, FABP4, FGFR4, HBA2, OCIAD2, PARP1, PLEKHH2, STX11, TCF21, TNNC1. These 12 key genes showed distinct differences in expression levels in LUAD samples and healthy samples. Notably, Of these, only OCIAD2 and PARP1 were found to be significantly highly expressed in tissues from LUAD samples, whereas the remaining 10 genes showed higher levels of expression in the control groups.

ADAMTS8 comes from integrins and metalloproteinases of the thrombospondin motif, and some studies show that ADAMTS8 is closely associated with vascular endothelial growth factor A (VEGFA), and some studies have found that ADAMTS8 expression in lung cancer is very low (30, 31). DPYSL2 is extremely highly associated with breast cancer, which can be expressed in breast cancer cells through axonal guidance. We can also use DPYSL2 to inhibit breast cancer progression and metastasis by inducing reversal. At the same time, numerous studies have demonstrated that phosphorylation of DPYSL2 and DPYSL2 is associated with drug resistance and tumor metastasis (32, 33). OCIAD2 belongs to the ovarian cancer immune response antigen (OCIA) domain family, which consists of 154 amino acids. It fulfills its role in tumor metastasis by promoting STAT3 activation and cell migration. And OCIAD2 is also highly expressed in lung adenocarcinoma but also ovarian mucinous tumors (33, 34). PARP1 is the central enzyme for cellular PAR production and a major target for polyadenosine diphosphate ribosylation during DNA damage. Upon DNA strand breaks, PARP1 performs DNA repair by covalently connecting the ADP-ribose moiety to the acceptor site of some amino acids on itself and other proteins (35, 36). Transcription factor 21 (TCF21) belongs to the class bHLHII superfamily of transcription factors and is expressed in various tissues and organs, it's not only related to different biological processes, such as the development of the reproductive system (support cell differentiation and sex determination), respiratory system, spleen development, it also involved in regulating RNA polymerase to transcription process and so on (37, 38). CD36 is a membrane glycoprotein, as well as a scavenger receptor, which is found in a wide variety of cells. CD36 plays a major role in regulating atherosclerosis *via* a variety of pathways (39, 40).

The above studies we performed showed that DEGS is inextricably linked with inflammatory response, immune response, various cytokines, chemokines, and IL-17 factors. In

this study, the infiltration of 28 immunocytes in the immune microenvironment of LUAD samples was investigated by the ssGSEA algorithm. The results showed that CD4 + T cells, CD4 + T cells, CD8 + T cells, natural killer (NK) cells, and Bcell were more infiltrated in LUAD samples than in normal samples. All of these cells are important in LUAD progression (24, 41, 42). However, following correlation analysis of HUB genes and infiltrating immune cells, in our study, most of these HUB genes were found to positively correlate with immune-infiltrating cells such as Macrophage, CD4 + T cells, CD8 + T cells, and NK cells. While CD8 + T cell has extensive anticancer effects (43). Macrophages play an immune role in a variety of tumors (lung cancer, breast cancer, liver cancer, etc.) (44, 45). Notably, OCIAD2 and PARP 1, which are inversely related to many immune cells, coincide with the results that these two genes are associated with the poor prognosis of lung adenocarcinoma. IL-17 mainly originates from Th17 cells, while Th17 cells mainly originate from CD4 + T cells, and high-level expression of IL-17 leads to inflammatory damage of inflammatory cells like neutrophils and leads to tumor vascular growth, both of which lead to the progression and metastasis of lung tumors. The enrichment of Tregs (regulatory T cell) is correlated with the occurrence, progression, metastasis, and prognosis of various malignancies, including lung cancer (46). Whereas the transcription factor Foxp 3 is the main regulator of Treg cell development and inhibitory activity, and this transcription factor is closely related to autoimmune diseases and a stable immune environment (47). In addition to producing plasma cells involved in the pathological process of LUAD, B cells can produce various cytokines that stimulate Tcell activation, thereby reducing the anti-inflammatory properties of regulatory Tcell and promoting the proliferation and differentiation of effector T cells. The above findings indicate that T cell homeostasis in the immune microenvironment is related to the occurrence, development, and prognosis of LUAD (48). Finally, to investigate the possible immune mechanisms during the development of LUAD, we used the immunological marker gene set in the MsigDB database as a reference for DSGS GSEA and found that activated CD8 T cells, NK Cells, CD4+T cells, monocytes, and regulatory T cells had enhanced expression in DEGS. This suggests that LUAD progression may be linked to the activation of T lymphocytes, monocytes, B lymphocytes, and various cytokines produced by themselves or by their interactions. These studies suggest that these HUB genes may have a potential relationship with the development of LUAD.

To conclude, we selected turquoise by WGCNA and LASSO regression analysis, combined with multiple bioinformatic analyses, and ultimately selected the 12 HUB genes with the highest correlation to LUAD (ADAMTS8, CD36, DPYSL2, FABP4, FGFR4, HBA 2, OCIAD2, PARP1, PLEKHH2, STX11, TCF21, TNNC1), and we analyzed and verified the functions of these genes in the present study. The results of this study will provide initial insights and novel insights into the underlying immunomodulatory mechanisms of LUAD. We will further investigate and explore the more sensitive and specific diagnostic markers of LUAD to provide new directions for LUAD diagnosis, treatment regimen, prognosis, and drug design.

Data availability statement

The original contributions presented in the study are included in the article/Supplementary Material. Further inquiries can be directed to the corresponding author.

Author contributions

AZ and DP designed this work. YZ performed the validation of the experiments. YF and SW integrated and analyzed the data. ZX, SS and XW wrote this manuscript. XG edited and revised the manuscript. All authors approved this manuscript.

Funding

This study was funded by Henan Provincial Health Commission (LHGJ20190422), Henan Provincial Health Commission (LHGJ20210486) and the Key Scientific Item of Henan Province Education Department (21A320037).

Conflict of interest

The authors declare that the research was conducted in the absence of any commercial or financial relationships that could be construed as a potential conflict of interest.

Publisher's note

Supplementary material

The Supplementary Material for this article can be found online at: https://www.frontiersin.org/articles/10.3389/fonc.2023.1199608/full#supplementary-material

SUPPLEMENTARY FIGURE 1
Prognostic relationships of 12 HUB genes and LUAD patients.

SUPPLEMENTARY TABLE 1
Enrichment analysis of GSEA immune signature gene sets.

References

1. Sung H, Ferlay J, Siegel RL, Laversanne M, Soerjomataram I, Jemal A, et al. Global cancer statistics 2020: GLOBOCAN estimates of incidence and mortality worldwide for 36 cancers in 185 countries. *CA Cancer J Clin* (2021) 71(3):209–49. doi: 10.3322/caac.21660

2. Cao W, Chen H-D, Yu Y-W, Li N, Chen W-Q. Changing profiles of cancer burden worldwide and in China: a secondary analysis of the global cancer statistics 2020. *Chin Med J (Engl)* (2021) 134(7):783–91. doi: 10.1097/CM9.0000000000001474

3. Collins LG, Haines C, Perkel R, Enck RE. Lung cancer: diagnosis and management. *Am Fam Physician* (2007) 75(1):56–63.

4. Rodriguez-Canales J, Parra-Cuentas E, Wistuba II. Diagnosis and molecular classification of lung cancer. *Cancer Treat Res* (2016) 170:25–46. doi: 10.1007/978-3-319-40389-2_2

5. Bade BC, Dela CC. Lung cancer 2020: epidemiology, etiology, and prevention. *Clin Chest Med* (2020) 41(1):1–24. doi: 10.1016/j.ccm.2019.10.001

6. Chen J, Fu Y, Hu J, He J. Hypoxia-related gene signature for predicting LUAD patients' prognosis and immune microenvironment. *Cytokine* (2022) 152:155820. doi: 10.1016/j.cyto.2022.155820

7. Lemjabbar-Alaoui H, Hassan OU, Yang YW, Buchanan P. Lung cancer: biology and treatment options. *Biochim Biophys Acta* (2015) 1856(2):189–210. doi: 10.1016/j.bbcan.2015.08.002

8. Nagano T, Tachihara M, Nishimura Y. Molecular mechanisms and targeted therapies including immunotherapy for non-small cell lung cancer. *Curr Cancer Drug Targets* (2019) 19(8):595–630. doi: 10.2174/1568009619666181210114559

9. Xu F, Cui W-Q, Wei Y, Cui J, Qiu J, Hu L-L, et al. Astragaloside IV inhibits lung cancer progression and metastasis by modulating macrophage polarization through AMPK signaling. *J Exp Clin Cancer Res* (2018) 37(1):207. doi: 10.1186/s13046-018-0878-0

10. Langfelder P, Horvath S. WGCNA: an r package for weighted correlation network analysis. *BMC Bioinf* (2008) 9:559. doi: 10.1186/1471-2105-9-559

11. Simon N, Friedman J, Hastie T, Tibshirani R. Regularization paths for cox's proportional hazards model *via* coordinate descent. *J Stat Softw* (2011) 39(5):1–13. doi: 10.18637/jss.v039.i05

12. Duan J, Soussen C, Brie D, Idier J, Wan M, Wang Y-P. Generalized LASSO with under-determined regularization matrices. *Signal Process* (2016) 127:239–46. doi: 10.1016/j.sigpro.2016.03.001

13. Ritchie ME, Phipson B, Wu D, Hu Y, Law CW, Shi W, et al. Limma powers differential expression analyses for RNA-sequencing and microarray studies. *Nucleic Acids Res* (2015) 43(7):e47. doi: 10.1093/nar/gkv007

14. Davis S, Meltzer PS. GEOquery: a bridge between the gene expression omnibus (GEO) and BioConductor. *Bioinformatics* (2007) 23(14):1846–7. doi: 10.1093/bioinformatics/btm254

15. Bindea G, Mlecnik B, Tosolini M, Kirilovsky A, Waldner M, Obenauf AC, Angell H, et al. Spatiotemporal dynamics of intratumoral immune cells reveal the immune landscape in human cancer. *Immunity* (2013) 39(4):782–95. doi: 10.1016/j.immuni.2013.10.003

16. Wu T, Hu E, Xu S, Chen M, Guo P, Dai Z, et al. clusterProfiler 4.0: a universal enrichment tool for interpreting omics data. *Innovation (Camb)* (2021) 2(3):100141. doi: 10.1016/j.xinn.2021.100141

17. Kinoshita T, Goto T. Molecular mechanisms of pulmonary fibrogenesis and its progression to lung cancer: a review. *Int J Mol Sci* (2019) 20(6):20061461. doi: 10.3390/ijms20061461

18. Park H, Li Z, Yang XO, Chang SH, Nurieva R, Wang YH, et al. A distinct lineage of CD4 T cells regulates tissue inflammation by producing interleukin 17. *Nat Immunol* (2005) 6(11):1133–41. doi: 10.1038/ni1261

19. Gu C, Wu L, Li X. IL-17 family: cytokines, receptors and signaling. *Cytokine* (2013) 64(2):477–85. doi: 10.1016/j.cyto.2013.07.022

20. Jin W, Dong C. IL-17 cytokines in immunity and inflammation. *Emerg Microbes Infect* (2013) 2(9):e60. doi: 10.1038/emi.2013.58

21. Majumder S, McGeachy MJ. IL-17 in the pathogenesis of disease: good intentions gone awry. *Annu Rev Immunol* (2021) 39:537–56. doi: 10.1146/annurev-immunol-101819-092536

22. Ouyang W, Kolls JK, Zheng Y. The biological functions of T helper 17 cell effector cytokines in inflammation. *Immunity* (2008) 28(4):454–67. doi: 10.1016/j.immuni.2008.03.004

23. Zitvogel L, Kroemer G. Lower airway dysbiosis exacerbates lung cancer. *Cancer Discovery* (2021) 11(2):224–6. doi: 10.1158/2159-8290.CD-20-1641

24. Joerger M, Finn SP, Cuffe S, Byrne AT, Gray SG. The IL-17-Th1/Th17 pathway: an attractive target for lung cancer therapy? *Expert Opin Ther Targets* (2016) 20 (11):1339–56. doi: 10.1080/14728222.2016.1206891

25. Salazar Y, Zheng X, Brunn D, Raifer H, Picard F, Zhang Y, et al. Microenvironmental Th9 and Th17 lymphocytes induce metastatic spreading in lung cancer. *J Clin Invest* (2020) 130(7):3560–75. doi: 10.1172/JCI124037

26. Reppert S, Boross I, Koslowski M, Türeci Ö, Koch S, Lehr HA, et al. A role for T-bet-mediated tumour immune surveillance in anti-IL-17A treatment of lung cancer. *Nat Commun* (2011) 2:600. doi: 10.1038/ncomms1609

27. Lin Q, Xue L, Tian T, Zhang B, Guo L, Lin G, et al. Prognostic value of serum IL-17 and VEGF levels in small cell lung cancer. *Int J Biol Markers* (2015) 30(4):e359–63. doi: 10.5301/jbm.5000148

28. Mason MJ, Fan G, Plath K, Zhou Q, Horvath S. Signed weighted gene co-expression network analysis of transcriptional regulation in murine embryonic stem cells. *BMC Genomics* (2009) 10:327. doi: 10.1186/1471-2164-10-327

29. Botía JA, Vandrovcova J, Forabosco P, Guelfi S, D'Sa K, Hardy J, et al. An additional k-means clustering step improves the biological features of WGCNA gene co-expression networks. *BMC Syst Biol* (2017) 11(1):47. doi: 10.1186/s12918-017-0420-6

30. Xia MD, Yu RR, Chen DM. Identification of hub biomarkers and immune-related pathways participating in the progression of antineutrophil cytoplasmic antibody-associated glomerulonephritis. *Front Immunol* (2021) 12:809325. doi: 10.3389/fimmu.2021.809325

31. Tang H, Lee M, Kim EH, Bishop D, Rodgers GM. siRNA-knockdown of ADAMTS-13 modulates endothelial cell angiogenesis. *Microvasc Res* (2017) 113:65–70. doi: 10.1016/j.mvr.2017.05.007

32. Wu Y-J, Nai A-T, He G-C, Xiao F, Li Z-M, Tang S-Y, et al. DPYSL2 as potential diagnostic and prognostic biomarker linked to immune infiltration in lung adenocarcinoma. *World J Surg Oncol* (2021) 19(1):274. doi: 10.1186/s12957-021-02379-z

33. Rmaileh AA, Solaimuthu B, Khatib A, Lavi S, Tanna M, Hayashi A, et al. DPYSL2 interacts with JAK1 to mediate breast cancer cell migration. *J Cell Biol* (2022) 221(7):202106078. doi: 10.1083/jcb.202106078

34. Maki M, JeongMin H, Nakagawa T, Kawai H, Sakamoto N, Sato Y, et al. Aberrant OCIAD2 demethylation in lung adenocarcinoma is associated with outcome. *Pathol Int* (2022) 72(10):496–505. doi: 10.1111/pin.13262

35. Spiegel JO, Van Houten B, Durrant JD. PARP1: structural insights and pharmacological targets for inhibition. *DNA Repair (Amst)* (2021) 103:103125. doi: 10.1016/j.dnarep.2021.103125

36. Alemasova EE, Lavrik OI. Poly(ADP-ribosyl)ation by PARP1: reaction mechanism and regulatory proteins. *Nucleic Acids Res* (2019) 47(8):3811–27. doi: 10.1093/nar/gkz120

37. Molkentin JD, Bugg D, Ghearing N, Dorn LE, Kim P, Sargent MA, et al. Fibroblast-specific genetic manipulation of p38 mitogen-activated protein kinase *In vivo* reveals its central regulatory role in fibrosis. *Circulation* (2017) 136(6):549–61. doi: 10.1161/CIRCULATIONAHA.116.026238

38. Ao X, Ding W, Zhang Y, Ding D, Liu Y. TCF21: a critical transcription factor in health and cancer. *J Mol Med (Berl)* (2020) 98(8):1055–68. doi: 10.1007/s00109-020-01934-7

39. Park YM. CD36, a scavenger receptor implicated in atherosclerosis. *Exp Mol Med* (2014) 46(6):e99. doi: 10.1038/emm.2014.38

40. Wang J, Li Y. CD36 tango in cancer: signaling pathways and functions. *Theranostics* (2019) 9(17):4893–908. doi: 10.7150/thno.36037

41. Roy-Chowdhuri S. Molecular pathology of lung cancer. *Surg Pathol Clin* (2021) 14(3):369–77. doi: 10.1016/j.path.2021.05.002

42. Paver E, O'Toole S, Cheng XM, Mahar A, Cooper WA. Updates in the molecular pathology of non-small cell lung cancer. *Semin Diagn Pathol* (2021) 38(5):54–61. doi: 10.1053/j.semdp.2021.04.001

43. van der Leun AM, Thommen DS, Schumacher TN. CD8(+) T cell states in human cancer: insights from single-cell analysis. *Nat Rev Cancer* (2020) 20(4):218–32. doi: 10.1038/s41568-019-0235-4

44. Choi J, Gyamfi J, Jang H, Koo JS. The role of tumor-associated macrophage in breast cancer biology. *Histol Histopathol* (2018) 33(2):133–45. doi: 10.14670/HH-11-916

45. Cheng K, Cai N, Zhu J, Yang X, Liang H, Zhang W. Tumor-associated macrophages in liver cancer: from mechanisms to therapy. *Cancer Commun (Lond)* (2022) 42(11):1112–40. doi: 10.1002/cac2.12345

46. Wang X, Xiao Z, Gong J, Liu Z, Zhang M, Zhang Z. A prognostic nomogram for lung adenocarcinoma based on immune-infiltrating treg-related genes: from bench to bedside. *Transl Lung Cancer Res* (2021) 10(1):167–82. doi: 10.21037/tlcr-20-822

47. Deng G, Song X, Fujimoto S, Piccirillo CA, Nagai Y, Greene MI. Foxp3 post-translational modifications and treg suppressive activity. *Front Immunol* (2019) 10:2486. doi: 10.3389/fimmu.2019.02486

48. Lee GR. The balance of Th17 versus treg cells in autoimmunity. *Int J Mol Sci* (2018) 19(3):19030730. doi: 10.3390/ijms19030730

frontiers | Frontiers in Immunology

TYPE Original Research
PUBLISHED 29 June 2023
DOI 10.3389/fimmu.2023.1188256

OPEN ACCESS

EDITED BY
Takaji Matsutani,
Repertoire Genesis, Inc., Japan

REVIEWED BY
Hanchen Xu,
Longhua Hospital Shanghai University of Traditional Chinese Medicine, China
Fei Peng,
University of Texas Southwestern Medical Center, United States

*CORRESPONDENCE
Jun Cheng
chengjundoctor@163.com
Youwen Deng
drywdeng@csu.edu.cn

RECEIVED 17 March 2023
ACCEPTED 07 June 2023
PUBLISHED 29 June 2023

CITATION
Pan B, Cheng X, Tan W, Liu R, Wu X, He J, Fan Q, Zhang Y, Cheng J and Deng Y (2023) Pan-cancer analysis shows that IBSP is a potential prognostic and immunotherapeutic biomarker for multiple cancer types including osteosarcoma. *Front. Immunol.* 14:1188256. doi: 10.3389/fimmu.2023.1188256

Pan-cancer analysis shows that IBSP is a potential prognostic and immunotherapeutic biomarker for multiple cancer types including osteosarcoma

Boyu Pan[1], Xiaoyun Cheng[2,3], Wei Tan[1], Renfeng Liu[1], Xin Wu[1], Jinpeng He[1], Qizhi Fan[1], Yan Zhang[3], Jun Cheng[1,4]* and Youwen Deng[1]*

[1]Department of Spine Surgery, The Third Xiangya Hospital, Central South University, Changsha, Hunan, China, [2]Department of Pulmonary and Critical Care Medicine, The Third Xiangya Hospital of Central South University, Changsha, Hunan, China, [3]Department of Respiratory Medicine, Xiangya Hospital, Central South University, Changsha, Hunan, China, [4]Department of Experimental Radiation Oncology, The University of Texas MD Anderson Cancer Center, Houston, TX, United States

Background: IBSP is a member of the small integrin-binding ligand N-linked glycoprotein (SIBLING) family that plays a vital role in bone formation, renewal and repair. Emerging evidence revealed that IBSP participated in the tumorigenesis and progression in some cancers. However, its significance in tumour prognosis and immunotherapy is still unknown.

Methods: In the current study, we studied the role of IBSP in tumorigenesis, tumor diagnosis, genomic heterogeneity, methylation modifications, immune infiltration, and therapy response in pan-cancer. In addition, we constructed a risk score model to assessed the prognostic classification efficiency of IBSP using the co-expression genes of IBSP in osteosarcoma (OS), and analyzed the expression and role of IBSP in OS through a series of assays *in vitro*.

Results: IBSP was upregulated in various cancers compared to the paired normal tissues, and it was strongly correlated with the prognosis, pathological stage, diagnostic accuracy, genomic heterogeneity, methylation modification, immune infiltration, immune and checkpoint. Moreover, the predictive model we established in combination with the clinical characteristics of OS patients showed high survival predictive power in these individuals. The assays in vitro showed that IBSP promoted the proliferation, migration and invasion of OS cells, which further confirmed IBSP's role in cancers.

Conclusions: Our research revealed the multifunctionality of IBSP in the tumorigenesis, progression and therapy in various cancers, which demonstrated that IBSP may serve as a potential prognostic biomarker and a novel immunotherapy target in pan-cancer.

KEYWORDS

IBSP, pan-cancer, prognosis, immunotherapy, osteosarcoma

1 Introduction

Osteosarcoma (OS) is the most prevalent primary malignant bone tumor, with an annual incidence of 3-4.5 cases per million individuals worldwide (1), and it occurs most frequently in children and adolescents, followed by the elderly over 60 (2). OS is a highly heterogeneous and aggressive malignancy that is prone to distant metastasis at an early stage, with the lungs being the most common metastasis site (3). Since the 1970s, neoadjuvant chemotherapy has been used clinically extensively, the five-year survival rate of OS patients with minimal lesions has increased dramatically from 20% to over 60% (4). However, the overall survival and prognosis of OS patients, particularly those with distant metastases and postoperative recurrence, haven't improved since then (5). Therefore, to ameliorate the prognosis and overall survival of OS patients, novel therapy targets are urgently required.

The integrin-binding sialic acid protein (IBSP) gene is located in the q28-q31 region of chromosome 4 (6). As a member of the small integrin-binding ligand N-linked glycoprotein (SIBLING) family, the secreted bone sialoprotein (BSP) encoded by it is the main structural protein of the bone matrix and is involved in the early process of regulating bone mineralization (7, 8). IBSP was initially found to play a role in promoting bone formation, bone renewal and repair in some studies (8), but some recent researches have revealed that the overexpression of IBSP is correlated to a poor prognosis in some cancers, such as breast cancer (9), colon cancer (10), esophageal cancer (11) and renal cell cancer (12). According to these studies, IBSP may be a promising biomarker for prognosis prediction in various cancers. However, no research has explored the pan-cancer analysis of IBSP using systematic multi-omics analysis.

In the current study, we performed a comprehensive pan-cancer analysis of IBSP using different bioinformatics approaches, we focused on the correlation of its overexpression with immune infiltration, epigenetic modifications and prognosis in various cancers. We also verified its role in OS using the experiments *in vitro*. In addition, we constructed a risk score model based on IBSP-related genes for OS patients and validated the model using the data from an external dataset.

2 Materials and methods

2.1 Data acquisition and differential expression analysis

RNA-Seq data from the Cancer Genome Atlas (TCGA) pan-cancer dataset (10,536 samples) and Genotype-Tissue Expression (GTEx) dataset (7,863 samples) were downloaded from the UCSC Xena (xena.ucsc.edu/). The "Primary Tumor" and "Solid Tissue Normal" data were extracted from the TCGA pan-cancer dataset and visualized by the R software (version 4.2.1). IBSP expression in tumor and normal tissues were explored using the Tumor Immune Estimation Resource 2.0 (TIMER2.0, http://timer.cistrome.org/). IBSP expression in pan-cancer were analyzed using the Sanger (http://sangerbox.com/). IBSP expression in different tumor stages were analyzed using the GEPIA 2 database (http://gepia2.cancer-pku.cn/). The data of OS patients were obtained from the GEO database (https://www.ncbi.nlm.nih.gov/geo/) and the GDC database (https://portal.gdc.cancer.gov/). The RNA-seq and clinical phenotype data about 88 patients were downloaded from the GDC database. The GEO database was searched for datasets containing "OS" and "Homo sapiens", with the inclusion criteria being the number of samples exceeded 50, the results are shown in GSE21257 (GPL10295). In addition, we obtained two datasets containing OS tissues and normal tissues from the GEO database (GSE16088 and GSE42352).

2.2 The correlation between IBSP and prognosis of pan-cancer

The association between IBSP and overall survival or disease-free survival (DFS) in pan-cancer were analyzed using the GEPIA2 database, patients were divided into high and low expression groups based on the median of IBSP expression value in the TCGA pan-cancer dataset. Meanwhile, R software was used to plot the connection between IBSP expression and pan-cancer prognosis, the Kaplan-Meier method was used to analyze overall survival, disease-free interval (DFI), disease-specific survival (DSS) and progression-free interval (PFI).

2.3 Genetic alterations of IBSP in pan-cancer

The IBSP mutation types and mutation frequencies of multiple cancers in the cBioPortal database (https://www.cbioportal.org/) were analyzed according to the TCGA pan-cancer dataset (32 cancers, a total of 10,967 samples). The frequency of IBSP mutations in TCGA tumor types was explored in the TIMER2.0 database. The Sanger was used to analyze the relationship between tumor mutation burden (TMB) and microsatellite instability (MSI) and pan-cancer IBSP expression.

2.4 Correlation and functional enrichment analyses

The Correlations of IBSP expression with StromalScore, ImmuneScore, and ESTIMATEScores were performed for each TCGA tumor type using the Sanger online site, the results were imported into R software, and radar plots were created using the "ggradar" package. Similarly, the correlation between IBSP and immune cell infiltration levels (Timer), RNA modification genes (m^6A, m^5C, m^1A) and immune checkpoint genes (ICP) in TCGA tumors was analyzed in Sanger.

Eighty-four samples in the TARGET-OS dataset and 53 samples in the GSE21257 dataset had corresponding clinical information, the sample information for the two datasets is shown in Table S1. The TARGET-OS dataset and the GSE21257 dataset were calculated separately, and genes with $|rho|>0.5$ and $p<0.05$ were extracted as IBSP-related genes using the "spearman" correlation method. The IBSP-related genes were imported into Cytoscape software (version 3.9.1) to plot the IBSP-related gene network. In the Metascape

database (https://metascape.org), investigations of Gene Ontology (GO) and Kyoto Encyclopedia of Genes and Genomes (KEGG) pathway enrichment were carried out. The Venn diagrams were plotted to extract the intersection of IBSP-related genes in the TARGET-OS dataset and the GSE21257 dataset.

2.5 Establishment and evaluation of predictive models in OS

The TARGET-OS dataset was used as the training set and the GSE21257 dataset was used as the external validation set. The univariate Cox analysis was performed on the IBSP-related genes shared by the two datasets, and the genes exhibiting significant differences in the univariate Cox analysis were screened using the Least Absolute Shrinkage and Selection Operator (LASSO) regression, and the risk score model was established based on the sum of the lasso regression coefficients and the product of gene expression. The median risk score value was used as the threshold of the high-risk and low-risk groups. Nomogram were constructed by combining the clinical characteristics of OS patients, and the model's predictive power was evaluated using calibration curves and time-dependent ROC curves.

The "estimate" package (13), "GSVA" package (14) and "IBOR" package (15) were used to calculate the ESTIMATE score, estimate the degree of immune cell infiltration for the high and low-risk groups. The correlation of risk score with ICP genes and ligand genes was analyzed in the TARGET-OS dataset by the "spearman" method, all ICP and ligand genes are shown in Table S2. Assessing the potential clinical efficacy of immunotherapy in different risk groups through the Tumor Immune Dysfunction and Exclusion online websites (TIDE, http://tide.dfci.harvard.edu/).

2.6 Cell culture and cell transfection

Human normal osteoblast (hFOB), normal liver cells (L-02), esophageal epithelial cells (H031), lung epithelial cells (BEAS-2B), renal epithelial cell (H193), breast epithelial cells (MCF 10A), lung epithelial cells (HCoEpiC) and all the cancer cell lines were obtained from Xiangya Medical College Cell Bank (Changsha, China). Saos-2 cells were cultured in McCoy's 5A medium (Gibco, Waltham, MA, USA), and the others were cultured in Dulbecco's Modified Eagle Medium (Gibco) with 10% FBS (Gibco). shRNAs were obtained from Genechem (Shanghai, China). The cells were transfected according to the recommended protocol, and screened using 2 ug/mL puromycin (Beyotime, China). The sequences of shRNA-IBSP were as follows:

shIBSP-1, forward 5'-GCCUAUGAAGAUGAGUACA-3',
reverse 5'-UGUACUCAUCUUCAUAGGC-3';
shIBSP-2, forward 5'-GGCACCUCGAAGACAACAA-3',
reverse 5'-UUGUUGUCUUCGAGGUGCC-3';
negative control (shNC), forward 5'-UUCUCCGAA CGUGUCACGU-3',
reverse 5'- ACGUGACACGUUCGGAGAA-3'.

2.7 Quantitative real-time PCR

PrimeScript RT kits (TaKaRa, Japan) were used for biosynthesis of cDNA. SYBR Premix ExTaq (TaKaRa, Japan) were used for qPCR. The detailed steps are carried out according to the recommended protocol. mRNA primers were as follows:

IBSP, forward 5'-AACAAGGCATAAACGGCACCAGTA-3',
reverse 5′-CGGTAATTGTCCCCACGAGGTT-3′;
GAPDH, forward 5′-CGGGAAGCTTGTCATCAATGG-3,
reverse 5′-GGCAGTGATGGCATGGACTG-3′.

2.8 Western blot analysis

The protein extraction and western blotting procedures used have been described in our previous study (16). The antibodies were as followed: GAPDH (1:2000; Cell Signalling Technologies, Danvers, MA, USA), IBSP (1:1000; Proteintech, Rosemont, IL, USA), MMP2 (1:1000; Proteintech) and MMP9 (1:1000; Proteintech).

2.9 Immunohistochemistry, immunofluorescence, CCK-8, wound healing assay, transwell assay and colony formation assay

The experimental procedure used has been described in detail in a previous study (16). The antibodies were as followed: IBSP (1:100; Proteintech).

2.10 Statistical analysis

All experiments *in vitro* were repeated three times independently. The results were reported as mean standard deviation, and the differences between the non-normally distributed variables were assessed using the Wilcoxon rank-sum test, which was performed using GraphPad Prism 9.0 and R software. Significance of differences between groups was assessed using Student's t-test ($p < 0.05$ indicates statistical significance).

3 Result

3.1 IBSP is overexpression in pan-cancer

The RNA-Seq analysis from TCGA revealed IBSP was overexpressed in 18 types tumors including breast invasive carcinoma (BRCA), bladder urothelial carcinoma (BLCA), cervical

10.3389/fimmu.2023.1188256

squamous cell carcinoma (CESC), colon adenocarcinoma (COAD), glioblastoma multiforme (GBM), cholangiocarcinoma (CHOL), esophageal carcinoma (ESCA), head and neck squamous cell carcinoma (HNSC), kidney renal papillary cell carcinoma (KIRP), kidney renal clear cell carcinoma (KIRC), kidney chromophobe (KICH), uterine corpus endometrial carcinoma (UCEC), liver hepatocellular carcinoma (LIHC), lung adenocarcinoma (LUAD), lung squamous carcinoma (LUSC), stomach adenocarcinoma (STAD), thyroid cancer (THCA) and rectal adenocarcinoma (READ) (Figure 1A). Analysis of IBSP expression in the TIMER2.0 database further validated our finding (Figure 1B). Combined analysis of TCGA and GTEx datasets, IBSP is also overexpressed in diffuse large B-cell lymphoma (DLBC), adrenocortical carcinoma (ACC), ovarian serous cystadenocarcinoma (OV), pancreatic adenocarcinoma (PAAD), brain Lower Grade Glioma (LGG), uterine carcinosarcoma (UCS), skin cutaneous melanoma (SKCM), thymoma (THYM), and prostate adenocarcinoma (PRAD) (Figures 1C, D). We further investigated the association between IBSP and the pathological stage

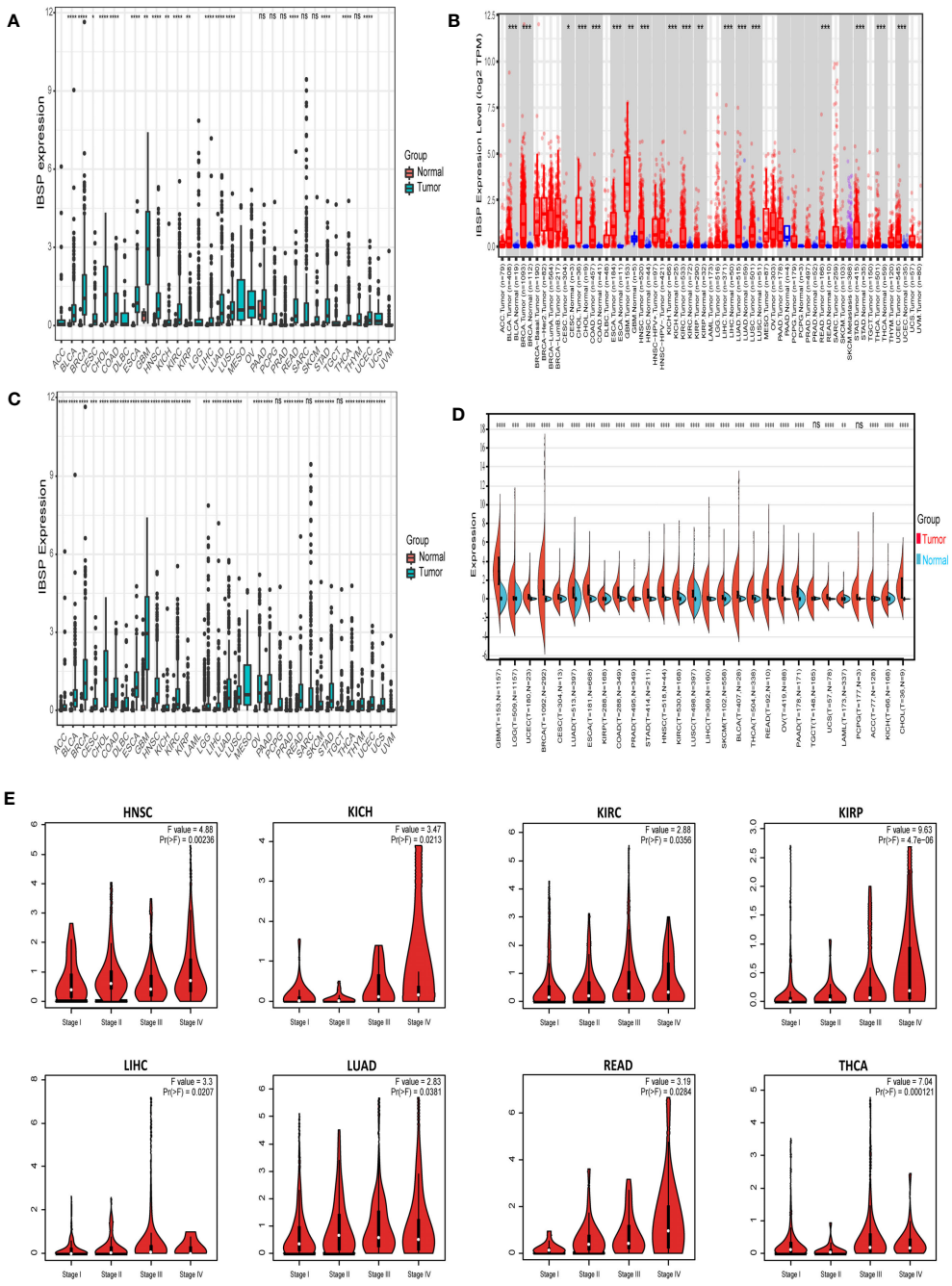

FIGURE 1
Different expression of IBSP in pan-cancer. **(A)** The mRNA expression of IBSP from the TCGA datasets. **(B)** The mRNA expression of IBSP from the TIMER database. **(C)** The mRNA expression of IBSP from the TCGA and GTEx datasets. **(D)** The mRNA expression of IBSP from the TCGA and GTEx datasets were analyzed using the Sanger. **(E)** The mRNA expression of IBSP in different tumor stages were analyzed in the GEPIA2 database. *P < 0.05, **P < 0.01, ***P < 0.001, ****P < 0.0001. ns, no significance.

in each tumor, the result revealed that elevated IBSP expression indicated advanced pathological stages in the following tumor types: KIRC, HNSC, KIRP, LUAD, KICH, LIHC, THCA and READ (Figure 1E). Moreover, the ROC curve analysis of the TCGA pan-cancer dataset revealed that IBSP had high diagnostic accuracy in CESC, BRCA, COAD, CHOL, HNSC, ESCA, LUSC, STAD and GBM; Moderate diagnostic accuracy was found in KICH, BLCA, LIHC, KIRC, PCPG, UCEC, LUAD, THCA, SARC and READ; Low diagnostic accuracy in KIRP, PAAD, PRAD, and THYM (Figure S1). These results suggested that IBSP was upregulated in various cancers, and it may be used as a biomarker for the diagnosis of cancers.

3.2 IBSP correlates with the prognosis of multiple tumors

Analysis of the GEPIA2 database suggested the overexpression of IBSP significantly reduced the overall survival in KIRC, KIRP, LIHC, LGG, READ and LUAD (Figure 2A). Additionally, IBSP overexpression decreased patients' DFS in ESCA, GBM, KIRC, LGG, LIHC, mesothelioma, PAAD and READ (Figure 2B). According to the classification of physiological system, COAD, CHOL, LIHC, ESCA, STAD, READ, PAAD, and PAAD belongs to the digestive system cancers, UCS, UCEC, TGCT, PRAD, OV, and CESC belongs to the reproductive system cancers, BLCA, KICH, KIRC, and KIRP belongs to the urinary system cancers, then survival analysis was performed in the GEPIA2 database according to this new classification. The results indicated that patients with IBSP overexpression in digestive system tumors, reproductive system tumors and urinary system tumors had shorter overall survival (Figure 2C). Similarly, patients with high IBSP expression had shorter DFS in digestive system tumors, reproductive system tumors and urinary system tumors (Figure 2D). Finally, survival analysis of the TCGA pan-cancer datasets revealed that IBSP overexpression was linked to a shorter overall survival, DFI, DSS and PFI in multiple cancers (Figures S2A–D). These data suggested IBSP overexpression is correlated to a poor prognosis in multiple cancers.

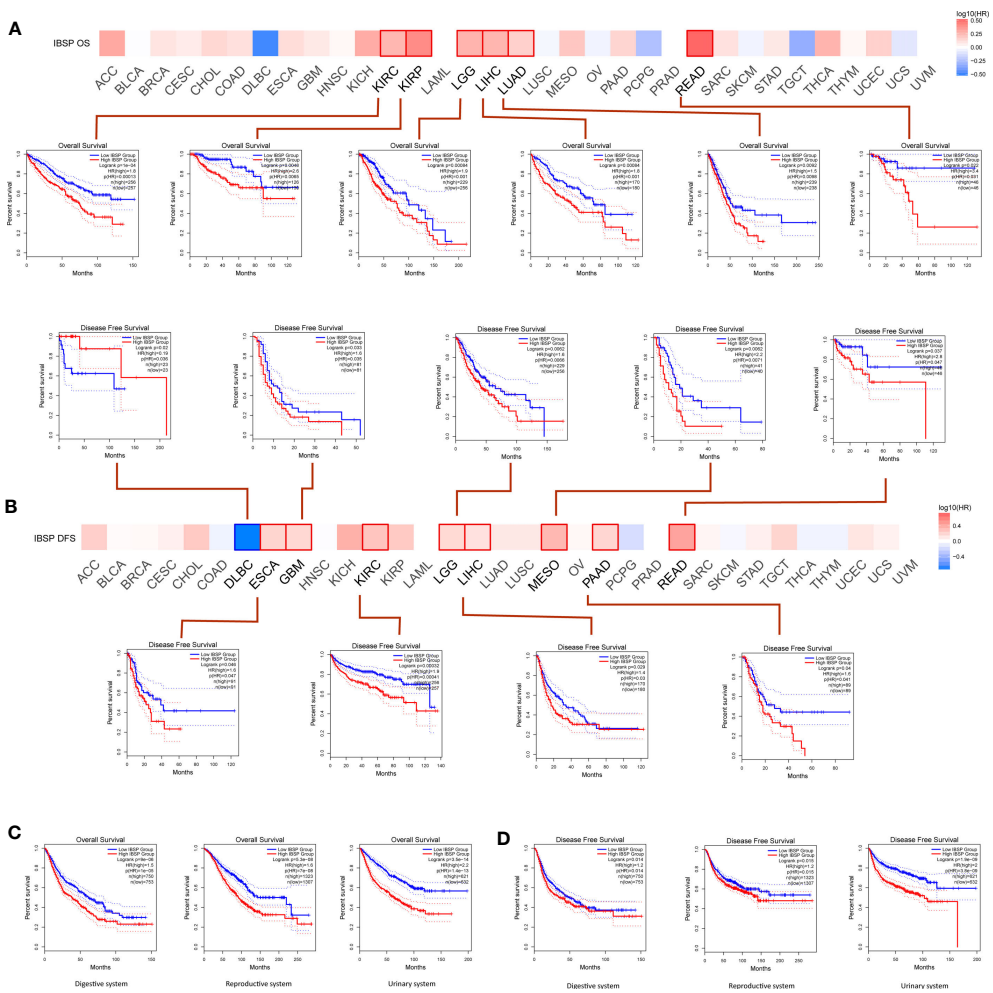

FIGURE 2
Effects of IBSP expression on the prognosis of pan-cancer. **(A)** Effects of pan-cancer IBSP expression on overall survival. **(B)** Effects of pan-cancer IBSP expression on disease-free survival. **(C)** Effects of IBSP expression on overall survival in digestive system tumors, reproductive system tumors and urinary system tumors. **(D)** Effects of IBSP expression on disease-free survival in digestive system tumors, reproductive system tumors and urinary system tumors.

3.3 The mutational landscape of IBSP in pan-cancer

The cBioPortal database was analyzed for the genetic alterations of IBSP, the results indicated that IBSP alterations occurred in 20 types cancer in total, among which UCEC having the highest level of alterations, along with "mutation" was the main type, while in BLCA and OV respectively, "amplification" and "deep deletion" were the main types (Figure 3A). Then the analysis of the Timer2.0 database showed that IBSP mutations occurred in 16 tumors, among which UCEC also having the highest level of mutation (Figure 3B). In addition, A total of 91 mutations sites were detected in IBSP, among which "missense" was the predominant type, followed by "truncating mutations" (Figure 3C). We also analyzed the TCGA pan-cancer dataset for the counts of IBSP mutation in the tumors, the result showed widespread genetic alterations of IBSP (Figure 3D). Furthermore, we analyzed the association between the IBSP mutation and the clinical outcomes of different tumors (Figures S3A-R), only PRAD patients with IBSP mutation had poor prognosis in overall survival (p = 9.320e-4) (Figures S3R). The relationship between IBSP and TMB/MSI of the tumors were analyzed by the Sanger, the results revealed that IBSP was positively related to TMB in 13 tumors and negatively related to KIRP (Figure 3E), and it was positively related to MSI in LUSC, STAD, COAD, LIHC and TGCT, and negatively related to LUAD (Figure 3F).

3.4 IBSP is associated immune infiltration and RNA modifying molecules in multiple tumors

Data analyzed by the Sanger suggested that IBSP in STAD and TGCT were negative correlated with ESTIMATEScores, which suggested that IBSP overexpression was associated with reduced stromal cell and immune cell in both tumors, resulting in higher tumor purity. However, in BLCA, COAD, GBM, HNSC, KICH, KIRC, KIRP, LGG, LUAD, OV, PAAD, PCPG, READ, SKCM, THCA and UVM, IBSP expression was positively correlated with the ESTIMATEScores (Figures 4A–C). Previous studies have verified that immune cell infiltration and RNA modification molecules are closely related to tumor development, metastasis and prognosis (17, 18). Therefore, we assessed the correlation of IBSP with pan-cancer immune cell infiltration and RNA modification molecules using the Sanger, the result suggested that IBSP was related to all six types of immune cells in LGG, TGCT, KIRP, KIRC, and BLCA (Figure 4D). We further explored the relationship between IBSP and 60 immune checkpoint genes

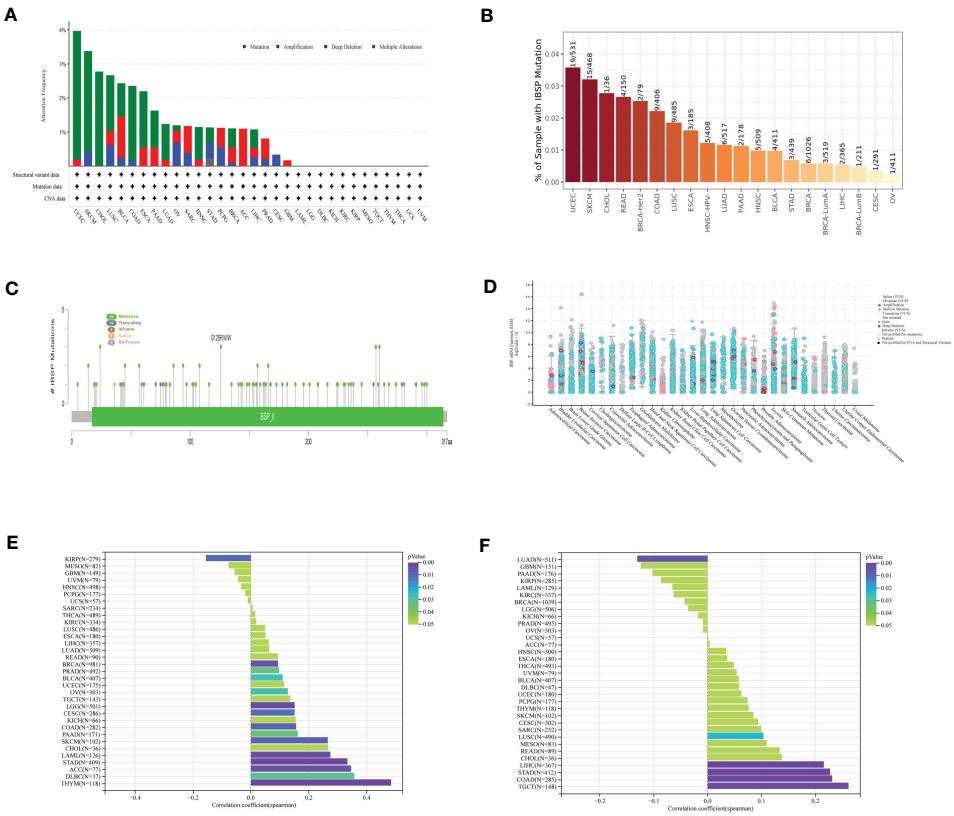

FIGURE 3
The mutational landscape of IBSP in pan-cancer. **(A)** The genetic alterations of IBSP in the cBioPortal database. **(B)** The genetic alterations of IBSP in The TIMER2.0 database. **(C)** The mutant sites and mutations types of IBSP. **(D)** The counts of IBSP mutation in the pan-cancer from the TCGA dataset. **(E, F)** The relationship between IBSP and TMB/MSI of pan-cancer were analyzed by the Sanger.

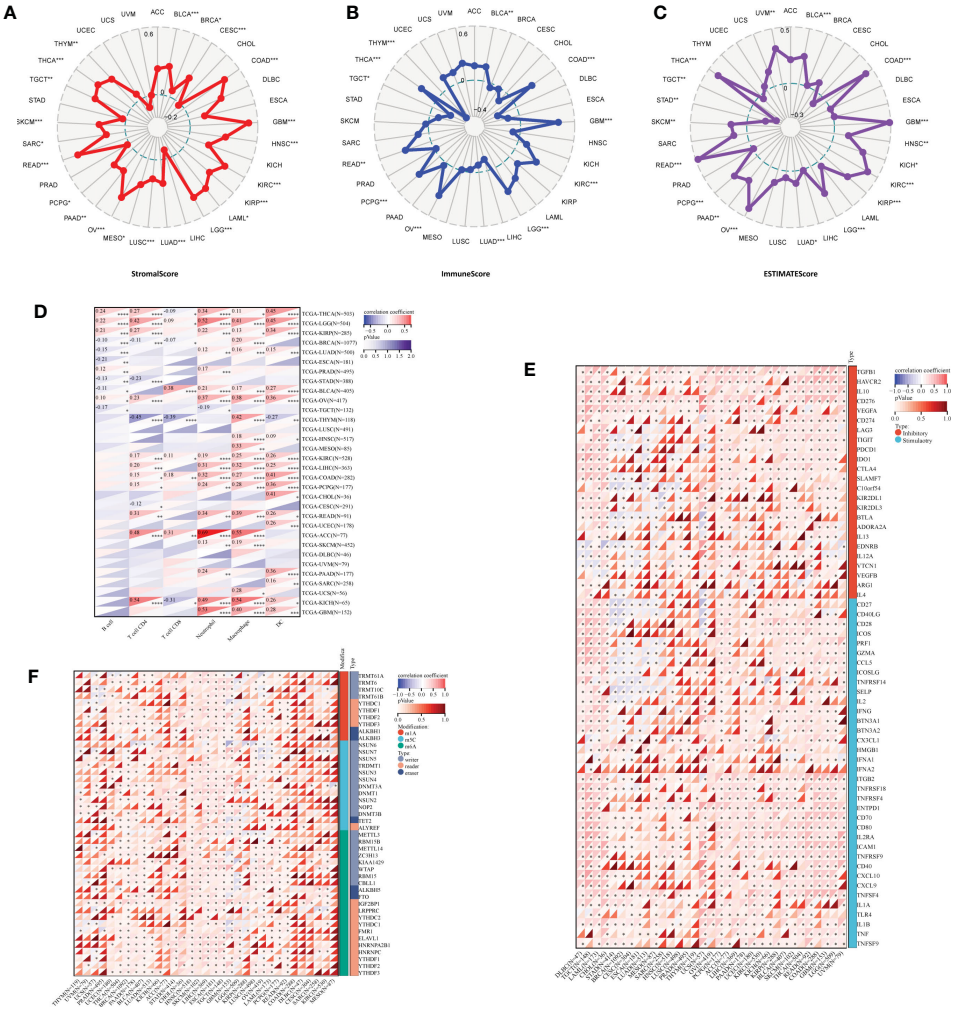

FIGURE 4
Correlation analysis for IBSP expression with immune cell infiltration levels, immune checkpoints, and RNA modification-related molecules. **(A–C)** The correlation between IBSP expression and StromalScore, ImmuneScore and ESTIMATEScore. **(D)** The correlation between IBSP expression and tumor infiltration levels was analyzed in the TIMER database. **(E)** Pan-cancer co-expression analysis for IBSP and immune checkpoint genes (ICP). **(F)** Co-expression analysis for IBSP and RNA modification-related molecules. *P < 0.05, **P < 0.01, ***P < 0.001, ****P < 0.0001.

(including 36 stimulatory and 24 suppressive genes), and found a substantial relationship between IBSP and five immune-suppressive checkpoint genes (TGFB1, HAVCR2, IL10, CD276, and VGEFA) in most tumors (Figure 4E). Meanwhile, the analysis on the relationship between IBSP and RNA modification showed that it was also substantially associated to three main types of RNA modification-related molecules (m^6A, m^5C and m^1A) in HNSC, SKCM, LIHC, ESCA, and TGCT (Figure 4F).

3.5 Enrichment and survival analysis of IBSP in OS

The aforementioned analysis showed that IBSP may be a potential tumor prognostic marker in various cancers. While, IBSP serve as an indicator of cancer bone metastasis (9, 19–23), its role and mechanism in the primary bone malignancies is still unknown, so we attempted to study its expression and function in OS. In the GSE16088 dataset and GSE42352 dataset, IBSP was significantly over-expressed in OS tissues than that in the paired normal tissues (Figures 5A, B). Moreover, OS patients with higher IBSP expression had shorter survival (Figures 5C, D). In the TARGET-OS dataset, the prediction accuracy of IBSP for the 1/3/5 years survival rates of OS patients was 0.552, 0.590, and 0.635 respectively (Figure 5E). In the GSE21257 dataset, the prediction accuracy of IBSP for the 1/3/5 years survival rates of OS patients was 0.643, 0.658, and 0.754 respectively (Figure 5F). It suggested that similar to other tumors, IBSP was a prognostic biomarker in OS, and it can predict patients' survival. To analyze the biological processes and signaling pathways of the IBSP co-expressed genes in OS, we performed correlation analysis on the two datasets, and 104 IBSP-related genes from the TARGET-OS dataset and 138 IBSP-related genes from the GSE21257 dataset were merged and imported into the Cytoscape software to plot a network diagram of IBSP-related genes (Figure 5G). The Enrichment analysis of the IBSP-related genes was performed through the Metascape dataset.

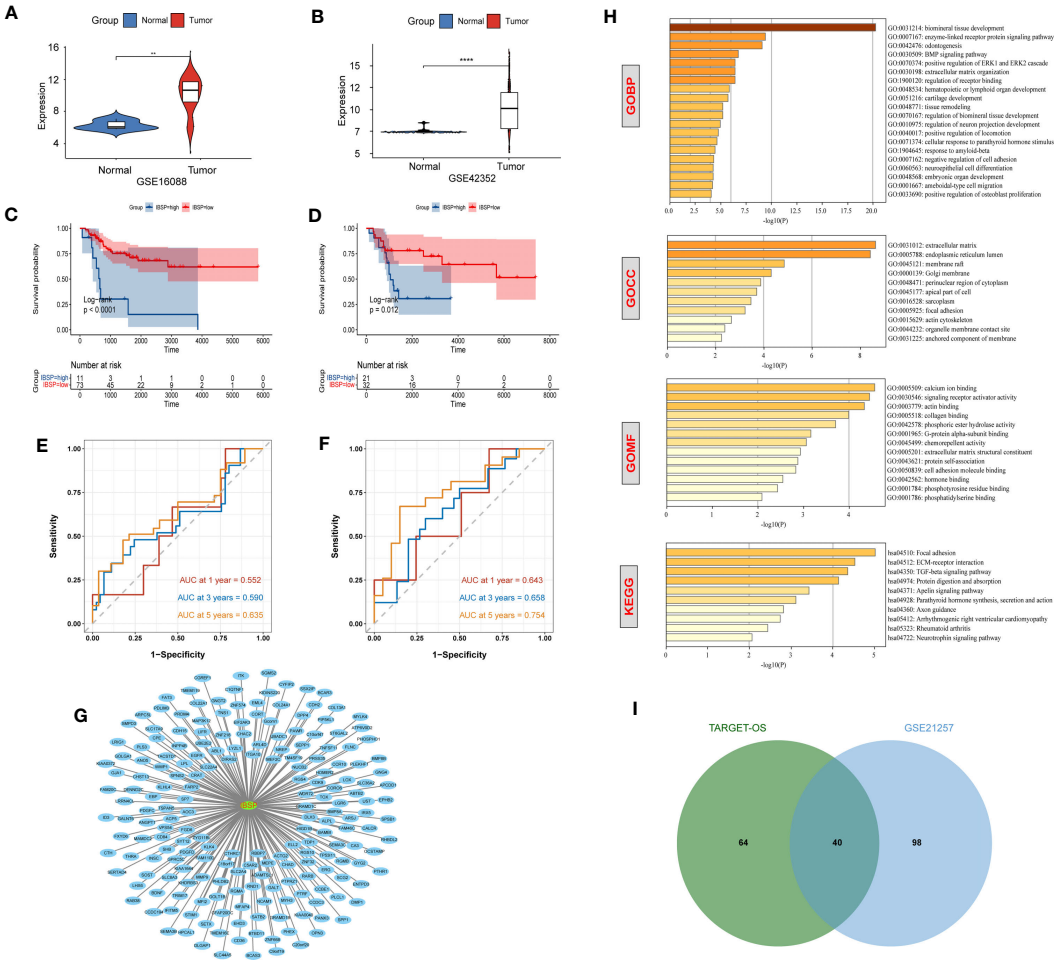

FIGURE 5
Enrichment and survival analysis of IBSP in OS. **(A, B)** The mRNA expression of IBSP from the GSE16088 and GSE42352 datasets. **(C, D)** Effects of IBSP expression on overall survival in the TARGET-OS and GSE21257 datasets. **(E, F)** The prediction accuracy of IBSP for the 1/3/5 years survival rates of OS patients in the TARGET-OS and GSE21257 datasets. **(G)** A network diagram of IBSP-related genes in the TARGET-OS and GSE21257 datasets. **(H)** GO and KEGG functional enrichment analysis of the molecules interacted with IBSP. **(I)** 40 intersection genes were screened from the TARGET-OS dataset and the GSE21257 dataset. **P < 0.01, ****P < 0.0001.

GO biological process (GO-BP) indicated that they were related to biomineral tissue formation, enzyme-linked receptor protein signaling pathway, tooth formation, and BMP signaling pathway. GO cell components (GO-CC) indicated that they were related to extracellular matrix and endoplasmic reticulum cavity. GO molecular function (GO-MF) showed that they were related to calcium ion binding, signal receptor activator activity and actin binding. KEGG enrichment analysis revealed that they were correlated to ECM-receptor interaction, local adhesion, TGF-β signaling pathway (Figure 5H). Finally, 40 intersection genes were screened from the TARGET-OS dataset and the GSE21257 dataset for subsequent analysis (Figure 5I).

3.6 Construction and evaluation of OS prediction model

Univariate Cox analysis of the 40 IBSP-related genes was performed in the training set TARGET-OS, the results showed that 24 genes exhibited differences in survival (Figure 6A). Then the 24 genes were subjected to the LASSO regression analysis, and three genes (CPE, CGREF1 and SOST) were screened out (Figure 6B). The risk score calculation formula was as follows: risk score=0.044*CPE +0.005*SOST+0.308*CGREF1. The relationship between IBSP and the three gene expressions and their risk scores in the TARGET-OS and GSE21257 datasets was evaluated using the "spearman" correlation method, the results revealed that IBSP was positively related to their expression and risk scores (Figures S4A, B). The risk scores of different clinical characteristics were calculated in the TARGET-OS dataset, the results showed that Female gender, age under 18, and tumor metastasis are risk factors for reduced survival (Figures S5A–D). In the TARGET-OS dataset, higher risk groups had shorter overall survival (Figure 6C), and the 1/3/5 years survival prediction accuracy of the risk score were 0.790, 0.790, and 0.759 respectively (Figure 6D). While in the GSE21257 dataset, overall survival was also significantly reduced in the higher risk group (Figure 6E), and the 1/3/5 years survival prediction accuracy were 0.694, 0.687, and 0.770 respectively (Figure 6F). Risk score and tumor

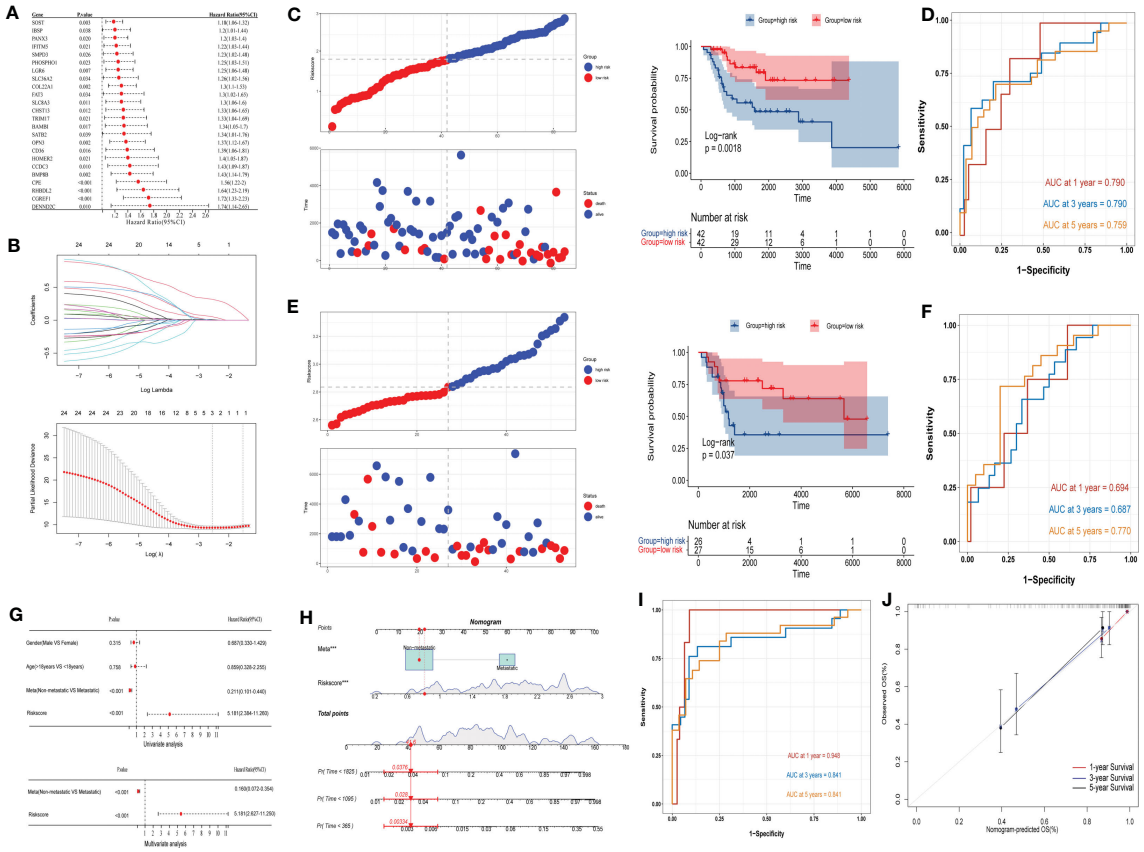

FIGURE 6
Construction and evaluation of OS prediction model. **(A, B)** Cox analysis and LASSO regression analysis were used to screen out the IBSP-related genes in the TARGET-OS dataset. **(C)** OS prediction model evaluated the overall survival in the high and low risk groups in the TARGET-OS dataset. **(D)** OS prediction model evaluated the accuracy for the 1/3/5 years survival rates of OS patients in the TARGET-OS. **(E)** OS prediction model evaluated the overall survival in the high and low risk groups in the GSE21257 dataset. **(F)** OS prediction model evaluated the accuracy for the 1/3/5 years survival rates of OS patients in the GSE21257 datasets. **(G)** Univariate and multivariate Cox analyses analyzed the clinical characteristics and risk scores. **(H–J)** The predictive model based on clinical characteristics and risk scores had a high predictive accuracy.

metastasis were both identified as independent prognostic factors by univariate and multivariate Cox analyses (Figure 6G). A nomogram was plotted based on these two indicators, and the value of AUC was used as a predictive indicator (Figure 6H). The results show that the 1/3/5 years survival prediction accuracy of this model are 0.948, 0.841, and 0.841 respectively (Figure 6I). The results above showed that the predictive model based on clinical characteristics and risk scores had a high predictive accuracy, and the 1/3/5-year survival predictive calibration curves further validated this model (Figure 6J).

3.7 Levels of immune infiltration and RNA modification analysis in OS

We evaluated the degree of immune cell infiltration in the TARGET-OS and GSE21257 datasets based on the ssGSEA algorithm, the result revealed that the levels of immune cells infiltration between the high and low risk groups is different (Figures 7A, B). Furthermore, we analyze immune cell infiltration using the EPIC, CIBERSORT, IPS, MCPCOUNTER, QUANTISEQ, TIMER and XCELL algorithm built into the IBOR package, the similar results are present (Figures S6A–B). In both datasets, the ESTIMATEScore of the high-risk group was lower than that of the low-risk group (Figures 7C, D), which meant that the cancers in the high-risk group were more purity, and the shorter survival time of the patients may be connected to the level of immune infiltration. In TARGET-OS dataset, risk scores were negatively correlated with ICP gene receptor CD27 and ligand TNFSF14, and positively correlated with ICP gene receptor CD47 (Figure 7E). Using the TIDE online website analysis, we found the low-risk group had higher TIDE scores, which suggested that the low-risk group had an increased potential for immune escape and may have a worse response to immunotherapy (Figure 7F). Moreover, the correlation of RNA modifications with IBSP and IBSP-related genes (SOST, CGREF1 and CPE) were analyzed in the OS prediction model, the results showed that multiple m^6A, m^1A and m^5C modification genes in the TARGET-OS dataset are closely related to IBSP and IBSP-related genes. In GSE21257 dataset, there are also multiple m^6A, m^1A, m^5C and M^7G modification genes that are closely related to IBSP and IBSP-related genes (Figures 7G, H).

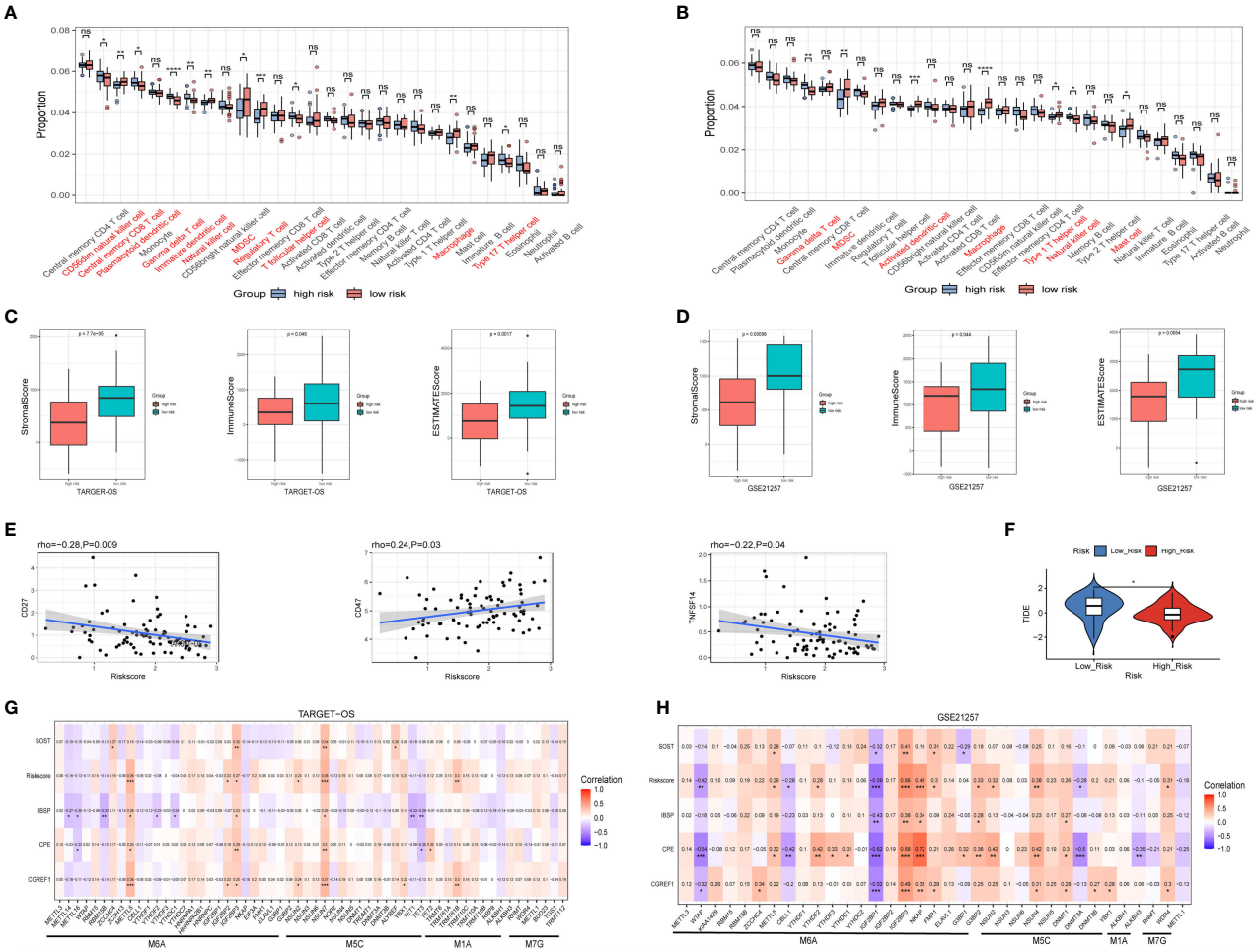

FIGURE 7
Relationship between IBSP expression and immune infiltration as well as RNA modification. **(A, B)** The levels of immune cells infiltration between the high and low risk groups in the TARGET-OS and GSE21257 datasets. **(C, D)** The StromalScore, ImmuneScore and ESTIMATEScore between the high and low risk groups in the TARGET-OS and GSE21257 datasets. **(E)** Relationship between risk score and ICP gene receptor as well as ICP ligand in the TARGET-OS dataset. **(F)** Analysis of immunotherapy response in the high- and low-risk groups from the TARGET-OS dataset. **(G, H)** The correlation of RNA modifications with IBSP and IBSP-related genes in the TARGET-OS and GSE21257 datasets. *P < 0.05, **P < 0.01, ***P < 0.001, ****P < 0.0001. ns, no significance.

3.8 IBSP is highly expressed in OS tissues and cell lines

Western blotting, immunohistochemistry, and qPCR assays were used to detected IBSP expression in tumor tissues and different cancer cell lines. Firstly, we detected its expression in several cancers with a high incidence, such as hepatic carcinoma, esophageal cancer, lung cancer, kidney cancer, breast cancer and colorectal cancer. The results showed IBSP was upregulated in these tumor tissues (Figures S7A–F). Then we validated its expression in the cancer cell lines, the results of qPCR demonstrated that its mRNA in the different cancer cell lines was elevated compared with the normal cells (Figures S7G–L); and the results of WB revealed its protein was overexpressed in the cancer cell lines as well (Figures S7M–R). Finally, we proceeded to detected its expression in OS tissues and cell lines. The results showed that OS tissues had higher levels of IBSP expression than the paired normal tissues, and that IBSP expression were elevated in advanced pathological stages (Figures 8A–C). qPCR and western blotting were used to detected the expression of IBSP in hFOB and OS cells, and it was upregulated in OS cells, especially in 143B and MG63, thus, they were selected for the further experiments (Figures 8D, E). In addition, we also examined the subcellular localization of IBSP in the OS cells, it showed that IBSP was mainly localized in the cytoplasm (Figure 8F).

3.9 IBSP knockdown suppresses OS proliferation, migration and invasion

To study the role of IBSP on the proliferation of OS, IBSP was knockdown in 143B and MG63 (Figures 9A, B). The data of CCK8 and clone formation assays revealed that IBSP knockdown inhibited OS cells proliferation in 143B (Figures 9C, D), and MG63 (Figures 9E, F). In addition, the transwell assay and the wound healing assay were carried out to clarify the role of IBSP in the metastasis of OS. The wound healing assay indicated that IBSP knockdown would reduce the closure in OS cells (Figures 10A, B). The results of transwell assays which included migration and

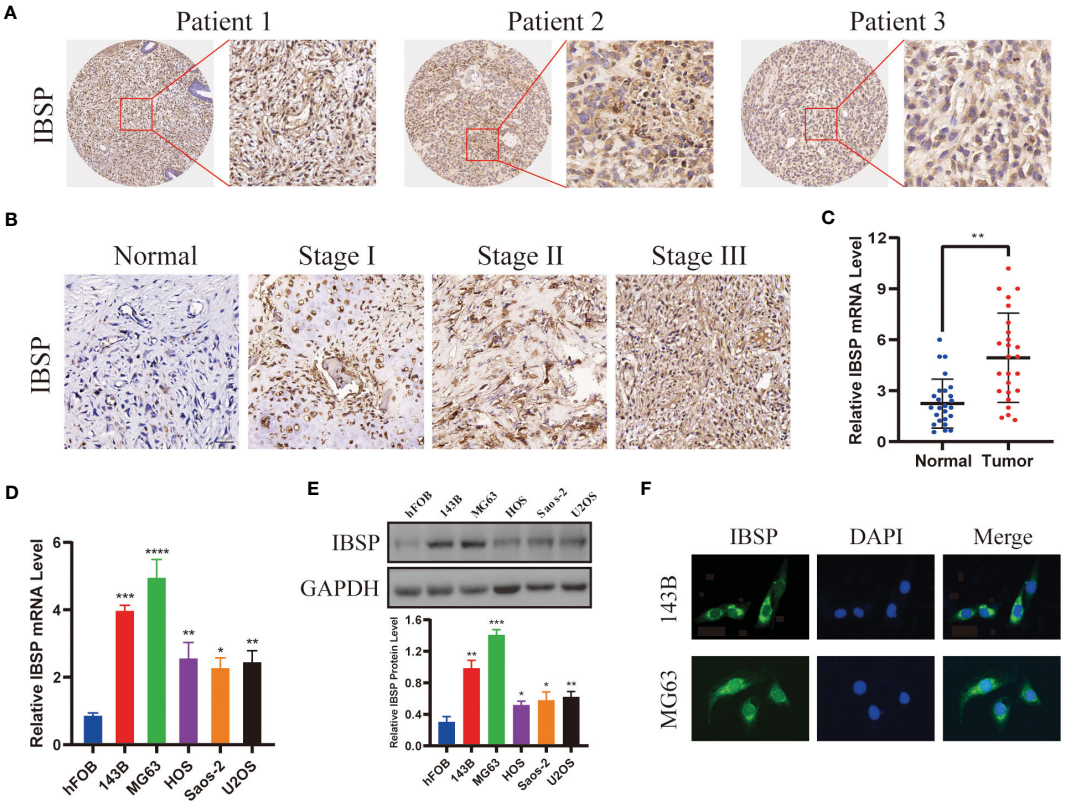

FIGURE 8
IBSP is overexpressed in OS. **(A)** IBSP expression in the OS tissues was detected by Immunohistochemistry (IHC). **(B)** IBSP expression in the OS tissues at different Enneking stages was detected by IHC. **(C)** IBSP mRNA was detected by qRT-PCR in the OS tissues and peritumor tissues (Normal). **(D, E)** IBSP mRNA and protein were detected by qRT-PCR in the OS cells. **(F)** Cellular localization of IBSP were detected by immunofluorescence (IF). *P < 0.05, **P < 0.01, ***P < 0.001, ****P < 0.0001.

invasion assays, suggested that OS cells permeating the membrane were reduced when IBSP was knocked down (Figures 10C–F). MMP2 and MMP9 are commonly used to indicate the metastatic potential of cancer cells. In our study, the expression of MMP2 and MMP9 were significantly reduced when IBSP was knockdown in OS cells (Figures 10G, H). The data together revealed that IBSP can promote the migration and invasion of OS cells *in vitro*.

4 Discussion

IBSP is a glycoprotein consisting of 301 amino acids, and its terminal Arg-Gly-Asp sequence can bind integrins, which play important roles in cell adhesion, angiogenesis, regulation of extracellular matrix, immune cell migration and infiltrated (24–26). Therefore, some studies have revealed that IBSP promotes bone metastasis of tumor cells in BRCA (9), PRAD (27), and non-small cell lung cancer (21). Recently, with the development of bioinformatics, some studies demonstrated that the expression of IBSP is upregulated in epithelial tumors such as laryngeal cancer (28) and BLCA (29), which is highly correlated with a poor prognosis. For malignant tumors of non-epithelial origin, such as GBM, IBSP can also promote tumor cell proliferation and migration (30). Therefore, IBSP is considered to be an oncogene and closely related to the bone metastasis.

Cancer has become a major threat to human health because of its indistinct symptoms, rapid development, and lack of effective treatment. Therefore, finding biomarkers of tumor progression can be beneficial to early diagnosis and early treatment of cancer patients, which is the main method to improve the efficiency of cancer treatment (31). In this study, based on TCGA data, we found that IBSP was upregulated in various malignant tumor tissues (BRCA, BLCA, CHOL, CESC, ESCA, COAD, KICH, GBM, HNSC, KIRP, KIRC, LUAD, LIHC, LUSC, READ, STAD, UCEC, THCA), and it was found to be significantly associated with poor prognosis of the patients with these malignant tumors. Meanwhile, based on the GTEx dataset, we further confirmed that IBSP was also overexpressed in ACC, DLBC, LGG, OV, PAAD, PRAD, SKCM, THYM and UCS. Furthermore, by analyzing the OS dataset, combined with the results of some assays *in vitro*, we determined that IBSP was overexpressed in OS and associated with a poor prognosis in OS patients.

The extracellular matrix (ECM) is a complex structure made up of numerous proteins and glycans, which was previously considered to act as a barrier for cells, providing mechanical pressure to maintain the normal tissue morphology of cells (32). However, some recent studies have revealed that changes in ECM compositional abundance and structural strength are inseparable to tumor occurrence, development, metastasis and chemotherapy resistance (33). In this study, our data revealed that the interaction

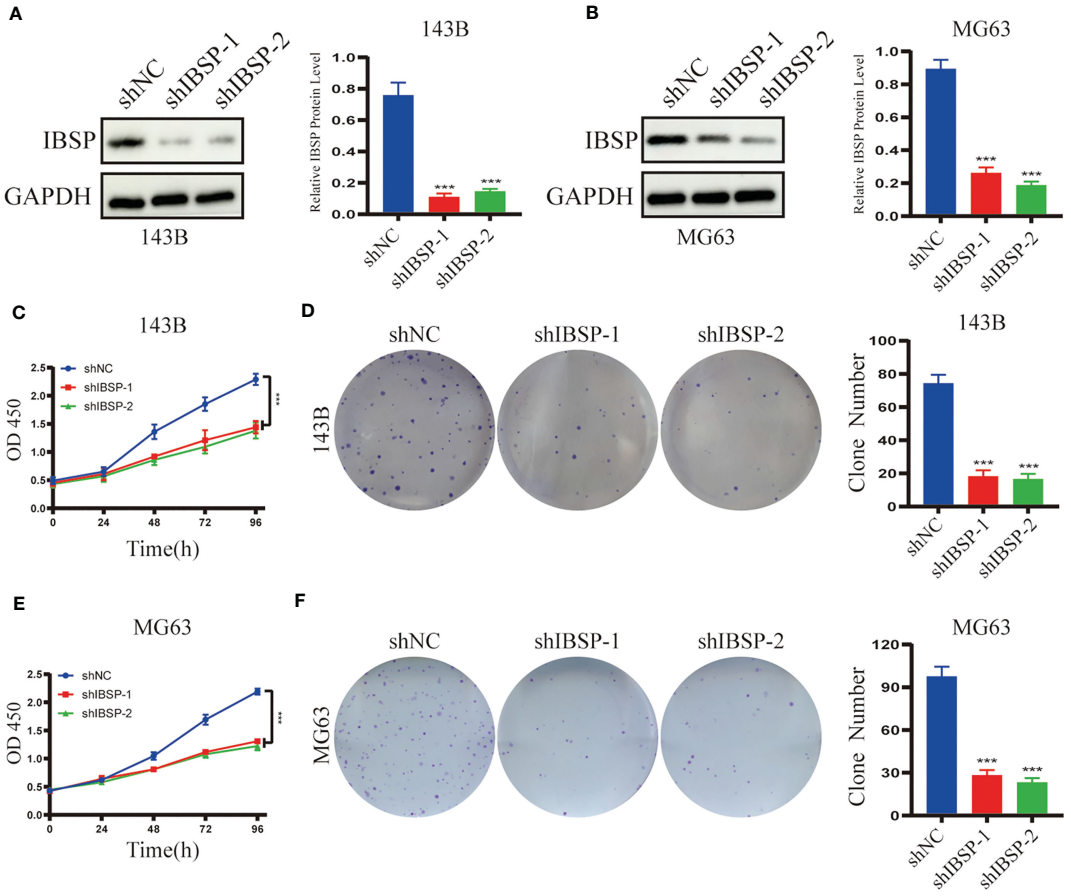

FIGURE 9
Silenced IBSP inhibits the proliferation of OS cells. **(A, B)** IBSP protein expression was detected in 143B and MG63 cells with IBSP knockdown or control. **(C, D)** Cell proliferation rate was detected by CCK-8 and clone formation assays in 143B. **(E, F)** Cell proliferation rate was detected by CCK-8 and clone formation assays in MG63. ***P < 0.001.

genes of IBSP have the function of regulating extracellular matrix, which is consistent with previous studies (10, 27). Moreover, the functional enrichment analysis demonstrated that IBSP and its interaction genes in OS were closely related to biomineral tissue development (GO-BP), extracellular matrix (GO-CC), calcium ion binding (GO-MF), and cell adhesion. Therefore, we speculate that the protein encoded by IBSP binds integrin through its RGD sequence, then recruits calcium ions to reduce the adhesion of OS cells, thereby promoting tumor cell metastasis. In order to verify our conjecture, some cell assays *in vitro* were performed, and the results confirmed that IBSP knockdown would inhibit the migration and invasion of OS cells, and the expression levels of tumor metastasis markers MMP2 and MMP9 were significantly weakened.

The tumor microenvironment contains a variety of immune cells and stromal components, and the occurrence, development, and metastasis of tumors are closely related to changes in the tumor microenvironment (34, 35). Our experiments confirmed that in a variety of tumors, the expression of IBSP was positively correlated with the infiltration of T cells, neutrophils, macrophages and dendritic cells (DC), especially the infiltration of macrophages. Increasing number of evidences showed that tumor-associated macrophages (TAM) are important regulators of tumorigenesis and metastasis, and their high infiltration rate is associated with chemotherapy resistance and poor prognosis (36). Similarly, different levels of immune cell infiltration in OS, including T cells, macrophages, and myeloid-derived suppressor cells, were also present in various risk subgroups, and ESTIMATEscores were lower in the high-risk subgroup than in the low-risk subgroup in both datasets. These differences may all be significant influencing factors resulting in various clinical outcomes in osteosarcoma patients. Immunotherapy is a viable new treatment option to take the place of traditional Chemoradiotherapy because it has demonstrated sufficient efficacy in the management of a range of cancers. Thus, we analyzed the expression of IBSP and ICP genes, and the results showed that IBSP was positively correlated with ICP genes such as VGEFA, HAVCR2, IL10, CD276, and TGFB1 in pan-cancer. In terms of OS, our study demonstrated that patients in the high-risk group not only had shorter survival durations than those in the low-risk group, but also had lower TIDE ratings. Hence, immunotherapy may enable the high-risk group to experience higher therapeutic benefit.

Finally, we contracted a risk score model consisting of three genes (CPE, CGREF1, SOST) that were significantly positively correlated with IBSP expression. Previous studies have confirmed

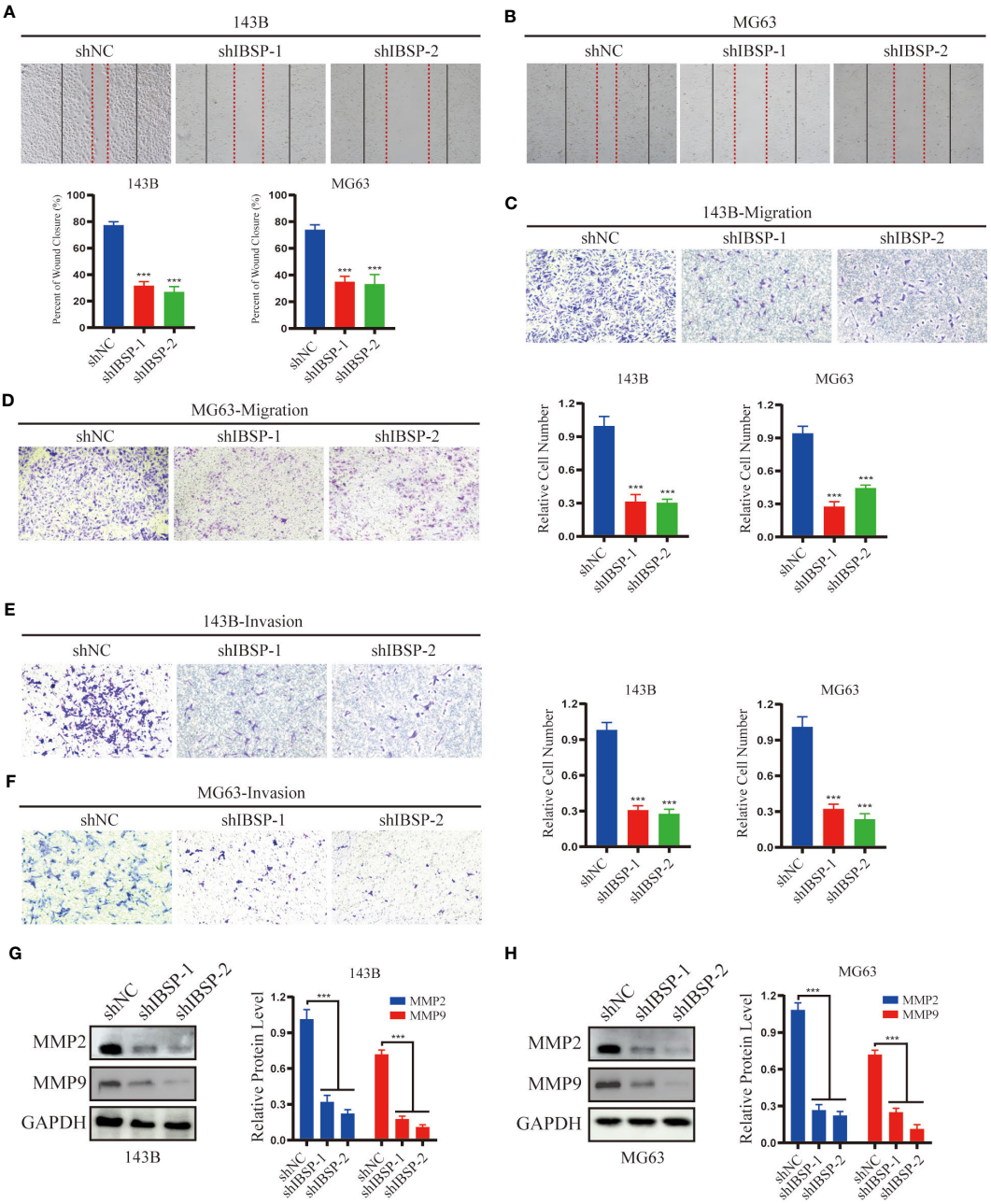

FIGURE 10
IBSP knockdown suppresses OS cells migration and invasion. **(A, B)** Cell migration rate was evaluated by wound healing assays in 143B and MG63 cells with IBSP knockdown or control. **(C, D)** Cell migration ability was evaluated by transwell assays in 143B and MG63 cells with IBSP knockdown or control. **(E, F)** Cell invasion ability was evaluated by transwell assays in 143B and MG63 cells with IBSP knockdown or control. **(G, H)** The expression of MMP2 and MMP9 was detected in 143B and MG63 cells with IBSP knockdown or control. ***P < 0.001.

that the three genes CPE, CGREF1, and SOST are closely related to the proliferation, metastasis, and drug resistance of OS (33–35), which imply that IBSP may play a role in the proliferation and migration of OS. Combined with external datasets, the reliability of the risk scoring model was confirmed. After incorporating clinically relevant features, we further established a clinical prediction model, which exhibited high accuracy in survival prediction, which will be helpful for the evaluation and management of OS patients.

However, our study also has some shortcomings. First, we didn't conduct further studies on the mechanism of IBSP in promoting OS progression; In addition, and we didn't conduct animal experiments to verify its function *in vivo*; Finally, we didn't generate IBSP overexpressed OS cells to further verify its role in OS.

In conclusion, we conducted a more comprehensive pan-cancer analysis of IBSP using multi-omics data, and found that IBSP is abnormally expressed in various tumors and highly related to a

poor prognosis. We also studied IBSP's function from the aspects of methylation modification, gene change, immune infiltration, and functional enrichment, which clarified the role of IBSP in tumor development and metastasis. Through bioinformatics methods and experiments *in vitro*, we revealed that IBSP could promote the proliferation and migration of OS cells. Taken together, our study demonstrates that IBSP is a potential prognostic biomarker and immunotherapy target in various tumors including OS.

Data availability statement

The datasets presented in this study can be found in online repositories. The names of the repository/repositories and accession number(s) can be found within the article/Supplementary Material.

Ethics statement

The study was approved by the ethics committee of the Third Xiangya Hospital, Central South University (Approval No.202023). All animal experiments were in compliance with the Experimental Animal Ethics Committee's guidelines and were approved by the Animal Experimental Committee of the Third Xiangya hospital (Grant number: 2021sydw0221).

Author contributions

BP, JC, WT and YD designed the research; BP, JC, XW collected and analyzed the data; JC, RL and YZ performed the research; BP, JH and QF analyzed the data; BP, JC and YZ wrote the paper; BP, XC and JC organized the original source data. All authors contributed to the article and approved the submitted version.

Funding

This work was supported by the Science and Technology Program of Hunan Province (2021RC4057); Postgraduate Scientific Research Innovation Project of Hunan Province (150110027).

Acknowledgments

We would like to thank our researchers for their hard work and reviewers for their valuable advice.

Conflict of interest

The authors declare that the research was conducted in the absence of any commercial or financial relationships that could be construed as a potential conflict of interest.

Publisher's note

Supplementary material

The Supplementary Material for this article can be found online at: https://www.frontiersin.org/articles/10.3389/fimmu.2023.1188256/full#supplementary-material

FIGURE S1
The diagnostic sensitivity of IBSP in the TCGA pan-cancer.

FIGURE S2
The survival analysis of the high and low IBSP expression groups in TCGA dataset, including overall survival **(A)**, disease-free interval **(B)**, disease-specific survival **(C)** and progression-free interval **(D)**.

FIGURE S3
Effect of IBSP gene mutation on overall survival of various tumors.

FIGURE S4
The relationship between IBSP and the three gene (CPE, CGREF1 and SOST) in the TARGET-OS **(A)** and GSE21257 **(B)**.

FIGURE S5
The risk factors for reduced survival in the TARGET-OS dataset **(A)**, which including gender **(B)**, age **(C)** and metastasis **(D)**.

FIGURE S6
The differences of immune infiltration between the high and low risk groups in the TARGET-OS **(A)** and GSE21257 **(B)** datasets.

FIGURE S7
The expression of IBSP in various cancer tissues and their cell lines **(A-F)**. The protein level of IBSP was detected in the tumor tissues (T) and adjacent normal tissues (N). **(G-L)** The mRNA of IBSP was detected in different cancer cell lines and their corresponding normal cell lines. **(M-R)** The protein level of IBSP was detected in different cancer cell lines and their corresponding normal cell lines.

References

1. Cole S, Gianferante DM, Zhu B, Mirabello L. Osteosarcoma: a surveillance, epidemiology, and end results program-based analysis from 1975 to 2017. *Cancer* (2022) 128(11):2107–18. doi: 10.1002/cncr.34163

2. Cundy T. Paget's disease of bone. *Metabolism: Clin Experimental* (2018) 80:5–14. doi: 10.1016/j.metabol.2017.06.010

3. Wang Z, Liang J, Jiang S, Zhao G, Lu J, Jiang B. The effect of miR-138 on the function of follicular helper T cells and the differentiation of b cells in osteosarcoma. *Comput Math Methods Med* (2021) 2021:2057782. doi: 10.1155/2021/2057782

4. Sampo M, Koivikko M, Taskinen M, Kallio P, Kivioja A, Tarkkanen M, et al. Incidence, epidemiology and treatment results of osteosarcoma in Finland - a

nationwide population-based study. *Acta Oncol (Stockholm Sweden)* (2011) 50 (8):1206–14. doi: 10.3109/0284186X.2011.615339

5. Gill J, Gorlick R. Advancing therapy for osteosarcoma. *Nat Rev Clin Oncol* (2021) 18(10):609–24. doi: 10.1038/s41571-021-00519-8

6. Kerr JM, Fisher LW, Termine JD, Wang MG, McBride OW, Young MF. The human bone sialoprotein gene (IBSP): genomic localization and characterization. *Genomics* (1993) 17(2):408–15. doi: 10.1006/geno.1993.1340

7. Ogata Y. Bone sialoprotein and its transcriptional regulatory mechanism. *J periodontal Res* (2008) 43(2):127–35. doi: 10.1111/j.1600-0765.2007.01014.x

8. Bellahcène A, Castronovo V, Ogbureke KU, Fisher LW, Fedarko NS. Small integrin-binding ligand n-linked glycoproteins (SIBLINGs): multifunctional proteins in cancer. *Nat Rev Cancer* (2008) 8(3):212–26. doi: 10.1038/nrc2345

9. Wu K, Feng J, Lyu F, Xing F, Sharma S, Liu Y, et al. Exosomal miR-19a and IBSP cooperate to induce osteolytic bone metastasis of estrogen receptor-positive breast cancer. *Nat Commun* (2021) 12(1):5196. doi: 10.1038/s41467-021-25473-y

10. Chen Y, Qin Y, Dai M, Liu L, Ni Y, Sun Q, et al. IBSP, a potential recurrence biomarker, promotes the progression of colorectal cancer via fyn/β-catenin signaling pathway. *Cancer Med* (2021) 10(12):4030–45. doi: 10.1002/cam4.3959

11. Wang M, Liu B, Li D, Wu Y, Wu X, Jiao S, et al. Upregulation of IBSP expression predicts poor prognosis in patients with esophageal squamous cell carcinoma. *Front Oncol* (2019) 9:1117. doi: 10.3389/fonc.2019.01117

12. Meng X, Yuan H, Li W, Xiao W, Zhang X. Biomarker screening and prognostic significance analysis for renal cell carcinoma. *Int J Gen Med* (2021) 14:5255–67. doi: 10.2147/IJGM.S325347

13. Yoshihara K, Shahmoradgoli M, Martínez E, Vegesna R, Kim H, Torres-Garcia W, et al. Inferring tumour purity and stromal and immune cell admixture from expression data. *Nat Commun* (2013) 4:2612. doi: 10.1038/ncomms3612

14. Hänzelmann S, Castelo R, Guinney J. GSVA: gene set variation analysis for microarray and RNA-seq data. *BMC Bioinf* (2013) 14:7. doi: 10.1186/1471-2105-14-7

15. Maeser D, Gruener RF, Huang RS. oncoPredict: an r package for predicting in vivo or cancer patient drug response and biomarkers from cell line screening data. *Briefings Bioinf* (2021) 22(6):bbab260. doi: 10.1093/bib/bbab260

16. Cheng J, Zhang Y, Wan R, Zhou J, Wu X, Fan Q, et al. CEMIP promotes osteosarcoma progression and metastasis through activating notch signaling pathway. *Front Oncol* (2022) 12:919108. doi: 10.3389/fonc.2022.919108

17. Lu C, Liu Y, Ali NM, Zhang B, Cui X. The role of innate immune cells in the tumor microenvironment and research progress in anti-tumor therapy. *Front Immunol* (2022) 13:1039260. doi: 10.3389/fimmu.2022.1039260

18. Liu Z, Zou H, Dang Q, Xu H, Liu L, Zhang Y, et al. Biological and pharmacological roles of m(6)A modifications in cancer drug resistance. *Mol Cancer* (2022) 21(1):220. doi: 10.1186/s12943-022-01680-z

19. Kayed H, Kleeff J, Keleg S, Felix K, Giese T, Berger MR, et al. Effects of bone sialoprotein on pancreatic cancer cell growth, invasion and metastasis. *Cancer Lett* (2007) 245(1-2):171–83. doi: 10.1016/j.canlet.2006.01.002

20. Tu Q, Zhang J, Fix A, Brewer E, Li YP, Zhang ZY, et al. Targeted overexpression of BSP in osteoclasts promotes bone metastasis of breast cancer cells. *J Cell Physiol* (2009) 218(1):135–45. doi: 10.1002/jcp.21576

21. Zhang L, Hou X, Lu S, Rao H, Hou J, Luo R, et al. Predictive significance of bone sialoprotein and osteopontin for bone metastases in resected Chinese non-small-cell lung cancer patients: a large cohort retrospective study. *Lung Cancer* (2010) 67(1):114–9. doi: 10.1016/j.lungcan.2009.03.017

22. Ogbureke KU, Nikitakis NG, Warburton G, Ord RA, Sauk JJ, Waller JL, et al. Up-regulation of SIBLING proteins and correlation with cognate MMP expression in oral cancer. *Oral Oncol* (2007) 43(9):920–32. doi: 10.1016/j.oraloncology.2006.11.011

23. Zhang JH, Tang J, Wang J, Ma W, Zheng W, Yoneda T, et al. Over-expression of bone sialoprotein enhances bone metastasis of human breast cancer cells in a mouse model. *Int J Oncol* (2003) 23(4):1043–8. doi: 10.3892/ijo.23.4.1043

24. Bouleftour W, Juignet L, Bouet G, Granito RN, Vanden-Bossche A, Laroche N, et al. The role of the SIBLING, bone sialoprotein in skeletal biology - contribution of mouse experimental genetics. *Matrix Biol* (2016) 52-54:60–77. doi: 10.1016/j.matbio.2015.12.011

25. Ludwig BS, Kessler H, Kossatz S, Reuning U. RGD-binding integrins revisited: how recently discovered functions and novel synthetic ligands (Re-)Shape an ever-evolving field. *Cancers* (2021) 13(7):1711. doi: 10.3390/cancers13071711

26. Pang X, He X, Qiu Z, Zhang H, Xie R, Liu Z, et al. Targeting integrin pathways: mechanisms and advances in therapy. *Signal transduction targeted Ther* (2023) 8(1):1. doi: 10.1038/s41392-022-01259-6

27. Gordon JA, Sodek J, Hunter GK, Goldberg HA. Bone sialoprotein stimulates focal adhesion-related signaling pathways: role in migration and survival of breast and prostate cancer cells. *J Cell Biochem* (2009) 107(6):1118–28. doi: 10.1002/jcb.22211

28. Zhang H, Zhao X, Wang J, Ji W. Development and validation of an immune-related signature for the prediction of recurrence risk of patients with laryngeal cancer. *Front Oncol* (2021) 11:683915. doi: 10.3389/fonc.2021.683915

29. Jiang Y, Zeng Z, Xiong S, Jiang M, Huang G, Zhang C, et al. New prognostic gene signature and immune escape mechanisms of bladder cancer. *Front Cell Dev Biol* (2022) 10:775417. doi: 10.3389/fcell.2022.775417

30. Ghochani Y, Muthukrishnan SD, Sohrabi A, Kawaguchi R, Condro MC, Bastola S, et al. A molecular interactome of the glioblastoma perivascular niche reveals integrin binding sialoprotein as a mediator of tumor cell migration. *Cell Rep* (2022) 41 (3):111511. doi: 10.1016/j.celrep.2022.111511

31. Soerjomataram I, Bray F. Planning for tomorrow: global cancer incidence and the role of prevention 2020-2070. *Nat Rev Clin Oncol* (2021) 18(10):663–72. doi: 10.1038/s41571-021-00514-z

32. Rais A, Husain A, Hasan GM, Hassan MI. A review on regulation of cell cycle by extracellular matrix. *Int J Biol macromol* (2023) 232:123426. doi: 10.1016/j.ijbiomac.2023.123426

33. Jiang Y, Zhang H, Wang J, Liu Y, Luo T, Hua H. Targeting extracellular matrix stiffness and mechanotransducers to improve cancer therapy. *J Hematol Oncol* (2022) 15(1):34. doi: 10.1186/s13045-022-01252-0

34. Bejarano L, Jordão MJC, Joyce JA. Therapeutic targeting of the tumor microenvironment. *Cancer discovery* (2021) 11(4):933–59. doi: 10.1158/2159-8290.CD-20-1808

35. Binnewies M, Roberts EW, Kersten K, Chan V, Fearon DF, Merad M, et al. Understanding the tumor immune microenvironment (TIME) for effective therapy. *Nat Med* (2018) 24(5):541–50. doi: 10.1038/s41591-018-0014-x

36. Liu M, Liu L, Song Y, Li W, Xu L. Targeting macrophages: a novel treatment strategy in solid tumors. *J Trans Med* (2022) 20(1):586. doi: 10.1186/s12967-022-03813-w

frontiers | Frontiers in Immunology

TYPE Original Research
PUBLISHED 29 June 2023
DOI 10.3389/fimmu.2023.1169144

OPEN ACCESS

EDITED BY
Eyad Elkord,
University of Salford, United Kingdom

REVIEWED BY
Reshmi Parameswaran,
Case Western Reserve University, United States
Said Dermime,
National Center for Cancer Care and Research, Qatar

*CORRESPONDENCE
Hong Zheng
hzheng@pennstatehealth.psu.edu

†These authors have contributed equally to this work

RECEIVED 18 February 2023
ACCEPTED 15 June 2023
PUBLISHED 29 June 2023

CITATION
Zhou H, Jia B, Annageldiyev C, Minagawa K, Zhao C, Mineishi S, Ehmann WC, Naik SG, Cioccio J, Wirk B, Songdej N, Rakszawski KL, Nickolich MS, Shen J and Zheng H (2023) CD26^{low}PD-1^{+} CD8 T cells are terminally exhausted and associated with leukemia progression in acute myeloid leukemia.
Front. Immunol. 14:1169144.
doi: 10.3389/fimmu.2023.1169144

CD26^{low}PD-1^{+} CD8 T cells are terminally exhausted and associated with leukemia progression in acute myeloid leukemia

Huarong Zhou[1,2†], Bei Jia[1†], Charyguly Annageldiyev[1], Kentaro Minagawa[1], Chenchen Zhao[1], Shin Mineishi[1], W Christopher Ehmann[1], Seema G. Naik[1], Joseph Cioccio[1], Baldeep Wirk[1], Natthapol Songdej[1], Kevin L. Rakszawski[1], Myles S. Nickolich[1], Jianzhen Shen[2] and Hong Zheng[1,3*]

[1]Penn State Cancer Institute, Penn State University College of Medicine, Hershey, PA, United States, [2]Fujian Institute of Hematology, Fujian Provincial Key Laboratory of Hematology, Fujian Medical University Union Hospital, Fujian Medical Center of Hematology, Fuzhou, China, [3]Department of Microbiology and Immunology, Penn State University College of Medicine, Hershey, PA, United States

Acute myeloid leukemia (AML) is a devastating blood cancer with poor prognosis. Novel effective treatment is an urgent unmet need. Immunotherapy targeting T cell exhaustion by blocking inhibitory pathways, such as PD-1, is promising in cancer treatment. However, results from clinical studies applying PD-1 blockade to AML patients are largely disappointing. AML is highly heterogeneous. Identification of additional immune regulatory pathways and defining predictive biomarkers for treatment response are crucial to optimize the strategy. CD26 is a marker of T cell activation and involved in multiple immune processes. Here, we performed comprehensive phenotypic and functional analyses on the blood samples collected from AML patients and discovered that CD26^{low}PD-1^{+} CD8 T cells were associated with AML progression. Specifically, the percentage of this cell fraction was significantly higher in patients with newly diagnosed AML compared to that in patients achieved completed remission or healthy controls. Our subsequent studies on CD26^{low}PD-1^{+} CD8 T cells from AML patients at initial diagnosis demonstrated that this cell population highly expressed inhibitory receptors and displayed impaired cytokine production, indicating an exhaustion status. Importantly, CD26^{low}PD-1^{+} CD8 T cells carried features of terminal exhaustion, manifested by higher frequency of T_{EMRA} differentiation, increased expression of transcription factors that are observed in terminally exhausted T cells, and high level of intracellular expression of granzyme B and perforin. Our findings suggest a prognostic and predictive value of CD26 in AML, providing pivotal information to optimize the immunotherapy for this devastating cancer.

KEYWORDS

AML, PD-1, CD26, t cell exhaustion, terminal exhaustion

Introduction

Acute myeloid leukemia (AML) is a devastating blood cancer with poor prognosis. Although treatment of AML has been significantly advanced recently with several novel targeting agents approved by FDA, five-year overall survival remains low at only 30.5% (1). Novel effective treatment is clearly an unmet need.

Multiple studies including ours have demonstrated the involvement of T cell exhaustion in AML pathogenesis (2–9). A recent study showed that T cell exhaustion may be a predominant process in AML at diagnosis and AML shaped CD8 T cell response *in vitro* (10). Up-regulation of PD-1 and other immune inhibitory pathways, the hallmark for T cell exhaustion, was found to be associated with AML progression (5). Importantly, PD-1 blockade enhanced T cell activity and reduced leukemia burden in mouse models of AML (6, 9). These observations suggest an important role of T cell exhaustion in AML. However, clinical studies applying PD-1 blockade to AML patients showed limited benefit (11–13). AML is highly heterogeneous. Identification of additional immune regulatory pathways and defining predictive biomarkers for treatment response are crucial to optimize treatment targeting T cell exhaustion and develop effective immunotherapy for AML.

CD26, also known as dipeptidyl peptidase 4 (DPP4), is a homodimeric type II transmembrane glycoprotein expressed on many cell types, including epithelial cells and immune components such as T cells, B cells, NK, and macrophages (14–18). CD26 is multifunctional and is involved in glucose homeostasis (19), stem cell homing (20), regulation of inflammatory diseases and multiple immune processes (21). CD26 is a marker for T cell activation. It acts as a costimulatory molecule enhancing interactions between antigen-presenting cells and T cells, subsequently initiating the signal transduction process and promoting T cell activation. Up-regulation of CD26 has been observed on both CD4 and CD8 T cells that are highly function in antiviral and anti-tumor response (22). However, the impact of T cell expression of CD26 on AML has not been studied. To fill this gap, we examined T cells of peripheral blood collected from a cohort of newly diagnosed AML patients (n=28). Subpopulations of T cells expressing different level of CD26 were further dissected for their phenotypic and functional status, as well as correlations with clinical outcome.

Materials and methods

Patient

Peripheral blood and bone marrow samples were collected from AML patients diagnosed per WHO criteria. All the patients were diagnosed at the Penn State Hershey Cancer Institute of Penn State University College of Medicine (Hershey, PA, USA). The study was approved by the Institutional Review Board of Penn State College of Medicine. Fully informed consent was obtained from all patients.

Isolation of PBMCs

Peripheral blood and bone marrow samples were collected from patients with newly diagnosed AML (n=28), AML patients in complete remission (n=15), and healthy donors (n=18). Peripheral blood mononuclear cells (PBMCs) and bone marrow mononuclear cells were isolated by density gradient centrifugation using Ficoll-Paque (Amersham Pharmacia Biotech, Stockholm, Sweden). Cells were preserved in fetal bovine serum containing 10% dimethyl sulfoxide (Gibco, Grand Island, NY, USA) and stored in liquid nitrogen.

Immunofluorescence staining and flow cytometry analysis

For surface staining, frozen PBMCs were thawed at 37°C and washed 2 times with phosphate-buffered saline containing 1% fetal bovine serum. Cells were incubated with Human BD Fc Block™ (10 minutes at room temperature) followed by staining with directly conjugated mAbs for 30 minutes at 4°C. Cells were then washed and resuspended in staining buffer before flow cytometry analysis. The monoclonal antibodies used were anti-human CD3-BV605, CD4-BV711, CD8-APC-H7, CD45RA-AF700, CD26-PE-CF594 or CD26-BV421, Ki67-AF488, Granzyme B-AF700, T-bet-PE, TCF-7/TCF-1-AF647, CD95-BV421, Annexin V-PE, hCD45-BV605 (BD Biosciences, San Diego, CA, USA), CCR7-BV421, PD-1-BV785, CD226-FITC, TIM-3-PE-Cy7, Perforin-APC (Biologend, San Diego, CA, USA), TIGIT-APC, Eomes-PE-eF610, TOX-PE, AITR/GITR-PE (invitrogen, Carlsbad, CA, USA) antibodies and corresponding isotype controls. Data were acquired using an LSR Fortessa flow cytometer (BD Biosciences) and analyzed with FlowJo software (Tree Star, Ashland, OR, USA).

In vitro stimulation and intracellular cytokine staining

PBMCs were cultured in RPMI-1640 medium (Gibco) containing 10% fetal bovine serum and stimulated with anti-CD3/CD28 (2 and 2.5 μg/mL) at the presence of Plus Golgiplug (BD Pharmingen, San Diego, CA, USA) for 5 hours. Cell viability was assessed using the Fixable viability dye eFluor™ 506 (invitrogen, Carlsbad, CA, USA). Cells were then surface stained with CD4-FITC, CD8-APC-H7, PD-1-BV785, and CD26-PE-CF594. After fixation and permeabilization, intracellular staining was performed with IL-2-PE-Cy7, TNF-α-BV421, IFN-γ-APC (BD Biosciences) antibodies.

Statistical analysis

All summary statistics (average values, s.d., s.e.m., significant differences between groups) were calculated using GraphPad Prism 9 (GraphPad Software Inc., San Diego, CA) or SPSS Statistics 26 as appropriate. For data distributed normally, the comparison of variables was performed using unpaired or paired Student t test. For data not distributed normally, the comparison of variables was performed with a Mann–Whitney U test or a Wilcoxon signedrank test for unpaired and paired data, respectively. Comparisons of

categorical patient characteristics were analyzed using Fisher exact test. The ROC curve was used to predict the reasonable grouping cutoff of low $CD26^{low}PD\text{-}1^{+}$ and high $CD26^{low}PD\text{-}1^{+}$ in newly diagnosed AML patients and healthy controls. The overall survival was analyzed by the log-rank (Mantel–Cox) test. For all analyses, a P value of < 0.05 was considered statistically significant.

Results

The proportion of $CD26^{low}PD\text{-}1^{+}$ CD8 T cells is significantly higher in blood of patients with untreated AML

Given its costimulatory function in T cell activation, we initially hypothesized that down-regulation of CD26 on T cells correlates with T cell hypofunction and subsequently AML progression. We performed flow cytometry analyses on PBMCs collected from AML patients at newly diagnosis (n=28) vs. that of healthy controls (n=18). The clinical characteristics of the AML patients are summarized in Table 1. Consistent with the heterogeneity of AML, there was wide variability in white blood cell (WBC) counts and blast percentages in the peripheral blood. The majority of patients carried intermediate or adverse cytogenetic features. Surprisingly, no significant differences in T cell expression of CD26 were observed (Supplemental Figure 1). However, when PD-1 was added to the analyses, in which $PD\text{-}1^{+}$ T cells were divided into 3 subsets based on the expression of CD26 (Figure 1A), we made striking observation that the frequency of $PD\text{-}1^{+}$ CD8 T cells expressing low level of CD26 ($CD26^{low}PD\text{-}1^{+}$) were significantly higher in newly diagnosed AML patients compared to that in healthy controls (31.45 ± 2.129% vs. 21.83 ± 2.541%, P=0.0062; Figures 1B, C). We further examined PBMCs from AML patients who have achieved complete remission (CR) after chemotherapy (n=15), and found that similar to healthy controls, $CD26^{low}PD\text{-}1^{+}$ CD8 T cells in these patients are significantly lower than that in newly diagnosed AML. In contrast, the frequency of CD8 T cells expressing intermediate level of CD26 ($CD26^{int}PD\text{-}1^{+}$) were lower in newly diagnosed AML compared to AML in CR or healthy controls (Figures 1B, C). Same analyses were performed on CD4 T cells and no significant differences were observed (Supplemental Figures 1, 2). These data suggest that $CD26^{low}PD\text{-}1^{+}$ CD8 T cells correlate with AML progression.

TABLE 1 Clinical feature of the AML patients.

Variable	Value
Age, y	
Median	63
Range	23-79
Gender, n (%)	
Male	10(36)
Female	18(64)
WBC, ×10^9/L	
Median	54.45
Range	3.6-361
PB blasts (%)	
Median	65
Range	12-94
Absolute blasts count, ×10^9/L	
Median	27.59
Range	0.71-315.88
Cytogenetics*, n (%)	
Favorable	2(7)
Intermediate	16(57)
Adverse	10(36)

WBC, white blood cell; PB, peripheral blood.
*Risk stratification is per '2022 ELN risk classification by genetics at initial diagnosis (23).

Terminally differentiated effector cells are significantly increased in $CD26^{low}PD\text{-}1^{+}$ CD8 T cells

We then focused our study on characteristic analyses of $CD26^{low}PD\text{-}1^{+}$ CD8 T cells. PBMCs from patients with newly diagnosed AML were examined. We first assessed the differentiation status of this cell population. Based on the expression of CD45RA and CCR7, T cells can be divided into four differentiation subsets (Figure 2A): naïve T cells (T_N, $CCR7^{+}CD45RA^{+}$), central memory T cells (T_{CM}, $CCR7^{+}CD45RA^{-}$), effector Memory T cells (T_{EM}, $CCR7^{-}CD45RA^{-}$) and terminally differentiated effector cells (T_{EMRA}, $CCR7^{-}CD45RA^{+}$). We performed multichannel flow cytometry analyses to dissect the distribution of all four differentiated subsets in $CD26^{low}PD\text{-}1^{+}$ CD8 T cells as well as the other two $PD\text{-}1^{+}$ CD8 T cell populations based on CD26 expression ($CD26^{int}PD\text{-}1^{+}$ and $CD26^{high}PD\text{-}1^{+}$). Consistent with the previous report that most $CD26^{int}$ T cells are naïve, we found a high frequency of naïve cells in $CD26^{int}PD\text{-}1^{+}$ CD8 T cells from our AML patients. In contrast, both $CD26^{low}PD\text{-}1^{+}$ and $CD26^{high}PD\text{-}1^{+}$ CD8 T cells are antigen experienced. Importantly, we observed a significantly higher frequency of T_{EMRA} cells in $CD26^{low}PD\text{-}1^{+}$ than $CD26^{high}PD\text{-}1^{+}$ CD8 T cells (48.74% vs. 22.28%, P<0.0001; Figures 2B, C). T_{EMRA} is considered to be a terminal effector cells with limited function. This data suggests an association of $CD26^{low}PD\text{-}1^{+}$ CD8 T cells with T cell dysfunction and AML pathogenesis.

Expression of inhibitory receptors is increased on $CD26^{low}PD\text{-}1^{+}$ CD8 T cells

We next examined the impact of CD26 expression on the inhibitory and stimulatory pathways in $PD\text{-}1^{+}$ CD8 T cells. To rule out potential confounding effect of Naïve T cells, we excluded Naïve-dominant $CD26^{int}PD\text{-}1^{+}$ CD8 T cells and focused our subsequent analyses on antigen experienced cells including $CD26^{low}PD\text{-}1^{+}$ and

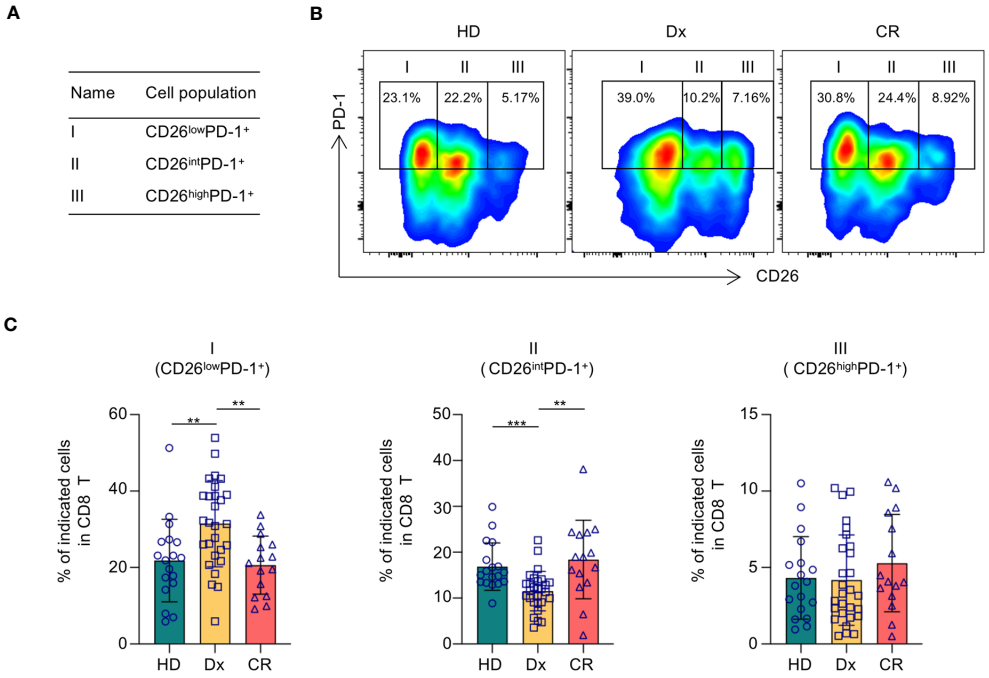

FIGURE 1
CD26^{low}PD-1^{+} CD8 T cells are significantly increased in AML patients at newly diagnosis. PBMCs collected from healthy donors, AML patients at newly diagnosis and in complete remission were assessed for CD26 and PD-1 expression on CD8 T cells by flow cytometry. **(A)** Based on the levels of CD26 and PD-1 expression, CD8 T cells are divided into three fractions. Shown is the schema of each fraction. **(B)** Representative flow data from healthy donors (HD), AML patient at newly diagnosis (Dx) and in complete remission (CR) displaying the percentage of CD26^{low}PD-1^{+}(fraction I), CD26^{int}PD-1^{+} (fraction II), CD26^{high}PD-1^{+} (fraction III) among CD8 T cells. **(C)** The frequencies of each fraction among CD8 cells in HD(n=18), AML patients at initial diagnosis (Dx, n=28) and AML patients in complete remission (CR, n=15). Each spot represents data of an individual patient or healthy donor. *P* values were obtained by unpaired Student t-test or Mann-Whitney test. ***P*<0.01, ****P*<0.001.

CD26^{high}PD-1^{+} CD8 T cells. When surface expression of a number of inhibitory receptors on these two cell populations was compared, we observed significantly higher expression of TIGIT and TIM-3 on CD26^{low}PD-1^{+} CD8 T cells, compared with that of CD26^{high}PD-1^{+} CD8 T cells (TIGIT: 46.09% vs. 5.71%, *P*<0.0001; TIM-3: 2.28% vs. 0.34%, *P*=0.0001; Figures 3A, B). In contrast, expression of the stimulatory receptor CD226 (counterpart of TIGIT) was significantly lower on CD26^{low}PD-1^{+} CD8 T cells (34.4% vs. 65.3%, *P*<0.0001, Figure 3C). Up-regulation of inhibitory receptors is a hallmark of T cell exhaustion. Our finding indicates that CD26^{low}PD-1^{+} CD8 T cells are likely in a more advanced exhaustive status, compared with CD26^{high}PD-1^{+} CD8 T cells.

CD26^{low}PD-1^{+} CD8 T cells express higher level of exhaustion related transcription factors

We further assessed the expression pattern of transcription factors in CD26^{low}PD-1^{+} CD8 T cells. Studies in models of chronic viral infection have demonstrated that several transcription factors including Eomes, T-bet, TOX, and TCF1 are important in regulating T cell exhaustion. We compared the intracellular expression of these transcription factors in CD26^{low}PD-1^{+} CD8 T cells to that in CD26^{high}PD-1^{+} CD8 T cells. As shown in Figure 4A, we observed a higher percentage of TOX expression in CD26^{low}PD-1^{+} CD8 T cells (79.77% vs. 64.55%, *P*<0.0001). In contrast, expression of TCF1 in CD26^{low}PD-1^{+} CD8 T cells was significantly lower (16.73% vs. 24.06%, *P*=0.0023, Figure 4B). When expression of Eomes and T-bet was assessed, we focused our analyses on the Eomes^{+}T-bet^{low} subset as our previous work showed that this subset was associated with poor clinical outcome in AML patients (4). As shown in Figure 4C, we observed a higher percentage of Eomes^{+}T-bet^{low} cells in CD26^{low}PD-1^{+} CD8 T cells, compared to that in CD26^{high}PD-1^{+} CD8 T cells (23.64% vs. 18.18%, *P*=0.0233). Collectively, we found that CD26^{low}PD-1^{+} CD8 T cells from untreated AML patients express higher level of TOX and Eomes, whereas lower level of TCF1. This transcription pattern is more consistent with terminal exhaustion.

CD26^{low}PD-1^{+} CD8 T cells exhibit functional defects

To assess the functional status of CD26^{low}PD-1^{+} CD8 T cells, we performed an *in vitro* assay to examine intracellular cytokine productions by CD8 T cells upon anti-CD3 and anti-CD28 stimulation. PBMCs from untreated AML patients were used in this study. CD8 T cells were gated by CD26^{low}PD-1^{+} vs. CD26^{high}PD1^{+} and intracellular production of IFN-γ, IL-2, and TNF-α by each cell subpopulation was assessed by flow cytometry analyses. As shown in Figures 5A–C, the CD26^{low}PD-1^{+} CD8 T cells had significantly lower production of IFN-γ, IL-2, and TNF-α compared with CD26^{high}PD-1^{+} CD8 T cells (IFN-γ:13.51% vs.

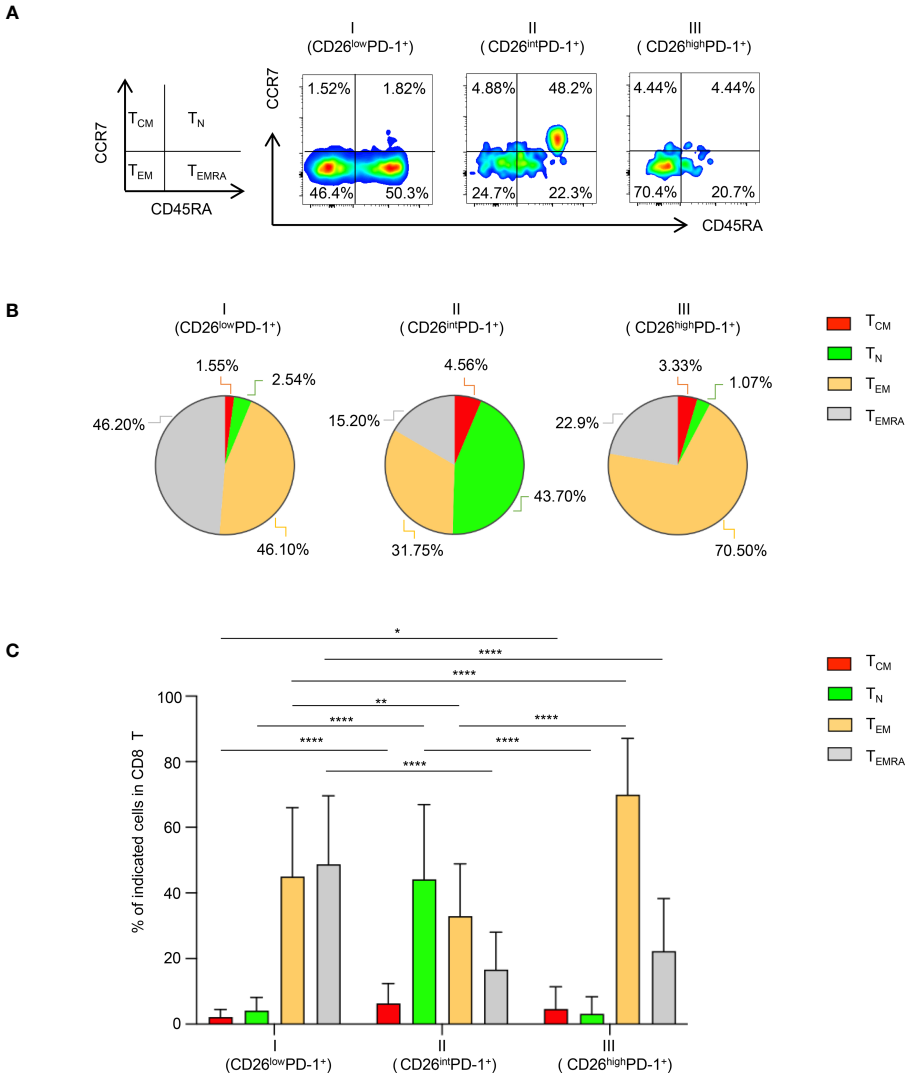

FIGURE 2
Terminally differentiated effector cells are significantly increased in CD26^{low}PD-1^{+} CD8 T cells. Flow cytometry analysis of surface expression of PD-1, CD26, CD45RA, CCR7 was performed on PBMCs collected from AML patients at initial diagnosis. **(A)** The gating strategy of Naïve (T_N), central memory (T_{CM}), effector memory (T_{EM}) and terminal differentiated cells (T_{EMRA}) in CD8 T cells was shown on the left. The representative flow images on the right show the distribution of the above subsets in CD26^{low}PD-1^{+} (fraction I), CD26^{int}PD-1^{+} (fraction II) and CD26^{high}PD-1^{+} (fraction III) in CD8 T **(B)** The pie chart depicts the distribution of T_N, T_{CM}, T_{EM} and T_{EMRA} in CD26^{low}PD-1^{+} (fraction I), CD26^{int}PD-1^{+} (fraction II) and CD26^{high}PD-1^{+} (fraction III) CD8 T cells. **(C)** Summary data for the distribution of naïve vs. memory in the three fractions of CD8 T cells. *P* values were obtained by paired Student t-test or Wilcoxon signed rank test. *P<0.05, **P<0.01, ****P<0.0001.

21.17%, P=0.003; IL-2:2.69% vs. 18.63%, P<0.0001; TNF-α: 5.27% vs. 8.05%, P=0.0163). We also evaluated the intracellular expression of Granzyme B and perforin in each cell subpopulation as an indication of killing capacity. Interestingly, we found a significantly increased level of Granzyme B and perforin in CD26^{low}PD-1^{+} CD8 T cells compared to that in CD26^{high}PD-1^{+} CD8 T cells (Figures 5D, E). The discrepancy between cytokine production and Granzyme B/perforin expression in the functional status of exhausted T cells has been observed in multiple studies (3, 24–27). It is suspected that terminally exhausted T cells may lose energy to secret Granzyme B/perforin, leading to the intracellular accumulation of these molecules (28, 29). Collectively, our data demonstrate that CD26^{low}PD-1^{+} CD8 T cells are functionally impaired demonstrated by reduced cytokine production, consistent with the status of exhaustion. In addition, they displayed higher intracellular expression of Granzyme B/perforin, suggesting a terminal exhausted status.

Discussion

In this study, we performed comprehensive phenotypic and functional analyses on the T cells of PBMCs collected from AML patients and healthy controls. We focused our study on the impact

10.3389/fimmu.2023.1169144

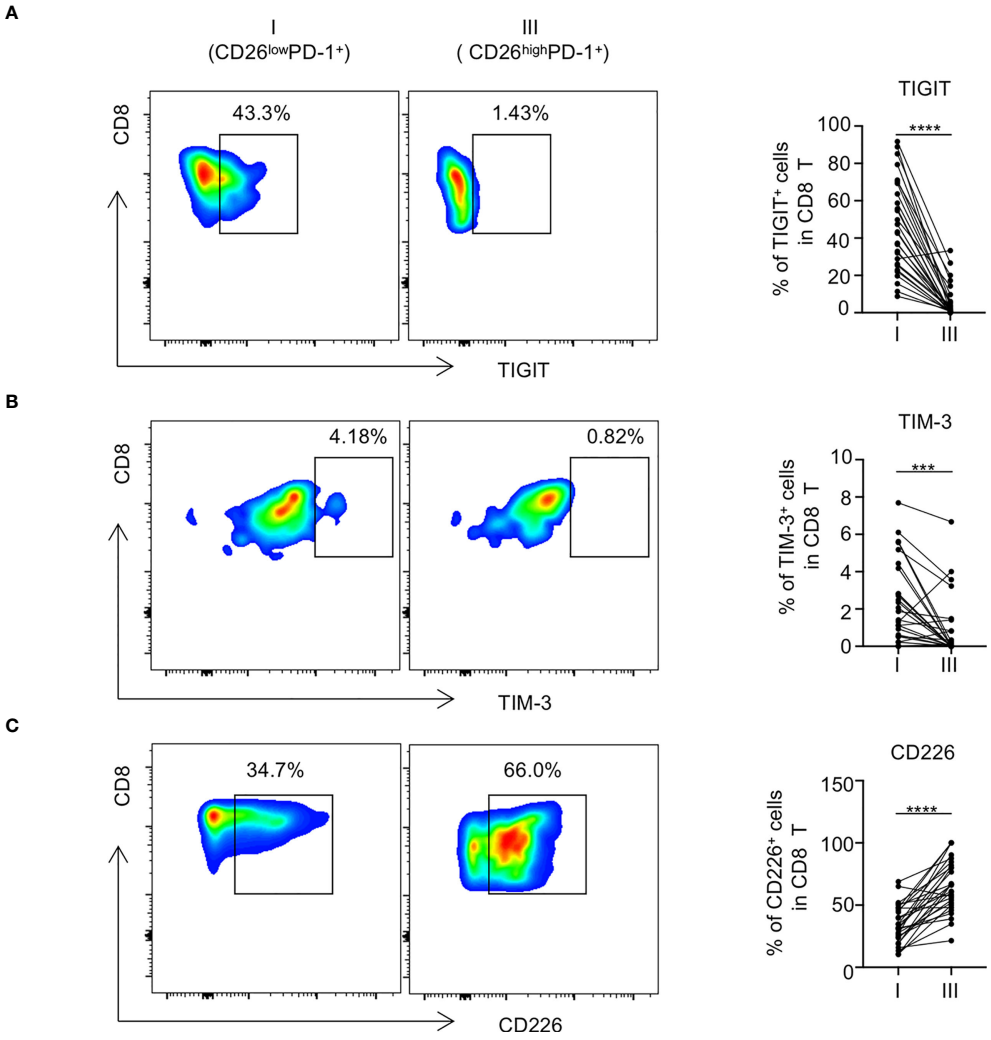

FIGURE 3
The expression of inhibitory receptors in CD26^{low}PD-1^{+} CD8 T cells in newly diagnosed AML patients was increased. PBMCs from AML patients at initial diagnosis were examined by flow cytometry(n=28). The expression of TIGIT [shown in **(A)**], TIM-3 [shown in **(B)**] and CD226 [shown in **(C)**] on CD8 T cell subpopulations [CD26^{low}PD-1^{+}(fraction I) and CD26^{high}PD-1^{+} (fraction III)] was assessed. **(A–C)** Shown are the representative flow data (left) and summary plots (right). P values were obtained by paired Student t-test or Wilcoxon signed rank test. ***P<0.001, ****P<0.0001.

of CD26 expression on T cells and discovered that CD26^{low}PD-1^{+} CD8 T cells were associated with AML progression. Specifically, the percentage of this cell fraction was significantly higher in patients with newly diagnosed AML (high leukemia burden) compared to that in patients who achieved CR (no leukemia) or healthy controls. Our subsequent studies on CD26^{low}PD-1^{+} CD8 T cells from newly diagnosed AML patients demonstrated that this cell population carries features of T cell exhaustion, manifested by higher frequency of T_{EMRA} differentiation, increased expression of inhibitory receptors and exhaustion-related transcription factors, and functional defects. To our knowledge, this is the first report to uncover the important role of CD26 expression on CD8 T cells in AML.

Increased expression of PD-1 is an essential marker for T cell exhaustion. Multiple studies including ours have demonstrated an up-regulation of PD-1 on T cells from AML patients who have disease relapse (2, 5, 8, 30–33). However, T cell expression of PD-1 was not increased in AML patients at initial diagnosis (32). It may be attributed to the heterogeneity of PD-1^{+} T cells at this particular disease status, thus PD-1 alone is inadequate to distinguish exhausted T cells from T cells of other functional status. In fact, elegant studies of mouse models of chronic viral infection have shown a higher frequency of PD-1^{+} CD8 T cells at activation phase short after viral infection as well as in the exhaustion status later in the chronic phase (34–36). It is possible that PD-1^{+} T cells in newly diagnosed AML patients are diverse in their functional status. In our current study, we further dissected PD-1^{+} CD8 T cells into three subpopulations based on their expression of CD26. We made novel findings that CD26^{low}PD-1^{+} CD8 T cells were phenotypically and functionally consistent with exhaustion status. Importantly, the frequency of CD26^{low}PD-1^{+} CD8 T cells was significantly higher in newly diagnosed AML patients compared to that in healthy controls or AML patients in CR. Therefore, two-dimensional analysis testing both CD26 and PD-1 on CD8 T cells provides an

10.3389/fimmu.2023.1169144

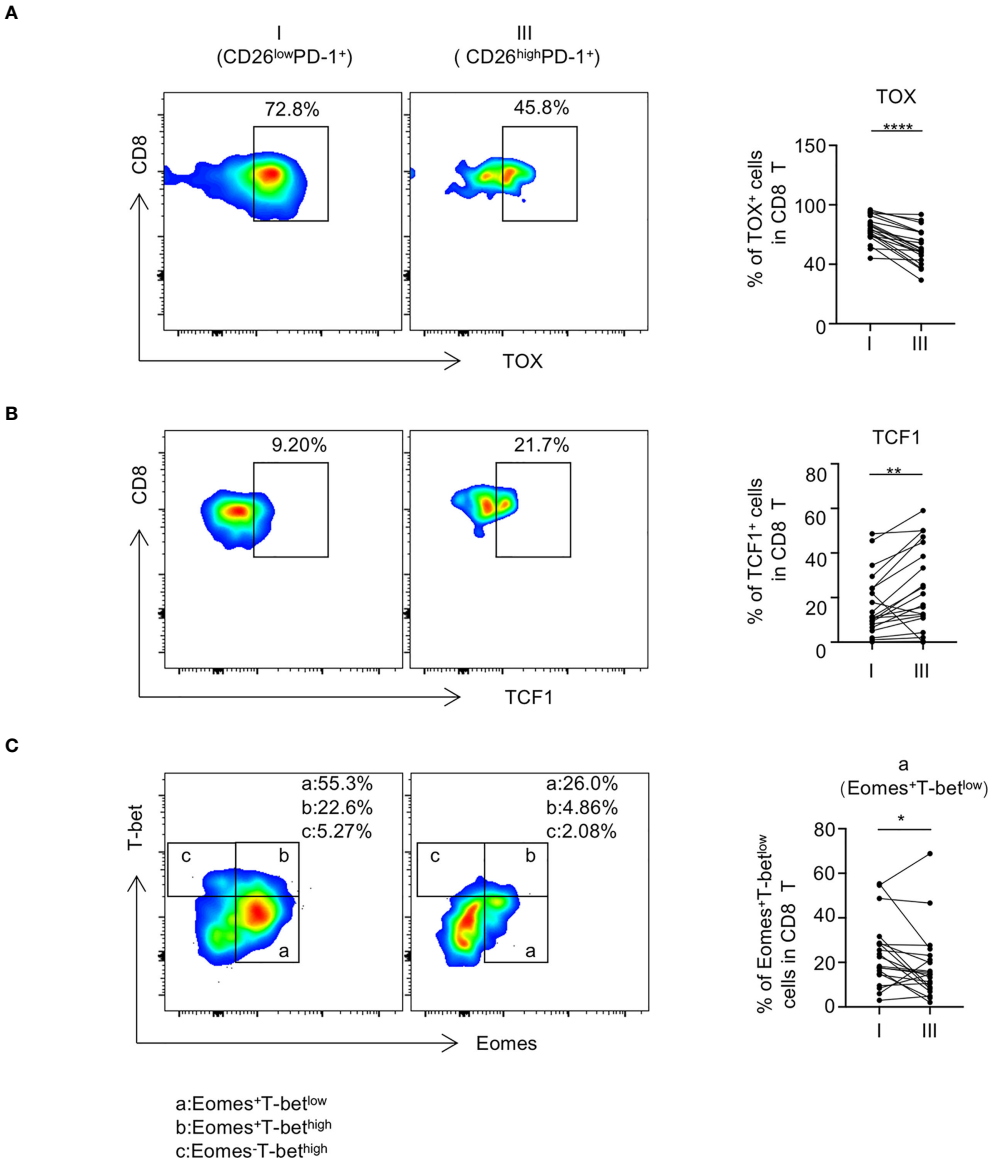

FIGURE 4
CD26^{low}PD-1^{+} CD8 T cells express higher level of exhaustion-related transcription factors. PBMCs collected from AML patients at initial diagnosis were assessed by flow cytometry (n=20). The expression of TOX [shown in **(A)**], TCF1 [shown in **(B)**] Eomes and T-bet [shown in **(C)**] on CD8 T cell subpopulations [CD26^{low}PD-1^{+} (fraction I) and CD26^{high}PD-1^{+} (fraction III)] was analyzed by flow cytometry. Upon the expression of Eomes and T-bet, CD8 T cells were divided into subsets of Eomes^{+}T-bet^{low}(a), Eomes^{+}T-bet^{high} (b) and Eomes^{-}T-bet^{high} (c), **(A–C)** Flow cytometry representative data were shown on the left and summary plots were shown on the right. *P* values were obtained by paired Student t-test or Wilcoxon signed rank test. *$P<0.05$, **$P<0.01$, ****$P<0.0001$.

optimal strategy to identify exhaustion T cells in newly diagnosed AML. With a hypothesis that higher frequency of exhausted T cells leads to poor prognosis due to compromised anti-leukemia immune response, we performed analyses on the data of newly diagnosed AML patients to determine the impact of CD26^{low}PD-1^{+} CD8 T cells on clinical outcome. Twenty-one AML patients whose overall survival (OS) were evaluable (medium follow-up time:1744 days) were divided into two groups based on their CD8 T cells expression level of CD26^{low}PD-1^{+}. We observed that patients with high percentage of CD26^{low}PD-1^{+} CD8 T cells displayed a trend of lower OS compared to that of low percentage subgroup (median: 372 vs. 1369 days; P=0.231; Supplemental Figure 3). No statistical significance was achieved likely due to limited sample size. Further studies in larger cohorts of patients are warranted to make a conclusion. If validated, CD26^{low}PD-1^{+} CD8 T cells could be a prognostic biomarker for newly diagnosed AML.

TOX has been considered as an essential transcription factor governing terminally exhausted T cells, whereas TCF1 is more functional in progenitor exhausted T cells (37–41). Our finding that CD26^{low}PD-1^{+} CD8 T cells expressed higher TOX and lower TCF1 suggests that these cells are more toward terminal exhaustion. Consistently, we observed that CD26^{low}PD-1^{+} CD8 T cells

10.3389/fimmu.2023.1169144

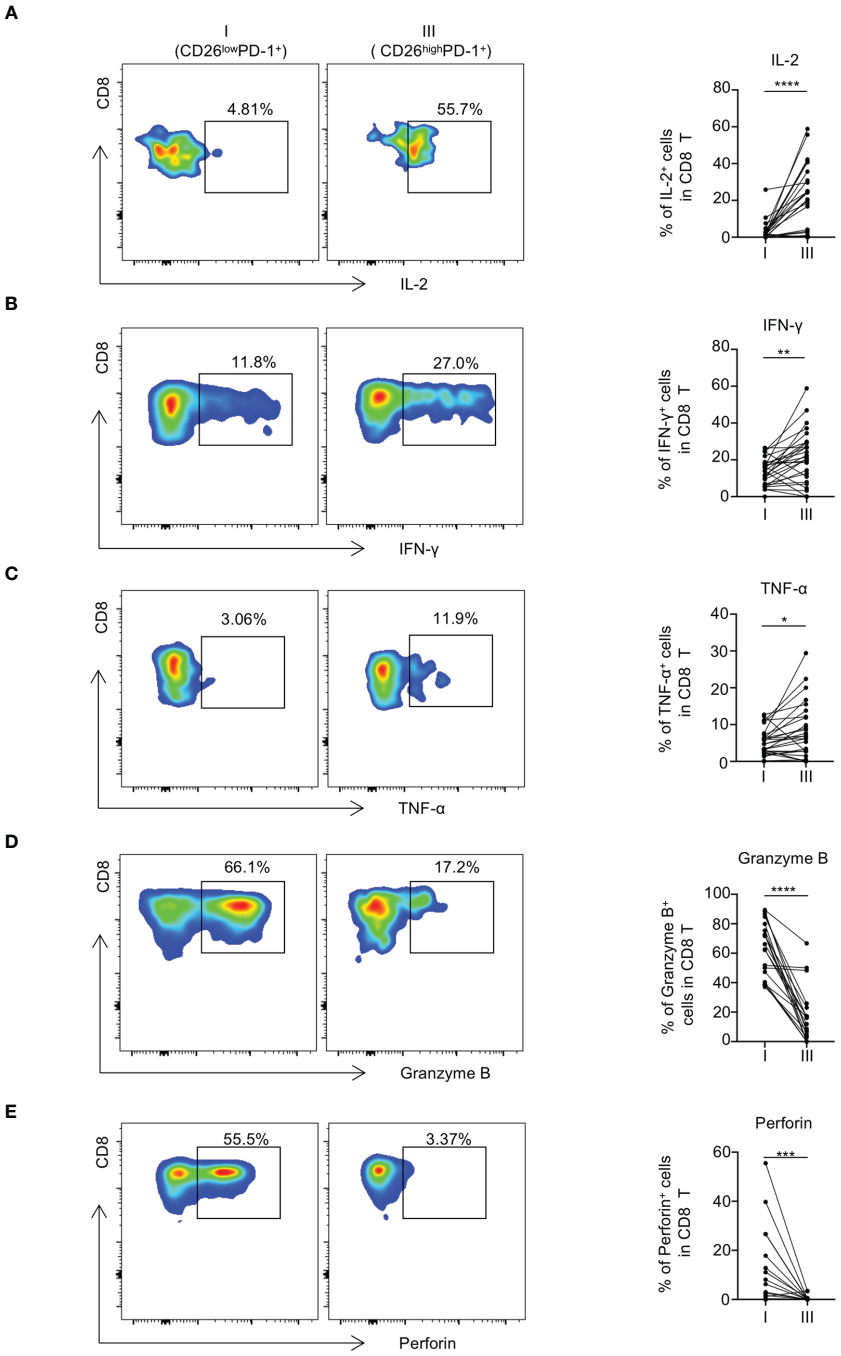

FIGURE 5
CD26^{low}PD-1^{+} CD8 T cells produce less cytokines and display decreased cytotoxic capacity in AML patients at initial diagnosis. **(A–C)** PBMCs collected from AML patients at initial diagnosis were stimulated *in vitro* with anti-CD3 and anti-CD28 before intracellular staining of IL-2, IFN-γ and TNF-α (n=28). Flow cytometry representative data (left) and summary plots (right) show the expressions of IL-2 **(A)**, IFN-γ **(B)** and TNF-α **(C)** in indicated CD8 subpopulations (CD26^{low}PD-1^{+} (fraction I) and CD26^{high}PD-1^{+} (fraction III)). **(D, E)** The expression of Granzyme B and perforin in each CD8 subpopulation. Representative data (left) and summary graphs (right) are shown. *P* values were obtained by paired Student t-test or Wilcoxon signed rank test. **P*<0.05, ***P*<0.01, ****P*<0.001, ****<0.0001.

contain higher frequency of Eomes^{+}T-bet^{low} cells, a pattern that is observed in terminal exhaustion. Furthermore, whereas being functionally impaired, evident by less cytokine production capacity, CD26^{low}PD-1^{+} CD8 T cells express more granzyme B and perforin, another feature of terminal exhausted CD8 T cells. Taking together, our data support the notion that CD26^{low}PD-1^{+} CD8 T cells in newly diagnosed AML represent a terminally exhausted T cell population. This finding has significant clinical impact. Multiple studies in preclinical models have demonstrated that reversing T cell exhaustion by PD-1 inhibition effectively

reduces leukemia burden (6, 9); however, results from clinical studies applying PD-1 blockade to AML patients are largely negative (11–13). An important strategy to improve treatments targeting T cell exhaustion is to define predictive biomarkers to identify patients who are likely to respond to the treatment. It becomes clear that terminally exhausted T cells have minimal response to PD-1 blockade, a main mechanism for resistance to checkpoint inhibitors (25, 35). Our novel finding that $CD26^{low}PD\text{-}1^{+}$ CD8 T cells are terminally exhausted is compelling: high frequency of this cell population in newly diagnosed AML may lead to poor response to PD-1-targeting agents. Therefore, optimizing clinical trial design by selecting patients with low percentage of $CD26^{low}PD\text{-}1^{+}$ CD8 T cells has a strong potential to improve efficacy of treatment with PD-1 blockade.

In contrast to $CD26^{low}PD\text{-}1^{+}$ CD8 T cells, we observed that $CD26^{high}PD\text{-}1^{+}$ CD8 T cells are highly functional evident by predominant differentiation stage of T_{EM} and potent cytokine release upon *in vitro* stimulation with anti-CD3/CD28. This is in line with the findings of Bailey et al. that $CD26^{high}$ CD4 T cells showed strong anti-tumor activity when transferred into mouse models of solid tumors (22). Given the fact that CD26 has a costimulatory function in activating T cells, sitagliptin, a CD26/DPP4 inhibitor, was applied to patients undergoing allogeneic stem cell transplantation as graft vs. host disease (GVHD) prophylaxis in a phase 2 clinical trial (42). Low incidence of grade II to IV acute GVHD was observed. A major concern is a decrease of graft vs. leukemia (GVL) effect due to CD26 inhibition. Encouragingly, one-year relapse rate was comparable with historical controls, indicating a preservation of GVL. However, longer follow-up and randomized studies are needed to draw a conclusion. It has been reported that CD26 is overexpressed on tumor cells and promotes metastasis of solid tumors (43–46). Several CD26 inhibitors have been tested for their direct cytotoxic effect against tumors in preclinical models (47–49). Although promising results were observed in some studies, most data were inconclusive or negative. It is possible that systemic treatment with CD26 inhibitors significantly suppresses T cell function and compromises the anti-tumor effect. Combining approaches of regaining T cell activity while inhibiting CD26 would be helpful to circumvent this obstacle. Further investigation of the mechanisms by which CD26 mediates T cell response is essential to identify such therapeutic targets.

Of note, we also examined the differentiation status (T_N, T_{CM}, T_{EM} and T_{EMRA}) in subsets of $CD26^{low}PD\text{-}1^{+}$, $CD26^{int}PD\text{-}1^{+}$ and $CD26^{high}PD\text{-}1^{+}$ CD8 T cells in healthy donor (HD) and CR groups. We observed that the differentiation status of each subset among HD and CR samples was similar to that in newly diagnosed samples (Dx) (Supplemental Figures 4A, B; Figure 2). In addition, expression patterns of TIGIT and CD226 in each subset among HD and CR samples was also similar to that in Dx samples (Supplemental Figures 4C, D). These observations indicate that each subset ($CD26^{low}PD\text{-}1^{+}$, $CD26^{int}PD\text{-}1^{+}$ or $CD26^{high}PD\text{-}1^{+}$ CD8 T cells) carries a unique feature that is not altered in different clinical settings (HD, Dx, or CR). Instead, the change in frequencies of the subsets reflects the disease specificity, thus we observed significantly increased frequency of $CD26^{low}PD\text{-}1^{+}$ CD8 T cells in Dx samples, compared to that in HD and CR (Figure 1).

It is unclear how $CD26^{low}PD1^{+}$ CD8 T cells are increased in AML progression. We examined the apoptosis of $CD26^{low}PD\text{-}1^{+}$ vs. $CD26^{high}PD\text{-}1^{+}$ CD8 T cells by evaluating the expression of CD95 and Annexin V. We observed no significant differences between the two subsets (Supplemental Figures 5A, B. In addition, when proliferation was assessed by evaluating the expression of Ki-67, no significant difference was observed either (Supplemental Figure 5C). Therefore the increased frequency of $CD26^{low}PD\text{-}1^{+}$ CD8 T cells in AML progression is unlikely due to increased apoptosis of $CD26^{high}$ T cells or altered proliferation in each subset. We further assessed the frequency of $CD26^{low}PD\text{-}1^{+}$, $CD26^{int}PD\text{-}1^{+}$ and $CD26^{high}PD\text{-}1^{+}$ CD8 T cells in the bone marrow of newly diagnosed AML patients, and observed that the percentage of each subset was comparable to peripheral blood (n=5, Supplemental Figure 6). So the increase of $CD26^{low}PD\text{-}1^{+}$ CD8 T cells is unlikely due to migration between blood and bone marrow. As the increase of $CD26^{low}PD\text{-}1^{+}$ T cells is associated with a decrease in $CD26^{int}PD\text{-}1^{+}$ T cells (Figure 1C), we suspect that differentiation of naïve $CD26^{int}PD\text{-}1^{+}$ T cells upon AML stimulation may be contributing. Our observation is different from the findings of Bozorgmehr et al, in which apoptosis of $CD26^{high}$ T cells is increased in CLL (50). The discrepancy is liked due to different disease context. This highlights the heterogeneity of T cell responses and importance of disease context-specific studies.

In summary, we made novel observations that $CD26^{low}PD\text{-}1^{+}$ CD8 T cells are increased in newly diagnosed AML patients, and their phenotypic and functional features are consistent with terminal exhaustion status. These findings suggest a prognostic and predictive value of CD26 in AML, providing pivotal information to optimize the immunotherapy for this devastating cancer.

Data availability statement

The raw data supporting the conclusions of this article will be made available by the authors, without undue reservation.

Ethics statement

The studies involving human participants were reviewed and approved by Penn State Hershey Medical Center. The patients/participants provided their written informed consent to participate in this study.

Author contributions

HuZ and BJ designed the experiments, performed the research, analyzed the results and wrote the manuscript. CA and CZ performed the research and analyzed the results. KM, SM, WE,

SM, JC, BW, NS, KR, and MN acquired samples, managed patients and discussed the data. JS discussed the data and reviewed the manuscript. HoZ conceived the concept, designed the experiments, oversaw the interpretation and presentation of the data, and wrote the manuscript. All authors contributed to the article and approved the submitted version.

Funding

This work was supported by the Penn State University Enhancing Health Initiative, the Kiesendahl Endowment funding, an Philanthropic Donation to our cancer research, and a Philanthropic Donation from Alan and Li Hao Colberg to our cancer research.

Acknowledgments

We thank all our patients for their trust, understanding, and willingness to provide their blood and bone marrow samples for our research.

Conflict of interest

The authors declare that the research was conducted in the absence of any commercial or financial relationships that could be construed as a potential conflict of interest.

Publisher's note

Supplementary material

The Supplementary Material for this article can be found online at: https://www.frontiersin.org/articles/10.3389/fimmu.2023.1169144/full#supplementary-material

References

1. National Cancer Institute Surveillance, Epidemiology, and End Results Program. *Cancer stat facts: leukemia-acute myeloid leukemia (AML)* (2022). Available at: https://seer.cancer.gov/statfacts/html/amyl.html (Accessed 5 January 2022).

2. Kong Y, Zhang J, Claxton DF, Ehmann WC, Rybka WB, Zhu L, et al. PD-1(hi) TIM-3(+) T cells associate with and predict leukemia relapse in AML patients post allogeneic stem cell transplantation. *Blood Cancer J* (2015) 5(7):e330. doi: 10.1038/bcj.2015.58

3. Kong Y, Zhu L, Schell TD, Zhang J, Claxton DF, Ehmann WC, et al. Zheng, h. T-cell immunoglobulin and ITIM domain (TIGIT) associates with CD8+ T-cell exhaustion and poor clinical outcome in AML patients. *Clin Cancer Res* (2016) 22 (12):3057–66. doi: 10.1158/1078-0432.CCR-15-2626

4. Jia B, Zhao C, Rakszawski KL, Claxton DF, Ehmann WC, Rybka WB, et al. Eomes (+)T-bet(low) CD8(+) T cells are functionally impaired and are associated with poor clinical outcome in patients with acute myeloid leukemia. *Cancer Res* (2019) 79 (7):1635–45. doi: 10.1158/0008-5472.Can-18-3107

5. Noviello M, Manfredi F, Ruggiero E, Perini T, Oliveira G, Cortesi F, et al. Bone marrow central memory and memory stem T-cell exhaustion in AML patients relapsing after HSCT. *Nat Commun* (2019) 10(1):1065. doi: 10.1038/s41467-019-08871-1

6. Zhou Q, Munger ME, Highfill SL, Tolar J, Weigel BJ, Riddle M, et al. Program death-1 signaling and regulatory T cells collaborate to resist the function of adoptively transferred cytotoxic T lymphocytes in advanced acute myeloid leukemia. *Blood* (2010) 116(14):2484–93. doi: 10.1182/blood-2010-03-275446

7. Mumprecht S, Schurch C, Schwaller J, Solenthaler M, Ochsenbein AF. Programmed death 1 signaling on chronic myeloid leukemia-specific T cells results in T-cell exhaustion and disease progression. *Blood* (2009) 114(8):1528–36. doi: 10.1182/blood-2008-09-179697

8. Norde WJ, Maas F, Hobo W, Korman A, Quigley M, Kester MG, et al. PD-1/PD-L1 interactions contribute to functional T-cell impairment in patients who relapse with cancer after allogeneic stem cell transplantation. *Cancer Res* (2011) 71(15):5111–22. doi: 10.1158/0008-5472.CAN-11-0108

9. Zhou Q, Munger ME, Veenstra RG, Weigel BJ, Hirashima M, Munn DH, et al. Coexpression of Tim-3 and PD-1 identifies a CD8+ T-cell exhaustion phenotype in mice with disseminated acute myelogenous leukemia. *Blood* (2011) 117(17):4501–10. doi: 10.1182/blood-2010-10-310425

10. Knaus HA, Berglund S, Hackl H, Blackford AL, Zeidner JF, Montiel-Esparza R, et al. Signatures of CD8+ T cell dysfunction in AML patients and their reversibility with response to chemotherapy. *JCI Insight* (2018) 3(21):e120974. doi: 10.1172/jci.insight.120974

11. Liu H. Emerging agents and regimens for AML. *J Hematol Oncol* (2021) 14 (1):49. doi: 10.1186/s13045-021-01062-w

12. Zeidan AM, Boss I, Beach CL, Copeland WB, Thompson E, Fox BA, et al. A randomized phase 2 trial of azacitidine with or without durvalumab as first-line therapy for older patients with AML. *Blood Adv* (2022) 6(7):2219–29. doi: 10.1182/bloodadvances.2021006138

13. Zheng H, Mineishi S, Claxton D, Zhu J, Zhao C, Jia B, et al. A phase I clinical trial of avelumab in combination with decitabine as first line treatment of unfit patients with acute myeloid leukemia. *Am J Hematol* (2021) 96(2):E46–e50. doi: 10.1002/ajh.26043

14. Gorrell MD, Gysbers V, McCaughan GW. CD26: a multifunctional integral membrane and secreted protein of activated lymphocytes. *Scandinavian J Immunol* (2001) 54(3):249–64. doi: 10.1046/j.1365-3083.2001.00984.x

15. Lambeir AM, Durinx C, Scharpé S, De Meester I. Dipeptidyl-peptidase IV from bench to bedside: an update on structural properties, functions, and clinical aspects of the enzyme DPP IV. *Crit Rev Clin Lab Sci* (2003) 40(3):209–94. doi: 10.1080/713609354

16. Thul PJ, Åkesson L, Wiking M, Mahdessian D, Geladaki A, Ait Blal H, et al. A subcellular map of the human proteome. *Science* (2017) 356(6340):eaal3321. doi: 10.1126/science.aal3321

17. Uhlén M, Fagerberg L, Hallström BM, Lindskog C, Oksvold P, Mardinoglu A, et al. Proteomics. tissue-based map of the human proteome. *Science* (2015) 347 (6220):1260419. doi: 10.1126/science.1260419

18. Waumans Y, Baerts L, Kehoe K, Lambeir AM, De Meester I. The dipeptidyl peptidase family, prolyl oligopeptidase, and prolyl carboxypeptidase in the immune system and inflammatory disease, including atherosclerosis. *Front Immunol* (2015) 6:387. doi: 10.3389/fimmu.2015.00387

19. Gerich J. Pathogenesis and management of postprandial hyperglycemia: role of incretin-based therapies. *Int J Gen Med* (2013) 6:877–95. doi: 10.2147/ijgm.S51665

20. Broxmeyer HE, Hoggatt J, O'Leary HA, Mantel C, Chitteti BR, Cooper S, et al. Dipeptidylpeptidase 4 negatively regulates colony-stimulating factor activity and stress hematopoiesis. *Nat Med* (2012) 18(12):1786–96. doi: 10.1038/nm.2991

21. Hatano R, Ohnuma K, Yamamoto J, Dang NH, Morimoto C. CD26-mediated co-stimulation in human CD8(+) T cells provokes effector function via pro-inflammatory cytokine production. *Immunology* (2013) 138(2):165–72. doi: 10.1111/imm.12028

22. Bailey SR, Nelson MH, Majchrzak K, Bowers JS, Wyatt MM, Smith AS, et al. Human CD26high T cells elicit tumor immunity against multiple malignancies via enhanced migration and persistence. *Nat Commun* (2017) 8(1):1961. doi: 10.1038/s41467-017-01867-9

23. Dohner H, Wei AH, Appelbaum FR, Craddock C, DiNardo CD, Dombret H, et al. Diagnosis and management of AML in adults: 2022 recommendations from an international expert panel on behalf of the ELN. *Blood* (2022) 140(12):1345–77. doi: 10.1182/blood.2022016867

24. Im SJ, Hashimoto M, Gerner MY, Lee J, Kissick HT, Burger MC, et al. Defining CD8+ T cells that provide the proliferative burst after PD-1 therapy. *Nature* (2016) 537 (7620):417–21. doi: 10.1038/nature19330

25. Paley MA, Kroy DC, Odorizzi PM, Johnnidis JB, Dolfi DV, Barnett BE, et al. Progenitor and terminal subsets of CD8+ T cells cooperate to contain chronic viral infection. *Science* (2012) 338(6111):1220–5. doi: 10.1126/science.1229620

26. Utzschneider DT, Charmoy M, Chennupati V, Pousse L, Ferreira DP, Calderon-Copete S, et al. T Cell factor 1-expressing memory-like CD8(+) T cells sustain the immune response to chronic viral infections. *Immunity* (2016) 45(2):415–27. doi: 10.1016/j.immuni.2016.07.021

27. Miller BC, Sen DR, Al Abosy R, Bi K, Virkud YV, LaFleur MW, et al. Subsets of exhausted CD8(+) T cells differentially mediate tumor control and respond to checkpoint blockade. *Nat Immunol* (2019) 20(3):326–36. doi: 10.1038/s41590-019-0312-6

28. Wherry EJ, Ha SJ, Kaech SM, Haining WN, Sarkar S, Kalia V, et al. Molecular signature of CD8+ T cell exhaustion during chronic viral infection. *Immunity* (2007) 27 (4):670–84. doi: 10.1016/j.immuni.2007.09.006

29. Wherry EJ. T Cell exhaustion. *Nat Immunol* (2011) 12(6):492–9. doi: 10.1038/ni.2035

30. Goswami M, Oetjen K, Mulé MP, Sheela S, Wong HY, Liu Q, et al. Increased frequencies of PD-1+ CD8+ marrow-infiltrating lymphocytes associated with highly clonal T-lymphocyte expansions in relapsed and refractory AML patients but not healthy adults. *Blood* (2016) 128(22):1644–4. doi: 10.1182/blood.V128.22.1644.1644

31. Hutten TJA, Norde WJ, Woestenenk R, Wang RC, Maas F, Kester M, et al. Increased coexpression of PD-1, TIGIT, and KLRG-1 on tumor-reactive CD8(+) T cells during relapse after allogeneic stem cell transplantation. *Biol Blood marrow Transplant* (2018) 24(4):666–77. doi: 10.1016/j.bbmt.2017.11.027

32. Schnorfeil FM, Lichtenegger FS, Emmerig K, Schlueter M, Neitz JS, Draenert R, et al. Cells are functionally not impaired in AML: increased PD-1 expression is only seen at time of relapse and correlates with a shift towards the memory T cell compartment. *J Hematol Oncol* (2015) 8:93. doi: 10.1186/s13045-015-0189-2

33. Toffalori C, Zito L, Gambacorta V, Riba M, Oliveira G, Bucci G, et al. Immune signature drives leukemia escape and relapse after hematopoietic cell transplantation. *Nat Med* (2019) 25(4):603–11. doi: 10.1038/s41591-019-0400-z

34. Youngblood B, Oestreich KJ, Ha SJ, Duraiswamy J, Akondy RS, West EE, et al. Chronic virus infection enforces demethylation of the locus that encodes PD-1 in antigen-specific CD8(+) T cells. *Immunity* (2011) 35(3):400–12. doi: 10.1016/j.immuni.2011.06.015

35. Blackburn SD, Shin H, Freeman GJ, Wherry EJ. Selective expansion of a subset of exhausted CD8 T cells by αPD-L1 blockade. *Proc Natl Acad Sci* (2008) 105 (39):15016–21. doi: 10.1073/pnas.0801497105

36. Barber DL, Wherry EJ, Masopust D, Zhu B, Allison JP, Sharpe AH, et al. Restoring function in exhausted CD8 T cells during chronic viral infection. *Nature* (2006) 439(7077):682–7. doi: 10.1038/nature04444

37. Khan O, Giles JR, McDonald S, Manne S, Ngiow SF, Patel KP, et al. TOX transcriptionally and epigenetically programs CD8+ T cell exhaustion. *Nature* (2019) 571(7764):211–8. doi: 10.1038/s41586-019-1325-x

38. Alfei F, Kanev K, Hofmann M, Wu M, Ghoneim HE, Roelli P, et al. TOX reinforces the phenotype and longevity of exhausted T cells in chronic viral infection. *Nature* (2019) 571(7764):265–9. doi: 10.1038/s41586-019-1326-9

39. Scott AC, Dündar F, Zumbo P, Chandran SS, Klebanoff CA, Shakiba M, et al. TOX is a critical regulator of tumour-specific T cell differentiation. *Nature* (2019) 571 (7764):270–4. doi: 10.1038/s41586-019-1324-y

40. Yao C, Sun HW, Lacey NE, Ji Y, Moseman EA, Shih HY, et al. Single-cell RNA-seq reveals TOX as a key regulator of CD8(+) T cell persistence in chronic infection. *Nat Immunol* (2019) 20(7):890–901. doi: 10.1038/s41590-019-0403-4

41. Beltra J-C, Manne S, Abdel-Hakeem MS, Kurachi M, Giles JR, Chen Z, et al. Developmental relationships of four exhausted CD8+ T cell subsets reveals underlying transcriptional and epigenetic landscape control mechanisms. *Immunity* (2020) 52 (5):825–41. doi: 10.1016/j.immuni.2020.04.014

42. Farag SS, Abu Zaid M, Schwartz JE, Thakrar TC, Blakley AJ, Abonour R, et al. Dipeptidyl peptidase 4 inhibition for prophylaxis of acute graft-versus-Host disease. *N Engl J Med* (2021) 384(1):11–9. doi: 10.1056/NEJMoa2027372

43. Okamoto T, Iwata S, Yamazaki H, Hatano R, Komiya E, Dang NH, et al. CD9 negatively regulates CD26 expression and inhibits CD26-mediated enhancement of invasive potential of malignant mesothelioma cells. *PloS One* (2014) 9(1):e86671. doi: 10.1371/journal.pone.0086671

44. Komiya E, Ohnuma K, Yamazaki H, Hatano R, Iwata S, Okamoto T, et al. CD26-mediated regulation of periostin expression contributes to migration and invasion of malignant pleural mesothelioma cells. *Biochem Biophys Res Commun* (2014) 447(4):609–15. doi: 10.1016/j.bbrc.2014.04.037

45. Donnenberg VS, Zhang JJ, Moravcikova E, Meyer EM, Lu H, Carson CT, et al. Antibody-based cell-surface proteome profiling of metastatic breast cancer primary explants and cell lines. *Cytometry A* (2018) 93(4):448–57. doi: 10.1002/cyto.a.23300

46. Pang R, Law WL, Chu AC, Poon JT, Lam CS, Chow AK, et al. A subpopulation of CD26+ cancer stem cells with metastatic capacity in human colorectal cancer. *Cell Stem Cell* (2010) 6(6):603–15. doi: 10.1016/j.stem.2010.04.001

47. Qin CJ, Zhao LH, Zhou X, Zhang HL, Wen W, Tang L, et al. Inhibition of dipeptidyl peptidase IV prevents high fat diet-induced liver cancer angiogenesis by downregulating chemokine ligand 2. *Cancer Lett* (2018) 420:26–37. doi: 10.1016/j.canlet.2018.01.064

48. Barreira da Silva R, Laird ME, Yatim N, Fiette L, Ingersoll MA, Albert ML. Dipeptidylpeptidase 4 inhibition enhances lymphocyte trafficking, improving both naturally occurring tumor immunity and immunotherapy. *Nat Immunol* (2015) 16 (8):850–8. doi: 10.1038/ni.3201

49. Pech V, Abusaada K, Alemany C. Dipeptidyl peptidase-4 inhibition may stimulate progression of carcinoid tumor. *Case Rep Endocrinol* (2015) 2015:952019. doi: 10.1155/2015/952019

50. Bozorgmehr N, Hnatiuk M, Peters AC, Elahi S. Depletion of polyfunctional CD26(high)CD8(+) T cells repertoire in chronic lymphocytic leukemia. *Exp Hematol Oncol* (2023) 12(1):13. doi: 10.1186/s40164-023-00375-5

frontiers | Frontiers in Immunology

TYPE Original Research
PUBLISHED 07 July 2023
DOI 10.3389/fimmu.2023.1158360

OPEN ACCESS

EDITED BY
Eyad Elkord,
University of Salford, United Kingdom

REVIEWED BY
Jiaheng Xie,
Nanjing Medical University, China
Philippe Gasque,
Centre Hospitalier Universitaire de La Réunion, France

*CORRESPONDENCE
Wei Ding
dingweigdwk@163.com
Lin Zhong
zhonglin1@medmail.com.cn

†These authors have contributed equally to this work and share first authorship

RECEIVED 03 February 2023
ACCEPTED 20 June 2023
PUBLISHED 07 July 2023

CITATION
Jiang Q, Kuai J, Jiang Z, Que W, Wang P, Huang W, Ding W and Zhong L (2023) CD93 overexpresses in liver hepatocellular carcinoma and represents a potential immunotherapy target.
Front. Immunol. 14:1158360.
doi: 10.3389/fimmu.2023.1158360

CD93 overexpresses in liver hepatocellular carcinoma and represents a potential immunotherapy target

Qianwei Jiang[1†], Jing Kuai[2†], Zhongyi Jiang[1†], Weitao Que[1], Pusen Wang[1], Wenxin Huang[1], Wei Ding[2*] and Lin Zhong[1*]

[1]Department of General Surgery, Shanghai General Hospital, Shanghai Jiao Tong University School of Medicine, Shanghai, China, [2]Department of Hepatobiliary Surgery, Weifang People's Hospital, Shandong, Weifang, Shandong, China

Background: Liver hepatocellular carcinoma (LIHC) is one of the malignant tumors with high incidence as well as high death, which is ranked as the sixth most common tumor and the third highest mortality worldwide. CD93, a transmembrane protein, has been widely reported to play an important role in different types of diseases, including many types of cancer by mainly functioning in extracellular matrix formation and vascular maturation. However, there are few researches focusing on the role and potential function of CD93 in LIHC.

Methods: In this study, we comprehensively analyzed the relationship between CD93 and LIHC. We not only discovered transcriptional expression of CD93 in LIHC by using the TIMER, GEPIA and UALCAN database, but also performed WB and IHC to verify the protein expression of CD93 in LIHC. Meantime, Kaplan-Meier Plotter Database Analysis were used to assess the prognosis of CD93 in LIHC. After knowing close correlation between CD93 expression and LIHC, there were STRING, GeneMania and GO and KEGG enrichment analyses to find how CD93 functions in LIHC. We further applied CIBERSORT Algorithm to explore the correlation between CD93 and immune cells and evaluate prognostic value of CD93 based on them in LIHC patients.

Results: The transcriptional and protein expression of CD93 were both obviously increased in LIHC by above methods. There was also a significant and close correlation between the expression of CD93 and the prognosis of LIHC patients by using Kaplan-Meier Analysis, which showed that LIHC patients with elevated expression of CD93 were associated with a predicted poor prognosis. We found that the functions of CD93 in different cancers are mainly related to Insulin like growth factor binding protein 7 Gene (IGFBP7)/CD93 pathway via STRING, GeneMania and functional enrichment analyses. Further, our data obtained from CIBERSORT Algorithm suggested CD93 was also associated with the immune response. There is a close positive correlation between CD93 expression and the infiltration levels of all six types of immune cells (B cells,

CD8+ T cells, CD4+ T cells, macrophages, neutrophils, and dendritic cells). Importantly, CD93 can affect the prognosis of patients with LIHC partially due to immune infiltration.

Conclusion: Our results demonstrated CD93 may be a candidate predictor of clinical prognosis and immunotherapy response in LIHC.

KEYWORDS

CD93, liver hepatocellular carcinoma, biomarker, immunotherapy target, immune infiltration

1 Introduction

Liver hepatocellular carcinoma (LIHC), the major subtype of liver cancer, is ranked as the sixth most common tumor and the third highest mortality among all malignancies, whose causes mainly arise from chronic liver disease and chronic hepatitis B and C viral infection (1, 2). There are a variety of mature and effective diagnosis and treatments for LIHC, including surveillance with imaging technology and α-fetoprotein plasma levels every 6 months and hepatic resection, liver transplantation, and transarterial chemoembolization (3–6). But most patients are usually diagnosed as advanced liver cancer because of insidious onset, so that they can't benefit from those treatments (7). In recent years, immunotherapy represented by immune checkpoint inhibitors has made huge and amazing breakthroughs to benefit more and more LIHC patients, particularly those with advanced cancer (8–10). However, there are still no clear and effective biomarkers to predict efficacy of immunotherapy for LIHC. Here, we found a potential gene, called CD93, to probably assume this important role.

CD93 is a transmembrane protein expressed in stem cells, monocytes, and endothelial cells, which consists of several domains, such as an extracellular domain with a C-type lectin domain (11–13). There are numerous studies that have found that CD93 plays a critical role in many diseases, including allergic asthma, diabetic wound healing, and many types of cancer (14–16). It's worth noting that CD93 is involved in angiogenesis in human primary tumors. The interaction between CD93 and its specific ligand, Multimerin 2 (MMRN2), can contribute to endothelial cell adhesion and migration, thus promoting pathological angiogenesis (17–19). CD93 can also function in vascular maturation and extracellular matrix formation by boosting β1 integrin activation and fibronectin to promote angiogenesis (20). Furthermore, CD93 can play a critical role in innate immunity (21). Recent clinical studies have shown that high CD93 expression had a close relationship with the poor effects of immunotherapy (22, 23). In addition, the blockage of the IGFBP7/CD93 pathway brings an extensive increase of effector T cells, making tumors sensitive to immune checkpoint therapy (24, 25).

Although CD93 has been wildly reported to play a critical role in many types of cancer, there are few studies to reveal the value of CD93 in LIHC. The aim of this study was to explore the promising predictive value of CD93 for LIHC prognosis and immunotherapy.

Abbreviations: LIHC, liver hepatocellular carcinoma; BLCA, Bladder urothelial carcinoma; BRCA, Breast invasive carcinoma; CESC Cervical squamous cell carcinoma and endocervical adenocarcinoma; CHOL, Cholangiocarcinoma; COAD, Colon adenocarcinoma; KICH, Kidney Chromophobe; KIRP, Kidney renal papillary cell carcinoma; LUAD, Lung adenocarcinoma; LUSC, Lung squamous cell carcinoma; UCEC, Uterine Corpus Endometrial Carcinoma; STAD, Stomach adenocarcinoma; GEO, Gene Expression Omnibus; TCGA, The Cancer Genome Atlas; GEPIA, Gene Expression Profiling Interactive Analysis; PPI, protein–protein interaction; GO, Gene Ontology; KEGG, Kyoto Encyclopedia of Genes and Genomes; BP, biological process; CC, cellular component; MF, molecular function; TF, transcription factor; DFS, disease-free survival; PFS, poor progression-free survival; OS, overall survival; TAMs, tumor-associated macrophages; NK, Natural killer

2 Materials and methods

2.1 Tumor samples and collection

Human LIHC tissues and paired normal tissues were recruited in Shanghai General Hospital from January 2016 to January 2021. All patients with LIHC underwent surgery for the first time and had not previously received radiotherapy or chemotherapy. Written informed consent was obtained from each patient. This study was approved by the ethics committee of Shanghai General Hospital (2021KSQ341).

2.2 Western blotting

Protein extracted from tissues was using RIPA buffer (Beyotime, Shanghai, China) mixed with PMSF (Beyotime, Shanghai, China) for 30 min on ice, and then centrifuged at 12,000 rpm for 10 min at 4°C. Protein lysates were separated by using SDS-PAGE and transferred to PVDF membranes. After incubating with 5% Bovine serum albumin (BSA) for 1 h at room temperature (RT), the membranes were incubated with primary antibodies (anti-CD93 antibody, sc-365172, Santa Cruz, USA; anti- anti-β-actin antibody, Sangon Biotech,

Shanghai, China) overnight at 4°C, washed with Tris Buffered Saline with Tween®20 (TBST) for 3 times, and further incubated with secondary antibodies (Sangon Biotech, Shanghai, China) for 1 h at RT, and developed using ECL solutions (Beyotime).

2.3 Immunohistochemistry staining and immunofluorescence staining

The samples were fixed in 10% paraformaldehyde for 24h and then embedded in paraffin wax. After deparaffinized and rehydrated, 5 μm thick slides were stained with hematoxylin & eosin (H&E) or primary antibodies (anti-CD93 antibody, sc-365172, Santa Cruz, USA), followed by incubation with horseradish peroxidase (HRP)-conjugated secondary antibody (Sangon, Shanghai, China). All the sections were observed using an AX-80 microscope (Olympus, Tokyo, Japan). The cells which were stained brown were considered positive (tumor tissue, $n = 6$; adjacent tissue, $n = 6$).

The samples were formalin-fixed and embedded in paraffin, then were deparaffinized, rehydrated, permeabilized, and rinsed. After those, we performed antigen repair in citrate buffer for 15 min and carried out the blocking in 5% BSA for 1 hour at room temperature. Then sections were stained with anti-CD93 (sc-365172, Santa Cruz, USA) anti-CD31/PECAM-1 (sc-18916, Santa Cruz, USA) and anti-IGFBP7 (171085, Abcam, USA) antibodies overnight at 4°C in a humidified box. Then, sections were incubated with secondary antibodies for 1 hour at RT and protected from light. After stain with DAPI, microscope images were taken of the sections.

2.4 Real-time PCR

Total RNA was extracted from human samples by using an Isolation Kit following the manufacturer's instructions. Then we performed the reverse transcription by using the reverse transcription kit. After those, Real-time PCR was carried out with the SYBR qPCR Master Mix kit. The primer sequences used for gene analysis were as follows: CD93-Forward: 5'-GCCCCAGA ATGCGGCAGACA-3', CD93-Reverse: 5'-GCAGTCTGTCCCA GGTGTCGGA-3'; β-actin-Forward: 5'-AGGATTCCTATGTG GGCGAC-3', β-actin-Reverse: 5'-ATAGCACAGCCTGGATA GCAA-3'.

2.5 Tumor immune estimation resource

TIMER (https://cistrome.shinyapps.io/timer/) is a comprehensive resource for performing systematical analysis of immune infiltrates across diverse cancer types (26). In this study, it was applied to evaluate the correlation between CD93 expression and the infiltration of immune cells and investigate the relationship between CD93 expression and different gene marker sets of immune cells.

2.6 Gene expression profiling interactive analysis

GEPIA (http://gepia.cancer-pku.cn/index.html) is a user-friendly web portal for gene expression analysis based on TCGA and GTEx data (27). In this study, it was used to explore the expression in HCC and clarify the relationships between CD93 and PD-1, PD-L1, CTLA-4, and VEGFA.

2.7 UALCAN

UALCAN (http://ualcan.path.uab.edu/) is a web-based tool for providing in-depth analyses of transcriptome data from The Cancer Genome Atlas (TCGA) and MET500 data (28). In this study, it is built to analyze the mRNA expression levels of CD93 in LIHC and the relationship between CD93 expression and patients' gender, individual cancer stages, and pathological grades.

2.8 Kaplan-Meier plotter database analysis

KM Plotter (http://kmplot.com) is an online database that contains gene expression data and survival information. In this study, it is used to analyze the prognostic value of CD93 in LIHC, including overall survival (OS), progression-free survival (PFS) and disease-free survival (DSS) with hazard ratios (HRs) with 95% confidence intervals (95% CIs) and log-rank p-values.

2.9 GeneMANIA

GeneMANIA (http://www.genemania.org) is a flexible, user-friendly tool for generating hypotheses about gene function (29). In this study, it is applied to construct the gene-gene interaction network.

2.10 STRING

STRING (https://string-db.org/) is an online database for searching known protein interaction relationships. In this study, it is used to collect, score, and integrate all publicly available sources of protein-protein interaction (PPI) data, and to complement these with computational predictions of potential functions.

2.11 Gene ontology term and Kyoto encyclopedia of genes and genomes pathway enrichment analysis and gene set enrichment analysis

GO and KEGG analyses were applied to explore the biological functions of CD93 in LIHC. In this study, GO analysis is a powerful bioinformatics tool to determine the biological processes (BPs), cellular components (CCs) and molecular functions (MFs) related

to CD93. GSEA was used to investigate the potential mechanisms of CD93.

2.12 Immune cell infiltration with the CIBERSORT algorithm

CIBERSORT (https://cibersort.stanford.edu/), is an established computational resource for characterizing the immune cell composition based on a validated leukocyte gene signature matrix containing 547 genes and 22 human immune cell subpopulations (30). In this study, it is applied to examine the correlations between CD93 expression and the immune cell subpopulation.

2.13 Statistical analysis

All statistical analyses were performed using R software 4.0.1. The results of Kaplan-Meier plots and GEPIA are displayed with HR and P or Cox P-values from a log-rank test. The correlation of CD93 gene expression was explored by Spearman's correlation and statistical significance. The heat map of the correlations was generated by the R software package pheatmap with Spearman's correlation. The P-values < 0.05 were considered statistically significant for all statistical analyses.

3 Results

3.1 Pan-cancer analysis of CD93 expression

To investigate the mRNA expression of CD93 in tumor and normal tissues, we utilized an online tool, Tumor Immune Estimation Resource (TIMER), to find that the expression of CD93 between various tumors and adjacent tissues was tremendously different (Figure 1A). Compared with the normal tissues, higher expression of CD93 was observed in Bladder urothelial carcinoma (BLCA), Breast invasive carcinoma (BRCA), Cervical squamous cell carcinoma, and endocervical adenocarcinoma (CESC), Cholangiocarcinoma (CHOL), Colon adenocarcinoma (COAD), Kidney Chromophobe (KICH), Kidney renal papillary cell carcinoma (KIRP), Liver hepatocellular carcinoma (LIHC), Lung adenocarcinoma (LUAD), Lung squamous cell carcinoma (LUSC), Stomach adenocarcinoma (STAD), and Uterine Corpus Endometrial Carcinoma (UCEC). Similarly, we confirmed that higher expression of CD93 in LIHC than in normal tissues from the gene expression profiling interactive analysis (GEPIA), the UALCAN databases, and The Cancer Genome Atlas (TCGA) and Gene Expression Omnibus (GEO), respectively (Figures 1B–D; Supplementary Figure 1A). Furthermore, there was a significantly increased mRNA expression of CD93 in 50 paired LIHC tissues compared to paired adjacent normal tissues (Figure 1E). Then, we performed the Real-time PCR to verify the above conclusion (Supplementary Figure 1B). These findings suggest that CD93 expression is increased in LIHC patients and that it may play a pivotal role in the occurrence and progression of LIHC.

We also investigated the protein expression of CD93 in LIHC tumor tissues and adjacent tissues. The results of Western Blot and Real-time PCR have demonstrated that CD93 was markedly upregulated in LIHC tumor tissues than in adjacent tissues (Figure 2A). Not coincidentally, immunohistochemistry and immunofluorescence staining of LIHC tumor tissue and adjacent tissues also demonstrated the same results (Figure 2B; Supplementary Figure 2).

3.2 CD93 expression and clinical parameters of LIHC

Since the expression of CD93 increased significantly in patients with LIHC, we further explored the relationships between CD93 expression levels and clinical outcomes according to different clinical parameters by using the UALCAN database. As shown in Figures 2C, D, there were significant differences in CD93 expression in tumors and normal tissues of LIHC patients by gender and age group. Based on the BCLC system (31), CD93 expression was higher in patients with LIHC classified as stages A, B, and C, which suggested that there was a close correlation between CD93 expression and tumor progression (Figure 2E). Regarding Edmondson's pathological grade of LIHC, a significant increase in CD93 expression was observed in LIHC patients in grades 1, 2, and 3 (Figure 2F). We then investigated the expression of CD93 in LIHC based on TP53 mutation status and found that the expression of CD93 in tumor tissues was higher than that in normal liver tissues regardless of TP53 mutation (Figure 2G). What's more, upregulated CD93 expression was observed in LIHC patients with nodal metastases (Figure 2H). These results suggest that the expression level of CD93 is closely related to the clinical progression of LIHC.

3.3 Elevated expression of CD93 indicates poor prognosis for LIHC

Based on our findings, we then examined the prognostic value of the CD93 gene by using the Kaplan Meier plotter database. According to the median expression of CD93, patients in the database were divided into high and low-expression subgroups. The results have shown that LIHC patients with higher expression of the CD93 gene who had no vascular invasion exhibited poor progression-free survival (PFS) (Figure 3B) and Disease-free survival (DFS) (Figure 3C), although there was no statistical difference in overall survival (OS) (Figure 3A). Moreover, we validated the prognostic value of CD93 according to various clinicopathological features using the Kaplan-Meier database. We found that high CD93 expression was significantly associated with poor OS in patients infected with the hepatitis virus, and with poor PFS when vascular invaded (Figures 3D, E). These results imply that CD93 expression possesses prognostic value in LIHC.

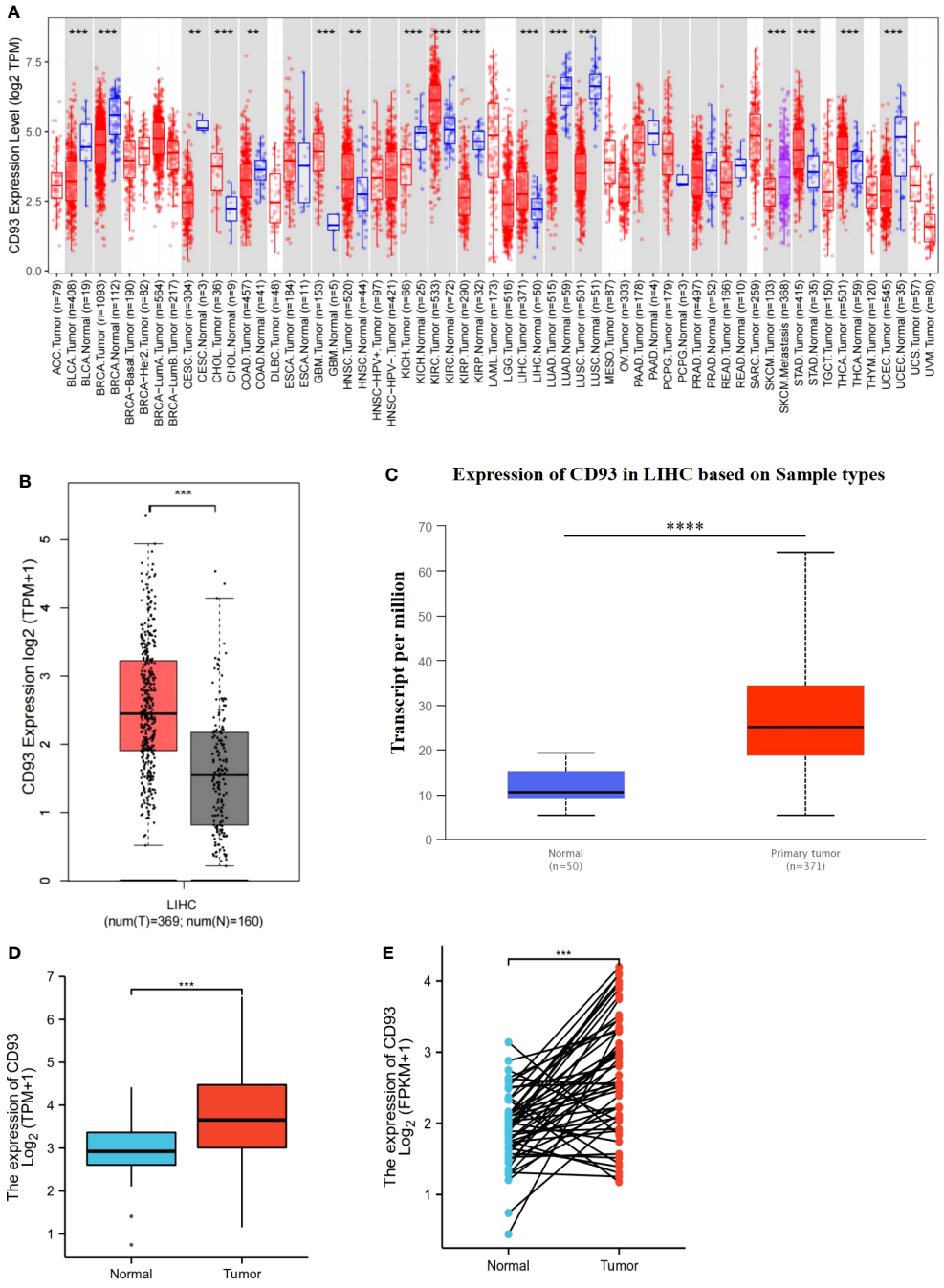

FIGURE 1
Transcriptional expression of CD93 in LIHC. **(A)** CD93 expression in different types of cancers was examined by using the TIMER database. **(B)** Increased expression of CD93 in LIHC compared to normal tissues in the GEPIA database. **(C)** Increased expression of CD93 in LIHC compared to normal tissues in the UALCAN database. **(D)** The expression of CD93 was higher in LIHC tissues by using the TCGA database. **(E)** CD93 was found to be highly expressed in LIHC tissues in 50 pairs of tumor tissues and paired adjacent tissues in the TCGA database. **p < 0.01, ***p < 0.001, ****p < 0.0001.

3.4 Identification of CD93 potential mechanism in LIHC

In addition to elucidating the prognostic value of CD93 expression in LIHC, we also focused on the potential mechanisms involved in CD93 in LIHC. We generated the gene-gene interaction network to explore the altered neighboring genes of CD93 via GeneMania (Figure 4A). The results showed that the 20 most frequently altered genes were closely correlated with CD93, including A-kinase anchor protein 13 (AKAP 13) and Collagen alpha-1(IV) chain (COL4A1). Functional analysis revealed that these genes were significantly associated with endothelium development and others. We also produced the protein-protein interaction (PPI) network of CD93 through the STRING database and obtained 48 edges and 11 nodes, which included PDZ domain-containing protein GIPC1 and Complement C1q subcomponent

10.3389/fimmu.2023.1158360

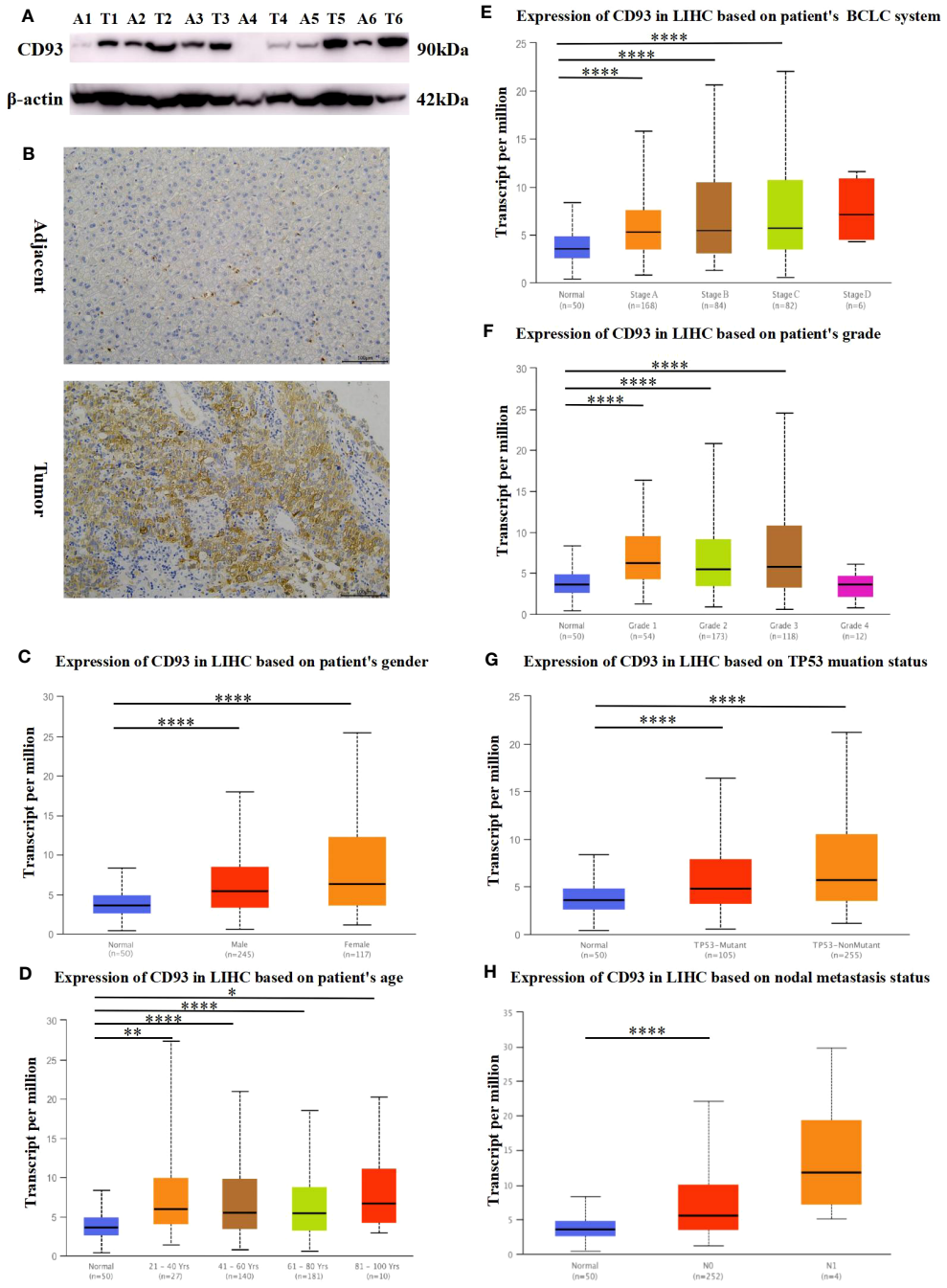

FIGURE 2
Protein expression of CD93. **(A)** Increased expression of CD93 in LIHC compared to normal tissues by WB. **(B)** Increased expression of CD93 in tumors compared to normal tissues by IHC.Box plots evaluating CD93 expression among different groups of patients based on clinical parameters using the UALCAN database. **(C)** gender, **(D)** age, **(E)** BCLC system, **(F)** Edmondson's pathological grade, **(G)** TP53 mutation status, **(H)** nodal metastasis status. *p < 0.05, **p < 0.01, ***p < 0.001, ****p < 0.0001.

subunit A (C1QA) (Figure 4B). Further, we investigated the correlation between CD93 and endothelial cell function-related genes based on the TCGA database (Figure 4C). As result, CD93 was positively and significantly correlated with Insulin-like growth factor-binding protein 7 (IGFBP7), post-GPI attachment to proteins inositol deacylase 1(PGAP1), and platelet and endothelial cell adhesion molecule 1 (PECAM1) whereas negatively correlated with fibronectin leucine rich transmembrane protein 3 (FLRT3), and dynein axonemal heavy chain 12 (DNAH12). In addition, we found that CD93 was correlated with vascular endothelial growth factor a (VEGFA) using the GEPIA and TIMER databases (Supplementary Figures 3A, B). We also performed IF staining to confirm the close contact between CD93 and IGFBP7 (Supplementary Figure 3C).

We further exploited the TCGA database to identify genes positively or negatively co-expressed with CD93. The top 50

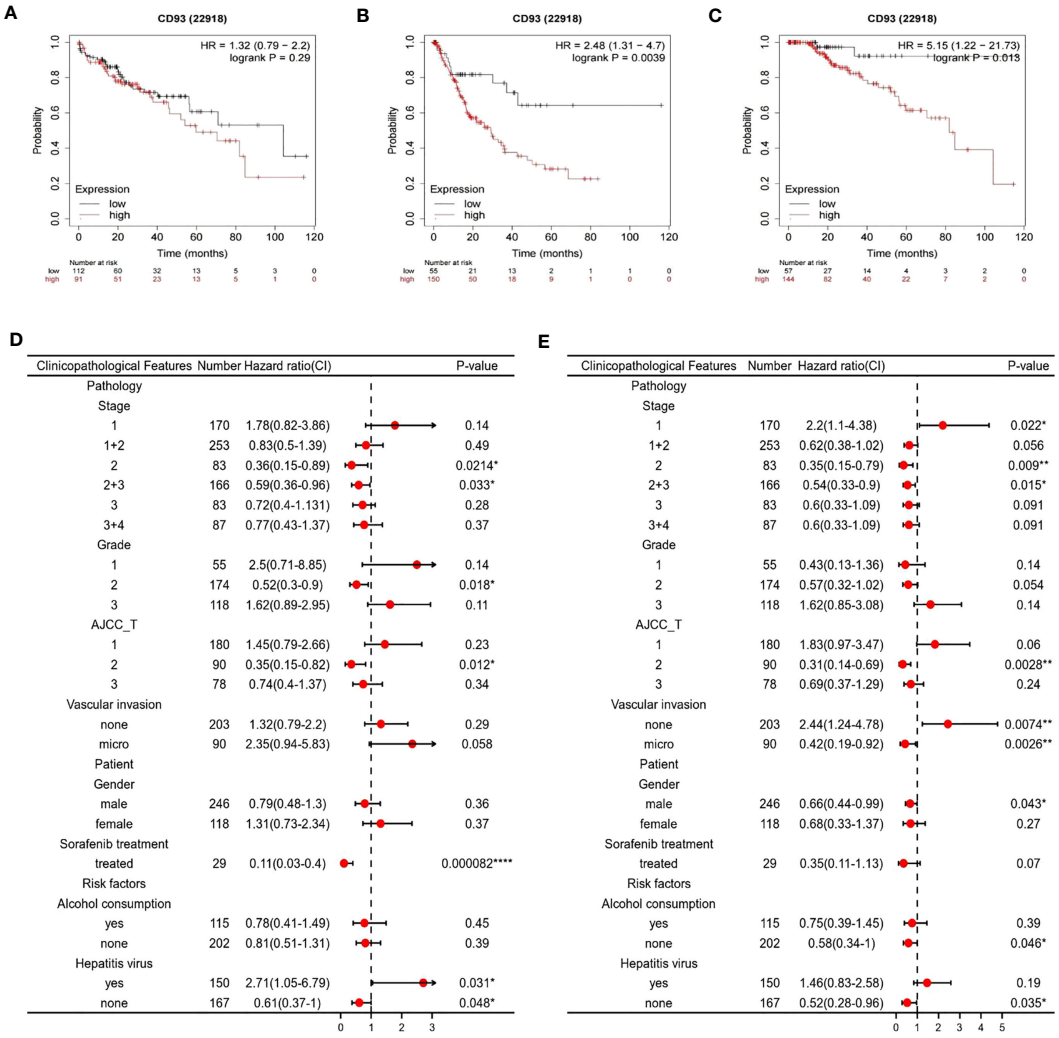

FIGURE 3
Survival curve evaluating the prognostic value of CD93. Survival curves using the Kaplan-Meier plotter are shown for **(A)** OS, **(B)** PFS, **(C)** DFS; A forest plot from the Kaplan-Meier database shows the correlation between CD93 expression and LIHC patients' clinicopathological parameters, such as **(D)** OS, **(E)** PFS. *p < 0.05, **p < 0.01, ****p < 0.0001.

genes that were positively and negatively correlated with CD93 in LIHC were shown in Figures 4D, E. To establish a clearer understanding of the biological functions and potential mechanisms involved in CD93 in the development of LIHC, we presented the top 20 significant terms by GO and KEGG functional enrichment analysis. As shown in the BP category, CD93 was enriched in the extracellular matrix organization, regulation of vasculature development, and regulation of angiogenesis (Figure 5A). Correspondingly, the enriched processes of MF were extracellular matrix structural constituent, cell adhesion molecule binding, and growth factor binding (Figure 5B), while the main enrichment of CC included collagen-containing extracellular matrix, cell-substrate junction, and collagen trimer (Figure 5C). Signaling pathway enrichment analysis demonstrated that high CD93 expression in LIHC was associated with the PI3K-Akt signaling pathway, ECM-receptor interaction, MAPK signaling pathway, etc. (Figure 5D).

3.5 Correlation analysis between CD93 expression and infiltrating immune cells

Given the complex hepatic immune microenvironment, we further evaluated the effect of CD93 expression in association with immune infiltrating cells on the occurrence and progression of LIHC using the TIMER database. We initially found a significant positive correlation between CD93 expression levels and the infiltration of six types of immune cells, including B cell, $CD8^+$ T cell, $CD4^+$ T cell, macrophage, neutrophil, and dendritic cell (Figure 6A). Furthermore, we estimated the associations of immune infiltration levels of immune cell subtypes with CD93 expression. As we showed, CD93 was notably positively correlated with the infiltration levels of endothelial cells, cancer-associated fibroblasts, M1/M2 macrophages, and activated Natural killer (NK) cells, whereas negatively correlated with the infiltration levels of Type 1 T helper cells, γδ T cells, central memory $CD4^+$ T cells (Figure 6B).

10.3389/fimmu.2023.1158360

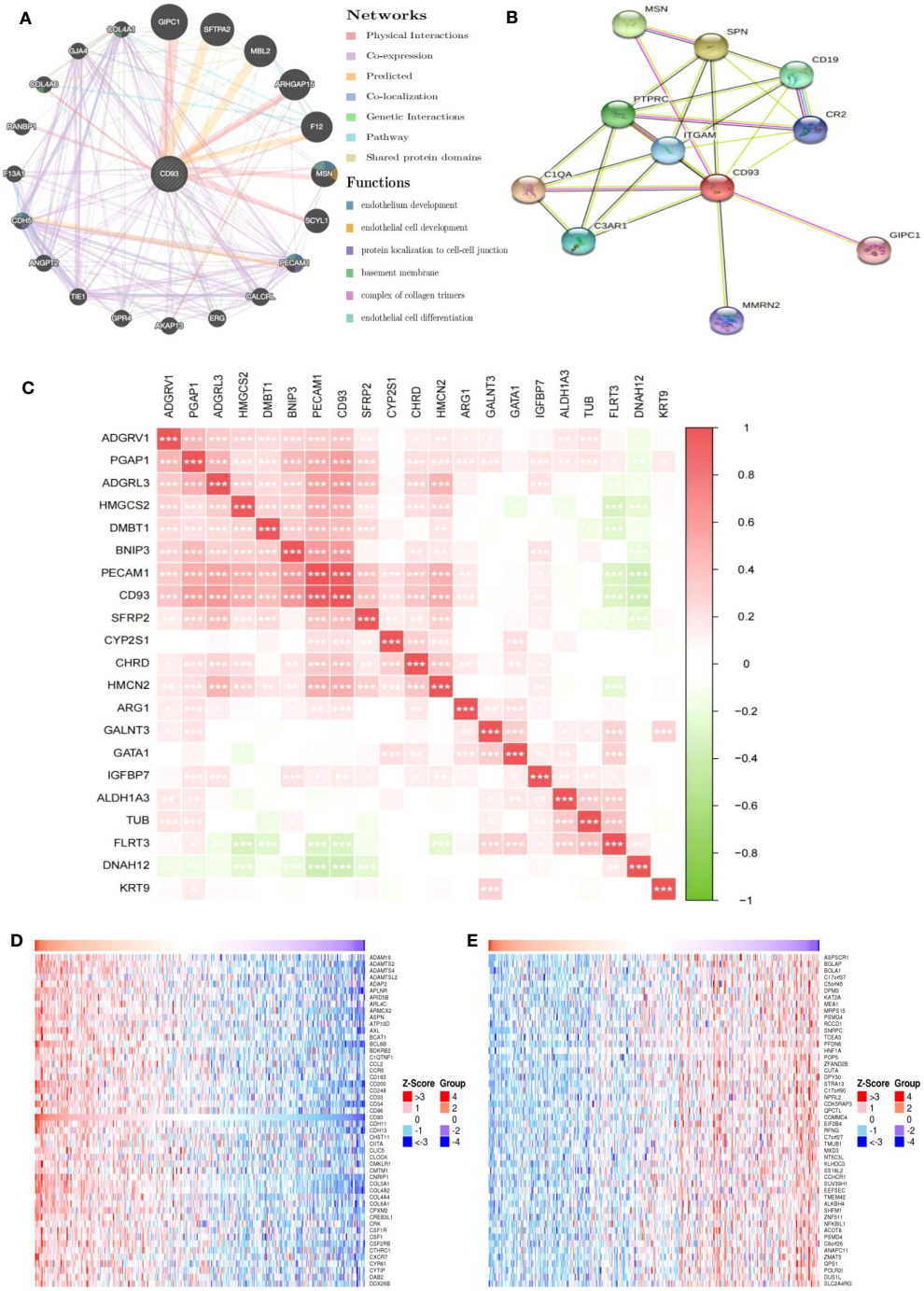

FIGURE 4
Genes and pathways closely related to CD93. **(A)** The gene-gene interaction network of CD93 was constructed using GeneMania. **(B)** The PPI network of CD93 was generated using STRING. **(C)** Heat maps showing the correlations between CD93 and other genes in LIHC. **(D)** Heat maps showing the top 50 genes positively correlated with CD93 in LIHC. **(E)** Heat maps showing the top 50 genes negatively correlated with CD93 in LIHC. *p < 0.05, **p < 0.01, ***p < 0.001.

3.6 Correlation between CD93 expression and diverse immune markers

To gain insight into the interaction between CD93 and immune responses, we utilized the TIMER database to verify the correlation between CD93 expression and various immune features in LIHC, including B cells, T cells, $CD8^+$ T cells, monocytes, tumor-associated macrophages (TAMs), M1/M2 macrophages, neutrophils, NK cells, and dendritic cells (Table 1). Based on calibrated tumor purity, we confirmed that CD93 expression correlated significantly with most of the representative markers in a variety of immune cells in LIHC (Table 1).

We further utilized the GEPIA database to exploit the interaction between CD93 expression and well-known immune checkpoints in immunotherapy, such as PD-1, PD-L1, and CTLA-4 (Figures 6C–E). These findings support the apparent

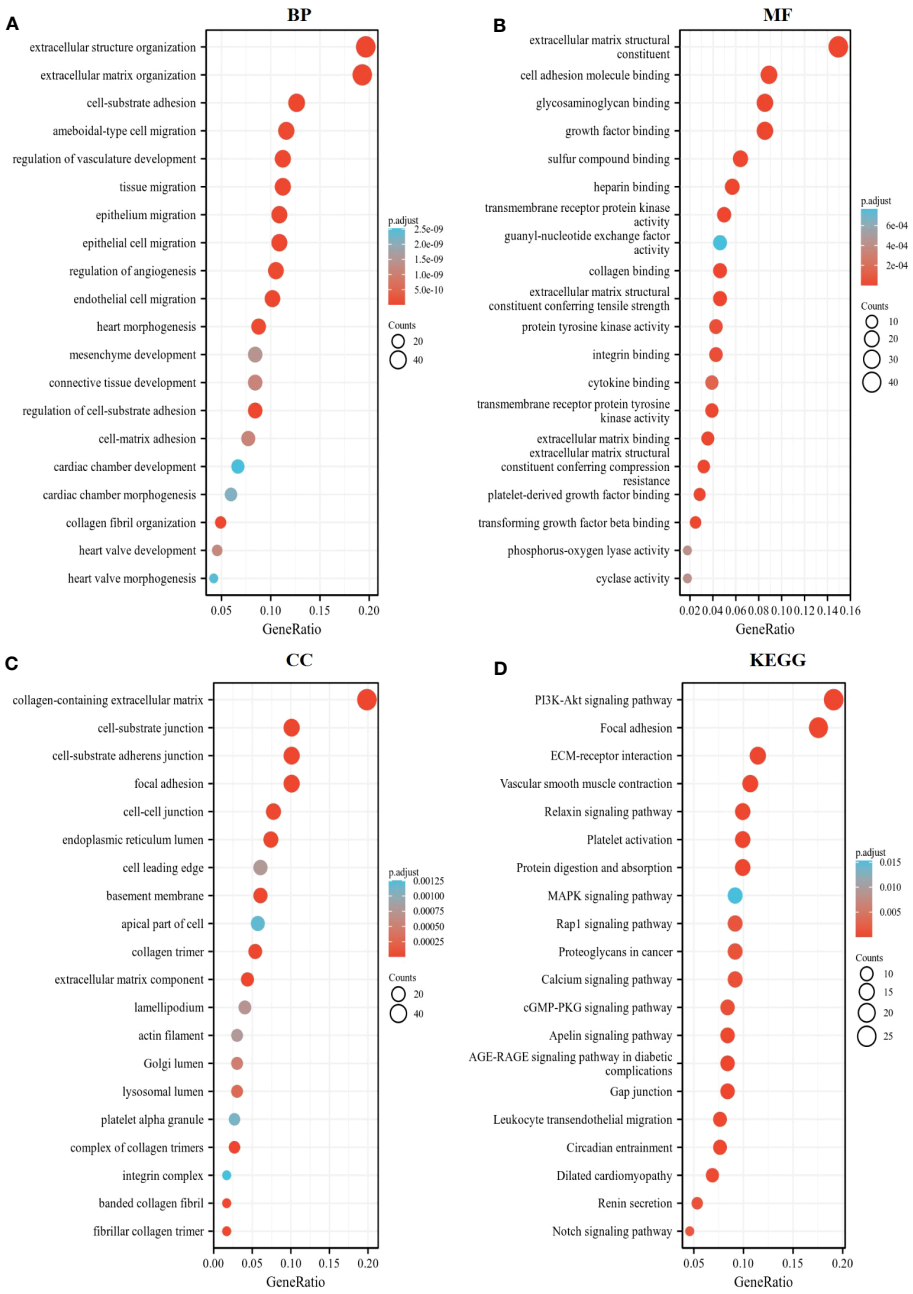

FIGURE 5
Enrichment analysis of CD93. The top 20 significant terms by GO and KEGG functional enrichment analysis showed in **(A)** BP, **(B)** MF, **(C)** CC, and **(D)** KEGG.

association of CD93 with immune infiltration of LIHC, which plays a key role in the immune response.

3.7 Prognostic evaluation of CD93 expression on the basis of immune cells in LIHC patients

With CD93 expression known to correlate with poor OS and PFS in LIHC, we further evaluated the impact of CD93 expression with the degree of infiltration of various immune cell subtypes on the prognosis of LIHC through prognostic analysis. The results of our analysis revealed a poor OS when LIHC patients with high expression of CD93 had decreased Regulatory T-cells, enriched Type 1 T-helper cells, and decreased Type 1 T-helper cells (Figure 7A). More details were shown in Figures 7C–E. In addition, LIHC patients with high expression of CD93 possessed poor PFS when there were enriched CD8+ T cells, enriched Type 1 T-helper cells, and enriched Type 2 T-helper cells (Figures 7B, F–H). These results suggest that CD93 affects the prognosis of patients with LIHC partially due to immune infiltration.

4 Discussion

LIHC is considered one of the most common malignancies with high morbidity and mortality worldwide (32, 33). To reduce the

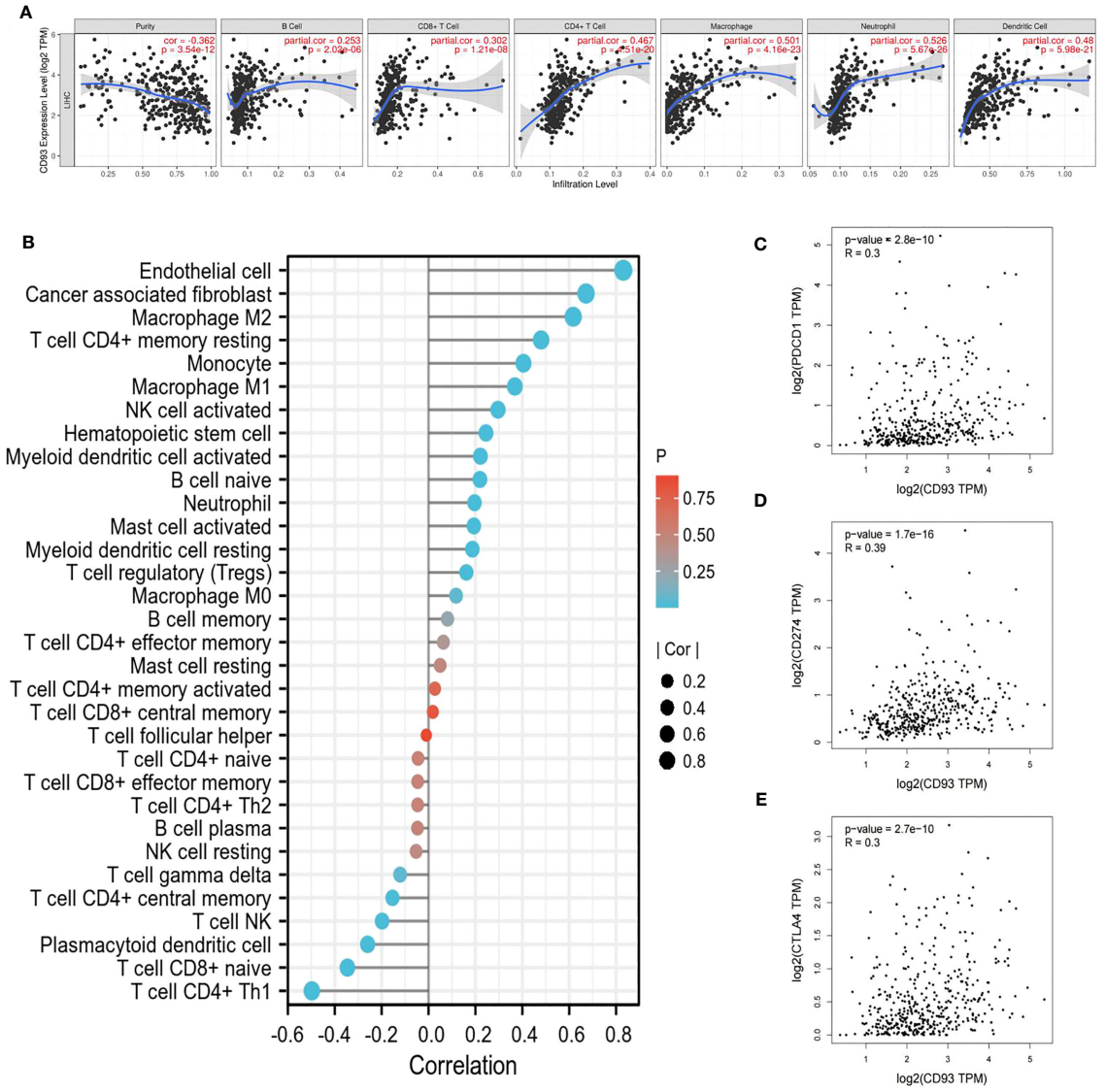

FIGURE 6
Relationship between CD93 and immune cells. **(A)** CD93 significantly associated with tumor purity and positively correlated with the infiltration of different immune cells using the TIMER database. **(B)** CD93 expression significantly correlated with the infiltration of immune cells in LIHC by using the CIBERSORT algorithm. **(C–E)** Scatterplots of the correlations between CD93 expression and **(C)** PD-1, **(D)** PD-L1 and **(E)** CTLA-4 in LIHC using the GEPIA database.

economic loss and life damage from LIHC, there emerge increasingly advanced and precise diagnoses and treatments. In particular, immunotherapy with tumor immune checkpoint inhibitors has revolutionized the treatment of many types of cancer, which brings the vast majority of patients too much real clinical benefit (34–37). However, LIHC is still diagnosed at an advanced stage and has a poor prognosis when it is found. Thus, it is urgently needed to clarify the mechanisms of hepatocarcinogenesis and identify useful prognostic biomarkers and potential immunotherapy targets of LIHC.

In this study, we found that CD93 could play an important role in LIHC by involving in endothelium development and angiogenesis. The researchers have reported that CD93 took part in the control of endothelial cell function through the cooperation between CD93 and dystroglycan, a laminin-binding protein, in malignant tumors (13, 38–40). CD93 overexpression was found in tumor vasculatures, and it influenced the survival of patients in PDAC, PNET, melanoma, and colon cancer (21, 41, 42). Our findings further demonstrated that CD93 was closely correlated with angiogenesis in LIHC, as among the most frequently altered genes closely associated with CD93 are many genes associated with tumor vascularization. In particular, IGFBP7 is a protein positively and significantly correlated with CD93 that has been identified to be up-regulated in tumor blood vessels and able to promote vascular angiogenesis. Hindering the CD93-IGFBP7 axis by CD93 or IGFBP7 mAb could normalize tumor vasculature to suppress tumor growth (21). Importantly, blocking the axis also increased immune cell infiltration to inhibit tumor progression (38).

Our study has shown that CD93 was positively correlated with six types of immune cells. There were a lot of studies that reported

10.3389/fimmu.2023.1158360

TABLE 1 Correlation analysis between CD93 and gene markers of immune cells in TIMER.

Description	Gene markers	LIHC			
		None		Purity	
		Cor	P	Cor	P
B cell	CD19	0.214692912	****	0.112166065	*
	CD79A	0.306124833	****	0.17127049	**
T cell (general)	CD3D	0.212227139	****	0.083895849	0.1199
	CD3E	0.398034483	****	0.277357047	****
	CD2	0.352582267	****	0.233499214	****
CD8+ T cell	CD8A	0.343579524	****	0.249149122	****
	CD8B	0.197541036	***	0.087212881	0.1059
Monocyte	CD86	0.548714213	****	0.480956881	****
	CSF1R	0.564914449	****	0.491071275	****
TAM	CCL2	0.568209815	****	0.484845407	****
	CD68	0.420702313	****	0.325439064	****
	IL10	0.430418027	****	0.324665302	****
M1	IRF5	0.348446454	****	0.377669482	****
	PTGS2	0.649824421	****	0.584545518	****
	NOS2	0.437941659	****	0.431980104	****
M2	CD163	0.565593305	****	0.502327393	****
	VSIG4	0.537297344	****	0.464709792	****
	MS4A4A	0.572326731	****	0.505990943	****
Neutrophils	CEACAM8	0.021500083	0.6798	-0.018706305	0.7292
	ITGAM	0.475869313	****	0.415199851	****
	CCR7	0.479802725	****	0.361253566	****
Natural killer cell	KIR2DL1	0.082681125	0.1119	0.075846689	0.1598
	KIR2DL3	0.176757483	***	0.131086101	*
	KIR2DL4	0.103274489	*	0.063190688	0.2417
	KIR3DL1	0.207017402	****	0.205497668	***
	KIR3DL2	0.128115099	*	0.079987159	0.1382
	KIR3DL3	0.032494912	0.5327	0.023996555	0.6569
	KIR2DS4	0.099460245	0.0556	0.109239811	*
Dendritic cell	HLA-DPB1	0.505105784	****	0.417565933	****
	HLA-DQB1	0.340864367	****	0.233194409	****
	HLA-DRA	0.527044652	****	0.451615068	****
	HLA-DPA1	0.559072889	****	0.488731572	****
	CD1C	0.506846064	****	0.4110962	****
	NRP1	0.634177992	****	0.630304624	****
	ITGAX	0.518528824	****	0.445647167	****

*p<0.05, **p<0.01, ***p<0.001, ****p<0.0001.

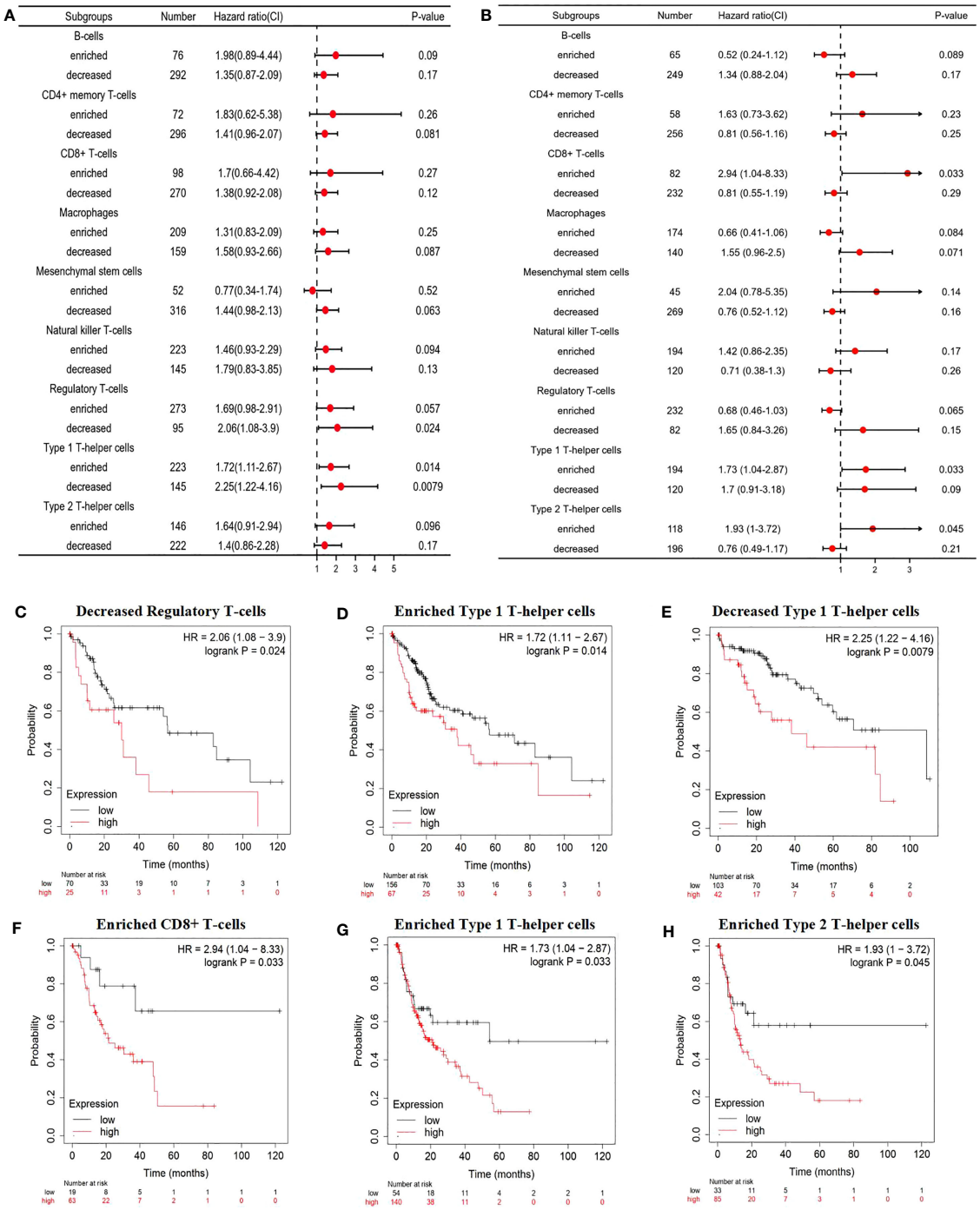

FIGURE 7
Prognostic evaluation of CD93 expression based on immune cells. A forest plot showing the correlations between **(A)** OS and **(B)** PFS and the CD93 expression according to different immune cell subgroups in LIHC patients. Correlations between CD93 expression and OS in **(C)** decreased Regulatory T-cells, **(D)** enriched Type 1 T-helper cells, **(E)** decreased Type 1 T-helper cells by Kaplan-Meier plotter; correlations between CD93 expression and PFS in **(F)** CD8+ T cells, **(G)** enriched Type 1 T-helper cells, and **(H)** enriched Type 2 T-helper cells.

that CD93 was involved in the regulation of the immune response in different cancers (43–46). We also found that there was a close and tight interaction between CD93 expression and well-known immune checkpoints in immunotherapy, such as PD-1, PD-L1, and CTLA-4, which were extensively reported to play an immune escape role by PI3K/Akt signaling pathway or MAPK signaling pathway (47–50). CD93 may interact with them through these pathways. In addition, we explored the impact of the relationship between immune infiltration and CD93 expression on the prognosis and survival of patients. Furthermore, subgroup analysis by immune cells showed that high CD93 expression with enriched immune cells such as CD8+ T cells, Type 1 T-helper cells or Type 2 T-helper was highly related to poor prognosis in LIHC patients. Sun et al. observed that blocking the CD93 pathway can sensitize tumors to

immunotherapy to promote the cancer immunotherapy effect and Riethe Huang et al. reported that CD93 could serve as an important regulator of leukemia stem cells and a potential therapeutic target (17, 20, 46, 51).

Above all these results, we can find that CD93 plays a role in LIHC through immune infiltration, and is expected to be a potential immunotherapy target.

Data availability statement

The original contributions presented in the study are included in the article/Supplementary Materials. Further inquiries can be directed to the corresponding authors.

Ethics statement

The studies involving human participants were reviewed and approved by the ethics committee of Shanghai General Hospita. The patients/participants provided their written informed consent to participate in this study.

Author contributions

QJ, JK, and ZJ wrote this manuscript and prepared the table and the figure. LZ and WD devised and supervised this project. WQ, PW, and WH assisted in the literature search and manuscript editing. All authors contributed to the article and approved the submitted version.

Funding

This study was partly supported by research grants from the National Natural Science Foundation of China (82070672), Science and Technology Commission of Shanghai Municipality (20ZR1445500, 20S31904800), and Three-year Action Plan for Clinical Skills and Clinical Innovation in Shanghai-level Hospitals (SHDC2020CR3035B).

Acknowledgments

We thank the National Natural Science Foundation of China, Science and Technology Commission of Shanghai Municipality, and Shanghai Shen-kang Hospital Development Center for the grant funding.

Conflict of interest

The authors declare that the research was conducted in the absence of any commercial or financial relationships that could be construed as a potential conflict of interest.

Publisher's note

Supplementary material

The Supplementary Material for this article can be found online at: https://www.frontiersin.org/articles/10.3389/fimmu.2023.1158360/full#supplementary-material

References

1. Llovet JM, Kelley RK, Villanueva A, Singal AG, Pikarsky E, Roayaie S, et al. Hepatocellular carcinoma. *Nat Rev Dis Primers* (2021) 7:6. doi: 10.1038/s41572-020-00240-3

2. Forner A, Reig M, Bruix J. Hepatocellular carcinoma. *Lancet* (2018) 391:1301–14. doi: 10.1016/S0140-6736(18)30010-2

3. Bruix J, Han K-H, Gores G, Llovet JM, Mazzaferro V. Liver cancer: approaching a personalized care. *J Hepatol* (2015) 62:S144–56. doi: 10.1016/j.jhep.2015.02.007

4. Verslype C, Rosmorduc O, Rougier P. Hepatocellular carcinoma: ESMO–ESDO clinical practice guidelines for diagnosis, treatment and follow-up. *Ann Oncol* (2012) 23:vii41–8. doi: 10.1093/annonc/mds225

5. Piñero F, Dirchwolf M, Pessôa MG. Biomarkers in hepatocellular carcinoma: diagnosis, prognosis and treatment response assessment. *Cells* (2020) 9:1370. doi: 10.3390/cells9061370

6. de Lope CR, Tremosini S, Forner A, Reig M, Bruix J. Management of HCC. *J Hepatol* (2012) 56:S75–87. doi: 10.1016/S0168-8278(12)60009-9

7. Anwanwan D, Singh SK, Singh S, Saikam V, Singh R. Challenges in liver cancer and possible treatment approaches. *Biochim Biophys Acta (BBA) - Rev Cancer* (2020) 1873:188314. doi: 10.1016/j.bbcan.2019.188314

8. Ruf B, Heinrich B, Greten TF. Immunobiology and immunotherapy of HCC: spotlight on innate and innate-like immune cells. *Cell Mol Immunol* (2021) 18:112–27. doi: 10.1038/s41423-020-00572-w

9. Rizvi S, Wang J, El-Khoueiry AB. Liver cancer immunity. *Hepatology* (2021) 73:86–103. doi: 10.1002/hep.31416

10. Greten TF, Lai CW, Li G, Staveley-O'Carroll KF. Targeted and immune-based therapies for hepatocellular carcinoma. *Gastroenterology* (2019) 156:510–24. doi: 10.1053/j.gastro.2018.09.051

11. Greenlee-Wacker M C, Galvan M D, S. Bohlson S. CD93: recent advances and implications in disease. *CDT* (2012) 13:411–20. doi: 10.2174/138945012799424651

12. Barbera S, Raucci L, Lugano R, Tosi GM, Dimberg A, Santucci A, et al. CD93 signaling via rho proteins drives cytoskeletal remodeling in spreading endothelial cells. *IJMS* (2021) 22:12417. doi: 10.3390/ijms222212417

13. Nativel B, Ramin-Mangata S, Mevizou R, Figuester A, Andries J, Iwema T, et al. CD 93 is a cell surface lectin receptor involved in the control of the inflammatory response stimulated by exogenous DNA. *Immunology* (2019) 158:85–93. doi: 10.1111/imm.13100

14. Park HJ, Oh E-Y, Han H-J, Park KH, Jeong K-Y, Park J-W, et al. Soluble CD93 in allergic asthma. *Sci Rep* (2020) 10:323. doi: 10.1038/s41598-019-57176-2

15. Khan KA, McMurray JL, Mohammed F, Bicknell R. C-type lectin domain group 14 proteins in vascular biology, cancer and inflammation. *FEBS J* (2019) 286:3299–332. doi: 10.1111/febs.14985

16. Jia J, Liu B, Wang D, Wang X, Song L, Ren Y, et al. CD93 promotes acute myeloid leukemia development and is a potential therapeutic target. *Exp Cell Res* (2022) 420:113361. doi: 10.1016/j.yexcr.2022.113361

17. Tosi GM, Neri G, Barbera S, Mundo L, Parolini B, Lazzi S, et al. The binding of CD93 to multimerin-2 promotes choroidal neovascularization. *Invest Ophthalmol Vis Sci* (2020) 61:30. doi: 10.1167/iovs.61.8.30

18. Galvagni F, Nardi F, Spiga O, Trezza A, Tarticchio G, Pellicani R, et al. Dissecting the CD93-multimerin 2 interaction involved in cell adhesion and migration of the activated endothelium. *Matrix Biol* (2017) 64:112–27. doi: 10.1016/j.matbio.2017.08.003

19. Liang Q, Su L, Zhang D, Jiao J. CD93 negatively regulates astrogenesis in response to MMRN2 through the transcriptional repressor ZFP503 in the developing brain. *Proc Natl Acad Sci USA* (2020) 117:9413–22. doi: 10.1073/pnas.1922713117

20. Lugano R, Vemuri K, Yu D, Bergqvist M, Smits A, Essand M, et al. CD93 promotes β1 integrin activation and fibronectin fibrillogenesis during tumor angiogenesis. *J Clin Invest* (2018) 128:3280–97. doi: 10.1172/JCI97459

21. Huang J, Lee H, Zhao X, Han J, Su Y, Sun Q, et al. Interleukin-17D regulates group 3 innate lymphoid cell function through its receptor CD93. *Immunity* (2021) 54:673–686.e4. doi: 10.1016/j.immuni.2021.03.018

22. Zhang Z, Zheng M, Ding Q, Liu M. CD93 correlates with immune infiltration and impacts patient immunotherapy efficacy: a pan-cancer analysis. *Front Cell Dev Biol* (2022) 10:817965. doi: 10.3389/fcell.2022.817965

23. Tong W, Wang G, Zhu L, Bai Y, Liu Z, Yang L, et al. Pan-cancer analysis identified CD93 as a valuable biomarker for predicting patient prognosis and immunotherapy response. *Front Mol Biosci* (2022) 8:793445. doi: 10.3389/fmolb.2021.793445

24. CD93 blockade stabilizes tumor vasculature to improve therapy response. *Cancer Discovery* (2021) 11:2368–8. doi: 10.1158/2159-8290.CD-RW2021-113

25. Sun Y, Chen W, Torphy RJ, Yao S, Zhu G, Lin R, et al. Blockade of the CD93 pathway normalizes tumor vasculature to facilitate drug delivery and immunotherapy. *Sci Transl Med* (2021) 13:eabc8922. doi: 10.1126/scitranslmed.abc8922

26. Li T, Fan J, Wang B, Traugh N, Chen Q, Liu JS, et al. TIMER: a web server for comprehensive analysis of tumor-infiltrating immune cells. *Cancer Res* (2017) 77:e108–10. doi: 10.1158/0008-5472.CAN-17-0307

27. Tang Z, Kang B, Li C, Chen T, Zhang Z. GEPIA2: an enhanced web server for large-scale expression profiling and interactive analysis. *Nucleic Acids Res* (2019) 47:W556–60. doi: 10.1093/nar/gkz430

28. Chandrashekar DS, Bashel B, Balasubramanya SAH, Creighton CJ, Ponce-Rodriguez I, Chakravarthi BVSK, et al. UALCAN: a portal for facilitating tumor subgroup gene expression and survival analyses. *Neoplasia* (2017) 19:649–58. doi: 10.1016/j.neo.2017.05.002

29. Franz M, Rodriguez H, Lopes C, Zuberi K, Montojo J, Bader GD, et al. GeneMANIA update 2018. *Nucleic Acids Res* (2018) 46:W60–4. doi: 10.1093/nar/gky311

30. Chen B, Khodadoust MS, Liu CL, Newman AM, Alizadeh AA. Profiling tumor infiltrating immune cells with CIBERSORT. In: von Stechow L, editor. *Cancer systems biology. methods in molecular biology*. New York, NY: Springer New York (2018). p. 243–59. doi: 10.1007/978-1-4939-7493-1_12

31. Llovet J, Brú C, Bruix J. Prognosis of hepatocellular carcinoma: the BCLC staging classification. *Semin Liver Dis* (1999) 19:329–38. doi: 10.1055/s-2007-1007122

32. Rebouissou S, Nault J-C. Advances in molecular classification and precision oncology in hepatocellular carcinoma. *J Hepatol* (2020) 72:215–29. doi: 10.1016/j.jhep.2019.08.017

33. Kulik L, El-Serag HB. Epidemiology and management of hepatocellular carcinoma. *Gastroenterology* (2019) 156:477–491.e1. doi: 10.1053/j.gastro.2018.08.065

34. Pinter M, Scheiner B, Peck-Radosavljevic M. Immunotherapy for advanced hepatocellular carcinoma: a focus on special subgroups. *Gut* (2021) 70:204–14. doi: 10.1136/gutjnl-2020-321702

35. Sim H-W, Knox J. Hepatocellular carcinoma in the era of immunotherapy. *Curr Problems Cancer* (2018) 42:40–8. doi: 10.1016/j.currproblcancer.2017.10.007

36. Yang JD, Hainaut P, Gores GJ, Amadou A, Plymoth A, Roberts LR. A global view of hepatocellular carcinoma: trends, risk, prevention and management. *Nat Rev Gastroenterol Hepatol* (2019) 16:589–604. doi: 10.1038/s41575-019-0186-y

37. Llovet JM, Montal R, Sia D, Finn RS. Molecular therapies and precision medicine for hepatocellular carcinoma. *Nat Rev Clin Oncol* (2018) 15:599–616. doi: 10.1038/s41571-018-0073-4

38. Kao Y-C, Jiang S-J, Pan W-A, Wang K-C, Chen P-K, Wei H-J, et al. The epidermal growth factor-like domain of CD93 is a potent angiogenic factor. *PloS One* (2012) 7:e51647. doi: 10.1371/journal.pone.0051647

39. Galvagni F, Nardi F, Maida M, Bernardini G, Vannuccini S, Petraglia F, et al. CD93 and dystroglycan cooperation in human endothelial cell adhesion and migration. *Oncotarget* (2016) 7:10090–103. doi: 10.18632/oncotarget.7136

40. Barbera S, Lugano R, Pedalina A, Mongiat M, Santucci A, Tosi GM, et al. The c-type lectin CD93 controls endothelial cell migration via activation of the rho family of small GTPases. *Matrix Biol* (2021) 99:1–17. doi: 10.1016/j.matbio.2021.05.006

41. Olsen RS, Lindh M, Vorkapic E, Andersson RE, Zar N, Löfgren S, et al. CD93 gene polymorphism is associated with disseminated colorectal cancer. *Int J Colorectal Dis* (2015) 30:883–90. doi: 10.1007/s00384-015-2247-1

42. Yi X, Zheng X, Xu H, Li J, Zhang T, Ge P, et al. IGFBP7 and the tumor immune landscape: a novel target for immunotherapy in bladder cancer. *Front Immunol* (2022) 13:898493. doi: 10.3389/fimmu.2022.898493

43. Bohlson S, Greenlee M, Sullivan S. CD93 and related family members: their role in innate immunity. *CDT* (2008) 9:130–8. doi: 10.2174/138945008783502421

44. Tarr J, Eggleton P. Immune function of C1q and its modulators CD91 and CD93. *Crit Rev Immunol* (2005) 25:305–30. doi: 10.1615/CritRevImmunol.v25.i4.40

45. Raedler D, Ballenberger N, Klucker E, Böck A, Otto R, Prazeres da Costa O, et al. Identification of novel immune phenotypes for allergic and nonallergic childhood asthma. *J Allergy Clin Immunol* (2015) 135:81–91. doi: 10.1016/j.jaci.2014.07.046

46. Baines KJ, Wood LG, Gibson PG. The nutrigenomics of asthma: molecular mechanisms of airway neutrophilia following dietary antioxidant withdrawal. *OMICS: A J Integr Biol* (2009) 13:355–65. doi: 10.1089/omi.2009.0042

47. Noorolyai S, Shajari N, Baghbani E, Sadreddini S, Baradaran B. The relation between PI3K/AKT signalling pathway and cancer. *Gene* (2019) 698:120–8. doi: 10.1016/j.gene.2019.02.076

48. Atefi M, Avramis E, Lassen A, Wong DJL, Robert L, Foulad D, et al. Effects of MAPK and PI3K pathways on PD-L1 expression in melanoma. *Clin Cancer Res* (2014) 20:3446–57. doi: 10.1158/1078-0432.CCR-13-2797

49. Liu M, Wei F, Wang J, Yu W, Shen M, Liu T, et al. Myeloid-derived suppressor cells regulate the immunosuppressive functions of PD-1–PD-L1+ bregs through PD-L1/PI3K/AKT/NF-κB axis in breast cancer. *Cell Death Dis* (2021) 12:465. doi: 10.1038/s41419-021-03745-1

50. Stutvoet TS, Kol A, Vries EG, Bruyn M, Fehrmann RS, Terwisscha van Scheltinga AG, et al. MAPK pathway activity plays a key role in PD-L1 expression of lung adenocarcinoma cells. *J Pathol* (2019) 249:52–64. doi: 10.1002/path.5280

51. Riether C, Radpour R, Kallen NM, Bürgin DT, Bachmann C, Schürch CM, et al. Metoclopramide treatment blocks CD93-signaling-mediated self-renewal of chronic myeloid leukemia stem cells. *Cell Rep* (2021) 34:108663. doi: 10.1016/j.celrep.2020.108663

frontiers | Frontiers in Immunology

TYPE Original Research
PUBLISHED 14 August 2023
DOI 10.3389/fimmu.2023.1202150

OPEN ACCESS

EDITED BY
Takaji Matsutani,
Repertoire Genesis, Inc., Japan

REVIEWED BY
Howard A. Young,
National Cancer Institute at Frederick (NIH), United States
Leonidas Salichos,
New York Institute of Technology, United States
Nayiyuan Wu,
Central South University, China

*CORRESPONDENCE
Wei Li
lw6666gx@aliyun.com

RECEIVED 07 April 2023
ACCEPTED 17 July 2023
PUBLISHED 14 August 2023

CITATION
Wei X, Ruan H, Zhang Y, Qin T, Zhang Y, Qin Y and Li W (2023) Pan-cancer analysis of IFN-γ with possible immunotherapeutic significance: a verification of single-cell sequencing and bulk omics research. *Front. Immunol.* 14:1202150. doi: 10.3389/fimmu.2023.1202150

Pan-cancer analysis of IFN-γ with possible immunotherapeutic significance: a verification of single-cell sequencing and bulk omics research

Xiaoying Wei[1], Hanyi Ruan[2], Yan Zhang[2], Tianyu Qin[2], Yujie Zhang[2], Yan Qin[1] and Wei Li[1]*

[1]Department of Health Management, The People's Hospital of Guangxi Zhuang Autonomous Region and Research Center of Health Management, Guangxi Academy of Medical Sciences, Nanning, China, [2]Department of Oncology, Guangxi Medical University Cancer Hospital, Nanning, China

Background: Interferon-gamma (IFN-γ), commonly referred to as type II interferon, is a crucial cytokine that coordinates the tumor immune process and has received considerable attention in tumor immunotherapy research. Previous studies have discussed the role and mechanisms associated with IFN-γ in specific tumors or diseases, but the relevant role of IFN-γ in pan-cancer remains uncertain.

Methods: TCGA and GTEx RNA expression data and clinical data were downloaded. Additionally, we analyzed the role of IFN-γ on tumors by using a bioinformatic approach, which included the analysis of the correlation between IFN-γ in different tumors and expression, prognosis, functional status, TMB, MSI, immune cell infiltration, and TIDE. We also developed a PPI network for topological analysis of the network, identifying hub genes as those having a degree greater than IFN-γ levels.

Result: IFN-γ was differentially expressed and predicted different survival statuses in a majority of tumor types in TCGA. Additionally, IFN-γ expression was strongly linked to factors like infiltration of T cells, immune checkpoints, immune-activating genes, immunosuppressive genes, chemokines, and chemokine receptors, as well as tumor purity, functional statuses, and prognostic value. Also, prognosis, CNV, and treatment response were all substantially correlated with IFN-γ-related gene expression. Particularly, the IFN-γ-related gene STAT1 exhibited the greatest percentage of SNVs and the largest percentage of SNPs in UCEC. Elevated expression levels of IFN-γ-related genes were found in a wide variety of tumor types, and this was shown to be positively linked to drug sensitivity for 20 different types of drugs.

Conclusion: IFN-γ is a good indicator of response to tumor immunotherapy and is likely to limit tumor progression, offering a novel approach for immunotherapy's future development.

KEYWORDS

IFN-γ, tumor microenvironment, immunotherapy, pan-cancer, single-cell transcriptome sequencing

Introduction

Cancer is one of the most feared diseases of the 21st century and has been rapidly increasing in prevalence over the past few decades. This can be attributed to changes in our lifestyles, habits, and the fact that people are living longer. As a result, cancer has become a major threat to human life and health. In the field of cancer treatment, there is now a strong focus on preserving the immune system, which has led to numerous advancements and breakthroughs in the area of immunotherapy. Some of the advanced immunotherapeutic strategies being employed today include the transfer of isolated activated T cells, the use of immunomodulatory monoclonal antibodies (MABs), and the development of cancer vaccines (1).

Cytokines (CK) are a class of proteins with a small molecular weight (typically <30kDa) and diverse biological functions. They are produced and released by immune cells as well as certain non-immune cells (such as fibroblasts, epidermal cells, and endothelial cells) in response to stimulation (2, 3). CKs are crucial components of the immune system and play a vital role in regulating both pathological conditions (such as cancer and autoimmune diseases) and maintaining physiological immunological balance (4, 5). CKs can be categorized into groups such as tumor necrosis factor (TNF), interferon (IFN), colony-stimulating factor (CSF), and interleukin (IL).When CKs bind to their respective receptor subunits, signaling is initiated through the formation of dimers or oligomers. This activation leads to the stimulation of pathways involving signal transducers and activators of transcription (STATs) and Janus kinases (JAKs). Additionally, specific gene expression programs and biological processes are activated (6, 7). The clustering of receptors triggers the activation of various kinases, which then phosphorylate tyrosine and serine residues in the cytoplasmic structural domain of the receptor. This phosphorylation event further activates transcriptional regulators, facilitating nuclear translocation and modulation of gene expression. Consequently, these processes exert the corresponding biological effects (8, 9).

Interferon-γ (IFN-γ), the sole member of the type II interferon family, plays a critical role as a cytokine. It is released by activated T lymphocytes, natural killer cells (NK), and γδT cells within the tumor microenvironment (TME). IFN-γ exhibits cytostatic, pro-apoptotic, and immune-inducing effects. Moreover, it performs a fundamental function in coordinating the anti-tumor immune process (10, 11). In addition to its function in the activation of cellular immunity and the enhancement of anti-tumor immunity, active IFN-γ signaling is linked to apoptosis and the arrest of the cell cycle in human cancer cells, both of which have the potential to have a direct impact on the fight against cancer (12). The role of IFN-γ in anti-tumor activities is best illustrated by the process known as cancer immunoediting. IFN-γ can induce multiple immunomodulatory pathways to achieve antitumor effects during the elimination phase of immunoediting as well as to maintain immune homeostasis (13). However, malignant tumor cells can also use IFN-γ as an inducer to suppress anti-tumor immunity and achieve immune escape of tumor cells *in vivo* (13, 14). Numerous research reports have demonstrated that active IFN-γ signaling is a characteristic that is shared by most tumors in the IFN-γ-tumor relationship through targeting cytotoxic T lymphocyte-associated antigen-4 (CTLA-4) and programmed cell death protein 1/programmed cell death 1 ligand 1 (PD-1/PD-L1) antibodies when subjected to immune checkpoint blockade (ICB) (15, 16). IFN-γ promotes the expression of the immunosuppressive metabolite indoleamine2,3-dioxygenase (IDO) in tumor cells and host bone marrow cells by driving the upregulation of PD-L1 in these cells, thus suppressing tumor-specific T cells and contributing to the development of an immunosuppressive TME (13).

Although the anti-cancer effects of IFN-γ have been demonstrated in various tumor studies, there is still a lack of research exploring its properties and mechanisms in pan-cancer. Additionally, there has been limited investigation into the positive and negative effects of IFN-γ in the anti-tumor process. To address this gap, we conducted a pan-cancer analysis using the Genotype-Tissue Expression (GTEx) and the Cancer Genome Atlas (TCGA) databases. This analysis focused on genes associated with IFN-γ across a range of tumors, examining their expression levels, prognostic outcomes, immune infiltration, tumor purity, single-cell levels, and tumor markers. By doing so, we aimed to provide valuable insights into the potential application of IFN-γ in tumor immunotherapy, expanding our understanding of its involvement in anti-cancer mechanisms.

Method

Data collection

We downloaded TCGA and GTEx RNA expression and clinical data by using the UCSC XENA database (http://xena.ucsc.edu/). TCGA (https://portal.gdc.cancer.gov/) is a platform with a sample size of over 10,000 and contains data on 33 common tumors and follow-up data (17, 18). Supplementary Table 1 displayed the full and abbreviated tumor names. TCGA was searched for methylation data and copy number variation (CNV). From the TCGA dataset, we retrieved RNA-Seq data that was presented in the form of transcripts per million (TPM). Additionally, we used the GTEx dataset for gene expression analysis in non-cancer tissues (19).

Evaluation of IFN-γ scores

IFN-γ-related gene was derived from Ayers et al (20). In their study, the IFN-γ 10 gene signature was identified based on data from different clinical studies using a learning-validation model. Calculation of IFN-γ scores based on single-sample gene-set enrichment analysis (ssGSEA) for the quantification of expression levels of these genes in each cancer (21). ssGSEA uses a method similar to GSEA enrichment analysis in which the enrichment score of the target gene set is calculated by ranking the target genes among the total genes. ssGSEA converts the gene expression profile of a single sample into a gene set enrichment profile. The enrichment score of a gene set represents the activity level of a biological process

that is synergistically upregulated or downregulated by the members of the gene set. This transformation allows researchers to characterize cell states in terms of the activity levels of biological processes and pathways, rather than by the expression levels of individual genes (22).

Construction of IFN-γ regulation Network and protein-protein interaction (PPI) analysis

Analysis of protein-protein interactions (PPI) was conducted on the IFN-γ-related genes after they were imported into the STRING database (https://string-db.org/). After downloading the txt file, an Excel copy of it was made for annotation purposes, after which it was imported into the Cytoscape program to develop the PPI network for the core genes. Cytoscape's network analysis feature was utilized to examine the topology of the network, and genes with degrees greater than IFN-γ were considered hub genes.

The analysis of IFN-γ function at the single-cell level

We investigated the association of IFN-γ with functional status in many malignancies utilizing the CancerSEA database. Single-cell analysis of 14 functional statuses of 10 IFN-γ-related genes across tumor types was conducted utilizing the Cancer Single Cell State Atlas (CancerSEA) database (http://biocc.hrbmu.edu.cn/CancerSEA/).

Single-cell transcriptome sequencing data analysis

Single-cell transcriptome sequencing data (GSE152938) was downloaded form GEO database. Prior literature has outlined the steps used to prepare single-cell suspensions (23). In brief, cold Hank's Balanced Salt Solution was utilized to transport freshly isolated tumor samples from the operating room to the lab (HBSS; Gibco, C11875500BT). Afterward, the samples were rinsed and sliced into 2-4 mm sections. For 30 minutes, several species of tissue were gently agitated in a digesting solution comprised of HBSS at 37°C. Before single-cell sequencing, samples were washed and filtered to remove red blood cells and determine cell viability. Two samples of kidney clear cell carcinoma (KIRC) were obtained from patients who underwent radical nephrectomy. Hiseq X10 (Illumina, San Diego, California) with standard settings was utilized to sequence all the samples. CellRanger (v3.0.2) was utilized to transform preliminary sequencing data (.bcl) into FASTQ files. To perform quality control (QC) and secondary analysis, we employed the R programming language (v3.5.2) together with the Seurat R package (v3.1.1). The GEO database (GSE152938) contains the datasets derived by single-cell sequencing (24).

Paraffin-embedded tissue collection

The matched malignancies and paracancerous tissues used in this study were derived from a total of 43 patients with breast cancer. Patients received a definite breast cancer diagnosis but had not yet undergone any kind of chemotherapy or radiotherapy. All patients were granted their written consent to participate. The affiliated Cancer Hospital of Guangxi Medical University's Ethics and Anthropology Committee granted its approval to the present research. All procedures and tests were carried out in conformity with all applicable guidelines and regulations.

Immunohistochemical staining of paraffin sections

The immunohistochemistry detection kit (EliVision plus) and DAB staining kit were purchased from Maixin Biotechnology Company in Fuzhou, China. Formalin was utilized to preserve all the tumor samples. To prepare the tissues for staining, they were first sectioned to a thickness of 5 micrometers and then put on glass slides, followed by routine dehydration, paraffin embedding, and consecutive sectioning with a thickness of 4μm. Deparaffinization was done using xylene, followed by gradient ethanol hydration. EDTA high-temperature high-pressure antigen retrieval, DAB staining, and counterstaining with hematoxylin were performed. The primary antibody was diluted at a concentration of 1:1000. Immunohistochemical staining was performed using the EnVision two-step method, and all experimental procedures strictly followed the instructions provided with the kit.

Survival analysis

Utilizing the R software, we carried out analyses of univariate Cox regression and Kaplan-Meier (KM) survival. The relevance of IFN-γ expression to patients with various cancers was assessed by using measurements of progression-free interval (PFI), disease-specific survival (DSS), and overall survival (OS) (25). Furthermore, both KM curves and univariate Cox proportional hazards regression were utilized to derive p-values, 95% confidence intervals (CIs), and hazard ratios (HRs) (26).

Correlation analysis between IFN-γ expression and immunity

Both tumor mutational burden (TMB) and microsatellite instability (MSI) have been proven in previous research to play a role in the prevention and treatment of tumors (27). TMB is a biological marker of immune response that characterizes the number of mutations that have occurred in tumor cells (28), calculated as the total number of errors in somatic gene coding, base substitution, gene insertions, or deletion that can be identified per million bases (29). The TMB score was determined by dividing

the sum of mutations by the size of the exome (the size of an exome was determined at 38 MB). MSI, induced by MMR defects, is related to patient prognosis (30). Data on somatic mutations were collected from TCGA (https://tcga.xenahubs.net) and used to compute MSI scores for all samples.

Furthermore, utilizing the TIMER database (http://cistrome.org/TIMER/), we examined the link between IFN-γ and tumor-infiltrating immune cells (TIICs). Through the use of ssGSEA, we studied how IFN-γ is linked to other immune-related factors such TIICs, immune-activating genes, immune suppressor genes, chemokines, and chemokine receptors. The immune score is a representation of the number of immune cells that have infiltrated the tumor tissue.

Tumor immune dysfunction and exclusion score analysis

TIDE is a mathematical framework that integrates and models data from 33,197 samples collected from 189 human cancer studies. When applied to malignancies, TIDE simulates the immune evasion mechanism by dampening the function of T cells in cancers with high cytotoxic T cell (CTL) infiltration and inhibiting the infiltration of T cells in tumors with lower CTL infiltration (31, 32). Following the tagging of defective markers on T cells, how the expression of certain genes in the tumor interacts with the amount of CTL infiltration was analyzed to determine how it will affect patient survival (33). TIDE is an effective predictor of ICBF response, and patients exhibiting elevated TIDE scores have a higher risk of the tumor evading the immune system. Consequently, they have a low likelihood of responding favorably to the ICBF scheme.

Drug sensitivity analysis

The Genomics of Drug Sensitivity in Cancer (GDSC) database was searched to obtain the data on the cell lines (n = 860), genes (n = 17419), and small molecules (n = 265). Using the methodology developed by Rees et al., we investigated the degree to which gene expression is correlated with drug responsiveness (34). The half maximum inhibitory concentration (IC50) values for medications as well as gene expression patterns for each tumor cell line were obtained from the GDSC. Calculations were made to determine the Pearson correlation coefficients between the transcript levels and the IC50 value (24).

Statistical analysis

The raw data obtained from TCGA and GTEx RNA were subjected to log2 transformation for normalization before further analysis. The Spearman correlation test was performed to assess the associations between gene expressions, and a significance level of $P < 0.05$ was used as the threshold for determining significant correlations. The Student's t-test was utilized to compare the differences in gene expression levels between normal and cancerous tissues. Kaplan-Meier (KM) survival curves were employed to evaluate the prognostic significance of the analyzed indexes. Cox proportional risk regression models were used to calculate adjusted risk ratios. A significance level of $P < 0.05$ was considered statistically significant.

Result

Differentially expressed IFN-γ-related genes in pan-carcinoma and their effect on prognosis

The Supplementary Figure 1 shows the flow chart of this study. Initially, we conducted an analysis of gene expression profiles associated with IFN-γ in various cancers and observed variations in their expression levels across different tumor types. Using a heat map, we examined the expression of 10 IFN-γ-associated genes in 33 distinct cancer types and discovered discrepancies in gene expression within the same tumor as well as across different tumor types. Notably, TGCT, LUSC, LUAD, KIRC, HNSC, DLBC, and CHOL exhibited high expression of the studied genes, while UVM, PCPG, LGG, KICH, and ACC showed low expression (Figure 1A). In terms of prognostic implications, we found that high expression of most of the selected 10 genes was associated with shortened progression-free survival (PFS), overall survival (OS), and disease-free survival (DSS) in patients with LGG and UVM, indicating increased risk. Conversely, SKCM patients with high gene expression had higher DSS, OS, and PFS, suggesting a protective effect (all $P < 0.05$). Additionally, high STAT1 expression was linked to higher DSS and OS in patients with PAAD or ACC (Figure 1B). These findings indicate that the expression of IFN-γ-associated genes is correlated with the prognosis of tumor patients, with the correlation depending on the specific tumor type.

Analysis of IFN-γ-related genes and gene mutations

To investigate the impact of gene mutations on gene expression, we analyzed the mutation status of IFN-γ-related genes in different tumors. Our study examined the genetic variations of genes associated with IFN-γ in 33 distinct cancers and found that in most malignancies, these genes were associated with copy number variation (CNV). Among the 9 genes we investigated, heterozygous amplification and heterozygous deletion were the most common mutations observed in the 33 distinct cancers. Specifically, heterozygous amplification was the most prevalent CNV type in IDO1, STAT1, and IFNG, while heterozygous deletion was the main CNV type for CCR5, CXCL11, CXCL10, CXCL9, PRF1, and GZMA across 25 tumors. Additionally, in cases of adrenocortical carcinoma (ACC), heterozygous amplification was the primary type of CNV (Figure 2A).

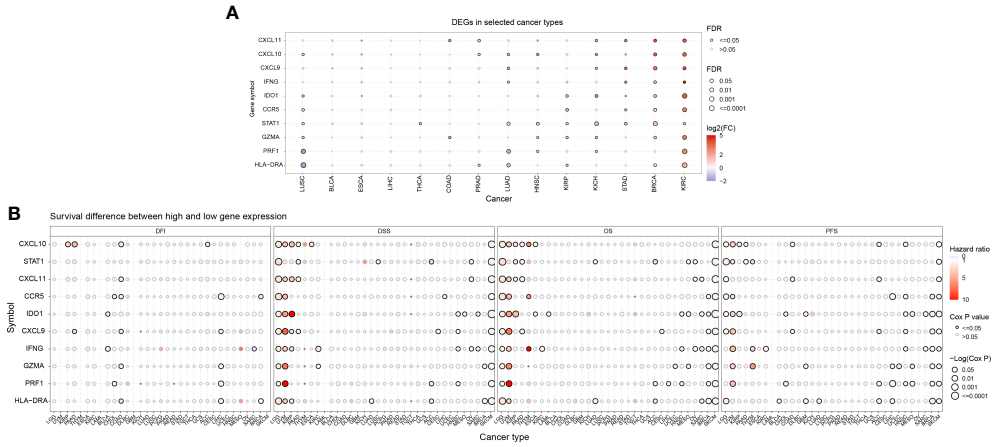

FIGURE 1
Prognostic significance of differential IFN-γ-related genes (IFN-γ-RGs) in various cancers. **(A)** Expression analysis of IFN-γ-RGs in 33 different types of cancer. Red indicates high expression genes, blue indicates low expression genes. **(B)** Survival differences between high and low gene expression levels. Red indicates high hazard ratio (HR). The size of the circles represents the significance level, with larger circles indicating lower p-values.

Furthermore, we conducted additional research to explore the relationship between relative linear copy number values and the mRNA expression levels of genes associated with IFN-γ. Our data revealed a strong positive correlation between the expression of CCR5, GZMA, IDO1, and PRF1 and CNV in both lung squamous cell carcinoma (LUSC) and head and neck squamous cell carcinoma (HNSC). Conversely, we observed a strong negative correlation between the expression of CXCL9, CXCL10, and CXCL11 and CNV in kidney renal papillary cell carcinoma (KIRP), which is a significant finding (Figure 2B). Additionally, we found a strong and favorable correlation between the expression of STAT1 and CNV.

We examined the mutations and types of variation in IFN-γ-related genes in each cancer type and discovered that uterine corpus endometrial carcinoma (UCEC) had the highest percentage (33%) of single nucleotide variations (SNVs) in STAT1, followed by skin cutaneous melanoma (SKCM), colon adenocarcinoma (COAD), stomach adenocarcinoma (STAD), rectum adenocarcinoma (READ), bladder urothelial carcinoma (BLCA), LUSC, and lung adenocarcinoma (LUAD). CASP1 had a high proportion of SNVs

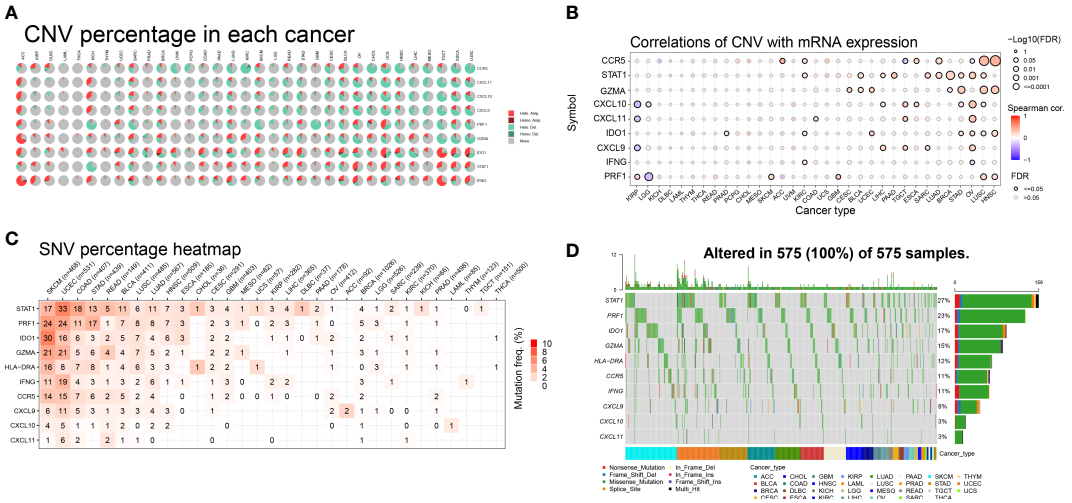

FIGURE 2
Pie charts illustrating the copy number variation (CNV) distribution of IFN-γ-related genes (IFN-RGs) in 33 different cancers. **(A)** Each CNV pie chart shows the relative frequency of homozygous/heterozygous IFN-γ-RG combinations in each tumor type. Different colored sections represent different CNV types. **(B)** Association between CNV and mRNA expression. The size of the dots represents the statistical significance, with larger dots indicating higher significance. P-values have been adjusted by false discovery rate (FDR) correction. **(C)** Color shading represents the intensity of mutation frequency. The size of the numbers indicates how frequently the associated mutated genes occur in a given tumor sample. No number indicates no mutation of that gene anywhere, "0" indicates no mutation in the coding region of the gene. **(D)** SNV Oncoplot. The side and top bar plots show the number of variations among samples or genes.

in UCEC, SKCM, LUSC, BLCA, and LUAD. In both SKCM and UCEC, the incidence of SNVs was higher in STAT1, PRF1, IDO1, GZMA, HLA-DRA, IFNG, and CCR5. The proportion of SNVs in CXCL10 and CXCL11 was lower (Figure 2C). These 10 genes mentioned above were the most common targets of missense mutations in pan-cancer single nucleotide polymorphisms (SNPs). The frequency of gene alterations was highest in patients with UCEC and SKCM, followed by those with STAD, COAD, BLCA, and pancreatic adenocarcinoma (PAAD). STAT1 had the highest proportion of SNPs (27%), followed by PRF1 (23%), IDO1 (17%), and GZMA (15%) (Figure 2D). These findings suggest that IFN-γ-related genes have a high frequency of mutations in various tumors and have the potential to be targeted further as therapeutic molecules.

Differential analysis of methylation of IFN-γ-related genes in pan-cancer

Abnormal DNA methylation may lead to abnormal gene expression and an increased risk of cancer. We studied the differential methylation of IFN-γ-related genes in 13 distinct types of cancers to learn more about how these genes impact tumorigenesis and uncover the mechanism of aberrant expression of these genes. IDO1 had high methylation levels in KIRP, LUAD, THCA, and ESCA, and significantly low methylation levels in LUSC and BRCA. Among the 10 genes studied, almost all of them showed low methylation levels in BRCA, KIRC, LIHC, and HNSC. Among 13 kinds of tumors, STAT1, IFNG, and CCR5 showed low methylation levels in BRCA, KIRC, LIHC, HNSC, UCEC, and BLCA (Figure 3A). For comprehending the relationship between methylation and IFN-γ mRNA expression, we discovered a strong inverse correlation in 31 cancer subtypes. Methylation was inversely associated with the expression of PRF1, CCR5, STAT1, GZMA, HLA-DRA, and CXCL10 in these malignancies. Conversely, methylation was positively linked to IDO1 expression in BRCA, THCA, SKCM, CESC, LUAD, PAAD, HNSC, STAD, BLCA, LIHC, COAD, READ, and ESCA (Figure 3B). These results suggest that the aberrant expression of IFN-γ-related genes is partly due to aberrant methylation regulation.

Differential expression of IFN-γ score and its association with tumor staging

Firstly, we found a positive link between genes associated with IFN-γ ($p<0.05$), indicating a close association between IFN-γ-RGs (Figure 4A). We also assessed the IFN-γ score between tumor and normal specimens for 33 malignancies using data from GTEx and TCGA. In contrast with normal samples, IFN-γ scores were remarkably elevated in carcinoma tissue samples, including in UCS, BRCA, UCEC, COAD, TGCT, OV, LIHC, LAML, PAAD, KIRC, PRAD, GBM, LGG, READ, ESCA, SKCM, DLBC, STAD, CESC, THCA, BLCA, and ACC. Twenty-two of thirty-three tumors had IFN-γ scores that were greater than those of normal tissues, implying that the inflammatory response in cancerous tissues was greatly enhanced (Figure 4B). The IFN-γ scores in pan-cancer at different stages were further investigated. The IFN-γ score was remarkably higher in the early stages of TGTC, HNSC, and COAD (All $P < 0.05$). The score of IFN-γ was higher in the late stage of KIRP (All $P < 0.05$). It can be inferred that IFN-γ may be a breakthrough in the early prevention and treatment of TGTC, HNSC, and COAD (Supplementary Figure 2).

Prognostic significance of IFN-γ score in tumor

We explored the predictive significance of IFN-γ in TCGA pan-cancer. Cox Regression analysis demonstrated that IFN-γ served a protective function among patients with SKCM, SARC, OV, MESO, LUAD, LIHC, HNSC, DLBC, CESC, BRCA, BLCA, THCA, and ACC (All $P< 0.05$, Figure 5A). The findings from DSS analysis confirmed the protective function of IFN-γ in BRCA, THCA, SARC, MESO, OV, CESC, LUAD, SKCM, BLCA, and ACC (All $P< 0.05$, Figure 5B). The findings from PFI analysis illustrated the protective

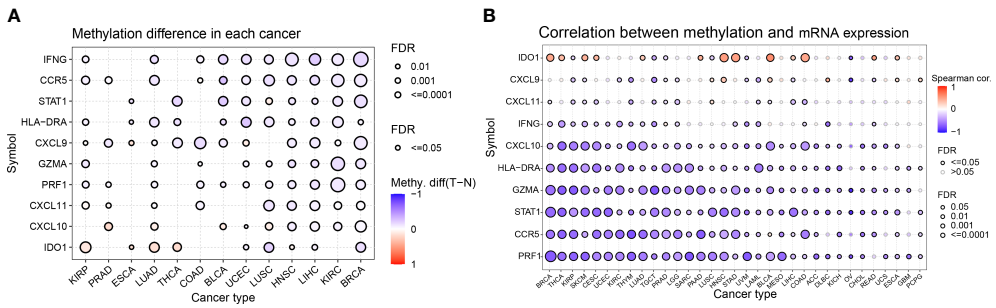

FIGURE 3
Differential methylation analysis of IFN-γ-related genes in pan-cancer. **(A)** Differential methylation of IFN-RGs in 13 different cancers. Different colors represent different methylation levels, red dots indicate higher methylation levels in cancer, blue dots indicate lower methylation levels. **(B)** Association between methylation and mRNA gene expression. Different colored linkages represent different associations, red dots and blue dots represent positive and negative associations, respectively. P-values have been adjusted by FDR correction.

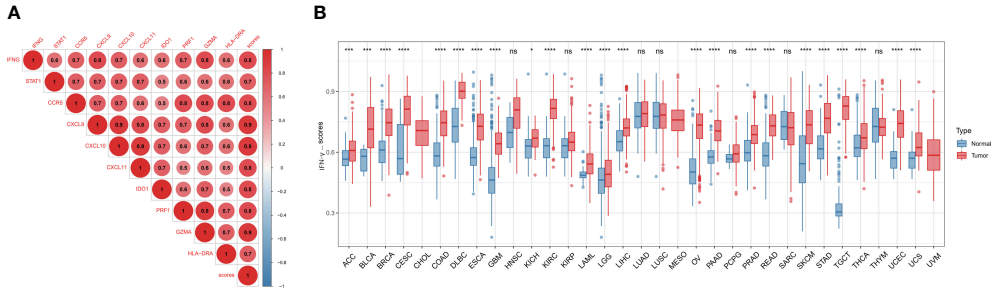

FIGURE 4
Differential expression of IFN-γ scores. **(A)** Association analysis between IFN-γ scores and IFN-γ-related gene expression. The hue of the colors represents the strength of the association, red dots and blue dots represent positive and negative associations, respectively. **(B)** Comparison of IFN-γ scores between 33 different types of tumors and normal tissues. *p < 0.05, ***p < 0.001, ****p < 0.0001, ns, no significance. P-values have been adjusted by FDR correction.

function of IFN-γ in BLCA, SKCM, LUAD, CESC, OV, LIHC, COAD, CHOL, BRCA, SARC, HNSC, and ACC (All P< 0.05, Figure 5C). Higher IFN-γ scores were linked to improved OS in ESCA, KIRC, LUAD, CESC, SARC, SKCM, STAD, and DLBC, as determined by KM analysis (Supplementary Figure 3). In MESO, LUSC, UCS, BRCA, OV, LUAD, CESC, HNSC, SARC, BLCA, SKCM, THCA, and ACC, higher IFN-γ expression was associated with improved OS and DSS (Supplementary Figure 4). Additionally, a longer PFI was associated with higher IFN-γ scores in OV, BLCA, STAD, HNSC, SKCM, CESC, LUSC, CHOL, LUAD, MESO, BRCA, COAD, LIHC, AD, and ACC (Supplementary Figure 5). From these findings, the IFN-γ score could improve the predictive significance of classical prognostic markers. Moreover, IFN-γ is strongly linked to the prognosis of many types of malignancies, suggesting that it may have a beneficial influence on the prognosis of patients with these tumors. In addition, we performed GSEA analysis of immune activation genes, immune suppression genes, immune checkpoints, chemokines, chemokine receptor gene sets and compared the variability between cancer and para-cancer (Supplementary Figures 6A–E). The results showed that the above gene set scores were either high or low in the tumors and lacked results similar to the consistency of IFN-γ-related genes. In addition, we performed 20 random samples of 10 genes each time for the above gene sets to obtain 20 random immune gene sets and perform GSEA analysis. The results were similar to previous results in that no gene sets were observed to have a consistent up- or down-regulation trend across tumors (Supplementary Figure 6F). The above results suggest that the expression status of IFN-γ-related genes in tumors is regulated by the biology behind it, and is not a coincidental result that can be obtained by an arbitrary set of immune genes.

Definition of hub genes and immunohistochemistry verification

In order to get the hub gene, the IFN- genes were imported into the Cytoscape program, and then a PPI network diagram was created. The proteins are denoted by the nodes, whereas the strength of the association between these proteins is denoted by the links. As can be seen, there are a total of 19 nodes in the PPI network, as well as 92 connections. The STAT1 gene is deemed to be the hub gene since it has the greatest degree of association (Figure 6). By means of IHC, we compared the expression of STAT1 in breast malignancies and paracancerous tissues and found that

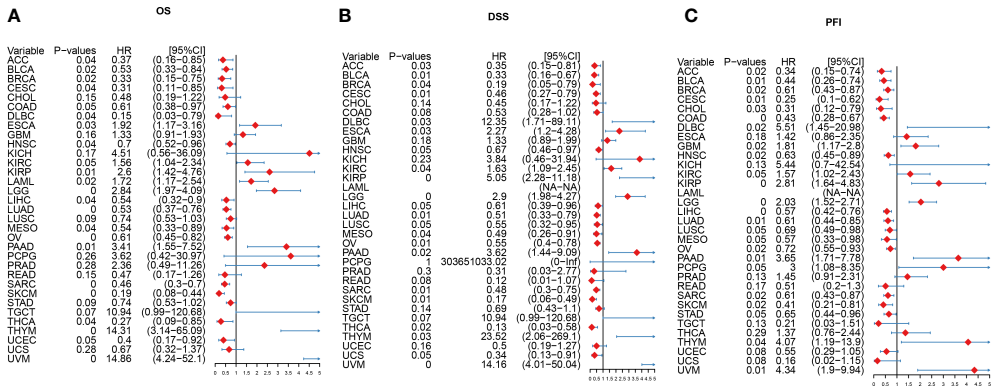

FIGURE 5
Forest plot of the results from univariate Cox regression analysis for IFN-γ. **(A)** Overall survival (OS). **(B)** Disease-specific survival (DSS). **(C)** Progression-free interval (PFI). P-values have been adjusted by FDR correction.

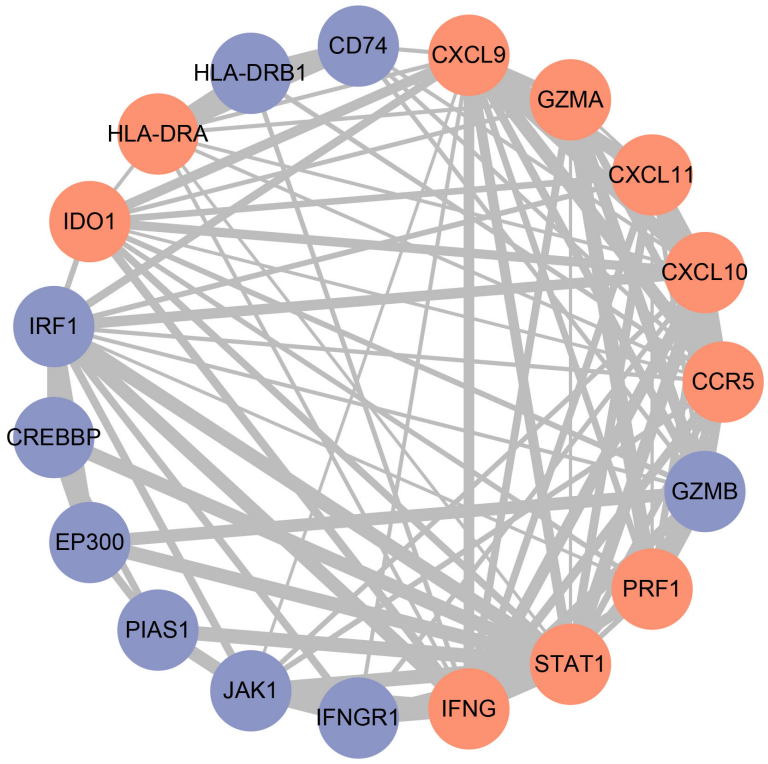

FIGURE 6
Construction of the protein-protein interaction (PPI) network. Red nodes represent IFN-γ-related genes, blue nodes represent other genes. The thickness of the lines indicates the strength of the evidence for the interaction.

STAT1 was considerably overexpressed in the malignant breast tissues (Figure 7, P=4.7e-6), which was in line with the findings of our investigation.

Single-cell functional analysis of IFN-γ

Through examining the CancerSEA dataset, we compared the IFN-γ score to 14 different functional statuses of cancers. In AML, the IFN-γ score was positively correlated with inflammation, invasion, quiescence, differentiation, angiogenesis, metastasis, EMT, and other functions, but negatively correlated with 13 functions in UM. In 11 types of tumors, there was a favorable correlation between the IFN-γ score and proliferation (Figure 8). Combined with the information on drug responsiveness from The Cancer Therapeutics Response Portal database and information on gene expression profiles of tumor cell lines, we found that twenty of thirty drugs' sensitivities were shown to be positively linked to STAT1. IFN-γ-related genes may serve as a target for research into these medications and targeted therapy for cancer (Supplementary Table 2).

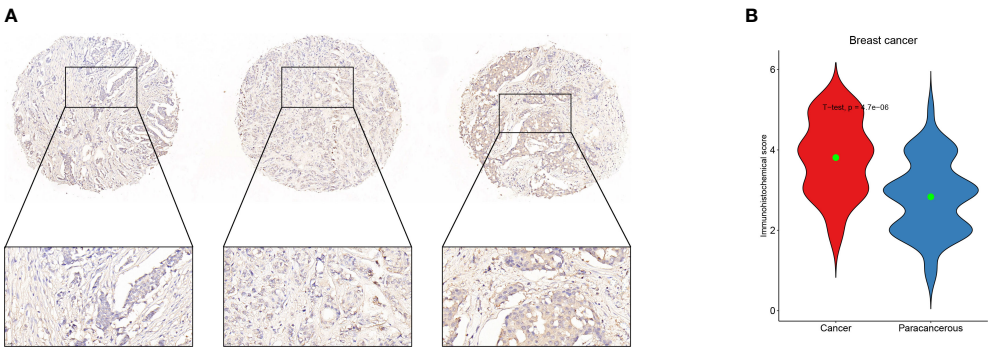

FIGURE 7
Validation of STAT1 expression in breast malignant tumors and adjacent tissues using immunohistochemistry. **(A)** Example of STAT1 expression in breast malignant tumor detected by immunohistochemistry. **(B)** Statistical analysis of STAT1 expression using Student's t-test to represent the mean values.

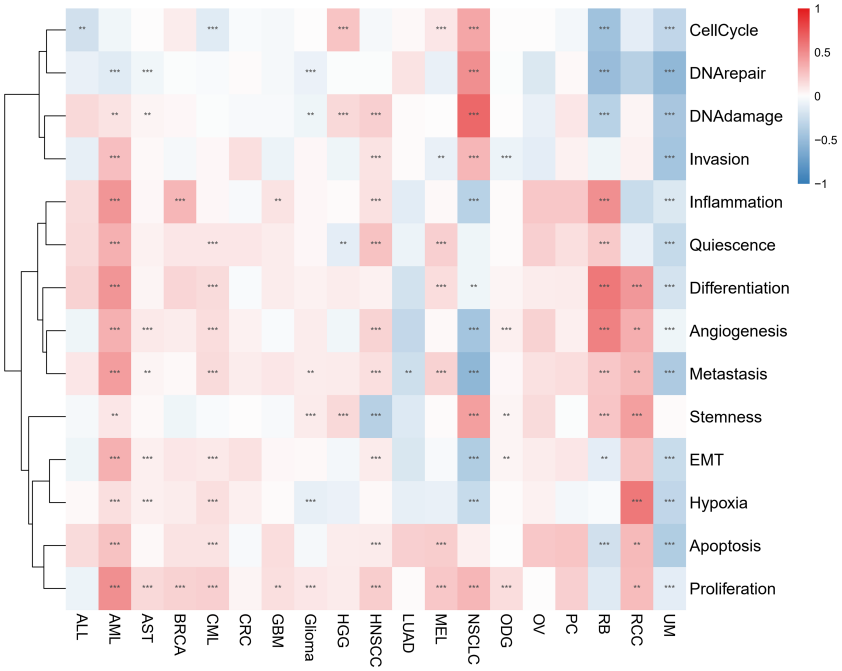

FIGURE 8
Associations between IFN-γ levels and 14 different functional states in various malignancies. Red and blue represent positive and negative associations, respectively. ** represents P<0.01, *** represents P<0.001.

The purity of tumors correlates with levels of IFN-γ

We evaluated 33 different types of tumors for determining associations between IFN-γ score and discovered a positive link between IFN-γ and M1 and M2 Macrophages, T cells follicular helper cells, activated NK cells, and CD8 T cells in most cancers. Also, the IFN-γ score showed an inverse association with T cell CD4 naïve and NK cell resting. (Figure 9). In the analysis of tumor immune score, the IFN-γ score was found to have a positive correlation with the degree of immune cell infiltration in most of the 33 tumors studied (P < 0. 05, Figure 10A, Supplementary Figure 7). For PCPG, LUSC, PAAD, SARC, READ, KIRP, COAD, GBM, UCS, KICH, THYM, CHOL, LGG, and ACC, IFN-γ score was positively linked to stromal cell score (Figure 10B). Additionally, the IFN-γ score had a positive link to the TME score of ACC, SKCM, UVM, THCA, SARC, UCS, KIRC, LGG, KIRP, TGCT, CESC, LIHC, BRCA, LUSC, KICH, LUAD, OV, LAML, READ, BLCA, MESO, HNSC, GBM, CHOL, COAD, UCEC, PAAD, PCPG, DLBC, PRAD, ESCA, STAD, and THYM (All P < 0. 05, Figure 10C). The above results indicate that IFN-γ is closely related to the immune status of tumors.

Association of IFN-γ score with genes involved in immunity

To investigate the involvement of IFN-γ in immune modulation, we investigated whether or not there was a correlation between the IFN-γ score and the presence of ICGs in human malignancies. The results of the association between IFN-γ score and ICG indicated that the IFN-γ scores of virtually all of the different cancers that were investigated had a positive association with the expression of TIGIT, IDO1, ICOS, CD86, CTLA4, HAVCR2, PDCD1LG2, and CD48 (Figure 11A). Further, we analyzed 23 immunosuppression genes for their association with the IFN-γ score. The expression levels of LAG3, TIGIT, CD96, IDO1, PDCD1, HAVCR2, CTLA4, PDCD1LG2, CD244, and CD244 were positively linked to IFN-γ scores in almost all evaluated cancer types. In 13 tumors, the IFN-γ score was inversely linked to VTCN1 expression, whereas in 16 tumors, it was inversely linked to KDR expression (Figure 11B). In 32 different cancers, the IFN-γ score was strongly linked to CD86, CD48, KLRK1, LTA, CD27, TNFSF13B, TNFRSF9, CD40LG, KLRC1, IL2RA, and CD80, out of a total of 46 immune activation genes in pan-cancer (All P < 0. 05, Figure 11C). Simultaneously, we explored the link between IFN-γ score and chemokines. The findings demonstrated a positive link between IFN- score and the expression of CCL5, CXCL11, CXCL9, CXCL10, CCL4, CXCL13, CCL3, CCL8, and CCL2 chemokine genes (Figure 11D). Positive correlations were observed between IFN-γ score and the chemokine receptor genes CXCR6, CCR1, CCR5, CCR2, and CXCR3, and negative correlations with CXCR2, CCR1, CCR9, and CCR10 (Figure 11E) Our results are consistent with previous studies which indicate that immune checkpoint genes (ICGs) perform a remarkable function in regulating the infiltration of immune cells as well as immunotherapy (35).

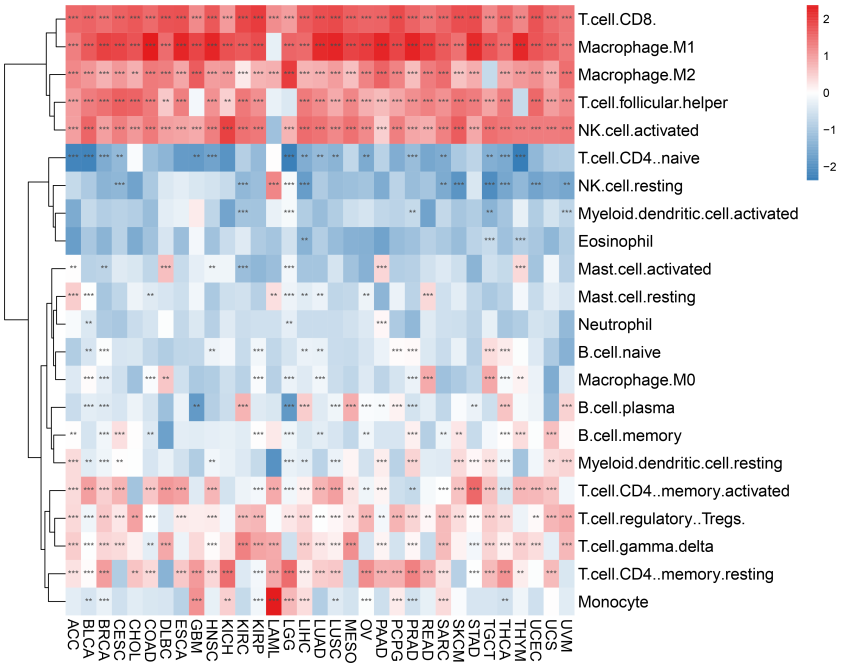

FIGURE 9
Correlation between IFN-γ scores and tumor-infiltrating immune cells. There is a correlation between IFN-γ scores and tumor-infiltrating immune cells in 33 different tumors. Red and blue represent positive and negative correlations, respectively. **p < 0.01, ***p < 0.001.

Correlation between IFN-γ score and immunotherapy response markers

Immunotherapy outcomes may be predicted by monitoring the tumor's immune escape process. For most cancers, we observed a favorable correlation between IFN-γ score and TMB. The TMB was strongly linked to IFN-γ score for PCPG, OV, LGG, LUSC, PRAD, THCA, LAML, COAD, ESCA, SARC, LIHC, CESC, BRCA, KIRP, MESO, PAAD, SKCM, BLCA, KIRC, UCEC, HNSC, KICH, LUAD, and UCS (All P<0.05, Figure 12A). Furthermore, we investigated whether or not the IFN-γ score was related to MSI. A higher IFN-γ score was associated with a lower prevalence of MSI in GBM, ACC, and BRCA (All P<0.05, Figure 12B). TIDE scores, like TMB and PD-L1, are one of the popular markers used to predict the effect of ICB treatment. Low ICB response was recorded in patients with elevated TIDE scores because of the

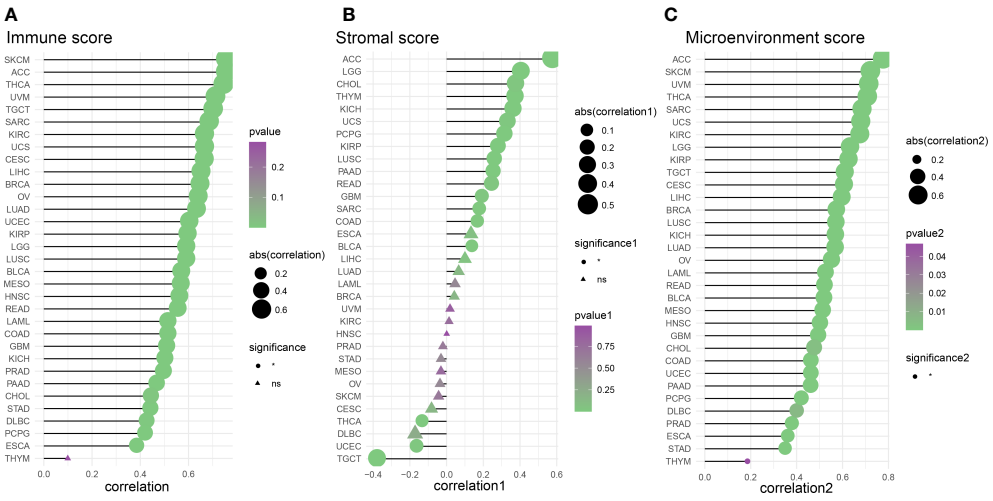

FIGURE 10
Analysis of the correlation between IFN-γ scores and tumor purity. **(A)** Tumor microenvironment score analysis based on the correlation between interferon-gamma levels and immune cell infiltration. **(B)** Tumor immune score analysis based on the correlation between IFN-γ levels and tumor microenvironment scores. **(C)** Analysis of the relationship between IFN-γ and tumor stromal scores (all P<0.05).

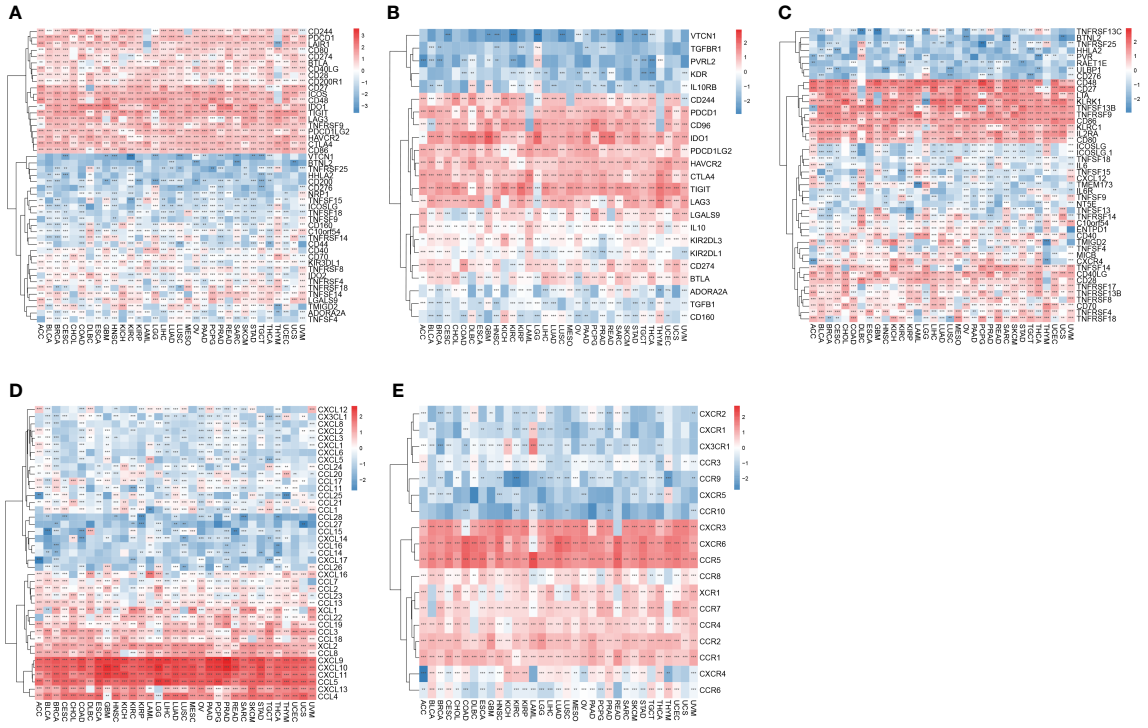

FIGURE 11
Relationship between IFN-γ levels and immune-related genes. **(A)** Association between immune checkpoint status and IFN-γ levels in human malignancies. **(B)** Association between immune inhibitory genes and interferon-gamma scores in human cancers. **(C)** Association between IFN-γ scores and expression of immune activation genes in human tumors. **(D)** Association between chemical factors and IFN-γ levels in human malignancies. **(E)** Association between IFN-γ scores and expression of chemical factor receptors in human tumors. **p < 0.01, ***p < 0.001.

increased risk of tumor immune evasion in these patients. In an examination of 22 cancers, the correlation between TIDE and IFN-γ scores was inverse in all 22 tumors. Evidence like this points to a link between IFN-γ expression and ICB response (Figure 12C, Supplementary Figure 8) This provides a basis for further investigation of whether the genes associated with IFN-γ can be used as potential markers of ICB therapy and modulators of immune checkpoint inhibition therapy.

Single-cell transcriptome analysis of IFN-γ in KIRC tumor microenvironment

Quality control was performed by Seurat, and then 13124 high-quality single-cell transcriptomic data were selected for further analyses. The aforementioned cells may be classified into 11 groups, as determined by a tSNE-based cell clustering analyses: monocyte1, monocyte2, KIRC1, KIRC2, KIRC3, macrophages,

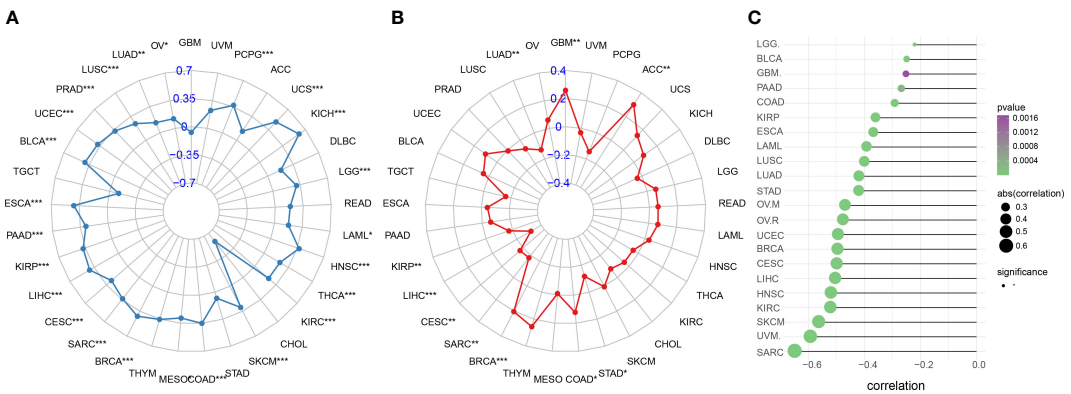

FIGURE 12
Immune therapy response indicators associated with IFN-γ in human malignancies. **(A)** Association between IFN-γ levels and tumor mutation burden in various cancers. **(B)** Association between microsatellite instability and interferon-gamma levels in cancers. **(C)** Association between IFN-γ scores and tumor immune dysfunction and exclusion scores. *p < 0.05, **p < 0.01, ***p < 0.001.

mast cells, endothelial cells, NK cells, CD4+T cells, and CD8+T cells (Figure 13A). Variations in marker gene expression were highly significant across cell types (Supplementary Figure 9). We also discovered that cancerous cells from two independent KIRC samples cluster together into the same cluster (KIRC3) as well as many other distinct clusters (KIRC1 and KIRC2). The above findings demonstrate the heterogeneity within the KIRC cell type (Figure 13B). To assess the variations in IFN-γ scores across cell types, we conducted ssGSEA to summarize the IFN- scores of cells in the KIRC TME. Notably, we found significant differences in IFN-γ scores among different cells (Figure 13C). KIRC cells had the least IFN-γ score, suggesting that this marker more accurately represented the TME than the tumor itself. IFN-γ scores varied significantly across KIRC cell subsets, suggesting that IFN-γ expression is a potential KIRC cell characteristic (Figure 13D). Based on this analysis, it appears that IFN-γ is significantly different among different cells of KIRC TME. As a consequence, targeting IFN-γ could represent a substantial step forward in TME regulation.

Discussion

IFN-γ is a protein that is produced by two polypeptide chains that are linked together in an antiparallel manner and are encoded by the IFNG gene (36). During the innate immune response, natural killer (NK) and natural killer T (NKT) cells are the primary cells involved in regulating IFN-γ synthesis. On the other hand, during the adaptive immunological response, CD8+ and CD4+ T cells are the primary paracrine producers of IFN-γ (37). IFN-γ maintains a steady level of coordination between pro-tumor and anti-tumor immune function in the tumor microenvironment (TME) (38, 39). IFN-γ is implicated in the eradication of cancer by preventing the growth of new blood vessels, suppressing the proliferation of existing cells, enhancing apoptosis, stimulating adaptive immunity, and improving antigen processing and presentation (40). Research indicates that IFN-γ may selectively and dosage-dependently trigger apoptotic death of stem cell-like carcinoma cells in colon cancer patients through JAK-STAT1-IRF1 signal transmission (41). IFN-γ- deficient animals were shown to develop lung epithelial tumors and lymphomas spontaneously, providing additional evidence that IFN-γ is involved in the immunity against tumors and validating IFN-γ's anti-cancer property (42, 43). Other immunosuppressive processes may be activated by IFN-γ because of its ability to induce the synthesis of indoleamine-2,3-dioxygenase (IDO) and immune checkpoint inhibitory molecules (44, 45). IFN-γ is important for cancer immunity and treatment. However, the relationship between IFN-γ and immunity is still the focus of the literature. Therefore, we

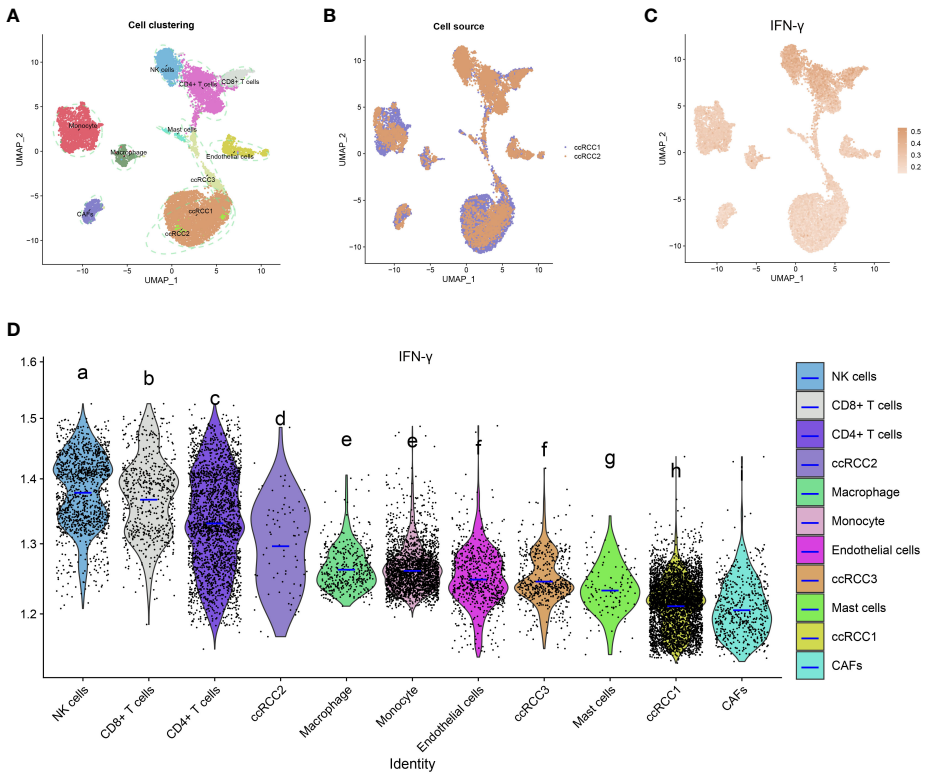

FIGURE 13
IFN-γ in the tumor microenvironment of KIRC. **(A)** t-distributed stochastic neighbor embedding (tSEN) plots showing 11 different cell types in KIRC samples. **(B)** tSEN plots of two KIRC samples. **(C)** IFN-γ scores of different cell types displayed on the tSEN plots. **(D)** Analysis of IFN-γ levels in different cell types in the tumor microenvironment of KIRC. The violin plots show the median of the IFN-γ scores. The letters at the top indicate whether there is a statistically significant difference between two cells. Different letters represent different levels of statistical significance.

conducted a systematic pan-cancer investigation of 10 IFN-γ-related genes using several databases. This research may provide the necessary strategy to maximize the anti-tumor effects of IFN-γ.

First, we analyzed the differential expression of IFN-γ-related genes in 33 tumors and found that these genes were upregulated in most tumors, especially in CESC, GBM, OV, SKCM, and TGCT. Additionally, tissue concentrations of IFN-γ were significantly higher in the cervical tissues of patients with cervical cancer (46). Also, evidence from human esophageal cancer samples demonstrated an increased level of IFN-γ in tumor tissue, which linked favorably to tumor growth and was in line with our findings (47). We analyzed the link between IFN-γ and survival rate to better understand its role in clinical risk stratification. According to the results of the survival study, OS, DSS, and PFI were all linked to IFN-γ overexpression. In the investigation of the prognostic implications of IFN-related gene expression, it was discovered that patients with COAD, LIHC, BRCA, SKCM, ACC, HNSC, and SARC had improved prognoses when IFN-γ expression levels were elevated (all $p<0.05$). In contrast, a worse prognosis was observed in individuals with LGG, UVM, KIRP, PAAD, and THYM who had elevated IFN-γ expression levels (all $p<0.05$). Previous studies found that IFN-γ inhibits the development of squamous cell carcinoma, which provided strong evidence for our findings (48).

We evaluated IFN-γ scores in tumor and normal samples of 33 cancers and found that most tumors had higher IFN-γ scores than normal tissue. INF-γ is a cytokine that promotes inflammation and is proven to be intimately linked to both innate and acquired immune responses (49, 50). Chronic inflammation can induce tumors, and the inflammatory microenvironment of tumors and exposure to tumor antigens trigger the infiltration of immune cells. Thus, IFN-γ scores are elevated in tumors that are closely associated with the inflammatory features of tumors. IFN-γ has antitumor effect. A previous study showed that M1 macrophages can be induced *in vitro* by IFN-γ, which can trigger a rapid pro-inflammatory response, and pathogen clearance and show anti-tumor activity (51). IFN-γ promotes migration of immune cells to TME by transcriptionally regulating the expression and secretion of CXCL9, CXCL10 and CXCL11 and their cognate receptor CXCR3 in T cells, NK cells, monocytes, DCs and cancer cells. The increase in chemotaxis of activated CTL towards TME enhances cytotoxic effects and limits tumor growth. In addition, IFN-γ can play an anti-tumor role by promoting macrophage activation, up-regulating the expression of antigen processing and presenting molecules, boosting the growth and activation of Th1 cells, facilitating the function of NK cells, and regulating the function of B cells. Therefore, IFN-γ promotes a severe inflammatory response in the tumor and shows a good prognosis. In addition, we observed large variation in IFN-γ scores across tumors, which may be related to differences in the inherent characteristics of different tumors. It has been found that IFN-γ is under transcriptional control and epigenetic control, such as chromosome access, DNA methylation and histone acetylation (52). There is variability in IFN-γ scores because the aforementioned functional activity varies among tumors.

To a large extent, TMB determines the immune response of cancer patients to treatment with immune checkpoint inhibitors (ICIs), either, anti-cytotoxic T cell-associated antigen 4 (CTLA-4) or anti-programmed cell death 1 (PD-1) (53–55). Researchers discovered that TMB has a significant role in tumor immunotherapy success. TMB is a good indicator of the effectiveness of immune checkpoint inhibitor (ICI), with larger values indicating better efficacy (56, 57). Additionally, we evaluated the link between IFN-γ scores and tumor immunity and discovered that, IFN-γ scores were positively correlated with TMB in most tumors. Numerous research reports have demonstrated that tumors with increased TMB are more likely to respond favorably to cancer immunotherapy (58). For instance, among non-small-cell lung cancer(NSCLC) patients treated with anti-PD-1/L1, patients with high TMB had longer associated PFS than those with low TMB (59). We found that IFN-γ scores were inversely linked to TIDE scores in most tumors. The lower the TIDE, the lower the possibility of immune escape, the higher the response rate to ICB treatment, and the better the clinical outcome of immunotherapy (24). Therefore, it can be inferred that IFN-γ is an indicator of a good response to tumor immunotherapy.

We examined the differential methylation of IFN-γ-related genes in 13 distinct cancers. We found variation in methylation patterns across tumors, and this phenomenon is similar to the findings of Saghafinia et al. (60) That may be caused by intrinsic differences in different tumors. In 13 different cancers, we discovered a statistically significant inverse association between the expression of most IFN-γ-related genes and methylation. Our findings were supported by data showing that the transcriptional activity of the entire IFN-γ promoter vector may be suppressed by its methylation (61, 62). Also, DNA hypermethylation in the IFN-γ promoter region was found in a vast number of cervical cancer samples, which may be linked to carcinogenesis in this disease. This suggests that methylation-mediated IFN-γ gene silencing contributes significantly to the mechanism of cervical carcinogenesis (63). However, we observed a significant positive correlation between the methylation level of IDO1 and RNA expression (64). Sailer and others similarly observed a significant positive correlation between IDO1 methylation levels and RNA expression in HNSCC (64). The reason for this phenomenon is mainly that methylation of IDO1 occurs mostly within the gene rather than the CPG island.

However, this research has several drawbacks. The current research only offers preliminary data on the association of IFN-γwith a wide range of tumor progression, and additional experimental work is required to clarify the specific molecular roles and processes of IFN-γ in carcinogenesis. Confirmation of our conclusions requires more research at the molecular and cellular levels. Meanwhile, the specific mechanisms involved in the regulation of immunity by IFN-γ remain unclear. In addition, there is a lack of specific and complete cases from which to draw inferences about the effectiveness of various medications in suppressing tumor development. Since IFN-γ processing can enhance tumor immunity by increasing T-cell and macrophage activity (65, 66), tumor cells resistant to IFN-γ may not necessarily be caused by their own drug resistance, but may be caused by the tumor promoting immune escape or creating an immunosuppressive microenvironment. We will further explore the mechanism of IFN-γ resistance in a subsequent study. Finally, the control group in this study

included non-cancer samples sourced from the GTEx database. However, GTEx consisted of tissues sampled from abruptly deceased individuals, which may impact the expression of immune genes and therefore influence the research findings.

Conclusion

This paper presents a pan-cancer analysis of IFN-γ in different tumors. Additionally, we presented novel concepts and perspectives for future tumor immunotherapy, highlighting the potential utility and application direction of IFN-γ for further tumor immunotherapy.

Data availability statement

The original contributions presented in the study are included in the article/Supplementary Materials, further inquiries can be directed to the corresponding author/s.

Ethics statement

This study was approved by The Affiliated Cancer Hospital of Guangxi Medical University's Ethics and Anthropology Committee. Written informed consent from obtained from the patients/participants.

Author contributions

HR, YZ, TQ, YJZ, XW, YQ, and WL conceived and designed the experiments; HR analyzed the data; YZ, TQ, YJZ, XW, YQ, and WL helped with reagents/materials/analysis tools; and XW, YQ, WL, YZ, TQ, and YJZ contributed to the writing of the manuscript. All authors reviewed the manuscript. All authors contributed to the article and approved the submitted version.

Funding

Guangxi Health Commission self-funded scientific research project (Z20200679) Guangxi Natural Science Foundation (2023GXNSFBA026070); Guangxi Health Commission self-funded scientific research project (Z-A20220031); Guangxi Natural Science Foundation (2022JJB140509) and Guangxi key research and development project (GuikeAB22080094); Guangxi Multidisciplinary Collaborative Health Management Talent Mini-Highland (guizutongzi:2019-85); Guangxi 14th Five-Year Major Science and Technology Special project (GuikeAA22096018) and Science and Technology Department Science and technology project (GuikeAD21220042).

Conflict of interest

The authors declare that the research was conducted in the absence of any commercial or financial relationships that could be construed as a potential conflict of interest.

Publisher's note

All claims expressed in this article are solely those of the authors and do not necessarily represent those of their affiliated organizations, or those of the publisher, the editors and the reviewers. Any product that may be evaluated in this article, or claim that may be made by its manufacturer, is not guaranteed or endorsed by the publisher.

Supplementary material

The Supplementary Material for this article can be found online at: https://www.frontiersin.org/articles/10.3389/fimmu.2023.1202150/full#supplementary-material

SUPPLEMENTARY FIGURE 1
Flow chart of this study.

SUPPLEMENTARY FIGURE 2
Stage-specific IFN-γ score for pan-cancer.

SUPPLEMENTARY FIGURE 3
Overall survival as determined by the Kaplan-Meier method for cancer patients with high and low IFN-γ expression levels.

SUPPLEMENTARY FIGURE 4
Kaplan-Meier survival curves of disease-specific survival in patients with cancer with high versus low expressions of the IFN-γ.

SUPPLEMENTARY FIGURE 5
Kaplan-Meier plots showing progression-free interval (PFI) survival rates in cancer patients having high and low levels of IFN-γ. Patients with an HR>1 have a dismal prognosis.

SUPPLEMENTARY FIGURE 6
(A–E) Comparison of immune activation genes, immune suppression genes, immune checkpoints, chemokines, chemokine receptor genes scores in cancer versus non-cancer. **(F)** Comparison of random sets of immune genes scores in cancer versus non-cancer. Red indicates that the score was significantly increased in tumors and FDR<0.05, blue indicates that the score was significantly decreased in tumors and FDR<0.05, and white indicates FDR>0.05.

SUPPLEMENTARY FIGURE 7
Link between immune score and IFN-γ score.

SUPPLEMENTARY FIGURE 8
There is a correlation between IFN-γ scores and markers of responsiveness to immunotherapy.

SUPPLEMENTARY FIGURE 9
Different cells in the kidney renal clear cell carcinoma tumor microenvironment express the IFN-γ marker genes.

References

1. Roy PS, Saikia BJ. Cancer and cure: A critical analysis. *Indian J Cancer* (2016) 53:441–2. doi: 10.4103/0019-509X.200658

2. Lin JX, Leonard WJ. Fine-tuning cytokine signals. *Annu Rev Immunol* (2019) 37:295–324. doi: 10.1146/annurev-immunol-042718-041447

3. Wang X, Lupardus P, Laporte SL, Garcia KC. Structural biology of shared cytokine receptors. *Annu Rev Immunol* (2009) 27:29–60. doi: 10.1146/annurev.immunol.24.021605.090616

4. Propper DJ, Balkwill FR. Harnessing cytokines and chemokines for cancer therapy. *Nat Rev Clin Oncol* (2022) 19:237–53. doi: 10.1038/s41571-021-00588-9

5. Broughton SE, Hercus TR, Lopez AF, Parker MW. Cytokine receptor activation at the cell surface. *Curr Opin Struct Biol* (2012) 22:350–9. doi: 10.1016/j.sbi.2012.03.015

6. Ihle JN, Witthuhn BA, Quelle FW, Yamamoto K, Silvennoinen O. Signaling through the hematopoietic cytokine receptors. *Annu Rev Immunol* (1995) 13:369–98. doi: 10.1146/annurev.iy.13.040195.002101

7. Levy DE, Darnell JEJr. Stats: transcriptional control and biological impact. *Nat Rev Mol Cell Biol* (2002) 3:651–62. doi: 10.1038/nrm909

8. Bonati L, Tang L. Cytokine engineering for targeted cancer immunotherapy. *Curr Opin Chem Biol* (2021) 62:43–52. doi: 10.1016/j.cbpa.2021.01.007

9. Spangler JB, Moraga I, Mendoza JL, Garcia KC. Insights into cytokine-receptor interactions from cytokine engineering. *Annu Rev Immunol* (2015) 33:139–67. doi: 10.1146/annurev-immunol-032713-120211

10. Gresser I. Biologic effects of interferons. *J Invest Dermatol* (1990) 95:S66–71. doi: 10.1111/1523-1747.ep12874776

11. Kursunel MA, Esendagli G. The untold story of IFN-γ in cancer biology. *Cytokine Growth Factor Rev* (2016) 31:73–81. doi: 10.1016/j.cytogfr.2016.07.005

12. Wall L, Burke F, Barton C, Smyth J, Balkwill F. IFN-gamma induces apoptosis in ovarian cancer cells in *vivo* and in vitro. *Clin Cancer Res* (2003) 9:2487–96.

13. Alspach E, Lussier DM, Schreiber RD. Interferon γ and its important roles in promoting and inhibiting spontaneous and therapeutic cancer immunity. *Cold Spring Harb Perspect Biol 11* (2019). doi: 10.1101/cshperspect.a028480

14. Castro F, Cardoso AP, Gonçalves RM, Serre K, Oliveira MJ. Interferon-gamma at the crossroads of tumor immune surveillance or evasion. *Front Immunol* (2018) 9:847. doi: 10.3389/fimmu.2018.00847

15. Sharma P, Pachynski RK, Narayan V, Fléchon A, Gravis G, Galsky MD, et al. Nivolumab plus ipilimumab for metastatic castration-resistant prostate cancer: preliminary analysis of patients in the checkMate 650 trial. *Cancer Cell* (2020) 38:489–499.e3. doi: 10.1016/j.ccell.2020.08.007

16. Ai L, Xu A, Xu J. Roles of PD-1/PD-L1 pathway: signaling, cancer, and beyond. *Adv Exp Med Biol* (2020) 1248:33–59. doi: 10.1007/978-981-15-3266-5_3

17. Tomczak K, Czerwińska P, Wiznerowicz M. The Cancer Genome Atlas (TCGA): an immeasurable source of knowledge. *Contemp Oncol (Poznan Poland)* (2015) 19:A68–77. doi: 10.5114/wo.2014.47136

18. Haeussler M, Zweig AS, Tyner C, Speir ML, Rosenbloom KR, Raney BJ, et al. The UCSC Genome Browser database: 2019 update. *Nucleic Acids Res 47* (2019), 47 (D1):D853–d858. doi: 10.1093/nar/gky1095

19. Zhang J, Jiang H, Du K, Xie T, Wang B, Chen C, et al. Pan-cancer analysis of genomic and prognostic characteristics associated with coronavirus disease 2019 regulators. *Front Med (Lausanne)* (2021) 8:662460. doi: 10.3389/fmed.2021.662460

20. Ayers M, Lunceford J, Nebozhyn M, Murphy E, Loboda A, Kaufman DR, et al. IFN-γ-related mRNA profile predicts clinical response to PD-1 blockade. *J Clin Invest* (2017) 127:2930–40. doi: 10.1172/JCI91190

21. Hanzelmann S, Castelo R, Guinney J. GSVA: gene set variation analysis for microarray and RNA-seq data. *BMC Bioinf* (2013) 14:7. doi: 10.1186/1471-2105-14-7

22. Subramanian A, Tamayo P, Mootha V, Mukherjee S, Ebert B, Gillette M, et al. Gene set enrichment analysis: a knowledge-based approach for interpreting genome-wide expression profiles. *Proc Natl Acad Sci U.S.A* (2005) 102:15545–50. doi: 10.1073/pnas.0506580102

23. Su C, Lv Y, Lu W, Yu Z, Ye Y, Guo B, et al. Single-cell RNA sequencing in multiple pathologic types of renal cell carcinoma revealed novel potential tumor-specific markers. *Front Oncol* (2021) 11:719564. doi: 10.3389/fonc.2021.719564

24. Qin Y, Pan L, Qin T, Ruan H, Zhang Y, Zhang Y, et al. Pan-cancer analysis of AIM2 inflammasomes with potential implications for immunotherapy in human cancer: A bulk omics research and single cell sequencing validation. *Front Immunol* (2022) 13:998266. doi: 10.3389/fimmu.2022.998266

25. Zhou X, Du J, Liu C, Zeng H, Chen Y, Liu L, et al. A pan-cancer analysis of CD161, a potential new immune checkpoint. *Front Immunol* (2021) 12:688215. doi: 10.3389/fimmu.2021.688215

26. Zhang H, Ding C, Li Y, Xing C, Wang S, Yu Z, et al. Data mining-based study of collagen type III alpha 1 (COL3A1) prognostic value and immune exploration in pan-cancer. *Bioengineered* (2021) 12:3634–46. doi: 10.1080/21655979.2021.1949838

27. Chan TA, Yarchoan M, Jaffee E, Swanton C, Quezada SA, Stenzinger A, et al. Development of tumor mutation burden as an immunotherapy biomarker: utility for the oncology clinic. *Ann Oncol Off J Eur Soc Med Oncol* (2019) 30:44–56. doi: 10.1093/annonc/mdy495

28. Choucair K, Morand S, Stanbery L, Edelman G, Dworkin L, Nemunaitis J. TMB: a promising immune-response biomarker, and potential spearhead in advancing targeted therapy trials. *Cancer Gene Ther* (2020) 27:841–53. doi: 10.1038/s41417-020-0174-y

29. Mo Z, Li P, Cao Z, Zhang S. A comprehensive pan-cancer analysis of 33 human cancers reveals the immunotherapeutic value of aryl hydrocarbon receptor. *Front Immunol* (2021) 12:564948. doi: 10.3389/fimmu.2021.564948

30. van Velzen MJM, Derks S, van Grieken NCT, Haj Mohammad N, van Laarhoven HWM. MSI as a predictive factor for treatment outcome of gastroesophageal adenocarcinoma. *Cancer Treat Rev* (2020) 86:102024. doi: 10.1016/j.ctrv.2020.102024

31. Gajewski TF, Schreiber H, Fu YX. Innate and adaptive immune cells in the tumor microenvironment. *Nat Immunol* (2013) 14:1014–22. doi: 10.1038/ni.2703

32. Spranger S, Gajewski TF. Tumor-intrinsic oncogene pathways mediating immune avoidance. *Oncoimmunology* (2016) 5:e1086862. doi: 10.1080/2162402X.2015.1086862

33. Jiang P, Gu S, Pan D, Fu J, Sahu A, Hu X, et al. Signatures of T cell dysfunction and exclusion predict cancer immunotherapy response. *Nat Med* (2018) 24:1550–8. doi: 10.1038/s41591-018-0136-1

34. Rees MG, Seashore-Ludlow B, Cheah JH, Adams DJ, Price EV, Gill S, et al. Correlating chemical sensitivity and basal gene expression reveals mechanism of action. *Nat Chem Biol* (2016) 12:109–16. doi: 10.1038/nchembio.1986

35. Topalian SL, Drake CG, Pardoll DM. Immune checkpoint blockade: a common denominator approach to cancer therapy. *Cancer Cell* (2015) 101130617:450–61. doi: 10.1016/j.ccell.2015.03.001

36. Zaidi MR, Merlino G. The two faces of interferon-γ in cancer. *Clin Cancer Res* (2011) 17:6118–24. doi: 10.1158/1078-0432.CCR-11-0482

37. Burke JD, Young HA. IFN-γ: A cytokine at the right time, is in the right place. *Semin Immunol* (2019) 43:101280. doi: 10.1016/j.smim.2019.05.002

38. Tau GZ, Cowan SN, Weisburg J, Braunstein NS, Rothman PB. Regulation of IFN-gamma signaling is essential for the cytotoxic activity of CD8(+) T cells. *J Immunol* (2001) 167:5574–82. doi: 10.4049/jimmunol.167.10.5574

39. Maimela NR, Liu S, Zhang Y. Fates of CD8+ T cells in tumor microenvironment. *Comput Struct Biotechnol J* (2019) 17:1–13. doi: 10.1016/j.csbj.2018.11.004

40. Levy EM, Roberti MP, Mordoh J. Natural killer cells in human cancer: from biological functions to clinical applications. *J BioMed Biotechnol* (2011) 2011:676198. doi: 10.1155/2011/676198

41. Ni C, Wu P, Zhu X, Ye J, Zhang Z, Chen Z, et al. IFN-γ selectively exerts pro-apoptotic effects on tumor-initiating label-retaining colon cancer cells. *Cancer Lett* (2013) 336:174–84. doi: 10.1016/j.canlet.2013.04.029

42. Lin CF, Lin CM, Lee KY, Wu SY, Feng PH, Chen KY, et al. Escape from IFN-γ-dependent immunosurveillance in tumorigenesis. *J BioMed Sci* (2017) 24:10. doi: 10.1186/s12929-017-0317-0

43. Li Q, Zhang XQ, Nie L, Chen GS, Li H, Zhang F, et al. Expression of interferon-gamma in human adrenal gland and kidney tumours. *Br J Cancer* (2007) 97:420–5. doi: 10.1038/sj.bjc.6603870

44. Mojic M, Takeda K, Hayakawa Y. The dark side of IFN-γ: its role in promoting cancer immunoevasion. *Int J Mol Sci 19* (2017). doi: 10.3390/ijms19010089

45. Zaidi MR, Davis S, Noonan FP, Graff-Cherry C, Hawley TS, Walker RL, et al. Interferon-γ links ultraviolet radiation to melanomagenesis in mice. *Nature* (2011) 469:548–53. doi: 10.1038/nature09666

46. Khorrami S, Zamani H, Hasanzadeh M, Mehramiz M, Soleimani A, Zare Marzouni H, et al. Association of a genetic variant in Interleukin-10 gene with increased risk and inflammation associated with cervical cancer. *Gene* (2022) 807:145933. doi: 10.1016/j.gene.2021.145933

47. Wang Y, Liu D, Chen P, Koeffler HP, Tong X, Xie D. Negative feedback regulation of IFN-gamma pathway by IFN regulatory factor 2 in esophageal cancers. *Cancer Res* (2008) 68:1136–43. doi: 10.1158/0008-5472.CAN-07-5021

48. Kaganoi J, Watanabe G, Okabe M, Nagatani S, Kawabe A, Shimada Y, et al. STAT1 activation-induced apoptosis of esophageal squamous cell carcinoma cells in vivo. *Ann Surg Oncol* (2007) 14:1405–15. doi: 10.1245/s10434-006-9274-7

49. Ucgun NI, Zeki-Fikret C, Yildirim Z. Inflammation and diabetic retinopathy. *Mol Vis* (2020) 26:718–21.

50. Urosevic M, Fujii K, Calmels B, Laine E, Kobert N, Acres B, et al. Type I IFN innate immune response to adenovirus-mediated IFN-gamma gene transfer contributes to the regression of cutaneous lymphomas. *J Clin Invest* (2007) 117:2834–46. doi: 10.1172/JCI32077

51. Zhou D, Huang C, Lin Z, Zhan S, Kong L, Fang C, et al. Macrophage polarization and function with emphasis on the evolving roles of coordinated regulation of cellular signaling pathways. *Cell Signal* (2014) 26:192–7. doi: 10.1016/j.cellsig.2013.11.004

52. Fenimore J. Regulation of IFN-γ Expression. *Adv Exp Med Biol* (2016) 941:1–19. doi: 10.1007/978-94-024-0921-5_1

53. McGranahan N, Furness AJ, Rosenthal R, Ramskov S, Lyngaa R, Saini SK, et al. Clonal neoantigens elicit T cell immunoreactivity and sensitivity to immune checkpoint blockade. *Science* (2016) 351:1463–9. doi: 10.1126/science.aaf1490

54. Smith KN, Llosa NJ, Cottrell TR, Siegel N, Fan H, Suri P, et al. Persistent mutant oncogene specific T cells in two patients benefitting from anti-PD-1. *J Immunother Cancer* (2019) 7:40. doi: 10.1186/s40425-018-0492-x

55. Hellmann MD, Nathanson T, Rizvi H, Creelan BC, Sanchez-Vega F, Ahuja A, et al. Genomic features of response to combination immunotherapy in patients with advanced non-small-cell lung cancer. *Cancer Cell* (2018) 33:843–852.e4. doi: 10.1016/j.ccell.2018.03.018

56. Chalmers ZR, Connelly CF, Fabrizio D, Gay L, Ali SM, Ennis R, et al. Analysis of 100,000 human cancer genomes reveals the landscape of tumor mutational burden. *Genome Med* (2017) 9:34. doi: 10.1186/s13073-017-0424-2

57. Goodman AM, Sokol ES, Frampton GM, Lippman SM, Kurzrock R. Microsatellite-stable tumors with high mutational burden benefit from immunotherapy. *Cancer Immunol Res* (2019) 7:1570–3. doi: 10.1158/2326-6066.CIR-19-0149

58. Nanda R, Chow LQ, Dees EC, Berger R, Gupta S, Geva R, et al. Pembrolizumab in patients with advanced triple-negative breast cancer: phase ib KEYNOTE-012 study. *J Clin Oncol* (2016) 34:2460–7. doi: 10.1200/JCO.2015.64.8931

59. Rizvi H, Sanchez-Vega F, La K, Chatila W, Jonsson P, Halpenny D, et al. Molecular determinants of response to anti-programmed cell death (PD)-1 and anti-programmed death-ligand 1 (PD-L1) blockade in patients with non-small-cell lung cancer profiled with targeted next-generation sequencing. *J Clin Oncol* (2018) 36:633–41. doi: 10.1200/JCO.2017.75.3384

60. Saghafinia S, Mina M, Riggi N, Hanahan D, Ciriello G. Pan-cancer landscape of aberrant DNA methylation across human tumors. *Cell Rep* (2018) 25:1066–1080.e8. doi: 10.1016/j.celrep.2018.09.082

61. Young HA, Ghosh P, Ye J, Lederer J, Lichtman A, Gerard JR, et al. Differentiation of the T helper phenotypes by analysis of the methylation state of the IFN-gamma gene. *J Immunol* (1994) 153:3603–10. doi: 10.4049/jimmunol.153.8.3603

62. Melvin AJ, McGurn ME, Bort SJ, Gibson C, Lewis DB. Hypomethylation of the interferon-gamma gene correlates with its expression by primary T-lineage cells. *Eur J Immunol* (1995) 25:426–30. doi: 10.1002/eji.1830250218

63. Ma D, Jiang C, Hu X, Liu H, Li Q, Li T, et al. Methylation patterns of the IFN-γ gene in cervical cancer tissues. *Sci Rep* (2014) 4:6331. doi: 10.1038/srep06331

64. Sailer V, Sailer U, Bawden EG, Zarbl R, Wiek C, Vogt TJ, et al. DNA methylation of indoleamine 2,3-dioxygenase 1 (IDO1) in head and neck squamous cell carcinomas correlates with IDO1 expression, HPV status, patients' survival, immune cell infiltrates, mutational load, and interferon γ signature. *EBioMedicine* (2019) 48:341–52. doi: 10.1016/j.ebiom.2019.09.038

65. Wieder T, Braumüller H, Kneilling M, Pichler B, Röcken M. T cell-mediated help against tumors. *Cell Cycle* (2008) 7:2974–7. doi: 10.4161/cc.7.19.6798

66. Zimmerman M, Yang D, Hu X, Liu F, Singh N, Browning D, et al. IFN-γ upregulates survivin and Ifi202 expression to induce survival and proliferation of tumor-specific T cells. *PloS One* (2010) 5:e14076. doi: 10.1371/journal.pone.0014076

frontiers | Frontiers in Immunology

TYPE Review
PUBLISHED 18 August 2023
DOI 10.3389/fimmu.2023.1223433

OPEN ACCESS

EDITED BY
Esra Akbay,
University of Texas Southwestern Medical Center, United States

REVIEWED BY
Yufei Luo,
Hunan University, China
Samantha Messina,
Roma Tre University, Italy

*CORRESPONDENCE
Ding Li
ld_sunshinev@163.com

RECEIVED 16 May 2023
ACCEPTED 31 July 2023
PUBLISHED 18 August 2023

CITATION
Wu X, Song W, Cheng C, Liu Z, Li X, Cui Y, Gao Y and Li D (2023) Small molecular inhibitors for KRAS-mutant cancers. *Front. Immunol.* 14:1223433. doi: 10.3389/fimmu.2023.1223433

Small molecular inhibitors for KRAS-mutant cancers

Xuan Wu[1,2], Wenping Song[3,4,5], Cheng Cheng[1], Ziyang Liu[2], Xiang Li[1], Yu Cui[1], Yao Gao[1] and Ding Li[3,4,5]*

[1]Department of Internal Medicine, The Affiliated Cancer Hospital of Zhengzhou University and Henan Cancer Hospital, Zhengzhou, China, [2]Academy of Medical Science, Zhengzhou University, Zhengzhou, China, [3]Department of Pharmacy, The Affiliated Cancer Hospital of Zhengzhou University and Henan Cancer Hospital, Zhengzhou, China, [4]Henan Engineering Research Center for Tumor Precision Medicine and Comprehensive Evaluation, Henan Cancer Hospital, Zhengzhou, China, [5]Henan Provincial Key Laboratory of Anticancer Drug Research, Henan Cancer Hospital, Zhengzhou, China

Three rat sarcoma (RAS) gene isoforms, KRAS, NRAS, and HRAS, constitute the most mutated family of small GTPases in cancer. While the development of targeted immunotherapies has led to a substantial improvement in the overall survival of patients with non-KRAS-mutant cancer, patients with RAS-mutant cancers have an overall poorer prognosis owing to the high aggressiveness of RAS-mutant tumors. KRAS mutations are strongly implicated in lung, pancreatic, and colorectal cancers. However, RAS mutations exhibit diverse patterns of isoforms, substitutions, and positions in different types of cancers. Despite being considered "undruggable", recent advances in the use of allele-specific covalent inhibitors against the most common mutant form of RAS in non-small-cell lung cancer have led to the development of effective pharmacological interventions against RAS-mutant cancer. Sotorasib (AMG510) has been approved by the FDA as a second-line treatment for patients with KRAS-G12C mutant NSCLC who have received at least one prior systemic therapy. Other KRAS inhibitors are on the way to block KRAS-mutant cancers. In this review, we summarize the progress and promise of small-molecule inhibitors in clinical trials, including direct inhibitors of KRAS, pan-RAS inhibitors, inhibitors of RAS effector signaling, and immune checkpoint inhibitors or combinations with RAS inhibitors, to improve the prognosis of tumors with RAS mutations.

KEYWORDS

RAS mutation, different isoform, RAS inhibitor, immunotherapy, combination strategy

1 Introduction

Rat sarcoma (RAS) genes have been recognized as the major oncogenes undergoing mutation for several decades (1, 2). Among the three isoforms (KRAS, NRAS, and HRAS), Kirsten rat sarcoma viral oncogene homolog (KRAS) is the common oncogene in a large percentage of cancers, including pancreatic cancer, non-small cell lung cancer (NSCLC), and colorectal cancer (3–6). Mutations in RAS lead to the dysfunction of its small GTPase activity, preventing it from properly breaking down GTP. The molecule remains in a

constant active state that triggers downstream pathways, including the mitogen-activated protein kinase (MAPK) and phosphatidylinositol 3-kinase (PI3K) pathways, leading to oncogenesis.

Attempts to develop effective agents that inhibit RAS mutations have been a failure for a long time (7, 8). In recent years, with the discovery of a new binding site beneath the effector binding switch-II region in RAS protein, several small-molecule agents targeting the KRAS-G12C single-nucleotide mutation (glycine-to-cysteine substitution at codon 12) have been developed and have shown promising efficacy in clinical trials (9–12). Sotorasib (AMG510) has been approved by the FDA as a second-line treatment for patients with KRAS-G12C mutant NSCLC who have received at least one prior systemic therapy (13, 14). Given that several excellent reviews have summarized the role of RAS signaling in oncogenesis and the advances in RAS inhibitors for anti-tumor therapy, we herein focus on KRAS mutations and summarize the promising new treatment options.

2 RAS mutations in human cancers

RAS mutations may represent the early onset of tumorigenesis and are essential for tumor maintenance, which has been validated by considerable evidence (15–17). The RAS mutation rates in various cancer types are shown in Supplemental Figure 1. Different single-base missense mutations result in different amino acid substitutions of the RAS oncogene (Figure 1A). KRAS, HRAS, and NRAS are the three most commonly mutated RAS isoforms with varying mutation rates in different cancers (18). KRAS mutations, more than 80% of which are G12 mutations, are frequently found in pancreatic ductal adenocarcinoma (> 90%), colorectal adenocarcinoma (> 40%), and lung adenocarcinoma (approximately 30%). NRAS mutations, which occur less frequently than KRAS mutations, mainly occur at codon 61 and are found in nearly 30% of cutaneous skin melanomas. HRAS mutations occurring at codon 12 or 61 are only found in a small subset of bladder urothelial carcinoma, head and neck squamous cell carcinoma, and thyroid carcinoma (19–21). The top ten predominant substitutions and frequencies with which they occur in the three RAS isoforms according to tissue type in common cancers are shown in Figure 1B. For pancreatic ductal adenocarcinoma and colorectal adenocarcinoma, the predominant amino acid substitution is G12D in KRAS. For lung adenocarcinoma, the predominant amino acid substitution is G12C in KRAS. However, for melanoma, the predominant substitution is Q61R in NRAS.

As the most frequently mutated isoform of the RAS family, KRAS has two splice variants, KRAS4A and KRAS4B, which differ in their fourth exon and encode two different proteins that differ only in their C-terminal membrane-targeting regions (22, 23). KRAS4B is the main mutant isoform in human cancer, whereas KRAS4A is commonly expressed in various cancer cell lines and colorectal cancer (24, 25). Certain mutations in the amino acid sequence of KRAS often result in distinct transformation properties and biological behaviors (26). For instance, KRAS-G12V mutations are associated with worse outcomes than KRAS-G12D mutations in patients with lung cancer. Over the last 30 years, the correlation

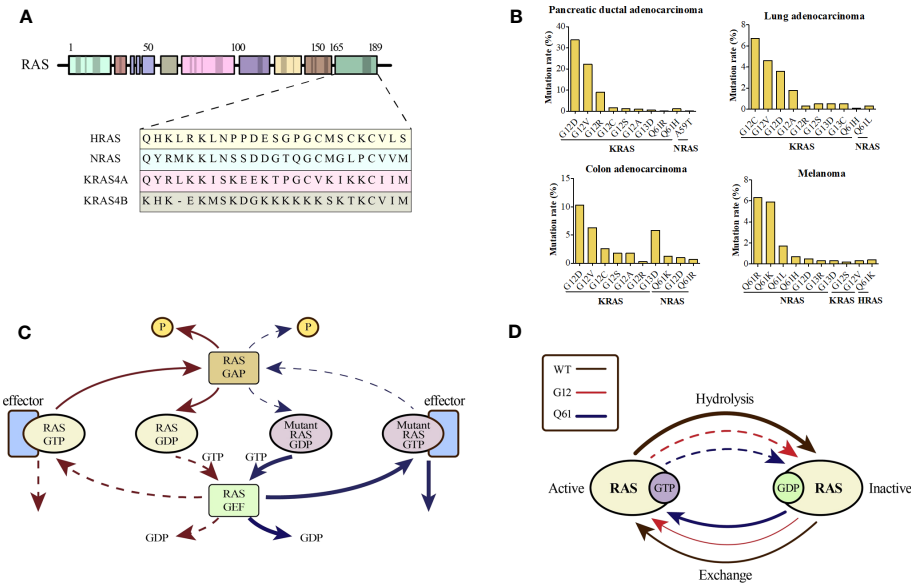

FIGURE 1
(A) An alignment of the carboxy terminus of the three RAS isoforms is shown. The RAS subtypes are highly conserved (~90%) with respect to the entire amino terminal GTPase domain (amino acids 1–166), which contains the GTP-GDP binding site and the interaction site of the effector protein; however, the carboxy terminal part differs and is called the hypervariable zone. **(B)** Percentages of KRAS mutations in codon 12 and NRAS mutations in codon 61 by tissue type for common cancers. **(C)** The canonical nature of RAS is characteristic of a small GTPase that usually circulates between the GTP-bound active state and GDP-bound inactive state, which is partly promoted by the GTP hydrolysis-stimulating GTPase activation protein (GAP). However, when the RAS protein is mutated, impaired GAP stimulation promotes the formation of a persistently GTP-bound RAS. **(D)** An overview of the general biochemical destruction of hydrolysis and guanine exchange after mutation of codon 12 or 61.

between biological behavior and specific RAS mutations has remained unclear (27–29). KRAS mutations are significantly associated with poor outcomes in patients with lung cancer (30, 31). However, a recent study suggested that for stages I-III, there was no statistical difference in overall survival (OS) between the mutant- and wild-type-carrying patients with NSCLC (32).

3 Domains and regions of KRAS

The RAS protein, cycling between inactive and active GDP-bound conformations, comprises three major domains: G-domain, C-terminal, and C-terminal CAAX motifs (33, 34). The G-domain is a highly conserved domain that includes switches I and II, which are responsible for the GDP-GTP exchange (33). The C-terminal region containing the CAAX motif varies considerably among different members of the RAS family. However, this motif is essential for post-translational modification (35). RAS is activated by guanine nucleotide exchange factors (GEFs) and transduces signals to downstream pathways.

KRAS encodes a membrane-bound GTPase that is inactive when bound to GDP and active when bound to GTP. The transition of KRAS to its active state is facilitated by GEFs such as SOS1. Once activated by extracellular stimuli, the active form of KRAS acts as a cellular switch, triggering downstream signaling pathways involved in fundamental cellular processes. Mutations in RAS block the binding of GTP to RAS and cause aberrant activation of downstream pathways (Figure 1C). RAS mutations may affect the intrinsic GTPase and GDP–GTP exchange rates (Figure 1D) (36). Mutations in KRAS at codons 12, 13, and 61 inhibit the ability of GTPase activation protein (GAP) to stimulate GTP hydrolysis. However, KRAS-G13D displays heightened intrinsic exchange activity compared to the wild-type RAS protein (37, 38). Despite the reduced p120 GAP-mediated hydrolysis rate, KRAS-G12C mutant exhibits almost wild-type intrinsic GTPase activity and has been used to develop covalent inhibitors (39).

4 KRAS inhibitors for patients with cancer

Despite over three decades of intensive efforts, no effective regimen to inhibit RAS-driven oncogenesis has been developed because of its inaccessible binding surface and picomolar affinity for GTP/GDP (7, 40). The high affinity of the RAS for cytoplasmic GTP renders competitive inhibition difficult to achieve. The absence of a drug-binding groove on the smooth surface of the RAS poses a challenge for targeted inhibitors. Multiple upstream and downstream regulators of RAS pathways contribute to drug resistance mechanisms and bypass signals, further limiting the effectiveness of combination strategies (41).

These complexities underscore the challenges in targeting RAS mutations. In 2013, with the identification of a new covalent pocket of the KRAS-G12C mutation located beneath the effector-binding switch-II region, Shokat et al. reported a novel strategy for overcoming these difficulties in a mutant-specific targeting manner (42). A series of small-molecule agents could irreversibly bind to the KRAS-G12C mutation and disrupt switch-I and switch-II to bind the mutation in the GDP-bound state, thereby blocking the association with Raf and other downstream tyrosine kinases (Figure 2).

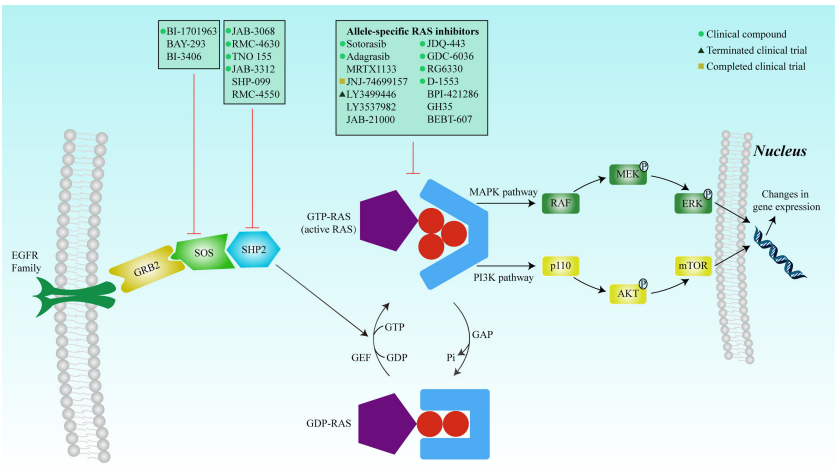

FIGURE 2
RAS mutation activates the protein, and the complex formed with GTP binds to the Ras-binding domain of the effector protein (RAF, PI3K, and RALGDS) to activate the MAPK and PI3K signaling pathways, respectively. The signals are transduced into the nucleus to regulate gene expression, thereby affecting cell proliferation and survival. Inhibition of SOS or SHP2 reduces the exchange rate between GDP and GTP and reduces the GTP-bound RAS population. Mutated RAS proteins accumulate in the GTP-bound state. Many inhibitors have been developed to directly inhibit RAS, including covalent allele-specific inhibitors that bind to KRAS-G12C.

4.1 Sotorasib (AMG510)

Sotorasib (AMG510) is an oral small-molecule inhibitor that specifically and irreversibly inhibits the KRAS-G12C mutation (43). A preclinical study showed that sotorasib potently impaired the viability of two KRAS-G12C mutant cell lines NCI-H358 and MIA PaCa-2. Xenograft models have shown that AMG-510 can induce the regression of KRAS-G12C mutant tumors (9). The CodeBreak 100 phase I/II clinical trial evaluated the efficacy, safety, tolerability, and pharmacokinetics of sotorasib in patients with KRAS-G12C-mutant solid tumors (10). Of the 129 patients who participated in the phase I cohort study, 73 (56.6%) experienced mainly low-grade adverse events related to treatment (10). No treatment-related death or dose-limiting toxic effects were observed. The objective response rates (ORR) were 32.2% and 7.1% in NSCLC and colorectal cancer, respectively, indicating a promising anti-tumor activity for sotorasib in NSCLC.

The phase II cohort-based study revealed that out of 126 individuals diagnosed with advanced KRAS-G12C-mutant NSCLC, sotorasib treatment resulted in confirmed ORR and disease control rates (DCR) of 37.1% and 80.6%, respectively. The median response time during treatment was 10 months (44). A phase III clinical trial designed to compare the efficacy of sotorasib when administered alone versus docetaxel administration in previously treated patients with KRAS-G12C-mutant NSCLC is ongoing (NCT04303780). The progression-free survival (PFS) times for sotorasib-treated cohort were significantly higher than those of docetaxel-treated cohort (p=0.0017); a more favorable safety profile was also observed (45). Currently, sotorasib (AMG510) is approved by the FDA as a second-line treatment for patients with KRAS-G12C-mutant NSCLC who have received at least one systemic therapy (13, 14).

4.2 Adagrasib (MRTX849)

Adagrasib (MRTX849) is a KRAS-G12C inhibitor (46). According to preclinical studies, adagrasib effectively and consistently blocks KRAS-dependent signaling pathways with long-lasting effects, resulting in substantial tumor regression in 17 out of 26 (65%) KRAS-G12C-positive cell line- and patient-derived xenograft models (47). In a phase I/II clinical study, the KRYSTAL-1 trial evaluated the safety, tolerability, and clinical activity of adagrasib in patients with advanced solid tumors and a KRAS-G12C mutation (NCT03785249). Preliminary results showed that adagrasib monotherapy exhibited promising clinical activity and an acceptable safety profile in pretreated patients with advanced solid tumors (48). Particularly, for patients with NSCLC, among 51 patients evaluated for its clinical activity, ORR was 45% (23/51) and DCR was 96% (49/51). According to the present data from Mirati Therapeutics, patients with NSCLC with active brain metastases experienced a 63% reduction in the size of the primary lesion, and some lesions even disappeared after several cycles of adagrasib monotherapy. Among 18 patients with colorectal cancer, the ORR and DCR were 17% (3/18) and 94% (17/18), respectively. Interestingly, some coexisting mutations, including those in TP53, STK11, and KEAP1, may influence the efficacy of this anti-tumor agent. Preliminary results of KRYSTAL-1 showed that patients with advanced NSCLC and co-mutations of KRAS-G12C and STK11 had an ORR of 64% (9/14) across the pooled cohorts of phase I/Ib and II studies. A phase III study evaluating the efficacy of adagrasib versus docetaxel in previously treated patients with metastatic NSCLC and KRAS-G12C mutation is ongoing (NCT04685135).

4.3 Other KRAS inhibitors

Another KRAS inhibitor MRTX1133 selectively and reversibly inhibits KRAS-G12D and is currently being investigated in investigational new drug (IND)-enabling studies. Preclinical models have demonstrated the selective inhibition of cell viability in KRAS-G12D mutant tumor cells with a long predicted half-life (~50 h) (48). JNJ-74699157 (ARS-3248), a new-generation KRAS-G12C inhibitor, was developed based on ARS-1620 (11). A phase I clinical trial to determine the preliminary anti-tumor activity and safety in patients with advanced solid tumors and KRAS-G12C mutation showed that no significant clinical benefit was observed, with the best response to stable disease in four patients (40%). Moreover, an unfavorable safety profile prevented further enrollment and clinical development (49). The ARS-853 is a version of the ARS-1620 (50). Although they both inhibit cell growth and downstream signaling of the MAPK pathway in KRAS-G12C mutant tumor cell lines, ARS-853 is not suitable for use in animal models because of its lack of chemical and metabolic stability (11). JDQ-443 is another KRAS-G12C inhibitor currently in phase Ib/II clinical trial that evaluates the safety and tolerability of monotherapy in combination with other treatment drugs (spartalizumab and TNO155) in patients with advanced solid tumors and KRAS-G12C mutation (NCT04699188). Other KRAS-G12C inhibitors, GDC-6036 (NCT04449874), RG6330, and D-1553 (NCT04585035), are under phase I/II clinical trials, and their results have not been published. BPI-421286, GH35, BEBT-607, and JAB-21000, are all the KRAS inhibitors used in IND-enabling studies (51). The clinical developments of single-agent RAS inhibitors are summarized in Table 1.

With the development of new small-molecule inhibitors, previously undruggable mutant KRAS could be targeted. However, the complexity of the RAS pathway makes the treatment of RAS-mutant tumors challenging. The heterogeneity of the response to the same KRAS inhibitor among different tumor types forces researchers to consider the difference in the same mutation isoform in downstream signaling pathways and the feedback effects of the various tumors (52), as not only are cells intrinsic factors but the tumor microenvironment, particularly inflammation, also has the potential to modify susceptibility to oncogenic RAS mutations. It has been observed that certain cells can have an anti-neoplastic response against oncogenic RAS due to the activation of tumor suppressor pathways, while others cannot. The role of cell lineage in this response is of significant importance (53). Moreover, one possible explanation for the heterogeneity is the

10.3389/fimmu.2023.1223433

TABLE 1 RAS inhibitor single agents and combination therapy in clinical development.

Drugs	Targets	ClinicalTrials.gov Number	Disease	Study Phase	Status	Interventions
Adagrasib (MRTX849)	KRAS-G12C	NCT03785249	Advanced solid tumors	I/II	Recruiting	Adagrasib
		NCT04685135	Advanced NSCLC	III	Recruiting	Adagrasib vs Docetaxel
MRTX1133	KRAS-G12D	/	/	/	Preclinical study	
JNJ-74699157 (ARS-3248)	KRAS-G12C	NCT04006301	Advanced solid tumors	I	Completed	JNJ-74699157
LY3499446	KRAS-G12C	NCT04165031	Advanced solid tumors	I/II	Terminated	LY3499446
LY3537982	KRAS-G12C	/	/	/	Preclinical study	
JDQ-443	KRAS-G12C	NCT04699188	Advanced solid tumors	Ib/II	Recruiting	JDQ443
GDC-6036	KRAS-G12C	NCT04449874	Advanced solid tumors	I	Recruiting	GDC-6036
RG6330	KRAS-G12C	/	/	I	Recruiting	RG6330
D-1553	KRAS-G12C	NCT04585035	Advanced solid tumors	I/II	Recruiting	D-1553
BPI-421286	KRAS-G12C	/	Advanced solid tumors	/	IND study	
GH35	KRAS-G12C	/	Advanced solid tumors	/	IND study	
BEBT-607	KRAS-G12C	/	NSCLC and colorectal cancer	/	IND study	
JAB-21000	KRAS-G12C	/	Advanced solid tumors	/	IND study	
Combination therapy of RAS inhibitor						
Sotorasib (AMG510)	KRAS-G12C	NCT03600883	Advanced solid tumors	I/II	Active	Sotorasib+PD-1/PD-L1 inhibitor
Adagrasib (MRTX849)	KRAS-G12C	NCT04613596	Advanced NSCLC	II	Recruiting	Adagrasib+ Pembrolizumab
		NCT03785249	Advanced solid tumors	I/II	Recruiting	Adagrasib+ Pembrolizumab/Afatinib (advanced NSCLC) Adagrasib+Cetuximab (Colorectal cancer)
		NCT04330664	Advanced solid tumors	I/II	Active	Adagrasib+TNO155
		NCT04793958	Colorectal cancer	IIII	Recruiting	Adagrasib+Cetuximab
LY3499446	KRAS-G12C	NCT04165031	Advanced solid tumors	I/II	Terminated	LY349944+ Abemaciclib/ Cetuximab/Erlotinib/Docetaxel
JDQ443	KRAS-G12C	NCT04699188	Advanced solid tumors	I/II	Recruiting	JDQ443+TNO155/ Spartalizumab/TNO155+ Spartalizumab
GDC-6036	KRAS-G12C	NCT04449874	Advanced solid tumors	I/II	Recruiting	GDC-6036+Atezolizumab (NSCLC) GDC-6036+Cetuximab (Colorectal cancer) GDC-6036+Bevacizumab (Advanced solid tumors) GDC-6036+Erlotinib (NSCLC)
D-1553	KRAS-G12C	NCT04585035	Advanced solid tumors	I/II	Recruiting	D-1553+other

existence of different signaling dependencies in different tumor types. While some tumors heavily rely on KRAS signaling for growth and survival, others may have acquired alternative signaling pathways to compensate for KRAS inhibition. These alternative pathways can bypass the need for KRAS signaling, rendering the KRAS inhibitor less effective. Moreover, the co-occurring genetic alterations in different tumor types can contribute to the heterogeneity of response (54).

In addition, most KRAS inhibitors have been developed to target the KRAS-G12C mutation, which constitutes only a portion of the KRAS mutations and is commonly found in lung cancer (55). Therefore, new approaches are warranted to effectively treat other KRAS mutations such as KRAS-G12D and KRAS-G12V.

5 Evidence for pan-RAS inhibitors in RAS-mutant cancers

Although covalent inhibitors that directly target specific KRAS mutations exhibit promising efficacy, inhibiting other RAS mutations is challenging. New inhibitors have been developed, regardless of the type of RAS mutation or protein. A multivalent small molecular inhibitor compound 3144 was designed to interact with adjacent sites on the KRAS surface and disrupt interactions between RAS proteins and their effectors (56). Preclinical models showed that compound 3144 was capable of binding to HRAS, KRAS, and NRAS and inhibited RAS signaling. Xenograft models also indicated that 3144 could prevent the growth of RAS-mutant mouse cancer xenografts derived from tumor cell lines and patients. Satchell et al. developed a pan-RAS biologic inhibitor by fusing the RAS-RAP1-specific endopeptidase to the diphtheria toxin, which could irreversibly cleave and inactivate intracellular RAS at picomolar concentrations and terminate downstream signaling and induce tumor shrinkage in mouse xenograft models driven by either wild-type or mutant RAS (57). Furthermore, a compound named cmp4 selectively binds to the Switch II pocket of both HRAS and KRAS proteins with different mutations. By interfering with the binding of RAS to GEFs and Raf effectors, cmp4 effectively reduced the intrinsic and GEF-mediated nucleotide dissociation and exchange processes of the Ras protein, ultimately leading to the inhibition of the mitogen-activated protein kinase signaling pathway and a decrease in cell viability. According to a mathematical model of the RAS activation cycle, cmp4 when combined with cetuximab reduces the proliferation of cetuximab-resistant cancer cell lines. However, the affinity of cmp4 for RAS is unsatisfactory, and this limits its application as an ideal clinical drug (58).

Unfortunately, all these compounds that could function as pan-RAS inhibitors have only been tested in preclinical studies. Given the essential role of RAS in normal cell signaling, it is unclear whether pan-RAS inhibitors are tolerated. Previous studies have revealed that homozygous deletion of KRAS is embryonically lethal in mice (59–61). Therefore, the toxicity of pan-RAS inhibitors should be investigated in future studies. In addition, acquired resistance to RAS inhibitors often prevents further clinical benefits. Awad et al. compared the genomic and histological landscapes of pretreatment samples and those obtained after the development of resistance. Acquired KRAS alterations included G12D/R/V/W, Q61H, R68S, and high-level amplification of the KRAS-G12C allele. Bypass mechanisms involve MET amplification, mutations in NRAS and BRAF, and the oncogenic fusion of ALK and RET. Loss-of-function mutations in NF1 and PTEN have been previously reported. Consequently, new therapeutic strategies are necessary to overcome and delay drug resistance in patients with cancer (62).

6 KRAS mutations and immune landscape

Specifically, mutant KRAS not only alters the behavior of cancer cells but also affects various cells in the tumor microenvironment (TME). KRAS activation increases the production of the neutrophil chemokines CXCL1, CXCL2, and CXCL5 (63). The upregulation of intercellular adhesion molecule 1 (ICAM1) by KRAS promotes the recruitment of pro-inflammatory M1 macrophages (in contrast, co-activation of KRAS and MYC increases the recruitment of anti-inflammatory M2 macrophages by releasing CCL9 and IL-23). KRAS-mediated secretion of TGFβ and IL-10 leads to the differentiation of immunosuppressive regulatory T cells (Tregs). It also enhances tumor-infiltrating myeloid-derived suppressor cells (MDSCs) through GM-CSF-dependent and IRF2/CXCL3-dependent mechanisms (64).

Moreover, different co-mutation statuses of KRAS can affect the TME and response to immune checkpoint inhibitors (ICIs). For example, tumors with KRAS/STK11 co-mutations often exhibit deficiencies in CD8+ T lymphocytes and a high abundance of T-regulatory cells in the microenvironment. In contrast, tumors with KRAS/p53 co-mutations tend to have an inflamed TME characterized by a higher number of CD8+ T lymphocytes. This can be attributed to p53 mutations, which tend to increase somatic tumor mutations and potentially lead to the development of tumor neoantigens (65).

A detailed understanding of these pleiotropic effects will facilitate the rational design of curative combination therapies. Leidner et al. reported a patient with metastatic pancreatic cancer who received a single infusion of genetically engineered autologous T-cells targeting mutant KRAS-G12D. This led to a 72% partial response at 6 months according to the currently ongoing Response Evaluation Criteria in Solid Tumors version 1.1. Engineered T cells constitute over 2% of the circulating T cells (66). The occurrence of distinct co-mutations affects the clinical efficacy of immunotherapies. In another study involving 536 patients with KRAS-mutant lung adenocarcinoma, both STK11 and KEAP1 mutations in the presence of a KRAS mutation were associated with poor response rates to anti-PD-L1 inhibitors. Median PFS and OS were significantly shorter for KRAS-mutant/STK11-mutant NSCLC (2.0 and 6.2 months, respectively) than that for KRAS-mutant/STK11-wildtype (4.8 and 17.3 months, respectively; HR 2.04, 95% CI 1.66–2.51, $p < 0.0001$) varieties.

Similarly, patients with KRAS-mutant/KEAP1-mutant NSCLC had lower PFS and OS (1.8 and 4.8 months, respectively) than those with KRAS-mutant/KEAP1-wildtype variety (4.6 and 18.4 months, respectively; HR 2.05, 95% CI 1.63–2.59, $p < 0.0001$) (67).

6.1 Immunotherapy in KRAS-mutant cancers

Immunotherapy has revolutionized the landscape of cancer therapy, especially ICIs, which have been aggressively tested in almost all cancer types. The discovery of immune checkpoints, including cytotoxic T lymphocyte protein 4 (CTLA4), PD-1, and PD-L1, was a breakthrough in cancer immunotherapy. Data obtained from human cancer studies and transgenic mouse models suggest that immune responses aimed at safeguarding the host can be overcome in RAS-driven cancers (47). A KRAS-G12D-induced mouse model also demonstrated that the initial immune response was inhibited, eventually leading to immune evasion. Therefore, resuscitation of the depressed immune surveillance system may be an efficient approach for the treatment of RAS-mutant cancers.

A good immunotherapy response is predicted by a high mutational burden, elevated PD-L1 expression, and an increased prevalence of tumor-infiltrating lymphocytes (TILs). KRAS-mutant NSCLC cells display a high mutational burden and are densely infiltrated by T-cells. In addition, a meta-analysis of 26 studies (n=7,541 patients) indicated that tumors with KRAS mutations had higher levels of PD-L1 than tumors without KRAS mutations; odds ratio (OR) =1.45, 95% CI, 1.18-1.80, P= 0.001) (68). Further, KRAS mutations can induce the upregulation of PD-L1. According to Coelho et al., PD-L1 expression in tumor cells can be influenced by activating the oncogenic RAS pathway, which is accomplished through post-transcriptional regulation of PD-L1 mRNA (69).

Thus, immunotherapy for KRAS-mutant lung cancer may show potential. A subgroup analysis of CheckMate-057 exhibited prolonged outcomes with ICIs than with docetaxel in patients with KRAS-mutant NSCLC (mean OS, 12.2 vs 9.4 months; P=0.002) (70). The exploratory analysis of KEYNOTE-042 revealed pembrolizumab monotherapy as the first-line therapy, which exhibited more pronounced benefits over chemotherapy in patients with KRAS mutations (mean OS, 28 vs 11 months; hazard ratio, 0.42; 95% CI, 0.22-0.81) than those with KRAS wild type (mean OS, 15 vs 12 months; hazard ratio, 0.86; 95% CI, 0.63-1.18). Recently, a retrospective study evaluated the correlation of KRAS status with outcomes following immunotherapy in patients with PD-L1≥50%. Among patients treated using ICI monotherapy, the KRAS variant was related to a superior survival than did KRAS wild-type (mean OS, 21.1 vs 13.6 months; P =0.03). The CCTG PA.7 study compared gemcitabine and nab-paclitaxel, with and without durvalumab and tremelimumab, in metastatic pancreatic ductal adenocarcinoma. Combination immunotherapy did not improve survival among the unselected patient population but improved survival for patients with wild-type KRAS tumors (NCT02879318) (71).

Many patients with KRAS-mutant NSCLC receive ICIs as first-line treatment because of their limited approval for second-line use. Combining KRAS inhibitors with ICIs is logical given the diverse mechanisms of mutant KRAS during immune response. Mouse models treated with sotorasib and ICIs showed pro-inflammatory changes in the TME and synergistic tumor cell killing. Adagrasib also induces a pro-inflammatory state and enhances immune cell infiltration. Combination therapy resulted in lasting anti-tumor and memory immune cell responses in mice. Future studies should explore combination therapies, predictive biomarkers, and mechanisms of resistance in KRAS-mutant cancers (9).

7 Combination therapy of RAS inhibitors for RAS-mutant cancers

In preclinical models, combination treatment with AMG510 caused regression of KRAS-G12C-mutant tumors and improved the anti-tumor efficacy of targeted agents and chemotherapy (9). When combined with immunotherapy, AMG510 induces complete and durable tumor regression. The improved efficacy of the combination therapy may be attributed to increased immune cell infiltration and activation. In preclinical models, the AMG510 monotherapy and combination therapy groups demonstrated a notable increase in CD8+ T cell infiltration, which was not observed in the anti-PD-1 monotherapy group. Additionally, AMG510 treatment increased the infiltration of macrophages and CD103+ cross-presenting dendritic cells, which play vital roles in T-cell priming, activation, and recruitment. Furthermore, the combination of AMG510 and anti-PD-1 therapy promoted the establishment of a memory T cell response and enhanced antigen recognition. Phase I/II clinical trials evaluating the efficacy and safety of sotorasib in combination with PD-1/PD-L1 inhibitors in patients with advanced solid tumors and KRAS-G12C mutations are ongoing (CodeBreaK 100/101).

Preclinical models have also demonstrated that human epidermal growth factor receptor (EGFR) family inhibitors, SHP2 inhibitors, mammalian target of rapamycin (mTOR) inhibitors, and inhibition of CDK4/6 could enhance the anti-tumor activity of MRTX849 and inhibit KRAS-dependent signaling pathways (46). Clinical trials were conducted to evaluate the efficacy and safety of combination therapy of adagrasib with pembrolizumab (a PD-1 inhibitor) or afatinib (an HER family inhibitor) in patients with NSCLC, with cetuximab in patients with colorectal cancer, and with TNO-155 in patients with advanced solid tumors. Preliminary results showed that more than 50 patients were treated with adagrasib in combination with either pembrolizumab (a PD-1 inhibitor) for NSCLC, cetuximab (an anti-EGFR antibody) for colorectal cancer, or TNO-155 (an SHP-2 inhibitor) for NSCLC or colorectal cancer. All the combination therapies were well tolerated by patients (48). A phase I-II clinical trial evaluated the efficacy and safety of adagrasib monotherapy or in combination with cetuximab in heavily pretreated patients with metastatic colorectal cancer and mutant KRAS-G12C. The results revealed that 19% of the 43 evaluated patients in the monotherapy group

responded, with a median response duration of 4.3 months and a median PFS of 5.6 months. However, the combination therapy group had a higher response rate (46%), with a median response duration of 7.6 months and a median PFS of 6.9 months (72). A phase II clinical trial evaluated the efficacy of adagrasib in patients with KRAS-G12C-mutant NSCLC previously treated with platinum-based chemotherapy and anti-PD-1 or PD-L1 therapy. The results showed that 48 of the 112 enrolled patients had a confirmed objective response, with a median response duration of 8.5 months and a median PFS of 6.5 months. The median OS was 12.6 months (73).

A phase Ib/II clinical trial to characterize the safety and tolerability of JDQ443 in combination with TNO155, spartalizumab (a PD-1 inhibitor), or TNO155 and spartalizumab in patients with advanced solid tumors and KRAS-G12C mutations is ongoing (NCT04699188) (74). Another phase I trial to assess the safety and preliminary activity of GDC-6036 in combination with atezolizumab (a PD-L1 inhibitor) or erlotinib in patients with NSCLC, cetuximab in patients with colorectal cancer, or bevacizumab in patients with advanced solid tumors is underway (NCT04449874). D-1553 is also the regimen used in clinical trials to assess the anti-tumor activity of combination therapy of RAS inhibitors with other treatments (NCT04585035). However, the results of these studies have not been reported. The combination therapies for RAS inhibitors used in clinical development are shown in Table 1.

8 Inhibitors of KRAS and associated molecular pathways

8.1 Upstream RAS pathways and KRAS inhibitors

Normal RAS upstream signaling requires activation by GEFs, membrane localization, effector binding, and nucleotide exchange and processing (75). Therefore, the disruption of any of these steps could indirectly inhibit RAS activation. Son of Sevenless (SOS) is a GEF that activates important cell signaling pathways and acts as a pacemaker for the RAS (76). Elimination of SOS1 specifically induces a decrease in the survival rate of tumor cells carrying a KRAS mutation, while exhibiting no significant impact on those with wild-type KRAS (77). BAY293, BI-3406, and BI-1701963 are SOS1 inhibitors developed to inhibit the protein-protein interactions of KRAS-SOS1 (78–80). However, preclinical studies have shown that BAY 293 only demonstrates modest antiproliferative effects, and no significant difference between KRAS mutation and wild-type was observed (78). BI-3406 exhibited more encouraging anti-tumor activity. It not only selectively inhibited the proliferation of KRAS-mutant cancer cells but also blocked the negative feedback reactivated by SOS1 (79). BI-1701963, an improved version of BI-3406, is currently in three phase I trials to determine the safety, tolerability, and pharmacokinetic parameters of BI-1701963 monotherapy or in combination with trametinib, BI-3011441 (a MEK inhibitor), or irinotecan in patients with KRAS-mutated cancers (NCT04111458, NCT04835714, and NCT04627142).

As a non-receptor protein tyrosine phosphatase, SHP2 is encoded by PTPN11, plays an important role in signal transduction downstream of various growth factors, and increases RAS nucleotide exchange by binding to GRB2 and SOS1 (81). The complete activation of the RAS-MAPK pathway requires SHP2; thus, the essential role of SHP2 in oncogenic signaling is established. The inhibition or deletion of SHP2 delays tumor progression in established tumors. SHP-099 and RMC-4550 are both potent and selective SHP2 allosteric inhibitors (82, 83). Both reduced cell proliferation, but the sensitivities differed among different KRAS-mutated cancer cells. Another study revealed that IACS-13909, a potent and specific allosteric inhibitor of SHP2, effectively inhibited tumor cell proliferation *in vitro* and caused regression of tumors *in vivo* in NSCLC models that exhibited resistance to osimertinib due to EGFR mutations (84). However, the anti-tumor activity of IACS-13909 against KRAS-mutant cancer cells has not yet been established.

Although SHP2 inhibitors offer a potential therapeutic solution for receptor tyrosine kinase-driven cancers, they may not adequately suppress tumor growth in KRAS-mutated cells when administered alone (83). In KRAS-mutant tumors, resistance to MEK inhibition is common owing to the activation of the receptor tyrosine kinase signaling pathway. However, combination treatment with MEK and SHP2 inhibitors resulted in the continued regression of tumor growth in xenograft models of pancreatic cancer and NSCLC derived from patients, indicating the clinical efficacy of dual SHP2/MEK inhibition for KRAS-mutant cancers (85).

RMC-4630 (SAR442720) is an SHP2 inhibitor under phase I/II trial that evaluates the safety, MTD, and RP2D of RMC-4630 in combination with cobimetinib in patients with relapsed/refractory solid tumors and combination with osimertinib in patients with EGFR-mutant locally advanced or metastatic NSCLC (NCT04000529). Another two phase I trial evaluating the safety of RMC-4630 monotherapy (NCT03634982) and in combination with pembrolizumab (NCT04418661) in advanced solid tumor patients presented in the AACR ANNUAL MEETING 2020 showed that the combination of RMC-4630 with cobimetinib has acceptable tolerability, and tumor reduction was observed in three of eight patients with KRAS-mutant colorectal cancer, including one unconfirmed PR at the data cut-off (86). TNO155 (NCT03114319, NCT04000529, NCT04330664, and NCT04699188), JAB-3068 (NCT04721223, NCT03518554, and NCT03565003), and JAB-3312 (NCT04121286 and NCT04045496) are all SHP2 inhibitors currently in clinical trials. However, the results of these studies have not yet been published.

In addition, complete RAS activation requires a post-translational process to associate with the membrane, protein oligomerization or dimerization, and effector binding. RAS can also self-associate to enhance scaffolding and signaling activities via dimerization. Disruption of any of these steps appears to effectively block RAS signaling. However, there remains a challenge that needs to be overcome. Enzymes involved in the post-translational process also process other membrane-associated proteins that can cause intolerable toxicity. Owing to the challenges in reconstituting RAS dimers and oligomers *in vitro*, the study of the molecular intricacies

of RAS-RAS interactions has been limited to a combination of computational modeling and experimental validation of protein interactions.

8.2 Downstream effectors of RAS pathways and KRAS inhibitors

Once activated, RAS interacts with a diverse array of downstream effectors, each of which plays a unique role in signal transduction. Some key effector pathways include the RAF-MEK-ERK, PI3K-AKT-mTOR, and RalGDS pathways. The RAF-MEK-ERK pathway is one of the most well-studied RAS effector pathways. It involves the activation of RAF kinases (such as ARAF, BRAF, and CRAF), which phosphorylate and activate MEK1/2. MEK1/2 then phosphorylates and activates ERK1/2, leading to the regulation of gene expression and cellular processes, such as proliferation, differentiation, and survival. The PI3K-AKT-mTOR pathway is an important RAS effector pathway. RAS activates phosphoinositide 3-kinase (PI3K), leading to the production of phosphatidylinositol-3,4,5-trisphosphate (PIP3). PIP3 recruits and activates protein kinase B (AKT), which regulates multiple downstream effectors involved in cell growth, metabolism, and survival. AKT also regulates the mammalian target of the rapamycin (mTOR) pathway, thereby influencing protein synthesis and cell proliferation. The RalGDS pathway involves the activation of the Ral guanine nucleotide dissociation stimulator (RalGDS) by RAS. RalGDS activates Ral GTPases that participate in diverse cellular processes, including cytoskeletal organization, membrane trafficking, and cell transformation. These downstream effectors represent only a fraction of the intricate network of signaling pathways regulated by RAS. The complexity and diversity of RAS signaling indicate its fundamental importance in cellular physiology and its role in various diseases, particularly cancer (87, 88).

Downstream effectors of the RAS pathway, particularly those in the RAF-MEK-ERK and PI3K-AKT-mTOR signaling pathways, have become attractive targets for anti-RAS mutation treatment. Numerous inhibitors targeting different constituents of the RAF-MEK-ERK and PI3K-AKT-mTOR effector pathways have been developed and are currently undergoing clinical assessment; however, their effectiveness appears to be limited (89–91). The RAF pathway plays a significant role in the promotion of RAS-driven cancer growth. Studies conducted in mouse models have indicated that only the constituents of the RAF-MEK-ERK pathway can compensate for the loss of RAS function and revive the growth of RAS-deficient mouse embryonic fibroblasts. However, inhibition with a single-component RAF, MEK, or ERK could lead to negative feedback, which might explain poor efficacy (92). Although the PI3K pathway may have a minimal effect on promoting RAS-dependent cancer growth, it complements the RAF-MEK-ERK cascade. Therefore, resistance to RAF pathway inhibitors may be mediated via the PI3K pathway. Thus, a combination strategy with other inhibitors as mentioned previously or immunotherapy might be required to completely suppress the signaling pathway as an effective strategy for RAS-mutant cancer.

Although the clinical data of immunotherapy are limited in other solid tumors with RAS mutations, the efficacy of a combinational strategy of immunotherapy with RAS inhibitors or inhibitors of downstream effectors of the RAS pathway, particularly the MAPK pathway, is worth anticipating, and the possible reason has been discussed previously. Clinical trials are ongoing, as previously discussed. The adoptive cell approach and cancer vaccines, two other immunotherapeutic approaches to treat RAS-driven cancers, have shown certain efficacy, but further research is still needed (93, 94).

9 Discussion

KRAS mutations have long been considered attractive targets for cancer therapy. After decades of effort, KRAS mutations are no longer considered undruggable. KRAS-G12C allele-specific inhibitors exhibit promising efficacy in clinical trials and have the potential to alter the treatment status of RAS-mutant cancers. Sotorasib and adagrasib have shown promising results in inhibiting KRAS-G12C and controlling tumor growth. Disease control was observed in a significant percentage of patients, and tumor shrinkage was also noted. However, some patients developed resistance mechanisms, such as mutations activating RAS or the RAS pathway, which rendered the drugs less effective. Combining KRAS-G12C inhibitors with other targeted therapies, like cetuximab or SHP2 inhibitors, has shown enhanced activity in preclinical studies. Resistance mutations were more frequent in patients with lung or colorectal cancer treated with adagrasib. Multiple types of lesions were identified, including mutations preventing drug binding, non-G12C activation of RAS, KRAS amplification, and activation of other pathway components. The presence of multiple and diverse resistance mechanisms poses a challenge to the efficacy of RAS inhibitors. However, similar mechanisms have been observed in resistance to other targeted therapies, indicating the need for further investigation. Despite these challenges, KRAS-G12C inhibitors have demonstrated clinical benefit and are likely to be useful as second-line treatments for lung cancer. Continued research and development are expected to lead to improved drugs and combination therapies that can enhance tumor-cell death and prevent adaptive resistance. Additionally, a new G12C inhibitor that targets active RAS-GTP is being developed and has shown effectiveness against KRAS-G12C tumor cells with resistance to previous inhibitors.

Even though the inhibition of the RAS pathway, including the MAPK and PI3K pathways, showed poor efficacy after monotherapy, a combinational strategy could be useful to improve efficacy. Patients with KRAS-mutant NSCLC can benefit from immunotherapy, and clinical trials evaluating the efficacy of adoptive cell therapy and cancer vaccines are ongoing.

Agents inhibiting RAS post-translational modifications during development have also been researched. Posttranslational modifications of RAS proteins include palmitoylation and depalmitoylation. Palmitoylation attaches palmitic fatty acids to specific amino acid residues, thereby promoting membrane associations and functionality. Depalmitoylation removes these

groups and redistributes RAS proteins to the active membrane sites. Inhibition of depalmitoylation has been proposed to hinder RAS membrane binding and functionality. Other modifications such as phosphorylation, nitrosylation, ubiquitination, and acetylation also regulate RAS localization and function. These modifications are potential targets for the development of anti-RAS drugs; however, their mechanisms of action and therapeutic relevance are still controversial. Further research is required to validate their feasibility and specificity for anticancer therapy (8).

Given the encouraging efficacy of KRAS-G12C allele-specific inhibitors, specific inhibitors may be the most promising therapeutic options. However, in addition to KRAS-G12C, other mutations, such as KRAS-G12D and KRAS-G12V, account for a large proportion of KRAS mutations. Therefore, the development of inhibitors targeting specific RAS mutations to provide personalized medicine may be a future direction. However, according to the presented results, the efficacy of sotorasib differs in NSCLC and colorectal cancer and drug resistance is inevitable (10, 52). In addition, combination therapies involving immunotherapy and other targeted therapies or chemotherapies may be worth exploring. The studies discussed in previous sections have shown promising outcomes when KRAS inhibitors were combined with ICIs or other targeted agents. Further investigations should focus on optimizing the treatment regimens, identifying predictive biomarkers, and understanding the mechanisms underlying the synergistic effects observed in preclinical models. Furthermore, understanding the TME and the role of immune cells in KRAS-mutant cancers is crucial. Exploring the factors influencing immune cell infiltration, activation, and recruitment can help in designing strategies to enhance anti-tumor immune responses. Investigating the mechanisms underlying immunotherapy resistance in KRAS-mutant cancers is an important area for future research. This knowledge can guide the development of novel therapeutic approaches to overcome drug resistance and improve patient outcomes. To address these unresolved issues, developing a comprehensive model that integrates the complex interactions between KRAS signaling, the immune system, and the tumor microenvironment would be valuable. Such a model could help explain the observed heterogeneity in treatment responses and potentially predict personalized treatment regimens and responses. This could also guide the design of clinical trials and treatment strategies. Therefore, exploring combination strategies for patients with distinct tumors is vital.

Author contributions

XW drafted the manuscript. WS and CC helped in the literature search. DL provided administrative and financial support, manuscript revision, and final approval of the manuscript. All authors contributed to the article and approved the submitted version.

Conflict of interest

The authors declare that the research was conducted in the absence of any commercial or financial relationships that could be construed as a potential conflict of interest.

Publisher's note

Supplementary material

The Supplementary Material for this article can be found online at: https://www.frontiersin.org/articles/10.3389/fimmu.2023.1223433/full#supplementary-material

References

1. Kirsten WH, Mayer LA. Morphologic responses to a murine erythroblastosis virus. *J Natl Cancer Institute* (1967) 39(2):311–35.

2. Moore AR, Rosenberg SC, McCormick F, Malek S. Ras-targeted therapies: Is the undruggable drugged? *Nat Rev Drug Discovery* (2020) 19(8):533–52. doi: 10.1038/s41573-020-0068-6

3. Cancer Genome Atlas Network. Comprehensive molecular characterization of human colon and rectal cancer. *Nature* (2012) 487(7407):330–7. doi: 10.1038/nature11252

4. Ma YS, Huang T, Zhong XM, Zhang HW, Cong XL, Xu H, et al. Proteogenomic characterization and comprehensive integrative genomic analysis of human colorectal cancer liver metastasis. *Mol Cancer* (2018) 17(1):139. doi: 10.1186/s12943-018-0890-1

5. Cancer Genome Atlas Research Network.Comprehensive molecular profiling of lung adenocarcinoma. *Nature* (2014) 511(7511):543–50. doi: 10.1038/nature13385

6. Cancer Genome Atlas Research Network. Integrated genomic characterization of pancreatic ductal adenocarcinoma. *Cancer Cell* (2017) 32(2):185–203.e13. doi: 10.1016/j.ccell.2017.07.007

7. Papke B, Der CJ. Drugging ras: Know the enemy. *Sci (New York NY)* (2017) 355 (6330):1158–63. doi: 10.1126/science.aam7622

8. Cox AD, Fesik SW, Kimmelman AC, Luo J, Der CJ. Drugging the undruggable ras: Mission possible? *Nat Rev Drug Discovery* (2014) 13(11):828–51. doi: 10.1038/nrd4389

9. Canon J, Rex K, Saiki AY, Mohr C, Cooke K, Bagal D, et al. The clinical kras (G12c) inhibitor amg 510 drives anti-tumour immunity. *Nature* (2019) 575(7781):217–23. doi: 10.1038/s41586-019-1694-1

10. Hong DS, Fakih MG, Strickler JH, Desai J, Durm GA, Shapiro GI, et al. Kras (G12c) inhibition with sotorasib in advanced solid tumors. *New Engl J Med* (2020) 383 (13):1207–17. doi: 10.1056/NEJMoa1917239

11. Janes MR, Zhang J, Li LS, Hansen R, Peters U, Guo X, et al. Targeting kras mutant cancers with a covalent G12c-specific inhibitor. *Cell* (2018) 172(3):578–89.e17. doi: 10.1016/j.cell.2018.01.006

12. Nagasaka M, Li Y, Sukari A, Ou SI, Al-Hallak MN, Azmi AS. Kras G12c game of thrones, which direct kras inhibitor will claim the iron throne? *Cancer Treat Rev* (2020) 84:101974. doi: 10.1016/j.ctrv.2020.101974

13. *FDA Grants Sotorasib Priority Review Designation For The Treatment Of Patients With KRAS G12C-Mutated Locally Advanced Or Metastatic Non-Small Cell Lung Cancer*. (2021). Retrieved February 16, 2021, Available at: https://www.prnewswire.com/news-releases/fda-grants-sotorasib-priority-review-designation-for-the-treatment-of-patients-with-kras-g12c-mutated-locally-advanced-or-metastatic-non-small-cell-lung-cancer-301229256.html.

14. FDA approves first KRAS inhibitor: Sotorasib. *Cancer Discov* (2021) 11(8):Of4. doi: 10.1158/2159-8290.Cd-nb2021-0362

15. Malumbres M, Barbacid M. Ras oncogenes: The first 30 years. *Nat Rev Cancer* (2003) 3(6):459–65. doi: 10.1038/nrc1097

16. Murugan AK, Grieco M, Tsuchida N. Ras mutations in human cancers: Roles in precision medicine. *Semin Cancer Biol* (2019) 59:23–35. doi: 10.1016/j.semcancer.2019.06.007

17. Johnson L, Mercer K, Greenbaum D, Bronson RT, Crowley D, Tuveson DA, et al. Somatic activation of the K-ras oncogene causes early onset lung cancer in mice. *Nature* (2001) 410(6832):1111–6. doi: 10.1038/35074129

18. Pylayeva-Gupta Y, Grabocka E, Bar-Sagi D. Ras oncogenes: Weaving a tumorigenic web. *Nat Rev Cancer* (2011) 11(11):761–74. doi: 10.1038/nrc3106

19. Cancer Genome Atlas NetworkComprehensive genomic characterization of head and neck squamous cell carcinomas. *Nature* (2015) 517(7536):576–82. doi: 10.1038/nature14129

20. Robertson AG, Kim J, Al-Ahmadie H, Bellmunt J, Guo G, Cherniack AD, et al. Comprehensive molecular characterization of muscle-invasive bladder cancer. *Cell* (2018) 174(4):1033. doi: 10.1016/j.cell.2018.07.036

21. Burd CE, Liu W, Huynh MV, Waqas MA, Gillahan JE, Clark KS, et al. Mutation-specific ras oncogenicity explains nras codon 61 selection in melanoma. *Cancer Discovery* (2014) 4(12):1418–29. doi: 10.1158/2159-8290.Cd-14-0729

22. Chen Z, Otto JC, Bergo MO, Young SG, Casey PJ. The C-terminal polylysine region and methylation of K-ras are critical for the interaction between K-ras and microtubules. *J Biol Chem* (2000) 275(52):41251–7. doi: 10.1074/jbc.M006687200

23. McGrath JP, Capon DJ, Smith DH, Chen EY, Seeburg PH, Goeddel DV, et al. Structure and organization of the human ki-ras proto-oncogene and a related processed pseudogene. *Nature* (1983) 304(5926):501–6. doi: 10.1038/304501a0

24. Plowman SJ, Berry RL, Bader SA, Luo F, Arends MJ, Harrison DJ, et al. K-ras 4a and 4b are co-expressed widely in human tissues, and their ratio is altered in sporadic colorectal cancer. *J Exp Clin Cancer Res CR* (2006) 25(2):259–67.

25. Tsai FD, Lopes MS, Zhou M, Court H, Ponce O, Fiordalisi JJ, et al. K-ras4a splice variant is widely expressed in cancer and uses a hybrid membrane-targeting motif. *Proc Natl Acad Sci United States America* (2015) 112(3):779–84. doi: 10.1073/pnas.1412811112

26. Keohavong P, DeMichele MA, Melacrinos AC, Landreneau RJ, Weyant RJ, Siegfried JM. Detection of K-ras mutations in lung carcinomas: Relationship to prognosis. *Clin Cancer Res* (1996) 2(2):411–8.

27. Kompier LC, Lurkin I, van der Aa MN, van Rhijn BW, van der Kwast TH, Zwarthoff EC. Fgfr3, hras, kras, nras and pik3ca mutations in bladder cancer and their potential as biomarkers for surveillance and therapy. *PloS One* (2010) 5(11):e13821. doi: 10.1371/journal.pone.0013821

28. Perentesis JP, Bhatia S, Boyle E, Shao Y, Shu XO, Steinbuch M, et al. Ras oncogene mutations and outcome of therapy for childhood acute lymphoblastic leukemia. *Leukemia* (2004) 18(4):685–92. doi: 10.1038/sj.leu.2403272

29. Rahul E, Goel H, Chopra A, Ranjan A, Gupta AK, Meena JP, et al. An updated account on molecular heterogeneity of acute leukemia. *Am J Blood Res* (2021) 11(1):22–43.

30. Califano R, Landi L, Cappuzzo F. Prognostic and predictive value of K-ras mutations in non-small cell lung cancer. *Drugs* (2012) 72 Suppl 1:28–36. doi: 10.2165/1163012-s0-000000000-00000

31. Slebos RJ, Kibbelaar RE, Dalesio O, Kooistra A, Stam J, Meijer CJ, et al. K-ras oncogene activation as a prognostic marker in adenocarcinoma of the lung. *New Engl J Med* (1990) 323(9):561–5. doi: 10.1056/nejm199008303230902

32. Shepherd FA, Domerg C, Hainaut P, Jänne PA, Pignon JP, Graziano S, et al. Pooled analysis of the prognostic and predictive effects of kras mutation status and kras mutation subtype in early-stage resected non-small-cell lung cancer in four trials of adjuvant chemotherapy. *J Clin Oncol* (2013) 31(17):2173–81. doi: 10.1200/jco.2012.48.1390

33. Vögler O, Barceló JM, Ribas C, Escribá PV. Membrane interactions of G proteins and other related proteins. *Biochim Biophys Acta* (2008) 1778(7-8):1640–52. doi: 10.1016/j.bbamem.2008.03.008

34. Saini DK, Chisari M, Gautam N. Shuttling and translocation of heterotrimeric G proteins and ras. *Trends Pharmacol Sci* (2009) 30(6):278–86. doi: 10.1016/j.tips.2009.04.001

35. Gao J, Liao J, Yang GY. Caax-box protein, prenylation process and carcinogenesis. *Am J Trans Res* (2009) 1(3):312–25.

36. Klimpel A, Stillger K, Wiederstein JL, Krüger M, Neundorf I. Cell-permeable caax-peptides affect K-ras downstream signaling and promote cell death in cancer cells. *FEBS J* (2021) 288(9):2911–29. doi: 10.1111/febs.15612

37. Hunter JC, Manandhar A, Carrasco MA, Gurbani D, Gondi S, Westover KD. Biochemical and structural analysis of common cancer-associated kras mutations. *Mol Cancer Res MCR* (2015) 13(9):1325–35. doi: 10.1158/1541-7786.Mcr-15-0203

38. Rabara D, Tran TH, Dharmaiah S, Stephens RM, McCormick F, Simanshu DK, et al. Kras G13d sensitivity to neurofibromin-mediated gtp hydrolysis. *Proc Natl Acad Sci United States America* (2019) 116(44):22122–31. doi: 10.1073/pnas.1908353116

39. Drugan JK, Rogers-Graham K, Gilmer T, Campbell S, Clark GJ. The ras/P120 gtpase-activating protein (Gap) interaction is regulated by the P120 gap pleckstrin homology domain. *J Biol Chem* (2000) 275(45):35021–7. doi: 10.1074/jbc.M004386200

40. Saxena N, Lahiri SS, Hambarde S, Tripathi RP. Ras: Target for cancer therapy. *Cancer Invest* (2008) 26(9):948–55. doi: 10.1080/07357900802087275

41. Stephen AG, Esposito D, Bagni RK, McCormick F. Dragging ras back in the ring. *Cancer Cell* (2014) 25(3):272–81. doi: 10.1016/j.ccr.2014.02.017

42. Ostrem JM, Peters U, Sos ML, Wells JA, Shokat KM. K-ras(G12c) inhibitors allosterically control gtp affinity and effector interactions. *Nature* (2013) 503(7477):548–51. doi: 10.1038/nature12796

43. Lanman BA, Allen JR, Allen JG, Amegadzie AK, Ashton KS, Booker SK, et al. Discovery of a covalent inhibitor of kras(G12c) (Amg 510) for the treatment of solid tumors. *J medicinal Chem* (2020) 63(1):52–65. doi: 10.1021/acs.jmedchem.9b01180

44. Hofmann MH, Gerlach D, Misale S, Petronczki M, Kraut N. Expanding the reach of precision oncology by drugging all KRAS mutants. *Cancer Discov* (2022) 12(4):924–37. doi: 10.1158/2159-8290.CD-21-1331

45. de Langen AJ, Johnson ML, Mazieres J, Dingemans AC, Mountzios G, Pless M, et al. Sotorasib versus docetaxel for previously treated non-small-cell lung cancer with kras(G12c) mutation: A randomised, open-label, phase 3 trial. *Lancet (London England)* (2023) 401(10378):733–46. doi: 10.1016/s0140-6736(23)00221-0

46. Fell JB, Fischer JP, Baer BR, Blake JF, Bouhana K, Briere DM, et al. Identification of the clinical development candidate mrtx849, a covalent kras(G12c) inhibitor for the treatment of cancer. *J medicinal Chem* (2020) 63(13):6679–93. doi: 10.1021/acs.jmedchem.9b02052

47. Hallin J, Engstrom LD, Hargis L, Calinisan A, Aranda R, Briere DM, et al. The kras(G12c) inhibitor mrtx849 provides insight toward therapeutic susceptibility of kras-mutant cancers in mouse models and patients. *Cancer Discovery* (2020) 10(1):54–71. doi: 10.1158/2159-8290.Cd-19-1167

48. Mirati Therapeutics Inc. *Mirati therapeutics reports investigational adagrasib (MRTX849) preliminary data demonstrating tolerability and durable anti-tumor activity as well as initial MRTX1133 preclinical data*. (2020). Available at: https://ir.mirati.com/press-releases/press-release-details/2020/Mirati-Therapeutics-Reports-Investigational-Adagrasib-MRTX849-Preliminary-Data-Demonstrating-Tolerability-and-Durable-Anti-Tumor-Activity-as-well-as-Initial-MRTX1133-Preclinical-Data/default.aspx.

49. Wang J, Martin-ROmano P, Cassier P, Johnson M, Haura E, Lenox L, et al. Phase I study of jnj-74699157 in patients with advanced solid tumors harboring the kras G12c mutation. *oncologist* (2022) 27(7):536–e53. doi: 10.1093/oncolo/oyab080

50. Patricelli MP, Janes MR, Li LS, Hansen R, Peters U, Kessler LV, et al. Selective inhibition of oncogenic kras output with small molecules targeting the inactive state. *Cancer Discovery* (2016) 6(3):316–29. doi: 10.1158/2159-8290.Cd-15-1105

51. Center for Drug Evalution, Nmpa . Available at: http://www.cde.org.cn/news.do?method=changePage&pageName=service&frameStr=25.

52. Dunnett-Kane V, Nicola P, Blackhall F, Lindsay C. Mechanisms of resistance to KRASG12C inhibitors. *Cancers (Basel)* (2021) 13(1):151. doi: 10.3390/cancers13010151

53. Li S, Balmain A, Counter CM. A model for ras mutation patterns in cancers: Finding the sweet spot. *Nat Rev Cancer* (2018) 18(12):767–77. doi: 10.1038/s41568-018-0076-6

54. Skoulidis F, Byers LA, Diao L, Papadimitrakopoulou VA, Tong P, Izzo J, et al. Co-occurring genomic alterations define major subsets of kras-mutant lung adenocarcinoma with distinct biology, immune profiles, and therapeutic vulnerabilities. *Cancer Discovery* (2015) 5(8):860–77. doi: 10.1158/2159-8290.Cd-14-1236

55. Nassar AH, Adib E, Kwiatkowski DJ. Distribution of kras (G12c) somatic mutations across race, sex, and cancer type. *New Engl J Med* (2021) 384(2):185–7. doi: 10.1056/NEJMc2030638

56. Welsch ME, Kaplan A, Chambers JM, Stokes ME, Bos PH, Zask A, et al. Multivalent small-molecule pan-ras inhibitors. *Cell* (2017) 168(5):878–89.e29. doi: 10.1016/j.cell.2017.02.006

57. Vidimar V, Beilhartz GL, Park M, Biancucci M, Kieffer MB, Gius DR, et al. An engineered chimeric toxin that cleaves activated mutant and wild-type ras inhibits tumor growth. *Proc Natl Acad Sci United States America* (2020) 117(29):16938–48. doi: 10.1073/pnas.2000312117

58. Tisi R, Spinelli M, Palmioli A, Airoldi C, Cazzaniga P, Besozzi D, et al. The multi-level mechanism of action of a pan-ras inhibitor explains its antiproliferative activity on cetuximab-resistant cancer cells. *Front Mol Biosci* (2021) 8:625979. doi: 10.3389/fmolb.2021.625979

59. Drosten M, Dhawahir A, Sum EY, Urosevic J, Lechuga CG, Esteban LM, et al. Genetic analysis of ras signalling pathways in cell proliferation, migration and survival. *EMBO J* (2010) 29(6):1091–104. doi: 10.1038/emboj.2010.7

60. Drosten M, Lechuga CG, Barbacid M. Genetic analysis of ras genes in epidermal development and tumorigenesis. *Small GTPases* (2013) 4(4):236–41. doi: 10.4161/sgtp.26905

61. Drosten M, Lechuga CG, Barbacid M. Ras signaling is essential for skin development. *Oncogene* (2014) 33(22):2857–65. doi: 10.1038/onc.2013.254

62. Awad MM, Liu S, Rybkin II, KC A, Dilly J, VW Z, et al. Acquired resistance to kras(G12c) inhibition in cancer. *N Engl J Med* (2021) 384(25):2382–93. doi: 10.1056/NEJMoa2105281

63. Hamarsheh S, Groß O, Brummer T, Zeiser R. Immune modulatory effects of oncogenic kras in cancer. *Nat Commun* (2020) 11(1):5439. doi: 10.1038/s41467-020-19288-6

64. Dias Carvalho P, Guimarães CF, Cardoso AP, Mendonça S, Costa ÂM, Oliveira MJ, et al. Kras oncogenic signaling extends beyond cancer cells to orchestrate the microenvironment. *Cancer Res* (2018) 78(1):7–14. doi: 10.1158/0008-5472.Can-17-2084

65. Arbour KC, Jordan E, Kim HR, Dienstag J, Yu HA, Sanchez-Vega F, et al. Effects of co-occurring genomic alterations on outcomes in patients with kras-mutant non-small cell lung cancer. *Clin Cancer Res* (2018) 24(2):334–40. doi: 10.1158/1078-0432.Ccr-17-1841

66. Leidner R, Sanjuan Silva N, Huang H, Sprott D, Zheng C, Shih YP, et al. Neoantigen T-cell receptor gene therapy in pancreatic cancer. *New Engl J Med* (2022) 386(22):2112–9. doi: 10.1056/NEJMoa2119662

67. Ricciuti B, Arbour KC, Lin JJ, Vajdi A, Vokes N, Hong L, et al. Diminished efficacy of programmed death-(Ligand)1 inhibition in stk11- and keap1-mutant lung adenocarcinoma is affected by kras mutation status. *J Thorac Oncol Off Publ Int Assoc Study Lung Cancer* (2022) 17(3):399–410. doi: 10.1016/j.jtho.2021.10.013

68. Lan B, Ma C, Zhang C, Chai S, Wang P, Ding L, et al. Association between pd-L1 expression and driver gene status in non-small-cell lung cancer: A meta-analysis. *Oncotarget* (2018) 9(7):7684–99. doi: 10.18632/oncotarget.23969

69. Coelho MA, de Carné Trécesson S, Rana S, Zecchin D, Moore C, Molina-Arcas M, et al. Oncogenic ras signaling promotes tumor immunoresistance by stabilizing pd-L1 mrna. *Immunity* (2017) 47(6):1083–99.e6. doi: 10.1016/j.immuni.2017.11.016

70. Borghaei H, Paz-Ares L, Horn L, Spigel DR, Steins M, Ready NE, et al. Nivolumab versus docetaxel in advanced nonsquamous non-small-cell lung cancer. *N Engl J Med* (2015) 373(17):1627–39. doi: 10.1056/NEJMoa1507643

71. Renouf DJ, Loree JM, Knox JJ, Topham JT, Kavan P, Jonker D, et al. The cctg pa.7 phase ii trial of gemcitabine and nab-paclitaxel with or without durvalumab and tremelimumab as initial therapy in metastatic pancreatic ductal adenocarcinoma. *Nat Commun* (2022) 13(1):5020. doi: 10.1038/s41467-022-32591-8

72. Yaeger R, Weiss J, Pelster MS, Spira AI, Barve M, Ou SI, et al. Adagrasib with or without cetuximab in colorectal cancer with mutated kras G12c. *New Engl J Med* (2023) 388(1):44–54. doi: 10.1056/NEJMoa2212419

73. Jänne PA, Riely GJ, Gadgeel SM, Heist RS, Ou SI, Pacheco JM, et al. Adagrasib in non-small-cell lung cancer harboring a kras(G12c) mutation. *New Engl J Med* (2022) 387(2):120–31. doi: 10.1056/NEJMoa2204619

74. Lorthiois E, Gerspacher M, Beyer KS, Vaupel A, Leblanc C, Stringer R, et al. Jdq443, a structurally novel, pyrazole-based, covalent inhibitor of kras(G12c) for the treatment of solid tumors. *J medicinal Chem* (2022) 65(24):16173–203. doi: 10.1021/acs.jmedchem.2c01438

75. Schlessinger J. Cell signaling by receptor tyrosine kinases. *Cell* (2000) 103 (2):211–25. doi: 10.1016/s0092-8674(00)00114-8

76. Freedman TS, Sondermann H, Friedland GD, Kortemme T, Bar-Sagi D, Marqusee S, et al. A ras-induced conformational switch in the ras activator son of sevenless. *Proc Natl Acad Sci United States America* (2006) 103(45):16692–7. doi: 10.1073/pnas.0608127103

77. Hall BE, Yang SS, Boriack-Sjodin PA, Kuriyan J, Bar-Sagi D. Structure-based mutagenesis reveals distinct functions for ras switch 1 and switch 2 in sos-catalyzed guanine nucleotide exchange. *J Biol Chem* (2001) 276(29):27629–37. doi: 10.1074/jbc.M101727200

78. Hillig RC, Sautier B, Schroeder J, Moosmayer D, Hilpmann A, Stegmann CM, et al. Discovery of potent sos1 inhibitors that block ras activation via disruption of the ras-sos1 interaction. *Proc Natl Acad Sci United States America* (2019) 116(7):2551–60. doi: 10.1073/pnas.1812963116

79. Hofmann MH, Gmachl M, Ramharter J, Savarese F, Gerlach D, Marszalek JR, et al. BI-3406, a potent and selective SOS1-KRAS interaction inhibitor, is effective in KRAS-driven cancers through combined MEK inhibition. *Cancer Discov* (2021) 11 (1):142–57. doi: 10.1158/2159-8290.CD-20-0142

80. Kessler D, Gerlach D, Kraut N, McConnell DB. Targeting son of sevenless 1: The pacemaker of kras. *Curr Opin Chem Biol* (2021) 62:109–18. doi: 10.1016/j.cbpa.2021.02.014

81. Shi ZQ, Yu DH, Park M, Marshall M, Feng GS. Molecular mechanism for the shp-2 tyrosine phosphatase function in promoting growth factor stimulation of erk activity. *Mol Cell Biol* (2000) 20(5):1526–36. doi: 10.1128/mcb.20.5.1526-1536.2000

82. Song Y, Zhao M, Wu Y, Yu B, Liu HM. A multifunctional cross-validation high-throughput screening protocol enabling the discovery of new shp2 inhibitors. *Acta Pharm Sin B* (2021) 11(3):750–62. doi: 10.1016/j.apsb.2020.10.021

83. Nichols RJ, Haderk F, Stahlhut C, Schulze CJ, Hemmati G, Wildes D, et al. Ras nucleotide cycling underlies the shp2 phosphatase dependence of mutant braf-, nf1- and ras-driven cancers. *Nat Cell Biol* (2018) 20(9):1064–73. doi: 10.1038/s41556-018-0169-1

84. Sun Y, Meyers BA, Czako B, Leonard P, Mseeh F, Harris AL, et al. Allosteric shp2 inhibitor, iacs-13909, overcomes egfr-dependent and egfr-independent resistance mechanisms toward osimertinib. *Cancer Res* (2020) 80(21):4840–53. doi: 10.1158/0008-5472.Can-20-1634

85. Ruess DA, Heynen GJ, Ciecielski KJ, Ai J, Berninger A, Kabacaoglu D, et al. Mutant kras-driven cancers depend on ptpn11/shp2 phosphatase. *Nat Med* (2018) 24 (7):954–60. doi: 10.1038/s41591-018-0024-8

86. Bendell J, Ulahannan S, Koczywas M, Brahmer J, Capasso A, Eckhardt SG, et al. Intermittent dosing of RMC-4630, a potent, selective inhibitor of SHP2, combined with the MEK inhibitor cobimetinib, in a phase 1b/2 clinical trial for advanced solid tumors with activating mutations of RAS signaling. *Eur J Cancer* (2020) 138:S8–S9. doi: 10.1016/S0959-8049(20)31089-3

87. Parikh K, Banna G, Liu SV, Friedlaender A, Desai A, Subbiah V, et al. Drugging kras: Current perspectives and state-of-art review. *J Hematol Oncol* (2022) 15(1):152. doi: 10.1186/s13045-022-01375-4

88. Liu C, Ye D, Yang H, Chen X, Su Z, Li X, et al. Ras-targeted cancer therapy: Advances in drugging specific mutations. *MedComm* (2023) 4(3):e285. doi: 10.1002/mco2.285

89. Mao C, Qiu LX, Liao RY, Du FB, Ding H, Yang WC, et al. Kras mutations and resistance to egfr-tkis treatment in patients with non-small cell lung cancer: A meta-analysis of 22 studies. *Lung Cancer (Amsterdam Netherlands)* (2010) 69(3):272–8. doi: 10.1016/j.lungcan.2009.11.020

90. De Roock W, Jonker DJ, Di Nicolantonio F, Sartore-Bianchi A, Tu D, Siena S, et al. Association of kras P.G13d mutation with outcome in patients with chemotherapy-refractory metastatic colorectal cancer treated with cetuximab. *Jama* (2010) 304(16):1812–20. doi: 10.1001/jama.2010.1535

91. Hatzivassiliou G, Song K, Yen I, Brandhuber BJ, Anderson DJ, Alvarado R, et al. Raf inhibitors prime wild-type raf to activate the mapk pathway and enhance growth. *Nature* (2010) 464(7287):431–5. doi: 10.1038/nature08833

92. Duncan JS, Whittle MC, Nakamura K, Abell AN, Midland AA, Zawistowski JS, et al. Dynamic reprogramming of the kinome in response to targeted mek inhibition in triple-negative breast cancer. *Cell* (2012) 149(2):307–21. doi: 10.1016/j.cell.2012.02.053

93. Cafri G, Gartner JJ, Zaks T, Hopson K, Levin N, Paria BC, et al. Mrna vaccine-induced neoantigen-specific T cell immunity in patients with gastrointestinal cancer. *J Clin Invest* (2020) 130(11):5976–88. doi: 10.1172/jci134915

94. Palmer DH, Valle JW, Ma YT, Faluyi O, Neoptolemos JP, Jensen Gjertsen T, et al. Tg01/gm-csf and adjuvant gemcitabine in patients with resected ras-mutant adenocarcinoma of the pancreas (Ct tg01-01): A single-arm, phase 1/2 trial. *Br J Cancer* (2020) 122(7):971–7. doi: 10.1038/s41416-020-0752-7

Frontiers in Immunology

Explores novel approaches and diagnoses to treat immune disorders.

The official journal of the International Union of Immunological Societies (IUIS) and the most cited in its field, leading the way for research across basic, translational and clinical immunology.

Discover the latest Research Topics

See more →

Frontiers

Avenue du Tribunal-Fédéral 34
1005 Lausanne, Switzerland
frontiersin.org

Contact us

+41 (0)21 510 17 00
frontiersin.org/about/contact